Journal of Pharmaceutical and Biomedical Analysis 66 (2012) 1–10

Contents lists available at SciVerse ScienceDirect

Journal of Pharmaceutical and Biomedical Analysis

journal homepage: www.elsevier.com/locate/jpba

Review

Application of the near-infrared spectroscopy in the pharmaceutical technology

Marzena Jamrógiewicz *

Medical University of Gdansk, Faculty of Pharmacy, Department of Physical Chemistry, Hallera 107, 80-416 Gdansk, Poland

ARTICLE INFO

Article history:
Received 4 October 2011
Received in revised form 5 March 2012
Accepted 7 March 2012
Available online 15 March 2012

Keywords:
Near-infrared spectroscopy
Pharmaceutical technology
Quantitative
Quality control
Multivariate analysis
PAT

ABSTRACT

Near-infrared (NIR) spectroscopy is currently the fastest-growing and the most versatile analytical method not only in the pharmaceutical sciences but also in the industry. This review focuses on recent NIR applications in the pharmaceutical technology. This article covers monitoring, by NIR, of many manufacturing processes, such as granulation, mixing or drying, in order to determine the end-point of these processes. In this paper, apart from basic theoretical information concerning the NIR spectra, there are included determinations of the quality and quantity of pharmaceutical compounds. Some examples of measurements and control of physicochemical parameters of the final medicinal products, such as hardness, porosity, thickness size, compression strength, disintegration time and potential counterfeit are included. Biotechnology and plant drug analysis using NIR is also described. Moreover, some disadvantages of this method are stressed and future perspectives are anticipated.

© 2012 Elsevier B.V. All rights reserved.

Contents

1. Introduction 1
2. Recommendations for NIR application in the pharmaceutical sciences 3
3. NIR in the pharmaceutical chemistry and physicochemistry 3
4. Steps of pharmaceutical technology, controlled by NIR 4
5. Plant drug analysis 4
6. Biotechnological medicinal products tested by NIR spectroscopy 4
7. Disadvantages of NIR spectroscopy 7
8. Conclusions 8
References 8

1. Introduction

Infrared spectral measurements have been used for a broad range of applications – from analysis of liquids, gas compositions and solid substances to detailed characterization of each physical state. One of the fundamental properties of chemical bonds is that they exhibit vibrations at distinct frequencies. The vibrational frequency of a chemical bond is intrinsic to the chemical bond of interest [1]. The electromagnetic energy of molecular vibration is defined as near-infrared (from 120 to 400 THz, from 2500 to 750 nm or from 12,500 to 4000 cm^{-1}), infrared, or mid-infrared (from 30 to 120 THz, from 2500 to 25,000 nm or from 4000 to 40 cm^{-1}) and far-infrared between 300 GHz and 30 THz (that is from 25,000 nm to 1,000,000 nm). Infrared radiation absorbed by an individual molecule causes particular bonds to vibrate in a manner which is similar to that of a diatomic oscillator. Therefore, it is convenient to start from the diatomic molecule as the simplest vibrating system and then extend the concept to polyatomic molecules. Changes in light energy between the three regions of infrared lead to varying absorptions of different molecules and bonds, inducing different types of vibrations. For instance, the least energetic far infrared region of light (FIR) is absorbed by heavy atoms, such as some inorganic and organometallic substances, while the mid infrared area (MIR) is used for organic chemical analyses.

Near-infrared (NIR) spectroscopy was not a popular technique until 1960s. The current triumph of this method is owed to Karl Norris who recognized the potential of the use of NIR in industrial practice for measurements of certain types of food, agricultural components [2] and product quality control. This method gained wide acceptance within the pharmaceutical industry, particularly for the analysis of intact dosage forms and process monitoring [3], and it could be applied for liquid, slurry, powdered or solid samples.

* Tel.: +48 58 349 16 56; fax: +48 58 349 16 52.
E-mail address: majam@gumed.edu.pl

0731-7085/$ – see front matter © 2012 Elsevier B.V. All rights reserved.
doi:10.1016/j.jpba.2012.03.009

A potential molecule, intended to be analyzed by NIR spectroscopy, should possess the change of dipole moment and also a large mechanical anharmonicity of the vibrating atoms [4]. Therefore, a large variety of compounds is appropriate for analysis in the range of near-infrared. Characteristic features of the NIR spectrum are overtones and combination bands of CH, OH and NH functionalities which dominate the spectrum, whereas the corresponding overtones resulting from the fundamental absorption values of the most intense MIR area are rarely represented [5]. Overtones (electron excitations to higher energy levels) are similar to octaves in a musical scale, like harmonics of the fundamental vibrational frequencies [6]. Combination bands are the sum of two different vibrations corresponding to different chemical bonds. Although the absorbance values of combination bands and overtones are smaller than transitions ones, in bulk materials (for example pharmaceuticals) this feature is an advantage because of the material's properties, which allow obtaining high absorbance values.

Unfortunately, because of the overlapping of overtones and combination of vibrations NIR spectra are much more complicated for interpretation [7]. The total NIR spectrum contains up to four overtones from the absorptions of methyl (C—H), methylene (C—H), methoxy (C—H), aromatic (C—H), carbonyl associated (C—H) groups, N—H from primary and secondary amides, N—H from amines (primary, secondary, and tertiary), N—H of amine salts, O—H (alcohols and water), S—H, or C=O groups [8]. In some papers clarification of spectroscopic signals and wavenumber ranges characteristic for each vibration–harmonics could be found [9].

Over the last few years near-infrared spectroscopy has developed into indispensable tool for academic research and industrial quality control in a wide field of applications, from the synthetic chemistry to the agriculture and from some life sciences to the environmental analysis. It is the crucial method also in the pharmaceutical area, mainly in such branches as technology, microbiology, toxicology, counterfeit detection, determination of physicochemical properties, stability testing and also quality control of a final product. Pharmaceutical technology needs NIR spectroscopy for implementation of *in-* and *on-line* processes control in many phases of manufacturing process (Fig. 1) [10–13].

The identification of specific wavelength regions is needed when changes in the signal obtained from the near-infrared spectrometer indicate the changes which are proportional to the concentration of chemical components of pharmaceuticals, or represent the physical characteristics of samples under analysis. Generally, qualitative and quantitative analysis performed by near-infrared spectroscopic methods requires the application of multivariate calibration algorithms (MCA), and, eventually, the usage of some chemometric methods essential for model spectral response to chemical or physical properties of a calibration or learning model set. It is possible and also quite recommended to create the spectral library of standard pharmaceutical materials using NIR spectroscopy as a rapid, non-invasive technique for compound identification [14]. Very useful information about characteristic bands of active pharmaceutical ingredients (APIs) or excipients is contained in recent publications [15]. There is also a need for verification and identification of such simple compounds or residual solvents as methanol and ethanol in pharmaceutical products. Two-dimensional (2D) correlation near-infrared spectroscopy sometimes is very useful for difficult and not typical analysis. This technique is useful for discovery of some special vibration modes that cannot be clearly seen in the original spectra. In example it is suited to distinguish between specific bands for methanol and ethanol which are not clearly observed in the combination vibration region of spectrum (5000–4500 cm^{-1}) [16].

NIR spectroscopy is a valuable diagnostic tool which can be used for elucidation of comprehensive structural information of numerous biological samples. The comprehensive vibrational

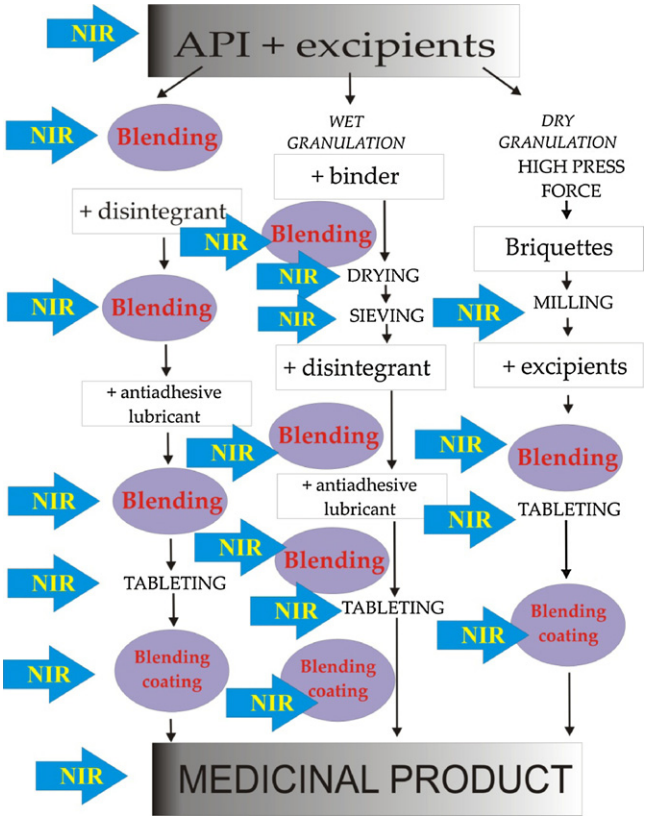

Fig. 1. Critical stages of pharmaceutical manufacturing process of medicinal products with the usage of NIR spectroscopy.

spectroscopic studies were performed for a group of newly developed synthetic biopolymers. In this case, NIR spectra result mainly from these vibrational regions which could be divided into:

- the first overtone of the hydroxyl stretching region;
- the second overtone of the C—H stretching mode, which could be found in the high wavenumber region between 9000 and 6500 cm^{-1};
- the first overtone of the C—H stretching vibrations, which could be found in the 5900–5350 cm^{-1} region;
- the combination of O—H stretching (mode) and second overtone of the C=O stretching mode, arising in the lower wavenumber region between 5300 and 4800 cm^{-1} [17].

The assignment of NIR absorption bands is important for simple band identification of active compound contained in a formulation [18], as well as for the recognition of reaction product and also for the monitoring in the synthesis reactor. Petter et al. presented a simple NIR spectroscopy method for monitoring of the peptide reaction between oxytocin and glutathione [19]. A qualitative model of analysis allowed rapid identification of newly produced conjugates, while a quantitative method was aimed at determination of the amount of oxytocin and glutathione degradation products.

A number of data and detailed spectra structure correlations have been presented in a comprehensive handbook by Workman and may be helpful during interpretation of NIR spectra [10]. Author described the increased interest of spectroscopists, particularly these involved in implementation of process of near-infrared measurements, in this spectral region. Moreover, some examples of useful near-infrared absorption bands are presented in a book about NIR implementation by Katherine Bakeev [9].

2. Recommendations for NIR application in the pharmaceutical sciences

Advanced medicinal products require new generations of pharmaceutical manufacture which must be ready for improved quality control of each step in the unit process of dosage form development [20]. In 2003, the Food and Drug Administration Agency (FDA) announced Pharmaceutical Current Good Manufacturing Practices (cGMPs) for the 21st century in order to modernize all the regulations and to get a better knowledge of the production processes. This document is recommended and respected all over the world. Generally, it is based on a risk approach of assurance of a pharmaceutical product quality and provides an implementation of Process Analytical Technology (PAT) in the process control of raw-materials, intermediate and final products [21,22]. Priority manners are focused on minimizing unwanted effects in the manufacturing process and on avoiding defects in the final products [23,24].

The reason for increasing industrial application of NIR spectroscopy in biomedical fields and pharmaceutical manufacture is the possibility of non-invasive mode of analysis [25]. It may be used in the determination of biochemicals in blood. Moreover, in spectrophotometric methods used for process control it is crucial to receive signals from different points along the production line and to obtain the information from each measuring point.

The implementation of the PAT system requires the identification of critical parameters for each technological stage. Analytical techniques chosen should allow the measurement of effects and statistical analysis in a very short time. Near-infrared spectroscopy belongs to these techniques [26] and is suitable for *on-*, *in-* and *at-line* process examinations. "*In-line*" means that process is monitored inside a reactor or a lyophilizer while "*on-line*" represents continuous control up to the end point (a sample flows through the outer tube). Spectrum registration not directly at the production line, but close to it, is called "*at-line*".

An additional advantage of NIR is the possibility to handle and control a great number of industrial/technological variables which must be optimized in manufacturing processes. In February 2009, the European Medicines Agency (EMA) published the draft of a revised guideline on the use of NIR by the pharmaceutical industry and the data requirements for new submission and variations involving this technique [27]. According to cGMP the use of NIR spectroscopy is recommended in analytical procedure of technological production of dosage forms.

3. NIR in the pharmaceutical chemistry and physicochemistry

Near-infrared spectroscopy provides a rapid analysis of a wide range of materials, giving a possibility of obtaining a large number of chemical and physicochemical parameters or even chemical composition of some formulations as well. Various pharmaceutical parameters from tablet technology, such as hardness, particle size, compaction force, dissolution rate, or water content, can be quantitatively analyzed by NIR spectroscopy [3,28]. Good standard of granulation step is acquired due to such quantity and quality tests as moisture content, particle size distribution and bulk density [29]. Tablets made of fine-grained powder are often smooth and easy to compress. The harder is a tablet, the smoother is its surface. Differences in properties cause reduction of light scattering and consequently build an upward shift in the spectral baselines for smooth surface (small particles powders). Similar situation is observed during determination of coating thickness in NIR reflectance spectra. When the coating arises on a tablet, the absorbance values of core components decrease, because NIR radiation reaching the tablet core decreases and radiation reflected by coating components increases [30,31].

The numerous possibilities of application of the NIR spectroscopy and chemometric methods in the pharmaceutical area, especially in the identification of raw materials, according to the quality control, as well as determination of moisture, are presented precisely in the review article written by Luypaert et al. [32].

The usage of NIR spectroscopy is very often based on a simple identification of active compound present in a drug. Civilization problem with counterfeit medicinal products is a plague not only in Asia [33]. Much harm is done to the customers because of taking up such drug products. The manufacturers suffer the greatest loss because of counterfeit drug products and therefore they have started to develop various anti-counterfeiting practices such as different analytical techniques, mainly NIR spectroscopy, thin layer chromatography (TLC) or methods based on colorimetric detection [34].

NIR spectroscopy allows selection of some characteristic spectral bands and comparison of specific spectrum of original drug product with unknown or doubtful one (e.g. with different pharmaceutical excipients). For example, when the spectra of Chinese Sildenafil [35,36] and Viagra® are compared, the major variability between 5500 cm^{-1} and 5000 cm^{-1} could be observed [37]. As another example could serve "high-quality" Metronidazole, which counterfeit and original could be detected only by means of chemometric NIR data [38]. NIR spectroscopy was also successfully applied during identification of confiscated drug blister, which proved to be bisoprolol-hemifumarate [39]. Important analyses of counterfeit confirmation are frequently performed on the basis of NIR libraries created.

Special pharmaceutical excipients added to pharmaceutical formulations create a unique composition which is difficult to identify by means of analytical methods recommended by Pharmacopoeias [40–42] for particular drug compound, such as infrared spectroscopy or liquid chromatography. Excipients obtained from different manufacturers sometimes possess dissimilar physical properties, particle size or purity. Therefore, there is a need of view into the structure of each ingredient of the drug product and of determination of its quality. For example, NIR spectroscopy may be used for recognition and confirmation of some compounds commonly used as tablet excipients, because in the process of manufacturing dosage forms all ingredients must be reliably identified. In the current literature some examples about the capability of FT-NIR spectroscopy to identify such substances as potassium sorbate, sodium starch glycolate, calcium ascorbate, calcium carbonate, candelilla wax, maltosextrin, monohydrated or anhydrous lactose could be found [15]. The discrimination between anhydrous and monohydrate form of lactose was done reliably inside USP vials. Specific NIR band of lactose monohydrate corresponds to 1991 nm, while the anhydrous form possesses no band in this region. Apart from complex mixtures analysis [43], all kinds of quantity [44–46] and quality determination are performed in case of detection [47] and location of chemical substances in a solid dosage forms [48]. The usage of NIR spectroscopy for comparison of manufacturing series and batches of pharmaceutical products is fast and simple due to chemometrics [49].

In a study conducted by Bittner et al. [50], the simultaneous identification and particle size determination of amoxicillin trihydrate in bulk materials was performed. NIR spectra of the observed particle range of 7–22 μm showed an inverse relationship between absorbance (baseline offset) and particle size. Similar observation about the increase of baseline offset with decreasing particle size of measured material was also done by Abebe et al. [51].

The use of infrared spectroscopy is suggested by a Q6A document of ICH as a way to perform and confirm the identification of tablets and to obtain high-throughput and accurate

multiparametric data collection, as presented for a coated solid dosage form – thiamazole tablets containing 2, 4 and 8% of active compound [52].

4. Steps of pharmaceutical technology, controlled by NIR

There are many industrial or scientific reports about the usage of near-infrared spectroscopy for API determination not only directly in a formulation, but also as a raw material or during different manufacturing processes [10–13]. The latter depends on homogeneity of the formulation and compound's stability. A non-destructive NIR method of drug content prediction has recently been presented in various aspects:

- determination of API in a case of powders with different particle size, which form agglomerates during blending. This research described the problems during tablet manufacture, when the presence of large agglomerates changes the content of API in the direct compressive process and powder tableting [47]. The usage of NIR-Chemical Imaging Spectroscopy method allows to see the influence of particle size on the frequency of agglomerates formation;
- monitoring of unstable dosage forms such as suppositories containing acetylsalicylic acid [53], finding an alternative method for nimesulide analysis in pharmaceutical formulation, which is easier and faster in comparison with potentiometric titration [44];
- quantification of low dosage pharmaceutical forms (for example syrup with acetaminophen, containing 16–24 mg/ml of the substance) which could be a very challenging task because of relatively low sensibility of NIR spectroscopy methods [54], development of a more suitable analytical method for oral solutions with dipyrone than iodometric titration [55];
- usage of appropriate NIR spectroscopy models for complex pharmaceutical matrixes, for example a hydroalcoholic gel containing ketoprofen and two preservatives [56], examination of suitability of a diffuse "transflection" technique for determination of diphenhydramine hydrochloride in pharmaceutical wafers with 2.5 cm diameter and a thickness of about 80 μm [57]. Samples during measurements are placed directly on the round window, covering the integrating sphere, and masked with a diffusely reflecting gold plate. NIR radiation after penetration through the sample is partially absorbed and partially reflected back into the sample, allowing the radiation to penetrate through the wafer twice;
- development of a method that allows the simultaneous identification and quantification of ranitidine in granulates for compression, cores (as intermediate) and coated tablets [18].

Japanese researches published some scientific reports about NIR spectroscopic analyses of two APIs, coexisting in one tablet or forming bilayer [58,59]. Due to irradiated NIR rays, penetrated through the tablet, a method developed was non-destructive and effective. The transmittance technique allows a simultaneous analysis of the two layers. A highly sensitive method for determination of tablet thickness fluctuation was also described [60].

The utility of near-infrared spectroscopy for simultaneous *in-line* drug and excipients quantification in manufacturing processes is presented in many publications (Table 1).

During the last few years, growing interest in the use of Near-Infrared Chemical Imaging (NIR-CI) method in the field of pharmaceutical analysis is observed. The reason for increasing popularity of this method is its ability to provide a wealth of information from a single sample, including the quantitative composition analysis and distribution of ingredients. For example, the content and homogeneity distribution of acetylsalicylic acid in commercial tablets were analyzed by applying quantitative algorithm to global hyperspectral image [86]. NIR-CI system was also used for analysis of ibuprofen location in calcium phosphate granules [87]. It was possible to investigate the chemical composition of some granules at high magnification and to gain useful knowledge of the spatial location of the components.

None of the authors have investigated the influence of fluctuations of environmental factors or time delay during spectra recording on the images obtained. NIR-CI allows observation of the contrast effect of the surface containing a number of ingredients and therefore this method may be compared with microscope techniques.

5. Plant drug analysis

In the last 40 years near-infrared spectroscopy became one of the most useful methods for analysis not only strictly pharmaceutical compounds but also proteins, dry matter of plant extracts or carbohydrates quantity in many agriculture related products and plant materials [3]. Some of them are intended to become medicinal products. Recently, the use of NIR spectroscopy in determination of some minor compounds such as alkaloids, tocopherols, phenolic and glycoside compounds, glucosinolates, or essential oils in plant materials has been reported [88,89]. In most cases authors claimed that the biggest challenge in the wider use of NIR spectroscopy is the interpretation of complex spectra obtained. Despite many multivariate analyses or chemometrics models used for the interpretation of spectra, the knowledge of the principles of molecular spectroscopy in natural products analysis is still the main barrier in understanding the basis and functionality of the models developed.

Pharmaceutical plants are often analyzed and classified due to the presence of some special marker compounds or medicinal compositions. Three species of *Dendrobium* (Orchidaceae), used for stomach nourishing, promotion of production of body fluid and fever reduction, were determined by NIR [90]. It was showed that the samples analyzed could be successfully verified on the basis of intensities of particular patterns of spectral bands at 5180 and 4900–4800 cm^{-1}. This study proved to be very useful and allows comprehensive evaluation of the different origins of *Dendrobium*, as well as estimation of their clinical efficacy.

Ginkgo biloba extract could be qualified as raw material intended for use in pharmaceutical products. Some quality specifications of *G. biloba* extract, intrinsic to its natural origin, show unpredicted and uncontrolled variability, which has influence on the manufacturing process of solid dosage forms (*viz*. granulation and compression). Some of these variabilities could not be determined by conventional quality control tests, therefore NIR method was used for qualification of the batches of *Ginkgo* extract, according to their different features, and for establishment of relationship between some of the manufacturing steps. Several approaches were evaluated, and the NIR method developed proved to be sensitive to changes in important quality specifications and therefore adequate for qualification of incoming batches of *G. biloba* extract [91]. Nowadays, medicinal plant preparations are produced with the highest quality control measurements, and each step of their manufacturing is also verified with PAT tools, such as NIR spectroscopy methods.

6. Biotechnological medicinal products tested by NIR spectroscopy

Apart from applications in pharmaceutical technology, chemistry or industry, near-infrared spectroscopy has also successfully been applied in the biotechnology field. Using near-infrared dyes, it is possible to analyze DNA and protein molecules [92], to detect some genetically modified organisms by comparison of their DNA

Table 1
The utility of NIR spectroscopy in the pharmaceutical technology processes.

Analyzed compound	Purpose	Range [cm^{-1}]	Description	Parameters	Ref.
Polymorphism					
Sulphathiazole	Comparison with other methods for the analysis of the solid-state forms of sulfathiazole polymorphic forms, such as DSC, XPRD, NMR, Raman spectroscopy	10,000–4000	Quality and quantity	Heating temp. 180 °C; drying temp. 105 °C Time of heating 30 min.	[61]
Acetaminophen	Polymorphic transformation monitored during a cooling crystallization process	14,000–4000	Quality, compared with crystallographic data, XRD and DSC	Cooling from 60 °C (1 °C/min)	[62]
Fluconazole	Determination of pure crystalline fluconazole form II in a binary polymorphic mixtures containing forms I and II comparing with XPRD	12,500–4000	Samples obtained by mixing known quantities of pure polymorphic forms II and III	A set of 12 samples covering a concentration range from 37.5 to 87.5% (37.5, 50, 62.5, 87.5% (w/w) was used to test	[63]
Crystallization					
Ibuprofen	Comparative study of attenuated total reflectance (ATR), Fourier transform infrared (FTIR), and Fourier transform (FT) near-infrared (NIR) spectroscopy for batch cooling crystallization of four different crystallization systems	12,000–4000	Quality and quantity	Cooling (0.5 °C/min)	[64]
Cephalexin	The crystallinity of cephalexin in microcrystalline cellulose was determined with the molecular interaction of a ground amorphous solid investigation. X-ray powder diffraction profiles were determinated	8500–8300	Quality and quantity	6 types of standard material with various degrees of crystallinity were prepared by the physical mixing	[65]
Trehalose	The phase behavior of sugars in ice and lyophilized solids was investigated for quantitate trehalose crystallization comparing with Raman spectroscopy	10,000–4000	Quality and quantity	Amorphous trehalose was prepared using aqueous trehalose solutions frozen at −70 °C and freeze-dried at −40 °C with pressure of approximately 100 mbar for 72 h	[66]
Particle size					
Dibasic calcium phosphate	Quantification of the median particle size of dry powders	9100–4550	Quality and quantity	Diameter of fractions: 53, 75, 106, 150, 180, 212, 250, 300 μm time of mixing 10 min	[67]
Particle size distribution					
Acetaminophen	Quantitative determination of acetaminophen in granulates, establishment of the particle size distribution and examination of average particle size was performed. The granulate samples were used to obtain laboratory tablets examined in the study. Particle size distribution was determined by using a PLS2 model allowing correlation between the spectral data matrix and more than one variable and prediction of various particle sizes with a single calibration model	9000–4000	Quality and quantity	Temp. 60 °C, compacting pressure 195–215 Mpa, time 180 min	[68]
Humidity/water content					
Unknown API	*In-line* measurement of water content during the fluid bed drying process of a drug product. This method is currently being applied on the commercial scale to control the drying end point	8500–4800	Quality and quantity	Time: 30 min, temp. 60 °C, air volume 1400–2300 m^3/h	[69]
Unknown API	Determination of moisture content ranging from 1% to 8%. The calibration protocol covered 6 different moisture levels: 0.5%, 1%, 2%, 4%, 8% and 10%. The entire calibration was performed within 2 days. Batches belonging to three different production campaigns were chosen. Each sample was measured with the NIR spectrometer in triplicate under two different temperature conditions: 5 and 25 °C.	12,500–3600	Quantity	Heating temp.: 105 °C, time: 90 min	[70]
Lyophilized allergen vaccine products	The small amount of samples (10 mg/vial), despite of low moisture content it was possible to use the NIR spectroscopy method	14,300–4000	Quality	–	[71]
Blending					
Acetaminophen	Distribution of mixture components and simulated chemical concentrations of samples in a small scale with the usage of chemical imaging	7140–6000	Quality and quantity	Time: 0.5, 1, 2, 5, 10, 15, 20, 24, 30, 40 min; Rotation: 25 rpm	[72]
Acetaminophen	Determination of blending end-point by the usage of a high rate of spectra collection (sensors positioned at the top and rotational axis of a bin-blender)	11,000–6000	Variation of concentration	Time: 90 min, 200 spectra	[73]

Table 1 (*Continued*)

Analyzed compound	Purpose	Range [cm^{-1}]	Description	Parameters	Ref.
Unknown API	A real-time noninvasive NIR quantitative method was developed for *on-line* blend uniformity analysis and transfer of the calibration model from laboratory to industrial scale	7400–6600; 6600–5500	Quantity	Rotation: 25 and 10 rpm; Time: 8, 20 min	[74]
Acetaminophen	Monitoring of the concentration of acetaminophen blends during the real time of the mixing process	8800–6000	Quantity	Rotation 1.000 rpm; Time: 2 min	[75]
Unknown API	Based on a powder blend study, it was shown that the current practice of calculating the % standard deviation for a given component within a specimen was not enough sensitive to assess blend uniformity	8300–4200	Quantity	Rpm = 12; Time: 3, 5, 7, 9, 11, 13, 15, 17, 19, 21, 23, 25, 27, 29, 60 min	[76]
Tobramycin base	Assessing blend uniformity in the context of the specific constraints of complex seven-component blends and small batches	10,000–4000	Quantity	Rotation: 67 rpm; Time: 19 min	[77]
Tabletting					
Micronized chlorphenira-mine maleate	*In-line* quantification enabled the content analysis of individual tablets in the production batch and detection of problems with content uniformity towards the end of the tabletting process. Furthermore, it provided the assurance of in-process monitoring of content uniformity of the particular excipients during the tabletting process	10,200–5200	Quality and quantity	5 kg powder batch; Time: 30 min; Rotary tabletting machine with 10 mm flat faced punches, operated at a speed of 10 rpm. Tablet weight: 530 mg	[45]
Compacts of lactose monohydrate with lubricant	Monitoring of the physical quality of tablets, control of tableting process and final ejection and production of density profiles by the usage of NIR-Chemical Imaging method	7100–4000	Quality and quantity	Lactose monohydrate was blended with 0%, 0.25%, or 1.0% MgSt for 30 s or 30 min. Compacts were prepared of each blend, with compaction forces monitored by load cell	[78]
Compression					
Metoprolol tartrate	Demonstration of physical changes due to compression differences (porosity, hardness)	7000–4000	Quality and quantity	Tablets prepared by direct compression and wet granulation. Time 10 s, pressure: 6.9–31 MPa	[79]
Production process of a new potent drug	Blend homogeneity, content uniformity, tablet coating thickness. A total of 720 tablets from five batches were used as calibration set. Target value was 2.98% (w/w). The validation set – 15 cores each compacted at 100–400 MPa	12,500–5800 and 12,500–3600	Quality and quantity	Duration of each mixing step: 25 min, rpm = 15, compression forces 100–400 MPa	[31]
Coating/film thickness					
Sulfanilamide-based tablets coated with HPMC, PEG mixture	*In-line* control of the coating thickness (3% deviation from the actual thickness), end-point determination for the fluid-bed coating process	7500–4800	Quality and quantity	Time: 160 min, number of tablets: 1.300, turnplate: 200 rpm, fan flow: 125 m^3/h, temp. 238 °C, humidity 40%, spraying rate 1.1 mL/min, shaking bag interval: 60 s	[80]
MCC, lactose monohydrate, PVP, PEG 400, HPMC, fluorescein sodium salt	Correlation between *in-line* NIR spectra from a fluid-bed pellet coating process and two separate methods for determination of coating thickness; laser diffraction particle size analysis and image analysis	7500–5000	Quality and quantity	Inlet air temp. 50 °C, air flow: 60 m^3/h, spray rate of coating solution: 1 mL/min, atomization pressure 5 psi	[81]
MCC, lactose, PVP, starch	Quantification of coat thickness for tablets coated at different process conditions with the use of optical microscopy, micrometer, X-ray fluorescence, Raman and NIR spectroscopy. Tablet weight, thickness and diameter, hardness, surface roughness and color were determined	9100–4000	Quality and quantity	Tablets (6 mm diameter), 15% (w/w) solids coating dispersion composed of 12% (w/w) hypromellose, 2% (w/w) polyethylene glycol, and 1% (w/w) iron oxide in water	[82]
PE and 0.1% Aerosil 200	A novel small-scale coating system as a method of preparation a calibration model used to predict the coating layer thickness. In-line coating analysis useful during the early stage of formulation studies when the amount of drug is limited and formulations are being tested on a small scale. Determination the coating thickness of tablets in a drum coating process was performed. High-density polyethylene used a strong NIR absorber to enable the detection of a core signal.	9100–4500	Quality and quantity	Tablets diameter between 7 and 11 mm, rotation speed 1 rpm, Six experiments with different rotations: 5, 10, 12, 15, 20, 25 resulting in thickness from 25 to 400 μm	[83]
Porosity					
Folic acid, microcrystalline cellulose, crosscarmellose sodium, magnesium stearate	Assessment of the effects of compaction variability in the tableting process on the performance of content prediction using NIR diffuse transmission mode. Examination of the effects of tablet thickness variation and/or porosity on the spectra. Elucidation of the proportional contribution of various areas of a tablet to the final NIR spectrum in diffuse transmission mode	11,520–6000	Quality and quantity	Time of mixing: 12 min, tablet mass: 200.46 mg, diameter 10 mm, thickness 2.39 mm, resistance to crushing 95.33 N, porosity 30.79%, dwell time 118.30 ms, upper compaction force 3.90 kN	[84]
Stability testing					
Metoprolol tartrate tablets	Presentation of differences in spectra obtained from metoprolol tartrate tablets packed in the original high density polyethylene containers or in USP Class A unit-dose blister packs	7000–4000	Quality and quantity	1. Temp. 25 °C, humidity: 60% 2. Temp. 40 °C, humidity 75%; Time: 13 and 52 weeks	[85]

fragments [93], and above all, to examine the activities and roles of a particular gene expression in some seed phenotypes with regard to their physiochemical composition [94]. Near-infrared spectroscopy characteristics have also been used for localization of some oxidative DNA damages [95].

The development of some new analytical tools, including spectroscopic sensors and data analysis, still continues. Miniaturized tools for remote environmental monitoring, based on integrated circuit technology, have recently been developed, leading to the marriage of biosensors and the lab-on-a-chip [23]. Near-infrared spectroscopy has many applications as a process monitoring and process supervision technique, also in the context of biomanufacturing. An industrial pilot-plant process of mammalian cell cultivation presented the use of *on-line* in situ NIR application by means of an immersion transflectance [96]. For animal cell culture processes, important recommendations for improving efficiency and for ensuring the quality of the final product were defined by PAT. An analytical procedure, using FT-NIR spectroscopy and chemometrics with multivariate techniques, was developed for the determination of the fruit authenticity and for the quantification of the fruit content [97]. Spectral information was correlated with the fruit content and gravimetric data obtained from sequential fractionation of the alcohol-insoluble residue. The contents of rhamnose, fucose, arabinose, xylose, mannose, galactose, and glucose in the hemicellulose fraction of apricots, peaches, and pumpkins were correlated and determined.

NIR is also an improved method for evaluation of the amount of physiologically acceptable polymer moieties (PEG) conjugated to a protein. None of the existing analytical methods (colorimetry, HPLC, phase-partitioning) are reliable enough for the quantitative determination of the amount of polymer molecules bound to a protein. This patented method [98] involves contact of the sample with a light source in the near-infrared spectrum and then measurement of relative absorbance levels. Inventors of the method claimed to determine over a range of the near-infrared wavelengths the number of polymer molecules, conjugated to the protein or protein complex. The essence and important advantage of the near-infrared spectroscopy is that this technique is useful in studies in which other methods are inadequate or ineffective.

A large number of biomolecules with potential pharmaceutical application are produced just as all medicinal products on the basis of Quality-by-Design (QbD) initiative [99]. Desired biological properties of the molecules are achieved during development of such factors as serum half-life, formulation, aggregation propensity, and immunogenicity, which are important for the production of the biologically active molecule.

7. Disadvantages of NIR spectroscopy

Near-infrared spectroscopy possesses several advantages over other analytical techniques used in the pharmaceutical technology but there are also some disadvantages of this method (Table 2).

One of the main disadvantages of NIR spectroscopy used in pharmaceutical technology is a problem with aqueous environment (solutions of medicinal products or active pharmaceutical ingredients alone) for direct quantity determinations. High absorbance of water, which leads to a broad peak on a spectrum, creates a limit of detection for other compounds that are present in the sample analyzed in smaller quantities. In situ NIR spectroscopy technique allows monitoring an activated sludge reactor by estimation of the nitrate and oxygen concentration ($N—NO_3^-$) and the amount of total suspended solids [100]. Characteristic spectra were collected with the use of immersion probes on the settler. This alternative method, both with UV–Vis spectroscopy, presents clear advantages during monitoring and controlling of wastewater treatment processes as well as provides a way of qualification. Such quantitative studies are very important also in toxicological measurements of wastes from pharmaceutical manufactures.

During work with samples which may suffer any kind of periodic or seasonal change, NIR operators should be aware of any changes in the reference method which may negatively impact the calibration process. Keeping the sample calibration pool updated by adding new samples when required and using standards for periodic examinations should be an obligatory practice by NIR calibrations, which means that standardization tasks are periodically unavoidable [101].

Scientific and academic groups of pharmacists and chemists are not especially involved in the applications of NIR method. This may be due to the fact that during academic work smaller amounts of samples are prepared in comparison with industrial conditions. Routine in work with reference methods is accepted and sufficient when a great number of samples are analyzed. Therefore, NIR spectroscopy is the most popular method used by people working or connected with industry, where PAT, FDA or Pharmacopoeias recommendations play a primary role.

A proper interpretation of results obtained after application of NIR spectroscopy in quality as well as quantity determination, which usually are numerous, chemometric data, is a difficult task. A person who operates NIR device must be well prepared to choose the best from many spectra obtained by pre-treatments steps, calibration and validation processes for further calculation. Apart from software developed for a method planning and setting for special analysis (establishment of API concentration, end-point determination or identification) NIR operator needs a harder view to manipulate spectra obtained in order to create good fitted mathematic results. Good analytical practice requires collaboration between analyst, chemist, technologist and also well-educated mathematician or statistician for proper calculation of all data.

NIR spectroscopy provides an alternative for validated conventional methods. Although, it is important to keep in mind restrictions about sensitivity and equipment or environmental specificity of this method. It cannot be repeated easily in official control laboratories, so the reference method needs to remain the important part of the official specifications. Current software allows development of NIR spectroscopy methods with minimal understanding of the relevant chemometrics, which creates a high risk of obtaining invalid results due to some unknown hidden variables [102].

Choice of proper parameters during pre-treatments operations or spectral pre-processing methods, which are needed during the near-infrared spectroscopy application, is regulated by a set of mathematical procedures before development of a calibration model. Mathematical pre-treatment of spectrum reduces noise or background information (smoothing techniques) and increases signal from the chemical compound analyzed (differentiation process). Any pre-treatment technique should succeed in a robust model with good predictive ability. In general, pre-processing methods can be defined as baseline correction–normalization, enhancement, and statistical filtering of the signal obtained. The effects of several pre-processing methods used on absorbance spectra obtained by reflectance mode instrument are presented by Agelet and Hurburgh [8]. The offset baseline correction could be observed when pre-processing method with SNV (standard normal variation) is used. With the usage of MSC (multiple scatter correction) and first and second Savitzky–Golay derivatives preprocessing methods, after elimination of scatter effects, the spectra obtained are more grouped together. In each case, the NIR operator is forced to choose a proper way to achieve satisfactory results. This step of analysis may cause some difficulties.

According to Lambert–Beer's law, in the case of calibration of spectroscopy method, the linear correlation between analyte or

Table 2
Several advantages and disadvantages of NIR spectroscopy application in the pharmaceutical technology and manufacturing.

Advantages	Disadvantages
Non-destructive and non-invasive method	Low sensitivity of the signal limit by the determination of substances with concentration below 0.1% (w/w)
Rapid spectral measurements (<1 min)	The initial high financial investment for the instrumentation
Low-cost of analysis – no chemical reagents needed, single operator can analyze a large number of samples	Development of calibration models requires high trained personnel
A possibility of scanning several spectra on the same object permits obtaining more representative sample composition and more accurate result of analysis	Accurate and robust calibration requires a large data set incorporated with large variation, which is often difficult to obtain
Sample requires minimal (drying and grinding) or no preparation	Requires a continuous maintenance of the calibration data set
Several constituents of the same sample can be measured at the same time	It is difficult to transfer calibration between instruments of the same manufacture or between different manufactures
Easily applicable in different environments such as industry or laboratory	It requires an accurate chemical and physical analysis of reference samples
Measurements can be carried out *on*/*in*/*at line*	
The possibility of using optical probes allows analysis of the sample in situ	
The availability of portable instruments permits obtaining spectra directly in the field, which is useful for following some active processes	
Ability to penetrate glass containers	
Can also be used for particulate level (e.g., particle size) and bulk level (e.g., water content) measurements with proper calibration	

property measured and its absorbance should be the first assumption. NIR calibration models correlate either raw or pre-processed spectra with one or more chemical-physical properties of a set of samples. As complicated as it may sound, there are several well-developed calibration methods which are proved to work with most of NIR applications and also are included in all chemometric software packages.

Unfortunately, NIR spectroscopy has received some bad publicity as a "black box" technique. Something is introduced into the black box and something out of this box is replaced without the knowledge of a mechanism or detailed calculation. Testing of a method is combined with verification and validation, while verification means checking the components of the system in terms of their compliance with the attached specifications. Moreover, it is often said that chemometric correlation requires a lot of faith in numbers that many spectroscopists do not possess [103]. Making a lot of analyses on a modern instrument without advanced courses about proper usage of complicated software may be in fact a totally bad experience.

NIR spectroscopy has increasingly been adopted as an analytical tool (PAT) in pharmaceutical industry, mainly on the step of pre-formulation and quality control of manufacturing process. The fast and harmless analysis performed and samples characterization as well as this method flexibility is the main reasons for popularity and particular usage of NIR.

8. Conclusions

There are many applications of near-infrared spectroscopy in the pharmaceutical technology. In addition, many difficult technological problems in the scientific or industrial field may be solved due to this popular PAT tool. NIR spectra band depends on the physical or chemical nature of the sample and allows its identification as well as determination of physical or chemical parameters of the sample. The advantages of NIR spectroscopy method are numerous: non-invasive and non-destructive techniques, no preparation of sample, high frequency of spectrum acquisition, as well as large number of molecules which could be quantified. NIR method is crucial not only in scientific, but also in practical sense. It requires cooperation between good chemists, pharmaceutical technologists and mathematics for chemometric calculations and results description, and this trend corresponds to the interdisciplinary of science also in other fields of manufacturing practice. NIR spectroscopy will certainly play a key role in the analysis of many industrial processes after implementation this method into the real-time process monitoring during continuous pharmaceutical production.

References

[1] P. Atkins, Physical Chemistry, fifth ed., Freeman, New York, 1994.
[2] J.R. Hart, K.H. Norris, C. Golumbic, Determination of the moisture content of seeds by near-infrared spectrophotometry of their methanol extracts, Cereal Chem. 39 (1962) 94–99.
[3] C.A. Anderson, J.K. Drennen, E.W. Ciurczak, Pharmaceutical applications of near-infrared spectroscopy, in: D.A. Burns, E.W. Ciurczak (Eds.), Handbook of Near-Infrared Analysis, Taylor & Francis Group, 2008, pp. 585–612.
[4] M.J. Pelletier, C.C. Pelletier, Spectroscopic theory for chemical imaging, in: S. Sasic, Y. Ozaki (Eds.), Raman, Infrared, and Near Infrared Chemical Imaging, Wiley, 2010, pp. 1–20.
[5] H.W. Siesler, Y. Ozaki, S. Kawata, H.M. Heine, Near-infrared Spectroscopy Principles, Instruments, Applications, fourth ed., Wiley, Weinhein, 2002.
[6] F.H. Long, Vibrational spectroscopic methods for quantitative analysis, in: K. Huynh-Ba (Ed.), Handbook of Stability Testing in Pharmaceutical Development, Springer Science, New York, 2009, pp. 224–228.
[7] E. Alm, R. Bro, S.B. Engelsen, B. Karlberg, R.J.O. Torgrip, Vibrational overtone combination spectroscopy (VOCSY) – a new way of using IR and NIR data, Anal. Bioanal. Chem. 388 (2007) 179–188.
[8] L.E. Agelet, C.R. Hurburgh, A tutorial on near-infrared spectroscopy and its calibration, Crit. Rev. Anal. Chem. 40 (2010) 246–260.
[9] M.B. Simpson, Near-infrared spectroscopy for process analytical technology: theory, technology and implementation, in: K.A. Bakeev (Ed.), Process Analytical Technology. Spectroscopic Tools and Implementation Strategies for the Chemical and Pharmaceutical Industries, John Wiley & Sons, New York, 2010, pp. 40–51.
[10] J. Workman Jr., A review of process near infrared spectroscopy: 1980–1994, J.Near Infrared Spectrosc. 1 (1993) 221–245.
[11] G. Reich, Near-infrared spectroscopy and imaging: basic principles and pharmaceutical applications, Adv. Drug Del. Rev. 57 (2005) 1109–1143.
[12] M. Blanco, J. Coello, H. Iturriaga, S. Maspoch, C. de la Pezuela, Near-infrared spectroscopy in the pharmaceutical industry, Analyst 123 (1998) 135R–150R.
[13] T. De Beer, A. Burggraeve, M. Fonteyne, L. Searens, J.P. Remon, C. Vervaet, Near infrared and Raman spectroscopy for the in-process monitoring of pharmaceutical production processes, Int. J. Pharm. 417 (2010) 32–47.
[14] J. Workman, L. Weyer, Practical Guide to Interpretive Near Infrared, Taylor and Francis, London, New York, 2008, pp. 117–286.
[15] H.R.H. Ali, H.G.M. Edwards, I.J. Scowen, Noninvasive in situ identification and band assignments of some pharmaceutical excipients inside USP vials with FT-near-infrared spectroscopy, Spectrochim. Acta A: Mol. Biomol. Spectrosc. 72 (2009) 890–896.
[16] I. Noda, Progress in two-dimensional (2D) correlation spectroscopy, J. Mol. Struct. 799 (2006) 2–15.
[17] R.K. Bista, R.F. Bruch, A.M. Covington, Vibrational spectroscopic studies of newly developed synthetic biopolymers, Biopolymers 93 (2010) 403–417.
[18] S.S. Rosa, P.A. Barata, J.M. Martins, J.C. Menezes, Development and validation of a method for active drug identification and content determination of ranitidine in pharmaceutical products using near-infrared reflectance spectroscopy: a parametric release approach, Talanta 75 (2008) 725–733.
[19] C.H. Petter, N. Heigl, S. Bachmann, V.A.C. Huck-Pezzei, M. Najam-ul-Haq, R. Bakry, A. Bernkop-Schnürch, G.K. Bonn, C.W. Huck, Near infrared spectroscopy compared to liquid chromatography coupled to mass spectrometry and capillary electrophoresis as a detection tool for peptide reaction monitoring, Amino Acids 34 (2008) 605–616.
[20] K.R. Morris, S.L. Nail, G.E. Peck, S.R. Byrn, U.J. Griesser, J.G. Stowell, S.-J. Hwang, K. Park, Advances in pharmaceutical materials and processing, PSTT 1 (1998) 235–245.
[21] M.C. Sarraguca, J.A. Lopes, Quality control of pharmaceuticals with NIR: From lab to process line, Vibr. Spectrosc. 49 (2009) 204–210.

[22] FDA. Guidance for industry: PAT – a framework for innovative pharmaceutical development. Manufacturing, and quality assurance, Pharmaceutical CGMPs, 2004.
[23] M. Blanco, M. Alcala, Use of near-infrared spectroscopy for off-line measurements in the pharmaceutical industry, in: K.A. Bakeev (Ed.), Process Analytical Technology, Spectroscopic Tools and Implementation, Strategies for the Chemical and Pharmaceutical Industries, Blackwell Publishing, New York, 2005, pp. 13–20, 362–376.
[24] R. Jachowicz, K. Woyna-Orlewicz, PAT – process analytical technology as a manufacturing process optimization strategy, Farm. Pol. 66 (2010) 209–214.
[25] M. Blanco, I. Villarroya, NIR spectroscopy: a rapid-response analytical tool, Trends Anal. Chem. 21 (2002) 240–250.
[26] J. Märk, M. Andre, M. Karner, ChW. Huck, Prospects for multivariate classification of a pharmaceutical intermediate with near-infrared spectroscopy as a process analytical technology (PAT) production control supplement, Eur. J. Pharm. Biopharm. 76 (2010) 320–327.
[27] EMEA, Guideline on the use of near-infrared spectroscopy by the pharmaceutical industry and the data requirements for new submissions and variations, European Medicines Agency, London, 16 (2009) 1–30.
[28] M.P. Freitas, A. Sabadin, L.M. Silva, F.M. Gianotti, D.A. do Couto, E. Tonhi, R.S. Medeiros, G.L. Coco, V.F.T. Russo, Prediction of drug dissolution profiles from tablets using NIR diffuse reflectance spectroscopy: a rapid and nondestructive method, J. Pharm. Biomed. Anal. 39 (2005) 17–21.
[29] M. Alcala, M. Blanco, M. Bautista, J.M. Gonzalez, On-line monitoring of a granulation process by NIR spectroscopy, J. Pharm. Sci. 99 (2010) 336–345.
[30] J.D. Kirsch, J.K. Drennen, Determination of film-coated tablet parameters by near-infrared spectroscopy, J. Pharm. Biomed. Anal. 13 (1995) 1273–1281.
[31] J.J. Moes, M.M. Ruijken, E. Gout, H.W. Frijlink, M.I. Ugwoke, Application of process analytical technology in tablet process development using NIR spectroscopy: Blend uniformity, content uniformity and coating thickness measurements, Int. J. Pharm. 357 (2008) 108–118.
[32] J. Luypaert, D.L. Massart, Y.V. Heyden, Near-infrared spectroscopy applications in pharmaceutical analysis, Talanta 72 (2007) 865–883.
[33] Y.C. Feng, X.B. Zhang, C.Q. Hu, Construction of identification system for non-invasive analysis of macrolides tablets using near infrared diffuse reflectance spectroscopy, J. Pharm. Biomed. Anal. 51 (2010) 12–17.
[34] K.T. Ram, P.S. Saumil, Y. Agrawal, Pharmaceutical counterfeiting and analytical authentication, Curr. Pharm. Anal. 7 (2011) 54–61.
[35] T. Liu, Y.C. Feng, D.Q. Song, C.Q. Hu, Selection of characteristic spectral bands for the analysis by the NIR correlation coefficient method, J. Chin. Pharm. Sci. 20 (2011) 83–91.
[36] B.J. Venhuis, G. Zomer, M.J. Vredenbregt, D. de Kaste, The identification of (−)-*trans*-tadalafil tadalafil, and sildenafil in counterfeit Cialis® and the optical purity of tadalafil stereoisomers, J. Pharm. Biomed. Anal. 51 (2010) 723–727.
[37] P.Y. Sacre, E. Deconinck, T. De Beer, P. Courselle, R. Vancauwenberghe, P. Chiap, J. Crommen, J.O. De Beer, Comparison and combination of spectroscopic techniques for the detection of counterfeit medicines, J. Pharm. Biomed. Anal. 53 (2010) 445–453.
[38] O.Y. Rodionova, A.L. Pomerantsev, NIR based approach to counterfeit-drug detection, Trends Anal. Chem. 29 (2010) 781–938.
[39] T. Puchert, D. Lochmann, J.C. Menezes, G. Reich, Near-infrared chemical imaging for counterfeit drug identification, J. Pharm. Biomed. Anal. 51 (2010) 138–145.
[40] European Pharmacopoeia 6.0, 2007.
[41] United States Pharmacopoeia, 2009.
[42] British Pharmacopoeia, 2007.
[43] D. Xiang, M. Konigsberger, B. Wabuyele, K. Hornung, J. Cheney, Development of robust quantitative methods by near-infrared spectroscopy for rapid pharmaceutical determination of content uniformity in complex tablet matrix, Analyst 134 (2009) 1405–1415.
[44] W.F.C. Rocha, A.L. Rosa, J.A. Martins, R.J. Poppi, Determination and validation of nimesulide in pharmaceutical formulation by near infrared spectroscopy, J. Braz. Chem. Soc. 21 (2010) 1929–1936.
[45] A.D. Karande, P.W.S. Heng, C.V. Liew, In-line quantification of micronized drug and excipients in tablets by near infrared (NIR) spectroscopy. Real time monitoring of tabletting process, Int. J. Pharm. 396 (2010) 63–74.
[46] C.V. Liew, A.D. Karande, P.W.S. Heng, In line quantification of drug and excipients in cohesive powder blends by near infrared spectroscopy, Int. J. Pharm. 386 (2010) 138–148.
[47] J. Mantanus, E. Ziémons, P. Lebrun, E. Rozet, R. Klinkenberg, B. Streel, B. Evrar, Ph Hubert, Active content determination of non-coated pharmaceutical pellets by near infrared spectroscopy: method development, validation and reliability evaluation, Talanta 80 (2010) 1750–1757.
[48] W. Li, A. Woldu, R. Kelly, J. McCool, R. Bruce, H. Rasmussen, J. Cunningham, D. Winstead, Measurement of drug agglomerates in powder blending simulation samples by near infrared chemical imaging, Int. J. Pharm. 350 (2008) 369–373.
[49] Y. Roggo, P. Chalus, L. Maurer, C. Lema-Martinez, A. Edmond, N. Jent, A review of near infrared spectroscopy and chemometrics in pharmaceutical technologies, J. Pharm. Biomed. Anal. 44 (2007) 683–700.
[50] L.K.H. Bittner, N. Heigl, C.H. Petter, M.F. Noisternig, U.J. Griesser, G.K. Bonn, C.W. Huck, Near-infrared reflection spectroscopy (NIRS) as a successful tool for simultaneous identification and particle size determination of amoxicillin trihydrate, J. Pharm. Biomed. Anal. 54 (2011) 1059–1064.
[51] S.B. Abebe, X.Z. Wang, R. Li, K.J. Roberts, X. Lai, The information content in NIR spectral data for slurries of organic crystals, Powder Technol. 179 (2008) 176–183.
[52] L. Alvarenga, D. Ferreira, D. Altekruse, J.C. Menezes, D. Lochmann, Tablet identification using near-infrared spectroscopy (NIRS) for pharmaceutical quality control, J. Pharm. Biomed. Anal. 48 (2008) 62–69.
[53] E. Otsuka, H. Abe, M. Aburada, M. Otsuka, A nondestructive prediction of the drug content of an aspirin suppository by near-infrared spectroscopy, Drug Dev. Ind. Pharm. 36 (2010) 839–844.
[54] E. Ziémons, J. Mantanus, P. Lebrun, E. Rozet, B. Evrard, Ph Hubert, Acetaminophen determination in low-dose pharmaceutical syrup by NIR spectroscopy, J. Pharm. Biomed. Anal. 53 (2010) 510–516.
[55] M.H. Ferreira, J.F.F. Gomes, M.M. Sena, Development and validation of multivariate calibration model for determination of dipyrone in oral solutions by near infrared spectroscopy, J. Braz. Chem. Soc. 20 (2009) 1680–1686.
[56] M. Blanco, M. Alcala, M. Bautista, Pharmaceutical gel analysis by NIR spectroscopy: Determination of the active principle and low concentration of preservatives, Eur. J. Pharm. Sci. 33 (2008) 409–414.
[57] M. Haag, M. Brüning, K. Molt, Quantitative analysis of diphenhydramine hydrochloride in pharmaceutical wafers using near infrared and Raman spectroscopy, Anal. Bioanal. Chem. 395 (2009) 1777–1785.
[58] Y. Dou, N. Qu, B. Wang, Y.Z. Chi, Y.L. Ren, Simultaneous determination of two active components in compound aspirin tablets using principal component artificial neural networks (PC-ANNs) on NIR spectroscopy, Eur. J. Pharm. Sci. 32 (2007) 193–199.
[59] M. Ito, T. Suzuki, S. Yada, H. Nakagami, H. Teramoto, E. Yonemochia, K. Terada, Development of a method for nondestructive NIR transmittance spectroscopic analysis of acetaminophen and caffeine anhydrate in intact bilayer tablets, J. Pharm. Biomed. Anal. 53 (2010) 396–402.
[60] M. Ito, T. Suzuki, S. Yada, A. Kusai, H. Nakagami, E. Yonemochi, K. Terada, Development of a method for the determination of caffeine anhydrate in various designed intact tablets by near-infrared spectroscopy: a comparison between reflectance and transmittance technique, J. Pharm. Biomed. Anal. 47 (2008) 819–827.
[61] Y. Hu, A. Erxleben, A.G. Ryder, P. McArdle, Quantitative analysis of sulphathiazole polymorphs in ternary mixtures by attenuated total reflectance infrared, near-infrared and Raman spectroscopy, J. Pharm. Biomed. Anal. 53 (2010) 412–420.
[62] I.-Ch. Wang, M.-J. Lee, D.-Y. Seo, H.-E. Lee, Y. Choi, W.-S. Kim, Ch-S. Kim, M.-Y. Jeong, G.J. Choi, Polymorph transformation in paracetamol monitored by in-line NIR spectroscopy during a cooling crystallization process, AAPS PharmSciTech. 12 (2011) 764–770.
[63] E. Ziemons, H. Bourichi, J. Mantanus, E. Rozet, P. Lebrun, E. Essassi, Y. Cherrah, A. Bouklouze, Ph Hubert, Determination of binary polymorphic mixtures of fluconazole using near infrared spectroscopy and X-ray powder diffraction: a comparative study based on the pre-validation stage results, J. Pharm. Biomed. Anal. 55 (2011) 1208–1212.
[64] S.S. Kadam, E. van der Windt, P.J. Daudey, H.J.M. Kramer, A comparative study of ATR–FTIR and FT-NIR spectroscopy for in situ concentration monitoring during batch cooling crystallization processes, Cryst. Growth Des. 10 (2010) 2629–2640.
[65] Y. Fukui, M. Otsuka, Determination of the crystallinity of cephalexin in pharmaceutical formulations by chemometrical near-infrared spectroscopy, Drug Develop. Ind. Pharm. 36 (2010) 72–80.
[66] B. Connolly, T.W. Patapoff, Y.J. Wang, J.M. Moore, T.J. Kamerzell, Vibrational spectroscopy and chemometrics to characterize and quantitate trehalose crystallization, Anal. Biochem. 399 (2010) 48–57.
[67] D.R. Ely, M. Thommes, M.T. Carvajal, Analysis of the effects of particle size and densification on NIR spectra, Colloids Surf. A: Physicochem. Eng. Aspects 331 (2008) 63–67.
[68] M. Blanco, R. Cueva-Mestanza, A. Peguero, Controlling individual steps in the production process of paracetamol tablets by use of NIR spectroscopy, J. Pharm. Biomed. Anal. 51 (2010) 797–804.
[69] A. Peinado, J. Hammond, A. Scott, Development, validation and transfer of a Near Infrared method to determine in-line the end point of a fluidized drying process for commercial production batches of an approved oral solid dose pharmaceutical product, J. Pharm. Biomed. Anal. 54 (2010) 13–20.
[70] J. Mantanus, E. Ziemons, P. Lebrun, E. Rozet, R. Klinkenberg, B. Streel, B. Evrard, Ph Hubert, Moisture content determination of pharmaceutical pellets by near infrared spectroscopy: method development and validation, Anal. Chim. Acta 642 (2009) 186–192.
[71] Y. Zheng, X. Lai, S.W. Bruun, H. Ipsen, J. Nedergaard, H. Løwenstein, I. Søndergaard, S. Jacobsen, Determination of moisture content of lyophilized allergen vaccines by NIR spectroscopy, J. Pharm. Biomed. Anal. 46 (2008) 592–596.
[72] H. Ma, C.A. Anderson, Characterization of pharmaceutical powder blends by NIR chemical imaging, J. Pharm. Sci. 97 (2008) 3305–3320.
[73] Z. Shi, R.P. Cogdill, S.M. Short, C.A. Anderson, Process characterization of powder blending by near-infrared spectroscopy. Blend end-points and beyond, J. Pharm. Biomed. Anal. 47 (2008) 738–745.
[74] Y. Sulub, B. Wabuyele, P. Gargiulo, J. Pazdan, J. Cheney, J. Berry, A. Gupta, R. Shah, H. Wu, M. Khan, Real-time on-line blend uniformity monitoring using near-infrared reflectance spectrometry: a noninvasive off-line calibration approach, J. Pharm. Biomed. Anal. 49 (2009) 48–54.
[75] A.U. Vanarase, M. Alcalà, J.I. Jerez Rozo, F.J. Muzzio, R.J. Romañach, Real-time monitoring of drug concentration in a continuous powder mixing process using NIR spectroscopy, Chem. Eng. Sci. 65 (2010) 5728–5733.

[76] M. Römer, J. Heinämäki, C. Strachan, N. Sandler, J. Yliruusi, Prediction of tablet film-coating thickness using a rotating plate coating system and NIR spectroscopy, AAPS PharmSciTech. 9 (2008) 1047–1053.
[77] T. Puchert, D. Lochmann, J.C. Menezes, G. Reich, A multivariate approach for the statistical evaluation of near-infrared chemical images using symmetry parameter image analysis (SPIA), Eur. J. Pharm. Biopharm. 78 (2011) 117–124.
[78] I. Storme-Paris, I. Clarot, S. Esposito, J.C. Chaumeil, A. Nicolas, F. Brion, A. Rieutord, P. Chaminade, Near infrared spectroscopy homogeneity evaluation of complex powder blends in a small-scale pharmaceutical preformulation process, a real-life application, Eur. J. Pharm. Biopharm. 72 (2009) 189–198.
[79] C.D. Ellison, B.J. Ennis, M.L. Hamad, R.C. Lyon, Measuring the distribution of density and tabletting force in pharmaceutical tablets by chemical imaging, J. Pharm. Biomed. Anal. 48 (2008) 1–7.
[80] R.B. Shah, M.A. Tawakkul, M.A. Khan, Process analytical technology: chemometric analysis of Raman and near infrared spectroscopic data for predicting physical properties of extended release matrix tablets, J. Pharm. Sci. 96 (2007) 1356–1365.
[81] M.-J. Lee, Ch-R. Park, A.-Y. Kim, B.-S. Kwon, K.-H. Bang, Y.-S. Cho, M.-Y. Jeong, G.-J. Choi, Dynamic calibration for the in-line NIR monitoring of film thickness of pharmaceutical tablets processed in a fluid-bed coater, J. Pharm. Sci. 99 (2010) 325–335.
[82] M.-J. Lee, D.-Y. Seo, H.-E. Lee, I.-C. Wang, W.-S. Kim, M.-Y. Jeong, G.J. Choi, In line NIR quantification of film thickness on pharmaceutical pellets during a fluid bed coating process, Int. J. Pharm. 403 (2011) 66–72.
[83] C. Cahyadi, A.D. Karande, L.W. Chan, P.W.S. Heng, Comparative study of non-descructive methods to quantify thickness of tablet coatings, Int. J. Pharm. 398 (2010) 39–49.
[84] M. Saed, S. Saner, J. Oelichmann, H. Keller, G. Betz, Assessment of diffuse transmission mode in near-infrared quantification – Part I: The press effect on low-dose pharmaceutical tablets, J. Pharm. Sci. 98 (2009) 4877–4886.
[85] Y. Yang, A. Gupta, A.S. Carlin, P.J. Faustino, R.C. Lyon, Ch.D. Ellison, B. Rothman, M.A. Khan, Comparative stability of repacked metoprolol tartrate tablet, Int. J. Pharm. 385 (2010) 92–97.
[86] J. Cruz, M. Blanco, Content uniformity studies in tablets by NIR-CI, J. Pharm. Biomed. Anal. 56 (2011) 408–412.
[87] E. Chevalier, M. Viana, S. Cazalbou, L. Makein, J. Dubois, D. Chulia, Ibuprofen-loaded calcium phosphate granules: Combination of innovative characterization methods to relate mechanical strength to drug location, Acta Biomater. 6 (2010) 266–274.
[88] D. Cozzolino, Near infrared spectroscopy in natural products analysis, Planta Med. 75 (2009) 746–756.
[89] D. Cozzolino, A review on the use of near infrared spectroscopy for plant analysis, Med. Plants – Int. J. Phytomed. Rel. Ind. 2 (2010) 1–8.
[90] C. Wang, B. Xiang, W. Hang, Application of two-dimentional near-infrared (2D-NIR) correlation spectroscopy to the discrimination of three species of *Dendrobium*, J. Chemometrics 23 (2009) 463–470.
[91] S.S. Rosa, P.A. Barata, J.M. Martins, J.C. Menezes, Near-infrared reflectance spectroscopy as a process analytical technology tool in *Ginkgo biloba* extract qualification, J. Pharm. Biomed. Anal. 47 (2008) 320–327.
[92] F.-F. Fu, R. Ye, S.-P. Xu, H.-W. Xue, Studies on rice seed quality through analysis of a largescale T-DNA insertion population, Cell Res. 19 (2009) 380–391.
[93] E. Michelini, P. Simoni, P. Cevenini, L. Mezzanotte, A. Roda, New trends in bioanalytical tools for the detection of genetically modified organisms: an update, Anal. Bioanal. Chem. 392 (2008) 355–367.
[94] L. Munck, B.M. Jespersen, From discovery of high lysine barley endosperm mutants in the 1960–70s to new holistic spectral models of the phenome and of pleiotropy in 2008, in: Q.Y. Shu (Ed.) Induced Plant Mutations in the Genomics Era, Rome, 2009, pp. 419–422.
[95] A. Capobianco, M. Carotenuto, T. Caruso, A. Peluso, The charge-transfer band of an oxidized Watson–Crick guanosine–cytidine complex, Angew. Chem. Int. Ed. 48 (2009) 9526–9528.
[96] J.G. Henriques, S. Buziol, E. Stocker, A. Voogd, J.C. Menezes, Monitoring mammalian cell cultivations for monoclonal antibody production using near-infrared spectroscopy, Adv. Biochem. Eng./Biotechnol. 116 (2009) 73–97.
[97] C. Kurz, M. Leitenberger, R. Carle, A. Schieber, Evaluation of fruit authenticity and determination of the fruit content of fruit products using FT-NIR spectroscopy of cell wall components, Food Chem. 119 (2010) 806–812.
[98] A. Weber, V. Hoefinfhoff, V. Siekmann, P. Turecek, Detection of physiologically acceptable polymer molecules using near infrared spectroscopy, United States Patent Application, US 2010/0152115 A1 (2010).
[99] C.-F. Mandenius, K. Graumann, T.W. Schultz, A. Premstaller, I.-M. Olsson, E. Petiot, C. Clemens, M. Welin, Quality-by-design for biotechnology related pharmaceuticals, Biotechnol. J. 4 (2009) 600–609.
[100] M.C. Sarraguça, A. Paulo, M.M. Alves, A.M.A. Dias, J.A. Lopes, E.C. Ferreira, Quantitative monitoring of an activated sludge reactor using on-line UV–visible and near infrared spectroscopy, Anal. Bioanal. Chem. 395 (2009) 1159–1166.
[101] V. Bellon-Maurel, E. Fernandez-Ahumada, B. Palagos, J.-M. Roger, A. McBratney, Critical review of chemometric indicators commonly used for assessing the quality of the prediction of soil attributes by NIR spectroscopy, Trends Anal. Chem. 29 (2010) 1073–1081.
[102] Feedback on FDA Validation Guideline., Regulatory highlights for March–August 2009, organic process research & development, Am. Chem. Soc. 13 (2009) 842–847.
[103] G.L. Bosco, L. James, Waters symposium 2009 on near-infrared spectroscopy, Trends Anal. Chem. 29 (2010) 197–208.

Journal of Pharmaceutical and Biomedical Analysis xxx (2012) xxx–xxx

Contents lists available at SciVerse ScienceDirect

Journal of Pharmaceutical and Biomedical Analysis

journal homepage: www.elsevier.com/locate/jpba

Review

HPTLC methods to assay active ingredients in pharmaceutical formulations: A review of the method development and validation steps

D.H. Shewiyo[a,b,c], E. Kaale[b], P.G. Risha[b], B. Dejaegher[c], J. Smeyers-Verbeke[c], Y. Vander Heyden[c,*]

[a] Tanzania Food and Drugs Authority, P.O. Box 77150, Dar es Salaam, Tanzania
[b] School of Pharmacy, Muhimbili University of Health and Allied Sciences, P.O. Box 65013, Dar es Salaam, Tanzania
[c] Department of Analytical Chemistry and Pharmaceutical Technology (FABI), Center for Pharmaceutical Research (CePhaR), Vrije Universiteit Brussel (VUB), Laarbeeklaan 103, 1090 Brussels, Belgium

ARTICLE INFO

Article history:
Received 21 February 2012
Accepted 16 March 2012
Available online xxx

Keywords:
HPTLC
Pharmaceutical analysis
Method development
Method validation
Active ingredient
Pharmaceutical formulation

ABSTRACT

High-performance thin-layer chromatography (HPTLC) is still increasingly finding its way in pharmaceutical analysis in some parts of the world. With the advancements in the stationary phases and the introduction of densitometers as detection equipment, the technique achieves for given applications a precision and trueness comparable to high-performance liquid chromatography (HPLC). In this review, the literature is surveyed for developed and validated HPTLC methods to assay active ingredients in pharmaceutical formulations published in the period 2005–2011. Procedures and approaches for method development, validation and quantitative assays are compared with the standard ways of conducting them. Applications of HPTLC in some other areas are also briefly highlighted.

© 2012 Elsevier B.V. All rights reserved.

Contents

1. Introduction 00
2. Thin-layer chromatographic methods and their classification 00
3. General steps in an HPTLC analysis 00
   3.1. Introduction 00
      3.1.1. Selection of the stationary phase 00
      3.1.2. Mobile phase selection and optimization 00
      3.1.3. Sample application 00
      3.1.4. Development (separation) 00
      3.1.5. Detection 00
   3.2. Quantitation 00
   3.3. HPTLC method validation for pharmaceutical analysis 00
      3.3.1. Classical validation approach 00
4. Other areas of HPTLC application 00
5. Conclusion 00
   Acknowledgements 00
   References 00

1. Introduction

Though being an old technique, today in some parts of the world, Thin-layer chromatography (TLC) is still increasingly finding its way in the assay of active ingredient(s) in pharmaceutical analysis. This is due to the evolution of the instrumentation, automization and the development of new adsorbents and supports [1]. Moreover, TLC features in a broad range of applications, such as the analysis of herbal medicines, dietary supplements, biological and clinical samples, food and beverages, environmental pollutants and chemicals [2].

Like all chromatographic techniques, TLC is based on a multistage distribution process, which involves a suitable "adsorbent" (the stationary phase), solvents or solvent mixtures (the mobile

* Corresponding author. Tel.: +32 2 477 47 34; fax: +32 2 477 47 35.
E-mail address: yvanvdh@vub.ac.be (Y.V. Heyden).

0731-7085/$ – see front matter © 2012 Elsevier B.V. All rights reserved.
doi:10.1016/j.jpba.2012.03.034

Please cite this article in press as: D.H. Shewiyo, et al., HPTLC methods to assay active ingredients in pharmaceutical formulations: A review of the method development and validation steps, J. Pharm. Biomed. Anal. (2012), doi:10.1016/j.jpba.2012.03.034

phase or eluent), and the sample molecules. high-performance thin-layer chromatography (HPTLC) is an advanced form of instrumental TLC, which does not only include the use of high performance adsorbent layers (e.g. silica gel with refined uniform particles, approximately 5 μm in diameter, as compared to 12 μm in TLC), but also adopted instrumentation e.g. the development chambers. It usually also implies a standardized methodology for development, optimization, documentation and the use of validated methods. The HPTLC technique is applied in qualitative and quantitative separations of compounds in mixtures, where the quantitative mode operates in a more optimized way (standardized with a given procedure), hence, applicable in the assay of compounds in samples.

There are several advantages of using HPTLC for the analysis of compounds as compared to other techniques, like HPLC, spectrometric, titrations, etc. [3,4]. Some of the advantages are:

- The separation process is easy to follow: especially with coloured compounds,
- Several samples can be separated in parallel on the same plate resulting in a high through-put, and a rapid low-cost analysis,
- Two-dimensional separations are easy to perform,
- Specific and sensitive colour reagents can be used to detect separated spots,
- HPTLC can combine and consequently use different modes of evaluation, allowing identification of compounds having different light-absorption characteristics or different colours,
- Contact detection allows radiolabelled compounds to be monitored and microbial activity in spots to be assessed,
- The TLC plates are disposable; therefore, neither regeneration nor essential clean-up are required, and
- Chromatographic development and detection of the separated spots on a plate are generally separate processes in time, therefore after separation, the plates can be stored for a long time, and detection performed at a later stage to obtain the analytical information.

Literature search reveals a large number of published papers that describe various usage of the (HP)TLC technique in many analytical fields. To emphasize on the importance, challenges and opportunities of the HPTLC technique, various older review papers are available in the literature [3,5,6]. In a recent (2011) review paper, Kaale et al. [7] reported the availability of a large number of publications on (HP)TLC methods that are developed, validated and applied in pharmaceutical analysis for the assay of active ingredient(s) and stability testing. The review in [7] gives a brief summary of the use of TLC in drug quality testing and therapeutic drug monitoring in resource-constrained settings in Africa and discusses the shortcomings associated with the use of TLC in Africa. It also gives a general overview of HPTLC methods and their application in drug testing in the above settings. In our review, we will focus on the quantitative mode of HPTLC as used in the assay of active ingredient(s) in pharmaceutical formulations. The different steps applicable to this technique during method development, validation and quantitative analysis will be discussed in relation to the practice observed in publications from 2005 to 2011. The paper is thus clearly different from [7].

Most of the reviewed publications were originating from Asia (mostly India), from some western European countries, and few, about twenty, were from Africa, where the technique has facilitated drug quality assurance, since the more sophisticated and costly analytical equipment, such as HPLC or liquid chromatography–mass spectrometry (LC–MS) is insufficiently available.

Given the context, one might expect to find many methods developed for quality assurance of drugs for diseases mostly affecting these areas, such as malaria, tuberculosis and HIV/AIDS. However, they were developed for many types of diseases. Table 1 shows pharmacological classes, which treat diseases, covered by some of the reviewed publications.

Table 1
Pharmacological classes, representing treated diseases, assayed with the reviewed methods.

Drugs	Pharmacological class	References
Lamivudine/stavudine/nevirapine	Antiretroviral	[15]
Clopidogrel	Cardiovascular agent	[16]
Trandolapril	Cardiovascular agent	[17]
Rapinirole hydrochloride	Anti-Parkinson's	[18]
Lamivudine/stavudine/nevirapine	Antiretroviral	[20]
Levocetirizine dihydrochloride/ montelukast sodium	Antihistamines	[21]
Nevibolol hydrochloride	Cardiovascular agent	[22]
Paracetamol/piroxicam	Analgesics/anti inflammatory	[23]
Tacrolimus	Immunosuppressant	[24]
Ranolazine	Cardiovascular agent	[25]
Dexibuprofen	Analgesics/anti inflammatory	[26]
Trigonelline	Cardiovascular agent	[27]
Steroids	Hormonal agents	[28]
Famotidine/domperidone	Gastrointestinal disorders	[29]
Risperidone	Antipsychotic/anticonvulsant/ anxiolytic	[30]
Duloxetine hydrochloride	Antipsychotic/anticonvulsant/ anxiolytic	[31]
Sumatriptan	Anti-migraine	[32]
Clotrimazole	Antifungals	[33]
Emtricitabine/tenofovir	Antiretroviral	[34]
Rabeprazole/itopride	Gastrointestinal disorders	[35]
Lamivudine/zidovudine	Antiretroviral	[36]
Sulfamethoxazole/trimethoprim	Antibiotics/anti infective	[37]
Isoniazid/rifampicin	Antibiotics/anti infective	[38]
Efavirenz	Antiretroviral	[39]
Ibuprofen	Analgesics/anti inflammatory	[40]
Cefetamet	Antibiotics/anti infective	[43]
Artemisinin	Antimalarial	[45]
Rabeprazole/domperidone	Gastrointestinal disorders	[47]
Telmisartan/ramipril	Cardiovascular agents	[49]
Atovastatine/ezetimibe	Cardiovascular agents	[50]
Cefuroxime axetil/ordinazole	Antibiotics/anti infective	[51]
Tenatoprazole	Gastrointestinal disorders	[53]
Fluconazole	Antifungals	[54]
Brominidine tartate	Ocular pressure	[56]
Lamivudine/tenofovir	Antiretroviral	[57]
Piperine	Anti-tussive	[58]
Amboxol hydrochloride	Expectorant	[59]
Azithromycin	Antibiotics/anti infective	[60]
Glucosamine	Anti arthritis	[61]

2. Thin-layer chromatographic methods and their classification

Thin-layer chromatographic techniques may be classified differently depending on the considered point of view. Reference [8] describes some of these classifications. One classification was based on the flow of the mobile phase through the stationary phase, i.e. capillary-flow layer chromatography, which is the classical mode, where capillary forces are responsible for the flow versus the Forced-Flow Planar Chromatography, where pressure is used to drive the mobile phase. A second classification was based on the nature of stationary phase, i.e. paper versus thin-layer chromatography. A third one divided the thin-layer chromatography according to the separation mechanisms, i.e. adsorption, partition, ion-exchange or size exclusion. A fourth one distinguished according to the polarity of the sorbent layer, i.e. normal-phase versus reversed-phase chromatography. A fifth classification was based

Please cite this article in press as: D.H. Shewiyo, et al., HPTLC methods to assay active ingredients in pharmaceutical formulations: A review of the method development and validation steps, J. Pharm. Biomed. Anal. (2012), doi:10.1016/j.jpba.2012.03.034

on the aim of the separation, i.e. qualitative or quantitative, and a last distinguishes on-line and off-line separation techniques.

HPTLC techniques may also be classified into classical, high-performance, ultra and preparative thin-layer chromatography, where the former three are analytical. They differ with classical TLC in the particle size distribution and thickness of the sorbent layers. The mean particles sizes are 12, 5, 25 μm for classical, high-performance and preparative thin-layer chromatography, respectively, whereas ultra-thin-layer chromatography does not have particles but a monolithic layer with 1–2 μm macropores [9,10]. Another difference is the layer thickness which is 250 μm, 200 μm, 10 μm and 0.5–2 mm, for classical, high-performance, ultra-thin and preparative sorbent layers, respectively. This review focuses on commonly used analytical HPTLC techniques with classical capillary mobile flow.

3. General steps in an HPTLC analysis

3.1. Introduction

According to Nyiredy [6], method development in thin-layer (planar) chromatography is one of the most critical steps for a qualitative and quantitative analysis. In [6] method development is divided into selection of the development mode, of the stationary phase, of the vapour phase, of suitable solvents, optimization of the mobile phase, transfer (occasionally) of the optimized mobile phase to an appropriate forced-flow planar chromatography (FFPC) method, and selection of other operating parameters. The transfer to a FFPC method however, is beyond the scope of this review and will not be discussed.

3.1.1. Selection of the stationary phase

To separate various pharmaceutical active ingredients, which apparently have different chemical properties, a number of stationary phases such as silica, alumina, kieselguhr, cellulose, gypsum and polyamides are available for HPTLC analysis [4,6]. In spite of this variety of stationary phases, it has been reported that about 90% of the separations are performed on silica either bare or modified [6,11]. In bare or unmodified silica the polar groups of the silica gel layer, i.e. the silanol groups, interact with analyte(s) in mixtures resulting in their separation. In modified silica, nonpolar and intermediately polar layers can be distinguished where in the former, the silica backbone bears, for instance, alkane (C8, C18), alkene or phenyl groups, and in the intermediately polar layers the silicagel layer bears, amino, cyano, diol or thiol groups, linked to the silica through short alpha chains, e.g. propyl, or substance-specific complexing ligands [6]. These layers interact with analyte(s) to cause separations. The interaction between analytes and the silanol groups in the unmodified silica, where the mobile phase is apolar (e.g. hexane based), is referred to as the normal-phase chromatography mode. The interaction with the apolar modified silica gel layer, where the mobile phases are polar (e.g. water based), is termed reversed-phase chromatography. The interaction of analytes with polar (modified) layers, as in normal-phase chromatography but in which the mobile phases are polar (e.g. methanol based) is called HILIC (hydrophilic interaction liquid chromatography).

During method development, stationary phase selection should be based on the type of compounds to be separated [12]. If the compounds are ionic, adsorption chromatography can be used. Ion-exchange chromatography in which ion-exchangers such as modified cellulose (e.g. aminoethyl cellulose, diethylaminoethyl cellulose and carboxymethyl cellulose) are used as layers, are applicable to the separation of ionic compounds, for instance, inorganic ions, purines and pyrimidines [12]. The difference with adsorption chromatography is small and is usually situated in the stationary phase applied, which is inorganic (e.g. bare silica) in adsorption chromatography and organic (see above) in ion-exchange chromatography. For macro-molecules like polymers and proteins, the thin-layer gel filtration may be used. When the compounds are water soluble, partition chromatography is the mode of choice.

Another approach of stationary phase selection for method development can be found in reference [6] where Nyiredy provided a flow chart illustrating a possible systematic approach for the selection of the appropriate separation mode and stationary phase (Fig. 1). In this flow chart, questions regarding the property of the sample mixture are asked and possible approaches to follow where a given property is present or not, have been suggested. If the sample mixture has compounds with a wide polarity then an automated multiple development (AMD) technique (*see* Section 3.1.4 *for description of AMD*) is proposed for separation. AMD is found to be suitable for the separation of complex mixtures, especially from plants extracts, which normally contain many compounds. In [13] alcoholic extracts from medicinal plants containing various compounds with varying polarities were separated on a silica gel stationary phase using the AMD technique. The plant extracts were from *Cinchona succirubra*, *Aesculus hippocastanum*, *Berberis vulgaris*, *Artemisia abrotanum*, *Carduus marianus*, *Thuja accidentalis*, *Baptisia tinctoria*, *Paulinia cupana*, *Lycopus europaeus* and *Echinacea angustifolia*.

According to the flow chart, for samples with extremely polar compounds or for sample solutions containing homologues the use of reversed-phase TLC is proposed. This approach is demonstrated by the method developed for the simultaneous analysis of levodopa, carbidopa and entacapone in a fixed-dose tablet formulation [14]. Levodopa and carbidopa are closely related compounds, which are not only structurally different from the entacapone, but also have different polarities to the latter drug. The three drugs were separated by reversed-phase HPTLC using silica gel 60 RP-18 F_{254} with a mobile phase consisting of acetonitrile, *n*-butanol, water and triethylamine (5:95:10:0.01, v/v/v/v).

An alumina (aluminium oxide) layer is indicated for the separation of samples containing dissociating compounds such as alkaloids, chlorinated hydrocarbons and steroids, since, alumina can exist as acidic, basic or neutral layer depending on the preparation procedure [10]. For the samples containing aromatic or isomeric compounds the use of a Reversed-Phase layer with buffer or, of ion-pair thin layer chromatography is indicated. If the sample mixture does not possess any of the above properties then the use of silica gel as a stationary phase for separation is suggested.

Despite the systematic possibilities in sequence as indicated in Fig. 1, it is a fact that the approach followed by most authors to decide on the type of stationary phase to use during method development is to search the literature in order to learn what others have used in a similar situation [12]. It is reported that unmodified silica has been used extensively [1,4,7,11]. We also observed this extensive use [15–61]. The preference for this stationary phase, as observed in the reviewed papers on pharmaceutical analysis, indicates its ability to solve current separation problems.

Despite the overwhelming use of bare silica, there are reports of the application of modified silica layers such as reversed stationary phase (see example higher).

Chiral separations also have been performed on TLC. For instance, on reversed-phase plates which were impregnated with complex forming molecules e.g. N,N-di-n-propyl-L-alanine/copper(II) complex and copper(II) complex of (2S, 4R, 2′RS)-4-hydroxy-1-(2′-hydroxydodecyl)-proline, chelate-complex forming compounds such as amino acids, and heterocyclic compounds were separated; cellulose phenyl carbamate phases resolved β-blocker enantiomers of propranolol and bupranolol, while molecularly imprinted polymers were used as chiral

Please cite this article in press as: D.H. Shewiyo, et al., HPTLC methods to assay active ingredients in pharmaceutical formulations: A review of the method development and validation steps, J. Pharm. Biomed. Anal. (2012), doi:10.1016/j.jpba.2012.03.034

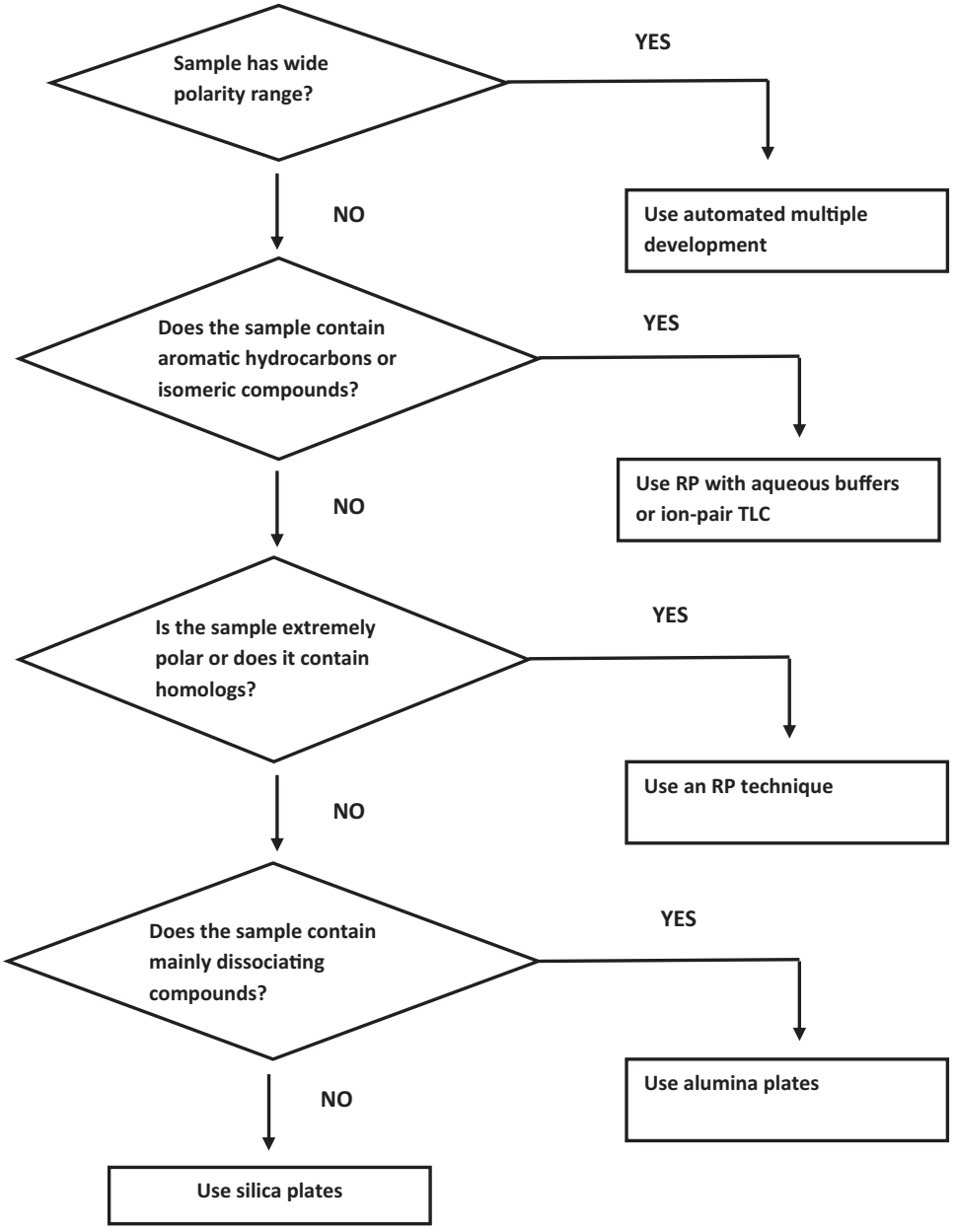

Fig. 1. Flow chart for the selection of the stationary phase and separation mode.

Source: Adapted from [6].

stationary phases for the separation of compounds, such as L- and D-phenylalanine anilide, and for adrenergic drugs, e.g. norepinephrine and epinephrine [62].

The use of the newly introduced ultra-thin layer chromatographic (UTLC) silica gel plates has been reported in [9] and [63]. This silicagel monolithic layer has a thickness of only 10 μm and small pore sizes of 3–4 nm for the mesopores and 1–2 μm for the macropores, as compared to a pore diameter of 0.6 μm for the classic TLC and HPTLC silica gel layers. Advantages of this layer include increased sensitivity, shorter migration distance (1–3 cm), shorter migration time (1–6 min) and consumption of less mobile phase (1–4 ml). Though Hauck and Schulz [63] reported the usefulness of this layer in pharmaceutical analysis, e.g. for the separation of bromazepam, diazepam and parazepam, we did not find any additional reported use of this stationary phase.

The support materials for the stationary phases as observed in the reviewed publications were glass [15,36,37] and aluminium materials [16–18,21–23,25,27,29,31,38–41,44,46,47,49–53,56,57,59]. These are known to be resistant to heat and chemicals as compared to other support materials for thin-layer chromatography layers, e.g. plastics [4]. Aluminium was used in most methods. This can be attributed to its lower cost, possibility of cutting to required sizes and ease of handling as compared to the glass support.

3.1.2. Mobile phase selection and optimization

It is a fact that mobile phase optimization is among the important steps that affect the quality of a separation in TLC method development [64]. Mobile phase components selection and optimization in many cases is done on a "trial and error" basis, or the analyst's experience or following hints from a literature search [2,4]. Manufacturers of HPTLC plates, such as Macherey–Nagel (MN), provide also information on mobile phases they have used

Please cite this article in press as: D.H. Shewiyo, et al., HPTLC methods to assay active ingredients in pharmaceutical formulations: A review of the method development and validation steps, J. Pharm. Biomed. Anal. (2012), doi:10.1016/j.jpba.2012.03.034

to separate given compounds on their layers [1]. This is another source that helps in mobile phase selection.

Based on Snyder's solvent classifications [65], Nyiredy [6,66] defined steps for the selection of individual solvents for the mobile phase. Snyder classified over 80 solvents into 8 groups for normal-phase chromatography (NPLC) according to their properties for proton acception, proton donation and dipole interaction. Out of the 80 solvents Nyiredy selected 27 commonly used solvents in planar chromatography, from which he indicated nine solvents that can be used individually for running a solution of a compound mixture on a silica TLC [66]. The selected solvents are diethyl ether, ethanol, tetrahydrofuran, acetic acid, dichloromethane, ethyl acetate, dioxane, toluene and chloroform. Each selected solvent is evaluated for its ability to cause movements of the compounds concerned. Migration of spots is recommended to be distributed in the region between 0.2 and 0.8 of the retardation factor (R_f), also called morbidity factor. This is the optimum region [2], which has been proven to have a high reproducibility of R_f values in planar chromatography [67]. The retardation factor (R_f) is a qualitative value which characterizes the position of a spot on the plate in thin-layer chromatography. It is the ratio of the distance travelled by the spot to the distance travelled by the solvent front. Depending on the migration of the compounds on the silica layer, the solvent strength of the solvent is either reduced or increased by addition of hexane (solvent strength = 0) or a small amount of water (solvent strength = 10.2 in NPLC), respectively, in order to make the spots migrate to the optimum R_f region. Finally, solvents giving best separation within this region are chosen for systematic mobile phase optimization [66]. In the latter, the mobile phase is optimized by mixing solvents in order to change the selectivity of the solvent mixture.

Nyiredy mentions possible systematic optimization methods for the mobile phase in planar chromatography, such as the window diagram, the sequential simplex method, Geiss's structural approach and the "PRISMA" model. The window diagram approach involves the determination of the worst results for all possible experimental conditions. i.e., for instance, for the different mixtures of two of the above solvents. Then from the set of worst results, one determines the experimental conditions resulting in the maximum value of the worst results. This value becomes the criterion for selecting the optimal experimental conditions [68,69].

The simplex method applies a sequential procedure in approaching the optimum composition of the mobile phase [70]. At the beginning of the simplex method, a simplex is defined. This is a geometrical figure consisting of a number of points equal to the number of variables to be examined plus one, e.g. for two variables the figure is a triangle and for three variables a tetrahedron. The vertices represent the experiments of a simplex. Specific rules are applied to determine the consecutive experiments. After executing a simplex the rules determine the next experiment. The worst experiment is dropped. The maintained and the new experiments form a new simplex. The above rules are applied on its results, etc. The changes caused by the rules are thus that one defines new experiments which make the simplex to move towards the optimum.

The Geiss's structural approach for mobile phase optimization considers selectivity and solvent strength as independent factors [71]. With a Vario KS chamber, a type of chamber that permits rapid mobile phase optimization, Geiss used three strong solvents, i.e. methyl tert-butyl ether, acetonitrile and methanol. These solvents are diluted with a weaker solvent e.g. 1,2 dichloroethane to obtain a series of solvent strengths ranging up to 0.70, with a gradual intermediate increase of 0.05. From these solvents an appropriate solvent strength for separation is determined. The fine tuning is performed by blending solvent mixtures, which have the appropriate solvent strength, but a different selectivity [71].

The PRISMA system is a three-dimensional geometrical design correlating the solvent strength and the selectivity of the mobile phase (Fig. 2). The approach has three parts in which part one, deals with the selection of the basic parameters such as the stationary phase and the individual solvents. Part two deals with the optimization of the compositions of the solvents selected in part one, to obtain the optimum combination for the separation of the compounds considered. In part three of the PRISMA approach the appropriate development mode is selected, e.g. FFPC, such as overpressured planar liquid chromatography (OPLC) or rotational planar chromatography (RPC), and HPTLC plates is possibilities. The development mode is also selected and finally application of the optimized mobile phase can be tested in various analytical and preparative circumstances.

From the literature search, we observed a frequent selection of solvents on a "readily available" basis and optimization by trial-and-error approaches [38]. Ekiert et al. [72] describe the source of the mobile phase used for the analysis of azole antifungal agents (ketoconazole, fluconazole, bifonazole and itraconazole) to be the Polish Pharmacopoeia VI, where it was designed for purity analysis of ketoconazole reference standard. The paper however, did not hint on the optimization procedure that was used to make the mobile phase fit for the new purpose.

Many authors did not discuss the solvent selection process but mentioned trial-and-error as the approach for mobile phase optimization [15,17,18,21–24,27,29,30,36–39,41,43–51,53,54,59,61]. Many other references [16,19,20,25,26,31–35,40,42,52,55–58,60] did not mention the origin of the solvent compositions nor any optimization method.

As mentioned earlier mobile phase components selection and optimization is done rarely based on a systematic approach but usually on a trial-and-error basis, the analyst's experience or a literature search. Since most pharmaceutical formulations typically analyzed on TLC have few active ingredients (often 1–3) that are to be analyzed, e.g. sulfamethoxazole/trimethoprim in tablets [15], rabeprazole/itopride in capsules [35] or cefuroxime axetil/ordinazole in tablets [51], the separations can be achieved relatively easily without systematic approach. Therefore, systematic optimization procedures do not seem to be applied often.

However, when sample composition becomes more complex, systematic optimization of the mobile phase becomes increasingly important [7]. This is demonstrated in [28] where during development of a method for the analysis of five androstane isomers by TLC, numerical taxonomy was used for the selection of the appropriate solvent system, and simplex or PRISMA approaches for mobile phase optimization. The numerical taxonomy utilizes a variety of related mathematical techniques in order to classify solvent systems into groups based on the R_f values [28]. Initially, seven mobile phases for the separation of the androstane isomers were obtained from the literature (from different papers) and were run to separate the compounds. R_f values were recorded and used as a basis for grouping the mobile phases due to separation similarities. The similarity between two mobile phases is characterized by the taxonomic distance, $d_{j,k}$, which is calculated by equation,

$$d_{j,k} = \sqrt{\sum_{i=1}^{n} \frac{(x_{i,j} - x_{i,k})^2}{n}} \quad (1)$$

where $x_{i,j}$ and $x_{i,k}$ are the R_f values of compound i in the mobile phases j and k, n is the number of analyzed compounds.

The smallest $d_{j,k}$ value is selected and the mobile phases having this taxonomic distance are the most similar systems, hence, forms a group p. The taxonomic distances between the new group p and other individual mobile phases q is then calculated.

Please cite this article in press as: D.H. Shewiyo, et al., HPTLC methods to assay active ingredients in pharmaceutical formulations: A review of the method development and validation steps, J. Pharm. Biomed. Anal. (2012), doi:10.1016/j.jpba.2012.03.034

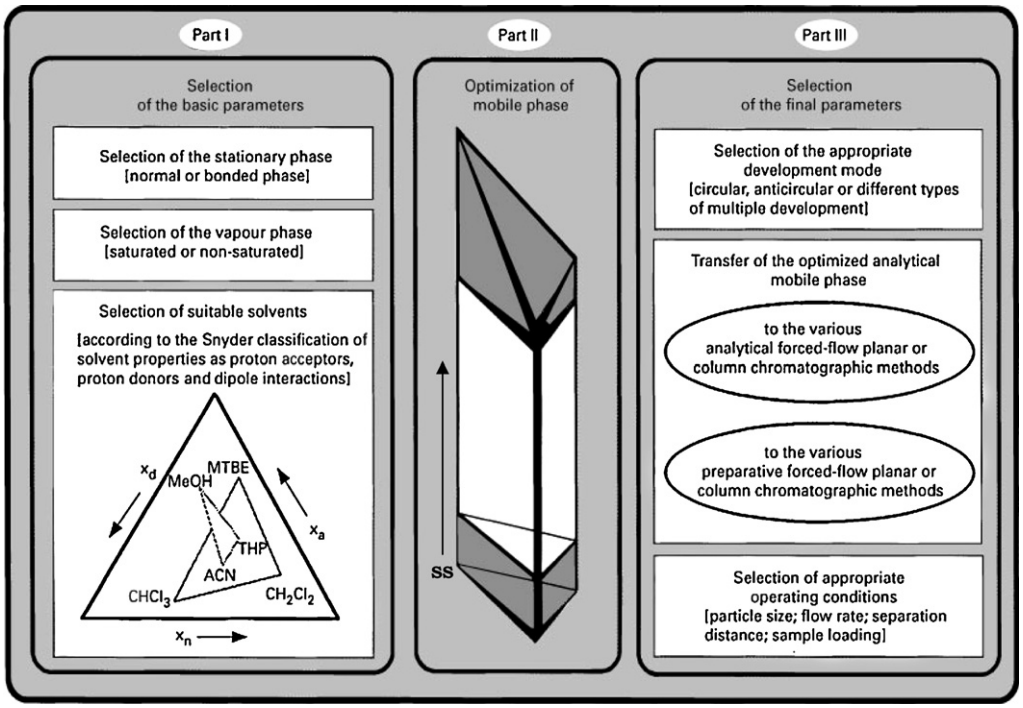

Fig. 2. The 'PRISMA' system for the systematic optimization of a planar chromatographic method.
Source: Reproduced with permission from [6] (NB: SS – solvent strength).

This is repeated until all mobile phases are clustered in one classification system containing hierarchy of non-overlapping groups. The selection of the most efficient mobile phase is carried out using the amount of information (I) and the objective function (F_{obj}), which are calculated using Eqs. (2) and (3), respectively.

$$I = -\sum \left(\frac{n_k}{n}\right) \log_2 \left(\frac{n_k}{n}\right) \quad (2)$$

where n_k is the number of separated compounds in a group and n is the number of investigated compounds.

$$F_{obj} = aI_p + \frac{b}{I} + \frac{c}{IR_c} + \frac{d}{RRP} \quad (3)$$

where a, b, c and d are arbitrary weighting coefficients ($a = 1$, $b = 10$, $c = 20$, $d = 20$), I_p is the performance index, and RRP is the relative resolution index. F_{obj} reflects the quality of the chromatogram separation by a single number, and it has a minimum value at the optimum system. The proper mobile phase is thus selected from I and F_{obj}. The reader is referred to references [28,73] for more elaborated explanation on the numeric taxonomy. Then, the best mobile phase obtained in the reference [28] was further optimized using two different approaches, i.e. simplex and PRISMA. The purpose was to compare the optimum compositions obtained by the simplex and PRISMA approaches, which turned out to be similar.

3.1.3. Sample application

Devices for application of sample solutions on the chromatographic layers are available from different manufacturers. Examples of such devices are the nanomat 4, the linomat 5 and the automatic TLC sampler 4 (ATS 4) (all CAMAG, Muttenz, Switzerland). Nanomat 4 is a manually operated spotwise sample application device where sample dosing is done with a disposable capillary pipette guided by a universal capillary holder, which can deliver between 0.5 and 5 μL/spot on the layer [74]. Linomat 5 is a bandwise application device for qualitative, quantitative and preparative separations which operates semi-automatically. It can hold sample dosage syringes of 100 and 500 μL capacities which can deliver 0.5–500 μL/spot. It uses the spray-on technique mostly with nitrogen gas during sample application [75]. The spray-on technique makes the solvent to evaporate immediately as sample is delivered on the plate. This allows formation of narrow bands and concentration of sample on the bands. Fully automated sample application is possible with the automatic TLC sampler 4, which has options for spot or bandwise application with the spray-on technique. Repeated application of different solutions on the same position on the layer is possible, e.g. for pre-chromatographic derivatization [76]. This device is appropriate in situations where many samples are to be applied on many TLC plates.

It is a fact that application of the sample is the most critical step to obtain good resolution for quantification in HPTLC. Sample solution applied as bands allows flexibility in terms of sample solvent (even polar solvents e.g. methanol and water can be used) and application volumes. When sample is applied as spots, larger spots which are formed due to broadening lead to poor resolution. This is not the case with band application.

The bandwise application, the precision of the applied volumes and the compactness of the application zones ensure the highest resolution, and therefore, they have impact on the final assay results. Consequently, automatic devices with band sample application are recommended for quantitative analyses [4]. Most publications indicated the use of the semi-automatic linomat 5 [15,18,19,22–24,26,27,29,32,34–40,42–45,47–49,51–53,55,56,60], linomat 4 [16,17,20,21,25,30,31,33,41,50,54,57–59], or Desaga AS 30 TLC applicators (Wiesloch, Germany) [41,61], while that of a micropipette was reported in [28]. Nanomat 4 or the automatic TLC samplers 4 were not reported in any of the reviewed publications.

3.1.4. Development (separation)

Chromatographic development techniques for HPTLC are described in detail in [4,8,77]. Some include ascending, descending, two-dimensional, multiple and stepwise development, radial, antiradial and forced flow planar chromatography. The ascending technique is the most commonly used type, where a spotted plate is introduced in a chamber with mobile phase which penetrates

the chromatograph layer upward due to capillary forces [77]. In doing so, the solute mixtures in the spotband migrate and separation takes place. For the descending technique, the plate is placed in a development chamber and the mobile phase is introduced into the chromatographic layer from the upper side of the plate. In two-dimensional developments, the plate is developed as in the ascending technique after spotting on one corner of the plate. However, after drying, the plate is turned a 90° angle and developed a second time with another solvent system (with a different solvent selectivity). Such technique improves separation capacity in cases where the mixture to be separated contains many compounds with closely related structures, such as amino acids, whose R_f values may be rather similar [77].

When after drying, the plate development is repeated with the same solvent, to the same distance, this is termed multiple run development. But when the repeated runs are done with different solvent systems, normally with decreasing solvent polarity and increased development distance, the mode is referred to as stepwise development. The aim of these procedures is to enhance efficiency of separation by concentrating separated compounds in the spots during each repeated run. Also the procedures improve detection in a small separated zone; and finally, the procedures are useful in separating compounds which have wide polarity such as plant extracts [77,78]. Automation of this mode is called automated multiple development (AMD). However, we did not find published papers describing the use of these techniques in the analysis of pharmaceutical formulations.

In the radial mode, sample solution is applied at the centre of a plate, which is circular in shape. Mobile phase similarly is applied to the plate at the centre using a wick which is in contact with mobile phase in its container. As the mobile phase moves radially, separation of compounds takes place in a similar manner forming circles with increasing diameter. Radial development is useful to separate compounds which have low R_f values when separated using the ascending development [8,77]. When the mobile phase enters the circular chromatographic plate from the circular sides towards the centre this technique is termed antiradial [8,77]. It is useful to resolve compounds with higher R_f values in the ascending development [8].

Forced flow planar chromatography is characterized by the use of pressure to influence the movement of mobile phase in the chromatographic layer. This technique can be divided into rotational planar chromatography (RPC), overpressured layer planar chromatography (OPLC) and electro-planar chromatography (EPC) [79,80]. The driving forces for the mobile phases through the chromatographic layers are centrifugal forces, pumps and electric fields for RPC, OPLC and EPC, respectively. The mobile phase flow in these FFPC techniques can be controlled, and thus, optimized for the required separation. They also offer high speed of method development, short run times, low consumption of mobile phases and reduced diffusion of analyte spots [77]. The advantage of FFPC can be demonstrated by an OPLC method developed for the analysis of five hormones (allylestrenol, estradiol, ethynodiol diacetate, levonorgestrel and norethisterone) in a cleaning validation procedure, to be used to ensure cleaning of production equipment after drug formulation manufacturing [81]. The chromatographic conditions used were a silicagel stationary phase, a mobile phase composed of diethyl ether and *n*-hexane (6:4, v/v), pressure for mobile phase flow was 5 MPa, development volume was 7000 μL. The time for the chromatography was 15 min. The mobile phase consumed was only 7 mL while for the normal HPTLC, up to 20 mL of mobile phase is usually used [9].

Despite all these options of chromatographic development modes, for an improved resolution of compounds, the ascending technique was found to be used in all methods reviewed.

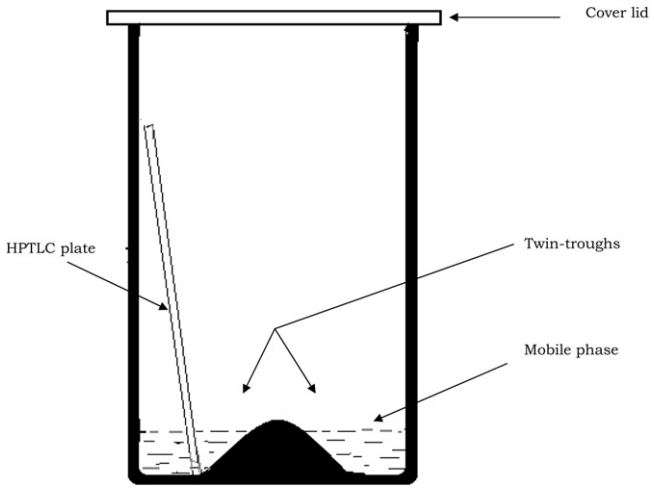

Fig. 3. A twin-trough chamber.

Major types of chambers available for HPTLC are the normal (N) type and the sandwich (S) type. When the distance between the chamber wall and the plate is more than 3 mm, it is referred to as the normal type. However, when this distance is less than 3 mm the chamber is referred to as the sandwich type. These types of chambers can further be divided depending on whether the chamber is saturated or not with mobile phase vapour. Many chamber types are available for various applications in method development for quantitative analysis, mobile phase optimization and transfer to other systems [4,7,8,66,73]. An important observation is the statement in [7,66] that, if the sample contains less than seven compounds to be quantitatively determined, saturated N chambers may be selected for method development; and if the sample contains more than seven substances, or the separation is very difficult (e.g. when compounds in sample solution are structurally related or have wide polarity), S chambers, which enable the transfer of the optimized mobile phase to the forced-flow, should be used.

Most pharmaceutical formulations are known to contain less than seven active compounds; hence, HPTLC methods are expected to fall under the first option of mainly using N chambers. We observed that the most commonly used chamber was the twin-trough chamber [15–18,21–39,44,45,47–51,53,54,56–59,61], which is the most versatile version of the normal N chamber [8]. Fig. 3 shows a twin-trough chamber. The twin-trough chamber is separated into two parts at the bottom by a glass ridge, where the mobile phase can be placed on one compartment to allow its vapour phase to saturate the chamber and equilibrate with the stationary phase which has been placed on the other compartment in the chamber. Then, solvent is allowed into the compartment where the plate had been placed and development begins. According to Kalasz and Bathori [3], twin-trough chambers offer several advantages to improve the result of plate development, including low mobile phase consumption (about 10–15 mL, since the bottom is divided into two compartments), and a reproducible pre-equilibration of the stationary phase, solvent system and vapour phase. The flat-bottom normal N chamber was reported in [47]. This N chamber is similar to the twin-trough chamber, except that it has a flat bottom where the mobile phase is placed and allowed to saturate the chamber, before the plate is placed inside.

3.1.5. Detection

Detection of separated compounds on the sorbent layers in HPTLC analysis is facilitated with the impregnation of fluorescence indicators with 254 and 366 nm excitation wavelengths, making an irradiated plate to fluorescence with green or blue colours,

Please cite this article in press as: D.H. Shewiyo, et al., HPTLC methods to assay active ingredients in pharmaceutical formulations: A review of the method development and validation steps, J. Pharm. Biomed. Anal. (2012), doi:10.1016/j.jpba.2012.03.034

respectively [77]. Fluorescence quenching by the (separated) UV-absorbing compounds enables detection. Electronic devices, such as densitometers are available to translate the intensity of the quenching by the detected compounds into chromatograms whose peak heights/areas can be used in a quantitative analysis [4]. The densitometers use monochromatic light and a rectangular slit of selectable length and width to scan the tracks of chromatograms. During scanning, light from a deuterium (UV) or a tungsten (vis) lamp strikes the sample spot at a right angle, and the reflected light is measured by a photomultiplier aligned at a 30° angle [76,77]. The light absorbed by the sample spot is measured as difference between the incident and reflected light. This mode of measurement in the densitometer is termed as reflectance/absorbance mode. It is also possible to perform measurement in transmission/absorbance where the photodiode for detection of the light transmitted through the sample spot on the adsorbent is positioned below the spot. Densitometry with slit scanning in the ultraviolet–visible (UV/vis) light range, in the reflectance/absorbance mode is observed to be the most commonly applied detection method [15–27,29–45,47–61]. The reflectance measurements give more precise and accurate measurements compared to the transmission measurements since the reflectance mode is not sensitive to variation in thickness and uniformity of the chromatographic layer [77].

Other possible detection techniques reported in the literature that could be used include video densitometry [82,83], mass spectrometry, Fourier transform infrared spectroscopy, Raman spectroscopy, near magnetic resonance and radio activity-based methods [84–86].

For the compounds that do no exhibit UV–vis absorbing properties, e.g. ethambutol, chemical derivatization is carried out [77]. However, many pharmaceutical active ingredients have UV-absorbing properties and are therefore easily detected without the need for derivatization.

3.2. Quantitation

Methods for the quantitative determination of separated compounds on the HPTLC plates include those in which the compounds are scraped from the stationary phase before being examined, and those in which separated compounds are examined directly on the stationary layer [8]. In the former, the scraped compound(s) are extracted from the layer using a suitable solvent, to obtain a solution that can be analyzed by conventional quantitative methods such as UV, HPLC, GC and Liquid Scintillation Counting. In the second group, optical densitometric scanners linked to computers are used for the in situ measurements of compounds directly on the layer.

The second approach is the one applied by all reviewed publications on formulation analysis [15–61]. It is easier than the first, where additional instrumentation for scraping off layer (containing compounds), and equipment for the analysis of extracted solutions are needed. Such equipment included the semi-automatic equipment for online extraction and injection to the mass spectrometer (MS), e.g. ChromeX-trakt (ChromAn, Holzhausen, Germany) [86] and TLC–MS interface (CAMAG, Muttenz, Switzerland) [87,88].

For successful quantitation in HPTLC, accurate and precise application of the sample is the most critical step [4], and as a rule sample and standard solutions should be chromatographed on the same plate [2,4]. This is important since it minimizes errors that may arise from variations across the layer on a plate or from plate-to-plate variations. After plate development and drying, measurement of separated spot bands areas is done with a suitable detector, usually a densitometer [15–27,29–45,47–61]. A calibration graph is constructed by plotting the peak areas/heights against the amounts of the standards (rather than concentrations). Straight line or quadratic relationships may be obtained and can be used to estimate the unknown amount of compound in a sample. Straight line calibration is preferred, though the use of a quadratic relationship was reported by [19,36].

Sample solution applied as bands by the spray-on technique result into a homogenous distribution of the sample across the bands, therefore, it is possible to measure only a portion of the band [76]. TLC scanner operation manuals direct the slit dimension of the densitometer to be set at 70–90% of the band size. If a band has a length of 6 mm, the slit dimensions (length × width) are 5.0 mm × 0.45 mm. This ensures that bands are scanned within approximately the same dimensions, so as to enhance the accuracy and precision of the scanning of the bands. Some scanners offer selectable slit dimensions ranging from 0.5 to 20 mm (length) and 0.025 to 1.2 mm (width) which can be combined in different ways depending on the size of the band; examples of such combinations are 5 mm × 0.45 mm or 4 mm × 0.1 mm.

It was observed that the majority of those who reported the slit dimension settings were within the 70–90% of the band sizes specified in their methods [15,17,21–25,27,29,32–37,40,43,45,48,49,51,53,56,57,59]. However, references [48,49] reported slit dimensions of 6 mm × 0.04 mm for bands with sizes 6 mm. Similarly, reference [60] applied samples as 8 mm bands and used slit dimension 8 mm × 0.6 mm during scanning. In these cases the slit dimensions covered 100% of the band size, hence, deviating from the manufacturer recommendation.

3.3. HPTLC method validation for pharmaceutical analysis

As is the case with all analytical methods for pharmaceutical analysis, HPTLC methods must be validated to ensure that they fit the intended purpose and meet the strict regulatory requirements for pharmaceuticals.

3.3.1. Classical validation approach

There are several sources of information in the literature describing validation procedures for analytical methods. Such information sources include the book on *Quality Assurance in Analytical Chemistry* [89], the ICH guidelines [90], the FDA Guidance for Industry [91], the US Pharmacopeia [92] and AOAC the guidelines for method validation for a single laboratory [93]. However, it is the ICH guidelines that have been referred to by most publications [15,17–19,21–24,26,27,29–32,34,36–44,46,48,50–57,60]. Other papers did not cite any reference.

Method performance parameters, i.e., specificity, linearity, precision, trueness, range, limits of detection and quantitation, and robustness are described and ways of evaluating them are proposed [68,90], but specifying acceptance criteria for each parameter is not evident and is certainly not generally done. Some fields of application (e.g. pharmaceutical analysis) or some methods (e.g. chromatography) specify criteria for some of the parameters in their guidelines (e.g. ICH).

In many occasions, a generally accepted value of a parameter, depending on the types of methods and samples, is adopted as criterion. For example, the percentage relative standard deviation for intermediate precision of a chromatographic method is widely accepted to be ≤5% in pharmaceutical analysis, as can be observed in some papers, e.g. [16,46]. A method is validated if all parameters comply with the set criteria.

The extent of validation differs among the case studies considered [15–61], and it is not clear whether this is always guided by the intended use of the method. While all publications validated for linearity, trueness and precision, the remaining parameters also suggested by ICH for validation of assay methods, i.e. specificity and

Please cite this article in press as: D.H. Shewiyo, et al., HPTLC methods to assay active ingredients in pharmaceutical formulations: A review of the method development and validation steps, J. Pharm. Biomed. Anal. (2012), doi:10.1016/j.jpba.2012.03.034

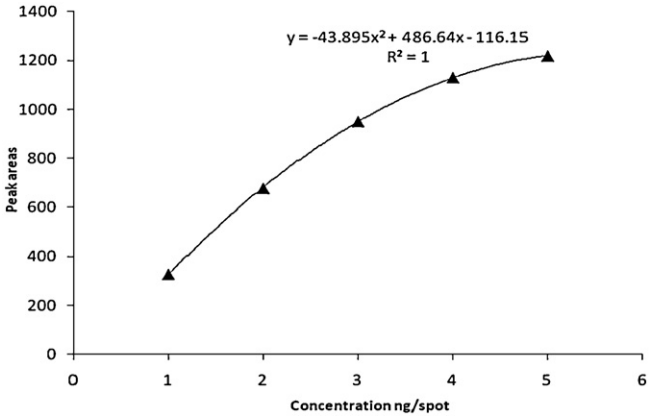

Fig. 4. A non-linear calibration curve showing a correlation coefficient $r = 1$.

range, were not evaluated by any. Range is anyway often not needed for formulation assays.

3.3.1.1. Linearity of calibration line. Analysts generally prefer to work with straight line equations for an easy estimation of the amount of ingredient(s) in samples. Therefore, many methods reviewed were optimized and validated at concentration ranges where a linear relationship between amount of active ingredient in solutions/spot bands and the peak heights/areas was demonstrated [15,20–27,29–31,33,35,37,38,40,42–60]. However, quadratic relationships were also reported to offer acceptable results. For instance, Habte et al. [36] developed and validated a method for the simultaneous separation and determination of lamivudine and zidovudine in pharmaceutical formulations. The calibration data fitted well to a quadratic model with $r^2 = 0.9997$ and 0.9996 for lamivudine and zidovudine, respectively, as compared to a straight-line model where the data did fit less well ($r^2 = 0.9776$ and 0.9616, respectively). The mean assay results obtained using the quadratic models were $99.74 \pm 0.84\%$ and $99.76 \pm 0.88\%$, for lamivudine and zidovudine, respectively. Kaale et al. [19] participated in an inter-laboratory investigation on the use of HPTLC to perform assays of lamivudine-zidovudine, metronidazole, nevirapine and quinine composite samples. A linearity study for each compound was performed at concentration levels covering 50–150% of the target concentration. The calibration data for all compounds fitted well to quadratic models with r^2 values above 0.998. The assay results obtained using the quadratic models for the participating laboratories for all compounds ranged from 97.0% to 102.7% with the percent relative standard deviation $\leq$3.21. In the two papers cited above, i.e. [19,36], the assay results obtained by using the straight line were not reported, and therefore, could not be compared to the results obtained using the quadratic equations. In both studies, a coefficient of determination (r^2) of at least 0.99 was considered as an indicator of the linearity of the calibration line.

However, this is not a good criterion since it has been demonstrated that values close to 1.0 can also be obtained for a nonlinear relationship [85,94–97]. Fig. 4 shows calibration data which gave an $r^2 = 1$ ($r = 1$), but the relationship is not straight. Therefore, visual observation of the plot of the response against the amount of the analyte is advised, and it may be followed by plotting the y-residual values against the concentration when there is a large number of measurements for calibration [68,94,96]. However, statistical tests, such as a lack-of-fit test (F-test) [68,82,84] and a test for the significance of the quadratic coefficient b_2 in the model, $y = b_0 + b_1x + b_2x^2$ [69], are most appropriate for evaluating the linearity. The publications [15,37] evaluated the linearity of the calibration lines using visual observation of the calibration graphs and the residual plots, and by lack-of-fit tests. The methods were developed and validated for the simultaneous analysis of lamivudine/stavudine/nevirapine and for sulfamethoxazole/trimethoprim in fixed-dose combination tablets, respectively. Reference [36] used a residual plot to evaluate the calibration models for a method for the simultaneous analysis of lamivudine and zidovudine. The residual plots showed that the data did not fit well to the straight line model which was initially selected. A quadratic model fitted well to the data.

3.3.1.2. Precision (repeatability and time-intermediate precision). The precision of an analytical procedure expresses the degree of closeness of agreement (degree of scatter) between a series of measurements obtained from multiple sampling of the same homogeneous sample under the prescribed conditions [90]. Regulatory guidelines stipulate repeatability, intermediate precision and reproducibility as possible types of precision to be evaluated [90,91]. Reproducibility evaluates precision between laboratories; therefore, it is not covered here as the considered case studies were validated within the development laboratories. Since analytical methods within a laboratory are used on different days and possibly by several analysts, sometimes also using different equipment, it is important that the repeatability and intermediate precision are evaluated. In reference [22] only repeatability was evaluated, which is insufficient to specify the precision of the method. Repeatability and intermediate precision were studied in publications [15,21–26,30,31,35,37,38,40,41,43–48,50–54] and the obtained percent relative standard deviations (%RSD), were $\leq$3% and $\leq$5% for repeatability and time-different intermediate precisions, respectively. These are comparable to those obtained by HPLC methods, which also should not exceed 5% [20,97].

The intermediate precision has to be estimated by measuring on several days, and possibly varying also the analysts and/or equipment [90]. The trend in the reviewed publications was to evaluate the time-different intermediate precision by measurements over several days. Some recommend the simultaneous evaluation of repeatability and intermediate precision using an experimental design with replicate, usually duplicate measurements at different days [68,90,98]. The analysis of variance (ANOVA) is used to estimate the variance components, i.e. variance due to repeatability (s_r^2) and variance due to between-days effects (s_{between}^2). Then time-different intermediate precision ($s_{I(t)}^2$) is estimated as $s_{I(t)}^2 = s_r^2 + s_{\text{between}}^2$.

In reference [98] underestimation of time-different intermediate precision when an experimental design is not used, is demonstrated. Without the experimental design and evaluation by ANOVA which considers the between-days effect, time-different intermediate precision was estimated as % RSD = 5.2 while with ANOVA it was estimated as % RSD = 6.0 for the same data set. With the exception of publications [15,37] in which ANOVA was used for the study of the two types of precision, other publications did not specify how the specified values were obtained.

For the repeatability study the proposed number of replicates is $n \geq 3$ for at least three concentration levels ($k \geq 3$) which cover 80–120% of the target concentration of the sample in the solution [69,90] was complied with in [15–18,21–27,30–33,36–41,43–45,47–53,56–59,61]. For the time-different intermediate precision, the study with $n \geq 2$, $k \geq 3$ with measurements for more than one day, was complied with in [15,17,18,21–27,30–33,36–40,43–45,47–53,56–59,61]. Some publications did not specify the number of measurement days during the study of the time-different intermediate precision while others did not clearly describe how the precision studies were conducted. The concentration levels used for the study of both precision types were not always described. Occasionally only a part of the method is evaluated and reported as repeatability, for instance, the repeatability of sample application on the

Please cite this article in press as: D.H. Shewiyo, et al., HPTLC methods to assay active ingredients in pharmaceutical formulations: A review of the method development and validation steps, J. Pharm. Biomed. Anal. (2012), doi:10.1016/j.jpba.2012.03.034

chromatographic plate or the repeatability of the measurement of the separated spots. This underestimates the method repeatability since it should include all steps of the method from the sample preparation to the final measurements.

3.3.1.3. Trueness. Trueness of an analytical method expresses the closeness of agreement between the mean value obtained from the series of measurements and the value which is accepted either as a conventional true value or an accepted reference value [99,100]. It is measured as recovery or bias [15,17,22,26,37,38,59,61]. ICH calls this accuracy, while others (ISO) consider accuracy as the combination of random (precision) and systematic (bias) errors.

All considered publications performed recovery tests after spiking with reference standard(s) to the prepared tablets matrix [15–17,61] or pre-analyzed samples, i.e. standard addition [18,20–27,29–31,33–36,38–45,47–49,51–54,56–60]. The ICH guidelines, which have been cited by many authors, indicate the recovery studies for the assay methods to be performed at a minimum of three concentration levels and three replicates at each level. Recoveries were mostly determined at 80%, 100% and 120% of the expected samples concentration [15–18,21–27,29–34,36–43,45–54,56,57,59–61]. In [35], where a method for simultaneous determination of rabeprazole and itopride hydrochloride in a fixed dose capsule was developed, the recoveries were performed at two concentration levels, i.e. 50% and 100%. A recovery study at only one concentration level was performed for a method developed to estimate cefetamet in tablets [43]. Almost all publications complied with the number of replicates ($n \geq 3$) at each of the concentration levels studied.

It has earlier been shown that the use of these above "point-interval" hypothesis tests is not the best way to proceed for the detection of bias. Therefore, "interval-hypothesis" testing has been proposed [101]. This approach requires the prior determination of an acceptance interval in which the bias at each concentration level is tested to fall within. However, none of the reviewed case studies applied this approach.

3.3.1.4. Range. According to the ICH guide [90], the range of a method is the interval between the upper and lower concentration of the analyte in samples (including these concentrations) where the method demonstrates a suitable level of precision, trueness and linearity. The ICH guidelines propose the concentration levels covering 80– 120% of the target concentration to be considered for evaluation as the range of a particular method to assay formulations. None of the reviewed papers, except [61], indicated the ranges of their methods. However, all reported the linear ranges which were the lower and upper concentrations of the calibration lines. The linear ranges usually exceed largely the 80–120% of the target sample concentration. For instance, the linear ranges for atorvastatin and ezetimibe were reported to cover 17–200% (0.4–2.4 ng/spot) of the target concentrations (1.2 ng/spot) in a method developed for their simultaneous determination in a tablet formulation [50].

In [61] where an HPTLC method was developed for the quantitative determination of glucosamine in herbal dietary supplements, and validated by using the accuracy profile approach, the range of the method was evaluated and reported.

An accuracy profile is a graphical tool that offers the possibility to visually comprehend the ability of the method to fulfil its objectives and to control the risk associated with its routine applications [102]. The bias and standard deviation of intermediate concentrations are determined at each concentration level during validation. Then the 95% tolerance limits of the total error (bias + intermediate precision) are calculated at each concentration level. The tolerance limits and the accepted bias limits (e.g. −5%, 5%, for active ingredient in pharmaceutical products) are used to construct the accuracy

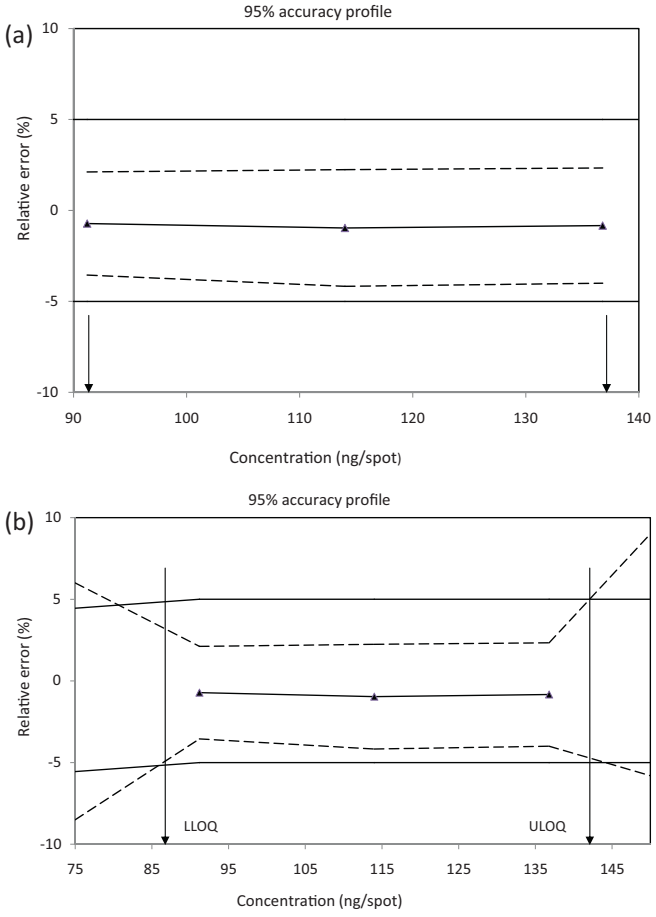

Fig. 5. Accuracy profiles. (a) The two arrows indicate the lower and the upper concentrations studied. (b) The arrows indicate the intersection between the 95% tolerance limits and the acceptance limits, and therefore, give the lower and the upper limits of quantitation (LLOQ and ULOQ, respectively).

profile [98,100,102,103]. Fig. 5a illustrates an accuracy profile. The continuous lines at −5 and 5% are the upper and lower acceptance limits. The dashed lines are the upper and lower 95% tolerance limits of the total error, the middle line is the relative error. The two arrows indicate the upper and the lower concentrations studied.

This accuracy profile easily shows the range since it corresponds to the lower and the upper concentrations which were studied and which lie within the acceptance limits specified, meaning that the accuracy (trueness + precision) at these levels is acceptable, and therefore, comply to the ICH definition for range.

3.3.1.5. Detection limit (DL) and quantitation limit (QL). According to the ICH guidelines, determination of DL and QL is generally not necessary for the assay methods [90]. Although most pharmaceutical formulations contain drug substances at high levels, and therefore, information regarding DL and QL is not useful, the limits were very often determined [22–25,27,30,33,35,38,40–46,48,51–53]. The approaches used often include the signal-to-noise ratio [24,27,35,44,45,48,53]. This approach is based on the measured signals from sample solutions with known low concentrations of sample and from blank solution [90]. The signal-to-noise ratios of 3:1 and 10:1 are generally considered acceptable for estimating the DL and the QL, respectively. A second approach used to determine the DL and the QL use the calibration curves [22,23,30,33,38,40,42,46,51,52]. According to [90],

$$\mathrm{DL} = \frac{3.3\sigma}{S}$$

$$QL = \frac{10\sigma}{S}$$

where σ is standard deviation of the response, S is slope of the calibration line.

The slope is estimated from the calibration curve of the sample. The estimates of σ may be obtained from the standard deviation of the signal from blank solutions. The σ may also be obtained from the standard deviation of the y-intercept of the regression line prepared by solutions with sample concentrations in the range of the corresponding DL and QL. The residual standard deviations of such regression lines may be used as estimates of σ.

A third approach used to determine the DL and the QL is the dilution of standard solution to the lowest detectable level [41]. Procedures used to determine DL and QL were not indicated in [25,43].

When using the accuracy profile to validate an analytical method, the intersections between the 95% expectation tolerance limits and the acceptance limits define the lower and upper quantitation limits [100], as illustrated in Fig. 5b. If these lines do not intersect, then the lower and the upper concentrations which were studied become the lower and upper quantitation limits (Fig. 5). Within these limits measurements can be performed with known accuracy [100].

4. Other areas of HPTLC application

HPTLC finds applications in many fields of analytical sciences. Apart from being used to active ingredients in pharmaceutical formulations it is also used for testing their stability. Ali et al. [38] developed and validated a stability indicating method for the separation of impurities and degradation products of a fixed-dose antituberculosis tablet formulation containing isoniazid and rifampicin. An aluminium backed silica gel 60 F_{254} plate with a mobile phase composed of *n*-hexane, 2-propanol, acetone, ammonia and formic acid (30:38:28:3:1, v/v/v/v/v) was used to separate the active compounds from their degradation products. Detection wavelength was set at 254 nm.

Chitlange et al. [26] reported a stability indicating HPTLC method for dexibuprofen in pharmaceutical dosage forms, in which the active ingredient was well resolved from the forced-degradation products. Chromatographic conditions were silica gel 60 F_{254} as the stationary phase, *n*-hexane, ethyl acetate and glacial acetic acid (7.5:2.5:0.2, v/v/v) as the mobile phase and detection wavelength set at 225 nm.

Ferenczi-Fodor et al. [104] published a comprehensive paper on how versatility, speed and flexibility of this technique can be employed for purity testing of pharmaceuticals. There is also a possibility of using HPTLC methods for the evaluation of the uniformity of content testing of tablets as reported by [4]. Another example is the publication by Machale et al. [105] where an HPTLC method was developed and validated for content uniformity of diazepam tablets (2 mg). Using an aluminium backed silica gel 60 F_{254}, 20 cm × 10 cm plate, 10 tablets were simultaneously analyzed within a short run time and the results were within USP specification of 85–115% for assay of individual tablets, with %RSD < 6%.

Applications in environmental analysis are also described in the literature, where residuals, soil and water analyses are performed. For instance, Morlock [106] describes a method for the simultaneous analysis of about 283 pesticide residuals in ground, raw drinking and mineral water. This method has been accepted as a German standard procedure. It is based on automated multiple development. HPTLC has also been utilized in the detection and quantitation of pesticide residuals in fruits, e.g. chlorpyrifos, imidaclopril and acephate pesticide residuals in brinjal fruits [107].

Potential usefulness and contribution of HPTLC in food analysis as a quantitative method is described in detail with various examples in [108]. In this reference the reliability of HPTLC is explained with some examples from published methods where it could be observed that %RSD for repeatability could achieve values between 1.5% and 6.4% which the author considered acceptable in food analysis. Other performance parameters, such as correlation coefficients for calibration are always above 0.998, though as described in (Section 3.3.1.1) above, this is not a good measure of linearity. Low detection limits, such as 1 mg/kg, could be obtained, which permit this technique to be used to check additives, such as sucralose, in some food products, e.g. milk-based confectionaries, according to the European legislature (where additions in the range of 10–3000 mg/kg are permitted depending on the type of food) [108].

Clinical laboratories also benefit from the advantage of HPTLC methods, e.g. in the area of drug monitoring, metabolism studies and doping control. Mennickent et al. [109] developed a method for the quantitative determination of the drug fluoxetine in human serum; a method which may be used for monitoring the drug in serum and to get information about the patients adherence to medication. In a 10 cm × 20 cm HPTLC plate, 33 spots (6 standard + 27 samples from 10 patients) were analyzed simultaneously. Sample preparation was a single-step precipitation of proteins from the plasma by using methanol. Jain et al. [110] developed a method for the determination of minocycline antibiotic in human plasma. Silica gel 60 F_{254} on aluminium plate, with a mobile phase composed of methanol, acetonitrile, isopropanol and water (5:4:0.5:0.5, v/v/v/v) were used for the separation. Detection was performed at 345 nm. Only a single-step precipitation of proteins was carried out with methanol to prepare the sample solutions. Trueness achieved was 95.8 ± 4.5%, the repeatability and the time-different intermediate precision (reported as %CV) were ≤3.49% and ≤4.14%, respectively. The limit of quantitation was 15.4 ng/spot band.

5. Conclusion

This review reveals that most of the HPTLC methods developed and validated comply with the general procedures pertaining to the quantitative mode of this technique. HPTLC is generally used with an unmodified silica layer as stationary phase on precoated plates and slit-scanning densitometry with UV–vis light as the detection technique. The most preferred way of mobile phase selection and "optimization" was found to be the trial- and error-approach and the analysts' own experiences. However, in case a complex mixture of drugs needs to be separated, we advocate for a systematic approach.

Acknowledgements

D.H. Shewiyo would like to express his sincere appreciations to the Belgium Technical Cooperation (BTC) for financial support. Bieke Dejaegher is a post-doctoral fellow of the Fund for Scientific Research (FWO), Flanders, Belgium.

References

[1] Thin Layer Chromatography, Macherey–Nagel, available at http://separations.co.za/fileadmin/themes/default/pdf/2.%20PRODUCT%20LINES/N.%20MACHEREY-NAGEL/iv.%20CHROMATOGRAPHY/4.%20TLC/MN%20TLC%20Catalogue.pdf (accessed on 10th December 2011).
[2] J. Sherma, Planar chromatography, review: planar chromatography, Anal. Chem. 80 (2008) 4243–4267.
[3] H. Kalasz, M. Bathori, Pharmaceutical applications of TLC, LC–GC Eur. 10 (2001) 311–321.
[4] P.D. Sethi, Quantitative Analysis of Pharmaceutical Formulations, High Performance Thin Layer Chromatography, CBS Publishers and Distributors, New Delhi, India, 1996.

[5] C.F. Poole, Layer chromatography: challenges and opportunities, J. Chromatogr. A 1000 (2003) 963–984.
[6] S. Nyiredy, Planar chromatographic method development using the PRISMA optimization system and flow charts, J. Chromatogr. Sci. 40 (2002) 553–563.
[7] E. Kaale, P. Risha, T. Layloff, An interlaboratory investigation on the use of high-performance thin layer chromatography to perform assay of Lamivudine-Zidovudine, Metronidazole, Nevirapine and Quinine composite samples, J. Chromatogr. A 1218 (19) (2011) 2732–2736.
[8] S. Nyiredy, in: E. Heftmann (Ed.), Chromatography, Joutrnal of Chromatography Library, vol. 51A, 5th ed., Elsevier, Amsterdam, 1992, pp. 109–150.
[9] G. Morlock, HPTLC steps from application to quantification: workshop presentation, available at http://www.hptlc.com/pdf/2006pdf/workshop/Morlock%20Workshop%201%20Part%201.pdf (accessed on 25th August 2011).
[10] S. Gocan, Stationary phases for thin-layer chromatography, J. Chromatogr. Sci. 40 (2002) 538–549.
[11] J. Sherma, J.C. Touchstone, M.F. Dobbins, in: J. Sherma, J.C. Touchstone (Eds.), Materials and Methods Densitometry in Thin Layer Chromatography: Practice & Applications, John Wileys & Sons, USA, 1979, pp. 25–120.
[12] R.M. Scott, The stationary phase in thin layer chromatography, J. Chromatogr. Sci. 2 (1973) 129–135.
[13] S. Gocan, G. Cimpan, L. Muresan, Automated multiple development thin-layer chromatography of some plants extracts, J. Pharm. Biomed. Anal. 14 (1996) 1221–1227.
[14] D.B. Gandhi, P.J. Mehta, Simultaneous RP-HPTLC method for determination of levodaopa, carbidopa and entocapone in combined tablet dosage form, J. Planar. Chromatogr.-Mod. TLC 24 (2011) 236–241.
[15] D.H. Shewiyo, E. Kaale, C. Ugullum, M.N. Sigonda, P.G. Risha, B. Dejaegher, J. Smeyers-Verbeke, Y. Vander Heyden, Development and validation of a normal-phase HPTLC method for the simultaneous analysis of Lamivudine, Stavudine and Nevirapine in fixed dose combination tablets, J. Pharm. Biomed. Anal. 54 (2011) 445–450.
[16] D. Antic, S. Filipic, D. Agbaba, A simple and sensitive TLC method for determination of Clopidogrel and its impurity SR 26334 in pharmaceutical products, Acta Chromatogr. 18 (2007) 199–206.
[17] R.J.R. Vikas, L. Sathiyanarayan, S.S. Yadav, Stability indicating HPTLC method for Trandolapril estimation in the bulk drug and dosage form, Indian J. Educ. Res. 44 (2010) 341–344.
[18] S.B. Bari, A.R. Bakhshi, P.S. Jain, S.J. Surana, Development and validation od stability – indicating TLC – denstitometric determination of Ropinirole hydrochloride in bulk and pharmaceutical dosage form, Pharm. Anal. Acta 2 (2011) 2–7.
[19] E. Kaale, P. Risha, E. Reich, T. Layloff, An interlaboratory investigation on the use of high-performance thin-layer chromatography to perform assays lamivudine-zidovudine, metronidazole, nevirapine, and quinine composite samples, J. AOAC Int. 93 (2010) 1836–1843.
[20] S. Anbazhagan, N. Indumathy, P. Shanmugapandigayan, S.K. Sridhar, Simultaneous quantification of Stavudine, Lamivudine and Nevirapine by UV spectroscopy, reversr phase HPLC and HPTLC in tablets, J. Pharm. Biomed. Anal. 39 (2005) 801–804.
[21] A.S. Rathore, L. Sathiyanarayanan, K.R. Mahadik, Develeopment of validated HPLC and HPTLC methods for simultaneous determination of levocetirizine dihydrochloride and montelukast sodium in bulk and pharmaceutical dosage form, Pharm. Anal. Acta – Open Access J. 1 (2010) 1–6, doi:10.4172/2153-2435.1000106.
[22] A.A. Shirkhedkar, P.M. Bugdane, S.J. Surana, Stability – indicating TLC – densitometric determination of nebivolol hydrochloride in bulk and pharmaceutical dosage form, J. Chromatogr. Sci. 48 (2010) 102–113.
[23] A.A. Shirkhedkar, A.M. Shaikh, S.J. Surana, Simultaneous determination of paracetamol and piroxicam in tablets by thin-layer chromatography combined with densitometry, Eurasian J. Anal. Chem. 3 (2008) 258–267.
[24] V.B. Borhade, H.A. Nair, D.D. Hegde, Development and validation of HPTLC method for estimation of tracolimus in formulations, Drug Dev. Ind. Pharm. 35 (2009) 440–448.
[25] R. Chakraborty, K. Pal, M. Shaiba, N. Sangepu, P. Sridevi, High performance thin-layer chromatographic estimation of ranolazine, Res. J. Pharm. Biol. Chem. Sci. 4 (2010) 152–157.
[26] S.S. Chitlange, N. Kumar, S.B. Wankhede, Stability – indicating HPTLC method for estimation of dexibuprofen in pharmaceutical dosage form, J. Pharm. Res. 9 (2009) 1542–1546.
[27] S. Chopra, F.J. Ahmad, R.K. Khar, S.K. Motwani, S. Mahdi, Z. Iqbal, S. Talegaonkar, Validated high performance thin-layer chromatography method for determination of trigonelline in herbal extract and pharmaceutical dosage form, Anal. Chim. Acta 577 (2006) 46–51.
[28] C. Cimpoiu, A. Hosu, S. Hodisan, Analysis of some steroids by thin-layer chromatography using optimum mobile phases, J. Pharm. Biomed. Anal. 41 (2006) 633–637.
[29] P. Deshpande, S. Gandhi, V. Bhavnani, R. Bandewar, A. Dhiware, V. Diwale, High performance thin-layer chromatographic determination of famotidine and domperidone in combined tablet dosage form, Res. J. Pharm. Biol. Chem. Sci. 4 (2010) 354–359.
[30] G. Devala Rao, S. Kathirvel, S.V. Satyanarayana, Development and validation of TLC-Densitometry method for the estimation of Anti-psychotic drug in bulk and tablet formulation, Int. J. ChemTech Res. 2 (2010) 2063–2069.
[31] S.S. Dhaneshwar, P. Deshpande, M. Patil, G. Vadnekar, S.R. Dhaneshwar, Development and validation of a HPTLC method for estimation of duloxetine hydrochloride in bulk drug and in tablet dosage form, Indian J. Pharm. Sci. 70 (2008) 233–236.
[32] C.R. Shah, B.N. Suhagia, N.J. Shah, R.R. Shah, Development and validation of a HPTLC method for the estimation of sumatriptan in tablet dosage forms, Indian J. Pharm. Sci. 70 (2008) 831–834.
[33] P. Parmar, A. Mehta, Development and validation of HPTLC method for the estimation of Clotrimazole in bulk drug and tablet formulations, Indian J. Pharm. Sci. 71 (2009) 451–454.
[34] M. Joshi, A.P. Nikalje, M. Shahed, M. Dehghan, HPTLC method for the simultaneous estimation of emtricitabine and tenovofiv in tablet dosage forms, Indian J. Pharm. Sci. 71 (2009) 95–97.
[35] A. Suganth, S. John, T.K. Ravi, Simultaneous HPTLC determination of rabeprazole and itopride hydrochloride from their combined dosage form, Indian J. Pharm. Sci. 70 (2008) 366–368.
[36] G. Habte, A. Hymete, A.M.I. Mohammed, Simultaneous separation and determination of lamivudine and zidovudine in pharmaceutical formulations using the HPTLC method, Anal. Lett. 42 (2009) 1552–1570.
[37] D.H. Shewiyo, E. Kaale, P.G. Risha, B. Dejaegher, J. Smeyers-Verbeke, Y. Vander Heyden, Development and validation of a normal-phase high-performance thin layer chromatographic method for the analysis of Sulfamethoxazole and Trimethoprim in Co-trimoxazole tablets, J. Chromatogr. A 1216 (2009) 7102–7107.
[38] J. Ali, N. Ali, Y. Sultana, S. Baboota, S. Faiyaz, Development and validation of a stability indicating HPTLC method for analysis of antitubercular drugs, Acta Chromatogr. 13 (2007) 168–179.
[39] L.V. Potale, A.S. Khodke, S.M. Patole, M.C. Damle, Development and validation of stability – indicating HPTLC method for determination of efavirenz as bulk drug and in pharmaceutical formulation, J. Adv. Pharm. Res. 1 (2010) 115–122.
[40] M. Starek, J. Krzek, TLC chromatographic–densitometric assay of ibuprofen and its impurities, J. Chromatogr. Sci. 48 (2010) 825–829.
[41] J. Krzek, A. Kwiecien, Application of densitometry for determination of beta-adrenergic-blocking agents in pharmaceutical preparations, J. Planar Chromatogr. 18 (2005) 308–313.
[42] V.B. Kshirsagar, U.A. Deokate, V.B. Bharkad, S.S. Khadabadi, HPTLC method development and validation for the simultaneous estimation of diosgenin and levodopa in marketed formulation, Asian J. Res. Chem. 1 (2008) 36–39.
[43] A. Lakshmana Rao, N. Prudhvi, K.P.C. Basavaraj, Y.N. Manohara, Development and validation of a HPTLC method for the estimation of cefetamet, Rasayan J. Chem. 2 (2009) 720–723.
[44] M.V. Mahadik, S.R. Dhaneshwar, Application of stability – indicating HPTLC method for the quantitative determination of ezetimibe in pharmaceutical dosage forms, Asian J. Pharm. Sci. 5 (2007) 182–190.
[45] S.P Agarwala, A. Ali, Y. Dua, S. Ahuja, Determinatin of Artemisinin in bulk and pharmaceutical dosage forms using HPTLC, Indian J. Pharm. Sci. 71 (2009) 98–100.
[46] G.A. Saleh, F.A. Mohamed, S.R. El-Shaboury, A.H. Rageh, Selective densitometric determination of four α-aminocephalosporins using ninhydrin reagent, J. Chromatogr. Sci. 48 (2010) 68–75.
[47] B.H. Patel, B.N. Suhagia, M.M. Patel, J.R. Patel, HPTLC determination of rabeprazole and domperidone in capsules and its validation, J. Chromatogr. Sci. 46 (2008) 304–307.
[48] R.B. Patel, M.R. Patel, K.K. Bhatt, B.G. Patel, Development and validation of a HPTLC method for estimation of Carbamazepine in formulations and is *in vitro* release study, Chromatogr. Res. Int. 2011 (2011) 1–8.
[49] V.A. Patel, P.G. Patel, B.G. Chaudhary, N.B. Rajgor, S.G. Rathi, Development and validation of HPTLC method for the simultaneous estimation of telmisartan and ramipril in combined dosage form, Int. J. Pharm. Biol. Res. 1 (2010) 18–24.
[50] S.S. Dhaneshwar, S.R. Daneshwar, P. Deshpande, M. Patil, Development anda validation of a method for the densitometric estimation of atorvastatin calcium and ezetimibe as the bulk drugs and tablet dosage forms, Acta Chromatogr. 19 (2007) 141–148.
[51] P.N. Ranjane, S.V. Gandhi, S.S. Kadur, K.G. Bothara, HPTLC determination of cefuroxime axetil and ordinazole in combined tablet dosage forms, J. Chromatogr. Sci. 48 (2010) 26–28.
[52] S.T. Kumbhar, G.K. Chougule, V.S. Tegeli, G.B. Gajeli, Y.S. Thorat, U.S. Shivsharan, A validated HPTLC method for simultaneous quantification of of nevibolol and hydrochlorothiazide in bulk and tablet formulation, Int. J. Pharm. Sci. Drug Res. 3 (2011) 62–66.
[53] S.R. Dhaneshwar, V.K. Bhusari, M.V. Mahadik, B. Santakumari, Application of a stability–indicating thin-layer chromatographic method to the determination of tenatoprazole in pharmaceutical dosage forms, J.AOAC Int. 92 (2009) 387–393.
[54] D.B. Meshram, S.B. Bagade, M.R. Tajne, A simple TLC method for analysis of fluconazole in pharmaceutical dosage forms, J. Planar Chromatogr. 21 (2008) 191–195.
[55] Z.A.J. Ebrahim, D. Balalau, D.L. Baconi, C.M. Gutu, M. Ilie, HPTLC method for the assay of tramadol and pentazocin from mixtures, Farmacia 59 (2011) 381–387.
[56] M. Anand, A. Fonseca, V.G. Santosh, B.P. Deshpande, Development and validation of a high-performance thin-layer chromatographic method for estimation of brimodine tartrate as bulk drug and ophthalmic solutions, Int. J. ChemTech Res. 2 (2010) 1376–1379.
[57] P. Chandra, A.S. Rathore, L. Sathiyanarayanan, K.R. Mahadik, Application of high-performance thin-layer chromatographic method for the simultaneous determination of Lamivudine and tenofovir disoproxil fumarate in pharmaceutical dosage form, J. Chil. Chem. Soc. 56 (2011) 702–705.

Please cite this article in press as: D.H. Shewiyo, et al., HPTLC methods to assay active ingredients in pharmaceutical formulations: A review of the method development and validation steps, J. Pharm. Biomed. Anal. (2012), doi:10.1016/j.jpba.2012.03.034

[58] P. Shanmugasundaram, R. Maheswari, M. Vijayaanandhi, Quantitative estimation of piperine in herbal cough syrup by HPTLC method, Rayasan J. Chem. 1 (2008) 212–217.
[59] P.S. Jain, Stability – indicating HPTLC determination of ambroxol hydrochloride in bulk drug and pharmaceutical dosage form, J. Chromatogr. Sci. 48 (2010) 45–48.
[60] A. Kwiecien, J. Krzek, L. Biniek, TLC – densitometric determination of azithromycin in pharmaceutical preparations, J. Planar Chromatogr. 21 (2008) 177–181.
[61] V. Esters, L. Angenot, V. Brandt, M. Frederich, M. Tits, C. Van Nerum, J-N Wauters, Ph. Hubert, Validation of a high-performance thin-layer chromatography/densitometry method for the quantitative determination of glucosamine in a herbal dietary supplement, J. Chromatogr. A 1112 (2006) 156–164.
[62] G. Gubitz, M.G. Schmid, Chiral separation by chromatographic and electromigration techniques, Biopharm. Drug Dispos. 22 (2001) 291–336.
[63] H.E. Hauck, M. Schulz, Ultrathin-layer chromatography, J. Chromatogr. Sci. 40 (2002) 1–3.
[64] F. Geiss, Fundamentals of Thin Layer Chromatography (Planar Chromatography), Dr. Alfred Huthig Verlag, Heidelberg, Germany, 1987.
[65] L.R. Snyder, Classification of the solvent properties of common liquids, J. Chromatogr. Sci. 16 (1978) 223–233.
[66] S. Nyiredy, Essential Guide to Method development in Thin-Layer (Planar) Chromatography, Academic Press, Budakalasz, Hungary, 2006, pp. 4652–4666.
[67] J.C. Touchstone, Practice of Thin Layer Chromatography, 3rd ed., John Wiley & Sons, New York, 1992.
[68] D.L. Massart, B.G.M. Vandeginste, L.M.C. Buydens, S. De Jong, P.J. Lewi, J. Smeyers-Verbeke, Handbook of Chemometrics and Qualimetrics: Part A, Elsevier, Amsterdam, 1997.
[69] M. Canales, in: I.W. Wainer (Ed.), Liquid Chromatography in Pharmaceutical Development, Aster Publishing, USA, 1985, p. 181.
[70] Y. Vander Heyden, LC.LG Asia Pacific (2006), available at http://chromatographyonline.findanalytichem.com/lcgc/article/articleDetail.jsp?id=445076&sk=&date=&pageID=2 (accessed on 12th December 2011).
[71] S. Nyiredy, in: E. Heftmann (Ed.), Chromatography, Joutrnal of Chromatography Library, vol. 69A, 6th ed., Elsevier, Amsterdam, 2004, pp. 253–296.
[72] R.J. Ekiert, J. Krzek, W. Rzesulko, Evaluation of a TLC densitometric method for analysis of azole atifungal agents, Chromatographia 67 (2008) 995–998.
[73] C. Cimpoiu, T. Hodisan, Application of numerical taxonomy techniques to the choice of optimum mobile phase in high-performance thin-layer chromatography (HPTLC), J. Pharm. Biomed. Anal. 21 (1999) 895–900.
[74] The system Camag Nanomat and Capillary Dispensor, Camag, Switzerland, available at http://www.kobis.si/material/Nanomat4brochure.pdf (assessed on 21st June 2011).
[75] Linomat 5, Bandwise sample application by spray-on technique for planar chromatography, Camag, Switzerland, http://www.instrument.com.cn/download.asp?url.pdf (accessed on 2nd January 2012).
[76] The Instrumental thin-layer chromatography, Catalogue 2010/11, Camag, Switzerland, available at http://www.camag.com/downloads/free/brochures/CAMAG_TLC10-11_E.pdf (accessed on 21st June 2011).
[77] S. Brainthwaite, F.J Smith, Chromatographic Methods, 5th ed., Kluwer Academic Publishers, London, 1999.
[78] G. Matysic, E. Soczewinski, Stepwise gradient development in thin-layer chromatography: II. Two-dimensional gradients for complex mixtures, J. Chromatogr. A 369 (1986) 19–25.
[79] S. Nyiredy, The bridge between TLC and HPLC: overpressured layer chromatography, (OPLC), Trends Anal. Chem. 20 (2001) 91–100.
[80] S. Nyiredy, Progress in forced-flow planar chromatography, J. Chromatogr. A 1000 (2003) 985–999.
[81] Z. Katona, L. Vincze, Z. Vegh, A. Trompler, K. Forenczi-Fodor, Cleaning validation procedure eased by using overpressured layer chromatography, J. Pharm. Biomed. Anal. 22 (2000) 349–353.
[82] I. Vovk, M. Prosek, Reproducibility of densitometric and image analyzing quantitative evaluation of thin-layer chromatograms, J. Chromatogr A 770 (1997) 329–336.
[83] S. Ebel, T. Henkel, Evaluation in HPTLC by use of imaging system. 1. Basic algorithms of image processing, J. Planar Chromatogr. 13 (2000) 248–253.
[84] G. Morlock, HPTLC–MS and other coupling techniques, available at http://nte-serveur.univ-lyon1.fr/afsep/fichier/271_14_11_2005.pdf (accessed on 15th September 2011).
[85] T. Yrjonen, Extraction and planar chromatographic separation technique in the analysis of natural products, Academic dissertation, Faculty of Pharmacy, University of Helsinki, November 2004.
[86] U. Jautz, G. Morlock, Efficacy of planar chromatography coupled to (tandem) mass spectrometry for employment in trace analysis, J. Chromatogr. A 1128 (2006) 244–250.
[87] G. Morlock, Hyphenations in HPTLC with UV/vis/FLD, MS, FTIR, NMR and bioassays, available at http://www.ilc.uni-hohenheim.de/joomla/images/stories/GM/Flyer%20TLC-MS%20Interface.pdf (accessed on 15th January 2012).
[88] T. Tuzimski, Application of different modes of thin-layer chromatography and mass spectrometry for the separation and detection of large and small biomolecules, J. Chromatogr. A 1218 (2011) 8799–8812.
[89] W. Funk, V. Dammann, G. Donnevert, Quality Assurance in Analytical Chemistry, 2nd ed., Wiley-VCH, Weinheim, 2007.
[90] Guidelines prepared within the International Conference on Harmonization of Technical Requirements for the Registration of Pharmaceuticals for Human use (ICH), Validation of Analytical Procedures: Text and Methodology, Q2 (R1), http://www.ich.org/, 2005, 1–13 (accessed on August 20th 2011).
[91] Food and Drugs Administration, Guidance for Industry, Analytical Procedures and Method Validation (Draft Guidance), 2000, available at http://www.fda.gov/downloads/Drugs/GuidanceComplianceRegulatoryInformation/Guidances/ucm122858.pdf (accessed on 25th August 2011).
[92] The United States Pharmacopeia 29, National Formulary 24, Unites States Pharmacopeia Convention, Rockville MD USA, 2006.
[93] AOAC Guidelines for Single Laboratory Validation of Chemical Methods for Dietary Supplements and Botanicals, available at http://www.aoac.org/Official_Methods/slv_guidelines.pdf (accessed on 16th September 2011).
[94] K. Ferenczi-Fodor, B. Renger, Z. Vegh, The frustrated reviewer–Recurrent failures in manuscripts describing validation of quantitative TLC/HPTLC procedures for analysis of pharmaceuticals, J. Planar Chromatogr. 23 (2010) 173–179.
[95] J. Van Loco, M. Elskens, C. Croux, H. Beernaert, Linearity of calibration curves: use and misuse of correlation coefficient, Accred. Qual. Assur. 7 (2002) 281–285.
[96] EURACHEM Guide, The Fitness for Purpose of Analytical Methods, 1998, available at http://www.eurachem.org/guides/pdf/valid.pdf (accessed on 25th August 2011).
[97] A.U. Kulikov, A.G. Verushkin, L.P. Loginova, Chromatographia 61 (2005) 455–463.
[98] E. Rozet, R.D. Marini, E. Ziemons, B. Boulanger, Ph. Hubert, Advance in validation, risk and uncertainty assessment of bioanalytical methods, J. Pharm. Biomed. Anal. 55 (2011) 848–858.
[99] International Organization for Standardization, Accuracy (Trueness and Precision) of Measurement Methods and Results, ISO:DIS 5725-1 to 5725-3, Geneva, 1994.
[100] Ph. Hubert, J.-J. Nguyen-Huu, B. Boulanger, E. Chapuzet, P. Chiap, N. Cohen, P.-A. Compagnon, W. Dewe, M. Feinberg, M. Lallier, M. Laurentie, N. Mercier, G. Muzard, C. Nivet, L. Valat, E. Rozet, Harmonization of strategies for the validation of quantitative analytical procedures: a SFSTP proposal – Part II, J. Pharm. Biomed. Anal. 45 (2007) 70–81.
[101] C. Hartmann, J. Smeyers-Verbeke, W. Pennickx, Y. Vander Heyden, P. Vankeerberghen, D.L. Massart, Reappraisal of hypothesis testing for method validation: detection of systematic error by comparing the means of two or of two laboratories, Anal. Chem. 67 (1995) 4491–4499.
[102] Ph. Hubert, J.-J. Nguyen-Huu, B. Boulanger, E. Chapuzet, P. Chiap, N. Cohen, P.-A. Compagnon, W. Dewe, M. Feinberg, M. Lallier, M. Laurentie, N. Mercier, G. Muzard, C. Nivet, L. Valat, Harmonization of strategies for the validation of quantitative analytical procedures: a SFSTP proposal – Part I, J. Pharm. Biomed. Anal. 36 (2004) 579–586.
[103] Ph. Hubert, J.-J. Nguyen-Huu, B. Boulanger, E. Chapuzet, N. Cohen, P.-A. Compagnon, W. Dewe, M. Feinberg, M. Laurentie, N. Mercier, G. Muzard, L. Valat, E. Rozet, Harmonization of strategies for the validation of quantitative analytical procedures: A SFSTP proposal – Part III, J. Pharm. Biomed. Anal. 45 (2007) 82–96.
[104] K. Ferenczi-Fodor, Z. Vegh, B. Renger, Thin-layer chromatography in testing the purity of pharmaceuticals, Trend. Anal. Chem. 25 (2006) 778–789.
[105] V.P. Machale, A.T. Gatade, R.T. Sane, Validated HPTLC content uniformity test for the determination of diazepam in tablet dosage form, Int. J. Pharm. Res. Dev. 3 (2011) 34–41.
[106] G.E. Morlock, Analysis of pesticide residuals in drinking water by planar chromatography, J. Chromatogr. A 754 (1996) 423–430.
[107] M. Hassan, F. Ahmad, M. Sagheer, M.F. Iqbal, M. Tariq, Residual persistence of chlorpyrifos, imidacloprid, and acephate in brinjal fruit, Pak. Entomol. 27 (2005) 53–55.
[108] G.E. Morlock, W. Schwack, The contribution of planar chromatography to food analysis, J. Planar Chromatogr. 20 (2007) 399–406.
[109] S. Mennickent, R. Fierro, M. Vega, M. De Diego, C.G. Godoy, Quantitative determination of fluoxetine in huma serum by high-performance thin-layer chromatography, J. Sep. Sci. 33 (2010) 2206–2210.
[110] G.K. Jain, N. Jain, Z. Iqbal, S. Talegaonkar, F.J. Ahmad, R.K. Khar, Development and validation of an HPTLC method for the determination of minocycline in human plasma, Acta Chromatogr. 19 (2007) 197–205.

Please cite this article in press as: D.H. Shewiyo, et al., HPTLC methods to assay active ingredients in pharmaceutical formulations: A review of the method development and validation steps, J. Pharm. Biomed. Anal. (2012), doi:10.1016/j.jpba.2012.03.034

Journal of Pharmaceutical and Biomedical Analysis 66 (2012) 24–32

Contents lists available at SciVerse ScienceDirect

Journal of Pharmaceutical and Biomedical Analysis

journal homepage: www.elsevier.com/locate/jpba

The development and application of a system for simultaneously determining anti-infectives and nasal decongestants using on-line solid-phase extraction and liquid chromatography–tandem mass spectrometry

Ghazanfar Ali Khan*, Richard Lindberg, Roman Grabic, Jerker Fick

Department of Chemistry, Umeå University, SE-901 87 Umeå, Sweden

ARTICLE INFO

Article history:
Received 18 November 2011
Received in revised form 9 February 2012
Accepted 12 February 2012
Available online 8 March 2012

Keywords:
Method development/validation
On-line solid-phase extraction
LC–MS/MS antibiotics
Anti-infectives
Nasal decongestants

ABSTRACT

A method for the simultaneous analysis of antibiotics, antiviral and nasal decongestants in treated sewage effluent and surface water has been developed and validated. The method uses on-line solid phase extraction (SPE) of injected high-volume samples in conjunction with liquid chromatography–tandem mass spectrometry (LC–MS/MS). This method includes a range of antibiotics (Trimethoprim, Oxytetracycline, Ofloxacin, Norfloxacin, Ciprofloxacin, Azithromycin, Doxycycline, Sulfamethoxazole, Erythromycin and Clarithromycin), an antiviral (Oseltamivir) and nasal decongestants (Naphazoline, Oxymetazoline and Xylometazoline). The method's detection limits (MDLs) ranged from (0.2 ng L^{-1}) to (3.1 ng L^{-1}), based on a 1 mL extraction volume. Its intra-day precision was determined by performing nine runs with 200 ng L^{-1} samples; the intra-day relative standard deviation (RSD) ranged from 1% to 19%. Inter-day precision was determined by analyzing samples in triplicate over the course of three days, yielding relative standard deviations ranging from <5% to <26%. The linearity (R^2) for all compounds tested was >0.90. Spike relative recoveries ranged from 40% to 157% and 40% to 152% for STP effluent and surface water samples, respectively. Finally, the method was used to analyze real effluent and surface water.

© 2012 Elsevier B.V. All rights reserved.

1. Introduction

Antibiotics are biologically active agents that are used to treat microbial diseases in humans and animals. In addition to their clinical uses, some antibiotics are also used in sub-therapeutic amounts as growth promoters and feed additives in livestock management, poultry production, and fish farming. Antibiotics, and other pharmaceuticals, are excreted in the urine and faeces of treated patients, either as the parent compounds or in the form of various metabolites and conjugates, many of which have been described in previous studies [1,2]. Active antibiotics and their derivatives are released into the environment from sources such as unused drugs that have been disposed of inappropriately, drug production facilities and also as a byproduct of veterinary use. They have been detected in waste water treatment plant (WWTP) effluents, hospital waste water, WWTP biosolids, surface water, ground water, drinking water, biota, and sediments at levels ranging from less than 1 ng L^{-1} up to a few μg/L [1–8]. There is substantial public and scientific concern regarding the potential ecotoxicological effects of estrogens released in this fashion [9–11], and also about the development of antibiotic resistance in microorganisms following uncontrolled exposure to antibiotics at very low concentrations. This phenomenon is particularly dangerous because of the potential for horizontal transfer of resistance to human pathogens [12].

Various methods have been used to detect and monitor levels of pharmaceuticals (including antibiotics), their metabolites and degradates. These typically involve liquid chromatography (LC) coupled to some specific detection technology; ultraviolet (UV) spectroscopy, fluorescence, and radioimmunoassays (RIA) have been used in some cases, but the most impressive progress in detecting ultra-trace concentrations of bioactive molecules in biological and environmental samples has been achieved with mass spectrometry [13,14]. Gas chromatography coupled to mass spectrometry (GC–MS) is suitable for detecting a limited number of non-polar volatile compounds, but polar compounds must generally be subjected to lengthy and irreversible derivatization processes before they can be separated by gas chromatography. Consequently, LC–MS and LC–MS/MS have become the techniques of choice for monitoring levels of pharmaceuticals and their metabolites [14,15].

The quantification of trace contaminants is a significant challenge in monitoring programs, and it is common for samples to be enriched by solid phase extraction (SPE) prior to analysis [16]. However, enrichment steps are labor-intensive and time-consuming, especially when dealing with high-volume samples. This problem

* Corresponding author. Tel.: +46 90 7869320; fax: +46 90 786 76 55.
E-mail addresses: ghazanfar.ali.khan@chem.umu.se, ghazanfaradc@hotmail.com (G.A. Khan).

0731-7085/$ – see front matter © 2012 Elsevier B.V. All rights reserved.
doi:10.1016/j.jpba.2012.02.011

could be addressed using an automated on-line SPE system coupled to an LC instrument via a column-switching system. This approach is more rapid, precise, and efficient than conventional techniques because it eliminates time-consuming evaporation and reconstitution steps and minimizes the need for sample handling. On-line SPE provides a number of significant advantages, including high sample throughput, minimal solvent utilization, and low sample preparation times; in addition, it can be done with comparatively small sample volumes. In one case, an on-line method was shown to be 16 times more cost-effective than an alternative off-line method [17].

A drawback of on-line SPE methods is that they are unsuitable for detecting trace compounds in surface- and drinking water because of their low preconcentration factor, which gives them relatively high method detection limits (MDLs). This can be addressed (albeit in a way that is not always practical) by increasing the preconcentration sample volume [18]. Nevertheless, a number of variations on the enrichment step have been described, and the technique has found significant use in the analysis of biological and environmental samples for trace concentrations of bioactive molecules, including anti-infectives [17–30] estrogens and androgens [31–33], drugs of abuse [34], biocides [35], pesticides [36], phthalates, phenols, and perfluorooctanesulfonate [37–39].

Matrix effects cause significant problems in quantitative analyses using liquid chromatography-HESI systems. They occur when substances co-elute, resulting in either signal suppression or enhancement, and must be taken into account when developing LC–MS/MS methods because they affect reproducibility and accuracy [40]. Numerous published studies have shown ion suppression to be the dominant matrix effect in ESI systems; it is believed to be caused by competition between analyte-derived ions and those originating from matrix components for access to the droplet surface during solvent evaporation [41,42]. There are numerous ways of minimizing the consequences of matrix effects; these include using diluted samples, pre-treating samples, using the standard addition method, matrix-matched calibration, and the use of analyte analogues or labeled internal standards. Each of these methods has its own merits and drawbacks [13].

The objective of the work reported herein was to develop and apply a sensitive, efficient and reliable method by using small preconcentration volume i.e. 1 mL for the simultaneous determination of antibiotics, antiviral, and nasal decongestants in two different matrices, using on-line SPE in conjunction with liquid chromatography tandem mass spectrometry (LC–MS/MS). In comparison to previous on-line study [26] where preconcentration volume used was 18 mL (loaded twice with 9.5 mL); developed method has a huge advantage using 1 mL preconcentration volume which also makes it rapid and more precise.

False positives were avoided by using confirmation techniques based on identification points [43]. The identity of each analyte was typically confirmed by means of selective reaction monitoring (SRM).

2. Materials and methods

2.1. Chemicals and standard

Trimethoprim (TRI), Oxytetracycline (OXY), Ofloxacin (OFL), Norfloxacin (NOR), Oseltamivir carboxylate (OC) (RO0640802-002; lot: 01007B243804), Ciprofloxacin (CIP), Naphazoline (NAP), Azithromycin (AZI), Cefotaxime (CEF), Doxycycline (DOX), Sulfamethoxazole (SUL), Oxymetazoline (OXYM), Erythromycin (ERY), Xylometazoline (XYL) and Clarithromycin (CLA) were purchased from Sigma Aldrich (Steinheim, Germany) and were classified as HPLC grade (>98%). Methanol, acetonitrile and water (Lichrosolv, Hypergrade) were obtained from Merck Darmstadt, Germany); formic acid (puriss pa) was acquired from Fluka (Steinheim, Germany). Sulphuric acid was obtained from Merck (Dramstadt, Germany). Purified water (resistivity: 18.2 MΩ cm) was prepared by passing water through an ELGA MAXIMA HPLC ultra-pure water system (ELGA, High Wycombe Bucks, England) equipped with a UV radiation source. The following internal standards were obtained from Cambridge Isotope Laboratories (Andover, MA, USA): $^{13}C_2$-Trimethoprim ($^{13}C_2$-TRI) (99%), $^{13}C_3$15N-Ciprofloxacin ($^{13}C_3$-CIP) (99%), $^{13}C_2$-Erythromycin ($^{13}C_2$-ERY) and $^{13}C_6$-Sulphamethoxazole ($^{13}C_6$-SUL). Oseltamivir carboxylate labeled with deuterium (OC_{D3}) (RO0604802-004; lot: 511-001-2197/4) was obtained from Roche (F. Hoffmann-La Roche Ltd., Basel, Switzerland). The properties, structure and uses of the compounds are given in Table 1.

2.2. Standard stock solutions

Standard stock solutions of individual compounds were prepared at concentrations ranging from 94 to 300 μg mL^{-1} by dissolution in methanol. The solubility of the fluoroquinolones was increased by adding a drop of sulphuric acid to their stock solutions, followed by ultrasonication for 10 min. Once prepared, the stock solutions were stored in darkness at −18 °C. Mixed solutions with concentrations of 1 μg mL^{-1} were prepared from the stock solutions for use in recovery experiments and for the preparation of calibration standards. Mixed solutions with concentrations of 0.1 μg mL^{-1} were prepared for use as internal standards. In recovery experiments, surface and effluent water samples were spiked with analytes at concentrations of 25 and 250 ng L^{-1}, respectively, to mimic the real environmental levels. Standard aqueous calibration solutions containing the target analyte at concentrations of 1, 5, 10, 25, 50, 100, 250, 500 and 1000 ng L^{-1} were prepared and augmented with an internal standard at a concentration of 0.1 ng mL^{-1} prior to injection into the LC system. Mixed and calibration standards were freshly prepared on a daily basis.

2.3. Sample collection and preparation

Surface water grab samples were collected from the river Ume in June 2010. Sampling was conducted at a location directly across the river from the Umeå Sewage Treatment Plant and also at a location upstream of the plant. In addition, effluent samples were collected in November 2009 from a sewage pipe at Umeå STP. Both the river and effluent samples were filtered through a 0.45 μm MF^{TM}-membrane filter (MF, Millipore, Sundbyberg, Sweden) and frozen at −18 °C. The samples were prepared for analysis with the help of syringe driven filter unit 0.45 μm (Millipore) attached to the syringe in 10 mL glass vials and then fortified by 0.1 ng mL^{-1} internal standards.

2.4. LC–MS

The liquid chromatography–tandem mass spectrometry (LC–MS) system used in this work was made by Thermo Fisher Scientific (Waltham, MA) and was used with a PAL HTC auto sampler (CTC Analytics AG, Zwingen, Switzerland). The liquid chromatography system consisted of a Surveyor LC-Pump (Thermo Fisher Scientific, San Jose, CA, USA), an on-line SPE Hypersil GOLD C18 column (20 mm × 2.1 mm i.d. × 12 μm, Thermo Fisher Scientific, Waltham, MA, USA), an Accela LC pump (Thermo Fisher Scientific, San Jose, CA, USA), and a Hypersil GOLD C18 column (50 mm × 2.1 mm i.d. × 3 μm particles, Thermo Fisher Scientific, San Jose, CA, USA) with a guard C18 column (2 mm × 2 mm i.d. × 3 μm particles, Thermo Fisher Scientific, San Jose, CA, USA). Hypersil GOLD columns are based on alkyl-bonded silica (end-capped) stationary phase which reduces peak tailing and enhances

Table 1
Pharmaceutical agents examined in this work and their uses, structures, and physical properties.

Compound (CAS No.)	Group/use	Structure	Mw (g mol^{-1})	Log K_{ow} KowWin (EPI Suite™ v1.67)	
				Est. values	Exp. values
TRI (738-70-5)	ATB/DRI	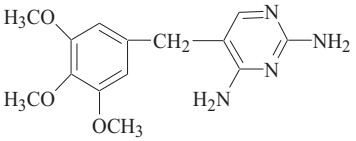	290.32	0.73	0.91
OXY (79-57-2)	ATB/TET	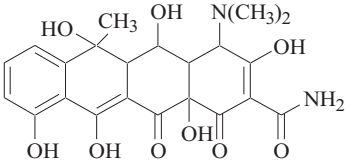	460.434	−2.87	−0.90
OFL (82419-36-1)	ATB/FQN	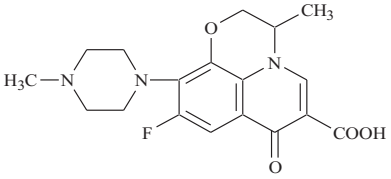	361.367	−0.20	−0.39
NOR (70458-96-7)	ATB/FQN	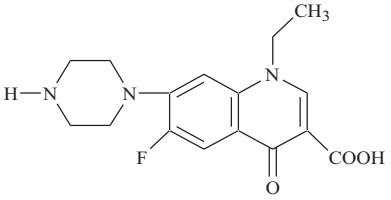	319.331	−0.31	−1.03
OC (187227-45-8)	ATV/NAI	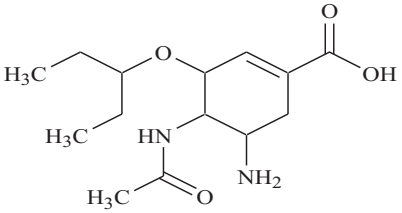	284.35	0.18	–
CIP (85721-33-1)	ATB/FQN	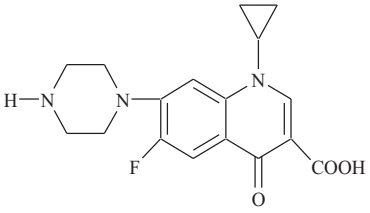	331.346	−0.00	0.28
NAP (835-31-4)	NDC	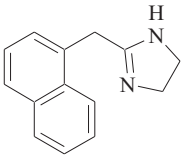	210.274	3.52	–
CEF (63527-52-6)	ATB/CEP	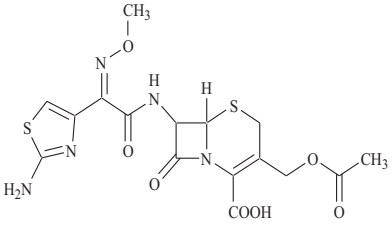	455.47	0.64	–

Table 1 (*Continued*)

Compound (CAS No.)	Group/use	Structure	Mw (g mol^{-1})	Log K_{ow} KowWin (EPI Suite™ v1.67)	
				Est. values	Exp. values
AZI (83905-01-5)	ATB/MAC	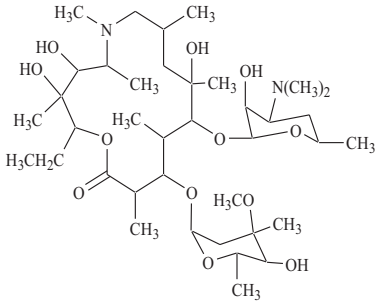	748.984	3.24	4.02
DOX (564-25-0)	ATB/TET	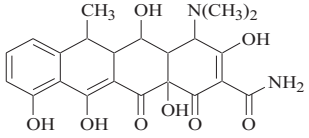	444.435	−1.36	−0.02
SUL (723-46-6)	ATB/SUL	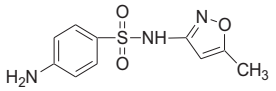	253.279	0.48	0.89
OXYM (1491-59-4)	NDC	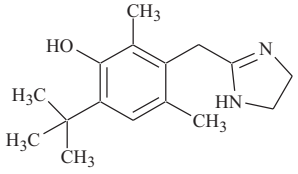	260.375	4.87	–
ERY (114-07-8)	ATB/MAC	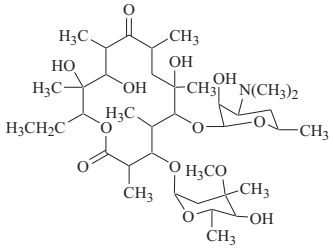	733.93	2.48	3.06
XYL (526-36-3)	NDC	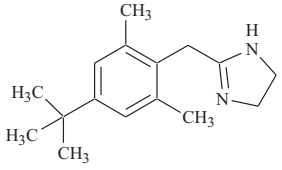	244.375	5.35	–
CLA (81103-11-9)	ATB/MAC	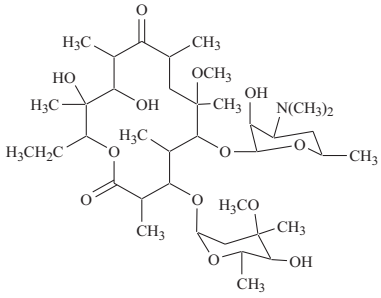	747.953	3.18	3.16

ATB, antibiotic; DRI, dihydrofolate reductase inhibitor; TET, tetracycline; FQN, fluoroquinolone; ATV, antiviral; NAI, neuroaminidase inhibitor; MAC, macrolide; CEP, cephalosporin; SUL, sulphonamide; NDC, nasal decongestant; Est., estimated value; Exp., experimental value.

resolution. The pH range for the columns is 1–11. The liquid chromatography system was coupled to a heated electrospray ionization (HESI) source and a Quantum Ultra triple quadrupole mass spectrometer.

The system relied on the column switching technique and featured a switching-column array made up of 6-port and 10-port switching valves manufactured by Valco Instruments Co. The valve settings used during injection, loading and elution are shown in Fig. 1; the arrows indicate the direction of the flow. A 1 mL loop was used, but 1.1 mL of sample was injected to ensure there was no void volume and that the loop was completely filled. The surveyor pump (S) was a load pump with a high flow rate; it was used to load the sample from the loop on to the SPE column over the course of 2 min with the divert valve remaining in the 'load position'. After 2 min, the divert valve was switched to the 'inject position' and the low flow rate Accela Pump (A) was used to elute the retained analytes from the SPE column by back-flushing the load column. The analytes were then loaded on to the analytical column for chromatographic separation and finally transferred to the ion source. The gradient elution program for both the Surveyor (load) and Accela (analytical) pumps is shown in Table 2.

The heated capillary temperature was set to 325 °C; the vaporizer temperature was 225 °C. The collision gas used was argon, at a flow rate of 1.5 mL/min. The MS parameters were optimized semi-automatically using a special-purpose software package. The sheath and auxiliary nitrogen gas flows were 60 and 25 (arbitrary units) respectively, and the source voltage was maintained at a constant 3.0 kV for all analytes. The capillary voltage and the collision energy (for fragmentation in MS/MS, see Table 3) were individually optimized for each substance. All compounds were detected using ESI-MS/MS in positive ion mode. Quantification was achieved using internal standard (IS) calibration; target analytes were identified on the basis of their similarity to the IS in terms of structure, retention time, or molecular weight. $^{13}C_2$-TRI was used as an internal standard for quantifying TRI, OXY, NAP, DOX; $^{13}C_3$-CIP was used for OFL, NOR and CIP; OC_{D3} was used against OC; $^{13}C_6$-SUL was used against CEP and SUL; and $^{13}C_2$-ERY was used against AZI, OXYM, ERY, XYL and CLA. Levels of the internal standards in native effluent and surface water samples were monitored in order to avoid underestimation of analyte concentrations. Instrumental blank samples consisting of HPLC-grade deionized water were injected regularly to reduce potential memory effects.

2.5. Method validation

The sensitivity of the method was evaluated by determining its method detection limits (MDLs) and method confirmation limits (MCLs). The MDL is defined as the 'the minimum concentration of a substance that can be identified, measured and reported with 99% confidence that the analyte concentration is greater than zero' and is calculated as the standard deviation of the concentrations (determined using the quantitation transition, SRM #1) of seven replicate measurements of a low concentration solution, multiplied by Student's t-value for a one-tailed test at the 99% confidence level and $n-1$ degrees of freedom [44]. Similarly, the MCL was calculated using the confirmation transition (SRM #2).

Retention times of the analytes have to match that of the calibration standard (±2.5%) and the relative retention time regarding analytes and internal standards have to correspond to that of the calibration standard (±2.5%). Each analyte is determined with a minimum of two transitions (1 precursor and 2 product ions) yielding at least 4 identification points according to the system used in the Decision 2002/657/EC of 17 August 2002 concerning the performance of analytical methods and the interpretation of results.

Relative recoveries (RR %) were determined by spiking Umeå STP effluent (STPE) and surface water (SW) from the river Ume with analytes at concentrations of 250 ng L^{-1} and 25 ng L^{-1} respectively, in quintuplicate ($n=5$). The MS/MS area response was then compared to that observed for solutions of the same analytes at the same concentration in hypergrade deionized water. Relative recoveries were calculated using the following expression:

$$\text{RR}\ \ (\%) = \frac{C_{sp} - C_0}{C_{hg}} \times 100$$

Here, C_{sp} is the measured concentration of the spiked analyte in the matrix, C_0 is the concentration of the analyte in the untreated matrix, and C_{hg} is the measured concentration of the spiked analyte solution in hypergrade deionized water.

Bench-top stability tests were conducted by comparing the results obtained when injecting fresh standard solutions at a concentration of 500 ng L^{-1} ($n=3$) to those achieved with solutions that had been stored at room temperature (24 °C) or 4 °C for 24 h.

Sample carryover is a memory effect from previous injection and needs to be minimized by adequate washing after each injection. It was determined by injecting hypergrade deionized water in-between sequence run both for samples and calibration curves.

3. Results and discussions

3.1. Optimization

The signal response for each analyte was optimized by direct injection into the ion source in both positive [M+H$^+$] and negative [M+H$^-$] MRM (multiple reaction monitoring) modes. Initially, a full scan was recorded to identify suitable precursor ions for each analyte. Full product ion scans of the selected precursor ions were then recorded by infusion of a 1 μg mL^{-1} standard solution at a flow rate of 250 μL min^{-1}. The Xcalibur software package (rev. 2.0 SP2, Thermo Fischer Scientific) was used for quantitative optimization by determining the product ions and their corresponding declustering potentials, collision energies and exit potentials. The product ion transition that yielded the most intense instrument response with the greatest sensitivity was taken as the quantitative transition; the transition with the second highest intensity was used as the confirmation transition. All of the compounds examined exhibited greater intensities in positive ion mode, so HESI(+) was utilized. The identities of the analytes were further confirmed by examining their LC retention times (supplementary material). The quantitative and confirmation transitions monitored for all analytes are listed in Table 3. The transitions are in agreement with those reported previously for TRI, OXYT, OFO, NOR, OC, CIP, AZI, DOX, SUL, ERY, and CLA, $^{13}C_2$-TRI, OC_{D3}, $^{13}C_3$-CIP, $^{13}C_6$-SUL and $^{13}C_2$-ERY and OXYM [5,7,19,45–47] however transitions for NAP and XYL were not found in the relevant articles.

3.2. Method validation

3.2.1. Relative recovery and matrix effects

Relative recovery (RR) and matrix effects were determined by fortifying effluent and surface water samples with analytes at concentrations of 250 ng L^{-1} and 25 ng L^{-1}, respectively. RR data for the STP effluent and surface water from the river Ume are presented in Table 4. The RR values for the STP effluent ranged from 30 ± 5% for NOR to 157 ± 14% for OXY; in the surface water, they ranged from 21 ± 3% for NOR to 152 ± 8% for OXY. For individual compounds, the RR values observed in the surface water did not generally differ from those in the effluent; the only exception was DOX, which

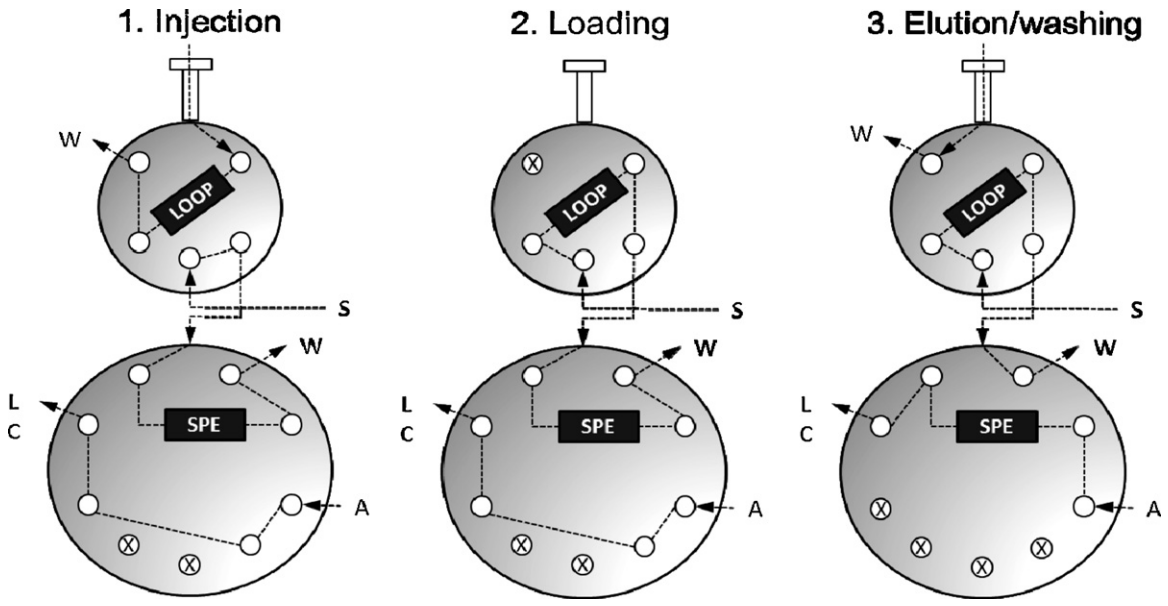

Fig. 1. On-line preconcentration setup. W: Waste; SPE: Enrichment LC; S: Surveyor LC pump; A: Accela LC pump; LC: Analytical LC; X: Not in use.

Table 2
On-line SPE and HPLC solvent gradient program.

Surveyor pump				Accela pump			
Time (min)	A %	B %	Flow (mL/min)	Time (min)	A[a] %	B %	Flow (μL min^{-1})
0.00	100.0	0.0	0.050	0.00	95.0	5.0	250.0
0.01	100.0	0.0	1.200	2.00	95.0	5.0	250.0
2.00	100.0	0.0	1.200	7.00	60.0	40.0	350.0
2.01	0.0	100.0	0.100	9.00	0.0	100.0	400.0
7.00	0.0	100.0	1.000	11.00	0.0	100.0	400.0
7.01	100.0	0.0	1.000	11.01	95.0	5.0	250.0
11.00	100.0	0.0	1.000	14.00	95.0	5.0	250.0
11.01	100.0	0.0	0.050				

A, purified water; B%, acetonitrile with 0.1% formic acid.
[a] Hypergrade water with 0.1% formic acid.

had an RR value of 126 ± 15% in the effluent and 40 ± 10% in the surface water. In general, the RR values for surface water samples were slightly higher than those for effluent. Notably, the target analytes for which isotopically labeled variants were available and that were used as internal standards (i.e. TRI, OC, SUL and ERY) had RR values above 80%, indicating that matrix effects were compensated for effectively with respective analytes other than CIP, which has a high affinity for metal ions.

Table 3
SRM transitions used for quantitation (SRM #1) and confirmation (SRM #2).

Compounds	SRM #1 (m/z)	Collision energy (v)	SRM #2 (m/z)	Collision energy (v)	Tube lens	Retention time (min)
TRI	291.00 → 230.10	23	291.00 → 123.20	25	106	5.44
OXY	461.00 → 426.20	18	461.00 → 443.20	13	130	5.60
OFL	362.10 → 318.20	17	362.10 → 261.10	25	138	5.68
NOR	320.00 → 302.10	20	320.00 → 233.10	23	114	5.71
OC	285.00 → 138.10	20	285.00 → 120.20	30	100	5.70
CIP	332.00 → 231.10	35	332.00 → 288.20	16	117	5.76
NAP	211.10 → 141.20	33	211.00 → 44.50	23	73	5.99
CEF	455.90 → 396.10	5	455.90 → 125.10	31	106	6.21
AZI	749.40 → 158.20	37	749.40 → 591.60	28	148	6.45
DOX	445.00 → 428.30	17	445.00 → 200.90	27	107	6.83
SUL	254.00 → 108.20	22	254.00 → 156.00	15	108	6.90
OXYM	261.10 → 205.20	25	261.10 → 135.20	33	93	7.21
ERY	734.30 → 576.60	19	734.30 → 158.10	29	154	7.30
XYL	245.10 → 189.20	26	245.10 → 119.30	35	91	7.60
CLA	748.40 → 158.10	27	748.40 → 590.50	17	156	7.88
Internal standards						
$^{13}C_2$-TRI	294.10 → 233.20	22	294.10 → 126.20	24	101	5.44
OC_{D3}	288.00 → 139.00	19	288.00 → 95.00	30	100	5.70
$^{13}C_3$-CIP	336.00 → 291.00	18	–		106	5.78
$^{13}C_6$-SUL	260.00 → 162.10	15	260.00 → 114.20	23	97	6.89
$^{13}C_2$-ERY	736.40 → 160.10	17	736.40 → 578.60	29	129	7.30

Table 4
Data on the performance of the new method for determining antibiotics in STP effluent and surface river water.

Compounds	R^2	MDLs (ng L^{-1})	MCLs (ng L^{-1})	Precision (% RSD)		Relative recovery (%)			
				Intra-day	Inter-day	Effluent water	SD	Surface water	SD
TRI	0.97	0.4	0.6	5	6	82	5.0	97	5.0
OXY	0.97	0.3	0.4	7	16	157	13.0	152	8.0
OFL	0.99	1.1	0.6	3	7	61	5.0	65	7.0
NOR	0.99	0.7	1.2	2	7	30	5.0	21	3.0
OC	0.97	1.4	1.9	4	5	85	9	89	6.0
CIP	0.98	1.0	1.9	1	7	75	8.0	66	10
NAP	0.97	0.3	0.6	3	8	52	3.0	49	2.0
CEF	0.97	0.8	0.5	19	17	98	8	98	18
AZI	0.97	3.1	4.2	6	26	62	14	88	26
DOX	0.96	0.3	0.5	8	5	126	15	40	10
SUL	0.97	2.7	0.7	2	7	88	6.0	98	4.0
OXYM	0.96	0.3	0.3	3	5	107	6.0	143	6.0
ERY	0.90	0.7	0.4	5	18	87	6.0	94	3.0
XYL	0.98	0.2	0.2	2	10	40	2.0	53	2.0
CLA	0.98	0.7	0.6	5	10	79	4.0	98	7.0

Intra-day precision is quantified in terms of % RSD and was determined by performing three analyses of the same sample on the same day. Inter-day precision ($n = 9$) was quantified by performing nine analyses of the same sample on three different days. Sample concentrations in both cases were 200 ng L^{-1}. Relative recovery (%) was determined by analysis of samples in quintuplicate ($n = 5$). R^2, correlation coefficient; MDL, method detection limit; MCL, method confirmation limits.

In off-line MS or MS/MS techniques, matrix effects are evaluated by using either post-extraction spikes or post-column infusions. In both cases, samples are initially extracted from the SPE cartridges and then spiked with a known amount of analyte before being injected onto the analytical column or infused directly into the ion-source [41]. However, the system used in this work made it impossible to retrieve samples after passage through the SPE column; as such, we were unable to evaluate the matrix effects by means of post-extraction spikes or post-column infusions. Instead, we spiked samples with known quantities of analytes and internal standards before they were injected. The addition of isotopically labeled internal standards that are chemically and structurally similar to the target analytes can be used to detect signal enhancement or signal suppression, since the standard and the target will behave similarly on the analytical column and in the ionization source, and will thus be suppressed or enhanced to approximately the same extent. This method has the drawback that isotopically labeled internal standards are often quite expensive and may not be commercially available for all of the target analytes. Matrix effects can also be detected and quantified by means of standard addition, but this is laborious and lengthy; since the objective of this work was to develop a rapid method which may be suitable for use in monitoring programs, we chose to use labeled internal standards (IS) instead.

3.2.2. *Linearity, MDL, inter/intra-day precision, bench top stability, SPE column lifetime and sample carry over*

Table 4 details the linearity, MDL, and the inter- and intra-day precision of the method for each compound and sample type tested. High linearity was observed in all cases ($R^2 > 0.90$). The method's MDL values ranged from 0.2 ng L^{-1} (for XYL) to 3.1 ng L^{-1} (for AZI); its MCL values ranged from 0.2 ng L^{-1} (for XYL) to 4.2 ng L^{-1} (for AZI).

The intra-day precision was determined by performing analyses in triplicate on the same day, using samples with a concentration of 200 ng L^{-1}; the relative intra-day standard deviation (RSD) ranged from 1% to 19%. Similarly, the inter-day precision was determined by performing analyses of 200 ng L^{-1} samples in triplicate on three different days; in this case, the relative standard deviation (RSD) ranged from 5% to 26%. While the inter-day precision values for OXY, AZI, CEF and ERY were higher than the target value of 15%, they remained within acceptable limits given the nature of the compounds and the complexity of the matrix [19,42].

Bench-top stability testing indicated that when using solutions with a concentration of 500 ng L^{-1}, the results obtained with fresh samples ($n = 3$) were statistically indistinguishable from those obtained with samples that had been stored at room temperature (24 °C) or at 4 °C for 24 h.

Table 5
Average concentrations ($n = 5$) of antibiotics in STP effluent and surface water samples collected in 2005, and in STP effluent samples from 2002, 2003, and 2004 (ng L^{-1}).

Compounds	Umeå STP effluent	Umeå surface water	Umeå STP effluent Lindberg et al.		
			2002 (45)	2003 (45)	2005 (46)
TRI	93.05	2.39	700	561	613–1880
OXY	49.75	22.67			
OFL	14.68	6.09	52	45	
NOR	96.61	3.64	37	7	46–71
OC	48.29	1.29			
CIP	82.74	17.78	7	14	38–54
NAP	2.05	1.32			
CEF	31.43	1.24			
AZI	6.92	<MDL			
DOX	83.18	32.64	424	64	
SUL	70.48	<MDL	304	–	
OXYM	1.00	0.83			
ERY	100.78	21.31			
XYL	5.23	2.88			
CLA	10.72	4.12			

Expected life time for SPE column was observed to be 500 samples without major change in peak area and retention time. Sample carry over was less than 0.1% both for samples and calibration curves.

3.3. Application to real samples: STP effluent and surface water from the river Ume

The method was applied to effluent samples from the Umeå STP and surface water samples from the river Ume; the results of these analyses are shown in Table 5. The analytes were much less abundant in the surface water samples than in the STP effluent. This suggests that there is little contamination of the river water by the effluent, since the river water was sampled at a location directly across the river from the sewage plant's outlet. Levels from previous analyses of the effluent from the Umeå STP [48,49], is given in Table 5. Previous publications on the levels of the studied compounds in STP effluents across Sweden [48–51] have reported concentrations of 40–1880 ng L^{-1} for TRI, 10–52 ng L^{-1} for OFL, 7–71 ng L^{-1} for NOR, 7–54 ng L^{-1} for CIP, 64–915 ng L^{-1} for DOX, and 70–304 ng L^{-1} for SUL. The concentrations of TRI, OFL, DOX and SUL measured in the effluent of the Umeå STP in this work were consistent with previous findings, but those of NOR and CIP were both greater than had previously been reported.

4. Conclusion

A rapid, reliable, selective and sensitive method for the simultaneous analysis of anti-infectives and nasal decongestants has been developed. The new method combines on-line solid phase extraction (SPE) of high-volume samples with liquid chromatography–tandem mass spectrometry (LC–MS/MS), and requires only a single extraction step with minimal sample preparation. Ion suppression/enhancement effects were observed for most of the analytes considered. Relative recoveries ranged from (40% to 157%) and (40% to 152%) for Umeå STP effluent and surface water, respectively. MDLs were in the low nanogram per liter range (0.2–3.1). The LC–MS/MS instrument was operated in SRM mode; high selectivity was obtained by monitoring both quantitation and confirmatory transitions. The use of on-line preconcentration and minimal sample handling made it possible to conduct individual analyses in less than 25 min, and the method was successfully applied to samples of effluent from the Umeå sewage treatment plant (STP) and surface water from the river Ume. The concentrations of the target analytes in these samples ranged from 1.00 to 100.78 ng L^{-1} and <MDL to 32.64 ng L^{-1}, respectively. The new method should be suitable for analysis of anti-infectives and nasal decongestants and is particularly well-suited for use in monitoring programs.

Acknowledgement

We thank FORMAS (The Swedish Research Council for Environment, Agricultural Sciences and Spatial Planning) for financial support.

Appendix A. Supplementary data

Supplementary data associated with this article can be found, in the online version, at doi:10.1016/j.jpba.2012.02.011.

References

[1] R. Hirsch, T. Ternes, K. Haberer, K.-L. Kratz, Occurrence of antibiotics in the aquatic environment, Sci. Total Environ. 225 (1999) 109–118.
[2] B. Halling-Sørensen, S. Nors Nielsen, P.F. Lanzky, F. Ingerslev, H.C. Holten Lützhøft, S.E. Jørgensen, Occurrence, fate and effects of pharmaceutical substances in the environment – a review, Chemosphere 36 (1998) 357–393.
[3] D.W. Kolpin, E.T. Furlong, M.T. Meyer, E.M. Thurman, S.D. Zaugg, L.B. Barber, H.T. Buxton, Pharmaceuticals, hormones, and other organic wastewater contaminants in U.S. streams, 1999–2000: a national reconnaissance, Environ. Sci. Technol. 36 (2002) 1202–1211.
[4] D.G.J. Larsson, C. de Pedro, N. Paxeus, Effluent from drug manufactures contains extremely high levels of pharmaceuticals, J. Hazard. Mater. 148 (2007) 751–755.
[5] J. Fick, H. Soderstrom, R.H. Lindberg, C. Phan, M. Tysklind, D.G.J. Larsson, Contamination of surface, ground, and drinking water from pharmaceutical production, Environ. Toxicol. Chem. 28 (2009) 2522–2527.
[6] M.S. Díaz-Cruz, M.J. López de Alda, D. Barceló, Environmental behavior and analysis of veterinary and human drugs in soils, sediments and sludge, TrAC: Trends Anal. Chem. 22 (2003) 340–351.
[7] R. Lindberg, P.-A. Jarnheimer, B. Olsen, M. Johansson, M. Tysklind, Determination of antibiotic substances in hospital sewage water using solid phase extraction and liquid chromatography/mass spectrometry and group analogue internal standards, Chemosphere 57 (2004) 1479–1488.
[8] A.J. Watkinson, E.J. Murby, D.W. Kolpin, S.D. Costanzo, The occurrence of antibiotics in an urban watershed: from wastewater to drinking water, Sci. Total Environ. 407 (2009) 2711–2723.
[9] S.R. Miles-Richardson, V.J. Kramer, S.D. Fitzgerald, J.A. Render, B. Yamini, S.J. Barbee, J.P. Giesy, Effects of waterborne exposure of 17 [beta]-estradiol on secondary sex characteristics and gonads of fathead minnows (*Pimephales promelas*), Aquat. Toxicol. 47 (1999) 129–145.
[10] F. Ingerslev, E. Vaclavik, B. Halling-Sorensen, Pharmaceuticals and personal care products: a source of endocrine disruption in the environment? Pure Appl. Chem. 75 (2003) 1881–1893.
[11] D.G.J. Larsson, M. Adolfsson-Erici, J. Parkkonen, M. Pettersson, A.H. Berg, P.E. Olsson, L. Förlin, Ethinyloestradiol – an undesired fish contraceptive? Aquat. Toxicol. 45 (1999) 91–97.
[12] J.L. Martínez, Antibiotics and antibiotic resistance genes in natural environments, Science 321 (2008) 365–367.
[13] F. Hernández, J.V. Sancho, M. Ibáñez, C. Guerrero, Antibiotic residue determination in environmental waters by LC–MS, TrAC: Trends Anal. Chem. 26 (2007) 466–485.
[14] S. Pérezand, D. Barceló, Application of advanced MS techniques to analysis and identification of human and microbial metabolites of pharmaceuticals in the aquatic environment, TrAC: Trends Anal. Chem. 26 (2007) 494–514.
[15] M. Gros, M. Petrović, D. Barceló, Multi-residue analytical methods using LC–tandem MS for the determination of pharmaceuticals in environmental and wastewater samples: a review, Anal. Bioanal. Chem. 386 (2006) 941–952.
[16] N. Le-Minh, S.J. Khan, J.E. Drewes, R.M. Stuetz, Fate of antibiotics during municipal water recycling treatment processes, Water Res. 44 (2010) 4295–4323.
[17] R.A. Trenholm, B.J. Vanderford, S.A. Snyder, On-line solid phase extraction LC–MS/MS analysis of pharmaceutical indicators in water: a green alternative to conventional methods, Talanta 79 (2009) 1425–1432.
[18] A. Garcia-Ac, P.A. Segura, L. Viglino, A. Fürtös, C. Gagnon, M. Prévost, S. Sauvé, On-line solid-phase extraction of large-volume injections coupled to liquid chromatography–tandem mass spectrometry for the quantitation and confirmation of 14 selected trace organic contaminants in drinking and surface water, J. Chromatogr. A 1216 (2009) 8518–8527.
[19] P.A. Segura, C. Gagnon, S. Sauvé, A fully automated on-line preconcentration and liquid chromatography–tandem mass spectrometry method for the analysis of anti-infectives in wastewaters, Anal. Chim. Acta 604 (2007) 147–157.
[20] A. Garcia-Ac, P.A. Segura, C. Gagnon, S. Sauve, Determination of bezafibrate, methotrexate, cyclophosphamide, orlistat and enalapril in waste and surface waters using on-line solid-phase extraction liquid chromatography coupled to polarity-switching electrospray tandem mass spectrometry, J. Environ. Monit. 11 (2009) 830–838.
[21] L. Viglino, K. Aboulfadl, A.D. Mahvelat, M. Prevost, S. Sauve, On-line solid phase extraction and liquid chromatography/tandem mass spectrometry to quantify pharmaceuticals, pesticides and some metabolites in wastewaters, drinking, and surface waters, J. Environ. Monit. 10 (2008) 482–489.
[22] J. Ding, N. Ren, L. Chen, L. Ding, On-line coupling of solid-phase extraction to liquid chromatography–tandem mass spectrometry for the determination of macrolide antibiotics in environmental water, Anal. Chim. Acta 634 (2009) 215–221.
[23] K.-J. Choi, S.-G. Kim, C.-w. Kim, S.-H. Kim, Determination of antibiotic compounds in water by on-line SPE-LC/MSD, Chemosphere 66 (2007) 977–984.
[24] M.J. García-Galán, M.S. Díaz-Cruz, D. Barceló, Determination of 19 sulfonamides in environmental water samples by automated on-line solid-phase extraction-liquid chromatography–tandem mass spectrometry (SPE-LC–MS/MS), Talanta 81 (2010) 355–366.
[25] M.J. García-Galán, T. Garrido, J. Fraile, A. Ginebreda, M.S. Díaz-Cruz, D. Barceló, Simultaneous occurrence of nitrates and sulfonamide antibiotics in two ground water bodies of Catalonia (Spain), J. Hydrol. 383 (2010) 93–101.
[26] K. Stoob, H.P. Singer, C.W. Goetz, M. Ruff, S.R. Mueller, Fully automated online solid phase extraction coupled directly to liquid chromatography–tandem mass spectrometry: quantification of sulfonamide antibiotics, neutral and acidic pesticides at low concentrations in surface waters, J. Chromatogr. A 1097 (2005) 138–147.
[27] R. Lopez-Serna, S. Perez, A. Ginebreda, M. Petrovic, D. Barcelo, Fully automated determination of 74 pharmaceuticals in environmental and waste waters by online solid phase extraction-liquid chromatography–electrospray-tandem mass spectrometry, Talanta 83 (2010) 10–424.

[28] O.J. Pozo, C. Guerrero, J.V. Sancho, M. Ibáñez, E. Pitarch, E. Hogendoorn, F. Hernández, Efficient approach for the reliable quantification and confirmation of antibiotics in water using on-line solid-phase extraction liquid chromatography/tandem mass spectrometry, J. Chromatogr. A 1103 (2006) 83–93.
[29] K. Vučićević-Prčetić, R. Cservenák, N. Radulović, Development and validation of liquid chromatography tandem mass spectrometry methods for the determination of gentamicin, lincomycin, and spectinomycin in the presence of their impurities in pharmaceutical formulations, J. Pharm. Biomed. Anal. 56 (2011) 736–742.
[30] K. Heinig, T. Wirz, F. Bucheli, V. Monin, A. Gloge, Sensitive determination of a pharmaceutical compound and its metabolites in human plasma by ultra-high performance liquid chromatography–tandem mass spectrometry with on-line solid-phase extraction, J. Pharm. Biomed. Anal. 54 (2011) 742–749.
[31] L. Viglino, K. Aboulfadl, M. Prévost, S. Sauvé, Analysis of natural and synthetic estrogenic endocrine disruptors in environmental waters using online preconcentration coupled with LC-APPI–MS/MS, Talanta 76 (2008) 1088–1096.
[32] A. Salvador, C. Moretton, A. Piram, R. Faure, On-line solid-phase extraction with on-support derivatization for high-sensitivity liquid chromatography tandem mass spectrometry of estrogens in influent/effluent of wastewater treatment plants, J. Chromatogr. A 1145 (2007) 102–109.
[33] W.J. Backe, C. Ort, A.J. Brewer, J.A. Field, Analysis of androgenic steroids in environmental waters by large-volume injection liquid chromatography tandem mass spectrometry, Anal. Chem. 83 (2011) 2622–2630.
[34] C. Postigo, M.J.L. de Alda, D. Barcelo, Fully automated determination in the low nanogram per liter level of different classes of drugs of abuse in sewage water by on-line solid-phase extraction-liquid chromatography–electrospray-tandem mass spectrometry, Anal. Chem. 80 (2008) 3123–3134.
[35] H. Singer, S. Jaus, I. Hanke, A. Luck, J. Hollender, A.C. Alder, Determination of biocides and pesticides by on-line solid phase extraction coupled with mass spectrometry and their behaviour in wastewater and surface water, Environ. Pollut. 158 (2010) 3054–3064.
[36] C. Janssonand, J. Kreuger, Multiresidue analysis of 95 pesticides at low nanogram/liter levels in surface waters using online preconcentration and high performance liquid chromatography/tandem mass spectrometry, J. AOAC Int. 93 (2010) 1732–1747.
[37] K. Kato, M.J. Silva, L.L. Needham, A.M. Calafat, Determination of 16 phthalate metabolites in urine using automated sample preparation and on-line preconcentration/high-performance liquid chromatography/tandem mass spectrometry, Anal. Chem. 77 (2005) 2985–2991.
[38] X.Y. Ye, Z. Kuklenyik, L.L. Needham, A.M. Calafat, Automated on-line column-switching HPLC–MS/MS method with peak focusing for the determination of nine environmental phenols in urine, Anal. Chem. 77 (2005) 5407–5413.
[39] M. Takino, S. Daishima, T. Nakahara, Determination of perfluorooctane sulfonate in river water by liquid chromatography/atmospheric pressure photoionization mass spectrometry by automated on-line extraction using turbulent flow chromatography, Rapid Commun. Mass Spectrom. 17 (2003) 383–390.
[40] H. Trufelli, P. Palma, G. Famiglini, A. Cappiello, An overview of matrix effects in liquid chromatography–mass spectrometry, Mass Spectrom. Rev. 30 (2011) 491–509.
[41] X. Zhaoand, C.D. Metcalfe, Characterizing and compensating for matrix effects using atmospheric pressure chemical ionization liquid chromatography–tandem mass spectrometry: analysis of neutral pharmaceuticals in municipal wastewater, Anal. Chem. 80 (2008) 2010–2017.
[42] M. Stüberand, T. Reemtsma, Evaluation of three calibration methods to compensate matrix effects in environmental analysis with LC–ESI-MS, Anal. Bioanal. Chem. 378 (2004) 910–916.
[43] Commission Decision (2002/657/EC) of 12 August 2002 concerning the performance of analytical methods and the interpretation of results, Off. J. Eur. Communities L221 (2002) 8–36.
[44] J.A. Glaser, D.L. Foerst, G.D. McKee, S.A. Quave, W.L. Budde, Trace analyses for wastewaters, Environ. Sci. Technol. 15 (1981) 1426–1435.
[45] C. Accinelli, M.L. Saccà, J. Fick, M. Mencarelli, R. Lindberg, B. Olsen, Dissipation and removal of oseltamivir (Tamiflu) in different aquatic environments, Chemosphere 79 (2010) 891–897.
[46] T. Ohmori, A. Suzuki, T. Niwa, H. Ushikoshi, K. Shirai, S. Yoshida, S. Ogura, Y. Itoh, Simultaneous determination of eight [beta]-lactam antibiotics in human serum by liquid chromatography–tandem mass spectrometry, J. Chromatogr. B 879 (2011) 1038–1042.
[47] I.P. Leader, J. Halket, P. Finch, Synthesis and identification of two potential oxidation degradants of oxymetazoline, Rapid Commun. Mass Spectrom. 18 (2004) 1645–1654.
[48] R.H. Lindberg, P. Wennberg, M.I. Johansson, M. Tysklind, B.A.V. Andersson, Screening of human antibiotic substances and determination of weekly mass flows in five sewage treatment plants in Sweden, Environ. Sci. Technol. 39 (2005) 3421–3429.
[49] R.H. Lindberg, U. Olofsson, P. Rendahl, M.I. Johansson, M. Tysklind, B.A.V. Andersson, Behavior of fluoroquinolones and trimethoprim during mechanical, chemical, and active sludge treatment of sewage water and digestion of sludge, Environ. Sci. Technol. 40 (2005) 1042–1048.
[50] S. Zorita, L. Mårtensson, L. Mathiasson, Occurrence and removal of pharmaceuticals in a municipal sewage treatment system in the south of Sweden, Sci. Total Environ. 407 (2009) 2760–2770.
[51] D. Bendz, N.A. Paxéus, T.R. Ginn, F.J. Loge, Occurrence and fate of pharmaceutically active compounds in the environment, a case study: Höje River in Sweden, J. Hazard. Mater. 122 (2005) 195–204.

Journal of Pharmaceutical and Biomedical Analysis 66 (2012) 33–39

Contents lists available at SciVerse ScienceDirect

Journal of Pharmaceutical and Biomedical Analysis

journal homepage: www.elsevier.com/locate/jpba

HPTLC method for the simultaneous determination of four indole alkaloids in *Rauwolfia tetraphylla*: A study of organic/green solvent and continuous/pulse sonication

Shikha Gupta, Karuna Shanker, Santosh K. Srivastava*

Analytical Chemistry Department, Central Institute of Medicinal and Aromatic Plants, Council of Scientific and Industrial Research (CSIR), Lucknow 226015, India

ARTICLE INFO

Article history:
Received 13 October 2011
Received in revised form 17 February 2012
Accepted 18 February 2012
Available online 8 March 2012

Keywords:
Reserpiline
α-Yohimbine
10-Methoxy tetrahydroalstonine
Rauwolfia tetraphylla
HPTLC-fingerprint

ABSTRACT

A new validated high-performance thin-layer chromatographic (HPTLC) method has been developed for the simultaneous quantitation of four antipsychotic indole alkaloids (IAs), reserpiline (RP, **1**), α-yohimbine (YH, **2**), isoreserpiline (IRP, **3**) and 10-methoxy tetrahydroalstonine (MTHA, **4**) as markers in the leaves of *Rauwolfia tetraphylla*. Extraction efficiency of the targeted IAs from the leaf matrix with organic and ecofriendly (green) solvents using percolation, ultrasonication and microwave techniques were studied. Non-ionic surfactants, viz. Triton X-100, Triton X-114 and Genapol X-80 were used for extraction and no back-extraction or liquid chromatographic steps were used to remove the targeted IAs from the surfactant-rich extractant phase. The optimized cloud point extraction was found a potentially useful methodology for the preconcentration of the targeted IAs. The separation was achieved on silica gel $60F_{254}$ HPTLC plates using hexane-ethylacetate-methanol (5:4:1, v/v/v) as mobile phase. The quantitation of IAs (**1**–**4**) was carried out using the densitometric reflection/absorption mode at 520 nm after post chromatographic derivatization using Dragendorff's reagent. The method was validated for peak purity, precision, accuracy, robustness, limit of detection (LOD) and quantitation (LOQ). Method specificity was confirmed using retention factor (R_f) and visible spectral (post chromatographic scan) correlation of marker compounds in the samples and standard tracks.

© 2012 Elsevier B.V. All rights reserved.

1. Introduction

Indole alkaloids are the secondary metabolites of plants and possess significant physiological activities such as anti-tumor, antihypertensive, antimalarial, central nervous system stimulant and anti-microbial [1]. *Rauwolfia tetraphylla* L. (Syn. *R. canescens/R. heterophylla/R. hirsuta*; Family – Apocynaceae) is popularly known as "Be still tree" or "Devil-pepper". It is an economically important medicinal plant and cultivated on commercial scale in India [2]. Various indole alkaloids viz. N(α)-demethylaccidine, tetraphylline, tetraphyllicine, aricine, isoreserpiline, tetrahydroalstonine, α-yohimbine and reserpiline are present in different parts of the plants [3–5]. The leaf extract is used in the treatment of cholera, intestinal disorders, diarrhea, dysentery, eye-disease, fever and as antihypertensive [6]. The plant is used for cardiovascular diseases, hypertension and various psychiatric diseases [7]. The plant extract mixed with castor oil is prescribed for refractory ailments while the bark decoction is used for chronic refractory, skin diseases and to destroy parasites [8]. The roots are used to stimulate uterine contractions hence recommended for use in difficult cases of childbirth [9]. Recently, antibacterial activity [10] has also been reported in *R. tetraphylla*. As roots yield an antihypertensive and tranquilizering drug deserpidine, they are often used as substitute or adulterant for *R. serpentina* alkaloids: ajmaline, ajmalcine, reserpine, serpentine etc.

Currently, ultrasonic-assisted extractions are used for rapid extraction of natural products [11–13], but it lacks preconcentration. Pre-treatment methods such as liquid–liquid extraction (LLE) and solid-phase extraction (SPE) usually require a large volume of toxic organic solvents [14]. Unfortunately, both of these pre-treatment processes suffer with the drawbacks of large sample volume, time-consuming procedure and sometimes compromised recovery [15]. Undoubtedly, the most popular extraction method is solvent extraction and the choice of solvent greatly depends on its properties [16]. Therefore, development of simple and environment friendly methods are highly desired in natural product research [17,18].

The micelle-mediated extraction and cloud-point preconcentration (CPE) methods offer a convenient alternative to the conventional extraction systems [19,20]. A plethora of reports have shown application of CPE in extracting and enriching

* Corresponding author at: Central Institute of Medicinal and Aromatic Plants, P.O. CIMAP, Lucknow 226015, India. Tel.: +91 522 2359623; fax: +91 522 2342666.
E-mail address: santoshkumar_1955@yahoo.com (S.K. Srivastava).

0731-7085/$ – see front matter © 2012 Elsevier B.V. All rights reserved.
doi:10.1016/j.jpba.2012.02.018

inorganic, organic and biological analytes prior to their analysis by spectroscopy, capillary electrophoresis or liquid chromatography [21,22], but there is very limited work on natural products [23–26].

Although, there are several analytical methods viz. TLC, fluorescence, HPLC-UV, MS/MS, GC–EI/MS and HPLC-UV–MS [27] for the qualitative and quantitative determination of an aphrodisiac indole alkaloid, yohimbine (an isomer of YH) in the clinical samples and commercially available aphrodisiacs, but HPTLC has several advantages over HPLC [27] such as: (i) samples and standards both are simultaneously processed under the same conditions leading to better analytical precision and accuracy, (ii) mobile phase consumption per sample is extremely low, (iii) thus reducing the acquisition and disposal cost, (iv) there is no possibility of interference from previous analysis as fresh stationary phase is used for each analysis, (v) instrumentation is simple, inexpensive and easy to handle and (vi) many samples can be analyzed at the same time. Therefore, HPTLC is rapidly gaining importance in pharmaceutical analysis, biochemistry and pharmacokinetics studies, but to the best of our knowledge there is only one report on the quantitative determination of aphrodisiac compound, yohimbine in *R. tetraphylla* leaf by HPTLC [28]. It would be worth mentioning at this point that neither Prof. Ashima Chatterjee nor we could isolate aphrodisiac compound, yohimbine in *R. tetraphylla* leaves. Both of us were able to isolate and characterize rauwolscin (α-yohimbine) an isomer of yohimbine, having quite different biological activities than yohimbine. Further, the reported HPTLC method seems ambiguous due to several reasons such as: (i) the color, intensity and R_f of the reference yohimbine does not match with the compound it has been shown in the leaf extract on HPTLC, (ii) it reports unbelievable high percentage of yohimbine (6.11%) in the leaves of *R. tetraphylla* and (iii) the reference itself is a mixture of many compounds. One of the reasons for this high yohimbine content may be the UV detection of TLC plat at 366 nm, which very clearly shows merging of compounds having close R_f values. In view of the above demerits, the reported HPTLC method [28] does not seems suitable for qualitative and quantitative determination of yohimbine.

Recently, we reported antipsychotic activity in the four leaf indole alkaloids, RP, YH, IRP and MTHA of *R. tetraphylla* [29] and developed new preparative-scale isolation and analytical methods for some bioactive molecules [30–34]. The objective of the present study was to assess the feasibility and effectiveness of organic and ecofriendly (green) solvents using percolation, ultrasonication and microwave techniques and develop a validated, rapid, sensitive and accurate HPTLC method for the simultaneous determination of four bioactive IAs RP, YH, IRP and MTHA in the leaves of *R. tetraphylla*.

2. Materials and methods

2.1. Plant materials

The plants of *R. tetraphylla* are maintained at the research farm of Central Institute of Medicinal and Aromatic Plants (CIMAP), Lucknow, India, located at 26.5°N, 80.5°E and 120 m above the main sea level, with an annual rainfall of 53.21 mm. The plants received normal intercultural operations (weeding, hoeing and irrigation as per requirement). The leaves of *R. tetraphylla* were collected in the month of January 2009. A voucher specimen (CIMAP No. 7671) was deposited in the Botany and Pharmacognosy Department of the institute. The leaves were powdered, packed in airtight container and stored at 20 °C until analysis.

2.2. Chemicals and reference compounds

Triton X-100 (polyethylene glycol mono [4-(1,1,3,3-tetramethylbutyl)-phenyl] ether) with an average ethylene oxide (EO) chain length of $n = 9.5$; TX-100, $C_{34}H_{62}O_{11}$ (MW 625 g/mol) 275 (λ_{max}, nm), 0.13–0.30 (CMC, mM); Triton X-114 (polyethylene glycol mono [4-(1,1,3,3-tetramethylbutyl)-phenyl] ether) with an average ethylene oxide (EO) chain length of $n = 7.5$; TX-114, $C_{30}H_{54}O_9$ (MW 537 g/mol) 223 (λ_{max}, nm), 0.20–0.35 (CMC, mM) and Genapol X-080 (isotridecyl poly ethylene glycol ether), GP-80, $C_{30}H_{62}O_{10}$ (MW 58 g/mol) 210 (λ_{max}, nm), 0.6–0.15 (CMC, mM) were purchased from Sigma–Aldrich (St. Louis, MO, USA) and were used without further purification. All other solvents used for extraction and chromatographic analysis were of analytical or HPLC grade (E. Merck Ltd., Mumbai, India). Prior to use, solvents were filtered through a 0.45 μm membrane (Millipore, Billerica, MA, USA). Pre-coated silica gel $60F_{254}$ glass HPTLC plates were purchased from Merck (Darmstadt, Germany). The sorbent, silica gel, used for flash chromatography was purchased from Qualigens Fine Chemicals, Mumbai, India. The standard antipsychotic compounds, RP (**1**), YH (**2**), IRP (**3**) and MTHA (**4**) were isolated (purity > 99% using HPLC) and characterized (Fig. 1) by us on the basis of their 1D and 2D NMR spectroscopic data.

2.3. Apparatus

Vario system, TLC Scanner, winCATS-III, Reprostar-3, twin trough chamber, immersion device-III, TLC plate heater (Camag, Muttenz, Switzerland) were used for digital image scanning, method development and validation. Ultrasonic extractions were performed in two modes; in the first mode, extraction was carried out on continuous ultrasonic bath (Microclean-109, Oscar Ultrasonics, Mumbai, India, 30.0 cm × 25.0 cm × 12.5 cm, 34 ± 3 kHz, PZT Sandwich Type Six Transducer, 250 W), while in second mode, extraction was carried out on pulsed acoustic waves (Sonics VCX-750, Vibra cell®, Sonics and Materials Inc., Newtown, CT, USA, 20 kHz, 750 W, 85% amplitude, 5 s/5 s pulse, sonic power 14.93 W/cm^2, PZT probe 13 mm dia). Microwave assisted extractions (MAE) were carried out in microwave oven (Whirlpool, New Delhi, India) having programmable heating power and pulse radiations (controlled temperature). The 300 MHz NMR (Avance, Bruker, Switzerland) was used to record ^{1}H and ^{13}C NMR spectra in C_5D_5N, CD_3OD with tetramethyl silane (TMS) as internal standard.

2.4. Extraction and isolation of indole alkaloids from R. tetraphylla

The shade dried and finely powdered leaves of *R. tetraphylla* (190 g) were exhaustively extracted with methanol (4× 3 l) in a percolator at room temperature (25 ± 2 °C). The pooled MeOH extract was distilled under vacuum at 40 °C until dryness. The crude MeOH extract (42 g) was then exhaustively extracted with 2% aqueous HCl solution (20× 150 ml) to dissolve IAs as their water-soluble hydrochloride salts. The combined acidic extract was successively defatted with hexane and $CHCl_3$ (4× 300 ml). The defatted acidic extract was then basified up to pH-9 at 0 °C with Na_2CO_3 and extracted with $CHCl_3$ (4× 500 ml). The pooled $CHCl_3$ extract so obtained was washed with water, dried over anhydrous sodium sulphate and the solvent removed under vacuum at 40 °C, which afforded a dark brown residue (3.2 g).

For the isolation of IAs, $CHCl_3$ extract (2.7 g) was subjected over flash chromatograph (FC) glass column (3 cm × 23 cm) packed with TLC grade silica (silica gel H, average particle size approx. 10 μm, 20 g). Gradient elution of the Flash was carried out with mixtures of solvents: hexane, EtOAc and methanol in increasing order of polarity. A total number of 186 fractions of 50 ml each were collected and pooled on the basis of their TLC profile after visualizing with Dragendorff's reagent. FC fractions 13–15, 17–21, 98–129 eluted with hexane: EtOAc (75:25) resulted in the isolation of IAs, MTHA, IRP and YH respectively. Similarly FC fractions 137–168 eluted with

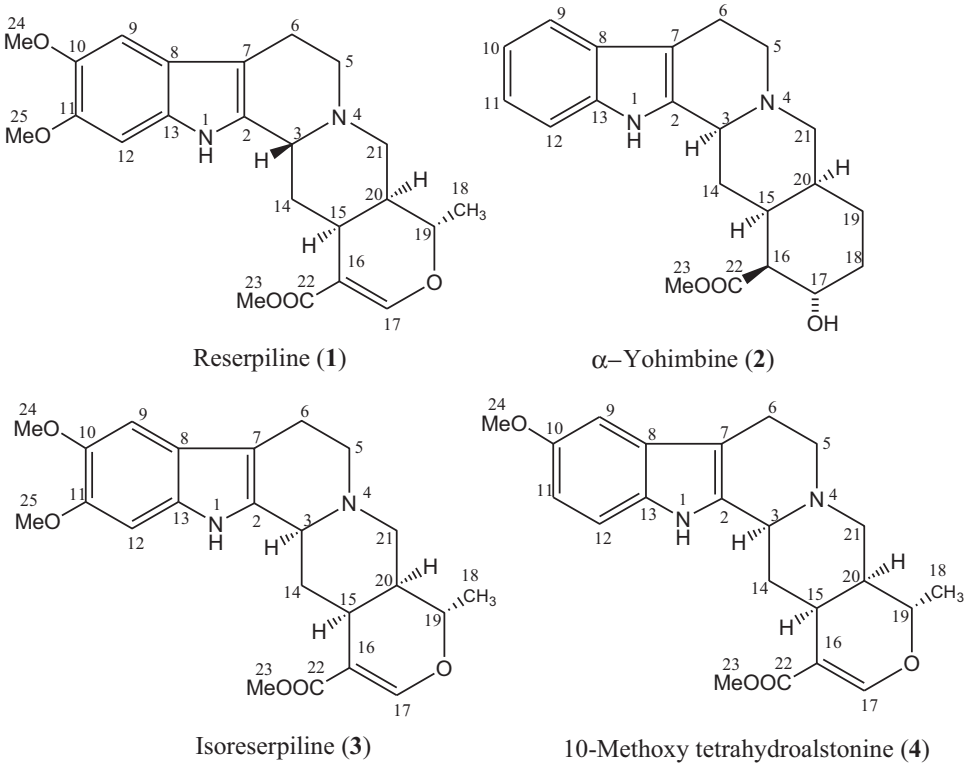

Fig. 1. Chemical structures of indole alkaloids.

hexane: EtOAc (6:4 and 4:6) resulted in the isolation of RP. The isolated IAs RP (1) and IRP (3) were stereo isomers and their structures were deduced mainly on the basis of their ^{13}C NMR spectroscopic data, which showed characteristic peaks at 131.7 (C-2), 55.1 (C-3), 52.5 (C-5), 19.4 (C-6), 31.0 (C-14), 26.2 (C-15), 37.8 (C-20), 50.8 (C-21) ppm for RP (1) and at 134.1 (C-2), 60.4 (C-3), 53.9 (C-5), 22.4 (C-6), 34.9 (C-14), 31.9 (C-15), 39.1 (C-20), 56.6 (C-21) ppm for IRP (3). These differences in chemical shifts of C-2, C-3, C-5, C-6, C-14, C-15, C-20 and C-21 may be accounted for the β and α orientation of the proton in RP (1) and IRP (3), respectively (Fig. 1). Since RP (1) and IRP (3) were stereoisomers hence showed same mass in ESI-MS (Fig. 1S), which were in complete agreement with the reported data for compounds **1** and **3** [35]. The structures of other IAs were characterized as YH (**2**) and MTHA (**4**) on the basis of their ^{1}H, ^{13}C, 2D NMR and ESI-MS (Fig. 1S) spectroscopic data, which were in complete agreement with the reported data [29,36]. The complete spectroscopic data of IAs **1**–**4** are given in supplementary file.

2.5. Standard stock solutions and sample preparation

Standard stock solutions of bioactive marker compounds, RP, YH, IRP and MTHA were prepared in 1.0 mg/ml concentration in methanol. Working stocks for calibration studies were prepared by dilution using Hamilton syringe (Bonaduz, Switzerland). The dried and milled leaf samples of *R. tetraphylla* (1 g each) were extracted separately with: methanol by cold percolation (3× 20 ml, 10 h extraction time at room temperature); hot extraction (3× 20 ml, 30 min extraction time at 50 °C); ultrasonication (waterbath, 3× 20 ml, 60 min extraction time); ultrasonication (pulse, 3× 20 ml, 5 s/5 s pulse mode at 60 °C for 50 min extraction time); microwave assisted extraction (3× 20 ml, at 350 W, 50 °C for 3 min extraction time). Each extract evaporated to dryness, re-dissolved in 1.0 ml of methanol, and centrifuged at 10,000 rpm for 10 min. The supernatants were pre-filtered with 0.45 μm and then used for HPTLC analysis.

2.6. Ultrasonic assisted micelle-mediated extraction

The powdered leaves of *R. tetraphylla* (1.0 g each) were accurately weighed and placed in 15 ml centrifuge tubes; 20 ml non-ionic surfactants (Genapol X-080, Triton X-100 and Triton X-114) solution (7%, v/v) were separately added to these centrifuge tubes. The tubes were capped and blended adequately and then placed in a ultrasonic cleaning bath for ultrasonic extraction. During the extraction, mixing was provided by an ultrasonic bath. For ultrasonic-assisted micelle-mediated extraction (UAMME), the extraction time was 1 h and the experiment was carried out at 50 ± 2 °C. After ultrasonic-assisted extraction, the extract of *R. tetraphylla* leaves was centrifuged at 4000 rpm for 20 min, and then the supernatant was collected and optimized for pre-concentration of IAs (**1**–**4**).

2.7. Cloud-point pre-concentration

To study the bi-phasic behavior of IAs in respective non-ionic surfactants, i.e. formation of a layer of organic-rich coacervate and large aqueous extract, the cloud point was achieved by adding salt. Sodium chloride (80 g/l) was added to the sample solution. The sample solution was then kept in a thermostatic water bath at 50 °C for 30–60 min until the solution completely separated out into two distinct phases. The upper phase was the small volume of surfactant-rich phase and the lower phase was the large volume of the aqueous phase. After centrifugation for 20 min at 4000 rpm, the aqueous phase was pipetted out, and the sticky surfactant-rich phase was left in the tube. A 1.0 ml aliquot of methanol was added to lower the viscosity of the surfactant-rich phase.

2.8. Chromatographic procedure

Chromatography was performed on a preactivated HPTLC plates (10 cm × 10 cm or 20 cm × 10 cm). The plates were washed with

methanol and activated at 120 °C for 20 min. Standard and sample solutions were applied in the form of band at 15 mm from both the lower and left edge with 20 mm space between two bands using a 100 μl syringe (Hamilton, Bonaduz, Switzerland). Linear ascending development was carried out in pre-saturated (optimized to 4 min for better resolution) vertical twin trough glass chambers (10 cm × 10 cm or 20 cm × 10 cm) saturated with the mobile phase. The mobile phase selection and optimization was carried out using the Vario System wherein different compositions consisting of different ratios of solvents of varying polarity were tried. Finally, a mobile phase consisting of organic layer of hexane: ethylacetate: methanol (50:40:10, v/v/v) was used as mobile phase and HPTLC separation of the four IAs was achieved without interference of sample matrix components under laboratory conditions (temperature 25 ± 3 °C and relative humidity 35–40%). After development, plates were dried and the components were visualized by Dragendorff's reagent using the immersion device (dipping time 2 s, dipping speed 5 cm/s) followed by air drying for 40 min. The plates were scanned and quantified densitometrically at 520 nm (maximum wavelength in the spectra of the derivative). TLC Scanner-III controlled by winCATS 1.4.2.8121 software (Camag) was used for quantitative evaluation. The densitometry scanning was performed in the reflectance/absorbance mode, slit width 8.00 mm × 0.40 mm, scanning speed 20 mm/s and data resolution 10 μm/step. Savitsky-Golay-7 was used for data filtering and the lowest slope for baseline correction in order to integrate the area. A tungsten lamp was used for recording of characteristic derivatized bands of standards RP, YH, IRP and MTHA and sample tracks in the range 400–800 nm. Reprostar 3 with cabinet cover and mounted digital camera (Canon PowerShot G5 with Neck Strap NS-DC2, Canon, Japan) was used for imaging and archiving the chromatograms. Quantitation was performed using linear regression equations of respective compounds.

3. Results and discussion

3.1. Optimization of extractability of indole alkaloids from sample matrix

For studying extraction efficiency of IAs from the leaves of *R. tetraphylla*, different extraction methodologies viz. cold percolation, hot extraction, ultrasonication, ultrasonic-assisted cloud point extraction and microwave extractions were carried out. During optimization, extraction of targeted IAs (**1**–**4**) at different operating conditions in sonicating bath (250 W, 40 kHz for 30, 45 and 60 min), ultrasonic pulse (5 s/5 s pulse mode at 60 °C for 10, 20, 30, 40, 50 and 60 min extraction time), microwave extraction (90, 160, 350, 650 W at 50 °C for 3 min extraction time) and ultrasonic-assisted cloud point extraction (7% solution of non-ionic surfactant Genapol X-080, Triton X-100 and Triton X-114 at 50 °C for 30–60 min extraction time) were studied. The result of extraction efficiency of solvents and suitability of extraction techniques are summarized in Table 1, which showed that optimum amount of targeted IAs (**1**–**4**) were obtained in ultrasonic bath (3× 20 ml, 60 min), ultrasonic pulse (3× 20 ml, 5 s/5 s pulse mode at 60 °C for 50 min), microwave (3× 20 ml at 350 W and 50 °C for 3 min) and ultrasonic-assisted cloud point (3× 20 ml, Triton X-100 at 50 °C for 30–60 min extraction time) at the operating conditions as given in parentheses.

The extracts were later concentrated under vacuum and redissolved in methanol for HPTLC analysis. All the samples and standard tracks were scanned at 520 nm after derivatization with Dragendorff's reagent. It is quite evident from Fig. 2 that no interfering compounds were eluted in the sample tracks, which can affect the quantitation of the targeted markers, RP, YH, IRP and MTHA, but showed variation in the extraction efficiency. For both qualitative and quantitative analysis, visible range was most suitable for scanning the spots after derivatization (Fig. 2) as it ruled out the possibility of merging of closet compounds. The spectra of RP, YH, IRP and MTHA in standard and sample track both were highly correlated (Table 2) and confirmed that the mode of scanning was sensitive and effective. It is for the first time, we have carried out a comparative study between methanol and non-ionic surfactants as extracting solvents for IAs in the conventional extraction process and the results have shown that methanol is the most suitable solvent for extracting IAs in *R. tetraphylla*.

3.2. Method validation

Method validation was performed on the parameters such as linearity, limit of sensitivities, specificity, precision, accuracy, recovery and robustness as per ICH [37] and IUPAC [38] guidelines. All the data were evaluated using standard statistical packages for Windows and GraphPad Prism 4.0 (GraphPad Software, Inc., USA). Statistical significance was considered at 95% probability level ($p < 0.05$). Pearson's coefficient (r^2) was used to evaluate the significance of correlations. Computing and comparing HPTLC standard curves with reference compounds and spiked samples curves were in compliance with the ICH validation requirements [39,40].

3.2.1. Calibration curves, limits of detection/quantification (LOD/LOQ)

Working stock solutions of RP, YH, IRP and MTHA were prepared by dilution with methanol to give the IAs concentrations 1.0, 2.0, 3.0, 4.0, and 5.0 mg/ml. Standard solution of each IA was spotted on

Table 1
Extraction efficiency of different solvents for chemical markers (IAs) from the leaves of *R. tetraphylla* on plant dry weight basis.

Techniques[a]/solvents	Amount of compound quantified (%, w/w)			
	Reserpiline (RP)	α-yohimbine (YH)	Isoreserpiline (IRP)	10-Methoxy tetrahydroalstonine (MTHA)
Cold percolation				
Methanol	0.0847	0.1028	0.0378	0.1250
Hot extraction				
Methanol	0.0979	0.1960	0.1030	0.1003
Microwave extraction				
Methanol	0.0580	0.0874	0.0319	0.0292
Ultrasonic extraction				
Methanol (Continuous)	0.0916	0.1459	0.1391	0.1655
Methanol (pulse)	0.1295	0.2195	0.1474	0.1910
CPE (Triton X-100)	0.0849	0.0500	0.0363	0.0500
CPE (Triton X-114)	ND	ND	ND	ND
CPE (Genopol X-80)	ND	ND	ND	ND

Values are average of three observations.
[a] The experimental conditions are described in Sections 2.5–2.7.

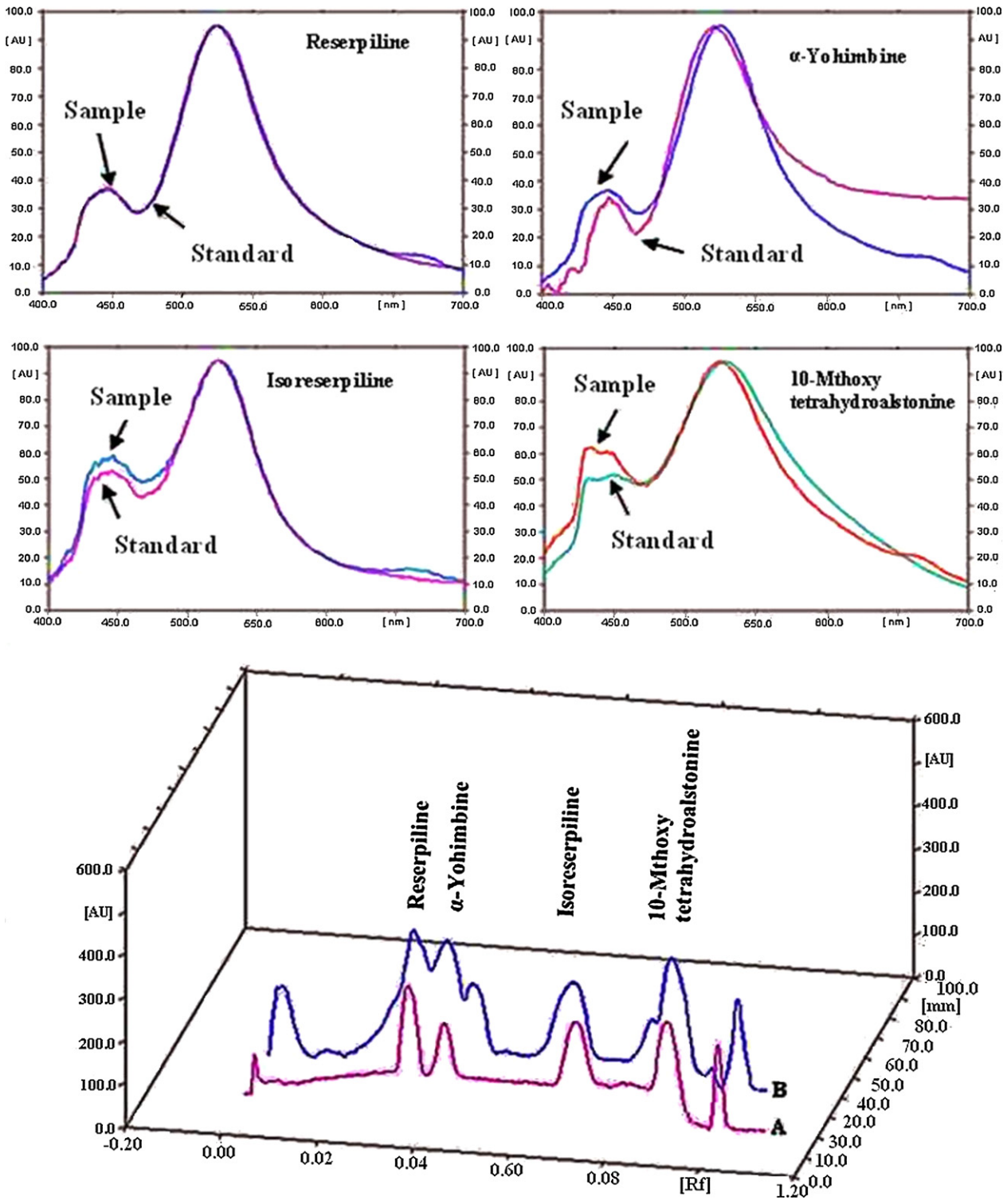

Fig. 2. Track A: mixture of four chemical markers reserpiline (RP, **1**) α-yohimbine (YH, **2**), isoreserpiline (IRP, **3**) and 10-methoxy tetrahydroalstonine (MTHA, **4**) and Track B: HPTLC chromatogram of methanolic extract of *R. tetraphylla* leaves (Ext) (concentration: Ext 1.0 g/ml; RP, YH, IRP and MTHA 1.0 mg/ml; sample loading: 4 μl/band; inset showing the comparison of visible spectra of respective compounds in sample and standard track).

HPTLC plate to give absolute amounts of 2, 4, 6, 8 and 10 μg/band for standards. Each concentration was spotted thrice. The calibration curves were prepared by the least-squares method using absolute amount (μg/band) as independent variable (X) and the peak area of IAs standards as dependent variable (Y). Regression analyses test of the compound was performed by GraphPAD Prism 4.0. The selection of working concentration range of respective IAs was based on their response. The curves (Table 2) confirmed linear relationship ($r^2 \geq 0.94$) between the working concentration and the peak areas. Linearity was checked for three consecutive days for the same concentration range (five data point in triplicate) from different stock solutions ($p \geq 0.28$). The intercept was not statistically significant ($p \geq 0.05$). A statistical residual analysis was also performed for each point of concentration range, which corresponded to the

Table 2
Analytical characteristics of the validated HPTLC method for the quantitation of IAs in *R. tetraphylla*.

Parameters	RP	YH	IRP	MTHA
R_f value	0.43 ± 0.02	0.60 ± 0.02	0.86 ± 0.01	0.95 ± 0.01
Densitometric linear relationship[a]				
Working concentration range	2–10 μg/band	2–10 μg/band	2–10 μg/band	2–10 μg/band
Regression equation	188.4*X* + 878.1	212.4*X* + 32.0	267.8*X* + 430.1	275.2*X* + 536.9
Correlation coefficient (r^2)	0.9977	0.9981	0.9948	0.9409
Accuracy (%)				
Repeatability (RSD %; n = 6) at 4 μg/band	0.45	0.62	0.90	0.97
Precision				
Intra-day (RSD %) (n = 3)	0.45	0.62	0.90	0.97
Inter-day (RSD %) (n = 3)	0.95	1.10	0.98	1.57
Recovery range (%)				
Spl (1.5,1.8,1.2 and 2.8 μg/band) + 2 μg/band (each Ref)	95–97	98–116	96–116	93–99
Specificity				
Peak purity[b]				
R (s,m)				
Standard track	0.9997	0.9949	0.9956	0.9993
Sample track	0.9980	0.9868	0.9850	0.9992
R (m,e)[c]				
Standard track	0.9998	0.9893	0.9897	0.9974
Sample track	0.9968	0.9864	0.9870	0.9896

[a] Digital scanning at 520 nm after post derivatization with Dragendorff's reagent and statistical relationship were established considering five data point each in triplicate; *X*, amount of compound (μl/band); *Y* peak area counts.
[b] Correlation of spectrum at start of peak with spectrum at the center of peak at 520 nm scanning.
[c] Correlation of spectrum at center of peak with spectrum at the end of peak at 520 nm scanning.

difference between estimated and mean concentrations. Residual plot analysis demonstrates that residuals were randomly distributed around the zero value. This further confirms for the choice of linear model.

LOD and LOQ were determined using the linear regression equations: LOD = $3S_{y,x}/b$ and LOQ = $10S_{y,x}/b$, where $S_{y,x}$ is the standard deviation of the *Y*-value distribution around the regression line and b is the slope of the calibration curve. LODs for RP, YH, IRP and MTHA were 0.20, 0.18, 0.30 and 1.05 μg/band, respectively and LOQs determined in the same way were 0.67, 0.61, 1.0 and 3.46 μg/band, respectively.

3.2.2. Specificity

The method specificity was assessed by comparing the R_f (RP 0.43, YH 0.60, IRP 0.86, MTHA 0.95) and absorption spectra of the reference compounds in sample and standard tracks. On comparison of spectra at peak start, peak apex and peak end positions of the band, an acceptable correlation (r^2 = 0.94–0.99) was obtained between standards and sample overlay spectra which confirms the purity of RP, YH, IRP and MTHA peaks in the sample tracks. The comparative elution study revealed that there is little peak broadening in MTHA, which resulted into different linear correlation.

3.2.3. Precision and accuracy

The repeatability of measurement (n = 6) for peak area of all IAs standards (**1**–**4**) has been expressed in terms of percent coefficient of variation (RSD %). The intra- and inter-day variations were also evaluated at 4 μg/band for RP, YH, IRP and MTHA. The results are shown in Table 2, which depict that the method is accurate and precise for the analysis of chemical test markers in *R. tetraphylla.*

3.2.4. Recovery

The accuracy of quantitation in terms of recovery was also assessed. For this purpose, leaf samples were extracted with methanol using ultrasonic pulse mode and amounts of IAs RP, YH, IRP and MTHA were estimated. Further, these samples were applied in triplicate on the plate. All standards (**1**–**4**) were spiked with 2 μg/band into samples to reach a final content within the working range of linear calibration. The recovery results were within acceptable limits (Table 2).

3.2.5. Robustness

To test robustness of the method, small changes in the chromatographic parameters were deliberately made, which may affect the performance of the method such as mobile phase composition, chamber saturation time, delay between spotting and plate development and delay in digital scanning after derivatization, but only negligible changes in the peak areas were found. The time gap between derivatization and scanning greatly affected the quantitation when the analysis was performed within 40 min of derivatization. After 40 min of derivatization time, it remained stable for 2 days under laboratory conditions. Quantitation was not significantly affected by changing scanning wavelength ±5 nm.

3.3. Quantitative evaluation of IAs

It is evident from Fig. 2 that the IAs in *R. tetraphylla* samples shows characteristic VIS-spectra after densitometry of HPTLC plates. The same figure shows that acceptable separation was achieved without any interference of the nearby components under the specified conditions. The most important advantages of HPTLC as a screening technique for phytomolecules are its low cost, methodological simplicity and high sample throughput [39]. That is why HPTLC is a globally accepted rational and practical solution to characterize the crude plant drug, pharmacologically active constituent enriched standardized extracts and their formulations [40]. The method validation data showed that this procedure is sensitive, selective, and reproducible. The applicability of the developed method was demonstrated. For the quantitative evaluation of IAs, pulsed acoustic waves extraction of *R. tetraphylla* leaves in methanol was best. Plant samples from three locations around the vicinity of Lucknow were collected. The analyses were performed in triplicate and the results are summarized in Table 3. The amount of marker was source dependent and varied. Several factors such as age, plant health, and environmental condition affect the content of plant secondary metabolites. These parameters are beyond control in wildly growing plants. The specificity of measurement of IAs was insured by corresponding R_f, and visible spectral matching of respective alkaloids in *R. tetraphylla* leaf samples. This standardized HPTLC procedure may be used effectively for the screening analysis as well as quality evaluation of the *R. tetraphylla*, extracts, fractions or its derived herbal products.

Table 3
Percent content of IAs in the leaves of *R. tetraphylla* (calculated on plant dry weight basis).

S. No.	Locations	Indole alkaloids amount quantified (%, w/w)			
		RP	YH	IRP	MTHA
1	CIMAP Campus, Lucknow	0.1295	0.2195	0.1474	0.1910
2	CISH Campus, Hardoi Road, Lucknow	0.1614	0.1002	0.1432	0.1453
3	CISH Campus, Raebareli Road, Lucknow	0.1476	0.1201	0.1293	0.1298

Values are average of three observations.

Acknowledgements

Financial support for this research by the Council of Scientific & Industrial Research (CSIR), New Delhi, India under the Network project NWP-37 is gratefully acknowledged. One of us (SG) is grateful to CSIR for providing Senior Research Fellowship. We also thanks Er. A.D. Nannaware, Scientist, CIMAP, Lucknow for extending pulsed acoustic waves extraction facility.

Appendix A. Supplementary data

Supplementary data associated with this article can be found, in the online version, at doi:10.1016/j.jpba.2012.02.018.

References

[1] R. Verpoorte, in: M.F. Roberts, M. Wink (Eds.), Alkaloids: Biochemistry, Ecology and Medicinal Applications, Plenum Press, New York, 1998, pp. 397–433.
[2] A.A. Farooqi, B.S. Sreeramu, Cultivation of Medicinal and Aromatic crops, University Press Ltd., India, 2001, pp. 210–211.
[3] J.A. Martinez, H. Velez, T. Santana, An alkaloid from two *Rauwolfia* spp., Phytochemistry 28 (1989) 961–962.
[4] C. Djerassi, J. Fishman, M. Gorman, J.P. Kutney, S.C. Prakashi, Alkaloids Studies. XVI. Alkaloids of *Rauwolfia tetraphylla* L. The structures of tetraphylline and tetraphyllicine, J. Am. Chem. Soc. 79 (1957) 1217–1222.
[5] R.P. Rastogi, B.N. Mehrotra, Compendium of Indian Medicinal Plants, vol. 3, 1980–1984.
[6] Anonymous, The Wealth of India. Publications and Information Directorate, vol. 8, CSIR, New Delhi, India, 1969.
[7] M. Faisal, M. Anis, Rapid in vitro propagation of *Rauvolfia tetraphylla* L.: an endangered medicinal plant, J. Physiol. Mol. Biol. Plants 8 (2002) 295–299.
[8] J.A. Parrota, Healing Plants of Penisular India, vol. 30, CABI Publishers, New York, USA, 2001, pp. 120–125.
[9] R. Villar, J.M. Calleja, C. Morales, A. Caceres, Screening of Guatemalan medicinal plants for platelet antisegregant activity, Phytother. Res. 11 (1998) 441–445.
[10] C. Alagesaboopathi, An investigation on the Antibacterial activity of *Rauvolfia tetraphylla* dry fruit extracts, Ethnobot. Leafl. 13 (2009) 644–650.
[11] K. Shanker, S.C. Singh, S. Pant, P. Srivastava, R. Pandey, R.K. Verma, M.M. Gupta, Quantitative TLC analysis of sterol (24b-ethylcholesta-5,22*E*,25-triene-3b-ol) in Agnimantha (*Clerodendrum phlomidis* Linn), Chromatographia 67 (2008) 269–274.
[12] R. Wu, Z.Q. Zhang, Microwave-assisted extraction and high performance liquid chromatography for simultaneous determination of osthole and isoimperatorin in *Libanotis buethorimensis*, Anal. Lett. 43 (2010) 34–44.
[13] A.K. Yadav, D. Yadav, K. Shanker, R.K. Verma, A.K. Saxena, M.M. Gupta, Flavone glycoside based validated RP-LC method for quality evaluation of Prishniparni (*Uraria picta*), Chromatographia 69 (2009) 653–658.
[14] C.W. Huie, A review of modern sample-preparation techniques for the extraction and analysis of medicinal plants, Anal. Bioanal. Chem. 373 (2002) 23–30.
[15] Y. Jiang, B. David, P. Tu, Y. Barbin, Recent analytical approaches in quality control of traditional Chinese medicines – a review, Anal. Chim. Acta 657 (2010) 9–18.
[16] H.K. Kim, R. Verpoorte, Sample preparation for plant metabolomics, Phytochem. Anal. 21 (2010) 4–13.
[17] K. Kiathevest, M. Goto, M. Sasaki, P. Pavasant, A. Shotipruk, Extraction and concentration of anthraquinones from roots of *Morinda citrifolia* by non-ionic surfactant solution, Sep. Purif. Technol. 66 (2009) 111–117.
[18] J. Zhou, X.L. Suna, S.W. Wang, Micelle-mediated extraction and cloudpoint preconcentration of osthole and imperatorin from *Cnidium monnieri* with analysis by high performance liquid chromatography, J. Chromatogr. A 1200 (2008) 93–99.
[19] R.C. Martınez, E.R. Gonzalo, J.D. Alvarez, J.H. Meındez, Cloud point extraction as a preconcentration step prior to capillary electrophoresis, Anal. Chem. 71 (1999) 2468–2474.
[20] Z. Wang, The potential of cloud point system as a novel two-phase partitioning system for biotransformation, Appl. Microbiol. Biotechnol. 75 (2007) 1–10.
[21] C.O. Bosch, F.R. Sanchez, Separation and preconcentration by a cloud point extraction procedure for determination of metals: an overview, Anal. Bioanal. Chem. 394 (2009) 759–782.
[22] R.M. Carabias, E.G. Rodriguez, B.C. Moreno, P.J.L. Perez, C.P. Garcia, E.L. Fernandez, Surfactant cloud point extraction and preconcentration of organic compounds prior to chromatography and capillary electrophoresis, J. Chromatogr. A 902 (2000) 251–265.
[23] M.P.K. Choi, K.K.C. Chan, H.W. Leung, C.W. Huie, Pressurized liquid extraction of active ingredients (ginsenosides) from medicinal plants using nonionic surfactant solutions, J. Chromatogr. A 983 (2003) 153–162.
[24] Q. Fang, H.W. Yeung, H.W. Leung, C.W. Huie, Micellemediated extraction and preconcentration of ginsenosides from Chinese herbal medicine, J. Chromatogr. A 904 (2000) 47–55.
[25] J. He, Z. Zhao, Z. Shi, M. Zhao, Y. Li, W. Chang, Analysis of isoflavone daidzein in *Puerariae radix* with micelle-mediated extraction and preconcentration, J. Agric. Food Chem. 53 (2005) 518–523.
[26] C. Sun, Y. Xie, Q. Tian, H. Liu, Analysis of glycyrrhizic acid and liquiritin in liquorice root with microwave-assisted micellar extraction and preconcentration, Phytochem. Anal. 19 (2008) 160–163.
[27] B. Zanolari, K. Ndjoko, J.R. Ioset, A. Marston, K. Hostettmann, Qualitative and quantitative determination of yohimbine in authentic yohimbe bark and in commercial aphrodisiacs by HPLC-UV–API/MS methods, Phytochem. Anal. 14 (2003) 193–201.
[28] A. Kumar, M.K. Bhardwaj, A.K. Upadhyay, A. Tiwari, B.D. Ohdar, Quantitative determination of yohimbine alkaloid in the different part of the *Rauvolfia tetraphylla*, J. Chem. Pharm. Res. 3 (2011) 907–910.
[29] S.K. Srivastava, A.K., Agrawal, S.C., Singh, V.K., Khanna, J., Singh, C., Nath, M.M., Gupta, S., Gupta, R.K., Verma, A., Pal, D.U.B., Bawankule, D., Sakia, A.K., Gupta, A., Maurya, S.P.S. Khanuja, Antipsychotic agents and standardized antipsychotic fractions from Rauwolfia tetraphylla and process of their isolation, 2010, WO/2010/113180.
[30] A. Maurya, S. Gupta, S.K. Srivastava, Preparative isolation of bioactive nitrile glycoside 'Niazirin' from the fruits of *Moringa oleifera* using fast centrifugal partition chromatography, Sep. Sci. Technol. 46 (2011) 1195–1199.
[31] A. Maurya, S.K. Srivastava, Preparative-scale separation of anticancer triterpenes from *Eucalyptus hybrid* by centrifugal partition chromatography, Sep. Sci. Technol. 46 (2011) 1189–1194.
[32] A. Maurya, S. Gupta, S. Negi, S.K. Srivastava, pH-Zone-refining centrifugal partition chromatography for preparative isolation and purification of steroidal glycoalkaloids from *Solanum xanthocarpum*, J. Sep. Sci. 32 (2009) 3126–3132.
[33] K. Shankar, S. Gupta, P. Srivastava, S.K. Srivastava, S.C. Singh, M.M. Gupta, Simultaneous determination of three steroidal glycoalkaloids in *Solanum xanthocarpum* by high performance-thin layer chromatography, J. Pharm. Biomed. Anal. 54 (2011) 497–502.
[34] K. Shankar, M.M. Gupta, S.K. Srivastava, D.U. Bawankule, A. Pal, S.P.S. Khanuja, Determination of bioactive nitrile glycoside(s) in drumstick (*Moringa oleifera*) by reverse phase HPLC, Food Chem. 105 (2007) 376–382.
[35] M.M. Qureshi, Isolation and structural studies on the chemical constituents of *Rhazya stricta*, *Alstonia macrophylla* and related medicinal plants, Thesis, University of Karachi/H.E.J. Research Institute of Chemistry, Pakistan, 1991, pp. 147–149, http://eprints.hec.gov.pk/730/1/571.htm.
[36] K. Honty, B.E. Gacs, G. Blasko, C. Szantay, Synthesis of yohimbines. 4. Synthesis of (±)-3-epi-alpha.-yohimbine and (±)-3,17-epi-alpha-yohimbine. carbon-13 NMR investigation of yohimbine stereoisomers, J. Org. Chem. 47 (1982) 5111–5114.
[37] ICH, Q2 (R1) validation of analytical procedures, in: Methodology in Proceeding of the International Conference on Harmonization, Geneva, Switzerland, 2005.
[38] IUPAC, Harmonized guidelines for single-laboratory validation of methods of analysis (IUPAC technical report), Pure Appl. Chem. 74 (2002) 835–855.
[39] V. Srivastava, M. Singh, R. Malasoni, K. Shanker, R.K. Verma, M.M. Gupta, A.K. Gupta, S.P.S. Khanuja, Separation and quantification of lignans in *Phyllanthus* species by a simple chiral densitometric method, J. Sep. Sci. 31 (2008) 47–55.
[40] A.K. Yadav, N. Tiwari, P. Srivastava, S.C. Singh, K. Shanker, R.K. Verma, M.M. Gupta, Iridoid glycoside-based quantitative chromatographic fingerprint analysis: a rational approach for quality assessment of Indian medicinal plant Gambhari (*Gmelina arborea*), J. Pharm. Biomed. Anal. 47 (2008) 841–846.

Journal of Pharmaceutical and Biomedical Analysis 66 (2012) 40–49

Contents lists available at SciVerse ScienceDirect

Journal of Pharmaceutical and Biomedical Analysis

journal homepage: www.elsevier.com/locate/jpba

Structural characterization of a novel degradant of the antifungal agent posaconazole

Wendy Zhong[a], Xi Yang[b], Weidong Tong[c], Gary E. Martin[a,*]

[a] Merck Research Laboratories, Discovery and Preclinical Sciences, Structure Elucidation Group, Summit, NJ 07901, United States
[b] Global Science and Technology Center, Merck Manufacturing Division, Summit, NJ 07901, United States
[c] Merck Research Laboratories, Discovery and Preclinical Sciences, Process Chemistry, Rahway, NJ 07065, United States

ARTICLE INFO

Article history:
Received 2 February 2012
Accepted 28 February 2012
Available online 10 March 2012

Keywords:
Posaconazole
Degradation product
LC/MS
NMR
1,1-ADEQUATE
HSQC-1,1-ADEQUATE

ABSTRACT

A number of degradants of the antifungal agent posaconazole have been isolated and characterized. Degradation chemistry occurs primarily in the piperazine moiety located near the center of the molecule and typically involves oxidative processes. At least one ring contraction product has also been fully characterized by MS and NMR methods. We report the isolation and characterization of a novel degradant of posaconazole in which remnants of the piperazine ring have been incorporated into a 1,4-benzodiazepine moiety. The structure of the novel degradant was unequivocally established through accurate mass measurements, MS/MS studies, H/D exchange, and a range of 2D NMR experiments that included 1,1-ADEQUATE and covariance calculated HSQC-1,1-ADEQUATE spectra.

© 2012 Elsevier B.V. All rights reserved.

1. Introduction

Posaconazole (**1**) is an antifungal agent with a broad spectrum of activity against a range of commonly encountered fungal pathogens including *Aspergillis*, *Candida*, and *Cryptococcus* species [1–4]. There have been several reports of the characterization of degradation products of the drug [5–7] as well as several NMR studies of the parent molecule [8–11]. The locus of degradation in the molecule has uniformly been the piperazine ring and has involved various oxidation products, and in one case a novel ring-contraction to a dihydroimidazolium-containing structure. A low level degradation product at around 0.05% (area%) was observed during the stability study in a drug formulation [7]. LC/MS accurate mass and LC/MS/MS experiments were initially conducted to characterize this unknown degradation product.

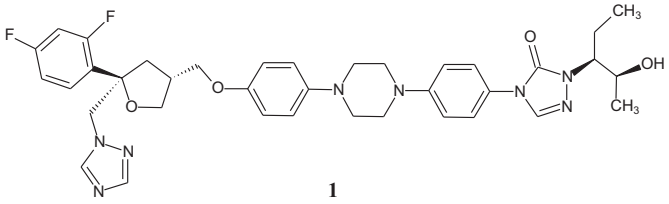

1

2. Materials and methods

2.1. LC/MS

LC/MS experiments were conducted using a Thermo LTQ^{TM}-Orbitrap instrument equipped with a Surveyor HPLC system. The high resolution LC/MS and LC/MS^n spectra were acquired in the FTMS mode of an Orbitrap instrument at a resolving power of 30,000 to obtain the elemental composition of each fragment ion. The electrospray ionization needle was held at 4.5 kV, and a nitrogen sheath gas (10 units) and a nitrogen auxiliary gas (20 units) were used to stabilize the spray. The heated capillary was set at 270 °C. All MS/MS experiments were conducted in the linear ion trap. Helium was introduced into the ion trap to improve the trapping efficiency and also serve as the collision gas for CID. Consequently, only helium can be used as collision gas with the Orbitrap instrument. The operational pressure after introducing helium was $\sim 2 \times 10^{-5}$ Pa in the linear ion trap.

* Corresponding author at: Merck Research Laboratories, Discovery and Preclinical Sciences, Structure Elucidation Group, 556 Morris Ave., S7-D1-1404, Summit, NJ 07901, United States. Tel.: +1 908 473 5378; fax: +1 908 473 6559.
E-mail addresses: gary.martin2@merck.com, lighthousephoto@gmail.com (G.E. Martin).

0731-7085/$ – see front matter © 2012 Elsevier B.V. All rights reserved.
doi:10.1016/j.jpba.2012.02.023

LC gradient conditions were 20% B to 100% B in 15 min at the flow rate of 200 μl/min. Mobile phase compositions were: (A) 0.1% formic acid in HPLC grade H_2O and (B) 0.1% formic acid in HPLC grade ACN. The sample was eluted using an XBridge C18 HPLC column, 2.1 mm × 150 mm, with 3.5 μm particle size. The sample was dissolved in ACN at the concentration of 1 mg/ml with the injection volume of 5 μl. On-line H/D exchange experiments were conducted *via* the same LC condition except that H_2O in mobile phase A was replaced by D_2O.

2.2. NMR spectroscopy

Preparative isolation yielded ~1 mg of the isolated degradant, **7**, albeit with a closely eluting 21% impurity present in the sample that was subsequently identified on the basis of accurate mass, MS/MS, and H/D exchange studies (see below) as **6**. The isolated degradant sample was dissolved in 35 μl of DMSO-d_6 (Cambridge Isotope Laboratories) and transferred to a Bruker 1.7 mm NMR tube using a 24G flexible Teflon™ needle and a Hamilton gas-tight syringe. All data were acquired using a Bruker 600 MHz AVANCE III, three channel NMR spectrometer equipped with a 1.7 mm MicroCryoProbe™.

NMR data for the confirmation of the structure of synthetically prepared **4**, included ^{1}H and ^{13}C reference spectra, COSY, multiplicity-edited HSQC (Fig. S1), 3, 5, and 8 Hz optimized ^{1}H–^{13}C HMBC spectra (see Fig. S2) and a 5 and 8 Hz optimized ^{1}H–^{15}N HMBC spectra (see Fig. S3). The data were acquired using a 2 mg sample dissolved in 200 μl of DMSO-d_6 (Cambridge Isotope Laboratories) and transferred to a 3 mm NMR (Wilmad) tube using a 19G flexible Teflon™ needle and a Hamilton gas-tight syringe. Data were acquired using a Varian 600 MHz three channel NMR spectrometer equipped with a 5 mm ColdProbe™ with the rf coil maintained at 20 K.

The ensemble of NMR spectra recorded for the isolated degradant sample, **7**, included one-dimensional ^{1}H and ^{13}C reference (6.5 h for the latter) spectra, COSY, multiplicity-edited HSQC (Fig. 3), 5 (Fig. 4) and 8 Hz (not shown) optimized ^{1}H–^{13}C HMBC, and a 4 Hz optimized ^{1}H–^{15}N HMBC spectrum (Supplemental Fig. S4). A 1,1-ADEQUATE spectrum [12–15] with the delays for $^1J_{CH}$ and $^1J_{CC}$ optimized for 145 and 60 Hz, respectively, was also acquired as a 2048 × 256 point file with 320 transients accumulated per t_1 increment using a 3 s interpulse delay, which gave an acquisition time of 72 h 28 m (see Fig. 5). The covariance calculated HSQC-1,1-ADEQUATE spectrum [15–19] was calculated using the generalized indirect covariance method of Snyder and Brüschweiler [20] to afford the spectrum shown in Fig. 6. Connectivities are traced for some of the structural fragments of the molecule in Supplemental Figs. S5 and S6.

3. Results and discussion

LC/MS accurate mass measurement of the protonated degradant molecule at RT = 8.8 min was *m/z* 687.32133, which corresponds to an empirical formula of $C_{36}H_{41}F_2N_8O_4$ $[M+H]^+$. Hence, the degradant, relative to the parent molecule with molecular formula of $C_{37}H_{43}F_2N_8O_4$ $[M+H]^+$, corresponds to the loss of a methylene. LC/MS/MS experiments were conducted in an attempt to obtain more structure information. Fig. 1A shows the MS/MS spectrum of the degradant from stressed drug product. The major fragment ion at *m/z* 669 is the water loss from the precursor ion. The fragment ion at *m/z* 278, **2**, is the result of the cleavage between the C–O connecting the tetrahydrofuran ring and phenyl ring. The fragment ion at *m/z* 516 was generated *via* the loss of the triazolone and aliphatic side chain represented by **3**. The MS/MS data localized the site of the degradation to the piperazine portion of the molecule, suggesting a ring-contraction, potentially to a tetrahydroimidazole, **4**, similar to

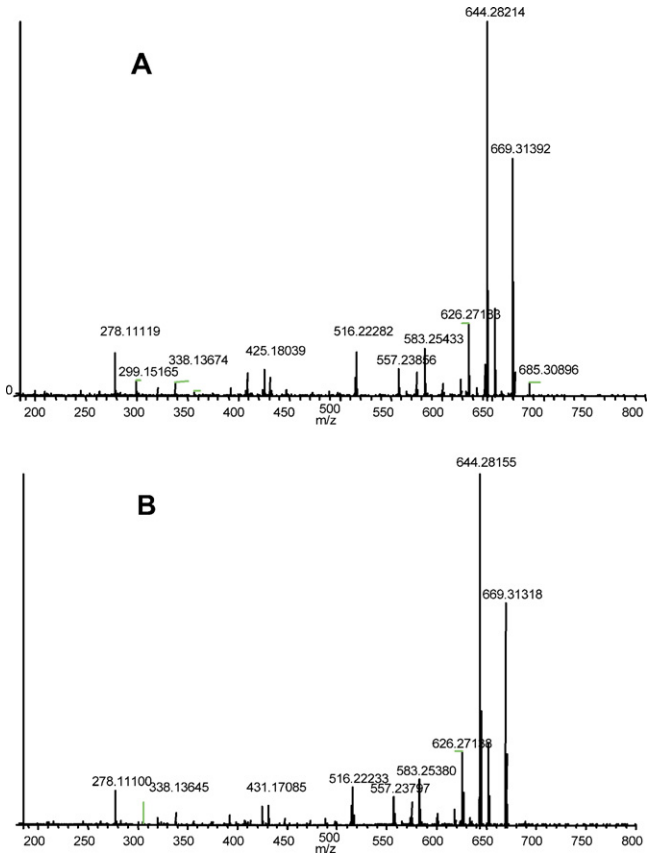

Fig. 1. (A) MS/MS spectrum of the degradation product, **7**, at RT = 8.8 min. (B) MS/MS spectrum of the synthetic compound, **4**, at RT = 11.14 min.

the dihydroimidazolium degradant recently reported [7,11]. Unfortunately, the initial sample was insufficient to obtain reliable LC/MS on-line H/D exchange data. Compound **4** was synthesized and subsequently characterized by MS and NMR methods. Despite the fact that the accurate mass data and MS/MS fragmentation data for **4** as shown in Fig. 1B are essentially identical to those of the degradation product at RT = 8.8 min. The retention time for **4** was significantly different than the degradation product at RT = 11.14 min.

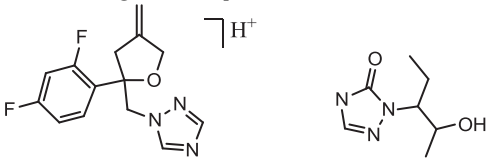

2 **3**

The lack of congruence between the retention time of synthetically prepared **4** and the actual degradant of posaconazole from stressed drug product sample observed chromatographically prompted further mass spectrometric experiments. Following the preparation of a suitable sample, H/D exchange was undertaken to gain further insight into the structure of the degradation product. The measured accurate mass for the deuterated degradation product at RT = 8.8 min is *m/z* 690.34427, which corresponds to an empirical formula of $C_{36}H_{38}D_3F_2N_8O_4$ $[M+H]^+$ with an error of 5.95 ppm. The measured accurate mass for the deuterated synthetic compound, **4**, is at *m/z* 689.33313, corresponding to an empirical formula of $C_{36}H_{39}D_2F_2N_8O_4$ $[M+H]^+$ with an error of −1.10 ppm. The data suggest that the degradation product eluting at RT = 8.8 min contains two exchangeable protons and one ionizing deuteron while the synthetic compound, **4**, has one exchangeable proton and one ionizing deuteron. The H/D exchange data preclude

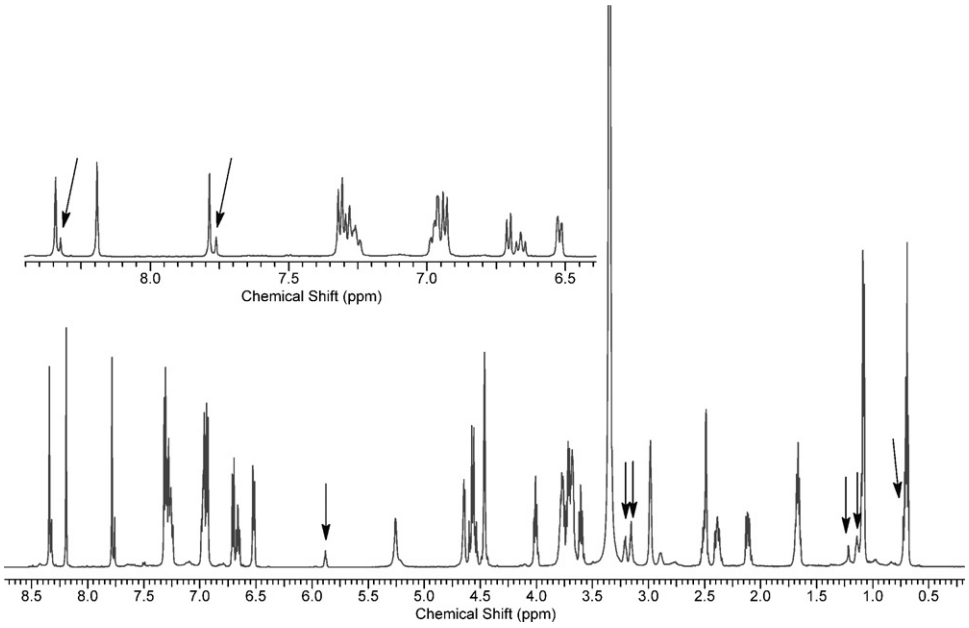

Fig. 2. 600 MHz ^{1}H NMR spectrum of the isolated degradant dissolved in 35 μl of DMSO-d_6. The spectrum was recorded using a Bruker Avance III three channel NMR spectrometer equipped with a 1.7 mm MicroCryoProbe™. Resolved resonances from the 21% impurity, **6**, contained in the sample are designated by arrows.

4 as the correct structure of the degradant. These observations spurred the consideration of alternative structural proposals in parallel with the preparative isolation of the degradant. The NMR spectral assignment of **4** was straightforward and readily accomplished from a standard suite of NMR experiments that included the one-dimensional ^{1}H and ^{13}C reference spectra, COSY, multiplicity-edited HSQC, 5 Hz optimized ^{1}H–^{13}C HMBC and 6 Hz optimized ^{1}H–^{15}N HMBC spectra. Complete NMR assignments for **4** are summarized in Table 1.

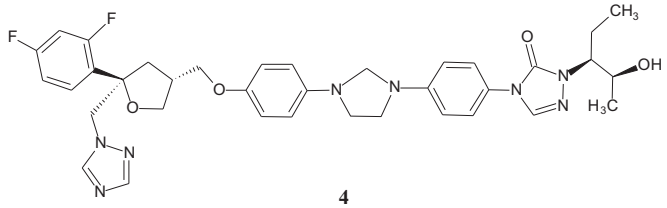

4

Based on both the empirical formula derived from the accurate mass measurements and the observed MS/MS fragmentation behavior the alternative ring-opened N-methyl structure, **5**, with an ethene linkage between the nitrogens were proposed, which could potentially account for the fragmentation and the H/D exchange data available. The structure of **5** shown is consistent with the MS/MS data. The alternative structure with the methyl group attached to the other piperidine-derived nitrogen can be excluded from consideration based on the MS/MS data.

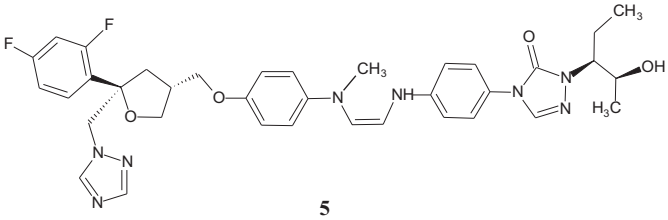

5

The 600 MHz ^{1}H reference spectrum recorded using a Bruker AVANCE III three channel 600 MHz NMR spectrometer equipped with a Bruker 1.7 mm MicroCryoProbe™ is shown in Fig. 2, with the resolved impurity resonances from **6**, which was identified by accurate mass and MS/MS measurements in comparison with authentic material. The resolved resonances from **6** in Fig. 2 are designated by arrows.

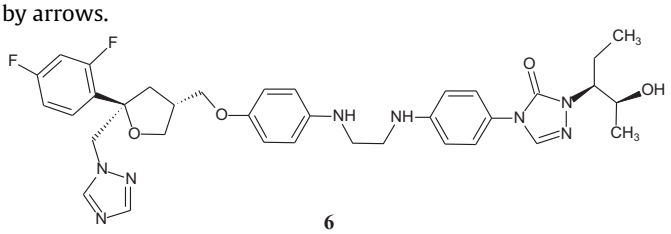

6

The lack of an N-methyl signal in the multiplicity-edited HSQC spectrum (Fig. 3) in conjunction with the ^{15}N shifts of the two piperazine-derived nitrogen resonances (62 and 70 ppm;

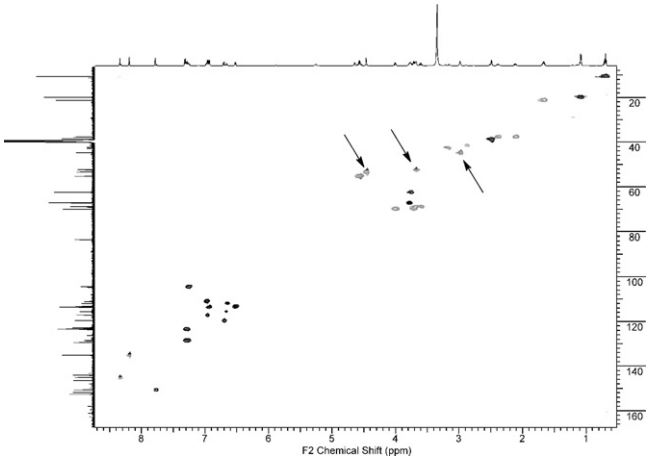

Fig. 3. Multiplicity-edited HSQC spectrum of the isolated posaconazole degradant, **7**. Methine/methyl resonances are plotted in black; methylene resonances have negative intensity and are plotted in gray. The three resonances designated by arrows arise from the three carbons of the remnants of the piperazine ring; the lack of a signal that could be assigned as the N-methyl resonance, in conjunction with the ^{15}N shifts (62 and 70 ppm see Supplemental Fig. S4) preclude the isomers of **5** as the structure of the degradation product.

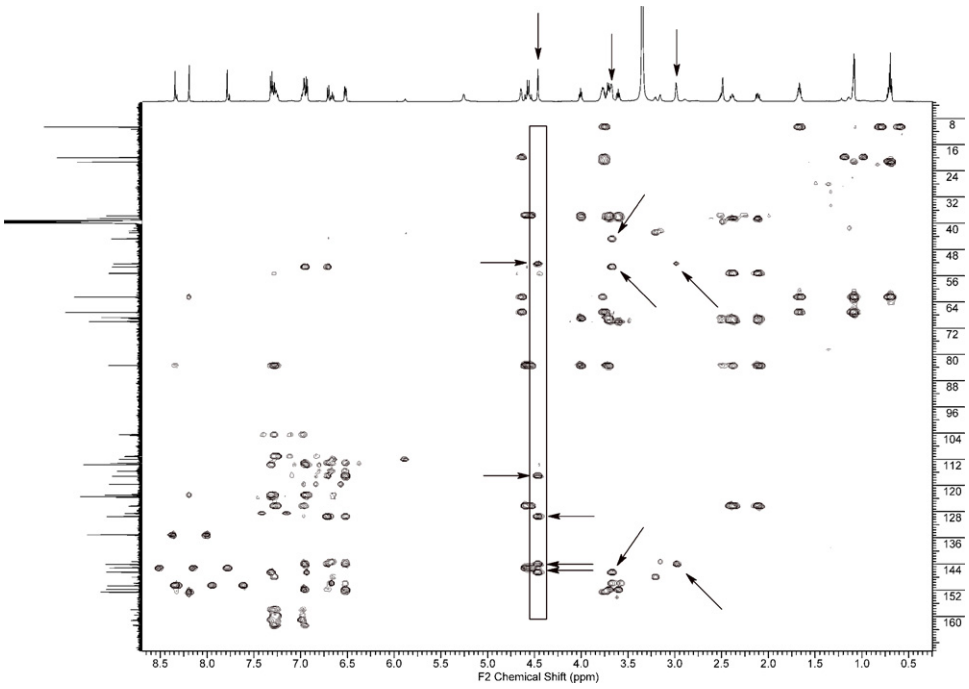

Fig. 4. The 5 Hz optimized $^{1}H–^{13}C$ HMBC spectrum of the isolated degradant, **7**. The data were acquired as a 4096 × 512 point matrix and were processed to afford the 2048 × 1024 point plot shown. The spectrum was acquired with 16 transients/t_1 increment, giving an acquisition time of 4 h 20 m. Correlations from the isolated methylene resonance at 4.47 ppm are contained in the boxed region and are designated by solid arrows; correlations form the vicinally coupled 3.67 and 2.98 ppm methylene resonances are designated by dashed arrows.

Supplemental Fig. S4) excluded structure **5** from consideration as the structure of the degradant [8]. Three methylene resonances attributable to the degradant were observed at 4.47/53.4 ($^{1}H/^{13}C$), 3.67/52.4, and 2.99/44.8 ppm, the latter two resonances corresponding to the ethylene bridge methylenes. In contrast, the corresponding methylenes of posaconazole resonate at 3.16/49.6 and 3.31/48.3 ppm while those of the tetrahydroimidazole analog, **4**, resonate at 4.55/66.4 for the methylene between the two

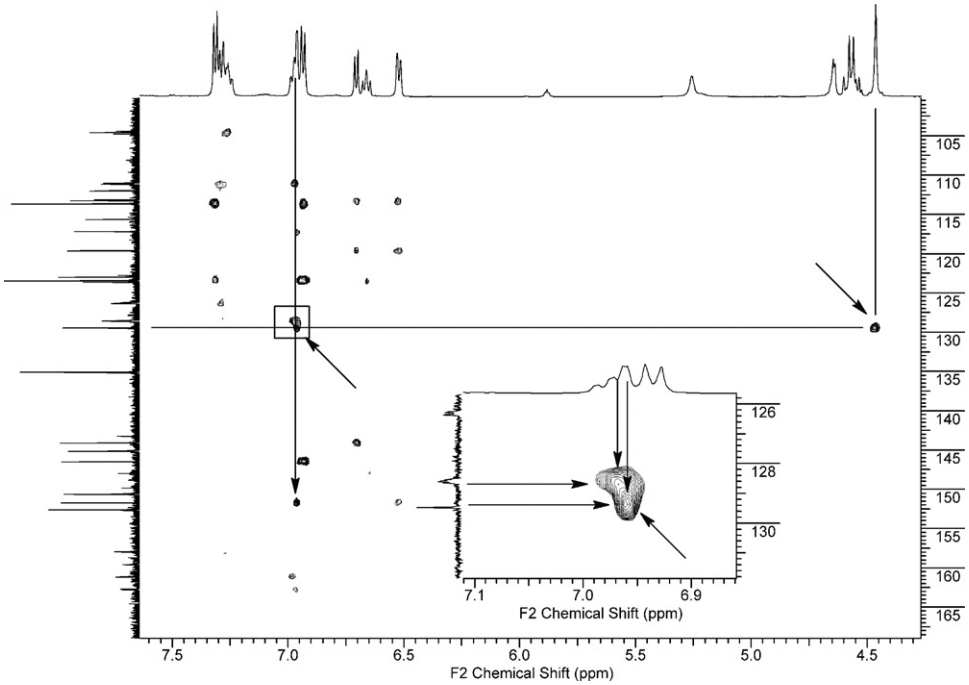

Fig. 5. Segment of the aromatic region of the 60 Hz optimized 1,1-ADEQUATE spectrum of the isolated degradant, **7**. The data were acquired with the sample dissolved in 35 μl of DMSO using a Bruker AVANCE III 600 MHz spectrometer equipped with a 1.7 mm MicroCryoProbe™. The data were acquired as a 2048 × 256 point file with 320 acquisitions accumulated per t_1 increment giving an acquisition time of 72 h 28 m. The data were processed to afford a final file that was 2048 × 1024 points. The correlation from the proton resonating at 4.47 ppm to the quaternary carbon resonating at 129.5 ppm is designated by an arrow. The correlation from the protonated aromatic carbon (6.99/117.2 ppm) to the non-protonated carbon is partially overlapped by another correlation as shown in the inset; the overlap in the inset is circumvented when the 1,1-ADEQUATE data are subjected to covariance processing with the multiplicity-edited HSQC spectrum as shown in Fig. 6.

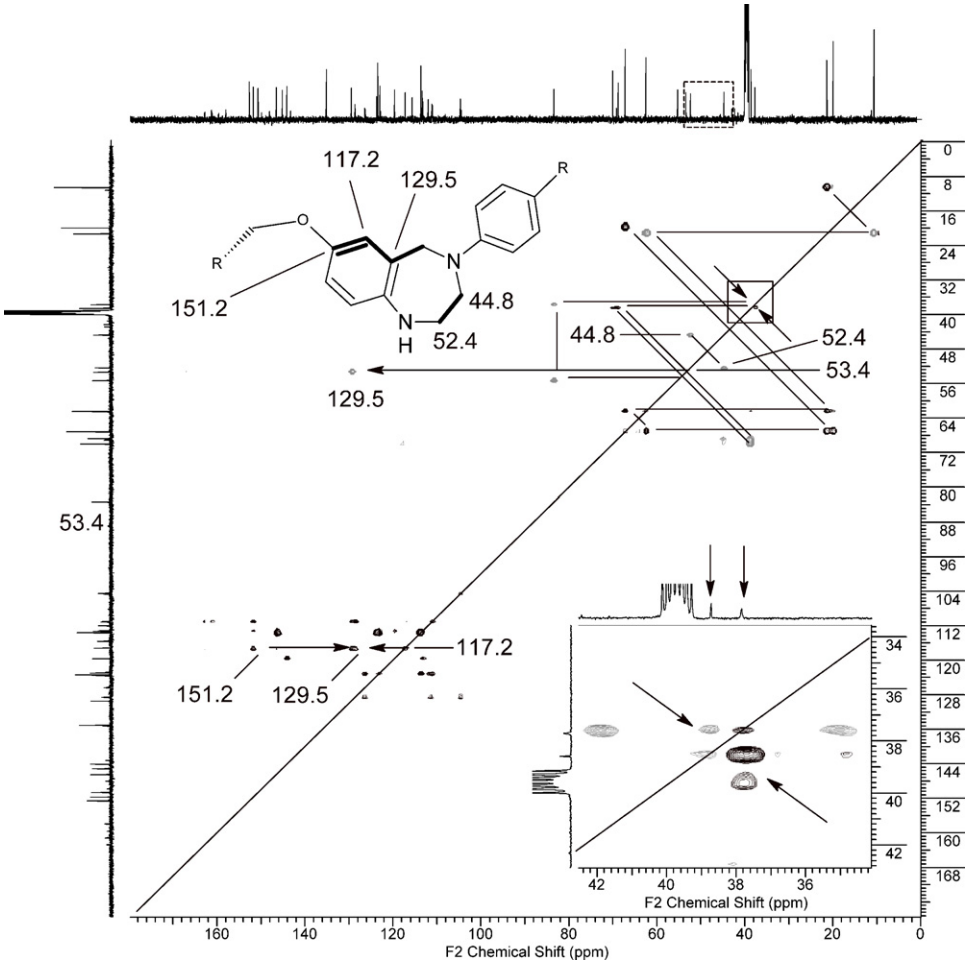

Fig. 6. The 60 Hz covariance calculated HSQC-1,1-ADEQUATE spectrum [15–19] of the isolated degradant, **7**, calculated using the generalized indirect covariance method [20], which was applied to the multiplicity-edited HSQC spectrum shown in Fig. 3 and the 60 Hz optimized 1,1-ADEQUATE spectrum shown in Fig. 5. The resulting covariance calculated HSQC-1,1-ADEQUATE spectrum is diagonally symmetric for protonated carbon pairs, *e.g.* the contiguous methylenes of the 1,4-benzodiazepine (C30 and C31; see Fig. 7 for the numbering scheme) and diagonally asymmetric for correlations between protonated and non-protonated adjacent carbons, *e.g.* the correlation from the 53.4 ppm methylene (C27) to the 129.5 ppm non-protonated aromatic carbon (C12) and the correlations from the 117.2 ppm protonated aromatic carbon (C13) and the flanking non-protonated carbons resonating at 129.5 and 151.2 ppm (C12 and C8, respectively). Through the series of correlations traced on the spectrum, the four carbon contiguous fragment designated by bolded bonds on the structure inset can be assembled. These correlations serve to establish that following ring-opening of the piperazine, the methylene reattached to the C12 aromatic carbon of the phenyl ring affording the 1,4-benzodiazepine structure shown, **7**. Cyclization in the other direction to the corresponding 1,4-benzodiazepine, **8**, can be conclusively ruled out based on the correlation from the 117.2 ppm protonated aromatic carbon to the oxygen-bearing non-protonated carbon resonating at 151.2 ppm. The three aliphatic carbons of the benzodiazepine ring (C27, C30, and C31) are contained within the dashed boxed region superimposed on the reference spectrum plotted above the contour plot. The inset region corresponds to the black boxed region astride the diagonal for the tetrahydrofuran moiety contained in the structure. Other correlations trace out the connectivity of the five carbon side chain (C46–C51) attached to the 1,2,4-triazolone ring, and the tetrahydrofuran moiety (C2–C6 and C20). Expansions showing the C2–C6 and C20 tetrahydrofuran and C46–C51 aliphatic side chain correlations are shown in Supplemental Figs. S5 and S6, respectively. The partial overlap of the correlation between the C12 and C13 in the 1,1-ADEQUATE spectrum (see inset, Fig. 5) is avoided in the covariance calculated HSQC-1,1-ADEQUATE spectrum.

nitrogens and at 3.60/46.3 and 3.53/46.9 ppm for the ethylene bridge methylene resonances.

Within the aromatic region of the multiplicity-edited HSQC spectrum, the three protonated carbon resonances associated with the triazole and triazolone rings were observed in the spectrum. Within the region of the spectrum generally associated with the two 1,4-disubstituted phenyl rings, there was one additional resonance observed. There are two possibilities to account for this observation. First, there could be an additional protonated carbon incorporated into the structure of the degradation product. This possibility was ruled out by the accurate mass data. Second, the symmetry of one of the two phenyl rings could have been disrupted by substitution causing the ring in question to exhibit three aromatic methine signals rather than the two normally observed for a 1,4-disubstituted phenyl. This later observation dovetails into the long-range correlations observed for the methylene carbon resonating at 4.47/54.3 ppm in the ^{1}H–^{13}C HMBC spectrum discussed below.

The 5 Hz optimized long-range ^{1}H–^{13}C HMBC spectrum was interesting in that it showed correlations for the methylene resonance at 4.47 ppm to carbons resonating at 52.4, 117.2, 129.5, 144.1, and 146.5 ppm (Fig. 4). The 52.4 ppm methylene was one of the methylenes derived from the remnant of the piperazine ring. The carbon resonating at 117.2 ppm is a protonated aromatic; the carbons resonating at 129.5, 144.1, and 146.5 ppm were all non-protonated aromatic carbons, the latter two exhibit ^{13}C chemical shifts consistent with carbons bound to the nitrogens derived from the piperazine ring. The latter two carbon shifts also established that the 4.47/53.4 ppm methylene must be contained in a ring structure to be able to exhibit

Table 1
^{1}H ^{13}C, and ^{15}N assignments for 4 in DMSO-d_6 at a regulated sample temperature of 30 °C. All data were recorded using a Bruker 600 MHz Avance III three channel spectrometer equipped with a TCI 1.7 mm MicroCryoProbe™. ^{13}C shifts were calculated using the v11.1 CNMR program; ^{15}N shifts were calculated using the NNMR program v11.1. Both programs were provided by ACDLabs. All chemical shifts were calculated using the neural network method.

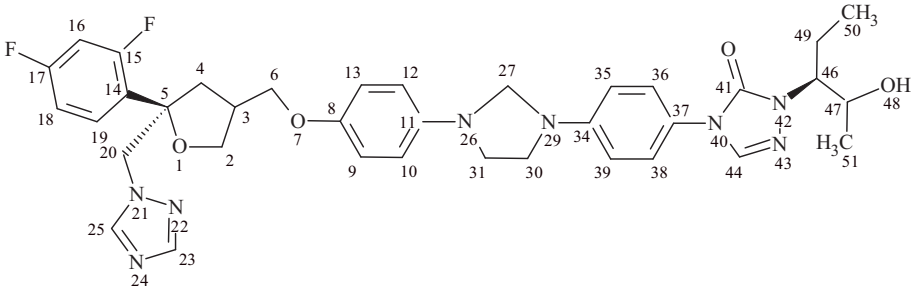

Position	$\delta^{1}H$ (ppm)	J_{CF} (Hz)	^{13}C (ppm)		^{15}N (ppm)	
			Obs.	Calc.	Obs.	Calc.
2	4.03, 3.75	–	69.9	70.1	–	–
3	2.52	–	38.4	40.0	–	–
4	2.39, 2.13	2.8	37.5	38.9	–	–
5	–	2.9	83.4	85.7	–	–
6	3.74, 3.65	–	69.0	70.7	–	–
8	–	–	151.2	153.9	–	–
9/13	6.72	–	114.1	114.9	–	–
10/12	6.84	–	115.5	116.4	–	–
11	–	–	141.4	141.6	–	–
14	–	13.0, 7.7	126.3	122.2	–	–
15	–	246.6, 12.1	158.8	160.8	–	–
16	7.29	27.0, 27.0	104.6	104.2	–	–
17	–	245.6, 12.1	162.0	163.9	–	–
18	7.00	20.5, 2.8	111.1	110.7	–	–
19	7.30	9.3, 5.6	128.4	128.6	–	–
20	4.61, 4.56	3.7	55.3	56.1	–	–
21	–	–	–	–	213	220
22	–	–	–	–	299	289
23	7.79	–	150.6	152.1	–	–
24	–	–	–	–	253	252
25	8.36	–	144.9	142.8	–	–
26	–	–	–	–	65	72
27	4.56	–	66.5	65.8	–	–
29	–	–	–	–	70	72
30	3.53[a]	–	47.1[a]	50.4	–	–
31	3.61[a]	–	46.5[a]	50.4	–	–
34	–	–	145.1	144.4	–	–
35/39	6.82	–	112.4	115.5	–	–
36/38	7.51	–	123.4	125.3	–	–
37	–	–	124.1	124.0	–	–
40	–	–	–	–	155	168
41	–	–	152.6	151.1	–	–
42	–	–	–	–	174	178
43	–	–	–	–	262	308
44	8.30	–	135.0	134.1	–	–
46	3.79	–	62.6	63.9	–	–
47	3.82	–	67.2	68.0	–	–
48-OH	4.64	–	–	–	–	–
49	1.70	–	21.3	22.2	–	–
50	0.74	–	10.7	11.6	–	–
51	1.11	–	20.0	19.8	–	–

[a] Assignments based on correlations observed to the flanking, nitrogen-bearing aromatic quaternary carbons in the 3 Hz optimized ^{1}H–^{13}C HMBC. Correlations from these resonances to the flanking nitrogen-bearing quaternary carbons were not observed in the 5 or 8 Hz optimized HMBC spectra.

long-range couplings to both nitrogen-bearing aromatic quaternary carbons.

Perhaps the most structurally definitive information was derived from a 60 Hz optimized 1,1-ADEQUATE [12–15] experiment performed on the sample that was subjected to generalized indirect covariance [20] processing to afford an covariance calculated HSQC-1,1-ADEQUATE spectrum [9,16–19]. Unlike the simple HMBC experiment, which does not provide unequivocal identification of adjacent carbon neighbors, *i.e.* those coupled *via* $^{2}J_{CH}$, in contrast, the 1,1-ADEQUATE experiment does exclusively that since magnetization transfers are *via* $^{1}J_{CH}$ and $^{1}J_{CC}$ couplings. The 60 Hz optimization of the 1,1-ADEQUATE experiment was based on work by Cheatham and co-workers [21], which demonstrated that better correlation intensity is observed for correlations between sp^2 and sp^3 carbons with 60 Hz optimization than for 40–50 Hz optimization. The $^{2}J^{3}J$-HMBC experiment [22] and H2BC experiment and variants [23–25] can identify adjacent protonated carbons *via* $^{2}J_{CH}$ couplings but not adjacent non-protonated carbons. From a sensitivity standpoint, the 1,1-ADEQUATE experiment is considerably less sensitive than HMBC and related experiments. Recent work by several labs, however, has shown that samples of a few milligrams can afford usable data when the sample is

Table 2
^{1}H, ^{13}C, and ^{15}N assignments for 7 in DMSO-d_6 at a regulated sample temperature of 30 °C. All data were recorded using a Bruker 600 MHz Avance III three channel spectrometer equipped with a TCI 1.7 mm MicroCryoProbe™. ^{13}C shifts were calculated using the v11.1 CNMR program; ^{15}N shifts were calculated using the NNMR program v11.1. Both programs were provided by ACDLabs. All chemical shifts were calculated using the neural network method. See Fig. 7 for the numbering scheme for 7.

Position	δ^{1}H (ppm)	J_{CF} (Hz)	^{13}C (ppm)		^{15}N (ppm)	
			Obs.	Calc.	Obs.	Calc.
2	4.02, 3.71	–	70.0	69.9	–	–
3	2.51	–	38.6	40.4	–	–
4	2.39, 2.12	–	37.7	39.0	–	–
5	–	3.6	83.4	85.7	–	–
6	3.71, 3.60	–	68.8	70.2	–	–
8	–	–	151.2	153.6	–	–
9	6.52	–	113.0	114.2	–	–
10	6.70	–	119.7	114.4	–	–
11	–	–	144.1	141.6	–	–
12	–	–	129.5	126.2	–	–
13	6.96	–	117.2	116.5	–	–
14	–	11.8, 3.6	126.3	122.2	–	–
15	–	247.0, 12.7	158.8	160.8	–	–
16	7.25	26.3, 26.3	104.6	104.2	–	–
17	–	246.1, 12.7	161.9	163.9	–	–
18	6.97	20.9, 3.6	111.1	110.7	–	–
19	7.28	9.1, 6.4	128.6	128.6	–	–
20	4.57	2.7	55.3	56.1	–	–
21	–	–	–	–	212	220
22	–	–	–	–	299	289
23	7.78	–	150.5	152.1	–	–
24	–	–	–	–	252	252
25	8.34	–	145.1	142.8	–	–
26	–	–	–	–	70	78
27	4.47	–	53.4	56.4	–	–
29	–	–	–	–	62	58
30	3.67	–	44.8	46.2	–	–
31	2.98	–	52.4	52.8	–	–
34	–	–	146.5	146.8	–	–
35/39	6.94	–	113.6	115.6	–	–
36/38	7.30	–	123.5	124.8	–	–
37	–	–	123.5	123.8	–	–
40	–	–	–	–	155	168
41	–	–	152.6	151.1	–	–
42	–	–	–	–	174	184
43	–	–	–	–	262	268
44	8.20	–	135.1	134.1	–	–
46	3.76	–	62.5	63.9	–	–
47	3.79	–	67.2	68.0	–	–
48-OH	5,43	–	–	–	–	–
49	1.67	–	21.2	22.2	–	–
50	0.70	–	10.6	11.6	–	–
51	1.08	–	20.0	19.8	–	–

dissolved in sufficient solvent for a 3 mm tube to be run coaxially in a 5 mm cryoprobe [15]; instruments equipped with 1.7 mm MicroCryoProbes™ can push sample requirements below 1 mg, particularly when the data will be subjected to unsymmetrical indirect covariance (UIC) [26] or generalized indirect covariance (GIC) processing [20] to calculate the corresponding covariance calculated HSQC-1,1-ADEQUATE spectrum [9,15–19].

The 60 Hz optimized 1,1-ADEQUATE spectrum of the isolated degradant is shown in Fig. 4; the covariance calculated HSQC-1,1-ADEQUATE spectrum calculated from the multiplicity-edited HSQC and the 1,1-ADEQUATE spectrum is shown in Fig. 5. Both spectra afford the same carbon–carbon correlation network generally with higher signal-to-noise and fewer problems associated with response overlap in the latter. Additionally, the former generally will need to be interpreted either side-by-side with a HSQC spectrum or with the two spectra superimposed [15] whereas the latter allows carbon–carbon connectivity to be determined directly from the spectrum.

The methylene resonant pair observed at 4.47/53.4 ppm was shown to be directly linked to the non-protonated aromatic carbon resonating at 129.5 ppm in the 1,1-ADEQUATE and covariance calculated HSQC-1,1-ADEQUATE spectra shown in Figs. 4 and 5, respectively. The 129.5 ppm quaternary carbon is correlated to a protonated aromatic carbon resonant pair at 6.99/117.2 ppm, which is, in turn, correlated to a non-protonated aromatic carbon resonating at 151.2 ppm. This series of carbon–carbon correlations irrefutably establishes the structure of the ring formed from the remnants of the piperazine ring as the 1,4-benzodiazepine structure shown in the inset in Figs. 5 and 6, and by **7**. The ADEQUATE-derived carbon–carbon correlation data also preclude the alternative isomeric benzodiazepine structure, **8**, that would arise from the formation of a carbon–carbon bond between the C27 methylene and the C35 aromatic carbon.

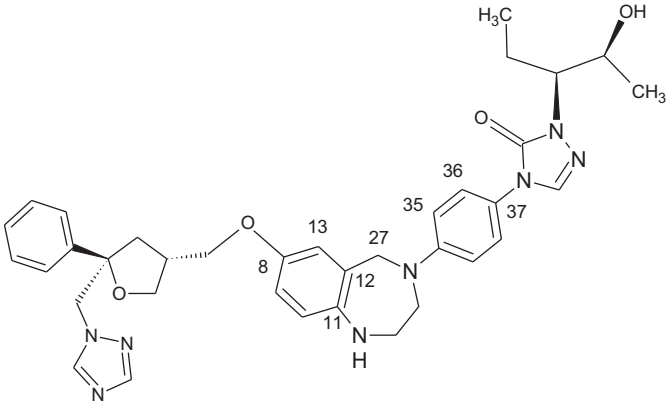

7

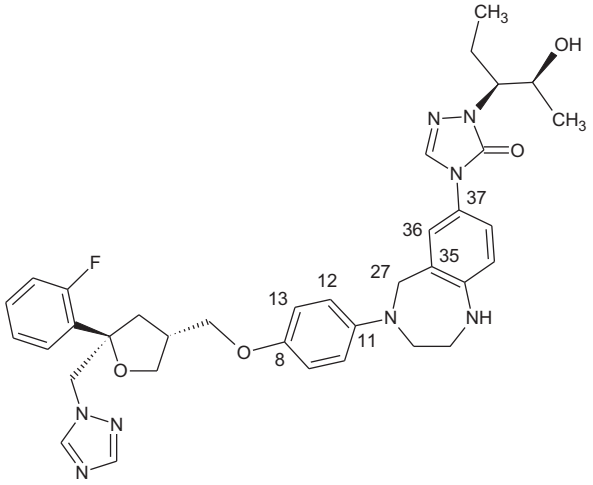

8

While the correlation from the 6.99/117.2 ppm protonated carbon to the 129.5 ppm non-protonated carbon is partially overlapped by another correlation in the conventional 1,1-ADEQUATE spectrum shown in Fig. 5 (see inset), that is not the case in the covariance calculated HSQC-1,1-ADEQUATE spectrum and the correlation is cleanly identifiable.

When the ADEQUATE data are considered in conjunction with the long-range ^{1}H–^{13}C and ^{1}H–^{15}N correlations as well as the proton–proton correlations from a 400 ms ROESY experiment, the constitution of the 1,4-benzodiazepine moiety in the structure of the degradant is rigorously established. The various long-range heteronuclear and homonuclear ROESY correlations, as well as the carbon–carbon correlations critical to the determination of the structure, are summarized in Fig. 7. Complete ^{1}H, ^{13}C, and ^{15}N NMR assignments for **7** are summarized in Table 2.

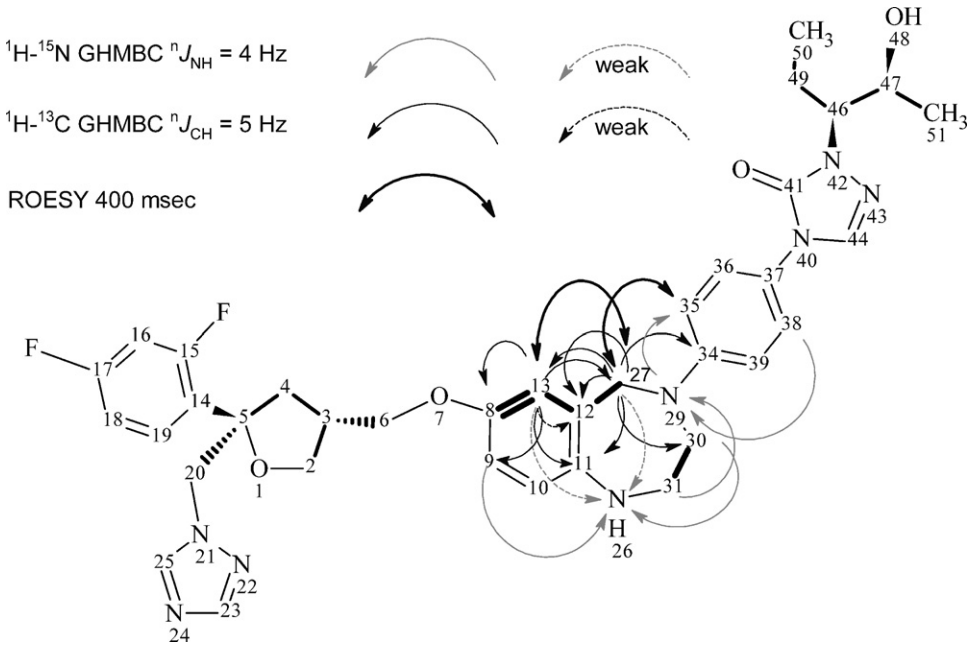

Fig. 7. Correlations used to establish the 1,4-benzodiazepine structure of the isolated posaconzole degradant, **7**. Various heteronuclear through bond and homonuclear through space (ROESY) correlations are designated by arrows between the correlated resonances. The bonds shown in bold were directly established from the 1,1-ADEQUATE/HSQC-1,1-ADEQUATE spectra.

The fragmentation pathways for the confirmed degradation product structure, **7**, at RRT = 8.8 min and synthetic compound **4** are shown in Schemes 1 and 2, respectively. The accurate masses of the major fragment ions for synthetically prepared **4** and the isolated degradant, **7**, were identical. Atypically, the relative intensities of the major fragment ions for the two molecules were also nearly the same. One major fragment ion at *m*/*z* 669 can be rationalized as the water loss from both molecules. The fragment ions at *m*/*z* 278 and *m*/*z* 516 do not involve the piperazine-derived structural moieties. One important fragment ion at *m*/*z* 425 is worth noting. The presence of the fragment ion at *m*/*z* 425 indicated that the methylene is connected to the phenyl ring to the "left" of the piperazine (as drawn) instead of the phenyl to the "right", which is consistent with **7** but not **8**. The fragment ions at *m*/*z* 669 and

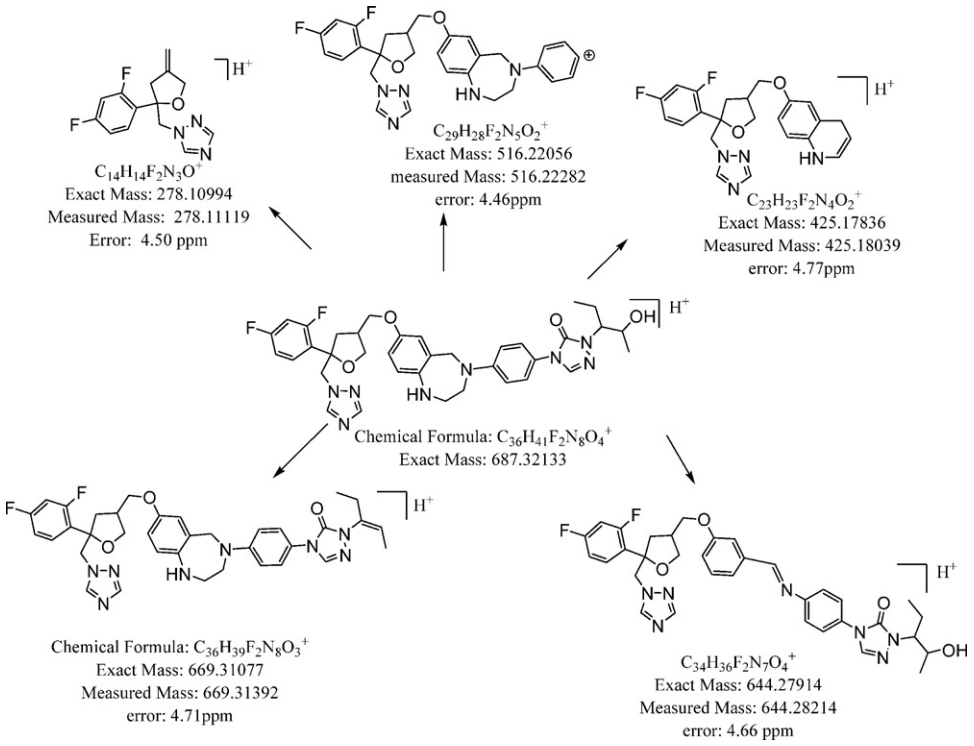

Scheme 1. The fragmentation pathway derived from MS/MS data of the degradant identified as **7** in this study.

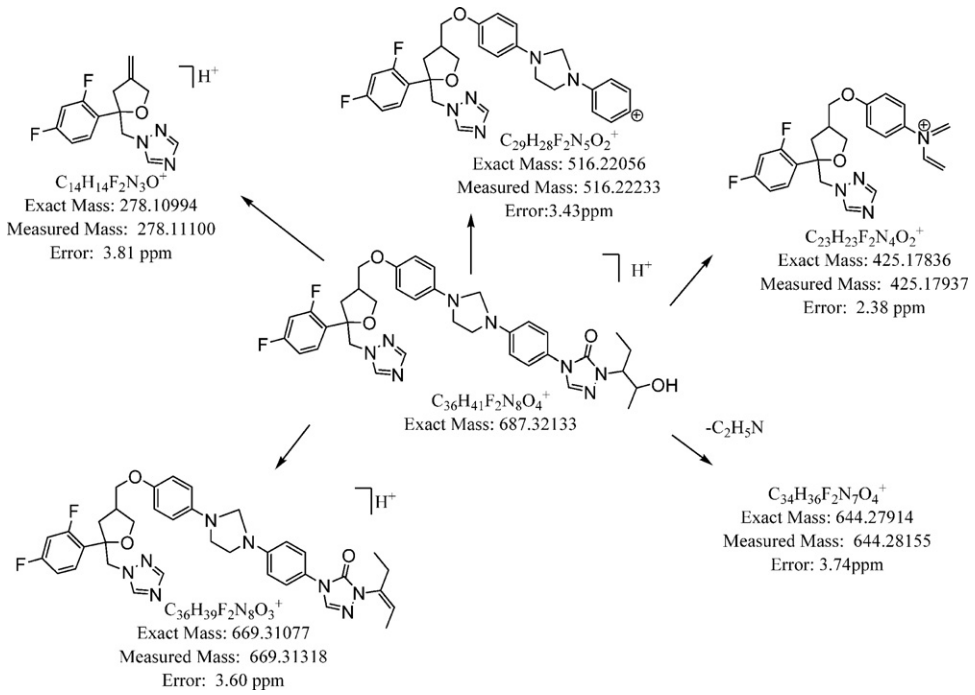

Scheme 2. The fragmentation pathway derived from MS/MS data of the synthesized compound **4** at RT = 11.14 min.

m/*z* 278 were also the important fragment ion in the posaconzole API itself [7]. Furthermore, the most dominant fragment ion present in MS/MS spectra of both unknown degradant and synthetic compound are at *m*/*z* 644. The measured accurate mass for this fragment ion at *m*/*z* 644 corresponds to an empirical formula of $C_{34}H_{36}F_2N_7O_4^+$, which is the result of the loss of C_2H_5N moiety from the precursor ion. The proposed structure of this fragment ion from structure **7** is shown in Scheme 1, while the location where the loss of C_2H_5N moiety occurred on structure **4** has not been determined.

4. Conclusions

The structure of a thermally induced degradant of the antifungal agent posaconazole (**1**) has been unequivocally assigned on the basis of accurate mass, MS/MS, H/D exchange, and an array of 2D NMR methods. The unequivocal determination of the structure relied on the acquisition of 1,1-ADEQUATE data that were subjected to generalized indirect covariance processing with a multiplicity-edited HSQC spectrum to afford the corresponding covariance calculated HSQC-1,1-ADEQUATE spectrum that allowed much of the carbon skeleton of the molecule to be directly traced out, confirming the novel formation of a 1,4-benzodiazepine moiety from the remnants of the piperazine moiety and one of the 1,4-disubstituted phenyl rings in the posaconazole structure as shown by **7**. The availability of these carbon–carbon connectivity data also allowed an alternative benzo-1,4-diazepine cyclization product, **8**, to be excluded as a possible structure for the degradant.

The fact that the fragmentation pattern and even the relative ion intensities of the various fragment ions for synthetically prepared **4** and the isolated degradant **7** are identical and nearly identical, respectively, serves to highlight the considerable challenge that can be encountered in the characterization of impurities and degradation products of complex pharmaceutical agents. This example further underscores the degree of care that must be taken to insure that such structures are unequivocally and rigorously characterized using both MS and NMR methods.

Appendix A. Supplementary data

Supplementary data associated with this article can be found, in the online version, at doi:10.1016/j.jpba.2012.02.023.

References

[1] K.L. Oakley, B.B. Moore, D.W. Denning, In vitro activity of SCH-56592 and comparison with activities of amphotericin B and itraconazole against *Aspergillus* spp., Antimicrob. Agents Chemother. 41 (1997) 1124–1126.
[2] D. Law, C.B. Moore, D.W. Denning, Activity of SCH-56592 compared with fluconazole and itraconazole against *Candida* spp., Antimicrob. Agents Chemother. 41 (1997) 2310–2311.
[3] J.R. Cox, G.M. Perfect, R.K. Dodge, W.A. Schell, In vitro and in vivo efficacies of the azole SCH-56592 against *Cryptococcus neoformans*, Antimicrob. Agents Chemother. 40 (1996) 1910–1913.
[4] Y. Koltin, C.A. Hitchcock, The search for new triazole antifungal agents, Curr. Opin. Chem. Biol. 1 (1997) 176–182.
[5] W. Feng, H. Liu, G. Chem, R. Malchow, F. Bennett, E. Liln, B. Pramanik, T.-M. Chen, Structural characterization of the oxidative degradation products of an antifungal agent SCH-56592 by LC-NMR and LC–MS, J. Pharm. Biomed. Anal. 25 (2001) 545–557.
[6] G. Chen, B.M. Warrack, A.K. Goodenough, Analysis of impurities and degradations in pharmaceuticals by high resolution tandem mass spectrometry and on-line H/D exchange LC/MS, Am. Pharm. Rev. 13 (2010) 20–27.
[7] W. Zhong, J. Yang, X. Yang, Structural determination of an unknown drug product using CASI technology in a Fourier transform ion cyclotron resonance mass spectrometer, Rapid Commun. Mass Spectrom. 25 (2011) 3651–3655.
[8] B.D. Hilton, W. Feng, G.E. Martin, Assignment of the ^{15}N resonances of the antifungal agent posaconazole, J. Heterocycl. Chem. 48 (2010) 948–951.
[9] G.E. Martin, Posaconazole application of HSQC-ADEQUATE from general indirect covariance processing, J. Heterocycl. Chem., in press.
[10] B.D. Hilton, G.E. Martin, The impact of long-range ^{1}H–^{15}N heteronuclear shift correlation data on computer-assisted structure elucidation: posaconzole, J. Heterocycl. Chem., in press.
[11] W. Feng, B.D. Hilton, W. Zhong, J. Yang, X. Yang, W. Tong, G.E. Martin, Characterization of an unusual ring-contraction degradant of the antifungal agent posaconazole, Magn. Reson. Chem., submitted.
[12] M. Köck, B. Reif, W. Fenical, C. Griesinger, Differentiation of HMBC two- and three-bond correlations: a method to simplify the structure determination of natural products, Tetrahedron Lett. 37 (1996) 363–366.
[13] B. Reif, M. Köck, R. Kerrsebaum, H. Kang, W. Fenical, C. Griesinger, ADEQUATE a new set of experiments to determine the constitute of small molecules at natural abundance, J. Magn. Reson. 118A (1996) 282–285.
[14] M. Köck, R. Kerrsebaum, W. Bermel, A broadband ADEQUATE pulse sequence using chirp pulses, Magn. Reson. Chem. 43 (2003) 65–69.

[15] G.E. Martin, Using 1,1- and 1,n-ADEQUATE 2D NMR data in structure elucidation protocols, in: G.A. Webb (Ed.), Ann. Rep. NMR Spectrosc., vol. 74, Elsevier, Amsterdam, 2011, pp. 215–291.
[16] G.E. Martin, B.D. Hilton, K.A. Blinov, HSQC-ADEQUATE correlation: a new paradigm for establishing a molecular skeleton, Magn. Reson. Chem. 49 (2011) 248–252.
[17] G.E. Martin, B.D. Hilton, M.R. Willcott III, K.A. Blinov, HSQC-ADEQUATE: an investigation of data requirements, Magn. Reson. Chem. 49 (2011) 350–357.
[18] G.E. Martin, D. Sunseri, Establishing the carbon skeleton of pharmaceutical agents using HSQC-ADEQUATE spectra, J. Pharm. Biomed. Anal. 55 (2011) 895–901.
[19] E.R. Zartler, G.E. Martin, The use of ^{1}H–^{31}P HMBC and covariance NMR to unambiguously determine phosphate ester linkages in complex polysaccharide mixtures, J. Biomol. NMR 51 (2011) 357–367.
[20] D.A. Snyder, R. Brüschweiler, Generalized indirect covariance NMR formalism for the establishment of multidimensional spin correlations, J. Phys. Chem. A 113 (2009) 12898–12903.
[21] S.F. Cheatham, M. Kline, R.R. Sasaki, K.A. Blinov, M.E. Elyashberg, S.G. Molodtsov, Enhanced automated structure elucidation by inclusion of two-bond specific data, Magn. Reson. Chem. 48 (2010) 571–574.
[22] V.V. Krishnamurth, D.J. Russell, C.E. Hadden, G.E. Martin, $^{2}J^{3}J$-HMBC: a new long-range heteronuclear shift correlation technique capable of differentiating $^{2}J_{CH}$ from $^{3}J_{CH}$ correlations to protonated carbons, J. Magn. Reson. 146 (2000) 232–239.
[23] N.T. Nyberg, J.Ø. Duus, O.W. Sørensen, Heteronuclear two-bond correlation: suppressing heteronuclear three-bon or higher NMR correlations while enhancing two-bond correlations even for vanishing $^{2}J_{CH}$, J. Am. Chem. Soc. 127 (2005) 6154–6155.
[24] N.T. Nyberg, J.Ø. Duus, O.W. Sørensen, Editing of H2BC NMR spectra, Magn. Reson. Chem. 43 (2005) 971–974.
[25] A.J. Benie, O.W. Sørensen, HAT-HMBC. A hybrid of H2BC and HMBC overcoming shortcomings of both, J. Magn. Reson. 184 (2007) 315–321.
[26] K.A. Blinov, N.I. Larin, A.J. Williams, M. Zell, G.E. Martin, Long-range carbon–carbon connectivity via unsymmetrical indirect covariance processing of HSQC and HMBC NMR data, Magn. Reson. Chem. 44 (2006) 143–147.

Journal of Pharmaceutical and Biomedical Analysis 66 (2012) 50–57

Contents lists available at SciVerse ScienceDirect

Journal of Pharmaceutical and Biomedical Analysis

journal homepage: www.elsevier.com/locate/jpba

Triprotic site-specific acid–base equilibria and related properties of fluoroquinolone antibacterials

Aura Rusu[a], Gergő Tóth[b], Levente Szőcs[b], József Kökösi[b], Márta Kraszni[b], Árpád Gyéresi[a], Béla Noszál[b,*]

[a] Department of Pharmaceutical Chemistry, University of Medicine and Pharmacy, 540139 Targu Mures, 38 Gh. Marinescu, Romania
[b] Department of Pharmaceutical Chemistry, Semmelweis University, Research Group of Drugs of Abuse and Doping Agents, Hungarian Academy of Sciences, Budapest H-1092, Hőgyes Endre u. 9, Hungary

ARTICLE INFO

Article history:
Received 11 January 2012
Received in revised form 27 February 2012
Accepted 28 February 2012
Available online 7 March 2012

Keywords:
NMR
Microspeciation
Fluoroquinolone
p*K*a
Protonation constant

ABSTRACT

The complete macro- and microequilibrium analyses of six fluoroquinolone drugs – ciprofloxacin, enrofloxacin, norfloxacin, pefloxacin, ofloxacin and moxifloxacin – are presented. Previous controversial literature data are straightened up, the protonation centers are unambiguously identified, and the protonation macro- and microconstant values are reported. The macroconstants were determined by ^{1}H NMR-pH titrations while the microconstants were determined by a multi-modal spectroscopic-deductive methodology, in which methyl ester derivatives were synthesized and their NMR-pH titration data contributed to the evaluation of all the microconstants. The full ^{1}H, ^{13}C and ^{15}N NMR assignments, NMR-pH profiles, macro- and microprotonation schemes and species-specific diagrams are included. Our studies show that the fluoroquinolones have three protonation centers: the carboxylate group, the N-1′ and N-4′ piperazine nitrogens and concentration of the uncharged microspecies is way below the values published earlier. The results could be well interpreted in terms of structural properties. The protonation macro- and microconstant values allow the pre-planned method development in techniques such as capillary zone electrophoresis and also, the interpretation of fluoroquinolone mechanism of biological action, including the pharmacokinetic properties, and antibacterial activities that are all heavily influenced by the states of protonation.

© 2012 Elsevier B.V. All rights reserved.

1. Introduction

Medicinal quinolones are synthetic antibacterial agents, introduced into the therapy in the early 1960s, when nalidixic acid was discovered for the treatment of urinary tract infections. A major therapeutic progress occurred with the insertion of a fluorine atom into the 6th position of the quinolone cycle, resulting in fluoroquinolone compounds (FQs) with broad antimicrobial activity, including Gram-negative, Gram-positive, anaerobe and highly resistant strains [1]. The addition of an extra ring or ring system, containing basic nitrogen to the C-7 position further improves the antibacterial activity and also, the pharmacokinetic properties. A number of subsequent structural and formulatory modifications have improved their therapeutic properties [2–5]. FQs poison the catalytic activity of the bacterial topoisomerase by a sterically effective interaction with the single-stranded DNA gyrase complex [6]. We studied 6 FQs, the structures of which are shown in Fig. 1.

It has long been known that the acid–base properties of drugs influence their pharmacokinetic behavior. In particular, the activity of FQs is reported to be pH-dependent, the binding of the bacterial DNA gyrase enzyme is therefore assumed to be dependent on the protonation states of FQs [7–9]. It is of crucial importance therefore to know the exact values of the protonation constants of FQs. The protonation of the compounds can be characterized in terms of protonation macroconstants and microconstants.

Macroscopic equilibrium constants (expressed either as dissociation constants p*K*a or protonation constants log *K*) of multiprotic molecules depict the acid–base properties of the compound as a whole. These are useful parameters to characterize large drug molecules [10]. The overall charge of the compound is primarily related to the macroscopic protonation constant, whereas the moieties and site-specific charges can be determined from the microscopic protonation constants. Latters are also primarily related to the interaction with the biological target. Microconstants describe the proton binding ability of the individual functional groups and are useful in calculating the pH-dependent concentrations of the

* Corresponding author at: Department of Pharmaceutical Chemistry, Semmelweis University, Budapest H-1092, Hőgyes Endre u. 9, Hungary.
Tel.: +36 06 1 217 0891; fax: +36 06 1 217 0891.
E-mail address: nosbel@gytk.sote.hu (B. Noszál).

0731-7085/$ – see front matter © 2012 Elsevier B.V. All rights reserved.
doi:10.1016/j.jpba.2012.02.024

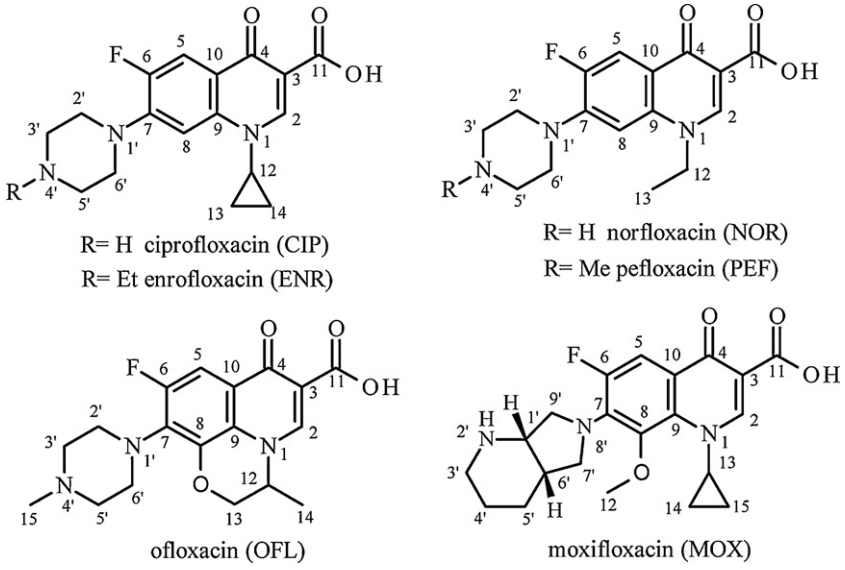

Fig. 1. The chemical structures and numbering of the six FQs studied.

different protonation isomers [11]. Protonation constants are also important to establish quantitative structure–activity relationships (QSAR) to design drugs of improved properties, and to develop selective analytical methods (e.g. capillary electrophoresis).

Unfortunately, however, the reported acid–base properties of FQs are highly controversial in the values of protonation constants and even in the number of basic sites. The reported conflicting values of norfloxacin are presented in Table 1.

The main objective of our research was either to identify all the basic sites in the FQs, or to determine the protonation macro- and microconstants, that play an important role in metal complexation and DNA gyrase binding of FQs [16]. We used ^{1}H NMR-pH titration for the determination of FQ macroconstants, and combined spectroscopic-deductive method for the determination of microconstants. To determine the protonation sites of FQs we synthesized and used model compounds that contain reduced number of basic sites.

Several important molecules have earlier been characterized by NMR-pH titration [17–19] due to the numerous advantages of the method: a number of compounds can be monitored simultaneously in one single solution and the accuracy of the log *K* determination is nowadays superior of the pH-potentiometric titrations, especially near the pH extrema, where potentiometric titrations are no longer applicable. Using *in tube* indicator molecules and in situ pH monitoring, ^{1}H NMR spectra can be acquired for single samples under circumstances of constant analyte concentration, ionic strength and gradually varied pHs. The protonation of one basic center can be followed selectively in many NMR-pH titrations [20].

In our FQ molecules all NMR nuclei are multiply influenced, their chemical shifts reflect to some extent the protonation of every basic center. Thus, to determine the site-specific protonation we also introduced model molecules of reduced number of basic centers. Model compounds are adequate to mimic the minor protonation isomer, and the macroconstants of the auxiliary compound can then be introduced into the microscopic protonation scheme of the parent compound. It has been shown [21,22] that the electronic effects of a carboxylic group and methyl ester; and those of an aromatic hydroxyl group and its phenol ether are virtually identical on the adjoining moieties. In conclusion the knowledge of the protonation macroconstants of the parent and model compounds can be an adequate set of data to calculate of all the protonation microconstants.

Although FQs have extensively been studied, a limited amount of microconstants is available only. Here we report a complete set of macro- and microconstants of six FQs, the data of which can be further utilized to interpret and improve biological activity and bioavailability during the development process of novel effective antibacterial FQs.

2. Materials and methods

2.1. Materials

The FQs were purchased as follows: ciprofloxacin hydrochloride (CIP) from Ranbaxy, ofloxacin (OFL), norfloxacin (NOR) from Smruthi Organics Ltd., pefloxacin mesylate (PEF) from Laropharm Romania, moxifloxacin hydrochloride (MOX) from Bayer Schering Pharma, enrofloxacin (ENR) and 1(2-fluorophenyl)piperazine monohydrochloride from Sigma–Aldrich. Other substances: dichloroacetic acid (Fluka), deuterium oxide (99.9%) and deuterium oxide (99.9%) containing 1% (w/w) 3-trimethylsilylpropane sulfonic acid (DSS) (Sigma–Aldrich), dimethyl sulfoxide-d_6 and thionyl chloride (Merck). All other reagents were of analytical grade. The deionized water was prepared with a Milli-Q Direct 8 Millipore system.

2.2. Synthesis of 7-chloro-6-fluoro-1-ethyl-4-oxo-1,4-dihydro-quinoline-3-carboxylic acid (model compound B)

Synthesis of 7-chloro-6-fluoro-1-ethyl-4-oxo-1,4-dihydro-quinoline-3-carboxylic acid was performed by a literature method [23]. Its chemical structure was checked by HRMS, ^{1}H NMR, ^{13}C NMR and ^{15}N NMR techniques (see supplementary data).

2.3. Synthesis of N-acetyl-ciprofloxacin (model compound D)

Synthesis of 7-(4-acetylpiperazin-1-yl)-1-cyclopropyl-6-fluoro-1,4-dihydro-4-oxoquinoline-3-carboxylic acid was performed by a literature method [24]. Its chemical structure was checked by HRMS, ^{1}H NMR, ^{13}C NMR and ^{15}N NMR techniques (see supplementary data).

Table 1
The reported protonation constants of NOR.

$\log K_1$	$\log K_2$	$\log K_3$	$\log K_4$	Technique	References
8.51	6.22	–	–	Potentiometry	[12]
8.45	6.25	5.00	–	CE	[13]
9.25	6.9	0.6	–	NMR	[14]
10.56	8.60	6.10	3.11	Potentiometry	[15]

2.4. Synthesis of CIP, ENR, MOX, NOR, OFL and PEF methyl esters

Methyl ester derivatives were prepared by a modified procedure of the synthesis of NOR-methyl ester [14]. First we prepared the appropriate acyl chloride derivatives. In this procedure we used only thionyl-chloride in excess for 60 min at 60 °C. Then the solvent was evaporated with benzene. In the last step we added methanol to the mixture and the mixture was stirred for 24 h at room temperature and finally it was evaporated. CIP-methyl ester was used as model compound C in latter experiment. The structure of the synthesized chloride salts were checked by HRMS, ^{1}H NMR and ^{13}C NMR (see supplementary data).

2.5. NMR-pH titrations and other NMR experiments

All NMR measurements were carried out on a Varian VNMRS spectrometer (599.9 MHz for ^{1}H, 150.9 MHz for ^{13}C and 60.8 for ^{15}N) with a dual 5 mm inverse-detection gradient (IDPFG) probehead. Standard pulse sequences and parameters were used to obtain 1D ^{1}H, ^{13}C, NOE, COSY, HSQC, HMBC and NOESY spectra.

Assignments were made in DMSO-d_6 solution (0.05–0.1 M). Spectra were referenced to internal TMS. The ^{15}N NMR chemical shifts were measured by ^{1}H–^{15}N HMBC. The spectra were referenced to external CH_3NO_2 (0.00 ppm), chemical shifts were obtained to a precision of 0.2 ppm.

The NMR-pH titrations were performed at 25.0 ± 0.1 °C at a constant ionic strength (I = 1 mol/dm^3, auxiliary electrolyte: KCl) in 5% D_2O–95% H_2O mixtures. This deuterium concentration proved to be enough for the spectrometer lock system. Using such a small amount of D_2O, the shift of pH-scale is within the deviation limit (0.02 pH unit), according to the Gross–Butler–Purlee theory [25,26]. The spectra were referenced to internal DSS that is known to be a pH independent NMR standard between pH 2 and 12 and was successfully applied in strong acidic solutions as well [27,28]. For the titration 1–3 mM solutions of FQs and their related compounds were used.

For pH measurement a combined glass electrode (Metrohm 6.0234.110) was used in the pH range 2–12. The pH data are pH meter readings based upon NIST primary standards: 0.05 M potassium tetraoxalate (pH = 1.68), 0.05 M potassium hydrogen phthalate (pH = 4.01), 0.025 M KH_2PO_4 + 0.025 M Na_2HPO_4 (pH = 6.87) and 0.01 M borax (pH = 9.18) [29]. In solutions of pH ≤ 2 the pH was determined using dichloroacetic acid (1 mM concentration) as an *in tube* pH-indicator to avoid the glass electrode acid error.

For the evaluation of protonation macroconstants Opium program and Origin 8.0 were used.

2.6. Potentiometric titration

The potentiometric titrations were carried out on a GLP conform computerized titration instrument (GLpKa) (Sirius Analitycal Instrument) using combination Ag–AgCl pH electrode. The titrations were carried out under N_2 atmosphere at constant (I = 0.15 M KCl) ionic strength and at standard temperature 25.0 ± 0.1 °C. The electrode was calibrated with "*four-parameter*"^{TM} calibration procedure that is based on alkalimetric titration of 0.5 M HCl [30]. *RefinementPro*^{TM} computer software was used for the calculation of the protonation macroconstants. Bjerrum difference curve was generated from the titration data. First approximate $\log_s K$ values were estimated at half-integer points of the difference curve and this "seed" value was refined by a nonlinear least squares procedure.

2.7. UV-pH titration

UV-pH titrations were carried out on a Jasco V-550 diode-array spectrometer with 10 mm cuvettes at 25.0 °C at 1 M ionic strength. The solution concentrations during the titrations were held constant, 0.075 mM for 1(2-fluorophenyl)piperazine monohydrochloride and 0.025 mM for 7-chloro-6-fluoro-1-ethyl-4-oxo-1,4-dihydro-quinoline-3-carboxylic acid. 10% methanol was used to dissolve each compound. In case of such solutions a glass electrode was calibrated with aqueous buffers and then these values were corrected with an appropriate value [31]. Absorption spectra were recorded between 210 and 400 nm, and for the evaluation of protonation constants a wavelength was chosen to achieve as much difference between the acidic and basic solutions as possible. Absorbance–pH datasets were fitted with Statistica 6.0.

2.8. HRMS analysis

The high resolution accurate masses were determined with an Agilent 6230 time-of-flight mass spectrometer. Samples were introduced by the Agilent 1260 Infinity LC system, the mass spectrometer was operated in conjunction with a Jet Stream electrospray ion source in positive ion mode. Reference masses of m/z 121.050873 and 922.009798 were used to calibrate the mass axis during analysis. Mass spectra were processed using Agilent MassHunter B.02.00 software.

3. Results and discussion

3.1. NMR analysis of the parent compounds

The proton assignment of the spectra was straightforward in most cases. The proton chemical shifts of FQs (except for MOX) with coupling constants are summarized in Table 2. Since the chemical structure of MOX is different from the other FQs studied, assignments of this compound are shown in Table 3.

In the aromatic region 3 signs occur, except for OFL and MOX, which have substitutions in C-8 position. The H-2 proton is of the largest chemical shift. The chemical shift of this nucleus and H-5 depend on the substituent in N-1 position; if this substituent is a cyclopropyl ring the H-2 chemical shift is reduced, while the H-5 chemical shift is increased. This phenomenon can be explained by the orientation and the magnetic anisotropy cone of cyclopropyl ring. The H-5 and H-8 signs are doublets because of the H–F coupling. The $^3J_{(H–F)}$ and the $^4J_{(H–F)}$ are approximately 13 and 7 Hz, respectively, in all compounds.

The piperazine protons can be assigned on the basis of integral values and only the H-6′ and H-2′ protons have cross peaks with the aromatic H-8 proton in the NOESY experiment. Furthermore, the ^{1}H NMR data and HSQC correlations unambiguously indicate the

Table 2
The ^{1}H NMR data (chemical shifts in ppm, multiplicities with coupling constants in Hz and relative intensities) of CIP, ENR, NOR, OFL and PEF (*tr.* = *trans*-methylene proton, *cys.* = *cys*-methylene proton, br. = broad, ax. = axial, eq. = equatorial).

	CIP	ENR	NOR	OFL	PEF
2	8.69 s 1H	8.66 s 1H	8.94 s 1H	8.96 s 1H	8.98 s 1H
5	7.96 d(12.98) 1H	7.90 d(12.97) 1H	7.90 d(13.00) 1H	7.58 d(12.42) 1H	7.97 d(12.91) 1H
8	7.58 d(7.16) 1H	7.56 d(7.06) 1H	7.15 d(7.15) 1H	–	7.28 d(7.15) 1H
2′, 6′	3.56 m 4H	3.32 m 4H	3.23 m 4H	3.29 m 4H	3.89 br. 2H ax. 3.55 br. 2H eq.
3′, 5′	3.31 m 4H	2.58 m 4H	2.89 m 4H	2.43 br. 4H	3.30 br. 4H
12	3.86 m 1H	3.82 m 1H	4.59 q(7.01) 1H	4.92 m 1H	4.62 q(7.00) 2H
13	1.33 m 2H (*tr.*)	1.31 m 2H (*tr.*)	1.42 t(7.01) 3H	4.58 dd(1.61, 11.40) 2H	1.43 t(7.00) 3H
14	1.20 m 2H (*cys.*)	1.18 m 2H (*cys.*)	–	1.45 d(7.01) 3H	2.32 s 3H
15	–	2.41 q(7.1) 2H	–	2.23 s 3H	
16	–	1.05 t(7.1) 3H	–	–	
					2.89 s 3H mesylate

chemical shifts of both types (2/6 and 3/5) of the methylene moieties of the piperazine ring. In some cases the piperazine methylene protons appear as broad peaks in DMSO-d_6 or in D_2O, because of ring motions. This fact depends on the protonation state of the piperazine rings. In acidic media (pH < 4) the H-3′/H-5′ protons appear as broad signals in FQs. In the PEF all piperazine protons have a broad signal and in the case of H-6′/H-2′ protons the axial and equatorial protons give separate peaks.

The proton assignment of pyrrolidino-piperidine ring (MOX) is more complex. In the literature no complete MOX NMR assignment was found. The pyrrolidino-piperidine protons can be assigned on the basis of multiplicity, coupling constants and integral values in ^{1}H spectra, ^{19}F–^{13}C coupling pattern in carbon spectra, and by COSY, HSQC, HMBC, NOESY as well as 1D NOE experiments with different mixing time. The anchor point of the assignment was that —O—CH_3 and the axial H-7′ and the protons in the same side of the ring are close in space, in agreement with the NOESY spectra of 500 ms mixing time.

The proton assignments of the cyclopropyl moiety in CIP, ENR and MOX were in accordance with earlier literature data [32,33]. In the cyclopropyl ring the *cys*- and *trans*-methylene protons give separate signals. The H-2 protons and the *cys*-methylene protons are in correlation in NOESY experiment; the distance between the *trans*-methylene proton and H-2 protons is larger. In the case of MOX all the cyclopropyl protons give a separate signal, because the —O—CH_3 group inhibits the rotation of the cyclopropyl ring.

The ^{13}C NMR assignment of FQs was deduced from the two-dimensional ^{1}H–^{13}C HSQC and HMBC experiments. Assignment of carbons was supported by the values of ^{13}C–^{19}F coupling constants. The carbon NMR assignments of FQs (except for MOX) with ^{13}C–^{19}F coupling constants are presented in Supplementary Table S1. The C–F coupling effect can also be observed at the piperazine C-2′ and C-6′ atoms. The value of this $^{4}J_{(C-F)}$ is about 5 Hz.

In all cases the ^{15}N chemical shifts were determined by means of the ^{1}H–^{15}N HMBC spectra. The main difference of the ^{15}N NMR spectra are in the chemical shift of outer piperazine nitrogen (N-4′ or N-8′) that can be explained by the hybridization state of nitrogen. The ^{15}N NMR assignments of FQs (except for MOX) are in Supplementary Table S2.

3.2. Identification of the protonation sites in FQs

In order to determine the correct protonation sites of FQs we used not only the parent molecules but also, some model compounds, such as 1(2-fluorophenyl)piperazine monohydrochloride **A**, 7-chloro-6-fluoro-1-ethyl-4-oxo-1,4-dihydro-quinoline-3-carboxylic acid **B**, CIP-methyl ester **C** and N4′-acetyl CIP **D**. These model compounds helped to identify the protonation sites of the appropriate moiety in the FQs. The structures of the model compounds are shown in Fig. 2.

In order to characterize the acid–base chemistry of FQs, we first titrated CIP, and its two derivatives that contain a reduced number of basic sites (carboxymethyl-CIP and N4′-acetyl-CIP (model compound C and D in Fig. 2)) by pH-potentiometry method. The advantage of potentiometric titration is that the titration steps are proportional to the number of protons bound/released. This

Table 3
^{1}H NMR, ^{13}C NMR and ^{15}N NMR data (chemical shifts in ppm, multiplicities with coupling constants in Hz, relative intensities and ^{19}F–^{13}C coupling constants in Hz in parentheses) of MOX (*tr.* = *trans*-methylene proton, *cys.* = *cys*-methylene proton, ax. = axial, eq. = equatorial).

atom	^{1}H	^{13}C	^{15}N	atom	^{1}H	^{13}C	^{15}N
1	–	–	−223.27	1′	3.88 m 1H	54.30	–
2	8.68 s 1H	150.31	–	2′	–	–	−316.19
3	–	106.31	–	3′ ax.	3.18 m 1H	41.40	–
4	–	175.90	–	3′ eq.	2.91 m 1H		–
5	7.68 d(13.21) 1H	106.44 (24.1)	–	4′ ax.	1.79 m 1H	20.31	–
6	–	152.37 (249.67)	–	4′ eq.	1.74 m 1H		–
7	–	136.53 (10.41)	–	5′ ax.	1.74 m 1H	17.34	–
8	–	140.21 (7.28)	–	5′ eq.	1.68 m 1H		–
9	–	134.45	–	6′	2.64 m 1H	36.34	–
10	–	117.20 (8.70)	–	7′ ax.	3.57 dd 1H	54.39 (10.28)	–
11	–	165.73	–	7′ eq.	4.05 dd(5.43, 12.13) 1H		–
12	3.60 s 3H	61.75	–	8′	–	–	−335.38
13	4.15 m 1H	40.51	–	9′ ax.	3.75 dd(5.11, 10.58) 1H	51.73 (9.07)	–
14 *tr.*	1.03 m 1H	9.56	–	9′ eq.	3.85 dd 1H		–
14 *cys.*	0.87 m 1H						
15 *tr.*	1.19 m 1H	8.30					
15 *cys.*	1.11 m 1H						

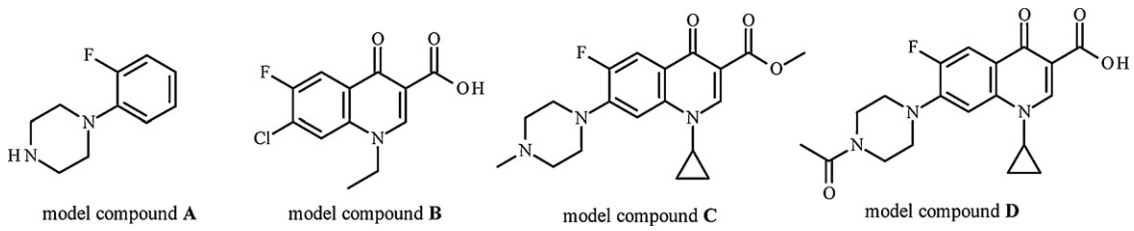

Fig. 2. The constitutional formulas of the model compounds.

method is also appropriate to determine how many basic centers are in a molecule in the 2–12 reliable range of pH-potentiometry. In the case of CIP the potentiometric titration curve shows two proton-association processes and the concomitant two basic centers and two protonation macroconstants ($\log K_1 = 8.54 \pm 0.01$, $\log K_2 = 6.18 \pm 0.01$ ($I = 0.15$ M)). The molecules with reduced number of basic sites have one basic center and one protonation constant only: $\log K = 8.48 \pm 0.01$ ($I = 0.15$ M) for carboxymethyl-CIP and $\log K = 6.30 \pm 0.01$ ($I = 0.15$ M) for N-acetyl-CIP, clearly indicating that FQs in the pH range 2–12 have two protonating sites: the carboxylate and the more basic piperazine N4′ nitrogen.

We then investigated whether the other two nitrogens (quinolone N1 and piperazine N1′) are able to protonate below pH 2. ^{1}H NMR-pH titration is a proper method to solve this problem. In our investigated compounds, however, all observed protons are multiply influenced by the protonation of every basic site. Their chemical shifts are composite ones. We used therefore two model compounds that contain one of the expected protonation sites only. The 1(2-fluorophenyl)piperazine monohydrochloride (model compound A in Fig. 2) contains the N-1′ nitrogen in the piperazine ring and the 7-chloro-6-fluoro-1-ethyl-4-oxo-1,4-dihydro-quinoline-3-carboxylic acid (model compound B in Fig. 2) contains the N-1 nitrogen in the quinolone ring as a possible basic center. We analyzed both model compounds by UV-pH titration and model compound A by NMR-pH titration. Model compound B could not be dissolved in the concentration range of the NMR-pH titration technique. The UV-pH and the NMR-pH titration curves of model compound A are shown in Supplementary Fig. S1. The absorbance of model compound B did not change during UV-pH titration in acidic media between pH 0–4. Consequently, only one macroconstant could be determined for this compound.

These investigations show that model compound A bears two basic centers; the N-1′ in piperazine ring protonates in very acidic media only. The protonation macroconstant values from NMR-pH titration: $\log K_1 = 8.99 \pm 0.02$ ($I = 1$ M) and $\log K_2 = 0.20 \pm 0.04$ ($I = 1$ M). Our results are different from those of Lin et al. [13] presented for the phenyl-piperazine compound. Model compound B has one basic center: the carboxylate group only. The $\log K$ for this compound from UV-pH titration is 6.08 ± 0.05 ($I = 1$ M).

In conclusion, FQs possess a total of three basic centers: the two nitrogens in the piperazine ring and the carboxylate group. The piperazine N1′ nitrogen protonates in acidic media in a well-separated manner from the other two basic centers. Thus the protonation of FQs can be depicted in terms of three macroconstants and four microconstants, as shown in Fig. 3.

3.3. Determination of the macroconstants of parent FQs and their derivatives

Evaluation of the protonation constants from ^{1}H NMR-pH titration curves was based on the principle that non-exchanging NMR nuclei near the basic site sense different electronic environments upon protonation. All carbon-bound protons could be observed. Since protonation processes are fast on the NMR time scale, the observed chemical shift of a nucleus can be expressed as a weighted average of chemical shifts of the protonated and unprotonated form. Weighting factors are the mole fractions.

$$\delta^{\text{obs.}} = \delta_{L^-}\chi_{L^-} + \delta_{HL}\chi_{HL} + \delta_{H_2L^+}\chi_{H_2L^+} = \frac{\delta_{L^-} + \delta_{HL}K_1[H^+] + \delta_{H_2L^+}K_1K_2[H^+]^2}{1 + K_1[H^+] + K_1K_2[H^+]^2} \quad (1)$$

where $\delta^{\text{obs.}}$ is the observed chemical shift, L^-, HL, and H_2L^+ are the non-protonated, mono- and diprotonated macrospecies, respectively, δ_{L^-}, δ_{HL}, $\delta_{H_2L^+}$ are the chemical shifts of the species in subscript.

The N-1′ nitrogen protonates in very acidic media where the glass electrode function is distorted by the well-known acidic error and the limiting chemical shift of the completely protonated form is beyond reach at the applied, 1 M ionic strength. In order to avoid the uncertainty of the glass electrode at $pH \leq 2$ we used dichloroacetic acid as an acidic NMR pH indicator. The pH of the solution was determined from the actual chemical shift of the indicator molecule, using Eq. (2):

$$pH = \log K_{\text{ind}} + \log \frac{\delta_{\text{ind}}^{\text{obs}} - \delta_{\text{Hind}}}{\delta_{\text{ind}} - \delta_{\text{ind}}^{\text{obs}}} \quad (2)$$

where $\log K_{\text{ind}}$ is the protonation constant of the indicator (1.14 for dichloroacetic acid), δ_{ind} and δ_{Hind} are the chemical shift of the species in subscript ($\delta_{\text{ind}} = 6.050$ ppm, $\delta_{\text{Hind}} = 6.345$ ppm for dichloroacetic acid,) $\delta_{\text{ind}}^{\text{obs}}$ is the observed chemical shift [28,34].

At this acidic pH equation (1) is not applicable to determine $\log K_3$, because the chemical shift of the fully protonated form cannot be measured at the applied ionic strength. Therefore, the Perrin–Fabian method was used to determine the most acidic macroconstants ($\log K_3$) [35].

$$\delta_{L}^{\text{obs.}} = \frac{\delta_{H_2L^+}(\delta_{\text{ind}}^{\text{obs}} - \delta_{\text{ind}}) + 10^{\Delta \log K}\delta_{HL}(\delta_{\text{Hind}} - \delta_{\text{ind}}^{\text{obs}})}{10^{\Delta \log K}(\delta_{\text{Hind}} - \delta_{\text{ind}}^{\text{obs}}) + (\delta_{\text{ind}}^{\text{obs}} - \delta_{\text{ind}})} \quad (3)$$

where $\Delta \log K = \log K_{\text{ind}} - \log K_L$.

Perrin and Fabian showed that relative protonation constants can be determined more precisely and accurately in a multicomponent NMR-pH titration than $\log K$ values themselves [35]. Orgován and Noszál [34] validated this method earlier and used for the quantitation of very high basicities where the limiting chemical shift could not be reached either.

The protonation macroconstants of all the parent molecules are shown in Table 4 and their derivatives in Table 5.

As an example Fig. 4 shows the NMR-pH profiles of ENR in the aromatic region. H-8 proton shows a so-called “wrong way” shift upfield. This upfield shift can be explained by pH-dependent conformational change of the piperazine ring.

The stepwise macroconstants show that the N-1′ nitrogen protonation takes place in highly separated manner, as indicated by the $\log K_3$ values of the parent molecules and $\log K_2$ values of the methyl ester derivatives. The largest $\log K_3$ value belongs to MOX that contains pyrrolidino-piperidine ring while the smallest $\log K_3$ value belongs to OFL due to the oxazine ring. The $\log K_2$ values of

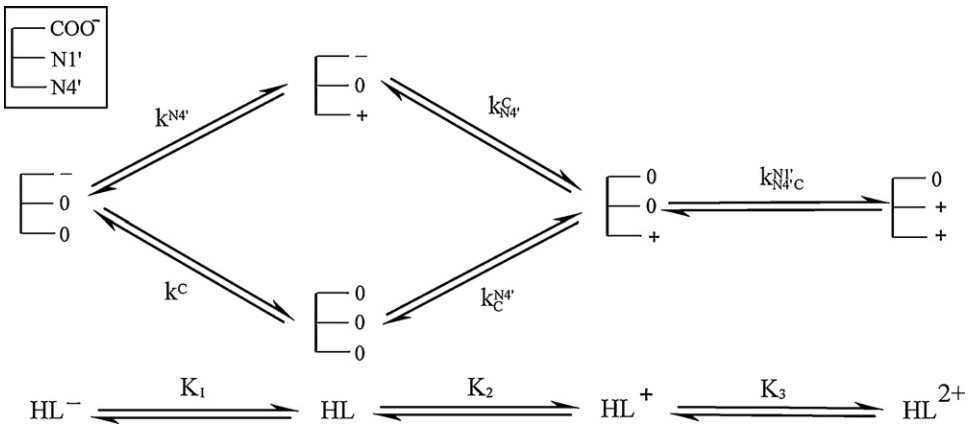

Fig. 3. The micro- and macroprotonation schemes of the FQs examined. Microconstants with superscript C, N4′ and N1′ belong to the carboxylate, piperazine N4′ nitrogen and N1′ nitrogen, respectively, and K_1, K_2, K_3 are stepwise macroconstants. The superscripts on the microconstant indicate the protonating site, while the subscript (if any) stand for the site already protonated.

Table 4
Protonation macroconstants of the parent molecules.

	CIP	ENR	MOX	NOR	OFL	PEF
$\log K_1$	8.61 ± 0.01	7.90 ± 0.02	9.35 ± 0.01	8.55 ± 0.01	8.21 ± 0.01	7.53 ± 0.01
$\log K_2$	6.30 ± 0.02	6.22 ± 0.02	6.31 ± 0.01	6.20 ± 0.03	6.13 ± 0.02	6.22 ± 0.02
$\log K_3$	−0.21 ± 0.10	−0.19 ± 0.09	−0.08 ± 0.07	−0.20 ± 0.07	−0.43 ± 0.14	−0.23 ± 0.10

Table 5
The protonation macroconstants of the carboxymethylated compounds (**1** = ciprofloxacin methyl ester, **2** = enrofloxacin methyl ester, **3** = moxifloxacin methyl ester, **4** = norfloxacin methyl ester, **5** = ofloxacin methyl ester, **6** = pefloxacin methyl ester).

	1	**2**	**3**	**4**	**5**	**6**
$\log K_1$	8.57 ± 0.01	7.78 ± 0.01	9.33 ± 0.01	8.50 ± 0.01	8.14 ± 0.01	7.38 ± 0.01
$\log K_2$	−0.23 ± 0.09	−0.16 ± 0.05	−0.09 ± 0.06	−0.21 ± 0.06	−0.38 ± 0.10	−0.24 ± 0.07

the parent compounds are similar with a maximum difference of 0.18 $\log K$ units. The $\log K_1$ values depend on the number of substituents at the N-4′ nitrogen, having relatively large values for secondary amino groups (NOR, CIP, MOX) and modest basicities for tertiary amino sites (OFL, ENR, PEF). This trend is known to be an effect of the different hydration states of the protonated forms of secondary and tertiary amines.

3.4. The complete microspeciation of FQs

Protonation microconstants can be determined by spectroscopy methods, provided that the concentrations of the related microspecies are commensurable. Earlier the carboxylate protonation microconstants of FQs were determined by UV-pH titration. Unfortunately the difference between the basicity of piperazine N-4′ and carboxyl groups is too large for reliable microconstant determinations. For example, differences between the MOX macroconstants exceed three $\log K$ units. Thus, the deductive method for the determination of FQ microconstants is more appropriate. In this investigation the protonation of the methyl ester derivatives mimic the protonation of N4′, when the carboxylate is in —COOH status. Thus, so the $\log K_1$ values of the esterified compounds are equal to the log $k_C^{N4'}$ microconstants of FQs. In accordance with the protonation scheme in Fig. 3, the following relationships between the micro- and macroconstants can be formulated:

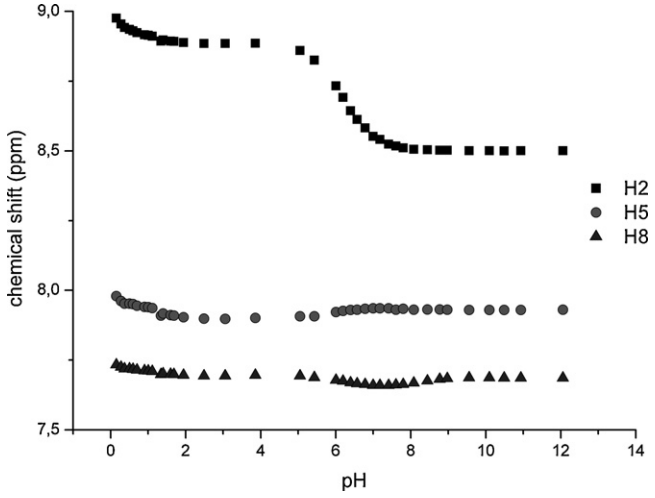

Fig. 4. NMR-pH titration curves of ENR in the aromatic region (H2, H5, H8 = chemical shifts of aromatic protons).

$$K_1 = k^{N4'} + k^{C} \tag{4}$$

$$\beta_2 = K_1 K_2 = k^{N4'} k^{C}_{N4'} = k^{C} k^{N4'}_{C} \tag{5}$$

Due to the large differences between the $\log K_3$ and $\log K_2$ macroconstants, the $\log k^{N1'}_{N4'C} = \log K_3$ equality can be set.

For further insight into the inter-moiety effects, the pair-interactivity parameter can be defined. The pair-interactivity parameter quantifies how much the protonation of a basic center reduces the basicity of the other basic site.

$$E^{N4'\text{-}C} = \frac{k^{N4'}}{k^{N4'}_{C}} = \frac{k^{C}}{k^{C}_{N4'}} \tag{6}$$

$$\log\ E^{N4'\text{-}C} = \log k^{N4'} - \log k^{N4'}_{C} = \log k^{C} - \log k^{C}_{N4'} \tag{7}$$

All the 24 determined microconstants and 6 interactivity parameters are shown in Table 6.

It can be seen that the values of $\log k^{C}_{N4'}$ and $\log k^{C}$ as well as the interactivity parameters differ from the previous literature values

Table 6
Protonation microconstants and interactivity parameters of FQs.

	CIP	ENR	MOX	NOR	OFL	PEF
$\log k^{N4'}$	8.61	7.89	9.35	8.55	8.21	7.50
$\log k^{C}$	6.34	6.34	6.33	6.25	6.20	6.37
$\log\ k_{C}^{N4'}$	8.57	7.78	9.33	8.50	8.14	7.38
$\log\ k_{C}^{N4'}$	6.30	6.23	6.31	6.20	6.14	6.25
$\log\ k_{N4'C}^{N1'}$	−0.21	−0.19	−0.08	−0.20	−0.43	−0.23
$\log E$	0.04	0.11	0.02	0.05	0.06	0.12

[12]. These data show that only the deductive method is appropriate to determine the protonation microconstants of FQ in the minor protonation pathway.

Comparing our analogous microconstants of the investigated FQs, the carboxylate microconstants are similar. These values show that the FQs have much weaker acid character than other aromatic carboxylic acid (for example benzoic acid $\log K = 4.19$ [36]). This property can be explained with the intramolecular H-bond between the 3-carboxyl and the 4-carbonyl groups, which stabilise the protonated form of the carboxyl group. The greatest differences can be observed in the protonation of the piperazine N4′. Substitution in the N-4′ position decreases the basicity of the compounds and the interpretation of this process is similar to those described for macroconstants. The interactivity parameters between the carboxylate and piperazine N4′ are low due to the relative large distance between these groups.

Using our microconstants the pH-dependent distribution diagrams of the 30 microspecies for the six FQs could be calculated. As examples the pH-dependent distribution diagram of ENR and MOX are shown in Fig. 5 and in Supplementary Fig. S2, respectively. The diagrams show that all compounds exist mainly in zwitterionic form at the pH of the blood. It can be seen that the concentration of the neutral microspecies at this pH are much below thus appeared in the previous literature data were shown. The neutral microspecies play a role in the transport mechanism and the zwitterionic ones in the binding of DNA gyrase. The distribution diagrams also show that the zwitterionic form fades away at acidic pH, while the cationic ones becomes predominant, which explains the pH-dependent activity of FQs [37]. In acidic media, at the pH of the stomach the monoprotonated form is overwhelmingly dominant in all molecules but our microconstants show the dicationic ones become also significant upon further lowering the pH.

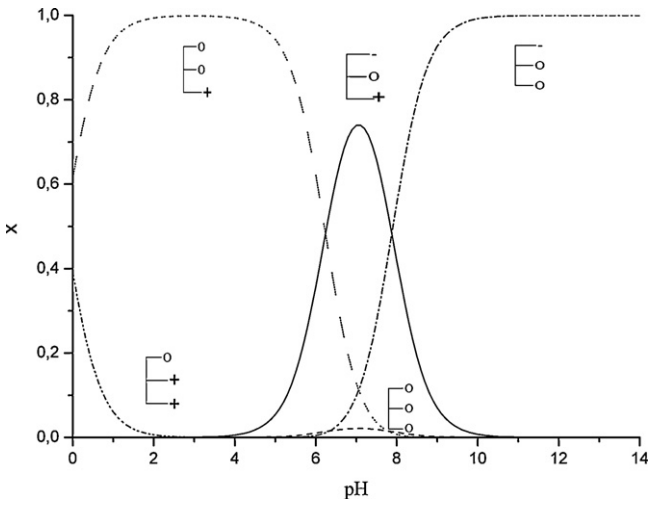

Fig. 5. The representative pH-dependent distribution of ENR microspecies.

4. Conclusions

We identified the protonation sites of FQs using the well-established therapeutic drugs and their model derivatives. Our results show that the FQs have three protonation sites: the 3-carboxylate group, the N-4′ and the N-1′ nitrogen in the piperazine ring. The N-1′ nitrogen protonates only in highly acidic media. By ^{1}H NMR-pH titrations we determined all the macroconstants, and by combination of NMR-pH titrations and a deductive method all the microconstants for the studied FQs. The pH-dependent distribution diagram of each FQ was calculated.

The site-specific acid base properties of FQs as distinctive properties significantly influence their pharmacokinetic behavior (absorption, distribution) and also, their protein/DNA-gyrase binding. On the basis of the determined macro- and microconstants capillary zone electrophoresis separation can be developed and the species-specific physicochemical properties can be interpreted and improved for further FQ drug candidates.

Acknowledgements

This work was supported by OTKA T 73804 Grant and an Erasmus scholarship for Aura Rusu funded by the European Union. The authors are grateful to Bayer Schering Pharma AG for providing the moxifloxacin hydrochloride and to Laropharm, Romania, for providing pefloxacin mesylate.

Appendix A. Supplementary data

Supplementary data associated with this article can be found, in the online version, at doi:10.1016/j.jpba.2012.02.024.

References

[1] J.A. O'Donnell, S.P. Gelone, Fluoroquinolones, Infect. Dis. Clin. North Am. 14 (2000) 489–513.
[2] M.I. Andersson, A.O. MacGowan, Development of the quinolones, J. Antimicrob. Chemother. 51 (2003) 1–11.
[3] P. Ball, The quinolones: history and overview, in: V.T. Andriole (Ed.), The Quinolones, 3rd ed., Academic Press, San Diego, CA, 2000, pp. 2–3.
[4] J.H. Block, J.M. Beale, Wilson and Gisvold's Textbook of Organic Medicinal and Pharmaceutical Chemistry, 11th ed., Lippincott Williams & Wilkins, Philadelphia, 2003, pp. 208–210.
[5] L. Budai, M. Hajdu, M. Budai, P. Gróf, S. Béni, B. Noszál, I. Klebovich, I. Antal, Gels and liposomes in optimized ocular drug delivery: studies on ciprofloxacin formulations, Int. J. Pharm. 343 (2007) 34–40.
[6] J.Y. Fan, D. Sun, H. Yu, S.M. Kerwin, L.H. Hurley, Self-assembly of a quinobenzoxazine-Mg2+ complex on DNA: a new paradigm for the structure of a drug–DNA complex and implications for the structure of the quinolone bacterial gyrase–DNA complex, J. Med. Chem. 38 (1995) 408–424.
[7] S. Lemaire, P.M. Tulkens, F. Van Bambeke, Contrasting effects of acidic pH on the extracellular and intracellular activities of the anti-gram-positive fluoroquinolones moxifloxacin and delafloxacin against *Staphylococcus aureus*, Antimicrob. Agents Chemother. 55 (2011) 649–658.
[8] J. Sun, S. Sakai, Y. Tauchi, Y. Deguchi, J. Chen, R. Zhang, K. Morimoto, Determination of lipophilicity of two quinolone antibacterials, ciprofloxacin and grepafloxacin, in the protonation equilibrium, Eur. J. Pharm. Biopharm. 54 (2002) 51–58.
[9] M. Neumann, A. Esanu, Gaps and perspectives of new fluoroquinolones, Drugs Exp. Clin. Res. 14 (1988) 385–391.
[10] K. Takacs-Novak, B. Noszal, M. Tőkes-Kövesdi, G. Szász, Acid–base properties and proton-speciation of vancomycin, Int. J. Pharm. 89 (1993) 261–263.
[11] B. Noszál, Acid–base properties of bioligands, in: K. Burger (Ed.), Biocoordination Chemistry: Coordination Equilibra in Biologically Active System, Ellis Horwood, Chichester, UK, 1990, pp. 18–41.
[12] K. Takács-Novák, B. Noszál, I. Hermecz, G. Keresztúri, B. Podányi, G. Szász, Protonation equilibria of quinolone antibacterials, J. Pharm. Sci. 79 (1990) 1023–1028.
[13] C.-E. Lin, Y.-J. Deng, W.-S. Liao, S.-W. Sun, W.-Y. Lin, C.-C. Chen, Electrophoretic behaviour and p*K*a determination of quinolones with a piperazinyl substituent by capillary zone electrophoresis, J. Chromatogr. A 1051 (2004) 283–290.
[14] D.A. Buckingam, C.R. Clark, A. Nangia, The acidity of norfloxacin, Aust. J. Chem. 43 (1990) 301–309.
[15] Z. Qiang, C. Adams, Potentiometric determination of acid dissociation constants (pK_a) for human and veterinary antibiotics, Water Res. 38 (2004) 2874–2890.

[16] D.S. Lee, H.J. Hun, K. Kim, W.B. Park, J.K. Cho, J.H Kim, Dissociation and complexation of fluoroquinolone analogues, J. Pharm. Biomed. Anal. 12 (1994) 157–164.
[17] A. Marosi, Z. Kovács, S. Béni, J. Kökösi, B. Noszál, Triprotic acid–base microequilibria and pharmacokinetic sequelae of cetirizine, Eur. J. Pharm. Sci. 37 (2009) 321–328.
[18] Z. Szakács, S. Béni, Z. Varga, L. Őrfi, G. Kéri, B. Noszál, Acid–base profiling of imatinib (Gleevec) and its fragments, J. Med. Chem. 48 (2005) 249–255.
[19] M. Kraszni, Z. Szakács, B. Noszál, Determination of rotamer populations and related parameters from NMR coupling constants: a critical review, Anal. Bioanal. Chem. 378 (2004) 1449–1463.
[20] Z. Szakács, M. Kraszni, B. Noszál, Determination of microscopic acid–base parameters from NMR-pH titrations, Anal. Bioanal. Chem. 378 (2004) 1428–1448.
[21] J.T. Edsall, J. Wyman, Biophysical Chemistry, Academic Press, New York, 1958, p. 487.
[22] L. Ebert, Determination of double ions in solutions of ampholytes, Z. Phys. Chem. 121 (1926) 385–400.
[23] H. Koga, A. Itoh, S. Muramaya, S. Suzue, T. Irikura, Structure–activity relationships of antibacterial 6,7-and 7,8-disubstituted 1-alkyl-1,4-dihydro-4-oxoquinoline-3-carboxylic acids, Eur. J. Med. Chem. 23 (1980) 1358–1363.
[24] J. Azéma, B. Guidetti, J. Dewelle, B. Le Calve, T. Mijatovic, A. Korolyov, J. Vaysse, M. Malet-Martino, R. Martino, R. Kiss, 7-((4-Substituted)piperazin-1-yl) derivatives of ciprofloxacin: synthesis and in vitro biological evaluation as potential antitumor agents, Bioorg. Med. Chem. 17 (2009) 5396–5407.
[25] E.L. Purlee, On the solvent isotope effect of deuterium in aqueous acid solutions, J. Am. Chem. Soc. 81 (1959) 263–272.
[26] P.K. Glasoe, F.A. Long, Use of glass electrodes to measure acidities in deuterium oxide, J. Phys. Chem. 64 (1960) 188–190.
[27] Z. Szakács, G. Hägele, R. Tyka, $^{1}H/^{31}P$ NMR pH indicator series to eliminate the glass electrode in NMR spectroscopic pK_a determinations, Anal. Chim. Acta 522 (2004) 247–258.
[28] Z. Szakács, G. Hägele, Accurate determination of low pK values by 1H NMR titration, Talanta 62 (2004) 819–825.
[29] European Pharmacopoeia, 7th ed., Council of Europe, Strasbourg, 2010, p. 367.
[30] A. Avdeef, J.E.A. Comer, S.J. Thomson, pH-metric log P: 3. Glass electrode calibration in methanol–water applied to pKa determination of water-insoluble substances, Anal. Chem. 65 (1993) 42–49.
[31] M. Roses, E. Bosch, Influence of mobile phase acid–base equilibria on the chromatographic behavior of protolytic compound, J. Chromatogr. A 982 (2002) 1–30.
[32] A. Zięba, A. Maślankiewicz, J. Sitkowski, Spectral assignments and reference data, ^{1}H, ^{13}C and ^{15}N NMR spectra of ciprofloxacin, Magn. Reson. Chem. 42 (2004) 903–904.
[33] U. Holzgrabe, S.K. Branch, 1H, 19F and 13C NMR spectral data of fifteen gyrase inhibitors and some metabolites, Magn. Reson. Chem. 32 (1994) 192–196.
[34] G. Orgován, B. Noszál, Electrodeless, accurate pH determination in highly basic media using a new set of 1H NMR pH indicators, J. Pharm. Biomed. Anal. 54 (2011) 958–964.
[35] C.L. Perrin, M.A. Fabian, Multicomponent NMR titration for simultaneous measurement of relative pKas, Anal. Chem. 68 (1996) 2127–2134.
[36] C.A. Hollingsworth, P.G. Seybold, C.M. Hadad, Substituent effects on the electronic structure and pKa of benzoic acid, Int. J. Quantum Chem. 90 (2002) 1396–1402.
[37] S. Lemaire, F.V. Bambeke, P.M. Tulkens, Activity of finafloxacin, a novel fluoroquinolone with increased activity at acid pH, towards extracellular and intracellular Staphylococcus aureus, Listeria monocytogenes and Legionella pneumophila, Int. J. Antimicrob. Agents 38 (2011) 52–59.

Journal of Pharmaceutical and Biomedical Analysis 66 (2012) 58–67

Contents lists available at SciVerse ScienceDirect

Journal of Pharmaceutical and Biomedical Analysis

journal homepage: www.elsevier.com/locate/jpba

Usefulness of reversed-phase HPLC enriched with room temperature imidazolium based ionic liquids for lipophilicity determination of the newly synthesized analgesic active urea derivatives

Jolanta Flieger[a,*], Anna Czajkowska-Żelazko[a], Marzena Rządkowska[b], Elżbieta Szacoń[b], Dariusz Matosiuk[b]

[a] Department of Analytical Chemistry, Medical University of Lublin, 4A Chodźki Street, 20-093 Lublin, Poland
[b] Chair and Department of Medical Chemistry, Medical University of Lublin, 4A Chodźki Street, 20-093 Lublin, Poland

ARTICLE INFO

Article history:
Received 14 December 2011
Received in revised form 27 February 2012
Accepted 28 February 2012
Available online 8 March 2012

Keywords:
Urea derivatives
Ionic liquids
RP-HPLC
Lipophilicity determination
Partition coefficient

ABSTRACT

Lipophilicity of several novel analgesic active 1-(1-arylimidazolidyn-2-ylidyn)-3-arylalkyl urea derivatives has been estimated by the use of chromatographic method. The investigated compounds were analyzed by reversed-phase high performance liquid chromatography (RP-HPLC) using mixtures of methanol or acetonitrile and water with addition of imidazolium based room temperature ionic liquids varying in an anion chaotropicity as the mobile phases. The relationships between log k values vs. concentration of organic solvent was used for determination of the log k_w values by extrapolation technique. The partition coefficients (log P) values were calculated by means of the Pallas 3.1.1.2. and Spartan 10.0 softwares and further correlated with log k_w measured experimentally in classical organic–aqueous eluent system and systems modified with ionic liquids addition. It was found that log k_w values measured in eluent system modified with butyl-methyl imidazoilum chloride correlate the best with the logarithm of partition coefficient calculated by Pallas software (log $P_{calc.}$). Furthermore, it was found that the examined compounds form H-bonding with imidazoilum cation of modifiers improving the chromatographic peak parameters (the symmetry factor, the theoretical plates number) especially when ionic liquid's anion was more chaotropic. Amphiphilic ionic liquid possessing longer alkyl chain substituent (OMIM BF_4) can be considered as a new cationic surfactant. Micellar conditions improved separation selectivity of chloro- and methoxy substituted derivatives.

© 2012 Elsevier B.V. All rights reserved.

1. Introduction

Since the pioneering work of Overton and Meyer [1,2] at the beginning of the 20th century and later Hansch' [3] studies, lipophilicity has become fundamental descriptor in quantitative structure–activity relationships (QSAR) examining the potential pharmacological effect of newly synthesized drug candidates.

Lipophilicity can be either predicted computationally (fragmental methods, models based on molecular properties, atomic contribution, surface area etc.) or measured in liquid–liquid and solid–liquid systems based on the Nernst's law of distribution. One of the oldest methods of lipophilicity determination is the shake-flask method. The modern versions of liquid–liquid extraction offer flow injection analysis (FIA) and counter-current chromatography (CCC). In turn, such chromatographic techniques as thin-layer chromatography (TLC), high-performance liquid chromatography (HPLC) or some of electrically driven separation methods use solid-liquid systems for lipophilicity determination [4–6].

Similarly to liquid–liquid extraction or crossing lipid barrier in the living organism, the main driving force in liquid chromatographic systems based on reversed-phase mode (RPLC) is partitioning of analytes between hydrophobic stationary phase and polar, usually organic, aqueous mobile phase. Relationship between retention factor (k) in chromatography and the partition coefficient ($P_{o/w}$) is expressed by Martin's equation [7]:

$$\log k = \log K + \log\left(\frac{V_s}{V_M}\right) \quad (1)$$

where log K is the chromatographic equilibrium constant, V_s, V_M are the volume of stationary and mobile phase. Assuming that the ratio $\log(V_s/V_m)$ is constant for a given chromatographic system and retention is governed by partition mechanism, we can expect that log k will be at least proportional to the distribution coefficient in its logarithmic form.

There are a few chromatographic lipophilicity parameters (log k_w, S φ_0). All of them are derived from Soczewinski–Wachtmeister

* Corresponding author. Tel.: +48 81 535 73 97; fax: +48 81 535 73 50.
E-mail address: j.flieger@umlub.pl (J. Flieger).

0731-7085/$ – see front matter © 2012 Elsevier B.V. All rights reserved.
doi:10.1016/j.jpba.2012.02.025

equation describing relationship between retention factor (k) and the volume fraction (φ) of organic modifier in the mobile phase [8]:

$$\log k = \log k_w - S\varphi \quad (2)$$

According to the above equations, log k_w is retention extrapolated to pure water ($\varphi = 0$), φ_0 represents mobile phase composition permitting to obtain a retention factor of unity (log $k = 0$), S is the slope of above relationship.

Among chromatographic lipophilicity parameters, log k_w appears to be the most similar in the order of magnitude to octanol–water log $P_{o/w}$ [9,10]. It should be stressed however that the correlation between log $P_{o/w}$ or log P obtained by the use of popular computational methods and chromatographically derived lipophilicity parameters are statistically significant mainly for congeneric group of neutral solutes.

The lipophilicity measurements using RPLC appear to be imperfect mainly due to the activity of residual silanols, influences of the organic modifier on the extrapolated log k_w values, structural diversity of solutes and presence of ionizable groups in the solutes structure.

This work studies the influence of addition of ionic liquids to acetonitrile-aqueous mobile phase on lipophilicity determination of the newly synthesized derivatives of urea which are active on central nervous system (CNS) and exhibit, in vivo, significant analgesic activities with relatively low acute toxicities. An opioid-like mechanism was confirmed by reversion of the antinociception by naloxon in the Witkin test [11–13]. Their LD_{50} values were found to be in the range from 1100 to over 2000 mg kg^{-1}. The strength of their activity depends on the nature of substituents.

The aim of the presented investigations was comparison of conventional reversed-phase high performance liquid chromatography (RP-HPLC) and RP-HPLC enriched with room temperature imidazolium based ionic liquids as for chromatographic behavior and agreement of obtained experimental lipophilicty parameters with theoretical values calculated by computer-assisted softwares. For the first time the existence of interaction between the cation of imidazolium based ionic liquid and unionized solutes, affecting the chromatographic behavior was demonstrated.

2. Experimental

2.1. Materials

The compounds: 1-(1-arylimidazolidyn-2-ylidyn)-3-arylalkyl urea derivatives investigated in the following study (Fig. 1) were synthesized in Department of Medical Chemistry, Medical University of Lublin. The synthesis procedure of this novel bioactive set of compounds was described in the Polish Patents [11–13]. The structures of all the investigated solutes were confirmed by ^{1}H NMR spectroscopy. Their purity was assessed by elemental analysis.

Ionic liquids: 1-butyl-3-methyl-imidazolium hexafluorophosphate (BMIM PF_6), 1-butyl-3-methyl-imidazolium chloride (BMIM Cl) and 1-butyl-3-methyl-imidazolium tetrafluoroborate (BMIM BF_4), 1-octyl-3-methyl imidazolium tetrafluoroborate (OMIM BF_4) were obtained from Fluka. The concentrations of the additives were in the range from 1 to 30 mmol l^{-1}, in the whole mobile phase. HPLC grade acetonitrile (ACN) and methanol (MeOH) were purchased from Merck (Darmstadt, Germany). HPLC water was obtained from Barnstead deionising system (Dubuque, IA, USA). All mobile phases were filtered with Nylon 66 membrane filter (0.45 μm) Whatman (Maidstone, England) by the use of a filtration apparatus.

2.2. HPLC apparatus

Experiments were performed using a LaChrom HPLC Merck Hitachi (E.Merck, Darmstadt, Germany) model equipped with diode array detector, column oven L-7350 and solvent degasser L-7612. The column (150 mm × 4.6 mm I.D.) was packed with 5-μm Zorbax Extend-C18 Agilent Technologies (Santa Clara, CA, USA); its void volume was determined to be 1.31 ml, by the injection of thiourea in acetonitrile–water (50:50) eluent system. Retention data were recorded at a flow-rate of 1 ml min^{-1}. The column was thermostated at 20 °C ± 0.1. Injected solutions were prepared at 0.1 mg ml^{-1} concentrations in aqueous methanol. The monitoring of the drugs was at 220 nm for organic aqueous eluent system and 265 nm for eluents modified with ionic liquids. Typical injection volumes were 2.5 μl. Duplicate injections were done.

2.3. RP-HPLC column

Extend-C18 column applied in this study offers a unique method of protection of the silica from dissolution at a wide range of eluent pH. Bidentate bonding technology combined with a double-endcapping process provides not only high pH stability but also prevents especially basic groups from any potential extremely disadvantageous silanophilic interactions.

Bonded phase	Pore size	Surface area	Temp. limits	pH range	End capped	Carbon load
ZORBAX Extend-C18	80 Å	180 m^2/g	60 °C	2.0–11.5	Double	12.5%

It should be noted that pH of the organic–aqueous eluent used in the present study independently of the modifier type can be generally referred to as pH 5–7. Even underivatized silanol groups will remain ionized taking into account their pK_a which is about 4.0. In turn at pH 5–7 the investigated compounds are neutral.

2.4. Calculation methods

Calculations devoted to theoretical plate number and asymmetry were performed using HSM program. The following equation was used to calculate the number of theoretical plates according to USP standards: $N = 16(R_T/W)^2$, where R_T stands for the actual full retention time of the appropriate peak, W equals the peak width obtained by drawing tangents to each side of the peak and by calculating the distance between the two points where the tangents meet the baseline. The HSM program uses the following equation to calculate asymmetry: A_s equals ½(1 + B/A), where A and B are evaluated at a 5% peak height of an appropriate peak. The capacity factor (k) was calculated as follows: $k = (t_r - t_0)/t_0$, where t_r stands for the actual retention time of the individual peak, t_0 is the elution of the unretained sample (thiourea).

Theoretical partition coefficients (log $P_{calc.}$) of the examined solutes were calculated using Pallas (version 3.1.1.2) software and Spartan (version 1.0.). Multivariate regressions were performed with Microsoft Office Excel 2007 and Statistica (version 5.1) respectively.

3. Results and discussion

3.1. Determination of chromatographic lipophilicity parameters on the basis of the relationships log k versus volume fraction of organic solvent in the mobile phase (φ)

Log k values were linearly extrapolated according to Eq. (2). In all cases very high correlation coefficients were obtained. Extrapolated log k_w values and the corresponding slopes (S) and φ_0 indices are presented in Table 1, along with their statistics.

Furthermore, existence of statistically significant correlations between log k_w and S either in acetonitrile or methanol containing mobile phase confirms structural similarity of investigated compounds and correctness of applied chromatographic method

for investigation of new synthesized derivatives' lipophilicity. These relationships can be expressed by the following equations expressed by regression analysis:

$$\log k_w(\mathrm{ACN}) = -0.9231(\pm 0.04)S - 0.9616(\pm 0.17) \quad (3)$$

$n = 20$, $R^2 = 0.9538$, $s_e = 0.18$; $F = 371.97$

$$\log k_w(\mathrm{MeOH}) = -1.0791(\pm 0.03)S - 1.2385(\pm 0.13) \quad (4)$$

$n = 20$, $R^2 = 0.9846$, $s_e = 0.14$; $F = 1157.72$

where numbers in parentheses denote the standard deviations of the individual regression coefficients, n is the number of analytes considered in deriving the regression equation, R^2 is the correlation coefficient, s_e is the standard error of estimate of the equation, F is the value of the Fisher test of significance, S is the slope in Soczewiński–Wachtmeister's equation.

The investigated compounds are not ionised at neutral pHs (except the pyridine derivative) in the examined conditions exhibiting simultaneously the greatest lipophilicity.

Obtained chromatographic lipophilicity parameters (log k_w, S and φ_0) can be directly compared to other lipophilicity scale (Table 2). One of them is offered by Pallas software using the weighted average of the log P values derived from three databases: ANNLOGP, ATOMIC6 and CDI-Rekker for log P estimation. Full set of structural descriptors was also determined by Spartan software.

The correlation of computer-assisted log P data (Pallas 3.1.1.2. software) with chromatographic lipophilicity parameters resulted in the following equations:

$$\log P(\mathrm{Pallas}) = 10.1063(\pm 0.99)\varphi_0(\mathrm{MeOH}) - 4.9277(\pm 0.75) \quad (5)$$

$n = 20$, $R^2 = 0.8516$, $s_e = 0.44$, $F = 103.61$

$$\log P(\mathrm{Pallas}) = 0.8681(\pm 0.12)\log k_w(\mathrm{MeOH}) - 0.0605(\pm 0.41) \quad (6)$$

$n = 20$, $R^2 = 0.7413$, $s_e = 0.58$, $F = 51.59$

$$\log P(\mathrm{Pallas}) = 1.1289(\pm 0.15)\log k_w(\mathrm{ACN}) + 0.01408(\pm 0.38) \quad (7)$$

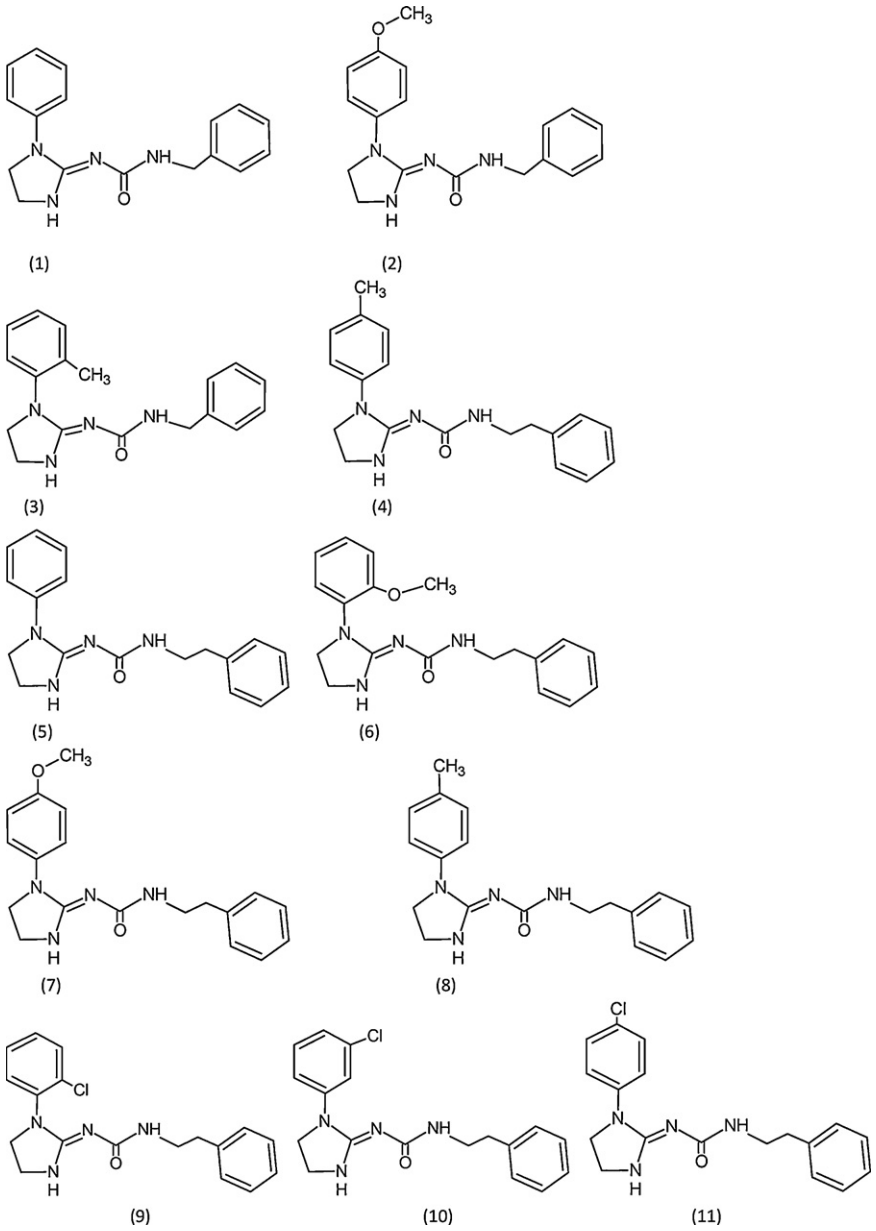

Fig. 1. Investigated compounds.

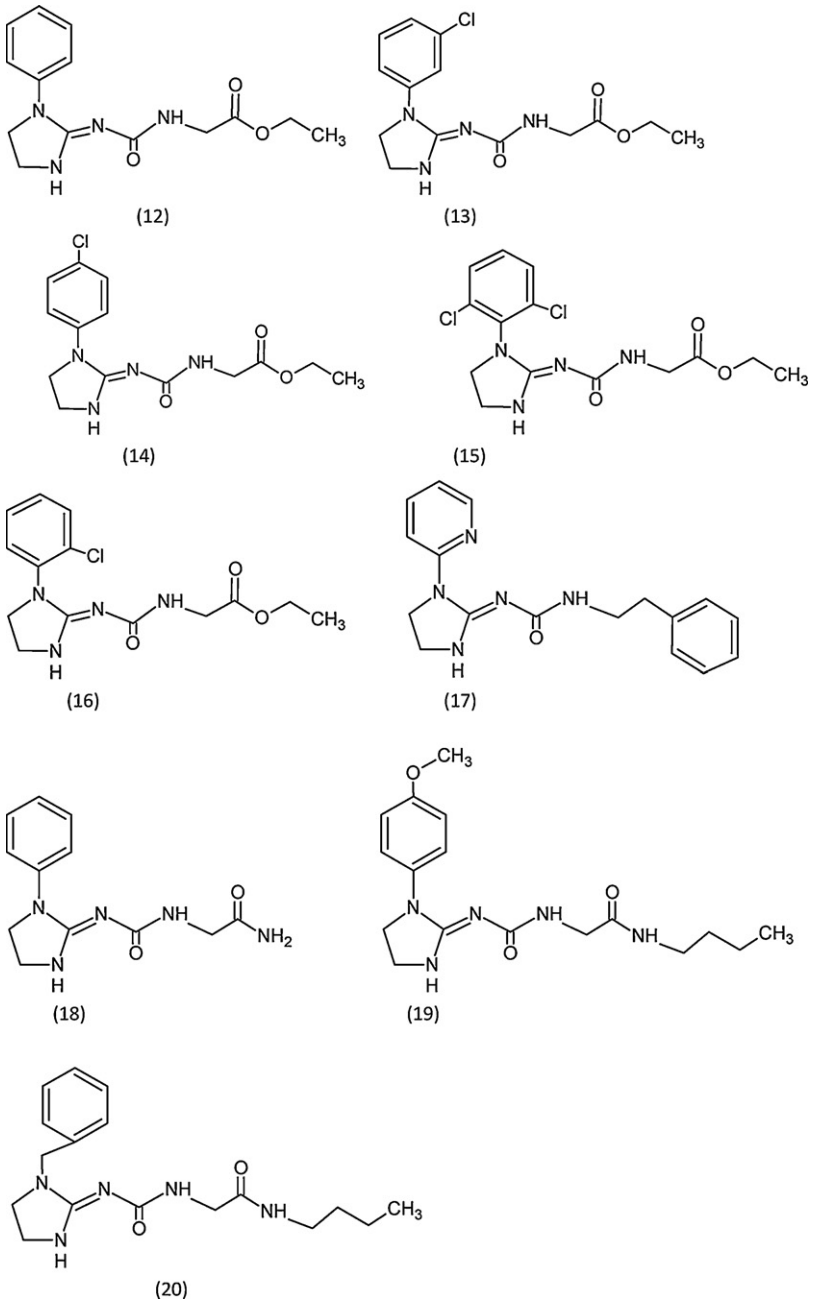

Fig. 1. (*Continued*).

$n = 20$, $R^2 = 0.7390$, $s_e = 0.58$, $F = 50.96$

$$\log P(\text{Pallas}) = 6.1719(\pm 0.98)\varphi_0(\text{ACN}) - 1.1360(\pm 0.62) \quad (8)$$

$n = 20$, $R^2 = 0.6445$, $s_e = 0.64$, $F = 39.55$

As it can be seen from the above, the obtained correlations are not satisfactory. The best statistical parameters were obtained for correlation of log *P* with φ_0 when methanol was used as an organic modifier. It ought to be stressed that methanol is preferred as an organic modifier of the mobile phase because it makes the reversed phase chromatographic system closer to the octanol/water partition system in their sensitivity to H-bond donor properties of the compounds. In the aqueous acetonitrile/reversed phase system H-bond donor groups significantly reduce retention.

In turn, advantages of φ_0 in comparison to other chromatographic hydrophobicity indices for lipophilicity estimation were proved. This observation is in consistence with already published papers suggesting φ_0 as a better model of the octanol–water partition in RP-HPLC [14]. The comprehensive studies show that this parameter is characteristic for all compounds and is independent of the type of reversed-phase packing and composition of the mobile phase.

Trials to use another software, for instance Spartan, for calculation of the log *P* values did not improve correlation with the lipophilicity parameters derived from chromatography.

Other method of checking lipophilicity is measuring the isocratic log *k* values. It appears that experimental chromatographic parameters correlate reasonably well with log *P* scale established by shake-flask method in 1-octanol–water system. This method saves time and improves correlation with lipophilicity parameter log $P_{o/w}$ especially when methanol is mixed with almost equal part

Table 1
Coefficients of Eq. (2) obtained by HPLC method for investigated compounds by the use of unmodified ACN/water and MeOH/water eluent systems.

No.	ACN/water				MeOH/water			
	log k_w	S	φ_0	R^2	log k_w	S	φ_0	R^2
1	2.342	−3.516	0.666	−0.994	2.952	−3.882	0.760	−0.998
2	2.251	−3.431	0.656	−0.993	3.249	−4.114	0.789	−0.998
3	2.215	−3.267	0.678	−0.993	3.209	−3.958	0.810	−0.996
4	2.720	−4.442	0.666	−0.998	3.839	−4.593	0.835	−0.997
5	2.598	−3.770	0.689	−0.992	3.984	−4.860	0.819	−0.998
6	2.393	−3.337	0.717	−0.986	3.343	−4.077	0.821	−0.997
7	2.470	−3.562	0.693	−0.989	3.827	−4.706	0.813	−0.997
8	2.924	−4.022	0.726	−0.989	4.553	−5.388	0.844	−0.995
9	3.205	−4.395	0.729	−0.990	4.831	−5.606	0.861	−0.999
10	3.208	−4.401	0.728	−0.990	4.784	−5.540	0.863	−0.999
11	3.219	−4.415	0.729	−0.990	4.656	−5.367	0.867	−0.999
12	1.590	−2.717	0.585	−0.997	2.359	−3.399	0.694	−0.996
13	2.083	−3.315	0.628	−0.992	3.318	−4.398	0.754	−0.996
14	2.087	−3.320	0.628	−0.992	3.321	−4.405	0.753	−0.996
15	1.834	−2.871	0.638	−0.994	2.651	−3.648	0.726	−0.998
16	1.088	−2.310	0.470	−0.997	1.786	−2.840	0.628	−0.996
17	3.626	−5.326	0.680	−0.999	1.756	−2.500	0.702	−0.984
18	0.105	−1.402	0.074	−0.993	0.997	−2.045	0.487	−0.992
19	2.051	−3.449	0.594	−0.991	2.536	−3.716	0.682	−0.995
20	1.071	−2.403	0.446	−0.999	1.623	−2.827	0.574	−0.992

of water. In this study, the isocratic log k values: log k_{MeOH} (50%) correlate the best with log P (Pallas) as can be seen below:

$$\log P(\text{Pallas}) = 2.03(\pm 0.19)\log k_{MeOH}(50\%) + 1.19(\pm 0.174) \quad (9)$$

$n = 20$, $R^2 = 0.8701$, $s_e = 0.42$, $F = 113.91$.

$$\log P(\text{Pallas}) = 2.2043(\pm 0.25)\log k_{ACN}(50\%) + 1.1887(\pm 0.20) \quad (10)$$

$n = 20$, $R^2 = 0.8104$, $s_e = 0.50$, $F = 76.94$.

For sure, this appears to be directly connected with the linearity of log k vs. φ relationships. To predict more precisely lipophilicity of the analyte by RP chromatography, plots log k versus φ must be linear also outside the working organic solvent range. In this context isocratic log k values are more advantageous to achieve more precise value of chromatographic lipophilicity.

3.2. Modification of aqueous–organic mobile phase by ionic liquid additives

To improve correlation of chromatographic lipophilicity parameters with computational lipophilicity scale, modification of chromatographic system by the use of ionic liquids has been proposed in this study. Three examples of room temperature ionic liquids with the same imidazolium cation differing in the anion chaotropicity were selected (BMIM Cl, BMIM BF_4 and BMIM PF_6). Investigated compounds do not change radically their spectrum in the range of 220–400 nm but the maximum at the shortness wavelengths was shifted towards the longer waves under influence of ionic liquid presence. As it can be seen on Fig. 2 this shift does not depend on the type of anion. The spectrum change might prove the H-bonding interaction. Fig. 3 illustrates superposition of 1-butyl-3-methylimidazolium cation (LUMO) and compound **8** (HOMO) orbitals. Minute difference between HOMO (−7.95 eV) and LUMO (−4.82 eV) energies equals about 3 eV confirms possibility of interactions between imidazoilum cation and 2-amino carbonyl fragment of molecules.

To our knowledge this is the first time when analyzed solutes interact with ionic liquid's cation during chromatographic process. So far cations were considered only as the stationary phase modifiers influencing slightly retention time of the solutes. Some papers demonstrated adsorption of ionic liquid's cation on hydrophobic surface [15]. The main force changing the retention time of ionized analytes with basic properties

Table 2
The structural parameters of the investigated compounds.

No	HOMO	LUMO	Dipol	E	log P Spartan	Area	Volume	PSA	log P Pallas
1	−8.17	3.88	3.2	−40.14	3.55	327.73	307.68	37.098	2.82
2	−8.02	3.93	3.32	−47.79	3.22	359.96	335.54	44.64	3.17
3	−8.71	3.84	3.95	−38.1	3.83	350.31	327.02	38.52	3.43
4	−7.96	3.92	3.29	−39.48	3.83	347.78	325.98	37.15	3.59
5	−8.17	3.88	3.3	−42.13	3.63	347.08	325.88	37.64	3.25
6	−8.56	3.76	2.92	−39.71	3.5	379.77	354.42	44.97	3.49
7	−8.02	3.92	3.25	−49.66	3.5	379.29	353.74	45.18	3.68
8	−7.95	3.92	3.41	−41.36	4.11	367.1	344.17	37.66	4.06
9	−8.65	3.39	3.93	−42.24	4.18	365.65	340.67	39.44	3.56
10	−8.48	3.53	1.38	−39.36	4.18	362.65	339.49	37.61	3.96
11	−8.33	3.51	3.54	−41.66	4.18	362.73	339.5	37.61	4.13
12	−8.24	3.79	4.98	−49.78	1.48	316.51	290.27	56.75	1.2
13	−8.55	3.45	3.61	−47.52	2.04	332.11	303.89	56.74	1.97
14	−8.4	3.43	4.45	−49.54	2.04	332.18	303.89	56.72	2.02
15	−9.46	2.96	6.64	−53.74	2.6	353.12	318.95	58.42	1.67
16	−9.2	3.34	5.62	−50.9	2.04	335.27	305.12	58.65	1.53
17	−8.53	3.57	2.56	−41.19	3	343.71	320.13	43.32	2.7
18	−8.39	3.63	7.78	−57.37	0.23	281.38	255.37	75.16	0.14
19	−7.88	3.82	6.23	−50.03	1.58	394.22	358.32	68.24	2.27
20	−9.19	3.73	8.17	−42.07	1.36	387.81	350.68	63.36	1.35

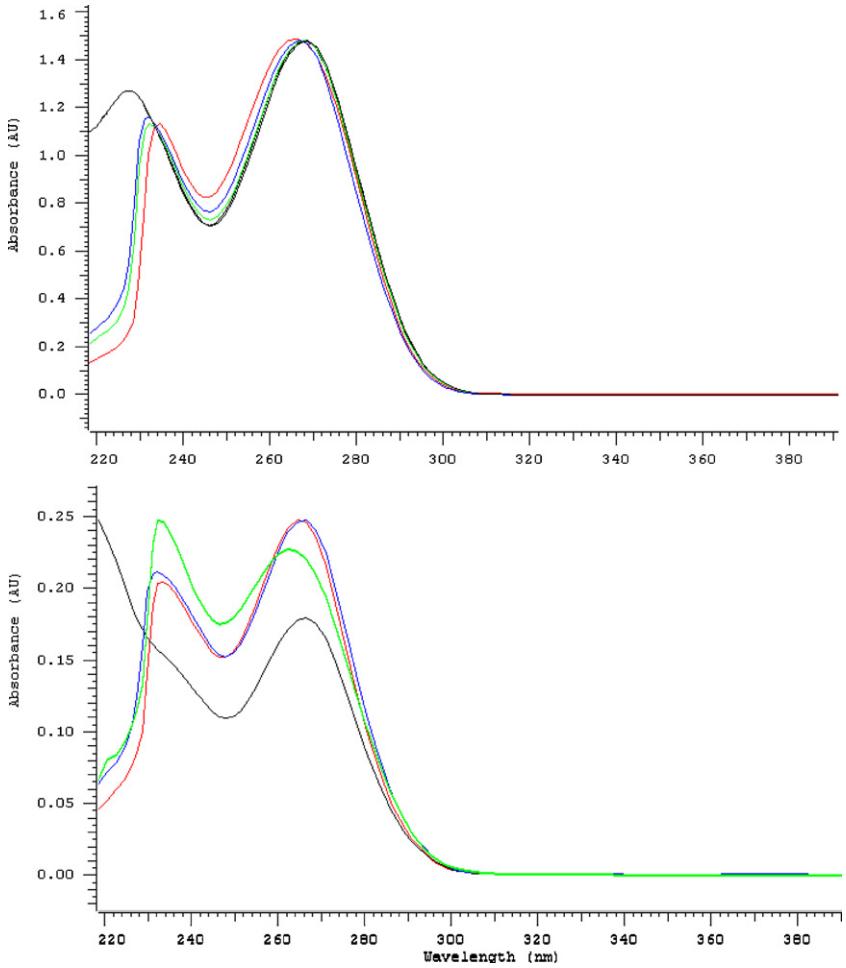

Fig. 2. Overlaid DAD spectra of compounds number **9** and **14** analysed by the use of 45% ACN (black) or with addition of 5 mM ionic liquids BMIM Cl (red), BMIM PF6 (blue), BMIMBF4 (green). (For interpretation of the references to colour in this figure legend, the reader is referred to the web version of this article.)

came from their interaction with ionic liquid's anion [16,17].

Detection of the analyzed compounds in eluent systems modified with ionic liquids was performed at 265 nm whereas in organic–aqueous eluent system without any additives detection was set at 220 nm.

Presence of ionic liquids in the mobile phase affected not only the spectrum shape but also the retention time, efficiency

Table 3
Comparison of the following peak parameters: *k*-retention parametr, A_s-tailing factor, *N*-theoretical plates number values for investigated compounds obtained in eluent systems studied.

No.	45%ACN/water			45%ACN/water 5 mM BMIM PF_6			45% ACN/water 5 mM OMIM BF_4			45% ACN/water + 5 mM BMIM Cl		
	k	A_s	*N*	*k*	A_s	*N*	*k*	A_s	*N*	*k*	A_s	*N*
1	5.91	1.44	3090	4.66	1.45	5400	4.39	1.19	6620	5.04	1.24	7680
2	4.96	3.05	622	3.97	1.18	5420	3.62	1.25	3510	3.75	2.05	3230
2	5.34	–	350	4.11	1.15	5270	3.61	1.41	1330	3.52	1.90	616
4	8.77	1.73	1320	7.47	1.14	5570	7.47	1.14	6670	7.86	1.59	4338
5	7.66	1.81	1850	6.59	1.16	5740	6.54	1.20	3160	6.85	1.58	2130
6	7.81	3.33	180	4.2	1.14	4670	3.15	1.5	530	3.02	1.84	511
7	7.11	–	616	5.31	1.14	5360	4.79	1.45	960	4.93	1.60	1310
8	12.41	1.76	1270	10.13	1.14	5210	10.07	1.36	1490	10.65	1.68	2660
9	16.04	1.16	7763	14.92	1.08	6020	14.75	1.09	5060	16.71	1.09	8980
10	16.05	1.16	7630	14.28	1.1	6010	14.64	1.10	8590	16.69	1.09	9210
11	16.17	1.12	5640	14.5	1.09	5980	14.5	1.14	6990	16.5	1.18	7820
12	2.24	1.08	7940	0.8	1.22	4080	0.13	1.25	750	0.19	1.28	6586
13	3.67	1.04	7041	2.17	1.15	5130	3.42	0.96	7970	2.17	1.12	8560
14	3.69	1.15	6730	3.41	1.15	5470	3.38	1.07	8110	3.78	1.09	8910
15	3.35	1.17	8070	3.16	1.3	5380	3.19	1.1	6180	3.46	1.09	9890
16	1.1	2.03	2985	0.91	1.18	4560	0.88	1.01	8600	0.93	1.22	6870
17	16.74	1.91	101	4.1	1.53	2720	1.65	1.12	3310	1.37	2.11	440
18	0.31	–	–	0.31	1.22	1500	0.31	1.05	3456	0.25	1.24	4450
19	2.94	1.13	6510	2.73	1.15	5480	2.72	1.07	9080	3.05	1.08	9410
20	0.99	1.19	4930	0.93	1.31	4130	0.93	1.1	8130	1.03	1.02	8900

Table 4
Coefficients of Eq. (2) obtained by RP-HPLC in eluent systems modified with 5 mM ionic liquids addition.

No.	ACN/water (BMIM PF_6)			ACN/water (BMIM Cl)			ACN/water (OMIMBF_4)		
	log k_w	S	R^2	log k_w	S	R^2	log k_w	S	R^2
1	2.219	−3.441	0.999	2.471	−3.870	0.996	1.862	−2.779	0.998
2	2.420	−4.099	0.989	2.839	−4.020	0.998	1.653	−2.590	0.992
3	2.314	−3.776	0.999	2.883	−4.002	0.995	1.448	−2.190	0.985
4	2.767	−4.199	0.999	2.915	−4.564	0.978	2.374	−3.418	0.998
5	2.430	−4.004	0.999	3.373	−4.281	0.991	2.193	−3.164	0.997
6	2.430	−4.004	0.999	3.018	−3.784	0.996	0.815	−1.007	0.990
7	2.576	−4.109	0.999	3.357	−4.222	0.996	1.694	−2.458	0.988
8	2.940	−4.302	0.999	3.767	−4.728	0.989	2.406	−3.263	0.996
9	3.302	−4.749	0.998	3.487	−5.069	0.993	3.278	−4.732	0.983
10	3.287	−4.727	1.000	3.482	−5.060	0.994	3.207	−4.511	0.998
11	3.304	−4.763	0.999	3.496	−5.115	0.990	3.168	−4.446	0.998
12	0.707	−1.788	0.998	1.368	−2.318	0.993	−0.871	−0.248	0.774
13	1.784	−3.229	0.999	1.780	−3.136	0.988	2.528	−4.451	0.989
14	2.144	−3.583	0.999	2.239	−3.718	0.995	2.089	−3.431	0.997
15	1.902	−3.127	0.999	1.975	−3.223	0.996	1.811	−2.901	0.991
16	1.114	−2.578	0.998	1.235	−2.862	0.987	0.856	−2.096	0.994
17	2.005	−3.151	0.985	2.474	−3.192	0.994	0.292	−0.695	0.996
18	−0.066	−0.968	0.999	−0.149	−0.802	0.992	0.525	−2.264	0.999
19	1.953	−3.386	0.998	2.093	−3.607	0.996	1.903	−3.222	0.998
20	1.281	−2.937	0.998	1.278	−2.842	0.997	1.149	−2.603	1.000

expressed as the theoretical plate's number and the peak symmetry. In all cases observed changes in experimental peak parameters are advantageous (Table 3).

The analyzed compounds exhibited retention decrease with the addition of ionic liquids to the mobile phase. The retention factor decrease was the smallest for BMIM Cl as an eluent modifier. However, the smallest changes in retention factor were connected with improvement of system efficiency visible in higher values of the theoretical plates' numbers. The influence of ionic liquid modifiers on retention, symmetry and efficiency of the peaks may be estimated on the basis of the examples of chromatograms obtained for compound number **6** (Fig. 4).

Appropriate choice of ionic liquid modifier concentration is also very important for further studies. The influence of ionic liquid BMIM PF_6 concentration on the retention of compound number **6** in 50% ACN is shown in Fig. 5.

As it was shown, major effects on the analyte retention were visible only at low ionic liquid concentration, where even slight amount of additive caused significant changes in retention, symmetry and efficiency.

Chosen compound shows decrease of its retention with increasing concentration of ionic liquid BMIM PF_6 in the mobile phase. This process is limited and achieves plateau level after which further increase of ionic liquid concentration causes no visible effect on peak parameters. This limited concentration of 5 mM was chosen for mobile phase modification in further study.

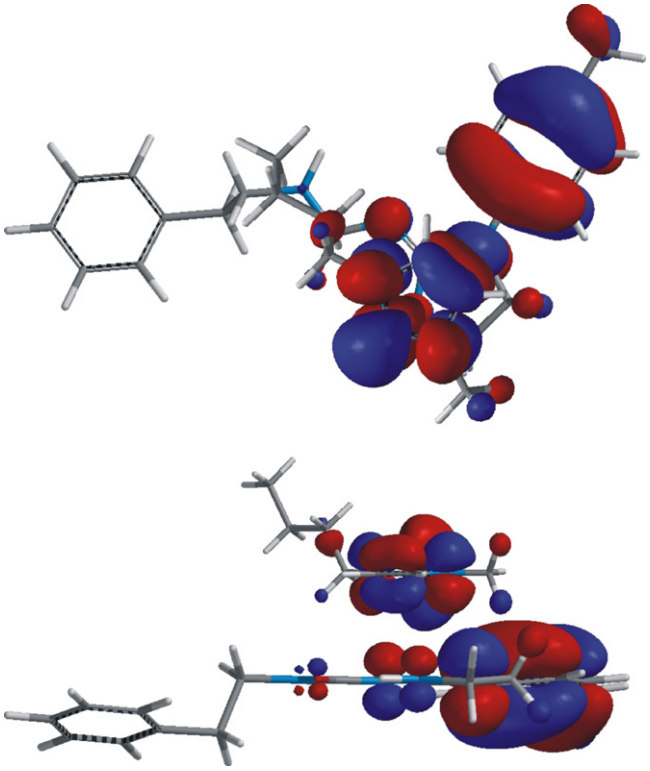

Fig. 3. Superposition of 1-butyl-3-methylimidazolinium cation (LUMO = −4.82 eV) and comp. 8 (HOMO = −7.95 eV) orbitals in top and side view, modeled by Spartan 10v1.0, ab initio method, DFT, B3LYP, 6-31G* basis set.

3.3. Determination of chromatographic lipophilicity parameters by the use of eluent system modified with ionic liquids

Changes in retention observed under increasing acetonitrile concentration varied from 40 to 55% in 5% increments in aqueous mobile phase enriched with constant concentration of ionic liquids: BMIM Cl and BMIM PF_6 can be satisfactory described by linear equation (Eq. (2)). Because relationships obtained for eluent modified with BMIM BF_4 were not linear we decided to change the cation into 1-octyl-3-methyloimidazolium. Addition of OMIM BF_4 at 5 mM concentration improved linearity of these correlations. For most dependences, the correlation coefficient was approaching 0.9 (Table 4) in the whole range of the investigated concentrations. On the basis of the experimentally obtained log k vs. volume fraction (φ) of acetonitrile containing 5 mM of ionic liquids relationships one can determine chromatographic lipophilicity parameters log k_w, by extrapolation techniques.

The correlation of computer-assisted log P data (Pallas 3.1.1.2. software) with chromatographic lipophilicity parameters obtained in system modified with BMIM Cl was the best and resulted in the following equation:

$$\log P(\text{Pallas}) = 1.0864(\pm 0.0616) \log k_w(\text{ACN} + 5 \quad \text{mM} \quad \text{BMIM Cl}) + 0.01655(\pm 0.1637) \qquad (11)$$

$n = 20$, $R^2 = 0.9452$, $r = 0.9722$, $s_e = 0.2696$, $F = 310.66$

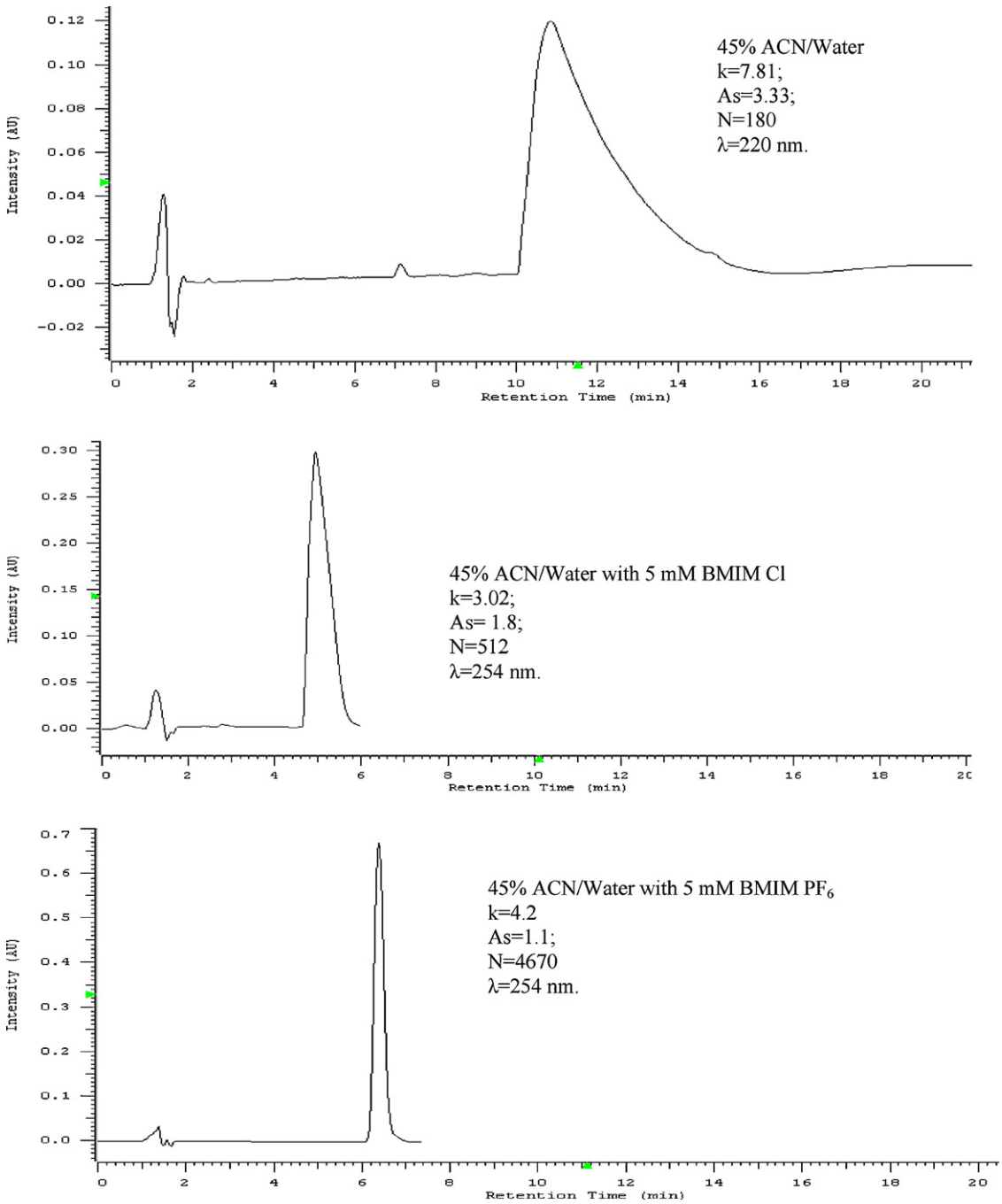

Fig. 4. Effect of ionic liquid addition to 45% ACN/water eluent system on peak parameters of compound number **6**.

whereas absence of ionic liquid addition resulted in Eq. (7) mentioned previously.

This suggests that not only the differences in hydrophobicity of analytes decide about differences in retention. Ionic liquid' cation undergo adsorption on hydrophobic surface as a lipophilic species creating new interphase. Obtained partition system composed on interphase and eluent system containing lipophilic ions simulate the best partition system for log *P* estimation. Not only the highest value of the correlation coefficient but also slope close to unity and small value of intercept of log *P* vs. log k_w (BMIM Cl) relationship prove similarity of compared values.

Summarizing the effectiveness of ionic liquids modifier according to their usefulness for prediction of lipophilicity one could arrange it as follows: BMIM Cl > BMIM PF_6 > OMIM BF_4.

By analysing the log k_w values in the series of investigated derivatives it is visible that the lipophilicity of compounds depends on the kind and position of the substituents in the phenyl ring. All chromatographic systems studied are more or less sensitive to these changes. However the greatest changes in log k_w values can be found in system modified with OMIM BF_4.

Let's consider the impact of ortho- and para- position of the electron-donating methyl group on the chromatographic lipophilicity parameters and calculated log *P* values. For compounds **3** and **4**, with 2-CH_3 and 4-CH_3 substituents, differences between experimental log k_w values obtained by the use of eluent systems modified with BMIM PF_6, BMIM Cl and OMIM BF_4 were found to be 0.45, 0.03 and almost 1.0 respectively whereas

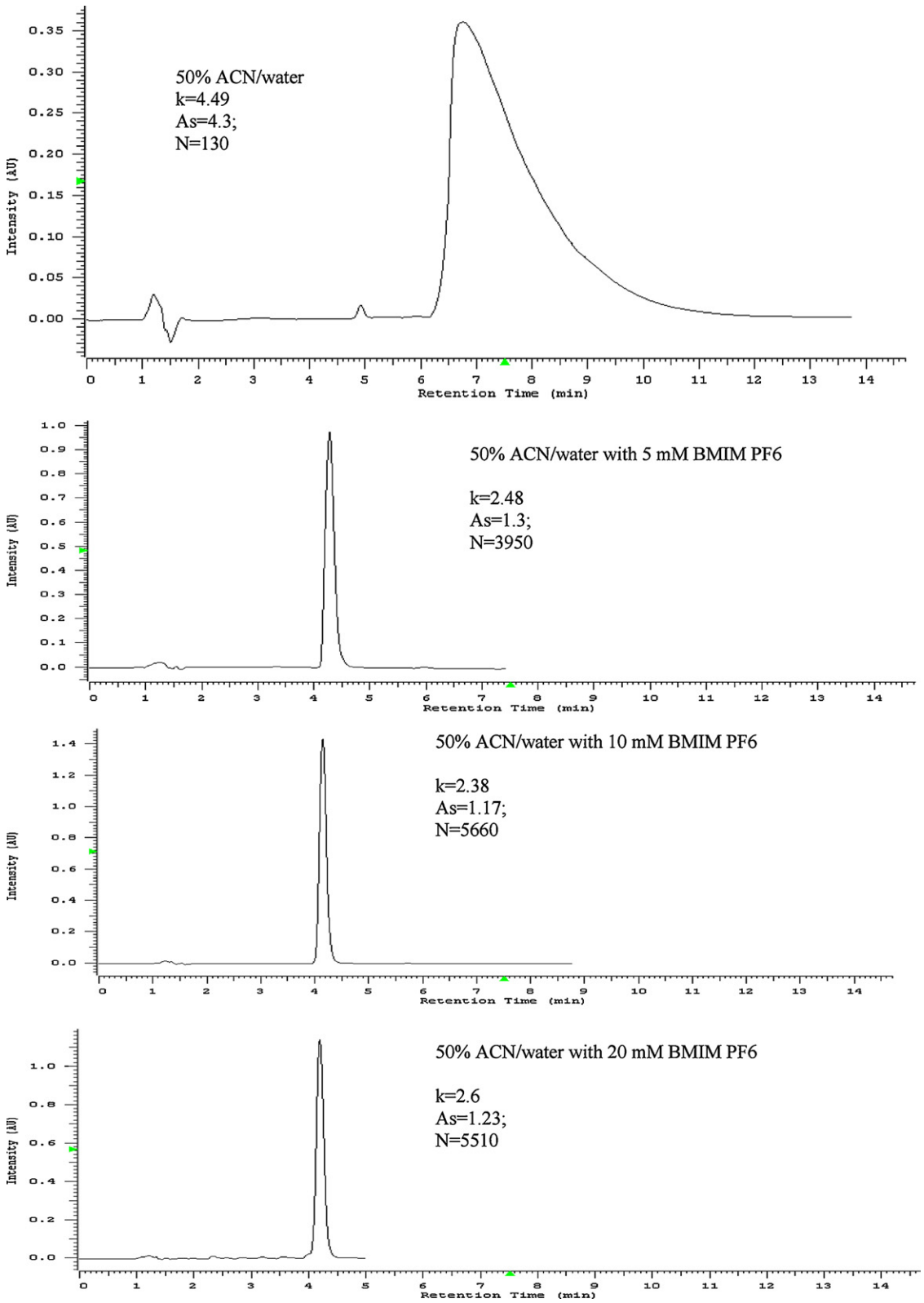

Fig. 5. Influence of BMIM PF_6 concentration in 50% ACN/water on the peak paramaters of compound number **6**.

differences between log *P* values predicted by Pallas and Spartan software were 0.16 and 0, respectively.

Considering the strong electron-donating CH_3O substituent in ortho and para-position (compounds number **6** and **7**) generally decrease in lipophilicity can be observed in relation to unsubstituted phenyl compound number **5**. Differences between experimental lipoophilicity indices estimated in eluents containing BMIM PF_6, BMIM Cl and OMIM BF_4 for ortho and para isomers were found to be 0.14, 0.34 and 0.88 in comparison to $\Delta \log P$ −0.19 and 0 predicted theoretically by Pallas and Spartan software.

The lipophilicity values of solutes **14**, **16** with electron-withdrawing monochloro-substituents caused the strongest

impact on the chromatographic lipophilicity values in comparison to those predicted by Spartan software for which there was no difference in log *P* values between above isomers. Furthermore, introduction of the second chlorine atom (compound number **15**) resulted in noticeable chromatographic lipophilicity variation. All modified eluent system studied arranged lipophilicity of chlorine derivatives in the following order: para-chloro > dichloro > otho-chloro substituted derivatives. OMIM BF_4 as the mobile phase modifier appeared to be also the most selective for separation of isomers **9**, **10**, **11** in comparison to other eluent systems unsensitive to the position of chlorine atom in the phenyl ring. Chromatographic lipophilicity of above chlorine derivatives can be arranged as follows: ortho > meta > para-chloro substituted derivatives in contrary to log *P* predicted by Pallas presenting completely reversed order and log *P* values calculated by Spartan where there are no differences between log *P* of ortho-, meta- and para-isomers.

On the basis of performed experiments one can conclude that modification of the mobile phase by the use of BMIM Cl improve correlation of chromatographic lipophilicity parameters with computational ones predicted theoretically for investigated 1-(1-arylimidazolidyn-2-ylidyn)-3-arylalkyl urea derivatives. Addition of BMIM PF_6 is the most advantageous for improvement of efficiency of the chromatographic system and peak symmetry. In turn, addition of small amount (5 mM) of OMIM BF_4 makes the system more sensitive for separation of isomers and derivatives differing in the substituent kind.

It should be mentioned here that additionally performed conductivity measurements of the eluent systems containing increasing OMIM BF_4 concentration showed the point of inflection of the obtained curve at 30 mM content of this ionic liquid. Considering amphiphilic properties of OMIM cation, micelle can be formed at such high concentration. At micellar conditions further improvement of separation can be achieved. Compounds number **6** and **19** differing in the position of methoxy-group in the phenyl ring improve their separation from 0.43 to 1.98 at micellar OMIM BF_4 concentration. Similarly, the pairs of chloro derivatives: **10**–**11** and **12**–**13** differing in the position of chlorine which were unseparated achieved Δk 0.52 and 1.92 respectively at higher OMIM BF_4 content.

4. Conclusion

In the present study the usefulness of room temperature imidazolium based ionic liquids as the mobile phase modifiers has been proved in RP-HPLC analysis of biologically active 1-(1-arylimidazolidyn-2-ylidyn)-3-aryl-alkyl urea derivatives. The presence of ionic liquids in the mobile phase was associated with creating of H-bonding between the ionic liquid's cation and tested compounds. It was found that ionic liquid's anion also play an important role in analytes' chromatographic behavior. For instance neutral anion (according to Hofmeister classification) improves correlation of chromatographically derived lipophilicity parameters with calculated ones, chaotropic anion improves peak parameters whereas tetrafluoroborates are sensitive for isomers separation. Furthermore this is the first time when ionic liquid (OMIM BF_4) was used as a surfactant agent creating micelle in RP-HPLC system.

References

[1] H. Mayer, Zur Theorie der Alkoholnarkose—Erste Mittheilung. Welche Eigenschaft der Anasthetica bedingt ihre narkotische Wirkung, Archiv fur Experimentelle Pathologie und Pharmakologie 42 (1899) 109–118.
[2] E. Overton, Studien ber die Narkose, zugleich ein Beitrag zur allgemeinen Pharmakologie, Gustav Fischer, Jena, Switzerland, 1901.
[3] C. Hansch, A. Leo, Substituent Constants for Correlation Analysis in Chemistry and Biology, Wiley/Interscience, New York, 1979.
[4] S. Gocan, G. Cimpan, J. Comer, Lipophilicity measurements by liquid chromatography, Adv. Chromatogr. 44 (2006) 79–176.
[5] R. Kaliszan, Chromatography and capillary electrophoresis in modelling the basic processes of drug action, Trends Anal. Chem. 18 (1999) 400–410.
[6] A. Berthod, S. Carda-Broch, Determination of liquid–liquid partition coefficients by separation methods, J. Chromatogr. A 1037 (2004) 3–14.
[7] A.J.P. Martin, A new form of chromatogram employing two liquid phases, Biochem. J. 35 (1941) 1358–1368.
[8] E. Soczewiński, C.A. Wachtmeister, The retention between the composition of certain ternary two-phase solvent systems and RM values, J. Chromatogr. 7 (1962) 311–320.
[9] G.L. Biaggi, M.C. Barbaro, A. Sapone, J. Recanatini, Determination of lipophilicity by means of reversed-phase thin-layer chromatography. I. Basic aspects and relationship between slope and intercept of TLC equations, J. Chromatogr. A 662 (1994) 341–361.
[10] J.G. Dorsey, M.G. Khaledi, Hydrophobicity estimations by reversed-phase liquid chromatography: implications for biological partitioning processes, J. Chromatogr. A 656 (1993) 485–499.
[11] E. Szacoń, M. Rządkowska, S. Fidecka, E. Kędzierska, D. Matosiuk, Polish Patent, PL, 207564.
[12] M. Rządkowska, E. Szacoń, D. Matosiuk, E. Kędzierska, S. Fidecka, Polish Patent, PL, 208540.
[13] E. Szacoń, M. Rządkowska, D. Matosiuk, E. Kędzierska, S. Fidecka, Polish Patent, PL, 208539.
[14] K. Valkó, C. Bevan, D. Reynolds, Chromatographic hydrophobicity index by fast-gradient RP-HPLC: a high-throughput alternative to log *P*/log *D*, Anal. Chem. 69 (1997) 2022–2029.
[15] X. Hu, J. Peng, Y. Huang, D. Yin, J. Liu, Ionic liquids as mobile phase additives for high-performance liquid chromatography separation of phenoxy acid herbicides and phenols, J. Sep. Sci. 32 (2009) 4126–4132.
[16] J. Flieger, Effect of ionic liquids as mobile-phase additives on chromatographic parameters of neuroleptic drugs in reversed-phase high-performance liquid chromatography, Anal. Lett. 42 (2009) 1632–1649.
[17] J. Flieger, A. Czajkowska-Żelazko, Ionic liquids as mobile phase additives in reversed-phase high performance liquid chromatography, J. Liq. Chromatogr. Relat. Technol. 34 (2011) 2224–2242.

Journal of Pharmaceutical and Biomedical Analysis 66 (2012) 68–74

Contents lists available at SciVerse ScienceDirect

Journal of Pharmaceutical and Biomedical Analysis

journal homepage: www.elsevier.com/locate/jpba

Quantification of main bioactive metabolites from saffron (*Crocus sativus*) stigmas by a micellar electrokinetic chromatographic (MEKC) method

Sándor Gonda[a], Péter Parizsa[a], Gyula Surányi[a], Gyöngyi Gyémánt[b], Gábor Vasas[a,*]

[a] University of Debrecen, Department of Botany, Division of Pharmacognosy, H-4010 Debrecen, Egyetem tér 1, Hungary
[b] University of Debrecen, Department of Inorganic and Analytical Chemistry; H-4010 Debrecen, Egyetem tér 1, Hungary

ARTICLE INFO

Article history:
Received 23 November 2011
Received in revised form 29 February 2012
Accepted 2 March 2012
Available online 10 March 2012

Keywords:
Crocus sativus
Secondary metabolites
Quality management
Micellar electrokinetic chromatography (MEKC)

ABSTRACT

Saffron is an expensive spice, cultivated in many regions of the world. Its chief metabolites include crocins, which are responsible for the coloring ability, safranal, which is the main essential oil constituent, and picrocrocin which is the main bitter constituent of the spice. A simple micellar capillary electrochromatographic (MEKC) method capable of quantifying all three types of main constituents was established. The pH, sodium dodecyl sulphate (SDS) content and electrolyte concentration of the background electrolyte was optimized. A simple extraction protocol was developed which can extract all metabolites of different polarity from the saffron stigmas. Optimal background electrolyte composed of 20 mM disodium phosphate, 5 mM sodium tetraborate, 100 mM SDS, pH was set 9.5. Optimal extracting solvent was the background electrolyte, incubated with the sample for 60 min. The proposed method allows quantification of picrocrocin, safranal, crocetin- Di-(β-D-gentiobiosyl) ester and crocetin (β-D-glycosyl)-(β-D-gentiobiosyl) ester within 17.5 min, with limit of detection values ranging from 0.006 to 0.04 mg/ml, from a single stigma.

© 2012 Elsevier B.V. All rights reserved.

1. Introduction

Saffron is an expensive spice cultivated in many regions of the world. The spice is the dried stigma of the plant *Crocus sativus* L. (*Iridaceae*). Its major cultivation regions giving high percent of the total world production are Iran, India, Spain, Greece and Morocco [1]. Besides its main application as a spice, it has recently gained interest as a potential source of pharmacologically active metabolites, which are also responsible for the spice characteristics of saffron. Being sterile, it could be only distributed throughout the region of cultivation by means of asexual reproduction, which led to a relative genetic homogeneity [2]. However, different techniques of drying and post-harvest treatment lead to different metabolite patterns [3], that is why the dried spice samples from different regions of cultivation do not have the same concentrations of main constituents. Saffron contains three different main metabolite groups, which are often analyzed by different methods and instruments. The presence of all three metabolite groups is important to achieve the desired organoleptic property of the spice, and all are linked to some potential therapeutic application, as discussed briefly below.

First, the dried stigma is well-known for its coloring ability, which was recognized already in ancient times. The coloring ability is due to the presence of the water-soluble carotenoids, crocins. The crocins are different glycosides (mono-glycosyl or di-glycosyl esters) of a C_{20} carotenoid aglycon crocetin (Fig. 1). Among the crocetin glycosides (CGs), crocetin digentiobiosyl ester is the most abundant in saffron. Crocetin is actually the precursor of crocin synthesis, its water-solubility is negligible compared to the crocin esters. The fruits of *Gardenia jasminoides* Ellis also contain some of these water-soluble carotenoids [4], but no other chief constituents of saffron are present. Being polyunsaturated, they act as natural antioxidants by efficiently scavenging reactive oxygen species [5]. This antioxidant activity can be one of the causes of the measured anti-inflammatory activity of saffron extracts, and CGs in particular. Several new potential uses have been established for saffron extracts, and crocins. Crocin and CGs were shown to have inhibitory effects on several cancer cell lines in vitro [6], and also in animal studies. The 80% ethanolic extract of saffron was shown to be effective in the treatment mild to moderate depression in randomized, placebo-controlled clinical trials on outpatients [7], but the active ingredients were not identified. Other results on effects of crocetin and its esters include anti-atherosclerotic effects, and anti-insulin resistance activity, measured mostly in rodent models [6]. The findings above make the spice an excellent candidate for being

Abbreviations: AUC, area under curve; BGE, background electrolyte; CE, capillary electrophoresis; CG, crocetin glycosides; DW, dry weight; LOD, limit of detection; LOQ, limit of quantification; MALDI-TOF, matrix assisted laser desorption and ionization – time-of-flight; MEKC, micellar electrokinetic chromatography; NACE, non-aqueos capillary electrophoresis; RSD, relative standard deviation; tCdG, trans-crocetin di-gentiobiosyl ester; tCGG, trans-crocetin gentiobiosyl glucosil ester.

* Corresponding author. Tel.: +36 52 512 900 62637; fax: +36 52 512 943 62772.
E-mail addresses: vasasg@tigris.klte.hu, vasas.gabor@science.unideb.hu (G. Vasas).

0731-7085/$ – see front matter © 2012 Elsevier B.V. All rights reserved.
doi:10.1016/j.jpba.2012.03.002

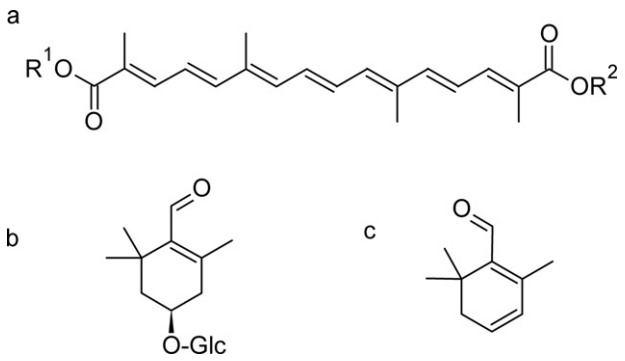

Fig. 1. Chemical structures of the studied saffron metabolites. (a) Crocetin: $R^1 = R^2 = H$, crocetin (β-D-glycosyl)-(β-D-gentiobiosyl) ester (tCGG): R^1 = glucosyl, R^2 = gentiobiosyl; crocetin di-(β-D-gentiobiosyl) ester (tCdG): $R^1 = R^2$ = gentiobiosyl; (b) picrocrocin; and (c) safranal.

a functional food. Crocetin and its esters are routinely analyzed by HPLC [8], and a non-aqueous capillary electrophoresis (NACE) method is also published for crocin separation [9]. Typical concentrations of total crocin are found to be as high as 6–16% of dry weight (DW) [6]. Other, more special methods, like Raman spectroscopy were described for estimation of these important compounds [10].

The main component responsible for the bitter taste in saffron is picrocrocin, a terpenoid glycoside (Fig. 1), which is present in 1–13% of DW in Croci stigma. Being bitter, picrocrocin is likely to be responsible for the digestion enhancing activity showed by the aqueous saffron extract on rats. It is also shown to contribute to the cytotoxic activity on some tumor cell lines [6]. Picrocrocin is quite polar, and can be analyzed by HPLC [11].

The characteristic odor of saffron is attributed to safranal (Fig. 1) content, the main compound of the saffron volatile oil (present in 30–70% in the essential oil) [6]. The essential oil also contains other compounds (probably also carotenoid breakdown-products) with similar structure [12,13]. Safranal is the product of natural deglycosylation of picrocrocin, dehydration is important in the release of safranal from picrocrocin via enzymatic activity. Safranal was shown to have anxiolytic activity in mice, and was also shown to inhibit some cancer cell lines [6]. Volatile constituents were typically determined by GC or GC–MS [12,13], but in some cases LC–MS is also employed. General (and official) methods of saffron quality management are often time consuming, expensive and many lack sufficient specificity [14].

Capillary electrophoresis (CE) separations, and micellar electrokinetic chromatography (MEKC)-related methods in particular, have major advantages. Frequently cited advantages include lower organic solvent consumption (compared to HPLC), the ability to separate compounds of very different polarity, the simplicity of sample preparation, and others which make CE and MEKC an excellent complementary method to HPLC [15].

Our aim was to develop a simple and environmentally friendly extraction protocol, and a single-run capillary MEKC method for routine screening and quality management of saffron samples, that requires only minimal amount of Croci stigma.

2. Materials and methods

2.1. Chemicals

Crocetin and safranal were purchased from Sigma–Aldrich. All used standard reagents (inorganic salts, solvents) etc. were of analytical quality (HPLC grade in the case of solvents) and were purchased from Spektrum-3D kft (Hungary). For all applications, bidistilled water was used.

2.2. Plant material

Dried plant material was obtained from local and internet markets; samples from the four main sites of production–Iran, Spain, Greece and Italy–were purchased. Residual moisture was removed from plant material with adsorbent silica.

2.3. Purification of pircocrocin and crocetin glycosides from saffron

CGs and picrocrocin were purified using a protocol based on [16]. To purify the CGs, the plant material was extracted with MeOH exhaustively, filtered, evaporated to dryness, reuptaken in 10% MeCN, and separated to fractions by RP-HPLC - Shimadzu SPD-M10A HPLC, semipreparative column: Supelco Supelcosil LC-18 column (25 cm × 10 mm, 5 μm), flow rate 3 ml/min, using a water-MeCN linear gradient (from 25 to 100%, 60 min, +0.1% TFA). Elution was monitored at 440 nm. Of the several CGs present, the fractions with the two most prominent ones were collected, and evaporated to dryness. The isolated compounds were identified by UV-Vis spectra, and MALDI-TOF analysis as described in [17]. The most prominent purified CG (31.0 min retention time) showed spectroscopic data identical to that of trans-crocetin di-(β-D-gentiobiosyl) ester (tCdG) (Fig. 1). Another purified fraction (28.5 min retention time) contained trans-crocetin (β-D-glycosyl)-(β-D-gentiobiosyl) ester (tCGG) (Fig. 1). Fragmentation patterns of glycosidic side chains helped to distinguish between possible isomers as described in [17]. Cis- and trans-crocetin glycosides were identified based on UV-Vis characteristics [18,19]. Among the CGs of saffron, these two were previously shown to be most prominent by LC/MS [19]. Other crocin fractions were also purified to determine their retention time in CE, but the amounts obtained were not enough for further identification.

Picrocrocin was purified from the same runs as described for crocin isolation. Retention time was 20.0 min, elution was monitored at 250 nm. Identification was done by UV-Vis spectrum and MALDI-TOF analysis.

2.4. Instrumentation, general settings

A PrinCE-C 700 capillary electrophoresis instrument with a diode array detector was used. A fused silica capillary (50 μm i.d., 375 μm o.d., total (effective) length: 60 cm (52 cm)) was used for the experiments. Before measurement with a new buffer, preconditioning was accomplished by washing the capillary with 0.1 M NaOH (3 min), water (3 min), and equilibration with the new BGE (10 min.). Between samples, capillary was washed with 0.1 M NaOH (3 min), water (3 min), and equilibrated with the BGE (4 min). Applied voltage was +25 kV. Samples were injected hydrodynamically, +50 mbar pressure was applied at the inlet for 0.1 min.

2.5. Optimization of analyte extraction from saffron stigmas

In order to obtain a method capable of extracting all analytes of interest, the plant material was extracted with different types of solvents, including water, methanol, and background electrolyte (optimized BGE: 20 mM disodium phosphate, 5 mM sodium tetraborate, 100 mM SDS, pH 9.5). A single dry stigma was accurately weighed (typical weight of few milligrams), reduced to powder and homogenized with 150 μl of extracting solvent. Thereafter, samples were allowed to stand at room temperature for 30 min, in darkness, followed by subsequent centrifugation at 13,000 rpm for 20 min. The supernatants were used for MEKC analysis directly. After choosing the solvent type (see Section 3.1), extraction time was optimized, i.e. incubation times of 15, 30, 60, 120 min were tested.

Linearity of extraction was also tested by extracting three different amounts of Croci stigma samples. Approximately 10, 20 and 30 mg DW/ml extracts were obtained ($n = 3$, each). Linearity was estimated by calculating the R^2 of the linear regression between the AUCs of the analytes of interest and DW of the samples.

Finally, a recovery study was carried out. Six samples of Croci stigma were extracted with MeOH, three samples with BGE. Three of the MeOH supernatants were evaporated to dryness, and reuptaken in the same amount of BGE. The three other MeOH samples were diluted with 2-fold concentrated BGE (40 mM disodium phosphate, 10 mM sodium tetraborate, 200 mM SDS in water) to obtain a BGE-like solvent. The three types of extracts were analysed with MEKC. The recovery study was done in triplicate.

2.6. MEKC method development

2.6.1. Effect of BGE composition on separation of Crocus metabolites

First, BGE pH was optimized. To test the effect of pH on the separation of the *Crocus* metabolites, a starting background electrolyte (25 mM disodium phosphate and 100 mM SDS) was set to different pHs, 6.0, 7.0, 8.0, 9.0, 9.5, 10.0. After optimization of pH, different concentrations of SDS were tested to achieve better separation of the analytes of interest. Concentrations 12.5, 25, 50, 75, 100 and 200 mM SDS were tested in a BGE containing 25 mM phosphate at pH 9.5 (1 M NaOH). To test the effect of phosphate concentration on the separation of the *Crocus* metabolites, a series of background electrolytes with pH 9.5, and 100 mM SDS was made, with phosphate concentrations 12.5, 25, 50 mM. Phosphate alone has very limited buffering capacity at pH 9.5, which may lead to pH shift in the inlet and outlet, and alteration of separation parameters [20]. After optimization of phosphate concentration, different phosphate/borate ratios were tested to achieve the same separation efficacy while increasing buffering capacity of the BGE. Different ratios of disodium phosphate/sodium tetraborate (in particular, 25/0, 20/5, 15/10, 10/15, 5/20, and 0/25 mM) concentrations were tested.

2.6.2. Testing performance of the proposed method

To test the method for the ability to separate common minor peaks in *Crocus sativus*, samples from different regions were tested with the described separation procedure, and their metabolite contents quantified. The method's ability to separate minor CG peaks from chief ones was tested by evaluation of HPLC and MEKC chromatograms in a high concentration range. A 25.0 mg of plant material was extracted exhaustively with MeOH ($3 \times 1000\,\mu l$), pooled, evaporated to dryness. A part of the dry extract was reuptaken in BGE so that the resulting solution was about 125 mg DW equivalent/ml concentrated. The supernatant was analyzed by the proposed MEKC method and checked for interfering CG peaks. Another part of the dry extract was analyzed by HPLC. The same instrumentation and main parameters were used, as described for metabolite purification, but a much smaller amount (equivalent DW: 100 μg, in 10 μl 20% MeCN) of the extract was injected.

2.6.3. Validation

For quantification, five-point standard calibration curves were used for all analytes, standards dissolved in BGE. Picrocrocin was detected at 250 nm, CGs and crocetin at 440 nm, safranal at 310 nm.

Precision was calculated as RSD values with respect to retention time and AUC. The values were determined in the range that contains the common concentrations of the real samples. Intraday repeatability was measured from 6 replicates. Interday repeatability was measured by calculating the RSD between the means of within-day results for both retention time and AUC, for all analytes', data of three days were used.

Sensitivity was expressed as LOD and LOQ values. Upper limit of quantification was assumed to be the most concentrated standard solution tested. Linearity was expressed as R^2 of the linear regression function between area under curve values and concentrations of standard solutions.

Accuracy was calculated by spiking the extracts with known amount of standards (50, 100 and 150% of the nominal concentrations, within linear range), and the recoveries calculated for all analytes ($n = 3$).

3. Results and discussion

3.1. Optimal extraction parameters

The saffron stigmas contain metabolites of a wide polarity spectrum, i.e. safranal is an apolar constituent, an essential oil compound immiscible with water, but picrocrocin and CGs are glycosidic (Fig. 1) and therefore dissolve excellently in water. Thus, different solvents were tested for extraction.

The background electrolyte (20 mM disodium phosphate, 5 mM sodium tetraborate, 100 mM SDS in water, pH 9.5) was found to extract most metabolites from the stigmas, whereas methanol and water extracted less metabolites, especially in the case of safranal. Direct injection of methanol extracts resulted in very poor general resolution. In water extracts, the peak of crocetin (present only in traces in BGE or MeOH extracts) was also not detected. Therefore, BGE was chosen as extracting solvent, and extraction time for BGE was optimized.

It was found, that the metabolite concentration–time functions follow a saturation curve. The 120 min extract contained equal amount of safranal, picrocrocin and only insignificantly more crocin esters than the 60 min extract ($p > 0.05$ for all analytes, ANOVA, $n = 3$). The plant material visibly lost its color at the end of the 60 min incubation. Shorter incubation times resulted in much less metabolite concentration in the supernatant. The 30 min extract contained 30–60% less metabolites (area under curve), than the 60 min extract. Therefore, 60 min extraction time was chosen for further experiments as a compromise.

Linearity of the extraction was tested by showing linear relationship between area under curve values of analytes and plant material DW mass in extracts of different concentrations (10, 20 and 30 mg DW/ml). Linearity was confirmed by the high R^2 values of the linear regression, R^2 values were 0.9932, 0.9934, 0.9908 and 0.9807 for picrocrocin, safranal, tCdG and tCGG, respectively ($p < 0.001$). Extraction was found to be linear at least up to 30 mg DW/ml.

Extraction efficiency using the proposed BGE was compared with that achieved using MeOH. MeOH extracts were evaporated to dryness, and the dried extract was reuptaken in BGE, and analysed with the proposed MEKC method. Safranal could not be recovered this way, because this volatile substance evaporated during vacuum drying of the MeOH extract, causing significant reduction of the recovered amount. Therefore, three other replicates of MeOH extracts were diluted with double-concentration BGE, and analysed. Presence of MeOH in the sample did not significantly alter the resolution of safranal. Recoveries were 107, 108, 119 and 116% for picrocrocin, safranal, tCdG and tCGG, respectively ($n = 3$). The BGE extraction solvent was found to be as efficient as MeOH–the difference was not found to be significant ($p > 0.05$).

Samples in BGE were found to be stable for at least 24 h after extraction, at room temperature, in darkness.

3.2. Separation of Crocus analytes

For method development, sample aliquots obtained from Croci stigma by extraction with BGE for 60 min were used. Metabolite identification was accomplished by standard addition to the plant samples.

3.2.1. Effect of pH on the separation of Crocus metabolites

First, experiments were run to determine the optimal pH for the separation of the metabolites of interest. A pH series including 6, 7, 8, 9, 9.5 and 10 was tested, the BGE contained 100 mM SDS and 25 mM phosphate. Changes in pH generally have great impact on EOF, dissociation of analytes and BGE components, complexes with BGE components, and thereby resolution [21].

As picrocrocin does not contain any dissociable functional groups, its retention time is only affected by interactions with micelles. The retention time of picrocrocin was not seriously affected by pH, it was around 5 min, but baseline separation from an unidentified impurity with higher retention time was not achieved at pHs 8 and 9.

Retention time of safranal was also not influenced by pH in the higher pH range. Safranal does not have any dissociable functional groups, its separation is only influenced by interactions with SDS micelles and EOF, but is relatively more apolar, than picrocrocin, resulting in more intensive micelle interaction and higher retention time.

Separation of CGs from each other was influenced by pH in spite of not being able to dissociate at the pH-s tested (Fig. 2). Resolution became a little better at higher pH-s between tCdG and tCGG (peaks 3 and 4 on Fig. 2), best separation of the crocin esters was achieved at pH 9.5 (Fig. 2d) and pH 10 (not shown). The retention time of an unidentified trans-crocin (peak 1 on Fig. 2) was more effected, at pH 10 this compound could not be separated from the main crocin esters (tCdG and tCGG), lower pH values resulted in lower retention times. Resolution between tCdG and an unidentified compound possessing cis-crocin UV-Vis spectrum (peak 2 in Fig. 2) was also best at high pH (9.5 or above, Fig. 2d). Finally, pH 9.5 BGE was selected for further experimentation because of increased resolution between the different crocins, and between picrocrocin and the impurities.

3.2.2. Effect of SDS concentration on the separation of Crocus metabolites

After optimization of pH, different SDS concentrations were tested. SDS concentration had great impact on retention times. In the case of picrocrocin, SDS concentration affected separation from impurities and retention time. At higher SDS concentration, higher retention times and better separation was obtained. Picrocrocin was separated from impurities at 50 mM SDS or higher concentration. As picrocrocin is uncharged and semipolar, its partition between the micellar and water phase greatly influences the retention time and separation.

The retention times of safranal was also influenced by SDS concentration. Higher SDS concentrations led to higher retention times. At the highest tested concentration (200 mM), safranal peak was not observed, retention time must have increased above total run time (30 min).

At lower concentrations (50 mM or below), crocin separation was not satisfactory (Fig. 3a–c). Higher concentrations of SDS increased the retention time of CGs. Resolution between tCdG and tCGG (peaks 3 and 4 on Fig. 3) was best at 100 mM SDS, as some other minor impurities (an unidentified cis-crocin, and other unidentified trans-crocins) merged into one or more crocin peak complexes at lower SDS concentrations (Fig. 3a–c). Separation of tCdG from an unidentified cis-crocin (peak 2 on Fig. 3) was only achieved at 100 mM SDS (Fig. 3d). Though unidentified, a method's capability of separating cis-crocins is important because abundance of these molecules (i.e. ratio of cis/trans crocins) can interfere with routine spectrophotometric quality management of the spice [22], as they have an absorption maximum around 330 nm. The paper [9] was also dealing with crocin separation, but no clear statement of cis-crocin separation was mentioned. At 200 mM, crocin esters were not detected, probably because retention time has increased above total run time. As a sum, 100 mM SDS was selected for further optimization, mainly because it separated CGs sufficiently.

3.2.3. Effect of phosphate concentration on the separation of Crocus metabolites

Changes in phosphate concentration did not alter retention time of picrocrocin, as it was expected. In the case of safranal, changes were also minimal. Higher phosphate concentration (50 mM)

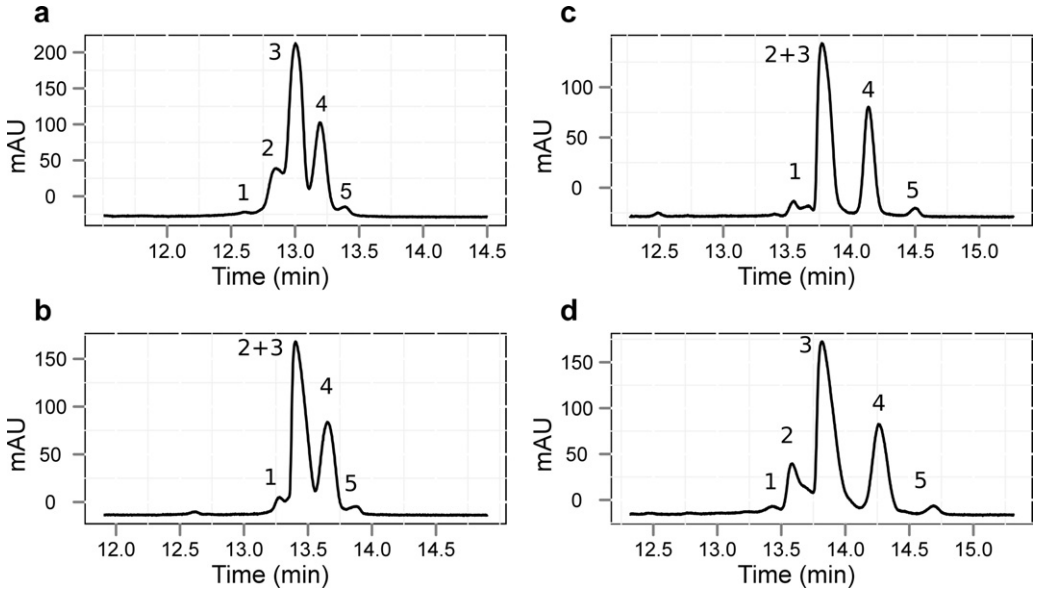

Fig. 2. Effect of background electrolyte pH on the separation of different crocetin glycosides. BGE contained 100 mM SDS and 25 mM phosphate. Detection was done at 440 nm. Subplots: (a) pH 7.0; (b) pH 8.0; (c) pH 9.0; and (d) pH 9.5. Metabolites: (1) unidentified trans-crocin; (2) unidentified cis-crocin; (3) tCdG; (4) tCGG; and (5) unidentified trans-crocin.

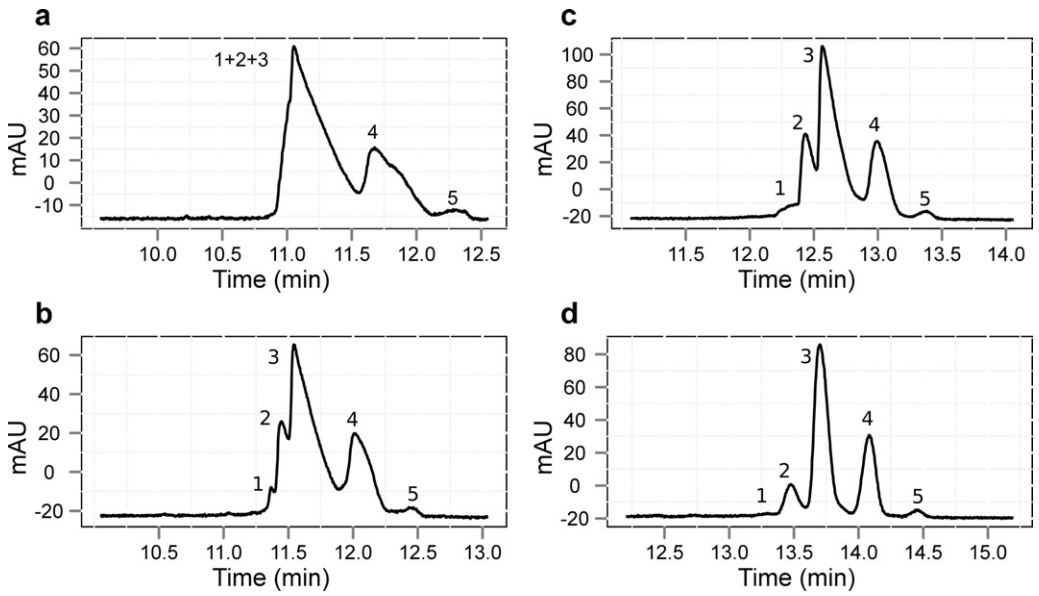

Fig. 3. Effect of SDS concentration on the separation of different crocetin glycosides. BGE contained 25 mM phosphate, pH was set 9.5. Detection was done at 440 nm. Subplots: (a) 12.5 mM SDS; (b) 25 mM SDS; (c) 50 mM SDS; and (d) 100 mM SDS. Metabolites: (1) unidentified trans-crocin; (2) unidentified cis-crocin; (3) tCdG; (4) tCGG; and (5) unidentified trans-crocin.

increased current, and resulted in a general loss of resolution. Lower phosphate concentrations (12.5 mM) resulted in loss of resolution between CGs. Thus, 25 mM phosphate was selected as optimal electrolyte concentration.

3.2.4. *Effect of disodium phosphate/sodium tetraborate ratio on the separation of Crocus analytes*

The phosphate-based BGE at pH 9.5 has very limited buffering capacity; therefore it may theoretically be susceptible to pH changes in the inlet and the outlet, thereby affecting reproducibility [20]. Shifts in pH need to be minimized to increase the amount of samples that can be run without changing the BGE. Though no significant shift in retention times after 10 sample determinations was observed, the BGE was further optimized to increase its buffering capacity. Borate also may offer increased selectivity due to complexation of sugar side-chains of glycosides [23].

As BGEs with higher total electrolyte concentrations could only be used at lower voltage, which leads to unwanted significant increase in retention times, this strategy was not tested. Instead, the BGE was further optimized by partially replacing disodium phosphate with sodium tetraborate, that has significant buffering capacity at this pH. All borate-containing BGEs were found to have significantly more (at least 20-fold) buffering capacity at pH 9.5 than the BGE based solely on disodium phosphate (determined by pH meter); detailed description of the issue is available in [24].

Replacing 25 mM phosphate with 20 mM phosphate and 5 mM borate did not influence the resolution of CGs. Higher borate concentrations (10 mM borate/15 mM phosphate), however, led to decreased resolution between the major cis-CG and the main trans-CGs, and also increased retention times of all analytes. Peak broadening also occurred at high sodium tetraborate concentrations. Major effects on other analytes' resolution were not observed.

It was hypothesized, that increased heating because of higher current (at higher borate concentration) may be in the background of resolution loss. However, lower concentration BGEs (e.g. 10 mM sodium tetraborate, 5 mM disodium phosphate, 100 mM SDS, pH 9.5) also produced poor resolution between CGs. Thus, it was concluded, that higher disodium phosphate concentrations are required for acceptable CG separation. A small concentration (5 mM) of sodium tetraborate was found to be necessary to increase the buffering capacity of the BGE to ensure long-term system stability. Final optimal BGE composition was: 20 mM disodium phosphate, 5 mM sodium tetraborate, 100 mM SDS, pH 9.5. A typical chromatogram of a real sample analysed with the final method is plotted in Fig. 4.

3.3. *Testing of the method*

Samples from dried spice products from Greek, Iranian, Italian and Spanian saffron were subjected to analysis using the extraction and MEKC method proposed above, the results are summarized in Table 1. Picrocrocin and safranal concentrations were comparable to those formerly described for *Crocus* stigmas [16]. Data on concentrations of individual crocetin glycosides (tCdG and tCGG) can be found in [9] and [25], the concentrations of these chief CGs were comparable to those measured in this work. The ratio of different CGs differs in the samples from different geographical sources, also the content of other metabolites was found to be related to the source. The quantitative comparative analysis of *Crocus* samples between production regions, and estimation of variance within regions was beyond the scope of this study. Our

Table 1
Results of a single-extraction screening of saffron samples from different regions. Values are given on dry weight basis. Presented data are mean ± SD from three determinations ($n = 3$). Abbreviations: tCGG: crocetin (β-D-glycosyl)-(β-D-gentiobiosyl) ester; tCdG: crocetin di-(β-D-gentiobiosyl) ester.

Analyte	Greek (%)	Iranian (%)	Italian (%)	Spanish (%)
Picrocrocin	3.993 ± 0.118	2.286 ± 0.153	5.809 ± 0.232	8.026 ± 0.261
tCdG	4.473 ± 0.146	2.208 ± 0.020	3.076 ± 0.073	6.370 ± 0.195
tCGG	0.715 ± 0.052	0.448 ± 0.032	0.919 ± 0.021	1.393 ± 0.033
Safranal	0.051 ± 0.002	0.019 ± 0.003	0.158 ± 0.003	0.081 ± 0.009

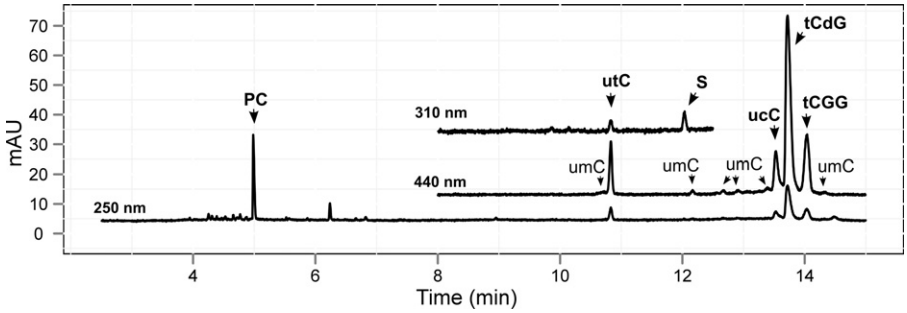

Fig. 4. MEKC chromatogram obtained from a Greek *Crocus* sample using the proposed analytical procedure. Detection was done on 250, 310 and 440 nm wavelengths. The 310 nm chromatogram is raised by a factor of 2, the chromatogram at 440 nm is reduced by a factor of 0.5 to allow better emplacement. Chief constituents are marked with arrows. Abbreviations: PC, picrocrocin; S, safranal; umC, unidentified minor crocin; utC, unidentified trans crocin; ucC, unidentified cis crocin, tCGG: crocetin (β-D-glycosyl)-(β-D-gentiobiosyl) ester; tCdG: crocetin di-(β-D-gentiobiosyl) ester.

Table 2
Analytical performance of the optimized capillary electrophoretic procedure for quantification of saffron chief metabolites. Abbreviations: AUC, area under curve; DW, dry weight; RSD, relative standard deviation; tCGG, crocetin (β-D-glycosyl)-(β-D-gentiobiosyl) ester; tCdG, crocetin di-(β-D-gentiobiosyl) ester; tR, retention time.

	Picrocrocin	Safranal	tCdG	tCGG
Accuracy (mean of recoveries, $n = 3 \times 3$)	105.3%	101.4%	106.7%	96.9%
Precision (tR, intraday, $n = 6$), RSD	0.67%	0.76%	0.70%	0.73%
Precision (tR, interday, $n = 3$), RSD	0.14%	1.03%	1.35%	1.42%
Precision (AUC, intraday, $n = 6$), RSD	2.65%	2.40%	2.29%	3.54%
Precision (AUC, interday, $n = 3$), RSD	2.27%	1.62%	0.44%	2.50%
Linear regression equation	$1.1411x - 0.0379$	$2.0379x - 0.0115$	$5.3137x + 1.1446$	$7.6559x + 0.0309$
Linearity (R^2 of linear regression)	0.9969	0.9999	0.9981	0.9999
LOD (mg/ml)	0.012	0.002	0.003	0.002
LOQ (mg/ml)	0.040	0.006	0.010	0.006
Range (upper limit of quantification) (mg/ml)	1.20	1.00	1.70	0.80
Typical extract content (1.5 mg DW/100 μl), (mg/ml)	0.3199	0.0363	0.8070	0.1681

main goal was achieved however, by showing that the proposed method separated impurities from analytes of interest – regardless of geographical origin.

Minor crocins could be also detected from a preconcentrated sample (equivalent to 125 mg DW/ml) at 440 nm, separated from the main crocins. Higher concentration was necessary to prove that the minor peaks have CG-like UV-Vis spectra. The electropherograms of samples with the proposed extraction concentration also show most of these minor CG peaks separated from the main analytes of interest (Fig. 4). The minor CG peaks made up only 9.7% of total 440 nm AUC. This concentration was within the linear range of determination.

The HPLC chromatograms of the concentrated MeOH extracts of the stigmas also showed four main crocins, that could be assigned to the four main peaks in the chromatogram (*Crocus* extracts were spiked with the purified, unidentified major CGs as well). The sum of the AUCs of the minor peaks in HPLC contributed very little to the total crocin AUC. The HPLC pattern found was comparable to that published in [19]. We concluded, that the minor CGs do not cause any significant interference during the determination of chief CG analytes.

The described method is also capable of detecting crocetin (extract spiked with standard). None of the stigma samples contained significant concentrations, some contained trace amounts. Crocins were well separated from crocetin, as crocetin dissociates at the BGE pH.

The validation results for the proposed analytical method are summarized in Table 2. The method showed acceptable reproducibility, the extraction protocol as well as the measurement method itself were shown to be efficient. LOD values and RSD values were comparable to those obtained by a NACE method for crocin determination [9]. The proposed method can be an inexpensive means of screening and quantification. It can be a complementary analytical procedure to the published HPLC methods [16,19], as it allows quantification of all main constituents (picrocrocin, the two main crocetin glycosides: tCdG and tCGG, and safranal) within reasonable time, from a single stigma of the *Crocus sativus* plant. The proposed method can thus be used for plant-to-plant variability studies.

4. Conclusions

A simple protocol for determination of all main saffron metabolite groups of high consumer interest was established. The proposed extraction method and subsequent MEKC quantification allows determination of two crocetin glycosides (responsible for coloring ability), picrocrocin (main bitter compound), and safranal (chief constituent of the essential oil, hence, smell). The protocol is carried out in an environmentally friendly fashion (uses no organic solvent), the used reagents are rather inexpensive. The short time required for analysis of a sample allows application as a routine screening and quality-management technique for saffron. The chromatogram pattern also helps estimating cis-crocin to trans-crocin ratios. The low sample demand (single stigma) of the proposed method allows it to be applied for studying plant-to-plant variability.

Acknowledgements

This work was supported by grants OTKA No. K 81370 and Baross_EA07_EA_ONKFI-_07_2008_0002. G. Vasas was financially supported by the Bolyai János Research scholarship.

References

[1] L. Maggi, M. Carmona, S.D. Kelly, N. Marigheto, G.L. Alonso, Geographical origin differentiation of saffron spice (*Crocus sativus* L. stigmas) – preliminary investigation using chemical and multi-element (H, C, N) stable isotope analysis, Food Chem. 128 (2011) 543–548.

[2] M.G. Caiola, P. Caputo, R. Zanier, RAPD analysis in *Crocus sativus* L. accessions and related Crocus species, Biol. Plant. 48 (2004) 375–380.
[3] M. Gregory, R. Menary, N. Davies, Effect of drying temperature and air flow on the production and retention of secondary metabolites in saffron, J. Agr. Food Chem. 53 (2005) 5969–5975.
[4] A. Ozaki, M. Kitano, N. Furusawa, H. Yamaguchi, K. Kuroda, G. Endo, Genotoxicity of gardenia yellow and its components, Food Chem. Toxicol. 40 (2002) 1603–1610.
[5] A.N. Assimopoulou, Z. Sinakos, V.P. Papageorgiou, Radical scavenging activity of *Crocus sativus* L. extract and its bioactive constituents, Phytother. Res. 19 (2005) 997–1000.
[6] J.P. Melnyk, S. Wang, M.F. Marcone, Chemical and biological properties of the world's most expensive spice: saffron, Food Res. Int. 43 (2010) 1981–1989.
[7] S. Akhondzadeh, H. Fallah-Pour, K. Afkham, A.-H. Jamshidi, F. Khalighi-Cigaroudi, Comparison of *Crocus sativus* L. and imipramine in the treatment of mild to moderate depression: a pilot double-blind randomized trial [ISRCTN45683816], BMC Complem. Altern. Med. 4 (2004) 12.
[8] H. Caballero-Ortega, R. Pereda-Miranda, F. Abdullaev, HPLC quantification of major active components from 11 different saffron (*Crocus sativus* L.) sources, Food Chem. 100 (2007) 1126–1131.
[9] M. Zougagh, B. Simonet, A. Rios, M. Valcarcel, Use of non-aqueous capillary electrophoresis for the quality control of commercial saffron samples, J. Chromatogr. A 1085 (2005) 293–298.
[10] E.G. Anastasaki, C.D. Kanakis, C. Pappas, L. Maggi, A. Zalacain, M. Carmona, G.L. Alonso, M.G. Polissiou, et al., Quantification of crocetin esters in saffron (*Crocus sativus* L.) using Raman spectroscopy and chemometrics, J. Agr. Food Chem. 58 (2010) 6011–6017.
[11] C.P. del Campo, M. Carmona, L. Maggi, C.D. Kanakis, E.G. Anastasaki, P.A. Tarantilis, M.G. Polissiou, G.L. Alonso, et al., Picrocrocin content and quality categories in different (345) worldwide samples of saffron (*Crocus sativus* L.), J. Agr. Food Chem. 58 (2010) 1305–1312.
[12] M. Jalali-Heravi, H. Parastar, H. Ebrahimi-Najafabadi, Characterization of volatile components of Iranian saffron using factorial-based response surface modeling of ultrasonic extraction combined with gas chromatography-mass spectrometry analysis, J Chromatogr. A 1216 (2009) 6088–6097.
[13] C.D. Kanakis, D.J. Daferera, P.A. Tarantilis, M.G. Polissiou, Qualitative determination of volatile compounds and quantitative evaluation of safranal and 4-hydroxy-2, 6, 6-trimethyl-1-cyclohexene-1-carboxaldehyde (HTCC) in Greek saffron, J. Agr. Food Chem. 52 (2004) 4515–4521.
[14] R.S. Verma, D. Middha, Analysis of saffron (*Crocus sativus* L. Stigma) components by LC–MS–MS, Chromatographia 71 (2010) 117–123.
[15] L. Suntornsuk, Recent advances of capillary electrophoresis in pharmaceutical analysis, Anal. Bioanal. Chem. 398 (2010) 29–52.
[16] M. Lage, C.L. Cantrell, Quantification of saffron (*Crocus sativus* L.) metabolites crocins, picrocrocin and safranal for quality determination of the spice grown under different environmental Moroccan conditions, Sci. Hortic. 121 (2009) 366–373.
[17] H. Zhang, Y. Zeng, F. Yan, F. Chen, X. Zhang, M. Liu, W. Liu, et al., Semi-preparative isolation of crocins from saffron (*Crocus sativus* L.), Chromatographia 59 (2004) 691–696.
[18] M.K. Assimiadis, P.A. Tarantilis, M.G. Polissiou, UV-Vis, FT-Raman and 1H NMR spectroscopies of cis – trans carotenoids from saffron (*Crocus sativus* L.), Appl. Spectrosc. 52 (1998) 519–522.
[19] P.A. Tarantilis, G. Tsoupras, M. Polissiou, Determination of saffron (*Crocus sativus* L.) components in crude plant extract using high-performance liquid chromatography-UV-visible photodiode-array detection-mass spectrometry, J. Chromatogr. A 699 (1995) 107–118.
[20] D. de Jesus, J. Brito-Neto, E. Richter, L. Angnes, I. Gutz, C. do Lago, Extending the lifetime of the running electrolyte in capillary electrophoresis by using additional compartments for external electrolysis RID B-3091-2008 RID G-5711-2011 RID A-1852-2008, Anal. Chem. 77 (2005) 607–614.
[21] S.E. Deeb, M.A. Iriban, R. Gust, MEKC as a powerful growing analytical technique, Electrophoresis 32 (2011) 166–183.
[22] M. Zougagh, A. Rios, M. Valcarcel, Determination of total safranal by in situ acid hydrolysis in supercritical fluid media: application to the quality control of commercial saffron, Anal. Chim. Acta 578 (2006) 117–121.
[23] P. Morin, F. Villard, M. Dreux, P. André, Borate complexation of flavonoid-O-glycosides in capillary electrophoresis. II. Separation of flavonoid-3-O-glycosides differing in their sugar moiety, J. Chromatogr. A 628 (1993) 161–169.
[24] J.C. Reijenga, T.P.E.M. Verheggen, J.H.P.A. Martens, F.M. Everaerts, Buffer capacity, ionic strength and heat dissipation in capillary electrophoresis, J. Chromatogr. A 744 (1996) 147–153.
[25] S.A. Ordoudi, M.Z. Tsimidou, Saffron quality effect of agricultural practices, processing and storage, in: R. Dris, S.M. Jain (Eds.), Production Practices and Quality Assessment of Food Crops: Preharvest Practice, Springer, 2004, pp. 209–260.

Journal of Pharmaceutical and Biomedical Analysis 66 (2012) 75–84

Contents lists available at SciVerse ScienceDirect

Journal of Pharmaceutical and Biomedical Analysis

journal homepage: www.elsevier.com/locate/jpba

A high pH based reversed-phase high performance liquid chromatographic method for the analysis of aminoglycoside plazomicin and its impurities

Li Tan[a,*], Kenneth B. Wlasichuk[a], Donald E. Schmidt Jr.[a], Robert L. Campbell[a], Pam Hirtzer[b], Lisa Cheng[c], Dane E. Karr[a]

[a] Department of Analytical Chemistry, Achaogen, Inc., 7000 Shoreline Court, Suite 371, South San Francisco, CA 94080, United States
[b] PharmDev Associates, LLC, 291 Scenic Ave, Piedmont, CA 94611, United States
[c] Biopharm Consulting Services, South San Francisco, CA 94080, United States

ARTICLE INFO

Article history:
Received 20 December 2011
Received in revised form 2 March 2012
Accepted 2 March 2012
Available online 10 March 2012

Keywords:
Aminoglycoside
Plazomicin (ACHN-490)
High pH based mobile phase
RP-HPLC
Mass spectrometry

ABSTRACT

A reversed-phase high performance liquid chromatographic (RP-HPLC) method has been developed for the aminoglycoside (AG) plazomicin (ACHN-490). This method employed a high pH mobile phase (pH > 11) with a gradient of 0.25 M ammonium hydroxide in water and acetonitrile, an XBridge C_{18} column and UV detection at 210 nm. Although the molar UV absorption of plazomicin is weak, the high pH conditions of this method allow for higher loadings, which compensates for the inherent low UV sensitivity. Under these high pH conditions, impurities and degradants were base line separated from plazomicin. The mobile phases used for this method allowed for on-line mass detection for the impurities and degradants.

The RP-HPLC method has been validated in terms of specificity, linearity and range, accuracy, and precision. The analytical method met specificity requirements of a homogenous peak with no interferences from the blank or from the known impurities in plazomicin. The linearity of the method for the plazomicin impurity determination was excellent, with a coefficient of determination (r^2) of 0.9993, over the freebase (FB) concentration range of 0.0025–3.0 mg/mL. The method is capable of detecting impurities down to 0.1% of the peak area of plazomicin. A single point standard at a concentration of 1.0 mg/mL FB was validated over the range of 50–150% for quantitation of the freebase content (the assay) in bulk drug substance. The mean recoveries of FB are in the range 98.6–102.0% with a mean RSD (relative standard deviation) <1.0%. The study also examined the method precision for purity, impurities and the assay with two instruments on two different days. The method showed adequate accuracy and precision for the intended use. This high pH method was successfully used to determine the impurity and measure the drug content in the final plazomicin drug substance. In addition, the method with an on-line mass spectrometry detector has been used to characterize the structures of the impurities in plazomicin.

© 2012 Elsevier B.V. All rights reserved.

1. Introduction

Aminoglycosides (AGs) are highly potent, broad-spectrum antibiotics used for treating serious bacterial infections and are frequently used empirically for treating complicated urinary tract infections, nosocomial respiratory tract infections, complicated intra-abdominal infections, and septicemia. Plazomicin is a broad-spectrum AG with differentiated activity against multidrug resistant Enterobacteriaceae and is being developed by Achaogen, Inc. as a first line treatment for resistant bacterial pathogens [1,2]. Plazomicin is a polar molecule of linked sugars that contain five amino groups (Fig. 1) with pK_a values 6.2, 7.3, 8.1, 8.8 and 9.7, as determined by titration. There is a need for an analytical method to determine the freebase content and monitor the impurities and degradants in plazomicin as a drug substance. Because of its extreme polarity, plazomicin is not well retained on conventional reversed phase columns. Furthermore, the weak UV active groups in the molecule prevent facile use of the convenient and robust UV detector.

Many different HPLC techniques have been developed to determine the impurity and content of aminoglycosides. Several methods are documented in the United States Pharmacopeia [3]. Sensitive conventional reversed phase methods employing fluorescence detection for gentamicin derivatized with o-phthalaldehyde and UV detection for tobramycin derivatized with 2,4-dinitrofluorobenzene are described. Derivatization is sensitive, but results can be hard to reproduce. Interference of the reagent or its products creates an overall tedious process. A low

* Corresponding author. Tel.: +1 6502434909; fax: +1 6502661130.
E-mail address: ltan@achaogen.com (L. Tan).

0731-7085/$ – see front matter © 2012 Elsevier B.V. All rights reserved.
doi:10.1016/j.jpba.2012.03.003

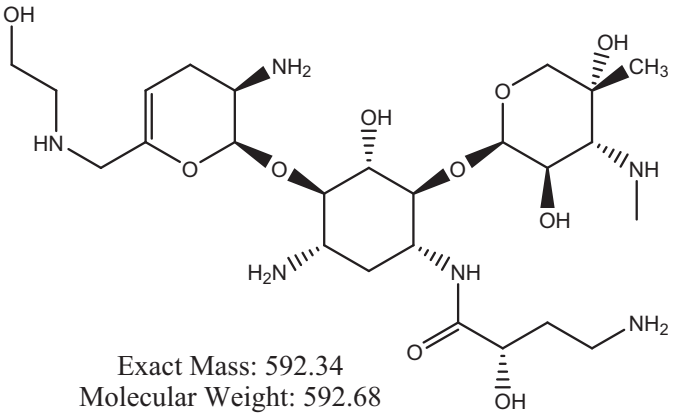

Fig. 1. Structures of plazomicin.

pH, reversed phase method with the ion pairing agent sodium heptanesulfonate in organic and aqueous mobile phases utilizing low wavelength detection at 205 nm is noted for netilmicin, but the method lacks sensitivity as the loading capacity is low [4,5].

With the introduction of new detectors, various methods for aminoglycoside analysis have been explored. A liquid chromatography–mass spectrometry (LC–MS) method using a 10 mM ammonium hydroxide mobile phase has been developed for tobramycin [6] concentration analysis in pharmaceutical formulations. Since ionization in the mass spectrometer is highly dependent upon mobile phase conditions, the method may lack robustness for impurity determination. Recently the highly sensitive pulsed amphoteric detector (PAD) [3,7,8] and the charged aerosol detector (CAD) [9] have been employed for the analysis of amikacin, kanamycin, netilmicin, gentamicin and neomycin. Since the CAD cannot be used with mobile phases with a pH greater than 7.5 [10], this detector is not suitable for separations at a high pH. Dionex demonstrated an improved high-performance anion-exchange chromatography with pulsed amperometric detection (HPAE-PAD) for neomycin purity analysis and its concentration determination in neosporin topical ointment, a complex over-the-counter pharmaceutical formulation [11]. Although this detector is suitable for impurity analysis, a potassium hydroxide containing mobile phase with a high performance anion exchange stationary phase or an octane sulfonic acid containing mobile phase with a reversed stationary phase precludes the easy use of a mass spectrometer as a detector for the identification of impurities.

This study describes the analysis of an aminoglycoside plazomicin that incorporates a robust UV detector and uses an on-line mass spectrometer for structural elucidation of impurities in plazomicin.

2. Experimental

2.1. Chemicals and reagents

Water, acetonitrile, and 28–30% ammonium hydroxide solutions were HPLC grade and were purchased from VWR International, USA (EMD brand). Heptafluorobutyric acid was from Pierce, USA. Plazomicin Reference Standard and research lots were synthesized as the sulfate salt and were produced in-house.

2.2. Instrumentations and conditions

The 1100 Series HPLC systems from Agilent Technologies (Santa Clara, CA, USA) were equipped with a binary or quaternary pump, autosampler, column heater, and diode array detector (DAD) or variable wavelength detector (VWD). Data were acquired and analyzed using Agilent ChemStation software. An XBridge C_{18}, 4.6 mm × 150 mm, 3.5 μm, P/N 186003034, column from Waters, Inc. (Milford, MA, USA) is used. Mobile phases A and B were prepared by adding 16.7 mL of 28–30% of ammonium hydroxide solution into 1 L of water and into 1 L of acetonitrile, respectively. The flow rate was 1.0 mL/min and the column temperature is 30 °C. The injection volume was 25 μL. The detection wavelength was 210 nm. The gradient was linear from 2% to 20% B in 25 min for separation followed by 2 min for washing with 95%B and then re-equilibration to 2%B. The total run time was 35 min. The mass spectrometry system for the HP 1100 was an LC-MSD SL from Agilent Technologies, and was run using electrospray ionization (ESI) in the positive ion mode with a scan range of *m*/*z* range 200–1200. The drying gas flow and the temperature were 12.0 psi and 350 °C, respectively. The capillary voltage was 3000 V and the nebulizer gas pressure was 50 psi. The tandem mass spectrometry experiments were performed using a 3200 Q Trap of AB SCIEX (Foster City, CA, USA) coupled to an LC instrument of Shimadzu's UFLC (Kyota, Japan). The ion source conditions are as follows: declustering potential 36.0 V, entrance potential 12.0 V, and ion spray voltage 2500 V. The temperature and pressure for both ion source gas 1, and gas 2 are 600 °C, and 60 psi, respectively. A fixed collision energy 35 eV was used for MS^2. The data obtained from the 3200 Q Trap were analyzed using Analyst software.

2.3. Sample preparation

Plazomicin sulfate samples were dissolved into HPLC grade water to prepare the target concentrations.

3. Results and discussion

3.1. HPLC method development

The structure of plazomicin is illustrated in Fig. 1. Plazomicin and its impurities are polar compounds that are not well retained on conventional reversed phase columns. In an initial study, acidic pH mobile phase conditions using 0.1% heptafluorobutyric acid (HFBA) in a water/acetonitrile mobile phase were investigated for plazomicin. Under these low pH conditions, some impurities cannot be separated. For the in-process samples, which have more impurities than the final purified product this makes the low pH method even more limiting. In addition, the sensitivity using UV detection at 210 nm was inadequate for the intended purpose of the method. This study describes a method that uses high pH methodology in which the pH of the mobile phase is maintained above 11 so that the neutral plazomicin is retained on the reversed phase column. Several reagents, including ammonium hydroxide, ammonium carbonate, sodium phosphate, and triethylamine, were investigated for the purposes of maintaining high pH. Among the reagents tried, ammonium hydroxide emerged as the preferred base due to its low UV absorbance and compatibility with a MS detector. The concentration of ammonium hydroxide was optimized at 0.25 M in both water and acetonitrile. The method used a shallow gradient on a Waters XBridge C_{18} column. The UV spectrum of plazomicin from 190 to 400 nm was collected on an Agilent 1100 instrument equipped with a DAD detector. The maximum absorption near 210 nm is the basis for setting the detection wavelength, in order to increase the sensitivity of the plazomicin analytical HPLC method. Unlike the initially investigated low pH method, the sensitivity of the high pH method was adequate for the purposes of the method. This probably arises because the load ability of an unionized molecule on reversed phase columns is as much as 20-fold greater than the ionized form [4]. To confirm

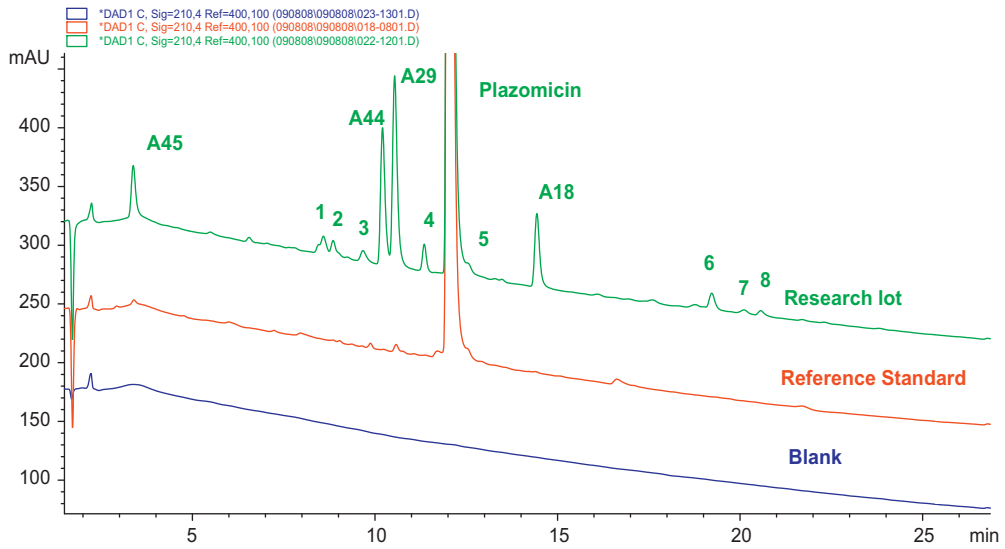

Fig. 2. Representative chromatograms of blank and plazomicin with two different purities. The blue, red and green traces represent blank, Reference Standard, and research lot of plazomicin. The HPLC condition is described in Section 2.2. (For interpretation of the references to color in this figure legend, the reader is referred to the web version of the article.)

Table 1
Comparison of column loading capacity, efficiency, and tailing factor with a low pH and high pH mobile phase for basic compound plazomicin.

Column loading	Mobile phase pH < 2		Mobile phase pH > 11	
Plazomicin (μg)	Plate	USP tailing factor	Plate	USP tailing factor
1.25	118,000	1.5	143,000	1.3
2.5	73,000	2.0	152,000	1.3
12.5	20,000	3.2	121,000	1.5
25	10,000	4.3	89,000	1.8

this finding, the column loading, efficiency, and tailing factor were studied in low pH (<2) mobile phases 0.1% HFBA in water and acetonitrile, and in high pH (>11) mobile phases on the X-Bridge column which has been designed for wide pH range conditions. The result of column loading, plate number, and the USP tailing factor for the plazomicin peak is summarized in Table 1. Plazomicin clearly overloads the column using the low pH mobile phase when 2.5 μg is injected onto the column. Plazomicin has a low loading capacity when low pH mobile phases are operated, which has a low sensitivity to monitor the impurities. The column plate number decreased and the USP tailing factor increased drastically when the loading increased. With the high pH mobile phase overloading was not observed. Hence, the high pH method was further validated.

The overlaid chromatograms of a blank and two lots of plazomicin with different impurity profiles are shown in Fig. 2. The early eluting impurity was identified as a hydrolysis product (A45). Impurities A45, A44, A29, and A18 (structure elucidation described in Section 3.3), as well as other unknown impurities are well separated from plazomicin. The columns were monitored to establish the life time in terms of the resolution between A44 and A29. It was observed that the column is able to maintain good resolution for at least 200 injections. The total ion chromatogram (TIC) from the research lot using on-line mass spectrometry detection is shown in Fig. 3. All peaks in the TIC (Fig. 3) also appear in the UV chromatogram of the research lot (Fig. 2), indicating that all impurities in the sample are detected using the UV detector. Since the mobile phase is also compatible for mass spectrometry, on-line mass analysis is an option to aid in the identification of impurities and can be readily implemented.

3.2. Method validation

Prior to using the method for analyses, two HPLC systems were evaluated for system suitability. The percent RSD of both peak areas

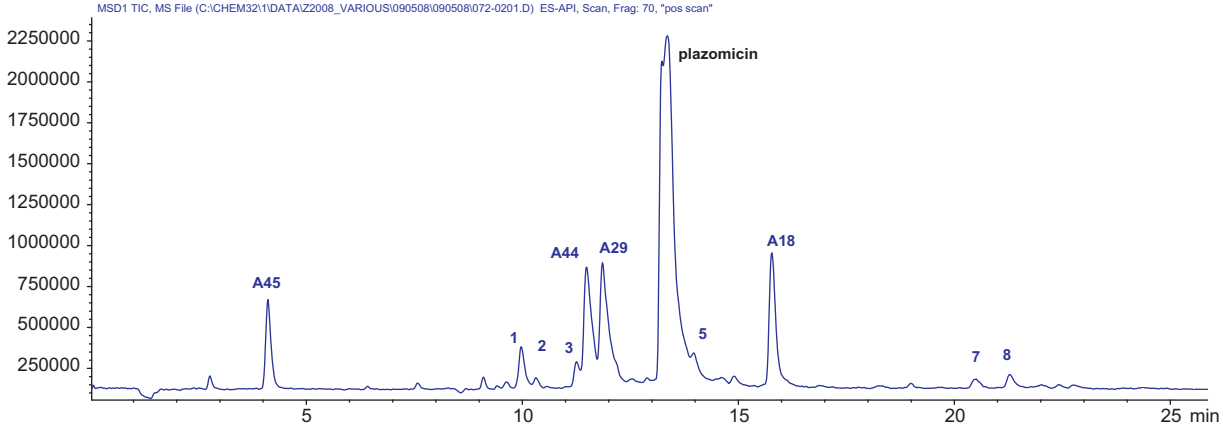

Fig. 3. TIC mass spectrum of plazomicin research lot using on-line LC/MSD SL.

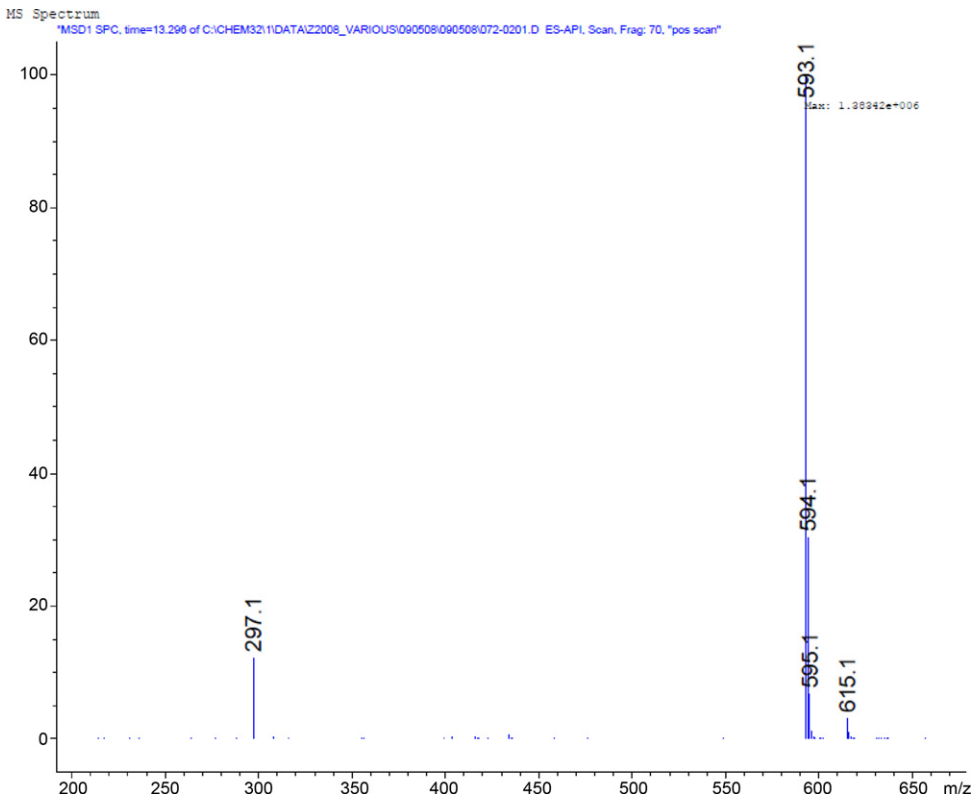

Fig. 4. ESI-MS(+) spectrum of plazomicin, The MS spectrum shows that plazomicin gives an $[M+H]^+$ ion at m/z 593.

and retention times of plazomicin are ≤0.4% from two HPLC instruments with either a DAD or VWD.

3.2.1. Specificity

The specificity of the method was evaluated by running a blank and a plazomicin sample. There are no peak interferences from the blank, the known impurities or the unknown impurities in the research lot with the plazomicin peak in the Reference Standard. To confirm the homogeneity of the plazomicin peak, the peak was evaluated for the degree of purity using photodiode array spectra. This experiment was conducted with a concentration of 0.5 mg/mL FB of plazomicin. An overlay of the normalized five different peak spectra shows that they exhibit identical profiles. Plazomicin is homogeneous based on the similarity curve having a purity factor of 999.775, which is within the threshold curve limit of 999.000, and the peak similarity factor being within the green band by a purity analysis of ChemStation software. In addition, direct mass spectrometry detection of Agilent MSD SL was carried out using ESI in positive ion mode. The MS data (Fig. 4) of the main peak shows an $[M+H]^+$ ion at m/z 593.1, an $(M+2H)^{+2}$ at m/z 297.1, and a sodium adduct $[M+Na]^+$ ion at m/z 615.1. This mass agrees with the proposed molecular weight of plazomicin. No other masses were detected in the main peak except for that of plazomicin. Therefore, the method demonstrates adequate specificity based on both UV and MS analyses.

3.2.2. Linearity and range

Linearity of the method for impurity determination was evaluated by preparing solutions of plazomicin sulfate from 0.0025 mg/mL to 3.0 mg/mL FB (0.1–120% of the test concentration at 2.5 mg/mL FB) and analyzing these samples by HPLC. Linear regression analysis was performed by calculating the coefficient of determination r^2, and the response factor of the UV response per unit concentration at each point (total $n = 9$). The representative regression equation was $y = 5.5503x + 105.84$. The resulting coefficient r^2 is 0.9993. The response factor over the range was flat, in which the calculated value is within ±7.0% of the theoretical value except for the two lowest concentrations at 0.0025 and 0.005 mg/mL (within 17% and 40%, respectively). Converting these errors to percent impurities results in 0.06% and 0.17% vs. theoretical values of 0.1% and 0.2%, both of which are acceptable for the assessment of low level impurities in early stage drug development. The percent RSD for three consecutive injections at the lowest concentration of 0.0025 mg/mL FB is 12.7%, meeting the criterion of less than 20%. The results demonstrate that the method is able to quantify an impurity at 0.1% (0.0025 mg/mL) of the total amount of the sample injected at 2.5 mg/mL FB.

The proposed assay concentration of 1.0 mg/mL FB, which provides a better linear range for the analysis of the freebase content of sulfate salts of plazomicin, was evaluated from the range of 50–150% of the targeted FB concentration. The validation of a single level calibration procedure requires that linearity using linear regression analysis for a multiple level calibration be demonstrated first, followed by analysis using the single level calibration. The same data set used for linear regression analysis was reanalyzed using single point calibration. Four parameters including the coefficient of determination, back-calculation of standards from a multiple level calibration, back-calculation of standards against a single level calibration, and Y-intercept error (IE) were determined. The IE is defined as the percentage of the Y-intercept of a multiple level calibration curve to the Y response in a multiple level calibration curve at the assay concentration, which reflects the significance of the intercept. The single point calibration can be used only if the residual is small.

Linear regression analysis was performed by plotting the freebase concentration of plazomicin at four levels ($n = 12$) against the

peak area of the UV response. The determined slope and *y*-intercept are 6060.5 (mau*s/(mg/mL) and 187.11 (mau*s), respectively. The coefficient of determination, r^2, for the linear regression analysis is 0.9996. Table 2 summarizes results of the back-calculation errors based on multiple and single level calibrations for the linearity. The back-calculation error from the multiple level linear curve is from −1.4% to 1.5%, which is within our criteria of ±5.0%. The linearity was further evaluated with a single calibration point at a nominal concentration 1.0 mg/mL FB. The back-calculation error from the single level calibration standard is in the range of −2.0% to 2.8% and the IE is 2.9% (IE calculation detailed in the bottom of Table 2), passing the criteria of 5% set for both.

Based on the result of the linearity coefficient, r^2, back-calculation errors from multiple linear curve and single level calibration standard, and IE, a single calibration standard can be used for the assay of plazomicin at 1.0 mg/mL FB.

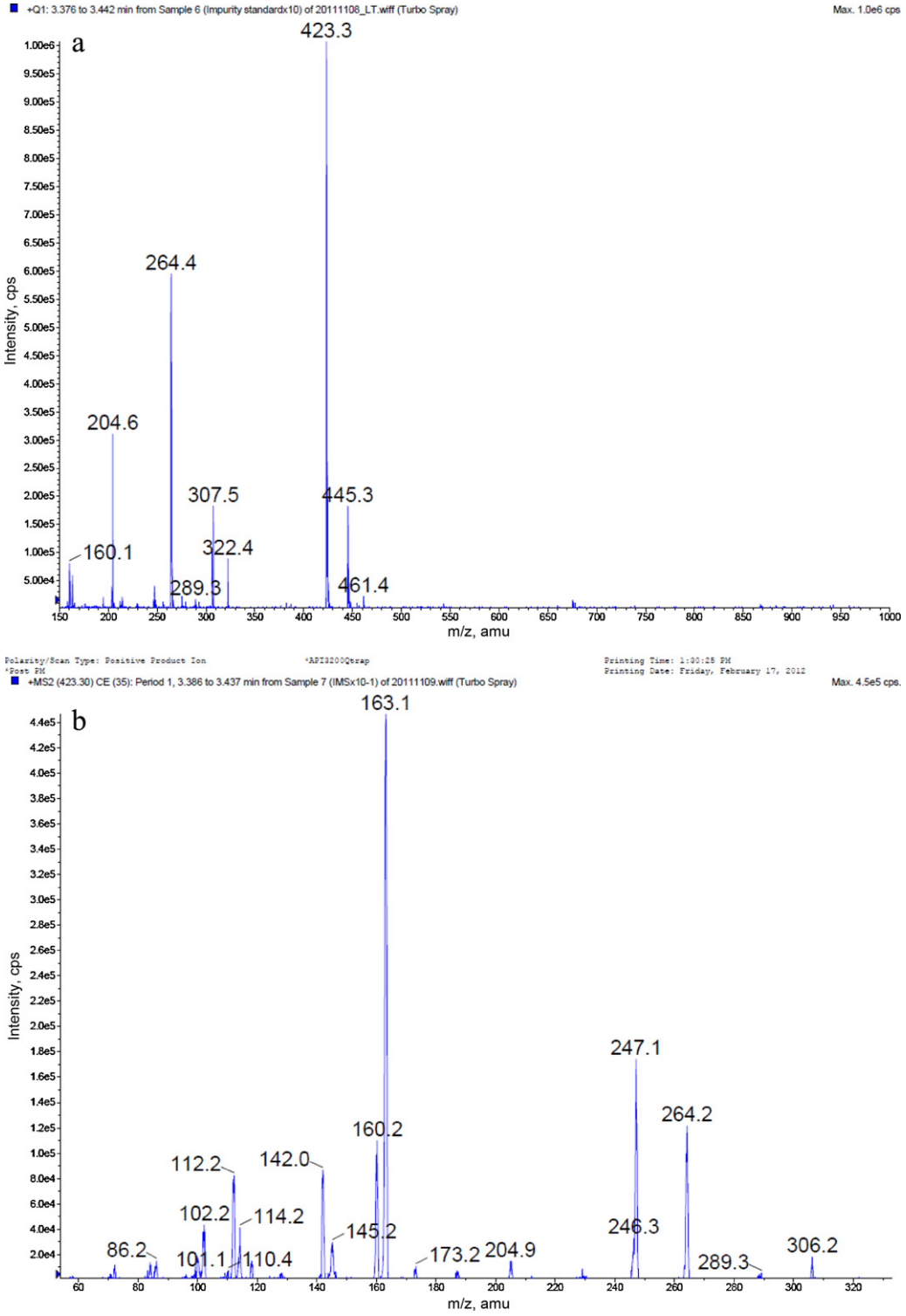

Fig. 5. The MS spectra of impurity A45 from (a) Q Trap and (b) MS^2, condition described in Section 2.2, the proposed structure shown in (c).

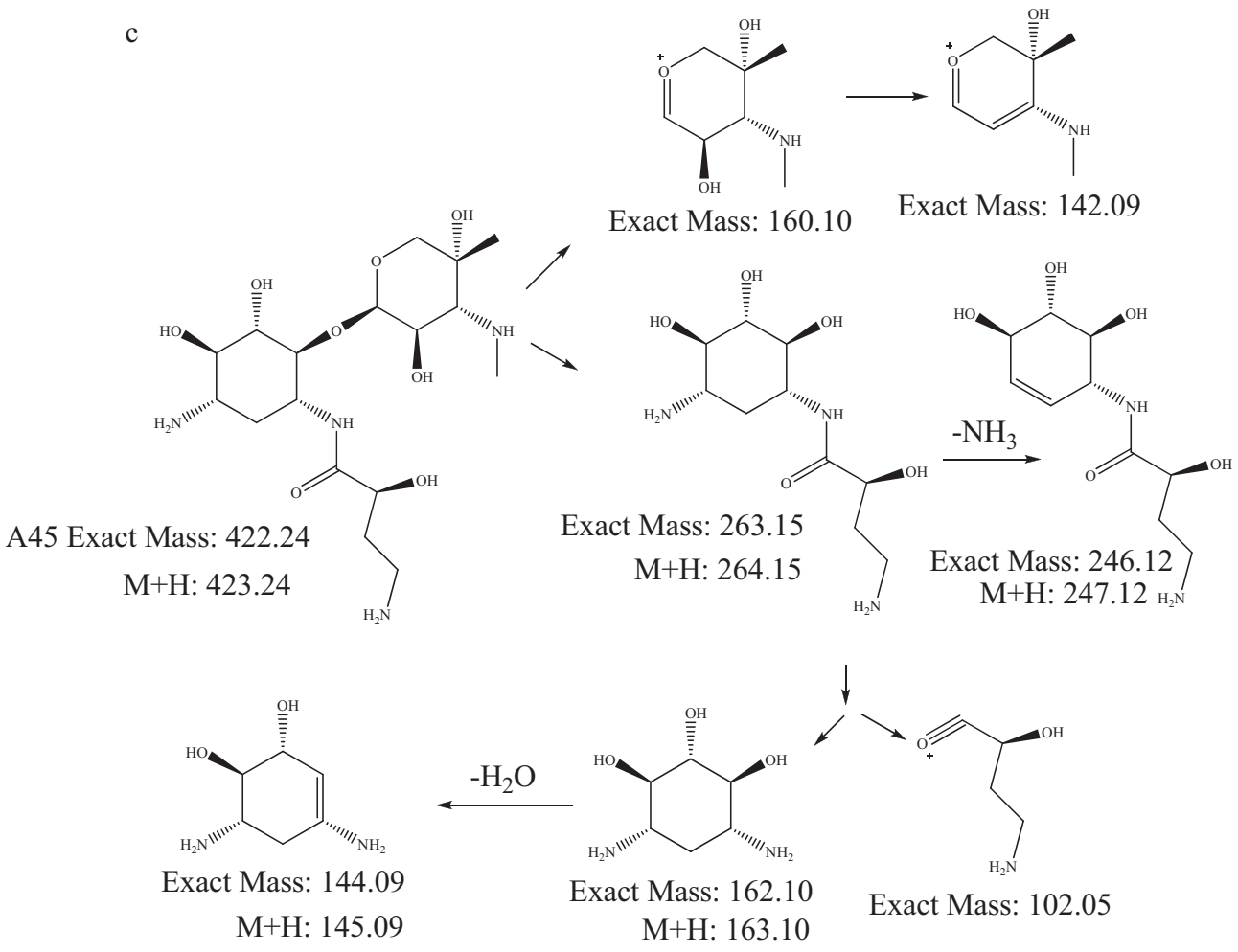

Fig. 5. (*Continued*).

3.2.3. Accuracy

To evaluate accuracy, samples of plazomicin were prepared in triplicate at four concentrations, 1.0, 1.5, 2.0 and 3.0 mg/mL of plazomicin sulfate salt. These salt concentrations correspond to 0.5–1.5 mg/mL of FB and cover the 50–150% range of the nominal FB assay concentration of 1 mg/mL FB. The samples were tested against the plazomicin Reference Standard prepared at 1.0 mg/mL FB to establish the accuracy of the method (Table 3). The recovery of each individual sample was calculated based on the mean free-base content of 51.0% as quantified by the Reference Standard. The percent recovery of individual samples at different concentrations is in the range of 98.0–102.8%, and the mean of the percent recovery for each concentration level ranged from 98.6% to 102.0%. The percent RSD of obtained concentrations at each level with three independent sample preparations is less than 1.0%.

Table 2
Summary of back-calculation with multiple and single level standard.

Preparation	Salt form (mg/mL)	Freebase (mg/mL)	Back-calculation error	
			Multiple levels (%)	Single level (%)
1	1.0	0.51	0.2	2.8
2	1.0	0.51	−1.4	1.2
3	1.0	0.51	−0.9	1.8
1	1.5	0.77	1.5	2.2
2	1.5	0.77	0.0	0.7
3	1.5	0.77	−0.4	0.3
1	2.0	1.02	1.1	0.8
2	2.0	1.02	−0.3	−0.6
3	2.0	1.02	0.1	−0.2
1	3.0	1.53	0.8	−0.5
2	3.0	1.53	−0.5	−1.8
3	3.0	1.53	−0.7	−2.0

IE = (*Y*-intercept/peak area of method concentration) × 100.
IE = ((187.11)/mean of (6438.0 + 6347.8 + 6374.6)) × 100 = 2.9%.

Table 3
Accuracy and precision of assay at concentration 1.0 mg/mL FB of plazomicin.

Preparation	Conc mg/mL salt	%Freebase	%RSD	%Recovery*	Mean
1	1.0	52.4		102.80	
2	1.0	51.6	0.77	101.25	102.0
3	1.0	51.9		101.82	
1	1.5	52.1		102.15	
2	1.5	51.4	0.97	100.74	101.1
3	1.5	51.1		100.28	
1	2.0	51.4		100.80	
2	2.0	50.7	0.73	99.39	100.0
3	2.0	50.9		99.81	
1	3.0	50.8		99.54	
2	3.0	50.1	0.83	98.23	98.6
3	3.0	50.0		98.04	

* Value pre-determined to be 51.0% by quantitation against the Reference Standard.

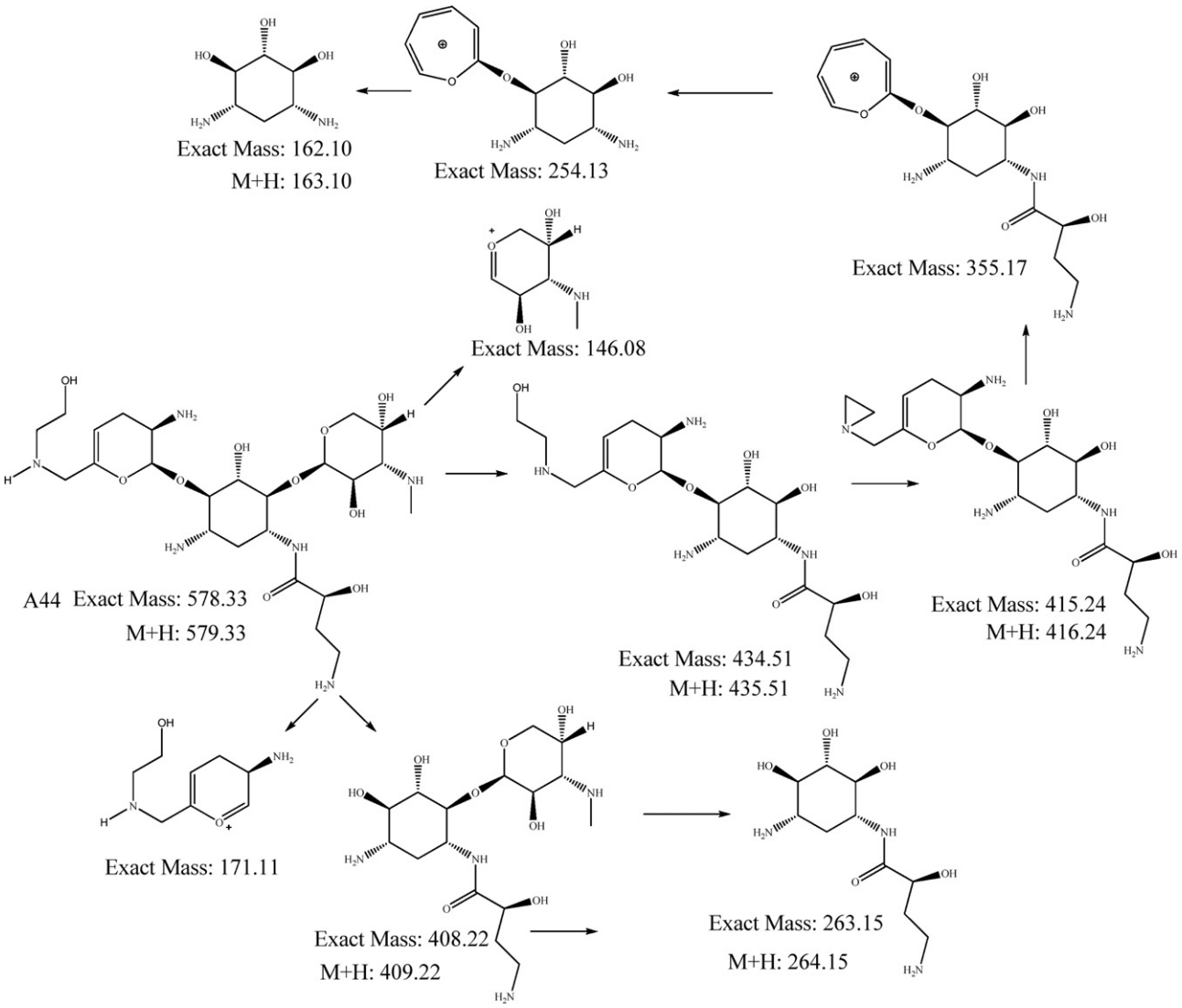

Fig. 6. Proposed structure of impurity A44 based on the MS spectra of Q Trap and MS^2, condition described in Section 2.2.

3.2.4. Precision

The precision for the assay was evaluated from the data generated in Table 3. The percent RSD of obtained concentrations at each level with three independent sample preparations is less than 1.0%.

An additional study was conducted using one lot of plazomicin across three experiments (three sample preparations for each experiment, $n = 9$ total). Results are listed in Table 4. The percent RSD of the intermediate precision for purity is ≤0.5%, and the percent RSD of the intermediate precision for the impurities A45, A44, A29 and A18 is ≤3.9%. The percent RSD of the assay across the three experiments is ≤0.6%.

3.3. Impurity structural elucidation by mass spectrometry

The tracking and characterizing impurities in plazomicin were performed by LC/MS/MS. This has been critical to develop and optimize chemistry by identifying the unique impurity patterns and levels of impurities specific to any reaction. Since plazomicin impurities were well-separated on LC, those impurities were analyzed individually by an on-line MS and MS^2 without interfering from each other.

The Q1 mass spectrum of early eluting impurity A45 shows the parent ion at *m/z* 423.3 (Fig. 5a). This ion was selected as a precursor ion for a product ion MS^2 experiment. The fragmentation pattern shown in Fig. 5b accounts for the key product ions proposed in Fig. 5c. The ions observed in the MS^2 experiment represent N1-HABA-2-deoxystreptamine at *m/z* 264.2, the major fragment ion 2-deoxystreptamine at *m/z* 163.1, sugar ring at *m/z* 160.2, and HABA group at *m/z* 102.2 with cleavage at the amide bond. The fragmentation of *m/z* 247.1 and 142.0 was observed due to loss of ammonia from N1-HABA-2-deoxystreptamine and H_2O from sugar ring. We concluded impurity A45 is a degradation product derived from glycosidic bond hydrolysis of plazomicin based on MS data. It was present in drug substance as an impurity from the synthesis or as a degradant in the drug product, especially at the low pH condition, which can be controlled by adjusting pH. The MS spectrum shows that A44 gives an $[M+H]^+$ ion at *m/z* 579.4, 14 less than a methyl group in parent plazomicin (mass spectra of A44, A29 and A18 in supplementary material). A44 was further dissociated by MS^2. The possible fragmentation pathway is summarized in Fig. 6. The signal of *m/z* 434.5 was observed from one sugar cleavage at *m/z* 145.8 with a missing methyl group compared to plazomicin. The fragmentation *m/z* 434.5 gives ions *m/z* 416.6,

Table 4
Impurity and assay method precisions of plazomicin across three experiments. Each data point is the mean of the results from three sample preparations and injections.

Day/instrument	Sample	%Purity	%A45	%A44	%A29	%A18	%w/w (assay)
Day 1/HPLC1	Mean	78.7	1.8	5.1	5.0	4.3	57.5
	Stdev	0.20	0.07	0.04	0.04	0.04	0.35
	%RSD	0.2	3.9	0.7	0.8	0.9	0.6
Day 2/HPLC1	Mean	78.7	1.5	5.1	5.0	4.2	57.6
	Stdev	0.05	0.04	0.03	0.03	0.00	0.18
	%RSD	0.1	2.4	0.5	0.7	0.1	0.3
Day 2/HPLC2	Mean	77.5	1.4	5.5	5.2	4.5	57.0
	Stdev	0.40	0.03	0.07	0.04	0.10	0.12
	%RSD	0.5	1.8	1.3	0.8	2.1	0.2

355.1, 254.2 and 163.2. The ions dissociated from glycosidic bond hydrolysis with an attached HABA at m/z 409.2 and 264.2, and from sugar ring with hydroxyethyl group at m/z 171.4 were obtained. A44 was carried over from the starting material sisomicin, which contains des-methyl sisomicin. It can be controlled by selecting a high purity sisomicin with a low percent des-methyl sisomicin as starting material.

The MS data of impurity A29 were collected and its proposed fragmentation pathway is summarized in Fig. 7. Fig. 8 represents A18 proposed fragmentation pathway. Several of the ions generated by the fragmentation of those two compounds are similar or identical to those from A44, cleaving from either one of two glycosidic bonds. For A29, the fragments obtained from MS2 are consistent with the proposed structure. The ion at m/z 127.2

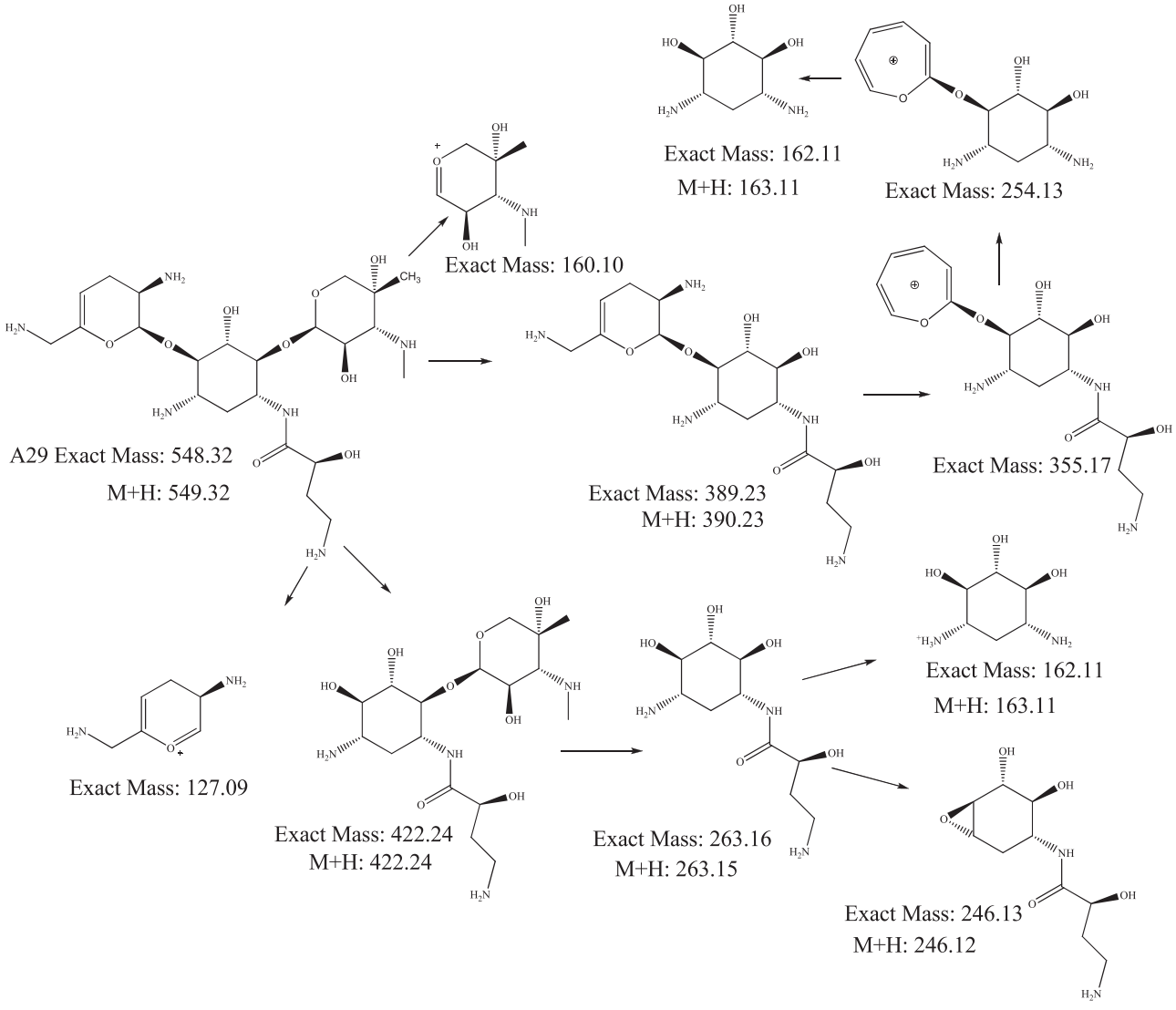

Fig. 7. Proposed structure of impurity A29 based on the MS spectra of Q Trap and MS^2, condition described in Section 2.2.

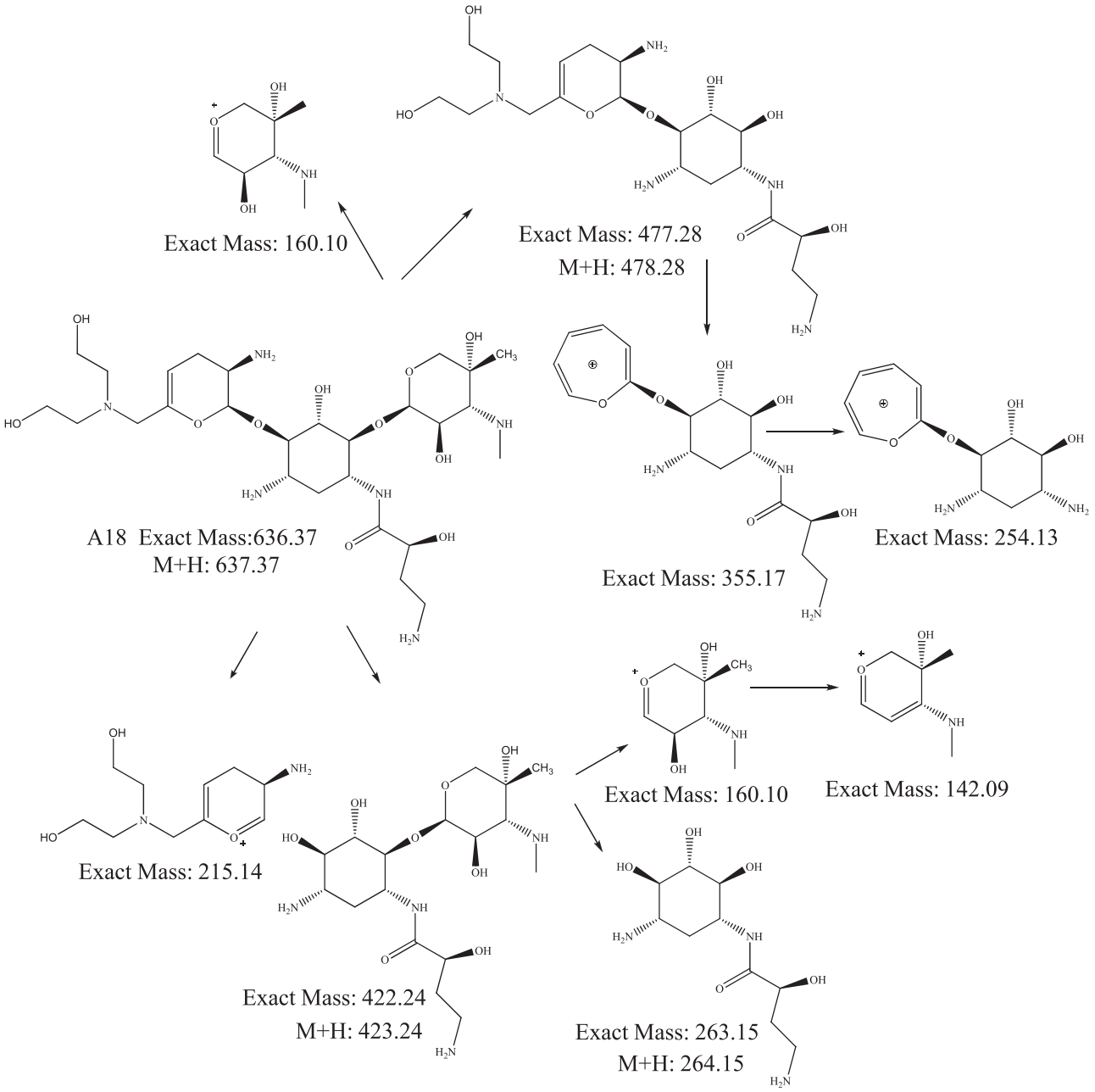

Fig. 8. Proposed structure of impurity A18 based on the MS spectra of Q Trap and MS^2, condition described in Section 2.2.

confirms a hydroxyethyl group is missing compared to plazomicin. Two hydroxyethyl groups are present in the ion at *m*/*z* 215.0 in A18. Two major process impurities, the A29 and the bisalkylated A18 are generated in the N-alkylation reaction.

4. Conclusion

In conclusion, an analytical method for the aminoglycoside plazomicin has been developed and validated successfully in terms of specificity, linearity, range, accuracy, precision, and quantitation limit. The structures of impurities were easily characterized via on-line MS spectrometry. The method is robust and is suitable for the purpose of measuring the impurities and quantifying plazomicin drug substance, as well as for elucidating the structures of the impurities. The method has the potential to be adapted for other aminoglycosides with weak UV absorbing groups used in pre-clinical or clinical studies.

Acknowledgements

The authors would like to thank Adam Goldblum and Raissa Trend for syntheses of plazomicin compounds and Raymond Diokno for pK_a measurements.

Appendix A. Supplementary data

Supplementary data associated with this article can be found, in the online version, at doi:10.1016/j.jpba.2012.03.003.

References

[1] J.B. Aggen, E.S. Armstrong, A.A. Goldblum, P. Dozzo, M.S. Linsell, M.J. Gliedt, D.J. Hildebrandt, L.A. Feeney, A. Kubo, R.D. Matias, S. Lopez, M. Gomez, K.B. Wlasichuk, R. Diokno, G.H. Miller, H.E. Moser, Synthesis and spectrum of the neoglycosie ACHN-490, Antimicrob. Agents Chemother. 54 (2009) 4636–4642.
[2] A. Endimiani, K.M. Hujer, A.M. Hujer, E.S. Armstrong, Y. Choudhary, J.B. Aggen, R.A. Bonomo, ACHN-490, a neoglycoside with potent in vitro activity against multidrug-resistant *Klebsiella pneumoniae* isolates, Antimicrob. Agents Chemother. 53 (2009) 4504–4507.
[3] U.S. Pharmacopeia/NF 2009, Vol. 2 1508–1509, 2489, 2734–2735, Vol. 3 3071–3072, 3756–3757.
[4] U.D. Neue, T.E. Wheat, J.R. Mazzeo, C.B. Mazza, J.Y. Cavanaugh, F. Xia, D.M. Diehl, Differences in preparative loadability between the charged and uncharged forms of ionizable compounds, J. Chromatogr. A 1030 (2004) 123–124.
[5] N.H. Davies, M.R. Euerby, D.V. McCalley, Study of overload for basic compounds in reversed-phase high performance liquid chromatography, J. Chromatogr. A 1119 (2006) 11–19.
[6] M.X. Guo, L. Wrisley, E. Maygoo, Measurement of tobramycin by reversed-phase high-performance liquid chromatography with mass spectrometry detection, Anal. Chim. Acta 571 (2006) 12–16.
[7] V. Manyanga, R.L. Dhulipalla, J. Hoogmartens, E. Adams, Improved liquid chromatographic method with pulsed electrochemical detection for the analysis of kanamycin, J. Chromatogr. A 1217 (2010) 3748–3753.
[8] V. Manyanga, J. Hoogmartens, E. Adams, Development and validation of an improved reversed-phase liquid chromatographic method combined with pulsed electrochemical detection for the analysis of netilmicin, J. Sep. Sci. 33 (2010) 1897–1903.
[9] A. Joseph, A. Rustum, Development and validation of a RP-HPLC method for the determination of gentamicin sulfate and its related substances in a pharmaceutical cream using a short pentafluorophenyl column and a charged aerosol detector, J. Pharm. Biomed. Anal. 51 (2010) 521–531.
[10] Operating & Maintenance Manual for Corana® CAD® detector, document#70-6258, esa.
[11] Dionex Application Note 66.

Journal of Pharmaceutical and Biomedical Analysis 66 (2012) 85–90

Contents lists available at SciVerse ScienceDirect

Journal of Pharmaceutical and Biomedical Analysis

journal homepage: www.elsevier.com/locate/jpba

Non-destructive detection of adulterated tablets of glibenclamide using NIR and solid-phase fluorescence spectroscopy and chemometric methods

Rafael da Silva Fernandes[a], Fernanda Saadna Lopes da Costa[a], Patrícia Valderrama[b], Paulo Henrique Março[b], Kássio Michell Gomes de Lima[a,*]

[a] Universidade Federal do Rio Grande do Norte, Instituto de Química, Grupo de Pesquisa em Quimiometria Aplicada, CEP 59072-970, Natal, RN, Brazil
[b] Universidade Tecnológica Federal do Paraná, Coordenação de Licenciatura em Química, BR 369, Km 0.5, CEP 87301-006, Campo Mourão, PR, Brazil

ARTICLE INFO

Article history:
Received 16 October 2011
Received in revised form 28 February 2012
Accepted 5 March 2012
Available online 14 March 2012

Keywords:
Glibenclamide
SIMCA
PLS-DA
UPLS-DA

ABSTRACT

This study describes a method for non-destructive detection of adulterated glibenclamide tablets. This method uses near infrared spectroscopy (NIRS) and fluorescence spectroscopy along with chemometric tools such as Soft Independent Modeling of Class Analogy (SIMCA), Partial Least Squares-Discriminant Analysis (PLS-DA) and Unfolded Partial Least Squares with Discriminant Analysis (UPLS-DA). Both brand name (Daonil) and generic glibenclamide tablets were used for analysis. The levels of glibenclamide in each type of tablet were evaluated by derivative spectrophotometry in the ultraviolet region. The results obtained from the NIR and fluorescence spectroscopy along with those obtained from multivariate data classification show that this combined technique is an effective way to detect adulteration in drugs for the treatment of diabetes. In the future, this method may be extended to detect different types of counterfeit medications.

© 2012 Elsevier B.V. All rights reserved.

1. Introduction

Glibenclamide is a second-generation sulfonylurea anti-diabetic used in tablet form for the treatment of diabetes mellitus [1]. There is only 5 mg of the active ingredient in each tablet, with the remainder consisting of excipients such as lactose, aerosil, starch and magnesium. Glibenclamide ($C_{23}H_{28}ClN_3O_5S$, molecular weight 494.01 g/mol) is usually found in the form of a white crystalline powder and is odorless and virtually tasteless. With a pK_a equal to 5.3, glibenclamide is a weak acid and has an oil/water partition coefficient (log P) of 3.53 [2]. Fig. 1 shows the structure for glibenclamide.

The dissemination of counterfeit drugs is a criminal activity that is escalating in many countries. A significant increase in counterfeit drugs has been noted in Brazil during the last few years. Many of the false products found on the market have altered composition in terms of both the amounts of active and inactive ingredients. According to the World Health Organization (WHO), counterfeit tablets are "a medicine, which is deliberately and fraudulently mislabeled with respect to identity and/or source. Counterfeit products may include products with the correct ingredients or with the wrong ingredients, without active ingredients, with insufficient active ingredients or with fake packaging" [3].

Several analytical methods have been described to detect counterfeit medicines, such as high performance liquid chromatography with UV detection (HPLC-UV) [4], mass spectrometry detection (HPLC–MS) [5], and nuclear magnetic resonance (NMR) [6]. However, despite the reliability of these techniques for the detection of adulterated tablets, they are inherently destructive, expensive and wasteful. In addition, some of these techniques, such as NMR, require specialized reagents and personnel, which limits the use of these techniques beyond the laboratory.

Rapid, non-destructive and reliable analytical methods for the detection of counterfeit tablets are desired by both industry and drug enforcement agencies [7]. In this regard, NIRS has been used quite successfully to detect counterfeit tablets [8,9], mainly because of its non-destructive nature and the possibility for online analysis. Storme-Paris et al. [8] used NIRS to test the ability of discrimination of the spectroscopy to analyze a number of pharmaceuticals containing the same active ingredient (API) with different excipients, with the goal being to analyze suspected counterfeit tablets. The results demonstrated that NIRS performs well for the detection of subtle differences in formulations. The authors were able to distinguish between 2.5 and 1.0% API (w/w) and between variations in excipient formulations having the same coating (<1%, w/w) and identical content. However, the detected amounts were close to the theoretical limit for sensitivity for NIR spectroscopy. Scafi [9] used NIRS to identify counterfeit drugs and evaluated the use of this technique for distinguishing between generic and brand-name tablets from different manufacturers and

* Corresponding author. Tel.: +55 84 3215 3828; fax: +55 84 3211 9224.
E-mail address: kassio@ufrnet.br (K.M.G. de Lima).

0731-7085/$ – see front matter © 2012 Elsevier B.V. All rights reserved.
doi:10.1016/j.jpba.2012.03.004

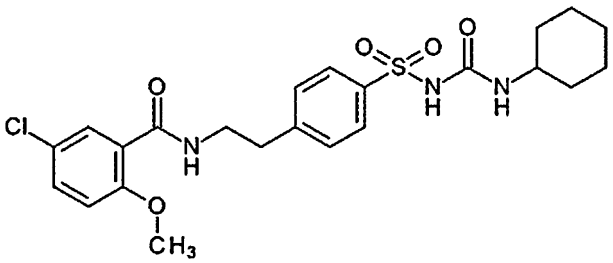

Fig. 1. Molecular structure of the compound glibenclamide.

between medicines containing the same active ingredient. Drugs evaluated included those in the packaging, drugs past the expiration date and drugs containing different amounts of the active ingredient.

In recent years, excitation and emission fluorescence spectroscopy have been used in conjunction with chemometric methods for the analysis of pharmaceutical formulations by solid-phase molecular fluorescence and second-order multivariate calibration [10,11]. Analysis by molecular fluorescence is an attractive option, due to its inherent sensitivity and ease of spectral acquisition. This is especially true for characterization of the solid phase, where reduced sample preparation is necessary. Solid-phase fluorescence spectroscopy allows for fast acquisition of data with minimal reagent consumption and low cost analysis. In addition, it does not generate residues and has good sensitivity and selectivity. Unfortunately, to date, this strategy has been rarely applied, most likely due to a lack of solid samples of pharmaceutical interest.

Several algorithms for the classification of data have been described in the literature as Soft Independent Modeling of Class Analogy (SIMCA) [12,13] and Partial Least Squares Discriminant Analysis (PLS-DA) [14] are more ideal classification methods, with the main difference between the two being that supervised SIMCA analysis produces more satisfactory results when the variability between groups is greater than the variability within groups. However, in cases where the variability within a group is greater than the variability among several groups, the SIMCA method does not distinguish between groups. For these cases, the PLS-DA method is an alternative. The PLS-DA method is a multivariate method used for the classification of samples when it is necessary to reduce the number of variables and it is unclear whether the differences between groups will dominate the total variability of the samples. When working with fluorescence data, the Unfolded Partial Least Squares (UPLS) method [15] with discriminant analysis may be a better alternative. Variable selection methods can be ultimately combined to obtain more robust models.

Theoretical and experimental evidence have shown that variable selection can improve multivariate models [16]. To improve these classification models, an alternative is to use a region presenting the most relevant information, thus eliminating spectral regions that do not have information directly correlated with the property of interest (such as noise, nonlinearities, or irrelevant information) and interferences and potential variables that generate a lower signal to noise ratio (indicative of low sensitivity) [17]. Some variable selection methods such as interval Partial Least Squares (iPLS) [18], Genetic Algorithm (GA) [19] and APS (the Successive Projections Algorithm) [20] use this type of strategy and have also been evaluated.

In this study, we report on the detection of adulteration in glibenclamide tablets by using NIR and solid-phase fluorescence spectroscopy along with chemometric tools.

2. Experimental

2.1. Tablets

The glibenclamide tablet that was used as the standard reference tablet was purchased from Sigma–Aldrich and had a purity greater than 99% (HPLC grade). Ethanol (99%, Merck) was used to prepare solutions of glibenclamide used for the construction of a calibration curve. A total of 366 tablets, all declared as having a glibenclamide content of 5 mg, were purchased from local traders in Natal, RN, Brazil. Among this group, 57 tablets were called reference (R) (Daonil®, 3 different batches), 58 were called generic 1 (G1, 3 different batches) and 251 tablets were called generic 2 (G2, 3 different batches).

2.2. Instrumentation

Spectra in the near infrared range of 1250–2500 nm were recorded in triplicate using an MB-160 D FT-NIR spectrometer (Bomem) with a spectral resolution of 8 cm^{-1}. Fifty scans were co-added, and the diffuse reflectance mode was used. The mean spectrum for each tablet was then calculated by averaging the triplicate spectra. The spectrum of a polytetrafluoroethylene (PTFE) sample was used as a background.

Data pre-treatment for SIMCA, PLS-DA and variable selection (iPLS, GA, SPA) models with NIR spectra were included calculating the first-order derivative spectra, applying the first-order Savitzky–Golay smoothing filter using nine points and normalization using the multiplicative scatter correction (MSC).

The excitation/emission fluorescence data were acquired in the range of wavelengths of 300–400 nm for excitation and 405–600 nm for emission, with steps of 5 and 2 nm for excitation and emission, respectively. A Perkin Elmer model LS-55 fluorescence spectrometer was used. The excitation and emission slits were set at 5 nm, the speed scan was set to the fastest mode, the photomultiplier tube was set to the medium level and a cell with a fiber optic reflectance probe was used. For model building, a range of 300–400 nm for excitation and 405–600 nm for emission was used, with steps of 25 and 0.5 nm used for excitation and emission, respectively. This resulted in a data matrix size of 5×392 for each sample. The instrument noise level was estimated based on 15 measurements of a blank solution.

An Agilent HP8453 UV/vis spectrophotometer with a single beam, automated variation in wavelength, and a quartz cuvette (10 mm path length) was used for characterization of the purchased glibenclamide tablets. In this case, 45 tablets were analyzed (12 R, 9 G1, and 24 G2), all of which were declared by their manufacturers as having a glibenclamide content of 5 mg. For the analysis, tablets were chosen randomly among the total set of 366 tablets for determination of drug content. A calibration curve made from standard solutions of glibenclamide in methanol was made based on first-order derivative spectrophotometry at 315 nm. Based on this UV characterization method, the R and G1 class tablets had concentrations of glibenclamide of 4.65 ± 0.22 and 4.73 ± 0.16 mg, respectively. The tablets referred to as class G2 had a concentration of 2.53 ± 0.32 mg. Recovery for the reference tablets was above 98%, with a relative standard deviation of less than 1%.

2.3. Chemometrics

2.3.1. PCA

A data set with many variables can be simplified by performing data reduction which makes the system more easily interpretable. Principal component analysis (PCA) [21] is a well-known way to

reduce the number of variables, in which the spectral matrix **X** is decomposed as:

$$\mathbf{X} = \mathbf{TP^t} + \mathbf{E} \quad (1)$$

where **X** is the $I \times J$ data matrix, **T** is the $I \times A$ matrix of score vectors, the score vectors $\mathbf{t}_a$ are orthogonal (i.e., $\mathbf{T^tT} = \mathrm{diag}(\lambda_a)$ and λ_a are eigenvalues of the matrix $\mathbf{X^tX}$), **P** is the $J \times A$ matrix of loading vectors, **E** is the $I \times J$ residual matrix, I is the number of objects, J is the number of variables, and A is the number of components calculated.

2.3.2. SIMCA

The SIMCA analysis method establishes a principal component model for each class and the corresponding models (the so-called disjointed class models or SIMCA boxes) are developed individually [22,23]. Unknown samples are then compared to the class models and assigned to classes according to their analogy with the calibration samples. A new sample will be recognized as a member of a class if it is enough similar to the other members; else it will be rejected. Each class is modeled using separate PCA models. A model distance limit $S_{\max}$ is used for classifying new samples and $S_{\max}$ is calculated for the class model m as follows (Eq. (1)):

$$S_{\max}(\mathrm{m}) = S_0(\mathrm{m})\sqrt{F_c} \quad (2)$$

where S_0 is the average distance within the model, and F_c (Fisher criterion) is the critical value provided by the Fisher–Snedecor tables. The F_c value depends on the percentage of risk, generally set to 5%. Class membership is defined at a significance level of 2.5% of $S_{\max}$. Mean centering is applied before modeling.

In this study, three classes of generic tablets were defined: (a) reference (R), (b) generic 1 (G1) and (c) generic 2 (G2). A total of 366 NIR spectra from the reference (R, 57 spectra), generic 1 (G1, 58 spectra) and generic 2 (G2, 251 spectra) tablets were imported into the SIMCA model, and the class cut-off limits were set at 5%. To validate the obtained SIMCA model, 18, 17, and 180 spectra from groups R, G1 and G2, respectively, were analyzed. Performance of the SIMCA model was evaluated by comparing the distance between the reference class and the generic classes with adulterants as seen in the two-dimensional principal component analysis scores plot, and the recognition and rejection rates of the samples were used to validate the model.

2.3.3. PLS-DA

PLS regression can be adapted for pattern recognition, giving rise to the PLS-DA method. PLS-DA is performed using an exclusive binary coding. During the calibration process, the PLS-DA method is trained to compute the "membership values", one for each class; the sample is then assigned to one class when the value is above a specific prediction threshold [14]. This method, adapted from PLS1 or PLS2 regressions, uses M spectral variables as predictors and q variables (0 or 1) as variable response [24]. The PLS-DA method was used to differentiate between the three different tablet classes and it requires that the data of interest be split into two data sets, a calibration set and a validation set. The PLS-DA was performed using a calibration step for 40, 40 and 166 tablets representing the classes R, G1 and G2, respectively. For external validation, 17, 18 and 85 tablets representing classes R, G1 and G2, respectively, were used. Cross validation was performed using random subsets, meaning that each test set was formed from a random selection of objects such that a single object is included in only one test set. In this way, the prediction error is said to be representative of that of the new samples. The number of latent variables selected for each model was determined using the smallest root mean squared error of prediction (RMSEP).

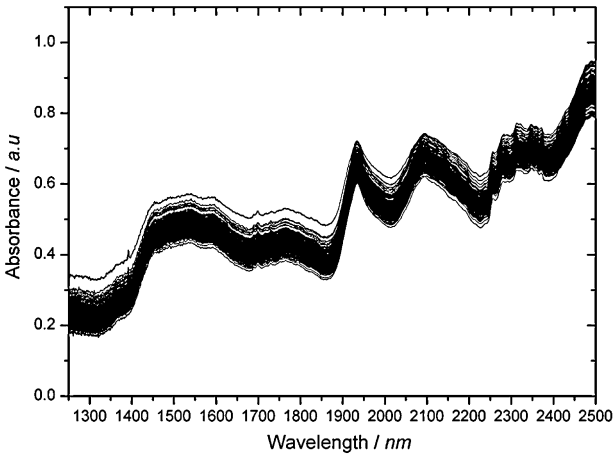

Fig. 2. Spectra of the original 38 tablets.

2.3.4. UPLS-DA

The UPLS model consists of the first-order calibration PLS model when it is applied to second-order data that have been unfolded into vectors, $\mathbf{V}_x$. With this $\mathbf{V}_x$ (JK, I) matrix, a usual PLS model is build, providing a set of loadings **P** and weight loadings **W**, both of size (JK, A), where A is the number of latent variables, as well as the loading vectors **q** (A, 1) that convert the scores t into the concentration values (y). The parameter A is usually selected by techniques such as cross-validation. If the calibration is precise, **q** could be employed to estimate the analyte concentrations in a test sample. The UPLS-DA model was built by unfolding the original data (the matrix containing the fluorescence for each sample), while the array of dependent variables contained the sample classes for different glibenclamide samples (R, G1 and G2). A linear relationship is established in this model between the scores of **X** (the vectorized matrix values for fluorescence of each sample) and the scores of **Y** (the matrix containing the different class types R, G1 and G2).

2.3.5. Software

Importing of the data, pre-treatment, variable selection (iPLS, GA, SPA) and the construction of chemometric classification models (SIMCA, PLS-DA UPLS-DA) were performed in MATLAB version 6.5 (Math-Works, Natick, USA) using the PLS-toolbox (Eigenvector Research, Inc., Wenatchee, WA, USA, version 5.8.2).

3. Results and discussion

Fig. 2 shows the NIR spectra of tablets from the three different classes (R, G1 and G2). It was difficult to find a difference in the raw NIR spectra between the different classes due to the high degree of band overlapping. However, some characteristic absorption peaks were observed and interpreted as follows: the region between 1480 and 2000 nm corresponds to the first stretch overtone of NH, the Ar—CH stretch and the second overtone of C=O. The region between 2150 and 2290 nm corresponds to a combination of fundamental transitions for the CONH functional group.

To reduce instrumental noise and light scattering that can affect the interpretation of the analytical signal, a series of pre-treatments were applied. The first pre-treatment used was a Savitzky–Golay smoothing using a window of nine points to eliminate the presence of random noise from the instrument. Then, a correction of light scattering (MSC) was performed to correct the effect of light scattering in the absorption spectra. Finally, the first derivative of the Savitzky–Golay smoothing was taken.

A PCA was performed on the array of pre-processed data. As seen in Fig. 3, a clear discrimination between the three classes can

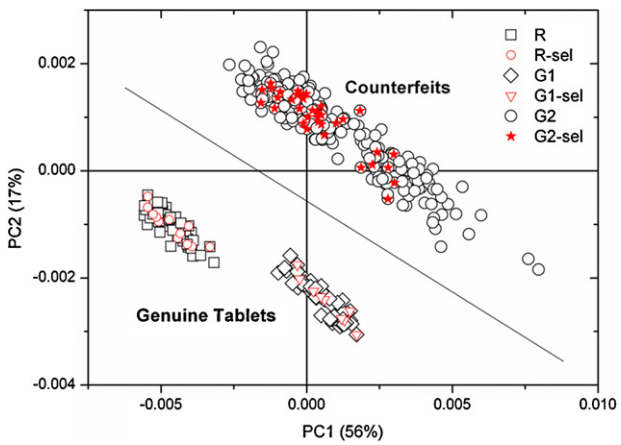

Fig. 3. First principal component against second principal component for classes R, G1 and G2. Genuine tablets under diagonal trace for classes R and G1. Counterfeit tablets above diagonal trace (G2 class).

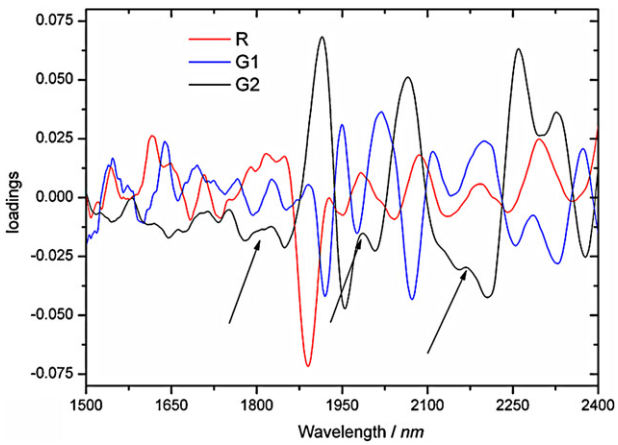

Fig. 4. Graph of loadings for the three classes of tablets investigated.

be observed, with 73% of the explained variance seen in PC1 versus PC2. There were three groups selected for analysis, and these are identified by their respective codes. In addition, a set of 45 tablets chosen at random within the total set was analyzed by derivative UV spectroscopy to investigate the composition of glibenclamide. In this case, samples belonging to class G2, where the detected levels of glibenclamide were below 5 mg, showed that the PCA scores resulting from the application of this technique to the NIR spectroscopy data were able to detect adulteration, as seen in the region bounded above the line plotted on the graph (indicating the spectra baseline).

Fig. 4 shows a plot of the absorption intensities observed for each of the three classes of tablets investigated. The intensities seen at the classes R and G1 were found to be similar for nearly every region of the studied NIR range. However, class G2 presented lower intensities for the bands representing three wavelengths: 1817, 1985 and 2168 nm. These bands refer mainly to the CONH group, and the low intensities seen for the G2 class confirm that this tablet class contained adulterated amounts of glibenclamide.

Full-spectrum SIMCA and PLS-DA models were built for each of the three classes using a total of 366 samples from different sources. There are two types of errors associated with the SIMCA model. Type I errors correspond to samples that were not included in their own class. Type II errors include samples that were categorized incorrectly. Classification of the different table types using the SIMCA model was 100% accurate, and both types of errors were avoided. This finding indicates that the SIMCA method was able to adequately distinguish between real and counterfeit tablets based on the amount of glibenclamide. The developed PLS-DA model also classified samples with an accuracy of 100%. These results show that the SIMCA and PLS-DA models are suitable for the detection of adulterated glibenclamide tablets.

Algorithms such as GA, iPLS and SPA were used in this study to construct classification models (SIMCA and PLS-DA) with a reduced number of variables. These algorithms were applied to the data matrix containing the mathematically corrected NIR spectra (1250–2500 nm), and the models were then built for classification. The type I and type II errors were determined for each model.

The number of latent variable used for the iPLS models was three and 200 selected variables. iPLS models showed that a narrow spectral region is enough to obtain satisfactory classification for each class. The strategy using SPA models has the advantage of using few variables (9) to build PLS-SPA models. The neural network (GA) was the third classification model using 219 selected variables. It was employed to verify if a non-linear procedure could produce better prediction results. For this model, the results obtained were slight better than other two classification models, confirming some non-linear behavior in the data set. Table 1 shows the results obtained with SIMCA and PLS-DA after using these algorithms for variable selection, with the type I and type II errors for each class highlighted. As seen in the figure, the SIMCA and PLS-DA models gave

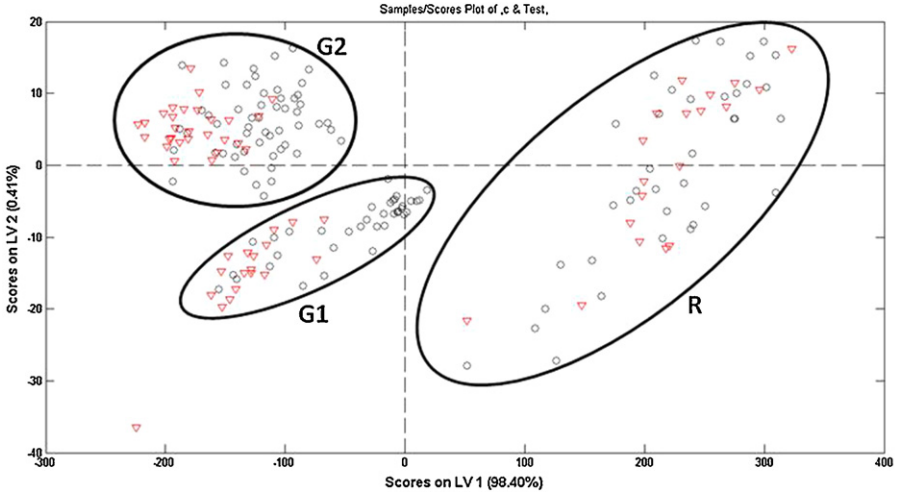

Fig. 5. Scores of UPLS-DA model: ○, calibration set; ∇, validation set.

Table 1
Results obtained for the models SIMCA and PLS-DA after the selection of variables.

Algorithm	Variables	SIMCA		PLS-DA	
		Error type I (%)	Error type II (%)	Error type I (%)	Error type II (%)
PLS-SPA	9	3.27	0	2.88	0
PLS-iPLS	200	0.55	9.56	0.24	6.58
PLS-GA	219	1.91	0	1.11	0

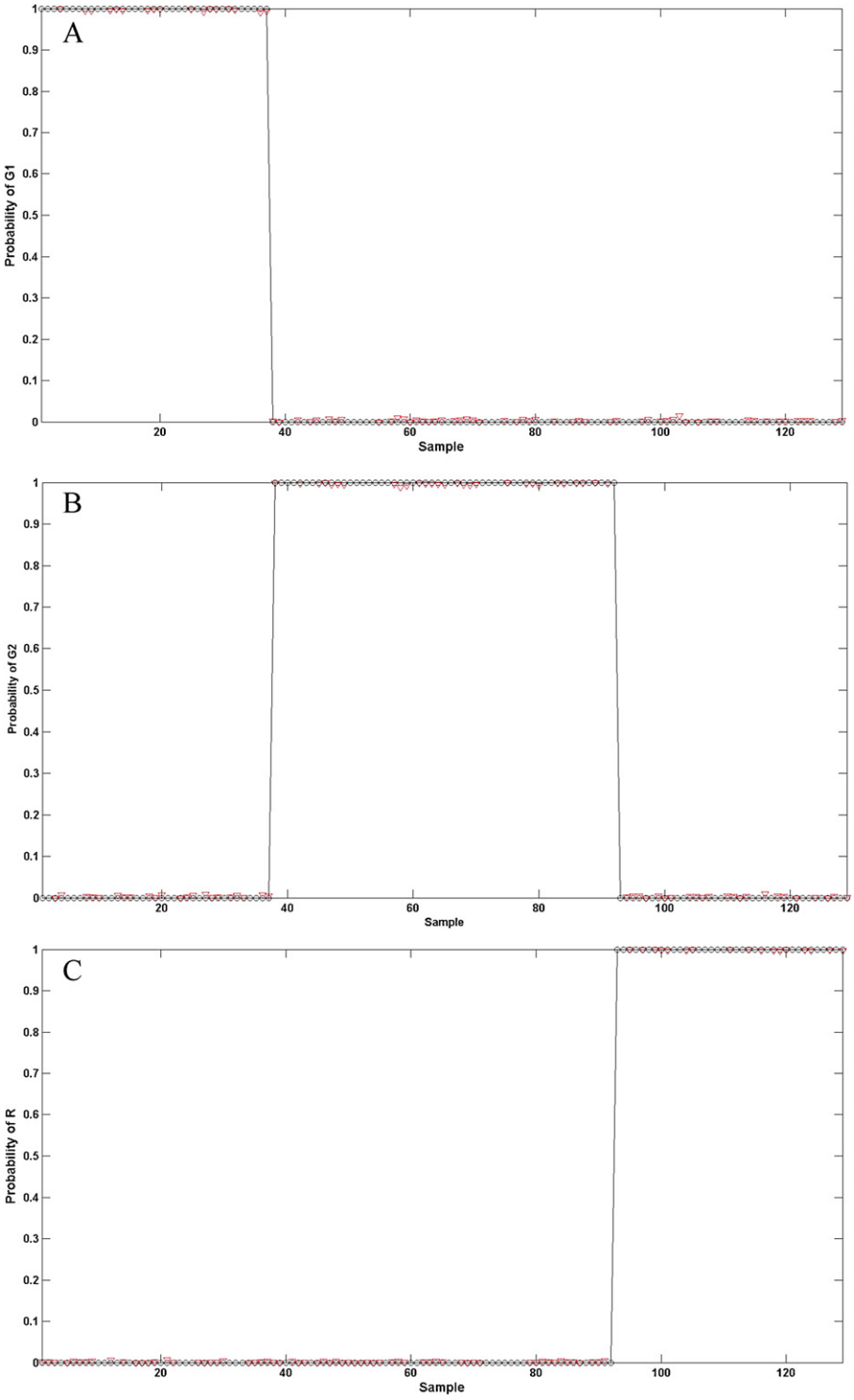

Fig. 6. Probability of classification (a) in class G1, (b) in class G2, (c) in the class R. ○, calibration set; ∇, validation set.

satisfactory results with respect to the accuracy of tablet classification for each class, since that, the real response and the response obtained by the proposed method are in agreement, as indicated by the definition for accuracy [16].

To construct second-order models for the purpose of classification, models of UPLS-DA type were developed from solid-phase molecular fluorescence data of all 366 tablets. Fig. 5 shows a clear separation between the three classes of pills investigated. The scores in this figure show that there is a clear distinction for the adulterated tablets, class G2. Fig. 6 confirms this correct classification and shows the probability of classification for the three classes evaluated in this study.

4. Conclusion

Near-infrared spectroscopy and solid-phase fluorescence in combination with chemometric tools proved to be highly effective for detecting adulterated glibenclamide tablets. These methods are advantageous over traditional analysis methods as NIR and fluorescence spectroscopy are non-destructive, offer feasible quick analysis, and do not create large amounts of waste. The classification models used (SIMCA and PLS-DA) accurately predicted the correct class (with 100% accuracy) using the NIR data, with or without the use of algorithms for variable selection (GA, SPA, and iPLS). The solid-phase fluorescence data and UPLS-DA scores showed 100% of correct discrimination for the different tablet classes. The results from this study suggest that the use of NIR and solid-phase fluorescence spectroscopy in combination with chemometric methods is a satisfactory approach for the classification and identification of counterfeit pharmaceuticals.

Acknowledgements

Rafael Fernandes and Fernanda Saada thank Propesq-UFRN for financial support. The authors also thank Claudia Martelli (UNICAMP) for collaboration with this work.

References

[1] D.S.M. Ribeiro, J.A.V. Prior, C.J.M. Taveira, J.M.A.F.S. Mendes, J.L.M. Santos, Automatic miniaturized fluorometric flow system for chemical and toxicological control of glibenclamide, Talanta 84 (2011) 1329–1335.
[2] C.G.C. Nery, M.A.S. Pires, G.A. Pianetti, C.D.V. Soares, Characterization of the hypoglycemic drug glibenclamide, Rev. Bras. Ciênc. Farm. 44 (2008) 61–73.
[3] WHO, Counterfeit Medicines, Fact Sheet 275, 2006. http://www.who.int/mediacentre/factsheets/fs275/en/print.html.
[4] A. Panusa, G. Multari, G. Incarnato, L. Gagliardi, High-performance liquid chromatography analysis of anti-inflammatory pharmaceuticals with ultraviolet and electrospray-mass spectrometry detection in suspected counterfeit homeopathic medicinal products, J. Pharm. Biomed. Anal. 43 (2007) 1221–1227.
[5] G.J. Schad, A. Allanson, S.P. Mackay, A. Cannavan, J.N. Tettey, Development and validation of an improved HPLC method for the control of potentially counterfeit isometamidium products, J. Pharm. Biomed. Anal. 46 (2008) 45–51.
[6] S. Trefi, C. Routaboul, S. Hamieh, V. Gilard, M. Malet-Martino, R. Martino, Analysis of illegally manufactured formulations of tadalafil (Cialis (R)) by ^{1}H NMR, 2D DOSY ^{1}H NMR and Raman spectroscopy, J. Pharm. Biomed. Anal. 47 (2008) 103–113.
[7] M. Laasonen, T. Harmia-Pulkkinen, C. Simard, M. Rasanen, H. Vuorela, Development and validation of a near-infrared method for the quantitation of caffeine in intact single tablets, Anal. Chem. 75 (2003) 754–760.
[8] I. Storme-Paris, H. Rebiere, M. Matoga, C. Civade, P.-A. Bonnet, M.H. Tissier, P. Chaminade, Challenging near infrared spectroscopy discriminating ability for counterfeit pharmaceuticals detection, Anal. Chim. Acta 658 (2010) 163–174.
[9] S.H.F. Scafi, C. Pasquini, Identification of counterfeit drugs using near-infrared spectroscopy, Analyst 126 (2001) 2218–2224.
[10] J.C.L. Alves, R.J. Poppi, Simultaneous determination of acetylsalicylic acid, paracetamol and caffeine using solid-phase molecular fluorescence and parallel factor analysis, Anal. Chim. Acta 642 (2009) 212–216.
[11] A.B. Moreira, I.L.T. Dias, G.O. Neto, E.A.G. Zagatto, L. Kubota, Solid-phase fluorescence spectroscopy for the determination of acetylsalicylic acid in powdered pharmaceutical samples, Anal. Chim. Acta 523 (2004) 49–52.
[12] T. Naes, T. Isaksson, T. Fern, T. Davies, A User-Friendly Guide to Multivariate Calibration and Classification, NIR Publications, UK, 2002.
[13] D.L. Massart, B.G.M. Vandeginste, S.N. Deming, Y. Michotte, L. Kaufman, Supervised Pattern Recognition, in: Chemometrics: A Textbook, Data Handling in Science and Technology, 1st edition, Elsevier Science Publisher B.V., Amsterdam, 1988, pp. 385–413.
[14] M. Barker, W. Rayens, Partial least squares for discrimination, J. Chemom. 17 (2003) 166–173.
[15] S. Wold, P. Geladi, K. Esbensem, J. Öhman, Local principal component models, rank maps and contextuallity for curve resolution and multi-way calibration inference, J. Chemom. 1 (1987) 273–281.
[16] P. Valderrama, J.W.B. Braga, R.J. Poppi, Variable selection, outlier detection, and figures of merit estimation in a partial least-squares regression multivariate calibration model. A case study for the determination of quality parameters in the alcohol industry by near-infrared spectroscopy, J. Agric. Food Chem. 55 (2007) 8331–8338.
[17] S.D. Osborne, R.B. Jordan, R. Kunnemeyer, Method of wavelength selection for partial least squares, Analyst 122 (1997) 1531–1537.
[18] L. Norgaard, A. Saudland, J. Wagner, J.P. Nielsen, L. Munck, S.B. Engelsen, Interval partial least-squares regression (iPLS): a comparative chemometric study with an example from near-infrared spectroscopy, Appl. Spectrosc. 54 (2000) 413–419.
[19] H.M. Cartwright, Applications of Artificial Intelligence in Chemistry, Oxford Science Publications, New York, 1995.
[20] M.C.U. Araujo, T.C.B. Saldanha, R.K.H. Galvao, T. Yoneyama, H.C. Chame, V. Visani, The successive projections algorithm for variable selection in spectroscopic multicomponent analysis, Chemom. Intell. Lab. Syst. 57 (2001) 65–73.
[21] M. Otto, Chemometrics, Wiley, Weinheim, 1999.
[22] K.R. Beebe, R.J. Pell, M.B. Deascholtz, Chemometrics: A Practical Guide, John Wiley & Sons Inc., New York, 1998.
[23] S.C. Park, S.J. Lee, H. Namkung, H. Chumg, S.H. Han, M.Y. Yoon, J.J. Park, J.H. Lee, C.H. Oh, Y.A. Woo, Feasibility study for diagnosis of stomach adenoma and cancer using IR spectroscopy, Vib. Spectrosc. 44 (2007) 279–285.
[24] R. Castillo, M. Otto, J. Freer, S. Valenzuela, Multivariate strategies for classification of *Eucalyptus globulus* genotypes using carbohydrates content and NIR spectra for evaluation of their cold resistance, J. Chemom. 22 (2008) 268–280.

Journal of Pharmaceutical and Biomedical Analysis 66 (2012) 91–99

Contents lists available at SciVerse ScienceDirect

Journal of Pharmaceutical and Biomedical Analysis

journal homepage: www.elsevier.com/locate/jpba

Comparison of solid phase microextraction versus spectroscopic techniques for binding studies of carbamazepine

Barbara Bojko, Dajana Vuckovic [1], Janusz Pawliszyn *

Department of Chemistry, University of Waterloo, Waterloo, Ontario, Canada N2L 3G1

ARTICLE INFO

Article history:
Received 2 January 2012
Received in revised form 2 March 2012
Accepted 6 March 2012
Available online 14 March 2012

Keywords:
Protein binding
Solid phase microextraction
Fluorescence
Nuclear magnetic resonance
In vivo

ABSTRACT

The binding of carbamazepine to human serum albumin was studied *in vitro* using solid-phase microextraction (SPME) with liquid chromatography–ultraviolet detection (LC–UV), as well as spectroscopic fluorescence and nuclear magnetic resonance (^{1}H NMR) techniques. We were able to recognize one high affinity binding site with both fluorescence and SPME methods. Additionally, SPME experiment showed the existence of one lower affinity binding site for carbamazepine at the range of concentrations studied with fluorescence. The analysis of Hill's plot indicated positive cooperativity between drugs located in these two binding sites. Two low affinity-binding sites have been found with SPME–LC–UV analysis performed in parallel to ^{1}H NMR study, which does not show any complex formation. In conclusion, the results of the studies with carbamazepine as a model drug showed the advantages of simultaneous use of solid phase microextraction and spectroscopic methods in protein binding studies and indicated complementary information, which can be obtained with the use of SPME. Furthermore, we show that SPME in combination with liquid chromatography–mass spectrometry permitted direct *in vitro* determination of plasma–protein binding and direct *in vivo* evaluation of inter-animal variability in free concentrations of carbamazepine at physiologically relevant concentrations, the type of experiments typically inaccessible by spectroscopic techniques due to poor sensitivity and different mode of implementation.

© 2012 Elsevier B.V. All rights reserved.

1. Introduction

Protein binding plays important role in drug distribution and pharmacological activity of pharmaceuticals. Only free fraction of the drug can transfer through the membranes, induce therapeutic response or can be metabolized and eliminated from the body. The most abundant protein in the blood is albumin, which covers most of transporting function in circulatory system. Albumin binds various exo- and endogenous compounds, *e.g.* fatty acids, hormones, bilirubin and drugs [1]. Single chain consists of 585 amino acids and 67% of the protein has α-helical structure. Three homologous subdomains I–III, each divided into two subdomains A and B, form a heart-shaped structure of the protein [2]. Among them, subdomain IIA and IIIA (site I and II according Sudlow's nomenclature, respectively) play primary role in drug binding. Subdomain IIA, also known as warfarin binding site, is preferably occupied by bulky heterocyclic anions or dicarboxylic acids, while IIIA (indole, ibuprofen or benzodiazepine binding site) by aromatic carboxylic acids with hydrophobic center and negatively charged acidic group at one end of the molecule [1]. Apart of these two subdomains, which are likely high affinity binding sites, albumin also has number of binding sites at lower affinity. Also, nonspecific interactions between ligands and polypeptide chain of the protein occur [3]. An important aspect of ligand–protein interaction is competitiveness in binding, since simultaneous binding of two or more ligands may affect their affinity and, as a consequence, change the ratio between free and bound fraction of the drug. Thus, determination of drug binding sites, evaluation of drug–protein binding parameters as well as influence of various parameters on the binding is a fundamental part of pharmacological studies [4].

Various analytical techniques can provide different information on ligand–protein binding. The most commonly used are: crystallography, fluorescence, magnetic nuclear resonance spectroscopy (NMR), circular dichroism (CD), Fourier transform infrared spectroscopy (FTIR), ultrafiltration, UV–VIS spectrophotometry, calorimetry, and biosensor technology [5,6]. For instance, ultrafiltration or equilibrium dialysis provides quantitative information about the extent of drug binding, while CD or FTIR provide details on protein structural changes. Fluorescence allows the determination of drug binding sites, while NMR allows to precisely point drug's atoms involved in interaction with protein. However, each technique has some limitations, such as concentration range of analyte or physical properties of the analyte allowing certain measurement (*i.e.* the presence of chromophores or fluorophores). Thus in order

* Corresponding author.
E-mail address: janusz@uwaterloo.ca (J. Pawliszyn).
[1] Current address: Donnelly carbamazepine for Cellular and Biomolecular Research, University of Toronto, Toronto, Ontario, Canada M5S 3E1.

0731-7085/$ – see front matter © 2012 Elsevier B.V. All rights reserved.
doi:10.1016/j.jpba.2012.03.005

to obtain complete information on the binding process, it is often required to employ different techniques.

SPME is a sample preparation technique where the amount of analyte extracted is proportional to free concentration of the analyte, thus permitting its use for binding studies. Although SPME binding studies were already reported in the literature [7–11], the results were validated against techniques other than spectroscopic ones and were focused on the comparison of the drug fraction bound to protein or number of existing binding sites and binding constant value. Since binding studies with the use of fluorescence and NMR are some of the most widely used methods, in the current studies we compared various binding parameters, including association constants, Hill's plots and plasma protein binding (PPB%) obtained on the basis of these two spectroscopic techniques and SPME–LC–UV or SPME–LC–MS. The interesting aspect of such comparison is substantially different principles of the methods, which determine the overall results of binding studies. Therefore, this study aims to show the types of binding results that can be obtained using different techniques in order to aid the user in the selection of the most appropriate technique for their given application. In contrast to spectroscopic methods, SPME can be used in binding studies under physiological conditions. Biocompatible SPME coating, such as employed in this study, protects the fiber surface from the adhesion of macromolecules, which can adversely affect the extraction efficiency of a given coating and cause inaccurate results. Due to the biocompatibility of the SPME probe it can be used both in simple protein solutions as well as in the case of complex matrices like plasma, urine or whole blood. The feasibility of this approach for bioanalysis was already presented [7,12–16]. *In vivo* pharmacokinetics studies of carbamazepine in mice performed with SPME coupled with LC–MS/MS platform enabled the determination of drug concentrations as low as 1 ng/mL (4.2 nM) without blood sample withdrawal and using short 2-min sampling times [13]. Full pharmacokinetic profile of the drug was presented on the basis of single rodent sampling and validated against two standard approaches: serial automated blood sampling and terminal blood collection [13]. In the current binding studies, plasma protein binding was performed at the same therapeutically relevant concentrations.

The comparison of drug binding obtained by SPME and standard spectroscopic methods is the first such study reported in the literature. Carbamazepine, a common antiepileptic drug, was investigated as the model drug in this study because monitoring of its free fraction is clinically important and can vary depending on underlying medical conditions and/or coadministration of other drugs capable to compete for binding [17]. We also show that SPME in combination with liquid chromatography–mass spectrometry (LC–MS) detection can be used to directly determine the free concentrations of carbamazepine and the extent of plasma–protein binding *in vivo*, and that percent of carbamazepine binding is higher than previously reported.

2. Experimental

2.1. Materials

Carbamazepine, chemicals used for phosphate-buffered saline (PBS) solution preparation, reference standard for NMR measurements, 4,4-dimethyl-4-silapentane-1-sulfonic acid (DSS), deuterated water (D_2O) and methanol-d4 (CD_4O) were purchased from Sigma–Aldrich (Oakville, ON, Canada). Acetonitrile (HPLC grade) and methanol (HPLC grade) were purchased from Caledon Laboratories Ltd. (Georgetown ON, Canada). Deionized water used for dilution of stock solutions and PBS preparation was from a Barnstead/Thermodyne NANO-pure ultra water system (Dubuque, IA, US). Carbamazepine-d10 (CBZ-d10) was used for on-fiber kinetic calibration and was purchased from Alltech (Deerfield, IL, USA) as a 100 μg/mL methanolic solution. Prototype biocompatible SPME C18 fibers were obtained from Supelco (Bellefonte, PA, USA) as research samples.

Phosphate-buffered saline (PBS) solution pH 7.4 was prepared by dissolving 8.0 g of sodium chloride, 0.2 g of potassium chloride, 0.2 g of potassium phosphate and 1.44 g of sodium phosphate in 1 L of purified water and adjusting the pH to 7.4, if necessary.

Stock solution of carbamazepine (CBZ, 50,000 μM) was prepared in methanol. Working solutions of CBZ at concentrations of 5000 and 500 μM were prepared by dilution of stock solution in methanol. Stock solution of human serum albumin (50 μM) was prepared in PBS pH 7.4. For NMR experiments deuterated solvents were used. All experiments were performed at 25 °C.

3. Methods

As in our previous study [13,16], prior to all binding experiments the drug was incubated with albumin or mouse plasma overnight at 4 °C in order to establish binding equilibrium.

3.1. Protein fluorescence quenching

For fluorescence measurement Perkin-Elmer LS55 fluorescence spectrometer was used. Excitation wavelength λ_{ex} was 280 nm, emission spectra were recorded in the range between 300 and 400 nm. Plastic disposable 1 cm × 1 cm × 4 cm cuvettes were used for the experiment. Concentrations of carbamazepine and human serum albumin (HSA) were 5–50 μM and 2.5 μM respectively. Series of CBZ–HSA solutions was prepared using three different concentrations of methanol: 1, 2 and 3% (v/v). For plasma binding experiment human albumin was spiked with 20,000 μM of CBZ. Final concentration of methanol was 1% (v/v).

3.2. Nuclear magnetic resonance (NMR)

^{1}H NMR experiment was performed on Bruker 300 MHz Ultrashield spectrometer with 5 mm BBO broadband probe and automatic tuning and matching. For water signal suppression presaturation method was used. Chemical shift of carbamazepine proton resonances was assigned with respect to resonance of internal standard, 4,4-dimethyl-4-silapentane-1-sulfonic acid (DSS). Spectra of CBZ at increasing concentrations (50–400 μM) were recorded in the presence of constant concentration of HSA 2.5 μM. The content of methanol (2%, v/v) was constant for all samples. Assignment of proton resonances of carbamazepine was done on the basis of Spectral Database for Organic Compounds [18]. For the analysis, proton resonances at the highest intensity (A and E in Fig. 1) were chosen.

3.3. Solid phase microextraction (SPME) coupled with liquid chromatography–UV spectrophotometry (LC–UV)

Solid phase microextraction experiment was performed with the use of biocompatible C18 fibers manufactured by Supelco. For SPME studies samples previously prepared for fluorescence and NMR experiments were used. NMR experiment samples were diluted 20 times to avoid fiber saturation. Additionally, for calibration purposes (evaluation of fiber constant) samples containing only carbamazepine in PBS at concentrations used for binding studies were also analyzed. The extraction time was 50 min and extraction sample volume was 1.8 mL. Fiber desorption was performed using 1.8 mL of acetonitrile:water 1:1 (v/v). Vortex agitation of 1000 rpm was used during extraction and desorption in order to speed up the time needed to reach extraction equilibrium. Using the

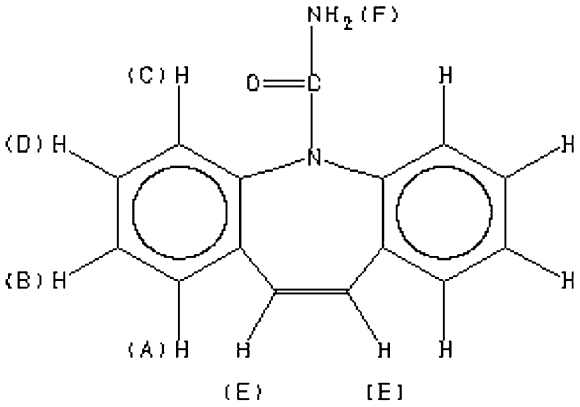

Fig. 1. Chemical structure of carbamazepine with assigned proton resonances of the drug used for analysis of ^{1}H NMR spectra.

stated desorption conditions, the analyte was effectively desorbed from the fiber with carry over less than 2%. Resulting samples were analyzed using LC–UV on Agilent 1100 Series system (Agilent Technologies, Palo Alto, CA) consisting of binary high pressure gradient pumps, vacuum solvent degasser, column thermostat and variable wavelength UV–VIS detector. Sample injection volume used was 20 μL, mobile phase consisted of acetonitrile:water 1:1 (v/v) with 0.1% acetic acid, flow rate 500 μL/min. Maximum absorption wavelength (λ_{max}) used for detection of carbamazepine was 290 nm. Chromatographic column used was Symmetry Shield RP18 with dimensions of 2.1 mm × 50 mm and 5 μm particles (Waters, Milford, MA, USA).

3.4. SPME coupled with liquid chromatography mass spectrometry (LC–MS/MS) for in vivo determination of free concentrations of CBZ

Two independent *in vivo* SPME experiments were performed using $n = 8$ (M1–8) and $n = 3$ mice (M9–11) respectively, according to validated procedures described in detail elsewhere [13]. Briefly, 2-min *in vivo* SPME extraction time was employed to sample the circulating mouse blood at 5, 15, 30 and 60-min time points after administration of a single 2 mg/kg i.v. dose of CBZ. Prior to sampling, the probes were pre-loaded with carbamazepine-d10 so that short pre-equilibrium extraction times could be used during *in vivo* experiment for better temporal resolution in combination with kinetic on-fiber standardization [14,15,19–21]. The amounts of CBZ extracted and carbamazepine-d10 loaded and remaining on the probe, were determined using liquid chromatography–mass spectrometry assay developed for CBZ and its main metabolite carbamazepine-10,11-epoxide [13]. Kinetic on-fiber standardization was used to accurately determine the equivalent amount of CBZ that would have been extracted if the extraction was performed at equilibrium using established validated kinetic calibration models. Finally, free CBZ concentration in circulating mouse blood was calculated on the basis of Eq. (6) using the fiber constant experimentally obtained after equilibrium extraction of a set of CBZ standards dissolved in phosphate-buffered saline (PBS, pH 7.4). In this case, PBS is used as an easily obtainable matrix which does not contain any binding proteins, and we have demonstrated in our previous studies that PBS is an appropriate substitute for protein-free plasma [22]. Calibration standards (0.3 mL sample volume in 0.3 mL capacity amber HPLC vial or 1.8 mL in 2 mL amber HPLC vial) were subjected to equilibrium SPME sampling procedure in parallel (16 h extraction, 200 rpm orbital agitation) using individual *in vivo* SPME probes for each standard. The calibration curve was obtained by $1/y$ weighted linear regression analysis using SigmaPlot 2004 for Windows (version 9.0) software.

3.5. Calculations and statistics

3.5.1. Solid phase microextraction

As mentioned in Section 1, the amount of analyte extracted by solid phase microextraction probe is proportional to free concentration of the analyte. The distribution of the analyte between sample and sorbent is described by the equation:

$$K_{fs} = \frac{C_{fibre}}{C_f} \quad (1)$$

where K_{fs} is partition coefficient for the analyte between SPME fiber and sample solution; C_{fiber} is the concentration of ligand at equilibrium in the fiber; C_f is the free concentration of ligand at equilibrium in sample solution.

The concentration of the ligand in the fiber can be calculated from the ratio of the amount extracted (n) and volume of the fiber (V_f)

$$C_{fibre} = \frac{n}{V_f} \quad (2)$$

The amount of drug extracted on the fiber can be expressed as:

$$n = C_0 \frac{K_{fs} V_s V_f}{K_{fs} V_f + V_s} \quad (3)$$

where C_0 is the initial concentration of the analyte in the sample.

At conditions of negligible depletion when the sample volume V_s is much larger than the product of $K_{fs}V_f$, Eq. (3) can be simplified to:

$$n = K_{fs} V_f C_0 \quad (4)$$

When we rearrange Eq. (4) we can express C_f as [23]

$$C_f = \frac{n}{K_{fs} \cdot V_f} \quad (5)$$

The parameters K_{fs} and V_f are difficult to determine experimentally, but the product of $K_{fs} \times V_f$, so called fiber constant, f_c, is constant for any given fiber and analyte, and can be easily calculated on the basis of extraction of the analyte from receptor-free solution. Thus, the final equation to calculate free concentration of the ligand at equilibrium conditions is given by Eq. (6) [23]

$$C_f = \frac{n}{f_c} \quad (6)$$

Detailed information about different calibration methods used to estimate free and total concentration of ligand, plasma binding and automation approaches to binding studies can be found elsewhere [7,8,12].

3.5.2. Determination of binding parameters

Association constant K_a was calculated by using the Scatchard method modified by Hiratsuka [24] and Lineweaver–Burk plot [25].

For Scatchard method Eq. (7) was used:

$$\frac{B}{C_f} = nK_a - K_a B \quad (7)$$

where B is the number of ligands bound to one protein molecule; C_f is the free (unbound) ligand concentration; n is the number of binding sites for the independent class of drug binding sites in albumin molecule which corresponds to the mean number of drug molecules bound in the independent class of drug binding sites in albumin molecule; K_a is the association constant.

Hill's plot was drawn on the basis of the following equation [26]:

$$\log[Y(1-Y)] = n_H \ \log C_f + n \log K \quad (8)$$

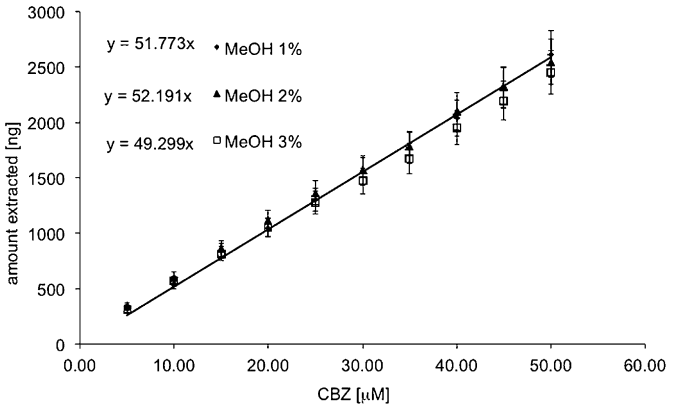

Fig. 2. Determination of SPME fiber constant for carbamazepine in the presence of 1, 2 and 3% (v/v) methanol in human plasma.

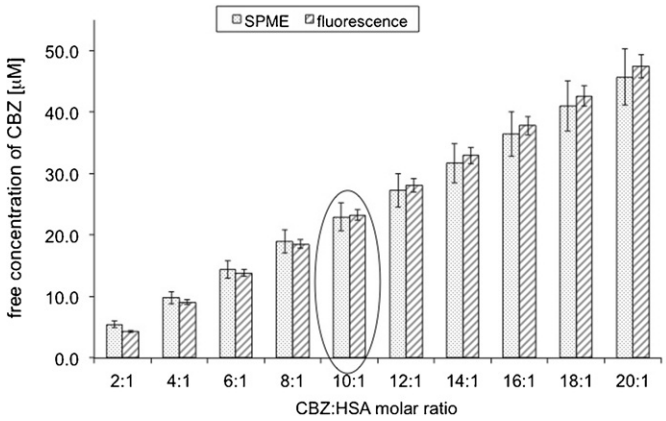

Fig. 3. Free concentration of carbamazepine–SPME *vs.* fluorescence data.

where Y is the fractional binding saturation; fraction of sites occupied with the ligand; $1 - Y$ is the number of free sites; n_H is the Hill's coefficient; K is the binding constant.

For fluorescence measurement:

$$Y(1 - Y) = \frac{Q}{Q_m - Q} \quad (9)$$

where $Q = (\mathrm{RFo} - \mathrm{RF})/\mathrm{RFo}$; $1/Q_m$ – intersect of OX axis on the plot $1/Q$ *versus* $1/C_f$.

3.5.3. Statistics

The mean and relative standard deviation was calculated from three independent experiments unless otherwise indicated.

4. Results and discussion

4.1. High affinity binding sites—fluorescence and SPME

To evaluate binding parameters with fluorescence technique drug (ligand):protein molar ratios must be adjusted to allow maximum quenching of protein fluorescence by the ligand. In the current study, maximum quenching of protein fluorescence by CBZ (60% of initial fluorescence intensity) was achieved at [CBZ]/[HSA] ratio 20:1. Further increase of CBZ concentration did not result in decrease of albumin fluorescence intensity.

In order to compare the binding results obtained using fluorescence and SPME–LC–UV, the above samples prepared for fluorescence studies were split into two portions and subsequently used for SPME experiment. LC–UV spectrometer linearity was found at the concentration range 0.064–4.24 μM ($y = 28.335x - 0.2359$; R^2 0.999). In the first step, extraction from CBZ buffered solution in the absence of HSA was performed. This experiment confirmed the lack of fiber saturation along the range of concentration used and allowed to calculate fiber constant, which is the slope of the graph amount extracted *versus* initial concentration of CBZ (Fig. 2). As it can be seen from Fig. 2 the amount of drug extracted and, as a consequence, fiber constant does not change within the range of investigated concentration of methanol in the solution.

The comparison of free concentration of CBZ calculated on the basis of fluorescence and SPME–LC–UV data is shown in Fig. 3. The figure shows that the free concentrations of CBZ calculated by the two methods are equivalent within the experimental error. (RSD%, 4% and 10% for fluorescence and SPME, respectively, $n = 3$; paired t-test showed no statistical differences $p > 0.21$). However, it can be seen that above [CBZ]/[HSA] molar ratio 10:1 free concentration of the drug calculated from SPME data is lower than fluorescence results. This trend was noted for all repeated experiments and further evaluation of the data obtained by both methods showed different binding properties of albumin toward CBZ observed with fluorescence and SPME.

Linear run of Scatchard plot for fluorescence data (Fig. 4A) indicates the existence of one class of binding site for CBZ on albumin molecule with association constant K_a $2.5 \times 10^4\ \mathrm{M}^{-1}$ (Table 1), while non-linear dependence is observed for SPME results (Fig. 4B) which suggests the existence of an additional class of binding site. Our fluorescence results are in agreement with the studies done recently by Kalanur et al. who characterized interaction of CBZ in IIA subdomain with the use of spectroscopic and volumetric techniques [27]. Additionally, the influence of drug molecule on mutual binding and allosteric heterogeneity in drug molecule binding was noted on the basis of sigmoidal shape of

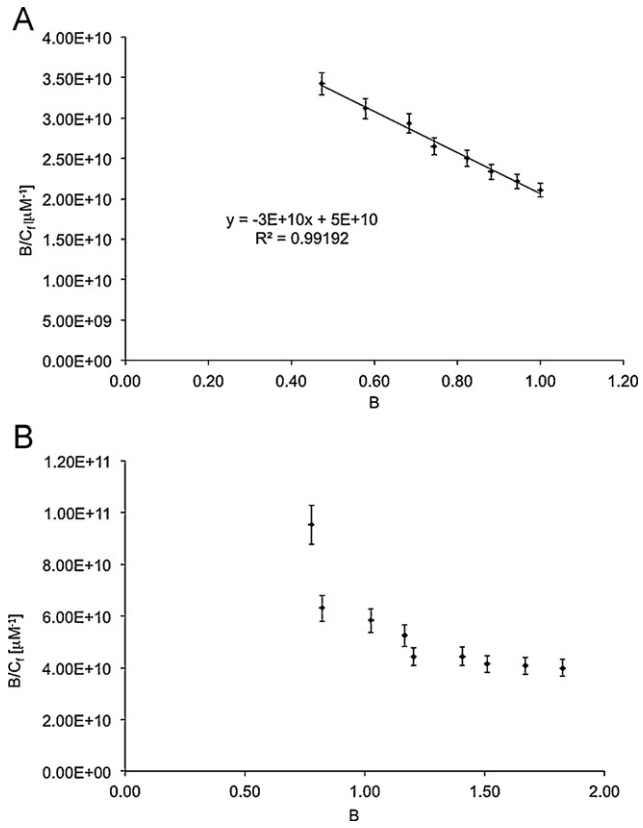

Fig. 4. Scatchard plot of carbamazepine–human serum albumin complex; fluorescence (A) and SPME (B) data.

Table 1
The binding constants calculated by Scatchard and Lineweaver–Burk equations and plasma protein binding (PPB%) obtained from fluorescence and SPME–LC–UV measurements.

MeOH (%)	Fluorescence		SPME		Fluorescence	SPME
	K_a (M^{-1}) Scatchard	K_a (M^{-1}) Lineweaver–Burk	K_a (M^{-1}) Lineweaver–Burk		PPB%	PPB%
1	2.54×10^4	3.00×10^4	3.38×10^4	7.50×10^3	5–9	4–9
2	2.67×10^4	2.95×10^4	3.06×10^4	1.38×10^4	5–9	3–17
3	2.65×10^4	2.98×10^4	3.26×10^4	1.90×10^4	5–9	2–14

semi-logarithmic Hill plot drawn for SPME data (Fig. 5A). According to Bindslev [28] Hill plot cannot be observed as a straight line (except for Hill coefficient equals 1) for multi-site complexes characterized by different affinity toward the ligand and each association constant must be considered separately according to general equation

$$Y = \sum_{r}^{n} a_r \frac{K_r x^r}{1 + K_r x^r} \quad (10)$$

where y is the total fractional occupancy, factor a_r is the maximal fraction of receptive units with a number of 'r' ligands bound, and K_r is the association constant for ligand binding with $r-1$ ligands already bound. The implications of equating K with subscript 'r' allow for co-operativity, as the association constants may vary independently [28]. Indeed, the existence of additional low affinity binding site is observed when analyzing Lineweaver–Burk plot created on the basis of SPME data (Fig. 5B). In contrast, the same relationship presented for fluorescence results confirms findings

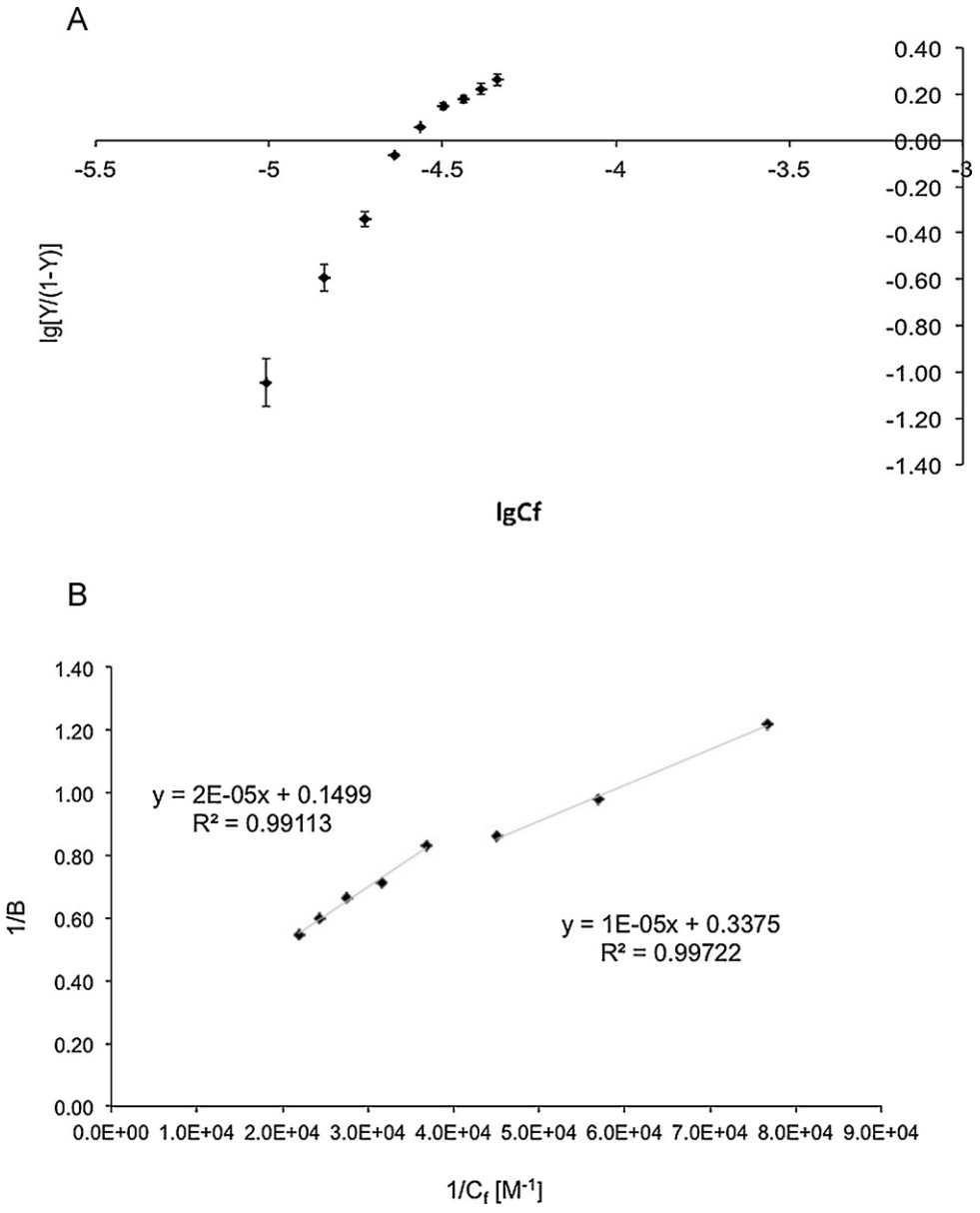

Fig. 5. Semi-log Hill's plot of carbamazepine–human serum albumin complex (A) and Lineweaver–Burk plot of carbamazepine–human serum albumin complex (B); SPME data.

obtained from Scatchard plot and shows the existence of only one class of high affinity binding site for CBZ in tertiary structure of HSA. The association constant for this binding site calculated on the basis of Lineweaver–Burk relationship is $3.0 \times 10^4\ M^{-1}$ (Table 1) and is in agreement with the constant previously calculated from Scatchard equation. The association constants calculated for two cooperating binding sites observed in Fig. 5B on the basis of SPME data are K_{aI} $3.4 \times 10^4\ M^{-1}$ and K_{aII} 3.9×10^3 M, respectively (Table 1). It can be noticed that K_{aI} value correlates to the one calculated from fluorescence results.

4.2. Plasma protein binding (PPB%)—fluorescence and SPME

Fraction of protein binding (PPB%) is also higher for SPME comparing to fluorescence data (Table 1), which is a result of the additional low affinity interactions. Significant discrepancy in PPB presented herein and by other authors [29] are due to the fact of great difference between the drug:protein molar ratios used in both experiments. In equilibrium dialysis binding studies by MacKichan and Zola [29] albumin concentration used was within the range 0.29×10^{-3} to 0.58×10^{-3} μM and CBZ concentration 0.02×10^{-3} to 5×10^{-3} μM, and the molar ratios were between 0.036 and 0.072, while in the current studies molar ratios adjusted to fluorescence method requirements were between 2 and 20. It can be concluded that in the situation when there is an excess of the drug molecules per one mole of albumin binding sites compared to situation where 10^{-2} mol compete for one binding site the fraction of CBZ bound must be lower unless binding capacity of the protein is large enough to associate with remaining free molecules of CBZ. The existence of additional binding site revealed in SPME experiment can be supported by results reported by Kim et al. using immobilized HSA column [30]. The authors investigated competition between CBZ and various HSA site probes and pointed out the direct competition with L-tryptophan at indole-benzodiazepine site, allosteric interaction with the warfarin-azaproprazone site and minor binding regions, *e.g.* digitoxin or tamoxifen site.

The differences reported arise from the fact of fundamentally different principles of the methods used. Solid phase microextraction provides quantitative information about the free fraction of drug extracted by the fiber. Thus, the knowledge about drug–protein interaction is 'global'. In case of fluorescence our observations are focused on certain regions of protein containing fluorophores, which become excited when 280 nm wavelength is used, *i.e.* tryptophanyl and tyrosil residues. As mentioned before, the main binding sites for drug are located in subdomains IIA and IIIA of human albumin. Both of these hydrophobic pockets contain at least one kind of the aforementioned amino acid residues, which may transfer energy to the ligand if the latter is in close proximity of the fluorophore (<10 nm) [31]. There is one tryptophan (Trp 214) and one tyrosine (Tyr 263) located in Sudlow's site I [1,2], which can be involved in drug binding. Although Trp 214 is the sole tryptophan in HSA structure, it plays primary role in interactions with ligands. Subdomain IIIA contains three tyrosines (Tyr 401, 411 and 497) [32], which can participate in energy transfer to the acceptor and the first two have been found as the amino acids, which stabilize binding of numerous ligands. To verify subdomain IIA of HSA as the specific binding site for CBZ quenching curves of HSA excited with both, 295 nm and 280 nm wavelengths in the presence of CBZ at increasing concentration were compared (data not shown). The overlap of the curves pointed that there is no difference in energy transfer between the protein and the ligand, *i.e.* only tryptophanyl residue is involved in interaction with CBZ. This allows identifying subdomain IIA as specific high affinity binding site for CBZ. This result corroborates recent spectroscopic reports on Sudlow's site I as primarily location of carbamazepine in albumin structure [27]. Considering these facts it can be concluded that the second class of binding site observed only in SPME–LC–UV experiment is probably set in the region of HSA where no fluorophore excited with λ_{ex} 280 nm is located.

The investigation of methanol influence on protein affinity toward CBZ indicated that CBZ–HSA complex formed in high affinity binding site is stable and methanol does not affect interaction between drug and macromolecule. Low affinity site observed in SPME experiment showed the increase of HSA affinity toward CBZ (K_a value increased almost 2.5-fold) and percentage of bound fraction (up to 14–17%) (Table 1). It can be surmized that methanol content above 1% (v/v) changes interaction between surface of the protein and/or regions more exposed to solvent effect than highly hydrophobic subdomain IIA.

4.3. Low affinity binding sites—NMR and SPME

In second experiment, the performance of SPME was compared to NMR. NMR enables the monitoring of interaction between macromolecule and ligand based on slow or fast exchange between free and bound ligand molecules, which corresponds to high (K_d < 1 μM; strong interaction), medium (K_d 1–100 μM) and low (K_d > 100 μM; weak interaction) affinity binding, respectively [33]. Although NMR is imaging method and SPME sample preparation and extraction technique, in both cases the measurement is based on the observation of ligand molecules, thus overview of all binding sites scattered in various regions of the albumin can be obtained. However, NMR requires relatively high concentration of the ligand, which can limit investigations of drug–albumin interactions. In our study no changes in chemical shift of CBZ proton resonances were observed with the increasing [CBZ]/[HSA] molar ratio, thus it can be concluded that no binding occurs within the studied range of concentration (Table 2).

The above samples used for NMR study could not be directly subjected to SPME–LC–UV analysis, because the extraction from the series of CBZ solution in PBS at the range of concentration corresponding to the one used for binding experiment showed saturation of C18 fibers due to the use of very high drug concentrations needed for NMR. The lack of linearity was noted for carbamazepine above concentration 252 μM. The problem of saturation can be avoided by replacing C18 coating with an appropriate sorbent having higher extraction capacity, *i.e.* PDMS, which are also commercially available or can be made in-lab, or with different geometry of C18 coating, *i.e.* thin film offering higher extraction volume. Another solution is the dilution of samples if the use of the same fibers is preferred, so in the current study 20-fold dilution of the samples with PBS was performed. SPME results showed changes in free concentration of CBZ and further analysis indicated existence of two low affinity classes of binding sites. The association constant calculated for the first and second class was $2.3 \times 10^3\ M^{-1}$ and $1.0 \times 10^3\ M^{-1}$, respectively. The fact that CBZ–HSA interaction was observed in SPME experiment and was not observed with NMR can be explained in two ways. One of the possible explanations

Table 2
Chemical shifts of chosen proton resonances of carbamazepine in the absence and the presence of human serum albumin.

[CBZ]/[HSA]	H1 (ppm)	H2 (ppm)
0	7.007	7.459
20	7.006	7.457
40	7.006	7.457
60	7.005	7.457
80	7.005	7.457
100	7.005	7.457
120	7.005	7.457
140	7.005	7.457
160	7.005	7.455

Table 3
The results of PBS calibration of carbamazepine for SPME method using two lots of C18 biocompatible SPME probes.

Experiment	Sample volume (mL)	Linear range (ng/mL)[a]	Number of standards	Slope	Std error – slope	*Y*-Intercept	Std error – *Y*-intercept	R^2	Fiber constant
1 (n = 8 mice)	0.3	0.8–300	7	**0.179**	0.0063	0.0463	0.128	0.994	**0.444**
2 (n = 3 mice)	1.8	0.6–300	8	**0.306**	0.012	0.267	0.195	0.992	**0.306**

The bold font refers to the parameters discussed in the text.
[a] Linear ranges given correspond to 0.003–1.26 μM and 0.002–1.26 μM; ng/mL units were used for better clarity of the data

relates to principles of NMR; for complexes where slow exchange between free and bound ligand molecule takes place two separate signals characterizing two ligand fractions can be observed, while in case of fast exchange chemical shift observed on NMR spectra is an average of the chemical shift of free and bound fraction of the drug [34]. Thus, if the percent of the drug bound is much lower than free drug, no significant changes can be noticed. It was previously reported for fluorouracil–bovine serum albumin complex that once the binding site(s) became saturated, the values of chemical shift of the observed proton resonances went back to the values characterizing free drug, due to the excess of unbound fraction [35]. Since PPB calculated from SPME data is low and varies between 12% and 17% the lack of changes in chemical shift suggesting no complex formation seems to be highly probable. The observed differences between SPME and NMR results can be also related to sample dilution, which likely changed equilibrium in drug–protein system. However, the influence of sample dilution on binding parameters is not unambiguous; some authors reported decrease of binding due to the lower concentration of available binding sites on protein [36], while others noted opposite phenomenon [37].

4.4. Plasma binding studies

The monitoring of free drug concentration in plasma, blood or other biological matrices and the determination of total plasma binding is an important step in drug development studies. Fluorescence technique is not used for this kind of studies due to the complexity of the matrix and low signal intensity. However, in order to verify the feasibility of the methods for the evaluation of drug–plasma binding short experiment with one concentration of CBZ equivalent to therapeutic dose (17–51 μM) [38] was performed. The results confirmed low fluorescence intensity of blank plasma observed in emission spectrum. As it was previously shown for CBZ–HSA binding, quenching of protein fluorescence required concentration of the drug higher than concentration of the albumin. As it was expected, addition of carbamazepine at therapeutic concentration (20 μM) did not change fluorescence intensity recorded for blank plasma sample.

In our ^{1}H NMR studies intensities of proton resonances of CBZ at therapeutic concentrations were too low to be analyzed. However, to enable NMR analyses and enhance efficiency of binding studies with NMR technique, analyses of isotopes different than proton can be performed (*e.g.* ^{19}F NMR, ^{31}P NMR, ^{13}C NMR) or/and isotopically labeled ligands can be used. NMR can be also used for localization of drug binding site on protein due to the changes in shielding of spins in binding site microenvironment [39].

As mentioned before, to obtain free concentration of the drug in the studied matrix calibration of fiber constant with the use of PBS buffer is required. The results for PBS calibrations performed during two independent experiments are summarized in (Table 3). The difference in fiber constants observed on two days is due to the differences in lot number of biocompatible C18 probes used for the two sets of experiments, and illustrates that calibration needs to be performed for each lot of probes employed in a given experiment, as significant lot-to-lot variability in the amount of extraction phase immobilized can be observed for different lots of probes. Furthermore, depending on the sample volume used for calibration, fiber constant can be obtained either directly from the slope of the calibration curve (1.8 mL sample volume used in experiment 2) or after applying appropriate correction for the use of non-negligible depletion conditions (0.3 mL sample volume used in experiment 1) to ensure accurate quantitation. *In vitro* experiment performed in triplicate with the use of pooled mouse plasma spiked with CBZ at concentration 0.45 μM showed 92% plasma binding. The precision of the method expressed as relative standard deviation (RSD) was less than 2%. Additionally, single determination of PPB% was performed in pooled mouse plasma across the range of carbamazepine concentrations (Table 4). As shown in Table 4 mean PPB% of the drug was 96.1% and was concentration-independent.

4.5. In vivo determination of free CBZ concentration and inter-animal variability in PPB binding

After showing that *in vitro* SPME can give results equivalent to fluorescence techniques for high concentrations of CBZ, we next demonstrated that SPME can be applied using *in vivo* sampling format to directly measure free concentrations during animal studies and estimate inter-animal variability at therapeutically relevant concentrations of CBZ. This type of information can be extremely valuable during drug discovery and development process, as only free concentration is biologically active and better correlates with observed pharmacological and toxicological effects.

Fig. 6A shows free concentration profiles of carbamazepine in whole blood in the interval from 5 to 60 min after single 2 mg/kg i.v. dose of CBZ to n = 11 mice in two independent experiments. The mean free concentration for all mice tested (n = 11) is overlaid with individual mouse profiles to show variability in binding observed with respect to time and individual. Carbamazepine induces its own metabolism, and elimination half-life after single dose can vary over three times [40], which can also induce inter-individual differences. Fig. 6B summarizes the extent of inter-animal variability observed at each time point and ranges from 53% to 40% across different time points, which correlates well with known inter-individual variability of 30% in free CBZ concentrations and CBZ PPB observed in humans [41]. Moreover, *in vivo* verification of the extent of binding may be particularly attractive for drugs

Table 4
Total and free concentration of carbamazepine, and plasma protein binding (PPB%) determined by SPME across the range of drug concentration.

C_{total} (after extraction) (μM)	C_{free} (μM)	PPB%
0.042	0.001	96.4
0.075	0.002	96.7
0.349	0.014	96.0
0.818	0.041	95.0
2.12	0.070	96.7
3.23	0.146	95.5
8.06	0.317	96.1
9.34	0.340	96.4
	Mean	96.1
	Std. dev.	0.6
	% RSD	0.6

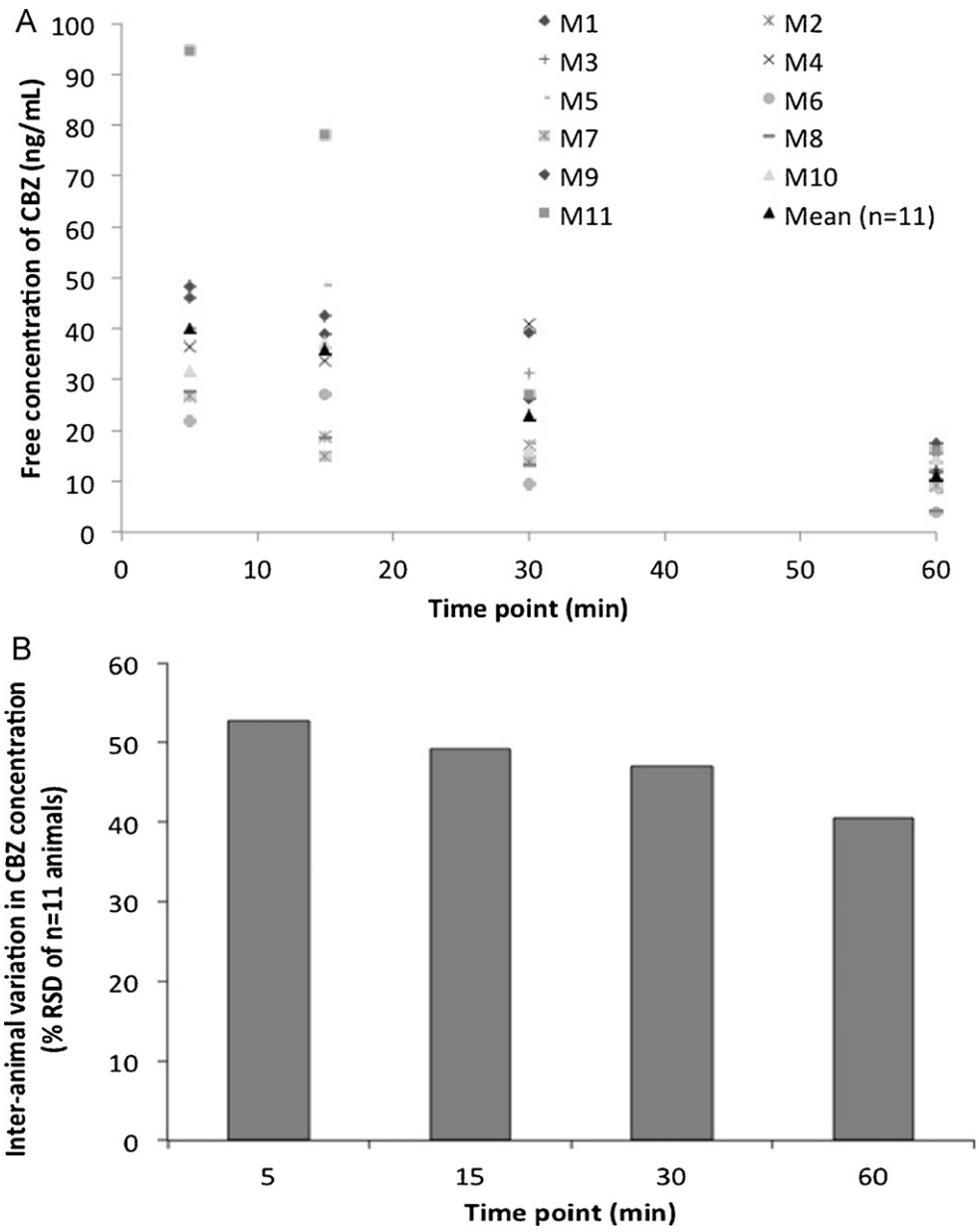

Fig. 6. Free concentration profiles of CBZ in mouse whole blood and mean CBZ free concentration ($n = 11$ mice) obtained using *in vivo* SPME at 5, 15, 30 and 60-min post-carbamazepine dose (A); inter-animal variability in free CBZ concentrations at different time points post-dose expressed as % RSD ($n = 11$ mice) (B).

known to bind to α1 acid glycoprotein (AAG) as previous studies have shown poor correlation of *in vitro versus in vivo* binding values for this protein, due to differences in the exact physiochemical properties of AAG employed *in vitro versus* native protein *in vivo* [42].

5. Concluding remarks

This study clearly illustrates the type of information that can be obtained during binding studies of human serum albumin with carbamazepine obtained with the use of three different analytical methods: protein fluorescence quenching, proton nuclear magnetic resonance and solid phase microextraction (SPME) coupled to LC–UV or LC–MS. Due to the different principles of the methods used, it is possible to collect information about local drug–amino acids interactions and global abilities of protein to form the complex. Although all techniques have some limitations, simultaneous analyses provide complementary information and allow better understanding of undergoing binding process. SPME, which is relatively new technique in bioanalysis, offers several advantages over standard methods used for binding studies, *i.e.* it can be used to study binding of drug to protein or other macromolecules or determination of free and/or total drug concentration in complex matrices like plasma or whole blood. Automated SPME system can be used for simultaneous determination of several drugs or interaction of the drug with different receptors in high-throughput format [9,12]. *In vivo* SPME can be used as rapid tool to estimate inter-animal variability in free concentrations of both drugs and their metabolites and to verify *in vitro* binding predictions at therapeutically relevant doses. SPME analysis is based on determination of amount of drug extracted by the probe, thus only quantitative data can be obtained from this measurement. This is in contrast to fluorescence or NMR studies, which provide us with the information about structural changes of protein structure or functional group of drug involved in complex formation, respectively. The combination of these techniques gives us the opportunity to obtain both,

qualitative and quantitative data, which characterizes microenvironment of binding site as well as quantitative data for the entire complex. Limitation of SPME such as saturation of the fiber, which may occur when high concentration of ligand is used may be overcome by using higher extraction capacity sorbent or by increasing the extraction phase surface by applying thin film geometry device. The simultaneous utilization of different chemistry coatings with multi-fiber sampler can enhance the throughput of analysis at early stage of drug development. In future studies, this type of approach can be further extended to monitor the effect of co-administration of drugs on binding characteristics of a given drug, to monitor the extent of inter-individual variability in binding in order to evaluate the necessity of therapeutic drug monitoring for a given drug and/or to improve understanding of factors that lead to this variability *in vivo*.

Acknowledgments

The authors thank the Natural Sciences and Engineering Research Council of Canada (NSERC) and Canada Research Chairs (CRC) for financial support of the project. Supelco is gratefully acknowledged for providing biocompatible SPME fibers and NoAb BioDiscoveries for the collaboration on *in vivo* experiment.

References

[1] U. Kragh-Hansen, V.T.G. Chuang, M. Otagiri, Practical aspects of the ligand-binding and enzymatic properties of human serum albumin, Biol. Pharm. Bull. 25 (2002) 695–704.
[2] X.M. He, D.C. Carter, Atomic-structure and chemistry of human serum-albumin, Nature 358 (1992) 209–215.
[3] I. Klotz, J. Ayers, Protein interactions with organic molecules, Discuss. Faraday Soc. (1953) 189–196.
[4] S. Schmidt, D. Gonzalez, H. Derendorf, Significance of protein binding in pharmacokinetics and pharmacodynamics, J. Pharm. Sci. 99 (2010) 1107–1122.
[5] H. Gao, L.D. Lei, J.Q. Liu, Q. Kong, X.G. Chen, Z.D. Hu, The study on the interaction between human serum albumin and a new reagent with antitumour activity by spectrophotometric methods, J. Photochem. Photobiol. A: Chem. 167 (2004) 213–221.
[6] C. Bertucci, G. Ascoli, G. Uccellobarretta, L. Dibari, P. Salvadori, The binding of 5-fluorouracil to native and modified human serum-albumin: UV, CD, and ^{1}H and ^{19}F NMR investigation, J. Pharm. Biomed. Anal. 13 (1995) 1087–1093.
[7] F.M. Musteata, J. Pawliszyn, M.G. Qian, J.T. Wu, G.T. Miwa, Determination of drug plasma protein binding by solid phase microextraction, J. Pharm. Sci. 95 (2006) 1712–1722.
[8] F.M. Musteata, J. Pawliszyn, Study of ligand–receptor binding using SPME: investigation of receptor, free, and total ligand concentrations, J. Proteome Res. 4 (2005) 789–800.
[9] D. Vuckovic, J. Pawliszyn, Automated study of ligand–receptor binding using solid-phase microextraction, J. Pharm. Biomed. Anal. 50 (2009) 550–555.
[10] H. Yuan, J. Pawliszyn, Application of solid-phase microextraction in the determination of diazepam binding to human serum albumin, Anal. Chem. 73 (2001) 4410–4416.
[11] G. Theodoridis, Application of solid-phase microextraction in the investigation of protein binding of pharmaceuticals, J. Chromatogr. B: Analyt. Technol. Biomed. Life Sci. 830 (2006) 238–244.
[12] D. Vuckovic, E. Cudjoe, F.M. Musteata, J. Pawliszyn, Automated solid-phase microextraction and thin-film microextraction for high-throughput analysis of biological fluids and ligand–receptor binding studies, Nat. Protoc. 5 (2010) 140–161.
[13] D. Vuckovic, I. de Lannoy, B. Gien, Y. Yang, F.M. Musteata, R. Shirey, L. Sidisky, J. Pawliszyn, In vivo solid-phase microextraction for single rodent pharmacokinetics studies of carbamazepine and carbamazepine-10,11-epoxide in mice, J. Chromatogr. A 1218 (2011) 3367–3375.
[14] X. Zhang, A. Es-haghi, F.M. Musteata, G. Ouyang, J. Pawliszyn, Quantitative *in vivo* microsampling for pharmacokinetic studies based on an integrated solid-phase microextraction system, Anal. Chem. 79 (2007) 4507–4513.
[15] F.M. Musteata, I. de Lannoy, B. Gien, J. Pawliszyn, Blood sampling without blood draws for *in vivo* pharmacokinetic studies in rats, J. Pharm. Biomed. Anal. 47 (2008) 907–912.
[16] D. Vuckovic, R. Shirey, Y. Chen, L. Sidisky, C. Aurand, K. Stenerson, J. Pawliszyn, In vitro evaluation of new biocompatible coatings for solid-phase microextraction: implications for drug analysis and in vivo sampling applications, Anal. Chim. Acta 638 (2009) 175–185.
[17] G.J.A. Macphee, J.R. Mitchell, L. Wiseman, A.R. Mclellan, B.K. Park, G.T. Mcinnes, M.J. Brodie, Effect of sodium valproate on carbamazepine disposition and psychomotor profile in man, Br. J. Clin. Pharmacol. 25 (1988) 59–66.
[18] http://riodb01.ibase.aist.go.jp/sdbs/ (accessed September 2010).
[19] Y. Chen, J. O'Reilly, Y. Wang, J. Pawliszyn, Standards in the extraction phase, a new approach to calibration of microextraction processes, Analyst 129 (2004) 702–703.
[20] Y. Chen, J. Pawliszyn, Kinetics and the on-site application of standards in a solid-phase microextration fiber, Anal. Chem. 76 (2004) 5807–5815.
[21] G. Ouyang, J. Pawliszyn, A critical review in calibration methods for solid-phase microextraction, Anal. Chim. Acta 627 (2008) 184–197.
[22] J.C. Yeung, D. Vuckovic, J. Pawliszyn, Comparison and validation of calibration methods for *in vivo* SPME determinations using an artificial vein system, Anal. Chim. Acta. 665 (2010) 160–166.
[23] J. Pawliszyn, Handbook of Solid Phase Microextraction, Chemical Industry Press, Beijing, 2009.
[24] T. Hiratsuka, Conformational changes in the 23-kilodalton NH_2-terminal peptide segment of myosin ATPase associated with ATP hydrolysis, J. Biol. Chem. 265 (1990) 18786–18790.
[25] J.T. Woosley, T.G. Muldoon, comparison of accuracy of Scatchard, Lineweaver–Burk and direct linear plots for analysis of steroid–protein interactions, J. Steroid Biochem. Mol. Biol. 8 (1977) 625–629.
[26] A. Hill, The possible effects of the aggregation of the molecules of haemoglobin on its dissociation curves, J. Physiol. 40 (1910) iv–vii.
[27] S.S. Kalanur, J. Seetharamappa, V.K.A. Kalalbandi, Characterization of interaction and the effect of carbamazepine on the structure of human serum albumin, J. Pharm. Biomed. Anal. 53 (2010) 660–666.
[28] N. Bindslev, Modeling theoretical tools to test and evaluate experimental equilibrium effects, Hill in Hell. (Chapter 10), in: Drug–acceptor interactions, 2008, Electronic ISBN: 978-91-977071-1-4 http://journals.sfu.ca/coactionbks/index.php/Bindslev/issue/current.
[29] J.J. MacKichan, E.M. Zola, Determinants of carbamazepine and carbamazepine 10,11-epoxide binding to serum-protein, albumin and alpha-1-acid glycoprotein, Br. J. Clin. Pharmacol. 18 (1984) 487–493.
[30] H.S. Kim, D.S. Hage, Chromatographic analysis of carbamazepine binding to human serum albumin, J. Chromatogr. B: Analyt. Technol. Biomed. Life Sci. 816 (2005) 57–66.
[31] B. Valeur, Molecular Fluorescence: Principles and Applications, Wiley-VCH, Weinheim, 2002, pp. 34–123.
[32] J. Kang, Y. Liu, M.X. Xie, S. Li, M. Jiang, Y.D. Wang, Interactions of human serum albumin with chlorogenic acid and ferulic acid, Biochim. Biophys. Acta Gen. Subj. 1674 (2004) 205–214.
[33] T. Carlomagno, Ligand–target interactions: what can we learn from NMR? Annu. Rev. Biophys. Biomol. Struct. 34 (2005) 245–266.
[34] L. Fielding, S. Rutherford, D. Fletcher, Determination of protein–ligand binding affinity by NMR: observations from serum albumin model systems, Magn. Reson. Chem. 43 (2005) 463–470.
[35] A. Sulkowska, B. Bojko, J. Rownicka, P. Rezner, W.W. Sulkowski, The competition of drugs to serum albumin in combination chemotherapy: NMR study, J. Mol. Struct. 744 (2005) 781–787.
[36] I. Kariv, H. Cao, K.R. Oldenburg, Development of a high throughput equilibrium dialysis method, J. Pharm. Sci. 90 (2001) 580–587.
[37] C.E. Ahlfors, Effect of serum dilution on apparent un-bound bilirubin concentration as measured by the peroxidase method, Clin. Chem. 27 (1981) 692–696.
[38] G.A. McMillin, J.M. Juenke, G. Tso, A. Dasgupta, Estimation of carbamazepine and carbamazepine-10,11-epoxide concentrations in plasma using mathematical equations generated with two carbamazepine immunoassays, Am. J. Clin. Pathol. 133 (2010) 728–736.
[39] U. Holzgrabe, I. Wawer, B. Diehl, NMR Spectroscopy in Drug Development and Analysis, John Wiley & Sons, Weinheim, 2008.
[40] S. Simon, Handbook of Epilepsy Treatment, Wiley-Blackwell, 2010.
[41] Y. Kodama, M. Kuranari, H. Kodama, I. Fujii, M. Takeyama, In vivo determinations of carbamazepine and carbamazepine-10, 11-epoxide binding parameters to serum-proteins in monotherapy patients, J. Clin. Pharmacol. 33 (1993) 851–855.
[42] J.M.H. Kremer, J. Wilting, L.H.M. Janssen, Drug-binding to human alpha-1-acid glycoprotein in health and disease, Pharmacol. Rev. 40 (1988) 1–47.

Journal of Pharmaceutical and Biomedical Analysis 66 (2012) 100–108

Contents lists available at SciVerse ScienceDirect

Journal of Pharmaceutical and Biomedical Analysis

journal homepage: www.elsevier.com/locate/jpba

Enantiomeric resolution of albendazole sulfoxide by semipreparative HPLC and *in vitro* study of growth inhibitory effects on human cancer cell lines

Kátia Roberta A. Belaz[a], Marina Denadai[a], Ana Paula Almeida[b,c], Raquel T. Lima[c,d], M. Helena Vasconcelos[d,e], M. Madalena Pinto[b,c], Quezia B. Cass[a], Regina V. Oliveira[a,*]

[a] *Chemistry Department, Federal University of São Carlos, São Carlos, SP, Brazil*
[b] *Laboratory of Organic and Pharmaceutical Chemistry, Department of Chemistry Sciences, Faculty of Pharmacy, University of Porto, Portugal*
[c] *CEQUIMED, Centro de Química Medicinal da Universidade do Porto, Faculty of Pharmacy, University of Porto, Portugal*
[d] *Cancer Drug Resistance Group, IPATIMUP, Institute of Molecular Pathology and Immunology of the University of Porto, Portugal*
[e] *Laboratory of Microbiology, Department of Biological Sciences, Faculty of Pharmacy, University of Porto, Portugal*

ARTICLE INFO

Article history:
Received 20 January 2012
Received in revised form 6 March 2012
Accepted 8 March 2012
Available online 15 March 2012

Keywords:
Albendazole sulfoxide
Semipreparative enantiomeric separation
Polysaccharide-based chiral stationary phases
Apoptosis
Tumor cell lines

ABSTRACT

Analytical and semipreparative high performance liquid chromatography methods using polysaccharide-based chiral stationary phases were developed for the enantiomeric resolution of albendazol sulfoxide. The enantioseparation of this compound was evaluated with four chiral stationary phases: cellulose and amylose *tris*(3,5-dimethylphenylcarbamate), amylose *tris*[(*S*)-1-phenylethylcarbamate] and amylose *tris*(3,5-dimethoxyphenylcarbamate), under three elution conditions: normal, reversed-phase and polar organic mode. The influences of the mobile phase and of the structure of the chiral stationary phase on the enantiomeric separation are discussed. The best chiral performances were achieved on an amylose *tris*(3,5-dimethylphenylcarbamate) phase under normal (R_s = 4.96) and polar organic mode (R_s = 2.60 and 3.09). A polar organic condition using methanol as mobile phase offered shorter retention factors (k_1 = 0.34) and was scaled up to semipreparative HPLC to obtain milligram quantities of both albendazole sulfoxide enantiomers for further *in vitro* studies. Optical rotation and circular dichroism of both enantiomers of albendazole sulfoxide was determined.

The compounds ABZ, ABZ-SO, (*R*)-(+)-ABZ-SO and (*S*)-(−)-ABZ-SO were all evaluated regarding their capacity to inhibit the *in vitro* growth of three human tumor cell lines: MCF-7 (breast adenocarcinoma), NCI-H460 (non-small cell lung cancer) and A375-C5 (melanoma). In addition, the effect of the (*R*)-(+)-ABZ-SO compound in the cell cycle profile and apoptosis of MCF-7 cells were also studied. Results indicated that compound ABZ was the most potent regarding cell growth inhibition and that the (+)-(*R*)-ABZ was a more potent inhibitor of cell growth than the (*S*)-(−)-ABZ-SO, particularly in the MCF-7 cell line. In addition, the (*R*)-(+)-ABZ-SO significantly increased the levels of apoptosis of the MCF-7 cells.

© 2012 Elsevier B.V. All rights reserved.

1. Introduction

Albendazole (ABZ), methyl-[(5-propylthio)-1*H*-benzimidazol-2-yl] carbamate, is a broad-spectrum anthelmintic agent widely used in both veterinary and human medicine for the prevention and treatment of infectious disease caused or transmitted by parasites [1–3]. ABZ has shown high efficacy in the treatment of neurocysticercosis [4,5], the most common parasitic infection of the central nervous system by the larval form of *Taenia solium* and the major cause of acquired epilepsy [6] in the Andean area of South America, Brazil, Central America and Mexico, China, the Indian subcontinent and South-East Asia, and sub-Saharan Africa, according to World Health Organization report [7].

Pharmacokinetic studies have shown that after ABZ oral administration to animal and humans species it rapidly undergoes first-pass metabolism by liver microsomal enzymes [8–11] originating its active metabolite albendazole sulfoxide (ABZ-SO), a chiral compound due to the asymmetrical substituted sulfoxide center [9,11]. Subsequently, ABZ-SO is further oxidized to an inactive metabolite, albendazole sulfone (ABZ-SO_2). The carbamate group of ABZ-SO_2 is further deacetylated to form albendazole 2-amino-sulfone (ABZ-SO_2NH_2). The interesting feature of this metabolic process is the formation of the chiral metabolite ABZ-SO. The chemical structures of albendazole and its metabolites are displayed in Fig. 1.

Chirality is an important concept in various fields of chemistry and biochemistry, and its importance has for a long time been recognized in relation to the biological activity of single enantiomers.

* Corresponding author at: Chemistry Department, Federal University of São Carlos, Rod. Washington Luiz, Km 235, 13565-905 São Carlos, SP, Brazil.
Tel.: +55 16 33518092; fax: +55 16 33518350.
E-mail addresses: oliveirarv@ufscar.br, oliveirarv1@gmail.com (R.V. Oliveira).

0731-7085/$ – see front matter © 2012 Elsevier B.V. All rights reserved.
doi:10.1016/j.jpba.2012.03.012

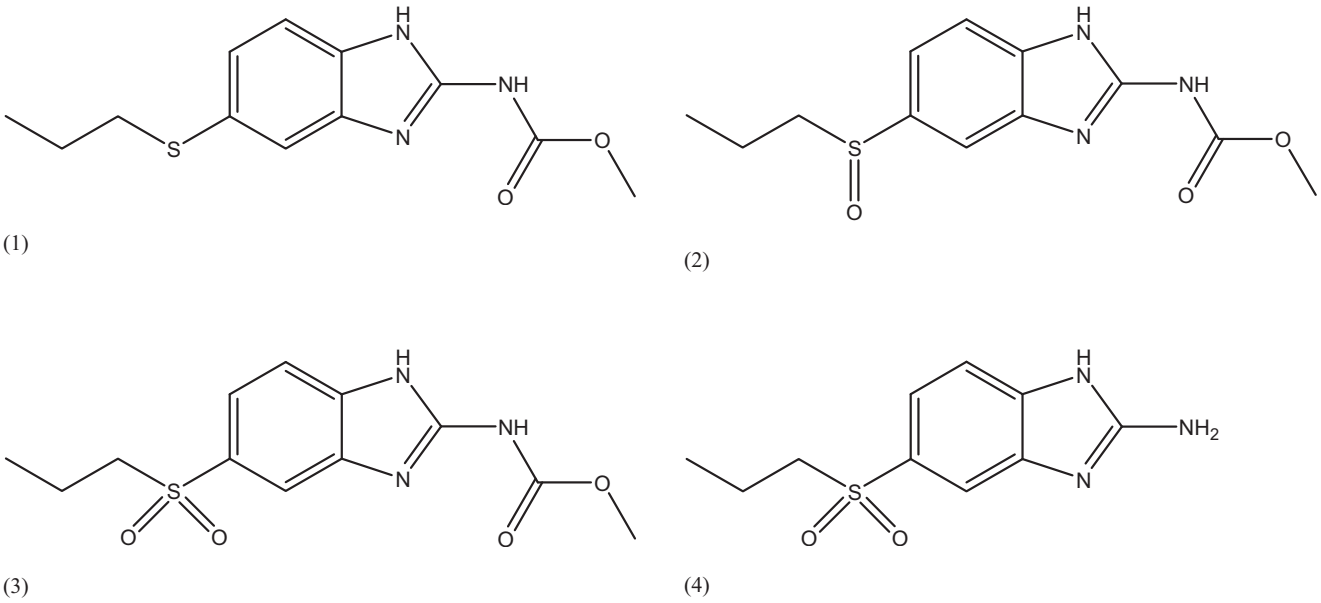

Fig. 1. Chemical structure of albendazole (1), albendazole sulfoxide (2), albendazole sulfone (3) and albendazole 2-amino-sulfone (4).

Living organisms, for example, are composed of chiral biomolecules such as amino acids, sugars, proteins and nucleic acids. In nature these biomolecules exist in only one of the two possible enantiomeric forms and, as a result of this stereoselective environment, two enantiomers may exert different pharmacodynamic, pharmacokinetic and toxicological activities in a biological system [12]. Ideally, the therapeutic activity would reside in both enantiomers. However, there is a range of possibilities, and the actions of the racemate may actually make the single enantiomer desirable [13].

The available pharmacokinetics studies for ABZ-SO have demonstrated that the enantiomeric proportions of (+)- and (−)-ABZ-SO differs among animal species [14–16] and parasite species [17] and it can also be related to age and gender differences [18,19]. Indeed, the (−)-ABZ-SO enantiomer was found to be predominant in rats and mice [14,15], whereas (+)-ABZ-SO was determined to be higher in sheep, goats, dogs, cattle and man [14,20–22]. These stereoselective differences observed among species, added to the possible influence of age and gender on the plasma disposition of ABZ-SO enantiomers and to the absence of detailed information about therapeutic and toxic properties of ABZ-SO enantiomers have attracted interest for pharmacokinetic, pharmacological and toxicological studies of these enantiomers.

Recently, studies conducted *in vitro*, in human tumor cells [23,24], as well as *in vivo*, using various human tumor xenograft mouse models [25] have provided evidence for the potential antitumor activity of ABZ, in particular by inducing apoptosis. Of particular interest is an *in vitro* study of the antitumor activity of ABZ and of ABZ-SO, which were both tested in the human colorectal cancer cell line HT-29. In this study, the IC_{50} values were calculated to be 0.12 μM for ABZ and 2.35 μM for ABZ-SO. In addition, ABZ was shown to induce apoptosis [23]. Moreover, in a phase I study carried out in thirty-six patients with advanced malignancies, the maximum-tolerated dosed for ABZ oral administration was 2.400 mg per day with myelosuppression being the main dose limiting toxicity [26].

Since ABZ is a pro-drug whose activity is due to its metabolite ABZ-SO and also considering that ABZ was previously shown anticancer activity in various tumor cells, the present study intended to investigate the difference in the activity, regarding the inhibition of tumor cell lines growth, of the (+)-ABZ-SO and (−)-ABZ-SO enantiomers.

Direct chromatographic enantioseparation on chiral stationary phases is considered to be the most efficient process to obtain individual enantiomers with the desired optical purity [27–29]. A large number of chiral stationary phases have been described in the literature, some of them being already commercially available. Among the most useful and versatile chiral columns are the polysaccharide-based columns [30–32]. Several studies have described the successful analytical [33–36] and semipreparative scale [37–39] resolution of chiral compounds on polysaccharide-based phases on multimodal elution under normal-phase, reverse-phase and organic polar mode.

The present work describes a full investigation of the resolution of albendazole sulfoxide (ABZ-SO) on arylcarbamate derivatives of cellulose and amylose (Fig. 2) as well as the influence of different mobile phases on enantiomeric separation using multimodal elution. A polar organic condition using methanol as mobile phase was scaled up to semipreparative HPLC to obtain milligrams quantities of (+)- and (−)-ABZ-SO compounds. Moreover, the effect of the ABZ and of its derivatives ABZ, ABZ-SO, (+)-ABZ-SO and (−)-ABZ-SO on the *in vitro* growth of three human tumor cell lines: MCF-7 (breast adenocarcinoma), NCI-H460 (non-small cell lung cancer) and A375-C5 (melanoma) was analyzed. The effect of the most active enantiomer was further evaluated in the MCF-7 cell line in what concerns effects on cell cycle profile and apoptosis.

2. Experimental

2.1. Equipment

The preparative HPLC system consisted of a Shimadzu LC-6AD pump, a Rheodyne 7725 injector fitted with a 500 μL loop and a SPD 10Avp variable wavelength UV–VIS detector with a CBM SCL-10A interface. Data acquisition was performed using LC-10 software.

The analytical HPLC system consisted of two Shimadzu LC-10 ADvp pumps, a SIL-10ADvp auto injector fitted with a 50 μL loop, and a SPD-10Avp UV-VIS detector with a SCL-10 AVvp interface. Data acquisition was performed using LAB SOLUTION software. A JASCO CD-2095 Plus circular dichroism (CD) detector was used for the identification of enantiomers. All HPLC analyses were performed at room temperature. The optical activity of the separated

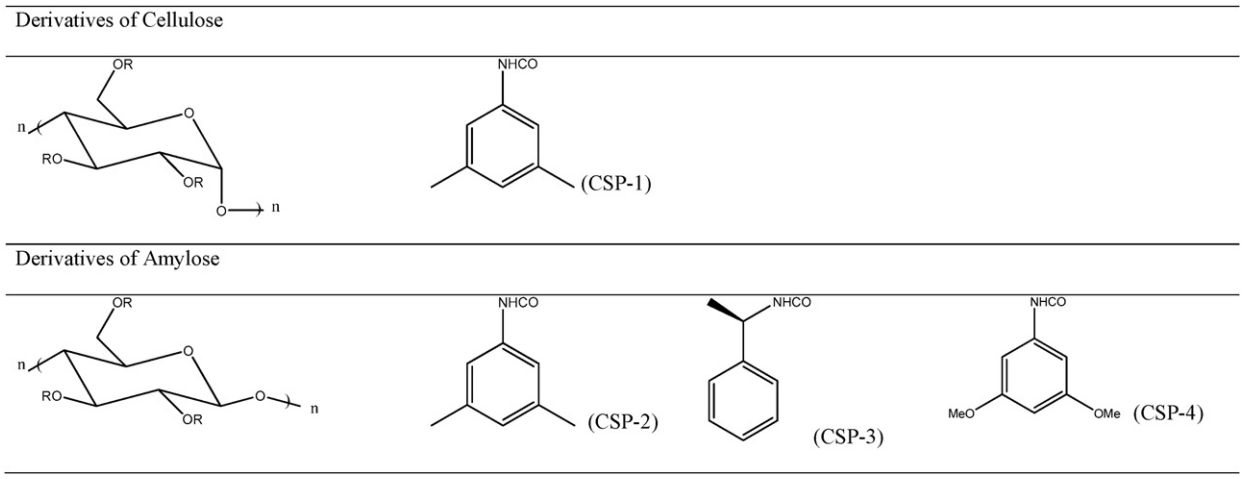

Fig. 2. Structure of chiral stationary phases. CSP-1: cellulose *tris*(3,5-dimethylphenylcarbamate); CSP-2: amylose *tris*(3,5-dimethylphenylcarbamate); CSP-3: amylose *tris*-[(*S*)-1-phenylethylcarbamate] and CSP-4: amylose *tris*(3,5-dimethoxyphenylcarbamate).

enantiomers was defined in methanol, at room temperature, using a Perkin-Elmer Model 241 polarimeter with a sodium lamp.

2.2. Materials and reagents

All solvents were of HPLC grade, purchased from Merck (Darmstadt, Germany) or Mallinckrodt Baker (St. Louis, USA). The mobile phases were prepared in a volume/volume ratio and degassed for 10 min in an ultrasonic bath prior to use. The ABZ-SO were generously supplied by Ouro Fino Saúde Animal (Ribeirão Preto, SP, Brazil).

2.3. Chiral stationary phases

The chiral columns were prepared at the UFSCar laboratory as previously described [40–43] and consisted of cellulose *tris*(3,5-dimethylphenylcarbamate) (CSP-1), amylose *tris*(3,5-dimethylphenylcarbamate) (CSP-2), amylose *tris*-[(S)-1-phenylethylcarbamate] (CSP-3) and amylose *tris*(3,5-dimethoxyphenylcarbamate) (CSP-4) coated onto APS-Nucleosil (500 Å, 7 μm, 20%, w/w) and packed into a stainless-steel 15 cm × 0.46 cm i.d. size column for analytical separation. The amylose *tris*(3,5-dimethylphenylcarbamate) were coated onto APS-Nucleosil (500 Å, 7 μm, 20%, w/w) and packed into a stainless-steel 20 cm × 0.70 cm i.d. size column for semipreparative separation (CSP-5). A Shandon HPLC packing pump was employed for all column packing.

2.4. Sample preparation

The stock solutions of ABZ-SO, 50 μg/mL and 10 mg/mL concentration, for analytical and semipreparative separation, respectively, were prepared by dissolving the appropriate amounts of the drug in methanol. All solutions were stored at −20 °C until analysis.

The analyses were performed on the four polysaccharide-based chiral columns with twelve mobile phases at a flow rate of 0.5 mL/min or 1.0 mL/min. Retention factor, selectivity and resolution of the three chromatographic modes were systematically observed; no degradation of column performance was observed.

2.5. Chromatographic conditions

Albendazole sulfoxide was detected at $\lambda = 290$ nm. The retention factors (k) were determined as $k = (t_r - t_0)/t_0$, where t_r and t_0 are retention time and dead time, respectively. The separation factors (α) were calculated as $\alpha = k_2/k_1$, where k_1 and k_2 are the retention factors for the first and second eluting enantiomer, respectively. Resolution (R_s) were calculated as $R_s = 1.18(t_2 - t_1)/(w_{(1/2)1} + w_{(1/2)2})$, where $w_{(1/2)1}$ and $w_{(1/2)2}$ are half-peak widths to the first and second eluting enantiomer, respectively. The dead time (t_0) was estimated using 1,3,5-tri-tert-butylbenzene for normal-phase and polar organic mode and acetonitrile for reverse-phase.

Semipreparative chromatographic separations were achieved through multiple injections fitted with a 500 μL loop at a flow rate of 2.5 mL/min. The collected fractions of each enantiomer were rotaevaporated at room temperature and analyzed using the analytical column to determine their enantiomeric purity (e.p.). The enantiomeric purity was calculated as for example the ratio between (+)-enantiomer area divided by the sum of the (+)- and (−)- area multiplied by 100 [44,45].

2.6. Biological assays

2.6.1. Effect in the in vitro growth of human tumor cell lines

Stock solutions of ABZ, ABZ-SO, (+)-ABZ-SO and (−)-ABZ-SO (60 mmol/L) were prepared in dimethyl sulfoxide (DMSO) and kept at −20 °C. Appropriate dilutions of the compounds were freshly prepared just before the assays. The compounds were tested in three human tumor cell lines; MCF-7 (ECACC, breast adenocarcinoma), NCI-H460 (a kind gift from NCI, Bethesda, USA, non-small cell lung cancer) and A375-C5 (ECACC, melanoma). Cells were routinely maintained in RPMI-1640 medium, supplemented with 5% inactivated FBS, at 37 °C in a humidified atmosphere containing 5% CO_2. The effect of ABZ, ABZ-SO, (+)-ABZ-SO and (−)-ABZ-SO on the *in vitro* growth of the three human tumor cell lines was evaluated according to the procedure adopted by the National Cancer Institute (NCI, USA) in the "*In vitro* Anticancer Drug Discovery Screen". This screen uses the protein binding dye sulforhodamine B (SRB) to indirectly assess cell growth [46]. Each cell line was plated at an appropriate density in 96-well plates and allowed to attach for 24 h [47]. Exponentially growing cells were further treated for 48 h with five serial dilutions (150; 75; 37.5; 18.75 and 9.37 μmol/L) of the compounds. Since the compound ABZ was very potent, the tested concentrations for this compound were further decreased (9.37; 4.68; 2.34; 1.17 and 0.58 μmol/L). Following this incubation period, cells were fixed with 10% trichloroacetic acid (final concentration), stained with SRB and washed with 1% acetic acid. The bound stain was solubilized with 10 mmol/L Tris–base and the absorbance was

Table 1
Separation performance of the CSP 1–4 for the ABZ-SO enantiomers.

Mobile phase	CSP											
	CSP-1			CSP-2			CSP-3			CSP-4		
	k_1	α	R_s	k_1	α	R_s	k_1	α	R_s	k_1	α	R_s
Hexane/ethanol (80:20)[a]	1.10	1	–	6.34	2.16	4.97	3.57	1	–	9.07	1.45	1.83
Hexane/2-propanol (80:20)[a]	3.38	1	–	6.57	1.45	<1	18.5	1	–	22.3	1.22	<1
Ethanol[a]	0.17	1	–	1.20	2.04	3.09	0.43	1	–	0.49	1.57	<1
2-Propanol	0.52	1	–	1.85	1.18	<1	2.29	1	–	2.15	1.16	<1
Acetonitrile[a]	3.68	1	–	14.7	1.75	1.36	10.4	1	–	0.45	1	–
Methanol[a]	0.63	1	–	0.34	3.50	2.60	0.05	1	–	2.22	1	–
Ethanol/water (50:50)	0.45	1	–	3.10	2.12	2.61	0.93	1	–	1.80	1.51	1.66
Ethanol/water (70:30)	0.23	1	–	0.98	2.26	2.44	3.31	1.59	<1.0	0.89	1.43	1.26
Acetonitrile/water (50:50)	0.25	1	–	0.96	2.28	2.63	0.29	1	–	0.57	1.26	<1
Acetonitrile/water (30:70)	0.46	1	–	2.34	1.86	1.84	0.79	1	–	1.44	1.35	1.41
Methanol/water (50:50)	1.77	1	–	R			3.13	1	–	6.63	1.44	<1
Methanol/methanol (70:30)	0.52	1	–	3.00	2.14	1.03	0.88	1	–	1.52	1.31	<1

R: retained.
[a] Flow rate, 1.0 mL/min.

measured at 492 nm in a microplate reader (BIORAD 680 model). The concentration of compound that inhibited cell growth by 50% (GI_{50}) was calculated as previously described [48].

2.6.2. Analysis of cell cycle profile and apoptosis in MCF-7 cells treated with the (R)-(+)-ABZ-SO

For analysis of the cell cycle profile, exponentially growing MCF-7 cells were incubated with medium (blank), vehicle of the compound (DMSO, control) or with the GI_{50} (13.4 μmol/L) of the (*R*)-(+)-ABZ-SO. Following 48 h incubation, cells were fixed in 70% ethanol for at least 12 h at 4 °C and further incubated with 5 μg/mL propidium iodide and 0.1 mg/mL RNase in PBS. Flow cytometry analysis of a minimum of 20,000 cells was performed using a flow cytometer (Epics XL – MCL, Beckman Counter, Brea, CA, USA). The percentage of cells in the G0/G1, S and G2/M phases of the cell cycle as well as in the sub-G1 peak was determined using the FlowJo 7.2 software (Three Star, Inc.) after excluding cell debris and aggregates. For the analysis of apoptosis, exponentially growing MCF-7 cells were treated for 48 h with medium (blank), vehicle of the compound (DMSO, control) or with the GI_{50} (13.4 μmol/L) of (*R*)-(+)-ABZ-SO, as described above. The levels of apoptosis were analyzed using the Human Annexin-V-FITC/PI apoptosis kit (Bender MedSystems, Vienna, Austria) according to the manufacturer's instructions. Analysis was carried out using a flow cytometer plotting at least 20,000 events per sample and data obtained from the flow cytometer was analyzed using the FlowJo 7.2 software (as above, for the cell cycle analysis) [49–51].

3. Results and discussion

In the last decades a vast number of new chiral stationary phases (CSPs) have been developed and are available for the separation of chiral drugs [52]. Based on published work [31,52,53] and on our own experience, the polysaccharide-based chiral columns are among the most useful and versatile chiral columns described for the analytical mode and preparative scale enantioseparation of a great number of chiral compounds. In addition, the polysaccharide-based chiral phases have shown an interesting versatility in that they can be used in multimodal elution mode (normal, reverse, and polar organic mode) for the enantioseparation of chiral sulfoxides [34,38,54]. These results prompted us to investigate the effects of different polysaccharide-based chiral stationary phases using multimodal elution on enantioselectivity and/or enantioresolution of ABZ-SO.

Initially, analytical HPLC analyses were carried out on four chiral columns: cellulose *tris*(3,5-dimethylphenylcarbamate) (CSP-1); amylose *tris*(3,5-dimethylphenylcarbamate) (CSP-2); amylose *tris*[(S)-1-phenylethylcarbamate] (CSP-3) and amylose *tris*(3,5-dimethoxyphenylcarbamate) (CSP-4). The chromatographic parameters such as retention factor (k), enantioselectivity (α) and enantioresolution (R_s) of ABZ-SO were systematically evaluated for all the compositions of mobile phases tested (Table 1).

3.1. Influence of the mobile phases and of the structure of the CSPs on chiral recognition of ABZ-SO

It is well known that the mobile phase plays an important role in the chiral interaction process, affecting the retention factor as well as the stereoselectivity of the polysaccharide-based chiral columns [27,55]. Thus, in order to verify the influence of the mobile phase on the enantioseparation and enantioresolution of ABZ-SO, the polysaccharide-base CSPs (1–4) were all operated under the normal-phase or reversed-phase conditions described below.

The normal phase conditions tested were as follows: a mixture of hexane:ethanol (80:20, v/v) was the starting mobile phase composition followed by hexane:2-propanol (80:20, v/v). The columns were then conditioned with 100% organic solvent as follows: 2-propanol, ethanol, methanol and acetonitrile and, after that, conditioned with the reversed-phase mode. The results are summarized in Table 1.

The selections of the mobile phases were made based on our previous work conducted to obtain the separation of chiral sulfoxides on polysaccharide-base CSPs [33,34,38,54]. It is important to note that no optimization for maximizing resolution or selectivity was performed and, in some cases, adjustments of flow rate were made in order to obtain satisfactory retention times.

The results obtained showed (Table 1) that CSP-2 and CSP-4 were the only columns capable of sufficiently resolving the ABZ-SO enantiomers. Under the same chromatographic conditions, CSP-2 showed higher values for enantioselectivity and enantioresolution compared to CSP-4. However, it is important to note that, to the best of our knowledge, this is the first chiral enantioseparation obtained using the CSP-4 in the normal mode of elution (Fig. 3A). Previous studies have demonstrated that the CSP-4 is able to provide high enantioselectivity for the series of drugs examined, when polar organic or reversed-phase chromatographic conditions were used [33,40,54]. However, none of the tested compounds could be enantioresolved by CSP-4 in the normal mode.

The CSP-2 showed excellent resolution (R_s = 4.97) and selectivity (α = 2.16) when hexane:ethanol (80:20, v/v) was used as the mobile phase. However, when ethanol was changed to 2-propanol, decreasing the solvent strength, the resolution was completely

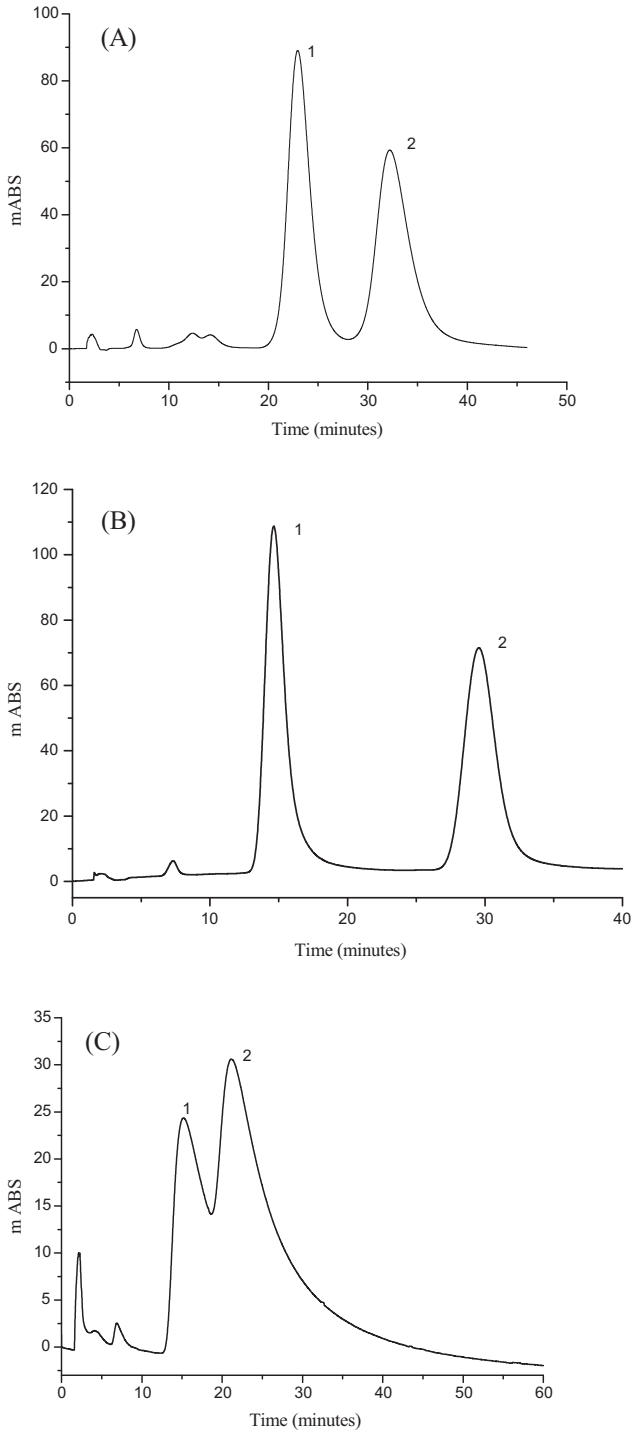

Fig. 3. Chromatograms of the separation of ABZ-SO enantiomers at CSP-4 (A) and CSP-2 (B) using both hexane:ethanol (80:20, v/v) and CSP-2 (C) using hexane:2-propanol (80:20, v/v) as mobile phase and flow rate at 1.0 mL/min, λ = 290 nm. 1 – first enantiomer; 2 – second enantiomer.

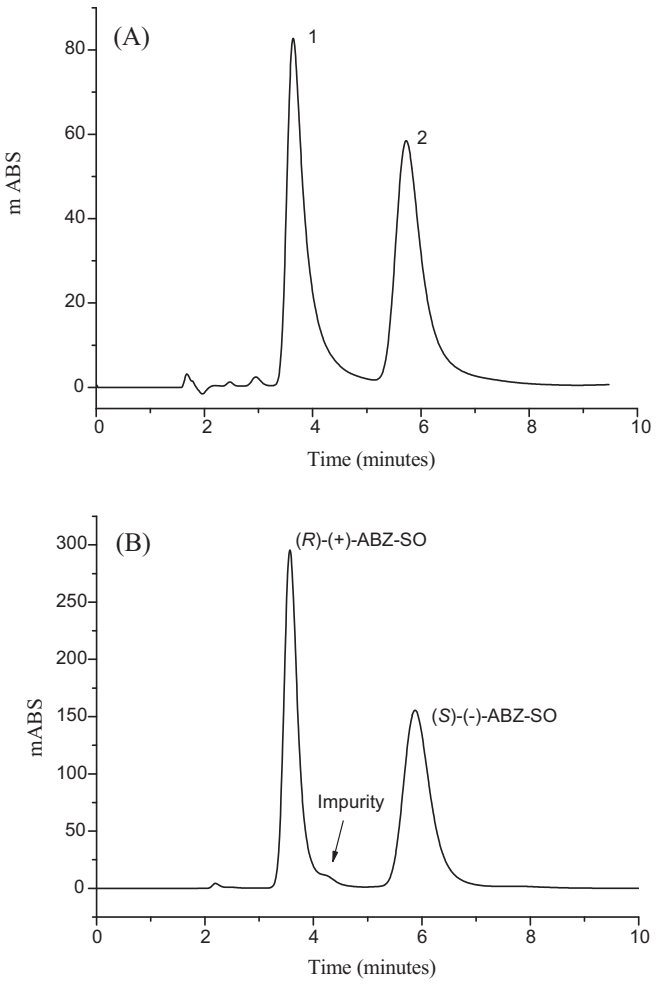

Fig. 4. Chromatograms of the separation of ABZ-SO enantiomers at CSP-2 with (A) ethanol and (B) methanol as mobile phase and a flow rate of 1.0 mL/min, λ = 290 nm. 1 – first enantiomer; 2 – second enantiomer.

lost and the selectivity decreased considerably ($\alpha = 1.45$). The chromatograms in Fig. 3(B and C) exemplify these differences in enantioresolution obtained using the two different normal-phase chromatographic conditions.

ABZ-SO showed excellent resolution ($R_s = 3.09$ and $R_s = 2.60$) and selectivity ($\alpha = 2.04$ and $\alpha = 3.50$) when 100% ethanol or methanol were used, respectively, as eluents in the polar organic mode. Representative chromatograms are shown in Fig. 4(A and B). However, partial resolution ($R_s \leq 1.36$) with median selectivity ($1.75 \geq \alpha \geq 1.18$) was observed using acetonitrile or 2-propanol as mobile phase.

The results obtained when the enantioseparation of ABZ-SO was evaluated under reversed-phase showed poor resolution using CPS-2 and methanol as the organic modifier ($R_s = 1.03$). However, when ethanol or acetonitrile was used in the mobile phase, good enantioselectivity ($\alpha = 1.86$–2.28) and resolution ($R_s = 1.84$–2.63) were obtained.

The analogous amylose phase (CSP-4) showed good resolution ($R_s = 1.83$) and median selectivity ($\alpha = 1.45$) for ABZ-SO enantiomers when ethanol (20%) was the organic modifier in normal elution mode (Fig. 3A). When the organic modifier was switched to 2-propanol only partial resolution ($R_s < 1$) was reached. No resolution and poor selectivity values ($1.0 \leq \alpha \leq 1.57$) were observed when CSP-4 was evaluated under polar organic mode. In reversed-phase mode, however, using ethanol (50%) or acetonitrile (30%) as organic modifiers, reasonable values for selectivity factor and resolution were obtained. These findings are in accordance with previous published results, which indicate that amylose *tris*(3,5-dimethoxyphenylcarbamate) chiral phase showed high enantioselectivity for a series of three chiral sulphoxides using reversed-phase mode [33].

No separation of ABZ-SO enantiomers was observed when CSP-1 and CSP-3 were tested with this multimodal elution system. The only exception was a medium selectivity and poor resolution

obtained when a mixture of ethanol:water (70:30, v/v) was tested as mobile phase and CSP-3.

In summary, the separation factor and resolution obtained for ABZ-SO in the CSP-2 were excellent in three different elution modes, which were the normal, reverse-phase and polar organic mode, while the CSP-4 demonstrated limited enantioresolution in most of the chromatographic conditions investigated, with the best chiral separation result being obtained in the normal elution mode. The CSP-1 and CSP-3 proved not to be appropriate for chiral separation of ABZ-SO using the chromatographic conditions tested in this work.

When the influence of the structure of the CSPs on the chiral recognition ability of ABZ-SO was examined, it was noted that the cellulose *tris*(3,5-dimethylphenylcarbamate) (CSP-1) did not show any discrimination ability for ABZ-SO enantiomers, while the corresponding chiral amylose *tris*(3,5-dimethylphenylcarbamate) (CSP-2) column, which was prepared using the same 3,5-dimethylphenylcarbamate moiety but with a distinct polysaccharide, presented the highest enantioselectivity power. Thus, the influence of the polysaccharide on chiral discrimination is clear. The differences observed in the results between the cellulose and amylose derivatives were already demonstrated by other authors [31,32] and could be explained by the conformation of the helix of the polysaccharide derivatives: left-handed three fold (3/2) and four-fold (4/1) for cellulose and amylose, respectively.

In addition, and accordingly to previous published studies [31,32,56], the influence of the chemical substituent introduced on the phenyl groups of the carbamate derivatives was also evident in our results. The CSP-2 (methyl group as substituents) showed higher chiral discrimination for ABZ-SO than CSP-4 (methoxy groups as substituents). Furthermore, CSP-4, which contains a methoxy group in the phenyl moiety, produced better enantioselectivity factors than CSP-3, which contains a 1-phenylethyl side chain. Thus, the enantioselectivity of the *tris*(phenylcarbamate) derivatives was significantly affected by the nature, position and number of substituents of the aromatic ring as well as the presence of chiral side-groups.

When a heteroatom substituent (such as the methoxyl) was present on the aromatic ring (CSP-4), there was a decrease on the chiral recognition of ABZ-SO. However, the presence of an electron-donating group, such as methyl (CSP-2), resulted in a higher chiral recognition for ABZ-SO.

The chromatograms in Fig. 5 exemplify the differences on the enantioresolution obtained for ABZ-SO when the CSP-2 and CSP-4 were evaluated under reverse-phase mode, respectively.

3.2. Multimilligram HPLC separation

When directing our experiments toward the production of multimilligram quantities of ABZ-SO enantiomers, the use of amylose *tris*-(3,5-dimethylphenylcarbamate) was selected as the best analytical method to scale up to semipreparative mode. This choice was made based not only on the best selectivity and enantioresolution factors but also in the fact that polar organic conditions offer the advantages of higher solubility for ABZ-SO and would therefore facilitate isolation of the enantiomers in preparative scale applications. Moreover, the use of a single solvent made easier the use of a recycle system, reducing even more the cost of the preparative separation. The enantiomeric separation of albendazole sulfoxide was also carried out by simulated moving bed chromatography with variable zones (VARICOL) and the absolute configuration of the (+)- and (−)-enantiomer obtained was determined by vibrational circular dichroism as (*R*)-(+)-ABZ-SO and (*S*)-(−)-ABZ-SO [57].

Albendazole sulfoxide was injected as a 10 mg/mL sample onto a semipreparative HPLC column (CSP-5) and the separation was performed at a flow rate of 2.5 mL/min using 100% methanol as

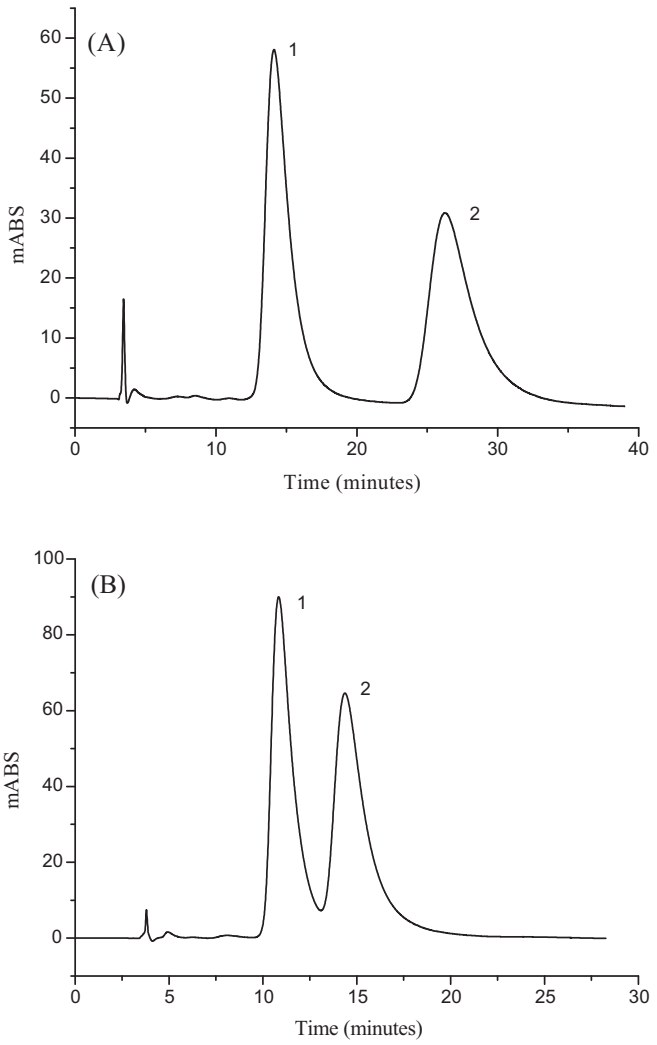

Fig. 5. Chromatograms of the separation of ABZ-SO enantiomers with ethanol:water (50:50, v/v) as mobile phase, flow rate of 0.5 mL/min and λ = 290 nm in (A) CSP-2 and (B) CSP-4. 1 – first enantiomer; 2 – second enantiomer.

mobile phase. The separation was monitored at λ = 290 nm. The chromatogram of the semipreparative separation is shown in Fig. 6.

Using this method the racemic mixture of ABZ-SO (10 mg/mL) was injected in 100 applications of 500 μL each. This method produced (*R*)-(+)-ABZ-SO (207.8 mg) and (*S*)-(−)-ABZ-SO (248.5 mg) isolated from 500 mg of racemic ABZ-SO. Individual fractions of enantiomers isolated were re-injected onto the analytical chiral column to determine their enantiomeric purity (e.p). The (*R*)-(+)-ABZ-SO was isolated with 83.1% recovery and an e.p. of 99.5% while the (*S*)-(−)-ABZ-SO was isolated with 99.4% recovery and an e.p. of 98.3%. Chromatograms of each enantiomer of ABZ-SO obtained after purification are given as examples in Fig. 7.

The recovery, enantiomeric purity, specific rotation and yield are summarized in Table 2.

Table 2
Recovery, enantiomeric purity, specific rotation and yield for ABZ-SO enantiomers.

	First enantiomer collected	Second enantiomer collected
Obtained mass (mg)	207.8	248.5
Enantiomeric purity (%)	99.5	98.3
Recovery (%)	83.1	99.4
$[\alpha]_{D\ (25\,^{\circ}C)}$, methanol	+112.8	−117.4
Yield (mg h^{-1})	12.5	14.9

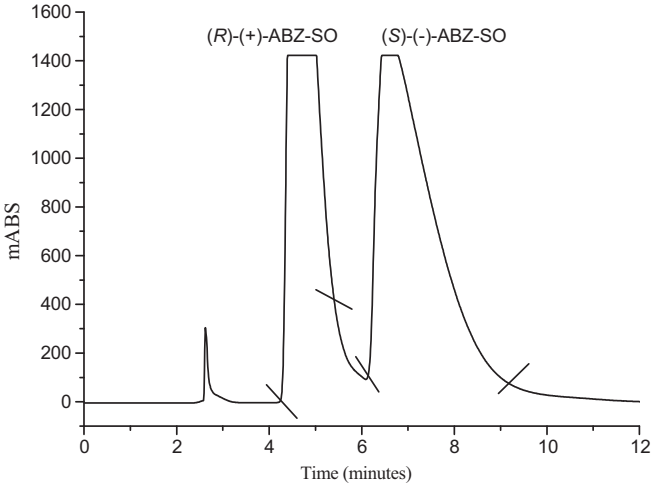

Fig. 6. Chromatogram of the semipreparative separation of ABZ-SO enantiomers at CSP-5 with methanol as mobile phase at a flow rate of 2.5 mL/min and λ = 290 nm.

The results show (Fig. 7) that the first eluted enantiomer could be isolated pure, but the second eluted enantiomer collected was contaminated with small quantities of the first eluted enantiomer. The impurity of the second eluted enantiomer may be explained in two ways. The first is due to the tailing of the first peak into the second peak and the second is due to the likely error associated with manual fraction collection. These issues were also addressed by other authors during semipreparative separation of mirtazapine [58].

The low recovery of the first eluted enantiomer isolated can be attributed to the presence of an impurity (Fig. 4), which interfered with collection of the second chromatographic band.

The optical rotations of the two enantiomers collected were also measured using a polarimeter ($[\alpha]_{D\ \text{methanol, } 25\,^{\circ}C}$). The results are given in Table 2.

In addition to optical rotation, circular dichroism (CD) was also performed on the racemate and on both enantiomers collected (Fig. 8). CD detection is based on an absorption difference between

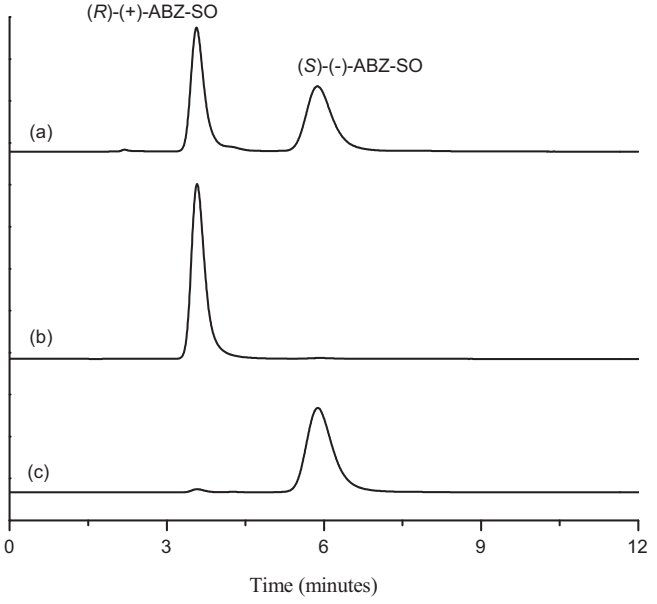

Fig. 7. Chromatograms of the ABZ-SO enantiomers isolated, re-injected in the analytical column CSP-2 using methanol as mobile phase at a flow rate of 1.0 mL/min and λ = 290 nm. (A) Racemate, (B) the first fraction isolated and (C) the second fraction isolated.

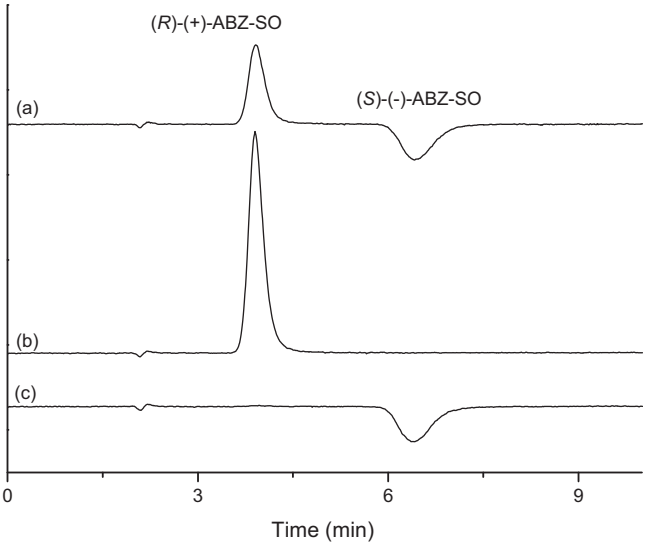

Fig. 8. The CD chromatograms of the ABZ-SO enantiomers isolated re-injected in the analytical column CSP-2 using methanol as mobile phase at a flow rate of 1.0 mL/min and λ = 290 nm. (A) Racemate, (B) the first fraction isolated and (C) the second fraction isolated.

right and left circularly polarized light. This type of detection is intrinsically stable throughout temperature and solvent changes [59]. The CD chromatograms of the two collected fractions exhibited completely opposite features, further confirming that they are enantiomers of each other. Also, the results show that the optical rotations of the isolated enantiomers are in agreement with the results observed using the CD detection.

3.3. *Effect of the compounds in the in vitro growth of human tumor cell lines*

The obtained compounds were evaluated for their capacity to inhibit the *in vitro* growth of three human tumor cell lines: MCF-7 (breast adenocarcinoma), NCI-H460 (non-small cell lung cancer) and A375-C5 (melanoma). The results are summarized in Table 3 and are discussed below.

The results show that ABZ was the most active of the compounds in all the cell lines studied, particularly in the A375-C5 cell line. The racemic mixture and the (*S*)-(−)-ABZ-SO showed the lesser activity, regarding their capacity to induce inhibition of cell growth of the studied cell lines. The most potent of the enantiomers studied was the (*R*)-(+)-ABZ-SO, particularly in the MCF-7 cell line. This may justify the activity found in the racemic mixture.

Given the good cell growth inhibitory activity of the (*R*)-(+)-ABZ-SO enantiomer, we also studied its effect in the cell cycle profile

Table 3
Cell growth inhibitory effect of ABZ, ABZ-SO, (+)-(*R*)-ABZ-SO and (−)-(*S*)-ABZ-SO in three human tumor cell lines.

Compound	Tumor cell line		
	MCF-7	NCI-H460	A375-C5
GI_{50} (μmol/L)			
ABZ	5.2 ± 2.0	8.7 ± 1.2	1.0 ± 0.2
ABZ-SO	41.3 ± 8.6	44.2 ± 8.5	36.3 ± 1.8
(*S*)-(−)-ABZ-SO	59.5 ± 4.8	58.8 ± 5.5	58.0 ± 3.8
(*R*)-(+)-ABZ-SO	13.4 ± 1.1	23.5 ± 7.2	23.0 ± 6.5

Results are given as the lowest concentrations causing 50% of cell growth inhibition (GI_{50}) after continuous treatment with the compounds for 48 h. Results are expressed as mean ± SEM of at least four independent experiments, performed in duplicate. Doxorubicin was used as a positive control (GI50: MCF-7 = 46.3 ± 4.8 nmol/L; NCI-H460 = 96.3 ± 7.3 nmol/L; A375-C5 = 80 ± 4.4 nmol/L).

Table 4
Cell cycle analysis, % of cells in the sub-G1 peak and % cells undergoing apoptosis following treatment of MCF-7 cells with the GI_{50} concentration of the (+)-(*R*)-ABZ-SO and with control treatments.

	Cells (%)				
	Cell cycle			Sub-G1 peak	Apoptosis
	G0/G1	S	G2/M		
Blank	56.8 ± 1.2	27.8 ± 1.4	16.5 ± 0.6	0.3 ± 0.5	6.2 ± 0.6
DMSO	56.1	25.6	18.7	0	8.1 ± 1.0
(*R*)-(+)-ABZ-SO	37.5 ± 4.0*	24.1 ± 2.0	16.4 ± 1.5	28.6 ± 4.0*	20.4 ± 0.7*

Cells were treated for 48 h with the (*R*)-(+)-ABZ-SO compound or with medium (blank) or compound vehicle (DMSO), as controls. Results are the mean ± SE of at least 3 independent experiments (except for the DMSO treatment which was only analyzed once for the cell cycle profile and sub-G1 peak analysis).
* $p \leq 0.01$ when compared to the Blank treatment.

and apoptosis in MCF-7 cells. The results from the cell cycle profile indicate that this enantiomer decreased the percentage of cells in G0/G1 phase and concomitantly increased the percentage of cells in the sub-G1 peak which is suggestive of apoptosis (Fig. 9, Table 4).

When performing a specific assay to determine the levels of apoptosis (the Annexin V assay), results confirmed that the (*R*)-(+)-ABZ-SO enantiomer significantly increased the levels of apoptosis of these cells (Table 4).

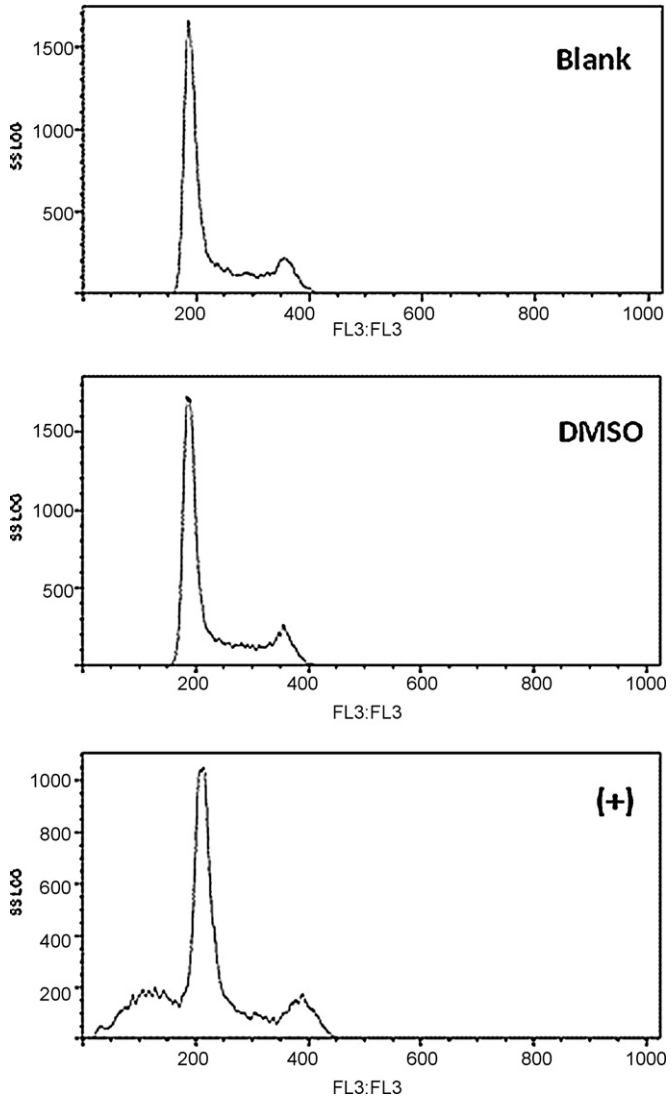

Fig. 9. Representative example of the effect of the (+)-(*R*)-ABZ-SO enantiomer and of the necessary controls treatments (blank and DMSO) in the cell cycle profile of MCF-7 cells. Results are representatitve of at least 3 independent experiments in which cells were incubated for 48 h with the various treatments.

4. Conclusions

The present work indicates that the applicability of the polysaccharide-based chiral phases could be widened by multimodal elution for the separation of ABZ-SO enantiomers. The CSP-2 showed excellent selectivity and enantioresolution in three different elution modes: the normal, reverse-phase and polar organic mode. Nevertheless, the CSP-1 and CSP-3 proved not to be appropriate for chiral separation of ABZ-SO using the chromatographic conditions tested in this work.

Results showed that multimilligrams of ABZ-SO enantiomers were obtained in high yield and with a high degree of enantiomeric purity. In addition, the ABZ was the most potent of the compounds tested, regarding the growth inhibition of three human tumor cell lines. Finally, the (*R*)-(+)-ABZ showed to be more potent than the (*S*)-(−)-ABZ-SO enantiomer, particularly in the MCF-7 cell line, and also to be a strong inducer of apoptosis in this cell line.

Acknowledgments

The authors acknowledge the financial support from Fundação de Amparo a Pesquisa do Estado de São Paulo (FAPESP). The grants from Conselho Nacional de Desenvolvimento Científico e Tecnológico (CNPq) and Coordenação de Aperfeiçoamento de Nível Superior (CAPES) are also acknowledged; Fundação para a Ciência e a Tecnologia under the project CEQUIMED-PEst-OE/SAU/UI4040/2011; under the project FCT-Grices/Capes 00770 29/05/08, FEDER funds through the COMPETE program. R.T.L. has a post-Doctoral grant (SFRH/BPD/68787/2010) from FCT IPATIMUP is an Associate Laboratory of the Portuguese Ministry of Science, Technology and Higher Education and is partially supported by FCT, the Portuguese Foundation for Science and Technology.

References

[1] L. Moreno, F. Echevarria, F. Muñoz, L. Alvarez, S. Sanchez Bruni, C. Lanusse, Dose-dependent activity of albendazole against benzimidazole-resistant nematodes in sheep: relationship between pharmacokinetics and efficacy, Exp. Parasitol. 106 (2004) 150–157.
[2] C. Urbani, M. Albonico, Anthelmintic drug safety and drug administration in the control of soil-transmitted helminthiases in community campaigns, Acta Trop. 86 (2003) 215–221.
[3] J. Horton, Albendazole: a review of anthelmintics efficacy and safety in humans, Parasitology 121 (2000) S113–S132.
[4] J. Sotelo, H. Jung, Pharmacokinetic optimisation of the treatment of neurocysticercosis, Clin. Pharmacokinet. 34 (1998) 503–515.
[5] I. Cruz, M.E. Cruz, F. Carrasco, J. Horton, Neurocysticercosis: optimal dose treatment with albendazole, J. Neurol. Sci. 133 (1995) 152–154.
[6] D.K. Pal, A. Carpio, J.W.A.S. Sander, Neurocysticercosis and epilepsy in developing countries, J. Neurol. Neurosurg. Psychiatry 68 (2000) 137–143.
[7] WHO, Fifty-Sixth World Health Assembly Provisional Agenda Item 14.2 A56/10 ed., 2003.

[8] H.C. Rawden, G.O. Kokwaro, S.A. Ward, G. Edwards, Relative contribution of cytochromes P-450 and flavin-containing monoxygenases to the metabolism of albendazole by human liver microsomes, Br. J. Clin. Pharmacol. 49 (2000) 313–322.
[9] A.D. Dayan, Albendazole, mebendazole and praziquantel. Review of non-clinical toxicity and pharmacokinetics, Acta Trop. 86 (2003) 141–159.
[10] J. Asteinza, R. Camacho-Carranza, R. Eugenia Reyes-Reyes, V. Dorado-González, J.J. Espinosa-Aguirre, Induction of cytochrome P450 enzymes by albendazole treatment in the rat, Environ. Toxicol. Pharmacol. 9 (2000) 31–37.
[11] P. Moroni, T. Buronfosse, C. Longin-Sauvageon, P. Delatour, E. Benoit, Chiral sulphoxidation of albendazole by the flavin adenine dinucleotide-containing and cytochrome P450-dependent monooxygenases from rat liver microsomes, Drug Metab. Dispos. 23 (1995) 160–165.
[12] S.W. Smith, Chiral toxicology: it is the same thing, only different, Toxicol. Sci. 110 (2009) 4–30.
[13] B. Waldeck, Three-dimensional pharmacology, a subject ranging from ignorance to overstatements, Pharmacol. Toxicol. 93 (2003) 203–210.
[14] P. Delatour, E. Benoit, S. Besse, A. Boukraa, Comparative enantioselectivity in the sulphoxidation of albendazole in man, dogs and rats, Xenobiotica 21 (1991) 217–221.
[15] P. Delatour, E. Benoit, M. Caude, A. Tambute, Species differences in the generation of the chiral sulfoxide metabolite of albendazole in sheep and rats, Chirality 2 (1990) 156–160.
[16] G. Virkel, A. Lifschitz, J. Sallovitz, A. Pis, C. Lanusse, Comparative hepatic and extrahepatic enantioselective sulfoxidation of abendazole and fenbendazole in sheep and cattle, Drug Metab. Dispos. 32 (2004) 536–544.
[17] H.D. Solana, J.A. Rodriguez, C. Lanusse, Comparative metabolism of albendazole and albendazole sulphoxide by different helminth parasites, Parasitol. Res. 87 (2001) 275–280.
[18] B.P.S. Capece, G. Castells, F. Pérez, M. Arboix, C. Cristòfol, Pharmacokinetics behaviour of albendazole sulphoxide enantiomers in male and female sheep, Vet. Res. Commun. 24 (2000) 339–348.
[19] A. Mirfazaelian, S. Dadashzadeh, M.R. Rouini, Effect of gender in the disposition of albendazole metabolites in humans, Eur. J. Clin. Pharmacol. 58 (2002) 403–408.
[20] P. Delatour, F. Garnier, E. Benoit, I. Caude, Chiral behaviour of the metabolites albendazole sulphoxide in sheep, goats and cattle, Res. Vet. Sci. 50 (1991) 134–138.
[21] C. Cristofol, G. Virkel, L. Alvarez, S. Sánchez, M. Arboix, C. Lanusse, Albendazole sulphoxide enantiomeric ratios in plasma and target tissues after intravenous administration of ricobendazole to cattle, Drug Metab. Pharmacokinet. Toxicol. 24 (2001) 117–124.
[22] E. Benoit, S. Besse, P. Delatour, Effect of repeated does of albendazole on enantiomerism of its sulfoxide metabolite in goats, Am. J. Vet. Res. 53 (1992) 1663–1665.
[23] M.H. Pourgholami, J. Akhter, L. Wang, Y. Lu, D.L. Morris, Antitumor activity of albendazole against the human colorectal cancer cell line HT-29: in vitro and in a xenograft model of pertoneal carcinomatosis, Cancer Chemother. Pharmacol. 55 (2005) 425–432.
[24] M.H. Pourgholami, L. Woon, R. Almajd, J. Akhter, P. Bowery, D.L. Morris, In vitro and in vivo suppression of growth of hepatocellular carcinoma cells by albendazole, Cancer Lett. 165 (2001) 43–49.
[25] M.H. Pourgholami, Z.Y. Cai, Y. Lu, L. Wang, D.L. Morris, Albendazole: a potent inhibitor of vascular endothelial growth factor and malignant ascites formation in OVCAR-3 tumor-bearing nude mice, Clin. Cancer Res. 12 (2006) 1928–1935.
[26] M.H. Pourgholami, M. Szwajcer, M. Chin, W. Liauw, J. Seef, P. Galettis, D.L. Morris, M. Links, Phase I clinical trial to determine maximum tolerated dose of oral albendazole in patients with advanced cancer, Cancer Chemother. Pharmacol. 65 (2010) 597–605.
[27] E.R. Francotte, Enantioselective chromatography as a powerful alternative for the preparation of drug enantiomers, J. Chromatogr. A 906 (2001) 379–397.
[28] L. Miller, C. Orihuela, R. Fronek, J. Chromatogr. A 849 (1999) 309–317.
[29] C.J. Shaw, P.J. Sanfilippo, J.J. McNally, S.A. Park, J.B. Press, J. Chromatogr. 631 (1993) 173–175.
[30] E. Yashima, Y. Okamoto, Chiral discrimination on polysaccharides derivatives, Bull. Chem. Soc. Jpn. 68 (1995) 3289–3307.
[31] E. Yashima, Polysaccharide-based chiral stationary phases for high-performance liquid chromatographic enantioseparation, J. Chromatogr. A 906 (2001) 105–125.
[32] Y. Okamoto, Y. Kaida, Resolution by high-performance liquid chromatography using polysaccharide carbamates and benzoates as chiral stationary phases, J. Chromatogr. A 666 (1994) 403–419.
[33] Q.B. Cass, A.L.G. Degani, N.M. Cassiano, Effects on enantioselectivity by the use of polysaccharide-based columns by multimodal elution, J. Liquid Chromatogr. Relat. Technol. 26 (2003) 2083–2101.
[34] Q.B. Cass, A.L.G. Degani, N.M. Cassiano, The use of a polysaccharide-based column on multimodal elution, J. Liquid Chromatogr. Relat. Technol. 23 (2000) 1029–1038.
[35] Q.B. Cass, V.V. Lima, R.V. Oliveira, N.M. Cassiano, A.L.G. Degani, J. Pedrazzoli Jr., Enantiomeric determination of the plasma levels of omeprazole by direct plasma injection using high-performance liquid chromatography with achiral–chiral column-switching, J. Chromatogr. B 798 (2003) 275–281.
[36] Q.B. Cass, R.V. Oliveira, A.C. De Pietro, Determination of gossypol enantiomer ratio in cotton plants by chiral higher-performance liquid chromatography, J. Agric. Food Chem. 52 (2004) 5822–5827.
[37] Q.B. Cass, R.V. Oliveira, Separation of multi-milligram quantities of gossypol enantiomers on polysaccharide-based stationary phases, J. Liquid Chromatogr. Relat. Technol. 25 (2002) 819–829.
[38] K.R.A. Belaz, M. Coimbra, J.C. Barreiro, A.C. Montanari, Q.B. Cass, Multimilligram enantioresolution of sulfoxide proton pump inhibitors by liquid chromatography on polysaccharide-based chiral stationary phase, J. Pharm. Biomed. Anal. 47 (2008) 81–87.
[39] M.E. Sousa, M.E. Tiritan, K.R.A. Belaz, M. Pedro, M.S.J. Nascimento, Q.B. Cass, M.M.M. Pinto, Multimilligram enantioresolution of low-solubility xanthonolignoids on polysaccharide chiral stationary phases using a solid-phase injection system, J. Chromatogr. A 1120 (2006) 75–81.
[40] S.A. Matlin, M.E. Tiritan, Q.B. Cass, D.R. Boyd, Enantiomeric resolution of chiral sulfoxides on polysaccharides phases by HPLC, Chirality 8 (1996) 147–152.
[41] E. Yashima, Polysaccharide-based chiral stationary phases for high-performance liquid chromatography enantioseparation, J. Chromatogr. A 906 (2001) 105–125.
[42] S.A. Matlin, M.E. Tiritan, A.J. Crawford, Q.B. Cass, D.R. Boyd, HPLC with carbohydrate carbamate chiral phases: influence of chiral phase structure on enantioselectivity, Chirality 6 (1994) 135–140.
[43] M.E. Tiritan, Q.B. Cass, A. Del Alamo, S.A. Matlin, S.J. Grieb, Preparative enantioseparation on polysaccharide phase using microporous silica as a support, Chirality 10 (1998) 573–577.
[44] R.E. Gawley, Do the terms % ee and % de make sense as expressions of stereoisomer composition or stereoselectivity? J. Org. Chem. 71 (2006) 2411–2416.
[45] L. Toribio, M.J. Nozal, J.L. Bernal, E.M. Nieto, Use of semipreparative supercritical fluid chromatography to obtain small quantities of the albendazole sulfoxide enantiomers, J. Chromatogr. A 1011 (2003) 155–161.
[46] V. Vichai, K. Kirtikara, Sulforhodamine B colorimetric assay for cytotoxicity screening, Nat. Protoc. 1 (2006) 1112–1116.
[47] A.P. Almeida, T. Dethoup, N. Singburaudom, R. Lima, M.H. Vasconcelos, M.P. Pinto, A. Kijjoa, The in vitro anticancer activity of the crude extract of the sponge-associated fungus *Eurotium cristatum* and its secondary metabolites, J. Nat. Pharmaceut. 1 (2010) 25–29.
[48] A. Kijjoa, S. Santos, T. Dethoup, L. Manoch, A.P. Almeida, M.H. Vasconcelos, A. Silva, L.H. Gales, Sartoryglabrins, analogs of ardeemins, from *Neosartorya glabra*, Nat. Prod. Commun. 6 (2011) 807–812.
[49] M.P. Neves, H. Cidade, M. Pinto, A.M. Silva, L. Gales, A.M. Damas, R.T. Lima, M.H. Vasconcelos, M.S. Nascimento, Prenylated derivatives of baicalein and 3,7-dihidroxyflavone: synthesis and study of their effects on tumor cell lines growth, cell cycle and apoptosis, Eur. J. Med. Chem. 46 (2011) 2562–2574.
[50] M.J. Queiroz, R.C. Calhelha, L.A. Vale-Silva, E. Pinto, R.T. Lima, M.H. Vasconcelos, Efficient synthesis of 6-(hetero)arylthieno[3,2-b]pyridines by Suzuki–Miyaura coupling: evaluation of growth inhibition on human tumor cell lines, SARs and effects on the cell cycle, Eur. J. Med. Chem. 45 (2010) 5628–5634.
[51] M.J. Queiroz, R.C. Calhelha, L.A. Vale-Silva, E. Pinto, G.M. Almeida, M.H. Vasconcelos, Synthesis and evaluation of tumor cell growth inhibition of methyl 3-amino-6-[(hetero)arylethynyl]thieno[3,2-b]pyridine-2-carboxylates. Structure–activity relationships, effects on the cell cycle and apoptosis, Eur. J. Med. Chem. 46 (2011) 236–240.
[52] Y. Okamoto, T. Ikai, Chiral HPLC for efficient resolution of enantiomers, Chem. Soc. Rev. 37 (2008) 2593–2608.
[53] I. Ali, K. Saleem, I. Hussain, V.D. Gaitonde, H.Y. Aboul-Enein, Polysaccharides chiral stationary phases in liquid chromatography, Sep. Purif. Rev. 38 (2009) 97–147.
[54] Q.B. Cass, F. Batigalhia, Enantiomeric resolution of a series of chiral sulfoxides by high-performance liquid chromatography on polysaccharide-based columns with multimodal elution, J. Chromatogr. A 987 (2003) 445–452.
[55] P. Piras, C. Roussel, J. Pierrot-Sanders, Reviewing mobile phases used on Chiralcel OD through an application of data mining tools to CHIRBASE database, J. Chromatogr. A 906 (2001) 443–458.
[56] Y. Kaida, Y. Okamoto, Optical resolution by high-performance liquid chromatography on benzylcarbamates of cellulose and amylose, J. Chromatogr. 641 (1993) 267–278.
[57] T.C. Lourenco, M.J. Batista Jr., M. Furlan, Y. Hec, L.A. Nafie, C.C. Santana, Q.B. Cass, Albendazole sulfoxide enantiomers: preparative chiral separation and absolute stereochemistry, J. Chromatogr. A 1230 (2012) 61–65.
[58] Z.D. Zhai, Y.P. Shi, T. Wang, Development and validation of HPLC methods for enantioseparation of mirtazapine enantiomers at analytical and semipreparative scale using polysaccharide chiral stationary phases, Anal. Chim. Acta 550 (2005) 123–129.
[59] A.L. Jenkins, W.A. Hedgepeth, Analysis of Chiral Pharmaceuticals using HPLC with CD Detection, Wiley-Liss, 2005, pp. S24–S29.

Journal of Pharmaceutical and Biomedical Analysis 66 (2012) 109–115

Contents lists available at SciVerse ScienceDirect

Journal of Pharmaceutical and Biomedical Analysis

journal homepage: www.elsevier.com/locate/jpba

Stability-indicating UPLC method for determination of Imatinib Mesylate and their degradation products in active pharmaceutical ingredient and pharmaceutical dosage forms

A. Nageswari [a,b,*], K.V.S.R. Krishna Reddy [a], K. Mukkanti [b]

[a] Aptuit Laurus Private Limited, ICICI Knowledge Park, Turkapally, Hyderabad 500078, India
[b] Department of Pharmaceutical Sciences, Jawaharlal Nehru Technological University, Kukatpally, Hyderabad 500072, India

ARTICLE INFO

Article history:
Received 29 December 2011
Received in revised form 9 March 2012
Accepted 12 March 2012
Available online 21 March 2012

Keywords:
UPLC
Imatinib Mesylate
Validation
Stability-indicating
Related substance

ABSTRACT

A simple, precise, accurate stability-indicating gradient reverse phase ultra-performance liquid chromatographic (RP-UPLC) method was developed for quantitative determination of purity of Imatinib Mesylate (IMM) drug substance and drug products in the presence of its process related impurities, and degradation products. The proposed RP-UPLC method utilizes Acquity UPLC BEH 50-mm, 2.1 mm and 1.7 μm C-18 column at 30 °C, with a gradient program of 9.0 min at a flow rate of 0.3 mL/min. The compounds of interest were monitored at 237 nm. Resolution for Imatinib and eight related components was found to be greater than 1.5 for any pair of components. The correlation coefficients ($r^2 > 0.9990$) obtained indicate clear correlations between the concentrations and their peak areas for the investigated compounds. RSD obtained for the repeatability and intermediate precision experiments, was less than 5.0%. Accuracy of the method was further ascertained by performing recovery studies through spiking experiments. The drug substance was subjected to hydrolytic, oxidative, photolytic and thermal stress conditions as per ICH. The developed method was validated according to the current ICH guidelines for specificity, limit of detection, limit of quantitation, linearity, accuracy, precision, ruggedness and robustness. The method is also suitable for the assay determination of IMM in pharmaceutical dosage forms.

© 2012 Elsevier B.V. All rights reserved.

1. Introduction

High pressure liquid chromatography (HPLC) is a well-known and widely used analytical technique which is prevalent throughout the pharmaceutical industry as a research tool for estimation of impurities in drug substances and drug products. Despite its prominence, HPLC possesses some disadvantages, most notably longer analysis time and large consumption of organic solvents. Ultra pressure liquid chromatography (UPLC) is a relatively new technique which offers better separation capabilities when compared to HPLC with added benefits of shorter run time and lower solvent consumption. One of the key developments which facilitate the new UPLC technology is sub 2-μm particles used as column packing material [1]. These particles withstand higher operating pressures and decreased flow rates to drastically increase the resolution, sensitivity and speed of analysis. Owing to its speed and sensitivity, this technique is gaining considerable attention in recent years for the analysis of pharmaceutical and biomedical compounds of interest. In the present work, this technique has been applied to the stability-indicating method development and method validation study of related substances and assay determination of IMM drug substance and dosage form. Imatinib Mesylate is an anticancer drug used to treat patients with hematological malignancies or malignant sarcomas such as Philadelphia positive chronic myeloid leukemia, chronic myeloid leukemia in blast crisis, acute lymphoblastic leukemia, aggressive systemic mastocytosis, gastrointestinal stromal tumors, and other diseases. Imatinib Mesylate is designated chemically as 4-[(4-methyl-1-piperazinyl)methyl]-N-[4-methyl-3-[[4-(3-pyridinyl)-2-pyrimidinyl]amino]-phenyl] benzamidemethanesulfonate (Fig. 1).

Stability testing forms an important part of the process of drug product development. The purpose of stability testing is to provide evidence on how the quality of a drug substance varies with time under the influence of a variety of environmental factors such as temperature, humidity and light, which enables recommendation of storage conditions, retest periods, and establishing shelf life. The content of related substances and assay of Imatinib Mesylate API (active pharmaceutical ingredient) and drug product is required to be determined using stability indicating method, as recommended

* Corresponding author at: Department of Pharmaceutical Sciences, Jawaharlal Nehru Technological University, Kukatpally, Hyderabad 500072, India.
Tel.: +91 7702201917.
E-mail addresses: nageswari.reddy@gmail.com, nageswarireddy@yahoo.co.in (A. Nageswari).

0731-7085/$ – see front matter © 2012 Elsevier B.V. All rights reserved.
doi:10.1016/j.jpba.2012.03.022

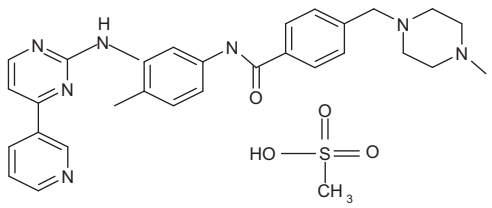

Imp-B: o-Toluidine.

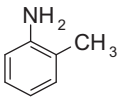

Imp-C: N-(5-amino-2-methylphenl)-4-(3-pyridyl)-2-pyrimidine amine

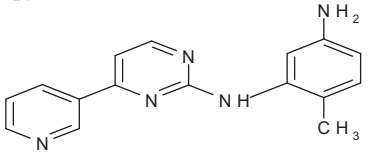

Imp-D: N-[4-Methyl-3-[[4-(1-oxido-3-pyridinyl)-2-pyrimidinyl]amino]phenyl]-4-[(4-methyl-1-piperazinyl)methyl]benzamide

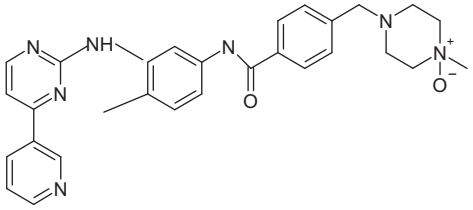

Imp-E: 4-[(4-methylpiperazin-1-yl)methyl]-N-[4-methyl-3-[4-(3-pyridinyl)-2-pyrimidinyl] chloromethylamino]phenyl]benzamide

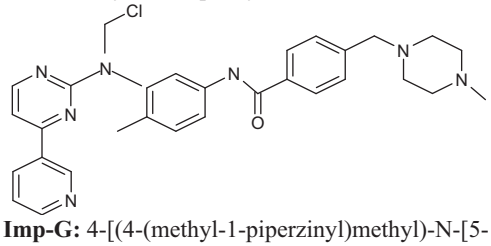

Imp-F: 4-[piperazinyl]methyl]-N-(4-methyl-3-[(4-pyridinyl)-2-pyrimidinylamino]phenyl] benzamide

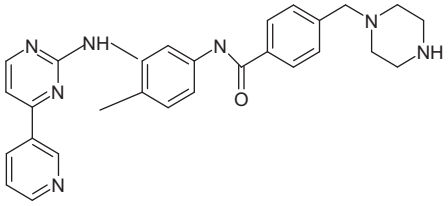

Imp-G: 4-[(4-(methyl-1-piperzinyl)methyl)-N-[5-methyl-4-[(4-pyridinyl)-2-pyrimidinyl-amino] phenyl]-benzamide

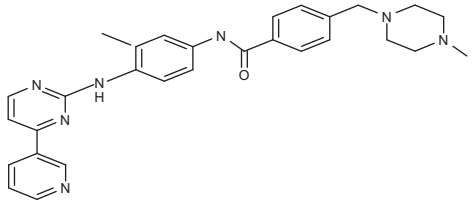

Imp-H: N-[4-Methyl-3-(4-pyridin-3-yl-pyrimidin-2-ylamino)phenyl]-4-chloromethyl benzamide

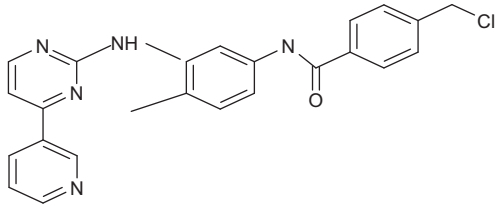

Fig. 1. Chemical structure of Imatinib Mesylate and its impurities.

by the International Conference on Harmonization (ICH) guidelines [2] and United State Pharmacopoeia (USP) [3].

Literature survey revealed few stability indicating analytical methods for quantification of IMM individually based on high performance liquid chromatography (HPLC) [4] and high performance thin layer chromatography (HPTLC) [5]. Vivekanand et al. [6] presented a validated LC method for IMM. There have been some RP-HPLC methods for estimation of IMM and impurities in Glivec capsules [7,8]. In the present work, in addition to reported impurities, other possible related substances and degradation products of IMM were considered for method development by UPLC. There are no official pharmacopoeial methods for estimation of related substances and assay of IMM. It is therefore felt necessary to develop a stability-indicating method for the determination of related substances and degradation products and quantitative estimation of IMM. For this study, we intend to opt for a faster chromatographic technique UPLC in order to assess whether UPLC can result in shorter analysis times without compromising on the resolution and sensitivity.

Hence, a stability-indicating RP-UPLC method was developed for the quantitative determination of IMM and its eight impurities and possible degradation products namely Imp-A, B, C, D, E, F, G and H (Fig. 1). This method was successfully validated according to the ICH guidelines (Validation of Analytical procedures: Test and Methodology Q2).

2. Experimental

2.1. Chemicals

Active pharmaceutical ingredient standards and samples were provided by Aptuit Laurus Private Limited, India. HPLC grade acetonitrile, methanol, ammonium acetate, AR grade ammonia solution purchased from Merck, Darmstadt, Germany. High purity water was prepared by using Millipore Milli-Q plus water purification system, Bedford, MA, USA.

2.2. Chromatographic conditions and equipments

Fast LC experiments were performed on a Waters Acquity UPLC with photo diode array detector. The output signal was monitored at a wavelength of 237 nm and processed using Empower

2 software; Version build 2154. The chromatographic column used was Acquity UPLC BEH C-18 50 mm, 2.1 mm and 1.7 μm particle size. The separation was achieved using a gradient method. Solvent A was 0.05 M ammonium acetate (pH 9.5); solvent B consisted a mixture of acetonitrile and methanol in a ratio of 40:60 (v/v). The flow rate was 0.3 mL/min with a gradient program of (T/%B) 0.01/42; 5/42; 7/80; 8/42; 9/42. The column temperature was maintained at 30 °C. The injection volume was 2.0 μL.

2.3. LC–MS conditions

LC–MS/MS system (Waters HPLC 2695 coupled with Waters Quattro Micro with Mass Lynx software, version 4.1, USA) was used for identification of degradants formed during forced degradation studies. Waters X-Bridge C18 (250 mm × 4.6 mm), 5 μm particle size column from Waters Corporation was used. Solvent A was 0.01 M ammonium acetate, pH was adjusted to 9.5 with ammonium hydroxide. Solvent B contains mixture of acetonitrile and methanol in the ratio of 40:60 (v/v). The flow rate of mobile phase was 1.5 mL/min.

The LC gradient program (T/%B) was set as 0.01/42; 25/42; 35/80; 40/42; 45/42. The column temperature was maintained at 30 °C. Solvent B was used as diluent and injection volume was 10 μL. The analysis was carried out by using electro spray ionization mode (+ve). Capillary voltage is 3.5 kV and cone voltage is 30 V. Desolvation temperature is 350 °C with desolvation gas flow rate 600 L/h.

2.4. Preparation of solutions

2.4.1. Preparation of standard solutions

Stock solutions were prepared by dissolving the respective standard substance in diluent to obtain a concentration of 1.0 mg mL^{-1} for IMM and a stock solution of impurity blend was prepared (mixture of Imp-A, Imp-B, Imp-C, Imp-D, Imp-E, Imp-F, Imp-G and Imp-H) at a concentration of 100 μg mL^{-1}.

2.4.2. Preparation of drug product solution

Glivec tablet (IMM) 400 mg was weighed and transferred to a clean and dry mortar and ground well. Tablet equivalent to 100 mg of the drug substance was dissolved in 100 mL of diluent and the resulting solution was filtered through a 0.22-μm nylon filter. This solution was analyzed by UPLC.

2.5. Stress studies

Specificity is the ability of the method to measure the analyte in the presence of its potential impurities. Specificity of the developed UPLC method for IMM was performed in the presence of impurities and degradation products. Stress studies were performed at concentration 1000 μg mL^{-1} of IMM drug substance to provide an indication of the stability indicating property and specificity of the proposed method. Degradation was attempted under stress condition of UV light (254 nm), heat (60 °C), acid (5.0 N HCl at 27 °C), base (5.0 N NaOH at 27 °C), hydrolytic (60 °C) and oxidation (2% H_2O_2 at 27 °C) to evaluate the ability of the proposed method to separate IMM from its degradation products. For heat and light studies, study period was 10 days whereas for acid hydrolysis approximately 40 h; base hydrolysis 30 h; hydrolytic 24 h and oxidation 2 h.

Peak purities of the stressed samples were checked by using PDA detector and the purity angle was found to be within the purity threshold limit in all stressed samples which demonstrates the homogeneity of analyte peak. Assay of stressed samples was performed by comparing with standard and mass balance (% assay + % impurities + % degradation products) was calculated for stressed samples. Assay was also calculated for spiked sample of IMM at 0.15% with respect to test concentration.

2.6. Method validation

The proposed method has been validated for assay and related substances by UPLC as per ICH guidelines [9].

2.6.1. Precision

Repeatability of the related-substances method was checked by analyzing six replicate samples of 1000 μg mL^{-1} IMM spiked with 0.15% of each of the impurities and degradants. The %RSD was calculated for each impurity for its content in terms of % area.

Intra-day, inter-day and analyst variations were studied to establish intermediate precision of the proposed method. Intra-day precision was determined by analyzing six replicate samples of 1000 μg mL^{-1} IMM spiked with 0.15% each of the eight impurities and degradation products. The same procedure was followed for three different days to study inter-day variation ($n = 18$). Different analysts prepared solutions on different days with different lots of AR and LR grade materials.

The %RSD was calculated for each impurity for its content in terms of % area.

The precision of the assay was evaluated by performing six independent assays of test samples of IMM and comparison with a reference standard. The %RSD of six results was calculated.

2.6.2. Sensitivity

Sensitivity of the method was proved by establishing the limit of detection (LOD) and limit of quantitation (LOQ) for IMM and its eight impurities and degradation products with a signal-to-noise ratio of 3:1 and 10:1, respectively. LOD and LOQ were determined by injecting a series of diluted solutions having known concentrations of drug substance and impurities. Precision study was also carried out at the LOQ level by injecting six individual preparations of IMM and impurities at LOQ concentration and by calculating the %RSD for the areas of each peak. Accuracy at LOQ level was verified by injecting three individual preparations of IMM spiked with impurities at LOQ level and by calculating % recoveries of each impurity.

2.6.3. Linearity and range

To establish linearity of the related substance method, solutions were prepared by diluting the impurity stock solution to obtain the required concentrations at seven different levels ranging from LOQ to 200% (i.e. LOQ, 0.075, 0.12, 0.15, 0.18, 0.225 and 0.30%) to the specification level, 0.15%. The correlation coefficient, slope and y-intercept of the calibration curve were calculated.

2.6.4. Accuracy

For the determination of accuracy of related substances method, recovery study was carried out by analyzing the spiked samples. Known amounts of impurities were spiked in triplicate at three different concentration levels of 0.75, 1.5 and 2.25 μg mL^{-1} to a previously analyzed drug substance sample The percentage of recoveries for eight impurities was calculated.

2.6.5. Robustness

The robustness study was carried out to evaluate the influence of small but deliberate variation in the chromatographic conditions. The factors chosen for this study which were critical sources of variability in the operating procedures such as temperature of the column (±5 °C), mobile phase pH (±0.5) and flow rate (±0.03 mL/min) were identified. Resolution between IMM and impurities was evaluated in the deliberately altered experimental conditions.

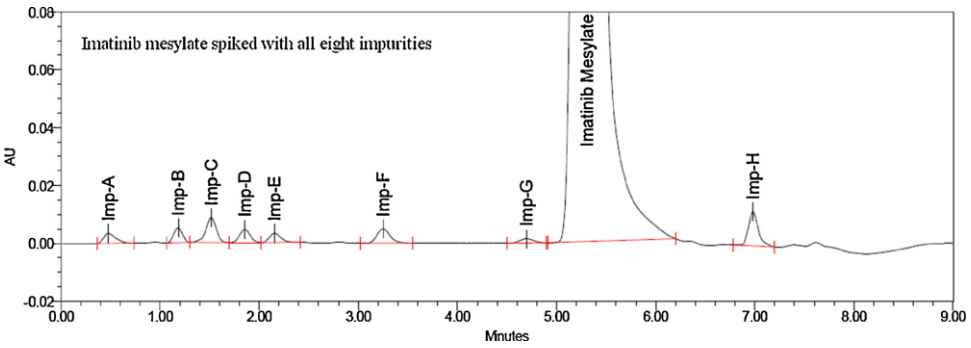

Fig. 2. Typical blend chromatogram of Imatinib Mesylate and its impurities.

3. Results and discussion

3.1. Method development

The main objective of the chromatographic method was to separate all the eight impurities from each other and IMM. A blend solution containing 1000 μg mL^{-1} of IMM and 1.5 μg mL^{-1} of each impurity dissolved in solvent B was used for method development. Initially, experiments were carried out based on the available isocratic HPLC method as per IP (Indian Pharmacopoeia) monograph by using Inertsil ODS-3V (250 mm × 4.6 mm), 5 μm column with mobile phase composed of 40 volumes of 1% (w/v) ammonium acetate and 60 volumes of acetonitrile. But in the method specified in the IP monograph, it was observed that Imp-G and IMM co-eluted with each other. Hence, a gradient program was employed with a runtime of 45 min using a mobile phase at pH 2.6 as specified in the available literature [7] and found that all the polar impurities namely Imp-A, Imp-B and Imp-C were not only merging with each other but also Imp-G co-eluted with IMM.

As IMM has a pK_a of 13.45 reported in the literature [10], to check the effect of pH on resolution of impurities in basic buffer, methods were tried using buffers at different pH ranging from 8 to 11 without disturbing the ionization pH range of IMM i.e. pK_a ± 1.5 [11]. For optimizing pH of the buffer, an HPLC column, Waters X-Bridge C18 (250 mm × 4.6 mm), 5 μm particle size, was selected, which can be used at broad pH ranges from 1 to 12. Blend solution was injected in the above mentioned buffers having different pH with gradient elution by using a mixture of methanol and acetonitrile in a ratio of 60:40 (v/v) as eluent B and it was observed that at pH below 9.0, Imp-E and Imp-F merged together. But separation was achieved for all the eight impurities and IMM at pH 9.5 ± 0.5.

In order to reduce the analysis time, HPLC method has been transferred to UPLC by using BEH C-18 100 mm, 2.1 mm and 1.7 μm particle size column with a runtime of 18 min which resulted in the separation between all the eight impurities and IMM with a resolution of >1.5 for any closely eluting pair. However, to further reduce the analysis time, UPLC BEH C-18 50 mm, 2.1 mm and 1.7 μm column was used with a gradient elution where the gradient program (T/%B) was set as 0.01/42; 5/42; 7/80; 8/42; 9/42 at a flow rate of 0.3 mL/min. Using these chromatographic parameters, desired separation for all the eight impurities and IMM was achieved within 9 min without compromising on resolution (>1.5) between any pair of impurities that were eluting closely when compared to 100 mm column. Retention time of IMM was 5.5 min. Typical blend chromatogram of IMM and its impurities is shown in Fig. 2. Placebo interference was also verified and found that no interference was observed at the retention time of any of the impurities and IMM.

In the optimized UPLC conditions, system suitability parameters were evaluated for IMM and its eight impurities (Fig. 2). Tailing factor for all the components was less than 1.5 and resolution between any pair components that were eluting closely was more than 1.5 (Table 1).

3.2. Method validation

3.2.1. Precision

The %RSD for peak areas of the eight impurities namely Imp-A, Imp-B, Imp-C, Imp-D, Imp-E, Imp-F, Imp-G and Imp-H in the study of the repeatability was within 1.5. Results for intermediate precision are within 4.0%. These results demonstrate that the method is precise (Table 2).

3.2.2. Limit of detection and quantitation

Limit of detection, limit of quantitation values for IMM and its impurities are reported in Table 2. The RSD for peak areas of IMM and its related eight impurities at limit of quantitation level are within 5.5%. The recoveries at LOQ level are in the range of 85–113%.

Table 1
System suitability parameters.

Compound	RT (min)[a]	RRT[b] (n = 6)[a]	USP resolution[c] (n = 6)[a]	USP tailing factor (n = 6)[a]
Imp-A	0.46	0.08 ± 0.01	–	1.01 ± 0.02
Imp-B	1.16	0.22 ± 0.00	4.02 ± 0.02	1.08 ± 0.01
Imp-C	1.51	0.28 ± 0.00	1.77 ± 0.01	1.14 ± 0.01
Imp-D	1.87	0.35 ± 0.00	1.63 ± 0.02	1.20 ± 0.02
Imp-E	2.28	0.43 ± 0.01	1.59 ± 0.01	1.50 ± 0.02
Imp-F	3.23	0.6 ± 0.00	3.16 ± 0.01	1.36 ± 0.01
Imp-G	4.77	0.89 ± 0.00	4.69 ± 0.02	1.03 ± 0.01
IMM	5.35	1.00 ± 0.00	1.57 ± 0.00	1.35 ± 0.01
Imp-H	6.97	1.30 ± 0.00	5.59 ± 0.03	0.94 ± 0.02

IMM, Imatinib Mesylate.
[a] Mean ± SD (n = 6 preparations).
[b] Relative retention time (RRT) was calculated against the retention time (RT) of IMM.
[c] Resolutions were calculated between two adjacent peaks.

Table 2
LOD, LOQ, regression and precision data.

Compound	LOD ($\mu g\,mL^{-1}$)	LOQ ($\mu g\,mL^{-1}$)	Regression equation (y)		Correlation coefficient	R^2 value	Precision (%RSD)[a]	Intermediate precision (%RSD)[a]
			Slope (b)	Intercept (a)				
Imp-A	0.06	0.20	16,479,305	975	1.000	0.9996	0.0	0.0
Imp-B	0.05	0.15	22,873,230	−23	1.000	1.0000	0.0	0.0
Imp-C	0.02	0.07	39,363,911	47	1.000	1.0000	0.0	1.5
Imp-D	0.05	0.15	18,043,902	−42	1.000	0.9999	4.0	0.0
Imp-E	0.09	0.30	15,456,338	−234	1.000	0.9999	2.6	3.2
Imp-F	0.05	0.17	24,996,280	45	1.000	0.9999	0.0	2.2
Imp-G	0.03	0.10	22,677,363	1278	0.999	0.9983	0.0	0.0
IMM	0.06	0.20	18,903,925	546	0.999	0.9978	0.0	0.0
Imp-H	0.05	0.16	16,555,477	−547	1.000	0.9999	3.2	2.6

Linearity range is LOQ–200% with respect to specification level i.e. 0.15%.
[a] Six preparations by using Imatinib with impurities spiked solution at 0.15%.

Table 3
Results of robustness study.

Parameter/variation	USP resolution (Rs)								
	Imp-A	Imp-B	Imp-C	Imp-D	Imp-E	Imp-F	Imp-G	IMM	Imp-H
As such conditions	–	4.0	1.8	1.6	1.6	3.2	4.7	1.6	6.0
Flow rate (mL/min)									
a. 0.27	–	4.4	1.8	1.6	1.6	3.1	4.7	1.6	4.2
b. 0.33	–	3.6	1.6	1.5	1.5	3.0	4.6	1.5	7.2
Temp. (°C)									
a. 25	–	3.9	1.7	1.6	1.6	3.0	4.6	1.6	5.4
b. 30	–	3.8	1.6	1.5	1.5	2.9	4.6	1.5	6.8
Buffer pH									
a. 9.0	–	3.1	1.8	1.9	1.3	2.3	6.1	1.8	7.7
b. 10.0	–	3.2	1.8	1.8	1.4	5.0	5.1	1.9	7.1

Table 4
Summary of forced degradation results.

Degradation condition	Time	Assay (%, w/w)	Mass balance (% assay + % deg. products)	RS by UPLC % degradation	Remarks/observation
HCl, 5.0 N (acid hydrolysis)	41 h	92.3	98.3	4.2	Imp-A, -C and -F degradation products were formed
NaOH, 5.0 N (base hydrolysis)	30 h	97.6	101.5	2.0	No significant degradation observed
Oxidation by 2.0% H_2O_2	2 h	93.9	98.8	3.0	Imp-B, -C and -D degradation products were formed
Thermal (60 °C) solid	10 days	97.9	100.0	0.1	No significant degradation observed
UV at 254 nm	10 days	98.0	99.9	0.1	No significant degradation observed

3.2.3. Accuracy

Recovery of impurities from drug substances in spiked studies ranged from 90 to 110% at three different levels.

3.2.4. Linearity

For all eight impurities of IMM, linear calibration curve was obtained in the concentrations ranging from LOQ to 0.30% and for IMM from LOQ to 200% (LOQ, 20, 50, 80, 100, 150 and 200%) of the nominal sample concentration ($1.0\,mg\,mL^{-1}$). The correlation coefficient obtained was >0.999 for all the components. The slope and y-intercept values are also provided in Table 2, which confirmed good linearity between peak areas and concentration.

3.2.5. Robustness

Under all the deliberately altered chromatographic conditions (flow rate, pH and column temperature), all peaks were adequately resolved and elution orders remained unchanged which indicate that the method is robust. Results of robustness study are provided in Table 3.

3.2.6. Results from forced degradation studies

Forced degradation samples under various conditions were analyzed at an initial concentration $1000\,\mu g\,mL^{-1}$ of IMM on UPLC using PDA detector to ensure homogeneity of IMM peak. Degradation was not observed when IMM was subjected to base hydrolysis (5.0 N NaOH for 30 h), water hydrolysis, light and heat conditions. Significant degradation was observed when the drug was subjected to oxidation (2% H_2O_2 for 2 h) leading to the formation of Imp-B, Imp-C and Imp-D and acid hydrolysis (5.0 N HCl approximately 40 h) leading to the formation of Imp-A, Imp-C and Imp-F. The degradation products that were formed during the stress studies were confirmed not only by co-injecting with the standard samples with stressed samples but also by LC–MS.

LC–MS analysis was performed as per experimental conditions given in Section 2.3. Stressed sample by oxidation exhibited molecular ions at m/z 108 amu $(M+H)^+$, 278 amu $(M+H)^+$, m/z 510 amu $(M+H)^+$ corresponding to Imp-B, Imp-C and Imp-D respectively. Stressed sample of acid hydrolysis exhibited molecular ions at m/z 235 amu $(M+H)^+$, 278 amu $(M+H)^+$ and 480 amu $(M+H)^+$ corresponding to Imp-A, Imp-C and Imp-F respectively. Mass spectral data of degradation products formed during stressed conditions of oxidation and acid hydrolysis are shown in Fig. 3. Results from forced degradation studies are presented in Table 4.

Assay studies were performed on stressed samples against IMM standard. Mass balance results were calculated for all stressed samples and were found to be in the range of 98.3–101.5% which confirms the stability-indicating nature of the proposed method.

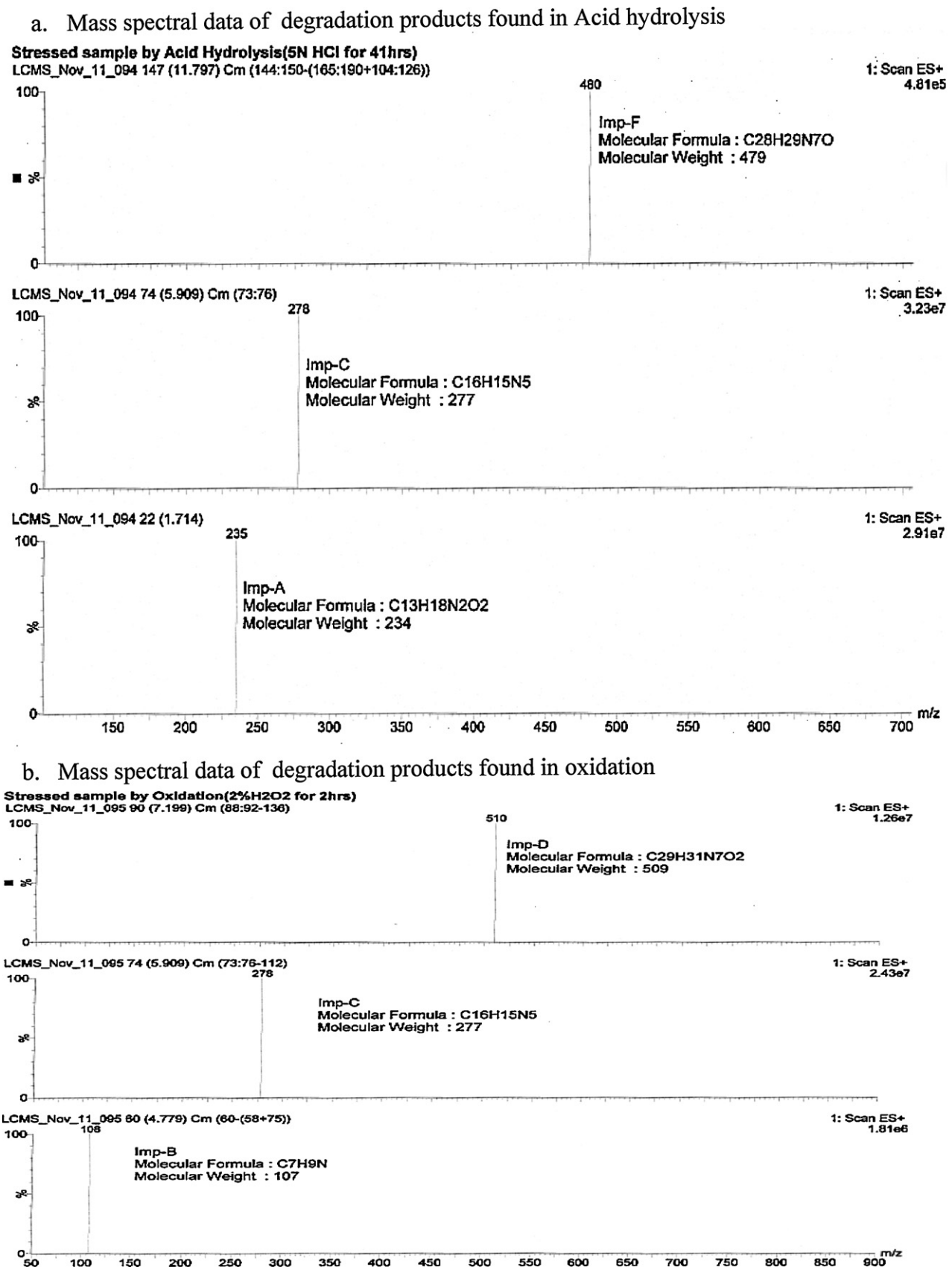

Fig. 3. LC–MS data of stressed samples. (a) Mass spectral data of degradation products found in acid hydrolysis. (b) Mass spectral data of degradation products found in oxidation.

4. Conclusion

The gradient RP-UPLC method developed for quantitative estimation of IMM and related substances in active pharmaceutical ingredient and dosage forms was found to be precise, accurate, linear, robust and specific. A runtime of 9 min enables quick determination of IMM, impurities and degradation products. The method is stability-indicating and can be used for routine analysis in quality control and also to test the stability of samples.

Acknowledgement

The authors wish to thank the management of Aptuit Laurus Private Limited for supporting this work.

References

[1] M.E. Swartz, UPLC: an introduction and review, J. Liq. Chromatogr. Relat. Technol. 28 (2005) 1253–1263.
[2] ICH Q1A (R2), Stability Testing of New Drug Substances and Products, 2003.
[3] The United States Pharmacopoeia, 26th ed., US Pharmacopoeia Convention, MD, 2003, pp. 1151–1154.
[4] B. Girish, K. Sivacharan, K. Venugopal, S. Ranendra, Development and validation of stability indicating RP-LC method for determination of Imatinib Mesylate, Chromatographia 66 (2007) 859–866.
[5] N. Vadera, G. Subramanian, P. Musmade, Stability-indicating HPTLC determination of Imatinib Mesylate in bulk drug and pharmaceutical dosage form, J. Pharm. Biomed. Anal. 43 (2007) 722–726.
[6] V.V. Vivekanand, D. Sreenivas Rao, G. Vaidhyanathan, N.M. Sekhar, S. Avijit Kelkar, P. Ramachandra Puranik, A validated LC method for Imatinib Mesylate, J. Pharm. Biomed. Anal. 33 (2003) 879–889.
[7] D. Ivanovic, M. Medenica, B. Jancic, A. Malenovic, Reversed-phase liquid chromatography analysis of Imatinib Mesylate and impurity product in Glivec® capsules, J. Chromatogr. B 800 (2004) 253–258.
[8] M. Medenica, B. Jancic, D. Ivanovic, A. Malenovic, Experimental design in reversed-phase high-performance liquid chromatographic analysis of Imatinib Mesylate and its impurity, J. Chromatogr. A 1031 (2004) 243–248.
[9] ICH Q2 (R1), Validation of Analytical Procedures: Text and Methodology, 2005.
[10] Drug Bank: Imatinib (DB00619).
[11] L.R. Snyder, J.J. Kirkland, J.L. Glajch, Practical HPLC Method Development, second ed., John Wiley & Sons, Inc., New York, USA, 1997, pp. 294–296.

Journal of Pharmaceutical and Biomedical Analysis 66 (2012) 116–125

Contents lists available at SciVerse ScienceDirect

Journal of Pharmaceutical and Biomedical Analysis

journal homepage: www.elsevier.com/locate/jpba

Voltammetric and RP-LC assay for determination of benidipine HCl

Nurgul Karadas[a,b], Senem Sanli[c], Mehmet Gumustas[a,b], Sibel A. Ozkan[b,*]

[a] Hitit University, Faculty of Science and Arts, Dept. of Chemistry, Corum, Turkey
[b] Ankara University, Faculty of Pharmacy, Dept. of Analytical Chemistry, 06100 Ankara, Turkey
[c] Usak University, Faculty of Science and Arts, Dept. of Chemistry, Usak, Turkey

ARTICLE INFO

Article history:
Received 11 January 2012
Received in revised form 13 March 2012
Accepted 14 March 2012
Available online 23 March 2012

Keywords:
Benidipine
Liquid chromatography
pK_a
Voltammetry
Stress conditions

ABSTRACT

The detailed electrooxidative behavior of benidipine (BEN) has been studied by using glassy carbon (GC) and boron-doped diamond (BDD) electrodes. Using cyclic voltammetry, depending on the pH values and the working electrodes, BEN showed one or two sharp and irreversible oxidation responses. The voltammetric experiments on some model compounds allowed elucidation of the oxidation mechanism of BEN. Highly sensitive, selective, rapid, and fully validated voltammetric methods for the determination of BEN in tablet dosage form were also presented. Under optimized conditions, the peak current showed a linear dependence with concentration in the range between 3.25 μg mL^{-1} and 54.20 μg mL^{-1} for GC and 1.08 μg mL^{-1} and 54.20 μg mL^{-1} for BDD electrodes by using differential pulse (DPV) and square wave (SWV) voltammetric techniques. In this study, acid dissociation constant (pK_a) value of BEN was determined by using the dependence of the retention factor on the pH of the mobile phase using reverse phase-liquid chromatographic (RP-LC) method. The effect of the composition of the mobile phase on the ionization constant was studied by measuring the pK_a at different acetonitrile–water mixtures, ranging between 50 and 65% (v/v). Also simple, accurate, precise and fully validated RP-LC method for the assay of BEN in dosage form has been developed. XTerra RP-18 column at 25 °C with the mobile phase of acetonitrile:water 55:45 (v/v) adjusted to pH 3.0 with 15 mM *o*-phosphoric acid was used. Isocratic elution was performed in less than 5.0 min with a flow rate of 1.0 mL min^{-1}. The RP-LC method allowed quantitation over the 0.25–15.00 μg mL^{-1} range for BEN. The proposed voltammetric and RP-LC methods allow a number of cost and time saving benefits. BEN was also exposed to thermal, photolytic, oxidative stress, acid–base catalyzed hydrolyses, and the stressed samples were detected by the proposed RP-LC method.

© 2012 Elsevier B.V. All rights reserved.

1. Introduction

Benidipine HCl (BEN), (±)-(R')-3-[(R')-1-benzyl-3-piperidyl] methyl 1,4 dihydro-2,6-dimethyl-4-(m-nitrophenyl)-3,5-pyridenecarboxylate hydrochloride (Scheme 1), is a dihydropyridine-derived calcium channel blocker with general properties similar to those of nifedipine. It has relatively high vascular selectivity and is expected to show protective effects on vascular endothelial cells. It is used orally in the management of hypertension and angina pectoris [1,2].

For the time being, few methods have been reported for quantification of this compound such as gas chromatographic [3–5] and LC–MS methods [6]. These published methods are time consuming and might have some limitations such as expensive instrumental set-up, and exact rigid experimental conditions like the amount of reagent, reaction temperature and time. So far, neither electroanalytical nor chromatographic report on quantitative determination of BEN in pharmaceutical formulations has been published. Also no information about the electrochemical redox properties, acid dissociation (pK_a) value, and degradation behavior of BEN by using LC method has been found in the literature. Moreover, no monograph of BEN has been published in the official pharmacopeias as of today.

Electroanalytical methods have proved to be very sensitive, selective and rapid for the determination of active pharmaceutical ingredients (APIs) in their dosage forms. The advantage of experimental electrochemical techniques in the field of quantitative analysis of drugs arise from their simplicity, low cost and relatively short analysis time as compared with other techniques. Voltammetric techniques are most suitable for investigation of the redox properties of APIs, and these techniques can give insight into the metabolic fate, in vivo redox process or pharmaceutical activity [7,8].

Owing to the widespread use of LC–DAD method in routine analyses, it is important that specific and thoroughly validated LC methods are developed for the analysis of APIs in their dosage forms

* Corresponding author. Tel.: +90 312 223 82 43; fax: +90 312 223 82 43.
E-mail address: ozkan@pharmacy.ankara.edu.tr (S.A. Ozkan).

0731-7085/$ – see front matter © 2012 Elsevier B.V. All rights reserved.
doi:10.1016/j.jpba.2012.03.025

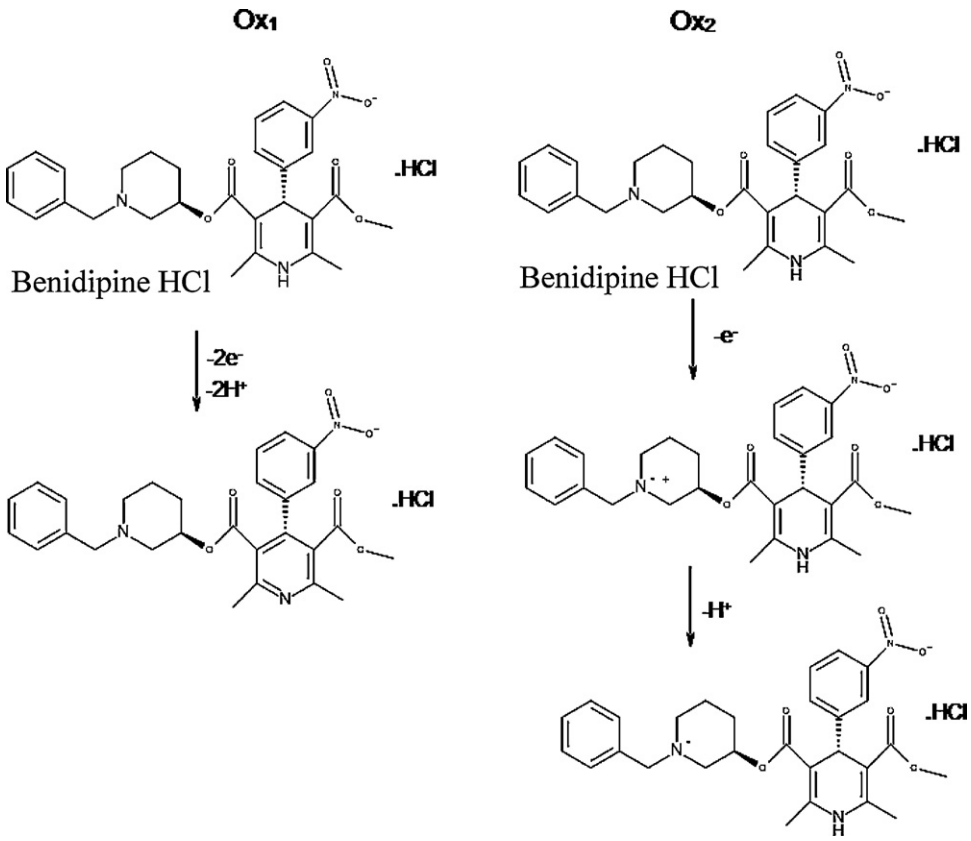

Scheme 1. The possible oxidation mechanisms of BEN.

[9]. LC–DAD methods offer important advantages, such as rapid set-up of instrumentation, versatility and low cost, and has proved to be a valuable method in the quality control of drugs.

The ionization constant (pK_a) is an important physico-chemical parameter of a drug. The relationship between pK_a and the structure may prove useful in drug design studies and in explaining the biopharmaceutical properties of a substance. The chromatographic retention and electrophoretic behavior of ionizable compounds strongly depend on the pK_a of the working compound and the pH of the mobile phase. A satisfactory knowledge of the acid–base behavior of substances in hydro-organic media, such as acetonitrile and water mixtures, is therefore essential to predict the influence of pH on selectivity, retention times, and also for optimization of analytical parameters [10,11].

This study has three-folds: first, carrying out a detailed investigation of electrochemical behavior of BEN; second, its quantitative determination at carbon-based electrodes by using cyclic (CV), linear sweep (LSV), and pulse voltammetric techniques and by using RP-LC with stability tests performing based on ICH standards; and third, determining the pK_a value of BEN by using RP-LC.

2. Experimental

2.1. Chemical and reagents

Benidipine HCl and its pharmaceutical dosage form Coniel® tablets were kindly donated by Deva Pharm. Ind. (Istanbul, Turkey). Model compounds and internal standard (IS), lacidipine (Glaxo Smithkline, Gebze, Turkey), nifedipine (Sanofi Aventis, Istanbul, Turkey), haloperidol (Ali Raif, Istanbul, Turkey) and indapamide (Sanovel, Istanbul, Turkey) (IS) were kindly supplied from different companies in Turkey.

Stock solution of BEN (1×10^{-3} M) was prepared in acetonitrile and kept in the dark in a refrigerator at about 4 °C. For voltammetric studies, working solutions of BEN were prepared by dilution of the stock solution with supporting electrolyte containing 30% acetonitrile for pH studies and 50% acetonitrile for analytical studies. Different supporting electrolytes, namely sulphuric acid (0.1 and 0.5 M; pH 1.0 and 0.3), phosphate buffer (0.2 M; pH 3.0–7.80), acetate buffer (0.2 M; pH 3.7–5.7), Britton–Robinson buffer (0.04 M; pH 2.14–12.03) were prepared in bidistilled water. The calibration curve for DPV and SWV analysis was constructed by plotting the peak current versus BEN concentration for both GC and BDD electrodes. The calibration graph was constructed by plotting the peak current versus corresponding BEN concentration in the range of 3.25–54.20 $\mu g\,mL^{-1}$ for both differential pulse (DPV) and square wave (SWV) voltammetric techniques.

All chemicals were analytical reagent grade and all solvents were HPLC grade. For the LC methods, HPLC grade acetonitrile (Merck, Darmstadt, Germany) was used as organic modifier. Sodium hydroxide (Merck, Darmstadt, Germany) and *o*-phosphoric acid (Riedel-de Haen, Germany) were used for pH adjustment. Water with conductivity lower than 0.05 $\mu S\,cm^{-1}$ for RP-LC studies was obtained with a Zeneer Power I (Human Corp.). Standard stock solutions of BEN and internal standard (IS) indapamide were prepared in acetonitrile at concentrations approximately 100 $\mu g\,mL^{-1}$ and working solutions were prepared by dilution using mobile phase. The concentration of BEN for LC studies was varied in the range of 0.25–15 $\mu g\,mL^{-1}$. The concentration of IS was maintained at a constant level of 2.0 $\mu g\,mL^{-1}$. The calibration curves for LC analysis were constructed by plotting the ratio of the peak area of the drug to that of IS versus drug concentration. The ruggedness and precision were checked at within day ($n = 5$) and between days ($n = 5$). Relative standard deviations (RSD) were calculated to check the ruggedness and precision of the method [12–14]. The

accuracy and precision of the developed methods were described in a quantitative fashion by the use of Bias % (relative error).

All stock and working solutions were protected from light and stored in fridge at about 4 °C. The responses of the sample solutions recorded a week period after preparation did not show any appreciable change in assay values.

2.2. Apparatus

All voltammetric measurements at a GC and BDDE were performed using a BAS 100W (Bioanalytical Systems, West Lafayette, IN, USA) electrochemical analyzer. The three electrode system contained either a BDDE (Windsor Scientific Ltd., Slough, Berkshire, UK; Ø: 3 mm, diameter) or GC (Bioanalytical Systems, West Lafayette, IN, USA; Ø: 3 mm, diameter) working electrodes, with a platinum wire auxiliary electrode and Ag/AgCl reference electrode (BAS; KCl 3M) and a standard one-compartment three-electrode cell of 10 mL capacity. Before each experiment, the GC or BDDE was polished manually with slurries prepared from 0.01 μm aluminum oxide on a smooth polishing pad (BAS velvet polishing pad), then rinsed with bidistilled water thoroughly. All measurements were performed at room temperature. For voltammetric studies, the pH measurements were carried out using a Model 538 pH-meter (WTW, Weilheim, Germany) with an accuracy of ±0.05 pH.

For analytical application the following parameters were employed for SWV: pulse amplitude, 25 mV; frequency, 15 Hz; scan increment, 4 mV; and for DPV: pulse amplitude, 50 mV; pulse width 50 ms; scan rate 20 mV s^{-1}.

The RP-LC analysis was carried out on a Shimadzu (Kyoto, Japan) HPLC system with a pump (LC-20AD), a DAD detection system (SPD-M 20A) and column oven (CTO20 AC). This equipment has a degasser system (DGU 20A). The chosen wavelength for the analysis of BEN was 238 nm. An XTerra (Waters Corp., Milford, MA, USA) RP-18 (250 × 4.6 mm ID × 5 μm) column was used as a stationary phase at 25 °C constant temperature. Mettler Toledo (Columbus, OH, USA) MA 235 pH/ion analyzer with Hanna HI 1332 (Smithfield, RI, USA) Ag/AgCl combined glass electrode was used for pH measurement in LC analyses and pK_a studies. Indapamide (IS) was used as the internal standard.

2.3. Chromatographic procedure

For pK_a studies, the mobile phases were assayed acetonitrile:water combination at 50, 55, 60 and 65% (v/v), containing 15 mM *o*-phosphoric acid. The pH of the mobile phase was adjusted between 2.8 and 8.0 by the addition of sodium hydroxide. The flow rate was maintained at 1.0 mL min^{-1} and injection volume was 20 μL. The column temperature was set at 25 °C during the experiments. The column was pre-conditioned at least 1 h at low flow rate (0.5 mL min^{-1}) with mobile phase at the corresponding pH before the first injection. The retention time values, t_R, were determined from three separate injections for each mobile phase composition at desired pH value. The most common procedure is to measure the pH of the aqueous buffer before mixing the mobile phase with the organic modifier. A more rigorous procedure, recommended by the IUPAC, is to measure the pH of the mobile phase after mixing the aqueous buffer and the organic modifier [15]. pH values have been previously determined in acetonitrile–water mixtures for the primary standard series of substances proposed by NIST, in accordance with the IUPAC rules. In this study, potassium hydrogen phthalate solutions (0.05 mol kg^{-1}) dissolved in the appropriate acetonitrile–water medium were used as primary standard buffer [16,17].

The dead time (t_0) was measured by injection of uracil solution (Sigma, USA, 0.1%, in water) which was established for each mobile phase composition and studied pH value. The pK_a values were determined by performing a non-linear fit using the NLREG program [18]. This is a general purpose program, where the function to be minimized and the parameters to be estimated can be defined by means of the built-in program editor. The ionic strength was determined from the amount of sodium hydroxide added to obtain the desired pH of the mobile phase, and in acidic solutions from the dissociation constant of the buffer.

2.4. Preparation of stress samples for establishment of stability-indicating assay

Degradation studies were attempt to stress condition of UV light, acid, base, oxidation and heat in oven (at 75 and 100 °C), to evaluate the ability of the proposed method to separate BEN from its degradation product [19]. Thermal and photo-degradation of BEN in raw material were carried out in solid state. After the degradation, stock solutions were prepared by dissolving in acetonitrile to achieve final concentration of 1 mg mL^{-1}.

From these solutions aliquot amounts were diluted with mobile phase to achieve a final concentration of 100 μg mL^{-1}. Peak purity test was performed for BEN peak by using DAD in stress samples. The optimized method was used to study the forced degradation behavior of BEN and may also be applied in stability testing of pharmaceutical dosage forms. Appropriate blank was injected before analysis of the stressed samples. For thermal stress testing, samples of drug substances were placed in a controlled-temperature oven at 75 and 100 °C for 24 h.

For acidic, alkaline, and oxidative degradation, solutions were prepared by dissolving raw material of BEN in acetonitrile. From this solution, aliquot amounts were diluted with HCl, NaOH and H_2O_2 to achieve a concentration of 100 μg mL^{-1} for each solution. Acid and alkaline hydrolyses of BEN in the solution state were conducted with 0.5 M and 1.0 M HCl and NaOH at 80 °C for 30 min, separately. For oxidative stress, sample solutions of BEN in the solution state with 3% and 30% H_2O_2 were kept at 75 °C for 30 min. For photolytic stress, samples of drug substances in the solid state were irradiated with UV radiation at 254 nm for 6 h and 24 h.

2.5. Tablet assay procedure and accuracy

For both electroanalytical and LC methods, 10 Coniel® (Deva Pharm. Int., Istanbul) tablets, each containing 4.0 mg BEN, were accurately weighed and crushed to a homogeneous fine powder in a mortar. An accurate weight of this powder equivalent to one tablet content was weighed, transferred into a 100 mL calibrated flask, diluted with acetonitrile, stirred for about 10 min and then completed to the volume with the same solvent. This solution was filtered and the clear filtrate was collected in a clean flask. Appropriate solutions were prepared by taking suitable aliquot of clear filtrate (for LC study, adding of the constant amount of IS (2.0 μg mL^{-1})) and diluting them with selected supporting electrolyte (final solution contains 50% acetonitrile) and with mobile phase for electroanalytical and LC methods, respectively, in order to obtain a final solution. The content amount of BEN was calculated from the corresponding regression equations.

In order to demonstrate the applicability of both methods, recovery experiments were performed by adding a known amount of pure BEN to pre-analyzed tablets. Known amounts of the pure BEN (and at a constant level of IS for LC method) were added to the tablet dosage form and the mixtures were analyzed. The percent recovery was calculated by comparing the concentration obtained from spiked samples with the actual added concentration. Thus, the effects of common excipients in tablet dosage form on voltammograms (e.g., shifting of peak potential or changing peak shape), and on chromatograms (e.g., tailing, broadening) were investigated.

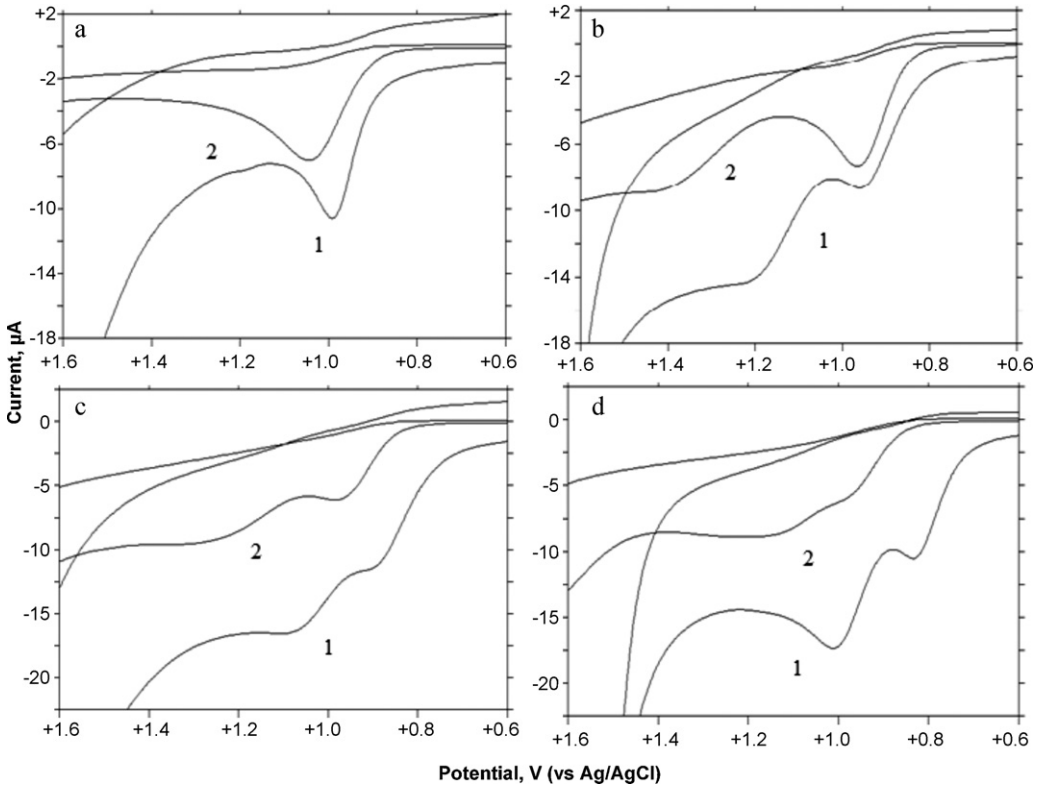

Fig. 1. Cyclic voltammograms of 1×10^{-4} M benidipine in 0.5 M H_2SO_4 (a); Britton–Robinson buffer at pH 3.50 (b); phosphate buffer at pH 4.00 (c); acetate buffer at pH 5.70 (d) with constant amount acetonitrile (30%). Scan rate, 100 mV s^{-1}. (1) GC and (2) BDD electrodes.

Recovery experiments from tablets also showed the reliability and suitability of both methods.

3. Results and discussion

3.1. Anodic behavior of BEN

No electrochemical information was found in the literature for the redox mechanism, and electroanalytical determination of BEN, using solid and mercury electrodes. To demonstrate the usefulness of the solid electrodes for determination of BEN that may offer advantages for the use of such electrodes as sensors, the electrochemical behaviors of BEN on GC and BDD electrodes were investigated. Voltammetric techniques such as LSV, CV, DPV and SWV were constructed to get information on the electrochemical oxidation mechanism of BEN.

In the first step, BEN was subjected to CV and LSV to achieve its anodic characterization on carbon-based electrodes. Oxidation of BEN was achieved on both GC and BDD electrodes in a broad pH range, producing one or two peaks depending on pH and the nature of the supporting electrolytes using CV (Fig. 1). The peak currents and peak potentials were determined in all supporting electrolytes that contain 30% acetonitrile (v/v) for solubility purposes and in all pH values There were two peaks observed for the oxidation of BEN when working with BDDE which overlapped at pH values higher than 5 and two new ill-defined waves appeared (Fig. 1c and d). On the other hand, two sharp anodic responses were obtained on GC electrode at pH > 2.5 (Fig. 1). In order to achieve the voltammograms the scanning was started at −0.20 V in the positive direction in 0.5 M H_2SO_4. The anodic oxidation of BEN did not occur until about +1.00 V on either of the electrodes. On reversing the direction of the applied potential at +1.80 V no reduction signal corresponding to the anodic response was observed. The fact that no reduction was observed in the reversed scan, hence, CV measurements proved an irreversible nature of the oxidation process. BEN peak decreased on the following cycles for both electrodes by repetitive CV. This phenomenon may be partly attributed to the consumption of adsorbed BEN on the electrode surface.

Comparison of the response at BDDE with that of GC electrodes reveals small potential shifts (to more positive potentials) of about 50 mV in 0.5 M H_2SO_4. Lower background currents were obtained when using BDDE (Fig. 1). However BEN was more easily oxidized on GC electrode than on BDDE electrode.

The effect of scan rate (ν) on the peak current (I_p) was studied in the range between 5 and 1000 mV s^{-1}. The potentials shifted to more positive potentials by about 94 mV for BDD and by about 84 mV for GC electrode to the anodic direction when the scan rate was increased. This shift also confirmed the irreversibility of the process for both electrodes. Scan rate studies were also carried out to understand whether the processes at BDD and GC electrodes were under diffusion or adsorption control. Using the concentration of 1×10^{-4} M in 0.5 M H_2SO_4 (30% acetonitrile), the voltammetric peak currents were obtained as the scan rate was varied over the range of 5–1000 mV s^{-1}. A linear response for both electrodes was achieved versus the square root of the scan rate and the values calculated are as follows:

$$I_p\,(\mu A) = 0.596\,\nu^{1/2}(\text{mV s}^{-1}) - 0.182\ (r = 0.999)\ \text{for GC}$$

and

$$I_p(\mu A) = 0.484\nu^{1/2}(\text{mV s}^{-1}) + 0.513\ (r = 0.999)\ \text{for BDD}$$

A plot of the logarithm of the peak current versus the logarithm of the scan rate gave also straight line with a slope of 0.50 and 0.46 for GC and BDD electrodes, respectively. These values were close to the theoretical value of 0.50, which would be expected for an ideal reaction of solution species [20]. Such linear dependence indicates that the oxidation of BEN was indeed diffusion controlled as would

be expected for an ideal reaction of solution species. The related equations are as follows:

$$\log I_p\,(\mu A) = 0.499 \log \nu(\text{mV s}^{-1}) - 0.235\ (r = 0.999) \text{ for GC}$$

and

$$\log I_p\,(\mu A) = 0.461 \log \nu(\text{mV s}^{-1}) - 0.184 (r = 0.999) \text{ for BDD.}$$

Next, the response of pH on the main voltammetric peak at GC and BDD electrodes was examined. The effect of pH on peak potential and peak current was studied using CV, DPV and SWV techniques for both electrodes, between pH 0.5 and 12.0. In all supporting electrolyte solutions and selected electrochemical techniques, BEN undergoes one main irreversible oxidation process and one additional peak or wave which was shifted towards less positive potentials was observed as the pH was increased for both electrodes. Thus the observed pH dependence on peak potential indicates that the electroactive group which corresponds to the main oxidation step of BEN has an acid–base equilibrium with pK_a about 7.0 for GC electrode. The intersection of the E_p–pH curves is located around pK_a value of the drugs. pH 7.34 corresponds to the pK_a value of BEN according to the literature [21] and our LC studies on pK_a which are described in the following sections. This break could be due to a change in protonation–deprotonation process of electroactive part of the molecule. At pH > pK_a, the conjugate base must be formed by a rapid dissociation of the protonated form. However, due to the overlap of both oxidation steps at pH values higher than 5.0 on BDDE, this intersection point and related equation could not be obtained clearly with this electrode.

Some disharmony was obtained between Britton–Robinson (0.04 M) and phosphate (0.2 M) buffers within working pH range. This may be due to the differences of the ionic strength and the ionic species of the buffers. The strictly linear segments between pH 2.0 and 7.0 can be expressed by the following equations in Britton–Robinson buffer for the main peak using GC electrode:

$$E_p = 1128.3 - 58.73\ \text{pH};\ r = 0.975 \text{ for GC (between pH 2.0 and 7.0)}$$

The slope of this equation is found as 58.74 mV/pH for GC electrode. This slope being close to the expected critical value of 59 mV/pH indicates that the number of electrons and protons involved in the oxidation of BEN are equal [7].

The study of influence of pH on peak currents was also carried out to determine the pH value for the maximum signal for both electrodes. Plots of pH vs. I_p and the experimental results for both electrodes showed that shapes of the curves and maximum peak currents were sharper, better in 0.5 M H_2SO_4 (Figure was not shown). The main peak appeared as a single response and became sharper without showing any shoulder using this supporting electrolyte. For this reason, 0.5 M H_2SO_4 with 50% constant amount of acetonitrile was chosen for the analytical studies.

Tafel analysis of voltammograms from the oxidation of 1×10^{-4} M BEN (at a scan rate of 5 mV s^{-1}) was conducted in 0.5 M H_2SO_4. The αn value of the anodic oxidation reaction corresponding to the oxidation peak was obtained using Tafel plot ($\log I$ vs. E_p). The value of 0.49 and 0.54 was obtained for GC and BDD electrodes, respectively. The intercepts for the $\log I = f(E)$ plot were obtained at −9.32 μA and −10.48 μA for GC and BDD electrodes, respectively. The exchange current densities were $I_0 = 4.84 \times 10^{-10}$ μA cm^{-2} for GC and 3.30×10^{-11} μA cm^{-2} for BDD electrodes. These values together with the absence of any cathodic response within the necessary potential ranges for reversible systems in CV (Fig. 1) confirmed the irreversibility of the oxidation process on both carbon-based electrodes.

When the logarithm of current at a potential of about +0.97 V for DPV and +0.99 V for SWV using GC and +1.05 V for DPV and +1.09 V for SWV using BDD electrodes was plotted against the logarithm of BEN in the concentration range of 3.25–54.20 μg mL^{-1} for GC and 1.08–54.20 μg mL^{-1} for BDD electrodes, in 0.5 M H_2SO_4 linear relationships were obtained. These equations were reported as follows:

$$\log I_p\,(\mu A) = 5.19 + 0.41 \log C(M)\ (r = 0.987;\ \text{DPV})$$

$$\log I_p\,(\mu A) = 4.72 + 0.24 \log C(M)\ (r = 0.983;\ \text{SWV}) \text{ for GCE}$$

$$\log I_p\,(\mu A) = 1.69 + 0.45 \log C(M)\ (r = 0.920;\ \text{DPV})$$

$$\log I_p\,(\mu A) = 1.21 + 0.32 \log C(M) (r = 0.956;\ \text{SWV}) \text{ for BDDE.}$$

The slopes of these equations give reaction order. These kinetic parameters and calculated reaction orders indicated that a mechanism due to the surface events could be proposed, and that the reactions seem to be first order.

The BEN molecule is extensively metabolized in vivo [1,2]. CV is the most suitable technique for investigating the redox behavior of the drug compounds which can give insights into its metabolic fate [7,22]. CV curves from the redox properties of drug active compounds [23–25] might have profound effects on the understanding of the redox mechanism related to the activity of BEN. Therefore, electrochemistry may be of value in the study of enzyme reactions in biological systems. BEN was compared with some selected compounds containing dihydropyridine or piperidine moieties to identify the grouping responsible for the oxidation. Even though the exact oxidation mechanism was not determined, some conclusions about the potentially electroactive centers under working conditions could be reached. In some cases, it has been suggested that the electrode mechanisms might mimic enzyme reactions.

The anodic oxidative behavior of BEN was comparable to those of 1–4 dihydropyridine and piperidine oxidations that were reported in our previous studies and in the literature [26,27]. To support the working hypothesis that 1–4 dihydropyridine (similar to nifedipine, lacidipine, amlodipine, lercanidipine oxidation step) and the piperidine groups (similar oxidation pathway pimozide, haloperidol, droperidol and sertindole) of BEN undergo oxidation, behavior of the first anodic peak I_{p1} (related to the 1–4 dihydropyridine moiety) and the second anodic peak I_{p2} (related to the piperidine moiety) of BEN was compared to some model compounds. 1–4 dihydropyridine oxidation response was found sharper and easier to measure for the determination of BEN than the piperidine oxidation step. Because of the bonded nitrogen atom of piperidine ring, oxidative response occurred with a small response and hence, it was assumed that the 1–4 dihydropyridine ring oxidation response was hindered in more acidic pH values. At pH > 5.0, both responses were more clearly obtained using GC electrode. However, in some supporting electrolytes these responses were obtained individually at pH < 5.0 (Fig. 1). This was due to the kinds of cations/anions, nature, composition, and concentration of the supporting electrolyte used. Comparative studies on selected model compounds were achieved by CV as a function of pH in order to identify the oxidation processes of BEN. Considering our results on BEN and the position of the break on the E_p vs. pH plot for the first process of BEN which is obtained at about pH 7.0, and bearing in mind the electrochemical behavior of 1–4 dihydropyridine moiety in BEN molecule at GC and BDD electrodes, we may assume that the first oxidation process is located on the nitrogen atom moiety [26,27] in the molecule similar to the peaks observed for the model compound. According to our results on BEN molecule, the main oxidation response (I_{p1}) of BEN is related with the 1–4 dihydropyridine ring which can undergo $2e^-$, $2H^+$ oxidation to generate the corresponding pyridine derivative as shown in Scheme 1 ox_1 pathway [26,27] and seems to be irreversible. Droperidol, benperidol, pimozide, haloperidol, sertindole, clonixin [23,24,28]

contain piperidine group in its chemical structure and we suggest that the second anodic reaction could be attributed to the oxidation of the nitrogen atom on the piperidine moiety (Scheme 1 ox_2 pathway) [28].

Our results on model compounds confirm that the electroactive centers corresponding to the I_{p1} and I_{p2} peaks were the nitrogen atom on the 1–4 dihydropyridine and piperidine moiety of the molecule, respectively.

3.2. Determination of dissociation constant (pK_a)

Before developing methods with LC, it is generally important to know various physico-chemical parameters, such as pK_a, solubility, and maximum wavelength, of pharmaceutically active compounds. The knowledge of pK_a value is more important than other parameters due to the absorption, evaluation and bioavailability of drugs in the body. The ionization value helps in selecting the pH of the buffer to be used in the mobile phase [9–11].

As can be seen from Scheme 1, BEN is a weak monoprotic base. In this study, the retention factors were determined for each mobile phase composition and pH studied. For this purpose, the effect of the pH of the mobile phase on the retention factors (k) was investigated and necessary values of BEN were calculated using NLREG 4.0 software from k/pH [18]. Typical sigmoidal curve was obtained for BEN. The obtained values of retention factors for the neutral and ionic forms of BEN in 50–65% (v/v) acetonitrile calculated by NLREG program in several acetonitrile:water mixtures are given in Table 1. This table also gives the pK_a values reported in the literature [21], together with those predicted by the program ACD Lab [29] and SPARC [30]. ACD Lab/pK_a is a software program that calculates accurate acid–base ionization constants under 25 °C and zero ionic strength conditions in aqueous solutions for almost any organic structure.

BEN has mainly three functional groups namely the nitro group, the secondary amine of the dihydropyridine ring and tertiary amine forming in the piperidine ring. The pK_a value of BEN was calculated as 7.34 by potentiometric method in a paper [21] where the detailed solvent system, temperature, ionic strength, etc. were not given. These types of parameters are critical because of their effectness on the resulting values. Thus, pK_a values in Table 1 agree in some instances with the values reported but in other cases are quite different due to the use of different methods and different solvents [15–17]. When the nitrogen group is deprotonated, there is no change in the number of charges involved in the process because the change is from a positively charged species to a neutral one and hydrogen ion is generated in the reaction. Therefore, a change in the polarity of the medium has a minor influence on the isoelectric dissociation reaction, which depends only on the solution of the different species by the solvent of the mixture.

All of the pK_a values which are obtained from LC and electroanalytical methods, SPARC and ACD-Lab programs and literature are in good agreement.

3.3. Assay methods for BEN

According to the obtained results by electrochemical and RP-LC studies, it was possible to apply these techniques to the quantitative analysis of BEN. Several pH values, supporting electrolytes, mobile phase composition were tested for obtaining the better peak shape, peak current and sharp response for both electroanalytical and RP-LC methods. Compounds like BEN could have problems, such as distorted peak shape, presence of peaks with shoulder, and long retention times. The selected IS (indapamide) is a different compound from BEN. Indapamide showed a shorter retention time with better peak shape and better resolution than those of BEN and other potential ISs, such as tested lacidipine, nifedipine,

Table 1
The pK_a values and the retention factors of benidipine in acetonitrile–water mixtures.

50% ACN			55% ACN			60% ACN			65% ACN			ACD Lab	SPARC
NLREG pK_a	K_{BH^+}	K_B	NLREG pK_a	K_{BH^+}	K_B	NLREG pK_a	K_{BH^+}	K_B	NLREG pK_a	K_{BH^+}	K_B		
6.989 ± 0.027	0.910 ± 0.106	21.770 ± 0.354	6.894 ± 0.037	0.664 ± 0.072	10.754 ± 0.227	6.801 ± 0.021	0.410 ± 0.025	6.254 ± 0.072	6.739 ± 0.031	0.251 ± 0.021	3.609 ± 0.059	7.34	7.90

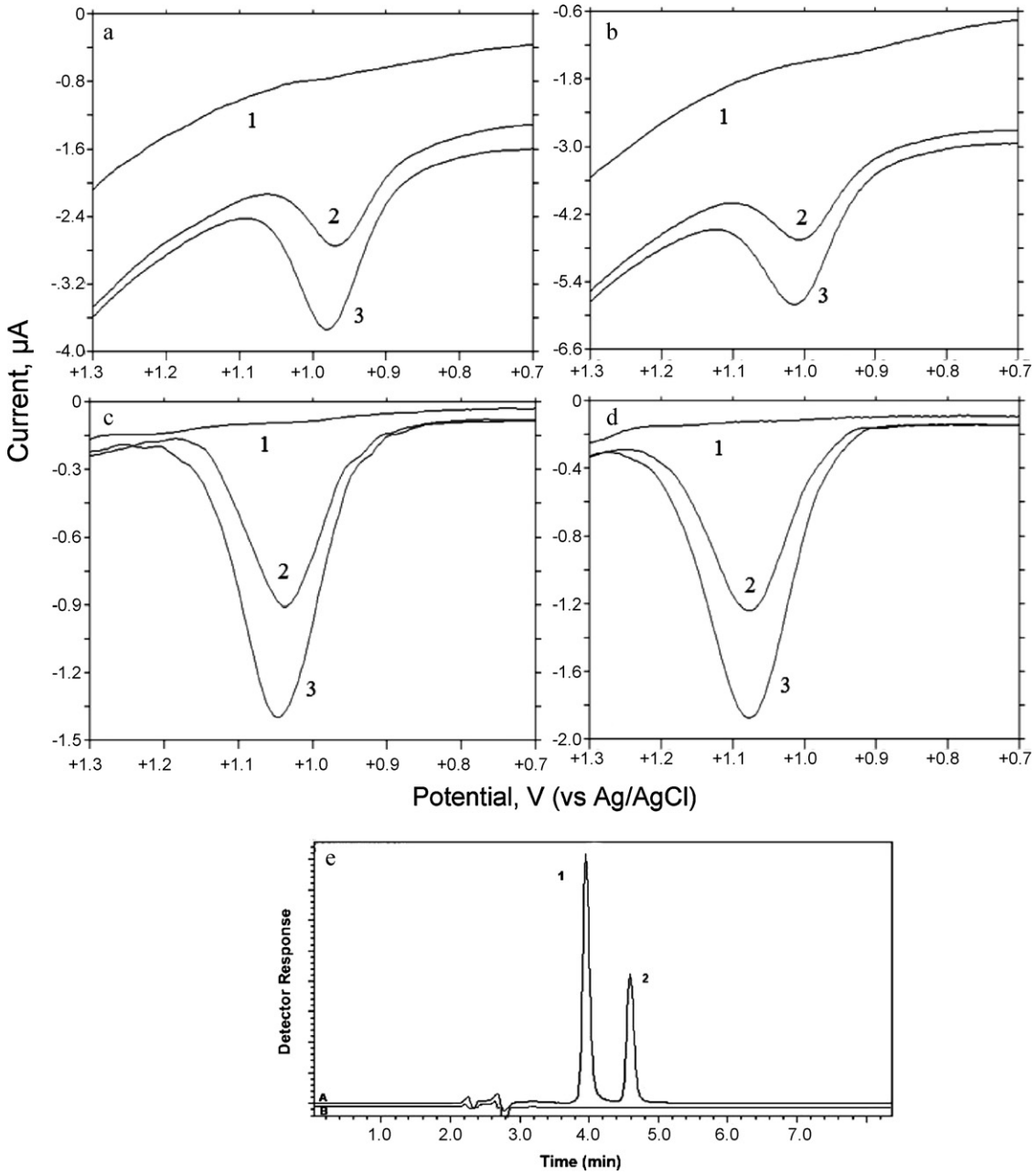

Fig. 2. DPV (a and c) and SWV (b and d) obtained for the determination of BEN using GC (a and b) and BDD (c and d) electrodes. (1) Supporting electrolyte; (2) 6×10^{-5} M and (3) 1×10^{-4} M BEN in 0.5 M H_2SO_4 solution with constant amount acetonitrile (50%). And (e) Typical LC chromatograms of pharmaceutical dosage form (A) of 4.0 μg mL^{-1} BEN (1) and 2.0 μg mL^{-1} IS (2) and mobile phase (B). Experimental conditions as in chromatographic procedure.

hydrochlorothiazide. The concentration of IS was maintained at a constant level of 2.0 μg mL^{-1}. Ionized strong bases can cause additional detrimental interactions in RP-LC separations hence 0.5 M H_2SO_4 (containing 50% acetonitrile) solution for electroanalytical techniques and 55% acetonitrile:water; v/v adjusted to pH 3.0 with 15 mM H_3PO_4 solution for RP-LC method were selected as the working medium. The column temperature was set at 25 °C.

In order to develop a voltammetric methodology for determining BEN, DPV and SWV methods were chosen. For these voltammetric studies, the effects of amount of acetonitrile on the peak current and potential were studied. As expected, the peak current decreased with changing ionic strength and viscosity of the medium. Some solubility problems occurred for high concentration of BEN when less than 50% acetonitrile was used. For analytical purposes, best response (with regard to peak current sensitivity, morphology, reproducibility and solubility) was obtained with 50% constant amount of acetonitrile in 0.5 M H_2SO_4 for both electrodes and methods. Under the chosen experimental conditions, the variation of peak current with increasing concentrations of BEN was analyzed by means of DPV and SWV for both electrodes (Fig. 2a–d). Good correlations were obtained for concentration values between 3.25 and 54.20 μg mL^{-1} for GC and 1.08 and 54.20 μg mL^{-1} for BDD electrodes for both techniques. The characteristics of the calibration equations and the related validation parameters are summarized in Table 2. The LOD and LOQ parameters were calculated according to the 3 s/m and 10 s/m criterions, respectively, where *s* is the standard deviation of the peak currents (five runs) and *m* is the slope of related calibration graph [12–14,25]. The precision and sensitivity of the proposed methods can easily be established from the low value of standard error (SE) of slope and intercept, LOD and LOQ

Table 2
Regression data of the calibration lines for quantitative determination of BEN by DPV and SWV for GC and BDD electrodes.

	GC		BDD		HPLC-UV method
	DPV	SWV	DPV	SWV	
Measured potential (V)/retention time (min)	1.092	1.112	1016	1044	3.947
Linearity range ($\mu g\,mL^{-1}$)	3.25–54.20	3.25–54.20	1.08–54.20	1.08–54.20	0.25–15.00
Slope	0.0296	0.036	0.025	0.032	0.416
Intercept	−0.057	−0.071	0.055	0.019	−0.016
Correlation coefficient	0.999	0.999	0.999	0.999	0.999
S.E. of slope ($\times 10^{-3}$)	0.300	0.700	0.400	0.300	4.000
S.E. of intercept ($\times 10^{-2}$)	0.910	1.900	0.930	0.850	2.500
LOD ($\mu g\,mL^{-1}$)	0.030	0.041	0.322	0.328	0.022
LOQ ($\mu g\,mL^{-1}$)	0.091	0.126	0.975	0.995	0.067
Repeatability of peak current/peak area (R.S.D.%)[a]	0.126	0.092	0.695	0.459	0.139
Repeatability of peak potential/retention time (R.S.D.%)[a]	0.340	0.393	0.705	0.475	0.058
Reproducibility of peak current/peak area (R.S.D.%)[a]	0.164	1.735	1.719	0.694	0.278
Reproducibility of peak potential/retention time (R.S.D.%)[a]	0.617	0.511	0.944	0.571	0.067

[a] Obtained from five experiments.

values and the greater value than 0.999 of correlation coefficient values.

On the other hand, with the RP-LC method different mobile phase compositions and ratios were employed for developing an efficient and reproducible result. The best resolution and peak shape was obtained by XTerra, C-18 (250 × 4.60 mm ID × 5 μm) column at 25 °C. This column has extended pH stability, is thermally more stable, and more efficient than the classical silica-based packing. The influence of pH on the mobile phase was examined in order to optimize the chromatographic conditions for RP-LC determination of BEN and IS. 238 nm wavelength was selected for the detection since it has a greater sensitivity and linearity than the others.

The precision and accuracy can be enhanced by the use of an appropriate IS, which also serves to correct fluctuations in the detector response. Generally sample preparation steps including reaction, filtration, precipitation, extraction or evaporation may cause unexpected results because of the sample losses. A properly chosen IS can be used to compensate for these sample losses when added prior to sample preparation. In this study indapamide was chosen as the IS because its peak showed a shorter retention time with a better peak shape and better resolution than those of the investigated compound and other potential ISs. After determining the optimum conditions, a satisfactory resolution and response were obtained in a short analysis time (5 min). The retention times of BEN and IS were 3.95 and 4.60 min, respectively (Fig. 2e).

The system suitability parameters have also been calculated for this system. Tailing factors and theoretical plate numbers were obtained as 1.206 and 6247 for BEN and 1.174 and 7873 for IS, respectively. Selectivity factor and resolution were 1.416 and 3.121, respectively, for this system. All obtained results are confirmed by the USP requirements for the system suitability tests.

The linearity was calculated by plotting the peak area ratio of BEN to IS vs. concentration of the compound in the range between 0.25 and 15 $\mu g\,mL^{-1}$. The developed RP-LC method was also validated according to the standard procedures [12–14,25] and the results were reported in Table 2 with the electroanalytical results.

The stability of reference substances and sample solutions was compared by analyzing prepared standard solution of BEN stored at +4 °C in the dark with freshly prepared sample using both electroanalytical and RP-LC methods. The results demonstrated that the working reference solutions were stable for at least 72 h.

The adequacy of the developed methods was evaluated by quantifying BEN in tablet dosage forms (labeled values 4.0 mg). Both electroanalytical and RP-LC methods can be used for the assay of BEN without prior separation of the excipients. The concentration of BEN determined in tablets using the proposed methods is reported in Table 3. The mean results for the determination of BEN using both electroanalytical and RP-LC methods were found very close to the declared value of 4.0 mg. The obtained results showed that the proposed methods could be applied with great success to BEN assay in tablets without any interference (Table 3).

For checking the accuracy, precision, and selectivity of the electroanalytical and RP-LC proposed methods and in order to know whether the excipients in tablets show any interference with the analysis, the recovery studies were evaluated after addition of known amounts of raw material of BEN. The obtained results from recovery studies indicated the absence of interference from commonly encountered pharmaceutical excipients and proved that the proposed methods had adequate precision and accuracy (Table 3).

Table 3
The results for the determination of BEN from dosage form and recovery experiments achieved by GC and BDD electrodes.

Parameters	GC		BDD		HPLC
	DPV	SWV	DPV	SWV	
Labeled claim (mg)	4.000	4.000	4.000	4.000	4.000
Amount found[a] (mg)	4.003	4.047	3.998	3.989	4.009
R.S.D.%	0.642	0.911	0.254	0.584	0.493
Bias %	−0.075	−1.175	0.300	0.275	−0.225
t_{value}	0.598	0.186	0.299	0.210	$t_{theoretical}$: 2.31
F_{value}	0.632	0.259	0.222	0.767	$F_{theoretical}$: 3.79
Added (mg)	4.000	4.000	4.000	4.000	4.000
Found[a] (mg)	3.987	3.995	4.003	4.036	4.001
Average recovered (%)	99.68	99.86	100.08	100.92	100.03
R.S.D.% of recovery	0.463	0.318	0.956	0.763	0.394
Bias %	0.325	0.125	−0.080	−0.920	−0.030

[a] Obtained from five experiments.

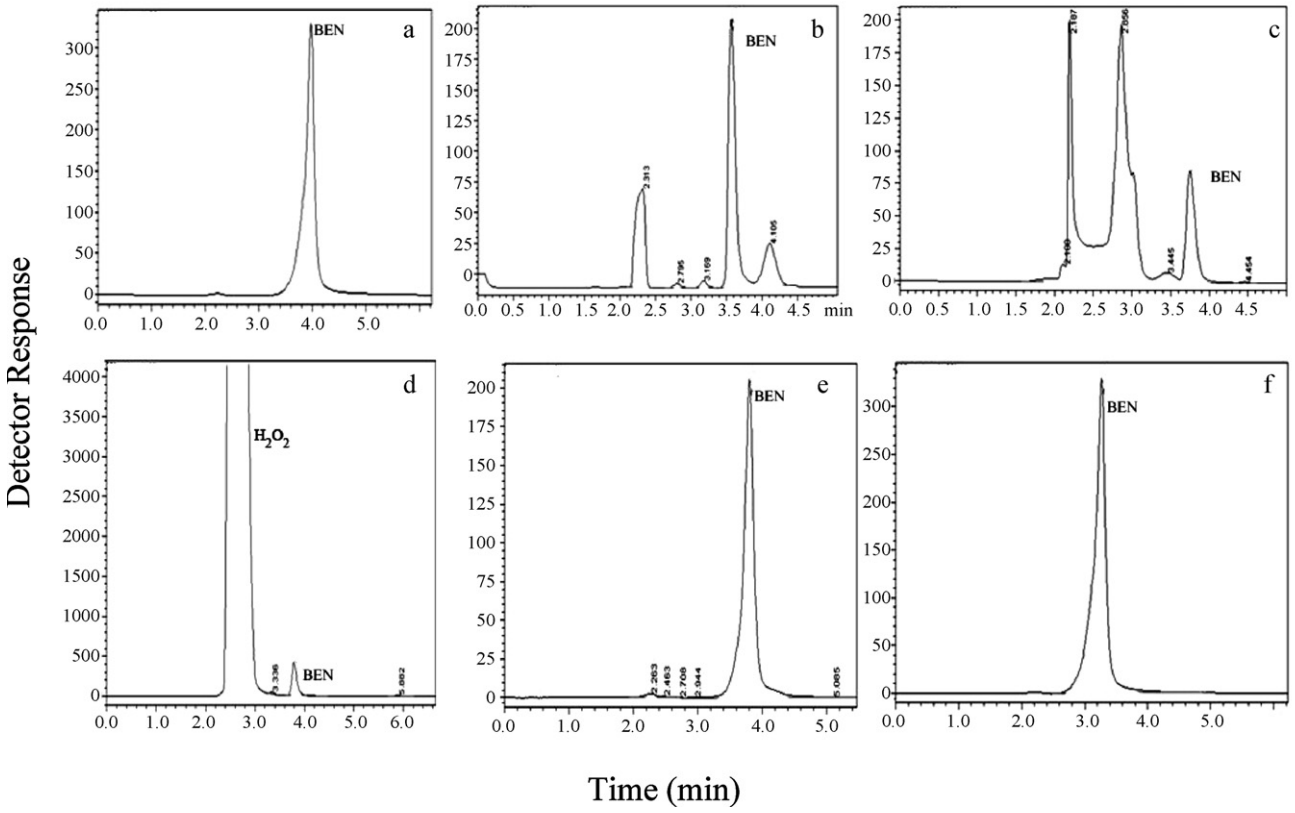

Fig. 3. Typical LC chromatograms of pure bulk sample of 100 μg mL^{-1} BEN (a) and drastic stressed conditions of samples: (b) 1 N HCl at 80 °C after 30 min; (c) 1 N NaOH at 80 °C after 30 min; (d) H_2O_2 30% at 80 °C after 30 min; (e) in UV light (254 nm) after 24 h; (f) at 100 °C after 24 h.

The precision value around the mean value should not exceed 5% of the RSD% [12–14,25].

To the best of our knowledge, no official or literature method is described related to the BEN analysis in tablets. For this reason, both electroanalytical and RP-LC methods were compared with each other using student-*t* and *F*-tests. At 95% of the confidence level, the values of *t*- and *F*-tests (calculated from experiments) were less than that of theoretical *t* and *F* values showing that there were no significant differences between the performances of both methods.

3.4. Specificity and stress-degradation studies

Stress-degradation studies of the drug substances can help identify the possible degradation products, which can in turn help establish the degradation pathways and the intrinsic stability of the molecule and validate the stability indicating power of the analytical procedures used. The specificity of the developed RP-LC method for BEN was assayed in the presence of its pharmaceutical formulations and degradation products. Generally, voltammetric methods do not enable separation of the degradation products and the main compounds. For this reason only RP-LC method was reported for the specificity studies. The chromatograms of BEN, after being subjected to different degradation conditions, were compared with blank solutions injected in a similar manner and with recently prepared solution. Degradation peaks for BEN were separated from the main response.

The results of specificity work using stress-testing studies in addition to that of monitoring standard solutions of BEN in the presence of its degradation products indicated a high degree of specificity of this method for BEN. The degradation product of the parent compound was found to be similar for both mild and drastic stress conditions. Typical chromatograms obtained following the assay of untreated standard samples and stressed samples using mild (not shown) and drastic conditions are shown in Fig. 3b–f. Possible degradation products were observed for the stressed samples of BEN that were subjected to light, oxidation, heat, acid and base hydrolysis. Some unknown degradation products of BEN were observed at acidic, basic and oxidation with H_2O_2 conditions (Table 4), especially when they were drastic (Fig. 3b–d). BEN was stable when exposed to UV light (254 nm) for 6 h and at 100 °C for 24 h. However, the retention time was shifted and peak became broader than the peak of the pure compound using UV-light stress conditions. Peak purity test results derived from DAD confirmed that the peak of BEN is homogenous and pure in nearly all analyzed stress samples except the ones under basic hydrolysis and oxidation with H_2O_2 conditions. The response of BEN was successfully resolved from those of the degradation products with the proposed RP-LC method, as shown in Fig. 3. The percentages of degraded compound amounts were reported in Table 4.

Table 4
The results of hydrolytic, oxidizing, thermal and photolytic hard stress conditions of drug.

The response of stress conditions	% Degradation of BEN
HCl (0.5 M)	9.10
HCl (1 M)	43.94
NaOH (0.5 M)	66.95
NaOH (1 M)	81.81
H_2O_2 (3%)	11.36
H_2O_2 (30%)	13.22
UV (6 h)	2.12
UV (24 h)	28.13
Heating (75 °C 24 h)	–
Heating (100 °C 24 h)	2.11

Each value is the mean of three experiments.

4. Conclusion

The electrochemical behavior and the determination of BEN in pharmaceutical dosage form were examined for the first time with this study. The anodic behavior of BEN at both GC and BDD electrodes was investigated in detail so that it could be used for analytical purposes, particularly as a sensor. The obtained results may possibly clarify and aid in understanding oxidation pathways of BEN. The electrooxidation processes of BEN on carbon-based electrodes are irreversible and diffusion controlled at all studied pH values in chosen supporting electrolytes.

The analytical results obtained from tablets using electroanalytical methods are in good agreement with those obtained by the RP-LC method. Both of the developed methods provide a sensitive, simple, rapid, experimentally convenient, cost-effective and high-throughout approach for the determination of BEN in pharmaceutical dosage form without the necessity of sample pretreatment, or any time-consuming evaporation or extraction steps prior to analysis. The amount of BEN can be determined within about 2 min after setting to instrument parameters.

The developed RP-LC method might serve as a versatile analytical tool suitable for the assay of BEN and interest quality control and therapeutic drug monitoring laboratories. The electroanalytical information and the obtained data might be used for the development of a RP-LC method with an electrochemical detection system.

This study presents a first study dealing with the determination of pK_a value of BEN by RP-LC method in acetonitrile:water binary mixtures. The lipophilicity, solubility and permeability of drug compounds are pK_a dependent. The pK_a value can also affect drug-receptor binding. Therefore pK_a value of BEN was determined and reported. The results of stress testing undertaken according to the ICH (International Conference on Harmonization) guidelines reveal that the method is selective, specific and stability indicating [13,19]. The proposed method has the ability to separate these drugs from their degradation products and related substances. The proposed RP-LC method can also be used for the routine and stability-indicating analysis of production samples and to check the stability of bulk samples of BEN.

References

[1] S.C. Sweetman (Ed.), Martindale, The Extra Pharmacopoeia, 35th ed., Pharmaceutical Press, London, 2007.
[2] K.D. Sanborn, Physicians Desk Reference (PDR), 61st ed., Medical Economics Co., Montvale, NJ, 2007.
[3] H. Magara, H. Kobayashi, S. Kobayashi, Determination of benidipine in human plasma by capillary column gas chromatography-negative chemical ionization mass spectrophotometry, J. Chromatogr. B 617 (1993) 59–63.
[4] Y. Uji, T. Sugimoto, S. Kobayashi, H. Kobayashi, Phase I clinical study of benidipine hydrochloride, Jpn. Pharm. Ther. 18 (1990) 7–20.
[5] H. Kobayashi, S. Kobayashi, A. Inoue, T. Oka, N. Nakamizo, Identification of benidipine hydrochloride metabolites in rats and dogs, Arzneimittel-Forschung/Drug Res. 38 (1988) 1730–1733.
[6] W. Kang, H.-Y. Yun, K.-H. Liu, K.-I. Kwon, J.-G. Shin, Analysis of benidipine enantiomers in human plasma by liquid chromatography–mass spectrometry using a macrocyclic antibiotic (vancomycin) chiral stationary phase column, J. Chromatogr. B 805 (2004) 311–314.
[7] J. Wang, Electroanalytical Techniques in Clinical Chemistry and Laboratory Medicine, VCH, New York, 1988.
[8] D. Kul, M. Gumustas, B. Uslu, S.A. Ozkan, Electroanalytical characteristics of antipsychotic drug ziprasidone and its determination in pharmaceuticals and serum samples on solid electrodes, Talanta 82 (2010) 286–295.
[9] M. Gumustas, S. Şanlı, N. Şanlı, S.A. Ozkan, Determination of pK_a values of some antihypertensive drugs by liquid chromatography and simultaneous assay of lercanidipine and enalapril in their binary mixtures, Talanta 82 (2010) 1528–1537.
[10] C.F. Poole, S.K. Poole, Chromatography Today, Elsevier, Amsterdam, 1991.
[11] E.C. Demiralay, G. Alsancak, S.A. Ozkan, Determination of pK_a values of non-steroidal antiinflammatory drug-oxicams by RP-HPLC and their analysis in pharmaceutical dosage forms, J. Sep. Sci. 32 (2009) 2928–2936.
[12] J. Ermer, J.H. Miller, Method Validation in Pharmaceutical Analysis, 1st ed., Wiley-VCH Pub, Germany, 2005.
[13] ICH, Topic Q2A validation of analytical procedures, methodology, PMP/ICH/281/95.
[14] M. Gumustas, S.A. Ozkan, The role of and the place of method validation in drug analysis using electroanalytical techniques, Open Anal. Chem. J. 5 (2011) 1–21.
[15] I. Canals, J.A. Portal, E. Bosch, M. Rosés, Retention of ionizable compounds on HPLC. 4. Mobile-phase pH measurement in methanol/water, Anal. Chem. 72 (2000) 1802–1809.
[16] J. Barbosa, I. Marqués, D. Barrón, V. Sanz-Nebot, The application of factor analysis to solvatochromic parameters and pHs values for the standardization of potentiometric sensors in mobile phases used in liquid chromatography, Trends Anal. Chem. 18 (1999) 543–549.
[17] S. Espinosa, E. Bosch, M. Rosés, Retention of ionizable compounds on HPLC. 12. The properties of liquid chromatography buffers in acetonitrile–water mobile phases that influence HPLC retention, Anal. Chem. 74 (2002) 3809–3818.
[18] P.H. Sherrod, NLREG, Nonlinear Regression Analysis and Curve Fitting Program, 2007, http://www.nlreg.com.
[19] ICH, Stability testing of new drug substances and products (Q1AR), in: International Conference on Harmonization IFPMA, Geneva, 2000.
[20] E. Laviron, A multilayer model for the study of space distributed redox modified electrodes. Part I. Description and discussion of the model, J. Electroanal. Chem. 112 (1980) 1–9.
[21] H.G. Brittain, Profiles of Drug Substances, Excipients and Related Methodology, vol. 33, 1st ed., Elsevier Pub., 2007, p. 93.
[22] J.P. Hart, Electroanalysis of Biologically Important Compounds, Ellis Horwood, London, 1990.
[23] J. Grimshaw, Electrochemical Reactions, Mechanism in Organic Chemistry, Elsevier Sci. Pub. Inc., New York, 2000.
[24] H. Lund, O. Hammerich, Organic Electrochemistry, 4th ed., Marcel Dekker Inc. Pub., New York, 2001.
[25] S.A. Ozkan (Ed.), Electroanalytical Methods in Pharmaceutical Analysis and their Validation, HNB Publishing, New York, 2012.
[26] Z. Şentürk, S.A. Özkan, Y. Özkan, Electroanalytical study of nifedipine using activated glassy carbon electrode, J. Pharm. Biomed. Anal. 16 (1998) 801–807.
[27] B. Turovska, J. Stradins, I. Turovskis, A. Plotniece, A. Shmidlers, G. Duburs, Electrochemical oxidation of compounds containing 1,4-dihydropyridine and pyridinium rings – Analogs of gene transfection agents, Chem. Heterocycl. Compd. 40 (2004) 753–758.
[28] A. Álvarez-Lueje, J.C. Sturm, L.J. Núñez-Vergara, J. Carbajo, J.A. Squella, Voltammetric behaviour of clonixin and its differential pulse polarographic determination in tablets, Anal. Lett. 33 (2000) 53–68.
[29] ACD/Labs, Advanced Chemistry Development Inc., 90 Adelaide Street, West Toronto, Ontario, M5H3V9, Canada, http://www.acdlabs.com/ilab/.
[30] Sparc On-Line Calculator, http://ibmlc2.chem.uga.edu/Sparc.

Journal of Pharmaceutical and Biomedical Analysis 66 (2012) 126–135

Contents lists available at SciVerse ScienceDirect

Journal of Pharmaceutical and Biomedical Analysis

journal homepage: www.elsevier.com/locate/jpba

Analysis of counterfeit Cialis® tablets using Raman microscopy and multivariate curve resolution

Kaho Kwok, Lynne S. Taylor*

Department of Industrial and Physical Pharmacy, College of Pharmacy, Purdue University, 575 Stadium Mall Drive, West Lafayette, IN 47907, USA

ARTICLE INFO

Article history:
Received 24 October 2011
Received in revised form 12 March 2012
Accepted 14 March 2012
Available online 24 March 2012

Keywords:
Counterfeit
Raman
Multivariate curve resolution
Chemometrics
Excipient

ABSTRACT

Counterfeit medicines have become a serious global problem. Consequently, analytical and pharmaceutical scientists have been active in developing and applying new methodologies to detect and analyze counterfeit medicines. Vibrational spectroscopy combined with chemometric methods is becoming a popular choice in this area of research. In this study, Raman microscopy was used to collect chemical images of counterfeit tadalafil tablets and multivariate curve resolution (MCR) was used to analyze the Raman spectra and reveal the identities of the excipients and active pharmaceutical ingredients (API) in each tablet. Resolved counterfeit tablet spectra were compared to the resolved genuine tablet spectra. Both similarities and dissimilarities were revealed by the analysis in terms of the identity of the excipients, the quantity of the API, and the distribution of the components. It was concluded that Raman microscopy combined with MCR is a powerful method to detect and analyze counterfeit tablets.

© 2012 Elsevier B.V. All rights reserved.

1. Introduction

Counterfeit products have been present since ancient times; the famous Greek mathematician Archimedes proved that a gold crown made for King Hiero II contained elements other than gold. Counterfeiting remains a serious problem in the modern society and counterfeit products can be found in a wide range of consumer goods, including clothing, media products, food and even automobiles. It has been reported that even the National Aeronautic and Space Association (NASA) may have purchased counterfeit materials [1]. Counterfeit products have detrimental effects on the economy and the Organisation for Economic Co-operation and Development (OECD) has estimated that the monetary value of the international trade in counterfeit products approached 200 billion in 2005 [2].

The pharmaceutical industry has been highly targeted by counterfeiters in recent years. The World Health Organization (WHO) defines counterfeit medications as follows [3]: "Counterfeit medicines are medicines that are deliberately and fraudulently mislabeled with respect to identity and/or source. The use of counterfeit medicines can result in treatment failure or even death. Counterfeit medicines may include products with the correct ingredients or with the wrong ingredients, without active ingredients, with insufficient or too much active ingredient, or with fake packaging". Counterfeit drugs are part of the broader phenomenon of substandard medicines. The WHO defines substandard medicines as follows: "Substandard medicines (also called out of specification (OOS) medicines) are genuine medicines produced by manufacturers authorized by the National Medicines Regulatory Authority (NMRA) which do not meet quality specifications set for them by national standards". The difference between counterfeit and substandard medicines is that the former are produced by unauthorized manufacturers who intend to deliberately mislead the consumer with respect to the origin of the product [3]. Besides the economic consequences of counterfeit products, counterfeit medicines can negatively impact the health of the consumer with the worst possible outcome being death. For example, diethylene glycol (DEG) contamination of paracetamol syrup was responsible for approximately 192,000 deaths in 2002 in China [4].

The seriousness of the counterfeit problem has motivated analytical and pharmaceutical scientists to develop and implement a variety of analytical techniques for the detection and analysis of counterfeit medicines. Among them, separation techniques such as thin layer chromatography (TLC) [5], high performance liquid chromatography (HPLC) [6,7] and capillary electrophoresis (CE) [8] are still the more common methods, but spectroscopic and imaging methods such as direct ionization mass spectrometry [9], near-infrared (NIR) spectroscopy [10,11], Raman spectroscopy [12,13], and nuclear magnetic resonance (NMR) spectroscopy [14] have been developed as they provide information on the molecular structural level and spatial distribution of the active pharmaceutical ingredients (API) and excipients. Raman spectroscopy has gained popularity for counterfeit analysis recently [12,13] because

* Corresponding author. Tel.: +1 765 496 6614; fax: +1 765 494 6545.
E-mail addresses: lstaylor@purdue.edu, ltaylor@pharmacy.purdue.edu (L.S. Taylor).

0731-7085/$ – see front matter © 2012 Elsevier B.V. All rights reserved.
doi:10.1016/j.jpba.2012.03.026

minimal or no sample preparation is required and even closely related molecules typically display spectral uniqueness. Raman spectroscopy is particularly suitable for analyzing solid dosage forms and can be used to detect different solid state forms of an API such as polymorphs [15], hydrate versus anhydrate [16] or amorphous versus crystalline drug [17]. Raman spectroscopy can be combined with microscopy to analyze microscopic features of a sample. A small but highly focused laser spot can be generated with the use of a high power objective and used to probe local microscopic features of a sample surface. Subsequently, a chemical image or map of the sample can be obtained when a large number of these spots are sampled and the spatial distribution of the chemical components can be generated and studied. Such an approach is especially useful and applicable to the analysis of tablets [18].

Over the past decade, the field of chemometrics has advanced tremendously [19] and numerous applications have been demonstrated [19–22]. Multivariate curve resolution (MCR) is a chemometric method that involves resolving a multicomponent system into individual pure components. In general, the process of MCR includes the decomposition of a data matrix that contains the response of a multicomponent system into a product of two matrices that contain pure component information in the row and column directions of the original data matrix [23]:

$$D = C \cdot S^T + E \quad (1)$$

where D is the original data matrix, C and S^T are the pure component matrices containing information in the row and column directions respectively, and E is the error matrix containing information irrelevant to the system. When MCR is being applied to spectroscopic data, C and S^T are usually referred to as the relative concentrations and spectral profiles of the pure components respectively. In order to obtain the resolved components, a number of algorithms are available. One of these algorithms is alternating least squares (ALS). This is an iterative least square process used to minimize the least square errors of the C and S^T matrices simultaneously. This process continues until a pre-defined convergence criterion is reached. No prior information is needed for MCR-ALS, only an initial estimate of either C or S^T is required to start the calculation. Constraints are often implemented into the calculation to better describe the chemical system and avoid ambiguous results.

The objective of this study was to combine Raman microscopy and multivariate curve resolution for the analysis of and comparison between genuine and counterfeit Cialis® tablets. Cialis is a phosphodiesterase 5 (PDE5) inhibitor used to treat erectile dysfunction. Counterfeit Cialis tablets have been studied by Raman and NMR spectroscopy [24], HPLC and NIR spectroscopy [25], and mass spectrometry [26]. In this research, detection and analysis of the excipients used in the counterfeit tablets was of interest, emphasis will be placed on the resolving and the spatial distribution of the excipients and API.

2. Experimental

2.1. Materials

Genuine Cialis® tablets (20 mg) (Eli Lilly, Indianapolis, IN) were purchased from the Purdue University Pharmacy (West Lafayette, IN). Counterfeit Cialis® tablets were obtained from Eli Lilly and Company. There are 11 excipients and one active pharmaceutical ingredient (API) present in the real tablets. The API in Cialis® is tadalafil while 11 excipients are lactose monohydrate (LMH), croscarmellose sodium (CMS), hydroxypropylcellulose (HPC), microcrystalline cellulose (MCC), sodium lauryl sulfate (SLS), magnesium stearate (MgSt) (in tablet core), LMH, hypromellose (HPMC), triacetin, titanium (IV) oxide (TiO_2), talc, and iron oxide (in tablet coating). LMH, SLS, MgSt, and talc were obtained from Spectrum Chemicals (Gardena, CA). CMS and HPC were obtained from Ashland Inc. (Covington, KY). MCC was obtained from FMC Biopolymer (Philadelphia, PA). HPMC was obtained from the Dow Chemicals and Company (Midland, MI). Triacetin and TiO_2 were obtained from the Sigma Aldrich Company (St. Louis, MO). Calcium sulfate was obtained from Alfa Aesar (Ward Hill, MA). Corn starch (Argo, ACH Food Companies, Cordova, TN) was obtained from a local grocery store. Tadalafil was obtained by recrystallization following extraction from the genuine Cialis® tablets using the following procedure: The coating of three Cialis® tablets was removed using a razor blade. The uncoated tablets were ground into a fine powder using a mortar and pestle. 30 ml of ethanol was added to the powder, thoroughly mixed and insoluble material was allowed to settle by gravity overnight. The solution was filtered using filter paper (No. 1, Whatman, Maidstone, UK). The resultant solution was filtered again using a syringe filter (0.2 μm PTFE, VWR, Radnor, PA) to remove smaller particulates. The supernatant was collected and the solvent was evaporated under ambient conditions yielding tadalafil crystals.

2.2. Methods

Raman microscopy was performed using a Renishaw Raman microscope (Model 1000, Renishaw plc., Gloucestershire, UK). The laser wavelength was 783 nm and the laser power was tuned to 24.5 ± 1.5 mW. The microscope objective has a magnification of 50 (0.75 N.A.) and the laser spot was focused to approximately 2–3 μm in diameter. The mapping mode of the data acquisition software (WiRE 1.3, Renishaw plc.) was used to collect the spectra. A 200 μm × 200 μm area was sampled for each tablet. The motorized stage (Prior Scientific, Rockland, MA) was set to move in 10 μm increments and spectra were acquired at each increment. The coating of the tablets was removed prior to all mapping experiments. The collected spectral range was from 250 to 1700 cm^{-1}. A silicon wafer was used to calibrate the Raman shift (accurate to within ± 1 cm^{-1}) axis prior to each experiment. Experimental parameters are summarized in Table 1.

Several data pre-processing steps were taken before subjecting the spectra to MCR analysis. The raw spectra were normalized

Fig. 1. Photographs of Cialis® tablets. From left to right: genuine, counterfeit A, counterfeit B.

Table 1
Experimental parameters.

Laser wavelength (nm)	783
Laser power (mW)	24.5 ± 1.5
Objective power	50×
Laser spot size (μm)	2–3
Sampling area (μm)	200 × 200
Scanning range (cm^{-1})	250–1700
Software	Renishaw WiRE 1.3

by the mean of each spectrum. The normalized spectra were then subjected to cosmic ray removal using the algorithm suggested by Cappel et al. [27]. Baseline correction and smoothing were performed on the corrected spectra using the method proposed by Lieber and Mahadevan-Jansen [28] and the Savitzky–Golay method [29], respectively. For the baseline correction, a fifth order polynomial was used to generate the estimated baseline and a minimum correlation coefficient of 0.9999 between the most recent baseline and the previous estimated baseline was used as the convergence criterion. For the smoothing, a third degree polynomial and a nine data point window were used. Final spectra were obtained by truncating the spectra to approximately 300–1650 cm^{-1} range to remove erratic behavior at the spectral extremes due to baseline correction and smoothing. All data pre-processing steps were performed using MATLAB (Version R2010a, Mathworks, Natick, MA).

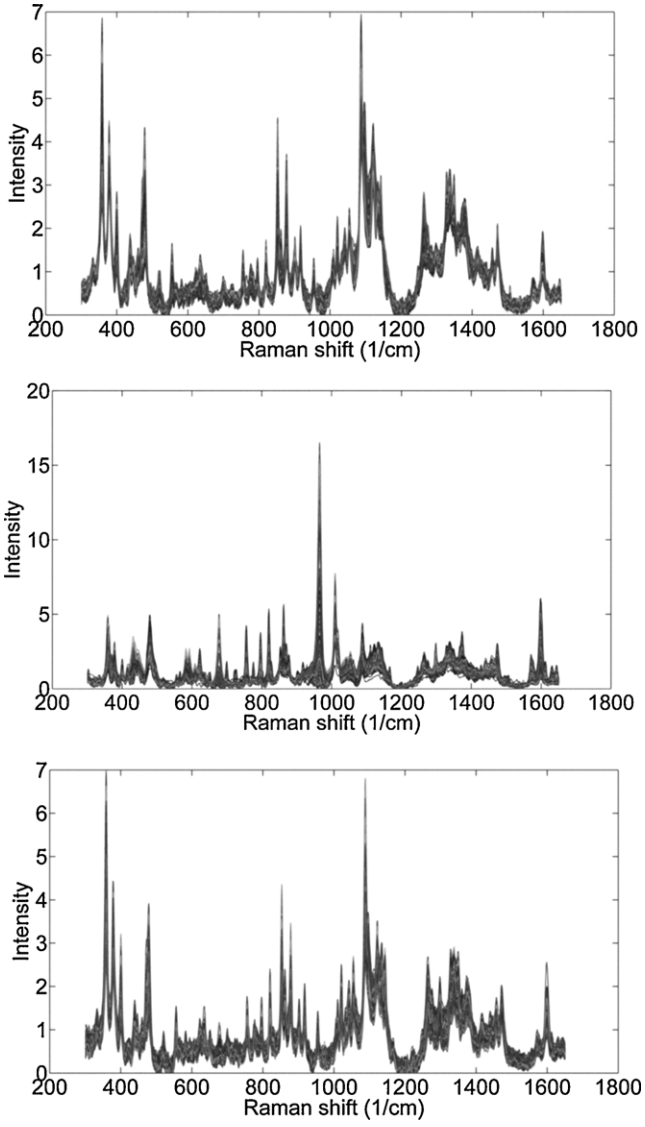

Fig. 2. Raman spectral sets from genuine tablet (top), counterfeit sample A (middle), and counterfeit sample B (bottom).

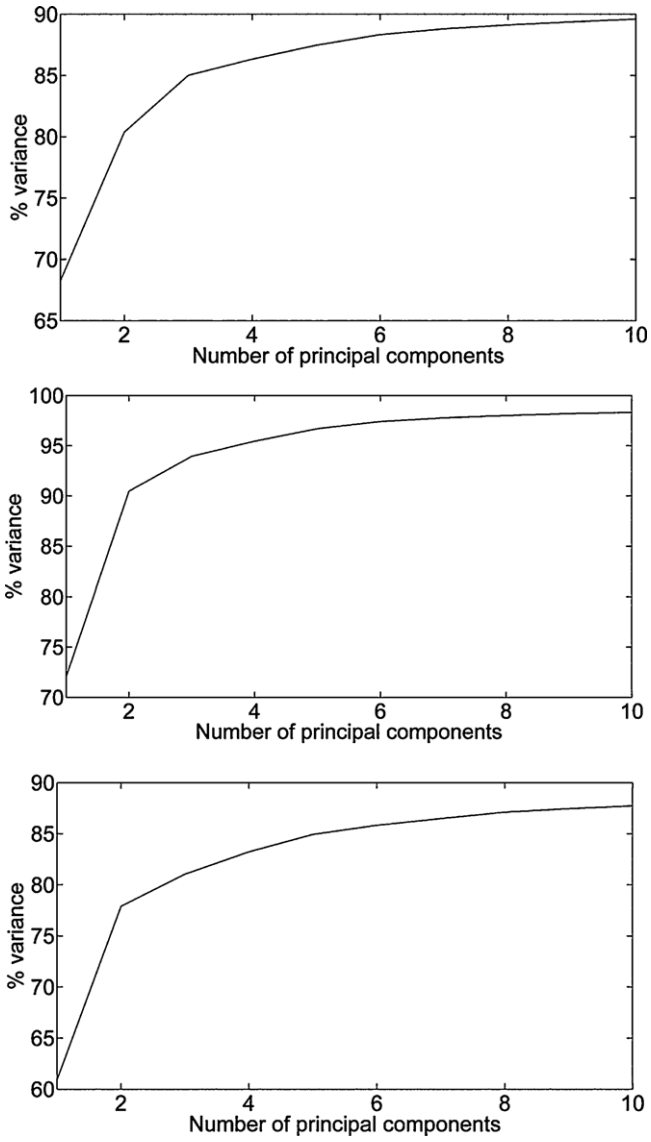

Fig. 3. Variance plots of genuine tablet data (top), counterfeit sample A data (middle), and counterfeit sample B data (bottom).

In order to estimate the number of pure components in each system, principal component analysis (PCA) and eigenstructure tracking analysis (ETA) were performed. PCA is an exploratory technique using eigenvectors to extract the significant variation of a multivariate data matrix. ETA is a modified PCA method that calculates the evolving eigenvalues for each principal component (PC) [30]. ETA was used as a complementary method to PCA to confirm the number of PCs. As mentioned in Section 1, constraints are usually required to obtain reasonable results in MCR. In this work, non-negativity for both spectra and concentration profiles and closure (total concentration is unity) were applied as the constraints in the MCR-ALS calculation. PCA and MCR were performed using Unscrambler (Version X, Camo, Woodbridge, NJ). The relative concentrations, C, of major components were obtained from the iterative least square process (ALS) which started with an estimate of the spectral matrix (S) and proceeded with the data matrix (D) as shown in Eq. (1). ETA was performed using MATLAB.

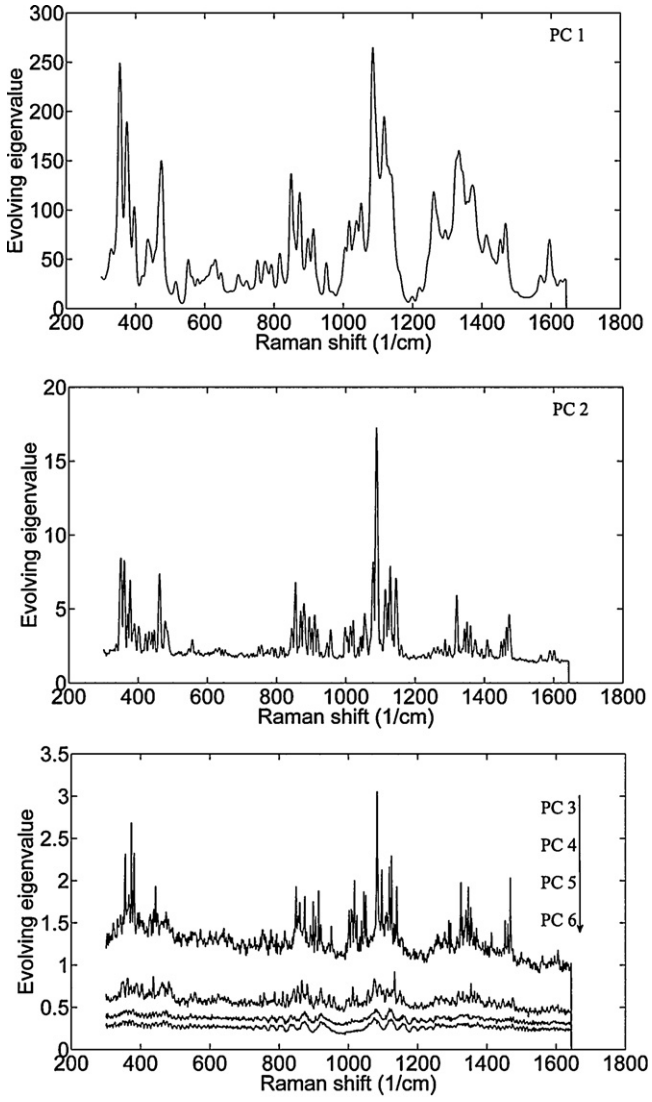

Fig. 4. ETA plots of genuine tablet data.

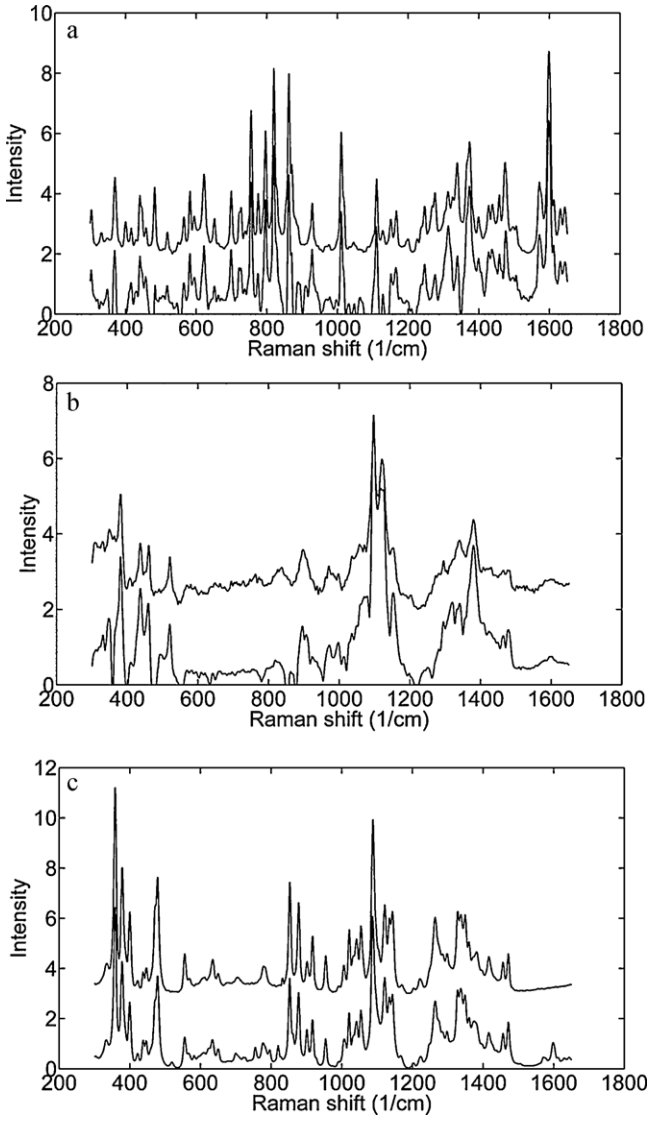

Fig. 5. Resolved spectra of genuine tablet data. The pure reference spectra were positively offset for clarity. (a) 1st component compared to tadalafil. (b) 2nd component compared to MCC. (c) 3rd component compared to lactose monohydrate.

3. Results and discussion

Genuine and two different counterfeit Cialis® tablets (Samples A and B) were analyzed. The photographs of these tablets are shown in Fig. 1. The genuine tablet is yellow with an almond shape and has the "C20" logo inscribed on one side of the tablet. The counterfeit tablets look very similar (size, shape, color, inscription) to the genuine tablets; it is rather difficult to distinguish between them using only appearance. However, the chemical details of these tablets were revealed by Raman microscopy and MCR-ALS.

3.1. Genuine tablets

The Raman spectra obtained from the genuine tablet are shown in Fig. 2. There are several recognizable peaks in the spectra. Several of the strongest peaks can be attributed to lactose monohydrate at 358, 378, 400 cm^{-1} (bending of the COC grouping [31]), and 1088 cm^{-1} (stretching of the COC grouping [31]), suggesting that lactose monohydrate is a major ingredient of this Cialis® formulation. An isolated peak at 1598 cm^{-1} arises from the API (stretching of the CC phenyl ring), with other API peaks located at 755 cm^{-1} and 820 cm^{-1}. Spectral features from many of the excipients cannot be found likely due to low concentrations while no TiO_2 or iron oxide peaks can be detected because these excipients are only present in the coating material of the tablet, which was removed prior to analysis.

The results of PCA can be summarized into a variance plot. A variance plot is the graphing of the percentage of the explained variance or accumulated eigenvalues versus the number of principal components. The more PCs utilized, the higher the % explained variance of the model. However, an optimum number of PCs often exists to describe the chemical system sought after and noise is modeled if too many PCs are used for the system. Therefore, it is important to determine the correct chemical rank or optimum number of PCs used to describe the system of interest. One way to determine the chemical rank is to use the variance plot. This plot for the spectra obtained from the genuine tablets is shown in Fig. 3. The optimum number of PCs is usually selected at the point where the curve of this plot starts to level off. In this case, 5–6 PCs (Fig. 3) appears to be optimal for this system. ETA is a chemometric method that relies on the evolving eigenvalues to determine the chemical rank of a multicomponent system. It has been used not only to determine the number of components in a system, but also can be used to reveal the noise pattern of a spectral profile [30,32].

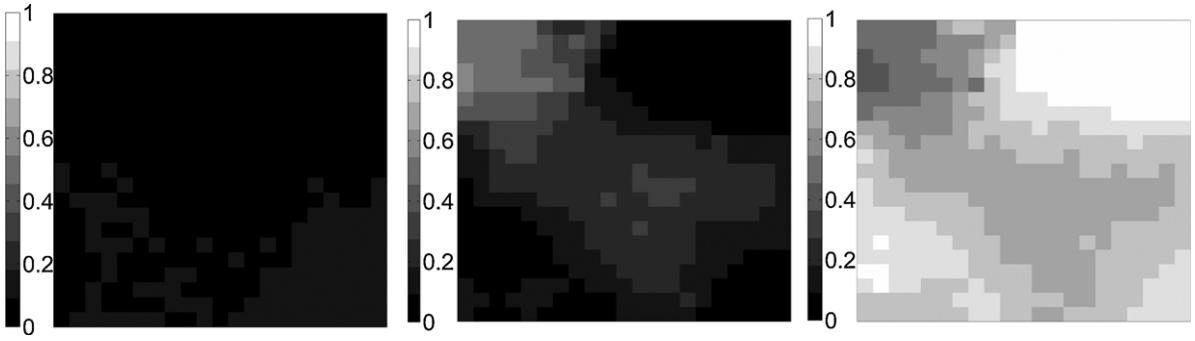

Fig. 6. Raman images of resolved components of the genuine tablet. From left to right: tadalafil, lactose monohydrate, MCC.

ETA is very similar to PCA as they both utilize a matrix decomposition technique called the singular value decomposition (SVD). However, ETA involves the division of the original data matrix into submatrices and SVD is applied to these submatrices to extract the evolving eigenvalues [30]. The evolving eigenvalues are then plotted against the independent variables (e.g. wavenumber), yielding an ETA plot which can be used for the examination of the eigenvalue structure and hence determination of the chemical rank. The ETA plots of the genuine tablet data are shown in Fig. 4. The ETA plots for the first four components show spectral features even though the noise level increases consistently from the first to the fourth component. The fifth and the sixth components show very little normal spectral features. Instead, these plots show more random noise and periodic fluctuations. Therefore, this analysis suggests that four components can be described in this system. However, MCR-ALS analysis revealed that only 3 components can be resolved for the genuine tablet spectra. The resolved spectra are shown in Fig. 5. The three resolved components are lactose monohydrate, MCC, and tadalafil. The resolved spectra compare well to the corresponding spectra of the pure components (Fig. 5). The correlation coefficients of the resolved spectra to their corresponding pure component spectra are all over 0.90. Despite the high correlations, there is some clear spectral mixing even in the resolved lactose monohydrate spectrum. For example, the tadalafil peaks at 1598 cm^{-1}, 820 cm^{-1}, and 755 cm^{-1} occur in this spectrum. This spectral mixing of the resolved component with another component is mainly due to the lack of selectivity of the sampling surface. The lack of selectivity arises when the sampling surface is highly homogeneous and/or the individual particle sizes are smaller comparing to the probing laser spot size. This suggests that the API is very homogeneously blended with the lactose in the tablet. Although there are 6 excipients and one API in the genuine tablet core, only two excipients and the API can be resolved by the MCR-ALS process. The reasons for this result include the lack of selectivity mentioned before and the fact that the relative concentrations of the undetected excipients are very low. The average relative concentrations of the resolved components are 77.4%, 16.8%, and 5.8% for lactose monohydrate, MCC, and tadalafil, respectively (Table 2). This implies that the relative concentrations of each undetected excipient are very likely much lower than 5%. The calculated API concentration is very close to the nominal concentration ($5.50 \pm 0.07\%$) calculated using the mass of three genuine tablets and the stated API content in each tablet (20 mg). The Raman images of the resolved components are shown in Fig. 6. The color of each pixel provides an indication of the relative concentration of the resolved component, based on the

Table 2
Average relative concentrations of the resolved components for each sample.

Component	Genuine (%)	Counterfeit A (%)	Counterfeit B (%)
1	5.8 (tadalafil)	4.4 (talc, SLS, MgSt)	2.2 (MCC)
2	16.8 (MCC)	19.5 (LMH, unknown)	5.8 (tadalafil)
3	77.4 (LMH)	20.3 (LMH)	73.1 (LMH)
4	NR[a]	23.9 (starch, $CaSO_4$)	3.6 (MgSt, MCC)
5	NR	24.2 (tadalafil)	1.6 (noise)
6	NR	7.7 (starch)	11.8 (tadalafil, MCC, MgSt)
7	NR	NR	1.4 (unknown)
8	NR	NR	0.5 (talc)

[a] Not relevant.

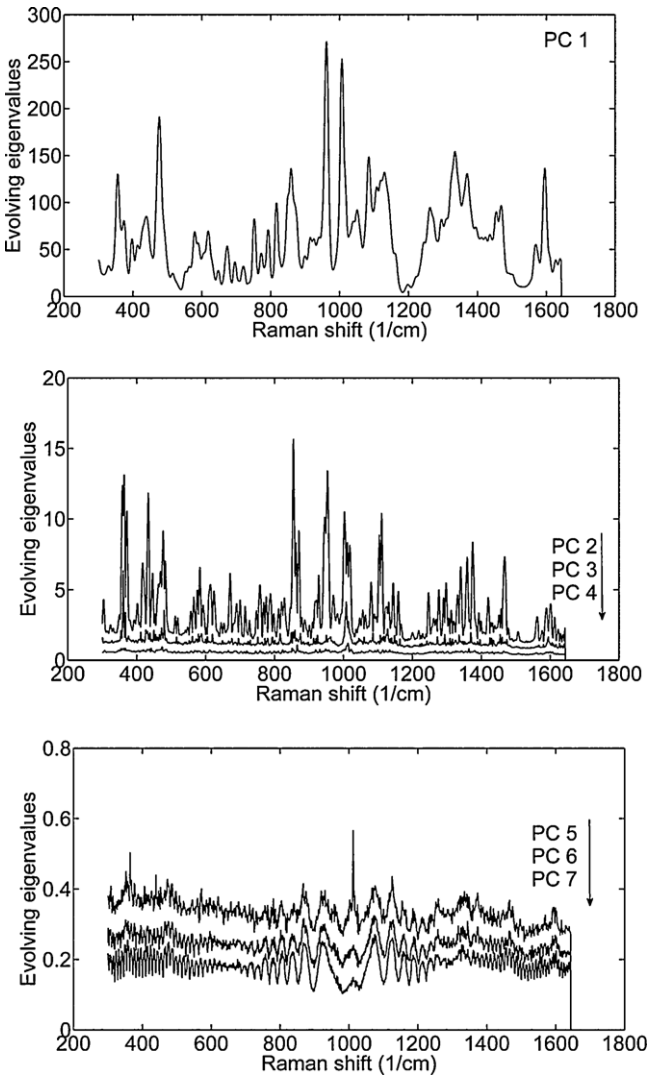

Fig. 7. ETA plots of counterfeit sample A.

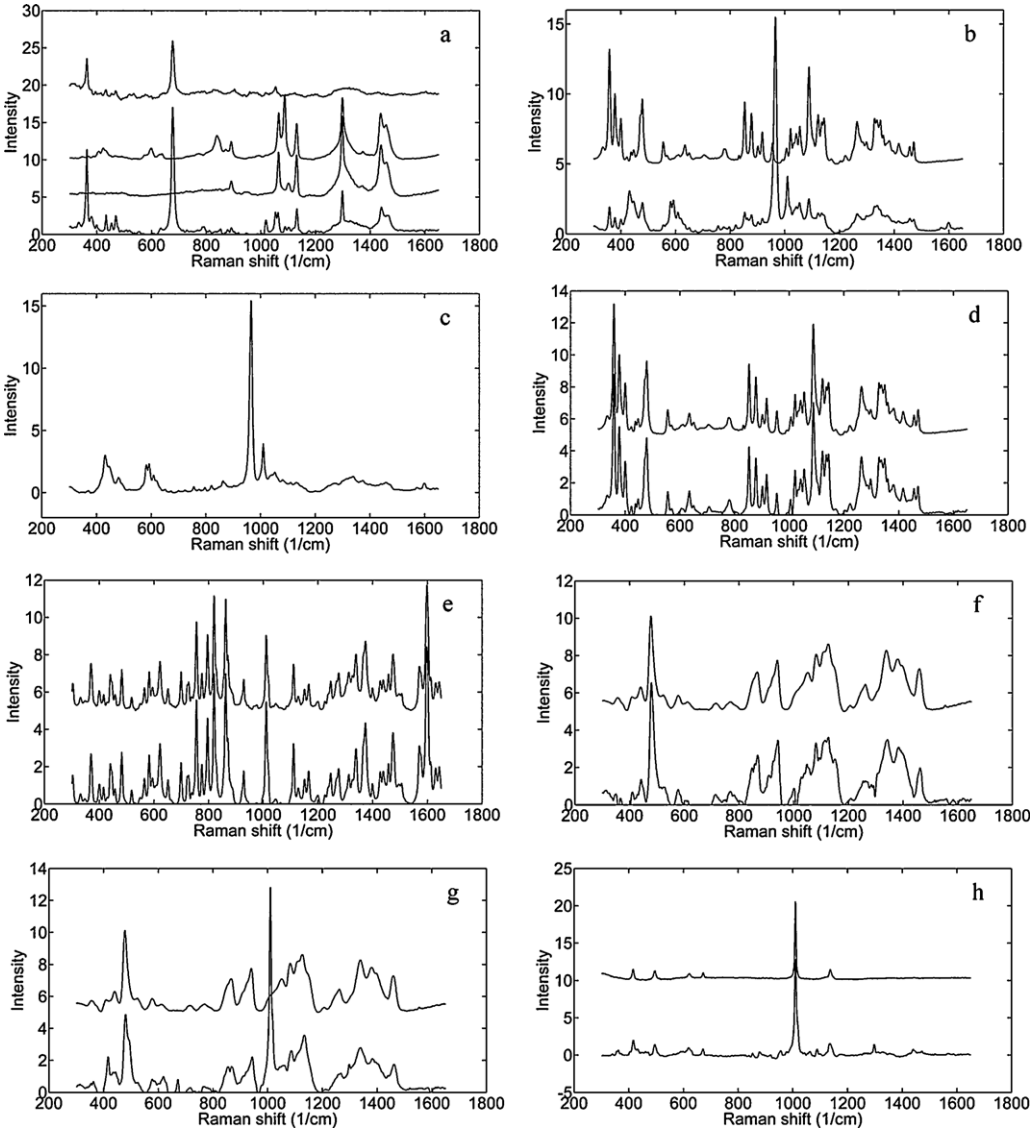

Fig. 8. Resolved spectra of counterfeit sample A. (a) 1st component compared to talc (top), SLS (second from top), and MgSt (second from bottom). (b) 2nd component compared to lactose monohydrate (top). (c) Corrected 2nd component. (d) 3rd component compared to lactose monohydrate (top). (e) 5th component compared to tadalafil (top). (f) 6th component compared to corn starch (top). (g) 4th component compared to corn starch (top). (h) Corrected 4th component compared to calcium sulfate (top).

scale shown with the images. The Raman images can often reveal information about the relative distribution of the resolved components. For example, the images of lactose monohydrate and MCC are very much negatively correlated. This implies that a region of the tablet that is rich in lactose monohydrate is deficient in MCC and vice versa.

3.2. Counterfeit tablets

3.2.1. Sample A

The Raman spectra of sample A are shown in Fig. 2. There are several peaks that are also found in the genuine tablet spectrum. Example peaks include the tadalafil peak at 1598 cm^{-1}, and the lactose monohydrate peaks at 358 cm^{-1}, 378 cm^{-1}, and 400 cm^{-1}. The relative magnitude of the API peak seems large in comparison to that observed for the genuine tablet spectra. This observation may suggest that there is a higher percentage of API in this counterfeit sample. However, there are also a number of new and unknown peaks in this spectral dataset. The most notable are the strong peaks located at 965 cm^{-1} and at 1010 cm^{-1}, neither of which is present in the genuine tablet spectra. In addition to these new and unknown peaks, there is also a larger variation in peaks among the spectra obtained at different locations than for the genuine tablet spectra.

The variance plot for sample A is shown in Fig. 3. This plot suggests that there should be 5–6 components in this system. ETA plots (Fig. 7) indicated that the system showed different degrees of spectral variations above the noise level until the 6th component. Therefore, around 5–6 components appears to be optimal for describing this particular system. MCR-ALS revealed that 6 components can be resolved for this counterfeit tablet. The first resolved component is actually a combination of three commonly used excipients: talc, magnesium stearate and sodium lauryl sulfate (Fig. 8). The presence of SLS is inferred based on the peak at 1090 cm^{-1}, and based on the peak intensity, only a very minute amount of this component is present in the tablet. All of these excipients should be present in the genuine tablets; however they were not resolved by MCR-ALS possibly due to lower concentrations or better distribution in the genuine tablets. The second component consists of some lactose monohydrate. However, the correlation coefficient between this spectrum and the pure lactose monohydrate spectrum is not very high. This indicates that there could be another compound contributing to this component.

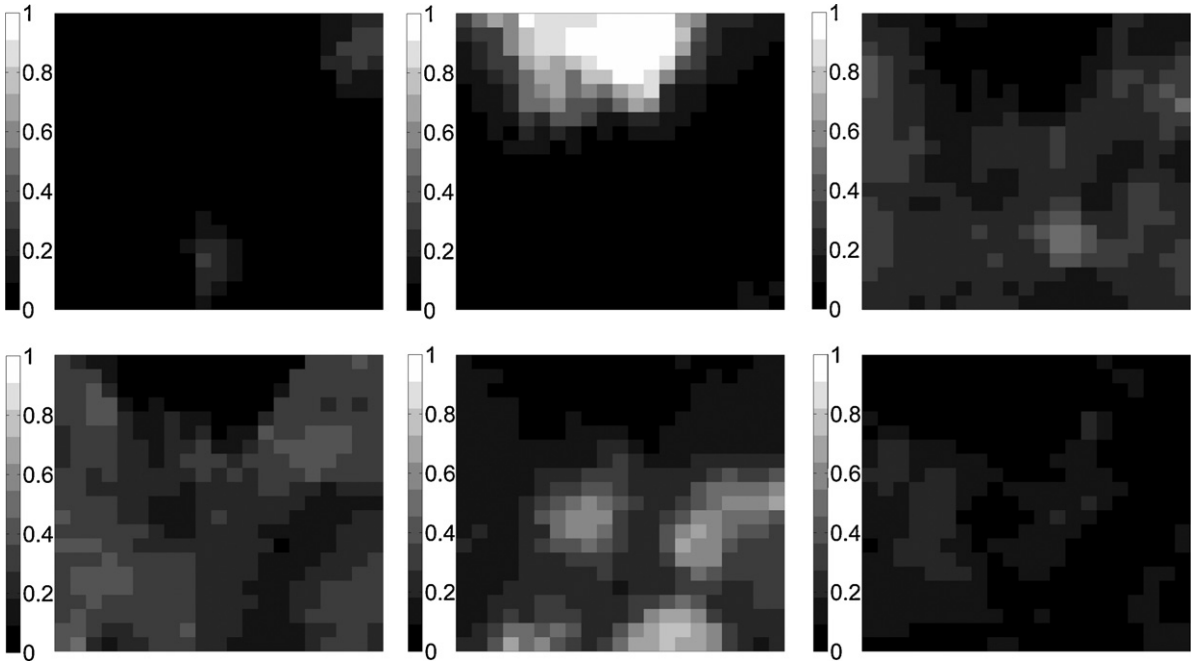

Fig. 9. Raman images of resolved components of counterfeit sample A. Top: 1st to 3rd components (left to right). Bottom: 4th to 6th components (left to right). 1st component: talc, SLS, MgSt; 2nd component: LMH, unknown; 3rd component: LMH; 4th component: starch, calcium sulfate; 5th component: tadalafil; 6th component: starch.

After a scaled subtraction (based on the 358 cm^{-1} LMH peak) from the pure lactose monohydrate spectrum, it is apparent that there is indeed another ingredient present in this component (Fig. 8). The identity of this ingredient is not clear at this time, although it is neither one of the excipients used in the genuine tablet nor is it a common excipient used in the pharmaceutical industry. From the spectrum itself, it appears to be a simple inorganic compound. Further forensic analysis is required to determine the exact identity of this unknown ingredient. The third resolved component is lactose monohydrate and it can be seen that it compares very well with the pure lactose monohydrate spectrum (Fig. 8) and the correlation coefficient between the two is 0.95. The fourth component will be discussed below. The fifth component is the API (Fig. 8). This component is also effectively resolved similar to the third component. The sixth component is a type of starch with a strong Raman peak at 485 cm^{-1} for the CC stretching of the ring system [33], and a comparison between the resolved spectrum and a Raman spectrum of corn starch is illustrated in Fig. 8. Since different types of starches possess very similar Raman spectra, it is not clear exactly what kind of starch is present in this counterfeit tablet. However, corn starch is probably a rather popular and an easily attained type of starch to be used by counterfeiters. Returning to the fourth component, a preliminary examination suggests that it does not appear to be any type of pharmaceutical excipient. However, if a scaled subtraction (based on the 485 cm^{-1} peak) from the sixth component (starch) is performed, it is clear that this component consists of starch and another ingredient. The other ingredient is calcium sulfate with a characteristic peak at 1010 cm^{-1} for the sulfate ion symmetric stretching vibration (Fig. 8), an inorganic compound commonly used as an excipient in pharmaceutical formulations, but not one that is in the genuine tablets. The average relative concentrations of the resolved components for this sample are summarized in Table 2. The average relative concentration of tadalafil (5th component) is 24.2% which is approximately four times that of the genuine tablet concentration. The chemical images (Fig. 9) of each component revealed that the distribution of each component is more heterogeneous than in the genuine tablet components, especially the unknown

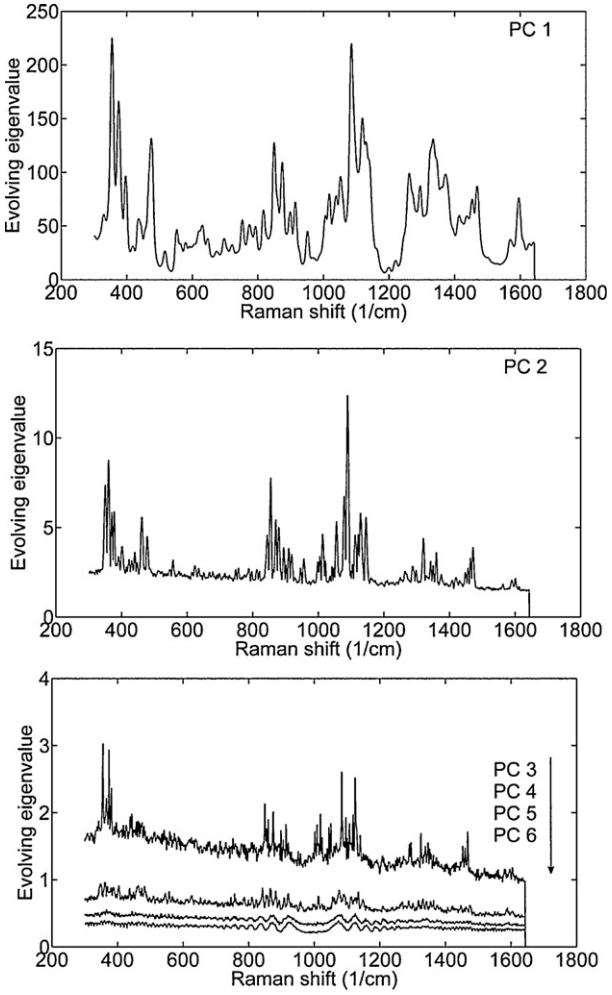

Fig. 10. ETA plots of counterfeit sample B.

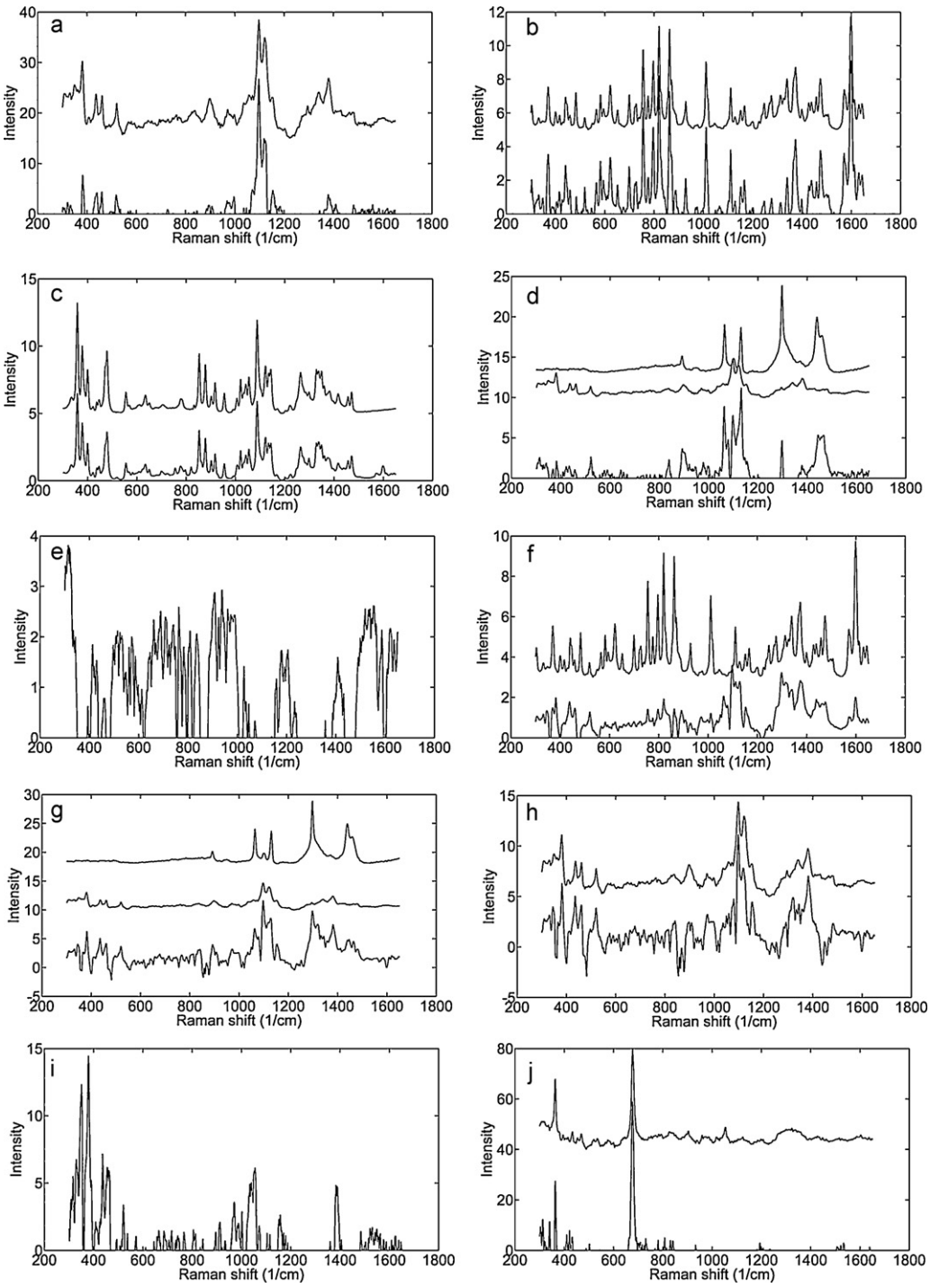

Fig. 11. Resolved spectra of counterfeit sample B. (a) 1st component compared to MCC (top). (b) 2nd component compared to tadalafil (top). (c) 3rd component compared to lactose monohydrate (top). (d) 4th component compared to magnesium stearate (top) and MCC (middle). (e) 5th component. (f) 6th component compared to tadalafil (top). (g) 6th component subtracted by tadalafil compared to magnesium stearate (top) and MCC (middle). (h) 6th component subtracted by tadalafil and MgSt compared to MCC (top). (i) 7th component. (j) 8th component compared to talc (top).

excipient and the API. This implies that the mixing process of the counterfeit tablets was poor and incomplete compared to that of genuine tablets.

3.2.2. Sample B

The Raman spectra of counterfeit sample B are shown in Fig. 2. These spectra look very similar to the genuine tablet spectra. The correlation coefficient between the average spectra of this counterfeit sample and the genuine tablet is 0.98, however, the overall spectral variation of this sample is slightly larger than that of the genuine tablet. From only a comparison of the raw spectra, it is difficult to distinguish between this sample and the genuine drug. However, further analysis using MCR-ALS should reveal more information about this counterfeit sample.

The variance plot of PCA (Fig. 3) showed that 5–6 components appear to be optimal for this system, while ETA analysis showed that 4 components are optimal (Fig. 10). These numbers are similar to those obtained from the genuine tablet data; however PCA and ETA are only the preliminary steps in analyzing these tablets. Examination of different models resulting from the MCR-ALS

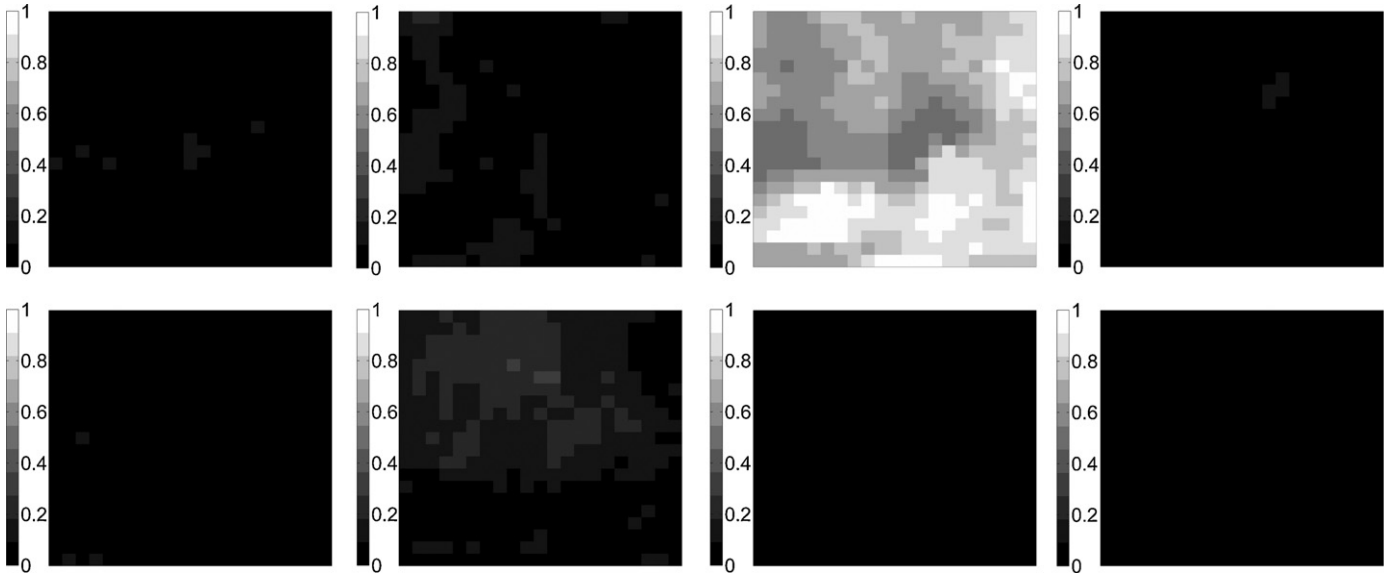

Fig. 12. Raman images of resolved components of counterfeit sample B. Top: 1st to 4th components (left to right). Bottom: 5th to 8th components (left to right). 1st component: MCC; 2nd component: tadalafil; 3rd component: LMH; 4th component: MgSt, MCC; 5th component: noise; 6th component: tadalafil, MgSt, MCC; 7th component: unknown; 8th component: talc.

process suggested that the model with eight components gave good spectral correlation to lactose monohydrate, MCC, and tadalafil which could be found in the first three components, respectively (see Fig. 11) while additional components could be correlated with other excipients. The 4th component resembles MCC and MgSt. For instance, the peaks at 1298 cm^{-1} and 1441 cm^{-1} belong to MgSt and the peaks at 1098 cm^{-1} and 1120 cm^{-1} belong to MCC. The 5th component resembles a random noise pattern and it does not match any of the pure component spectra. The 6th component resembles the API spectrum with additional peaks at 1098 cm^{-1} and 1298 cm^{-1} that are assigned to MCC and MgSt. The spectra obtained from scaled subtractions of the corresponding pure excipient spectra clearly showed that these are the excipients that contributed to this component. The 7th component does not resemble any of the pure component spectra ($R < 0.3$), and is most likely an impurity or contaminant. Finally, the two peaks at 363 cm^{-1} and 677 cm^{-1} of the 8th component resemble the two distinct peaks of talc. The average relative concentration for each component is shown in Table 2. The average relative concentration for the resolved tadalafil (2nd component) is 5.8%, which is the same as found for the genuine tablet. This particular counterfeit thus appears to be a good imitation with respect to the amount of the API present. The relative concentration of lactose monohydrate (3rd component) (73.1%) is also very close to the genuine tablet result. The concentration of the 6th component is 11.8% and spectral analysis showed that this component consists of MCC, MgSt, and the API. The concentrations of the other components are under 4% as can be seen from the Raman images (Fig. 12). Although these relative concentrations were derived from a relatively small sampling area (200 μm × 200 μm), they were verified as being representative of the table as a whole, by comparing to the Raman spectrum obtained by using a large spot size probe (6 mm diameter, Kaiser Optical Systems, Ann Arbor, MI). The peak area ratios between the API and three excipients (LMH (358 cm^{-1}), MgSt (1298 cm^{-1}), MCC (1120 cm^{-1})) were calculated from this "bulk" spectrum and the average spectrum of all the pixels from the mapping experiments. The API:LMH, API:MgSt, and API:MCC peak area ratios are 0.57 and 0.52, 1.84 and 2.20, 1.21 and 1.02 for the "bulk" spectrum and the average mapping spectrum, respectively.

The resolved components of all samples are summarized in Table 3. The major differences between sample B and the genuine tablet are the fact that magnesium stearate and talc can be resolved and that there is an unknown contaminant or impurity present in this counterfeit sample. In retrospect, it can be seen with visual observation from the average spectrum that the MgSt peak at 1441 cm^{-1} and the talc peak at 677 cm^{-1} are more intense in the average counterfeit spectrum than in the average spectrum of the genuine tablet (Fig. 13). Other than these subtle differences, this counterfeit Cialis® tablet closely resembles the genuine tablet. This analysis thus demonstrates the power of MCR-ALS in revealing subtle differences but also reveals the sophistication of some counterfeit products, which are hard to distinguish from the genuine products.

Table 3
Identity of resolved compounds for each sample.

Resolved compound	Genuine	Counterfeit A	Counterfeit B
Lactose monohydrate	×	×	×
Microcrystalline cellulose	×		×
Tadalafil	×	×	×
Magnesium stearate		×	×
Talc		×	×
Sodium lauryl sulfate		×	
Starch		×	
Calcium sulfate		×	
Unknown[a]		×	×

[a] The unknown compound in sample A is not the same as that in sample B.

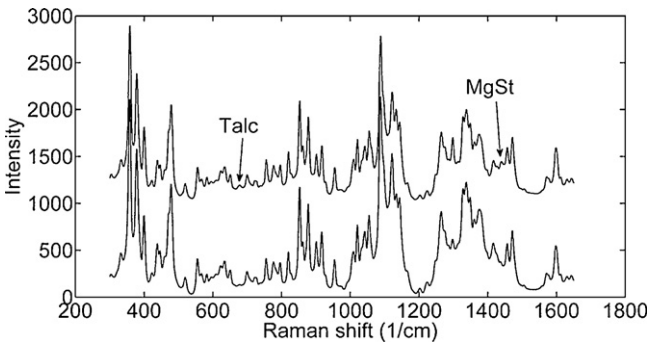

Fig. 13. Comparison between average genuine tablet spectrum (bottom) and average counterfeit sample B spectrum (top).

4. Conclusions

Raman microscopy combined with MCR-ALS was used to successfully analyze genuine and counterfeit Cialis® tablets. For the genuine tablets, two excipients and the API were resolved. The homogeneous nature of the genuine tablet most likely explains why only the three major components could be resolved. For counterfeit sample A, seven excipients, the API, and an unknown compound were resolved. Two of the excipients present are not found in the genuine tablets. The API content was more than four times that of the genuine tablets. For counterfeit sample B, four excipients, the API, and an unknown chemical were resolved. This sample is very similar to the genuine tablet chemically. The subtle differences could not easily be detected without the aid of the MCR-ALS analysis. Both counterfeit products showed more scattered spatial distribution of the components, especially sample A. This study has demonstrated the feasibility of MCR-ALS combined with Raman microscopy for the analysis of counterfeit pharmaceuticals. Combining the advantages of MCR-ALS (no prior information about composition needed) and Raman microscopy (spectral uniqueness) thus provides a powerful method in analyzing counterfeit tablets.

Acknowledgments

This work was supported by a grant from the Lilly Endowment Inc. to the College of Pharmacy and a research fellowship from United States Pharmacopeia to K.K.

References

[1] "The spread of counterfeiting: Knock-offs catch on | The Economist" The Economist. http://www.economist.com/node/15610089 (accessed 22.07.11).
[2] Organisation for Economic Co-operation and Development, The Economic Impact of Counterfeiting and Piracy, OECD Publishing, New York, 2008.
[3] "WHO | Medicines: Counterfeit Medicines" The World Health Organization. http://www.who.int/mediacentre/factsheets/fs275/en/index.html (accessed 22.07.11).
[4] H. Hill, Counter medicines – how much of a risk to public health are they? Pharm. J. 275 (2005) 520.
[5] "GPHF | The GPHF-Minilab® – Protection Against Counterfeit Medicines" The Global Pharma Health Fund. http://www.gphf.org/web/en/minilab/index.htm (accessed 13.10.11).
[6] X. Fan, Y. Cheng, Z. Ye, R. Lin, Z. Qian, Multiple chromatographic fingerprinting and its application to the quality control of herbal medicines, Anal. Chim. Acta 555 (2006) 217–224.
[7] K.E. Arthur, J. Wolff, D.J. Carrier, Analysis of betamethasone, dexamethasone and related compounds by liquid chromatography/electrospray mass spectrometry, Rapid Commun. Mass Spectrom. 18 (2004) 678–684.
[8] R.D. Marini, E. Rozet, M.L.A. Montes, C. Rohrbasser, S. Roht, D. Rheme, P. Bonnabry, J. Schappler, J.L. Veuthey, P. Hubert, S. Rudaz, Reliable low-cost capillary electrophoresis device for drug quality control and counterfeit medicines, J. Pharm. Biomed. Anal. 53 (2010) 1278–1287.
[9] F.M. Fernandez, R.B. Cody, M.D. Green, C.Y. Hampton, R. McGready, S. Sengaloundeth, N.J. White, P.N. Newton, Characterization of solid counterfeit drug samples by desorption electrospray ionization and direct-analysis-in-real-time coupled to time-of-flight mass spectrometry, ChemMedChem 1 (2006) 702–705.
[10] F.E. Dowell, E.B. Maghirang, F.M. Fernandez, P.N. Newton, M.D. Green, Detecting counterfeit antimalarial tablets by near-infrared spectroscopy, J. Pharm. Biomed. Anal. 48 (2008) 1011–1014.
[11] M.J. Vredenbregt, L. Blok-Tip, R. Hoogerbrugge, D.M. Barends, D. de Kaste, Screening suspected counterfeit Viagra® and imitations of Viagra® with near-infrared spectroscopy, J. Pharm. Biomed. Anal. 40 (2006) 840–849.
[12] M. de Veij, A. Deneckere, P. Vandenabeele, D. de Kaste, L. Moens, Detection of counterfeit Viagra® with Raman spectroscopy, J. Pharm. Biomed. Anal. 46 (2008) 303–309.
[13] M. de Veij, P. Vandenabeele, K.A. Hall, F.M. Fernandez, M.D. Green, N.J. White, A.M. Dondorp, P.N. Newton, L. Moens, Fast detection and identification of counterfeit antimalarial tablets by Raman spectroscopy, J. Raman Spectrosc. 38 (2007) 181–187.
[14] U. Holzgrabe, M. Malet-Martino, Analytical challenges in drug counterfeiting and falsification – the NMR approach, J. Pharm. Biomed. Anal. 55 (2011) 679–687.
[15] D. Pratiwi, J.P. Fawcett, K.C. Gordon, T. Rades, Quantitative analysis of polymorphic mixtures of ranitidine hydrochloride by Raman spectroscopy and principal components analysis, Eur. J. Pharm. Biopharm. 54 (2002) 337–341.
[16] J. Rantanen, H. Wikström, F.E. Rhea, L.S. Taylor, Improved understanding of factors contributing to quantification of anhydrate/hydrate powder mixtures, Appl. Spectrosc. 59 (2005) 942–951.
[17] M. Savolainen, K. Kogermann, A. Heinz, J. Aaltonen, L. Peltonen, C. Strachan, J. Yliruusi, Better understanding of dissolution behaviour of amorphous drugs by in situ solid state analysis using Raman spectroscopy, Eur. J. Pharm. Biopharm. 71 (2009) 71–79.
[18] L. Zhang, M.J. Hansen, S.S. Sekulic, Multivariate data analysis for Raman imaging of a model pharmaceutical tablet, Anal. Chim. Acta 545 (2005) 262–278.
[19] B. Lavine, J. Workman, Chemometrics, Anal. Chem. 82 (2010) 4699–4711.
[20] M. Kansiz, P. Heraud, B. Wood, F. Burden, J. Beardall, D. McNaughton, FTIR spectroscopy as a tool to discriminate between cyanobacterial strains, Phytochemistry 52 (1999) 407–417.
[21] D. Ollivier, J. Artaud, C. Pinatel, J.P. Durbec, M. Guerere, Triacylglycerol and fatty acid compositions of french virgin olive oils. Characterization by chemometrics, J. Agric. Food Chem. 51 (2003) 5723–5731.
[22] J. Rantanen, H. Wikstrom, R. Turner, L.S. Taylor, Use of in-line near-infrared spectroscopy in combination with chemometrics for improved understanding of pharmaceutical processes, Anal. Chem. 77 (2005) 556–563.
[23] R. Tauler, A. de Juan, Multivariate curve resolution, in: P. Gemperline (Ed.), Practical Guide to Chemometrics, Taylor and Francis Group, Boca Raton, FL, 2006, pp. 417–473.
[24] S. Trefi, C. Routaboul, S. Hamieh, V. Gilard, M. Malet-Martino, R. Martino, Analysis of illegally manufactured formulations of tadalafil (Cialis®) by H-1 NMR, 2D DOSY H-1 NMR and Raman spectroscopy, J. Pharm. Biomed. Anal. 47 (2008) 103–113.
[25] M. Shin, R.D. Jee, K. Chae, A.C. Moffat, Identification of counterfeit Cialis®, Levitr® a and Viagra® tablets by near-infrared spectroscopy, J. Pharm. Pharmacol. 57 (2005) S11.
[26] A.C. Moffat, R.B. Cody, R.D. Jee, A.J. O'Neil, Identification of counterfeit Cialis® tablets by direct analysis in real time (DART) time-of-flight mass spectrometry, J. Pharm. Pharmacol. 59 (2007) A26.
[27] U.B. Cappel, I.M. Bell, L.K. Pickard, Removing cosmic ray features from Raman map data by a refined nearest neighbour comparison method as a precursor for chemometric analysis, Appl. Spectrosc. 64 (2010) 195–200.
[28] C.A. Lieber, A. Mahadevan-Jansen, Automated method for subtraction of fluorescence from biological Raman spectra, Appl. Spectrosc. 57 (2003) 1363–1367.
[29] A. Savitzky, M.J.E. Golay, Smoothing and differentiation of data by simplified least squares procedures, Anal. Chem. 36 (1964) 1627–1639.
[30] J. Toft, O.M. Kvalheim, Eigenstructure tracking analysis for demonstration of heteroscedastic noise in instrumental profiles—application to transmittance and absorbance IR, Chemometr. Intell. Lab. Syst. 19 (1993) 65–73.
[31] H. Susi, J.S. Ard, Laser-Raman spectra of lactose, Carbohydr. Res. 37 (1974) 351–354.
[32] F.C. Sanchez, J. Toft, O.M. Kvalheim, D.L. Massart, Eigenstructure tracking analysis for assessment of peak purity in HPLC-DAD, Anal. Chim. Acta 314 (1995) 131–139.
[33] O. Piot, J.-C. Autran, M. Manfait, Spatial distribution of protein and phenolic constituents in wheat grain as probed by confocal Raman microspectroscopy, J. Cereal Sci. 32 (2000) 57–71.

Journal of Pharmaceutical and Biomedical Analysis 66 (2012) 136–143

Contents lists available at SciVerse ScienceDirect

Journal of Pharmaceutical and Biomedical Analysis

journal homepage: www.elsevier.com/locate/jpba

Characterization of physicochemical properties of hydroxypropyl methylcellulose (HPMC) type 2208 and their influence on prolonged drug release from matrix tablets

S. Devjak Novak[a], E. Šporar[a], S. Baumgartner[b], F. Vrečer[a,b,*]

[a] Krka, d.d., Novo mesto, Šmarješka cesta 6, 8501 Novo mesto, Slovenia
[b] University of Ljubljana, Faculty of Pharmacy, 1000 Ljubljana, Slovenia

ARTICLE INFO

Article history:
Received 24 January 2012
Received in revised form 15 March 2012
Accepted 16 March 2012
Available online 26 March 2012

Keywords:
HPMC
Particle-size
NIR
Calibration models
SEM
Drug release

ABSTRACT

The key physicochemical properties of functional excipients should be identified, and the influence of their variability on the properties of the final dosage form should be evaluated during the development phase. Excipients produced by different manufacturers and/or by different manufacturing processes should have comparable properties. Hydroxypropyl methylcellulose (HPMC) with a high molecular weight is a functional excipient often used in solid matrix systems with prolonged release of active pharmaceutical ingredients (API). This study investigates whether HPMC manufactured by two manufacturers using different chemical procedures differs in particle-size distribution, particle shape, particle morphology, chemical composition, and dissolution of diclofenac sodium as a model drug. NIR spectroscopy was introduced and calibration models were developed to detect physical differences among HPMC batches from two different origins. The physical differences between HPMC samples were additionally confirmed with scanning electron microscopy (SEM), gas chromatography (GC) measurements, and dissolution testing of hydrophilic matrix tablets. Our results prove that, even if HPMC polymers manufactured from two different sources comply with the pharmacopeial specification, they significantly differ in physicochemical properties and thus influence the properties of the formulated dosage forms.

© 2012 Elsevier B.V. All rights reserved.

1. Introduction

Hypromellose, hydroxypropyl methylcellulose (HPMC) with a molecular weight ranging from 10,000 to 1,500,000, is one of the most frequently used polymers for the preparation of hydrophilic matrix tablets with prolonged release of active pharmaceutical ingredients (API). There are many reasons for the popularity of HPMC as an excipient: it is nontoxic, easy to handle, relatively cheap, easy to compact, and able to accommodate high levels of drug loading; moreover, the process variables show little effect on drug release [1]. Commercial HPMC is available in different viscosity (polymerization) and substitution grades with specifications included in United States (USP) and European (Ph. Eur.) pharmacopeia. The pharmacopeial specifications are broad and provide only average values of the polymer quality with respect to polymerization and substitution parameters. HPMC used as a pharmaceutical excipient is typically prepared by batch processes; that is, discrete quantities of powder are produced according to standard procedures rather than on a continuous basis [2]. Production begins with starting material of natural origin (i.e., wood or cotton). Minor batch-to-batch differences in the polymer manufacturing conditions can result in variation in the physical properties of the product. These batch variations are generally small, but if a formulation is not robust enough, or if batch variation is large, this could lead to a product that does not meet required specifications. Another source of variability of polymer properties and its functionality could be the raw materials from which HPMC is produced [2,3]. There are two major suppliers of pharmaceutical-quality HPMC that use different manufacturing procedures and raw materials, even though HPMC of the same grade from both manufacturers complies with the same pharmacopoeial monographs. Batch-to-batch variations within HPMC grades have also previously been reported [4–6].

The factors influencing drug release from hydrophilic matrix systems include viscosity and particle-size distribution of the polymer, ratio of the polymer to drug, polymer grade or use of mixtures of HPMC of different grades, compression pressure, thickness of the tablet, particle size of the drug, entrapped air in the tablets, molecular size of the drug, molecular geometry of the drug, solubility of the drug, the presence of excipients, and the mode of incorporation of these substances [7,8]. Polymer particle size is one of the

* Corresponding author at: Krka, d.d., Novo mesto, Šmarješka cesta 6, 8501 Novo mesto, Slovenia. Tel.: +386 7 331 3608; fax: +386 7 331 3751.
E-mail address: franc.vrecer@krka.biz (F. Vrečer).

0731-7085/$ – see front matter © 2012 Elsevier B.V. All rights reserved.
doi:10.1016/j.jpba.2012.03.032

polymer properties that has been indicated as responsible for the rate of polymer hydration. It has been claimed that small (fine) particle size ensures more rapid hydration and also gives rise to a more continuous gel layer formation. On the other hand, coarse fractions hydrate too slowly to form a fast-growing and continuous gel layer, and therefore excessively rapid initial release is more expressed [9,10].

NIR spectroscopy was found to offer many possibilities for industrial analytical applications. This is a very fast technique because spectra can be recorded in only a few seconds. The most interesting advantage of the technique is the non-destructive character of the analysis and its simplicity because a sample can be analyzed either without preparation or with only minimal sample preparation. In the pharmaceutical industry NIR has been successfully used for material identification, determining endpoints during powder mixing, moisture determination, tablet assay and crushing strength determination, predicting dissolution from tablets, determining moisture in lyophilized products through the bases of vials, detecting various polymorphic forms of the same compound, and particle-size determination [11–15]. Generally, NIRs and chemometrics are used to classify or quantify samples with regard to reference measurements [15]. It is well known that particle size affects the characteristics of NIR diffuse reflection spectra. Particle-size measurements with NIR spectroscopy have been reported and various chemometric approaches have been suggested for correlating particle size with NIR spectra [13]. One reference method for linking particle-size distribution with NIR spectra is laser diffraction. This method is also rapid, requires a small sample volume, provides information about particle-size distribution, does not need external calibration, shows high reproducibility, and can be performed in wet and dry conditions [16].

This study demonstrates how various commonly used characterization techniques (i.e., particle size analysis, NIR spectroscopic method in combination with multivariate data analysis, gas chromatography (GC) and scanning electron microscopy (SEM)) can be used to extend the quality control of incoming batches of HPMC raw material and how the differences correlate with the dissolution profiles from the final drug product. For this purpose, seven HPMC batches from two widely used sources were investigated: Methocel and Metolose. Although all the HPMC batches investigated have similar pharmacopeial specifications, the intention was to determine whether there are physicochemical differences between HPMC batches from the same source and from two different sources.

2. Materials and methods

2.1. Materials

Seven HPMC batches of the same substitution (USP type 2208) and viscosity grade (the nominal viscosity of 2% aqueous solution is 4000 mPa s) were used in the study. All of the samples used and their characteristics are listed in Table 1. HPMC batches were produced by Dow (Dow Chemical Co., USA) and Shin-Etsu (Shin-Etsu Chemical Co., Ltd., Tokyo, Japan).

Table 1
HPMC batches and viscosity of 2% (w/w) solutions in mPa s. All samples were USP 2208 substituent grade. Data were obtained by suppliers.

HPMC batches	Manufacturer	Viscosity (2% w/w) (mPa s)
A (Metolose)	Shin-Etsu Chemical Co., Ltd.	3940
B (Metolose)	Shin-Etsu Chemical Co., Ltd.	4140
C (Metolose)	Shin-Etsu Chemical Co., Ltd.	3740
D (Methocel)	Dow Chemical Co.	3580
E (Methocel)	Dow Chemical Co.	4386
F (Metolose)	Shin-Etsu Chemical Co., Ltd.	3630
G (Methocel)	Dow Chemical Co.	4124

2.2. Sieving of different HPMC batches

HPMC batches were mechanically sieved to selected particle-size fractions. An AS200 Digit Retsch (Japan) vibrational sieving apparatus was used. Thirty grams of each HPMC sample was passed through eleven sieves: 200 μm, 180 μm, 150 μm, 125 μm, 100 μm, 75 μm, 71 μm, 63 μm, 53 μm, 45 μm, and 32 μm. Sieving was carried out under ambient humidity and temperature. The agitation time was 20 min.

Twelve sieved fractions of HPMC batches from A to E were used as calibration samples and sieved fractions of HPMC-F and HPMC-G were subjected to the NIR models to prove its prediction ability.

2.3. Determination of particle-size distribution by laser diffraction as a reference method

Laser diffraction analysis was used as a reference method to determine particle-size distribution. Laser diffraction measurements were performed using a Mastersizer S (Malvern Instruments, UK). The instrument was equipped with a wet dispersion module with a stirrer (1500 rpm) to homogenize samples before measurements. Approximately 300 mg of each HPMC fraction was dispersed in 150 ml of anhydrous ethanol, where HPMC is practically insoluble. The results of each HPMC fraction was based on the volume-weight mean diameter $D(4,3)$, where each result was an average of three consecutive measurements.

2.4. Degree of substitution of HPMC batches investigated

The degree of substitution of all HPMC batches investigated was determined according to the Ph. Eur. procedure. The degree of substitution was determined after reaction with hydroiodic acid with an Agilent 6890, GC 4 apparatus equipped with a thermal conductivity detector. The carrier gas was helium for chromatography with a flow rate of 2 ml/min. The length of the column used was 1.8 m and its temperature was 100 °C. The column was filled with a stationary phase: diatomaceous earth for gas chromatography impregnated with 20% of poly(dimethyl)(75)(diphenyl)(25) siloxan. Adipic acid, isopropyl iodide, methyl iodide, and octane were used as reference solutions.

2.5. Recording of NIR spectra and development of calibration models

NIR reflectance spectra were measured using a fully calibrated multipurpose analyzer (MPA®) Fourier transform near-infrared spectrometer (Bruker Optics, Germany), which was equipped with an indium gallium arsenide (InGaAs) detector. The spectrum of each sample (the average of 32 scans) was recorded in triplicate with a resolution of 8 cm^{-1}. Bruker OPUS software (version 6.5) was used for all data collection and data analysis, in which the Optimizer function was used to obtain the optimal PLS models with optimal selection of the preprocessing technique and wavelength regions. All HPMC fractions were directly measured after sieving (no sample preparation was needed) using the diffuse reflectance mode by placing the powdered samples in glass vials and using a ceramic plate as reference. Sieved HPMC fractions of different batches and of two different origins were used in cross validation to build partial least squares (PLS) models. In PLS, calibration involves correlating the data in the spectral matrix X with the data in the matrix Y, representing the particle size of the analyte. The calibration function b correlates to property Y (the property of the analyte) of a

system with an experimentally observable X (the spectrum) (Eq. (1)) [16,17]:

$$b = (X^T X)^{-1} X^T Y \quad (1)$$

where X and Y are written in matrix form and function b is called the b-coefficient or regression coefficient. With this function the unknown property of an analyte can be calculated using the following equation (Eq. (2)):

$$Y = Xb \quad (2)$$

The overall predictability of the PLS calibration model could be expressed in terms of the root mean square error of cross validation (RMSECV) (Eq. (3)):

$$\mathrm{RMSECV} = \sqrt{\frac{1}{M}\sum_{i=1}^{M}(Y_i^{\mathrm{meas}} - Y_i^{\mathrm{pred}})^2} \quad (3)$$

where Y_i^{meas} is the cross validation estimate of sample i, Y_i^{pred} is an actual analyte property such as the particle size of the sample, and M is the number of calibration samples.

Another statistical parameter characterizing the PLS model is Bias (Eq. (4)). It is calculated by averaging all particular deviations of the samples inside the data sets:

$$\mathrm{Bias} = \frac{\sum_{i=1}^{M} Y_i^{\mathrm{meas}} - Y_i^{\mathrm{pred}}}{M} \quad (4)$$

RPD (residual prediction deviation) is a qualitative measure for assessing validation results. RPD is the quotient of the standard deviation of the reference values (SD) and the bias-corrected mean error of prediction of the validation ($\mathrm{SEP_{bias}}$) (Eqs. (5)–(7)):

$$\mathrm{RPD} = \frac{\mathrm{SD}}{\mathrm{SEP_{bias}}} \quad (5)$$

with

$$\mathrm{SD} = \sqrt{\frac{1}{M-1}\sum_{i=1}^{M}(Y_i^{\mathrm{meas}} - Y_m)^2} \quad (6)$$

and

$$\mathrm{SEP_{bias}} = \sqrt{\frac{1}{M-1}\sum_{i=1}^{M}(Y_i^{\mathrm{meas}} - Y_i^{\mathrm{pred}} - \mathrm{bias})^2} \quad (7)$$

The smaller the $\mathrm{SEP_{bias}}$ compared to the variance of the reference values, the better the model; that is the larger the RPD, the better the calibration. The results also show how good the predictability is because the most capable model is the one with the lowest RMSECV value and the highest RPD value.

The coefficient of determination (R^2) gives the percentage of variance present in the component values, which is reproduced in the prediction (Eq. (8)). This is often called explained variance. The higher is the coefficient, the better is the correlation between the particle size and spectral data.

$$R^2 = \left(1 - \frac{1}{\mathrm{RPD}^2}\right) \times 100 \quad (8)$$

For the analysis of particle sizes of new unknown samples, the Mahalanobis distance (Mahal.-dist.) was calculated. The Mahal.-dist. is a quantitative measure for the quality of an analysis and it is defined as the difference of the measured spectrum of the analyte to the mean value of all spectra in the calibration data set that was used when constructing the spectral data matrix for the given number of samples. If the values lie within the threshold, it is guaranteed that the analysis result is reliable and there it is also checked how well the spectra of the analyte fit the spectra of the calibration data set. On the other hand, if the values lie outside the threshold then the results are detected as an outlier. If the spectral data are factorized according to Eqs. (1) and (2), the Mahal.-dist. h_i is determined as (Eq. (9)):

$$h_i = t_i^T (X^T X)^{-1} t_i \quad (9)$$

where single-score vectors t_i are calculated from a calibration spectrum.

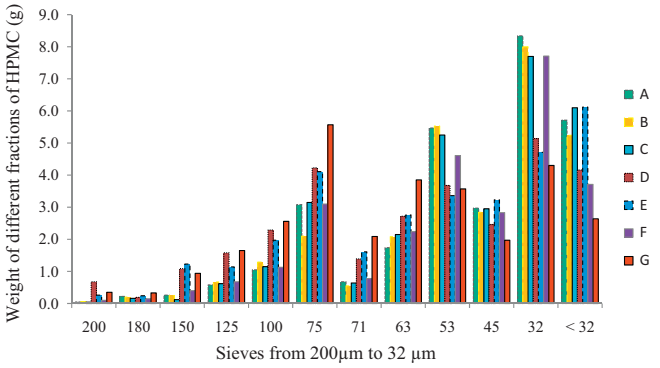

Fig. 1. Particle size distribution curves of all investigated HPMC batches named A, B, C, D, E, F and G.

2.6. Scanning electron microscopy (SEM)

Scanning electron microscopy was used to visually comparison of HPMC powders. (SEM, Carl Zeiss Ultra Plus, Germany), operated at an accelerated voltage of 1 kV with a secondary detector. The distance between the samples and detector was 2.4 mm and the aperture size was 30 μm.

2.7. Preparation of tablets by direct compression and dissolution testing

The composition of tablets made of different HPMC-C and HPMC-D size fractions is presented in Table 2. HPMC was used as matrix-forming agent, lactose monohydrate as a filler, magnesium stearate as a lubricant, and diclofenac sodium as model drug. Powders were homogeneously blended and tablets were made by direct compression, using a Killian Pressima compression machine equipped with 10 mm flat-faced punches; the compression force was 15 ± 0.5 kN and the tablet weight was 300 ± 15 mg.

The drug-release studies were performed on a fully calibrated dissolution apparatus using the paddle method (apparatus 2, Van Kel 7025 dissolution test station, USA) at 50 rpm, using 900 ml of phosphate buffer solution (pH 6.8) at 37 °C ± 0.5 °C. JP13 Japanese sinkers were used to prevent adhesion of the HPMC tablet types investigated to the vessels. Ten ml of filtered samples were taken each hour and the UV absorbance was measured at 276 nm. The amount of released drug was calculated using a calibration curve. Dissolution tests were performed on six tablets for each tablet type.

3. Results and discussion

3.1. Sieving of different HPMC batches and determination of particle-size distribution by laser diffraction

In this study the samples investigated were HPMC-A to HPMC-G. All samples were sieved and particle-size distribution curves were constructed (Fig. 1). Some differences could be seen from the particle-size distribution curves. Methocel samples had a distribution of particles in the full range from 32 to 200 μm, whereas Metolose samples had only a small amount of larger particles

Table 2
Composition in tablet formulations investigated in present study.

HPMC tablet type	Size of HPMC particles (μm)	Amount of HPMC (mg)	Amount of diclofenac sodium (mg)	Amount of magnesium stearat (mg)	Amount of Lactose monohydrate (mg)	Methoxy/ hydroxypropyl ratio
HPMC-C	32–45 μm	90	107.4	3	99.6	2.7
HPMC-C	100–125 μm	90	107.4	3	99.6	2.7
HPMC-C	Unsieved[a]	90	107.4	3	99.6	2.5
HPMC-D	32–45 μm	90	107.4	3	99.6	3.1
HPMC-D	100–125 μm	90	107.4	3	99.6	3.2
HPMC-D	Unsieved[a]	90	107.4	3	99.6	3.1

[a] Sample of HPMC as supplied (untreated).

(>125 μm). Practically no material was found in sieves with an opening greater than 125 μm in the case of Metolose samples. This was also in line with the manufacturer's data for particle size, in which the maximum particle size of Metolose samples was stated as being below 125 μm, which was confirmed by our results. Furthermore, it could be seen that sieved Metolose fractions had more homogenous particle-size distribution and lower batch-to-batch variability in comparison with the Methocel fractions, where particle-size distribution was less homogenous and larger batch-to-batch variability could be observed.

The volume-weighted mean diameter $D(4,3)$ for every sieved fraction of HPMC was determined by laser diffraction (data not shown).

Due to the small sample quantities of Metolose fractions with a particle size larger than 125 μm, the volume-weighted mean diameter $D(4,3)$ was not determined for these fractions. Only well-defined particle-size fractions and fractions with a sufficient amount of samples were used for recording NIR spectra and building PLS calibration models. The volume-weighted mean diameter $D(4,3)$ of each sieved HPMC fraction was used as a reference method in PLS calibration models.

3.2. Determination of degree of substitution by gas chromatography

In spite of the fact that all HPMC batches investigated were specified to be of the same viscosity and substitution grade, we sought to determine whether there were differences in methoxyl and hydroxypropoxyl content between the HPMC batches investigated (Table 3). From the results obtained it could also be seen that all Metolose samples have a higher hydroxypropoxyl content in comparison to Methocel samples. On the other hand, there were minor differences in methoxyl content between all HPMC samples investigated. The methoxy/hydroxypropoxyl ratio for Metolose batches was between 2.4 and 2.5 and for Methocel between 2.7 and 3.1. Again, the Methocel batches regarding methoxy/hydroxypropoxyl ratio differed more among each other than from the Metolose batches.

We also investigated whether there were differences between the methoxy and hydroxypropoxy content of different HPMC size fractions within one HPMC batch. Therefore two fractions of HPMC-C and HPMC-D were analyzed, one fraction with particles in a range from 32 to 45 μm and one fraction with particles in a range from 100 to 125 μm, respectively. The results showed that the methoxy/hydroxypropoxyl ratio between the HPMC-C sample with particles from 32 to 45 μm and the HPMC-C sample with particles from 100 to 125 μm was equal (2.7) or higher than for the unsieved HPMC-C sample (2.5). That difference arose from lower hydroxypropyl content (8.5%) in the case of sieved fractions of HPMC-C samples. On the other hand, there were only small differences between sieved and unsieved HPMC-D samples.

Although there were minor differences in the methoxy/hydroxypropoxyl ratio between Methocel and Metolose materials, these differences were not negligible.

3.3. Calibration models obtained from NIR spectra

The NIR spectra were recorded over a wavelength range from 12,500 to 3500 cm^{-1}. The spectral range below 3500 cm^{-1} can easily be affected by edge effects and noise, and therefore we did not select a spectral range below 3500 cm^{-1}. The spectra obtained exhibited characteristic overlapping combinations and overtones, revealing a high content of chemical and physical information at the same time through the entire spectral range [16]. In the first part of developing the PLS models, our intention was to recorded the original NIR spectra of various HPMC particle-size fractions and from various manufacturers to determine whether the NIR spectrum could be affected by variability in particle size with regard to sieve analysis. The NIR spectra of all fractions from 32 to 200 μm are shown in Fig. 2. It can be seen that all spectra profiles were identical in shape. All recorded spectra were separated as expected, whereby bigger particles show stronger light absorption than smaller ones, as has also been previously reported [16,18–20]. In addition, the NIR spectra for all HPMC batches investigated show vibrational groups at the same frequency, indicating the presence of the identical chemical composition of each sieved fraction.

3.3.1. Development of a universal calibration model using Metolose and Methocel HPMC samples

First, we tried to build a universal calibration model of all sieved batches of HPMC-A, HPMC-B, HPMC-C, HPMC-D, and HPMC-E from both origins. The calibration details (pretreatments and frequency regions used) are summarized in Table 4. The method was validated by cross validation, which allows evaluation of the model from the calibration data alone; that is, each sample omitted from the calibration set once, the calibration set was remodeled, and the volume-weight mean diameter $D(4,3)$ of the left out sample was predicted using the new calibration model. This cycle was repeated until each spectrum of the sieved fraction was correlated with the corresponding volume–weight mean diameter $D(4,3)$ obtained for each sieved fraction by wet dispersion laser diffraction. The statistical parameters of the universal PLS calibration model are presented in Table 4 and we classified them as too high. When analyzing the unknown samples (unsieved and sieved fractions of HPMC-F and HPMC-G) for determining the $D(4,3)$, three of the sieved fractions were classified as outliers, which means that these samples deviated from the predicted value and were recognized as statistically significant different (the values of the Mahal.-dist. were greater than the set limit; data not shown).

Although all HPMC batches used were chemically comparable, and were of the same substitution type (2208) and viscosity grade (4000 mPa s), they differ in the starting materials for polymer

Table 3
Degree of substitution and methoxy/hydroxypropyl ratio of investigated HPMC batches.

HPMC batches	Hydroxypropyl content (% w/w)	Methoxyl content (% w/w)	Methoxy/hydroxypropyl ratio
A (Metolose)	9.6	23.0	2.4
B (Metolose)	9.7	22.8	2.4
C (Metolose)	9.3	22.9	2.5
D (Methocel)	7.5	23.4	3.1
E (Methocel)	7.6	22.7	3.0
F (Metolose)	9.5	23.0	2.4
G (Methocel)	8.5	22.9	2.7
C (particles from 32 μm to 45 μm)	8.5	22.8	2.7
C (particles from 100 μm to 125 μm)	8.5	23.1	2.7
D (particles from 32 μm to 45 μm)	7.4	23.0	3.1
D (particles from 100 μm to 125 μm)	7.2	23.3	3.2

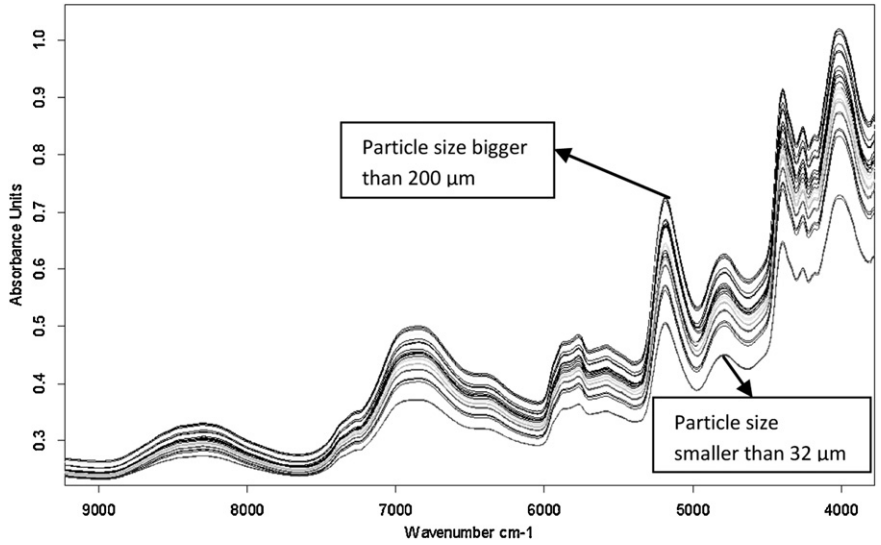

Fig. 2. Original NIR spectra of different particle size fractions of HPMC.

manufacturing: for Metolose, cellulose fibers from wood pulp was the starting material, whereas for Methocel it was cotton [21]. We have also proved that HPMC samples from both manufacturers differ in particle-size distribution and in their methoxy/hydroxypropoxy ratio because all chemical properties have an influence on the NIR spectra and PLS calibration models. Our hypothesis was that the outliers obtained were attributable to the influence of sample chemical history (i.e., manufacturing procedure) on the NIR spectra of the HPMC samples. All of these differences in starting material and process parameters may also influence particle-size distribution, particle shape, particle morphology, and methoxy/hydroxypropoxy ratio, which was seen in the universal calibration model. Evidently the universal calibration model did not cover all the characteristics of samples used in cross validation. Therefore we separated the sieved fractions into two groups with regard to their origin and built two separate PLS calibration models.

3.3.2. Development of calibration model according to HPMC origins

Sieved samples of Metolose HPMC-A, HPMC-B, and HPMC-C in a range from 32 to 125 μm were used to build a new PLS regression model. The values of all statistical parameters (Table 4) were better in comparison to those obtained from the universal calibration PLS model, especially values of Bias and RPD, where determining $D(4,3)$ for the unknown Metolose samples (unsieved and sieved fractions of HPMC-F) no outliers were found, all values of the Mahal.-dist. were within specified limits, and predicted values were comparable to results obtained by laser diffraction (data not shown). The results obtained show better correlation between spectral data and volume-weighted mean diameter $D(4,3)$ in comparison to the universal PLS calibration model. With the PLS model obtained, we also tried to determine $D(4,3)$ for the Methocel HPMC-G sample. Three of the sieved samples were found as outliers (data not shown).

Further sieved samples of Methocel HPMC-E and HPMC-F (Methocel batches) in a range from 32 to 200 μm were used to build another PLS regression model. No outliers were found when analyzing the unknown samples of unsieved and sieved fractions of Methocel HPMC-G samples. Again, the PLS obtained model shows better predictability than the universal calibration model (Table 4). As before, we tried to determine $D(4,3)$ for Metolose fractions of the HPMC-F sample. In this case no outliers were found and the predicted $D(4,3)$ values were comparable to the $D(4,3)$ values determined (data not shown).

Table 4
Summary of calibration data for the PLS models.

PLS models	Pretreatments	Frequency regions (cm^{-1})	R^2	RMSECV (%)	Bias	RPD
Universal model	Vector normalization	9828.4–8046.3; 7159.1–6264.3; 5380.9–3598.9	95.84	13.8	0.419	4.91
Metolose model	First derivative	11606.6–8933.5; 8046.3–6264.3; 4489.9–3598.9	98.51	6.3	0.0901	8.2
Methocel model	Constant offset elimination	8046.3–7155.3; 4489.9–3598.9	98.15	9.5	0.255	7.36

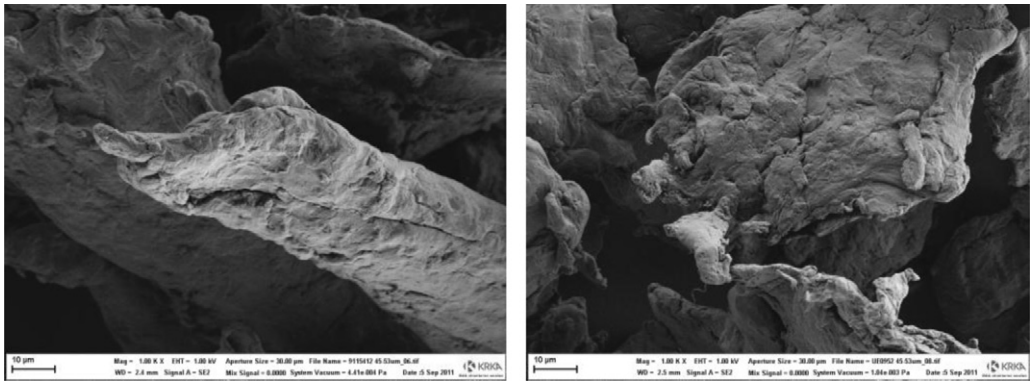

Fig. 3. SEM results of both HPMC fraction in the range from 32 to 45 μm. Left fraction (HPMC-C) and right fraction (HPMC-D). Magnitude ×1000.

Both separated models are improved and give better predictions in comparison to the universal calibration PLS model. First of all, the Methocel HPMC batches (HPMC-D, HPMC-E, and HPMC-G) have wider particle-size distribution (32–200 μm), whereas the Metolose batches (HPMC-A, HPMC-B, HPMC-C, and HPMC-F) have a narrower particle-size distribution (32–125 μm). From the data in the literature, it is known that particle size has an impact on the NIR scattering properties of the powder. The radiation penetrates more deeply into the sample with larger particles leading to less reflection, weak band characteristics, and a high over-all absorption signal. Strong differences in particle size were limiting and therefore the spectral reproducibility may lead to non-linearities in the PLS calibration model [22] seen as high RMSECV values in the case of the Methocel batches. On the other hand, the calibration model with a narrower particle-size distribution yielded lower RMSECV values and higher RPD values. However, this relationship does not necessarily apply in all cases and is also dependent on the particle shape and the material's refractive index [19]. Based on the calculated statistical parameters, we assumed that particles from two different origins differ not only in particle-size distribution but also in particle shape and particle morphology. A higher RMSECV and Bias could be attributable to variability of the methoxy/hydroxypropoxy ratio between Methocel batches whose variability was not included in the Methocel PLS model, which is also the reason for outliers when testing the Metolose PLS model with Methocel HPMC-G. For reducing the RMSECV and Bias even more, more Methocel batches should be used, which makes the PLS model more robust.

Both separated PLS models were improved, and they offer better prediction in comparison to the universal calibration PLS model. Thus, determination of particle sizes $D(4,3)$ of unknown HPMC samples is possible using separated models according to HPMC origin.

3.4. Scanning electron microscopy (SEM)

Scanning electron microscopy (SEM) was used to find out whether differences in the particle shape of HPMC size fractions from two different origins can be observed. Samples of Metolose C and Methocel D were imaged using SEM. Particle-shape differences were found for samples HPMC-C and HPMC-D with particle size in the range from 32 to 45 μm (Fig. 3). Metolose HPMC-C had more fiber-shaped particles, whereas Methocel HPMC-D had more irregularly shaped particles. It was suggested that the observed morphological differences influenced the NIR spectra, the PLS models presented, and their prediction capability. Particle-shape differences among HPMC batches from two origins were previously noticed and a non-homogeneous particle shape was observed particularly in the case of the Methocel batches [6]. Interestingly, a difference in particle shape between two batches of different origin was not observed for larger particles; that is, for particles in the size range from 100 to 125 μm (Fig. 4). Irregularly shaped particles were observed in both samples; thus it is not possible to distinguish between two HPMC origins on the basis of SEM pictures. This observation was quite surprising because differences in particle morphology in the entire particle-size range of Metolose HPMC-C and Methocel HPMC-D were expected.

Although each HPMC origin has its own calibration model for predicting particle-size distribution, the reduced RMSECV is still quite large (6.3% and 9.5%, respectively). Irregularly shaped particles of both HPMC origins in the range from 125 to 150 μm could explain the high RMSECV values obtained for both separated PLS calibration models to some extent. Based on these observations, it can be concluded that particle shape is an important parameter in the value of the prediction model for HPMC particle size and has an influence on NIR spectra.

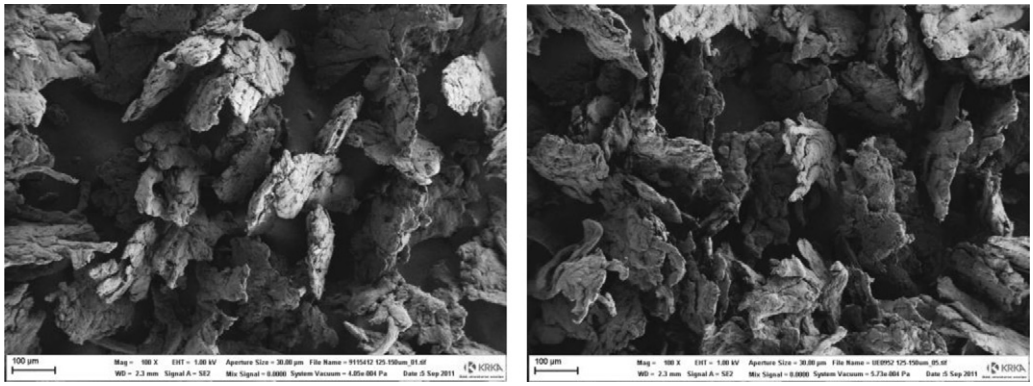

Fig. 4. SEM results of both HPMC fractions in the range from 100 to 125 μm. Left fraction (HPMCC) and right fraction (HPMC-D). Magnitude ×100.

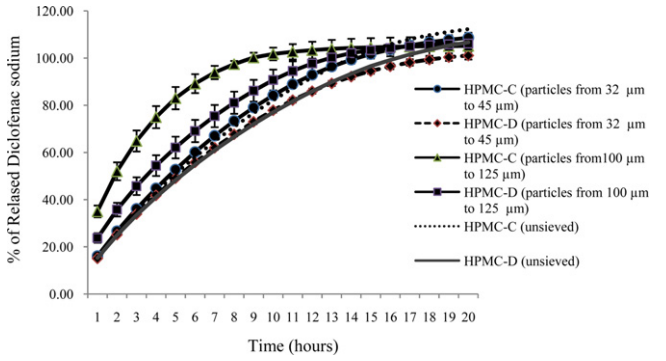

Fig. 5. Comparison of dissolution profiles of model drug diclofenac sodium. The symbols denote the calculated average value of six tablets and the error bars show the standard deviation from the mean value.

3.5. Dissolution testing of model drug diclofenac sodium

Based on the physical and chemical differences studied above between Metolose HPMC-C and Methocel HPMC-D fractions, the dissolution profiles of the model drug diclofenac sodium from prepared tablets were investigated (Table 2). Six tablet types were prepared in order to emphasize the influence of particle size and the methoxy/hydroxypropoxyl ratio of HPMC on drug dissolution. The percent of HPMC in all formulations was fixed at 30%.

The results in Fig. 5 showed that all six tablet types enable prolonged drug release irrespective of the HPMC particle-size fraction used. Formulations with HPMC particles in a size range from 100 to 125 μm showed faster drug release in comparison with formulations made of unsieved HPMC fractions or made of HPMC fractions in a size range from 32 to 45 μm. However, detailed examination of dissolution curves showed additional differences. The fastest drug-release profile was from tablets from HPMC-C particles with a size from 100 to 125 μm and the slowest from tablets made of HPMC-D with unsieved particles and HPMC-D with particles from 32 to 45 μm, which were practically identical. These suggest that the release of diclofenac sodium from tablets made of HPMC-C particles in the size range from 100 to 125 μm started before the continuous gel layer was formed. The burst effect was the most pronounced from these tablets. The difference in release profiles from tablets made of smaller particles and unsieved particles were very small. These results were statistically proved with the calculated similarity factor f_2. For a dissolution profile to be considered similar, the value of f_2 should be between 50 and 100 [4]. The f_2 value for tablets with incorporated HPMC-C and HPMC-D with particles from 32 to 45 μm was 61, which indicates that both dissolution profiles were similar. In the case of larger particles of both HPMC samples (HPMC-C and HPMC-D) with particles from 100 to 125 μm, the f_2 value is 45, which indicates that the dissolution profiles were not similar. Furthermore, there was also no statistical difference between incorporated unsieved particles of HPMC-C and HPMC-D (the f_2 value was 76).

The question still remains why tablets made of HPMC-C with larger particles enabled faster release of the model drug compared to tablets made of HPMC-D of the same particle size. One possible reason is the formation of a homogeneous gel layer. This is influenced by the heterogeneity of the substitution of HPMC [23] and it could also be influenced by the methoxy/hydroxypropoxyl ratio. For the formation of a homogeneous gel layer, not only a high amount of hydrophilic hydroxypropoxy substituent is needed, but it seems that the appropriate methoxy/hydroxypropoxyl ratio is even more important. It can be concluded that various physical parameters had a different impact on low soluble drug-release profiles. The critical parameter is particle size and, within particles larger than 100 μm, the influence of methoxy/hydroxypropoxyl ratio is even more expressed.

4. Conclusion

This study shows that there are several differences in the physicochemical characteristics of the Methocel and Metolose HPMC batches. These differences include particle-size distribution, particle morphology, particle shape, methoxy/hydroxypropoxyl ratio, and the quality of the PLS calibration models obtained using NIR spectroscopy. Based on our results, it can be concluded that PLS calibration models for predicting the particle size of unknown sources cannot be simply built because of the presence of different physicochemical properties of HMPC batches that affect NIR spectra data and PLS calibration models. However, we succeeded in developing PLS calibration models that are capable of predicting the particle size of HPMC of a known source. Moreover, our results confirm that the release rate of diclofenac sodium from hydrophilic HPMC matrix tablets is mainly influenced by HPMC particle size, although the methoxy/hydroxypropoxyl ratio of the HPMC polymer must also be considered in the case of HPMC particles larger than 100 μm.

Although all the HPMC batches investigated were supplied as equivalent with regard to chemical and physical properties, both manufacturers and users must be aware of the polymer characteristics, which could generate great variation in the behavior of end-product formulations made from HPMC of the same commercial grade.

Acknowledgments

Colorcon (The Dow Chemical Co.) and Harke Pahrma (Shin-Etsu Chemical Co.) are acknowledged for providing cellulose samples. The experimental work was carried out at Krka, d.d. and at the Faculty of Pharmacy, Ljubljana, Slovenia.

References

[1] A. Viridén, B. Wittgren, A. Larsson, Investigation of critical polymer properties for polymer release and swelling of HPMC matrix tablets, Eur. J. Pharm. Sci. 36 (2009) 297–309.
[2] M.D. Ticehurst, P. York, R.C. Rowe, S.K. Dwivedi, Characterization of the surface properties of [alpha]-lactose monohydrate with inverse gas chromatography, used to detect batch variation, Int. J. Pharm. 141 (1996) 93–99.
[3] A. Viridén, B. Wittgren, T. Andersson, A. Larsson, The effect of chemical heterogeneity of HPMC on polymer release from matrix tablets, Eur. J. Pharm. Sci. 36 (2009) 392–400.
[4] S.D. Novak, V. Kuhelj, F. Vrečer, S. Baumgartner, The influence of HPMC viscosity as FRC parameter on the release of low soluble drug from hydrophylic matrix tablets, Pharm. Dev. Technol., doi:10.3109/10837450.2011.609991, in press.
[5] A. Viridén, A. Larsson, B. Wittgren, The effect of substitution pattern of HPMC on polymer release from matrix tablets, Int. J. Pharm. 389 (2010) 147–156.
[6] C. Gustafsson, C. Nyström, H. Lennholm, M.C. Bonferoni, C.M. Caramella, Characteristics of hydroxypropyl methylcellulose influencing compactibility and prediction of particle and tablet properties by infrared spectroscopy, J. Pharm. Sci. 92 (2003) 494–504.
[7] M.E. Campos-Aldrete, L. Villafuerte-Robles, Influence of the viscosity grade and the particle size of HPMC on metronidazole release from matrix tablets, Eur. J. Pharm. Biopharm. 43 (1997) 173–178.
[8] C. Maderuelo, A. Zarzuelo, J.M. Lanao, Critical factors in the release of drugs from sustained release hydrophilic matrices, J. Control. Release 154 (2011) 2–19.
[9] M.V. Velasco, J.L. Ford, P. Rowe, A.R. Rajabi-Siahboomi, Influence of drug: hydroxypropylmethylcellulose ratio, drug and polymer particle size and compression force on the release of diclofenac sodium from HPMC tablets, J. Control. Release 57 (1999) 75–85.
[10] S.A. Mitchell, K.M. Balwinski, Investigation of hypromellose particle size effects on drug release from sustained release hydrophilic matrix tablets, Drug Dev. Ind. Pharm. 33 (2007) 952–958.
[11] J. Luypaert, D.L. Massart, Y. Vander Heyden, Near-infrared spectroscopy applications in pharmaceutical analysis, Talanta 72 (2007) 865–883.
[12] M. Blanco, I. Villarroya, NIR spectroscopy: a rapid-response analytical tool, TrAC Trends Anal. Chem. 21 (2002) 240–250.
[13] G. Reich, Near-infrared spectroscopy and imaging: basic principles and pharmaceutical applications, Adv. Drug Deliv. Rev. 57 (2005) 1109–1143.

[14] M.P. Freitas, A. Sabadin, L.M. Silva, F.M. Giannotti, D.A. do Couto, E. Tonhi, R.S. Medeiros, G.L. Coco, V.F.T. Russo, J.A. Martins, Prediction of drug dissolution profiles from tablets using NIR diffuse reflectance spectroscopy: a rapid and nondestructive method, J. Pharm. Biomed. Anal. 39 (2005) 17–21.
[15] Y. Roggo, C. Roeseler, M. Ulmschneider, Near infrared spectroscopy for qualitative comparison of pharmaceutical batches, J. Pharm. Biomed. Anal. 36 (2004) 777–786.
[16] L.K.H. Bittner, N. Heigl, C.H. Petter, M.F. Noisternig, U.J. Griesser, G.K. Bonn, C.W. Huck, Near-infrared reflection spectroscopy (NIRS) as a successful tool for simultaneous identification and particle size determination of amoxicillin trihydrate, J. Pharm. Biomed. Anal. 54 (2011) 1059–1064.
[17] A. Candolfi, R. De Maesschalck, D. Jouan-Rimbaud, P.A. Hailey, D.L. Massart, The influence of data pre-processing in the pattern recognition of excipients near-infrared spectra, J. Pharm. Biomed. Anal. 21 (1999) 115–132.
[18] M. Blanco, A. Peguero, An expeditious method for determining particle size distribution by near infrared spectroscopy: comparison of PLS2 and ANN models, Talanta 77 (2008) 647–651.
[19] A.J. O'Neil, R.D. Jee, A.C. Moffat, The application of multiple linear regression to the measurements of the median particle size of drugs and pharmaceutical excipients by near-infrared spectroscopy, Analyst 123 (1998) 2297–2302.
[20] E.W. Ciurczak, R.P. Torlini, M.P. Demkowicz, Determination of particle size of pharmaceutical raw materials using near-infra-red reflectance spectroscopy, Spectroscopy (Springfield, Oreg.) 1 (1986) 36–39.
[21] J. Herder, Å. Adolfsson, A. Larsson, Initial studies of water granulation of eight grades of hypromellose (HPMC), Int. J. Pharm. 313 (2006) 57–65.
[22] J. Märk, M. Andre, M. Karner, C.W. Huck, Prospects for multivariate classification of a pharmaceutical intermediate with near-infrared spectroscopy as a process analytical technology (PAT) production control supplement, Eur. J. Pharm. Biopharm. 76 (2010) 320–327.
[23] A. Viridén, S. Abrahmsén-Alami, B. Wittgren, A. Larsson, Release of theophylline and carbamazepine from matrix tablets—consequences of HPMC chemical heterogeneity, Eur. J. Pharm. Biopharm. 78 (2011) 470–479.

Journal of Pharmaceutical and Biomedical Analysis 66 (2012) 144–153

Contents lists available at SciVerse ScienceDirect

Journal of Pharmaceutical and Biomedical Analysis

journal homepage: www.elsevier.com/locate/jpba

Determination of carotenoids in *Taraxacum formosanum* by HPLC–DAD–APCI-MS and preparation by column chromatography

T.H. Kao[a], C.H. Loh[a], B. Stephen Inbaraj[a], B.H. Chen[a,b,*]

[a] Department of Food Science, Fu Jen University, Taipei 242, Taiwan
[b] Graduate Institute of Medicine, Fu Jen University, Taipei 242, Taiwan

ARTICLE INFO

Article history:
Received 17 February 2012
Received in revised form 15 March 2012
Accepted 16 March 2012
Available online 28 March 2012

Keywords:
Taraxacum formosanum
Carotenoids
HPLC–DAD–APCI-MS
Preparative column chromatography

ABSTRACT

The objectives of this study were to determine the variety and content of carotenoids in *Taraxacum formosanum*, a traditional Chinese herb possessing vital biological activities, by developing an HPLC–DAD–APCI-MS method and a preparative column chromatographic method for carotenoid isolation. A total of 25 carotenoids were resolved within 66 min by employing a YMC C30 column and a gradient mobile phase of methanol–acetonitrile–water (79:14:7, v/v/v) and methylene chloride (100%) with flow rate at 1.0 mL/min and detection at 450 nm. All-*trans*-canthaxanthin was shown to be an appropriate internal standard for quantitation, with all-*trans*-β-carotene and its *cis* isomers present in largest amount (413.6 μg/g), followed by all-*trans*-violoxanthin and its *cis* isomers (209.5 μg/g), all-*trans*-lutein and its *cis* isomers (212.4 μg/g), all-*trans*-neoxanthin and its *cis* isomers (134.6 μg/g), antheraxanthin (16.5 μg/g), all-*trans*-β-cryptoxanthin and its *cis* isomers (5.8 μg/g), all-*trans*-zeaxanthin (3.6 μg/g) and neochrome (0.1 μg/g). For preparative chromatography, with a glass column containing 52 g of magnesium oxide-diatomaceous earth (1:3, w/w) as adsorbent, the carotenoid fraction was eluted with 300 mL of ethyl acetate with flow rate at 10 mL/min. Some more epoxides and *cis* isomers of carotenoids were generated during preparative column chromatography. Nevertheless, the carotenoids isolated from *T. formosanum* may be used as raw material for possible production of health food in the future.

© 2012 Elsevier B.V. All rights reserved.

1. Introduction

Taraxacum officinale, commonly known as dandelion, is a popular Chinese herb widely used throughout the world, especially Taiwan and China. Dandelion has been shown to contain several species, in which *Taraxacum formosanum* is the dominant one in Taiwan [1]. Besides being used as medicinal plant, dandelion can be consumed as vegetable as well because of its abundance in nutrients [1]. It has been well documented that the intake of dandelion can be protective against liver and lung damage in mice [2,3]. This important biological activity can be attributed to the presence of many functional components such as taraxacerin, triterpenoid, chlorogenic acid, saponin and carotenoid [4]. However, the amount and variety of carotenoids in *T. formosanum* remain uncertain.

Like green plants, carotenoids are widely distributed in nature representing a vital class of pigments with color ranging from yellow to red. The lipid-soluble carotenoids can be divided into carotene and xanthophyll, with the former comprising only hydrocarbon and the latter being oxygenated derivative [5,6]. Among the various carotenoids, both lutein and lycopene have received great attention in the past decade due to their potential beneficial effects in the treatment of chronic diseases such as age-related macular degeneration and prostate-associated disease [7]. In addition, the impact of some other carotenoids like zeaxanthin and β-carotene on human health has been illustrated in the literature [8]. Thus, to develop a reliable method for determination of variety and amount of carotenoids in *T. formosanum* with maximum accuracy is deemed to be necessary.

The extraction of carotenoids has been routinely carried out by organic solvents such as hexane, acetone, ethanol or methanol or in combination of these solvents [5,6], and a high yield of carotenoids can often be achieved by employing a mixture of low-polarity and high-polarity solvents [9]. More recently, Shi et al. [10] used supercritical carbon dioxide to extract carotenoids from pumpkin, and a high yield of total carotenoids (109.6 μg/g) was attained with 10% ethanol as modifier and temperature at 40 °C and pressure at 35 MPa. Nevertheless, a much higher amount of total carotenoids (148.8 μg/g) was obtained by organic solvent extraction [10]. Following extraction, the various carotenoids can be separated by thin-layer chromatography (TLC) or high-performance liquid chromatography (HPLC), with the former being frequently used for preparation and purification for subsequent analysis by HPLC–MS [6,11]. Compared to TLC, HPLC can provide a better resolution

* Corresponding author at: Department of Food Science, Fu Jen University, Taipei 242, Taiwan. Tel.: +886 2 29053626; fax: +886 2 29051215.
E-mail address: 002622@mail.fju.edu.tw (B.H. Chen).

0731-7085/$ – see front matter © 2012 Elsevier B.V. All rights reserved.
doi:10.1016/j.jpba.2012.03.035

power, and thereby is the technique used most often for carotenoid separation [6]. Also, a gradient mobile phase and a C30 column are often adopted for simultaneous separation of positional and geometrical carotenoid isomers, as poor resolution has been shown for isocratic mobile phase and C18 column. For instance, Marinova and Ribarova [12] determined carotenoids in blackberry by a C18 column and a gradient mobile phase, and only 5 carotenoids were separated within 20 min. In a later study, a total of 27 carotenoids in concentrated orange juice was separated within 60 min with a C30 column and a gradient mobile phase [11]. However, the resolution remained inadequate. Likewise, a total of 14 carotenoids in orange juice were also resolved by a C30 column (5 μm particle size) and a similar gradient mobile phase [13]. As the number in carotenoid separation is still limited, it is pivotal to develop a better HPLC method for carotenoid separation in dandelion. The objectives of this study were to develop an improved HPLC–DAD–APCI-MS method and column chromatography for determination and preparation of carotenoids in *T. formosanum*.

2. Materials and methods

2.1. Materials and instrumentation

2.1.1. Materials

T. formosanum was procured from a local Chinese herb medicine store in Taipei city, Taiwan. Spinach (*Spinacea oleracea*) was purchased from a traditional market in New Taipei City, Taiwan and then subjected to cutting, freeze drying and grinding into powder for subsequent isolation of carotenoids by TLC. Carotenoid standards, including all-*trans*-zeaxanthin and all-*trans*-β-cryptoxanthin were obtained from Extrasynthese Co. (Genay, France), while all-*trans* forms of α-carotene, β-carotene and lutein were from Sigma (St. Louis, MO, USA). Internal standard all-*trans*-canthaxanthin was also from Sigma. All-*trans*-neoxanthin was procured from ChromaDex Co. (Santa Ana, CA, USA), but was found indeed to be 9- or 9′-*cis*-neoxanthin based on presence of a *cis* peak in absorption spectrum, and comparison of MS data and *Q*-ratio reported in the literature. The HPLC-grade solvents including methanol, ethanol, ethyl acetate, hexane, acetonitrile, methylene chloride, acetone and toluene were from Lab-Scan Co. (Gliwice, Poland). Deionized water was made using a Milli-Q water purification system from Millipore Co. (Bedford, MA, USA). The adsorbent magnesium oxide was from Sigma and diatomaceous earth from J.T. Baker Co. (Phillipsburg, NJ, USA). Anhydrous sodium sulfate was from Nacalai Tesque Co. (Kyoto, Japan). A polymeric reversed-phase C30 column (250 mm × 4.6 mm I.D., particle size 5 μm) used to separate carotenoids was from Waters Co. (Milford, MA, USA).

2.1.2. Instrumentation

The HPLC–MS instrument (1100 series) is composed of a column temperature controller (G1316A), degasser (G1379A), quaternary pump (G1311A), binary pump (G1312A), photodiode-array detector (G1315B), and quadrupole MS detector with multi-mode ion source (ESI and APCI) from Agilent (Agilent Technologies 1100 series, Palo Alto, CA, USA). The Eyela rotary evaporator (N-1) and vacuum pump (A-3S) was from Tokyo, Japan. The low-temperature circulating water tank was from Li-Tsen Co. (Taoyuan, Taiwan). The sonicator (2210R-DTH) was from Branson Co. (Danbury, CT, USA), and the freeze dryer (FD-24) from Chin-Ming Co. (Taipei, Taiwan). The low-temperature incubator (TL 520R) was from Shen-Long Co. (Taiwan), and the spectrophotometer (DU 640) from Beckman Co. (Fullerton, CA, USA).

2.2. Methods

2.2.1. Extraction of carotenoids

A method based on Inbaraj et al. [9] was modified to extract carotenoids from *T. formosanum*. Initially, 1 g of dried *T. formosanum* sample was mixed with 30 mL of hexane/ethanol/acetone/toluene (10:6:7:7, v/v/v/v) in a flask and shaken for 1 h, after which 2 mL of 40% methanolic potassium hydroxide was added for saponification for 16 h in the dark under nitrogen. Then, 15 mL of hexane was added and the solution shaken for 10 min, followed by adding 15 mL of 10% sodium sulfate solution and shaken for 1 min. The supernatant was collected and 15 mL of hexane was added to the residue and shaken for 10 min. Again, the supernatant was collected. This procedure was repeated 4 times until the residue became colorless. All the supernatants were pooled, evaporated to dryness, dissolved in 5 mL of methanol–methylene chloride (1:1, v/v), filtered through a 0.2-μm membrane filter and 20 μL injected for HPLC–DAD–APCI-MS analysis.

2.2.2. Isolation of carotenoids by TLC

A method based on Inbaraj et al. [9] was modified to prepare neoxanthin and violaxanthin standards from spinach by TLC. In the beginning 20 g of freeze-dried spinach powder was mixed with 250 mL of hexane in a flask and the mixture shaken for 1 h, after which 25 mL of 40% methanolic potassium hydroxide was added and shaken for 1 min. Then the solution was saponified in the dark for 16 h under nitrogen, followed by adding 150 mL of hexane and shaken for 1 min. Again, 50 mL of 10% sodium sulfate solution was added and shaken for 1 min. Next, the mixture was allowed to stand in the dark for 1 h until two layers were formed. The supernatant layer was collected, evaporated to dryness and dissolved in 10 mL of hexane for TLC analysis. Prior to TLC separation, the TLC plates (20 cm × 20 cm, silica gel 60 F254, 0.5 mm thickness) were activated in 100 °C oven for 1 h and then cooled, after which 150 mL of methanol–acetone–hexane (1:29:70, v/v/v) was poured into a glass tank lined with a filter paper and covered with a lid. After equilibrating at room temperature for 30 min for saturation with solvent vapor, 1 μL of spinach extract was spotted at a distance of about 3 cm from the bottom of the plate for a total of 12 spots each plate. After solvent front reached a distance of about 18 cm from the bottom of the plate, both neoxanthin and violaxanthin bands were scratched with a razor and dissolved in acetone separately. A total of 30 TLC plates were used for collection of neoxanthin and violaxanthin bands. After evaporation to dryness, both neoxanthin and violaxanthin were dissolved in ethanol separately for absorbance measurement at 439 and 443 nm, respectively, based on Beer's law and extinction coefficient of 2243 and 2550 [9]. The contents of neoxanthin and violaxanthin were calculated to be 3.62 and 37.8 μg/mL, respectively.

2.2.3. Preparation of photoisomerized carotenoid standards

The photoisomerization was performed by preparing 100 μg/mL each of all-*trans* forms of lutein, β-carotene and β-cryptoxanthin standards and 50 μg/mL of all-*trans*-zeaxanthin standard. One mL of each solution was collected and poured into a vial and mixed with 100 μL of 0.01% iodine solution to accelerate isomerization, after which all the vials were placed in a 25 °C incubator and illuminated under fluorescent light for 1 h with the following condition: 4 fluorescent tubes with 55-cm long and 20 W each, illumination distance 30 cm and light intensity 2000–3000 lux. After illumination, each standard solution was filtered through a 0.2 μm membrane filter and 20-μL injected for absorption spectra and HPLC–MS analysis. The total-ion scanning mode with APCI was used for detection with the following condition: scanning range 400–1200 *m*/*z*, drying gas flow 7 L/min, nebulizer pressure 10 psi, dry gas temperature 330 °C, vaporizer

temperature 230 °C, capillary voltage 2000 V, charging voltage 2000 V, fragmentor voltage 200 V and corona current 4 μA.

2.2.4. Chromatographic conditions

A method based on Inbaraj et al. [9] was modified to separate the various carotenoids in *T. formosanum*. After several trial studies, a mobile phase system of methanol/acetonitrile/water (79:14:7, v/v/v) (A) and methylene chloride (B) was found appropriate with the gradient condition being 95% A in the beginning and maintained for 9 min, decreased to 85% A in 23 min, 83% A in 33 min, 71% A in 35 min, 70% A in 45 min, 66% A in 66 min and returned to original ratio in 71 min. A C30 column and a flow rate of 1 mL/min with detection at 450 nm were used. The separation efficiency was evaluated based on k value (retention factor) and α value (selectivity). The identification of carotenoids was carried out by comparing retention time, absorption spectra and mass spectra of unknown peaks with reference standards. For *cis* isomers of carotenoids, they were identified based on absorption spectra characteristics as described in several previous studies [7,9]. Additionally, the photoisomerized carotenoid standards were used for comparison of retention time and absorption spectra with unknown peaks.

2.2.5. Method validation

For quantitation, the internal standard all-*trans*-canthaxanthin was used and prepared in methylene chloride for a concentration of 100 μg/mL. Six concentrations of 0.6, 1, 5, 8, 10 and 20 μg/mL were each prepared for all-*trans*-zeaxanthin and all-*trans*-β-cryptoxanthin standards separately, while 0.2, 1, 5, 10, 20 and 50 μg/mL for all-*trans*-lutein standard, and 1, 5, 8, 10, 20 and 50 μg/mL for all-*trans*-β-carotene standard. Likewise, 6 concentrations of 0.08, 1.3, 1.95, 3.25, 5.19 and 6.49 μg/mL were prepared for 9 or 9′-*cis*-neoxanthin standard, whereas 0.47, 0.95, 1.89, 3.78, 4.73 and 9.45 μg/mL for violaxanthin standard. Then all the standard solutions were mixed with internal standard with each standard solution containing all-*trans*-canthaxanthin at 10 μg/mL. Each standard solution was injected into HPLC twice and the standard curves were prepared by plotting concentration ratio (standard versus internal standard) against its area ratio, and the regression equation and correlation coefficient (R^2) of each standard curve was obtained automatically with an EXCEL software system.

The intra-day variability was carried out by measuring carotenoid concentration in *T. formosanum* in the morning, afternoon and night with 3 determinations each on the same day for a total of 9 determinations. Similarly, the inter-day variability was performed by measuring carotenoid concentrations on the 1st, 2nd and 3rd day with 3 determinations each day for a total of 9 determinations. Both limit of detection (LOD) and limit of quantitation (LOQ) were determined by preparing the following 3 low concentrations of carotenoid standards and each concentration injected into HPLC 3 times: 0.2, 0.6 and 1 μg/mL for all-*trans*-β-cryptoxanthin and all-*trans*-lutein; 1, 5 and 8 μg/mL for all-*trans*-β-carotene; 0.5, 0.9 and 1.9 μg/mL for violaxanthin; 0.08, 0.16 and 0.33 μg/mL for 9- or 9′-*cis*-neoxanthin. Each standard curve was prepared by plotting concentration against peak height, with the slope (S) and the maximum noise height ($N\rho - \rho$) being obtained for calculation of LOD and LOQ by using the following formula:

$$\delta = N\rho - \rho/5$$

$$\mathrm{LOD} = 3.3 \times \delta/S$$

$$\mathrm{LOQ} = 3 \times \mathrm{LOD}$$

The recovery was determined by adding 50 μL or 100 μL of all-*trans*-lutein and all-*trans*-β-carotene (1000 μg/mL each) to 1 g of freeze-dried *T. formosanum* sample separately for extraction and HPLC analysis, while 30 μL or 100 μL of all-*trans*-zeaxanthin and all-*trans*-β-cryptoxanthin (100 μg/mL each) were added to 1 g of the same sample. Similarly, 552 μL or 2209 μL of neoxanthin (3.62 μg/mL each) were added to 0.1 g of *T. formosanum* sample for extraction and HPLC analysis, whereas 264.5 μL or 1058.2 μL of violaxanthin (37.8 μg/mL each) added to 1 g of the same sample. After quantitation by HPLC–DAD, the recovery of each carotenoid was calculated based on the ratio of the amount of carotenoid standard after HPLC relative to that before HPLC (spiked amount). Because of unavailability of commercial standards, the *cis* isomers of carotenoids were quantified using the recovery of their corresponding all-*trans* forms. The various carotenoids in *T. formosanum* were then quantified using a formula as described in several previous studies [5,6,9].

2.2.6. Statistical analysis

Triplicate analyses were performed and the data were subjected to analysis of variance by ANOVA and Duncan's multiple range test for statistical significance ($P < 0.05$) in mean comparison based on SAS [14].

2.2.7. Preparation of carotenoids by column chromatography

A method based on Inbaraj et al. [5] and Tsai et al. [8] was modified to prepare carotenoids from *T. formosanum*. A 10-g of freeze-dried *T. formosanum* sample was mixed with 80 mL of hexane/ethanol/acetone/toluene (10:6:7:7, v/v/v/v) in a flask and the mixture was shaken for 1 h, after which 80 mL of hexane was added and shaken for 10 min, followed by adding 30 mL of 10% sodium sulfate solution and standing until separation into two layers. The supernatant (upper layer) containing carotenoids and chlorophylls was collected, while the lower layer was repeatedly extracted with hexane for 4 times until colorless. All the supernatants were combined, evaporated to dryness and dissolved in 10 mL of hexane for column chromatography. Then 3 mL of crude extract was collected and poured into a glass column (400 mm × 42 mm I.D.) containing 52 g of magnesium oxide and diatomaceous earth (1:3, w/w), which was previously activated with 500 mL of hexane and anhydrous sodium sulfate added to form a layer of 1 cm above the adsorbent, followed by adding 300 mL of ethyl acetate (100%) for elution of carotenoids at a flow rate of 10 mL/min. The chlorophyll fraction remained uneluted under this condition as several green bands still retained in the column. The carotenoid fraction was then evaporated to dryness under vacuum, dissolved in 5 mL of methanol/methylene chloride (1:1, v/v), filtered through a 0.2-μm membrane filter, and 20 μL injected for HPLC–DAD–APCI-MS analysis.

3. Results and discussion

3.1. HPLC analysis

It has been well established that a C30 column can provide a much better resolution than a C18 column in separating carotenoids and their geometrical isomers [5,9]. Initially a gradient solvent system of methanol/acetonitrile/water (84:14:2, v/v/v) and methylene chloride developed by Inbaraj et al. [9] was used to separate the various carotenoids in *T. formosanum* by a YMC C30 column (250 mm × 4.6 mm I.D., particle size 5 μm). However, several carotenoid peaks overlapping occurred, which should be due to a high strong solvent strength of this mobile phase. Thus, it is necessary to decrease solvent strength through increase of mobile phase polarity. After various studies, a gradient mobile phase of methanol/acetonitrile/water (79:14:7, v/v/v) (A) and methylene chloride (B) as described in Section 2.2 was developed to separate 25 carotenoids and their geometrical isomers within 66 min (Fig. 1),

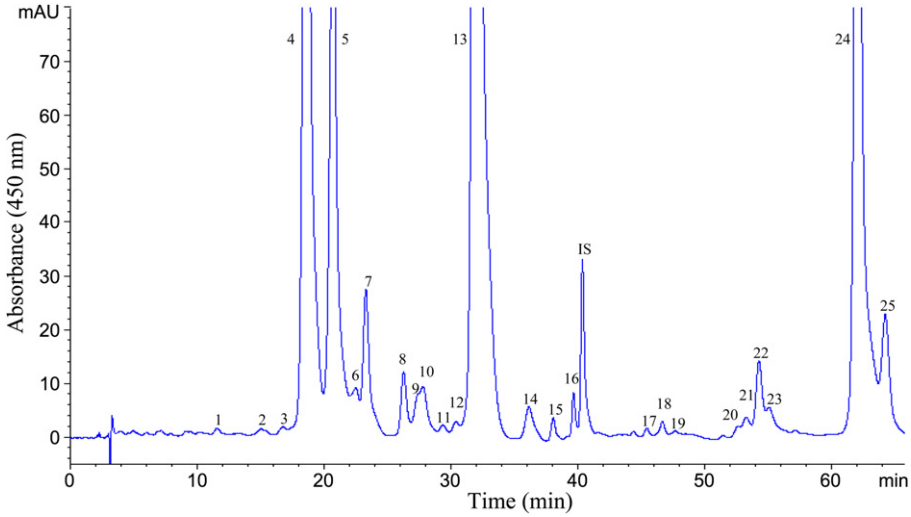

Fig. 1. HPLC chromatogram of carotenoids extracted from *T. formosanum* (column: C_{30}, mobile phase: (A) methanol–acetonitrile–water (79:14:7, v/v/v), (B) methylene chloride, flow rate: 1 mL/min, detection wavelength: 450 nm). Peak identification shown in Table 1.

with the retention times ranging from 11.54 to 64.22 min, retention factor from 2.51 to 18.57, separation factor from 1.01 to 1.44 and peak purity from 88.3 to 99.8% (Table 1). Most carotenoid peaks were adequately resolved (Fig. 1), implying both solvent strength and selectivity of mobile phase to sample components were properly controlled.

3.2. TLC analysis

As the amount of 9- or 9′-*cis*-neoxanthin standard was inadequate, as shown by a small concentration at 0.649 mg/L, and the commercial unavailability of violaxanthin standard, both neoxanthin and violaxanthin standards were also prepared from spinach by TLC using a procedure described in Section 2.2. Following collection of neoxanthin and violaxanthin bands, they were identified by adding one drop of 0.1 N HCl solution (in methanol) to both extracts and the absorption spectra measured with a spectrophotometer. A color change from yellow to green, accompanied by a hypsochromic shift of about 20 nm indicated the presence of neoxanthin. But for violaxanthin, a color change from yellow to blue and a hypsochromic shift of about 40 nm was observed [6]. Both neoxanthin and violaxanthin were further subjected to HPLC–DAD–APCI-MS analysis for positive identification.

3.3. Photoisomerization of standards

For further identification of carotenoids in *T. formosanum*, the various carotenoid standards were illuminated to accelerate *cis* isomers formation by using a procedure described in the preceding section. Fig. 2 shows the HPLC chromatograms of photoisomerized carotenoid standards, including lutein (Fig. 2A), zeaxanthin (Fig. 2B), β-cryptoxanthin (Fig. 2C) and β-carotene (Fig. 2D). Following the same approach in identifying carotenoid *cis* isomers, a total of 9 *cis* isomers of lutein and all-*trans*-lutein (peak 6) were shown in Fig. 2A, with the retention times ranging from 22.08 to 40.53 min, *k* value from 5.59 to 11.10 and peak purity from 97.8 to 99.9%. Similarly, a total of 5 *cis* isomers of zeaxanthin and all-*trans*-zeaxanthin (peak 3) were present in Fig. 2B, with the retention times ranging from 30.21 to 42.06 min, *k* value from 8.27 to 11.90 and peak purity from 93.0 to 99.9%, as were 9 *cis* isomers of β-cryptoxanthin and all-*trans*-β-cryptoxanthin (Peak 7) in Fig. 2C, with the retention times ranging from 39.61 to 49.22 min, *k* value from 11.03 to 13.96 and peak purity from 99.2 to 99.9%. In Fig. 2D, a total of 5 *cis* isomers of β-carotene and all-*trans*-β-carotene (peak 5) were found, with the retention times ranging from 52.39 to 64.21 min, *k* value from 14.55 to 18.05 and purity from 93.9 to 99.9%. Next, as mentioned before, the retention time, absorption spectra and mass spectra characteristics of each carotenoid isomer were compared with unknown peaks on the HPLC chromatogram in *T. formosanum* samples for identification.

3.4. Identification of carotenoids in T. formosanum

Table 2 shows the tentative identification data containing both absorption and mass spectra as well as reported values [5,9,11,15–23]. In Fig. 1, peak 1 was identified as 9- or 9′-*cis*-violaxanthin based on epoxide test and hypsochromic shift of about 2 nm when compared to all-*trans*-violaxanthin as well as a weak absorption peak at 348 nm [15]. Additionally, the characteristic ions $[M+H]^+$ 601.5 and $[M+H-18]^+$ 583.4 were the same as that reported by de Faria et al. [21]. Peak 2 was identified as neochrome as a hypsochromic shift of about 20 nm was found when compared to neoxanthin prepared by TLC and *m*/*z* $[M+H]^+$ 601.5 with that reported by de Faria et al. [21]. Both peaks of 3 and 4 were identified as all-*trans* forms of neoxanthin and violaxanthin, respectively, based on epoxide text, absorption spectra and mass spectra characteristics, as well as comparison with those prepared by TLC and those reported in the literature [11,15,21]. Peak 5 was identified as 9- or 9′-*cis*-neoxanthin as a hypsochromic shift of about 6 nm and a weak absorption band at 326 nm occurred when compared to all-*trans*-neoxanthin prepared by TLC. In addition, a hypsochromic shift of 18 nm was shown after epoxide test, and both absorption spectra and mass spectra were in agreement with those reported by Melendez-Martinez et al. [15] and de Faria et al. [21]. Both peaks 6 and 10 were identified as luteoxanthin based on absorption spectra and mass spectra characteristics and compared with that reported by Chen et al. [16] and Dugo et al. [19]. Also, a hypsochromic shift of 20 nm occurred for both peaks after epoxide test, indicating its further conversion to auroxanthin upon treatment with acid. Following the same approach, peaks 7 and 9 were identified as *cis*-violaxanthin and 9 or 9′-*cis*-violaxanthin, respectively [15,17,21]. However, the *cis* position of violaxanthin (peak 7) was not assigned as the absorption spectrum was the same as all-*trans*-violaxanthin (peak 4). Peak 8 was identified as antheraxanthin based on a hypsochromic shift of about 20 nm after adding a drop of 0.1 N HCl, indicating its further conversion to

Table 1
Retention time, retention factor (k), separation factor (α), purity and content of carotenoids in *T. formosanum*.

Peak no.	Compound	t_R (min)	Retention factor (k)	Separation factor (α)	Peak purity (%)	Content (μg/g)[b]	
						Intra-day variability (RSD, %)	Inter-day variability (RSD, %)
1	9-or 9′-*cis*-Violaxanthin	11.54	2.51	1.44 (1, 2)[a]	88.3	1.4 ± 0.1 (0.7)	1.2 ± 0.1 (1.6)
2	Neochrome	15.17	3.62	1.14 (2, 3)	92.9	0.1 ± 0.0 (4.5)	0.1 ± 0.0 (6.5)
3	All-*trans*-neoxanthin	16.86	4.14	1.13 (3, 4)	96.2	0.2 ± 0.0 (0.7)	0.3 ± 0.1 (4.9)
4	All-*trans*-violaxanthin	18.65	4.68	1.13 (4, 5)	91.7	181.7 ± 3.8 (1.9)	184.2 ± 4.5 (2.0)
5	9-or 9′-*cis*-Neoxanthin	20.65	5.29	1.10 (5, 6)	96.8	134.4 ± 3.3 (3.2)	137.9 ± 4.1 (5.5)
6	Luteoxanthin	22.54	5.87	1.04 (6, 7)	93.7	8.0 ± 0.1 (1.3)	8.7 ± 0.6 (5.7)
7	*cis*-Violaxanthin	23.35	6.11	1.14 (7, 8)	92.6	21.3 ± 0.5 (0.2)	21.4 ± 1.4 (5.4)
8	Antheraxanthin	26.27	7.00	1.04 (8, 9)	92.7	16.5 ± 0.1 (2.2)	16.2 ± 0.4 (6.2)
9	9-or 9′-*cis*-Violaxanthin	27.31	7.32	1.02 (9, 10)	95.4	5.1 ± 0.2 (3.5)	4.6 ± 0.3 (5.3)
10	Luteoxanthin	27.80	7.47	1.06 (10, 11)	96.6	8.4 ± 0.2 (1.6)	8.2 ± 0.5 (5.1)
11	13-or 13′-*cis*-Lutein	29.39	7.96	1.03 (11, 12)	95.3	0.4 ± 0.0 (2.1)	0.4 ± 0.0 (5.9)
12	13 or 13′-*cis*-Lutein	30.33	8.24	1.06 (12, 13)	93.4	0.7 ± 0.0 (3.5)	0.8 ± 0.1 (5.8)
13	All-*trans*-lutein	31.97	8.74	1.14 (13, 14)	97.0	209.4 ± 2.8 (1.6)	205.4 ± 8.0 (4.2)
14	All-*trans*-zeaxanthin	36.09	10.00	1.06 (14, 15)	90.9	3.6 ± 0.1 (3.5)	3.4 ± 0.2 (4.8)
15	9-or 9′-*cis*-Lutein	38.05	10.60	1.04 (15, 16)	96.6	0.6 ± 0.0 (4.8)	0.5 ± 0.1 (6.4)
16	9-or 9′-*cis*-Lutein	39.60	11.07	1.01 (16, IS)	92.8	1.3 ± 0.0 (1.7)	1.4 ± 0.1 (7.2)
IS	All-*trans*-canthaxanthin	40.34	11.29	1.13 (IS, 17)	99.8	–	–
17	All-*trans*-β-cryptoxanthin	45.48	12.86	1.03 (17, 18)	92.2	1.8 ± 0.1 (2.0)	1.7 ± 0.2 (4.4)
18	9-or 9′-*cis*-β-Cryptoxanthin	46.83	13.27	1.15 (18, 19)	95.2	2.3 ± 0.4 (1.8)	2.4 ± 0.4 (5.2)
19	9-or 9′-*cis*-β-Cryptoxanthin	47.66	13.53	1.11 (19, 20)	91.8	1.7 ± 0.1 (3.6)	1.5 ± 0.2 (6.9)
20	15 or 15′-*cis*-β-Carotene	52.64	15.04	1.01 (20, 21)	98.8	6.1 ± 0.2 (4.2)	6.9 ± 0.3 (6.5)
21	9-or 9′-*cis*-β-Carotene	53.37	15.27	1.02 (21, 22)	92.6	9.7 ± 0.3 (3.0)	8.9 ± 0.3 (3.4)
22	15-or 15′-*cis*-β-Carotene	54.52	15.62	1.01 (22, 23)	94.3	24.7 ± 0.9 (4.1)	24.2 ± 1.2 (5.3)
23	13-or 13′-*cis*-β-Carotene	55.36	15.87	1.03 (23, 24)	98.1	13.0 ± 0.5 (4.4)	12.6 ± 0.8 (6.6)
24	All-*trans*-β-carotene	62.11	17.93	1.03 (24, 25)	97.4	312.2 ± 5.0 (2.1)	316.3 ± 15.2 (6.6)
25	9-or 9′-*cis*-β-Carotene	64.22	18.57	1.03 (24, 25)	90.5	47.9 ± 1.5 (4.8)	46.1 ± 2.3 (7.2)

[a] Numbers in parentheses represent values between two neighboring peaks.
[b] Average of duplicate analyses ± standard deviation.

mutatoxanthin. In addition, the absorption spectra and mass spectra characteristics of peak 8 were coincided with that reported by Dugo et al. [19]. Peaks 13, 14, 17 and 24 were positively identified as all-*trans* forms of lutein, zeaxanthin, β-cryptoxanthin and β-carotene, respectively, with their *cis* isomers being tentatively identified based on the same criteria and comparison with those of photoisomerized carotenoid standards [5,9,20,21,23]. In several similar studies the major carotenoids, including neoxanthin, violaxanthin, β-carotene, zeaxanthin, β-cryptoxanthin and antheraxanthin were also detected in dandelion (*Taraxacum officinale* F. Weber ex Wiggers), a different variety of *Taraxacum* [24], as was neoxanthin in another variety of *Taraxacum* [25]. Nevertheless, the kind of carotenoid may be varied as some more carotenoids like neochrome and luteoxanthin were detected in *T. formosanum* samples in our study, which should be due to difference in analytical method or growth condition and location.

3.5. Method validation

As mentioned in the preceding section, an internal standard all-*trans*-canthaxanthin was used for preparation of carotenoid standard curves for subsequent quantitation by HPLC–DAD. The regression equations for all-*trans* forms of lutein, zeaxanthin, β-cryptoxanthin, β-carotene and violaxanthin as well as 9- or 9′-*cis*-neoxanthin were $y = 4.1596x + 0.0627$, $y = 4.4076x - 0.086$, $y = 3.6381x - 0.1415$, $y = 1.0935x - 0.1299$, $y = 2.5019x - 0.0433$ and $y = 1.7349x + 0.0727$, respectively, with R^2 being all higher than 0.99. The LOD of all-*trans* forms of lutein, zeaxanthin, β-cryptoxanthin, β-carotene and violaxanthin, and 9- or 9′-*cis*-neoxanthin were 0.06, 0.06, 0.03, 0.29, 0.05 and 0.03 μg/mL, respectively, whereas the LOQ were 0.18, 0.18, 0.09, 0.87, 0.09 and 0.15 μg/mL. Table 1 shows the precision data of various carotenoids in *T. formosanum* with the intra-day variability being ranged from 0.2 to 4.8% and the inter-day variability from 1.6 to 7.2%, demonstrating that a high reproducibility was achieved by using this method. The accuracy of this method was assessed by determining recovery of all-*trans* forms of lutein, zeaxanthin, β-cryptoxanthin, β-carotene and violaxanthin, and 9- or 9′-*cis*-neoxanthin, with a mean value of 91.4, 96.1, 90.6, 97.7, 86.6 and 85.6% being attained, respectively. Compared to the other carotenoids, both violaxanthin and neoxanthin showed a slightly lower recovery, which should be due to their susceptibility to form some other derivatives like epoxides and *cis* isomers or undergo degradation in the presence of oxygen, light or acid [6].

3.6. Contents of carotenoids in T. formosanum

The contents of various carotenoids in *T. formosanum* are shown in Table 1, in which all-*trans*-β-carotene and its *cis*-isomers were present in largest amount (413.6 μg/g), followed by all-*trans*-lutein and its *cis* isomers (212.4 μg/g), all-*trans*-violaxanthin and its *cis* isomers (209.5 μg/g), all-*trans*-neoxanthin and its *cis* isomers (134.6 μg/g), antheraxanthin (16.5 μg/g), luteoxanthin (16.4 μg/g), all-*trans*-β-cryptaxanthin and its *cis* isomers (5.8 μg/g), all-*trans*-zeaxanthin (3.6 μg/g) and neochrome (0.1 μg/g), with a total amount being 1012.5 μg/g. Comparatively, all-*trans* forms of β-carotene, lutein, violaxanthin, as well as 9- or 9′-*cis*-neoxanthin were present at a much larger amount than their corresponding *cis* isomers. As most carotenoids occur naturally in all-*trans* form, the formation of 9- or 9′-*cis*-neoxanthin is probably due to extraction or chromatography. According to literature reports, neoxanthin, violaxanthin, lutein and β-carotene are widely present in green plants, but the amount can be varied with type and variety. For instance, neoxanthin was present in abundant amount (185.0 μg/g) in *Bacopa monnieri*, while in *Aloe vera*, neoxanthin was only present in small amount (22.7 μg/g) [26]. Similarly, violaxanthin was present at 97.0 μg/g in *Datura stramonium* [26]. Compared to neoxanthin and violaxanthin, lutein and β-carotene were often

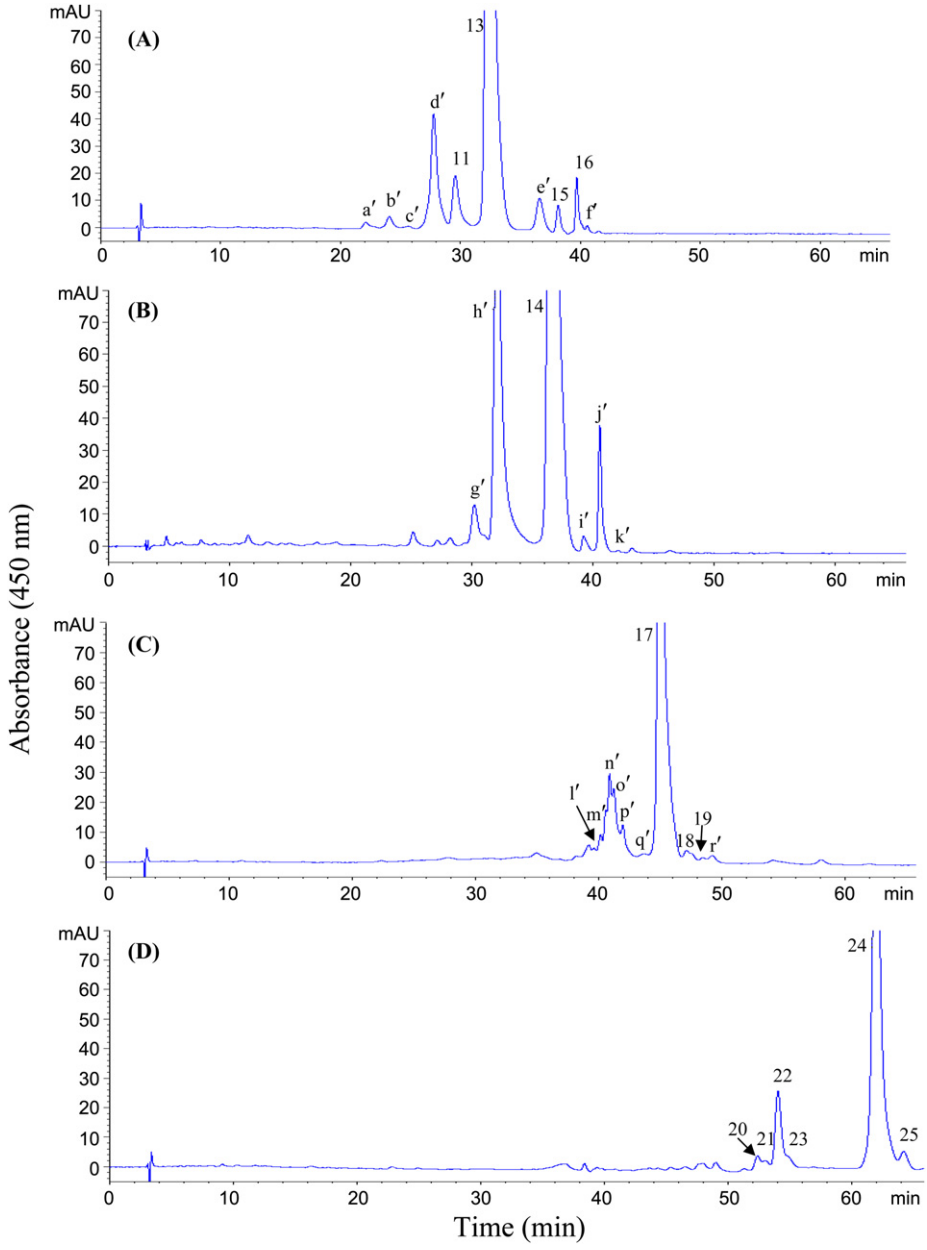

Fig. 2. HPLC chromatogram of lutein standard and its *cis* isomers (A), zeaxanthin standard and its *cis* isomers (B), β-cryptoxanthin standard and its *cis* isomers (C) and β-carotene standard and its *cis* isomers (D) after iodine-catalyzed illumination at 25 °C for 1 h (A, B, C) and 30 min (D). Peak identification for (A): a′, *cis*-lutein; b′, *cis*-lutein; c′, 13- or 13′-*cis*-lutein; d′, 13- or 13′-*cis*-lutein; 11, 13- or 13′-*cis*-lutein; 13, all-*trans*-lutein; e′, 9- or 9′-*cis*-lutein; 15, 9- or 9′-*cis*-lutein; 16, 9- or 9′-*cis*-lutein; f′, *cis*-lutein. Peak identification for (B): g′, 13- or 13′-*cis*-zeaxanthin; h′, 15- or 15′-*cis*-zeaxanthin; 14, all-*trans*-zeaxanthin; i′, 9- or 9′-*cis*-zeaxanthin; j′, 9- or 9′-*cis*-zeaxanthin; k′, 9- or 9′-*cis*-zeaxanthin. Peak identification for (C): l′, 15- or 15′-*cis*-β-cryptoxanthin; m′, 15- or 15′-*cis*-β-cryptoxanthin; n′, 15- or 15′-*cis*-β-cryptoxanthin; o′, 13- or 13′-*cis*-β-cryptoxanthin; p′, 15- or 15′-*cis*-β-cryptoxanthin; q′, 15- or 15′-*cis*-β-cryptoxanthin; 17, all-*trans*-β-cryptoxanthin; 18, 9- or 9′-*cis*-β-cryptoxanthin; 19, 9- or 9′-*cis*-β-cryptoxanthin; r′, 9- or 9′-*cis*-β-cryptoxanthin. Peak identification for (D): 20, 15- or 15′-*cis*-β-carotene; 21, 9- or 9′-*cis*-β-carotene; 22, 15- or 15′-*cis*-β-carotene; 23, 13- or 13′-*cis*-β-carotene; 24, all-*trans*-β-carotene; 25, 9- or 9′-*cis*-β-carotene.

present at a much larger content in green plants. For example, a large level of 298.3 and 4840 μg/g of lutein were shown to be present in *Cassia augustifolia* and *Cynodon dactylon*, respectively [27]. Likewise, a high level of β-carotene (146.0 μg/g) was found in *Cyphostemma digitatum* [28]. Conversely, both β-cryptoxanthin and antheraxanthin were usually present at a much smaller amount in green plants, as evident by 6.7 μg/g in *Cyphostemma digitatum* for the former [28] and being undetected in *Arabidopsis thaliana* for the latter [29]. Zeaxanthin showed a similar trend with a moderate amount of 94.6 μg/g in *Cyphostemma digitatum* [28] and a small amount of 1.6, 7.5 and 15.8 μg/g in *Vitex negundo*, *Acalypha indica* and *Ocimum sanctum*, respectively [26]. All these outcomes further demonstrated that a much larger amount of total carotenoids were present in *T. formosanum*, which can be used as a major source of carotenoids for possible production of functional food in the future.

3.7. Preparation of carotenoids from T. formosanum by column chromatography

Initially a preparative column chromatographic method developed by Tsai et al. [8] was adopted to isolate carotenoids from *T. formosanum*. However, carotenoids were co-eluted with a portion of chlorophylls based on band color present on the column and HPLC–DAD analysis, and thereby the preparative column

Table 2
Identification data for all-*trans* and *cis* forms of carotenoids in Fig. 1.

Peak no.	Compound	λ (nm, inline)[a]	λ (nm, reported)	Epoxide test (hypsochromic shift)	Q-ratio[k] found	Q-ratio reported	*m*/*z* found	*m*/*z* reported
1	9-or 9′-*cis*-Violaxanthin	348, 412, 438, 464	326, 412, 436, 464[b]	420, 442	0.12	0.125[b]	601.5[M+H]$^+$, 583.4[M+H−18]$^+$	601[M+H]$^+$, 583.4[M+H−18]$^{+l}$
2	Neochrome	332, 404, 422, 450	332, 398, 422, 446[c]	400, 418, 442	0.25	0.22[c]	601.5[M+H]$^+$	601[M+H]$^{+l}$
3	All-*trans*-neoxanthin	336, 414, 442, 470	418, 440, 468[d]	400, 418, 442	0.03	–	601.5[M+H]$^+$, 583.4[M+H−18]$^+$	601[M+H]$^+$, 583[M+H−18]$^{+l}$
4	All-*trans*-violaxanthin	328, 416, 440, 468	416, 440, 468[b]	400, 422, 448	0.06	–	601.5[M+H]$^+$, 583.4[M+H−18]$^+$, 565.4[M+H−18−18]$^+$, 491.3[M+H−18−92]$^+$	601[M+H]$^+$, 583[M+H−18], 565[M+H−18−18]$^+$, 491.3[M+H−18−92]$^{+l}$
5	9-or 9′-*cis*-neoxanthin	326, 412, 436, 464	326, 414, 436, 464[d]	394, 418, 446	0.08	0.08[d]	601.4[M+H]$^+$, 583.4[M+H−18]$^+$, 565.4[M+H−18−18]$^+$, 491.3[M+H−18−92]$^+$	601[M+H]$^+$, 583[M+H−18]$^+$, 565[M+H−18−18]$^+$, 491.3[M+H−18−92]$^{+l}$
6	Luteoxanthin	330, 400, 422, 448	399, 423, 447[e]	382, 402, 426	0.07	0.16[e]	601.4[M+H]$^+$, 583.4[M+H−18]$^+$	601[M+H]^m
7	*cis*-Violaxanthin	326, 416, 440, 468	328, 414, 438, 466[f]	392, 418, 448	0.06	–	601.5[M+H]$^+$, 583.4[M+H−18]$^+$	601[M+H]$^+$, 583[M+H−18]$^{+l}$
8	Antheraxanthin	348, 418, 442, 472	421, 443, 470[i]	402, 422, 448	0.08	–	585.4[M+H]$^+$	585[M+H]^m
9	9-or 9′-*cis*-Violaxanthin	330, 412, 438, 464	326, 412, 436, 464[b]	398, 422, 448	0.20	0.125[b]	601.5[M+H]$^+$	601[M+H]$^{+l}$
10	Luteoxanthin	332, 394, 422, 448	399, 423, 447[e]	382, 402, 426	0.20	0.16[d]	601.5[M+H]$^+$	601[M+H]^m
11	13-or 13-*cis*-Lutein	330, 416, 442, 470	332, 415, 440, 464[c]		0.41	0.44[c]	551.4[M+H−18]$^+$	551.5[M+H−18]$^{+n}$
12	13 or 13′-*cis*-Lutein	330, 418, 438, 464	332, 415, 440, 464[c]		0.06	0.44[c]	551.4[M+H−18]$^+$	551.5[M+H−18]$^{+n}$
13	All-*trans*-lutein	334, 422, 446, 472	332, 423, 446, 470[c]		0.05	0.12[c]	569.4[M+H]$^+$, 551.4[M+H−18]$^+$, 533.4[M+H−18−18]$^+$, 459.3[M+H−18−92]$^+$	569.9[M+H]$^+$, 551.5[M+H−18]$^+$, 533.4[M+H−18−18]$^+$, 459.3[M+H−18−92]$^{+l}$
14	All-*trans*-zeaxanthin	424, 452, 478	344, 427, 452, 476[c]		–	0.11[c]	569.4[M+H]$^+$, 551.4[M+H−18]$^+$	569.7[M+H]$^+$, 551.4[M+H−18]$^{+o}$
15	9-or 9′-*cis*-Lutein	322, 414, 442, 472	332, 416, 440, 470[c]		0.05	0.13[c]	551.4[M+H−18]$^+$	551.5[M+H−18]$^{+n}$
16	9-or 9′-*cis*-Lutein	344, 414, 442, 470	332, 416, 440, 470[c]		0.20	0.13[c]	551.4[M+H−18]$^+$	551.5[M+H−18]$^{+n}$
IS	All-*trans*-canthaxanthin	480	–		–		–	–
17	All-*trans*-β-cryptoxanthin	334, 424, 452, 478	450, 476[j]		0.04	–	553.4[M+H]$^+$, 535.4[M+H−18]$^+$	553.4[M+H]$^+$, 535.4[M+H−18]$^{+l}$
18	9-or 9′-*cis*-β-Cryptoxanthin	334, 420, 446, 476	342, 446, 470[j]		0.07	0.08[j]	553.4[M+H]$^+$	553[M+H]$^{+l}$
19	9-or 9′-*cis*-β-Cryptoxanthin	330, 422, 448, 474	342, 446, 470[j]		0.04	0.08[j]	553.4[M+H]$^+$	553[M+H]$^{+l}$
20	15- or 15′-*cis*-β-Carotene	338, 424, 450, 474	421, 445, 474[g]		0.32	0.38[g]	537.4[M+H]$^+$	537[M+H]$^{+l}$
21	9-or 9′-*cis*-β-Carotene	340, 430, 450, 474	421, 452, 476[g]		0.08	0.25[g]	537.4[M+H]$^+$	537[M+H]$^{+l}$
22	15-or 15′-*cis*-β-Carotene	340, 422, 446, 470	421, 445, 474[g]		0.38	0.38[g]	537.5[M+H]$^+$	537[M+H]$^{+l}$
23	13-or 13′-*cis*-β-Carotene	338, 422, 444, 472	342, 422, 448, 474[h]		0.40	0.43[h]	537.4[M+H]$^+$	537[M+H]$^{+l}$
24	All-*trans*-β-carotene	454, 480	426, 456, 480[h]		–	0.09[h]	537.4[M+H]$^+$	537[M+H]$^{+l}$
25	9-or 9′-*cis*-β-Carotene	332, 452, 474	344, 428, 452, 476[c]		0.08	0.20[c]	537.4[M+H]$^+$	537[M+H]$^{+l}$

[a] A gradient mobile phase of methanol–acetonitrile–water (79:14:7, v/v/v) and methylene chloride (from 95:5, v/v to 66:34, v/v) was used.
[b] A mobile phase of methanol (solvent A), MTBE (solvent B) and water (solvent C) (from 90:5:5, v/v/v to 50:50:0, v/v/v) was used by Meléndez-Martínez et al. [15].
[c] A mobile phase of methanol–acetonitrile–water (84:14:2, v/v/v) and methylene chloride (from 100:0, v/v to 45:55, v/v) was used by Inbaraj et al. [9].
[d] A mobile phase of methanol (solvent A), MTBE (solvent B) and water (solvent C) (from 90:5:5, v/v/v to 50:50:0, v/v/v) was used by Meléndez-Martínez et al. [11].
[e] A mobile phase of methanol–2-proponol (99:1, v/v) and methylene chloride (from 100:0, v/v to 70:30, v/v) was used by Chen et al. [16].
[f] A mobile phase of MeCN–MeOH (75:25, v/v, solvent A), MTBE (solvent B) and water (solvent C) (from 95:0:5, v/v/v to 26:74:0, v/v/v) was used by Lee [17].
[g] A mobile phase of methanol–acetonitrile–water (84:14;2, v/v/v) and methylene chloride (from 80:20, v/v to 45:55, v/v) was used by Liu et al. [18].
[h] A mobile phase of methanol–acetonitrile–water (81:14:5, v/v/v) and methylene chloride (from 84:16, v/v to 75:25, v/v) was used by Inbaraj et al. [5].
[i] A mobile phase of 2-propanol and water–acetonitrile (20:80, v/v) (from 5:95, v/v to 70:30, v/v) was used by Dugo et al. [19].
[j] A mobile phase of methanol (solvent A), MTBE (solvent B) and water (solvent C) (from 90:5:5, v/v/v to 50:50:0, v/v/v) was used by Meléndez-Martínez et al. [20].
[k] Q-ratio is defined as the height ratio of the *cis* peak to the main absorption peak.
[l] Based on a report by de Faria et al. [21].
[m] Based on a report by Dugo et al. [19].
[n] Based on a report by Lakshminarayana et al. [22].
[o] Based on a report by Nakagawa et al. [23].

Table 3
Retention time, UV data, mass data and contents of carotenoids in carotenoid fraction prepared from *T. formosanum* by column chromatography.

Peak no.[*]	Compound	t_R (min)	λ (nm, inline)[a]	λ (nm, reported)	*Q*-ratio[k] found	*Q*-ratio reported	*m*/*z* found	*m*/*z* reported	Content (μg/g)[o]
A	Auroxanthin	6.99	328, 382, 398, 422	338, 374, 398, 422[c]	0.64	0.52[c]	601[M+H]$^+$	601[l]	2.87 ± 1.88
B	Auroxanthin	7.44	338, 380, 398, 422	338, 374, 398, 422[c]	0.62	0.52[c]	601[M+H]$^+$, 583[M+H−H_2O]$^+$	601, 583[l]	2.26 ± 1.42
C	Auroxanthin	8.87	328, 382, 400, 422	338, 374, 398, 422[c]	0.63	0.52[c]	601[M+H]$^+$	601[l]	1.61 ± 0.04
1	9-or 9′-*cis*-Violaxanthin	11.27	336, 412, 438, 460	326, 412, 436, 464[b]	0.31	0.13[b]	601[M+H]$^+$, 583[M+H−H_2O]$^+$	601, 583[m]	1.28 ± 0.05
D	13-or 13′-*cis*-neoxanthin	13.43	328, 414, 434, 460	328, 412, 434, 460[d]	0.27	0.39[d]	601[M+H]$^+$, 583[M+H−H_2O]$^+$	601, 583[m]	0.49 ± 0.37
2	Neochrome	14.98	328, 404, 428, 456	332, 398, 422, 446[c]	0.36	0.22[c]	601.5 [M+H]$^+$	601[m]	5.90 ± 0.55
3	All-*trans*-neoxanthin	16.80	328, 416, 440, 468	418, 440, 468[d]	0.24	–	601[M+H]$^+$, 583[M+H−H_2O]$^+$	601, 583[m]	5.20 ± 0.44
4	All-*trans*-violaxanthin	18.72	328, 416, 440, 468	416, 440, 468[b]	0.09	–	601[M+H]$^+$, 583[M+H−H_2O]$^+$	601, 583[m]	161.74 ± 2.65
5	9-or 9′-*cis*-neoxanthin	20.74	328, 414, 436, 464	326, 414, 436, 464[d]	0.08	0.08[d]	601[M+H]$^+$, 583[M+H−H_2O]$^+$	601, 583[m]	114.70 ± 1.18
6	Luteoxanthin	22.67	330, 402, 422, 448	399, 423, 447[e]	0.06	0.16[e]	601[M+H]$^+$, 583[M+H−H_2O]$^+$	601, 583[n]	17.54 ± 0.97
7	*cis*-Violaxanthin	23.44	328, 418, 440, 468	328, 414, 438, 466[f]	0.06	–	601[M+H]$^+$	601[m]	10.51 ± 1.05
E	Violaxanthin	24.48	330, 422, 440, 470	–	0.11	–	601[M+H]$^+$	–	2.85 ± 0.49
8	Antheraxanthin	26.40	328, 418, 444, 472	422, 442, 470[i]	0.20	–	585[M+H]$^+$	585[n]	10.74 ± 0.84
9	9-or 9′-*cis*-Violaxanthin	27.56	330, 414, 438, 464	326, 412, 436, 464[b]	0.28	0.13[b]	601[M+H]$^+$, 583[M+H−H_2O]$^+$	601, 583[m]	6.61 ± 0.22
10	Luteoxanthin	27.75	330, 414, 438, 464	399, 423, 447[e]	0.38	0.16[e]	601[M+H]$^+$, 583[M+H−H_2O]$^+$	601, 583[n]	5.58 ± 0.26
11	13-or 13′-*cis*-Lutein	29.56	330, 412, 440, 466	332, 415, 440, 464[c]	0.58	0.44[c]	569[M+H]$^+$, 551[M+H−H_2O]$^+$	569, 551[m]	3.76 ± 0.51
12	13-or 13′-*cis*-Lutein	30.47	334, 414, 440, 464	332, 415, 440, 464[c]	0.24	0.44[c]	551[M+H−H_2O]$^+$	551[m]	0.90 ± 0.74
13	All-*trans*-lutein	32.12	334, 420, 446, 474	332, 423, 446, 470[c]	0.05	0.12[c]	569[M+H]$^+$, 551[M+H−H_2O]$^+$	569, 551[m]	100.08 ± 3.70
14	All-*trans*-zeaxanthin	36.21	342, 428, 454, 480	344, 427, 452, 476[c]	0.28	0.11[c]	569[M+H]$^+$, 551[M+H−H_2O]$^+$	569, 551[l]	2.07 ± 0.18
15	9-or 9′-*cis*-Lutein	38.10	330, 420, 440, 470	332, 416, 440, 470[c]	0.11	0.13[c]	551[M+H−H_2O]$^+$	551[m]	1.82 ± 0.14
16	9-or 9′-*cis*-Lutein	39.64	330, 420, 440, 470	332, 416, 440, 470[c]	0.14	0.13[c]	569[M+H]$^+$	569[m]	1.34 ± 0.24
IS	All-*trans*-canthaxanthin	40.38	480	–	–	–	–	–	–
17	All-*trans*-β-cryptoxanthin	45.52	342, 428, 450, 482	450, 476[j]	0.08	–	553[M+H]$^+$	553[m]	2.26 ± 0.42
18	9-or 9′-*cis*-β-Cryptoxanthin	46.99	320, 420, 446, 478	342, 446, 470[j]	0.03	0.08[j]	553[M+H]$^+$	553[m]	2.96 ± 0.07
19	9-or 9′-*cis*-β-Cryptoxanthin	48.11	320, 418, 438, 468	342, 446, 470[j]	0.60	0.08[j]	553[M+H]$^+$	553[m]	3.79 ± 0.03
20	15-or 15′-*cis*-β-Carotene	52.60	342, 424, 442, 472	421, 445, 474[g]	0.46	0.38[g]	537[M+H]$^+$	537[m]	10.17 ± 1.47
21	9-or 9′-*cis*-β-Carotene	53.44	336, 424, 454, 476	344, 422, 452, 476[c]	0.37	0.26[c]	537[M+H]$^+$	537[m]	13.24 ± 1.78
22	15-or 15′-*cis*-β-Carotene	54.60	340, 422, 446, 472	421, 445, 474[g]	0.42	0.38[g]	537[M+H]$^+$	537[m]	17.87 ± 4.25
23	13-or 13′-*cis*-β-Carotene	55.49	342, 424, 446, 474	422, 446, 476[g]	0.50	0.46[g]	537[M+H]$^+$	537[m]	15.33 ± 5.12
F	9-or 9′-*cis*-β-Carotene	59.79	332, 422, 446, 470	342, 424, 446, 472[f]	0.08	–	537[M+H]$^+$	537[m]	12.70 ± 1.72
24	All-*trans*-β-carotene	62.25	454, 478	426, 456, 480[h]	–	0.09[h]	537[M+H]$^+$	537[m]	289.53 ± 48.16
25	9-or 9′-*cis*-β-Carotene	64.36	348, 450, 474	344, 428, 452, 476[c]	0.11	0.20[c]	537[M+H]$^+$	537[m]	55.29 ± 15.78

[*] Peak numbers with alphabetical letters (A–F) indicate additional carotenoids identified in carotenoid fraction isolated by column chromatography, while 1–25 denote the same carotenoids identified originally in the sample extract.

[a] A gradient mobile phase of methanol–acetonitrile–water (79:14:7, v/v/v) and methylene chloride (from 95:5, v/v to 66:34, v/v) was used.

[b] A mobile phase of methanol (solvent A), MTBE (solvent B) and water (solvent C) (from 90:5:5, v/v/v to 50:50:0, v/v/v) was used by Meléndez-Martínez et al. [15].

[c] A mobile phase of methanol–acetonitrile–water (84:14:2, v/v/v) and methylene chloride (from 100:0, v/v to 45:55, v/v) was used by Inbaraj et al. [9].

[d] A mobile phase of methanol (solvent A), MTBE (solvent B) and water (solvent C) (from 90:5:5, v/v/v to 50:50:0, v/v/v) was used by Meléndez-Martínez et al. [11].

[e] A mobile phase of methanol–2-proponol (99:1, v/v) and methylene chloride (from 100:0, v/v to 70:30, v/v) was used by Chen et al. [16].

[f] A mobile phase of MeCN–MeOH (75:25, v/v, solvent A), MTBE (solvent B) and water (solvent C) (from 95:0:5, v/v/v to 26:74:0, v/v/v) was used by Lee [17].

[g] A mobile phase of methanol–acetonitrile–water (84:14;2, v/v/v) and methylene chloride (from 80:20, v/v to 45:55, v/v) was used by Liu et al. [18].

[h] A mobile phase of methanol–acetonitrile–water (81:14:5, v/v/v) and methylene chloride (from 84:16, v/v to 75:25, v/v) was used by Inbaraj et al. [5].

[i] A mobile phase of 2-propanol and water–acetonitrile (20:80, v/v) (from 5:95, v/v to 70:30, v/v) was used by Dugo et al. [19].

[j] A mobile phase of methanol (solvent A), MTBE (solvent B) and water (solvent C) (from 90:5:5, v/v/v to 50:50:0, v/v/v) was used by Meléndez-Martínez et al. [20].

[k] *Q*-ratio is defined as the ratio of the *cis* peak to the main absorption peak.

[l] Based on a report by Zepka and Mercadante [30].

[m] Based on a report by de Faria et al. [21]

[n] Based on a report by Dugo et al. [19].

[o] Average of duplicate analyses ± standard deviation based on sample weight.

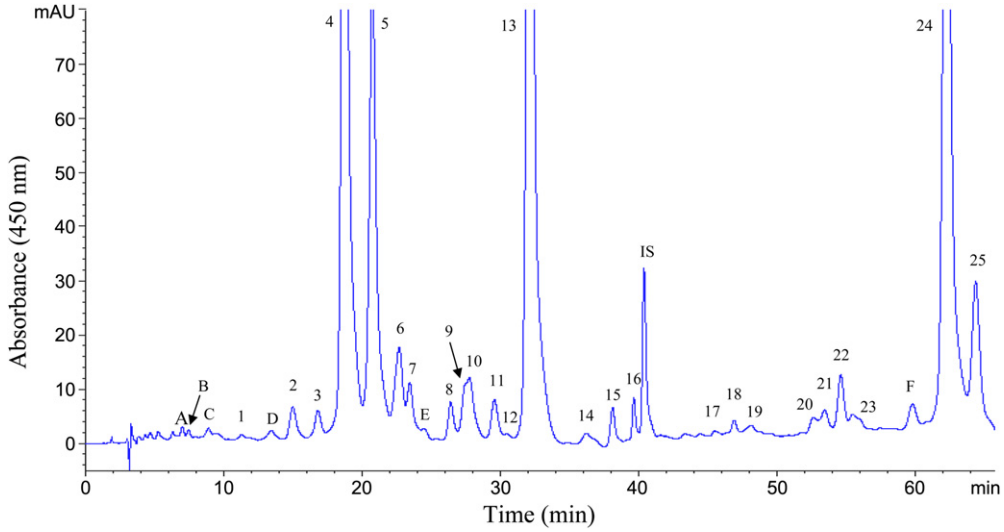

Fig. 3. HPLC chromatogram of carotenoid fraction isolated from *T. formosanum*. Peak identification shown in Table 3. Peak numbers with alphabetical letters (A–F) indicate additional carotenoids identified in carotenoid fraction isolated by column chromatography, while 1–25 denote the same carotenoids identified originally in the sample extract.

chromatographic method has to be modified. After various studies, the most appropriate condition as described in Section 2.2 was developed. After separation and collection, the eluted carotenoid fraction was evaporated to dryness, dissolved in 5 mL of methylene chloride-methanol (1:1, v/v), filtered through a 0.2-μm membrane filter and 20-μL injected for HPLC–DAD–APCI-MS analysis by using the same condition shown in the preceding section.

Fig. 3 shows the HPLC chromatogram of various carotenoids in carotenoid fraction isolated from *T. formosanum*. Following the same identification and quantitation criteria, a total of 31 carotenoids were separated and identified [5,9,11,15–21,30], in which all-*trans*-β-carotene and its *cis* isomers dominated (414.13 μg/g), followed by all-*trans*-violaxanthin and its *cis* isomers (182.99 μg/g), all-*trans*-neoxanthin and its *cis* isomers (120.39 μg/g), all-*trans*-lutein and its *cis* isomers (107.90 μg/g), luteoxanthin (23.12 μg/g), antheraxanthin (10.74 μg/g), all-*trans*-β-cryptoxanthin and its *cis* isomers (9.01 μg/g), auroxanthin (6.74 μg/g), neochrome (5.90 μg/g) and all-*trans*-zeaxanthin (2.07 μg/g) (Table 3). Comparatively, several carotenoids including auroxanthin, 13- or 13′-*cis*-neoxanthin, violaxanthin and 9- or 9′-*cis*-β-carotene were generated in carotenoid fraction after column chromatography, implying that the epoxidation or isomerization of carotenoids may occur during the lengthy preparative procedure. In addition, a loss of 129.5 μg/g (12.8%) of total carotenoids was found after column chromatography, revealing that the carotenoid degradation may also occur. Nevertheless, the column chromatography can still be adopted as a reference technique to isolate a large amount of carotenoids from *T. formosanum* for possible production of health food in the future with carotenoids as raw material.

4. Conclusion

In conclusion, an HPLC gradient mobile phase of methanol/acetonitrile/water (79:14:7, v/v/v) and methylene chloride (100%) was developed to separate 25 carotenoids and their isomers in *T. formosanum* within 66 min by employing a C-30 column with flow rate at 1.0 mL/min and detection at 450 nm. All-*trans*-β-carotene and its *cis* isomers were present in largest amount, followed by all-*trans*-lutein and its *cis* isomers, all-*trans*-violaxanthin and its *cis* isomers, all-*trans*-neoxanthin and its *cis* isomers, antheraxanthin, luteoxanthin, all-*trans*-β-cryptoxanthin and its *cis* isomers, all-*trans*-zeaxanthin and neochrome, with a total amount being 1012.5 μg/g. By using a preparative column containing 52 g of magnesium oxide-diatomaceous earth (1:3, w/w) as adsorbent, a large amount of carotenoids was eluted with 300 mL of ethyl acetate (100%) at a flow rate of 10 mL/min. However, both epoxidation and isomerization as well as degradation occurred during preparative column chromatography, resulting in 12.8% loss of total carotenoids.

References

[1] Y.S. Bajaj, Medicinal and Aromatic Plants, Springer, 1994, pp. 356–365.
[2] J.B.R. Domitrovic, H. Jokovac, Z. Romic, D. Rahelic, Z. Tadic, Antifibrotic activity of *Taraxacum officinale* root in carbon tetrachloride-induced liver damage in mice, J. Ethanopharmacol. 130 (2010) 569–577.
[3] L. Liu, H. Xiong, J. Ping, Y. Ju, X. Zhang, *Taraxacum officinale* protects against lipopolysaccharide-induced acute lung injury in mice, J. Ethanopharmacol. 130 (2010) 392–397.
[4] S. Shi, Y. Zhao, H. Zhou, Y. Zhang, X. Jiang, K. Huang, Identification of antioxidants from *Taraxacum mangolicum* by high-performance liquid chromatography-diode array detection-radical-scavenging detection-electrospray ionization mass spectrometry and nuclear magnetic resonance experiments, J. Chromatogr. A 1209 (2008) 145–152.
[5] B.S. Inbaraj, H. Lu, C.F. Hung, W.B. Wu, C.L. Lin, B.H. Chen, Determination of carotenoids and their esters in fruits of *Lycium barbarum* Linnaeus by HPLC–DAD–APCI-MS, J. Pharmaceut. Biomed. Anal. 47 (2008) 812–818.
[6] T.H. Kao, C.J. Chen, B.H. Chen, Carotenoid composition in *Rhinacanthus nasutus* (L.) Kurz as determined by HPLC–MS and affected by freeze-drying and hot-air-drying, Analyst 136 (2011) 3194–3202.
[7] A.V. Rao, L.G. Rao, Carotenoids and human health, Pharmacol. Res. 55 (2007) 207–216.
[8] Y.C. Tsai, W.B. Wu, B.H. Chen, Preparation of carotenoids and chlorophylls from *Gynostemma pentaphyllum* Makino and their antiproliferation effect on hepatoma cell, J. Med. Food 13 (2010) 1431–1442.
[9] B.S. Inbaraj, J.T. Chien, B.H. Chen, Improved high performance liquid chromatographic method for determination of carotenoids in the microalga *Chlorella pyrenoidosa*, J. Chromatogr. A 1102 (2006) 193–199.
[10] J. Shi, C. Yi, X.Q. Ye, S. Xue, Y.M. Jiang, Y. Ma, D.H. Liu, Effects of supercritical CO_2 fluid parameters on chemical composition and yield of carotenoids extracted from pumpkin, LWT-Food Sci. Technol. 43 (2010) 39–44.
[11] A.J. Melendez-Martinez, G. Britton, I.M. Vicario, F.J. Heredia, The complex carotenoid pattern of orange juices from concentrate, Food Chem. 109 (2008) 546–553.
[12] D. Marinova, F. Ribarova, HPLC determination of carotenoids in Bulgarian berries, J. Food Comp. Anal. 20 (2007) 370–374.
[13] A. Fratianni, L. Cinquanta, G. Panfili, Degradation of carotenoids in orange juice during microwave heating, LWT-Food Sci. Technol. 43 (2010) 871–876.
[14] SAS, SAS Procedures and SAS/Graph User's Guide, Version 6, SAS Institute Inc., Cary, NC, USA, 2009.
[15] A.J. Melendez-Martinez, I.M. Vicario, F.J. Heredia, Geometrical isomers of violaxanthin in orange juice, Food Chem. 104 (2007) 169–175.

[16] J.P. Chen, C.Y. Tai, B.H. Chen, Improved liquid chromatographic method for determination of carotenoids in Taiwanese mango (*Mangifera indica* L.), J. Chromatogr. A 1054 (2004) 261–268.
[17] H.S. Lee, Characterization of carotenoids in juice of red navel orange (Cara Cara), J. Agric. Food Chem. 49 (2001) 2563–2568.
[18] S.C. Liu, J.T. Lin, D.J. Yang, Determination of cis- and trans-α- and β-carotenoids in Taiwanese sweet potatoes (*Ipomea batatas* (L.) Lam.) harvested at various times, Food Chem. 116 (2009) 605–610.
[19] P. Dugo, M. Herrero, T. Kumm, D. Giuffrida, G. Dugo, L. Mondello, Comprehensive normal-phase x reversed-phase liquid chromatography coupled to photodiode array and mass spectrometry detection for the analysis of free carotenoids and carotenoids esters from mandarin, J. Chromatogr. A 1189 (2008) 196–206.
[20] Melendez-Martinez, G. Britton, I.M. Vicario, F.J. Heredia, Identification of zeinoxanthin in orange juices, J. Agric. Food Chem. 53 (2005) 6362–6367.
[21] A.F. de Faria, P.N. Hasegawa, E.A. Chagas, R. Pio, E. Purgatto, A.Z. Mercadante, Cultivar influence on carotenoid composition of loquats from Brazil, J. Food Comp. Anal. 22 (2009) 196–203.
[22] R. Lakshminarayana, G. Aruna, R.K. Sangeetha, N. Bhaskar, Possible degradation/biotransformation of lutein in vitro and in vivo: isolation and structural elucidation of lutein metabolites by HPLC and LC–MS (atmospheric pressure chemical ionization), Free Radic. Biol. Med. 45 (2008) 982–993.
[23] K. Nakagawa, T. Kiko, K. Hatade, A. Asai, F. Kimura, P. Sookwong, T. Tsuduki, H. Arai, T. Miyazawa, Development of a high-performance liquid chromatography-based assay for carotenoids in human red blood cells: application to clinical studies, Anal. Biochem. 381 (2008) 129–134.
[24] G. Britton, I.M. Vicario, F.J. Heredia, HPLC analysis of geometrical isomers of lutein epoxide isolated from dandelion (*Taraxacum officinale* F. Weber ex Wiggers), Phytochemistry 67 (2006) 771–777.
[25] H. Nitsche, C. Pleugel, Neoxanthin from *Helianthus*, *Taraxacum* and *Impatiens*, Phytochemistry 11 (1972) 3383–3385.
[26] R.K. Sangeetha, V. Baskaran, Carotenoid composition and retinol equivalent in plants of nutritional and medicinal importance: efficacy of β-carotene from Chenopodium album in retinol-deficient rats, Food Chem. 119 (2010) 1584–1590.
[27] A. Loranty, E. Rembialkowska, E.A.S. Rosa, R.N. Bennett, Identification, quantification and availability of carotenoids and chlorophylls in fruit, herb and medicinal teas, J. Food Comp. Anal. 23 (2010) 432–441.
[28] M. Al-Duais, J. Hohbein, S. Werner, V. Bohm, G. Jetschke, Contents of vitamin C, carotenoids, tocopherols, and tocotrienols in the subtropical plant species *Cyphostemma digitatum* as affected by processing, J. Agric. Food Chem. 57 (2009) 5420–5427.
[29] K.L. Taylor, A.E. Brackendridge, M.A. Vivier, A. Oberholster, High performance liquid chromatography profiling of the major carotenoids in *Arabidopsis thaliana* leaf tissue, J. Chromatogr. A 1121 (2006) 83–91.
[30] L.Q. Zepka, A.Z. Mercadante, Degradation compounds of carotenoids formed during heating of a simulated cashew apple juice, Food Chem. 117 (2009) 28–34.

Journal of Pharmaceutical and Biomedical Analysis 66 (2012) 154–161

Contents lists available at SciVerse ScienceDirect

Journal of Pharmaceutical and Biomedical Analysis

journal homepage: www.elsevier.com/locate/jpba

Chemical profile and seasonal variation of phenolic acid content in bastard balm (*Melittis melissophyllum* L., Lamiaceae)

Ewa Skrzypczak-Pietraszek[a,*], Jacek Pietraszek[b]

[a] *Chair and Department of Pharmaceutical Botany, Collegium Medicum, Jagiellonian University, 9 Medyczna Str., 30-688 Kraków, Poland*
[b] *Institute of Applied Informatics, Cracow University of Technology, 37 Jana Pawła II, 31-864 Kraków, Poland*

ARTICLE INFO

Article history:
Received 10 March 2012
Accepted 19 March 2012
Available online 28 March 2012

Keywords:
Melittis melissophyllum L.
Bastard balm
Lamiaceae
Phenolic acids
HPLC-DAD
SPE

ABSTRACT

Melittis melissophyllum L. is an old medicinal plant. Nowadays it is only used in the folk medicine but formerly it has been applied in the official medicine as a natural product described in French Pharmacopoeia. *M. melissophyllum* herbs used in our studies were collected from two localities in Poland in May and September. Methanolic plant extracts were purified by means of solid-phase extraction and then analysed by HPLC-DAD for their phenolic acid profile. Eleven compounds were identified in all plant samples and quantitatively analysed as: protocatechuic, chlorogenic, *p*-hydroxybenzoic, vanillic, caffeic, syringic, *p*-coumaric, ferulic, sinapic, *o*-coumaric and cinnamic acid. Plant materials contained free and bound phenolic acids. The main compounds were: *p*-hydroxybenzoic acid (30.21–54.16 mg/100 g dw and 37.04–56.75 mg/100 g dw, free and bound, respectively) and *p*-coumaric acid (40.48–80.55 mg/100 g dw and 28.09–40.85 mg/100 g dw, free and bound, respectively). The highest amounts of the investigated compounds were found in all samples collected in September, e.g. *p*-hydroxybenzoic acid (September 51.72–54.16 mg/100 g dw vs. May 30.21–34.07 mg/100 g dw), *p*-coumaric acid (September 77.14–80.55 mg/100 g dw vs. May 40.48–43.25 mg/100 g dw). Multivariate statistical and data mining techniques, such as cluster analysis (CA) and principal component analysis (PCA), were used to characterize the sample populations according to the geographical localities, vegetation period and compound form (free or bound). To the best of our knowledge we report for the first time the results of quantitative analysis of *M. melissophyllum* phenolic acids and seasonal variation of their content. Plant herbs are usually collected at flowering for plant derived medical preparations. Our results show that it is not always the optimal time for the highest contents of active compounds.

© 2012 Elsevier B.V. All rights reserved.

1. Introduction

Phenolic acids are the important group of secondary plant metabolites widely spread in the plant kingdom showing a broad spectrum of pharmacological activities such as antiphlogistic, antioxidant, immunostimulating, antiseptic, cholagogic, spasmolytic and others (e.g. [1–3]). Crude methanolic plant extract contain numerous polar metabolites and various nonpolar ballast compounds often interfering with the process of HPLC determination of phenolic acids. Głowniak et al. [4] developed solid-phase extraction (SPE) procedure for isolation and purification of phenolic acid fraction. The described two-step method is based on reversed-phase chromatography followed by ion-exchange chromatography. SPE procedure is especially useful for isolation of phenolic acid fractions from numerous small plant samples.

Melittis melissophyllum is a perennial plant growing in thermophilous copse broadleaf woodlands in Europe [5,6]. In Poland *M. melissophyllum* grows is scattered places and from 2004 is protected by law, but in other countries (e.g. Italy, Serbia) occurs in numerous localities.

M. melissophyllum has been known as a medicinal plant for centuries. In 1542 *Melittis* was described for the first time by Leonard Fuchs [7] because of its medicinal properties. Nowadays *Melittis* is not mentioned as a pharmacopoeial natural product, but was included in earlier editions of French Pharmacopoeia [8,9]. *M. melissophyllum* is described as a plant used in the folk medicine especially in Italy and in Serbia. *Melittis* was mentioned by Guarrera [10], Idolo et al. [11] and Jarić [12] in their ethnopharmacobotanical studies published in recent years. *M. melissophyllum* is described to be used as antispasmodic; against insomnia and eye inflammations [10], as digestive and to treat cough and sore throat [11]; sedative for nervous anxiety and insomnia [12]. *Melittis* is also used as beverage. Fresh and dry leaves are used to prepare aromatic tea for drinking after meals as digestive and antispasmodic [11]. Results of biological investigations have shown antioxidant

* Corresponding author. Tel.: +48 605 697292.
E-mail address: ewa.skrzypczak-pietraszek@uj.edu.pl (E. Skrzypczak-Pietraszek).

0731-7085/$ – see front matter © 2012 Elsevier B.V. All rights reserved.
doi:10.1016/j.jpba.2012.03.037

Table 1
Collection localities of the studied *Melittis melissophyllum* L. samples.

Collection site	Sample	Date of collection	GPS coordinates	Altitude (m)
Tyniec (near Kraków)	T-1(M)	May 2003	N 50°0′49″ E 19°48′50″	233
	T-1(S)	September 2003		
Botanical Garden in Poznań	P-1(M)	May 2003	N 52°25′06″ E 16°52′51″	82
	P-1(S)	September 2003		
	P-2(M)	May 2010		
	P-2(S)	September 2010		

activity of *M. melissophyllum* extracts [13,14]. On the basis of in vitro and in vivo tests it was concluded that water extracts had the highest protective activity against free radicals [14].

M. melissophyllum chemical content is only partly known. Coumarin has been found [15,16] and quantitatively analysed [17]. Iridoids from *M. melissophyllum* were isolated and their structure was established as: ajugoside and ajugol [18], melittoside [19], monomelittoside [20], harpagide and harpagide acetate [21]. Phenolic acids in *M. melissophyllum* were only partly investigated—Świątek and Chybowski [22] made preliminary qualitative analysis of that chemical group using 2D paper chromatography. *M. melissophyllum* essential oil was analysed in plant material collected in Greece [23], Spain [24], Italy [25–27] and Slovakia [27]. *M. melissophyllum* essential oil contains a mushroom-like flavour of potential food industry interest [28,29].

Authors of this paper have been interested in *M. melissophyllum* plant and in vitro cultures for many years [30–33]. Water-soluble polysaccharides from *M. melissophyllum* L. herb and callus tissue were isolated, fractionated by IEC and GPC and the respective fractions were analysed concerning sugar composition and linkage characteristics. The dominant structures were type-II arabinogalactans with a $(1 \rightarrow 3)$-galactose backbone and arabinose–galactose side chains [31].

To the best of our knowledge we report for the first time the results of quantitative analysis of *M. melissophyllum* phenolic acids and seasonal variation of their content. Plant material has been collected from two different localities in Poland during the flowering period (May) and at the end of the vegetative stage (September). Plant extracts were purified by means of SPE and then analysed by HPLC-DAD for their phenolic acid profile.

2. Materials and methods

2.1. Plant materials

Aerial parts of *M. melissophyllum* were collected at flowering in May and then in September (at the end of the vegetative stage). They were gathered in Poland in a woody place near Kraków (Tyniec) and from Botanical Garden in Poznań (Table 1). Plant material was air dried at room temperature, tightly packed and stored at fridge conditions (4–10 °C). Plants were identified by Dr. Skrzypczak-Pietraszek using available literature. Voucher specimens were deposited in the Department of Pharmaceutical Botany, Jagiellonian University, Collegium Medicum, Kraków, Poland.

2.2. Chemicals

Methanol and acetic acid (both of HPLC grade) were purchased from Merck (Darmstadt, Germany). Reagents used for sample preparation and SPE procedure (methanol, ethyl acetate, hydrochloric acid, sodium bicarbonate, phosphoric acid) all of analytical standard grade were purchased from POCh (Gliwice, Poland). Phenolic acid standards: *p*-coumaric, ferulic, *p*-hydroxybenzoic and vanillic acid were from Fluka (Chemie AG); caffeic, chlorogenic, cinnamic, *o*-coumaric, protocatechuic, sinapic and syringic acid were from Sigma (St. Louis, MO, USA). Water was purified by redistillation followed by filtration through Millipore 0.22-μm filters. Standard solutions or studied samples were filtered through 0.22-μm syringe filters (Millipore, Millex-GP) before injection to HPLC.

2.3. Sample preparation

Dry plant materials were manually grounded in a mortar to fine powders.

2.3.1. Extraction

The extraction process was carried out as follows: 2 g of each powdered plant material were twice extracted with 100 ml of boiling methanol (at 67.4 °C) for 2 h under reflux condensor. Combined extracts (200 ml) were concentrated to dryness using a rotary vacuum evaporator (Büchi) at 40 °C. Residues were dissolved in 10 ml of 30% (v/v) methanol. Extract samples contained free phenolic acids and other methanol soluble substances from plant material.

2.3.2. Hydrolysis

The hydrolysis process was carried out as follows: 2 g of each powdered plant material was hydrolysed with 100 ml of 2 M hydrochloric acid for 2 h at 100 °C. Hydrolysates were extracted with ethyl acetate (5 times with 50 ml of ethyl acetate). Acetate extracts were combined (250 ml) and concentrated to dryness in a rotary vacuum evaporator (Büchi) at 40 °C. Hydrolysed samples contained all phenolic acids present in plant material: free and earlier bound with other plant metabolites.

2.4. Sample purification—SPE

Solid-phase extraction (SPE) method was used to isolate and purify phenolic acid fractions from all studied samples (Sections 2.3.1 and 2.3.2). The applied SPE procedure was developed by Głowniak et al. [4]. Briefly, methanolic (30%, v/v) plant extracts were passed through previously conditioned micro-columns (octadecyl, 500 mg, J.T.Baker, Phillipsburg, NJ, USA) to remove nonpolar ballast compounds. The columns were inserted into a vacuum manifold processor (system Baker SPE-12 G, J.T.Baker, Phillipsburg, NJ, USA). The eluates (adjusted to pH 7.0–7.2 with aqueous solution of sodium bicarbonate) were passed through quaternary amine microcolumns (500 mg, J.T.Baker, Phillipsburg, NJ, USA). Phenolic acids remained on the sorbent beds were finally eluted from columns with 0.2 M H_3PO_4–MeOH (1:1, v/v) mixture. The collected eluates were analysed by HPLC.

2.5. HPLC and HPLC-DAD analysis

HPLC method was performed according to the procedure developed by Ellnain-Wojtaszek and Zgórka [34] with our modifications. Qualitative and quantitative HPLC analyses of phenolic acids were conducted using Hitachi apparatus with L-7100 pump, L-7400 UV Detector ($\lambda = 254$ nm) and Purospher® RP-18e column (250 mm × 4 mm, 5 μm) thermostated at 25 °C. A mobile phase was composed of methanol–0.5% acetic acid (1:4, v/v) as solvent A and methanol (solvent B). The following gradient elution scheme

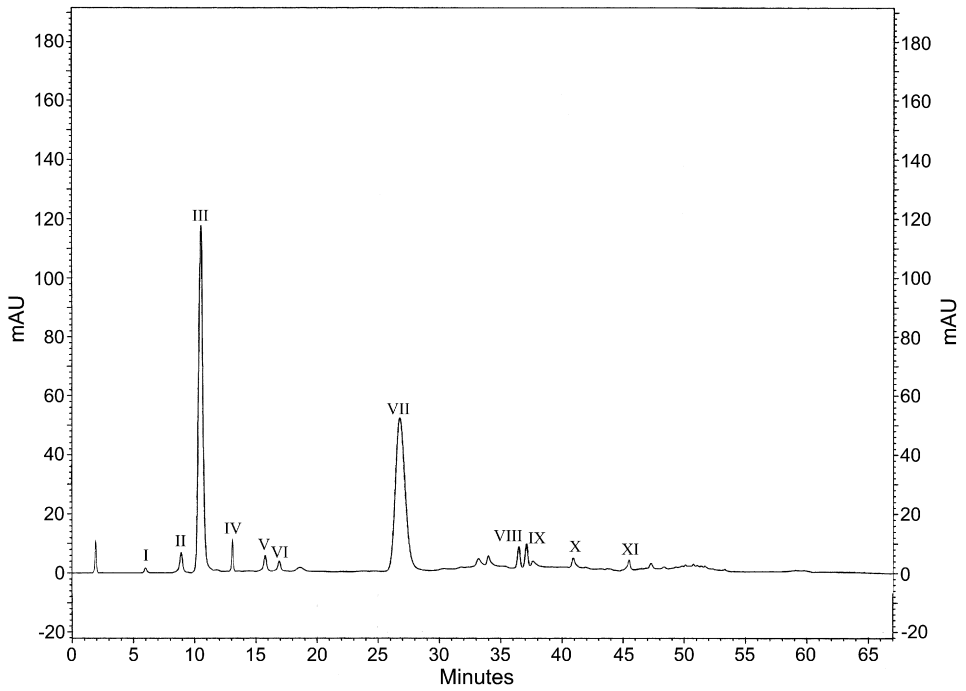

Fig. 1. HPLC chromatogram of free phenolic acid fraction from *Melittis melissophyllum* L. (sample without hydrolysis). Plant material collected in Poznań in September 2010 (P-2(S)). Identified acids: I—protocatechuic, II—chlorogenic, III—*p*-hydroxybenzoic, IV—vanillic, V—caffeic, VI—syringic, VII—*p*-coumaric, VIII—ferulic, IX—sinapic, X—*o*-coumaric, XI—cinnamic.

was used (A:B ratio): 100%:0% $t = 0$–25 min; 70%:30% $t = 35$ min; 50%:50% $t = 45$ min; 0%:100% $t = 50$–55 min; 100%:0% $t = 57$–67 min. Analyses were repeated once in the same conditions, using new HPLC VWR Hitachi apparatus (autosampler L-2200, pump L-2130, column oven L-2350, diode array detector (DAD) L-2455) at UV range 200–400 nm. The comparison of UV spectra and retention times with standard compounds enabled the identification of phenolic acids presented in the analysed samples. Qualitative analyses were supplemented with internal standard method. Identified phenolic acids were quantified against their external standards (the calibration curve method). Two examples of the representative chromatograms are shown in Figs. 1 and 2.

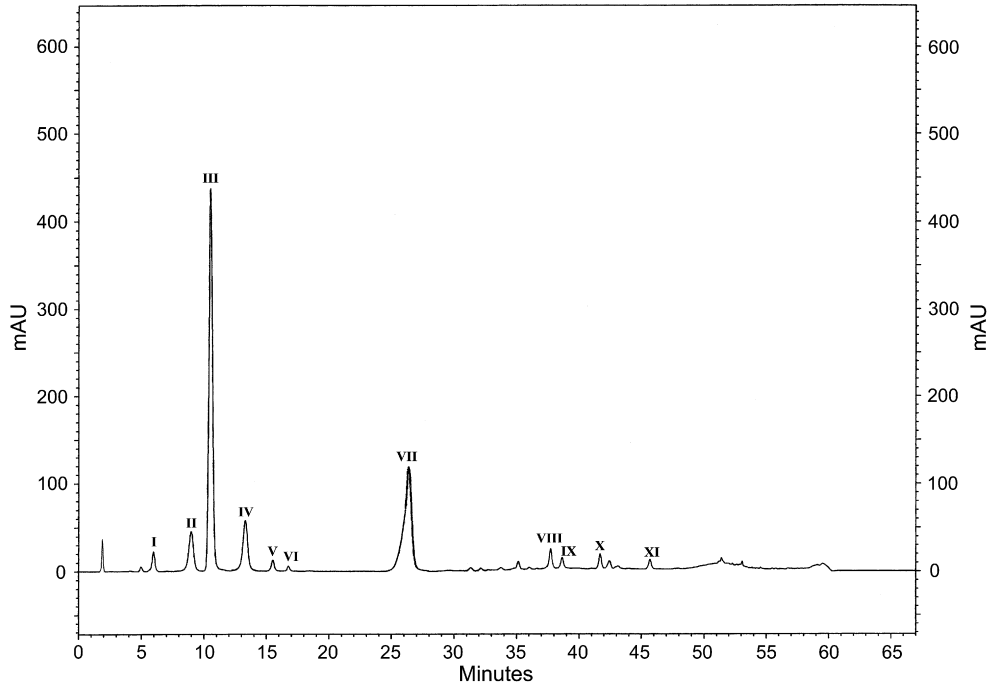

Fig. 2. HPLC chromatogram of total phenolic acid fraction from *Melittis melissophyllum* L. (sample after hydrolysis). Plant material collected in Poznań in September 2010 (P-2(S)). Identified acids: I—protocatechuic, II—chlorogenic, III—*p*-hydroxybenzoic, IV—vanillic, V—caffeic, VI—syringic, VII—*p*-coumaric, VIII—ferulic, IX—sinapic, X—*o*-coumaric, XI—cinnamic.

Table 2
Contents (mg/100 g dw) of phenolic acids in *Melittis melissophyllum* plant samples.[a]

Phenolic acid	T-1(M)[a]	T-1(S)	P-1(M)	P-1(S)	P-2(M)	P-2(S)
	mg/100 g dw					
(I) Protocatechuic						
Free[b]	tr[b]	5.41 ± 0.14	tr	5.29 ± 0.16	tr	5.71 ± 0.15
Total[b]	2.33 ± 0.09	7.92 ± 0.19	2.10 ± 0.09	7.88 ± 0.20	2.40 ± 0.09	8.22 ± 0.21
(II) Chlorogenic						
Free	tr	8.37 ± 0.24	tr	7.12 ± 0.23	tr	9.25 ± 0.29
Total	4.52 ± 0.20	15.16 ± 0.51	4.24 ± 0.17	14.72 ± 0.49	4.66 ± 0.19	16.43 ± 0.71
(III) *p*-Hydroxybenzoic						
Free	31.11 ± 1.10	52.16 ± 2.16	30.21 ± 2.01	51.72 ± 3.01	34.07 ± 4.02	54.16 ± 5.10
Total	68.27 ± 4.82	104.14 ± 8.21	67.25 ± 3.25	99.25 ± 7.15	70.03 ± 5.42	110.91 ± 6.23
(IV) Vanillic						
Free	3.84 ± 0.12	11.41 ± 0.57	3.72 ± 0.17	10.15 ± 0.52	3.97 ± 0.16	12.09 ± 0.53
Total	4.27 ± 0.18	19.15 ± 0.82	4.19 ± 0.18	18.28 ± 0.84	4.30 ± 0.15	20.13 ± 0.60
(V) Caffeic						
Free	0.91 ± 0.04	2.72 ± 0.12	0.87 ± 0.10	2.68 ± 0.11	1.15 ± 0.04	2.81 ± 0.13
Total	1.44 ± 0.05	3.35 ± 0.13	1.31 ± 0.04	3.23 ± 0.12	1.52 ± 0.06	3.47 ± 0.11
(VI) Syringic						
Free	tr	1.52 ± 0.08	tr	1.47 ± 0.06	tr	1.64 ± 0.06
Total	2.29 ± 0.09	3.11 ± 0.12	2.19 ± 0.08	3.03 ± 0.12	2.31 ± 0.09	3.25 ± 0.09
(VII) *p*-Coumaric						
Free	42.28 ± 1.54	79.45 ± 2.75	40.48 ± 1.36	77.14 ± 2.68	43.25 ± 1.29	80.55 ± 2.32
Total	70.92 ± 2.36	114.87 ± 3.83	68.57 ± 3.36	118.19 ± 2.56	72.17 ± 2.24	121.40 ± 4.24
(VIII) Ferulic						
Free	2.13 ± 0.08	4.94 ± 0.20	2.05 ± 0.08	4.89 ± 0.20	2.38 ± 0.15	5.05 ± 0.32
Total	7.47 ± 0.35	9.08 ± 0.45	7.34 ± 0.33	8.83 ± 0.36	7.87 ± 0.32	9.24 ± 0.39
(IX) Sinapic						
Free	0.81 ± 0.04	1.12 ± 0.06	0.91 ± 0.05	1.10 ± 0.06	1.01 ± 0.04	1.22 ± 0.06
Total	2.13 ± 0.12	2.90 ± 0.17	2.23 ± 0.13	3.05 ± 0.21	3.03 ± 0.12	3.15 ± 0.19
(X) *o*-Coumaric						
Free	tr	0.72 ± 0.03	tr	0.65 ± 0.04	tr	0.81 ± 0.03
Total	0.71 ± 0.04	2.44 ± 0.15	0.63 ± 0.04	2.36 ± 0.14	0.72 ± 0.04	2.61 ± 0.15
(XI) Cinnamic						
Free	tr	0.49 ± 0.02	tr	0.42 ± 0.03	tr	0.57 ± 0.03
Total	0.51 ± 0.03	2.10 ± 0.15	0.45 ± 0.03	2.04 ± 0.12	0.61 ± 0.02	2.26 ± 0.16

[a] Data are expressed as mean ± standard error ($n = 3$); plant samples collected in Tyniec (T) or in Poznań (P); in 2003 (1) or in 2010 (2); in May (M) or in September (S)—details described in Table 1.
[b] tr: traces; free: free phenolic acid present in plant (samples without hydrolysis—Section 2.3.1); total: total content of phenolic acid present in plant, free and bound (samples after hydrolysis Section 2.3.2).

2.6. Statistical methods

The HPLC analyses were repeated in triplicate. Next, the standard statistical procedures were conducted: evaluation of means and associated standard errors (standard deviations of means). All calculations, also mentioned below, were performed in the environment of Statsoft STATISTICA version 10 [35].

To statistically interpret the phenolic acids profile characteristics, hierarchical cluster analysis (CA) [36] and principal component analysis (PCA) [37] methods were established to study the obtained experimental data.

CA is unsupervised technique that reveals the natural groupings existing between sample populations characterized by the values of a set of measures. The handled data unit was mg/100 g dw. Data with values detected as traces (abbreviation 'tr' in Table 2) were substituted for the purpose of statistical analyses as 0.01 mg/100 g dw. Data were subjected to CA. The specific CA method CLC (complete linkage clustering) with the Euclidean distance as dissimilarity coefficient was applied to contents of phenolic acids. Then the multivariate method, principal component analysis (PCA) based on covariance matrix, was used to identify principal components, which are responsible most to the variability of the studied set. The scree plot was used to identify the number of significant PCA factors. Next, the experimental samples data were projected onto the plane of two main PCA factors. Additionally, classic three-way analysis of variance (ANOVA) was used to simultaneously compare means of experimental data categorized into groups by plant material source, month of the year and kind of acid. The threshold for statistical significance was set at value of 0.05.

3. Results

3.1. HPLC-DAD analysis

All plant samples showed the identical phenolic acid profile—the same eleven phenolic acids were detected in all samples (Table 2) as protocatechuic, chlorogenic, *p*-hydroxybenzoic, vanillic, caffeic, syringic, *p*-coumaric, ferulic, sinapic, *o*-coumaric and cinnamic acid. All acids were present as free and bound compounds in *M. melissophyllum* herb—the concentrations of studied compounds were much higher after hydrolysis than before. The main components of all plant samples were: *p*-hydroxybenzoic acid (max. amount 54.16 mg/100 g dw before hydrolysis and 110.91 mg/100 g dw after hydrolysis) and *p*-coumaric (80.55 mg/100 g dw and 121.40 mg/100 g dw, respectively). There is no single ratio pattern for free and bound form of phenolic acids. All samples collected in May (T-1(M), P-1(M), P-2(M)) contained five phenolic acids mostly in bound forms: protocatechuic acid 2.09–2.39 mg/100 g dw, chlorogenic acid 4.23–4.65 mg/100 g dw, syringic acid 2.18–2.30 mg/100 g dw, *o*-coumaric acid 0.44–0.60 mg/100 g dw and cinnamic acid 0.44–0.60 mg/100 g dw. Free forms of these compounds occurred only in trace amounts. The ratio of free and bound form of *p*-hydroxybenzoic acid was close to 1:1. The dominant forms of vanillic acid and caffeic acid were free ones. All samples

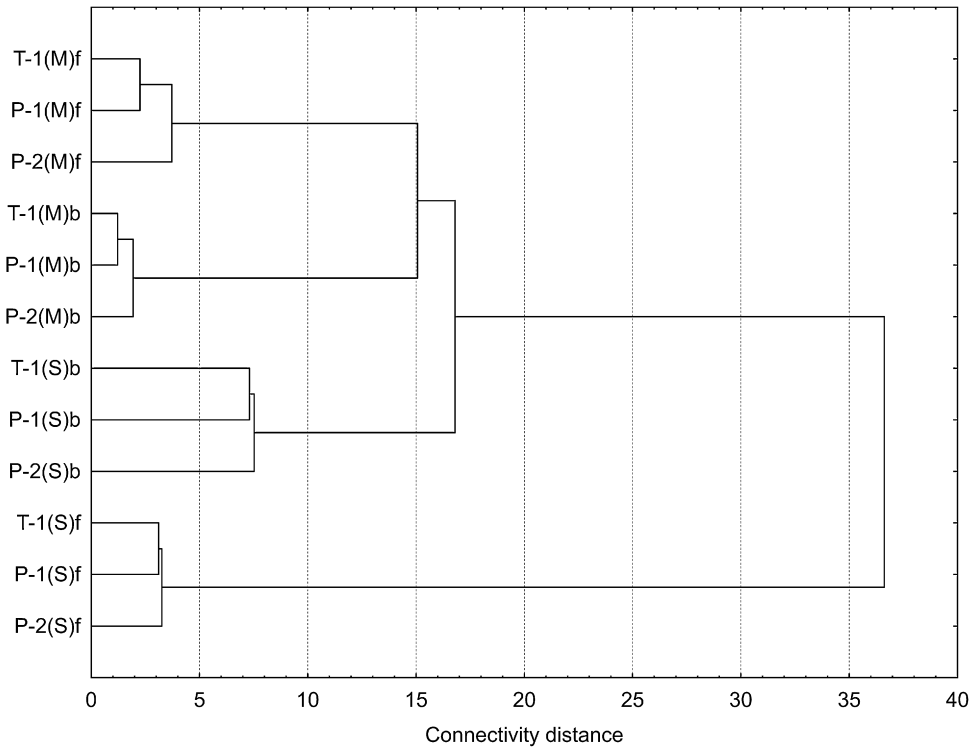

Fig. 3. Dendrogram obtained by hierarchical cluster analysis of contents (mg/100 g dw) of phenolic acids in *Melittis melissophyllum* plant samples. Clustering method based on CLC with the Euclidean distance as dissimilarity coefficient. Plant samples collected in Tyniec (T) or in Poznań (P); in 2003 (1) or in 2010 (2); in May (M) or in September (S); free (f) and bound (b) form of phenolic acids. Details described in Table 1.

collected in September contained free and bound forms of protocatechuic acid in ratio close to 2:1.

3.2. Statistical analysis

The results obtained from standard statistical analysis are expressed in Table 2 in the format: mean ± standard error. The results were compared taking into account localities (Tyniec or Poznań), year of collection (2003 or 2010), vegetation state (flowering in May and ending of vegetation in September) and phenolic acid form (free or bound).

The results of CA method with CLC variant are shown as the dendrogram (Fig. 3). From this dendrogram, four main groups could be delineated: the first group, formed by free phenolic acids derived from material collected in May; the second group, formed by bound phenolic acids derived from material collected in May; the third group, formed by free phenolic acids derived from material collected in September; the fourth group, formed by bound phenolic acids derived from material collected in September. Interestingly, the third group formed a cluster which is linked to the others at the largest distance value indicating a very significant difference.

As the first step in PCA, the number of significant PCA factors was identified due to the scree plot (Fig. 4). This plot shows that two main PCA factors explain 99.8% of observed variability. It means that collected data are almost two-dimensional in formally eleventh-dimensional space of experiment. Next, the experimental samples data were projected onto the plane of two main PCA factors (Fig. 5). The projection shows the same groups as detected by cluster analysis. It allowed to evaluate the significant differences for two grouping factors: vegetation season (May or September) and form of acids (free or bound).

Passing on now from statistical analysis to interpretation, it could be said that phenolic acid contents in plant samples collected in May were significantly lower than in September of the same year, in the same locations. Plant samples collected in Tyniec contained higher amounts of phenolic acids than corresponding samples from Botanical Garden in Poznań. The results showed also higher contents of studied compounds in samples collected in 2010 than in 2003. In both cases those differences were not statistically significant.

4. Discussion

SPE method [4] has proved to be very useful to isolate and purify phenolic acid fraction. This article shows for the first time the results of quantitative analysis of phenolic acids in *M. melissophyllum* herb. Świątek and Chybowski [22] did only the approximate qualitative analysis of these compounds using 2D paper chromatography. Their results are similar to qualitative aspects of ours, but not the same.

There are numerous literature data on seasonal changes of secondary metabolite contents in different plant species [17,38–50]. Content of essential oils and their chemical composition seem to be unstable and dependent on different factors. Maggi et al. [27] reported that various physicochemical changes of aromatic volatiles (e.g. oxidation and evaporation) took place during the drying process. As a result, the dried whole aerial parts of *M. melissophyllum* contained the lower amounts of monoterpene and sesquiterpene hydrocarbons in comparison with fresh frozen material. On the other hand, that decrease was accompanied by an increase in oxygenated products. The essential oil content and composition usually changes during a vegetative period [38,39]. The young herb of *Tanacetum parthenium* [38] yielded a relatively high percentage of oil (0.53%, v/w), then the oil content sharply declined (to 0.30%, v/w) to increase again in full bloom (0.83%, v/w). The content of some oil constituents rosed (e.g. camphor—from 28% to 48%) but of other ones decreased (e.g. chrysanthenyl acetate—from 30% to 22%). On the other hand, Papageorgiou et al. [40] have

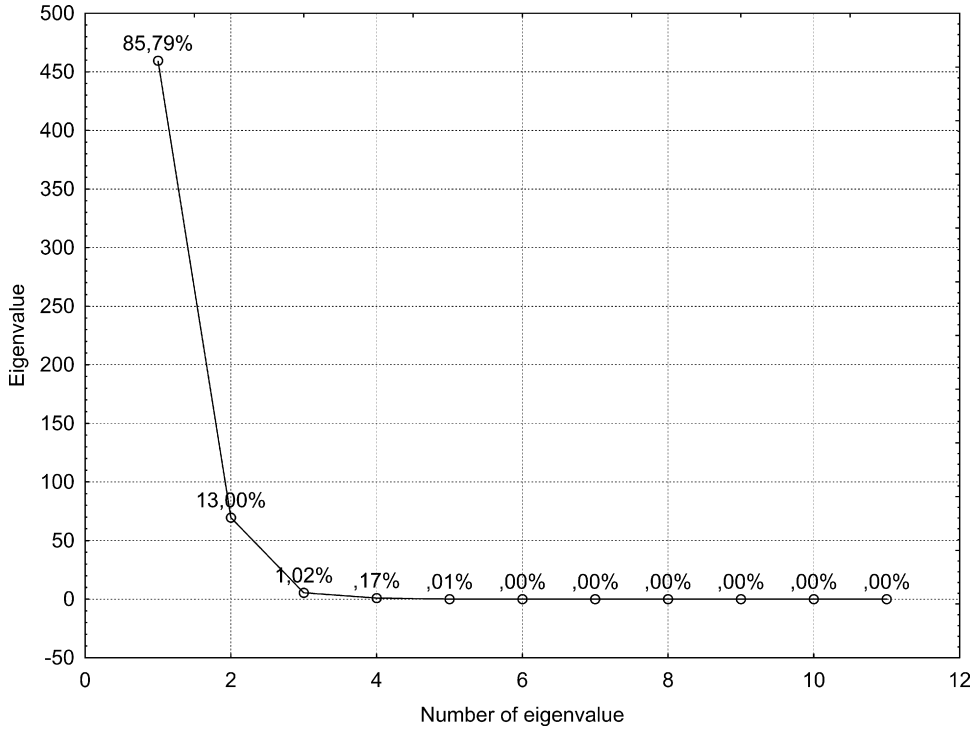

Fig. 4. Scree plot obtained for principal component analysis of contents (mg/100 g dw) of phenolic acids in *Melittis melissophyllum* plant samples. The first two principal components contain ca. 98.79% information.

stated, that *Rosmarinus officinalis* and *Salvia fruticosa* did not show great seasonal variations in terms of their essential oil composition. Authors [40] assumed that the chemical oil profile between the same plant populations is more or less defined by their genetic features.

The levels of total coumarin in *M. melissophyllum* samples [17] varied during the phenological cycle both in fresh and dry plant material. The maximum contents were observed at the beginning of cycle (May) and the lowest values—at the later stages of cycle (August). The total coumarin content was significantly higher in

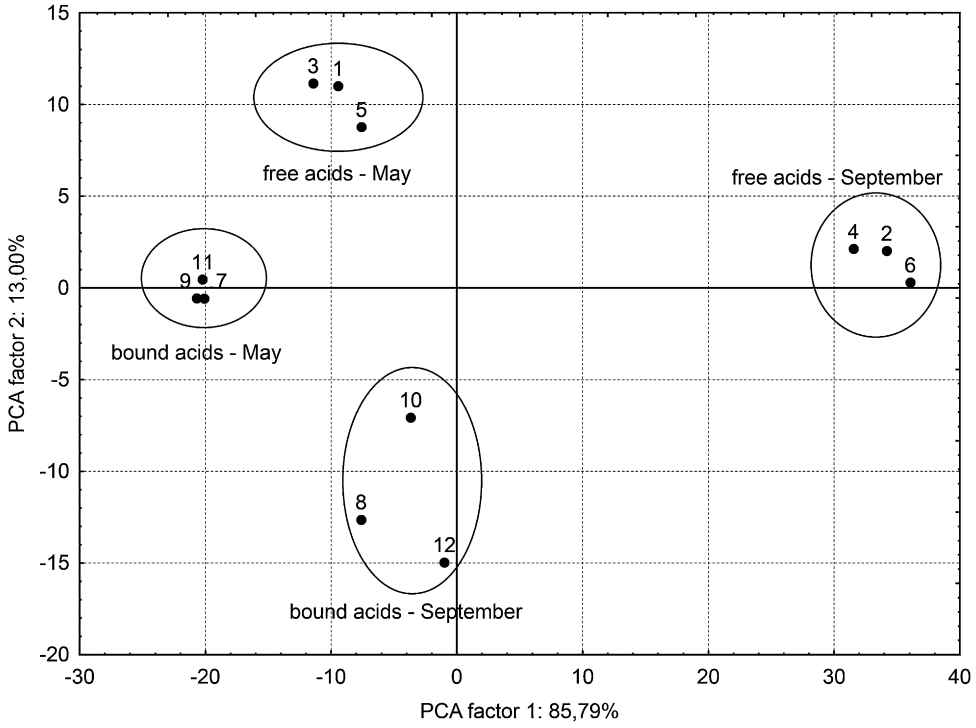

Fig. 5. Projection of samples onto the plane of two main PCA (principal component analysis) factors obtained for contents (mg/100 g dw) of phenolic acids in *Melittis melissophyllum* plant samples. Labels: 1—T-1(M)free, 2—T-1(S)free, 3—P-1(M)free, 4—P-1(S)free, 5—P-2(M)free, 6—P-2(S)free, 7—T-1(M)bound, 8—T-1(S)bound, 9—P-1(M)bound, 10—P-1(S)bound, 11—P-2(M)bound, 12—P-2(S)bound. Details described in Table 1.

fresh samples compared with the corresponding dry ones. Zheng et al. [41] obtained similar results. They studied distribution and seasonal variation of coumarins in leaves and roots of *Dendrobium thyrsiflorum*. Relative quantity of coumarins reached the highest level during profuse flowering period and significantly lower one at the end of vegetative cycle. On the other hand, content of coumarins determined in *Artemisia scoparia* herb [42] did not have any relationship to vegetation period except of one compound: scoparone. The content of that compound increased significantly in autumn. The coumarin glucosides – esculin and fraxin – were investigated in stem and bark of *Aesculus hippocastanum* [43]. The highest levels of both compounds were found in early spring and late autumn.

Pěnčikova et al. [44] studied seasoned variation of alkaloid contents in *Macleaya microcarpa* herb and roots. The proportion of individual alkaloids significantly changed during the vegetation period. The main alkaloids of the new spring leaves were sanguinarine and chelerythine whose content was more than twice higher than in autumn. The content of alkaloids in the roots culminated during June and July for most compounds.

The taxol content in the needles of *Taxus brevifolia* grown in Hungary [45] is considerably highest in the winter months and lowest in June. *Ballota nigra* leaves [46] produced three main phenylopropanoids (caffeoyl-malic acid, forsythoside B and verbascoside) with the highest quantities during early flowering period (May) and then levels of the compounds significantly decreased.

Seasonal variations of flavonoid and phenolic acid contents were studied for several plants, e.g. *Arnica chamissonis* (flower heads) [39], *Artemisia capillaris* (herb) [40], *Bellis perennis* (flower heads) [47], *Ficus cariaca* (fruits) [48], *Ginkgo biloba* (leaves) [34,49], *Origanum vulgare* (leaves) [50], *R. officinalis* (herb) [40] and *S. fruticosa* (herb) [40]. Most of the results show that contents of flavonoids and phenolic acids are lowest at the beginning of vegetative period and increase during summer to achieve the highest amounts at the end of phenological cycle [34,48–50]. Our results on phenolic acids in *M. melissophyllum* herb suit to that pattern. Papageorgiou et al. [40] showed similar dependence for phenolic acids in *R. officinalis* and *S. fruticosa* but stated the highest levels of flavonoids (except rutin) in May and lowest ones in August. On the other hand, Tan et al. [42] obtained for Asiatic species – *A. scoparia* – quite opposite results: lowest contents of phenolic acids and highest levels of flavonoids at the end of vegetative period. Contents of phenolic acids and flavonoids in *A. chamissonis* [39] and *B. perennis* [47] flower heads were relatively constant during the year and did not depend on the time of collection.

5. Conclusions

To our best knowledge, we showed for the first time the results of quantitative analysis of phenolic acids in *M. melissophyllum* herb and their seasonal variation. According to literature data [17,38–50], there is no single pattern for seasonal variation of secondary metabolites in different plant species even for the same group of chemical compounds.

We found that the main constituents of *M. melissophyllum* phenolic acid fraction were *p*-hydroxybenzoic acid and *p*-coumaric acid. According to literature data *p*-hydroxybenzoic acid shows antimicrobial, antifungal and antimutagenic activities (e.g. [2]) and *p*-coumaric acid has antioxidant activities [3]. Kaurinovic et al. [14] investigated antioxidant activities of *M. melissophyllum* extracts and *p*-coumaric acid can be the one of compounds responsible for these properties. Maggi et al. [17] performed quantitative analysis of coumarin in *M. melissophyllum*. This compound is known to possess hepatotoxic activity [51]. It was stated [17] that contents of coumarin was lowest at the end of plant vegetation. Combining this information with our results associated with phenolic acids, it is worth to mention that August/September can be recommended as the best time for collecting of *M. melissophyllum* L. herb because of the lowest content of coumarin and highest content of phenolic acids.

Plant herbs are usually collected at flowering for plant derived medical preparations. Literature data and our results show that it is not always the optimal time for the highest contents of active compounds.

References

[1] A. Gaspar, M. Martins, P. Silvia, E.M. Garrido, J. Garrido, O. Firuzi, R. Miri, L. Saso, F. Borges, Dietary phenolic acids and derivatives. Evaluation of the antioxidant activity of sinapic acid and its alkyl esters, J. Agric. Food Chem. 58 (2010) 11273–11280.
[2] S. Khadem, R. Marles, Monocyclic phenolic acids: hydroxy- and polyhydroxybenzoic acids—occurrence and recent bioactivity studies, Molecules 15 (2010) 7985–8005.
[3] P. Terpinc, T. Polak, N. Šegatin, A. Hanzlovsky, P.N. Ulrih, H. Abramovič, Antioxidant properties of 4-vinyl derivatives of hydroxycinnamic acids, Food Chem. 128 (2011) 62–69.
[4] K. Głowniak, G. Zgórka, M. Kozyra, Solid-phase extraction and reversed-phase high-performance liquid chromatography of free phenolic acids in some *Echinacea* species, J. Chromatogr. A 730 (1996) 25–29.
[5] P.W. Ball, *Melittis* L., in: T.G. Tutin, V.H. Heywood, N.A. Burges, D.M. Moore, D.H. Valentine, S.M. Walters, D.A. Webb (Eds.), Flora Europea, vol. 3, Cambridge University Press, Cambridge, 1972, p. 143.
[6] H. Meusel (Ed.), Vergleichende Chorologie der Zentraleuropäischen Flora, Gustav Fischer Verlag, Jena, 1978, p. 375.
[7] G. Hegi, Illustrierte Flora von Mittel-Europa, Bd. V/4, Carl Hanser Verlag, München, 1964, pp. 2468–2472.
[8] A. Imbesi, Index Plantarum quae in omnium populorum Pharmacopoeis sunt adhuc receptae, Principato, Messina, 1964, p. 470.
[9] G. Penso, Index plantarum medicinalium totius mundi eorumque synonymorum, O.E.M.F., Milano, 1983.
[10] P.M. Guarrera, Traditional phytotherapy in Central Italy (Marche, Abruzzo and Latium), Fitoterapia 76 (2005) 1–25.
[11] M. Idolo, R. Motti, S. Mazzoleni, Ethnobotanical and phytomedicinal knowledge in a long-history protected area, the Abruzzo, Lazio and Molise National Park (Italian Apennines), J. Ethnopharmacol. 127 (2010) 379–395.
[12] S. Jarić, Z. Popović, M. Mačukanović-Jocić, L. Djurdjević, M. Mijatović, B. Karadžić, M. Mitrović, P. Pavlović, An ethnobotanical study on the usage of wild medicinal herbs from Kopaonik Mountain (Central Serbia), J. Ethnopharmacol. 111 (2007) 160–175.
[13] J.L. Lamaison, C. Petitjean-Freytet, F. Duband, A.P. Carnat, Rosmarinic acid content and antioxidant activity in French Lamiaceae, Fitoterapia 62 (1991) 166–171.
[14] B. Kaurinovic, M. Popovic, S. Vlaisavljevic, M. Raseta, Antioxidant activities of *Melittis melissophyllum* L. (Lamiaceae), Molecules 16 (2011) 3152–3167.
[15] R. Salgues, Les variations du taux de la coumarine chez le *Melittis melissophyllum* L., Rev. Gener. Sci. 52 (1942) 35–41.
[16] M. De Vincenzi, E. Mancini, M.R. Dessi, Monographs on botanical flavouring substances used in food, Fitoterapia 68 (1997) 49–61.
[17] F. Maggi, L. Barboni, G. Caprioli, F. Papa, M. Ricciutelli, G. Sagratini, S. Vittori, HPLC quantification of coumarin in bastard balm (*Melittis melissophyllum* L., *Lamiaceae*), Fitoterapia 82 (2011) 1215–1221.
[18] M. Guiso, R. Marini-Bettolo, A. Agostini, Iridoids-XIII: Ajugoside and ajugol: structure and configuration, Gazz. Chim. Ital. 104 (1974) 25–33.
[19] M.L. Scarpati, P. Esposito, Iridoidi (III): struttura e configurazione del melittoside, Gazz. Chim. Ital. 97 (1967) 211–218.
[20] M.L. Scarpati, P. Esposito, Iridoidi (IV): monomelittoside, Ric. Sci. 37 (1967) 840–845.
[21] M.L. Scarpati, M. Guiso, L. Panizzi, I. Iridoids, Harpagide acetate from *Melittis melissophyllum* L., Tetrahedron Lett. 6 (1965) 3439–3443.
[22] L. Świątek, J. Chybowski, Identification of chemical components of *Melittis melissophyllum* L., Annales Universitatis Mariae Curie-Sklodowska, Sectio D: Medicina 37 (1982) 163–170.
[23] H. Skaltsa-Diamantidis, E. Tsitsa-Tzardi, O. Tzakou, N. Argiriadou, Analysis of the essential oil of *Melittis melissophyllum* L. subsp. *albida* Guss., J. Essent. Oil Res. 3 (1991) 367–368.
[24] A. Velasco-Negueruela, J. Sanz, M.J. Pérez-Alonso, J. Palá-Paúl, The volatile components of the aerial parts of *Melittis melissophyllum* L. subsp. *melissophyllum* gathered in Spain, Bot. Complutensis 28 (2004) 133–136.
[25] F. Maggi, F. Papa, G. Cristalli, G. Sagratini, S. Vittori, C. Giuliani, Histochemical localization of secretion and composition of the essential oil in *Melittis melissophyllum* L. subsp. *melissophyllum* from Central Italy, Flavour Frag. J. 25 (2010) 63–70.
[26] F. Maggi, F. Conti, G. Cristalli, C. Giuliani, F. Papa, G. Sagratini, S. Vittori, Chemical differences in volatiles between *Melittis melissophyllum* L. subsp. *melissophyllum* and subsp. *albida* (Guss.) P. W. Ball (Lamiaceae) determined by solid-phase microextraction (SPME) coupled with GC/FID and GC/MS, Chem. Biodivers. 8 (2011) 325–343.

[27] F. Maggi, P. Mártonfi, F. Conti, G. Cristalli, F. Papa, G. Sagratini, S. Vittori, Volatile components of whole and different plant parts of bastard balm (*Melittis melissophyllum* L., Lamiaceae) collected in central Italy and Slovakia, Chem. Biodivers. 8 (2011) 2057–2079.
[28] F. Maggi, T. Bílek, D. Lucarini, F. Papa, G. Sagratini, S. Vittori, *Melittis melissophyllum* L. subsp. *melissophyllum* (Lamiaceae) from Central Italy: a new source of a mushroom-like flavour, Food Chem. 113 (2009) 216–221.
[29] F. Maggi, F. Papa, G. Cristalli, G. Sagratini, S. Vittori, Characterisation of the mushroom-like flavour of *Melittis melissophyllum* L. subsp. *melissophyllum* by headspace solid-phase microextraction (HS-SPME) coupled with gas chromatography (GC-FID) and gas chromatography–mass spectrometry (GC–MS), Food Chem. 123 (2010) 983–992.
[30] E. Skrzypczak, L. Skrzypczak, The tissue culture and chemical analysis of *Melittis melissophyllum* L., Acta Hortic. 330 (1993) 263–267.
[31] E. Skrzypczak-Pietraszek, A. Hensel, Polysaccharides from *Melittis melissophyllum* L. herb and callus, Pharmazie 55 (2000) 768–771.
[32] E. Skrzypczak-Pietraszek, A. Szewczyk, A. Piekoszewska, H. Ekiert, Biotransformation of hydroquinone to arbutin in plant in vitro cultures preliminary results, Acta Physiol. Plant. 27 (2005) 79–87.
[33] J. Pietraszek, E. Skrzypczak-Pietraszek, A comparison of statistical analysis and fuzzy analysis related to an example of callus tissue growth of *Melittis melissophyllum* L. with various variants of Murashige and Skoog's medium, Pol. J. Environ. Stud. 18 (3B) (2009) 290–293.
[34] M. Ellnain-Wojtaszek, G. Zgórka, High-performance liquid chromatography and thin-layer chromatography of phenolic acids from *Ginkgo biloba* L. leaves collected within vegetative period, J. Liq. Chromatogr. Relat. Technol. 22 (1999) 1457–1471.
[35] STATISTICA (Data Analysis Software System), Version 10, Tulsa, Statsoft Inc., 2011, http://www.statsoft.com.
[36] B.S. Everitt, S. Landau, M. Leese, D. Stahl, Cluster Analysis, John Wiley & Sons, Chichester, 2011, pp. 71–110.
[37] I.T. Jolliffe, Principal Component Analysis, Springer, New York, 2002.
[38] H. Hendriks, R. Bos, H.J. Woerdenbag, The essential oil of *Tanacetum parthenium* (L.) Schultz-Bip., Flavour Frag. J. 11 (1996) 367–371.
[39] N. Roki, N. Menkovic, K. Savikin-Fodulovic, D. Krivokuca-Dokic, M. Ristic, D. Grubisic, Flavonoids and essential oil in flower heads of introduced *Arnica chamissonis*, J. Herbs Spices Med. Plants 4 (2001) 19–27.
[40] V. Papageorgiou, C. Gardeli, A. Mallouchos, M. Papaioannou, M. Komaitis, Variation of the chemical profile and antioxidant behavior of *Rosmarinus officinalis* L. and *Salvia fructicosa* Miller grown in Greece, J. Agric. Food Chem. 56 (2008) 7254–7264.
[41] Y. Zheng, L. Xu, Z. Wang, C. Zhang, Distribution and dynamic change of coumarins in leaf and root of *Dendrobium thyrsiflorum*, Zhongguo Zhongyao Zazhi 24 (2009) 1071–1074.
[42] X. Tan, Q. Li, X. Chen, Z. Wang, Z. Shi, K. Bi, Y. Jia, Simultaneous determination of 13 bioactive compounds in Herba *Artemisiae Scopariae* (Yin Chen) from different harvest seasons by HPLC-DAD, J. Pharm. Biomed. Anal. 47 (2008) 847–853.
[43] G. Matysik, K. Głowniak, E. Soczewiński, M. Garbacka, Chromatography of esculin from stems and bark of *Aesculus hippocastanum* L. for consecutive vegetative periods, Chromatographia 38 (1994) 766–770.
[44] K. Pěnčikova, J. Urbanová, P. Musil, E. Táborska, J. Gregorová, Seasonal variation of bioactive alkaloid contents in *Macleaya microcarpa* (Maxim.) Fedde, Molecules 16 (2011) 3391–3401.
[45] V. Németh-Kiss, E. Forgács, T. Cserháti, G. Schmidt, Determination of taxol in *Taxus* species grown in Hungary by high-performance liquid chromatography-diode array detection effect of vegetative period, J. Chromatogr. A 750 (1996) 253–256.
[46] E. Tóth, G. Janicsák, I. Máthe, G. Blunden, Determination of phenylpropanoids in three *Ballota* species, J. Planar Chromatogr. 22 (2009) 293–296.
[47] T. Siatka, M. Kašparová, Seasonal variation in total phenolic and flavonoid contents and DPPH scavenging activity of *Bellis perennis* L. flowers, Molecules 15 (2010) 9450–9461.
[48] R. Veberic, M. Colaric, F. Stampar, Phenolic acids and flavonoids of fig fruit (*Ficus carica* L.) in the northern Mediterranean region, Food Chem. 106 (2008) 153–157.
[49] M. Ellnain-Wojtaszek, Z. Kruczyński, J. Kasprzak, Analysis of the content of flavonoids, phenolic acids as well as free radicals from *Ginkgo biloba* L. leaves during the vegetative cycle, Acta Pol. Pharm. 58 (2001) 205–209.
[50] G. Zgórka, E. Lutostańska, K. Głowniak, Seasonal variations of phenolic acids in *Origanum vulgare* leaves, Pharm. Pharmacol. Lett. 7 (1997) 187–190.
[51] K. Abraham, F. Wöhrlin, O. Lindtner, G. Heinemeyer, A. Lampen, Toxicology and risk assessment of coumarin: focus on human data, Mol. Nutr. Food Res. 54 (2010) 228–239.

Journal of Pharmaceutical and Biomedical Analysis 66 (2012) 162–169

Contents lists available at SciVerse ScienceDirect

Journal of Pharmaceutical and Biomedical Analysis

journal homepage: www.elsevier.com/locate/jpba

Thermal analysis and FTIR spectral curve-fitting investigation of formation mechanism and stability of indomethacin-saccharin cocrystals via solid-state grinding process

Gang-Chun Zhang, Hong-Liang Lin*, Shan-Yang Lin**

Department of Biotechnology, Yuanpei University, Hsin Chu, Taiwan, ROC

ARTICLE INFO

Article history:
Received 31 December 2011
Received in revised form 19 March 2012
Accepted 19 March 2012
Available online 28 March 2012

Keywords:
Curve-fitting
DSC
Cocrystal
Cogrinding
Indomethacin
Saccharin
Formation mechanism
Thermal effect
Stability

ABSTRACT

The cocrystal formation of indomethacin (IMC) and saccharin (SAC) by mechanical cogrinding or thermal treatment was investigated. The formation mechanism and stability of IMC–SAC cocrystal prepared by cogrinding process were explored. Typical IMC–SAC cocrystal was also prepared by solvent evaporation method. All the samples were identified and characterized by using differential scanning calorimetry (DSC) and Fourier transform infrared (FTIR) microspectroscopy with curve-fitting analysis. The physical stability of different IMC–SAC ground mixtures before and after storage for 7 months was examined. The results demonstrate that the stepwise measurements were carried out at specific intervals over a continuous cogrinding process showing a continuous growth in the cocrystal formation between IMC and SAC. The main IR spectral shifts from 3371 to 3,347 cm^{-1} and 1693 to 1682 cm^{-1} for IMC, as well as from 3094 to 3136 cm^{-1} and 1718 to 1735 cm^{-1} for SAC suggested that the O—H and N—H groups in both chemical structures were taken part in a hydrogen bonding, leading to the formation of IMC–SAC cocrystal. A melting at 184 °C for the 30-min IMC–SAC ground mixture was almost the same as the melting at 184 °C for the solvent-evaporated IMC–SAC cocrystal. The 30-min IMC–SAC ground mixture was also confirmed to have similar components and contents to that of the solvent-evaporated IMC–SAC cocrystal by using a curve-fitting analysis from IR spectra. The thermal-induced IMC–SAC cocrystal formation was also found to be dependent on the temperature treated. Different IMC–SAC ground mixtures after storage at 25 °C/40% RH condition for 7 months had an improved tendency of IMC–SAC cocrystallization.

© 2012 Elsevier B.V. All rights reserved.

1. Introduction

More than 90% of drugs approved from 1995 and about 40% of active new chemical entities (NCEs) have poor solubility, poor permeability, or both [1,2]. Since the bioavailability of orally administered drugs markedly depends on drug's solubility in aqueous medium, thus the solubility behavior of drugs is one of the most challenging tasks in the oral dosage form design. The Biopharmaceutical Classification System (BCS) is an available developed guidance for predicting the gastrointestinal drug absorption based on solubility and permeability of drugs [3,4]. This guidance may be also used to establish the correlation between in vitro dissolution and in vivo bioavailability of drug products in early drug development [5,6]. According to this classification system, how to improve the solubility of active pharmaceutical ingredients (APIs) is a critical issue in the preformulation study for solid dosage form development.

Traditional methods such as particle size reduction, salt formation, micellar solubilization, cyclodextrin complexation, solid dispersion and others, have extensively been approached in pharmaceutical industry to enhance the solubility and bioavailability of the poorly water-soluble APIs [7,8]. However, there are several practical limitations to these techniques and the desired bioavailability enhancement may not always be achieved [9,10]. Recently, the cocrystallization is a relatively unique technology and offers a platform for improving physicochemical and biopharmaceutical properties of APIs. This technology applied in the pharmaceutical industry through the development of new class of crystalline solids, called pharmaceutical cocrystals [11–14]. Although cocrystals have long been studied in chemistry, the practical usage of cocrystals in the pharmaceutical industry has recently emerged as new interesting alternatives. The pharmaceutical cocrystals have already proven to be useful in enhancing the solubility, dissolution rate, stability, and bioavailability of APIs [11–14].

Pharmaceutical cocrystals consist of an API (host) and a pharmaceutically acceptable compound (guest, coformer), which are

* Corresponding author. Fax: +886 3 6102312.
** Corresponding author. Fax: +886 3 6102328.
E-mail addresses: hllin@mail.ypu.edu.tw (H.-L. Lin), sylin@mail.ypu.edu.tw (S.-Y. Lin).

0731-7085/$ – see front matter © 2012 Elsevier B.V. All rights reserved.
doi:10.1016/j.jpba.2012.03.039

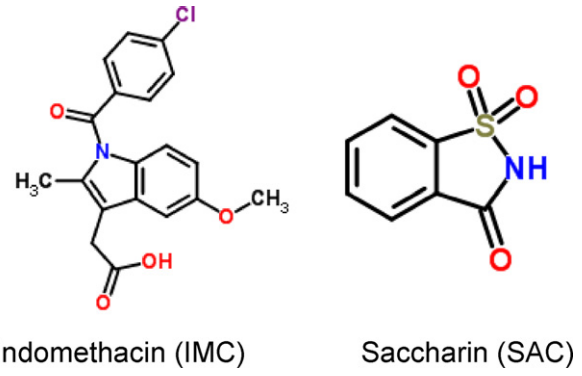

Fig. 1. The chemical structures of indomethacin (IMC) and saccharin (SAC).

structurally homogeneous crystalline phase with defined stoichiometry and contain two or more different neutral molecular components in a crystal lattice [11–14]. It has been described in the literatures as a molecular complex or solid-state complex by stabilizing through a variety of different intermolecular interactions such as hydrogen bonds, aromatic π-stacking, or van der Waals forces [11,15]. The hydrogen bonding is one of the most important interactions in forming the cocrystals [16]. Different methods for forming cocrystals have been demonstrated, including the solid-based method (neat or solvent-assisted grinding) or solution-mediated method (reaction crystallization, slurring, solvent evaporation, cooling or anti-solvent addition, etc.) [11–14]. In addition, cocrystal formation may also offer the opportunity of intellectual property protection and the possibility of extending the life cycles of old APIs in the pharmaceutical industry [17,18].

In our previous study, we first reported by using a powerful differential scanning calorimetry-Fourier transform infrared (DSC-FTIR) combined microspectroscopic system to simultaneously and rapidly screen and detect the cocrystal formulation in real time [19]. This one-step approach is a quick and easy cocrystal screening method for indomethacin-saccharin (IMC–SAC) or nicotinamide, carbamazepine-glutaric acid or urea, piroxicam-saccharin, theophylline-citric acid or nicotinamide, etc. In order to achieve the industrial-based development, a scalable method for mass production of cocrystals should be established. In common, the cocrystals may be easily produced on large scale via cogrinding two constituents together by machine [20–23]. More recently, solvent-assisted grinding has been developed as a more improved method to make the cocrystals [23,24]. These mechanical grinding methods seem to be more effective than solution methods to prepare the cocrystals, since only the grinding machine is necessary. Although the IMC–SAC cocrystal had been investigated [25–28], but the detailed formation mechanism of this cocrystal in the mechanical cogrinding process and the cocrystal stability of ground mixture were rarely studied. In the present study, IMC and SAC were selected as API and coformer. The chemical structures of IMC and SAC used are shown in Fig. 1. The cocrystal formation mechanism of IMC–SAC ground mixtures via mechanical cogrinding process was thoroughly examined by using the curve-fitting analytical technique from the FTIR spectra. Moreover, the stability of different IMC–SAC ground mixtures was also investigated.

2. Materials and methods

2.1. Materials

Indomethacin (IMC, γ-form) and saccharin (SAC) were purchased from Sigma–Aldrich Chem. Co. (St. Louis, MO, USA) and identified by FTIR microspectroscopy. Both raw materials were used without further purification but vacuum-dried at 60 °C for 24 h before use. The KBr crystals were obtained from Jasco Co. (Tokyo, Japan).

2.2. Preparation of different ground mixtures of IMC, SAC or IMC–SAC by neat cogrinding

The raw material of IMC or SAC as well as the physical mixture of IMC–SAC (molar ratio = 1:1) were ground in an oscillatory ball mill (Mixer Mill MM301, Retsch GmbH & Co., Germany) with 20 Hz oscillation frequency, respectively. About 0.2 g powder sample was placed into a 25 ml volume stainless steel milling jar containing two 12 mm diameter stainless steel balls by grinding for 30 min at ambient temperature [29]. In the neat grinding process, the sample ground was withdrawn at the prescribed intervals and kept in 25 °C/40%RH storage condition for further examination. The 25°/40%RH storage condition was controlled by a programmable temperature & humidity chamber (King Son Instru. Tech. Co. Ltd., Taipei, Taiwan).

2.3. Preparation of intact IMC–SAC cocrystal

The preparation of IMC–SAC cocrystal was modified by slow evaporation of an acetone solution containing the same molecular ratio of IMC and SAC at ambient temperature [25,27]. After evaporation for one day, the precipitates were vacuum-dried and stored at the same storage condition.

2.4. Thermal treatment of IMC–SAC physical mixture

A certain amount of physical mixture of IMC–SAC (molar ratio = 1:1) was respectively pre-heated from 30 °C to the predetermined temperature at 140, 150, 157 or 165 °C by DSC with a heating rate of 3 °C/min, and then cooled to room temperature. The cooled sample was then re-examined by DSC and FTIR determinations.

2.5. Stability of IMC–SAC ground mixtures

The stability of four IMC–SAC ground mixtures prepared by neat cogrinding for 3, 10, 15 or 30 min was examined after storage at 25 °C/40%RH condition. These different ground samples before and after storage for 7 months were analyzed by FTIR determination with curve-fitting technique.

2.6. Thermal analysis of different samples

All the samples were directly determined by using a DSC analytical technique (DSC, Q 20, TA Instruments, Inc., New Castle, DE, USA) at a heating rate of 3 °C/min with an open pan system in a stream of N_2 gas from 30 to 250 °C. The instrument was calibrated for temperature and heat flow using indium as standards.

2.7. FTIR microspectroscopic study

A trace powder of each different sample was respectively sealed into two pieces of KBr pellets (without any grinding with KBr powders) and then directly compressed with an IR spectrophotometric hydraulic press (Riken Seiki Co., Tokyo, Japan) under 400 kg/cm$_2$ for 15 s. The compressed KBr disc was respectively determined by FTIR microspectroscopy (IRT-5000-16/FTIR-6200, Jasco Co., Tokyo, Japan) with a mercury cadmium telluride (MCT) detector by transmission technique. FTIR spectra were generated by co-addition of 256 interferograms collected at 4 cm^{-1} resolution.

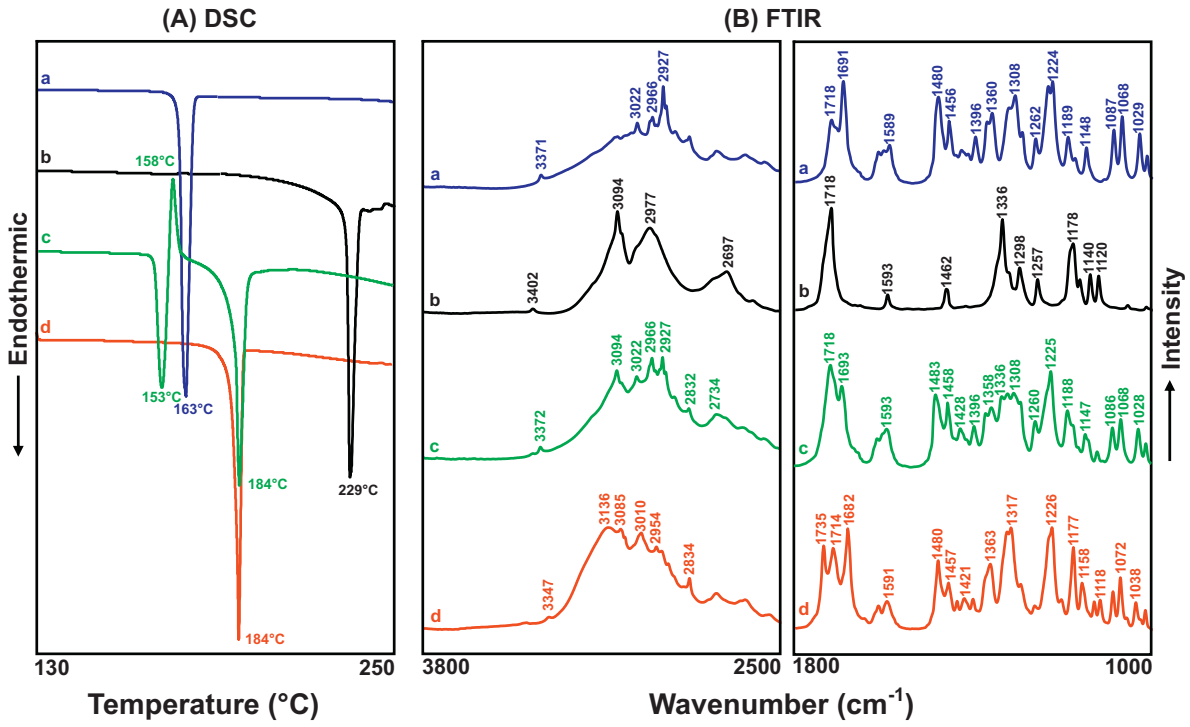

Fig. 2. DSC thermograms and FTIR spectra of indomethacin (IMC, a), saccharin (SAC, b), IMC–SAC physical mixture (c) and solvent-evaporated IMC–SAC cocrystal (d).

2.8. Curve-fitting analysis of FTIR spectra of different IMC–SAC samples

The components and relative compositions of different ground mixtures or temperature-treated samples of IMC–SAC were estimated quantitatively in the 1800–1650 cm^{-1} region of FTIR spectra by a curve-fitting algorithm with a Gaussian–Lorenzian function [29,30]. The best curve-fitting procedure was performed by iterative fits toward a minimum standard error. Because the analysis depends on the positions and intensities of the components of the contour, substantial attention was paid to obtaining the best possible fit with the minimum number of component bands. The relative proportion of a component was computed to be the fractional area of the corresponding peak, divided by the sum of areas of all the peaks. The raw material of IMC or SAC, and intact IMC–SAC cocrystal were also estimated.

3. Results and discussion

3.1. Identification of different raw materials and mixed samples

Fig. 2 shows the DSC curves and FTIR spectra of IMC (a), SAC (b), physical mixture (c) and solvent-evaporated (d) sample of IMC–SAC. One endothermic peak at 163 °C and another peak at 229 °C were observed in the DSC curves, the former was the melting of IMC (a) and the latter was attributed to the fusion of SAC (b), respectively. While two endothermic peaks at 153 and 184 °C as well as one exothermic peak at 158 °C were also found in the DSC curve of the IMC–SAC physical mixture (c). The peak appeared at 153 °C might be due to the fusion of eutectic mixture [31,32], but the peak at 184 °C might be corresponded to the melting of IMC–SAC cocrystal (d) following the exothermic peak at 158 °C [19,25,26]. The appearance of exothermic peak at 158 °C might be due to a new form recrystallized from the eutectic melt at 153 °C to cause the cocrystal formation [33,34]. Since the sample was a physical mixture without any pretreatment, thus this exothermic peak did not attribute to the amorphous recrystallization [35,36]. The solvent-evaporated sample showed a clear sharp endothermic peak at 184 °C (d). The endothermic peak at 184 °C with 82.8 kJ/mole for solvent-evaporated sample was close to the melting point at 184.2 °C with 79.4 kJ/mole of IMC–SAC cocrystal reported by Basavoju et al. [25].

Since the cocrystal was formed between IMC and SAC, a significant IR spectral difference was also observed between the physical mixture (c) and solvent-evaporated sample (d) of IMC–SAC. Particularly, several unique IR peaks at 3347, 3136, 3085, 3010, 2954, 1735, 1714, 1682 and 1317 cm^{-1} were observed in the IR spectrum of the solvent-evaporated sample (d) of IMC–SAC, as shown in Fig. 2. The representative FTIR spectra of IMC and SAC are also displayed. Several characteristic IR absorption bands and their assignments of IMC or SAC were respectively indicated as follows:

3371 and 2900–3400 (carboxylic O—H), 1718 (C=O of carboxylic acid dimmer), 1691 (benzoyl C=O), 1625–1575 and 1480 (C=C of aromatic rings), 1308 (C—O of acidic group), 1270–1200 (=C—O of ether group), 1068 cm^{-1} (C—Cl) for IMC [37–39]; 3402 and 3094 (N—H), 2977 (C—H), 2697 (N—H), 1718 (C=O), 1336 and 1178 cm^{-1} (asymmetric and symmetric SO_2) for SAC [40,41]. It clearly indicates that the IR spectrum of IMC–SAC physical mixture was superimposed by all the IR spectral peaks of each individual IMC or SAC, suggesting that there was no any interaction occurred in their physical mixture. The IR spectrum for solvent-evaporated IMC–SAC sample was markedly different from that of the IMC–SAC physical mixture. Several new unique IR absorption peaks at 3347, 3136, 3085, 3010, 2954, 1735, 1714, 1682 and 1317 cm^{-1} were observed in the IR spectrum of the solvent-evaporated IMC–SAC sample (d). The appearance of these new IR peaks was due to the occurrence of cocrystal formation via intermolecular interaction between IMC and SAC, which was almost consistent with the IR spectrum of IMC–SAC cocrystal [25]. From the results of DSC and FTIR, the solvent-evaporated IMC–SAC sample in this study may be confirmed as an IMC–SAC cocrystal.

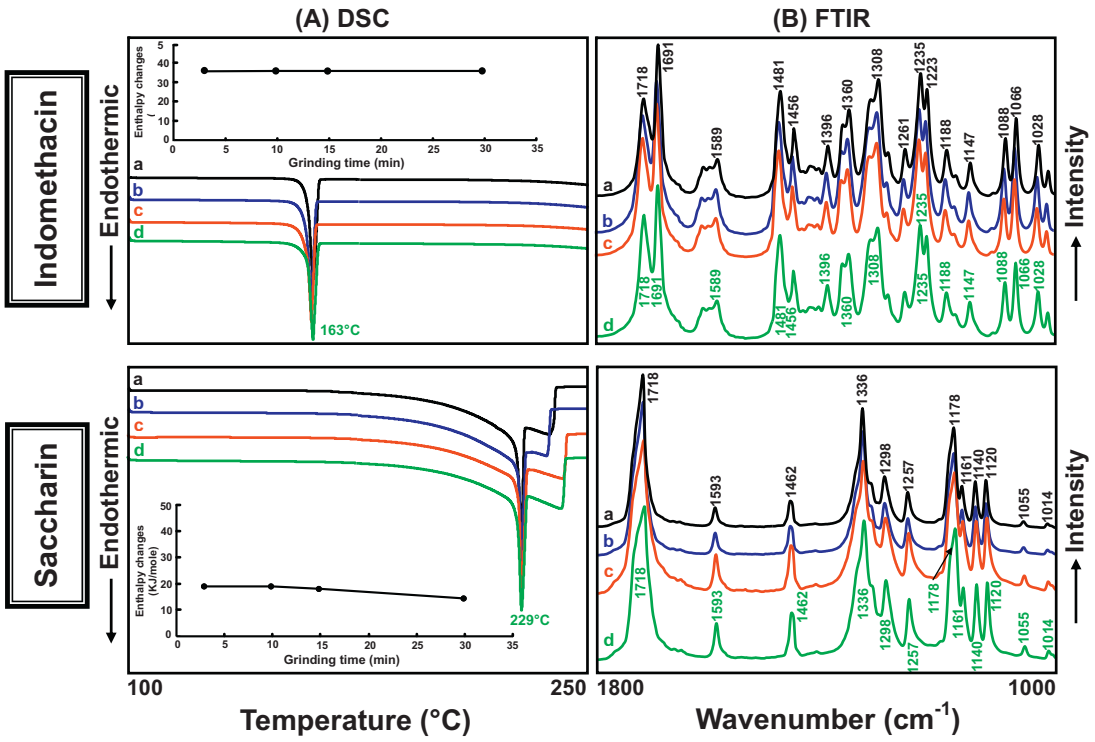

Fig. 3. Effect of grinding on the changes in DSC curves and FTIR spectra of IMC or SAC. Key, Grinding time: a, 3 min; b, 10 min; c, 15 min; d, 30 min.

3.2. Grinding effect on the raw material of IMC or SAC and IMC–SAC physical mixture

The effect of grinding on the changes in DSC curves and FTIR spectra of raw material of IMC or SAC is displayed in Fig. 3. Obviously, both DSC thermograms and FTIR spectra for these two raw materials almost maintained the same shape as that of the ungrounded sample and did not alter with the increase of grinding time. The enthalpy of endothermic peaks at 163 and 229 °C in both DSC curves was only slightly reduced with grinding time, indicating that solid-state IMC or SAC alone was less influenced by a mechanical grinding process. However, the cogrinding process did clearly cause the changes in both DSC curves and FTIR spectra for the IMC–SAC ground mixture, as shown in Fig. 4. It is

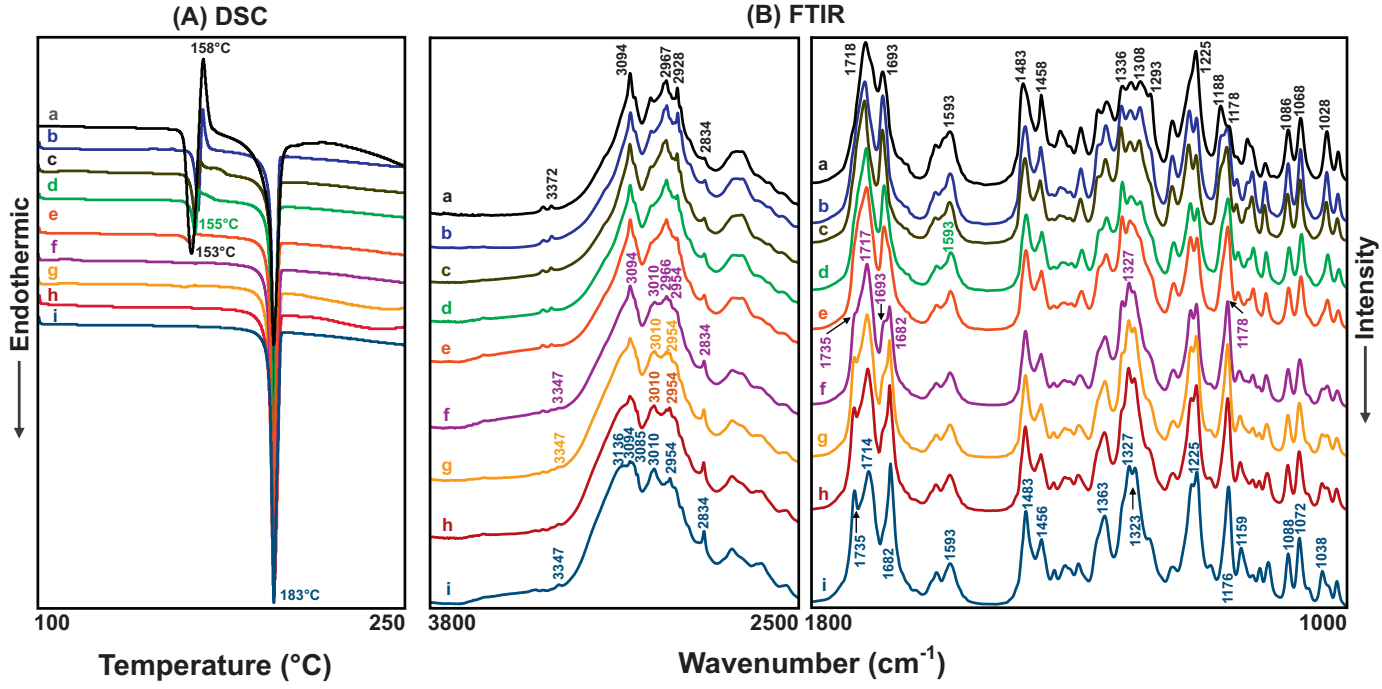

Fig. 4. The changes in DSC curves and FTIR spectra of the IMC–SAC physical mixture before and after cogrinding process. Key: Cogrinding time: a, 0 min; b, 1 min; c, 3 min; d, 5 min; e, 10 min; f, 15 min; g, 20 min; h, 25 min; i, 30 min.

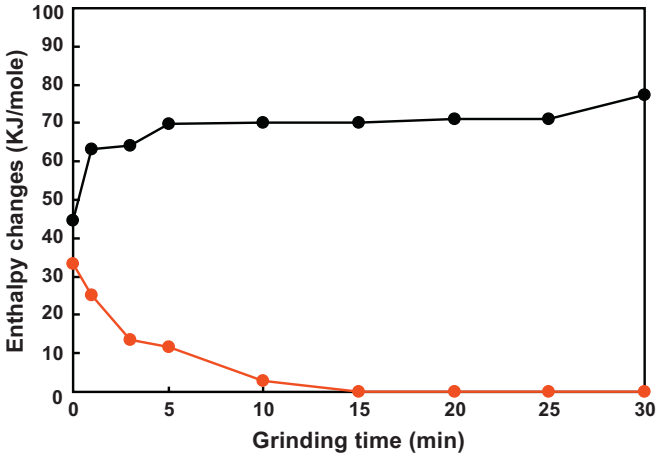

Fig. 5. Cogrinding-induced enthalpy changes of the DSC endothermic peaks at 153 °C (●) and 183 °C (●).

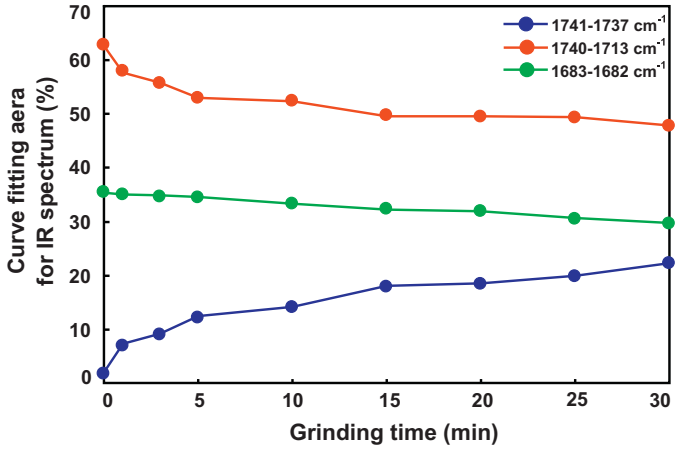

Fig. 7. Cogrinding time-dependent changes in the curve-fitted FTIR spectra peak areas for the IMC–SAC ground mixture from Fig. 6 in the 1800–1600 cm^{-1} region.

clearly evident that the endothermic peak intensity at 153 °C corresponded to the fusion of eutectic point of IMC–SAC physical mixture was gradually reduced with the increase of cogrinding time. While another endothermic peak intensity at 183 °C due to the cocrystal formation of IMC–SAC was increased with the cogrinding time. The former endothermic peak at 153 °C disappeared after mechanical cogrinding for 15 min, but the latter sharp endothermic peak at 183 °C was apparently obtained with cogrinding time (Fig. 4A). This sharp DSC endothermic peak was close to that of the melting of solvent-evaporated IMC–SAC cocrystal and the IMC–SAC cocrystal reported [25]. The intensity of exothermic peak at 158 °C was also reduced with cogrinding time. The gradual disappearance and stronger appearance of both endothermic peaks at 153 and 183 °C might be due to the cogrinding-induced cocrystal formation between IMC and SAC. This implies that the IMC–SAC cocrystal was formed after mechanical cogrinding for 15 min. Moreover, the cogrinding-induced enthalpy changes of both endothermic peaks at 153 and 183 °C are also displayed in Fig. 5. Obviously, the enthalpy for the former peak at 153 °C was gradually reduced but for the latter peak at 183 °C due to cocrystal formation was markedly increased and maintained with cogrinding time. This strongly suggests that mechanical cogrinding process may gradually induce the cocrystal formation between IMC and SAC.

The changes in FTIR spectra also agreed the DSC results. The time-dependent FTIR spectral changes of the IMC–SAC ground mixtures are also displayed in Fig. 4B. Particularly, the IR spectral ranges within 3800–2500 and 1800–1600 cm^{-1} were gradually altered beyond cogrinding for 15–20 min. In the spectral range of 3800–2500 cm^{-1}, five new IR peaks near at 3347, 3136, 3085, 3010 and 2954 cm^{-1} assigned to N—H and O—H stretching vibrations appeared as a shoulder beyond cogrinding for 15 min but were apparently observed after 30 min-cogrinding. In the meantime, another three new IR peaks at 1735, 1714, and 1682 cm^{-1} also gradually appeared and became sharper with the increase of

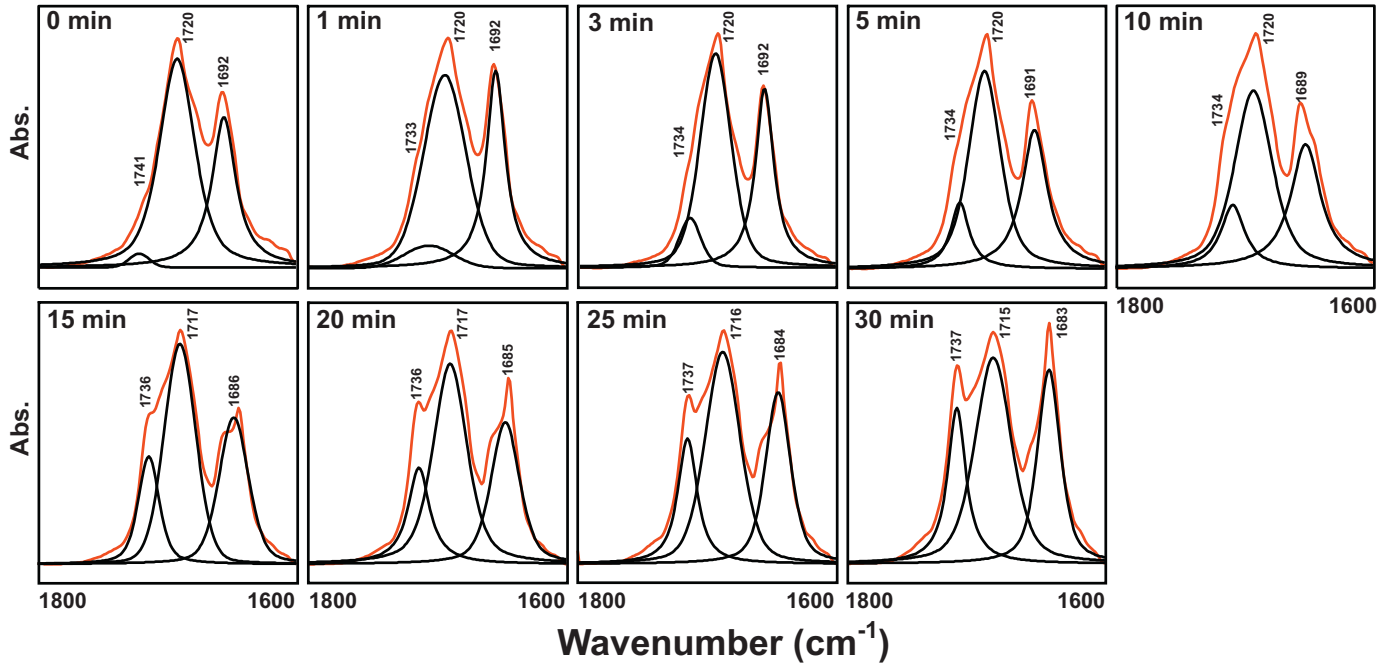

Fig. 6. The best curve-fitted profiles for the IMC–SAC ground mixture from the IR spectra of Fig. 4 in the 1800–1600 cm^{-1} region.

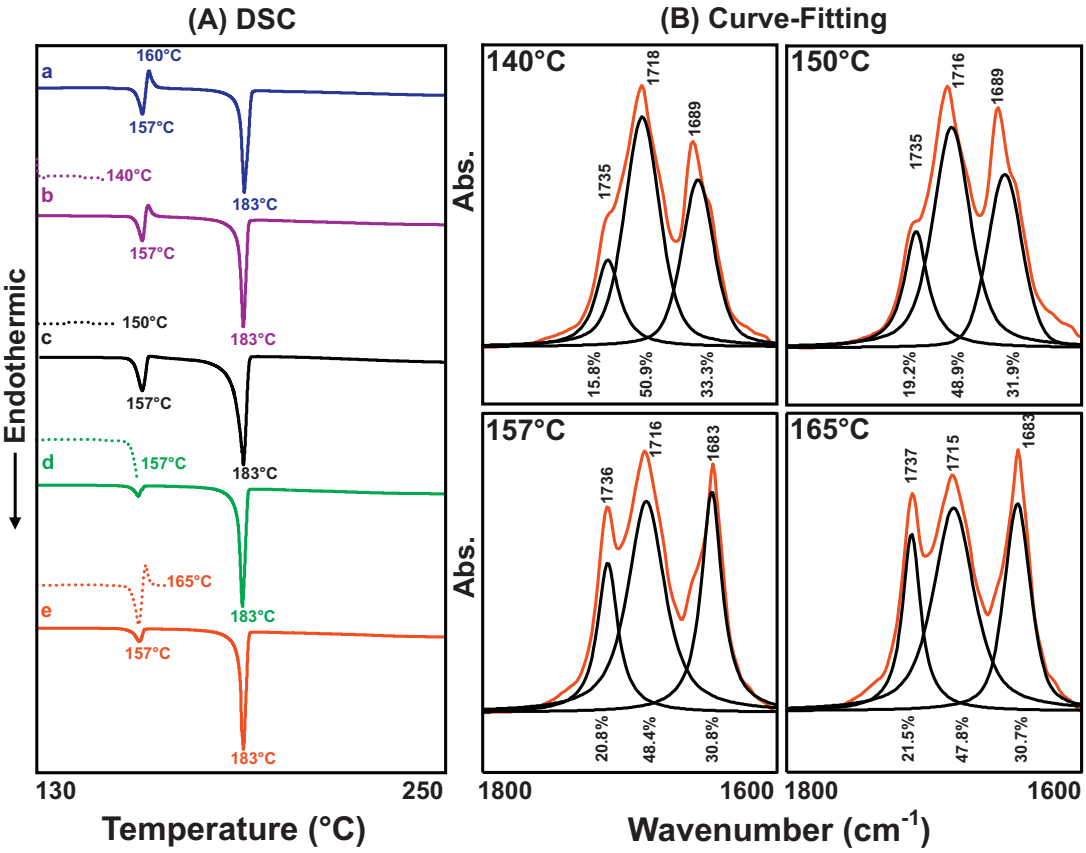

Fig. 8. Changes in DSC curves and FTIR spectra of the IMC–SAC physical mixture after pre-heating to different predetermined temperatures. Key: preheating temperature: a, without pretreatment; b, 140 °C; c, 150 °C; d, 157 °C; e, 165 °C.

the cogrinding time. This might be attributed to the intermolecular interaction occurred between IMC and SAC.

Both FTIR spectral peaks at 3347 and 3136 cm^{-1} were also found in the IR spectrum of 30 min-ground mixture of IMC–SAC. According to the Basavoju's study [25], these might be due to the spectral shift from 3371 (carboxylic O—H of IMC) and 3094 cm^{-1} (N—H of SAC), respectively. The spectral shift of the O—H stretching vibration from 3371 cm^{-1} in IMC structure to 3347 cm^{-1} of IMC–SAC cocrystals implies that the O—H group was participating in a hydrogen bonding. Similarly, the spectral shift of the N—H stretching vibration from 3094 cm^{-1} in the imide dimer of SAC to 3136 cm^{-1} of IMC–SAC cocrystals also suggests that the N—H group was also taken part in a hydrogen bonding. Another FTIR spectral shifts from 1693 cm^{-1} to 1682 cm^{-1} for IMC and 1718 cm^{-1} to 1735 cm^{-1} for SAC further explain the formation of IMC–SAC cocrystals. The IR peaks at 1327 and 1176 cm^{-1} (asymmetric and symmetric SO_2 stretching modes of SAC) shifted from 1336 and 1178 cm^{-1} were also observed in the IR spectra of IMC–SAC cocrystal, implying the influence of intermolecular interaction between IMC and SAC. This strongly demonstrates that the cogrinding process could gradually cause the cocrystal formation of IMC and SAC via intermolecular interaction between IMC and SAC.

3.3. Quantitative curve-fitting analysis of time-dependent cocrystal formation after cogrinding

The IR absorption spectra for many large biological macromolecules or heterogeneous matrix are well known to be frequently comprised of multi-component bands which overlapped into a broad unresolved absorption, leading to difficult interpretation of the data [42,43]. Spectral data analyses such as Fourier self-deconvolution (FSD), partial least squares (PLS) and/or curve-fitting analysis have been developed to resolve these complex multi-component absorptions [44]. By using the curve fitting analysis, it can not only easily resolve the individual component bands and facilitate data interpretation, but may also calculate the area from each of the individual bands [45,46]. Here, the curve-fitting analysis was applied to combine with a nonlinear deconvolution technique to probe the nature and extent of structural changes in the IR spectra of different samples. The best curve-fitted IR spectral components and areas of IMC, SAC or IMC–SAC cocrystal prepared by slow solvent evaporation were listed as follows: IMC (1719 cm^{-1}, 37.6%; 1707 cm^{-1}, 3.6%; 1692 cm^{-1}, 58.8%); SAC (1737 cm^{-1}, 13.7%; 1730 cm^{-1}, 14.9%; 1720 cm^{-1}, 71.4%); IMC–SAC cocrystal (1737 cm^{-1}, 26.1%; 1713 cm^{-1}, 46.5%; 1682 cm^{-1}, 27.4%), respectively.

The best curve-fitted profiles for the IMC–SAC ground mixture from the IR spectra of Fig. 3 in the 1800–1650 cm^{-1} region are displayed in Fig. 6. Here, the IR spectral region of 1800–1650 cm^{-1} was selected due to the most sensitive changes in this region. The changes in the curve-fitted FTIR spectral areas for each component peak with cogrinding times are also revealed in Fig. 7. It is evident that the IR spectral position and area of the IMC–SAC physical mixture were gradually changed with the increase of cogrinding time. After cogrinding for 15 min, particularly the peak position and the compositional area were markedly altered. Three new peak positions at 1737, 1713 and 1682 cm^{-1} due to the contribution of IMC–SAC cocrystal formation were observed. The peak position and compositional area of the 30 min-ground mixture (1737 cm^{-1}, 22.3%; 1713 cm^{-1}, 47.9%; 1682 cm^{-1}, 29.8%) were closely similar to that of the solvent-evaporated cocrystal (1737 cm^{-1}, 26.1%; 1713 cm^{-1}, 46.5%; 1682 cm^{-1}, 27.4%), indicating again that the

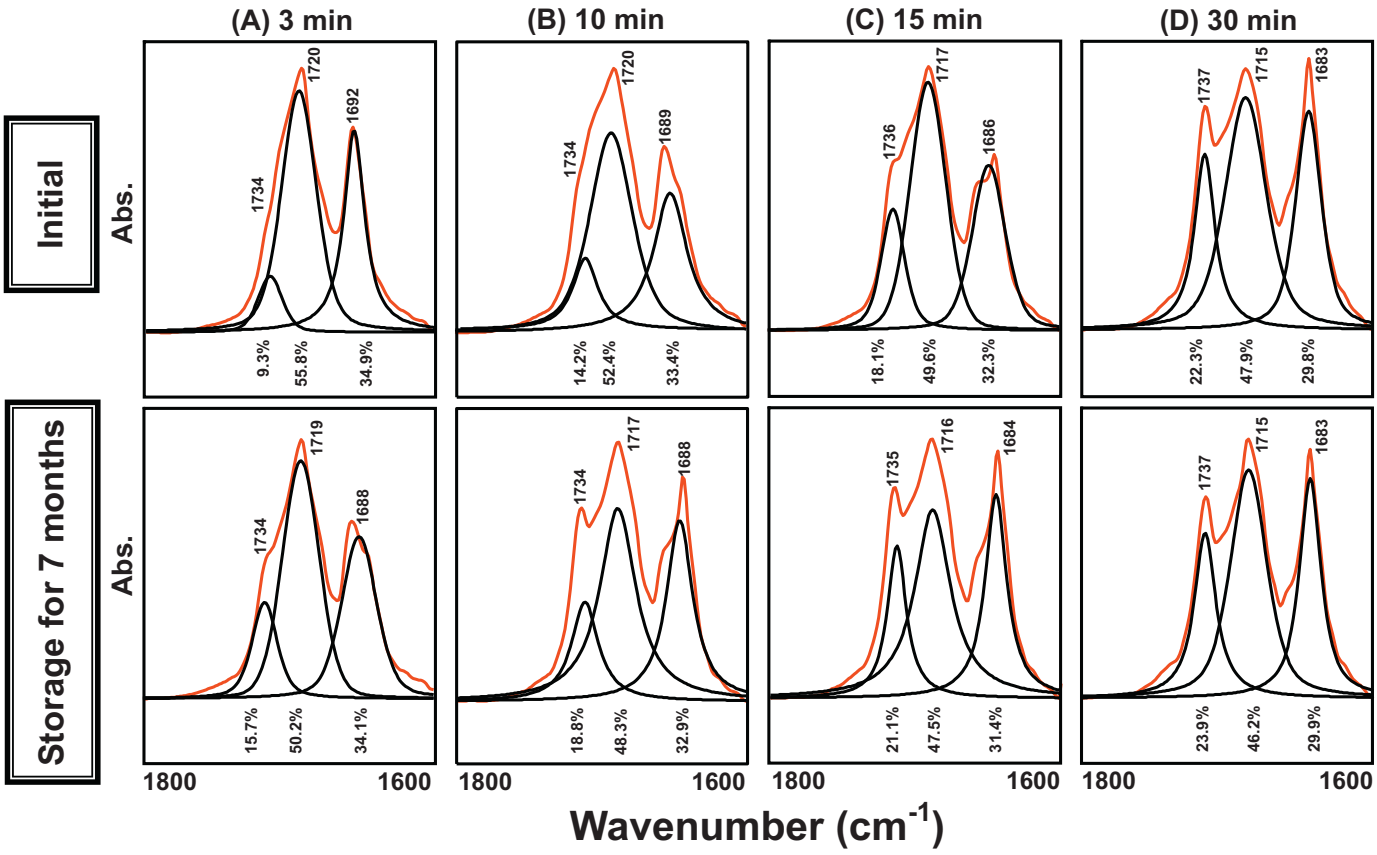

Fig. 9. Changes in FTIR spectra of the physical mixture and 60 min-ground mixture of IMC–SAC after storage at 25 °C/40% RH condition.

cogrinding process can availably cause the cocrystal formation between IMC and SAC. The gradual changes in IR spectral position and area of the IMC–SAC ground mixture might explain the formation mechanism of IMC–SAC cocrystals.

3.4. Thermal-induced formation of IMC–SAC cocrystal

In order to examine the thermal effect on the cocrystal formation of IMC and SAC, the physical mixture of IMC–SAC (molar ratio = 1:1) was respectively pre-heated to each predetermined temperature. Fig. 8 reveals the changes in DSC curves and the best curve-fitted FTIR profiles of the IMC–SAC physical mixture after different pre-thermal treatments. The pre-treated samples were analyzed by DSC and FTIR determinations, again. Obviously, two endothermic peaks at 157 (fusion of eutectic mixture) and 183 °C (cocrystal formation) and one exothermic peak at 160 °C (recrystallization from eutectic melt) obtained from the DSC curve of IMC–SAC physical mixture did not alter after pre-heating the physical mixture to 140 °C, but which curve-fitted FTIR data was similar to that of the 10 min-ground sample (Fig. 6). Once the IMC–SAC physical mixture was pre-heated to 150 °C, the peak intensities at 150 and 160 °C were reduced and its curve-fitted FTIR spectrum was near to that of the 15 min-ground mixture. When the IMC–SAC physical mixture was pre-heated to 157 or 165 °C, a small endothermic peak at 157 °C was still seen in the DSC curve and their curve-fitted FTIR spectra were more closely to the result of 25 or 30 min-ground mixture. The peak position and compositional area of the 165 °C-pretreated sample (1737 cm^{-1}, 21.5%; 1715 cm^{-1}, 47.8%; 1683 cm^{-1}, 30.7%) were also near to that of the solvent-evaporated IMC–SAC cocrystal (1737 cm^{-1}, 26.1%; 1713 cm^{-1}, 46.5%; 1682 cm^{-1}, 27.4%), indicating again that the cocrystal formation between IMC and SAC can also be induced by thermal treatment.

3.5. Stability of different IMC–SAC ground mixtures

Pharmaceutical stability testing is well known to provide evidence on how the quality and quantity of a drug substance or drug product after storage under appropriate conditions [47,48]. Stability testing is one of the methods to predict the pharmaceutical product throughout its lifetime. In common, stability testing includes long-term, accelerated and intermediate stability studies. Here, the long-term stability of different ground mixtures of IMC–SAC was examined before and after storage for 7 months at 25 °C/40%RH conditions.

Fig. 9 shows the curve-fitted FTIR spectral changes of different IMC–SAC ground mixtures before and after storage at 25 °C/40% RH for 7 months. It clearly indicates that the peak positions and compositional areas for all the ground mixtures at the initial stage were markedly different from that of the ground mixtures after storage for 7 months. All the ground mixtures after storage at 25 °C/40% RH conditions for 7 months exhibited a good tendency to cocrystal formation. In particular, the 10 or 15-min ground mixture of IMC–SAC showed a more improved cocrystal formation from initial to 7 months. The compositional areas of 30 min-ground mixture of IMC–SAC after storage 7 months were also found to be close to that of the data of IMC–SAC cocrystal prepared by solvent evaporation, indicating that the long-term storage might improve the IMC–SAC cocrystal formation from different ground mixtures of IMC–SAC. The partially intermolecular interaction of IMC–SAC induced by mechanical cogrinding process under such storage condition might

be responsible for the improvement of cocrystal formation between IMC and SAC.

4. Conclusions

The results of this study reveal that mechanical cogrinding process may gradually induce the cocrystal formation between IMC and SAC via an intermolecular interaction by hydrogen bonding. The 30-min ground mixture of IMC–SAC was found to show the similar components and contents to that of the solvent-evaporated IMC–SAC cocrystal by using a curve-fitting analysis. The IMC–SAC cocrystal formation was also dependent on the temperature of thermal treatment. In addition, different IMC–SAC ground mixtures after storage at 25 °C/40% RH condition for 7 months also exhibited an improved tendency of IMC–SAC cocrystallization.

Acknowledgements

This work was supported by National Science Council, Taipei, Taiwan (NSC 100-2320-B-264-001-MY3).

References

[1] D.J. Hauss, Oral lipid-based formulations, Adv. Drug Deliv. Rev. 59 (2007) 667–676.
[2] R.D. Connors, E.J. Elder, Using a portfolio of particle growth technologies to enable delivery of drugs with poor water solubility, Drug Deliv. Technol. 4 (2004) 78–83.
[3] US FDA, The Biopharmaceutics Classification System (BCS) Guidance, 2009, http://www.fda.gov/AboutFDA/CentersOffices/CDER/ucm128219.htm.
[4] G.L. Amidon, H. Lennernäs, V.P. Shah, J.R. Crison, A theoretical basis for a biopharmaceutics drug classification: the correlation of in vitro drug product dissolution and in vivo bioavailability, Pharm. Res. 12 (1995) 413–420.
[5] J. Emami, In vitro–in vivo correlation: from theory to applications, J. Pharm. Pharm. Sci. 9 (2006) 169–189.
[6] R.S. Uppoor, Regulatory considerations for in vitro/in vivo correlations, Am. Pharm. Rev. 8 (2005) 42–45.
[7] T. Loftsson, P. Jarho, M. Másson, T. Järvinen, Cyclodextrins in drug delivery, Expert Opin. Drug Deliv. 2 (2005) 335–351.
[8] V.R. Vemula, V. Lagishetty, S. Lingala, Solubility enhancement techniques, Int. J. Pharm. Sci. Rev. Res. 5 (2010) 41–51.
[9] D.A. Wadke, A.T.M. Serajuddin, H. Jacobson, Preformulation testing, in: H.A. Lieberman, L. Lachman, J.B. Schwartz (Eds.), Pharmaceutical Dosage Forms: Tablets, vol. 1, Dekker, New York, 1989, pp. 1–73.
[10] A.T.M. Serajuddin, Solid dispersion of poorly water-soluble drugs: early promises, subsequent problems and recent breakthroughs, J. Pharm. Sci. 88 (1998) 1058–1066.
[11] P. Vishweshwar, J.A. McMahon, J.A. Bis, M.J. Zaworotko, Pharmaceutical co-crystals, J. Pharm. Sci. 95 (2006) 499–516.
[12] N. Schultheiss, A. Newman, Pharmaceutical cocrystals and their physicochemical properties, Cryst. Growth Des. 9 (2009) 2950–2967.
[13] I. Miroshnyk, S. Mirza, N. Sandler, Pharmaceutical co-crystals—an opportunity for drug product enhancement, Expert Opin. Drug Deliv. 6 (2009) 333–341.
[14] N. Qiao, M. Li, W. Schlindwein, N. Malek, A. Davies, G. Trappitt, Pharmaceutical cocrystals: an overview, Int. J. Pharm. 419 (2011) 1–11.
[15] R.E. Davis, K.A. Lorimer, M.A. Wilkowski, J.H. Rivers, Studies of relationship in cocrystal systems, ACA Trans. 39 (2004) 41–61.
[16] K. Shiraki, N. Takata, R. Takano, Y. Hayashi, K. Terada, Dissolution improvement and the mechanism of the improvement from cocrystallization of poorly water-soluble compounds, Pharm. Res. 25 (2008) 2581–2592.
[17] A.V. Trask, An overview of pharmaceutical cocrystals as intellectual property, Mol. Pharm. 4 (2007) 301–309.
[18] N. Shan, M.J. Zaworotko, The role of cocrystals in pharmaceutical science, Drug Discov. Today 13 (2008) 440–446.
[19] T.K. Wu, S.Y. Lin, H.L. Lin, Y.T. Huang, Simultaneous DSC-FTIR microspectroscopy used to screen and detect the co-crystal formation in real time, Bioorg. Med. Chem. Lett. 21 (2011) 3148–3151.
[20] A.V. Trask, W. Jones, Crystal engineering of organic cocrystals by the solid-state grinding approach, Top. Curr. Chem. 254 (2005) 41–70.
[21] T. Friščić, W. Jones, Recent advances in understanding the mechanism of cocrystal formation via grinding, Cryst. Growth Des. 9 (2009) 1621–1637.
[22] G. Kaupp, Mechanochemistry: the varied applications of mechanical bond-breaking, CrystEngComm 11 (2009) 388–403.
[23] N. Shan, F. Toda, W. Jones, Mechanochemistry and co-crystal formation: effect of solvent on reaction kinetics, Chem. Commun. (2002) 2372–2373.
[24] S. Karki, T. Friscić, W. Jones, W.D. Motherwell, Screening for pharmaceutical cocrystal hydrates via neat and liquid-assisted grinding, Mol. Pharm. 4 (2007) 347–354.
[25] S. Basavoju, D. Boström, S.P. Velaga, Indomethacin-saccharin cocrystal: design, synthesis and preliminary pharmaceutical characterization, Pharm. Res. 25 (2008) 530–541.
[26] L. Padrela, M.A. Rodrigues, S.P. Velaga, H.A. Matos, E.G. de Azevedo, Formation of indomethacin–saccharin cocrystals using supercritical fluid technology, Eur. J. Pharm. Sci. 38 (2009) 9–17.
[27] M. Allesø, S. Velaga, A. Alhalaweh, C. Cornett, M.A. Rasmussen, F. van den Berg, et al., Near-infrared spectroscopy for cocrystal screening. A comparative study with Raman spectroscopy, Anal. Chem. 80 (2008) 7755–7764.
[28] M.S. Jung, J.S. Kim, M.S. Kim, A. Alhalaweh, W. Cho, S.J. Hwang, et al., Bioavailability of indomethacin–saccharin cocrystals, J. Pharm. Pharmacol. 62 (2010) 1560–1568.
[29] S.Y. Lin, C.H. Hsu, M.T. Sheu, Curve-fitting FTIR studies of loratadine/hydroxypropyl-beta-cyclodextrin inclusion complex induced by co-grinding process, J. Pharm. Biomed. Anal. 53 (2010) 799–803.
[30] W.T. Cheng, S.Y. Lin, S.L. Wang, Differential scanning calorimetry with curvefitting program used to quantitatively analyze the polymorphic transformation of famotidine in the compressed compact, Drug Dev. Ind. Pharm. 34 (2008) 1368–1375.
[31] M.A. Mohammad, A. Alhalaweh, S.P. Velaga, Hansen solubility parameter as a tool to predict cocrystal formation, Int. J. Pharm. 407 (2011) 63–71.
[32] E. Lu, N. Rodriguez-Hornedo, R. Suryanarayanan, A rapid thermal method for cocrystal screening, CrystEngComm 10 (2008) 665–668.
[33] O.L. Évora, R.A.E. Castro, T.M.R. Maria, M.T.S. Rosado, M.R. Silva, A.M. Beja, et al., Pyrazinamide-diflunisal. A new dual-drug co-crystal, Cryst. Growth Des. 11 (2011) 4780–4788.
[34] E. Zaini, Y.C. Sumirtapura, S.N. Soewandhi, A. Halim, H. Uekusa, K. Fujii, Cocrystalline phase transformation of binary mixture of trimethoprim and sulfamethoxazole by slurry technique, Asian J. Pharm. Clin. Res. 3 (2010) 26–29.
[35] P. Mura, M. Cirri, M.T. Faucci, J.M. Ginès-Dorado, G.P. Bettinetti, Investigation of the effects of grinding and co-grinding on physicochemical properties of glisentide, J. Pharm. Biomed. Anal. 30 (2002) 227–237.
[36] D. Giron, Thermal analysis, microcalorimetry and combined techniques for the study of pharmaceuticals, J. Therm. Anal. Calorim. 56 (1999) 1285–1304.
[37] Y. Umeda, T. Fukami, T. Furuishi, T. Suzuki, M. Makimura, K. Tomono, Molecular complex consisting of two typical external medicines: intermolecular interaction between indomethacin and lidocaine, Chem. Pharm. Bull. (Tokyo) 55 (2007) 832–836.
[38] F. Wang, H. Hui, T.J. Barnes, C. Barnett, C.A. Prestidge, Oxidized mesoporous silicon microparticles for improved oral delivery of poorly soluble drugs, Mol. Pharm. 7 (2010) 227–236.
[39] M. Del Arco, E. Cebadera, S. Gutiérrez, C. Martín, M.J. Montero, V. Rives, et al., Mg, Al layered double hydroxides with intercalated indomethacin: synthesis, characterization, and pharmacological study, J. Pharm. Sci. 93 (2004) 1649–1658.
[40] G. Jovanovski, The SO_2 stretching vibrations in some metal saccharinates: spectra–structure correlations, Spectrosc. Lett. 28 (1995) 1095–1109.
[41] I.G. Binev, B.A. Stamboliyska, E.A. Velcheva, The infrared spectra and structure of o-sulfobenzimide (saccharin) and of its nitranion: an ab initio force field treatment, Spectrochim. Acta Part A 52 (1996) 1135–1143.
[42] M.C. Manning, Use of infrared spectroscopy to monitor protein structure and stability, Expert Rev. Proteom. 2 (2005) 731–743.
[43] C.P. Sherman Hsu, Infrared spectroscopy, in: F.A. Settle (Ed.), Handbook of Instrumental Techniques for Analytical Chemistry, Prentice-Hall, Inc, New Jersey, 1998, pp. 247–283.
[44] K.A. Oberg, A.L. Fink, Methods for collecting and analyzing attenuated total reflectance FTIR spectra of proteins in solution, Tech. Protein Chem. 6 (1995) 475–484.
[45] V.A. Lórenz-Fonfría, E. Padrós, Curve-fitting of Fourier manipulated spectra comprising apodization, smoothing, derivation and deconvolution, Spectrochim. Acta. A: Mol. Biomol. Spectrosc. 60 (2004) 2703–2710.
[46] J.G. Dodd, L.K. DeNoyer, Curve-fitting: modeling spectra, in: J.M. Chalmers, P.R. Griffiths (Eds.), Handbook of Vibrational Spectroscopy, vol. 3, 2nd ed., John Wiley & Sons Ltd, Chichester, UK, 2002, pp. 2215–2223.
[47] S. Kopp, Stability testing of pharmaceutical products in a global environment, RAJ Pharm. 16 (2006) 291–294.
[48] K.C. Waterman, The application of the Accelerated Stability Assessment Program (ASAP) to quality by design (QbD) for drug product stability, AAPS PharmSciTech 12 (2011) 932–937.

Journal of Pharmaceutical and Biomedical Analysis 66 (2012) 170–175

Contents lists available at SciVerse ScienceDirect

Journal of Pharmaceutical and Biomedical Analysis

journal homepage: www.elsevier.com/locate/jpba

Simultaneous quantification of coumarins, flavonoids and limonoids in Fructus Citri Sarcodactylis by high performance liquid chromatography coupled with diode array detector

Jun Chu[a,b], Song-Lin Li[a,b,c], Zhi-Qi Yin[d,**], Wen-Cai Ye[e], Qing-Wen Zhang[a,b,*]

[a] State Key Laboratory of Quality Research in Chinese Medicine (University of Macau), Macao
[b] Institute of Chinese Medical Sciences, University of Macau, Macao
[c] Department of Metabolomics and Key Laboratory of New Drug Delivery System of Chinese Materia Medica, Jiangsu Province Academy of Chinese Medicine, Nanjing 210028, China
[d] Department of Natural Medicinal Chemistry, China Pharmaceutical University, Nanjing 210009, China
[e] Institute of Traditional Chinese Medicine and Natural Products, Jinan University, Guangzhou 510632, China

ARTICLE INFO

Article history:
Received 6 January 2012
Received in revised form 19 March 2012
Accepted 19 March 2012
Available online 28 March 2012

Keywords:
Citrus medica var. *sarcodactylis*
Coumarin
Flavonoid
HPLC-DAD
Limonoid

ABSTRACT

A high performance liquid chromatography coupled with diode array detector (HPLC-DAD) method was developed for simultaneous quantification of eleven major bioactive components including six coumarins, three flavonoids and two limonoids in Fructus Citri Sarcodactylis. The analysis was performed on a Cosmosil 5 C_{18}-MS-II column (4.6 mm × 250 mm, 5 μm) with water–acetonitrile gradient elution. The method was validated in terms of linearity, sensitivity, precision, stability and accuracy. It was found that the calibration curves for all analytes showed good linearity ($R^2 > 0.9993$) within the test ranges. The overall limit of detection (LOD) and limit of quantification (LOQ) were less than 3.0 and 10.2 ng. The relative standard deviations (RSDs) for intra- and inter-day repeatability were not more than 4.99% and 4.92%, respectively. The sample was stable for at least 48 h. The spike recoveries of eleven components were 95.1–104.9%. The established method was successfully applied to determine eleven components in three samples from different locations. The results showed that the newly developed HPLC-DAD method was linear, sensitive, precise and accurate, and could be used for quality control of Fructus Citri Sarcodactylis.

© 2012 Elsevier B.V. All rights reserved.

1. Introduction

Citrus medica L. var. *sarcodactylis* (Noot.) Swingle (commonly named bergamot) is a native plant of southern Asia and grown on a large scale in China. Fructus Citri Sarcodactylis, the fruit of *C. medica* var. *sarcodactylis* is widely used as food ingredient and traditional Chinese medicinal herb [1]. This herb has been reported having activities of antiasthma [2,3], cytotoxicity [4], anti-inflammatory [5,6], immune enhancement [7,8], hypolipemic and hypoglycaemic [9], antioxidant [10,11], antimicrobial [12], and antiobesity [13]. Phytochemical studies showed that flavonoids such as 3,5,6-trihydroxy-3′,4′,7-trimethoxyflavone, diosmin, hesperidin and diosmetin [14–16], coumarins such as 5,7-dimethoxycoumarin [7,8,17–20], and limonoids such as limonin, nomilin and limonexic acid [4,21] are major bioactive components of Fructus Citri Sarcodactylis.

Qualitative and quantitative analysis of major bioactive components is very important for the quality control of Fructus Citri Sarcodactylis. To date, only one or two components, such as 5,7-dimethoxycoumarin [7,8,17–20] and hesperidin [1,20], were used as chemical markers for the quality control of Fructus Citri Sarcodactylis. It is well known that herbal medicines exert its activities through multiple components at multiple targets, and determination of multiple components has also been well accepted for the quality control of medicinal herbs. However, to the best of our knowledge, no method has been developed for simultaneous analysis of coumarins, flavonoids and limonoids in Fructus Citri Sarcodactylis.

As a continuous work on the quality research in commonly used Chinese medicinal herbs, a high performance liquid chromatography coupled with diode array detector (HPLC-DAD) method was developed for simultaneous quantification of three different types of ingredients, i.e., flavonoids, coumarins and limonoids, in Fructus Citri Sarcodactylis. Eleven compounds, including isoscopoletin (**1**), scopoletin (**2**), 7-hydroxycoumarin

* Corresponding author at: Institute of Chinese Medical Sciences, University of Macau, Macao. Tel.: +853 8397 4879; fax: +853 2884 1358.
** Co-corresponding author. Tel.: +86 25 86185371.
E-mail addresses: chyzq2005@126.com (Z.-Q. Yin), qwzhang@umac.mo (Q.-W. Zhang).

0731-7085/$ – see front matter © 2012 Elsevier B.V. All rights reserved.
doi:10.1016/j.jpba.2012.03.041

Table 1
Linearity and sensitivity of the assay.

Analyte	RT (min)	Calibration curve	R^2	Test range (μg/ml)	LOD[b] (ng)	LOQ[c] (ng)
1	9.52	$y = 34.4729x - 0.3099$[a]	1.0000	0.14–35.00	0.4	1.4
2	10.26	$y = 31.0882x - 0.5423$	1.0000	0.16–20.00	0.5	1.6
3	11.06	$y = 43.0959x + 5.6546$	0.9998	0.16–40.00	0.5	1.6
4	12.28	$y = 10.7024x - 0.9523$	0.9993	0.63–40.00	2.0	6.3
5	12.97	$y = 14.8670x + 5.4972$	0.9999	0.39–50.00	0.7	2.1
6	16.89	$y = 36.4464x + 7.1467$	0.9998	0.15–38.00	0.5	1.5
7	30.36	$y = 43.2944x + 19.3511$	0.9998	0.20–100.00	0.6	2.0
8	31.39	$y = 40.6628x + 10.2006$	0.9999	0.12–62.00	0.4	1.2
9	31.99	$y = 19.6955x - 8.6986$	0.9997	1.00–16.00	3.0	10.0
10	33.27	$y = 7.1098x + 3.4677$	0.9999	0.87–111.70	2.6	8.7
11	34.96	$y = 5.8203x + 3.6074$	0.9999	1.02–130.80	3.0	10.2

[a] y = peak area and x = concentration (μg/ml).
[b] Limit of detection (S/N = 3).
[c] Limit of quantification (S/N = 10).

(**3**), diosmin (**4**), hesperidin (**5**), 6,7-dimethoxycoumarin (**6**), 5,7-dimethoxycoumarin (**7**), bergapten (**8**), 3,5,6-trihydroxy-3′,4′,7-trimethoxyflavone (**9**), limonin (**10**) and nomilin (**11**) were used as the chemical markers for this analysis. The contents of these components in samples collected from different locations were compared.

2. Materials and methods

2.1. Materials and chemicals

Fructus Citri Sarcodactylis samples were collected from Puning (GFS-A) and Guangzhou (GFS-B and GFS-C), Guangdong Province, China. The botanical origin of the materials was authenticated at the College of Pharmacy, Jinan University, Guangzhou, China.

Isoscopoletin (**1**), scopoletin (**2**), 7-hydroxycoumarin (**3**), diosmin (**4**) and 6,7-dimethoxycoumarin (**6**) were purchased from Yuanye Company (Shanghai, China). Hesperidin (**5**) was supplied from Nature Standard Company (Shanghai, China) and bergapten (**8**) was supplied from Zelang Company (Nanjing, Jiangsu, China). 5,7-dimethoxycoumarin (**7**) and 3,5,6-trihydroxy-3′,4′,7-trimethoxyflavone (**9**), limonin (**10**) and nomilin (**11**) were previously isolated from this herb in our laboratory refereeing to the methods reported in the literature [14–16,21,22]. Deionized water was prepared using a Millipore Milli Q-Plus system (Millipore, Bedford, MA, USA). Acetonitrile for HPLC was purchased from Merck (Darmstadt, Germany).

2.2. Sample preparation

Pressurized liquid extraction (PLE) is a commonly used sample preparation method for plant analysis owing to its high extraction speed, low extraction solvent assumption and high extraction efficiency. PLE was performed on a Dionex ASE 200 system (Dionex Corp., Sunnyvale, CA, USA) under optimized conditions. In brief, dried powder of Fructus Citri Sarcodactylis (0.5 g) mixed with diatomaceous earth at the ratio of 1:1 was put into an 11 ml stainless steel extraction cell. The conditions of the PLE method were: solvent, methanol; temperature, 90 °C; particle size, 0.125–0.15 mm; static extraction time, 5 min; pressure, 1500 psi.; static cycle, 1; number of extraction, 1; and 40% of the flush volume. PLE extract solution was transferred into a 25 ml volumetric flask which was filled up to its volume with the same solvent and filtered through a 0.45 μm Econofilter (Agilent Technologies) before injecting into the HPLC system.

2.3. HPLC analysis

Analysis was performed on an Agilent 1200 HPLC system (Palo Alto, CA, USA), equipped with vacuum degasser, quaternary gradient pump, autosampler and DAD, connected to an Agilent ChemStation software. A Cosmosil 5 C_{18}-MS-II column (4.6 mm × 250 mm, 5 μm) was used. A binary gradient elution system consisted of water (A) and acetonitrile (B). The gradient program was: 0–10 min, 18–23% B; 10–15 min, 23% B; 15–30 min, 23–50% B; 30–40 min, 50–100% B; and finally, reconditioning the column with 18% B isocratic for 5 min. The flow-rate was 1.0 ml/min and the column temperature was 25 °C. The injection volume was 10 μl with needle wash. The UV detection wavelengths were set at 210 nm, 254 nm, 280 nm, 320 nm and 340 nm.

2.4. Calibration curves

Methanol stock solution containing isoscopoletin (**1**), scopoletin (**2**), 7-hydroxycoumarin (**3**), diosmin (**4**), hseperidin (**5**), 6,7-dimethoxycoumarin (**6**), 5,7-dimethoxycoumarin (**7**), bergapten (**8**), 3,5,6-trihydroxy-3′,4′,7-trimethoxyflavone (**9**), limonin (**10**) and nomilin (**11**) was diluted with methanol to obtain a series concentrations of working solutions, and subjected to HPLC analysis. The calibration curves of compound **1** to compound **11** were constructed by plotting the peak areas versus the concentrations respectively.

2.5. Sensitivity and stability

The sensitivity study was completed by analyzing the limit of detection (LOD) and limit of quantification (LOQ) which were determined at a signal-to-noise (S/N) ratio of about 3 and 10, respectively.

The stability was tested by analyzing the sample of GFS-A and peak areas of eleven analytes at 0, 2, 4, 8, 12, 24 and 48 h were recorded and compared.

2.6. Precision and accuracy

Intra- and inter-day variations were chosen to determine the precision of the developed method. The relative standard deviation (RSD) was taken as a measure of precision. Intra- and inter-day repeatability was determined on six replicates within one day and three consecutive days, respectively.

Spike recovery was used to evaluate the accuracy of the assay. Known amount of individual standards was added into accurately weighed samples (GFS-A, purchased from Puning, Guangdong province). The mixtures were extracted and analyzed in triplicate using the method described in Section 2.2.

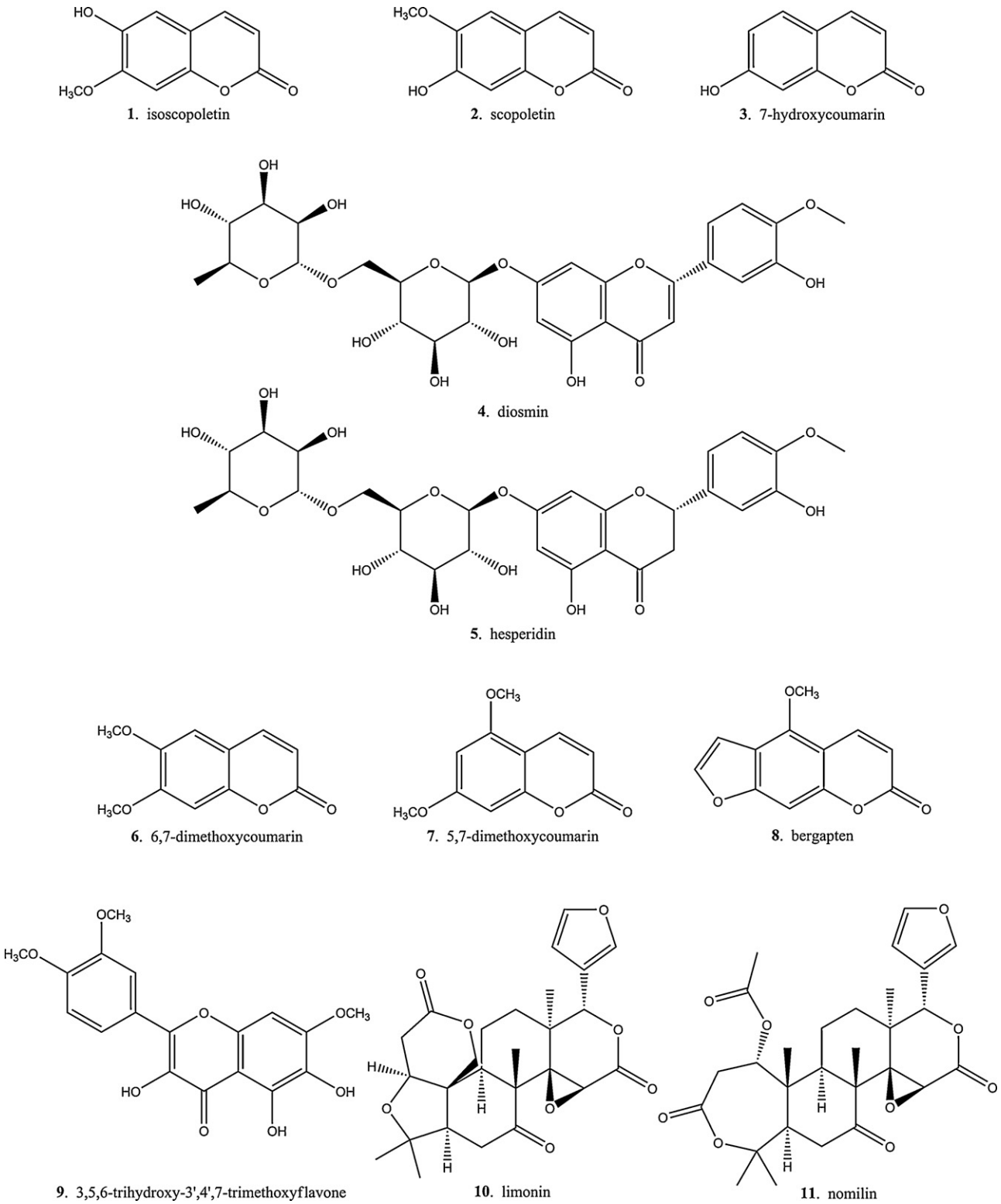

Fig. 1. Structures of eleven investigated components in Fructus Citri Sarcodactylis.

3. Results and discussion

3.1. Optimization of HPLC conditions

Although the eleven analytes belong to three different types, i.e., flavonoids, coumarins and limonoids, those belonging to the same type have very similar chemical structure (Fig. 1), so baseline separation of all eleven analytes is a challenge issue for the development of this method. Different mobile phases and elution programs were tested in order to obtain good resolution. At last, on a Cosmosil 5 C_{18}-MS-II column (4.6 mm × 250 mm, 5 μm), all eleven analytes were eluted with baseline separation (Fig. 2) by using elution program of water (A) and acetonitrile (B). The gradient program is described in Section 2.3.

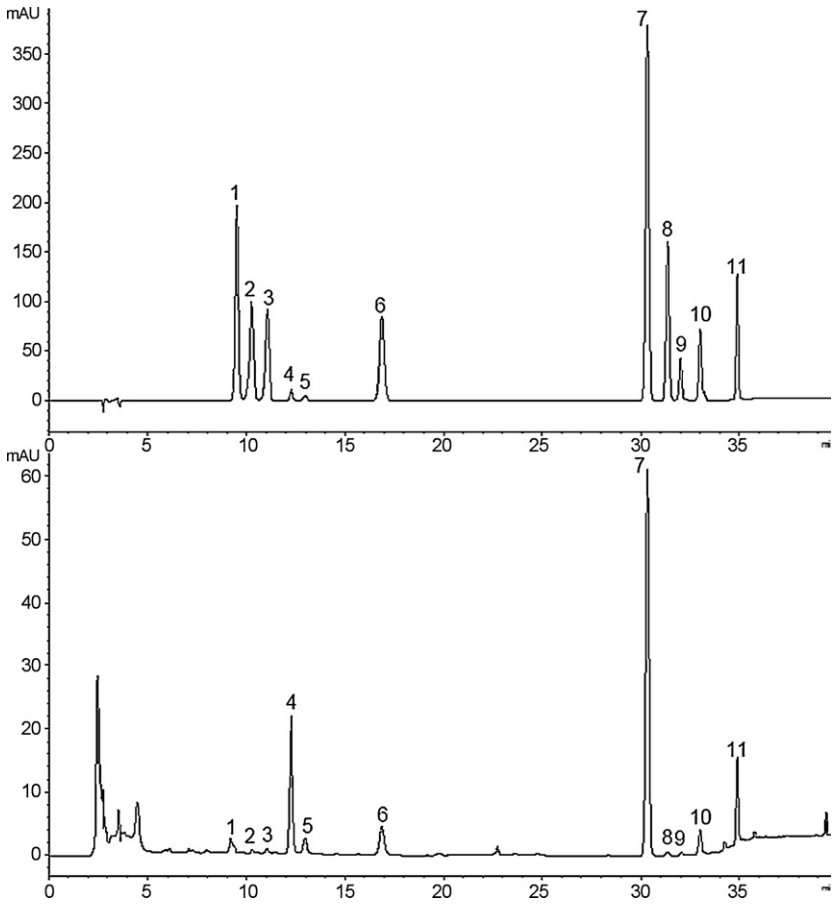

Fig. 2. HPLC-DAD chromatograms of reference compounds. (A) **1**: isoscopoletin, 63.06 μg/ml; **2**: scopoletin, 53.56 μg/ml; **3**: 7-hydroxycoumarin, 40.23 μg/ml; **4**: diosmin, 13.51 μg/ml; **5**: hesperidin, 30.36 μg/ml; **6**: 6,7-dimethoxycoumarin, 38.79 μg/ml; **7**: 5,7-dimethoxycoumarin, 106.47 μg/ml; **8**: bergapten, 35.07 μg/ml; **9**: 3,5,6-trihydroxy-3′,4′,7-trimethoxyflavone, 21.70 μg/ml; **10**: limonin, 94.13 μg/ml; **11**: nomilin, 152.77 μg/ml and (B) extract of sample GFS-A.

Considering the different UV λ_{max} values of different compounds, the UV detection wavelengths were set at 254 nm for 3,5,6-trihydroxy-3′,4′,7-trimethoxyflavone (**9**), 280 nm for hesperidin (**5**), 320 nm for 5,7-dimethoxycoumarin (**7**), 7-hydroxycoumarin (**3**) and bergapten (**8**), 340 nm for 6,7-dimethoxycoumarin (**6**), isoscopoletin (**1**), scopoletin (**2**) and diosmin (**4**), and 210 nm for limonin (**10**) and nomilin (**11**). Typical chromatograms are shown in Fig. 2. In order to obtain a distinct chromatogram, we used the function DAD Timetable. The program changes in the DAD wavelength were: 0–31 min, 340 nm; 31–32.5 min, 254 nm; 32.5–36 min, 210 nm; 36–40 min, 340 nm.

3.2. Validation of the developed method

The method was validated in terms of linearity, sensitivity, precision, stability and accuracy. Table 1 summarizes the linearity, test range, limit of detection (LOD) and limit of quantification (LOQ) of the analytes. It was found that the calibration curves for all analytes showed good linearity ($R^2 > 0.9993$) within the test range. The overall LODs and LOQs were less than 3.0 and 10.2 ng for DAD, indicating that this method is sufficiently sensitive. The relative standard deviations (RSDs) for intra- and inter-day repeatability are shown in Table 2. It was found that overall intra- and inter-day variations were not more than 4.99% and 4.92% respectively, suggesting that the developed method was precise. The spike recoveries of eleven components were 95.1–104.9%, demonstrating that this method was also very accurate. Furthermore, the sample was stable for at least 48 h.

3.3. Sample determination

The established method was applied for the quantification of three Fructus Citri Sarcodactylis samples from different collections. The contents of the eleven compounds are shown in Table 3. From Table 3, it was found that diosmin (**4**), hesperidin (**5**), 5,7-dimethoxycoumarin (**7**), limonin (**10**) and nomilin (**11**) are five major components of Fructus Citri Sarcodactylis, while the contents of isoscopoletin (**1**), scopoletin (**2**), 7-hydroxycoumarin (**3**), 6,7-dimethoxycoumarin (**6**) are relatively lower, and the contents of bergapten (**8**) and 3,5,6-trihydroxy-3′,4′,7-trimethoxyflavone (**9**)

Table 2
Precision test of the assay.

Analyte	Intra-day repeatability ($n = 6$)		Inter-day repeatability ($n = 6$)	
	Content (μg/g)	RSD[a] (%)	Content (μg/g)	RSD (%)
1	64.2 ± 1.9	2.99	65.6 ± 1.8	2.72
2	11.5 ± 0.3	2.23	11.4 ± 0.2	1.56
3	7.7 ± 0.4	4.56	7.8 ± 0.4	4.92
4	1214.3 ± 12.2	1.01	1222.0 ± 22.0	1.80
5	669.8 ± 11.7	1.74	672.4 ± 14.3	2.13
6	99.1 ± 1.4	1.40	99.5 ± 1.7	1.71
7	882.1 ± 0.4	0.05	876.7 ± 4.7	0.53
8	ND[b]	ND	ND	ND
9	ND	ND	ND	ND
10	223.4 ± 11.4	4.99	227.3 ± 5.8	2.56
11	789.1 ± 22.2	2.82	801.3 ± 21.1	2.64

[a] RSD (%) = 100 × S.D./mean.
[b] ND, not detected.

Table 3
Contents of eleven compounds in samples from different collections ($n = 3$, μg/g).

	1	2	3	4	5	6	7	8	9	10	11
GFS-A	58.8 ± 0.4	12.7 ± 0.1	7.5 ± 0.4	1223.5 ± 1.2	666.8 ± 2.0	100.5 ± 0.2	897.7 ± 0.6	–[a]	–	236.9 ± 5.6	801.2 ± 4.3
GFS-B	34.2 ± 0.3	15.5 ± 0.2	13.4 ± 0.1	1204.8 ± 1.4	801.6 ± 18.8	35.8 ± 0.3	779.0 ± 7.3	1.7 ± 0.0	–	973.1 ± 1.8	3199.9 ± 27.5
GFS-C	20.6 ± 0.2	36.8 ± 1.5	12.7 ± 0.1	462.3 ± 7.7	243.4 ± 4.4	16.0 ± 0.1	1206.6 ± 11.7	–	51.3 ± 0.5	546.2 ± 2.1	274.0 ± 2.7

[a] –, beyond LOQ.

were too low to be quantified in some samples. It should be noticed that although the content of 5,7-dimethoxycoumarin (**7**) was consistent among three samples analyzed, the contents of other components, in particular that of nomilin (**11**) were markedly different among three samples, ranging from 274.0 to 3199.9 μg/g for nomilin (**11**), suggesting that although all these samples were collected from the genuine locations of Guangdong Province of China, the quality difference still existed.

4. Conclusion

An HPLC-DAD method was developed for the quantification of eleven major components in Fructus Citri Sarcodactylis. Compared with previously reported methods, the newly established method could simultaneously determine three different types of major components, including six coumarins (isoscopoletin, scopoletin, 7-hydroxycoumarin, 6,7-dimethoxycoumarin, 5,7-dimethoxycoumarin and bergapten), three flavonoids (diosmin, hesperidin, and 3,5,6-trihydroxy-3′,4′,7-trimethoxyflavone) and two limonoids (limonin and nomilin) in Fructus Citri Sarcodactylis. Furthermore, different wavelengths were chosen to ensure the high sensitivity of the assay, so that the established method could be successfully applied for the "holistic" quality control of Fructus Citri Sarcodactylis.

Acknowledgments

We are grateful to Mr. Leon Lai from our institute for his technical assistance. The research was supported by grants from Macau Science and Technology Development Fund (013/2008/A1 to Dr. Zhang and SKL/QRCM/EST/11-Y1/ICMS for state key lab), the Team Project of the Natural Science Foundation of Guangdong (8351063201000003 to Dr. Ye), and the Research Starting Fund (RC1101) and the Open Fund (No. 2011NDDCM02003) to Dr. Li from Jiangsu Province Academy of Chinese Medicine.

References

[1] E. Committee, Pharmacopoeia of the People's Republic of China, China Medical Science Press, Beijing, 2010, p. 167.
[2] H.P. Yin, S.M. Xu, Effect of ethyl acetate extract from bergamot in asthmatic mouse model, Health Res. 29 (2009) 92–94.
[3] H.P. Yin, G.-H. Lin, L.-P. Yu, H. Yuan, Experimental study on antitussive and expectorant effects of ethyl acetate extract from bergamot, J. Hangzhou Teach. Coll. (Med. Ed.) 27 (2009) 377–379.
[4] Y.Y. Chan, T.S. Wu, Y.H. Kuo, Chemical constituents and cytotoxicity from the stem bark of *Citrus medica*, Heterocycles 78 (2009) 1309–1316.
[5] J.Y. Wang, C.C. Shi, W.P. Zhu, W.H. Huang, Tests on anti-inflammation and acute toxicity of Jinhua finger citron volatile oil, Res. Pract. Chin. Med. 18 (2004) 46–48.
[6] Y.Y. Chan, C.H. Li, Y.C. Shen, T.S. Wu, Anti-inflammatory principles from the stem and root barks of *Citrus medica*, Chem. Pharm. Bull. 58 (2010) 61–65.
[7] L. Huang, Z.Y. Kuang, M. Zhang, Effect of CMPS on cytokine of mice induced by cyclophosphamide, Mod. J. Integr. Tradit. Chin. Western Med. 9 (2000) 871–872.
[8] L. Huang, Z.Y. Kuang, M. Zhang, Y. Li, Effect of Fructus Citri Sarcodactylis polysaccharide on IL-6 in macrophages of cyclophosphamide-treated mice, J. Guangzhou Univ. Tradit. Chin. Med. 17 (2000) 58–59.
[9] V. Mollace, I. Sacco, E. Janda, C. Malara, D. Ventrice, C. Colica, V. Visalli, S. Muscoli, S. Ragusa, C. Muscoli, D. Rotiroti, F. Romeo, Hypolipemic and hypoglycaemic activity of bergamot polyphenols: from animal models to human studies, Fitoterapia 82 (2011) 309–316.
[10] A. Wei, T. Shibamoto, Antioxidant/lipoxygenase inhibitory activities and chemical compositions of selected essential oils, J. Agric. Food Chem. 58 (2010) 7218–7225.
[11] D. Ramful, T. Bahorun, E. Bourdon, E. Tarnus, O. Aruoma, Bioactive phenolics and antioxidant propensity of flavedo extracts of Mauritian citrus fruits: potential prophylactic ingredients for functional foods application, Toxicology 278 (2010) 75–87.
[12] G. Mandalari, R.N. Bennett, G. Bisignano, D. Trombetta, A. Saija, C.B. Faulds, M.J. Gasson, A. Narbad, Antimicrobial activity of flavonoids extracted from bergamot (*Citrus bergamia* Risso) peel, a byproduct of the essential oil industry, J. Appl. Microbiol. 103 (2007) 2056–2064.

[13] C.H. Peng, Y.B. Ker, C.F. Weng, C.C. Peng, C.N. Huang, L.Y. Lin, R.Y. Peng, Insulin secretagogue bioactivity of finger citron fruit (*Citrus medica* L. var. *sarcodactylis* Hort, Rutaceae), J. Agric. Food Chem. 57 (2009) 8812–8819.
[14] H.Y. He, L.Q. Ling, Chemical studies of a Chinese traditional drug fingered citron, *Citrus medica* L. var *sarcodactylis* (Noot.) Swingle, Acta Pharm. Sin. 20 (1985) 433–435.
[15] Y.K. Nogata, K. Sakamoto, H. Siratsuchi, T. Ishii, M. Yano, H. Ohta, Flavonoid composition of fruit tissues of citrus species, Biosci. Biotechnol. Biochem. 70 (2006) 178–192.
[16] F. Yin, L. Cheng, F.C. Lou, Studies on the constituents of *Citrus medica* L. var. *sarcodactylis* (Noot.) Swingle, Chin. J. Nat. Med. 2 (2004) 149–151.
[17] L.W. Lin, L. Jiang, D.Q. Hao, G.D. Zheng, X. Yang, Determination of 5,7-dimethoxycoumarin in Fructus Citri Sarcodactylis from Guangdong at different collecting times, Res. Pract. Chin. Med. 22 (2009) 15–17.
[18] Y.H. Gao, Y.M. Diao, X.S. Peng, H.H. Xu, Determination of 5,7-dimethoxycoumarin in Fructus Citri Sarcodactylis by HPLC, Tradit. Chin. Drug Res. Clin. Pharmacol. 14 (2003) 250–251.
[19] R.F. Zhang, Y.H. Gao, H.H. Cui, S.L. Liang, Fingerprints of Fructus Citri Sarcodactylis from Guangdong by HPLC, Chin. Tradit. Herb. Drugs 38 (2007) 1075–1077.
[20] L.W. Lin, L. Jiang, D.Q. Hao, G.D. Zheng, X. Yang, Q. Wang, J.Y. Zhang, HPLC fingerprint of Fructus Citri Sarcodactylis from Guangdong province, Chin. Tradit. Patent Med. 31 (2009) 1805–1808.
[21] H.Y. He, L.Q. Ling, G.P. Shi, N. Zhang, Q.M. Mao, Studies on the chemical constituents of Chinese traditional drug fingered citron, China J. Chin. Mater. Med. 13 (1988) 352–354.
[22] F. Yin, F.C. Lou, Studies on the constituents of *Citrus medica* L. var. *sarcodactylis*, Chin. Pharm. J. 39 (2004) 20–21.

Journal of Pharmaceutical and Biomedical Analysis 66 (2012) 176–182

Contents lists available at SciVerse ScienceDirect

Journal of Pharmaceutical and Biomedical Analysis

journal homepage: www.elsevier.com/locate/jpba

Development and validation of an HPLC/UV assay for separation and quantification of peptide antigens from a liposomal vaccine delivery platform

Andrea Penwell*, Kendall Sharp, Marc Mansour, Leeladhar Sammatur

Immunovaccine Inc., 1344 Summer Street, Suite 411, Halifax, NS, Canada B3H 0A8

ARTICLE INFO

Article history:
Received 29 February 2012
Received in revised form 23 March 2012
Accepted 24 March 2012
Available online 1 April 2012

Keywords:
Reversed-phase HPLC
Peptide
Liposome formulation
DepoVax™
Validation

ABSTRACT

The development and validation of an HPLC method for the quantification of eight peptide antigens from the therapeutic cancer vaccine DPX-0907 is described. The antigens were formulated in DepoVax™, a patented liposomal vaccine delivery platform used in a phase 1 study for breast, ovarian, and prostate cancers. A gradient reversed-phase method with UV detection was optimized for separating and quantifying the peptide mixture. Several extraction methods investigated to extract the peptides from the lipids led to poor recovery of one or more of the peptides. A simple, reproducible, and high-recovery extraction procedure for the simultaneous quantification of hydrophilic and hydrophobic peptides was discovered using a liquid–liquid extraction with water–saturated n-butanol and sodium bicarbonate (0.1 M). The method was found to be specific, linear, accurate, precise, and reliable within the range of 50–150% of the nominal concentration for DPX-0907. The validated method was successfully applied to the assay of peptide content in pre-clinical and clinical batches of DPX-0907.

© 2012 Elsevier B.V. All rights reserved.

1. Introduction

DepoVax™ is a patented vaccine enhancement and delivery platform comprising disease specific antigens, a proprietary oligonucleotide adjuvant, liposomes consisting of phospholipids and cholesterol, and a hydrophobic carrier (oil diluent) [1,2]. The formulation of immunogens in liposomes is lyophilized for stable storage and reconstituted in the oil diluent prior to injection. The lipid-based platform bypasses the need for emulsification in the clinic and is well suited for delivering antigens with poor immunogenicity. The DepoVax platform is a highly versatile delivery system and can accommodate a wide variety of antigens, including recombinant proteins and synthetic peptides. This provides the flexibility to develop many different vaccine products using a single platform.

An assay was required to separate and quantify a mixture of eight peptide antigens from DPX-0907, a DepoVax therapeutic cancer vaccine, which has successfully completed a phase 1 clinical trial [3]. Seven of the antigens have been identified as over-expressed cytotoxic T lymphocyte (CTL) epitopes bound to major histocompatibility complex (MHC) class I molecules from the surface of ovarian, breast, and prostate cancer cells, but not found on normal cells [4]; the eighth is a T-helper peptide epitope from tetanus toxoid and has been used in the clinic extensively by others [5] (Table 1).

The aim of the present work was to develop and validate an RP-HPLC method to be applied to the quality control analysis and stability studies of the seven short peptide antigens and the T-helper peptide A16L in DepoVax, contributing therefore to the quality control and safety of the vaccine.

A literature survey revealed few analytical methods for extracting peptides from liposomes [6–10]. Samuel et al. [10] evaluated several extraction solvents for extracting a panel of eight therapeutic peptides from liposomal formulations, but found that the total amount of peptide accounted for was considerably less than 100% for many of the peptides after the optimal extraction solvent was chosen. The study herein reports a simple, reproducible, and high-recovery extraction procedure for the simultaneous quantification of hydrophilic and hydrophobic peptides from the lipid-based vaccine DPX-0907. An RP-HPLC method was developed and validated for the quantification of the peptides at the 50, 100, and 150% levels as per ICH guidelines [11]. Recoveries of all peptides were between 90 and 110%. The method has successfully been transferred to a contract manufacturing site for in-process and release testing and is currently being used in-house for routine stability testing for assay of pre-clinical and clinical batches of DPX-0907.

2. Experimental

2.1. Chemicals and reagents

Peptides were manufactured by PolyPeptide Laboratories (San Diego, CA, USA). The sequences can be found in Table 1.

* Corresponding author. Tel.: +1 902 421 5735; fax: +1 902 492 0888.
E-mail address: apenwell@imvaccine.com (A. Penwell).

0731-7085/$ – see front matter © 2012 Elsevier B.V. All rights reserved.
http://dx.doi.org/10.1016/j.jpba.2012.03.046

Table 1
DPX-0907 peptide antigens.

Peptide name	Protein name	Peptide sequence	Range	Average hydrophobicity[a]	Net charge at pH 7.0[b]
P3	BAP31 (CDM protein)	KLDVGNAEV	167–175	−0.09	−1.0
P5	Integrin β8 subunit precursor	ALMEQQHYV	662–670	−0.37	−0.9
P4	Topoisomerase II α	FLYDDNQRV	828–836	−1.00	−1.0
P7	Abl-binding protein C3	ILDDIGHGV	145–153	0.67	−1.9
P13	TACE/ADAM17	YLIELIDRV	250–258	0.89	−1.0
P14	Junction plakoglobin	NLMEQPIKV	5–13	−0.18	0.0
P15	EDDR1	FLAEDALNTV	904–913	0.70	−2.0
A16L	Tetanus toxoid	AQYIKANSKFIGITEL	830–843	0.14	1.0

[a] Average hydrophobicity was calculated using the sum of all hydrophobicity values [12] for the given sequence divided by the sequence length. The higher the value, the more hydrophobic the peptide.
[b] Net charge was calculated using an online peptide property calculator (www.innovagen.se).

The lipids used were a 10:1 (w/w) mixture of dioleoylphosphatidyl choline (DOPC) and cholesterol, manufactured by Lipoid GmbH (Ludwigshafen, Germany). The oligonucleotide adjuvant was manufactured by Eurofins MWG Operon (Huntsville, Alabama, USA). Water was purified in-house by a 2121A deionization system from Aqua Solutions (Jasper, GA, USA). Acetonitrile (HPLC grade), n-butanol (HPLC grade), trifluoroacetic acid (TFA, ≥99%), acetic acid (ACS grade), hydrogen peroxide (30%), and sodium bicarbonate (USP grade) were purchased from Fisher Scientific (Nepean, ON, Canada). Sodium dihydrogen phosphate monohydrate ($NaH_2PO_4{\cdot}H_2O$) and disodium hydrogen phosphate (Na_2HPO_4) were obtained from VWR (Ville-Mont-Royal, QC, Canada), both USP grade. Sodium hydroxide was purchased from Bio Basic Inc. (Toronto, ON, Canada).

Water–saturated n-butanol was prepared by mixing n-butanol with water in a 4:1 (v/v) ratio, vortexing vigorously for 3 min, and then centrifuging at 4000 rpm for 10 min.

2.2. Instrument

The liquid chromatographic system consisted of an Agilent 1100 Series HPLC System equipped with thermostatted autosampler, UV detector, degasser, and quaternary pump (GenTech Scientific, NY, USA). The HPLC parameters were controlled by ChemStation Software Rev.A.09.03.

2.3. Liquid chromatographic conditions

Analysis was carried out at 215 nm with a Phenomenex Luna C8 (2) 5 μm, 150 mm × 4.6 mm, 100 Å column (Torrance, CA, USA). The temperature of the column heater was set to 25 °C, while the temperature of the sample chamber was set to 10 °C. The injection volume was 50 μl, for a sample concentration of 50 μg/ml for each peptide antigen and 25 μg/ml for A16L. Solvent A was prepared by combining water, acetonitrile, and trifluoroacetic acid in

Table 2
Study results for determining the absolute phase change volume during extraction.

Sample	Mass aqueous layer (before extraction) (mg)	Mass aqueous layer (after extraction) (mg)	Volume[a] aqueous layer (before extraction) (μl)	Volume[a] aqueous layer (after extraction) (μl)	Volume (after)/volume (before)
Mean	1004.9	1064.8	1013.1	1094.6	1.1 (dilution factor)
S.D.	7.2	6.3	7.4	6.3	
%RSD	0.7	0.6	0.7	0.6	

[a] Volume was calculated by dividing the mass of the aqueous layer by its density. Density was determined by weighing the mass of each aqueous layer in a 1 ml volumetric flask.

Table 3
System suitability study.[a]

	P3	P5	P4	P7	P14	P15	A16L	P13
Peak area (mAU*s)								
Mean (n = 6)	925.60	2193.08	2097.32	1707.83	1500.72	1517.13	742.10	1480.97
S.D.	2.85	13.94	4.37	4.05	5.21	3.88	11.68	10.58
%RSD	0.31%	0.64%	0.21%	0.24%	0.35%	0.26%	1.57%	0.71%
Retention time (min)								
Mean (n = 6)	10.453	11.379	12.282	12.951	14.470	16.337	17.281	20.808
S.D.	0.004	0.004	0.003	0.004	0.003	0.003	0.003	0.003
%RSD	0.037	0.032	0.023	0.029	0.021	0.016	0.016	0.014
USP tailing factor								
Mean (n = 6)	1.330	1.350	1.343	1.382	1.362	1.296	1.269	1.406
S.D.	0.010	0.004	0.004	0.004	0.004	0.005	0.008	0.008
%RSD	0.733	0.302	0.291	0.320	0.295	0.382	0.615	0.559
Resolution								
Mean (n = 6)	–	4.787	4.520	3.287	7.444	9.163	4.715	16.960
S.D.	–	0.025	0.031	0.015	0.032	0.046	0.029	0.055
%RSD	–	0.530	0.690	0.468	0.433	0.497	0.605	0.324

[a] Acceptance criteria: peak area %RSD ≤ 5%; retention time %RSD ≤ 5%; USP tailing factors < 2; resolution between peaks > 2.

a 900:100:1 (v/v/v) ratio; solvent B was prepared by combining water, acetonitrile, and trifluoroacetic acid in a 600:400:1 (v/v/v) ratio. Both mobile phases were degassed by sonication for 10 min. The solvent program was a gradient starting with 100% solvent A and linearly increasing to 100% solvent B in 25 min. The mobile phase composition was ramped back to 100% solvent A for equilibration prior to the next injection for a total run time of 35 min. The flow rate was set to 1.0 ml/min.

2.4. Preparation of liposome samples

Samples of DPX-0907 vaccine were formulated in-house as described previously [2]. Briefly, stock solutions of each peptide antigen were prepared separately in sodium bicarbonate (0.1 M). The seven stock solutions were then added sequentially to a solution of phosphate buffer (0.2 M; pH 7) and oligonucleotide adjuvant. The DOPC/cholesterol lipid mixture was added to the solution, along with 20–30 glass beads (3 mm, Fisher Scientific, Nepean, ON, Canada), and shaken vigorously for 30 min on a mechanical shaker to form the liposomes. The solution was subsequently diluted with water to give 88 mg/ml DOPC/cholesterol, 0.67 mg/ml peptide antigens, and 0.27 mg/ml oligonucleotide. Next, the liposomes were extruded by passing through 0.2 and 0.1 μm polycarbonate membranes using an Avestin C5 extruder (Ottawa, ON, Canada). Following the sizing of liposomes to a particle size < 120 nm (PDI < 0.1), a mixture of A16L in 0.25% acetic acid was added to give 100% of final volume. The final concentrations of all components were as follows: 66 mg/ml DOPC/cholesterol, 0.5 mg/ml each peptide antigen, 0.25 mg/ml A16L, 0.2 mg/ml oligonucleotide adjuvant, and 0.05 M phosphate buffer (pH 7). The solution was sterile filtered, aliquoted into vials, and lyophilized to form a uniformly dry cake. In the clinic, the vaccine was reconstituted with oil to give 1 mg/ml each peptide antigen and 0.5 mg/ml A16L.

The placebo was prepared by combining DOPC/cholesterol, the oligonucleotide adjuvant, 0.25% acetic acid, sodium bicarbonate (0.1 M), sodium phosphate buffer (0.2 M; pH 7), and water in the appropriate amounts.

2.5. Standard preparation

Standard stock solutions for the seven peptide antigens were prepared separately in sodium bicarbonate (0.1 M) at concentrations of 25 mg/ml (with the exception of P13, which was prepared at 10 mg/ml). A16L was prepared in 0.25% acetic acid at a concentration of 5 mg/ml. A mixed stock solution (3000 μl) was prepared by adding the stock solutions and diluents in the following order: 0.25% acetic acid (600 μl), A16L (150 μl), sodium phosphate buffer (0.2 M; pH 7) (750 μl), P4 (60 μl), P5 (60 μl), P7 (60 μl), P13 (150 μl), P14 (60 μl), P15 (60 μl), P3 (60 μl), and water (990 μl). The solution was gently mixed after the addition of each component. The concentrations were 0.5 mg/ml for the peptide antigens and 0.25 mg/ml for A16L. Calibration standards were prepared at concentrations of 25, 37.5, 50, 62.5, and 75 μg/ml peptide antigens by diluting an appropriate volume of the mixed stock solution in 5 ml volumetric flasks with solvent A (2500 μl) and diluting to volume with sodium bicarbonate (0.1 M). The concentrations for A16L in the calibration standards were consequently 12.5, 18.8, 25, 31.3, and 37.5 μg/ml. The third calibration standard (50 μg/ml peptide antigens; 25 μg/ml A16L) was used for system suitability testing. Preliminary studies showed that all analytes were stable in solution for at least 48 h at room temperature.

2.6. Sample preparation (liquid–liquid extraction method)

A single sample preparation used to quantitate all eight peptides was prepared by reconstituting the lyophilized cake of DPX-0907

Table 4
Results of the regression analysis of the linearity data.

	Mean ± S.D. (n = 6)							
	P3	P5	P4	P7	P14	P15	A16L	P13
Correlation coefficient (r^2)	0.99996 ± 0.00004	0.99998 ± 0.00003	0.99998 ± 0.00003	0.99998 ± 0.00003	0.99989 ± 0.00021	0.99998 ± 0.00002	0.99945 ± 0.00016	0.99998 ± 0.00001

with an appropriate amount of distilled water to yield a concentration of 0.5 mg/ml peptide antigens and 0.25 mg/ml A16L. The sample was homogenized by adding glass beads and vortexing for 30 s. A portion of the sample (200 mg) was accurately weighed in a centrifuge tube and diluted with sodium bicarbonate (0.1 M, 800 μl). The lipids were extracted by adding water–saturated n-butanol (1000 μl), shaking vigorously for 10 min, and then centrifuging at 3000 rcf for 10 min. 200 μl of the aqueous (bottom) layer was taken and diluted 1:1 with solvent A. The final dilution factor was 11× instead of 10× due to a slight increase in volume of the aqueous layer after extraction with water–saturated n-butanol (see Section 3.1 for explanation).

2.7. Method validation

2.7.1. Specificity

Specificity was determined by evaluating the presence of components in the placebo and stressed placebo that may interfere with the peptide analytes. The placebo contained liposomes and oligonucleotide adjuvant without the peptides. Stressed placebos were obtained from three different conditions: (1) shaken at 37 °C for 2 h; (2) shaken with 0.5 M NaOH for 2 h; and (3) shaken with 3% H_2O_2 for 2 h. Samples were prepared as described in Section 2.6.

2.7.2. System suitability

The system suitability was assessed by six replicate analyses of Calibration Standard 3. The acceptance criteria were as follows: ≤5% for the percent relative standard deviation (%RSD) for the peak areas and retention times, <2 for the tailing factor, and >2 for the resolution between any two peaks.

2.7.3. Linearity (calibration curves)

The calibration curves were constructed with five concentrations ranging from 25 to 75 μg/ml for the peptide antigens and 12.5–37.5 μg/ml for A16L. The linearity was evaluated by linear regression analysis, which was calculated by the least square regression method.

2.7.4. Accuracy and precision

Accuracy of the assay method was evaluated by the determination of the recovery of peptides from spiked placebos covering 50–150% of the nominal sample concentration. The lipid and oligonucleotide concentrations remained constant at 66 mg/ml and 0.2 mg/ml, respectively. A minimum of three extractions were performed on each spiked sample. Precision of the assay was determined by repeatability (intra-day) and intermediate precision (inter-day, different instrument, and different analyst) on a pre-clinical batch of DPX-0907.

3. Results and discussion

3.1. Method development and optimization

In order to develop and validate a simple and reliable RP-HPLC method for the simultaneous determination of all eight peptides in DPX-0907, the following parameters were optimized: mobile phase composition, selection of column, resolution, run time, and sample preparation. The conventional mobile phases of water–TFA (99:0.1, v/v) (solvent A) and acetonitrile–TFA (99:0.1, v/v) (solvent B) were selected for the initial separation studies. A linear gradient of 10% solvent A to 40% solvent B in 45 min on a Phenomenex Jupiter C18 column gave the best resolution between the peptides, however also gave a noisy baseline. The solvents were then pre-mixed as described in Section 2.3 and a linear gradient of 100% solvent A to 100% solvent B was used to resolve the baseline issue. Several columns (C18 and C8) were investigated to optimize the resolution and run time. The Phenomenex Luna C8 (150 mm × 4.6 mm, 5 μm particle size) afforded the best peak resolution, lowest back pressure, and shortest retention times with a run time of 25 min.

The main analytical challenge was developing an extraction method that would give high recoveries of all eight peptides, as well as acceptable peak shapes. Total solubilization of the liposome mixture required solvents such as methanol or ethanol, mixed with appropriate volumes of water or solvent A. This required a ratio of at least 80:20 (v/v) of methanol (or ethanol) to water for complete dissolution of lipids, which led to poor peak shapes

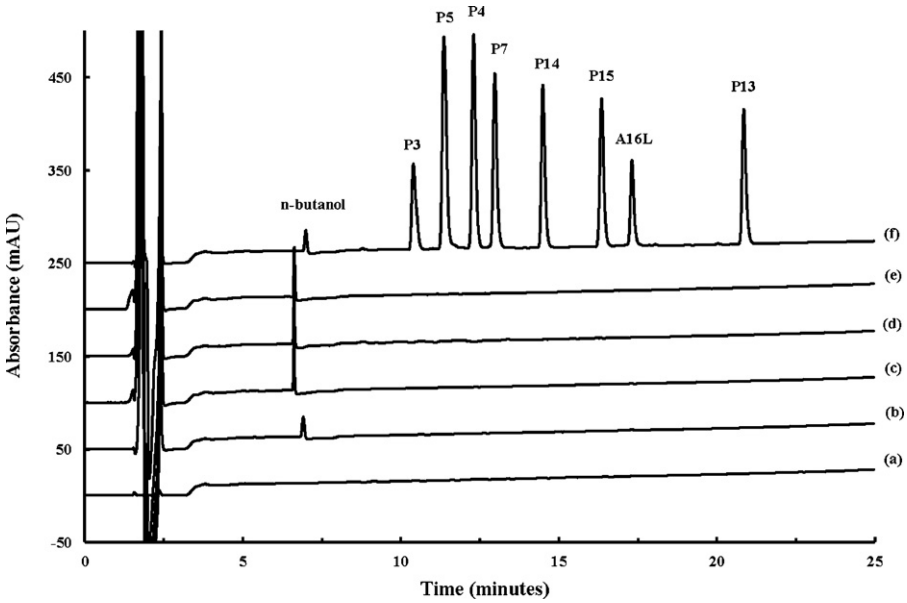

Fig. 1. HPLC chromatograms of placebo and DPX-0907 solutions: (a) blank diluent, (b) placebo, (c) heat-stressed placebo, (d) placebo treated with base, (e) placebo treated with hydrogen peroxide and (f) spiked sample (100%).

Table 5
Results of determination of accuracy, recovery, and precision for spiked samples.

Approximate level	Mean recovery (%RSD)							
	P3	P5	P4	P7	P13	P14	P15	A16L
50% (n = 3)	100.58 (0.53)	100.30 (0.36)	99.56 (0.07)	100.79 (0.65)	91.17 (0.85)	99.61 (0.50)	100.85 (0.83)	108.67 (0.57)
100% (n = 6)	101.97 (1.18)	101.83 (1.12)	101.94 (1.21)	101.15 (1.39)	93.48 (1.54)	100.54 (1.27)	101.84 (1.14)	107.41 (1.16)
150% (n = 3)	101.53 (0.93)	101.52 (0.83)	100.71 (0.79)	101.84 (0.83)	92.32 (0.64)	100.45 (0.67)	101.43 (1.01)	107.88 (0.61)

Table 6
Intra- and inter-day precision of peptides in a pre-clinical batch of DPX-0907 vaccine.

Analyte	Concentration limits (μg/ml)	Intra-day[a]			Inter-day[b]		
		Mean calculated concentration (μg/ml)	S.D. (n = 6)	%RSD	Mean calculated concentration (μg/ml)	S.D. (n = 12)	%RSD
P3	400–600	537.19	21.78	2.03	526.21	27.86	2.65
P5	400–600	541.00	13.28	1.23	525.20	34.51	3.29
P4	400–600	523.22	12.92	1.23	513.06	23.53	2.29
P7	400–600	572.92	18.08	1.58	553.17	43.67	3.95
P14	400–600	522.08	17.18	1.65	516.65	17.40	1.68
P15	400–600	496.41	13.88	1.40	488.03	20.54	2.10
A16L	200–300	259.60	8.73	1.68	266.74	16.87	3.16
P13	400–600	532.60	23.86	2.24	513.67	42.84	4.17

[a] Intra-day precision was determined with six replicate sample preparations from a DPX-0907 vial.
[b] Inter-day precision was determined with twelve replicates (lab 1, n = 6; lab 2, n = 6).

due to incompatibility of the sample solvent with the HPLC system. Extraction of the peptides from the lipids using a 2% formic acid–MeOH–CH_2Cl_2 (or $CHCl_3$) mixture gave good recoveries of the seven peptide antigens (92–110%), but inconsistent recovery of A16L. The reproducibility of A16L recovery continued to be an issue when switching the formic acid for sodium bicarbonate (0.1 M) or switching from methanol to ethanol; the peptide would often precipitate at the interface of the two layers.

Water–saturated n-butanol is a solvent that has been used extensively for the isolation of lipids in food science [13]. By diluting the sample with sodium bicarbonate (0.1 M) and then extracting the lipids with water–saturated n-butanol, excellent and reproducible recoveries (Table 4) were obtained for all peptides, including A16L (see Section 2.6 for detailed extraction procedure). Both layers were clear with no precipitation occurring at the interface. The bottom aqueous layer was further diluted with solvent A (1:1) to ensure compatibility with the HPLC system. This extraction procedure was found to be the optimal method for achieving high recoveries of all eight peptides, despite each having different physicochemical properties. On a side note, the procedure was also applicable to other therapeutic peptides, including those with higher molecular weights (>30 amino acids).

It was observed, however, that during the extraction procedure the organic layer decreased in volume, whereas the aqueous layer increased in volume by about 10%. This altered the concentration of analytes in the aqueous phase, which in turn affected the accuracy of the assay. These changes could be attributed to the low, yet significant, solubility of n-butanol in the aqueous layer, coupled with the decreased solubility of water in n-butanol as the hydrophobic lipid molecules entered that phase.

A study was conducted to calculate the absolute phase change by mass and by volume. Briefly, 0.2 ml of rehydrated liposomes was combined with 0.8 ml of sodium bicarbonate (0.1 M) and mixed in a 2.0 ml centrifuge tube (six replicate samples). The actual mass of liquid added to each tube was recorded, and then water–saturated n-butanol (1.0 ml) was added. The samples were spiked with crystal violet solution to color the organic layer. The tubes were shaken vigorously for 10 min, and then centrifuged for 10 min at 3000 rcf. The aqueous layers from the six samples were transferred to tared centrifuge tubes and the liquids weighed. The approximate density

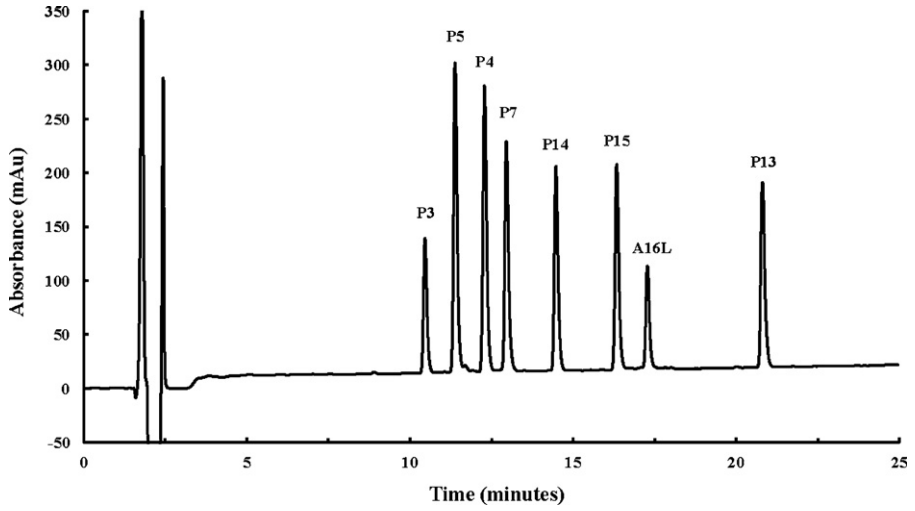

Fig. 2. HPLC chromatogram of a system suitability standard.

Table 7
Peptide assay results on DPX-0907 clinical batch.

Peptide	Specifications (mg/ml)	Content vial 1 (mg/ml)	Content vial 2 (mg/ml)	Average content (mg/ml)	Pass/fail
P3	0.80–1.20	1.00	0.99	1.00	Pass
P5	0.80–1.20	0.95	0.94	0.95	Pass
P4	0.80–1.20	0.96	0.96	0.96	Pass
P7	0.80–1.20	0.93	0.93	0.93	Pass
P13	0.80–1.20	0.95	0.95	0.95	Pass
P14	0.80–1.20	0.97	0.96	0.96	Pass
P15	0.80–1.20	1.01	1.01	1.01	Pass
A16L	0.40–0.60	0.50	0.51	0.51	Pass

was calculated for the aqueous layer; the mass values were then converted to volume values. The average volume after extraction divided by the average volume before extraction afforded an extra dilution factor of 1.1× due to the phase change (Table 2). The final dilution factor for the extraction and subsequent 2× dilution with solvent A was therefore 11× (1 ml/0.2 ml × 1.1 × 2).

Despite having a small amount of n-butanol present in the aqueous layer, the extraction procedure was found to be very efficient at removing the lipids. Analysis of the aqueous layer using a separate HPLC assay for analyzing DOPC and cholesterol content demonstrated that >99.9% of the lipids were extracted into the n-butanol layer. This was important for preventing lipid build-up on the column. The same column was used for hundreds of analyses using this protocol and no lipid contamination was observed, demonstrating excellent method robustness. As well, since the gradient only reaches 40% aqueous acetonitrile, the column was routinely washed with 100% methanol after long sequences to ensure complete removal of lipids and any other impurities.

3.2. Method validation

3.2.1. Specificity

The specificity of the analytical method was indicated in Fig. 1, where the placebo and stressed placebo samples did not have any peaks that interfered with the retention times of the peptide analytes. A small peak from residual n-butanol was observed around 7 min. All lipids and lipid degradants remained in the organic layer. The oligonucleotide adjuvant was not retained on the column and eluted with the solvent front around 2 min.

3.2.2. System suitability

Six analyses of the system suitability solution prepared as described in the experimental part were performed to test the system suitability. The %RSD of peak area and retention time for all peptides were <1.57% indicating the suitability of the system. As well, the USP tailing factors were <1.5 and the resolution between each peptide was >4.76. All the values were within the acceptability criteria (Table 3). An example of a system suitability standard chromatogram is shown in Fig. 2.

3.2.3. Linearity

Calibration plots were constructed after analysis of five peptide solutions in the range of 50–150% of the normal working concentration. Linearity of the calibration plot data was verified by linear regression analysis by plotting detector response (peak area) against analyzed concentration. The correlation coefficients (r^2) for calibration curves generated on six different days were consistently greater than 0.999 (Table 4). The results indicated that the method was linear over the range of 25–75 μg/ml for the seven peptide antigens and 12.5–37.5 μg/ml for A16L.

3.2.4. Accuracy and recovery

Accuracy and recovery of the assay method was demonstrated by analyzing the data obtained from spiked placebos covering 50–150% of the nominal sample concentration (500 μg/ml for the peptide antigens and 250 μg/ml for A16L). Spiked placebos were prepared at the 50, 100, and 150% levels. The mean recoveries for each component at each level and the respective %RSDs are shown in Table 5. All acceptance criteria were met (peptide recovery should lie within the range of 90–110% and %RSD less than 5%).

3.2.5. Precision

Precision was evaluated by determining the %RSD of the repeatability and intermediate precision for six measurements at 100% of the test concentration. For repeatability, six measurements were carried out using spiked samples (Table 5), as well as samples of a pre-clinical batch of DPX-0907 (Table 6). Samples were extracted from liposomes as described in Section 2.6 under the same conditions (same analyst, apparatus, identical reagents and short time interval). For the evaluation of intermediate precision, the determination was carried out on a different day, at a different site, by a different investigator, with a different HPLC instrument and column, using the same batch of DPX-0907. The average peptide content in the DPX-0907 vials is shown in Table 6. The %RSD of repeatability and intermediate precision was less than 4.17%, which complied with the proposed acceptance criteria (%RSD < 5%).

Upon completion of validation, this method was transferred from the development laboratory to a contract manufacturing site for the in-process and release testing of clinical batches of DPX-0907.

3.3. Application of the method to release testing of DPX-0907

The HPLC method developed is specific, accurate, and precise for the quantitative determination of all eight peptides in DPX-0907 and has been applied for the assay of peptide content (1 mg/ml P3, P4, P5, P7, P13, P14, P15; 0.5 mg/ml A16L) in a clinical batch. Two vials of DPX-0907 vaccine manufactured at a cGMP facility (Albany Molecular Research, Inc., Burlington, MA, formerly Hyaluron Contract Manufacturing) were evaluated for the amount of each peptide present in the formulation. The peptide content, along with the specifications are shown in Table 7. All release testing criteria were met and the batch was successfully used in a phase 1 trial for advanced breast, ovarian, and prostate cancer patients.

4. Conclusions

The goal of this work was achieved by separating and quantifying a mixture of eight therapeutic peptides in DPX-0907, an investigational cancer vaccine, by high performance liquid chromatography with UV detection. While the liposomal formulation presented challenges with peptide extraction, a simple liquid–liquid extraction method was developed to achieve excellent recoveries of each peptide. The method was developed and validated for the simultaneous determination of all eight peptides and had acceptable specificity, linearity, accuracy, and precision for

phase 1 studies. It uses a simple mobile phase composition and gradient to separate the peptide analytes with acceptable resolution in a short run time of 25 min. The method has been successfully transferred to a contract facility for the cGMP manufacture of DPX-0907 and is currently being used to test the stability of pre-clinical and clinical batches. The extraction procedure has also been applied to DepoVax formulations containing other promising therapeutic peptides.

Acknowledgments

The authors wish to thank Mr. Antar Fuentes-Ortega for preparation of pre-clinical batches of DPX-0907 vaccine.

References

[1] M. Mansour, L. Sammatur, L.D. MacDonald, M. Karkada, G.M. Weir, A. Fuentes-Ortega, Compositions comprising liposomes, an antigen, a polynucleotide and a carrier comprising a continuous phase of a hydrophobic substance, US Patent 2011/0070298 A1, 24 March 2011.

[2] M. Karkada, G.M. Weir, T. Quinton, L. Sammatur, L.M. MacDonald, A. Grant, R. Liwski, R. Juskevicius, G. Sinnathamby, R. Philip, M. Mansour, A novel breast/ovarian cancer peptide vaccine platform that promotes specific type-1 but not Treg/Tr1-type responses, J. Immunother. 33 (2010) 250–261.

[3] ImmunoVaccine Technologies, Inc., A phase I study of two different doses of the subcutaneous administration of an immunotherapeutic vaccine, DPX-0907 in advanced stage patients with ovarian, breast or prostate cancer, in: ClinicalTrials.gov [Internet], National Library of Medicine (US), Bethesda, MD, 2010. Available from: <http://clinicaltrials.gov/show/NCT01095848 NLM Identifier: NCT01095848> (cited 21.02.12).

[4] V. Ramakrishna, M.M. Ross, M. Petersson, C.C. Gatlin, C.E. Lyons, C.L. Miller, H.E. Myers, M. McDaniel, L.R. Karns, R. Kiessling, G. Parmiani, D.C. Flyer, Naturally occurring peptides associated with HLA-A2 in ovarian cancer cell lines identified by mass spectrometry are targets of HLA-A2-restricted cytotoxic T cells, Int. Immunol. 15 (2003) 751–763.

[5] C.L. Slingluff Jr., G. Yamshcikov, P. Neese, H. Galavotti, S. Eastham, V.H. Engelhard, D. Kittlesen, D. Deacon, S. Hibbits, W.W. Grosh, G. Petroni, R. Cohen, C. Wiernasz, J.W. Patterson, B.P. Conway, W.G. Ross, Phase I trial of a melanoma vaccine with gp100(280-288) peptide and tetanus helper peptide in adjuvant: immunologic and clinical outcomes, Clin. Cancer Res. 7 (2001) 3012–3024.

[6] H. Grohganz, O. Schläfli, M. Rischer, M. Brandl, Development and validation of a HPLC method for routine quantification of the decapeptide Cetrorelix in liposome dispersions, J. Pharm. Biomed. Anal. 34 (2004) 963–969.

[7] J. Turánek, D. Záluská, J. Neča, Linkup of a fast protein liquid chromatography system with a stirred thermostated cell for sterile preparation of liposomes by the proliposome–liposome method: application to encapsulation of antibiotics, synthetic peptide immunomodulators, and a photosensitizer, Anal. Biochem. 249 (1997) 131–139.

[8] A. Shibata, K. Nakajima, S. Ueno, T. Yamashita, Preparation and characterization of liposomes incorporating hydrophobic poly(amino acid)s with different secondary structure, Chem. Pharm. Bull. 42 (1994) 1151–1153.

[9] Q. Ye, J. Asherman, M. Stevenson, E. Brownson, N.V. Katre, DepoFoam technology: a vehicle for controlled delivery of protein and peptide drugs, J. Control. Release 64 (2000) 155–166.

[10] M.E.C. Lutsiak, G.S. Kwon, J. Samuel, Analysis of peptide and lipopeptide content in liposomes, J. Pharm. Pharm. Sci. 5 (2002) 279–284.

[11] ICH Guidelines, Q2 (R1), Validation of analytical procedures: test and methodology, November 2005.

[12] J. Kyte, R.F. Doolittle, A simple method for displaying the hydropathic character of a protein, J. Mol. Biol. 157 (1982) 105–132.

[13] Y. Pomeranz, C.E. Meloan, Food Analysis: Theory and Practice, third ed., Springer, New York, 1994.

Journal of Pharmaceutical and Biomedical Analysis 66 (2012) 183–190

Contents lists available at SciVerse ScienceDirect

Journal of Pharmaceutical and Biomedical Analysis

journal homepage: www.elsevier.com/locate/jpba

Release of pamidronate from poly(ethyleneimine)/cellulose sulphate complex nanoparticle films: An in situ ATR-FTIR study

M. Müller[a,b,*], B. Keßler[a]

[a] Leibniz-Institut für Polymerforschung Dresden e.V. (IPF), Department Polyelectrolytes and Dispersions, Hohe Straße 6, 01069 Dresden, Germany
[b] Technische Universität Dresden (TUD), Fachrichtung Chemie und Lebensmittelchemie, 01062 Dresden, Germany

ARTICLE INFO

Article history:
Received 26 January 2012
Received in revised form 23 March 2012
Accepted 24 March 2012
Available online 5 April 2012

Keywords:
Bisphosphonate
Polyelectrolyte complex
Drug delivery
In situ ATR-FTIR

ABSTRACT

In situ ATR-FTIR spectroscopy was used as a screening method to quantify the relative release of pamidronate (PAM) from films of polyelectrolyte (PEL) complex (PEC) particles. Stable colloid PEC particles consisting of poly(ethyleneimine) (PEI) and cellulose sulphate (CS) loaded with PAM were obtained by PEL complexation featuring hydrodynamic radii between 60 and 90 nm and a cationic or anionic surface charge dependent on the mixing ratio $n-/n+ = 0.9$ or 1.1, respectively. Respective bare unloaded PEC particles showed smaller hydrodynamic radii. PAM loaded PEC particles were casted from dispersion onto Ge model substrates and dried forming stable films in contact to water. By in situ ATR-FTIR spectroscopy it could be shown, that PAM/PEC particle films contacting to water resulted in a time dependent retarded release of PAM from the PEC matrix, while PAM from a pure drug film was immediately released. Cationic PAM loaded PEC particles of PEI/CS showed smaller initial burst and long term release compared to anionic one at similar PAM/PEI ratios. With increasing PAM/PEI ratio the initial burst could be minimized to around 30% and the residual long term amount of PAM optimized to 50% for PAM/PEC samples casted from 0.002 M dispersions. A further improvement of the release performance was achieved either by prerinsing the dry film in H_2O or by rising the PEC concentration from 0.002 M to 0.01 M revealing an initial burst of around 5% and long term residual PAM content of around 75%. ATR-FTIR and TRANS-FTIR analysis of the PAM release from equivalent PEC samples revealed similar kinetic courses and parameters justifying the use of the Ritger/Peppas two parameter model. Applying this model PAM/PEC samples casted from 0.002 M dispersions revealed exponent values of $b \ll 0.5$ suggesting PAM dissolution in the PEC matrix, while for those casted from 0.01 M b values close to 0.5 were obtained suggesting hindered dissolution and diffusion. A model describing different retention modalities of PAM in PEC particle is suggested.

© 2012 Elsevier B.V. All rights reserved.

1. Introduction

Elder people suffering from osteoporosis often happen to break bones by accident, so that in severe cases the usage of bone substituting materials (BSM) or implants is indicated. Currently, one of the main tasks is to directly equip BSM with local and retarded release functions for bone therapeutic agents, instead of administering them systemically. Released agents can be Ca^{2+} or Sr^{2+} ions, drugs like bisphosphonates (BP), statins (STA) or proton pump inhibitors (PPI), which all influence bone formation and resorption via the delicate osteoblast/osteoclast equilibrium. This contribution is related to the controlled release or elution of BPs from BSM via an attachable and interfacial polymer based drug delivery system. Pamidronate (PAM) was chosen as a well available model BP and germanium (Ge) as an analytically well accessible planar model substrate material. Several concepts of BP delivery systems have been reported in the literature like calcium phosphate compounds [1,2], acrylic bone cement [3] or iron oxide particles, the latter of which rather for clinical imaging purposes [4]. Our general solution concept for that purpose is based on nanoparticular polyelectrolyte (PEL) complexes (PECs) formed in the presence of the drug. Bare PECs can be prepared by mixing polycations and polyanions in non-stoichiometric ratios (related to their charged monomers), which is well known from initial work of Kabanov [5], Tsuchida [6] and Dautzenberg [7]. Recently, nanoparticular PEC systems could be optimized by certain refinement steps with respect to reproducibility and size distribution [8]. We use the PEL complexation technique for entrapment of drugs, since it is simple, uses mild conditions, allows to involve biorelated components, which might enhance biocompatibility, and is based on aqueous media. The loading and release of drugs from PEC particles have been initially described in the open literature by Tiyaboonchai [9] using a PEC system of PEI

* Corresponding author.
E-mail address: mamuller@ipfdd.de (M. Müller).

0731-7085/$ – see front matter © 2012 Elsevier B.V. All rights reserved.
http://dx.doi.org/10.1016/j.jpba.2012.03.047

and dextran sulphate (DS) and amphotericin, a systemically effecting fungicid drug. However, therein the release of drug loaded PECs from an interfacial adhesive PEC layer was not treated.

Herein we report results on PAM loaded PEC nanoparticles, which have been deposited as adhesive films onto planar Ge model substrates showing a retarded release of PAM under conservation and adhesive stability of the bare PEC particle film matrix [10]. Analytically, drug release from a given drug loaded matrix, film or surface can be determined either by probing selectively the actual drug content (depletion) in or at such a material or by probing the enrichment of the drug in the release medium in dependence of time, respectively. Commonly, the latter (enrichment) concept is realized by UV/VIS or fluorescence spectroscopy monitoring the intensity increase of a diagnostic absorption or emission band of the drug. However, BP like PAM are lacking appropriate UV/vis and fluorescence chromophores. Alternatively, manageable but more sophisticated techniques like fluorescence detection of derivatized BP [11], NMR spectroscopy [12] or ion pair reverse phase liquid chromatography (IP-RP-LC) [13] may be routinely applied to follow the enrichment concept.

Herein we liked to follow the detection concept of drug depletion in an interfacial material by applying in situ-ATR-FTIR spectroscopy on PAM loaded PEC particles deposited at model surfaces. Up to now this surface sensitive method was widely applied by us to analyze sorption and conformation processes of PEC layers (e.g. [14,15]), melanin-like films [16], chiral model drug compounds [17], lipids [18], peptides [19] and proteins (e.g. [20]). The main task of this study is to establish an ATR-FTIR based analytical screening system to evaluate and learn on modalities of the desorption or release of a model BP from a PEC based drug delivery system. Especially, the influence of PAM/PEC ratio and PEC concentration were of prime interest.

A PEL system based on poly(ethyleneimine) (PEI) and cellulose sulphate (CS) was used, since these compounds are well available. While CS is a biorelated PEL and might be expected as "biocompatible", there has been some debate on the "biocompatibility" of PEI. PEI/DNA complexes in solution to be used as gene vectors are reported to be cytotoxic (e.g. [21]), while layers of PEI/heparin (HEP) complexes are claimed to have positive effects on cell adhesion and viability in dependence of the PEI/HEP composition [22]. Pamidronate (PAM) was selected due to its availability. Furthermore, the results obtained for this PAM/PEC system should be transferred and applied on other drugs, other PEC systems as well as directly on BSM like calcium phosphate modified silicon/collagen xerogels [23] or calcium phosphate based cements [24].

2. Experimental

2.1. Materials

Branched poly(ethyleneimine) (PEI, 750,000 g/mol, BASF) and cellulose sulphate (CS, 200,000 g/mol, degree of substitution DS = 3.0, ACROS) were dissolved to 0.002–0.01 M solutions related to their monomer units. To get the concentration of truly charged monomer units, colloid titration (PCD) was applied (see below). Respective factors for PEI and CS were $F = 0.63$ and 2.90. Pamidronate (PAM, Sigma) and calcium chloride ($CaCl_2 \times H_2O$, Sigma) were dissolved to 0.01 M stock solutions, respectively.

2.2. Preparation of drug loaded polyelectrolyte complex (PEC) particles

Defined volumes (optionally 1–5 ml) of PEI solutions having concentrations $c_{PEL} = 0.002$–0.01 M were incubated with varying volumes of a 0.01 M PAM solution under stirring to get stoichiometric ratios PAM/PEI of 1:4 to 1:20. To these PEI/PAM solutions defined volumes of 0.002–0.01 M CS solutions were mixed under stirring to get a stoichiometric ratio CS/PEI of $n-/n+ = 0.9$. Such prepared PEC samples are denoted as PAM/PEI-1:4/CS-0.9 or PAM/PEC-0.9-1:4 or PAM/PEC-0.9-1:4-0.002 M (for $c_{PEL} = 0.002$ M). Unloaded and PAM loaded PEI/CS-1.1 dispersions were prepared and denoted analogously, whereby at first PAM solutions were also given to PEI solutions, but these PAM/PEI solutions (minority component) were dosed into CS solutions (majority component) to get a stoichiometric ratio of $n-/n+ = 1.1$. Finally, 10 μl of 0.01 M $CaCl_2$ solution were added to 200 μl of the PAM/PEI/CS dispersions.

2.3. Deposition of drug loaded PEC particles

50 μl of the respective PAM/PEI/CS/$CaCl_2$ mixture were solution casted onto the Ge model substrate to homogeneous films and dried at 50 °C in the vacuum oven for 30 min. Some of the samples were prepared by casting consecutively multiple PEC layers of PAM/PEI/CS on top of the dried initial PAM/PEI/CS film and subsequent drying. In further sets of experiments the Ge IRE with the final dried PAM/PEI/CS film was shortly dipped into a beaker with Millipore water for 5 s, withdrawn and immediately dried. This sample is further termed "prerinsed".

2.4. Determination of the loaded and released PAM amount

The actual bound PAM amount was determined in the deposited PAM/PEC film in contact to release medium by in situ ATR-FTIR spectroscopy (see below) at various times. Optionally the total released PAM was determined by TRANS-FTIR on the equivalent PAM/PEC samples at various times after drying.

2.5. Quantitative ATR-FTIR spectroscopy

Characterization of PAM/PEC films deposited onto Ge internal reflection elements (IRE) was performed by in situ-ATR-FTIR spectroscopy using the SBSR concept [25] to obtain well compensated ATR-FTIR spectra, as it is described therein [14]. The ATR-FTIR attachment (OPTISPEC, Zurich, Switzerland) was operated on the IFS 55 Equinox spectrometer (BRUKER Optics GmbH, Ettlingen, Germany) equipped with globar source and MCT detector. 100 scans were collected at a spectral resolution of 2 cm^{-1} using Happ-Gänzel apodisation for each recorded spectrum.

According to Harrick and Fringeli [25,26] quantification of concentrations c of or in polymer films by ATR-FTIR spectroscopy is based on the absorbance or integral A of a given IR band using a modified Lambert–Beer law given in Eq. (1)

$$A = N\varepsilon c d_E \quad (1)$$

Importantly, Eq. (1) includes the number of reflections $N = 11$, absorption coefficient ε of the given band and the effective thickness d_E instead of the true sample thickness d in TRANS-FTIR. Values of d_E can be calculated straight forward knowing the refractive indices n_1, n_2, n_3 of the IRE, polymer and bulk medium, respectively, depth of penetration d_P and incident angle θ of the IRE. It has been shown earlier, that band integrals from ATR-FTIR spectra are directly proportional to the molar amount of IR absorbing monomer units or components in polymer films, if the thickness of the polymer film does not exceed around 300 nm (thin film case) [27]. In our case of casted PEC films this assumption was valid.

2.6. Quantitative transmission (TRANS) FTIR spectroscopy

PAM/PEC films and the release of PAM were additionally measured by TRANS-FTIR. A homebuilt sample holder (IPF Dresden) was used, into which the coated Ge-IRE was clamped allowing to

measure directly the transmission intensity I. The naked Ge-IRE was used as the reference to measure I_0. Ratioing these intensities and calculating the logarithm gave absorbance spectra according to $A = -\log(I/I_0)$. Quantification of concentrations c in polymer films is based on the Lambert–Beer law $A = \varepsilon c d$, wherein A and ε have been introduced in Eq. (1) and d denotes the true film thickness. Generally, applying TRANS-FTIR the Ge/PAM/PEC sample is completely crossed by IR light and the respective TRANS-FTIR spectrum (i.e. diagnostic band) reflects the PAM concentration over the whole PEC matrix. Whereas, ATR-FTIR senses rather the interfacial region between Ge and the PAM/PEC film due to the exponentially decaying evanescent IR field amplitude [26]. For thick films (thickness $d \gg 1\,\mu m$) and above a certain depth of penetration d_P the evanescent IR field amplitude approaches zero and no longer detects PAM in outermost zones of the PEC matrix. However, for thin films ($d < 300$ nm), like they were used herein, the respective ATR-FTIR spectrum (i.e. diagnostic band) reflects the PAM concentration in the whole matrix (like the TRANS-FTIR spectrum) without any sampling depth dependence. The advantage of ATR-FTIR over TRANS-FTIR is the higher sensitivity. For dry organic films ($n_2 = 1.5$, $d \approx 200$ nm) onto Ge ($n_1 = 4.0$) in contact to air ($n_3 = 1$) N times effective thickness for ATR-FTIR has a value of $N\ d_E = 1690$ nm, which is around eight times higher compared to the true film thickness $d \approx 200$ nm valid for TRANS-FTIR.

2.7. Curve fitting analysis and quantification of actual PAM content

The diagnostic but highly overlapped ATR-FTIR spectral region between 1300 and 900 cm^{-1} on PAM/PEC films was analysed by a curve fitting procedure reported initially and applied to spectral data on polypeptides [19] or on polyelectrolyte multilayers [27]. Briefly, the lineshape of selected ATR-FTIR spectra was fitted by the sum of ten Lorentzian/Gaussian (50/50%) band components, which were freely relaxed in their individual parameters wavenumber position ν_0, half width h_0 and integrated absorbance A_0 to give optimum fits, respectively. Five ATR-FTIR spectra recorded in the initial (0 min) and end (1200 min) dry state and the initial (5 min), intermediate (60 min) and end (1200 min) wet state, respectively, were selected. Then the found values for ν_0 and h_0 were averaged among these five selected ATR-FTIR spectra for each of the ten components. Finally, intensity fits were performed on all measured ATR-FTIR spectra of a kinetic series under fixation of the averaged ν_0 and h_0 values to get A_0 values for each component. Typical curve fitting results are shown in Fig. 1 for a PAM/PEI-1:4/CS-0.9 sample in the initial and end dry end state after PAM release. While the component at 1064 cm^{-1} (ν(O=P=O) vibration) could be identified and assigned to phosphate moieties of PAM, the band component at 1255 cm^{-1} (ν(O=S=O) vibration) was assigned to sulphate groups of CS. For both components the respective A_0 values were read out for the further analysis (see below). This was done for all corresponding spectra on PAM/PEC samples as well as for spectra on PEC samples without PAM (pure PEC). A_0 values of PAM/PEC samples were further denoted as $A^{1064}_{PAM/PEC}$ and $A^{1255}_{PAM/PEC}$ and A_0 values of PAM free PEC samples as A^{1064}_{PEC} and A^{1255}_{PEC}, respectively.

The ratio A_{PAM} was used as a measure for the *relative PAM content* in the PEC according to the following formalism (Eqs. (2)–(4)):

$$A_{PAM} = \frac{A^{1064/1255}_{ACTUAL}}{A^{1064/1255}_{INITIAL}} \times 100\% \quad (2)$$

$$A^{1064/1255}_{INITIAL} = \frac{A^{1064}_{PAM/PEC}}{A^{1255}_{PAM/PEC}} - \frac{A^{1064}_{PEC}}{A^{1255}_{PEC}} \quad \text{for} \quad t = 0\,\text{min} \quad (3)$$

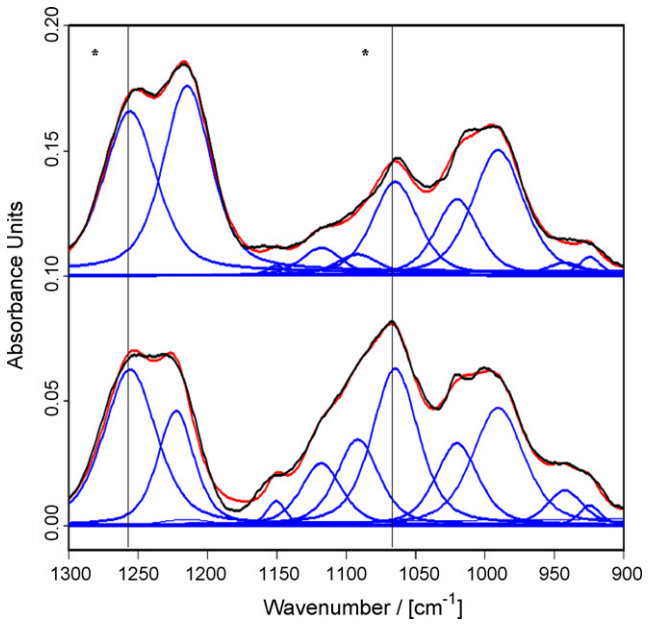

Fig. 1. Typical curve fitting results on ATR-FTIR spectra of a dry PAM/PEI-1:4/CS PEC sample directly after casting and drying (lower panel) and after contact to release medium and drying (upper panel). The experimental ATR-FTIR spectrum (black), simulated ATR-FTIR spectrum (red) and the underlying components of the ATR-FTIR spectrum (blue) are shown. The diagnostic PAM component (ν(O=P=O)) and PEC (CS) component (ν(O=S=O)) are marked by asterisks (*). (For interpretation of the references to color in this figure legend, the reader is referred to the web version of the article.)

$$A^{1064/1255}_{ACTUAL} = \frac{A^{1064}_{PAM/PEC}}{A^{1255}_{PAM/PEC}} - \frac{A^{1064}_{PEC}}{A^{1255}_{PEC}} \quad \text{for} \quad t = \text{actual time} \quad (4)$$

The ratio $A^{1064}_{PAM/PEC}/A^{1255}_{PAM/PEC}$ is related to PEC samples with drug and that of $A^{1064}_{PEC}/A^{1255}_{PEC}$ to PEC samples without drug (blank ratio). Subscripts INITIAL and ACTUAL denote values corresponding to $t = 0$ min (initial dry state) and to actual times (wet state). For $t = 0$ min the relative PAM content $A_{PAM} = 100\%$ ($A^{1064/1255}_{ACTUAL}/A^{1064/1255}_{INITIAL} = 1$) and for $t > 0$ min $A_{PAM} < 100\%$ ($A^{1064/1255}_{ACTUAL}/A^{1064/1255}_{INITIAL} < 1$) due to drug release.

2.8. Stability of PEC films

The determination of the stability of PEC films in contact to the release medium was based on the band component at 1255 cm^{-1}. In principal the "self release" of the PEC is determined based on the relative pure PEC content C_{PEC} defined in Eq. (5). Thereby, the initial value ($t = 0$, dry state) of the 1255 component is normalized to 100%. Whereas, the actual values (t = actual time, wet state) were corrected by the ratio of the effective thickness for polymer films in contact to air and in contact to water $Q = d_E^{AIR}/d_E^{H_2O} = 0.93$, which is an empirical constant, according to:

$$C_{PEC} = Q \times \frac{A^{1255}_{PAM/PEC}(\text{actual time})}{A^{1255}_{PAM/PEC}(t = 0)} \times 100\% \quad (5)$$

2.9. Dynamic light scattering

PAM/PEC and PEC particle sizes were determined by dynamic light scattering (DLS). DLS data were measured by the Jianke Portable Particle Sizer (Jianke Instruments Co. Ltd., Wuhu, PR China) at the scattering angle of 90°. The samples were held in 10 mm cuvettes with circular bottom. The hydrodynamic radius R_H was estimated using the Stokes–Einstein equation. Intensity weighted

DLS data were considered, as it was applied earlier therein [8]. Errors of R_H are related to the standard deviation of at least three different measurements. The ALV-5000/E/EPP-Software of ALV GmbH, Langen, Germany was used for calculations of DLS parameters.

2.10. Colloid titration

The true concentration of the charged monomer units of PELs used in this study was determined by the Particle Charge Detector (PCD, Mutek, Herrsching, Germany) according to standard protocols using low molecular 0.001 M PDADMAC or 0.001 M PVS solutions as titrating solutions. The true concentration of charged monomer units in the PEL solutions, whose initial concentration was 0.002–0.01 M, related to their both charged and uncharged monomer units, was calculated from the consumed amount of the titrator solution. The true concentration of charged monomer units was always smaller compared to the monomer unit concentration of 0.002–0.01 M. The ratio between true charged monomer and monomer concentration can be expressed by the factor F (see above).

3. Results

3.1. Colloidal characterization

3.1.1. Dynamic light scattering

Before the interfacial characterization as drug eluting adhesive films the colloidal properties of drug loaded and unloaded PEC particles were studied by dynamic light scattering (DLS) and colloid titration (particle charge detection, PCD). Herein we focussed on the fixed mixing ratios of $n-/n+ = 0.9$ and $n-/n+ = 1.1$, which is related to the ratio of charged monomer units of the polyanion (PA) CS and polycation (PC) PEI. At these mixing ratios it is known, that no large amount of excess PC or PA is present in the dispersion, which is an important point in view of applications for in vitro cell culture experiments or in vivo ones in the animal body. Basic colloidal parameters of the selected PEC systems can be found in Table 1.

Generally, low polydispersity values of around PDI = 0.1 (not shown) and ranges of the count rate CR = 143–300 kHz and of the hydrodynamic particle radius R_H = 60–87 nm were obtained. Unloaded PEC particles of PEI/CS-1.1 (63 nm) had the same size compared to those of PEI/CS-0.9 (60 nm). Generally, there was an increase of both CR and R_H values for PEC particles loaded with PAM in comparison to the bare PEC particles for all measured systems. Qualitatively, with increasing PAM content the particle size of PAM/PEI/CS-0.9 was increasing. Increasing the PEL concentration from c_{PEL} = 0.002 to 0.01 M did not alter the size dramatically for the PAM free and loaded PEI/CS-0.9 particles.

Table 1
Colloidal parameters of various PAM/PEI/CS samples. PEL concentration c_{PEL} = 0.002 M was used, if not further indicated.

Sample	Count rate [kHz]	Hydrodyn. radius [nm]	Charge sign (+/−) (titrated amount)
PEI/CS-0.9	155 ± 28	60 ± 10	(+)
PAM/PEI-1:20/CS-0.9	257 ± 44	69 ± 7	(+)
PAM/PEI-1:12/CS-0.9	300 ± 62	82 ± 6	(+)
PAM/PEI-1:4/CS-0.9	296 ± 61	87 ± 9	(+)
PEI/CS-0.9, 0.01 M	154 ± 43	53 ± 7	(+)
PAM/PEI-1:20/CS-0.9, 0.01 M	221 ± 43	82 ± 7	(+)
PEI/CS-1.1	143 ± 44	63 ± 6	(−)
PAM/PEI-1:12/CS-1.1	150 ± 44	66 ± 7	(−)

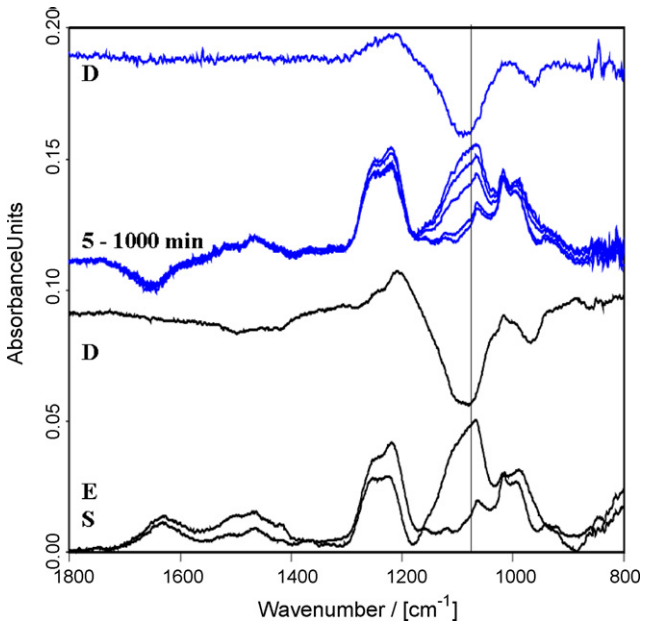

Fig. 2. In situ ATR-FTIR spectra of a casted film of PAM/PEI-1:4/CS (PEC-0.9). The black spectra correspond to the dry start (S) and end (E) state and their difference (D). The blue spectra correspond to the wet state after the release times 5, 10, 20, 60 and 1000 min and the difference between state after 1000 and 5 min (D). (For interpretation of the references to color in this figure legend, the reader is referred to the web version of the article.)

3.1.2. Colloid titration

For the unloaded PEC-0.9 nanoparticles of PEI/CS titrated amounts of 0.064 ml (PVS) and for the respective PEC-1.1 nanoparticles those of 0.024 ml (PDADMAC) were obtained by colloid titration. Hence it can be concluded, that PEC-0.9 dispersions contain weakly positively charged and PEC-1.1 ones weakly negatively charged PEC nanoparticles, respectively. The addition of PAM either to PEC-0.9 or PEC-1.1 preserved the cationic or anionic net charge sign of the PEC nanoparticles, respectively, for all PAM/PEI ratios 1:20–1:4.

3.2. Interfacial characterization

Herein, the release of PAM from adhesive films of PEC particles and its modalities are described using in situ ATR-FTIR spectroscopy. Thereby, an analytical approach sensitive to drug depletion in an interfacial material is followed, which should be complimentary to commonly used other approaches sensitive to drug enrichment in the release medium. At first we present typical in situ ATR-FTIR spectra (Section 3.2.1) and secondly relative PAM release profiles based on these data are given (Section 3.2.2). Several influences like the mixing ratio and PAM/PEC ratio, concentration and the usage of multiple PEC layers are shown. Thirdly, from quantitative kinetic analysis of these data kinetic parameters based on the Ritger/Peppas model are provided (Section 3.2.3). Finally, ATR-FTIR data are compared with TRANS-FTIR data on a same selected PAM/PEC sample to justify the analytical approach in this report (Section 3.2.4).

3.2.1. ATR-FTIR spectra

In Fig. 2 typical in situ ATR-FTIR spectra of solution casted PAM loaded PEC particles of PEI/CS are shown, where the PAM/PEI ratio is 1:4. In the bottom half (black) ATR-FTIR spectra recorded on the initial or start (S) PEC film and those recorded after contact to the release medium at the end (E) both in contact to air (dry state) are given. In the upper half (blue) ATR-FTIR spectra on the

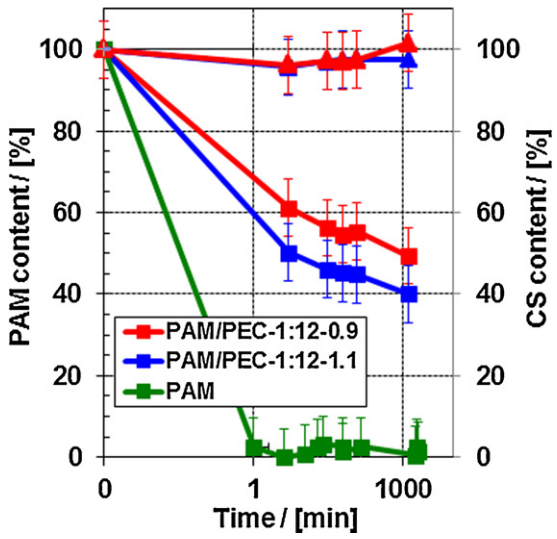

Fig. 3. Percentage release profiles of PAM from deposited PEC-0.9 and PEC-1.1 particle films of PAM/PEI-1:12/CS at Ge based on the time course of $A_{ACTUAL}^{1064/1255}$ (Eq. (4)) and from a deposited pure PAM film at Ge (left ordinate axis, cubes). Percentage change of PEC film matrix based on the time course of the diagnostic band component at 1255 cm^{-1} due to sulphate moieties from CS for respective PAM loaded PEC samples (right ordinate axis, triangles).

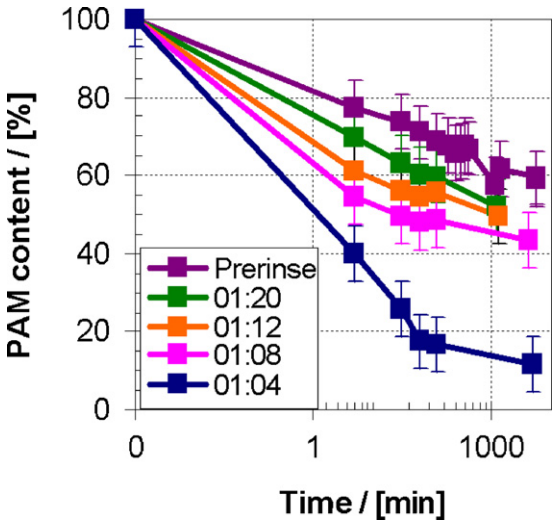

Fig. 4. Percentage release profiles of PAM from solution casted single PEC films of PAM/PEI-X/CS-0.9 at 0.002 M for various PAM/PEI molar ratios X = 1:4, 1:8, 1:12, 1:20 (from bottom to top). The uppermost curve is related to casted PAM/PEI-1:4/CS-0.9 film prerinsed in H_2O and dried before release experiment.

PEC/PAM film in contact to aqueous medium (wet state) recorded after 5–1000 min are given.

A stepwise decrease of the band at around 1070 cm^{-1} assigned to the ν(O=P=O) vibration due to PAM, is found, which is a qualitative hint for a retarded release of PAM from PAM loaded PEC particles. Furthermore, other bands like that around 1250 cm^{-1} assigned to the ν(O=S=O) vibration due to CS, stayed nearly constant, which is a qualitative hint for the stability of the PEC matrix during PAM release.

3.2.2. Quantitative analysis of PAM release

As the main diagnostic quantitative parameter A_{PAM} denoting the relative PAM content (%) in PAM/PEC films based on the ratio of the 1064 cm^{-1} and 1255 cm^{-1} component integrals is used, which is introduced in Eqs. (2)–(4) and explained in Section 2.

3.2.2.1. Influence of the mixing ratio. Typical kinetic courses based of A_{PAM} for PAM/PEI-1:12/CS films are shown in Fig. 3 (left ordinate axis) for the mixing ratios $n-/n+$ = 0.9 and 1.1, respectively.

Thereby, PAM was given to the PEI solution at a fixed molar ratio (related to PEI monomer units) of 1:12 and the resulting solutions were then mixed with CS solution, so that in principle also the PAM/PEC ratio was varied. The PAM/PEI-1:12/CS-0.9 system showed a slightly lower release from 100 to around 50% after around one day (1440 min) in comparison to the PAM/PEI-1:12/CS-1.1 system, which ended at 40% after the same period. Furthermore the difference in the relative PAM content between 0 min (100%) and 5 min (actual percentage) ("initial burst") was around 40% for the PEC-0.9 and 50% for the PEC-1.1 system. Hence, we chose PEC-0.9 systems of PAM/PEI/CS for further PAM release studies. For comparison in Fig. 3 the release profile of PAM from a deposited pure PAM film is given. No retention of PAM and an initial burst close to 100% can be observed even after 1 min.

3.2.2.2. Stability of the drug/PEC films. A very important property of such PEC based drug releasing systems is the adhesive stability of the PEC matrix upon releasing the drug. Principally, no PEC or PEL material should be lost during drug release to minimize adverse responses or reactions in a given in vitro or in vivo system. PEC film stability was checked by plotting C_{PEC}, which is a measure of the relative CS as it is introduced in Eq. (5) and explained in Section 2, versus time. In Fig. 3 the kinetic course of C_{PEC} for the PAM/PEI-1:12/CS system in contact to water is shown (right ordinate axis). In the analytical error limit practically no loss of the initial CS content was found for both PAM/PEC-0.9 and PAM/PEC-1.1 films. Therefore, we assume, that the PEC matrix stays intact during the release of PAM in contact to water, which is an important condition for the applicability of drug loaded PEC systems.

3.2.2.3. Influence of the PAM/PEI ratio. As a further parameter the molar PAM/PEI ratio in PEC particles of PEI/CS was varied from 1:4 to 1:20. The results are given in Fig. 4 in logarithmic scale. Significantly, the initial burst could be minimized from 60% for PAM/PEI = 1:4 to 30% for PAM/PEI = 1:20. Furthermore, the residual PAM content after around one day could be maximized from 10% (1:4) to 50% (1:20). Interestingly, a further minimization of the initial burst to around 20% and a maximization of the residual PAM content to around 60% could be achieved by prerinsing the dried PAM/PEI/CS film (PAM/PEI = 1:4) in water followed again by drying. Hence, it seems, that the prerinse treatment takes away this amount of PAM, which would be released very quickly without prerinse.

3.2.2.4. Influence of the PEC concentration. Another significant influence on the release properties of PAM/PEC-0.9 particles played also the concentration, which was varied by mixing PEL solutions at the concentrations of c_{PEL} = 0.002 M, 0.005 M and 0.01 M. In all three cases a constant PAM/PEI ratio of 1:20 was kept. Part results are shown in Fig. 5. While the PAM/PEC-1:20 sample casted from 0.002 M dispersion showed an initial burst of around 60% and a residual PAM content of around 10% (1200 min), the initial burst could be further minimized to around 5% and the residual PAM content maximized to around 75% for a PAM/PEC-1:20 sample casted from 0.01 M dispersion. For 0.005 M the initial burst was also lower (≈30%) and the residual PAM content higher (≈55%) compared to 0.002 M. Conclusively, for 0.01 M the highest release retardation was obtained.

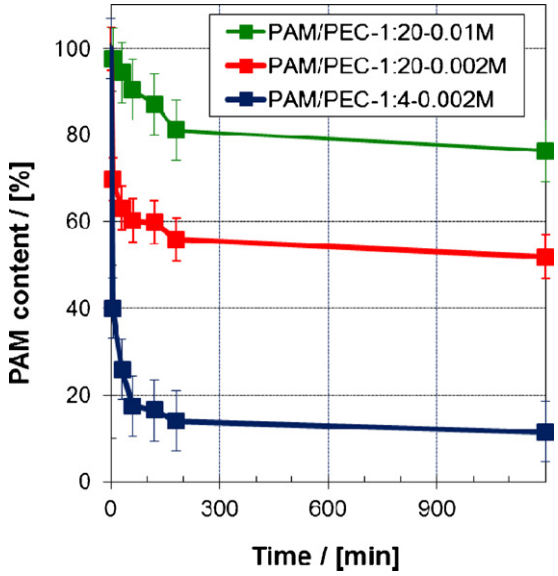

Fig. 5. Release profiles of PAM from solution casted PEC films for various samples from bottom to top: single casted PAM/PEC-1:4 at 0.002 M, single casted PAM/PEC-1:20 at 0.002 M, single casted PAM/PEC-1:20 at 0.01 M and triple casted PAM/PEC-1:4 at 0.002 M.

3.2.3. Kinetic analysis

3.2.3.1. Ritger/Peppas model. For the description of kinetic drug release data from hydrogel like materials the Ritger/Peppas equation [28] is frequently used according to

$$C_{DRUG}(t) = at^b \tag{6a}$$

where $C_{DRUG}(t)$ is the actual concentration of a drug at a given time t, a is an empirical prefactor and b is the exponent diagnostic for the release type. This model accounts for porous structure in a releasing (hydrogel) matrix. If the pores are rather large in comparison to the drug size, drug release is dominated by free diffusion and the exponent b should be close to 0.5. If the pores are rather small with respect to the drug size, drug release is hindered and b should be closer to 1 defining a zero order kinetics. Adapting this model to ATR-FTIR release data is not straight forward: $C_{DRUG}(t)$ is not directly proportional to the band integral $A_{DRUG}(t)$, since due to the exponentially decaying field amplitude of the evanescent wave there is an additional dependence on the distance x of the drug in direction of the IRE surface normal, which has to be described by $A_{DRUG}(x, t)$. However for rather thin films, the exponential decay contribution in kinetic ATR-FTIR data can be neglected in a first order approximation. Then the experimental $A_{PAM}(t)$ data shown, e.g. in Figs. 3–5 may be directly fitted by a modified analytical function with respect to Eq. (6b):

$$A_{PAM}(t) = 100 - at^b(\%) \tag{6b}$$

Therein A_{PAM} is defined in Eq. (2) as a measure of the actual relative PAM content in the PEC film. The values of a and b determined for various PAM/PEC samples are summarized in Table 2.

Obviously, for all PEC samples casted from 0.002 M dispersions the kinetic parameter b did not show a significant dependence on the PAM/PEI ratio and ranged between $b \approx 0.11$–0.17, which was significantly lower than the critical value of $b = 0.5$. This might be interpreted rather by a dissolution process of locally dried or concentrated PAM amounts regions than by free diffusion of PAM out of pores. Whereas, the PEC sample casted from 0.01 M PEC dispersion revealed a value of $b = 0.44$, which is close to the critical value of $b = 0.5$ indicating rather Fickian diffusion. However, a zero order kinetics characterized by values $b \gg 0.5$ was not obtained with the present PAM/PEC samples. Furthermore, the

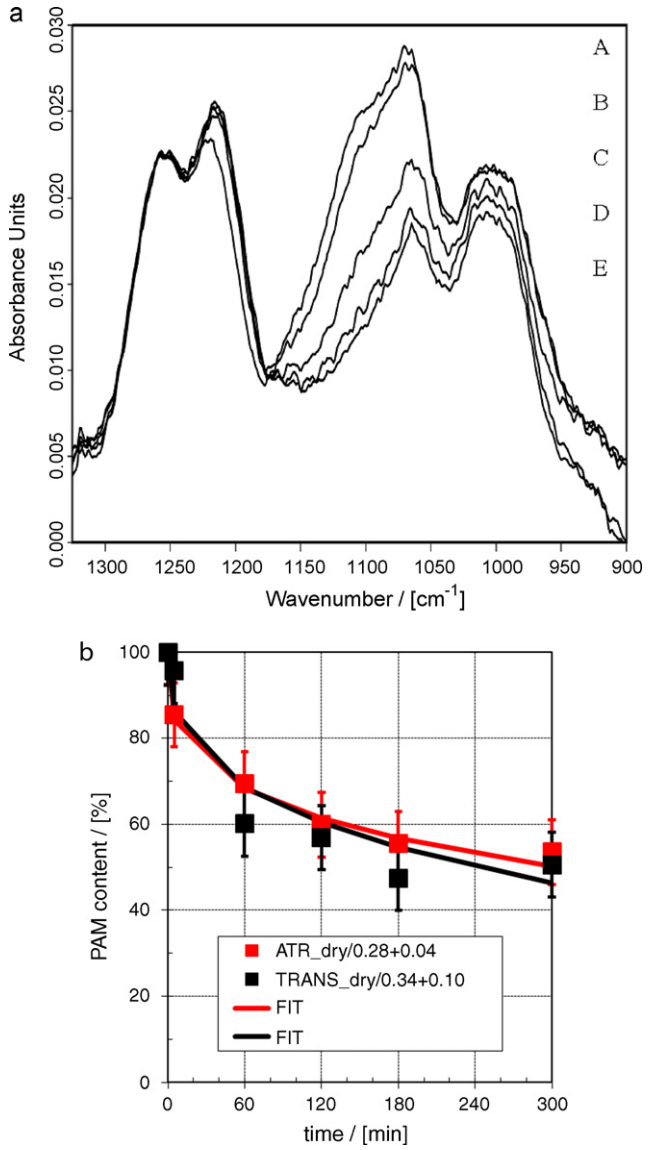

Fig. 6. (a) TRANS-FTIR spectra of a casted film of PEI/CS (PEC-0.9) loaded with PAM (1:4). The initial spectrum in the dry state (A, top) and the spectra after contact to release medium for 5 min (B), 60 min (C), 120 min (D), and 300 min (E) after drying, respectively, are shown. (b) Relative PAM content determined using Eqs. (2)–(4) from ATR-FTIR spectra (red) and TRANS-FTIR spectra (black) on the $[PAM/PEI\text{-}1{:}4/CS]_3$ sample in dependence of time. ATR-FTIR and TRANS-FTIR release data were fitted by the Ritger/Peppas model (Eqs. (6a) and (6b)). Found parameters are given in Table 2.

parameter a gives an information on the relative released drug amount, which was largest for the single PAM/PEC-1:4 sample casted from 0.002 M ($a = 51.29\,cm^{-1}$) and smallest for the PAM/PEC-1:20 sample casted from 0.01 M ($a = 2.55\,cm^{-1}$) dispersions, respectively. This was accompanied with an increase of b from 0.11 to 0.44, respectively, due to the retardation of PAM release. Prerinsing a PEC-0.9 of PAM/PEC-1:4-0.002 M with release medium results in a decreased relative released PAM amount from $a = 51.29\,cm^{-1}$ to $18.09\,cm^{-1}$, but in no increase of the kinetic parameter b ($b = 0.11$ for both original and prerinsed PAM/PEC-1:4-0.002 M sample). This clearly shows, that by prerinsing only the initial burst presumably due to rapid PAM dissolution can be minimized but not the long term release kinetics, since the retention properties of the PEC matrix does not change.

Table 2
Kinetic parameters *a*, *b* (see Eqs. (6a) and (6b)) according to the Ritger/Peppas model [28] concerning PAM release from films of PAM loaded PEI/CS-0.9 particles.

Samples	FTIR technique	a [cm^{-1}] (by Eq. (6b))	b (by Eq. (6b))
PAM/PEC-1:4-0.002 M	ATR	51.29 ± 2.73	0.11 ± 0.01
PAM/PEC-1:12-0.002 M	ATR	24.69 ± 5.88	0.15 ± 0.06
PAM/PEC-1:20-0.002 M	ATR	19.87 ± 4.06	0.17 ± 0.05
PAM/PEC-1:4-0.002M-prerinse	ATR	18.08 ± 1.34	0.11 ± 0.02
PAM/PEC-1:20-0.01 M	ATR	2.55 ± 0.40	0.44 ± 0.04
$[PAM/PEC\text{-}1{:}4\text{-}0.002\ M]_3$	ATR	10.07 ± 1.49	0.28 ± 0.04
$[PAM/PEC\text{-}1{:}4\text{-}0.002\ M]_3$	TRANS	8.15 ± 4.49	0.34 ± 0.10

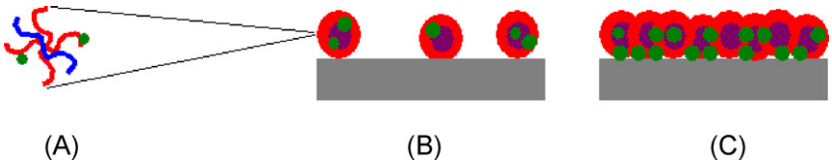

Fig. 7. Proposed scheme on the locations and retention types of PAM (green) at PEC particles (red with violet core) consisting of PEI (red) and CS (blue). (For interpretation of the references to color in this figure legend, the reader is referred to the web version of the article.)

3.2.4. Comparison between ATR and transmission FTIR data

In order to compare ATR-FTIR data on PAM release from PEM with another technique, we performed additional TRANS-FTIR experiments. Both methods were applied on an identical sample, which was a triple coated $[PAM/PEC\text{-}1{:}4]_3$ (0.002 M) film onto the Ge substrate providing sufficient band intensities also in the spectra recorded by TRANS-FTIR technique. Unlike the measurement concept for the in situ ATR-FTIR mode, the PAM/PEC sample film onto a Ge-IRE was measured in the dry initial state and then put into a beaker filled with release medium (50 ml). After 5, 60, 120, 180 and 300 min, respectively, the PEC/PAM coated Ge-IRE was removed, immediately dried and measured in the dry state. The corresponding spectra are shown in Fig. 6a and the course of the relative PAM content together with the fitted curve are given in Fig. 6b.

Obviously, the kinetic ATR- and TRANS-FTIR data on the relative PAM content [%] revealed quite similar courses. This finding has two important consequences. Firstly, both methods measure the relative drug depletion from the PEC film meaning, that the drug is really out of (i.e. released from) the PEC matrix and *not* located in considerable portions at some outer zones according to a concentration gradient (see Section 2.6). Secondly, the Ritger/Peppas model is adequate for both TRANS and ATR-FTIR data. Fitting ATR-FTIR ($b = 0.28 \pm 0.04$) and TRANS-FTIR data ($b = 0.34 \pm 0.10$) to this simple model revealed values for b, which in the error limit are quite similar. These values are also included in Table 2. The obviously slower PAM release from the triple $[PAM/PEC\text{-}1{:}4]_3$ compared to the single system [PAM/PEC-1:4] is due to the better entrapment of inner PAM amounts by two additional outer protecting layers.

4. Discussion

As it has been shown in Section 3 the PAM release was most retarded for the highly concentrated PAM/PEC-1:20 system at 0.01 M and for the triple casted PAM/PEC system in contrast to the single casted PAM/PEC systems at 0.002 M, respectively. Since no dramatic differences have been found in the size of the PEC particles in dependence of concentration by DLS we conclude, that rather the degree of surface aggregation as well as the internal structure of the PEC particles may play a crucial role for the binding or retention of PAM. Two main interaction types might prevail between PAM and PEC matrix. One interaction type is ionic binding of the bivalent low molecular counteranion PAM via the phosphonate groups to oppositely charged free cationic PEI sites of the PEC, which are not compensated by CS. This might be seen in the classical picture of counterion (PAM) condensation at oppositely charged PEL [29], which serves as a considerable binding force for charged drugs. On the other hand based on the classical scrambled egg model of Michaels [30] claiming a high number of oppositely charged polyelectrolyte chains to be densely packed in a PEC the physical entrapment of PAM within the PEC phase is very likely. Presumably, ionic interaction causes stronger retention of PAM in comparison to the pure unspecific physical entrapment of PAM within an aggregated and dried PEC phase. This would explain the high initial bursts and rapid releases, especially when high relative PAM/PEC loadings at lower PEC concentrations were applied. Whereas, for lower PAM/PEC loadings at higher PEC concentrations the structural density, which is on the order of 0.43 mg/ml according to Dautzenberg [31], as well as the drug/surface area ratio is increased causing more specific PAM/PEC interaction and thus lower initial bursts and slower releases.

Future studies will address structural changes related to polymer segment density and pore size in the PEC matrix to be responsible for the different drug release properties associated with hindered diffusion. Such an approach was followed by Rubner [32] at polyelectrolyte multilayers (PEM) loaded with anticoagulant cytochalasin, which are structurally related to the drug loaded PEC particle films shown herein. These authors found from fits of their release curves values of $b \approx 0.5$ for microporous and those of $b \approx 1$ for nanoporous PEM, which could be distinguished by SFM. Also related to our studies are ones of Bohidar [33] on encapsulation of salbutamol (bronchodilator) in a PEC coacervate phase prepared by mixing anionic and cationic gelatine in the presence of the drug. They claim, that the salbutamol release from the coacervate phase could not be described by known release models, since too many factors like dissolution, permeation of solvent into the matrix and non-Fickian drug diffusion in a crowded environment play a role.

Finally, we suggest, that the studied deposited PAM/PEC particle films exhibit three structural levels of retention for PAM, which is schemed in Fig. 7: a molecular one based on charged drug binding/condensation at free uncomplexed PEI sites within PEC particles (A), an intraparticular nanoscopic one due to entrapment of PAM within single PEC particles of complexed cationic PEI and anionic CS (B) and an interparticular mesoscopic one due to the entrapment of PAM within the zone formed by aggregated PEC particles (C).

5. Conclusions

- Mixing PEI, CS and PAM solutions resulted in dispersed, colloidally stable PAM loaded PEC nanoparticles with hydrodynamic radii of around 60–90 nm (PAM/PEC). The respective bare unloaded PEC particles showed smaller radii.
- PAM/PEC particles were casted from dispersion onto Ge model substrates and dried forming stable films in contact to water.
- By in situ ATR-FTIR spectroscopy combined with spectral lineshape analysis the retarded release of PAM from PAM/PEC particle films in contact to water could be quantified.
- Cationic PAM loaded PEC-0.9 particles showed smaller initial burst and long term release of PAM compared to anionic PAM loaded PEC-1.1 particles at similar PAM/PEI ratios. Casted pure PAM films were immediately dissolved in contact to water.
- With increasing PAM/PEI ratio the initial burst could be minimized to around 30% and the residual relative PAM content maximized to around 50% for PAM/PEC samples cased from 0.002 M dispersions. Further improvement was achieved by prerinsing PAM/PEC films in H_2O and drying resulting in an initial burst of 20% and a residual long term relative PAM content of 60%.
- Rising the concentration from 0.002 M to 0.01 M, PAM/PEC-1:20 samples showed an initial burst of only around 5% and a long term residual relative PAM content of around 75%, which actually features the best release properties and performance.
- Kinetic analysis based on the Ritger/Peppas model revealed values of $b \ll 0.5$ for PAM/PEC samples casted from 0.002 M dispersions suggesting dissolution of dried PAM in the PEC matrix. Whereas, PAM/PEC samples casted from 0.01 M dispersions revealed values of b close to 0.5 suggesting hindered dissolution and diffusion due to a denser PEC matrix and lower drug/surface area ratio.
- ATR-FTIR and TRANS FTIR data on the PAM release from an identical $[PAM/PEC]_3$ sample revealed similar courses and similar a and b values, which justifies the Ritger/Peppas model.
- A model describing different retention modalities of PAM in PEC particle films is suggested.

Acknowledgements

This work was sponsored and carried out in the framework of the Special Research Area/Transregional 79 (TRR 79, part project M7) entitled Materials for Tissue Regeneration in Systemically Diseased Bones by Deutsche Forschungsgemeinschaft (DFG) involving universities and research institutes in Gießen, Heidelberg and Dresden, Germany.

DRESDEN concept linking research activities of IPF Dresden and TU Dresden is gratefully acknowledged.

References

[1] S. Josse, C. Faucheux, A. Soueidan, G. Grimandi, D. Massiot, D. Alonso, P. Janvier, P. Pilet, O. Gauthier, G. Daculsi, J. Guicheux, B. Bujoli, J.M. Bouler, Novel biomaterials for bisphosphonate delivery, Biomaterials 26 (2005) 2073–2080.
[2] C. Faucheux, E. Verron, A. Soueidan, S. Josse, M.D. Arshad, P. Janvier, P. Pilet, J.M. Bouler, B. Bujoli, J. Guicheux, Controlled release of bisphosphonate from a calcium phosphate biomaterial inhibits osteoclastic resorption in vitro, J. Biomed. Mater. Res. 89A (2009) 46–56.
[3] N.Y.C. Yu, A.J. Ruys, M. Zenios, C. Godfrey, M. McDonald, P. Kiely, K. Mikulec, D.G. Little, A. Schindeler, Bisphosphonate-laden acrylic bone cement: mechanical properties, elution performance, and in vivo activity, J. Biomed. Mater. Res. Part B: Appl. Biomater. 87B (2008) 482–491.
[4] R.T.M de Rosales, R. Tavare, A. Glaria, G. Varma, A. Protti, P.J. Blower, (99m)Tc-bisphosphonate-iron oxide nanoparticle conjugates for dual-modality biomedical imaging, Bioconjugate Chem. 22 (2011) 455–465.
[5] V.A. Kabanov, A.B. Zezin, Soluble interpolyelectrolyte complexes as ne class of synthetic polyelectrolytes, Pure Appl. Chem. 56 (1984) 343–354.
[6] E. Tsuchida, Y. Osada, H. Ohno, Formation of interpolymer complexes, J. Macromol. Sci. B 17 (1980) 683–714.
[7] B. Philipp, H. Dautzenberg, K.J. Linow, J. Kötz, W. Dawydoff, Polyelectrolyte complexes – recent developments and open problems, Prog. Polym. Sci. 14 (1989) 91–172.
[8] M. Müller, B. Keßler, S. Richter, Preparation of monomodal polyelectrolyte complex nanoparticles of PDADMAC/poly(maleic acid-alt-alpha-methylstyrene) by consecutive centrifugation, Langmuir 21 (2005) 7044–7051.
[9] W. Tiyaboonchai, J. Woiszwillo, C.R. Middaugh, Formulation and characterization of amphotericin B-polyethylenimine-dextran sulfate nanoparticles, Pharm. Sci. 90 (2001) 902–914.
[10] DE 10 2010 003 615 A1 & WO 2011/121019 A2.
[11] J.A. Wong, K.W. Renton, J.F.S. Crocker, P.A. O'Regan, P.D. Acott, Determination of pamidronate in human whole blood and urine by reversed-phase HPLC with fluorescence detection, Biomed. Chromatogr. 18 (2004) 98–101.
[12] J. Chou, R. Shimmon, B. Ben-Nissan, Bisphosphonate determination using (1)H-NMR spectroscopy for biomedical applications, J. Tissue Eng. Regen. Med. 3 (2009) 92–96.
[13] B.M. Rao, M.K. Srinivasu, C.S. Rani, S.S. Kumar, P.R. Kumar, K.B. Chandrasekhar, M. Veerender, Validated stability indicating ion-pair RP-LC method for zoledronic acid, J. Pharm. Biomed. Anal. 39 (2005) 781–790.
[14] M. Müller, T. Rieser, K. Lunkwitz, S. Berwald, J. Meier-Haack, D. Jehnichen, An in situ ATR-FTIR study on polyelectrolyte multilayer assemblies on solid surfaces and their susceptibility to fouling, Macromol. Rapid Commun. 19 (1998) 333–336.
[15] T.F. Keller, M. Müller, W. Ouyang, J.T. Zhang, K.D. Jandt, Templating alpha-helical poly(l-lysine)/polyanion complexes by nanostructured uniaxially oriented ultrathin polyethylene films, Langmuir 26 (2010) 18893–18901.
[16] M. Müller, B. Keßler, Deposition from dopamine solutions at Ge substrates: an in situ ATR-FTIR study, Langmuir 27 (2011) 12499–12505.
[17] W. Ouyang, M. Müller, D. Appelhans, B. Voit, In situ ATR-FTIR investigation on the preparation and enantiospecificity of chiral polyelectrolyte multilayers, ACS Appl. Mater. Interfaces 1 (2009) 2878–2885.
[18] M. Müller, I. Grosse, H.J. Jacobasch, P. Sams, Surfactant adsorption and water desorption on thin cellulose films monitored by in situ ATR FTIR spectroscopy, Tenside Surfact. Det. 35 (1998) 354–435.
[19] H.H. Bauer, M. Müller, J. Goette, H.P. Merkle, U.P. Fringeli, Interfacial adsorption and aggregation associated changes in secondary structure of human calcitonin monitored by ATR-FTIR spectroscopy, Biochemistry 33 (1994) 12276–12282.
[20] M. Müller, B. Keßler, N. Houbenov, K. Bohata, Z. Pientka, E. Brynda, PH dependence and protein selectivity of poly(ethyleneimine)/poly(acrylic acid) multilayers studied by in situ ATR-FTIR spectroscopy, Biomacromolecules 7 (2006) 1285–1294.
[21] F. Alexis, S.L. Lo, S. Wang, Covalent attachment of low molecular weight poly(ethylene imine) improves tat peptide mediated gene delivery, Adv. Mater. 18 (2006) 2174–2178.
[22] M.S. Niepel, D. Peschel, X. Sisquella, J.A. Planell, T. Groth, pH-dependent modulation of fibroblast adhesion on multilayers composed of poly(ethylene imine) and heparin, Biomaterials 30 (2009) 4939–4947.
[23] S. Heinemann, C. Heinemann, R. Bernhardt, M. Meyer, A. Reinstorf, B. Nies, H. Worch, T. Hanke, Bioactive silica-collagen composite xerogels modified by calcium phosphate phases with adjustable mechanical properties for bone replacement, Acta Biomater. 5 (2009) 1979–1990.
[24] M. Nair, A. Bernhardt, A. Reinstorf, C. Heinemann, S. Thieme, T. Hanke, H.K. Varma, M. Gelinsky, A.J. John, A bioactive triphasic ceramic-coated hydroxyapatite promotes proliferation and osteogenic differentiation of human bone marrow stromal cells, J. Biomed. Mater. Res. A 90 (2009) 533–542.
[25] U.P. Fringeli, in: J.C. Lindon, G.E. Tranter, J.L. Holmes (Eds.), Encyclopedia of Spectroscopy and Spectrometry, Academic Press, 2000.
[26] N.J. Harrick, Internal Reflection Spectroscopy, Harrick, Ossining, NY, 1981.
[27] M. Müller, S. Paulik, *in situ*-ATR-FTIR and AFM studies on the influence of adsorption time on deposition and nanostructure of poly(ethyleneimine)/poly(acrylic acid) multilayers, Macromol. Symp. 265 (2008) 77–88.
[28] P.L. Ritger, N.A. Peppas, A simple equation for description of solute release. I. Fickian and non-Fickian release from non swellable devices in the form of slabs, spheres, cylinders or discs, J. Control. Release 5 (1987) 23–36.
[29] G.S. Manning, Limiting laws and counterion condensation in polyelectrolyte solutions. I. Colligative properties, J. Chem. Phys. 51 (1969) 924–933.
[30] A.S. Michaels, R.G. Miekka, Polycation-polyanion complexes – preparation and properties of poly(vinylbenzyltrimethylammonium)/poly(styrenesulfonate), Phys. Chem. 65 (1961) 1447–1455.
[31] H. Dautzenberg, Physical Chemistry of Polyelectrolytes, Surfactant Science Series 99, Radeva, 2001, pp. 743–792.
[32] M.C. Berg, L. Zhai, R.E. Cohen, M.F. Rubner, Controlled drug release from porous polyelectrolyte multilayers, Biomacromolecules 7 (2006) 357–364.
[33] A. Tiwari, S. Bindal, H.B. Bohidar, Kinetics of protein–protein complex coacervation and biphasic release of salbutamol sulfate from coacervate matrix, Biomacromolecules 10 (2009) 184–189.

Journal of Pharmaceutical and Biomedical Analysis 66 (2012) 191–196

Contents lists available at SciVerse ScienceDirect

Journal of Pharmaceutical and Biomedical Analysis

journal homepage: www.elsevier.com/locate/jpba

Inhibition of myeloperoxidase and antioxidative activity of *Gentiana lutea* extracts

Branislav Nastasijević[a,*], Tamara Lazarević-Pašti[a], Suzana Dimitrijević-Branković[b], Igor Pašti[c], Ana Vujačić[a], Gordana Joksić[a], Vesna Vasić[a]

[a] Department of Physical Chemistry, Vinča Institute of Nuclear Sciences, University of Belgrade, P.O. Box 522, 11001 Belgrade, Serbia
[b] Department of Bioengineering and Biotechnology, Faculty of Technology and Metallurgy, University of Belgrade, Karnegijeva 4, 11120 Belgrade, Serbia
[c] Faculty of Physical Chemistry, University of Belgrade, Studentski Trg 12-16, 11158 Belgrade, Serbia

ARTICLE INFO

Article history:
Received 27 January 2012
Received in revised form 27 March 2012
Accepted 28 March 2012
Available online 6 April 2012

Keywords:
Cyclic voltammetry
DPPH test
Gentiana lutea
Gentiopicoside
Myeloperoxidase
UPLC

ABSTRACT

The aim of this study was to investigate the inhibitory activity of *Gentiana lutea* extracts on the enzyme myeloperoxidase (MPO), as well as the antioxidant activity of these extracts and their correlation with the total polyphenol content. Extracts were prepared using methanol (100%), water and ethanol aqueous solutions (96, 75, 50 and 25% v/v) as solvents for extraction. Also, isovitexin, amarogentin and gentiopicroside, pharmacologically active constituents of *G. lutea* were tested as potential inhibitors of MPO. Antioxidant activity of extracts was determined using the 2,2-diphenyl-1-picrylhydrazyl (DPPH) scavenging test and also using cyclic voltammetry (CV). Among all extracts, the antioxidant capacity of 50% ethanol aqueous extract was the highest, both when measured using the DPPH test, with IC_{50} = 20.6 μg/ml, and when using CV. Also, 50% ethanol extract, showed the best inhibition of MPO activity in comparison with other extracts. In the group of the selected *G. lutea* constituents, gentiopicroside has proved to be the strongest inhibitor of MPO, with IC_{50} = 0.8 μg/ml. Also, the concentration of *G. lutea* constituents were determined in all extracts, using Ultra Performance Liquid Chromatography (UPLC).

© 2012 Elsevier B.V. All rights reserved.

1. Introduction

Gentiana lutea belongs to family of *Gentianaceae*, flowering plants comprising approximately 70–80 genera and 900–1200 species. It is a perennial herb commonly growing in mountainous areas of central and southern Europe and in western Asia [1,2]. It grows naturally on uncultivated ground in France, Spain and the Balkan mountains [3]. *Gentian radix* is an official drug in many pharmacopoeias and it is present commercially in the form of dried fermented rhizomes and roots. The active principles of *Gentiana* possess different pharmacological activities, ranging from anti-inflammatory to diuretic [1,4]. These properties can be attributed mainly to secoiridoid bitter compounds, such as gentiopicroside, amarogentin, swertiamarin and group of xanthones such as isovitexin and isogentisin [5–7]. It was shown in animal studies that roots of *G. lutea* demonstrate antihelmintic properties, while in rats, intragastric and intraduodenal administration of gentian extracts stimulates bile production [8–10].

In terms of enzyme inhibition *G. lutea* extracts and some of its constituents (isogentisine and isovitexin) showed inhibitory effects on monoamine oxidase type A and B and xanthine oxidase [6,11,12]. However, taking into account the anti-inflammatory properties of *Gentiana* extracts, it was desirable to explore its inhibitory effects on MPO activity. MPO (EC 1.11.2.2.) is a peroxidase enzyme released during degranulation of neutrophils and monocytes. Through catalyzing chloride ion oxidation to hypochlorous acid, MPO enables microbicidal action of neutrophils. However, in contrast to its beneficial activity, MPO also contributes to the development of many disorders, such as cardiovascular, inflammatory, neurodegenerative and immune-mediated diseases. Its impact on the process of athrogenesis, as well its role in the pathogenesis of lung cancer, Alzheimer's disease and multiple sclerosis has been previously reported [13–17].

MPO catalyzes the oxidation of various substrates with hydrogen peroxide (H_2O_2), producing oxidizing and halogenating agents [18,19]. Numerous nonsteroidal and anti-inflammatory drugs, anilines, and phenols inhibit MPO reversibly [20]. Therefore, alongside testing the extracts, some of *G. lutea* constituents were also investigated as potential inhibitors of MPO. For these purposes, gentiopicroside, amarogentin and isovitexin were selected, since they possess pharmacological activity.

For determining the antioxidative capacity of extracts, the DPPH scavenging test and CV were used. Thus, the results obtained using different antioxidative tests could be correlated to each other as well as with the total polyphenol content, with great accuracy. The content of total polyphenols was also determined, since

* Corresponding author. Tel.: +381 11 3408 872; fax: +381 11 8066 434.
E-mail address: branislav@vinca.rs (B. Nastasijević).

0731-7085/$ – see front matter © 2012 Elsevier B.V. All rights reserved.
http://dx.doi.org/10.1016/j.jpba.2012.03.052

numerous polyphenols, belonging to the class of iridoids, secoiridoids, xanthones and flavonoids are present in *G. lutea* root [21].

2. Materials and methods

2.1. Chemicals

Gentiopicroside (5-Ethenyl-6-(β-D-glucopyranosyloxy)-5,6-dihydro-1*H*,3*H*-pyrano[3,4-*c*] pyran-1-one), amarogentin (2-4aS-(4aα,5ß,6α))-3,3′,5-Trihydroxy-(1,1′-biphenyl)-2-carboxylate) and isovitexin (6-ß-D-Glucopyranosyl-5,7-dyxidroxy-2-(4-hydroxyphenyl)-4H-1-benzopyran-4-one) were purchased from ChromaDex (Irvine, USA). Acetonitrile and methanol were HPLC grade obtained from J.T. Baker (Deventer, Netherlands) and trifluoroacetic acid (TFA) was spectrophotometric grade (Aldrich). DPPH was obtained from Fluka Chemie AG Buchs (St. Louis, USA). Folin–Ciocalteu reagent used for total polyphenol content was bought from AppliChem-Biochemica (Darmstadt, Germany) and Gallic acid from Sigma–Aldrich. MPO from human neutrophils was obtained from Planta Natural Products (Vienna, Austria). It was purified to an Rz (A_{430}/A_{280}) 0.84, and its concentration was calculated using $\varepsilon_{430} = 91{,}000\ M^{-1}\ cm^{-1}$ per hemeHydrogen peroxide working solutions were prepared daily by diluting a 30% (w/v) stock solution and concentration was determined using $\varepsilon_{240} = 43.6\ M^{-1}\ cm^{-1}$ [22]. *O*-dianisidine dihydrochloride was purchased from Sigma–Aldrich (St. Louis, USA).

2.2. Plant material and extracts preparation

G. lutea roots were purchased from the Institute of Medicinal Plant Research "Dr Josif Pancic", Belgrade, Serbia. Five grams of grounded *Gentiana* roots were extracted with methanol, ethanol aqueous (96%, 75%, 50% and 25% v/v) solutions and water, in the ratio 1:5 (w/v). Extraction with ethanol aqueous solutions and with methanol was performed at room temperature, for 48 h, with occasional shaking. Water extract was prepared by heating in a boiling water bath for ten minutes. After filtering through 0.45 μm filter (Millipore Co. Ltd.) extracts were concentrated using a rotavapor at 35 °C and stored in sample tubes until analysis, in a dry place.

2.3. MPO inhibition

Peroxidase enzyme activity was monitored by the *o*-dianisidine assay at 25 °C. In the inhibition experiments, MPO (3 nM) was mixed with 50 mM phosphate buffer, pH 6.0. Extracts were incubated for 10 and 15 min with MPO and in both cases five minutes in the presence 0.53 mM *o*-dianisidine as enzyme substrate. The reaction was started by adding hydrogen peroxide, to a final concentration of 0.15 mM in the final volume of 700 μl assay mixture. The temperature in the cell was kept at 25 ± 1 °C by means of a thermostated-controlled water bath. Reference measurements were performed without inhibitors (control value). The spectrophotometric measurements were performed on a Perkin Elmer Lambda 35 UV–vis spectrophotometer, using 1 cm path length cuvettes. Absorbance at 460 nm was monitored for 1 min. The activity was determined from the linear slope of the progress curves obtained with an extinction coefficient of $\varepsilon_{460} = 11.3\ mM^{-1}\ cm^{-1}$ [22].

2.4. UPLC separation of G. lutea extracts

Waters ACQUITY Ultra Performance Liquid Chromatography (UPLC) system coupled with a TUV detector controlled by the Empower software was used. Extracts, as well gentiopicroside, were separated on an ACQUITY UPLCTM BEH C18 column (1.7 μm, 100 mm × 2.1 mm) in gradient mode, with the mobile phase consisting of solvent (A) TFA (0.1% v/v in water) and (B) acetonitrile–methanol mixture (85:15 v/v) starting from 5% to 95% of B, within 7 min, at room temperature. Absorbance was measured at 250 nm. The eluent flow rate was 0.3 ml/min, the injection volume was 10 μl. All extracts were standardized to a concentration of 0.1 mg/ml, and filtered through 0.22 μm nylon filter (Phenomenex) before injection.

2.5. DPPH radical-scavenging activity

The free radical scavenging capacity of the extracts, based on the scavenging activity of the DPPH free radical was determined by the method described by Brand Williams [23]. DPPH (7.8 mg) was dissolved in methanol (100 ml) to obtain a concentration of 78 μg/ml. The following concentrations of extracts were prepared: 0.1, 0.5, 1, 2.5, 5 and 10 mg/ml. Then, 50 μl of these extracts were diluted with methanol up to 4 ml, and then mixed with 1 ml of DPPH (0.2 mM solution). After 30 min, absorbance was measured at λ = 517 nm using a control prepared with water instead of extracts, against methanol as a blank. The inhibition of DPPH was calculated as:

$$\text{Inhibition}(\%) = 100 \times \frac{A_{\text{DPPH}} - A_{\text{sample}}}{A_{\text{DPPH}}}$$

where A_{DPPH} is the absorption of the DPPH control solution against the blank, and A_{sample} is the absorption of the extract against the blank. The extract concentration providing 50% of antioxidant activity (EC_{50}) was obtained by plotting the DPPH inhibition against the plant extract concentration.

2.6. Determination of total polyphenol content using Folin–Ciocalteu method

The total content of polyphenolics was determined by a colorimetric method described by Singleton and Rossi [24]. Extracts were diluted to a concentration of 1 mg/ml. Oxidation with Folin–Ciocalteu reagent (500 μl), was performed by mixing with 100 μl of each extract solution, followed by the addition of 2 ml of 15% Na_2CO_3. Reaction mixtures were diluted up to 10 ml with distilled water. Absorption was measured after 2 h at λ = 750 nm, against a blank, prepared with water, using the same procedures as for samples. Quantification of total polyphenols in the extracts, was made using gallic acid to establish a calibration curve, covering a range from 2 to 200 μg/ml. The results were expressed as mg of gallic acid equivalents per 100 g of dry weight of plant extract.

2.7. Cyclic voltammetry

CV measurements were performed at room temperature using a Gamry PCI-4/750 system (Gamry, USA) in one-compartment three-electrode electrochemical cell with glass carbon (GC) disk (base surface area 0.19625 cm^2) as a working electrode, and a saturated calomel electrode (SCE) as a reference one. Pt foil was used as a counter electrode large area. Prior to each measurement the GC disk was polished with diamond paste (1–2 μm particles) and thoroughly washed with ethanol and deionized water. Reproducibility of electrode preparation was confirmed by recording background currents in inert electrolyte, namely 0.1 M K_2SO_4 solution, prior to each measurement. Plant extracts (1 ml, concentration 20 mg/ml) were diluted in 0.1 M K_2SO_4 solution (10 ml) and these solutions were subjected to electrochemical measurements. Cyclic voltammograms were recorded at a scan rate 100 mV s^{-1}, in the potential window between −0.4 and 1.2 V *vs.* SCE. Prior to and during each experiment solutions were purged with high-purity N_2.

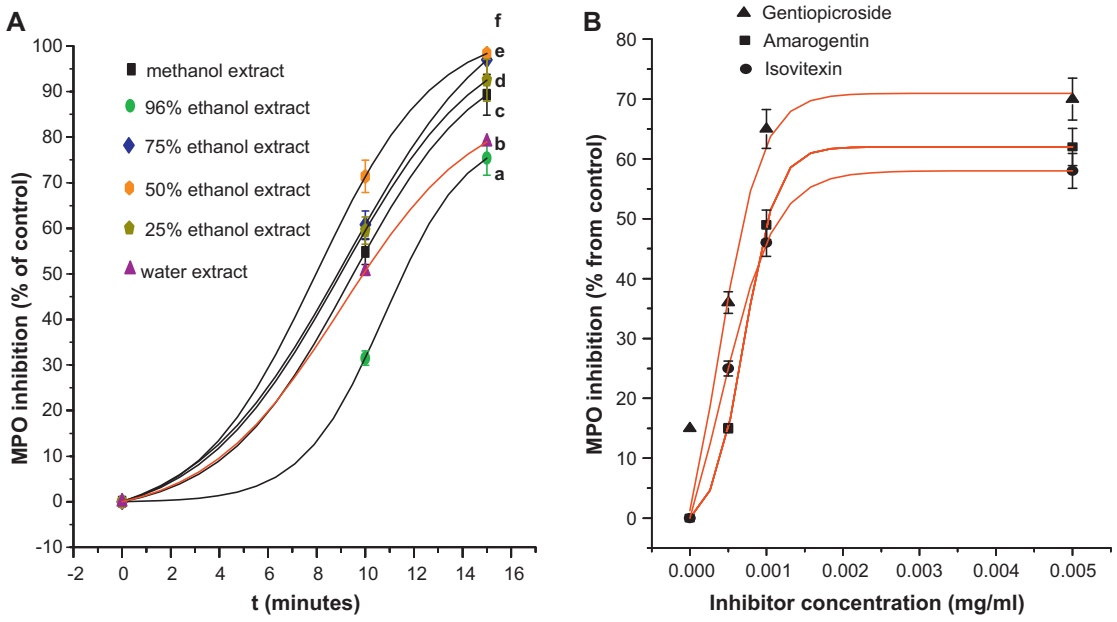

Fig. 1. Inhibition of MPO activity (as a function of the time (A) and of inhibitor concentration (B)) by the: (A) *Gentiana lutea* extracts (0.01 mg/ml) in the presence of 53 mM *o*-dianisidine as substrate in: (a) 96% ethanol-aqueous, (b) water extract, (c) methanol, (d) 25% ethanol-aqueous, (e) 75% ethanol-aqueous, (f) 50% ethanol-aqueous extract; and by (B) gentiopicroside; isovitexin and amarogentin, in the presence of 53 mM *o*-dianisidine. The inhibition curves of constituents were obtained for concentrations ranging from 1×10^{-5} to 1×10^{-3} mg/ml. IC_{50} values were calculated from equations obtained by sigmoidal curve fitting. The results present the mean values obtained in three experiments performed in duplicate.

3. Results and discussion

Investigation of MPO inhibition activity, antiradical activity and total polyphenol content was directed mainly toward *G. lutea* extracts which are traditionally used in folk medicine and as an auxiliary means of healing in alternative medicine. Consequently, except methanol extract, all other extracts were prepared with ethanol or water as solvents, due their common usage in alcohol tinctures, and alcoholic beverages, as well in the form of tea (water decoctions).

3.1. Inhibition of MPO activity

The influence of *G. lutea* extracts on MPO activity was investigated at a concentration of 0.01 mg/ml for each extract as the function of the incubation time in the intervals of 15 min. The results, presented as percentage of inhibition of control are shown in Fig. 1A. They indicate that the percent of enzyme inhibition increased with incubation time, reaching a plateau after 15 min incubation. Among all the extracts tested, the most potent MPO inhibitors were 50% ethanol-aqueous extract and 75% ethanol extract, since they induced almost 100% inhibition of the enzyme activity, respectively, after 15 min of exposure. However, results of MPO inhibition obtained for shorter incubation times enable clearer insight of the enzyme inhibition and revealed that 50% ethanol extract is the strongest inhibitor of MPO among the extracts examined. It inhibits 71% of MPO activity after 10 min of exposure, in contrast with 96% ethanol extract which inhibits only 31% of MPO activity for the same incubation time. Previous studies have demonstrated that some anti-inflammatory drugs may inhibit MPO activity. Therefore the inhibitory ability of *Gentiana* extracts toward MPO leads to the conclusion that these extracts can be considered to exert an anti-inflammatory effect [25]. This information may be useful in the preparation process of products based on *Gentiana* root for its traditionally use in folk medicine.

In addition to anti-inflammatory drugs with inhibition ability toward MPO, numerous phenolic acids derivatives as quercetin, curcumin, ferulic, caffeic and gallic have demonstrated a strong MPO inhibition [26]. Accordingly to that, it was desirable to examine whether some *Gentiana* constituents would exhibit a similar effect. Hence, gentiopicroside, isovitexin and amarogentin were selected as potential MPO inhibitors, since these pharmacologically active compounds are usually present in *G. lutea* extracts. IC_{50} values, which represent the inhibitor concentrations that induced 50% inhibition of MPO activity, were obtained from the analysis of sigmoid shaped inhibition curves. In the group of the selected compounds, gentiopicroside showed the highest level of inhibition with $IC_{50} = 0.8 \pm 0.1$ μg/ml, followed by isovitexin ($IC_{50} = 2.2 \pm 0.1$ μg/ml) and amarogentin ($IC_{50} = 2.4 \pm 0.1$ μg/ml).

In order to determine the contribution of the aforementioned constituents to MPO inhibition, mixtures of gentiopicroside, isovitexin and amarogentin were investigated as inhibitors. The results obtained were compared with the results of MPO inhibition obtained with each of these constituents separately and they are shown in the Table 1. Results show that mixture of isovitexin and amarogentin is significantly less potent MPO inhibitor than the three other mixtures. It is evident that the presence of gentiopicroside in the mixtures leads to an increase in the degree (% from control) of inhibition.

Table 1
Inhibition of MPO activity obtained with the single constituents and their mixtures: (I) Amarogentin and Isovitexin, (II) Amarogentin and Gentiopicroside, (III) Isovitexin and Gentiopicroside and (IV) Amarogentin, Isovitexin and Gentiopicroside. Concentration of each constituent individually and each of them in the mixtures was 0.001 mg/ml, within 10 minutes of incubation with enzyme.

Type of inhibitor	MPO inhibition (% from control)
Amarogentin	49 ± 2
Isovitexin	46 ± 2
Gentiopicroside	65 ± 3
I	18 ± 1
II	44 ± 2
III	46 ± 2
IV	43 ± 2

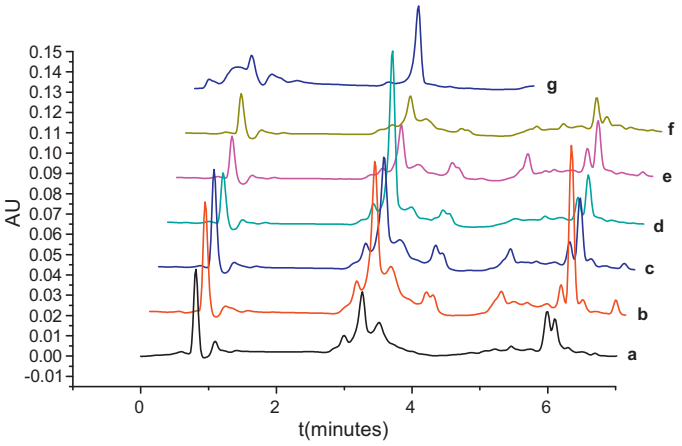

Fig. 2. UPLC chromatograms of *Gentiana lutea* extracts and gentiopicroside standard: (a) 25% ethanol-aqueous, (b) 50% ethanol-aqueous, (c) 75% ethanol-aqueous, (d) 96% ethanol-aqueous, (e) methanol, (f) water extract and (g) Gentiopicroside (0.01 mg/ml). A peak with the retention time of 3.25 min was identified in all extracts, and was ascribed to gentiopicroside.

This is in accordance with the results obtained with the inhibition of MPO with an individual constituent (Fig. 1B) which also show that gentiopicroside has the strongest inhibitory activity against MPO. In addition, the obtained IC_{50} values for the investigated constituents can be compared with the inhibitory activity of the other polyphenolic compounds such as quercetin, whose IC_{50} is 0.33 μg/ml [20]. This data could be interesting for further investigations since the capability of enzyme inhibition could be structure dependent, as quercetin belongs to a class of flavonoids while gentipoicroside belongs to secoiridoids, the predominating class of compounds in *Gentiana* root [21].

3.2. UPLC analysis

Since gentiopicroside exerted the strongest inhibitory activity against MPO, the amount of this compound was determined in all *G. lutea* extracts. For this purpose UPLC was used and a novel method for its separation was developed. An additional explanation for elution method is given in Section 2.4. Extracts were run at concentrations of 0.1 mg/ml and their UPLC chromatograms are presented in the Fig. 2a–f. Standard solutions of gentiopicroside were run in concentrations from 0.005 to 0.03 mg/ml. Quantification of gentiopicroside was done by comparing retention times and peak areas of samples to peak areas of standards. It is obvious that all ethanolic extracts contained higher concentration of gentiopicroside than water and methanol extracts. The highest amount of gentiopicroside was present in 96% and 50% ethanol aqueous extracts (18.08 and 13.92%, respectively) while the water and methanol extracts contained 7.79 and 6.53% of gentiopicroside, respectively. That was also confirmed in other studies where the highest amount of gentiopicroside was extracted with a mixture of ethanol and water (55:45 v/v). At the same time the efficiency of gentiopicroside extraction was correlated with increasing of extraction temperatures [27].

Finally, it is also likely that increased inhibitory activity of ethanolic extracts, toward MPO, could be dependent on higher concentration of gentiopicroside. This hypothesis is supported by our results obtained for MPO inhibition with the mixture of *Gentiana* constituents.

3.3. DPPH radical-scavenging capacity and total phenolic content

The scavenging activity of the DPPH free radical test revealed that 50% and 75% ethanol water extracts have the highest antiradical activity with the IC_{50} values of 20.6 μg/ml and 25.4 μg/ml, respectively. Water and 96% ethanol extracts had the lowest antiradical activity (Table 2). For comparison, other studies have shown the antioxidant capacity of other compounds, determined with DPPH test and expressed as IC_{50}: 3.2 μg/ml for quercetin, 10.62 μg/ml for α-tocopherol and 9.4–40.1 μg/ml for ethanolic extracts of *Salvia fruticosa* IC_{50} [28,29]. The antioxidant activity of *Gentiana* root is, however only moderate in comparison with some other plant extracts which contain higher amounts of flavonoids. *Gentiana* in contrast, contains mainly secoiridoides, xanthones, and isoflavonoids and dihydroxybenzoic acids [21,30–32]. Similar results were obtained by Kintizos et al. in a comparative study using the DPPH antioxidant test and cell based biosensor [33]. The total phenolic content of *Gentiana lutea* extracts was determined using the Folin–Ciocalteau method which allows the estimation of all flavonoids, anthocyanins and nonflavonoid phenolics present in the samples. As shown in the Table 2, water extract, as well 50% ethanol-aqueous extract had the highest phenolic content. Generally, increasing solvent polarity results in an improved extraction of polyphenols from plants [34]. Moreover, in some cases, depending on the plant material and its polyphenol composition larger amounts of polyphenols can be extracted with a mixture of ethanol and water than those extracted only with water [35].

Table 2
Antiradical activity of *Gentiana lutea* extracts obtained by the DPPH test and total polyphenol content of these extracts.[a]

Type of extract	DPPH IC_{50} inhibition (μg/ml)	Total polyphenol content[b] (mg/g)
25% ethanol	36.1 ± 0.6	78.1 ± 0.4
50% ethanol	20.6 ± 0.4	96.1 ± 1.2
75% ethanol	25.4 ± 0.9	74.4 ± 0.6
96% ethanol	82.4 ± 1.1	58.3 ± 0.4
Methanol	48.4 ± 0.4	51.1 ± 0.5
Water extract	77.2 ± 0.8	99.6 ± 0.9

[a] Data are represented as means ± standard deviation of three independent experiments.
[b] Total phenolic content was expressed as mg of Gallic acid equivalents per 100 g dry weight of extracts.

Regardless of that, it was expected that the higher content of polyphenols in the extracts entails their greater antioxidant capacity. However, this was not confirmed by measuring of DPPH inhibition activity in all cases. A weak linear correlation between the total polyphenols content and DPPH inhibition was observed ($r = -0.18$). Furthermore, strong DPPH inhibition by the water extract was expected, since it had a high content of total polyphenols (Table 2). Therefore, the antioxidant capacity of the extracts was also determined using CV. Using more than one method for determination of the antioxidative capacity is also justified because of the limitations of each test [33,36]. Namely, even though the DPPH assay is widely used for measuring and comparing of the antioxidant status of phenolic compounds, the results obtained, should be carefully interpreted. The absorbance of DPPH radical at 517 nm, after reaction with antioxidants is changeable with light, oxygen, pH, and type of solvent [37]. A difference between the antioxidative capacity when it has been determined by chemical test and by biological test, such as cell based biosensor method, has been observed [33]. Therefore, it is essential to determine the antioxidative activity using at least two methods, and then make a final and more comprehensive evaluation of their activity.

3.4. CV measurement of antioxidant capacity

CV did not revealed any faradaic processes at potentials lower than ~330 mV *vs.* SCE, for any of the plant extract solutions studied here. Furthermore, the electrochemical response was not observed

Table 3
Electrochemical characteristics of anodic oxidation processes of the plant extracts studied (E_{onset} – potential at which oxidation processes start, $E_{p,a}$ – potential of the first anodic peak, Q_1 – charge associated with oxidation process between E_{onset} and 600 mV *vs*. SCE, Q_{tot} – total charge under anodic wave).

Sample	E_{onset}/mV *vs*. SCE	$E_{p,a}$/mV *vs*. SCE	Q_1/μC	Q_{tot}/μC
25% EtOH extract	355	486	2.63	45.3
50% EtOH extract	334	484	4.03	37.0
75% EtOH extract	359	527	2.18	19.7
96% EtOH extract	395	–	0.52	17.4
MeOH extract	400	–	0.43	11.7

in the case of the water extract. Hence, that sample will not be discussed further in this section. Oxidation processes were observed to start in the potential window between 330 and 400 mV *vs*. SCE (E_{onset}; Table 3). Some samples revealed a small anodic peak at potentials below 600 mV *vs*. SCE, while the others displayed monotonic increase of anodic current with no distinct characteristics. The CV curves obtained here displayed irreversible behavior with no reverse cathodic peaks observable. Where possible, the first anodic peak was characterized in terms of the peak potential ($E_{p,a}$) (Table 3). In CV experiments, the antioxidant capacity of a particular compound or a complex mixture is related to the low potentials at which the oxidation commences.

In relation to the appropriateness of parameters derived from CV experiments for the assessment of antioxidant capacity, Chevion et al. proposed that the total charge under anodic peaks should be used as a measure of the content of low-molecular-weight antioxidants, especially when more than a single molecule contributes a specific anodic wave and the identities of the components of a wave are not known [38]. Therefore, $E_{p,a}$ of the first anodic peak is considered as a relevant measure of the antioxidant capacity. In addition to the parameters listed above, we also integrated recorded CV curves up to 600 mV *vs*. SCE (Q_1) and included the results obtained, summarized in Table 3 and presented in Fig. 3. We consider this parameter to be appropriate for the assessment of both antioxidant capacity and total polyphenol concentration. The rationale is found in the theory of CV and linear sweep voltammetry. Results obtained by CV were correlated to the ones obtained by the DPPH test (in terms of DPPH IC_{50} values, Section 3.3) and the ones regarding total polyphenol content (Section 3.3), which is usually considered to be responsible for the antioxidant capacity and was found to correlate well with DPPH radical scavenging activity [39]. It should be noted that the correlation between these parameters was performed without taking into account the water extract, since its electrochemical signal was not detected.

It was clear that Q_1 values correlated strongly IC_{50} DPPH values, with Pearson correlation coefficient $r = -0.80$, which was somewhat better than correlation with the total polyphenol content ($r = -0.73$). E_{onset} values were also very well correlated to DPPH IC_{50} values, giving $r = 0.81$. Q_{tot} values showed much lower correlation with DPPH IC_{50} values, with $r = -0.49$. Excellent correlation of Q_1 values to total polyphenol content ($r = 0.99$) was noticed, while Q_{tot} correlated to the total polyphenol content with $r = 0.78$. An additional explanation, about correlation between DPPH IC_{50} values with CV parameters (Q_1 and Q_{tot} values) as well their correlation between total polyphenol content is given in the Supplementary material. The results obtained confirmed that only electrochemical response at low potentials, in terms of charge passed is important for estimation of the antioxidant capacity of a complex mixture and that rather simple CV measurements can be used for rapid evaluation of the antioxidative activity of the plant constituents studied.

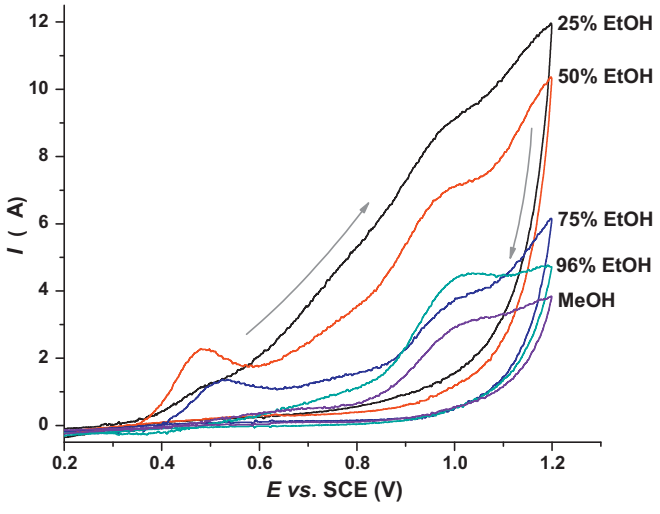

Fig. 3. Background-corrected cyclic voltammograms of plant extracts in 0.1 M K_2SO_4 solution, recorded on GC electrode, sweep rate 100 mV s^{-1}. Only the potential window between 0.2 and 1.2 V *vs*. SCE is shown as electrochemical response is located in this potential window.

4. Conclusion

Results demonstrate that 50% ethanol extract has the best inhibition activity toward MPO, and the highest antioxidant activity with the lowest IC_{50} = 20.6 μg/ml (DPPH determined). Its antioxidant activity could be attributed to the increased content of total polyphenols. This dependence was also confirmed by results obtained with CV, where the highest Q_1 potential under first anodic peak corresponds to high phenolic content of 50% ethanol extract. Among the group of selected *G. lutea* constituents, gentiopicroside is the most potent inhibitor of MPO, with IC_{50} = 0.8 μg/ml. Additional studies are needed to demonstrate whether the MPO inhibitory activity of *Gentiana* extracts depends mainly on gentiopicorside or whether it is due to synergistic effects of several components. Since inhibition of MPO is associated with antiinflamatory effects, our results obtained could be useful for the future rapid evaluation of the healing properties of *Gentiana* root. This is particularly important since this method of extraction (with alcohol and water) is commonly used in traditional medicine.

Acknowledgments

The authors would like to thank to the Ministry of Education and Science of the Republic of Serbia for their financial support, Project No 172023, as well as to the FUNCFOOD (FP7) project.

Appendix A. Supplementary data

Supplementary data associated with this article can be found, in the online version, at http://dx.doi/org10.1016/j.jpba.2012.03.052.

References

[1] A. Singh, Phytochemicals of gentianaceae: a review of pharmacological properties, Int. J. Pharm. Sci. Nanotechnol. 1 (2008) 33–36.
[2] European Medicines Agency (EMA), Assessment report on *Gentiana lutea* L., radix, Doc. Ref.: EMA/HMPC/578322/2008, 2009.
[3] R. Hänsel, O. Sticher, Pharmakognosie – Phytopharmazie, 8th ed., Springer Medizin Verlag, Heidelberg, 2007.
[4] A. Mathew, A.D. Taranalli, S.S. Torgal, Evaluation of anti-inflammatory and wound healing activity of *Gentiana lutea* rhizome extracts in animals, Pharm. Biol. 42 (2004) 8–12.
[5] N. Ozturk, S. Korkmaz, Y. Ozturk, K.H.C. Baser, Effects of Gentiopicroside, sweroside and swertiamarine, secoiridoids from gentian (*Gentiana lutea* ssp. symphyandra), on cultured chicken embryonic fibroblasts, Planta Med. 72 (2006) 289–294.

[6] C.M. Lin, C.T. Chen, H.H. Lee, J.K. Lin, Prevention of cellular ROS damage by isovitexin and related flavonoids, Planta Med. 68 (2002) 365–367.
[7] A. Schmieder, S. Schwaiger, A. Csordas, A. Backovic, B. Messner, G. Wick, H. Stuppner, D. Bernhard, Isogentisin – a novel compound for the prevention of smoking-caused endothelial injury, Atherosclerosis 194 (2007) 317–325.
[8] C. Lans, N. Turner, T. Khan, G. Brauer, Ethnoveterinary medicines used to treat endoparasites and stomach problems in pigs and pets in British Columbia, Canada, Vet. parasitol. 148 (2007) 325–340.
[9] Radix *Gentianae luteae*, in: WHO Monographs on Selected Medicinal Plants, World Health Organisation, Geneva, 2007, pp. 150–159.
[10] Z.W. Liu, C.X. Chen, R.M. Jin, G.Q. Shi, C.Q. Song, Z.B. Hu, Studies on liver-protecting and bile secretion-promoting effects of Gentiopicroside, Zhong Cao Yao 33 (2002) 47–50.
[11] H. Haraguchi, Y. Tanak, A. Kabbash, T. Fujioka, T. Ishizu, A. Yagi, Monoamine oxidase inhibitors from *Gentiana lutea*, Phytochemistry 65 (2004) 2255–2260.
[12] O. Suzuki, Y. Katsumata, M. Oya, V.M. Chari, R. Klapfenberger, H. Wagner, K. Hostettmann, Inhibition of type A and type B monoamine oxidase by isogentisin and its 3-o-glucoside, Planta Med. 39 (1980) 19–23.
[13] J.D. Smith, Myeloperoxidase, inflammation, and dysfunctional high-density lipoprotein, J. Clin. Lipido. 4 (2010) 382–388.
[14] S.J. Klebanoff, Myeloperoxidase: friend and foe, J. Leukos. Biol. 77 (2005) 598–625.
[15] I. Chevrier, I. Stücker, A.M. Houllier, S. Cenée, P. Beaune, P. Laurent-Puig, M.A. Loriot, Myeloperoxidase: new polymorphisms and relation with lung cancer risk, Pharmacogenetics 13 (2003) 729–739.
[16] W.F. Reynolds, M. Hiltunen, M. Pirskanen, A. Mannermaa, S. Helisalmi, M. Lehtovirta, I. Alafuzoff, H. Soininen, MPO and APOEε4 polymorphisms interact to increase risk for AD in Finnish males, Neurology 55 (2000) 1284–1290.
[17] R.M. Nagra, B. Becher, W.W. Tourtellotte, J.P. Antel, D. Gold, T. Paladino, R.A. Smith, J.R. Nelson, W.F. Reynolds, Immunohistochemical and genetic evidence of myeloperoxidase involvement in multiple sclerosis, J. Neuroimmunol. 78 (1997) 97–107.
[18] T. Lazarevic-Pašti, M. Čolović, J. Savić, T. Momić, V. Vasić, Oxidation of diazinon and malathion by myeloperoxidase, Pestic. Biochem. Physiol. 100 (2011) 140–144.
[19] T. Lazarević-Pašti, B. Nastasijević, V. Vasić, Oxidation of chlorpyrifos, azinphos-methyl and phorate by myeloperoxidase, Pestic. Biochem. Physiol. 101 (2011) 220–226.
[20] T. Momić, Z. Vujčić, V. Vasić, Kinetics of inhibition of peroxidase activity of MPO by quercetin, Int. J. Chem. Kinet. 40 (2008) 384–394.
[21] A. Aberham, V. Pieri, E.M. Croom Jr., E. Ellmerer, H. Stuppner, Analysis of iridoids, secoiridoids and xanthones in Centaurium erythraea, Frasera caroliniensis and *Gentiana lutea* using LC–MS and RP-HPLC, J. Pharm. Biomed. Anal. 54 (2011) 517–525.
[22] P.P. Bradley, D.A. Priebat, R.D. Christensen, G. Rothstein, Measurement of cutaneous inflammation: estimation of neutrophil content with an enzyme marker, J. Invest. Dermatol. 78 (1982) 206–209.
[23] W. Brand-Williams, M.E. Cuvelier, C. Berset, Use of a free radical method to evaluate antioxidant activity, Lebensmittel Wissenschaft und Technologie, Food Sci. Technol. 28 (1995) 25–30.
[24] V.L. Singleton, A. Rossi, Colorimetry of total phenolics with phosphomolybdic-phosphotungstic acid reagents, Am. J. Enol. Viticult. 16 (1965) 144–158.
[25] T.O. Vieira, I. Seifriz, C.C.T. Charao, S.Q. Oliveira, T.B. Creczynski-Pasa, Antioxidant effects of crude extracts from *Baccharis* species: inhibition of myeloperoxidase activity, protection against lipid peroxidation, and action as oxidative species scavenger, Rev. Bras. Farmacogn. 21 (2011) 601–607.
[26] Y. Kato, A. Nagao, J. Terao, T. Osawa, Inhibition of myeloperoxidase-catalyzed tyrosylation by phenolic antioxidants in vitro, Biosci. Biotechnol. Biochem. 67 (2003) 1136–1139.
[27] A. Arino, I. Arberas, J. Leiton, M. de Renobales, J.B. Dominguez, The extraction of yellow gentian root (*Gentiana lutea*), Z. Lebensm Unters. Forsch. A 205 (1997) 295–299.
[28] Pasias, E. Farmaki, N. Thomaidis, E. Piperaki, Elemental content and total antioxidative activity of Saliva Fruticosa, Food Anal. Method 3 (2010) 195–204.
[29] I. Gulcin, R. Elias, A. Gepdiremen, K. Taoubi, E. Koksal, Antioxidative secoiridoids from fringe three (*Chionantus virginicus* L.), Wood Sci. Technol. 43 (2009) 195–212.
[30] C.A. Calliste, P. Trouillas, D.P. Allais, A. Simon, J.L. Duroux, Free radical scavenging activities measured by electron spin resonance spectroscopy and B16 cell antiproliferative behavior of seven plants, J. Agric. Food Chem. 49 (2001) 3321–3327.
[31] N. Menković, K. Šavikin-Fodulović, K. Savin, Chemical composition and seasonal variations in the amount of secondary compounds in *Gentiana lutea* leaves and flowers, Planta Med. 66 (2000) 178–180.
[32] S. Khadem, R.J. Marles, Monocyclic phenolic acids, hydroxy- and polyhydroxybenzoic acids: occurrence and recent bioactivity studies, Molecules 15 (2010) 7985–8005.
[33] S. Kintzios, K. Papageorgiou, I. Yiakoumettis, D. Baričević, A. Kušar, Evaluation of the antioxidants activities of four Slovene medicinal plant species by traditional and novel biosensory assays, J. Pharm. Biomed. Anal. 53 (2010) 773–776.
[34] N. Turkmen, Y.S. Velioglu, F. Sari, G. Polat, Effect of extraction conditions on measured total polyphenol contents and antioxidant and antibacterial activities of black tea, Molecules 12 (2007) 484–496.
[35] D. Franco, J. Sineiro, M. Rubilar, M. Sánchez, M. Jerez, M. Pinelo, N. Costoya, M.J. Núñez, Polyphenols from plant materials: extraction and antioxidant power, Eur. J. Environ. Agric. Food Chem. 7 (2008) 3210–3216.
[36] R. Apak, K. Guclu, B. Demirata, M. Ozyurek, S.E. Celik, B. Bektasoglu, K.I. Berker, D. Ozyurt, Comparative evaluation of various total antioxidant capacity assays applied to phenolic compounds with the CUPRAC assay, Molecules 12 (2007) 1496–1547.
[37] B. Ozcelik, J.H. Lee, D.B. Min, Effects of light, oxygen, and pH on the absorbance of 2,2-diphenyl-1-picrylhydrazyl, J. Food Sci. 68 (2003) 487–490.
[38] S. Chevion, M. Chevion, P.B. Chock, G.R. Beecher, Antioxidant capacity of edible plants: extraction protocol and direct evaluation by cyclic voltammetry, J. Med. Food 2 (1999) 1–10.
[39] C. Anesini, G.E. Ferraro, R. Filip, Total polyphenol content and antioxidant capacity of commercially available tea (*Camellia sinensis*) in Argentina, J. Agric. Food Chem. 56 (2008) 9225–9229.

Journal of Pharmaceutical and Biomedical Analysis 66 (2012) 197–203

Contents lists available at SciVerse ScienceDirect

Journal of Pharmaceutical and Biomedical Analysis

journal homepage: www.elsevier.com/locate/jpba

Development of an ultrasonic slurry sampling method for the determination of Cu and Mn in antibiotic tablets by electrothermal atomic absorption spectrometry

Carlos Eduardo R. de Paula, Luiz Fernando S. Caldas, Daniel M. Brum, Ricardo J. Cassella *

Departamento de Química Analítica, Universidade Federal Fluminense, Outeiro de São João Batista s/n, Centro, Niterói, RJ, 24020-141, Brazil

ARTICLE INFO

Article history:
Received 5 March 2012
Received in revised form 30 March 2012
Accepted 31 March 2012
Available online 7 April 2012

Keywords:
Pharmaceuticals
Slurry sampling
Electrothermal atomic absorption spectrometry
Copper
Manganese

ABSTRACT

A new method is described for simple, efficient and rapid determination of Cu and Mn in tablets of antibiotics (ciprofloxacin and cephalexin) by electrothermal atomic absorption spectrometry (ETAAS) using slurry sampling. In order to optimize the procedure, several variables that could affect the performance of the method were investigated. In the best conditions, the tablets could be analyzed by introducing into the graphite tube 20 μl of a slurry prepared with approximately 90–100 mg of the sample and 2 ml of a solution containing 5% m/v of Triton X-114 and 2.8 M of HNO_3. Before the introduction, the slurries were sonicated for 15 min at 40% of amplitude (130 W maximum power) with an ultrasonic probe. The developed method was applied in the determination of Cu and Mn in four samples, and the results were compared with those obtained by focused microwave acid digestion with aqua regia (1:3 mixture of HNO_3:HCl). There was no statistical difference between the obtained values at 95% confidence level when a paired Student *t*-test was applied.

© 2012 Elsevier B.V. All rights reserved.

1. Introduction

One of the most important steps in the production of pharmaceuticals is the quality control, which is the step that ensures their safe use [1]. According to the Brazilian Pharmacopeia [2], three assays must be carried out to attest the quality of a medicine: (i) identification, (ii) dosing of the active principle and (iii) purity. The tests to verify the presence of inorganic contaminants such as chlorides, sulfates and metals are included in these assays and make part of the common analysis of the raw materials and final products.

Manganese and copper are considered essential elements for living organisms [3]. However, their ingestion (or exposure) in high amounts can cause serious problems to the human health. Manganese is associated with neurological dysfunctions and pulmonary problems [4,5], while copper can damage the liver and kidneys [6].

Brazilian Pharmacopeia [2] indicates that the determination of metals in medicines can be performed by two different approaches. The first approach is a non-selective and semi-quantitative assay that is based on the precipitation of metallic cations with sulfide ion. In this assay, a visual comparison between the standard (precipitate of PbS) and the sample is carried out to decide if the limit (20 $\mu g\,g^{-1}$, total metal content) is achieved or not. Obviously, several problems can be pointed out for this kind of procedure such as the lack of selectivity and the great influence that the experience of the analyst has on the results [7–9]. Another possibility is to determine the metals in the samples using atomic spectrometric techniques. In this case, the methods are selective for each element of interest and have convenient sensitivity, making possible the identification and quantification of individual species in the samples. Recently, the Brazilian Pharmacopeia has established a limit for the content of Cu and Mn, among other metals, in oral medicines and in parenteral solutions that are 250 $\mu g\,g^{-1}$ and 25 $\mu g\,g^{-1}$, respectively, for both elements.

In general, the employment of atomic spectrometric techniques for the determination of metals in solids (as some tablets of antibiotics) requires a previous step of treatment of the samples that should be applied to convert them into a convenient form before introduction into the instrument. This step is, in most cases, laborious and time-consuming. Besides, it is subjected to some problems such as the contamination of the samples during their handling and losses [10]. Several strategies have been used to decompose (or dissolve) solid samples of pharmaceuticals for the analysis by atomic spectrometric techniques. Classical procedures commonly used for this task are the acid digestion with conventional or microwave assisted heating, and the dry ashing at high temperatures [11–13].

The use of the slurry sampling approach can be considered a good alternative to the decomposition of the samples because it does not require the destruction of the matrix, which simplifies

* Corresponding author. Tel.: +55 21 2629 2222; fax: +55 21 2629 2143.
E-mail address: cassella@vm.uff.br (R.J. Cassella).

0731-7085/$ – see front matter © 2012 Elsevier B.V. All rights reserved.
http://dx.doi.org/10.1016/j.jpba.2012.03.057

Table 1
Operational conditions employed in the determination of Cu and Mn in the slurries by ETAAS.

Parameter	Copper	Manganese
Wavelength (nm)	324.8	403.1
Lamp current (mA)	4	5
Slit width (nm)	0.5	0.2
Purge gas	Argon	Argon

the whole procedure. The main advantages of the slurry sampling strategy are the simplification of the sample treatment, the minimization of contamination risks and analytes losses, the use of less aggressive reagents and the possibility of application to organic and inorganic samples [14].

Nowadays, there are a number of papers regarding the application of the slurry sampling approach to the direct analysis of different kinds of solid samples, such as geological materials [15–17], glasses [18], foods [19–21], biological materials [22–24] and others [25–28], by ETAAS. However, to the best of our knowledge, there is no application of such strategy in the determination of trace metals in solid medicine samples as the tablets of antibiotics analyzed in this present work. So, the goal of this work was to optimize a method for the determination of trace concentrations of Cu and Mn, as contaminants, in tablets of some antibiotics (cephalexin and ciprofloxacin) using the slurry sampling approach and ETAAS. Also, a study was performed to evaluate the influence of the sonication (time and power) of the slurry on the performance of the method.

2. Experimental

2.1. Apparatus

All measurements were carried out with a Varian (Mulgrave, Australia), model AA240Z, electrothermal atomic absorption spectrometer equipped with a Varian GTA 120 atomizer unit and a Varian PSD 120 autosampler. The background correction was performed with a Zeeman effect-based background corrector with a constant magnetic field strength of 0.8 T.

The atomization was carried out directly from walls of the graphite tubes using a tubes made of electrolytic graphite covered with pyrolytic graphite also supplied by Varian. Monoelementar hollow cathode lamps of copper and manganese were used as light sources and Argon (99.99% grade), supplied by Linde Gases (Macaé, Brazil), was employed as protective gas. The operational conditions of the instrument for the measurements are summarized in Table 1.

The slurries were prepared with the aid of an ultrasound processor, furnished by Sonics (Newtown, CT, USA), model VCX 130, equipped with a titanium probe with 6 mm diameter.

The acid dissolution of the samples was carried out with a focused microwave oven supplied by CEM (Matthews, NC, USA), model Star 2, using quartz flasks. It is important to remark that the microwave oven was coupled to a scrubber unit in order to avoid the emission of acid gases.

An analytical balance with 0.1 mg precision, model AY-220, from Shimadzu (Tokyo, Japan) was employed.

2.2. Reagents and solutions

All solutions and slurries were prepared with purified water (18.2 MΩ cm) obtained with a DirectQ-3 system, supplied by Millipore (Bedford, MA, USA).

Analytical solutions of Cu and Mn were prepared from adequate dilution of the individual standard stock solutions with 1000 mg l^{-1} concentration of each metal, supplied by Tedia (Fairfield, OH, USA).

Table 2
Heating program employed in the acid dissolution of the samples.

Stage	Temperature (°C)	Ramp (min)	Hold (min)
1	90	3	10
2	110	1	15

Diluted nitric acid solutions were prepared by convenient dilution of concentrated HNO_3 (P.A. grade), furnished by Tedia, using purified water.

The aqueous solution used in the preparation of the slurries (5% m/v Triton X-114 in 2.8 M HNO_3) was prepared by dissolving 5 g of Triton X-114 (Acros Organics, St. Louis, USA) in approximately 50 ml of 2.8 M HNO_3 solution. After total dissolution of the surfactant and foam decrease, the obtained solution was transferred to a 100 ml volumetric flask and the volume was completed to the mark with the 2.8 M HNO_3 solution.

The solution used in the acid dissolution of the samples was prepared by gentle mixing of 90 ml of concentrated HCl (P.A. grade, Tedia) with 30 ml of concentrated HNO_3. The mixture was continuously cooled in an ice bath during the preparation of this solution.

2.3. Sample processing

The samples analyzed in this present work were purchased in the local market and ground with an agate mortar in order to obtain samples with a convenient homogeneity in terms of particle size. Each sample was a set of 20 tablets.

2.4. Acid dissolution of the samples

The acid dissolution of the samples was performed employing a mixture of concentrated nitric and hydrochloric acids (1:3 ratio). For this task, approximately 400 mg of the samples were weighed directly into the microwave oven flask and 5 ml of the oxidant mixture was added. The condenser was adapted to the flask, which was adjusted to the cavity of the oven, and the heating program (Table 2) was run. After running the heating program, the quartz flask was taken out of the microwave oven cavity and kept on the bench (inside the fume hood) for cooling to room temperature. Then, it was opened, the content was quantitatively transferred to a 25 ml volumetric flask and the volume was completed to the mark with purified water. The final solution obtained was employed in the determination of Cu and Mn by ETAAS, using the same temperature program employed for the analysis of the slurries (Table 3). When necessary, this solution was filtered, in order to eliminate residual amounts of amorphous silica, and diluted with purified water. All determinations were made in triplicate by the standard addition method and the content of Cu and Mn in the reference sample was 8.1 ± 0.9 μg g^{-1} and 2.1 ± 0.5 μg g^{-1}, respectively.

2.5. Slurry preparation and measurement

The slurries used in the determination of Cu and Mn in the antibiotic tablets were prepared by dispersing approximately

Table 3
Program of temperatures employed for the determination of Cu and Mn by ETAAS.

Step	Temperature (°C)	Ramp (s)	Hold (s)	Ar flow rate (ml min^{-1})
Drying	85	5	0	300
	95	40	0	300
	120	10	0	300
Pyrolysis	1100 (Cu); 1000 (Mn)	2	6	300
Atomization	2300 (Cu); 2400 (Mn)	1	4	0
Cleaning	2400 (Cu); 2500 (Mn)	2	0	300

90–100 mg of the samples in 2 ml of a solution containing 5% m/v Triton X-114 and 2.8 M HNO_3. The slurry was sonicated for 15 min at 40% amplitude of the probe. The homogeneous slurry obtained was transferred to the vial of the ETAAS and the metals were measured by sampling 20 μl and running a convenient temperature program (Table 3), which was optimized in the present work.

Since there are no certified reference materials of medicines for metals content, one sample was analyzed after the acid dissolution and the values were taken as reference in the optimization process and in the preparation of the reference slurry utilized in the quantification of the analytes in the samples.

The calibration procedure was carried out with the reference sample in the quantification of Cu and Mn. In this case, the slurry used in the calibration was prepared exactly as described previously and different volumes (10–30 μl) of the reference slurry were introduced into the instrument in order to change the mass of each element measured. The analytical curves were constructed taking into account the mass of the analytes (determined after acid dissolution) inserted into the graphite tube. All determinations were made in triplicate.

2.6. Material decontamination

All glassware and plastic flasks were decontaminated before use. They were firstly washed with large amounts of tap water and rinsed with purified water. After that, they were soaked in a 10% v/v HCl solution for 24 h. Just before their use, the flasks and glasses were taken out from the acid bath, rinsed with purified water and dried at ambient temperature in a dust-free environment.

3. Results and discussion

The present work was developed following the univariate optimization strategy, where each variable considered was optimized separately. Firstly, the temperature program for the measurement of Cu and Mn by ETAAS was evaluated through the construction of pyrolysis and atomization curves. Once established the temperature program, the effect of some parameters that could affect the method was investigated. The parameters were the HNO_3 and Triton X-114 concentrations in the solution used in the slurry preparation, the sonication time and the amplitude of the probe applied in the sonication step, and the mass of sample used in the slurry preparation.

3.1. Pyrolysis and atomization curves

As mentioned previously, the first part of the work was the evaluation of the temperature program, which was performed by constructing pyrolysis and atomization curves. The drying step of the temperature program was set taking into consideration only the elimination of water, since an aqueous solution was used for the sample dispersion in the preparation of slurries. So, a conventional step with maximum temperature of 120 °C (enough to ensure water vaporization) was employed [29].

The curves of pyrolysis and atomization for Cu and Mn were constructed using aqueous standards (10 μg l^{-1} of each metal) and a slurry prepared by dispersing approximately 90 mg of the reference sample in 2 ml of a 10% m/v Triton X-114 solution. The slurry was sonicated for 20 min at 50% amplitude of the probe. No chemical modifier was added in the measurement of the metals. The results are presented as normalized signals in order to facilitate their analysis.

The main objective of this experiment was to compare the profiles observed for the thermal behavior of the analytes in the aqueous solution and in the slurry. With this information it was possible to select correct pyrolysis and atomization temperatures

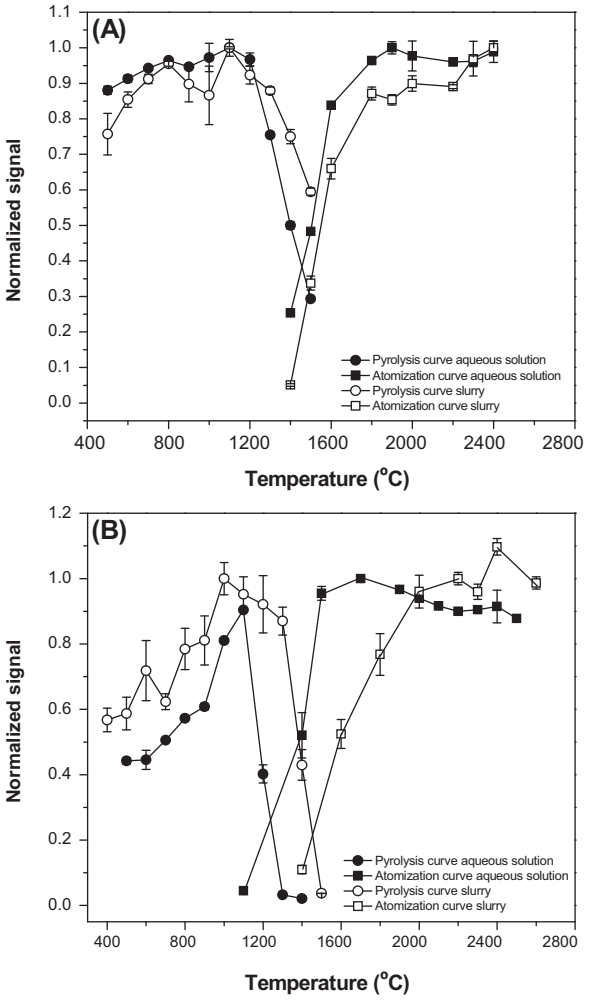

Fig. 1. Pyrolysis and atomization curves for (A) Cu and (B) Mn in aqueous medium and in the slurry. The concentration of both Cu and Mn in the standard solution was 10 μg l^{-1}. The slurry was prepared by dispersing approximately 90 mg of the reference sample (Cu = 8.1 ± 0.9 μg g^{-1} and Mn = 2.1 ± 0.5 μg g^{-1}) in 2 ml of a 10% m/v Triton X-114 solution.

for the temperature program. As it can be seen in Fig. 1, for Cu, a very similar profile was observed for the pyrolysis and atomization curves when either aqueous standard solution or slurry were introduced into the graphite tube. This fact evidenced that the thermal behavior of Cu is similar when it is present as free ion in solution or in the bulk of the pharmaceutical product used to prepare the slurry. It is important to notice that the background signals were always low and were easily corrected by the Zeeman effect-based corrector. The temperatures of pyrolysis and atomization for Cu were set at 1100 and 2300 °C, respectively.

On the other hand, the behavior of Mn was slightly different. When the slurry was introduced, both optimum pyrolysis and atomization temperatures were displaced to values higher than those observed in solution, which indicated that the Mn is possibly retained in the solid matrix of the pharmaceutical product used in the slurry preparation during the atomization step. Taking this fact into consideration, the optimum temperatures of pyrolysis and atomization for Mn were chosen using the curves constructed with the slurry, which were 1000 and 2400 °C, respectively.

3.2. Effect of the sonication conditions

Once established the temperature program, the parameters related to the slurry preparation were investigated. Initially, the

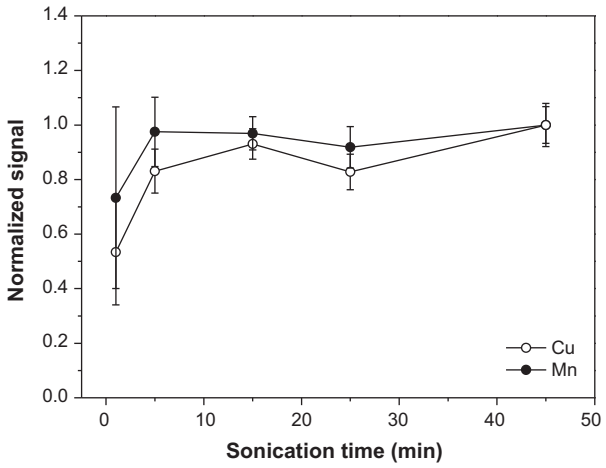

Fig. 2. Effect of the sonication time on the measurement of (○) Cu and (●) Mn in the slurry. The slurry was prepared by dispersing approximately 90 mg of the reference sample in 2 ml of a 10% m/v Triton X-114 solution and the amplitude applied to the probe was 50%.

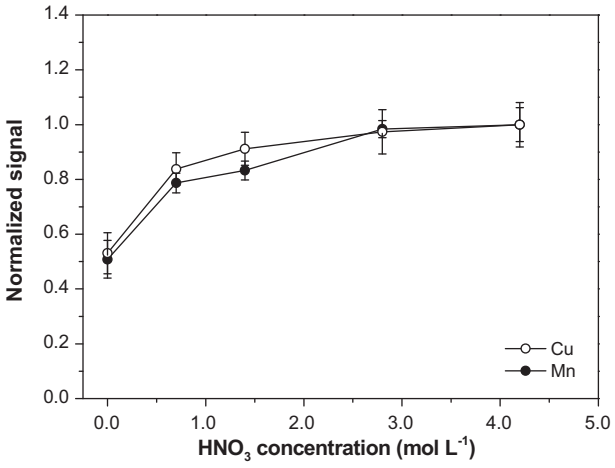

Fig. 3. Effect of the HNO_3 concentration on the measurement of (○) Cu and (●) Mn in the slurry. The slurry was prepared by dispersing approximately 90 mg of the reference sample in 2 ml of a 10% m/v Triton X-114 solution. The amplitude applied to the probe was 40% and the sonication time was 15 min.

sonication conditions (sonication time and amplitude applied to the probe) were tested.

In the first experiment, the amplitude applied to the probe was kept constant (50%) and the sonication time was varied in the range of 1–45 min. The slurries were always prepared by dispersing approximately 90 mg of the reference sample in 2 ml of a 10% m/v Triton X-114 solution. The results obtained in this experiment are shown in Fig. 2.

The most prominent effect of the sonication time was noted on the precision of the measurements. This observation is related to an important aspect of the slurry sampling procedure, which is its inherent low precision. The low precision comes from the fact that the slurry is not, in principle, a homogeneous system. So, although the average signals increased with the increase of the sonication time, for both Cu and Mn, the high dispersion of the measurements (expressed as standard deviation of five measurements) for the sonication times of 1 and 5 min made impossible to conclude that this increase was due to the variation of this parameter. On the other hand, the standard deviation of the measurements clearly decreased with the increase of the sonication time. When a sonication time of 15 min was employed, the relative standard deviation was approximately 6% for both elements, which was considered satisfactory for this type of procedure. This behavior can be explained by the effect of the sonication on the disaggregation of the solid particles. The increase of the sonication time resulted in the formation of smaller particles in the slurry, which were more easily suspended in the medium chosen for the slurry preparation, thus increasing the homogeneity of the system and, consequently, the precision of the measurements. Therefore, a sonication time of 15 min was chosen for the slurry preparation.

The effect of the amplitude applied to the probe was also studied, since this parameter is related to the amount of energy transferred to the system through the ultrasonic waves. It was varied in the range of 30–60% while the sonication time was fixed at 15 min. All other conditions were the same used in the evaluation of the sonication time. The amplitude of the probe did not affect the magnitude of the signals for Cu and Mn and, similarly to the sonication time, only affected the precision of the measurements. Improved precision (relative standard deviation always better than 7%) was observed when the amplitude applied to the probe was 40% or higher. So, the amplitude applied to the probe was fixed at 40% for the method.

3.3. Effect of the HNO_3 concentration in the solution used in the preparation of the slurry

The use of acidic solutions for the preparation of slurries is a very common strategy when solid samples are analyzed using the slurry sampling approach [11]. Diluted solutions of HNO_3 (containing other components) are the most employed diluents for the analysis of both organic [30,31] and inorganic matrices [32,33]. Different functions are attributed to the HNO_3 when used in the slurry preparation. According to Robles and Aller [30], it can act as a chemical modifier, enhancing the sensitivity of the measurements by ETAAS. Also, it is considered that HNO_3 is able to extract the analytes from the solid particles, which improves the stability of the slurries and the precision of the measurements [14]. Taking these facts into account, the concentration of HNO_3 in the solution used in the preparation of the slurries was evaluated.

In this experiment, the slurries were prepared with 90 mg of the reference sample dispersed in the solutions containing 10% m/v Triton X-114 and variable concentrations of HNO_3 (0–4.2 M). Before the measurement of Cu and Mn by ETAAS, the slurries were sonicated for 15 min at 40% amplitude.

The results obtained in this study showed that the HNO_3 plays an important role in the process. The analytical signal for Cu and Mn increased with the increase of HNO_3 concentration up to 2.8 M (Fig. 3). After this concentration the signals remained constant, indicating that they do not depend on the HNO_3 concentration anymore. As the profiles of the curves for both elements were similar, it was considered that the extraction ability of the HNO_3 was the most important effect on the slurries. So, a concentration of HNO_3 of 2.8 M was chosen for the method.

3.4. Effect of the Triton X-114 concentration in the solution used in the preparation of the slurry

The addition of stabilizers to the slurries in analytical methods based on slurry sampling is associated to their ability in maintaining the particles in suspension and/or to avoid the formation of agglomerates with the solid particles present in the medium [34]. In this work, Triton X-114 was employed to prevent these drawbacks and its effect was investigated through the evaluation of the slurry stability. The slurries were prepared as described previously, using the optimized conditions, and the concentration of Triton

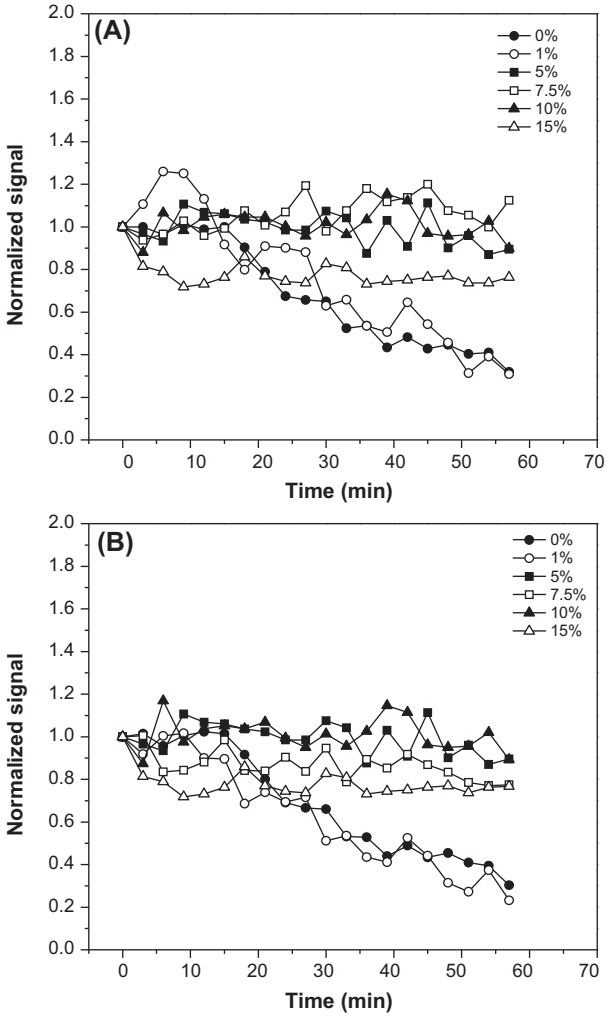

Fig. 4. Influence of the Triton X-114 concentration on the stability of the slurries for the measurements of (A) Cu and (B) Mn along the time. The slurries were prepared by dispersing approximately 90 mg of the reference sample in 2 ml of a solution containing the Triton X-114 and 2.8 M of HNO_3. The amplitude applied to the probe was 40% and the sonication time was 15 min.

X-114 in the solution was varied between 0 (no addition of surfactant) and 15% m/v.

As expected, the addition of Triton X-114 presented a significant effect on the slurry stability, which was assessed by measuring the analytical signal along the time for each element of interest. The relative standard deviation (RSD) observed for the measurements of Cu and Mn by ETAAS along the time (60 min) was satisfactory when 5% m/v Triton X-114 was added to the solutions used to prepare the slurries (Fig. 4). In this case, for Cu signals, a RSD of 7.6% was observed after processing the 20 measurements executed during the 60 min, while for Mn a RSD of 7.7% was observed.

The addition of a concentration of Triton X-114 (or no use) lower than 5% m/v resulted in a continuous and significant decrease of the analytical signals of Cu and Mn with time, which is inappropriate for routine determinations, especially when a number of slurries should be measured. This effect can be credited to the fast sedimentation rate of the solid particles. On the other hand, when the concentration of the surfactant was higher than 5% m/v, the signal of the blank was elevated, which deteriorated the limits of detection and quantification. It is important to highlight that there was no noticeable difference in the magnitude of the signals (always comparing the first analytical signal recorded, at time zero) with the variation of the concentration of Triton X-114. So, a

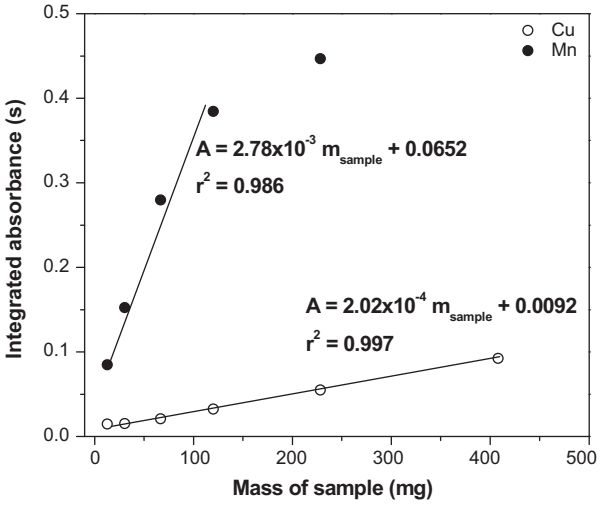

Fig. 5. Influence of the mass of sample used in the slurry preparation on the measurements of (○) Cu and (●) Mn in the slurry. The slurries were prepared by dispersing approximately 90 mg of the reference sample in 2 ml of a solution containing the 5% m/v of Triton X-114 and 2.8 M of HNO_3. The amplitude applied to the probe was 40% and the sonication time was 15 min.

concentration of Triton X-114 of 5% m/v was always added to the solutions used in the preparation of the slurries.

3.5. Effect of the mass of sample used to prepare the slurries

The evaluation of the mass/volume ratio employed in the preparation of the slurry is of fundamental importance in this kind of procedure because it affects the sensitivity of the method and, sometimes, the precision of the measurements [35]. Also, it is important to consider that the stability of the slurry could also be affected by this parameter, once the increase of the mass results in the increase of the number of particles that must be maintained in suspension. If the increase of the mass of sample added does not affect the method, a linear relationship should be expected between the analytical signal and the mass used for the preparation of the slurry for a constant volume of diluent.

In this work, the volume of diluent solution (5% m/v Triton X-114 + 2.8 M HNO_3) was always 2 ml and the mass of sample was changed in the range of 10–400 mg. For both analytes, a linear relationship was observed between the mass and the analytical signal (Fig. 5). For Cu, this linear relationship was observed until 400 mg of sample, while for Mn, the linear relationship was observed until 120 mg. However, as it can be seen in Fig. 5, the analytical signals for Mn were considerably higher than those observed for Cu, certainly because of the higher concentration of Mn in the reference sample than the Cu and the highest sensitivity verified for the measurement of Mn. This fact indicated that the deviation from linearity for Mn could be attributed to the deviation from the Beer's law and not due to the high mass of sample used to

Table 4
Results obtained in the construction of the analytical curves used for comparison of different calibration strategies (A is the integrated absorbance and m_x is the mass of each metal injected into the graphite tube in ng).

Method of calibration	Analyte	
	Cu	Mn
Aqueous solutions	$A = 0.2001\, m_{Cu} + 0.0194$ $r^2 = 0.998$	$A = 0.3427\, m_{Mn} + 0.0116$ $r^2 = 0.995$
Reference slurry	$A = 0.0158\, m_{Cu} + 0.0252$ $r^2 = 0.977$	$A = 0.1026\, m_{Mn} + 0.0057$ $r^2 = 0.988$

Table 5
Determination of Cu and Mn in the samples by ETAAS, using the slurry sampling procedure developed in this work. Results are expressed as mean ± standard deviation ($n = 3$).

Sample	Active principle	Cu ($\mu g\,g^{-1}$)		Mn ($\mu g\,g^{-1}$)	
		Slurry sampling	Acid dissolution	Slurry sampling	Acid dissolution
S1	Ciprofloxacin	4.4 ± 0.1	5.3 ± 0.2	3.9 ± 0.4	3.7 ± 0.3
S2	Ciprofloxacin	1.9 ± 0.2	1.6 ± 0.1	1.7 ± 0.1	2.0 ± 0.2
S3	Cephalexin	1.6 ± 0.1	1.7 ± 0.1	0.92 ± 0.11	0.91 ± 0.07
S4	Cephalexin	1.2 ± 0.1	1.4 ± 0.2	1.3 ± 0.2	1.6 ± 0.1
$t_{calculated}$[a]		0.905		0.791	

[a] Value of t calculated in the application of a paired Student t-test, at 95% confidence level, in the comparison of the results obtained by slurry sampling and acid dissolution ($t_{critical} = 3.182$).

prepare the slurries, once the same deviation was not observed for Cu when the highest mass of sample was used to prepare the slurries. Additionally, the very high signal observed for Mn (peak height higher than 1.0 absorbance units) is typically out of the linear range delimited by the Beer's law in the atomic absorption technique.

As the other experiments of optimization were carried out using a mass of sample of approximately 90 mg in 2 ml of diluent solution, the slurries used in the quantification of Cu and Mn in the unknown samples were always prepared with 90–100 mg in the same 2 ml of diluent. This condition seemed to be suitable for calibration purposes, when different volumes of the standard slurry were introduced in the spectrometer, and for the analysis of the samples.

4. Evaluation of the calibration strategy and analytical features

One of the main challenges in the application of slurry sampling methodologies is to use a correct approach for calibration. Several works report the use of aqueous solutions of the analytes for calibration [36–40]. Sometimes, the use of slurries made with certified reference materials is necessary, in order to simulate the behavior of the analytes in the slurries of the samples [41,42]. The election of one or other strategy is based on the similarity of the analytical signals generated by the standards with the analytical signals obtained with the samples.

In the present work, the two methods were tested. In the first, aqueous solutions of Cu and Mn were used as standards. In the second method, a slurry with known content of Cu and Mn was prepared using the reference sample, which was previously analyzed by the conventional method based on the acid dissolution of the sample. In this case, the calibration was performed by introducing increasing volumes (10–30 μl) of the reference slurry and measuring the resulting analytical signal, which was proportional to the mass of each analyte inserted into the graphite tube. The theoretical amount of Cu and Mn introduced was calculated taking into account the concentrations of Cu and Mn in the reference sample, which were $8.1 \pm 0.9\,\mu g\,g^{-1}$ and $2.1 \pm 0.5\,\mu g\,g^{-1}$, respectively, as mentioned previously. The equations and the coefficients of determination of the analytical curves constructed in the application of both methods are shown in Table 4. In all equations, the mass of the elements introduced into the graphite tube was considered for a convenient comparison.

As it can be seen, the slopes of the analytical curves constructed using the method under study were very different, which evidenced the possible occurrence of matrix interferences on the determination of the metals by the slurry sampling approach, in spite of the fact that, for Cu, the thermal behavior was not different when aqueous solutions or slurries are measured (see Section 3.1). Therefore, the methodological calibration with the reference slurry was mandatory to avoid the effect of these interferences on the accuracy of the developed method.

The limits of detection and quantification were calculated taking into account slurries prepared through the dispersion of 100 mg of sample in 2 ml of diluent. Also, a volume of 20 μl was considered. In this case, the limits of detection (3 s) and quantification (10 s) for Cu were 0.095 and $0.32\,\mu g\,g^{-1}$, respectively. For Mn the limit of detection was $0.013\,\mu g\,g^{-1}$ and the limit of quantification was $0.044\,\mu g\,g^{-1}$. The RSD calculated from ten measurements of 20 μl of the reference slurry was 6.8 for Cu and 6.7% for Mn.

5. Application of the proposed methodology

In order to test the accuracy of the procedure, four samples were analyzed by the proposed method and after total dissolution, used as reference method. The accuracy was tested this way because there are no certified reference materials for metals in medicines available.

Firstly, the accuracy of the reference method was evaluated by performing a recovery test with the samples S_2 (ciprofloxacin as active principle) and S_4 (cephalexin as active principle). Spikes of $10\,\mu g\,l^{-1}$ of each metal were done on the sample before the application of the digestion method. Then, the resulted solutions were analyzed by standard addition method and the amount of the analytes recovered was calculated in relation to the amount found without spiking. In the case of Cu, recovery percentages of 106 ± 5% and 109 ± 7% were obtained in the experiments with the samples S_2 and S_4, respectively. For Mn, the recovery percentages were 104 ± 5% and 93.5 ± 4% in the experiments with the samples S_2 and S_4, respectively.

Once the accuracy of the reference method was proved, the samples were analyzed by the proposed and the reference methods for comparison. The results obtained in the determination of Cu and Mn by both methods are shown in Table 5. There were no statistical differences (paired Student t-test at 95% confidence level [43]) between the results, which indicated that the use of the slurry sampling approach developed in this work is equivalent to the conventional method, based on the acid dissolution of the samples, for the quantification of trace concentrations of Cu and Mn in the tablets of antibiotics.

6. Conclusions

The slurry sampling method investigated in this work showed to be a good alternative to conventional methods based on the total dissolution of the samples for Cu and Mn determination in tablets of antibiotics. The method is simple, fast and requires minimum sample handling, which makes it very attractive for routine analysis of this kind of sample.

In the optimized conditions, the slurries were prepared by dispersing approximately 90–100 mg of the powdered sample in 2 ml of a solution containing 5% m/v of Triton X-114 and 2.8 M of HNO_3. Before introduction, the slurries were sonicated for 15 min at 40% amplitude of the probe in order to enhance the homogeneity of the system. The slurries prepared by this procedure were stable for a

minimum of 60 min and provided precise measurements of Cu and Mn by ETAAS. The RSD observed for the measurement of both metals was always better than 7%, which is satisfactory for this kind of procedure.

Acknowledgments

The authors are grateful to Coordenação de Aperfeiçoamento de Pessoal de Nível Superior (CAPES), Fundação Carlos Chagas Filho de Apoio à Pesquisa do Estado do Rio de Janeiro (FAPERJ) and to Conselho Nacional de Desenvolvimento Científico e Tecnológico (CNPq) for providing grants, scholarships and financial support.

References

[1] D.K. Sarker, Quality Systems and Control for Pharmaceuticals, John Wiley & Sons, Chichester, UK, 2008.
[2] Brazilian Pharmacopeia, V. edition, Part I, 2010.
[3] C.G. Fraga, Relevance, essentiality and toxicity of trace elements in human health, Mol. Aspects Med. 26 (2005) 235–244.
[4] K.M. Erikson, K. Thompson, J. Aschner, M. Aschner, Manganese neurotoxicity: a focus on the neonate, Pharmacol. Ther. 113 (2007) 369–377.
[5] L.E. Pascal, D.M. Tessier, Cytotoxicity of chromium and manganese to lung epithelial cells in vitro, Toxicol. Lett. 147 (2004) 143–151.
[6] J.Y. Uriu-Adams, C.L. Keen, Copper oxidative stress and human health, Mol. Aspects Med. 26 (2005) 268–298.
[7] S. Görög, The importance and the challenges of impurity profiling in modern pharmaceutical analysis, Trends Anal. Chem. 25 (2006) 755–757.
[8] N. Lewen, S. Mathew, M. Schenkenberger, T. Raglione, A rapid ICP-MS screen for heavy metals in pharmaceutical compounds, J. Pharm. Biomed. Anal. 35 (2004) 739–752.
[9] J. Huang, X. Hu, J. Zhang, K. Li, Y. Yan, X. Xu, The application of inductively coupled plasma mass spectrometry in pharmaceutical and biomedical analysis, J. Pharm. Biomed. Anal. 40 (2006) 227–234.
[10] E. Oliveira, Sample preparation for atomic spectroscopy: evolution and future trends, J. Braz. Chem. Soc. 14 (2003) 174–182.
[11] N. Niemela, H. Kola, K. Eilola, P. Peramaki, Development of analytical methods for the determination of sub-ppm concentrations of palladium and iron in methotrexate, J. Pharm. Biomed. Anal. 35 (2004) 433–439.
[12] H.H. Ang, E.L. Lee, K. Matsumoto, Analysis of lead content in herbal preparations in Malaysia, Human Exp. Toxicol. 22 (2003) 445–451.
[13] L. Qi, L. Huirong, Determination of lead in natural herbal medicines by flame atomic absorption spectrometry with a slotted, sputtered quartz tube, J. Anal. Atom. Spectrom. 13 (1998) 1203–1205.
[14] M.J. Cal-Prieto, M. Felipe-Sotelo, A. Carlosena, J.M. Andrade, P. Lopez-Mahıa, S. Muniategui, D. Prada, Slurry sampling for direct analysis of solid materials by electrothermal atomic absorption spectrometry (ETAAS). A literature review from 1990 to 2000, Talanta 56 (2002) 1–51.
[15] M. Felipe-Sotelo, A. Carlosena, E. Fernández, P. López-Mahía, S. Muniategui, D. Prada, Microwave-assisted extraction and ultrasonic slurry sampling procedures for cobalt determination in geological samples by electrothermal atomic absorption spectroscopy, Talanta 63 (2004) 735–742.
[16] R. Dobrowolski, A. Adamczyk, M. Otto, J. Dobrzyńska, Determination of antimony in sediments and soils by slurry sampling graphite furnace atomic absorption spectrometry using a permanent chemical modifier, Spectrochim. Acta Part B 66 (2011) 493–499.
[17] M.W. Hinds, K.E. Latimer, K.W. Jackson, Determination of lead in soil by slurry electrothermal atomic absorption spectrometry with fast temperature program, J. Anal. Atom. Spectrom. 6 (1991) 473–476.
[18] N.J. Miller-Ihli, Ultrasonic slurry sampling graphite furnace atomic absorption spectrometry: analytical considerations for analysis of a high density glass material, Spectrochim. Acta Part B 52 (1997) 431–436.
[19] R. Dobrowolski, I. Pawlowska-Kapusta, J. Dobrzynska, Chromium determination in food by slurry sampling graphite furnace atomic absorption spectrometry using classical and permanent modifiers, Food Chem. 132 (2012) 597–602.
[20] R.G.O. Araujo, N. Oleszczuk, R.T. Rampazzo, P.A. Costa, M.M. Silva, M.G.R. Vale, B. Welz, S.L.C. Ferreira, Comparison of direct solid sampling and slurry sampling for the determination of cadmium in wheat flour by electrothermal atomic absorption spectrometry, Talanta 77 (2008) 400–406.
[21] E.G.P. da Silva, V. Hatje, W.N.L. dos Santos, L.M. Costa, A.R.A. Nogueira, S.L.C. Ferreira, Fast method for the determination of copper, manganese and iron in seafood samples, J. Food Compos. Anal. 21 (2008) 259–263.
[22] P. Bermejo-Barrera, A. Moreda-Piñeiro, J. Moreda-Piñeiro, A. Bermejo-Barrera, Determination of aluminium and manganese in human scalp hair by electrothermal atomic absorption spectrometry using slurry sampling, Talanta 45 (1998) 1147–1154.
[23] Z. Arslan, J.F. Tyson, Slurry sampling for determination of lead in marine plankton by electrothermal atomic absorption spectrometry, Microchem. J. 86 (2007) 227–234.
[24] L.M. Marcó P, E.A. Hernández-Caraballo, C. Pascusso, J. Alvarado, Determination of manganese in brain samples by slurry sampling graphite furnace atomic absorption spectrometry, Talanta 59 (2003) 897–904.
[25] M.M. Silva, M.G.R. Vale, E.B. Caramão, Slurry sampling graphite furnace atomic absorption spectrometry: determination of trace metals in mineral coal, Talanta 50 (1999) 1035–1043.
[26] D. Baralkiewicz, H. Gramowska, M. Kózka, A. Kanecka, Determination of mercury in sewage sludge by direct slurry sampling graphite furnace atomic absorption spectrometry, Spectrochim. Acta Part B 60 (2005) 409–413.
[27] N. Tokman, The use of slurry sampling for the determination of manganese and copper in various samples by electrothermal atomic absorption spectrometry, J. Hazard. Mater. 143 (2007) 87–94.
[28] M.C. Santos, J.A. Nóbrega, N. Baccan, S. Cadore, Determination of toxic elements in plastics from waste electrical and electronic equipment by slurry sampling electrothermal atomic absorption spectrometry, Talanta 81 (2010) 1781–1787.
[29] D.J. Butcher, J. Sneddon, A Practical Guide to Graphite Furnace Atomic Absorption Spectrometry, John Wiley & Sons, New York, USA, 1998.
[30] L.C. Robles, A.J. Aller, Determination of cadmium in biological and environmental samples by slurry electrothermal atomic absorption spectrometry, Talanta 42 (1995) 1731–1744.
[31] A.J. Aller, L.C. Robles, Determination of selenocystamine by slurry sampling electrothermal atomic absorption spectrometry after a selective preconcentration by living *Pseudomonas putida*, J. Anal. Atom. Spectrom. 13 (1998) 469–476.
[32] H.M. Dong, V. Krivan, B. Welz, G. Schlemmer, Determination of trace impurities in titanium dioxide by slurry sampling electrothermal atomic absorption spectrometry, Spectrochim. Acta B 52 (1997) 1747–1762.
[33] V. Krivan, A. Heger, S. Hauptkorn, Slurry sampling electrothermal atomic absorption spectrometry for trace element analysis of high-purity tungsten trioxide, Fresen. J. Anal. Chem. 360 (1998) 167–174.
[34] P. Bermejo-Barrera, A. Moreda-Piñeiro, J. Moreda-Piñeiro, A. Bermejo-Barrera, Determination of traces of silver in human scalp hair slurries by electrothermal atomic absorption spectrometry, Mikrochim. Acta 129 (1998) 71–76.
[35] N.J. Miller-Ihli, Influence of slurry sampling preparation on the accuracy of ultrasonic slurry electrothermal atomic absorption spectrometry, J. Anal. Atom. Spectrom. 9 (1994) 1129–1134.
[36] W. Fuyi, J. Zucheng, Direct determination of cadmium in solid biological materials by slurry sampling electrothermal atomic absorption spectrometry with polytetrafluoroethylene as a chemical modifier, Anal. Chim. Acta 391 (1999) 89–94.
[37] D.G. da Silva, G.D. Matos, A.M.P. dos Santos, R.D. Fiuza, R.M. de Jesus, A procedure using slurry sampling for the determination of manganese in corn flour by ET AAS, Anal. Methods 3 (2011) 2625–2629.
[38] R. Dobrowolski, M. Otto, A. Adamczyk, Determination of tin in marine sediments by slurry sampling atomic absorption spectrometry with electrothermal atomization using a permanent modifier, Microchim. Acta 168 (2010) 355–362.
[39] L.A. Pereira, I. Amorim, J.B.B. da Silva, Determination of cadmium, chromium and lead in marine sediment slurry samples by electrothermal atomic absorption spectrometry using permanent modifiers, Talanta 68 (2006) 771–775.
[40] I. López-Garcia, P. Viñas, R. Romero-Romero, M. Hernádez-Córdoba, Fast determination of phosphorus in honey, milk and infant formulas by electrothermal atomic absorption spectrometry using a slurry sampling procedure, Spectrochim. Acta Part B 62 (2007) 48–55.
[41] I. Kradjova, P. Mandjukov, S. Tsakovsky, V. Simeonov, J.A. Stratis, G.A. Zachariadis, Determination of mercury by electrothermal atomic absorption spectrometry using different chemical modifiers or a slurry technique, J. Anal. Atom. Spectrom. 10 (1995) 1065–1068.
[42] K. Danzer, W. Schron, B. Dressler, K.U. Jagemann, Matrix sensitivity of solid sampling AAS. Determination of zinc in geological samples, Fresen. J. Anal. Chem. 361 (1998) 710–713.
[43] J.N. Miller, J.C. Miller, Statistics for Analytical Chemistry, 3rd ed., Ellis Horwood PTR Prentice Hall, Chichester, UK, 1993.

Journal of Pharmaceutical and Biomedical Analysis 66 (2012) 204–210

Contents lists available at SciVerse ScienceDirect

Journal of Pharmaceutical and Biomedical Analysis

journal homepage: www.elsevier.com/locate/jpba

Evidence for the genotoxic effect of daunomycin in multipotent hematopoietic cells of mouse bone marrow: Chromatin proteins analysis

Asieh Aramvash[a], Azra Rabbani-Chadegani[a,*], Mahvash Khodabandeh Shahraki[b]

[a] Department of Biochemistry, Institute of Biochemistry and Biophysics, University of Tehran, Tehran, Iran
[b] Industrial and Environmental Biotechnology Group, National Institute of Genetic Engineering and Biotechnology, Tehran, Iran

ARTICLE INFO

Article history:
Received 22 October 2011
Received in revised form 19 February 2012
Accepted 20 February 2012
Available online 3 March 2012

Keywords:
Bone marrow
Multipotent hematopoietic cells
Histones
HMG proteins
Chromatin

ABSTRACT

Severe bone marrow suppression and anemia are the main side effects of using chemotherapeutic agents like daunomycin. In this study the effect of daunomycin on viability and chromosomal proteins of multipotent hematopoietic cells (MHCs) of mouse bone marrow was investigated. The cells were separated from mature cells according to their adherence, incubated in the absence and presence of various concentrations of daunomycin and viability was determined by trypan blue exclusion and MTT assay. The histones and high mobility group (HMG) proteins were extracted by acid and salt, respectively and analyzed on SDS-PAGE and immunoblot. The results revealed that daunomycin exhibited time and dose dependent cytotoxicity on the cells and upon increasing the concentrations of drug, the extractability of histone and HMG proteins decreased. Agarose gel electrophoresis showed aggregation of DNA in the presence of drug. Flow cytometry analysis suggested that there are differences in type and amount of histones H2A and H2B of these cells in comparison with thymus histones. Moreover histone H3 was not subjected to trimethylation at lysine 9 and daunomycin decreased H3K9 dimethylation and H3K9 acetylation in these cells in a dose-dependent manner. From these results it is concluded that the binding of daunomycin to chromatin precedes chromatin of multipotent hematopoietic cells of bone marrow into compaction/aggregation and beside DNA, histones and HMG proteins also play an important role in this process.

© 2012 Elsevier B.V. All rights reserved.

1. Introduction

Bone marrow is a tissue in which hematopoiesis occurs. Hematopoiesis is a complex process in which multipotent hematopoietic cells (MHCs) differentiate into special circulating erythroid, granulocyte, macrophage, megakaryocytic and lymphoid blood cells [1]. In vivo toxicity studies on hematopoietic cells, especially in terms of stem cell depletion, and direct in vitro exposure to chemotherapeutic agents like anthracyclines has showed a reduction in progenitor survival [2,3].

Daunomycin is one of the most active antitumor compounds widely used in clinical oncology, especially in the treatment of acute leukemias [4]. It mainly acts by intercalation of its planar aglycan chromophore between DNA base pairs, and its amino sugar ring lies in the minor groove of the double helix [5,6]. Although, large body of evidence introduces DNA as a main cellular target of daunomycin and its in vitro binding to DNA has been extensively studied in the past, there is no single mechanism of action responsible for all of the observed clinical and cellular effects of this drug.

As we know, in the cell nucleus, DNA exists as a complex structure called chromatin. It is associated with DNA binding proteins such as histones and nonhistone proteins building repeating units named "nucleosomes". These consist of 145 bp DNA wrapped around an octamer of basic proteins (core histones). There are five main histones in chromatin structure; a linker histone H1 and four core histones (H2A, H2B, H3 and H4) are arranged in an octamer form [7,8]. High mobility group (HMG) nonhistone chromosomal proteins are diverse, ubiquitous nuclear proteins which are existed in three subfamilies: HMGA, HMGB and HMGN [9]. HMGB subfamily is abundant and highly conserved nonhistone proteins that may exist in all eukaryotic cells nuclei [10]. Therefore the presence of these chromosomal proteins may affect and modulate the binding of daunomycin to DNA.

Abbreviations: BSA, bovine serum albumin; Gmean, geometric means; PAGE, polyacrylamide gel electrophoresis; SDS, sodium dodecyl sulfate; EDTA, ethylenediaminetetraacetic acid; PBS, phosphate buffer saline; FITC, fluorescein isothiocyanate; TCA, trichloroacetic acid; DMEM, Dulbecco's Modified Eagle Medium; Ub, ubiquitin; H3K9me2, histone H3 lysine 9 dimethylation; H3K9Ac, histone H3 lysine 9 acetylation; MTT, 3-(4,5-dimethylthiazal-2-yl)-2,5-diphenyltetrazolium bromide.

* Corresponding author at: Department of Biochemistry, Institute of Biochemistry and Biophysics, University of Tehran, P.O. Box: 13145-1384, Tehran, Iran.
Tel.: +98 21 66499422; fax: +98 21 66404680.
E-mail address: rabbani@ibb.ut.ac.ir (A. Rabbani-Chadegani).

0731-7085/$ – see front matter © 2012 Elsevier B.V. All rights reserved.
doi:10.1016/j.jpba.2012.02.019

As stated bone marrow is the main site of daunomycin cytotoxicity [2,11]. Although several attempts in this direction have already been carried out but the effect of daunomycin on cytotoxicity and chromatin of bone marrow cells are still poorly understood. In the present study, in order to elucidate the biological mechanism of daunomycin action, the effect of daunomycin on cytotoxicity and chromatin proteins of multipotent hematopoietic cells of mouse bone marrow cells was investigated. The results show that apart from lower content of H2A and H2B in these cells, daunomycin as an anticancer drug prevents extractability of histones and non-histone proteins via condensation of chromatin.

2. Materials and methods

2.1. Reagents

Daunomycin was purchased from Helale Ahmar Pharmacy (Tehran, Iran, manufactured by Pharmacia) and used without further purification. Stock solution of the drug was prepared in sterile distilled water at a concentration of 2 mg/ml and stored at −20 °C in the dark. Before use it was diluted to desired concentrations with 0.1 M PBS, pH = 7.4. Trypan blue, MTT, proteinase K, ECoRI-Hind III digested DNA marker, cocktail protease inhibitor, FITC or HRP-conjugated IgG were purchased from Sigma–Aldrich Chemical Company (St. Louis, MO, USA). DMEM with 2 mM L-glutamine (Gibco, Invitrogen, Carlsbad, CA, USA) was supplemented with 3.7 g/l $NaHCO_3$, 15% heat-inactivated fetal calf serum (Faculty of Veterinary Medicine, University of Tehran, Tehran, Iran) 30 mg/l asparagine, 100 U/ml penicillin and 10 μg/ml streptomycin (Gibco, Invitrogen, Carlsbad, CA, USA).

Anti H3, H4, H2A, H2B, H3K9me2, H3K9me3, H3K9Ac and ubiquitin antibodies were purchased from Abcam (Cambridge, UK). Histones (H1 and core histones) and HMG proteins were prepared according to the procedures of Johns [12] and Goodwin et al. [13], respectively and used as a marker. Antibodies against H1, core histones and HMG proteins were prepared in IBB Laboratory (Tehran, Iran).

Male Balb/c mice weighting 20–25 g (6–8 weeks old) were obtained from the Laboratory Animal Center of IBB (Tehran, Iran). They were maintained in conventional pathogen free conditions in a temperature (22–23 °C), humidity (50–70%), and photoperiod (12 h dark/light cycle) controlled room.

2.2. Isolation of multipotent hematopoietic cells of bone marrow

Total bone marrow from each femur and tibia pair was eluted aseptically with 1 ml syringe and 25-gauge needle into 1 ml DMEM and aliquot of the cell suspension was diluted in 3% acetic acid to lyse red blood cells. The total nucleated cells were counted and the viability was determined by trypan blue exclusion assay. The bone marrow cells were cultured overnight in DMEM at the density of 10^6 cells per ml at 37 °C with 5% CO_2 and full humidified condition. Nonadherent cells which are the population of hematopoietic stem and progenitor cells were collected and used for further investigation [14].

2.3. Drug treatment and viability assay

Nonadherent multipotent hematopoietic cells of bone marrow (10^6 cells/ml) were cultured in the absence and presence of various concentrations of daunomycin for 4 h (time course study revealed that 4 h is a best incubation time). Daunomycin was added directly at the onset of the culture and the cultures without daunomycin were used as control. Viability of the cells was determined as is described below.

Trypan blue: Drug treated and the control was mixed with an isotonic solution of trypan blue (0.4%, w/v) and viability of the cells was determined by trypan blue exclusion assay.

MTT assay: The method of Mossman [15] was used with some modifications. The cells (8×10^4 cells/well) were seeded into a 96-well plate (Nunclon, Denmark) and incubated with a series of drug concentrations for 4 h (to control wells only culture medium was added). Then 10 μl of MTT (5 mg/ml in H_2O) was added to each well and the cells were incubated at 37 °C with 5% CO_2 for 4 h. Then the medium was aspirated and replaced with 100 μl DMSO per well in order to dissolve the formed violet formazan crystals within the metabolically viable cells. The plates were gently shaken for 5 min at room temperature to allow complete dissolving of the formazan and the absorbance was read at 570 nm with a BioTek ELISA microplate reader (Model Power Wave XS2, Bio Tek, USA). The relative viability of the treated cells was expressed as the percent of the control.

2.4. Extraction of histones, HMG proteins and DNA

Histones and nonhistone proteins extraction: Multipotent hematopoietic cells of bone marrow (2×10^6) were incubated in the absence and presence of various concentrations of daunomycin as described above. Total histones (all five histones) and ubiquitin were isolated from the cells with 0.3 N HCl as described by Johns [12]. High mobility group (HMG) proteins were isolated with 0.35 M NaCl as described by Goodwin et al. [13]. After precipitation with 12% TCA, the proteins were dissolved in the SDS gel loading buffer for polyacrylamide gel electrophoresis.

DNA extraction: Drug treated and the controls were washed twice with ice-cold PBS and resuspended in DNA lysis buffer (10 mM Tris–HCl, pH 8.0, 1 mM EDTA, 100 mM NaCl, 1% SDS and 50 μg/ml proteinase K), followed by incubation at 56 °C for 4 h. Subsequently, equal volume of phenol was added to each solution, and the aqueous phase was recovered using a mixture of chloroform–isoamyl alcohol (24:1). Sodium acetate (3 M) (1/10 volume) and absolute ethanol (2 volumes) were added and incubated at −20 °C for 2 h. The samples were then eppendorfed for 5 min at 4 °C, washed with ethanol and air dried. DNAs were resuspended in TE buffer (10 mM Tris–HCl, pH 7.4, 1 mM EDTA) and DNA sample solvent, heated at 65 °C and electrophoresed on agarose gel.

2.5. Gel electrophoresis and western blot

SDS-PAGE: The protein samples were analyzed on 15% SDS polyacrylamide gel electrophoresis as described by Laemmli [16]. The samples (100 μl) were directly equilibrated with SDS sample buffer or precipitated with 12% TCA and then after added sample buffer loaded. The gel was run for 1.5 h at 100 V, stained with 0.1% Coomassie brilliant blue R 250, destained in 10% methanol/acetic acid and photographed.

Western blot: The protein samples were run on 15% polyacrylamide gel at 100 V for protein separation. The proteins were then transferred onto a nitrocellulose membrane [17]. The membrane with the immobilized protein bands was incubated for 1 h at 37 °C with 1% (w/v) gelatin in Tris–NaCl buffer (50 mM Tris–HCl pH 7.4, 150 mM NaCl), referred to as blocking buffer, and washed three times of 5 min with Tris–NaCl buffer. The membrane was then incubated overnight with overall anti rabbit specific antibodies (e.g. total histones and HMG proteins) or anti rabbit specific anti histones (H2A, H2B, H3, H4, Ub) individually at 4 °C. After three times washing the membrane with Tris–NaCl/Tween somehow 20 (0.05%), it was incubated with peroxidase-conjugated goat anti rabbit IgG for 2 h at room temperature. After washing (three times), the membrane was incubated with the substrate solution (1.2 ml of 0.3% 4-chloro-1-naphtol in methanol was mixed with 20 ml

Tris–NaCl buffer and 20 ml H_2O_2) for 30 min at 37 °C and the reaction was stopped by adding distilled water. The membrane was then dried and photographed.

Agarose gel: Agarose (1.2%) gel electrophoresis was carried out in TBE buffer (89 mM Tris–borate, 2 mM EDTA (pH 8)) at a constant voltage of 90 V for 1 h [18]. The gel was then stained with ethidium bromide (5 μg/ml in distilled water) and photographed.

2.6. Analysis of bone marrow histone content by flow cytometry

Multipotent hematopoietic cells of bone marrow at a density of 2×10^6 cells were fixed for 15 min in 4% paraformaldehyde in PBS on ice and subsequently washed with PBS plus 1% BSA and 0.1% Tween-50 for 10 min at room temperature. After washing, the samples were incubated with H2A, H2B, H3 and H4 mouse monoclonal antibodies (1:50 dilution). Detection was done by incubation with a FITC-conjugated sheep anti mouse IgG for 1 h. Flow cytometry analysis was performed using FAC Scan flow cytometer (Becton Dickinson, San, CA, USA) and the data were conducted using WinMDI software. Fluorescence intensity, in arbitrary units, was expressed relative to the isotype control, cell population which was stained with FITC-conjugated antibody. The populations of histone labeled cells were gated according to the control histograms to determine the percentage of the cells labeled with histones antibody.

3. Results and discussion

3.1. Toxicity of daunomycin on multipotent hematopoietic cells of bone marrow

To investigate the potential effects of daunomycin on survival of the multipotent hematopoietic cells, both conventional trypan blue exclusion and MTT assays were used for comparison. Fig. 1A shows time and concentration dependent cell toxicity of daunomycin. The cells in the absence of daunomycin show more than 90% viability up to 6 h of incubation (e.g. 95%, 92.3% and 90.5% viability for 1, 4 and 6 h, respectively). Upon addition of daunomycin, the cell viability is reduced to 90%, 84% and 77.9%, at 10 μM of drug until it reaches to 70.8%, 42.6% and 21.5% at 300 μM of drug at 1, 4 and 6 h, respectively. As shown in Fig. 1A, upon increasing drug concentrations, the viability is decreased for 1, 4 and 6 h incubation time in a dose dependent manner and even very small amount of drug shows toxicity for these cells. There is considerable decrease in the cell viability within 6 h culture and in 1 h culture daunomycin did not have enough time to affect these cells. Therefore, through this time course study, 4 h incubation time was used throughout the experiments. Fig. 1B represents dose response curves for both MTT and trypan blue assays after 4 h of incubation. As is seen precise correlation is observed in the cell viability curve in both assays. In MTT assay about 30% decrease in the cell viability is obtained by enhancement of daunomycin increased, whereas in trypan blue exclusion assay, 50% cytotoxicity is recorded as compared to the control.

The result suggests that daunomycin has dose dependent cytotoxicity on these cells even at low concentration of daunomycin (10 μM) with exposure time of 4 h (IC50 = 150 μM). The effect of daunomycin on cancer cells especially leukemia cell line has been studied in detail [19] different IC50 values reported according to cell type, incubation time, cell sensitivity and number of the cells (e.g. for K562 after 24 h ~810 μM). Our data is in consistent with previous report that daunomycin causes dose dependent apoptotic cell death and may be considered as the side effect of this drug on bone marrow cells [20].

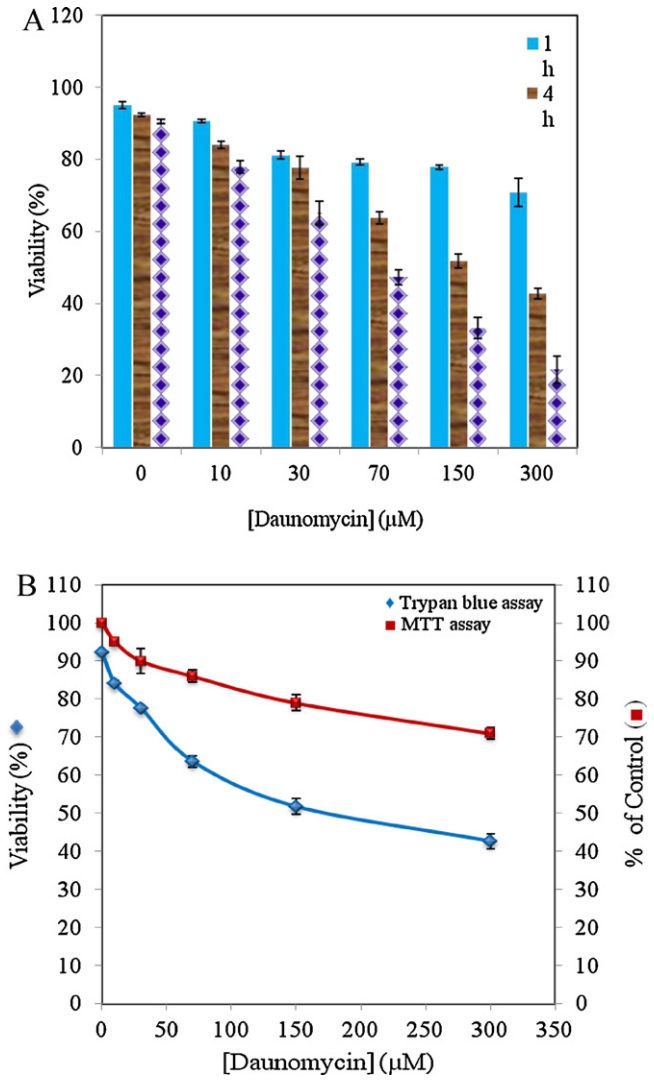

Fig. 1. (A) Effect of daunomycin on the viability of multipotent hematopoietic cells of bone marrow after 1 h ( ), 4 h ( ) and 6 h ( ) of exposure to various concentration of daunomycin. (B) Comparison of viability assay obtained from trypan blue exclusion ( ) and MTT ( ) assay. The cells (10^6/ml) were incubated with various concentrations of daunomycin for 4 h. Data are represented as means ± SD. (For interpretation of the references to color in this figure legend, the reader is referred to the web version of the article.)

3.2. Daunomycin prevents extractability of histone proteins

Concerning previous studies revealing that daunomycin, apart from DNA, interacts with histones and nonhistone proteins [7,21] it was interested to see whether daunomycin has any effect on chromatin proteins in these cells. To this end, histone proteins (H1, H1°, H2A, H2B, H3 and H4) were extracted from the cells cultured in the absence and presence of various concentrations of daunomycin and analyzed on SDS-PAGE. Confirmation studies were taken by immunoblot using anti mouse antibodies against H1, H2B, H2A, H3, H4 and H1°. Fig. 2 represents the pattern of histone proteins in comparison to calf thymus histones used as a reference. As is seen, the control (lane 1, in the absence of drug) exhibits slightly different pattern of histone proteins compared to thymus histones. In thymus all five main histones (H1, H2A, H2B, H3 and H4) are existed in the cell whereas in multipotent hematopoietic cells of bone marrow H1, H3 and H4 are seen as thick bands on the gel and there is a faint band in the position of histones H2A and H2B.

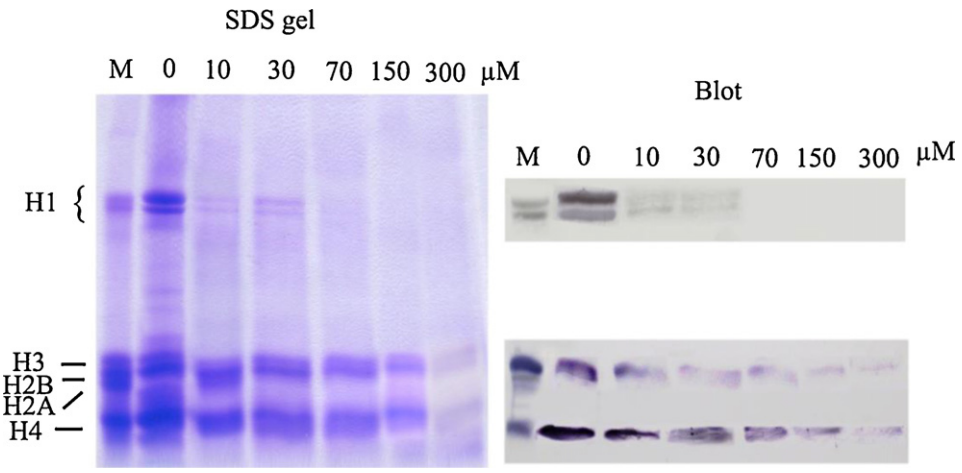

Fig. 2. SDS-polyacrylamide gel electrophoresis (15%) and immunoblots of the histone proteins extracted from the cells cultured in the absence and presence of various concentrations of daunomycin. The cells (2×10^6 cells) were extracted with equal volume of 0.25 N HCl and equal volumes were loaded. Daunomycin concentration in μM is shown on top of each lane. M: calf thymus histones as a standard. Western blot analysis has also been presented in the right ($n = 3$).

Immunoblot in Fig. 2 (signed as blots) shows that between the histone proteins extracted from bone marrow cells, only histones H1, H3 and H4 are reacted with the antibodies and represent a defined band on the nitrocellulose membrane, but no band is observed in the histones H2A and H2B position. In the presence of daunomycin (Fig. 2) histone H1 is the most sensitive histone against daunomycin action and its content is significantly decreased upon addition of low concentration of drug (<10 μM). The content of histones H3 and H4 remain unchanged up to 10 μM and then the contents are decreased until they are disappeared on the gel as daunomycin concentration is increased. Upon increasing drug concentration, the amount of extracted histone proteins is decreased. This observation with previous studies clearly suggest that daunomycin binds to chromatin and produces a compact structure possibly via forming cross links between the chromatin components [7] therefore, extractability of histone proteins decreases upon increasing daunomycin concentration in these cells. This is evidently shown by the disappearance of histones on the gel. Moreover daunomycin represents higher affinity to histone H1 compared to core histones. This is in agreement with the results reported previously that histone H1 is a suitable target for anticancer drugs such as daunomycin [21].

Moreover another protein that was analyzed was histone H1°, a subtype of histone H1 which is present preliminary in cells with little or no cell division, and its level appears to be related to the degree of differentiation [22]. Analysis of the extracted proteins on SDS gel and immunoblot did not show this protein in these cells (data not shown). The result is in consistent with the results indicating that this protein has a role in the organization of chromatin in arrested and differentiated cells. However, it is not a general rule, for example histone H1° has also been reported to be absent from lymphocytes as differentiated cells [23].

3.3. Identification of histone proteins by flow cytometry

Histones are structural and global proteins of chromatin that are found in all eukaryotic cells. The absence of H2A and H2B in multipotent hematopoietic cells of bone marrow is a strange case needed further investigation. For this purpose, the histone proteins of the multipotent hematopoietic cells were stained with FITC-conjugated antibody indirectly and analyzed by flow cytometry. Fig. 3A shows single stained histograms from isotype control and staining samples with H4, H3, H2B, H2A and ubiquitin antibodies. In general histograms shifted to right of M1 region which is indicative of isotype control (negative peak of the control) reflecting the intensity of each protein. The great the difference between the isotype control and the samples, the more histone proteins are expressed per cell and the more positive the population.

To compare the histones quantities, the resulting histograms are characterized as monophasic; therefore the Gmean fluorescence ratio was calculated using relative histones fluorescence intensities by WinMDI software. The geometric mean for each histogram of histones H4, H3, H2B, H2A and ubiquitin was 22.31, 21.83, 12.77, 9.52, and 10.36, respectively.

It can be demonstrated that these cells have equal amounts of histones H3 and H4 (34 and 33%, respectively) whereas the amount of histones H2A and H2B is much lower (14 and 19%, respectively) than histones H3 and H4 (or H2A and H2B in thymus). We know that distinct histone variants might have evolved to confer structural or regulatory heterogeneity on chromatin and histones H2A and H2B are more variable among different tissues than histones H3 and H4. Probably, some other variants of these proteins exist in multipotent hematopoietic cells which need to be elucidated. The presence of H2AZ as a variant of H2A which incorporates in decondensation of chromatin and make it transcriptionally active [24] was also analyzed but this protein was absent in these cells under the experimental condition used.

Ubiquitin is a small regulatory protein that has been found in almost all tissues of eukaryotic organisms. Our flow cytometry data shows the presence of this protein in these cells and its level is comparable to histones H2A and H2B (approximately equal).

3.4. Effect of daunomycin on HMGB/N proteins

After histones, high mobility group proteins (HMG) are the most abundant proteins which have role in inactive and active chromatin domains and control the expression of a limited number of genes specifically in processes such as development and differentiation [10]. Concerning identification of chromosomal proteins, HMG proteins were extracted from the multipotent hematopoietic cells of bone marrow, cultured in the absence and presence of various concentrations of daunomycin and analyzed on SDS-PAGE and immunoblot. Fig. 4 represents the pattern of HMG proteins in comparison to calf thymus HMGB and N proteins (lane M) used as a marker. As is seen, in these cells, HMGB proteins exhibit bands on the gel but no band is seen in the position of HMGN proteins.

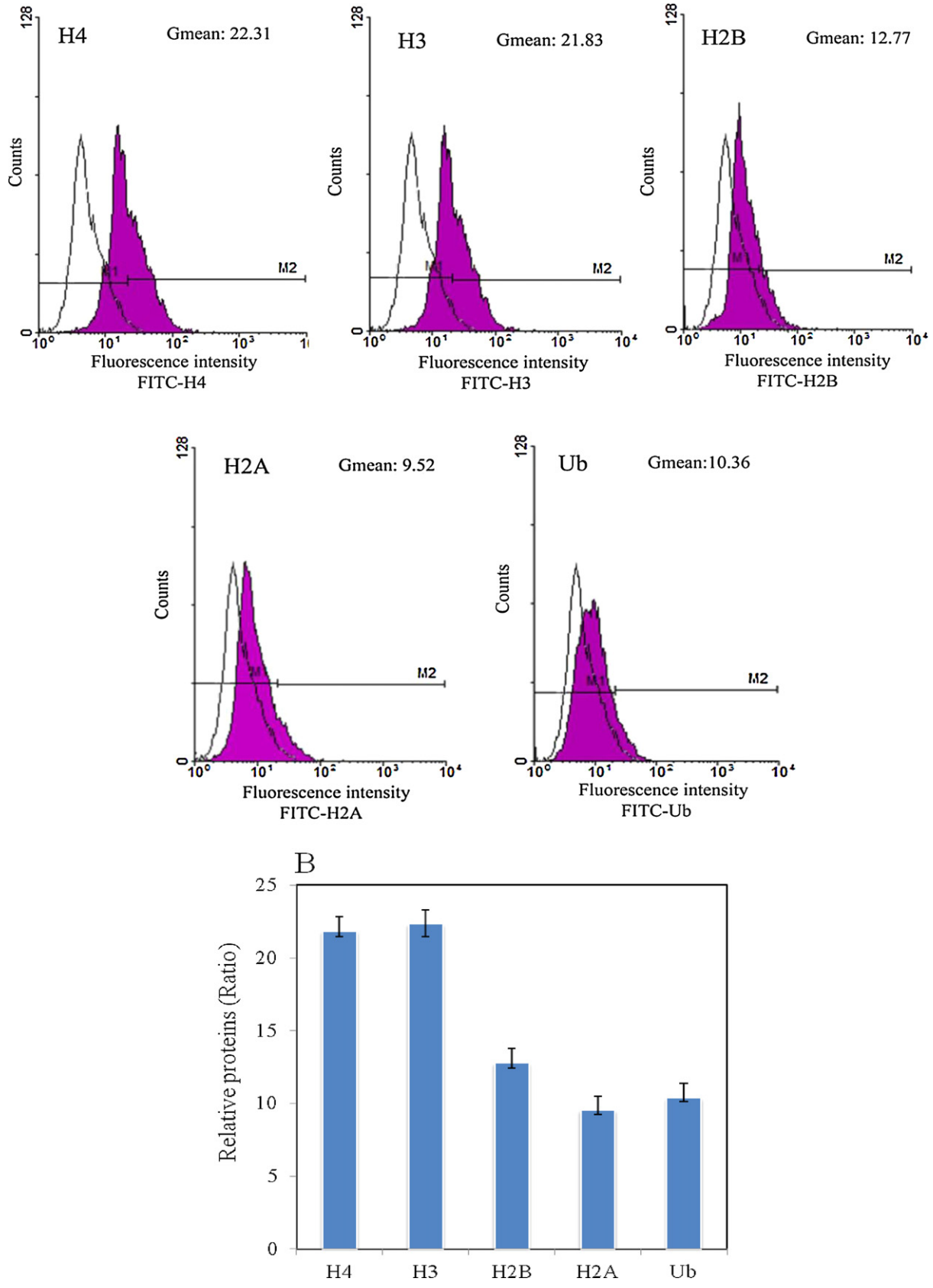

Fig. 3. (A) Single stained histogram of core histones and ubiquitin in bone marrow multipotent hematopoietic cells. The cells were fixed by paraformaldehyde and stained with: mouse H3, H4, H2B, H2A and ubiquitin antibodies. Region M1 (plain) corresponds to the isotype control which stained only with FITC-conjugated secondary antibody. Region M2 (pink) corresponds to expression of each protein. Movement in relative position of histograms represents histones intensities. (B) Relative intensities of histone proteins determined by the ratio of Geometric mean values from histograms describing the different protein expression. (For interpretation of the references to color in this figure legend, the reader is referred to the web version of the article.)

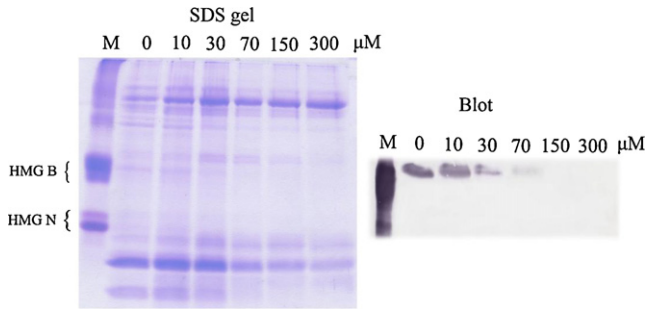

Fig. 4. SDS-polyacrylamide gel electrophoresis (15%) and immunoblot of HMG proteins extracted from the multipotent hematopoietic cells of mouse bone marrow (2×10^6 cells) incubated in the absence and presence of various concentrations of daunomycin. Daunomycin concentration in μM is shown on the top of each lane. M: calf thymus HMG proteins as a standard ($n = 3$).

Immunoblots data also confirmed the result. At low concentrations of daunomycin (<10 μM), the level of HMGB proteins on the gel is similar to the control but upon enhancement of drug concentration, the content of HMGB proteins is decreased until they become faded. Consistent with other researches that HMGB subfamily is ubiquitous in all eukaryotic cells [10]. HMGBs are found in multipotent hematopoietic cells of mouse bone marrow, but the absence of HMGN differ from studies by Mohamed et al. [25] which have demonstrated that HMGN expression is found in continuously renewing cell types and during mouse embryogenesis two HMGN are progressively down regulated through differentiation. Possibly because these cells are transcriptionally inactive the amount of this protein is low or does not express the case that needs further investigation of the stages of the cell cycle and mRNA expression of HMGN in these cells.

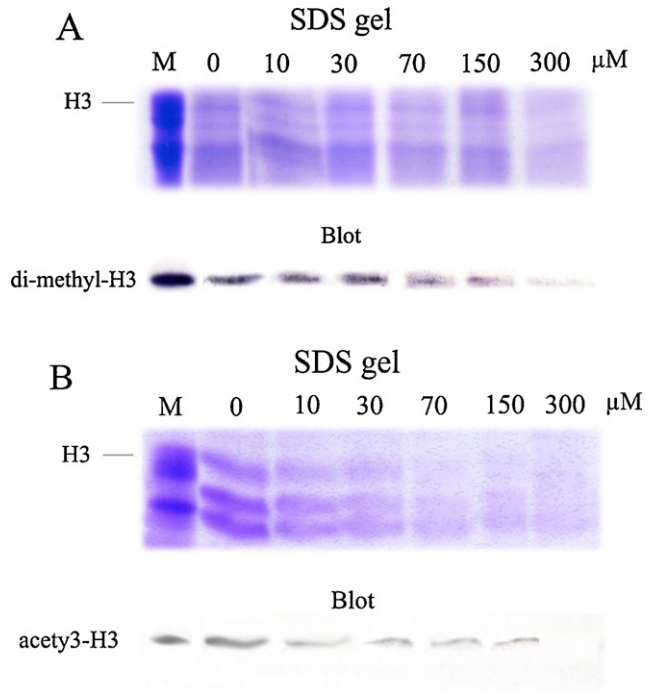

Fig. 5. SDS-gel and western blots of H3K9me2 and H3K9Ac modifications in the histones extracted from the multipotent hematopoietic cells of mouse bone marrow which were incubated with various concentrations of daunomycin. The histones were extracted with equal volumes of acid and equal volumes were analyzed on SDS-PAGE and transferred onto nitrocellulose for western blot analysis performed using both rabbit anti mouse H3K9me2 (A) and rabbit anti mouse H3K9Ac (B) each experiment was performed in triplicate.

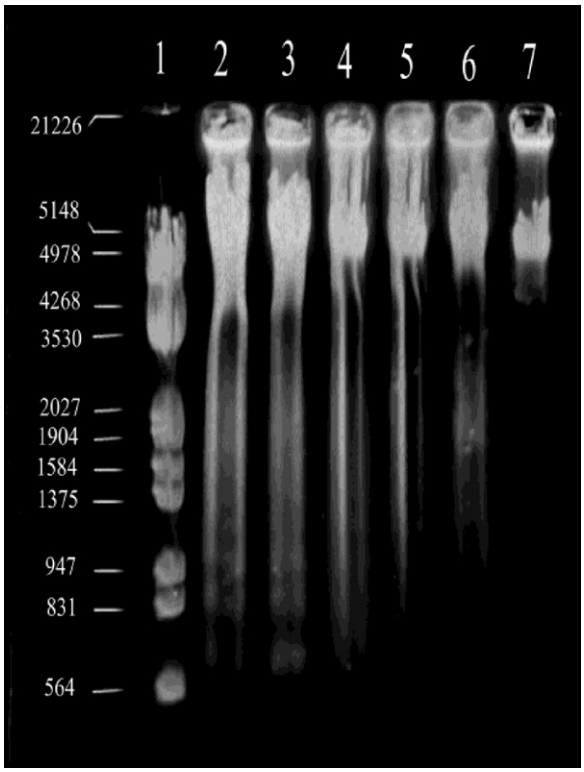

Fig. 6. Agarose gel (1.2%) electrophoresis of DNA extracted from the multipotent hematopoietic cells of mouse bone marrow treated with various concentration of daunomycin. After phenol extraction in the same experimental condition, DNA sample buffer were added and loaded. Lane 1, EcoRI, HindIII digested DNA marker. Lanes 2–7 are 0, 10, 30, 70, 150 and 300 μM of daunomycin, respectively. Number of experiments was 3.

3.5. Effect of daunomycin on acetylation and methylation of H3K9

Acetylation (H3K9Ac) and methylation (H3K9me2 and H3K9me3) of histone H3 are the most well known epigenetic markers of silence and active chromatin. However, H3K9Ac is associated with transcriptionally active chromatin [26,27]. In order to analyze epigenetic effect of daunomycin on histone H3, the cells were treated with different concentrations of daunomycin and the possible modifications were analyzed by SDS gel electrophoresis and immunoblot against anti H3K9me2, H3K9me3 and H3K9Ac antibodies. Fig. 5 represents an accumulation of H3K9me2 and H3K9Ac in the control (lanes 0 in A and B). In the presence of daunomycin the pattern of H3K9me2 is unaffected up to 30 μM of drug but is gradually diminished as drug concentration is increased (Fig. 5A). Daunomycin shows pronounced effect on the H3K9Ac thus at 10 μM the content of H3K9Ac is decreased on the gel and the band is completely disappeared as drug concentration is increased (Fig. 5B). H3K9 trimethylation could be identified neither in the control nor in the drug treated samples (data not shown). Other studies have revealed that H3K9Ac occur in promoter region of the genome and may serve to maintain transcriptionally competent regions of the genome by blocking methylation of H3K9 and preventing the downstream assembly of heterochromatin [27]. Whether existence of dimethylation and acetylation but not trimethylation in H3K9 have a role in transcriptional regulation and are involved in the establishment or maintenance of lineage progenitors or this modification occurs in different part of the genome is not known and remain to be elucidated.

3.6. Effect of daunomycin on DNA profile

Condensation of chromatin under daunomycin binding in these cells also is confirmed by analysis of DNA molecule. In this case, the cells were treated with daunomycin in the way and condition described for histones and analyzed on agarose gel. As is shown in Fig. 6 the cells treated with low concentrations of daunomycin (lanes 3–4 corresponding to 10–30 μM daunomycin) did not undergo any significant changes and their DNA pattern is similar to the control (lane 2). But upon increasing drug concentration low molecular weight bands are disappeared and only high molecular weight DNA bands located at the top of the gel are observed with lower content compared to the control. This observation clearly demonstrate compaction/aggregation of chromatin somehow that renders DNA to be unextractable. Our results come in support of the notion that apart from DNA, the protein component of chromatin can also be considered as a target for the activity of this antitumor drug. Whether daunomycin interacts directly with the histones or cross-linking occurs between the DNA and chromosomal proteins is still unknown.

4. Conclusions

Daunomycin is an anthracycline antibiotic which principally interacts with chromatin in nucleus. In this study, we attempted to report the effect of this drug on multipotent hematopoietic cells of bone marrow. Based on the results obtained, it is concluded that: (1) daunomycin has toxicity on multipotent hematopoietic cells of mouse bone marrow at very low concentrations and this can be considered as a side effect for cancers in which daunomycin is used especially in leukemia. (2) Daunomycin induces chromatin condensation/aggregation in which prevents extraction of chromosomal proteins by manual procedures. This can be achieved by cross-linking of drug with DNA and chromatin proteins introducing a compact structure preventing accessibility of histones to the extraction. (3) In addition, after treatment of the cells with daunomycin, H3K9me2 and H3K9Ac modifications are decreased in a dose dependent manner. (4) Multipotent hematopoietic cells of bone marrow represent lower amount of standard histones H2A and H2B compared to histones H3 and H4.

As the mechanism of bone marrow poisoning with daunomycin and nucleosomes component of multipotent hematopoietic cells of mouse bone marrow is not clear at this stage, these results can be useful for better understanding of this aspect at the chromatin level, however, many questions still remain to be elucidated which are subjects of ongoing studies in our laboratory.

Acknowledgment

The work was financially supported by a grant (# 6401017/6/12) of the Research Office of the University of Tehran to A.R.

References

[1] A. Valeri, M.E. Alonso-Ferrero, L. Cerrato, S. Martínez, J.A. Bueren, B. Albella, Development of an in vitro model for the simultaneous study of the efficacy and hematotoxicity of antileukemic compounds, Toxicol. Lett. 199 (2010) 317–322.
[2] S.J. Schomaker, F.A.S. Clemo, D.E. Amacher, Analysis of rat bone marrow by flow cytometry following in vivo exposure to cychlohexanone oxime or daunomycin HCl, Toxicol. Appl. Pharmacol. 185 (2002) 48–54.
[3] P. Crivori, G. Pennella, M. Magistrelli, P. Grossi, A.M. Giusti, Predicting myelosuppression of drugs from in silico models, J. Chem. Inf. Model. 28 (2011) 434–445.
[4] X. Zhu, Y. Ma, D. Liu, Novel agents and regimens for acute myeloid leukemia: 2009 ASH annual meeting highlights, J. Hematol. Oncol. 3 (2010) 17–26.
[5] J.B. Chaires, N. Dattagupta, D.M. Crothers, Binding of daunomycin to calf thymus nucleosomes, Biochemistry 22 (1983) 284–292.
[6] F. Belloc, F. Lacombe, P. Dumain, F. Lopez, P. Bernard, M.R. Boisseau, J. Reifers, Intercalation of anthracyclines into living cell DNA analyzed by flow cytometry, Cytometry 13 (1992) 880–885.
[7] A. Rabbani, R.M. Finn, J. Ausio, The anthracycline antibiotics: antitumor drugs that alter chromatin structure, Bioassays 27 (2005) 50–56.
[8] E.M. Bradbury, K.E. Van Holde, in: J. Zlatanova, S.H. Leuba (Eds.), Chromatin Structure and Dynamics: A Historical Perspective in Chromatin Structure and Dynamics: State of the Art, Elsevier, Amsterdam, The Netherlands, 2004.
[9] M. Bustin, Revised nomenclature for high mobility group (HMG) chromosomal proteins, Trends Biochem. Sci. 26 (2001) 152–153.
[10] M.E. Bianchi, A. Agresti, HMG proteins: dynamic players in gene regulation and differentiation, Curr. Opin. Genet. Dev. 15 (2005) 496–506.
[11] D. Parent-Massin, N. Hymery, Y. Sibiril, Stem cells in myelotoxicity, Toxicolology 12 (2010) 112–117.
[12] E.W. Johns, Studies on histone: preparative methods for histone fractions from calf thymus, Biochem. J. 92 (1964) 55–59.
[13] G.H. Goodwin, C. Sanders, E.W. Johns, A new group of chromatin-associated proteins with a high content of acidic and basic amino acids, Eur. J. Biochem. 38 (1973) 14–19.
[14] D.R. Clohisy, J.C. Chappel, S.L. Teitelbaum, Bone marrow-derived mononuclear phagocytes autoregulate mannose receptor expression, J. Biol. Chem. 264 (1989) 5370–5377.
[15] T. Mossman, Rapid colorimetric assay for cellular growth and survival: application to proliferation and cytotoxicity assays, J. Immunol. Methods 65 (1983) 55–63.
[16] U.K. Laemmli, Cleavage of structural proteins during the assembly of the head of bacteriophage T4, Nature 227 (1970) 680–685.
[17] A. Demaio, Protein blotting and immunoblotting using nitrocellulose membranes, in: B.S. Dunbar (Ed.), Protein Blotting, Oxford University Press, Oxford, 1996, pp. 11–32.
[18] J. Sambrook, E.F. Fritsch, T. Maniatis, Molecular Cloning: A Laboratory Manual, Cold Spring Harbor Laboratory Press, Cold Spring Harbor, NY, 1989.
[19] X. Yang, L. Yang, H. Chang, R.Q. Zhou, H.Y. Xing, B.H. Zheng, The anti-leukemic effects of imatinib, daunomycin and bortezomib on two leukemia cell lines with Ph (+), Sichuan Da Xue Bao Yi Xue Ban 41 (2010) 793–796.
[20] J. Li, H.K. Law, Y.L. Liu, G.C. Chan, Effect of cisplalin, toopotecan, daunorubicin and hydroxyurea on human mesenchymal stem cells, Zhongguo Shi Yan Xue Ye Xue Za Zhi 18 (2010) 991–996.
[21] A. Rabbani, R.M. Finn, A.A. Thambirajah, J. Ausio, Binding of antitumor antibiotic daunomycin to histones in chromatin and in solution, Biochemistry 43 (2004) 16497–16504.
[22] N.N. Kostova, L.N. Srebreva, A.D. Bogdanova, I.R. Lindner, D.V. Markov, Immunohistochemical demonstration of histone H1° in human breast carcinoma, Histochem. Cell Biol. 124 (2005) 435–443.
[23] O. Valiron, C. Gorka, Histone H1° expression is restricted to progenitor cells during human hepatopoiesis, Eur. J. Cell Biol. 72 (1997) 39–45.
[24] J.Y. Fun, F. Gordon, K. Luger, J.C. Hansen, D.J. Tremethick, The essential histone variant H2A.Z regulates the equilibrium between different chromatin conformational states, Nat. Struct. Biol. 9 (2002) 172–176.
[25] O.A. Mohamed, M. Bustin, H.J. Clarke, High-mobility group proteins 14 and 17 maintain the timing of early embryonic development in the mouse, Dev. Biol. 229 (2001) 237–249.
[26] J. Fuchs, D. Demidov, A. Houben, I. Schubert, Chromosomal histone modification patterns – from conservation to diversity, Trends Plant Sci. 11 (2006) 199–208.
[27] J.C. Rice, C.D. Allis, Histone methylation versus histone acetylation: new insights into epigenetic regulation, Curr. Opin. Cell Biol. 13 (2001) 263–273.

Journal of Pharmaceutical and Biomedical Analysis 66 (2012) 211–217

Contents lists available at SciVerse ScienceDirect

Journal of Pharmaceutical and Biomedical Analysis

journal homepage: www.elsevier.com/locate/jpba

Liquid chromatography–tandem mass spectrometric assay for the light sensitive calcium channel antagonist lacidipine in human plasma

Vijaya Kumari Karra[a], Nageswara Rao Pilli[a], Srinivasa Rao Polagani[b], Jaswanth Kumar Inamadugu[c], J.V.L.N. Seshagiri Rao[d,*]

[a] University College of Pharmaceutical Sciences, Jawaharlal Nehru Technological University, Kukatpally, Hyderabad 500 085, India
[b] Research Studies, Rayalaseema University, Kurnool 518 002, India
[c] Analytical and Environmental Chemistry Division, Sri Venkateswara University, Tirupathi 517 502, India
[d] University College of Pharmaceutical Sciences, Andhra University, Visakhapatnam 530 003, India

ARTICLE INFO

Article history:
Received 19 November 2011
Received in revised form 25 February 2012
Accepted 27 February 2012
Available online 6 March 2012

Keywords:
Lacidipine in human plasma
Solid-phase extraction (SPE)
Liquid chromatography–tandem mass spectrometry
Method validation
Pharmacokinetic studies

ABSTRACT

A novel, rapid and sensitive liquid chromatography/tandem mass spectrometry method was developed and validated for the quantification of calcium channel antagonist lacidipine in human plasma. Carbamazepine was used as an internal standard. Analyte and the internal standard were extracted from human plasma by solid-phase extraction technique. The reconstituted samples were chromatographed on a C_{18} column by using a mixture of acetonitrile–ammonium acetate buffer (5 mM) (80:20, v/v) as the mobile phase at a flow rate of 1.0 mL/min. The calibration curve obtained was linear ($r^2 \geq 0.9990$) over the concentration range of 0.05–12.5 ng/mL. The multiple reaction-monitoring mode was used for quantification of ion transitions at m/z 456.2/354.2 and 237.1/194.1 for the drug and the internal standard, respectively. The results of the intra- and inter-day precision and accuracy studies were well within the acceptable limits. A run time of 2.2 min for each sample made it possible to analyze more than 300 plasma samples per day. The proposed method was found to be applicable to clinical studies.

© 2012 Elsevier B.V. All rights reserved.

1. Introduction

Lacidipine is a calcium channel antagonist and developed for the treatment of hypertension [1–3]. In addition to its antihypertensive effect, lacidipine has also shown anti-atherosclerotic and antioxidant effects [4,5]. It has long duration of action because of its high degree of lipophilicity [6,7]. Lacidipine undergoes extensive first-pass hepatic metabolism and has a mean absolute bioavailability of about 10% (range 3–59%). It is completely metabolized in the liver by cytochrome P450 3A4 (CYP3A4) to pharmacologically inactive metabolites [2,3]. Therefore, the determination of the level of unchanged drug in plasma requires an analytical method with high sensitivity.

For the determination of lacidipine in biological fluids some high-performance liquid chromatographic methods [8–11] and liquid chromatography-mass spectrometric methods [12–14] were reported. Of all the above, only two methods are comparable with the present work. Ramakrishna et al. [13] reported a method with plasma concentration range of 0.1–25 ng/mL using 1.0 mL plasma sample volume. This method employs tedious liquid–liquid extraction; however, not sensitive enough for the determination of lacidipine concentrations for pharmacokinetic/bioequivalence studies. Another method proposed by Tang et al. [14] for quantification of lacidipine in human plasma (LLOQ of 0.025 ng/mL) also utilizes 1.0 mL plasma sample volume, which is very high compared to the present work.

In the present investigation, we have developed a method having a shorter run time with simple solid-phase extraction technique. The following are the advantages of the proposed method over those reported earlier: (1) because of the use of less plasma volume (250 μL), the volume of the sample to be collected per time point from an individual during the study is reduced significantly. This allows inclusion of additional points; (2) employing a simple solid-phase extraction procedure allows higher recoveries and the elimination of possible interference from endogenous and exogenous components; (3) greater sensitivity is achieved even with low plasma volumes and the method is well suited for pharmacokinetic analysis; (4) the rapid sample turnaround time of 2.2 min makes it an attractive procedure in high-throughput bioanalysis of lacidipine in human plasma.

* Corresponding author at: Department of Pharmaceutical Analysis, College of Pharmaceutical Sciences, Andhra University, Visakhapatnam 530 003, India. Tel.: +91 949 1766577/891 2535316.
E-mail address: jvlnsrao@rediffmail.com (J.V.L.N. Seshagiri Rao).

0731-7085/$ – see front matter © 2012 Elsevier B.V. All rights reserved.
doi:10.1016/j.jpba.2012.02.022

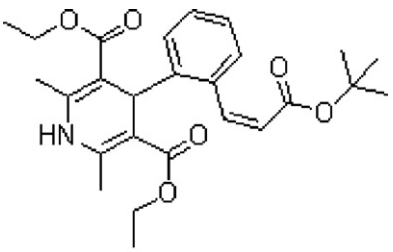

Lacidipine

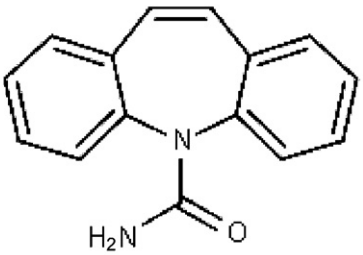

Carbamazepine (IS)

Fig. 1. Chemical structures of lacidipine and carbamazepine (IS).

2. Experimental

2.1. Chemicals

Lacidipine reference standard (98.8% pure) was obtained from Clearsynth Labs Limited (Mumbai, India). Carbamazepine (99.2% pure) was employed as an internal standard (IS) and was obtained from Vivan Life Sciences Limited (Mumbai, India). Chemical structures are presented in Fig. 1. Drug free human plasma containing K2. EDTA as an anticoagulant was obtained from the Cauvery Diagnostics (Hyderabad, India). HPLC-grade LiChrosolv methanol, LiChrosolv acetonitrile were from Merck (Darmstadt, Germany). Ammonium acetate, formic acid and ethyl acetate were from Merck (Worli, Mumbai, India). HPLC Type I water from a Milli-Q system (Millipore, Bedford, MA, USA) was used. All other chemicals were of analytical grade.

2.2. LC–MS/MS instrument and conditions

An HPLC system (Shimadzu, Kyoto, Japan) consisting of a Zorbax XDB-Phenyl column (75 mm × 4.6 mm, 3.5 μm; Agilent Technologies, Santa Clara, CA, USA), a binary LC-20AD prominence pump, an auto sampler (SIL-HTc) and a solvent degasser (DGU-20A_3) was used for the study. Aliquot of 10 μL of the processed samples were injected into the column, which was kept at room temperature (25 °C). An isocratic mobile phase consisting of a mixture of acetonitrile–ammonium acetate buffer (5 mM) (80:20, v/v) was used to separate the analyte and delivered at a flow rate of 1.0 mL/min into the electrospray ionization chamber of the mass spectrometer. Quantification was achieved with MS–MS detection in positive ion mode for the analyte and the internal standard using an MDS Sciex API-4000 mass spectrometer (Foster City, CA, USA) equipped with a Turboionspray™ interface at 500 °C. The ion spray voltage was set at 5000 V. The source parameters viz. the nebulizer gas (GS1), auxiliary gas (GS2), curtain gas and collision gas were set at 54, 35, 45, and 10 psi, respectively. Dwell time was set at 200 ms. The compound parameters viz. the declustering potential (DP), collision energy (CE), entrance potential (EP) and collision cell exit potential (CXP) were 72, 16, 10, 11 V for lacidipine and 75, 27, 10, 4 V for carbamazepine. Detection of the ions was carried out in the multiple-reaction monitoring mode (MRM), by monitoring the transition pairs of m/z 456.2 precursor ion to the m/z 354.2 for lacidipine and m/z 237.1 precursor ion to the m/z 194.1 product ion for the IS. Quadrupoles Q_1 and Q_3 were set on unit resolution. The analysis data obtained were processed by Analyst Software™ (version 1.4.2).

2.3. Preparation of plasma standards and quality controls

Standard stock solutions of lacidipine (1 mg/mL) was prepared in 1% formic acid in methanol, where as the IS (1 mg/mL) was prepared in methanol. Working solutions for calibration and controls were prepared by appropriate dilution in water–methanol (40:60, v/v; diluent). All the solutions were prepared under yellow monochromatic light and stored in dark to protect form photodegradation. The IS working solution (4 ng/mL) was prepared by diluting its stock solution with water–methanol (40:60, v/v; diluent).

Calibration samples were prepared by spiking 950 μL of control human plasma with the 50 μL working standard solution of the analyte as a bulk, to obtain lacidipine concentration levels of 0.05, 0.1, 0.41, 1.28, 2.57, 5.13, 7.6, 10 and 12.5 ng/mL. Similarly, quality control (QC) samples were also prepared as a bulk based on an independent weighing of standard drug, at concentrations of 0.05 (LLOQ), 0.15 (low), 1.91 (middle 1), 6.35 (middle 2) and 10.77 ng/mL (high) as a single batch at each concentration. The calibration and control bulk samples were divided into aliquots in micro centrifuge tubes (Tarson, 2 mL) and stored in the freezer at −70 °C until analyses.

2.4. Sample processing

A 250 μL aliquot of human plasma sample was mixed with 25 μL of the internal standard working solution (4 ng/mL of carbamazepine). To this, 250 μL of extraction buffer (0.5% formic acid in 100 mM ammonium acetate) was added after vortex mixing for 10 s. The sample mixture was loaded onto a Oasis HLB cartridge (30 mg/1 mL, Make: Waters Corporation) that was pre-conditioned with 1.0 mL of methanol followed by 1.0 mL water. The extraction cartridge was washed with 1.0 mL extraction buffer followed by 1.0 mL of water. Analyte and internal standard were eluted with 2.0 mL of dichloromethane and evaporated to dryness at 40 °C under a stream of nitrogen. The dried extract was reconstituted in 500 μL of mobile phase and transferred into amber-colored injector vials. From these, a 10 μL aliquot was injected into the chromatographic system. The entire sample processing and further LC–MS/MS analysis were carried out as soon as possible, under yellow monochromatic light in order to prevent the degradation of the lacidipine by light.

2.5. Bioanalytical method validation

The validation of the above method was carried out as per US FDA guidelines [17]. The parameters determined were selectivity, matrix effect, linearity, precision, accuracy, recovery, stability and dilution integrity. Selectivity was assessed by comparing the chromatograms of six different batches of blank plasma obtained from six different sources including one lipemic and hemolyzed plasma. Sensitivity was determined by analyzing six replicates of plasma samples spiked with the lowest level of the calibration curve concentrations. Matrix effect was checked with six different lots of K2. EDTA plasma. Three replicate samples each of LQC and HQC were prepared from different lots of plasma (36 QC samples in total). For checking the linearity standard calibration curves containing at least 9 points (non-zero standards) were plotted. In

addition, blank plasma samples were also analyzed to confirm the absence of direct interferences. Intra-day precision and accuracy were determined by analyzing six replicates at five different QC levels on two different days. Inter-day precision and accuracy were determined by analyzing six replicates at five different QC levels of five different runs. Recoveries of analyte and IS was determined by comparing the peak area of extracted analyte standard with the peak area of non-extracted standard. Recoveries of lacidipine was determined at a concentrations of 0.15 (low), 6.35 (middle 2) and 10.77 (high) ng/mL, whereas for IS was determined at concentration of 4 ng/mL. Dilution integrity was performed to extend the upper concentration limit with acceptable precision and accuracy. Six replicates each at a concentration of about 1.7 times of the uppermost calibration standard were diluted two- and four-fold with blank plasma. The diluted samples were processed and analyzed.

Stability tests were conducted to evaluate the analyte stability in stock solutions and in plasma samples under different conditions. The stock solution stability at room temperature and refrigerated conditions (2–8 °C) was performed by comparing the area response of the analyte (stability samples) with the response of the sample prepared from fresh stock solution. Bench top stability (8 h), processed samples stability (autosampler stability for 46 h, wet extract stability for 28 h and reinjection stability for 24 h), freeze–thaw stability (three cycles), long-term stability (60 days) were performed at LQC and HQC levels using six replicates at each level. Samples were considered to be stable if assay values were within the acceptable limits of accuracy (±15% SD) and precision (≤15% RSD).

2.6. Pharmacokinetic study design

A pharmacokinetic study on drug was performed in healthy male subjects ($n = 6$). The Ethics Committee (Hyderabad Independent Ethics Committee, Hyderabad, India) approved the protocol and the volunteers provided with informed written consent. Blood samples were collected under yellow monochromatic lamps following oral administration of a tablet of lacidipine (4 mg) at pre-dose and 0.25, 0.5, 0.75, 1, 1.25, 1.5, 1.75, 2, 2.25, 2.5, 2.75, 3, 3.5, 4, 5, 6, 8, 10, 12, 16, 24, 48, 72 and 96 h, in K2. EDTA vacutainer collection tubes (BD, Franklin, NJ, USA). The tubes were centrifuged at 3200 rpm for 10 min and the plasma was collected. The collected plasma samples were stored at −70 °C till their use. Plasma samples were spiked with the IS and processed as per the extraction procedure described earlier. Along with the clinical samples, the QC samples at low, middle 1, middle 2 and high concentration levels were also assayed in triplicate. Plasma concentration-time profile of lacidipine was analyzed by non-compartmental method using WinNonlin Version 5.1.

3. Results and discussion

3.1. Method development

In order to develop a method with the desired LLOQ (0.05 ng/mL), it was necessary to use MS/MS detection, as MS/MS method provides improved limit of detection for trace-mixture analysis. The inherent selectivity of MS/MS detection was also expected to be beneficial in developing a selective and sensitive method. The product ion mass spectrum of lacidipine and the IS are shown in Fig. 2. Protonated form of analyte and IS, $[M+H]^+$ ion was the parent ion in the Q_1 spectrum and was used as the precursor ion to obtain Q_3 product ion spectra. The most sensitive mass transition was observed from m/z 456.2 to 354.2 for lacidipine and from m/z 237.1 to 194.1 for the IS. LC-MRM is a very powerful technique for pharmacokinetic studies since it provides sensitivity and selectivity requirements for analytical methods. Thus, the MRM technique was chosen for the assay development. The MRM state file parameters were optimized at a concentration of 5 ng/mL to maximize the response for the analyte.

Chromatographic conditions, especially the composition of the mobile phase were optimized through several trials to achieve good resolution and increased intensity of the signals of the analyte, as well as short run time. It was found that a mixture of acetonitrile and 5 mM ammonium acetate (80:20, v/v) could achieve this purpose and was finally adopted as the mobile phase. Zorbax XDB-Phenyl (75 mm × 4.6 mm, 3.5 μm) column gave good peak shapes and response even at lowest concentration level for the analyte and IS. The mobile phase was operated at a flow rate of 1.0 mL/min. The retention times of analyte and the IS were low enough (1.3 and 0.95 min) allowing a short run time of 2.2 min. A simple solid-phase extraction (SPE) technique was employed for the sample preparation in this work and provides high recoveries of the drugs. For an LC–MS/MS analysis, utilization of stable isotope-labeled drugs as internal standards proves to be helpful when a significant matrix effect is possible. Isotope-labeled analyte was not obtainable to serve as IS, so, in the initial stages of this work, several compounds were investigated to find a suitable IS and finally carbamazepine was found to be best for the present purpose.

3.2. Selectivity and chromatography

The selectivity of the method was examined by analyzing blank human plasma extract (Fig. 3A) and an extract spiked only with the IS (Fig. 3B). As shown in Fig. 3A, no significant direct interference in the blank plasma traces was observed from endogenous substances in drug-free human plasma at the retention time of the analyte and IS. Similarly, Fig. 3B shows the absence of direct interference from the IS to the MRM channel of the analyte. Figs. 3C and 4 depict a representative ion-chromatogram for the LLOQ sample (0.05 ng/mL) and MRM chromatogram resulting from the analysis of a subject plasma sample after the administration of a 4 mg oral single dose of lacidipine.

3.3. Sensitivity

The lowest limit of reliable quantification for the analyte was set at the concentration of the LLOQ. The precision and accuracy of analyte at LLOQ concentration was found to be 2.34% and 93.0%, respectively.

3.4. Matrix effect

No significant matrix effect was observed in all the six batches of human plasma for the analyte at low and high quality control concentrations. The precision and accuracy for lacidipine at LQC concentration were found to be 0.97% and 100%, and at HQC level they were 0.33% and 96.1%, respectively.

3.5. Linearity

The nine-point calibration curve was found to be linear over the concentration range of 0.05–12.5 ng/mL for lacidipine. After comparing the two weighting models ($1/x$ and $1/x^2$), a regression equation with a weighting factor of $1/x^2$ of the drug to the IS concentration was found to produce the best fit for the concentration–detector response relationship for both the analytes in human plasma. The mean correlation coefficient of the weighted calibration curves generated during the validation was ≥0.9990.

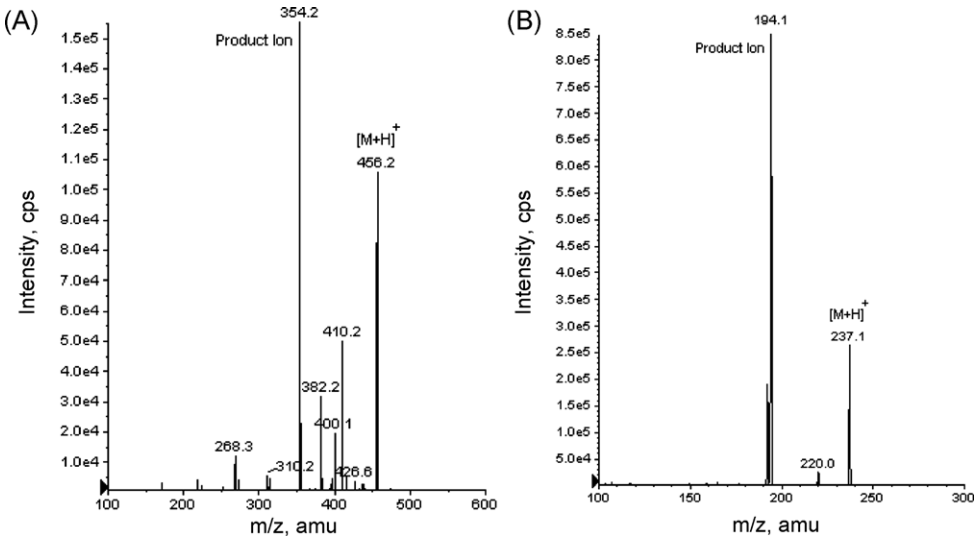

Fig. 2. Full scan positive mode product ion mass spectrum of (A) lacidipine and (B) carbamazepine (IS).

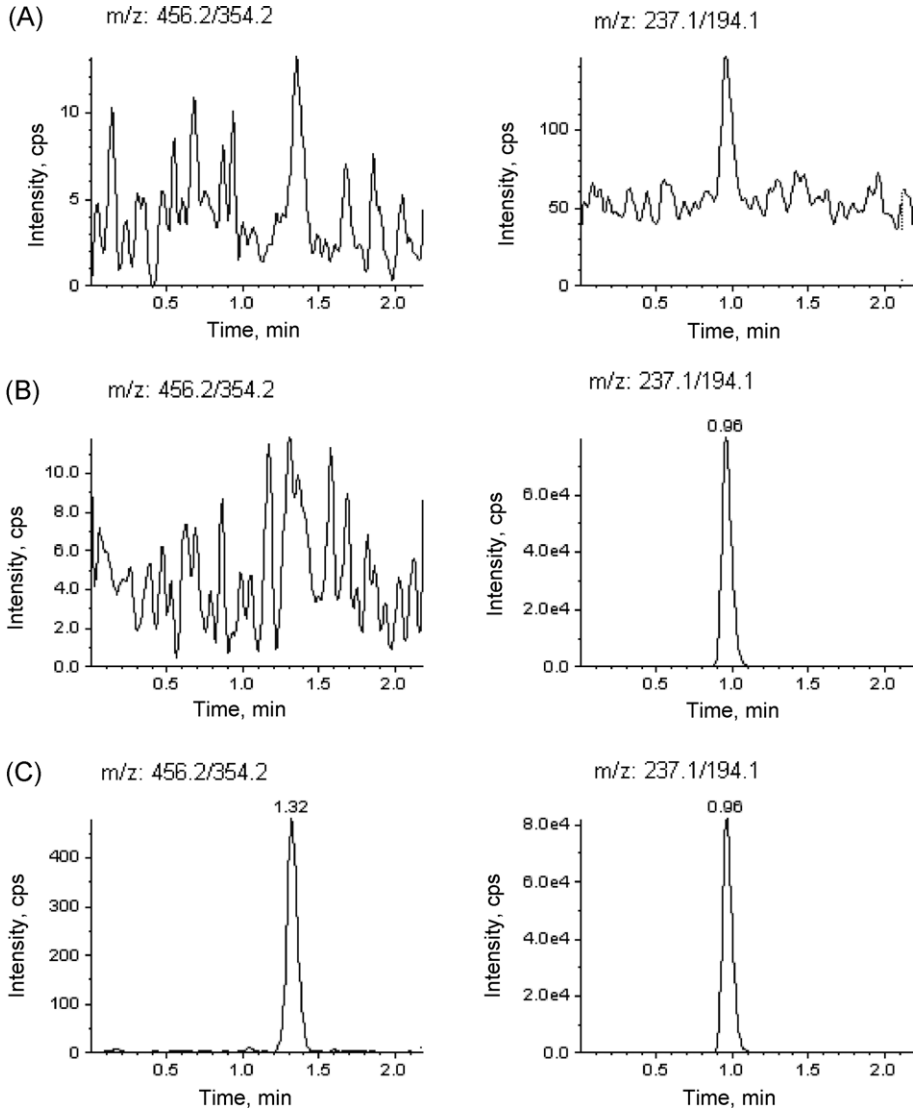

Fig. 3. Typical MRM chromatograms of lacidipine (left panel) and IS (right panel) in (A) human blank plasma (B) human plasma spiked with IS (C) a LLOQ sample along with IS.

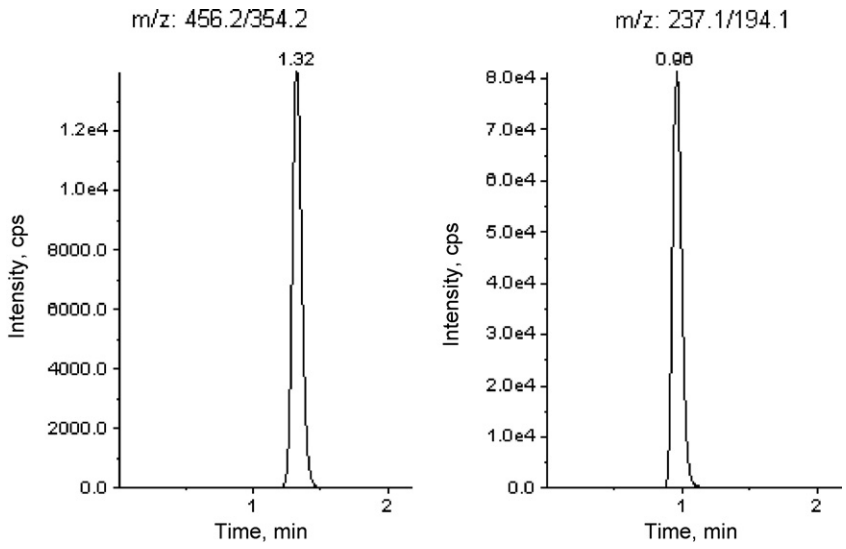

Fig. 4. MRM chromatograms resulting from the analysis of subject plasma sample after the administration of a 4 mg oral single dose of lacidipine. The sample concentration was determined to be 1.8266 ng/mL.

3.6. Precision and accuracy

The results for intra-day and inter-day precision and accuracy in plasma quality control samples are summarized in Table 1. The intra-day and inter day precision deviation values were all within 15% of the relative standard deviation (RSD) at low, middle 1, middle 2 and high quality control level, whereas within 20% at LLOQ QCs level. The intra-day and inter-day accuracy deviation values were all within 100 ± 15% of the actual values at low, middle 1, middle 2 and high quality control level, whereas within 100 ± 20% at LLOQ QCs level. The results revealed good precision and accuracy.

3.7. Extraction efficiency

Solid phase extraction with HLB cartridge proved to be robust and provided the cleanest samples. The recoveries of analyte and IS was good and reproducible. The mean overall recovery of analyte and IS is summarized in Table 2.

3.8. Dilution integrity

The upper concentration limit of lacidipine can be extended to 21.3 ng/mL for by 1/2 and 1/4 dilutions with screened human blank

Table 1
Precision and accuracy data for lacidipine.

Quality control	Run	Concentration found (mean ± SD; ng/mL)	Precision (%)	Accuracy (%)
Intra-day variations (n = 6)				
	1	0.045 ± 0.01	12.7	84.8
	2	0.054 ± 0.00	3.74	102
LLOQ	3	0.046 ± 0.00	2.98	86.8
	4	0.048 ± 0.00	6.46	91.5
	5	0.052 ± 0.00	8.79	98.4
	1	0.13 ± 0.01	6.09	86.5
	2	0.15 ± 0.00	2.86	96.0
LQC	3	0.14 ± 0.00	2.32	94.0
	4	0.15 ± 0.00	2.51	100
	5	0.15 ± 0.01	6.32	96.9
	1	1.85 ± 0.05	2.94	96.9
	2	1.82 ± 0.02	1.36	95.6
MQC1	3	1.82 ± 0.02	0.93	95.4
	4	1.79 ± 0.05	2.88	94.0
	5	1.85 ± 0.04	2.20	97.0
	1	5.96 ± 0.32	5.41	93.9
	2	5.98 ± 0.06	0.96	94.2
MQC2	3	6.00 ± 0.08	1.34	94.5
	4	6.27 ± 0.32	5.05	105
	5	6.48 ± 0.39	5.94	108
	1	9.51 ± 0.68	7.17	88.4
	2	9.95 ± 0.18	1.78	92.4
HQC	3	9.84 ± 0.09	0.95	91.4
	4	10.1 ± 0.54	5.34	93.4
	5	10.6 ± 0.41	3.92	98.1
Inter-day variations (n = 30)				
LLOQ	0.049 ± 0.00	10.2	92.8	
LQC	0.14 ± 0.01	6.32	94.7	
MQC1	1.82 ± 0.04	2.36	95.8	
MQC2	6.14 ± 0.33	5.29	96.7	
HQC	10.0 ± 0.54	5.36	92.7	

Spiked concentrations of LLOQ, LQC, MQC1, MQC2 and HQC are 0.05, 0.15, 1.91, 6.35 and 10.8 ng/mL, respectively.

Table 2
Mean overall recoveries of lacidipine and IS ($n = 6$).

Analyte	Sample concentration (ng/mL)	Response unextracted (mean ± SD)	Response extracted (mean ± SD)	Recovery (%)	Mean ± SD (% CV)
Lacidipine	0.15	22,234 ± 262	20,330 ± 934	91.44	91.91 ± 0.44 (0.48%)
	6.35	228,263 ± 3214	210,713 ± 12,393	92.31	
	10.77	383,749 ± 1160	352,922 ± 13,589	91.97	
Carbamazepine (IS)	4.00	328,897 ± 7674	281,965 ± 6496	85.73	–

Table 3
Stability data for lacidipine in plasma ($n = 6$).

Stability test	QC (spiked concentration (ng/mL)	Mean ± SD (ng/mL)	Accuracy/stability (%)	Precision (%)
Process[a]	0.15	0.15 ± 0.01	101	4.03
	10.8	10.4 ± 0.60	96.7	5.75
Process[b]	0.15	0.15 ± 0.01	101	4.03
	10.8	10.3 ± 0.51	95.3	4.92
Bench	0.15	0.15 ± 0.01	100	4.04
top[c]	10.8	10.3 ± 0.54	95.4	5.23
FT[d]	0.15	0.16 ± 0.00	102	3.04
	10.8	10.3 ± 0.54	95.5	5.29
Reinjection[e]	0.15	0.15 ± 0.01	97.7	3.45
	10.8	10.7 ± 0.38	99.2	3.57
Long-term[f]	0.15	0.14 ± 0.00	92.9	3.11
	10.8	9.92 ± 0.81	92.1	8.12

[a] After 46 h in autosampler at 10 °C.
[b] After 28 h in refrigerator at 2–8 °C.
[c] After 8 h at room temperature.
[d] After three freeze and thaw cycles.
[e] After 24 h of reinjection.
[f] At −70 °C for 60 days.

plasma. The mean back-calculated concentrations for 1/2 and 1/4 dilution samples were within 85–115% of their nominal value. The coefficients of variation (%CV) for 1/2 and 1/4 dilution samples were less than 5%.

3.9. Stability studies

All the stability experiments were conducted under a yellow monochromatic lamp as the lacidipine was found to be light sensitive [13,15,16]. In the different stability experiments carried out viz. bench top stability (8 h), autosampler stability (46 h), repeated freeze-thaw cycles (3 cycles), reinjection stability (24 h), wet extract stability (28 h at 2–8 °C) and long term stability at −70 °C for 60 days the mean % nominal values of the analyte was found to be within ±15% of the predicted concentrations for the analyte at their LQC and HQC levels (Table 3). Thus, the results were found to be within the acceptable limits during the entire validation.

Stock solutions of lacidipine and IS were found to be stable for 20 days at 2–8 °C. The percentage stability (with the precision range) of lacidipine and IS were 97.2% (1.40–3.54%) and 103% (0.86–5.85%), respectively.

3.10. Pharmacokinetic study results

In order to verify the sensitivity and selectivity of this method in a real-time situation, the present method was used to test for lacidipine in human plasma samples collected from healthy male volunteers ($n = 6$). The mean plasma concentrations vs time profile of lacidipine is shown in Fig. 5 and corresponding pharmacokinetic parameters are listed in Table 4. These values were in close proximity when compared with earlier reported values [14].

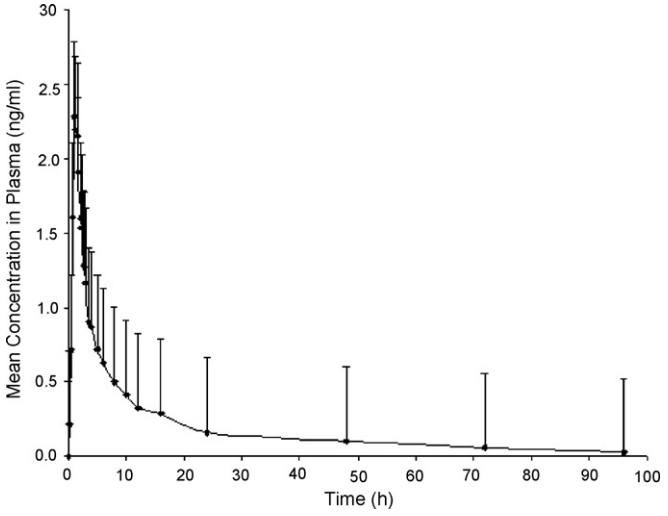

Fig. 5. Concentration–time profile of lacidipine in human plasma after a single oral dose of 4 mg.

Table 4
Pharmacokinetic parameters of lacidipine ($n = 6$, mean ± SD).

Parameter	Estimate value
C_{max} (ng/mL)	2.40 ± 0.52
t_{max} (h)	1.25 ± 0.32
AUC_{0-t} (ng h/mL)	18.6 ± 9.55
AUC_{0-inf} (ng h/mL)	19.9 ± 9.96
$t_{1/2}$ (h)	24.7 ± 13.64

4. Conclusions

The LC–MS/MS assay presented in this paper is rapid, simple, specific and sensitive for quantification of lacidipine in human

plasma and is fully validated according to commonly acceptable FDA guidelines. The method showed suitability for pharmacokinetic studies in humans. The extraction method gave high, consistent and reproducible recoveries for the analyte and IS from plasma. The cost-effectiveness, simplicity of the assay and usage of solid-phase extraction and sample turnover rate of less than 2.2 min per sample, make it an attractive procedure in high-throughput bioanalysis of lacidipine.

Acknowledgment

The authors gratefully acknowledge Wellquest Clinical Research Laboratories for providing necessary facilities to carry out this work.

References

[1] C.R. Lee, H.M. Bryson, Lacidipine: a review of its pharmacodynamic and pharmacokinetic properties and therapeutic potential in the treatment of hypertension, Drugs 48 (1994) 274–296.
[2] P.L. McCormack, A.J. Wagstaff, Lacidipine: a review of its use in the management of hypertension, Drugs 63 (2003) 2327–2356.
[3] P. Tcherdakoff, J.M. Mallion, K.H. Rahn, French large-scale study evaluating the tolerability and efficacy of lacidipine, J. Cardiovasc. Pharmacol. 25 (1995) S27–S32.
[4] G.Y. Anacak, L. Ustünes, O.Y. Dilsiz, A. Ergul, Lacidipine has antiatherosclerotic effects independent of its actions on lipid metabolism and blood pressure, Vascul. Pharmacol. 53 (2010) 193–199.
[5] R. Toniolo, F.D. Narda, G. Bontempelli, F. Ursini, An electroanalytical investigation on the redox properties of lacidipine supporting its anti-oxidant effect, Bioelectrochemistry 51 (2000) 193–200.
[6] G. Leonetti, Comparative study of lacidipine and nicidipine SR in the treatment of hypertension: an Italian multicenter study, J. Cardiovasc. Pharmacol. 17 (1991) S31–S34.
[7] M. Dino, R. Emiliangelo, G. Toson, G. Giovanni, Pharmacology of lacidipine, a vascular-selective calcium antagonist, J. Cardiovasc. Pharmacol. 17 (1991) S1–S8.
[8] A.B. Baranda, N. Etxebarria, R.M. Jimenez, R.M. Alonso, Development of a liquid–liquid extraction procedure for five 1,4-dihydropyridines calcium channel antagonists from human plasma using experimental design, Talanta 67 (2005) 933–941.
[9] J.A. Lopez, V. Martınez, R.M. Alonso, R.M. Jimenez, High-performance liquid chromatography with amperometric detection applied to the screening of 1,4-dihydropyridines in human plasma, J. Chromatogr. A 870 (2000) 105–114.
[10] M. Pellegatti, S. Braggio, S. Sartori, Validation of a high-performance liquid chromatographic-radioimmunoassay method for the determination of lacidipine in plasma, J. Chromatogr. Biomed. Appl. 573 (1992) 105–111.
[11] V.R. Kharat, K.K. Verma, J.D. Dhake, Determination of lacidipine from urine by HPTLC using off-line SPE, J. Pharm. Biomed. Anal. 28 (2002) 789–793.
[12] P. Rossato, M. Scandola, P. Grossi, Investigation into lacidipine and related metabolites by high-performance liquid chromatography–mass spectrometry, J. Chromatogr. 647 (1993) 155–166.
[13] N.V.S. Ramakrishna, K.N. Vishwottam, S. Puran, S. Manoj, M. Santosh, M. Koteshwara, Simple, sensitive and rapid liquid chromatographic/electrospray ionization tandem mass spectrometric method for the quantification of lacidipine in human plasma, J. Mass Spectrom. 39 (2004) 824–832.
[14] J. Tang, R. Zhu, R. Zhao, G. Cheng, W. Peng, Ultra-performance liquid chromatography–tandem mass spectrometry for the determination of lacidipine in human plasma and its application in a pharmacokinetic study, J. Pharm. Biomed. Anal. 47 (2008) 923–928.
[15] F.P. De, E. Bovina, R.L. Da, J. Fiori, V. Cavrini, Photodegradation studies on lacidipine in solution: basic experiments with a *cis–trans* reversible photoequilibrium under UV-A radiation exposure, J. Pharm. Biomed. Anal. 27 (2002) 803–812.
[16] A.B. Baranda, R.M. Alonso, R.M. Jimenez, W. Weinmann, Instability of calcium channel antagonists during sample preparation for LC–MS–MS analysis of serum samples, Forensic Sci. Int. 156 (2006) 23–34.
[17] Food and Drug Administration, Guidance for Industry, Bioanalytical Method Validation, 2001.

Journal of Pharmaceutical and Biomedical Analysis 66 (2012) 218–224

Contents lists available at SciVerse ScienceDirect

Journal of Pharmaceutical and Biomedical Analysis

journal homepage: www.elsevier.com/locate/jpba

β-Cyclodextrin enhanced on-line organic solvent field-amplified sample stacking in capillary zone electrophoresis for analysis of ambroxol in human plasma, following liquid–liquid extraction in the 96-well format

Ji Li[a,b], Youwei Bi[a,b,c], Li Wang[a,b,d], Fanlu Sun[a,b], Zhao Chen[a,b], Guili Xu[e,*], Guorong Fan[a,b,**]

[a] Department of Pharmaceutical Analysis, School of Pharmacy, Second Military Medical University, No. 325 Guohe Road, Shanghai 200433, PR China
[b] Shanghai Key Laboratory for Pharmaceutical Metabolite Research, No. 325 Guohe Road, Shanghai 200433, PR China
[c] School of Medicine, Shanghai Jiaotong University, No. 800 Dongchuan Road, Shanghai 200240, PR China
[d] Department of Pharmaceutical Analysis, China Pharmaceutical University, Nanjing 210009, PR China
[e] Department of Pharmacy, Kunming General Hospital of Chengdu Military Command, No. 212 Daguan Road, Kunming, Yunnan 650032, PR China

ARTICLE INFO

Article history:
Received 5 November 2011
Received in revised form 27 February 2012
Accepted 28 February 2012
Available online 8 March 2012

Keywords:
Ambroxol hydrochloride
CZE
Plasma
Field-amplified sample stacking
96-Well format LLE

ABSTRACT

A field-amplified sample stacking (FASS) and capillary zone electrophoresis (CZE) method is described for the quantification of ambroxol hydrochloride in human plasma, following liquid–liquid extraction in the 96-well format. The separation was carried out at 25 °C in a 31.2 cm × 75 μm fused-silica capillary with an applied voltage of 15 kV. The background electrolyte (BGE) was composed of 6.25 mM borate–25 mM phosphate (pH 3.0) and 1 mM β-cyclodextrin. The detection wavelength was 210 nm. Clean-up and preconcentration of plasma biosamples were developed by 96-well format liquid–liquid extraction (LLE). In this study, FASS in combination with β-cyclodextrin enhanced the sensitivity about 60–70 fold in total. The method was suitably validated with respect to stability, specificity, linearity, lower limit of quantitation, accuracy, precision, extraction recovery and robustness. The calibration graph was linear for ambroxol hydrochloride from 2 to 500 ng/ml. The lower limit of quantification was 2 ng/ml. The intra- and inter-day precisions of lowest limit of quantification (LLOQ) were 9.61 and 11.80%, respectively. The method developed was successfully applied to the evaluation of clinical pharmacokinetic study of ambroxol hydrochloride tablet after oral administration to 12 healthy volunteers.

© 2012 Published by Elsevier B.V.

1. Introduction

Ambroxol (trans-4-(2-amino-3, 5-dibromobenzyl)-aminocyclohexanol, Fig. 1), a metabolite of bromhexine [1], is an expectorant and mucolytic agent, which could reduce the bronchial hyper-reactivity, stimulate the cellular surfactant production and increase the amount of antibiotic penetration [2–6]. In addition to the mucolytic action, it has also been reported to have a cough-suppressing effect, antioxidant and anti-inflammatory action [1,7,8]. Ambroxol is administered as hydrochloride in a daily dose of 30–120 mg using oral, rectal, inhalation and intravenous routes, which produces good results in the treatment of chronic bronchitis [9].

In order to carry out clinical pharmacokinetic studies of ambroxol hydrochloride, a rapid and sensitive analytical method was needed, which could allow its determination in plasma. Common separation methods had been reported for the determination of ambroxol in various matrices based on HPLC determinations with UV [10], electrochemical [11,12] and mass spectrometric detection [13–16], and gas chromatography determinations with electron capture [17,18] and mass spectrometric detection [19]. Some of these methods suffered from inadequate sensitivity or long analysis time. Although LC–MS/MS method can provide excellent sensitivity and short run time, the apparatus is expensive and the matrix effects are difficult to overcome. Capillary electrophoresis (CE) is rapidly developing as an alternative analytical tool with different separation mechanism to HPLC, because of its high efficiency, rapid separation, extremely low solvent consumption compared with HPLC, and small sample volume requirement [20]. What is more, the cost of capillaries is far cheaper than that of HPLC columns. Up to date, only Pérez-Ruiz et al. reported two CE methods for clinical analysis of ambroxol [9,21]. Disadvantages

Abbreviations: CZE, capillary zone electrophoresis; CE, capillary electrophoresis; FASS, field-amplified sample stacking; BGE, background electrolyte; LLE, liquid–liquid extraction; EOF, electroosmotic flow; HD, hydrodynamic; EK, electrokinetic; LC–MS/MS, liquid chromatography tandem mass spectrometry; UV, ultraviolet; HPLC, high-performance liquid chromatography; LLOQ, lower limit of quantification; IS, internal standard; QC, quality control sample.

* Corresponding author. Tel.: +86 871 5414186; fax: +86 871 5414186.
** Corresponding author at: School of Pharmacy, Second Military Medical Univ., No. 325 Guohe Road, Shanghai 200433, PR China. Tel.: +86 21 8187 1260; fax: +86 21 8187 1260.
E-mail addresses: guilixukm@163.com (G. Xu), guorfan@yahoo.com.cn (G. Fan).

0731-7085/$ – see front matter © 2012 Published by Elsevier B.V.
doi:10.1016/j.jpba.2012.02.026

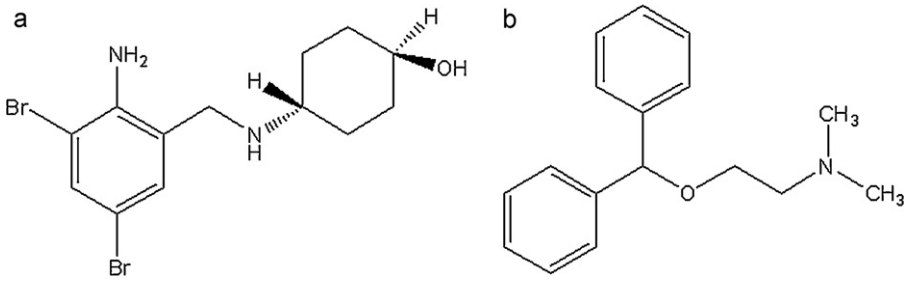

Fig. 1. Chemical structures of ambroxol (a) and internal standard diphenhydramine (b).

of these are tedious derivatization process [9] and low detection sensitivity and long analysis time [21], respectively.

To solve the problem of low sensitivity, field-amplified sample stacking (FASS) is usually employed as a simple and efficient technique in capillary zone electrophoresis (CZE), first introduced by Mikkers et al. [22,23]. It is based on a mismatch between the electric conductivity of the sample and that of the running buffer. When compared to injection from a nonstacking sample, conventional FASS provided a sensitivity enhancement of about 10- to 20-fold [24]. Shihabi [25] reported that some water-miscible organic solvents, especially acetonitrile and acetone, bring along greater degrees (~30 times) of stacking for the compounds compared to that for aqueous buffers or water. However, sometimes FASS could result in peak tailing and poor reproducibility, which is attributed to the introduction of matrix in large amount. Therefore, β-cyclodextrin which normally acts as carrier electrolyte additive in capillary electrophoretic (CE) techniques and chiral selector was reported to be used for improving peak shape and separation efficiency and obtaining good reproducibility of migration times [26].

In this paper, we tried to enhance sensitivity by means of organic solvent field-amplified sample stacking combined with β-cyclodextrin in capillary zone electrophoresis for the determination of ambroxol hydrochloride in human plasma. The method was evaluated in terms of selectivity, sensitivity, linearity, accuracy, precision and stability in accordance to the recommendations published by the FDA [27], and when combined with 96-well format liquid–liquid extraction, it was successfully applied to the analysis of ambroxol hydrochloride in clinical pharmacokinetic studies in 12 healthy volunteers.

2. Experimental

2.1. Chemicals and reagents

Ambroxol hydrochloride (99.4% purity) and the tablet formulation of ambroxol hydrochloride (30 mg, lot08030151) were from Jiangsu Hengrui Pharmaceutical Co. Ltd. (Jiangsu, PR China). Diphenhydramine hydrochloride (99.0% purity) was used as the internal standard (IS, Fig. 1) obtained from National Institute for the Control of Pharmaceutical and Biological Product (Beijing, PR China). $Na_2B_4O_7$, NaH_2PO_4 and β-cyclodextrin were acquired from China Medicine (Group) Shanghai Chemical Reagent Corporation (Shanghai, PR China). Human control plasma (sodium heparin as an anticoagulant) was obtained from Kunming General Hospital of Chengdu Military Command (Yunnan, PR China). Water was deionized and purified by using a Milli-Q system (Millipore, Milford, MA, USA) and was used to prepare all aqueous solutions.

2.2. Instrumentation

The employed CE system consisted of a Beckman P/ACE MDQ instrument (Beckman Coulter, Brea, CA) equipped with a photodiode array detection detector (PDA) and P/ACE System MDQ Software. Detection was performed at 210 nm, where ambroxol had the maximum absorption. Fused-silica capillaries (31.2 cm × 75 μm i.d., effective length 21 cm) were obtained from Hebei Yongnian Optical Fiber Factory (Hebei, China). 96-Well plate refrigerated centrifuge (Model SC210A, Thermo Electron, USA) was also used. The 2.0 ml Oasis® 96-well plates were purchased from Waters Corporation (Milford, USA).

2.3. Capillary electrophoretic conditions

The background electrolyte (BGE) used in this study was composed of 25 mM borate–25 mM phosphate (pH 3.0) and 1 mM β-cyclodextrin. It was prepared by accurately weighing 0.39 g phosphate and 0.24 g borate and making up to 100 ml with deionized water. After that, buffer pH was adjusted to 3.0 with 10% phosphoric acid. Then 0.1135 g β-CD was weighed and added into the borate–phosphate buffer. The capillary temperature was maintained at 25 °C and the separation voltage was 15 kV with the current of about 70 μA. The sample was introduced by using electrokinetic (7.5 kV × 15 s) injection modes. BGE were prepared freshly every day and filtered through a 0.45 μm hydrophilic cellulose membrane filter prior to use. A new capillary was conditioned by rinsing with 1 M NaOH, 0.1 M NaOH, H_2O and 0.1 M HCl (30 min each) sequentially. Daily conditioning before start-up was water (2 min), 0.1 M NaOH (10 min), water (2 min), and running buffer (10 min) in regular sequences. Between runs, the capillary was rinsed with 0.01 M NaOH, H_2O and separating buffer (2 min each) sequentially.

2.4. Preparation of stock solutions, calibration samples and quality control samples

Stock solutions of ambroxol hydrochloride and the IS were prepared in methanol at concentrations of 2 mg/ml and 1 mg/ml, respectively. The ambroxol hydrochloride stock solution was diluted with distilled water to working solutions ranging from 20 to 5000 ng/ml. A 250 ng/ml IS working solution was obtained by diluting the stock solution of IS with distilled water. All described solutions were protected from light, stored at 4 °C.

Calibration samples were obtained by diluting standard working solutions (20 μl) with drug-free human control plasma (180 μl), to span a calibration standard range of 2–500 ng/ml (2, 5, 10, 20, 50, 100, 200, and 500 ng/ml). Quality control (QC) samples (5, 20, 400 ng/ml) were independently prepared by spiking appropriate amount of the working standard solution in drug-free human control plasma.

2.5. Sample preparation

Samples were prepared using LLE in 96-well format plates. An eight-channel 300 μl electronic pipetting tool and an eight-channel 1200 μl electronic pipetting tool (Eppendorf Xplorer®, Eppendorf AG, Hamburg, Germany) were used for liquid transfer steps. Subject plasma samples were thawed at room temperature. 200 μl of

subject plasma samples, standard curve samples and QC samples were added individually into a 2 ml deep 96-well plate spiked by an eight-channel pipetting tool. Aliquots of 30 μl internal standard solution (250 ng/ml) were added, except to the well designated for the double blank plasma. Then 60 μl 1 M sodium hydroxide were added to each well of the plate, and vortexed for 30 s. After adding 1.0 ml of N-hexane, the plate was covered with a mat, vortexed for 5 min, and centrifuged 10 min at 3500 rpm. The mats were carefully removed and 800 μl of the supernatant organic layer was transferred from the original sample plates into the respective positions of new 2.0 ml deep 96-well plates. The height of the transfer stage was carefully chosen so that only the organic layer was aspirated by an eight-channel pipetting tool. The plates were then placed into a self-constructed 96-well plate evaporator, and the organic extracts were evaporated to dryness with a nitrogen flow at 30 °C. All dry residues were reconstituted by addition of 50 μl ACN–water (80:20, v/v). Finally, the plates were vortex mixed for 5 min, then centrifuged for 10 min at 12,000 rpm, and the supernatant was transferred to the autosampler for injection onto the CE.

2.6. Clinical pharmacokinetic study

The method was applied to determine plasma concentrations of ambroxol hydrochloride from a clinical trial in which 12 healthy volunteers received a single oral dose of 90 mg of ambroxol hydrochloride tablet. About 1 ml of blood samples were collected in heparinized tubes before administration (0 h) and 0.25, 0.50, 1.0, 1.5, 2.0, 2.5, 3.0, 4.0, 6.0, 9.0, 12.0, 15.0 and 24.0 h after dosing and centrifuged at 3500 rpm for 10 min to separate the plasma fraction. The obtained plasma samples were stored at −20 °C until analysis. The study was approved by a local ethics committee and performed after obtaining written consent from the subject.

3. Results and discussion

3.1. Method development

In this study, we explored the optimization and validation of preconcentration process and separation mode. Both ambroxol and IS have strong UV absorption at 210 nm. Therefore the detection wavelength was set at 210 nm.

3.1.1. Optimization of borate–phosphate buffer concentrations and pH and voltage

Borate–phosphate buffer (pH 3.0) in different concentrations (3.125 mM borate–12.5 mM phosphate, 6.25 mM borate–25 mM phosphate, 12.5 mM borate–50 mM phosphate) was studied. Higher concentrations of buffer caused the increase in current and reduction in the EOF, leading to more Joule heating and longer analysis time. However, lower concentrations of electrolyte decreased the ionic strength of the buffer, which could lower the sensitivity. In order to get the best running time and sensitivity of the analytes, 6.25 mM borate–25 mM phosphate buffer was selected.

Based on the p*K*a value (8.2) of ambroxol [28], measurements were carried out at pH values lower than 7.0. Running buffer containing 6.25 mM borate–25 mM phosphate was studied at different pH to observe the influence on electrophoretic behavior of ambroxol and IS in terms of separation efficiency and migration time. The increase of the pH from 2.5 to 6.0 shortened the migration time of both ambroxol and IS and worsened the resolution. Better resolution and analysis time were obtained when pH < 4, so we chose a running buffer containing 6.25 mM borate–25 mM phosphate with a pH of 3.0.

Various voltages were tested, including 10, 15, 20, and 25 kV. Due to the big inner diameter (75 μm) and short length (31.2 cm) of capillary, too large separation voltage in our experiment induced certain current problems, such as appreciable Joule heating. 15 kV was chosen because it provided optimal separation and efficiency.

3.1.2. Selection of injection modes and sample solvent

The sample is usually introduced into the capillary either by hydrodynamic (HD) or electrokinetic (EK) injection. Under the former, all components were introduced without discrimination, resulting in more endogenous interference when conducting biosample analysis. To avoid those interferences in the CZE mode, the latter was considered a better option for the better sensitivity and selectivity of basic drugs. Furthermore, in our experiment, the peak shapes of both ambroxol and IS in the latter was better than those in the former. In addition, EK is reported suitable for online FASS [29]. Therefore the electrokinetic injection was chosen as the optimum.

In order to enhance the response of ambroxol, the compositions of sample solvent (10% buffer, distilled water, ACN–distilled water) were investigated. As shown in Fig. 2, using ACN–distilled water as sample solvent was good at improving sensitivity. The mechanism of transient pseudo-isotachophoresis has been proposed for acetonitrile stacking, in which fast moving anions in the salts serve as leading ions, whereas water-miscible organic solvents act as the slower moving “terminating ions” [30,31]. For further exploration of ACN on ambroxol stacking, different ratios of ACN to distilled water (70%, 80%, 90%) were also investigated. With the increase of acetonitrile concentration, ambroxol was stacked more effectively. However, 90% acetonitrile caused the current drop to zero, so we chose 80% ACN–distilled water as sample solvent.

3.1.3. Concentrations of β-CD

Although the sensitivity of the analytes was improved over 30-fold, FASS resulted in peak tailing of plasma sample. In our experiment, β-CD was added to improve peak shape and reproducibility of analytes. Moreover, during this process, the sensitivity of the analytes was improved another 2–3 fold.

In our experiment, using β-CD could get better peak shape and higher sensitivity. Therefore the effects of β-CD at concentrations of 0.0, 1.0, 2.0 mM were investigated. As shown in Fig. 3, a running buffer containing 1.0 mM β-CD was chosen as the optimum.

3.1.4. Pre-treatment of sample

The extraction of plasma samples was optimized in our preliminary studies by comparing liquid–liquid extraction, solid-phase extraction and protein precipitation. Protein precipitation is not suitable for amboxol extraction from plasma because of lower sensitivity, and more interference of endogenous components in human plasma. Solid-phase extraction was time consuming and wasteful. However, the results were satisfactory when N-hexane was used in liquid–liquid extraction. A 60 μl aliquot of 1 M sodium hydroxide was added to 200 μl plasma, which enhanced the extraction efficiency of ambroxol and the IS. In order to increase sample throughput, the LLE 96-well format plates were used, resulting in a shorter sample preparation time.

3.2. Method validation

Analytical method validation was carried out according to the recommendations published by the FDA [27].

3.2.1. Specificity

Specificity of the method was investigated by both peak purity and spiking experiments with pure standard compounds. Peak purity was evaluated by means of the P/ACE System MDQ Software. The total peak purity values of ambroxol hydrochloride and

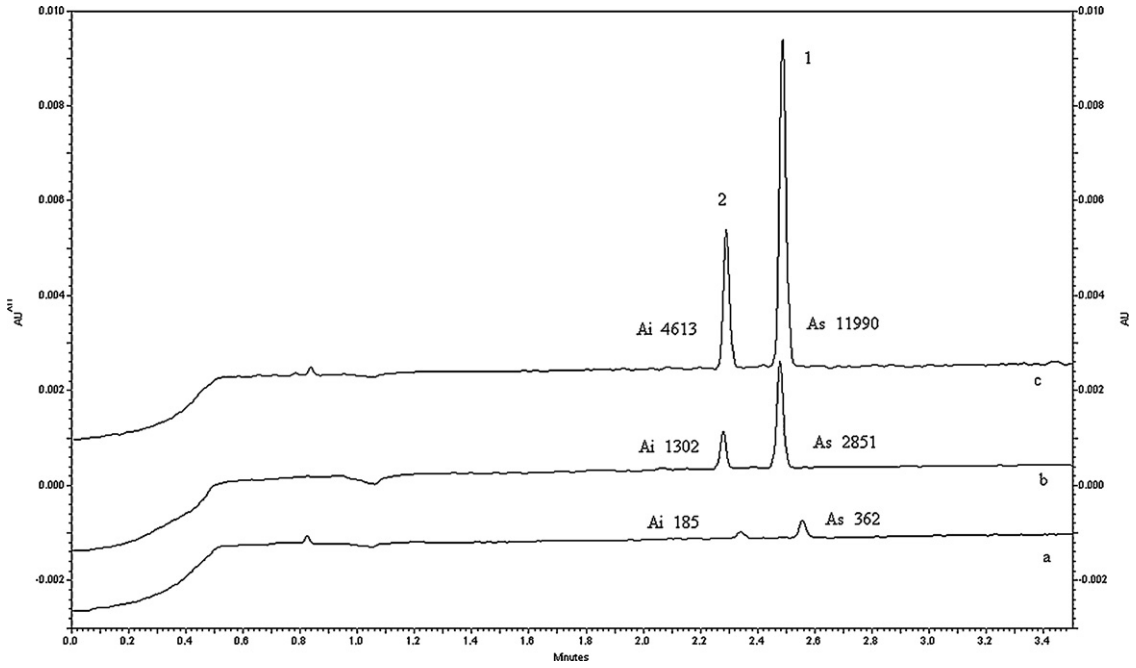

Fig. 2. The effect of different sample solvents on FASS of ambroxol hydrochloride (400 ng/ml) standard and IS (750 ng/ml). Running buffer, 25 mM phosphate–6.25 mM borate (pH 3.0); capillary, 31.2 cm × 75 μm i.d., effective length 21 cm, uncoated; applied voltage, 15 kV (+) → (−); column temperature, 25 °C; detection 210 nm; electrokinetic injection, 7.5 kV × 15 s. Electropherograms: (a) 10% buffer; (b) distilled water; (c) 80% ACN–distilled water. Peaks: 1, ambroxol hydrochloride; 2, the IS.

the IS were 1.0000. There appeared to be no interference from the endogenous substance, which were analyzed under the same optimized condition (Fig. 4).

3.2.2. Linearity of calibration curves and lower limits of quantification (LLOQ)

A weighted $(1/x)$ linear regression was used to perform standard calibration. The mean calibration equation was $y = 0.02817$ ($n = 5$, RSD = 0.85%) $x + 0.06351$ ($n = 5$, RSD = 4.76%) and $r^2 = 0.9998$ ($n = 5$, RSD = 0.01%). In this equation, y represents the peak area ratios of the analyte to the IS and x represents the plasma concentration of analyte in ng/ml. Calibration curves showed excellent linearity in the range 2–500 ng/ml. The LLOQ, which is determined as the lowest concentration on the standard curve, of ambroxol hydrochloride in human plasma was found to be 2 ng/ml with accuracy of 91.03% and precision of 9.61% ($n = 5$).

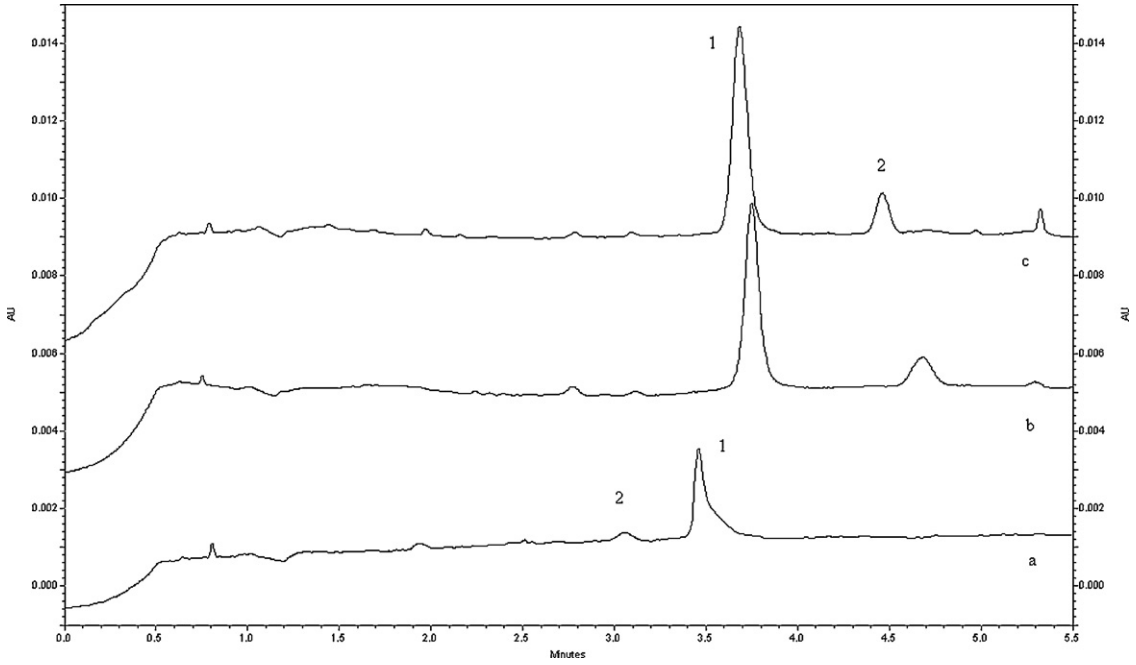

Fig. 3. The effect of different concentrations of β-CD on the peak shape and sensitivity of ambroxol hydrochloride (50 ng/ml) and IS (250 ng/ml) in plasma. Electrokinetic injection: 7.5 kV × 15 s. Electropherograms: (a) 0 mM β-cyclodextrin; (b) 2 mM β-cyclodextrin; (c) 1 mM β-cyclodextrin. Peaks: 1, ambroxol hydrochloride; 2, the IS. See Fig. 2 for other CZE conditions.

Table 1
Within- and between-run accuracy and precision in spiked plasma samples.

Sample level	Low QC 5 ng/ml	Medium QC 20 ng/ml	High QC 400 ng/ml
Within-run accuracy and precision			
Validation run 1			
Mean ± SD (ng/ml)	5.32 ± 0.43	20.52 ± 0.89	385.87 ± 30.17
Accuracy (%)	106.50 ± 8.63	102.58 ± 4.45	96.47 ± 7.54
RSD (%)	8.10	4.33	7.81
N	5	5	5
Validation run 2			
Mean ± SD (ng/ml)	4.92 ± 0.45	20.30 ± 2.12	392.08 ± 31.49
Accuracy (%)	98.41 ± 9.04	101.55 ± 10.58	98.02 ± 7.87
RSD (%)	9.19	10.42	8.03
N	5	5	5
Validation run 3			
Mean ± SD (ng/ml)	4.97 ± 0.30	19.42 ± 1.13	389.56 ± 9.07
Accuracy (%)	97.51 ± 5.97	97.04 ± 5.65	97.37 ± 2.27
RSD (%)	6.12	5.82	2.33
N	5	5	5
Between-run accuracy and precision			
Mean ± SD (ng/ml)	5.04 ± 0.41	20.07 ± 1.37	389.17 ± 22.43
Accuracy (%)	100.80 ± 8.15	100.39 ± 6.87	97.29 ± 5.60
RSD (%)	8.08	6.84	5.76
N	15	15	15

3.2.3. Accuracy, precision and extraction recovery

Five replicate samples at each QC concentrations were analyzed in three separate runs. Accuracy was determined by calculating the ratios of the predicted concentrations to the spiked values and with the precision expressed as RSD. The results in Table 1 show that the within- and between-day variances at three QC levels were all below 10.42%. It was shown that the accuracy was from 96.47% to 106.50%. The extraction recovery (Table 2) was found to be 78.12 ± 10.79%, 81.46 ± 3.52% and 85.81 ± 1.76% at the concentration of 5, 20 and 400 ng/ml, respectively. The extraction recovery of IS was 82.63 ± 5.22%.

Table 2
Recoveries of ambroxol hydrochloride and IS in spiked plasma samples ($n = 5$).

Compound	Concentration (ng/ml)	Recovery (%) (mean ± SD)	RSD (%)
Ambroxol	5	78.12 ± 10.79	13.81
	20	81.46 ± 3.52	4.32
	400	85.81 ± 1.76	2.05
IS	250	82.63 ± 5.22	6.32

3.2.4. Stability

Analyte stability determinations comprised short-term temperature stability, long-term stability, autosampler stability and freeze–thaw cycles stability, which were evaluated by analyzing three QC levels in quintuple. The mean values and standard deviations of the ratios between the concentrations found and initial concentration were used for stability evaluation. The results (Table 3) show that ambroxol hydrochloride had an acceptable

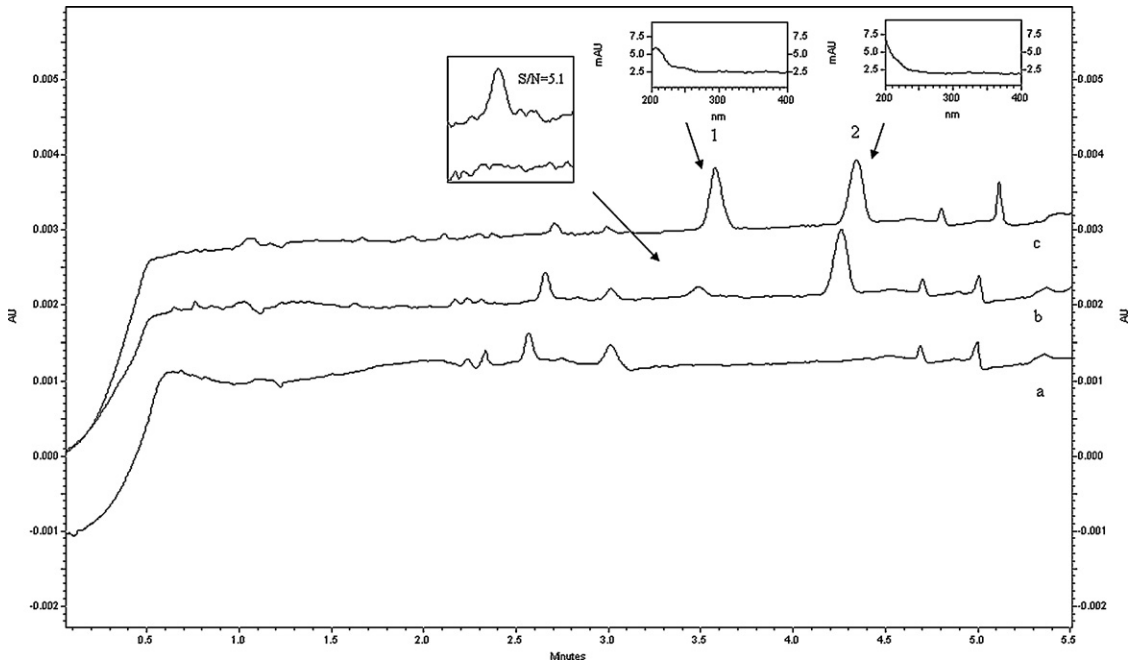

Fig. 4. Typical chromatograms of blank plasma (a); blank plasma spiked with 2 ng/ml (LLOQ) ambroxol hydrochloride and 250 ng/ml IS (b); test plasma spiked with 250 ng/ml of IS at 0.5 h after the dose of 90 mg (c). Peak 1: ambroxol hydrochloride; peak 2: the IS.

Table 3
Stability results of ambroxol hydrochloride in spiked plasma samples ($n = 5$).

Sample condition	Nominal concentration (ng/ml)	Measured concentration (ng/ml) (mean ± SD)	Accuracy (%)	RSD (%)
Freeze–thaw stability[a]	5	4.71 ± 0.64	94.30	13.60
	20	20.80 ± 0.92	104.01	4.44
	400	387.44 ± 31.51	96.86	8.13
30-day stability[b]	5	4.53 ± 0.33	90.52	7.31
	20	19.70 ± 1.21	98.49	6.15
	400	392.95 ± 30.60	98.24	7.79
Bench top stability[c]	5	4.96 ± 0.32	99.26	6.41
	20	18.69 ± 1.03	93.44	5.53
	400	407.88 ± 22.26	101.97	5.46
Autosampler stability[d]	5	5.10 ± 0.37	102.08	7.25
	20	20.43 ± 1.39	102.15	6.82
	400	388.34 ± 9.40	97.09	2.42

[a] After three freeze–thaw cycles.
[b] Stored at −20 °C.
[c] Exposed at ambient temperature (25 °C) for 8 h.
[d] Kept at ambient temperature (25 °C) for 8 h.

Table 4
The robustness data of the analytical method upon variation of CZE separation condition (ambroxol hydrochloride (MQC) = 20 ng/ml, $n = 5$).

Parameter	Experimental electrophoretic plate (N)[a]		Resolution[a]	Found (RSD%) (ng/ml)[a]
	Ambroxol hydrochloride	IS		
Optimum condition (separation voltage 15 kV; buffer pH 3.0; β-CD concentration 1 mM)	4063 ± 154	3606 ± 96	4.11 ± 0.98	19.44 ± 1.29 (6.64)
Separation voltage 13.5 kV	3866 ± 182	3584 ± 132	4.77 ± 0.61	18.63 ± 0.85 (4.56)
Separation voltage 16.5 kV	3892 ± 146	3585 ± 85	4.50 ± 0.34	19.01 ± 2.09 (10.99)
Buffer pH 2.7	3948 ± 125	3627 ± 92	4.26 ± 0.52	19.87 ± 2.23 (11.22)
Buffer pH 3.3	4084 ± 103	3559 ± 102	3.81 ± 0.51	20.61 ± 0.90 (4.37)
β-CD concentration 0.9 mM	4021 ± 112	3706 ± 127	3.48 ± 0.31	19.26 ± 1.33 (6.91)
β-CD concentration 1.1 mM	3932 ± 101	3667 ± 143	5.02 ± 0.45	20.98 ± 1.65 (7.86)

Statistical test results: small changes in experimental conditions have no effect on the determination of ambroxol hydrochloride (t-test, $p > 0.05$). Each mean value was compared with the mean value obtained by standard conditions.
[a] Mean ± standard error; RSD, relative standard deviation.

stability at room temperature for 8 h, at −20 °C for 1 month, in the autosampler at room temperature for 8 h after liquid–liquid extraction and after three freeze–thaw cycles with the values 93.44–101.97%, 90.52–98.49%, 97.09–102.15% and 94.30–104.01%, respectively, at the three concentrations studied.

3.2.5. Robustness

The robustness of the method was evaluated by deliberate variation of the method parameters, such as pH, concentration of β-CD and voltage. Analyses were carried out in quintuplicate and only one parameter was changed in the experiments at a time. The determination of 20 ng/ml ambroxol hydrochloride and 250 ng/ml IS spiked plasma samples was performed under various conditions (Table 4). The statistical comparison was done with t-test and no difference was found between results ($p > 0.05$). Hence, the method was considered robust and reliable.

3.3. Application to clinical pharmacokinetic study

The developed and validated CZE method was used to analyze pharmacokinetic profiles of ambroxol hydrochloride in 12 healthy volunteers after a single oral dose of 90 mg of ambroxol hydrochloride tablet. Profiles of the mean plasma concentration of ambroxol versus time are shown in Fig. 5. The value of T_{max} and C_{max} were 1.80 ± 0.80 h and 204.55 ± 35.41 ng/ml, respectively. The elimination half-life of ambroxol was 8.14 ± 1.94 h. The AUC_{0-24} and $AUC_{0-\infty}$ values were 1280.51 ± 450.43 ng h/ml and 1496.45 ± 601.37 ng h/ml, respectively. Our results of pharmacokinetic parameters were similar to those results obtained by LC/MS/MS [13–16] though the dose of administration was different.

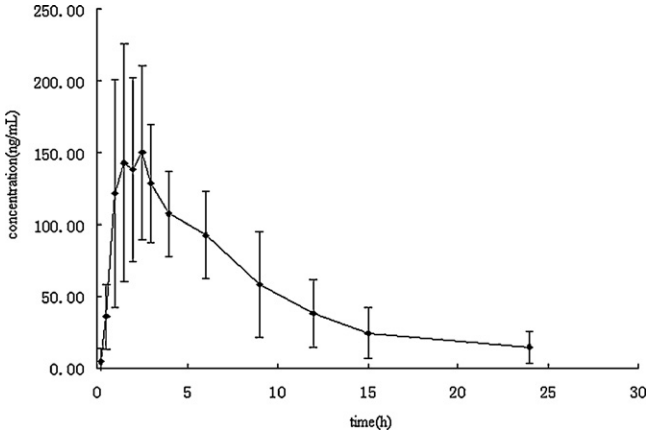

Fig. 5. Mean plasma concentration–time curve in 12 healthy Chinese subjects when administered oral dose of 90 mg of ambroxol hydrochloride.

4. Conclusion

This work illustrates that preparing the sample in water-miscible organic solvents yields better stacking than that in aqueous buffers, and β-cyclodextrin has an effect on improving

sensitivity and reproducibility. Under the proper condition, this stacking CZE method provided a sensitivity enhancement of about 60–70 fold in comparison with the same sample dissolved in 10% buffer and separated in buffer without β-cyclodextrin. The method was validated for the determination of ambroxol hydrochloride in 12 healthy volunteers after a single oral administration of ambroxol hydrochloride. The combination of the CZE with 96-well format LLE greatly simplified the preparation process and decreased the time of sample preparation. Furthermore, it saved a great amount of cost of solvent for the determination of large numbers of samples. The in vivo analysis process and pharmacokinetic parameters confirmed that the CZE method was an alternative method for routine analysis of ambroxol hydrochloride in plasma comparing with the reference method [10,14–16]. The method possessed good characteristics of specificity, sensitivity, precision and accuracy and proved to be reliable. It is expected that this approach can be applied to the extraction and analysis of numerous samples in clinical therapy and pharmacokinetic studies of ambroxol hydrochloride.

Acknowledgements

This work was supported by Pharmacokinetic Platform of the Innovation Drug Research founded by Ministry of Science and Technology of PR China (2009ZX09301-011-07). The authors gratefully acknowledge laboratory colleagues, Fangyuan Gao and You Li for the valuable discussion for article composition.

References

[1] E. Nemceková, G. Nosálóvá, S. Franová, Ambroxol and protective reflexes of the respiratory tract, Bratisl. Lek. Listy 99 (1998) 111–115.
[2] F. Paganin, O. Bouvet, P. Chanez, D. Fabre, M. Galtier, P. Godard, F.B. Michel, F. Bressolle, Evaluation of the effects of ambroxol on the ofloxacin concentrations in bronchial tissues in COPD patients with infectious exacerbation, Biopharm. Drug Dispos. 16 (1995) 393–401.
[3] J.C. Wiemeyer, Influence of ambroxol on the broncopulmonary level of antibiotics, Arzneim.-Forsch. 31 (1981) 974–976.
[4] M.S. Hwang, S. Cho, H. Chung, Y.A. Woo, Nondestructive determination of the ambroxol content in tablets by Raman spectroscopy, J. Pharm. Biomed. Anal. 38 (2005) 210–215.
[5] J. Spátola, J.J. Poderoso, J.C. Wiemeyer, M. Fernández, R.B. Guerreiro, C. Corazza, Influence of ambroxol on lung tissue penetration of amoxicillin, Arzneim.-Forsch. 37 (1987) 965–966.
[6] K.A. Shaikh, S.D. Patil, A.B. Devkhile, Development and validation of a reversed-phase HPLC method for simultaneous estimation of ambroxol hydrochloride and azithromycin in tablet dosage form, J. Pharm. Biomed. Anal. 48 (2008) 1481–1484.
[7] V. Stetionová, V. Herout, J. Kvetina, In vitro and in vivo antioxidant activity of ambroxol, Clin. Exp. Med. 4 (2004) 152–159.
[8] S. Pfeifer, G. Zissel, K. Kienast, J. Müller-Quernheim, Reduction of cytokine release of blood and bronchoalveolar mononuclear cells by ambroxol, Eur. J. Med. Res. 2 (1997) 129–132.
[9] T. Pérez-Ruiz, C. Martínez-Lozano, A. Sanz, E. Bravo, Sensitive method for the determination of ambroxol in body fluids by capillary electrophoresis and fluorescence detection, J. Chromatogr. B. 742 (2000) 205–210.
[10] M. Nobilis, J. Pastera, D. Svoboda, J. Kvêtina, K. Macek, High-performance liquid chromatographic determination of ambroxol in human plasma, J. Chromatogr. 581 (1992) 251–255.
[11] F.J. Flores-Murrieta, C. Hoyo-Vadilo, E. Hong, G. Castañeda-Hernandezet, Assay of ambroxol in human plasma by high-performance liquid chromatography with amperometric detection, J. Chromatogr. 490 (1989) 464–469.
[12] H.J. Lee, S.K. Joung, Y.G. Kim, et al., Bioequivalence assessment of ambroxol tablet after a single oral dose administration to healthy male volunteers, Pharmacol. Res. 49 (2004) 93–100.
[13] W.Q. Hu, Y. Xu, F. Liu, A.X. Liu, Q.X. Guo, Rapid and sensitive liquid chromatography tandem mass spectrometry method for the quantification of ambroxol in human plasma, Biomed. Chromatogr. 22 (2008) 1108–1114.
[14] F.L. Su, F. Wang, W. Gao, H.D. Li, Determination of ambroxol in human plasma by high performance liquid chromatography–electrospray ionization mass spectrometry (HPLC–MS/ESI), J. Chromatogr. B 853 (2007) 364–368.
[15] A.D. Wen, T.J. Hang, S.N. Chen, Z.R. Wang, L.K. Ding, Y. Tian, M. Zhang, X.X. Xu, Simultaneous determination of amoxicillin and ambroxol in human plasma by LC–MS/MS: validation and application to pharmacokinetic study, J. Pharm. Biomed. Anal. 48 (2008) 829–834.
[16] H. Kim, J.Y. Yoo, S.B. Han, H.J. Lee, K.R. Lee, Determination of ambroxol in human plasma using LC–MS/MS, J. Pharm. Biomed. Anal. 32 (2003) 209–216.
[17] J. Schmid, Assay of ambroxol in biological fluids by capillary gas–liquid chromatography, J. Chromatogr. 414 (1987) 65–75.
[18] L. Colombo, F. Marcucci, G.M. Marini, P. Pierfederici, E. Mussini, Determination of ambroxol in biological material by gas chromatography with electron-capture detection, J. Chromatogr. 530 (1990) 141–147.
[19] C.E. Uboh, J.A. Rudy, L.R. Soma, M. Fennell, L. May, R. Sams, F.A. Railing, J. Shellenberger, M. Kahler, Characterization of bromhexine and ambroxol in equine urine: effect of furosemide on identification and confirmation, J. Pharm. Biomed. Anal. 9 (1991) 33–39.
[20] K. Ohyamaa, N. Kishikawa, H. Nakagawa, N. Kuroda, M. Nishikido, M. Teshima, H. To, T. Kitahara, H. Sasaki, Simultaneous determination of mycophenolic acid and its acyl and phenol glucuronide metabolites in human serum by capillary zone electrophoresis, J. Pharm. Biomed. Anal. 47 (2008) 201–206.
[21] T. Pérez-Ruiz, C. Martínez-Lozano, A. Sanz, E. Bravo, Determination of bromhexine and ambroxol in pharmaceutical dosage forms, urine and blood serum, J. Chromatogr. B 692 (1997) 199–205.
[22] F.E.P. Mikkers, F.M. Everaerts, T.P.E.M. Verheggen, High-performance zone electrophoresis, J. Chromatogr. 169 (1979) 11–20.
[23] C.C. Chen, S.M. Wu, Y.H. Huang, W.K. Ko, H.S. Kou, H.L. Wu, On-line field-amplified sample stacking in capillary electrophoresis for analysis of amitriptyline and its metabolite nortriptyline in plasma, Anal. Chim. Acta 517 (2004) 103–110.
[24] M.C. Breadmore, Recent advances in enhancing the sensitivity of electrophoresis and electrochromatography in capillaries and microchips, Electrophoresis 28 (2007) 254–281.
[25] Z.K. Shihabi, Organic solvent high-field amplified stacking for basic compounds in capillary electrophoresis, J. Chromatogr. A 1066 (2005) 205–210.
[26] S. Razee, A. Tamura, T. Masujima, Improvement in the determination of food additive dyestuffs by capillary electrophoresis using β-cyclodextrin, J. Chromatogr. A 715 (1995) 179–188.
[27] Guidance for Industry, Bioanalytical Method Validation, US Department of Health and Human Services, Food and Drug Adiministration, Center for Drug Evaluation and Research (CDER), Center for Veternary Medicine (CVM), 2001, Available at: http://www.fda.gov/cder/guidance/4252fnl.htm.
[28] S. Jacob, A. Shirwaikar, Preparation and evaluation of microencapsulated fast melt tablets of ambroxol hydrochloride, India J. Pharm. Sci. 71 (2009) 276–284.
[29] Z. Krivácsy, A. Gelencsér, J. Hlavay, G. Kiss, Z. Sárvári, Electrokinetic injection in capillary electrophoresis and its application to the analysis of inorganic compounds, J. Chromatogr. A 834 (1999) 21–44.
[30] Z.K. Shihabi, Transient pseudo-isotachophoresis for sample concentration in capillary electrophoresis, Electrophoresis 23 (2002) 1612–1617.
[31] M. Wang, Z.W. Cai, L. Xu, Coupling of acetonitrile deproteinization and salting-out extraction with acetonitrile stacking in chiral capillary electrophoresis for the determination of warfarin enantiomers, J. Chromatogr. A 1218 (2011) 4045–4051.

Journal of Pharmaceutical and Biomedical Analysis 66 (2012) 225–231

Contents lists available at SciVerse ScienceDirect

Journal of Pharmaceutical and Biomedical Analysis

journal homepage: www.elsevier.com/locate/jpba

Sensitive detection of carcinoembryonic antigen with magnetic nano-bead and upconversion nanoparticles-based immunoassay

Zhaohui Huang[a,*], Shijia Wu[b], Nuo Duan[b], Dong Hua[a], Yu Hu[a], Zhouping Wang[b,**]

[a] Oncology Institute, The Fourth Affiliated Hospital of Soochow University, Wuxi 214062, China
[b] State Key Laboratory of Food Science and Technology, School of Food Science and Technology, Jiangnan University, Wuxi 214122, China

ARTICLE INFO

Article history:
Received 17 December 2011
Received in revised form 28 February 2012
Accepted 29 February 2012
Available online 7 March 2012

Keywords:
Carcinoembryonic antigen
Immunoassay
Magnetic nanoparticles
Upconversion nanoparticles
Colorectal cancer

ABSTRACT

A novel magnetic nanobead-based immunoassay was developed for the quantification of carcinoembryonic antigen (CEA) in human serum in this study. Amine-functionalized Fe_3O_4 magnetic nanoparticles (MNPs) were conjugated with capture *anti*-CEA antibodies and amine-functionalized $NaY_{0.78}F_4$:$Yb_{0.20}$, $Ho_{0.02}$ upconversion nanoparticles (UCNPs) were synthesized and conjugated with detection *anti*-CEA antibodies, respectively. Based on a sandwich-type immunoassay format, the detection limit for CEA under optimal conditions was as low as 2.5 pg/mL, and the linear range of CEA detection was from 2.5×10^{-12} to 1×10^{-8} g/mL ($I = 406.19 \log X + 428.81$) with a correlation coefficient equal to 0.9987. The established method was successfully applied to measure CEA in human serum samples and more sensitive than a commercially available chemiluminescence method. The precision expressed as the relative standard deviation of CEA detection was equal to 5.19% (1 ng/mL) or 4.36% (5 pg/mL), indicating that the developed method exhibited good reproducibility. The results demonstrate that the method offers potential advantages of sensitivity and good reproducibility for the determination of CEA, and is applicable to the determination of CEA in serum samples.

© 2012 Elsevier B.V. All rights reserved.

1. Introduction

Carcinoembryonic antigen (CEA) is a member of immunoglobulin superfamily and function as an intracellular adhesion molecule. CEA is a commonly used tumor marker associated with many human cancers, including colorectal, pancreatic, gastric, and cervical arcinomas [1–5]. The published methods for the detection of CEA include enzyme-linked immunosorbent assays (ELISA) [6], radioimmunoassays (RIA) [7,8], chemiluminescence [9]. One drawback of conventional ELISA is its relatively low sensitivity. In addition, active enzymes are often needed to be stored at cold conditions. In spite of high specificity and sensitivity, RIA has some disadvantages such as the use of radioisotopes, waste disposal problems, short half-life, and conjugate radiolysis. Chemiluminescence assays require careful manipulation, and ultra-pure water and materials is needed in the experiment in order to eliminate the potential interfering factors. Consequently, persistent endeavor has been tried to establish new improved methods using different materials or signal amplication systems [10–19] including integrated bead-bed immunoassay [11], piezoelectric immunosensor [12], Raman scattering-based [13], microchip electrophoresis-based surface-enhanced assay [14], electrochemical immunoassay [15], or nanomaterials-based assays [16–19]. The characters of materials are the key determining the analytical performance of these new methods.

Although conventional downconversion fluorescent materials, such as semiconductor nanocrystals [20], organic dyes [21], dye-coupled hybrid materials (carbon nanotubes) [22] and mesoporous silica [23], are commonly used in biomedical studies and clinical application. However, these materials usually emit one lower-energy photon after absorption of a higher-energy ultraviolet or visible photon, and the use of higher-energy light may result in several significant disadvantages, including low light-penetration depth, potential severe photodamage to living organisms, and the autofluorescence (noise) of some biological samples.

The rapidly evolving field of nanoscience and nanotechnology has opened up a new and promising era. Increasing attention has been paid to study the potential bioanalytical applications of nanomaterials. In our previous work, we developed a novel magnetic nanobead-based immunoassay for the fluorescence detection of biomoleculars [24]. In contrast to conventional downconversion fluorescent materials, this kind of upconversion nanoparticles (UCNPs) exhibits unique luminescent properties, including the

Abbreviations: CEA, carcinoembryonic antigen; MNP, magnetic nanoparticle; UCNPs, upconversion nanoparticles; ELISA, enzyme-linked immunosorbent assays; RIA, radioimmunoassays; PBS, phosphate-buffered saline; XRD, X-ray diffraction; TEM, transmission electron microscope.

* Corresponding author. Tel.: +86 510 88682900; fax: +86 510 88682900.
** Corresponding author. Tel.: +86 510 85917023; fax: +86 510 85917023.
E-mail addresses: hzhwxsy@126.com (Z. Huang), wangzp@jiangnan.edu.cn (Z. Wang).

0731-7085/$ – see front matter © 2012 Elsevier B.V. All rights reserved.
doi:10.1016/j.jpba.2012.02.027

ability to convert a longer wavelength radiation to shorter wavelength fluorescence via a two-photon or multi-photon mechanism, is emerging as a new class of fluorescent biolabels. Their advantages including high quantum yields very narrow emission peak, large Stokes shifts, sharp emission bandwidths, high chemical stability, and low toxicity. More importantly, the excitation of UCNPs often requires near-infrared radiation, thus the signal-to-noise ratio and sensitivity of the detection can be improved owing to the absence of autofluorescence.

In this sandwich-type immunoassay, the *anti*-CEA antibodies modified magnetic nanoparticles (MNPs) were employed as capture probes, and the *anti*-CEA antibodies modified UCNPs were used as detection probes, then the antibodies-functionalized UCNPs were linked to the surface of the antibodies-functionalized MNPs by antibody–antigen affinity. Based on the new system, in the present study, we further developed a novel method to detect the levels of CEA in sera samples. The results were highly correlated with that of the commercially available chemiluminescence method.

2. Materials and methods

2.1. Reagents and apparatus

Rare-earth oxides used in this work, including yttrium oxide (Y_2O_3), ytterbium oxide (Yb_2O_3), erbium oxide (Er_2O_3), and thulium oxide (Tm_2O_3) were of 99.99% purity; hydrofluoric acid (HF), 25% ammonia ($NH_3{\cdot}H_2O$), sodium hydroxide (NaOH), nitric acid (HNO_3), cetyltrimethyl ammonium bromide (CTAB), ethylene diamine tetraacetic acid (EDTA), phosphate-buffered saline (PBS), 25% glutaraldehyde ($OHC(CH_2)_3CHO$) and tetraethyl orthosilicate (TEOS) were of analytical grade; all these chemicals above were purchased from Sinopharm Chemical Reagent Co. Ltd. (Shanghai, China). 98% 3-aminopropyltrimethoxysilane (APTES) was purchased from Alfa Aesar (Ward Hill, MA).

The size and morphology of nanoparticles were observed on a JEM-2100HR transmission electron microscope (TEM) (JEOL Ltd., Tokyo, Japan), using an accelerating voltage of 200 kV. X-ray diffraction (XRD) measurements were performed on a D8-advance (Bruker AXS Ltd., Karlsruhe, Germany) with graphite-monochromatized Cu Kα radiation (λ = 0.15406 nm). The operation voltage and current were kept at 40 kV and 40 mA, respectively. A 2θ range from 10° to 70° was covered in steps of 0.02° with a count time of 2 s. UCNPs fluorescence spectra were measured on an F-7000 fluorescence spectrophotometer (Hitachi Co., Tokyo, Japan) attached to an external 980 nm laser (Beijing Hi-Tech Optoelectronic Co., Beijing, China) instead of the internal excitation source. The maximum power of the laser was 1300 mW. Ultraviolet–visible (UV–vis) absorption spectra were recorded by using a Shimadzu UV-2300 UV–vis spectrophotometer (Shimadzu, Japan). FTIR spectra of the amino-functionalized NPs were conducted with a Nicolet Nexus 470 Fourier transform infrared spectrophotometer (Thermo Electron Co., Waltham, MA) by using the KBr method. The suspension of NPs was prepared by using an ultrasonic bath KJ-300 (Wuxi Kejie Electron Instruments Co., Wuxi, China). CEA antigen (L2C010) *anti*-CEA antibodies (L1C00202/L1C00205) were obtained from Shanghai Linc-Bio Science Co. LED (Shanghai, China).

2.2. Synthesis and surface modification of $NaY_{0.78}F_4$:$Yb_{0.20}$, $Ho_{0.02}$ upconversion nanoparticles (UCNPs)

$NaY_{0.78}F_4$:$Yb_{0.20}$, $Ho_{0.02}$ UCNPs were synthesized according to the method described by our previous work [24] with some modifications. Briefly, a mixture of 0.440 g Y_2O_3 (78%), 0.19704 g Yb_2O_3 (28%) and 0.01889 g Ho_2O_3 (2%) was dissolved in nitric acid with heating, and the solvent was evaporated to form the rare-earth nitrate powder and then dissolved in 10 mL deionized water. The transparent EDTA–Ln^{3+} solution was acquired by adding 1.8612 g EDTA and adjusting the pH to weak basic conditions (pH 8.0). Then 0.4 g CTAB was added to 25 mL glycol increase the amount of carbon in the reaction system to prevent the nanoparticles from aggregating. Under vigorous stirring, 10 mL of the EDTA–Ln^{3+} solution was added dropwise, followed by the addition of 2 mL hydrofluoric acid (HF) as the fluorine source and 3.5 mL of nitric acid. The mixed solution was transferred into a Teflon lined autoclave and heated to 195 °C for 24 h. The autoclave was allowed to cool to room temperature, during which the UCNPs were deposited at the bottom of the vessel. They were washed with hot water into a beaker, dispersed ultrasonically for 15 min, and allowed to stand for several minutes after which the supernatant was discarded; this process was repeated three times. The UCNPs were purified by centrifugation, washed with ethanol three times, and dried at 60 °C for 12 h.

Surface modification of $NaY_{0.78}F_4$:$Yb_{0.20}$, $Ho_{0.02}$ UCNPs was completed by using an advanced Stöber-based method [25] to cap silica onto the surface of the UCNPs. In a 250 mL flask, 60 mg of UCNPs were dispersed in 60 mL of 3-propanol by sonication and agitation for 40 min, then 2.5 mL of ammonia and 20 mL of water were added to the flask, and the mixture was maintained at 35 °C under vigorous stirring. A solution containing 20 mL of 3-propanol and 60 μL of TEOS was added dropwise to the mixture over a period of 1 h. The reaction was maintained for another 3 h. A solution containing 20 mL of 3-propanol and 200 μL of APTES was then added dropwise into the suspension. The reaction was maintained for 1 h. When the reaction terminated the product was aged for 2 h at room temperature. The precipitate was then separated by centrifugation, washed three times with ethanol, and then dried at 60 °C for 12 h to obtain the amino-modified $NaY_{0.78}F_4$:$Yb_{0.20}$, $Ho_{0.02}$ UCNPs.

2.3. Preparation of amine-functionalized Fe_3O_4 magnetic nanoparticles

Amine-functionalized Fe_3O_4 MNPs were prepared as previously described [26]. Briefly, a solution of 6.5 g 1,6-hexanediamine, 2.0 g anhydrous sodium acetate and 1.0 g $FeCl_3{\cdot}6H_2O$ as a ferric source in 30 mL glycol was stirred vigorously at 50 °C to give a transparent solution. This solution was then transferred to a Teflon lined autoclave and reacted at 198 °C for 6 h. The MNPs were then rinsed with water and ethanol (2 or 3 times) to effectively remove the solvent and unbound 1,6-hexanediamine, and then dried at 50 °C before characterization and application. During each rinsing step, the nanoparticles were magnetically separated from the supernatant.

2.4. Preparation of antibodies-conjugated nanoparticles

The coupling of nanoparticles with proteins used the same method as our previous work [24]. Typically, 10 mg of MNPs were dispersed in 5 mL of 10 mM PBS solution (pH 7.4) by ultrasonication for 20 min. 1.25 mL of 25% glutaraldehyde and 100 mg of $NaBH_4$ were then added to the mixture. The mixture was shaken slowly at room temperature for 1 h, and the Fe_3O_4 MNPs were separated by an external magnetic field and washed with PBS solution three times to remove the physically adsorbed glutaraldehyde. Subsequently, 5 mL of the capture *anti*-CEA antibodies at a concentration of 0.1 mg/mL was added into a suspension of Fe_3O_4 MNPs in PBS. The mixture was shaken slowly for 6 h at room temperature. The surplus proteins were removed by magnetic separation of the particles from the solution. The capture *anti*-CEA antibodies conjugated MNPs were treated with 5 mL BSA in PBS at a concentration of 10 mg/mL at room temperature for 6 h to block the unreacted and nonspecific sites. Finally, the as-prepared capture probes were

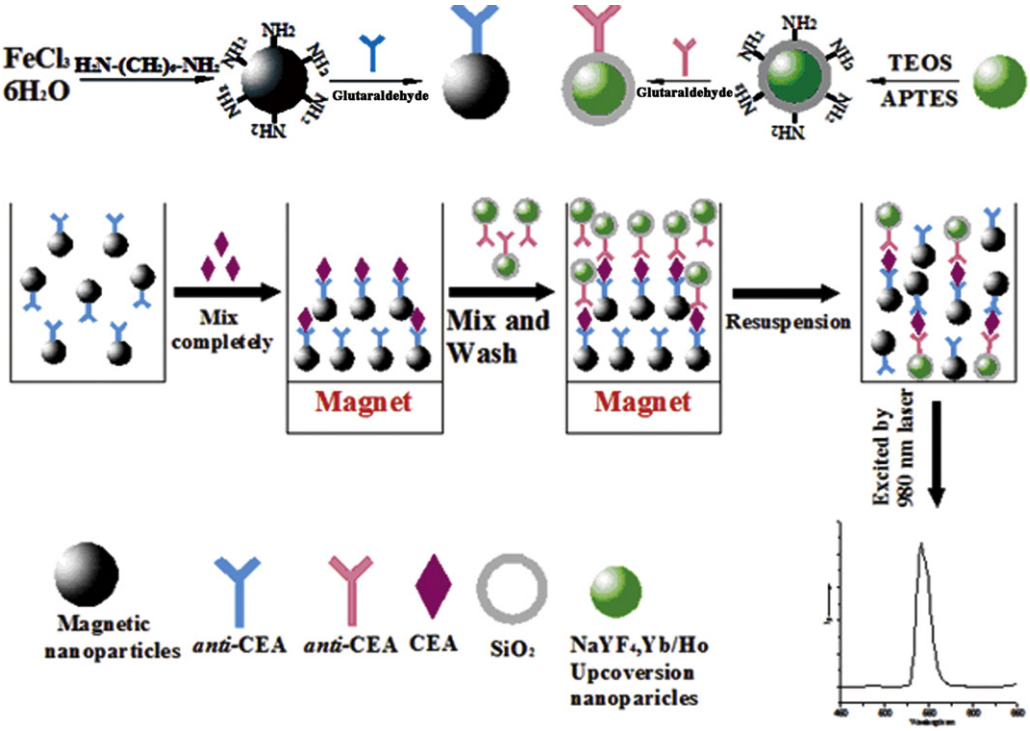

Fig. 1. Schematic representation of the sandwich-type immunoassay with the assistance of magnetic force and upconversion fluorescent detection.

stored in 5 mL of 0.01 M PBS at 4 °C prior to use. The biofunctionalization of amino-modified, silica-capped UCNPs conjugated with detection *anti*-CEA antibodies (0.15 mg/mL), namely the preparation of the signal probes, was similar to that of the capture *anti*-CEA antibodies conjugated MNPs described above. The resultants were characterized by UV spectrum.

2.5. Sandwich-type immunoassay for CEA

A schematic view of the reaction steps for detection of CEA is shown in Fig. 1. This is a sandwich type of detection with the assistance of magnetic force and upconversion fluorescent detection. MNPs labeled with the capture *anti*-CEA antibodies are used to react with the CEA in a pseudo-homogenous condition. With the assistance of magnetic force, the resulting complexes can be easily separated from unreacted substances. UCNPs labeled with the detection *anti*-CEA antibodies are used to react with the CEA of affinity complex to form sandwich nanoparticles and serve as detection probes. Thus, the fluorescent intensities of sandwich nanoparticles are proportional to the CEA in the samples.

One hundred μL of CEA with different concentrations ranging from 10^{-8} to 10^{-12} g/mL were added into each tube which contained 100 μL of 0.1 mg/mL *anti*-CEA-labeled magnetic nanoparticles, and the two solutions were mixed completely and separated by external magnet for 5 min to settle down the complex from unreacted species. These procedures were repeated during each washing step. After magnetic nanoparticles were attracted to the bottom of the tube, the supernatant was removed. The resulting complexes on the magnetic nanoparticles were washed three times with 100 μL of PBS solutions to remove unreacted CEA. Then, 100 μL of 0.15 mg/mL *anti*-CEA-labeled fluorescent nanoparticles were added into each tube and mixed completely with the capture *anti*-CEA/CEA complex to form the capture *anti*-CEA/CEA/detection *anti*-CEA sandwich nanoparticles in buffer solutions. The unreacted fluorescent nanoparticles were removed by washing three times with PBS buffer. The sandwich nanoparticles were resuspended in 100 μL of PBS solutions and were transferred to another tailor-made cuvette for the measuring of the fluorescent intensity.

3. Results and discussion

3.1. Characterization of UCNPs and MNPs

In this work, the monodispersed nanoparticles emit strong and pure green fluorescence with symmetric and narrow emission spectrum excited at a single wavelength (980 nm laser).

To the best of our knowledge, the hexagonal phase $NaYF_4$ is reported as one of the most efficient hosts for performing infrared to visible photon conversion when activated by Yb, Er/Tm/Ho ion-pairs [27]. In Yb^{3+} and Ho^{3+} co-doped systems, Yb^{3+} ions act as sensitizers and Ho^{3+} ions as activators. In Fig. 2, only one emission line appears, peaking at 542 which is assigned to the $^5S_2$–$^5I_8$ (green) transitions of Ho^{3+} ions. The size and morphology of the bare and surface-modified upconversion and magnetic nanoparticles were characterized with transmission electron microscopy (TEM) and XRD analysis.

Typical TEM image of the bare UCNPs synthesized before silica coating is shown in Fig. 3a, the UCNPs were well-dispersed and uniform in size with an average diameter of about 50 nm. It should be noted that the UCNPs synthesized even under relatively stringent conditions present a regular spherical shape, which is beneficial to their further application in biomolecule. After surface modification by SiO_2, the size of the UCNPs was increased to about 55 nm due to the formation of a thin silica layer on the surface of the bare UCNPs (Fig. 3b). Meanwhile, the XRD results (Supplementary Fig. 2) can be easily indexed to hexagonal β-phase $NaYF_4$ (JCPDS no. 16-0034).

The $NaYF_4$:Yb, Ho UCNPs were synthesized by hydro-thermal method and there was no intrinsic aqueous solubility and lack functional groups (such as —COOH and —NH_2) on their surface. Therefore, they are no water-soluble and surface modification is necessary before their use in biological detections. So they were first coated by a silica shell and further functionalized with APTES

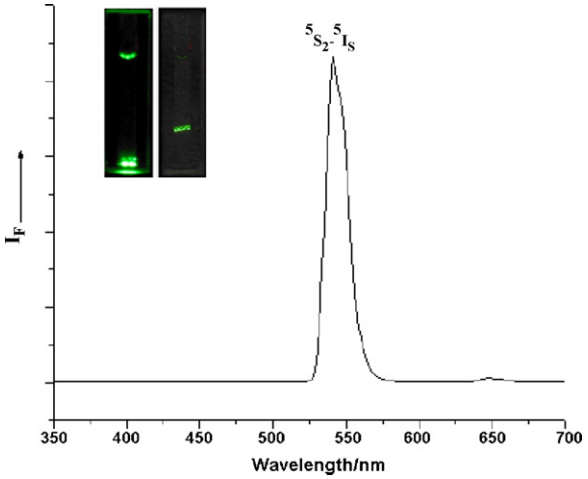

Fig. 2. Fluorescence spectra of $NaY_{0.78}F_4$:$Yb_{0.20}$, $Ho_{0.02}$ upconversion nanoparticles and photograph of naked-eye visible green upconversion luminescence of the $NaY_{0.78}F_4$:$Yb_{0.20}$, $Ho_{0.02}$ UCNPs (inset). (For interpretation of the references to color in this figure legend, the reader is referred to the web version of the article.)

to form an amino-terminated surface via a typical Stöber-based modification method [25]. The functional groups on the surfaces of the amino-modified and pure $NaYF_4$:Yb, Ho UCNPs were identified by FT-IR spectra (Fig. 3c and d).

The amine-functionalized magnetic nanoparticles applied here were prepared with onepot synthesis. TEM, FT-IR and XRD were demonstrated to characterize the as-synthesized magnetic nanoparticles (Supplementary Fig. 2).

3.2. Characterization of antibodies-conjugated nanoparticles

The antibodies molecules of CEA were directly conjugated onto the nanoparticles surfaces by using the amino-amino reaction as illustrated in Scheme. The preparation process included surface activation and chemical modification, as above mentioned. To verify the formation of the bionanoparticles, UV–vis absorption spectroscopy was utilized to monitor the reaction products in each derivatization step (Fig. 4). A strong absorption peak at 280 nm was observed when nanoparticles were incubated with *anti*-CEA antibodies. The absorbance of the supernatant at 280 nm was observed to be weaker than that of the preliminary *anti*-CEA antibodies solution was at that wavelength. These results indicated that some

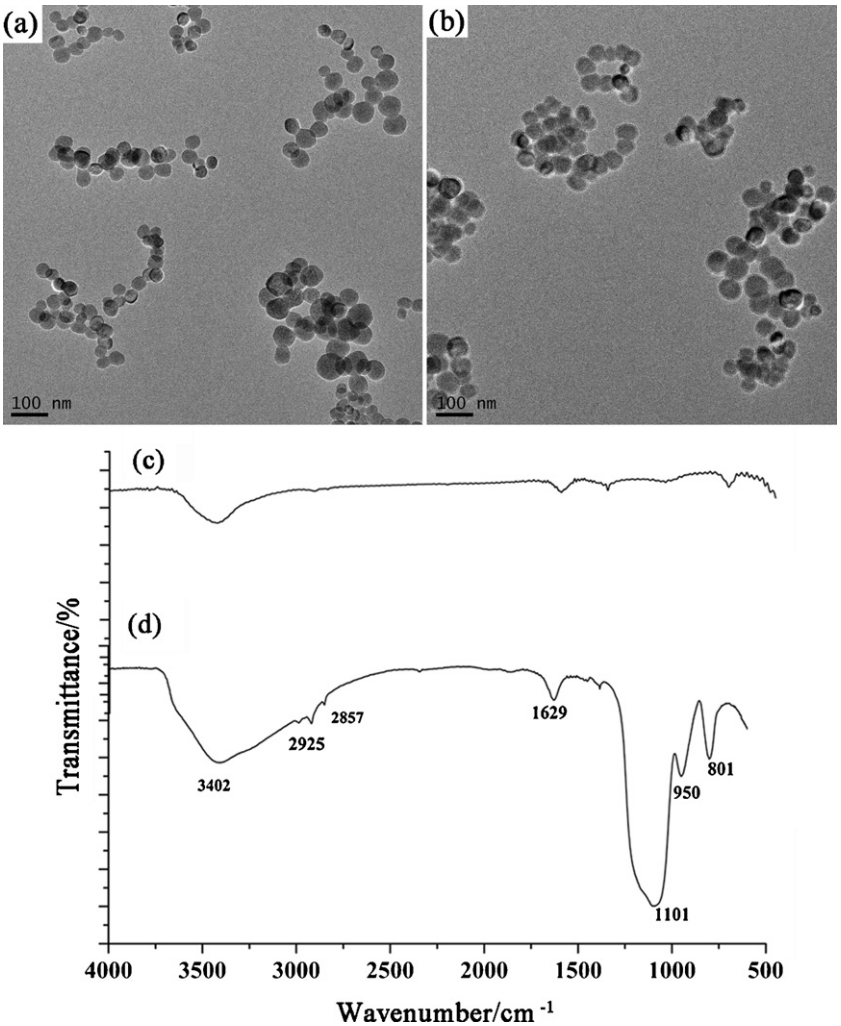

Fig. 3. TEM images of hexagonal phase $NaY_{0.78}F_4$:$Yb_{0.20}$, $Ho_{0.02}$ UCNPs (a) and silica-coated $NaY_{0.78}F_4$:$Yb_{0.20}$, $Ho_{0.02}$ UCNPs (b), FT-IR spectra of the hydrothermal-prepared upconversion nanoparticles (c) and the amino-modified upconversion nanoparticles (d).

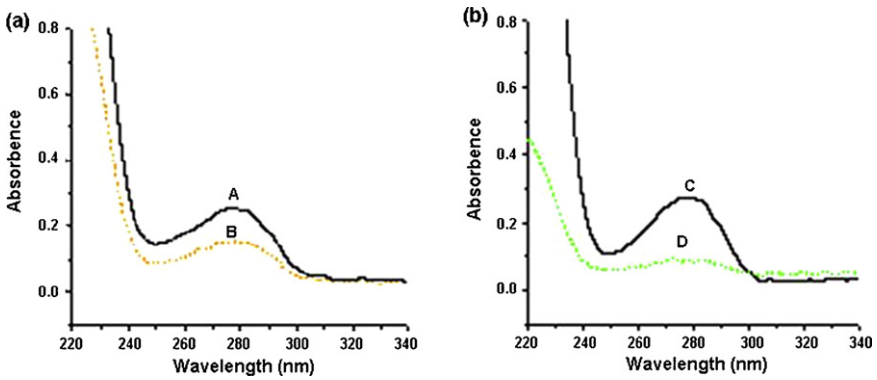

Fig. 4. UV–vis absorption spectra of capture *anti*-CEA antibodies stock solution 0.1 mg/mL (A) or solution 0.15 mg/mL (C), supernatant solution after incubated with amino-modified magnetic nanoparticles (B) or $NaY_{0.78}F_4:Yb_{0.20}$, $Ho_{0.02}$ UCNPs (D).

of the antibodies had been immobilized onto the surface of the nanoparticles.

3.3. Optimization of antibodies concentration

Fig. 5 shows the effect of capture and detection antibodies concentration on the efficiency of the magnetic and upconversion nanoparticles. The absorbance of the supernatant at 280 nm was monitored to optimize the concentration of antibodies binding with nanoparticles. The highest efficiency of capture antibodies was 0.1 mg/mL and detection antibodies was 0.15 mg/mL. It was observed that the amount of antibodies played an important role in the analytical procedure.

3.4. Effect of the amount of antibodies–MNPs conjugates

It was found that the amount of capture antibodies–MNPs conjugates greatly influenced the fluorescence intensity of the final sandwich nanoparticles complexes. Fig. 6 shows the fluorescence intensity with error bars of CEA (0.5 ng/mL) for eight samples measured using 20, 40, 60, 80, 100, 120, 140 and 160 μL of capture antibodies–MNPs conjugates, respectively. It was observed that an increase in the amount of capture antibodies-MNPs conjugates results in increased fluorescence intensity. However, excess MNPs will deepen the color of the solution (brown into black), thereby leading to decreased fluorescence intensity. Based on these observations, an optimal volume of 100 μL capture antibodies was chosen in the present work.

3.5. Analytical performance

By following the sandwich-type immunoassay protocol described in Section 2, the upconversion and magnetic nanoparticle tagged immunocomplexes formed. The nanoparticles were then concentrated and separated by magnetic separation. We chose to monitor CEA at 542 nm. The luminescent intensity was weakest in the absence of CEA, and the fluorescent signals of the nanocomposites gradually increased with increasing the concentrations of CEA. Under optimal conditions, the linear range of CEA detection was from 2.5×10^{-12} to 1×10^{-8} g/mL ($I = 406.19 \log X + 428.81$) with a correlation coefficient equal to 0.9987. To investigate the reproducibility of our assay, we repeatedly assayed 7 times for two different concentrations of CEA (1 ng/mL and 5 pg/mL). The precision expressed as the relative standard deviation of CEA detection was equal to 5.19% (1 ng/mL, $n = 7$) or 4.36% (5 pg/mL, $n = 7$), indicating that the developed method exhibited good reproducibility. The detection limit was 2.5 pg/mL deduced from the signal to noise ratio of three. These values are desirable for detection CEA, more sensitive than most current existing methods [9–12,14–17]. The detection limit of the present assay was similar to that of Chon et al. (1–10 pg/mL) [13], Tang et al. (1.5 pg/mL) [19] or Tsai et al. (1.8 pg/mL) [18]. Of these published methods, several nanomaterials-based assays

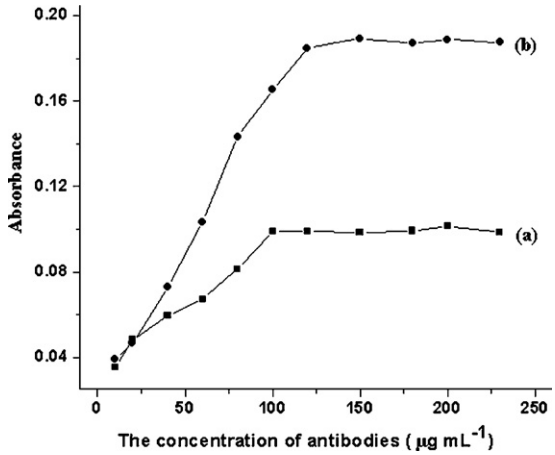

Fig. 5. Absorbance of UV recorded for various concentrations of antibodies after incubation with nanoparticles: (a) capture antibodies incubated with magnetic nanoparticles (2 mg/mL); (b) detection antibodies incubated with upconversion nanoparticles (2 mg/mL).

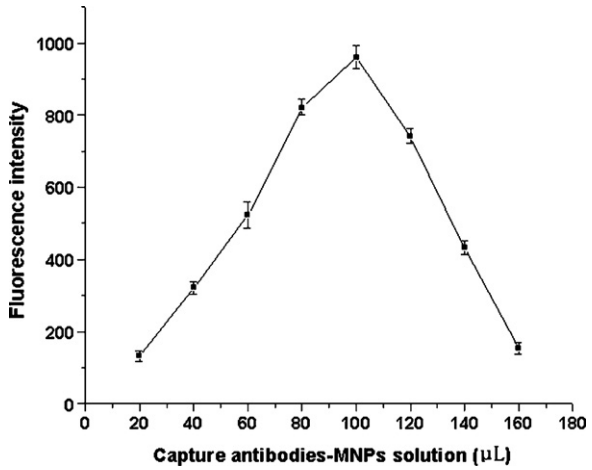

Fig. 6. Fluorescence intensity recorded for signal probes after incubation with various amounts of capture antibodies–MNPs conjugates: 100 μL of detection antibodies-UCNPs as signal probes for 0.5 ng/mL CEA.

Table 1
Analytical results of CEA in human serum samples.

Samples	The available chemiluminescence method (ng/mL)	The developed method (ng/mL)
Serum 1	0.54	0.46
Serum 2	1.20	0.75
Serum 3	1.49	1.04
Serum 4	1.22	0.98
Serum 5	10.3	9.62
Serum 6	627	454
Serum 7	1233	1189
NE 1[a]	n.d.[b]	n.d.
NE 2	n.d.	n.d.

[a] NE, phosphate-buffered saline.
[b] n.d., not detected.

[16–19] also showed different analytical performance because of their different material modifications or signal detection systems. Tang et al. [19] described a horseradish peroxidase-encapsulated nanogold hollow microspheres (HRP-GHS)-based electrochemical immunoassay for the detection of CEA with high sensitivity. Compared to the time-consuming feature and difficulty in electrode fabrication of electrochemical immunoassay, our assay may be more stable, simple and time-saving. In addition, Tsai et al. [18] also reported a high similar method as ours using different functional magnetic nanoparticles. However, UCNPs used in our assay have inherent advantages (such as high stability, no autofluorescence) over the fluorescent dye-doped silica nanoparticles used in their method [24].

3.6. Analytical application

The feasibility of the developed sandwich type immunoassay for the detecting of CEA was further evaluated using seven serum samples obtained from The Fourth Affiliated Hospital of Soochow University. Two samples of PBS buffer were used as negative controls. The results revealed that the concentrations of CEA in these serum samples were ranged from 0.46 ng/mL to 1189 ng/mL (Table 1), which were highly comparable to these of an available chemiluminescence method (Roche Diagnosis) and no significant difference was found between the results of the two methods (paired t-test, $P = 0.248$). In addition, the results of the two methods were also highly correlated ($R = 0.9929$, $P < 0.0001$). The standardization of a new test is also a key factor for its clinical application; and the measurement traceability should be performed before this new detection system is clinically used.

4. Conclusions

In summary, this study describes a sensitive, competitive fluorescence-based immunoassay method for quantification of CEA in human sera using antibodies-modified magnetic nanoparticles as capture probes, and antibodies-functionalized $NaY_{0.78}F_4{:}Yb_{0.20}$, $Ho_{0.02}$ upconversion nanoparticles as detection probes. The method showed high sensitivity and reproducibility for the determination of CEA in serum samples, suggesting its potential application value. Meanwhile, the developed detection system can be easily modified for detection of other tumor markers or for multi-analytes detection of other tumor markers.

Acknowledgments

This work was partly supported by grants from National Natural Science Foundation of China (No. 81000867), "Medical Key Professionals Program" and "333 Project" of Jiangsu Province (for Dr. Zhaohui Huang), Science and Technology Supporting Project of Jiangsu Province (BE2011621), Research Fund for the Doctoral Program of Higher Education (for Prof. Zhouping Wang), and Program for New Century Excellent Talents in University (for Prof. Zhouping Wang).

Appendix A. Supplementary data

Supplementary data associated with this article can be found, in the online version, at doi:10.1016/j.jpba.2012.02.027.

References

[1] J.E. Shively, V. Spayth, F.F. Chang, G.E. Metter, L. Klein, C.A. Presant, C.W. Todd, Serum levels of carcinoembryonic antigen and a tumor-extracted carcinoembryonic antigen-related antigen in cancer patients, Cancer Res. 42 (1982) 2506–2513.
[2] J. Kos, H.J. Nielsen, M. Krasovec, I.J. Christensen, N. Cimerman, R.W. Stephens, N. Brunner, Prognostic values of cathepsin B and carcinoembryonic antigen in sera of patients with colorectal cancer, Clin. Cancer Res. 4 (1998) 1511–1516.
[3] P. Dhar, T. Moore, N. Zamcheck, H.Z. Kupchik, Carcinoembryonic antigen (CEA) in colonic cancer. Use in preoperative and postoperative diagnosis and prognosis, J. Am. Med. Assoc. 221 (1972) 31–35.
[4] C.G. Moertel, J.R. O'Fallon, V.L. Go, M.J. O'Connell, G.S. Thynne, The preoperative carcinoembryonic antigen test in the diagnosis, staging, and prognosis of colorectal cancer, Cancer 58 (1986) 603–610.
[5] M. Tatsuta, H. Yamamura, S. Noguchi, M. Ichii, H. Iishi, S. Okuda, Values of serum carcinoembryonic antigen and elastase 1 in diagnosis of pancreatic carcinoma, Gut 25 (1984) 1347–1351.
[6] H. Kitagawa, E. Ohkouchi, A. Fukuda, K. Imai, A. Yachi, Characterization of carcinoembryonic antigen-specific monoclonal antibodies and specific carcinoembryonic antigen assay in sera of patients, Jpn. J. Cancer Res. 77 (1986) 922–930.
[7] J.M. MacSween, N.L. Warner, A.D. Bankhurst, I.R. Mackay, Carcinoembryonic antigen in whole serum, Br. J. Cancer 26 (1972) 356–360.
[8] M. Herlyn, M. Blaszczyk, H.F. Sears, H. Verrill, J. Lindgren, D. Colcher, Z. Steplewski, J. Schlom, H. Koprowski, Detection of carcinoembryonic antigen and related antigens in sera of patients with gastrointestinal tumors using monoclonal antibodies in double-determinant radioimmunoassays, Hybridoma 2 (1983) 329–339.
[9] W. Dungchai, W. Siangproh, J.M. Lin, O. Chailapakul, S. Lin, X. Ying, Development of a sensitive micro-magnetic chemiluminescence enzyme immunoassay for the determination of carcinoembryonic antigen, Anal. Bioanal. Chem. 387 (2007) 1965–1971.
[10] S. Wang, X. Zhang, X. Mao, Q. Zeng, H. Xu, Y. Lin, W. Chen, G. Liu, Electrochemical immunoassay of carcinoembryonic antigen based on a lead sulfide nanoparticle label, Nanotechnology 19 (2008) 435501.
[11] K. Sato, M. Tokeshi, H. Kimura, T. Kitamori, Determination of carcinoembryonic antigen in human sera by integrated bead-bed immunoassay in a microchip for cancer diagnosis, Anal. Chem. 73 (2001) 1213–1218.
[12] G.Y. Shen, H. Wang, T. Deng, G.L. Shen, R.Q. Yu, A novel piezoelectric immunosensor for detection of carcinoembryonic antigen, Talanta 67 (2005) 217–220.
[13] H. Chon, S. Lee, S.W. Son, C.H. Oh, J. Choo, Highly sensitive immunoassay of lung cancer marker carcinoembryonic antigen using surface-enhanced Raman scattering of hollow gold nanospheres, Anal. Chem. 81 (2009) 3029–3034.
[14] F. Ye, M. Shi, Y. Huang, S. Zhao, Noncompetitive immunoassay for carcinoembryonic antigen in human serum by microchip electrophoresis for cancer diagnosis, Clin. Chim. Acta 411 (2010) 1058–1062.
[15] J. Li, H. Gao, Z. Chen, X. Wei, C.F. Yang, An electrochemical immunosensor for carcinoembryonic antigen enhanced by self-assembled nanogold coatings on magnetic particles, Anal. Chim. Acta 665 (2010) 98–104.
[16] M. Liu, C. Jia, Q. Jin, X. Lou, S. Yao, J. Xiang, J. Zhao, Novel colorimetric enzyme immunoassay for the detection of carcinoembryonic antigen, Talanta 81 (2010) 1625–1629.
[17] L. Chen, Z. Zhang, P. Zhang, X. Zhang, A. Fu, An ultra-sensitive chemiluminescence immunosensor of carcinoembryonic antigen using HRP-functionalized mesoporous silica nanoparticles as labels, Sens. Actuators B: Chem. 155 (2011) 557–561.
[18] H.Y. Tsai, C.Y. Chang, Y.C. Li, W.C. Chu, K. Viswanathan, C. Bor Fuh, Detection of carcinoembryonic antigen using functional magnetic and fluorescent nanoparticles in magnetic separators, J. Nanopart. 13 (2011) 2461–2467.
[19] D. Tang, R. Yuan, Y. Chai, Ultrasensitive electrochemical immunosensor for clinical immunoassay using thionine-doped magnetic gold nanospheres as labels and horseradish peroxidase as enhancer, Anal. Chem. 80 (2008) 1582–1588.
[20] M. Bruchez Jr., M. Moronne, P. Gin, S. Weiss, A.P. Alivisatos, Semiconductor nanocrystals as fluorescent biological labels, Science 281 (1998) 2013–2016.
[21] M. Zhang, M. Yu, F. Li, M. Zhu, M. Li, Y. Gao, L. Li, Z. Liu, J. Zhang, D. Zhang, T. Yi, C. Huang, A highly selective fluorescence turn-on sensor for cysteine/homocysteine and its application in bioimaging, J. Am. Chem. Soc. 129 (2007) 10322–10323.
[22] N. Nakayama-Ratchford, S. Bangsaruntip, X. Sun, K. Welsher, H. Dai, Noncovalent functionalization of carbon nanotubes by fluorescein–polyethylene glycol:

supramolecular conjugates with pH-dependent absorbance and fluorescence, J. Am. Chem. Soc. 129 (2007) 2448–2449.
[23] I.I. Slowing, B.G. Trewyn, V.S. Lin, Mesoporous silica nanoparticles for intracellular delivery of membrane-impermeable proteins, J. Am. Chem. Soc. 129 (2007) 8845–8849.
[24] S. Wu, N. Duan, C. Zhu, X. Ma, M. Wang, Z. Wang, Magnetic nanobead-based immunoassay for the simultaneous detection of aflatoxin B(1) and ochratoxin A using upconversion nanoparticles as multicolor labels, Biosens. Bioelectron. 30 (2011) 35–42.
[25] W. Stöber, A. Fink, E. Bohn, Controlled growth of monodisperse silica spheres in the micron size range, J. Colloid Interface Sci. 26 (1968) 62–69.
[26] L. Wang, J. Bao, F. Zhang, Y. Li, One-pot synthesis and bioapplication of amine-functionalized magnetite nanoparticles and hollow nanospheres, Chemistry 12 (2006) 6341–6347.
[27] J.H. Zeng, J. Su, Z.H. Li, R.X. Yan, Y.D. Li, Synthesis and upconversion luminescence of hexagonal-phase $NaYF_4$:Yb, Er^{3+} phosphors of controlled size and morphology, Adv. Mater. 17 (2005) 2119–2123.

Journal of Pharmaceutical and Biomedical Analysis 66 (2012) 232–239

Contents lists available at SciVerse ScienceDirect

Journal of Pharmaceutical and Biomedical Analysis

journal homepage: www.elsevier.com/locate/jpba

Quantitative determination and pharmacokinetic study of the novel anti-Parkinson's disease candidate drug FLZ in rat brain by high performance liquid chromatography–tandem mass spectrometry

Jinfeng Hou, Feng Qu, Caisheng Wu, Qiang Ren, Jinlan Zhang*

State Key Laboratory of Bioactive Substances and Functions of Natural Medicines, Institute of Materia Medica, Chinese Academy of Medical Sciences and Peking Union Medical College, Beijing 100050, People's Republic of China

ARTICLE INFO

Article history:
Received 17 December 2011
Received in revised form 1 March 2012
Accepted 2 March 2012
Available online 10 March 2012

Keywords:
High performance liquid chromatography–tandem mass spectrometry
FLZ
Rat brain
Pharmacokinetics
Anti-Parkinson's disease

ABSTRACT

FLZ (N-[2-(4-hydroxy-phenyl)-ethyl]-2-(2,5-dimethoxy-phenyl)-3-(3-methoxy-4-hydroxyphenyl)-acrylamide) is a novel anti-Parkinson's disease candidate drug. A sensitive and specific high performance liquid chromatography–tandem mass spectrometry (HPLC–MS/MS) method was developed and validated for the quantification of FLZ in rat brain. Carbamazepine was selected as the internal standard. Sample preparation involved double liquid–liquid extraction by n-hexane and ethyl acetate with high extraction efficiency. The chromatographic separation was achieved on a Zorbax SB-C_{18} column (100 mm × 2.1 mm, 3.5 μm) with an isocratic elution system comprised of acetonitrile and 0.3% aqueous acetic acid at a flow rate of 0.3 ml/min. The elutes were detected under positive electrospray ionization (ESI) and the target analytes were quantified by multiple reaction monitoring (MRM) mode. The method was sensitive with the lowest limit of quantification (LLOQ) at 1.0 ng/g brain tissue. Good linearity ($r > 0.99$) was obtained over the range of 1.0–400 ng/g. The intra- and inter-day precision ranged from 0.68% to 12%, while the accuracy between 92.7% and 111%. In addition, the stability, recovery and matrix effect involved in this method were also validated. The method was used to investigate the pharmacokinetics of FLZ in rat brain successfully after intravenous administration. The brain distribution studies showed that the brain distribution of FLZ was limited with the penetration ratio less than 0.1 in rats, with no target effect in the seven collected regions. Inhibition of P-glycoprotein (P-gp) by zosuquidar·3HCl ((2R)-1-{4-[(1aR,10bS)-1,1-difluoro-1,1a,6,10b-tetrahydrodibenzo[a,e]cyclopropa[c][7]annulen-6-yl]-1-piperazinyl}-3-(5-quinolinyloxy)-2-propanol trihydrochloride) resulted in a significant increase in brain-to-plasma ratio, while no significant increase by inhibition of breast cancer resistance protein (BCRP) by ko143 (2-methyl-2-propanyl 3-[(3S,6S,12aS)-6-isobutyl-9-methoxy-1,4-dioxo-1,2,3,4,6,7,12,12a-octahydropyrazino[1′,2′:1,6]pyrido[3,4-b]indol-3-yl]propanoate). The results indicated that FLZ had poor penetration to the brain due to the P-gp transport system.

© 2012 Elsevier B.V. All rights reserved.

1. Introduction

FLZ, N-[2-(4-hydroxy-phenyl)-ethyl]-2-(2,5-dimethoxy-phenyl)-3-(3-methoxy-4-hydroxyphenyl)-acrylamide (Fig. 1) is a synthetic novel derivative of squamosamide from *Annona glabra* [1]. Previous studies have indicated that FLZ has potent neuroprotective effect, anti-Parkinson's disease (PD) activity [2–7] and anti-Alzheimer's disease (AD) activity [8,9]. Brain is the pathological site of PD and AD. The blood–brain barrier (BBB) and blood–cerebrospinal fluid barrier are the main functional interfaces which regulate the transfer of solutes between the systemic circulation and brain [10]. Both of them express a wide variety of efflux transport proteins, such as P-glycoprotein (P-gp) and breast cancer resistance protein (BCRP), which can actively extrude a variety of structurally diverse drugs and drug metabolites [11–15]. This presents a huge challenge for effective delivery of therapeutics to the central nervous system (CNS) [16,17]. Therefore, the CNS drug candidates should have both optimal pharmacokinetic properties (absorption, metabolism, elimination and plasma binding) and the ability to cross the protective barriers of the brain. In previous study, a HPLC method was established and applied to pharmacokinetic research of FLZ in rats [18]. However, the penetration of FLZ to brain and the distribution of FLZ in target site have not been studied yet.

In order to understand the value of FLZ in the early-medium prevention of Parkinson's disease, we developed, optimized, and validated a high performance liquid chromatography–tandem mass spectrometry (HPLC–MS/MS) method to examine the FLZ

* Corresponding author. Tel.: +86 10 83154880; fax: +86 10 63017757.
E-mail address: zhjl@imm.ac.cn (J. Zhang).

0731-7085/$ – see front matter © 2012 Elsevier B.V. All rights reserved.
doi:10.1016/j.jpba.2012.03.001

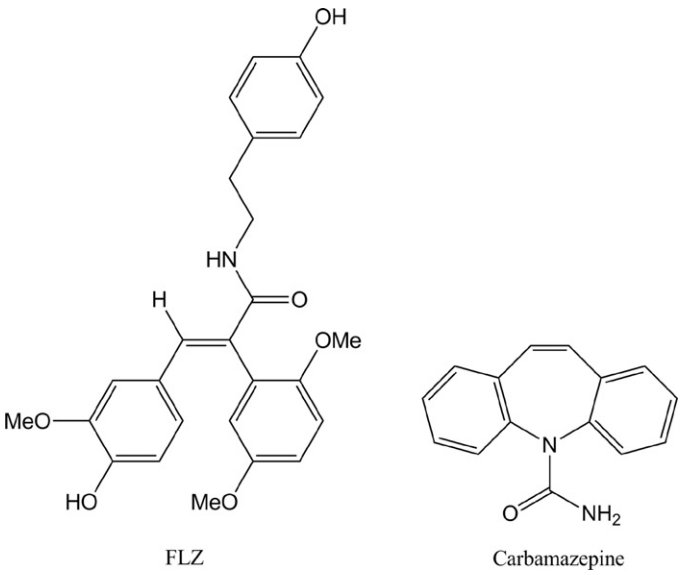

Fig. 1. Structure representation of FLZ and carbamazepine (IS).

levels in rat brain after an intravenous dosing. Our study was aimed to contribute to the understanding of the transport efficiency of FLZ across the blood–brain barrier (BBB) and to investigate the role of P-glycoprotein (P-gp) and breast cancer resistance protein (BCRP) in modulating the CNS penetration of FLZ. The pharmacokinetic characterization of FLZ at the site of action and its regional distribution can help us to enhance insight into the pharmacokinetic–pharmacodynamic relationships.

2. Materials and methods

2.1. Chemicals and materials

FLZ (purity 99.6%, $pK_a = 13.75 \pm 0.46$, lipophilic and poor water solubility) was supplied by Prof. Ping Xie (Institute of Materia Medica, Chinese Academy of Medical Sciences, Beijing, China) and carbamazepine (internal standard (IS)) was obtained from National Institutes for food and drug Control (Beijing, China). Zosuquidar trihydrochloride and ko143 (purity >98%) were purchased from Shanghai Haoyuan Chemexpress Co. Ltd. (Shanghai, China). Acetonitrile of MS grade was obtained from Honeywell Burdick and Jackson Inc. (Muskegon, MI, USA). Methanol of HPLC grade was purchased from Burdick and Jackson Inc. (Ulsan, Korea). HPLC grade ethyl acetate and n-hexane were obtained from Mallinckrodt Baker Inc. (Phillipsburg, NL, USA). Other chemicals were all of analytical grade. Deionized water was purified using a Millipore water purification system (Millipore, Billerica, MA, USA). Drug free brain tissue and plasma were obtained from the male rats (wistar, weighing 200 ± 20 g) purchased from Vital River Laboratories (Beijing, China).

2.2. Instrumentation and chromatographic conditions

The assay was performed on a 6410B triple quadrupole LC–MS system (Agilent Corporation, MA, USA) consisting of an Agilent 1200 RRLC system (Agilent Co.) connected to a triple quadrupole MS analyzer with an electrospray ionization (ESI) interface usable in either positive-ionization or negative-ionization mode. Chromatographic separation was achieved on a Zorbax SB-C_{18} column (2.1 mm × 100 mm, 3.5 μm, Agilent Co.) with a SB-C8 pre-column (2.1 mm × 12.5 mm, 5 μm, Agilent Co.). 5 μl of the sample solution was injected and the analytes were eluted using acetonitrile and water containing 0.3% acetic acid (37:63, v/v) at a flow rate of 0.3 ml/min. The isocratic separation run was completed within 5.5 min at 30 °C. After each injection, the injection needle was washed with methanol for 10 s to reduce carry-over.

The ESI instrumental settings were optimized for the analysis and the appropriate MRM transitions and MS/MS parameters were determined for individual compounds by direct infusion into the mass spectrometer. The following were the optimum operating parameters of the ESI interface in positive mode: nebulizer, 45 psi; dry gas, 9 l/min; dry temp, 325 °C; capillary voltage, 4000 V; delta EMV, 300 V; the LC eluent flow during the period from 0.0 to 1.6 min was switched to waste before introducing to the mass spectrometer for data acquisition. The following precursor-to-product ion transitions were subjected to multiple reaction monitoring: for FLZ, m/z 449.9 → 136.9 (fragmentor, 135 V, collision energy, 10 V) and m/z 449.9 → 312.8 (fragmentor, 135 V, collision energy, 25 V) as the quantitative and qualitative ion-pairs, respectively; for carbamazepine (IS), 236.9 → 194.0 (fragmentor, 120 V, collision energy, 18 V) as the quantitative ion-pairs. All dwell times were 100 ms. Data acquisition and processing were performed using MassHunter workstation (Agilent Co., MA, USA).

2.3. Preparation of stock solutions, calibration standards and quality control (QC) samples

Stock solutions of FLZ and carbamazepine (IS) were prepared separately in methanol at a target concentration of 1 mg/ml and diluted in 80% methanol to create working solutions of FLZ at the concentrations of 5, 10, 15, 50, 150, 500, 1500 and 2000 ng/ml and the IS at the concentration of 100 ng/ml. All solutions were stored in glass tubes at 4 °C and protected from light less than two months until analysis. Calibration standards of FLZ at eight levels (1.0, 2.0, 3.0, 10, 30, 100, 300 and 400 ng/g) were prepared by spiking the pooled drug free brain homogenate (plasma) with the appropriate working standard solution of FLZ. Quality control (QC) samples were prepared using the working solutions from the same stock solution at four concentration levels (1.0 ng/g (LLOQ), 3.0 ng/g (QC low), 30 ng/g (QC medium) and 300 ng/g (QC high)) representing the entire range of concentrations.

2.4. Sample preparation

In this study, a double liquid–liquid extraction (LLE) method was applied to extract FLZ and IS from rat brain. All samples were thawed at room temperature before analysis. To 0.5 ml of the brain homogenate were added 20 μl of the IS working solution. The mixture was vortex-mixed for 20 s and evaporated to dryness with a gentle stream of nitrogen gas at 36 °C and the sample was reconstituted with 100 μl 80% methanol. Then, 400 μl of water was added to the reconstitution. After adding 1.5 ml of n-hexane, the mixture was vortex-mixed for 90 s and centrifuged at 1721 × g for 10 min, then the n-hexane layer was removed and discarded. The remainder was extracted with 1.5 ml ethyl acetate by vortex-mixing for 90 s. After centrifuging at 1721 × g for 10 min, the organic layer was transferred into another test tube and evaporated to dryness again. The residue was reconstituted in 50 μl 80% methanol by ultrasonic method for 180 s and centrifuged at 16,654 × g for 10 min. Finally, 5 μl supernatant was injected to HPLC–MS/MS system.

For the plasma samples, 20 μl of the IS working solution was added to 100 μl plasma and then 500 μl methanol after a vortex-mixing. The mixture was vortex-mixed for 90 s, centrifuged at 16,654 × g for 10 min, and the methanol extraction solution was treated using the same procedure as brain homogenate.

2.5. Method validation

The assay validation was performed to meet the acceptance criteria according to the guidance concerning bioanalytical method validation (EMA, Guideline on bioanalytical method validation, 21 July 2011). The assay was validated in terms of specificity, matrix effect, recovery from spiked brain homogenate samples, calibration curve, precision and accuracy (intra- and inter-day), lower limit of quantification (LLOQ), stability (short and long term, autosampler and freeze–thaw) and dilution integrity.

2.5.1. Specificity

The specificity of the method was investigated by analyzing six different of drug-free rat brain homogenate for the exclusion of any potential endogenous interference. They were compared to those brain samples spiked with FLZ at known concentrations. All the brain homogenate samples were pre-treated and analyzed under the same procedure as described in Section 2.4.

2.5.2. Matrix effect and recovery

The absolute matrix effect was determined by comparing the peak responses of the analytes resolved in the blank brain homogenate that from six different rats with those of the analytes resolved in the 80% methanol containing equivalent amounts of the analytes. The IS-normalized MF was calculated by dividing the MF of the analyte by the MF of IS. The CV of the IS-normalized MF calculated from the 6 lots of matrix should not be greater than 15%.

The extract recovery of the analyte was determined by comparing the responses of the analyte from QC samples with the responses of analyte resolved in the 80% methanol at same concentration level.

2.5.3. Calibration curve

Brain homogenate calibration curves were constructed using the peak area ratios of FLZ to IS versus the concentration of FLZ in eight sets of matrix matched calibration standards, and applying a weighted ($1/x^2$) least squares linear regression analysis. To evaluate the linearity of the method, calibration curves were prepared and assayed on three different days. The back calculated concentrations of the calibration standards should be within ±15% (±20% at the lower limit of quantitation, LLOQ) of the nominal value. At least 75% of the calibration standards, with a minimum of six calibration standard levels, must fulfill this criterion.

2.5.4. Precision and accuracy

Intra-day accuracy and precision were determined in quintuplicate by analyzing QC samples at LLOQ, low, medium and high concentrations across the linear range. Inter-day accuracy and precision were evaluated on three separate days. Precision was expressed as the relative standard deviation of the determined concentrations. Accuracy was calculated using the following equation: (mean measured concentration/nominal concentration) × 100. The criteria for acceptability of the data included accuracy within 85–115%, and precision with RSD less than 15%, except for LLOQ, with accuracy within 80–120%, and precision with RSD less than 20%.

2.5.5. Stability

The stability of FLZ in rat brain was evaluated by using QC samples (3.0, 30 and 300 ng/g) with three samples for each concentration. The stability of FLZ was tested under the following conditions: (1) freeze–thaw stability of FLZ in rat brain homogenate through three freeze–thaw cycles between −80 °C and ambient temperature; (2) short-term stability of FLZ in rat brain homogenate at room temperature for 12 h; (3) long-term stability of FLZ in rat brain homogenate stored at −80 °C for 45 days; (4) post-preparative stability of FLZ during storage in the auto-sampler at room temperature for 48 h.

2.5.6. Dilution integrity

In order to demonstrate the accuracy to dilute and analyze samples containing FLZ concentrations above the upper limit of quantitation (ULOQ), a set of spiked brain homogenate samples were prepared with FLZ concentrations at 0.3, 3 and 30 μg/g. The spiked samples were diluted 100 times with methanol, and then processed according to the sample preparation procedure described in Section 2.4 and analyzed with the developed methodology. Dilution integrity was also validated in rat plasma diluted 500 times at 1.5, 15 and 150 μg/ml and 100 times at 0.3, 3 and 30 μg/ml with saline in the same way.

2.6. Pharmacokinetic study (PK) in rats and statistics

Male Wistar rats (weighing 200 ± 20 g) were purchased from Vital River Laboratories (Beijing, China) and maintained under temperature-controlled conditions with a 12-h light/dark cycle and fed with food and water ad libitum. All rats were allowed to acclimatize for a minimum 3 days upon arrival before experimentation. All protocols and procedures involving animals were approved by the Animal Care and Welfare Committee of Institute of Materia Medica, Chinese Academy of Medical Sciences & Peking Union Medical College (Beijing, China).

All rats received FLZ by intravenous administration in the tail vein at a dose of 35 mg/kg. The study involved the following five study groups.

2.6.1. PK profile in blood, brain and different districts of brain

Two groups and each of sixty rats were dosed of FLZ at 35 mg/kg which was dissolved in a mixture solvent of dimethyl sulfoxide, polyethylene glycol 400 and sodium chloride injection 1:4:5 (v/v/v), respectively. For one group, five rats per time point were exsanguinated and decapitated at 0.25, 2, 4, 7, 10, 20, 30, 45, 60, 90 and 180 min. Whole brain was immediately harvested, rinsed with ice-cold saline to remove extraneous blood, then transferred to a labeled and pre-weighed tissue tube which wrapped in aluminum foil. In the mean time, blood was collected to a heparinized test tube and centrifuged at 1721 × *g* for 10 min. Plasma was obtained and stored at −80 °C until analysis. For another group, the rats were treated in the same way, and then the whole brain was put on a glass plate resting on a bed of ice. Using a scalpel, the brain was dissected and the following regional tissues were collected: cerebral cortex, cerebellum, medulla oblongata, thalamus (including hypo-thalamus), midbrain, striatum and hippocampus. Each tissue was placed in a pre-weighed tube. An anatomical map of the rat brain [19] was used as a reference to help identify the anatomical boundaries of these brain areas.

All the brain samples were homogenized with methanol (1:5, w/v) using a homogenizer (Kimble & Kontes, NJ, USA), respectively, then centrifuged at 16,654 × *g* for 10 min and the brain homogenate was stored at −80 °C until analysis. The whole brain free of FLZ was collected as blank sample for generating standard curve and QC samples.

2.6.2. Effects of P-gp and BCRP inhibitors on penetration of FLZ to rat brain

Seventy-two rats were divided into three groups and all of the rats were given continuously two intravenous injections in tail vein. The first injection consisted of 2.5 ml/kg vehicle, zosuquidar (20 mg/kg, dissolved in 20% ethanol–saline) or ko143 (7.5 mg/kg, dissolved in solutol HS15-ethanol–saline, 1:2:7, v/v/v), and the second injection consisted of 3.5 ml/kg FLZ (35 mg/kg). The time between two injections was 10 min. The rats were sacrificed at 0.25,

4, 10 and 30 min post-dose ($n = 6$ per group). Whole brain and blood samples were collected as the procedure described in Section 2.6.1.

2.6.3. Calculations and statistical analysis

Brain concentrations were corrected for residual blood volume using 15 μl/g of brain tissue as the vascular space [20]. Values were expressed as mean ± SD for five rats at each time point or in each group. To determine the pharmacokinetic parameters of FLZ, the concentration–time data were analyzed by the DAS (Drug and Statistics for Windows) software package (version 2.0, Chinese Pharmacological Association, China) generated by a non-compartmental model (statistical moment). The penetration ratio of FLZ to BBB was presented by the partition coefficient (R_i) which was calculated as the FLZ AUC in whole brain divided by the FLZ AUC in blood ($R_i = AUC_{brain}/AUC_{blood}$) [21]. Distribution of FLZ in various rat brain regions was estimated by $AUC_{(0-\infty)}$.

For the inhibitor treated groups, the brain penetration was estimated by the brain-to-plasma concentration ratio (B/P ratio) using the corrected brain concentrations. The significance between control group and inhibitor treated group was determined by Student's *t*-test at $p < 0.05$ significance level.

3. Results and discussion

3.1. Chromatography and mass spectrometry

In order to develop the ESI-MS/MS method for the determination of FLZ, the full scan precursor and product ion spectra of the analyte and IS were tried both in positive and negative ion mode. The result demonstrated that both of them presented greater ionization efficiency in positive rather than in negative ESI mode, giving rise to $[M+H]^+$ ion peak at *m/z* 449.9 for FLZ and *m/z* 236.9 for IS in positive mode. The fragmentor voltage for the fragmentation of the selected precursor ions of FLZ and IS was optimized over the range of 80–180 V with a 5 V step, and 135 V provided optimum fragmentation of FLZ, whereas the corresponding value for IS was found to be 120 V. The product ion mass spectrometry of FLZ showed predominant ions at *m/z* 136.9 and 312.8, corresponding to the fragment ions after the fragmentation of amide linkage, respectively, while the predominant ion of IS was shown at *m/z* 194.0. For the selective and sensitive quantification of FLZ in positive ESI-MS/MS mode the transitions of 449.9 → 136.9 and 312.8 were monitored for FLZ, whereas the 236.9 → 194.0 for IS. And after the optimization of the collision energy voltage of the three ion-pairs over the range of 5–40 V, 10, 25 and 18 V were showed giving better ion efficiency, respectively. The ESI interface parameters were also optimized under the chromatographic condition.

The chromatographic condition was optimized to get the rapid and efficient separation of FLZ and IS from brain samples. Through comparing different columns and mobile phases, a Zorbax SB-C_{18} column and acetonitrile–water were chosen. Further optimization was performed by adding acetic acid in mobile phase and changing the column temperature, which may improve the peak shape of the analyte, accelerate the analysis time and enhance ionization. Finally, addition of 0.3% acetic acid to the mobile phase was found to improve separation and enhance detection under the positive ionization mode. Under the optimal LC conditions, FLZ was eluted at 3.84 min, and the IS was at 2.80 min, with a total chromatographic run time within 5.5 min.

3.2. Sample preparation and extraction efficiency

In this study, methanol was used as the extraction solvent. It showed better efficiency of extraction for FLZ from the brain than other aqueous solutions such as saline. In order to avoid the matrix effect, the extract of FLZ was subjected to further preparation methods such as solid phase extraction and liquid–liquid extraction. Solid phase extraction was jammed by extraction solution due to the endogenous lipid-soluble substances in brain. Although ethyl acetate showed good extraction for FLZ, the extract solution contained lipid-soluble substances from the brain and were visually so turbid and oleaginous that the analytical column was contaminated and lost column efficiency. The endogenous lipid-soluble substances could be extracted by n-hexane, while FLZ will not be extracted. So a double liquid–liquid extraction with n-hexane and ethyl acetate could avoid matrix effect and contamination, and improve the sensitivity. During the pre-treatment, the addition of water (400 μl) was necessary to get a good phase separation between the aqueous and organic layers.

3.3. Method validation

3.3.1. Specificity

No apparent interferences were observed around FLZ or IS in blank rat brain and rat brain sample obtained after intravenous administration of FLZ (Fig. 2). These results supported the high specificity and selectivity of this method in analysis of FLZ.

3.3.2. Matrix effect and recovery

The matrix effect of FLZ was from 1.02 to 1.25 at the four concentration levels with the precision less than 12%, while the IS-normalized MF was from 0.93 to 1.14 (Table 1). The mean extract recovery was higher than 96%.

3.3.3. Linearity and LLOQ

Table 2 showed the back-calculated concentrations of FLZ (range: 1.0–400 ng/g) and the parameters obtained from the corresponding calibration curves. The mean accuracy (%) of back-calculated concentrations ranged from −6.0% to +2.3% and the precision was below 12% except one concentration level at 2.0 ng/g was 20%. The mean coefficient of correlation (r) was 0.9956. The LLOQ was established at 1.0 ng/g, which was the lowest point of the standard curve. A $1/x^2$-weighting scheme was used for each day of the validation and analysis for FLZ.

3.3.4. Precision and accuracy

The results of intra-day and inter-day accuracy and precision were presented in Table 3. The intra-day and inter-day precisions were less than 12% for brain and less than 11% for plasma. Over the range of concentrations from 1.0 to 400 ng/g, the average accuracy ranged from 92.7% to 111% for brain and from

Table 1
Matrix effect (ME, $n = 6$) and extraction recovery (RE, $n = 5$) of FLZ in rat brain homogenate.

	Concentration (ng/g)	RE (mean ± SD (%))	RSD (%)	ME (mean ± SD)	IS-normalized MF	RSD (%)
FLZ	1.0			1.14 ± 0.10	1.04	8.8
	3.0	96.1 ± 6.1	6.4	1.25 ± 0.15	1.14	12
	30	109 ± 7	6.5	1.05 ± 0.02	0.95	2.0
	300	114 ± 4	3.6	1.02 ± 0.004	0.93	0.4
IS	20			1.10 ± 0.02		1.9

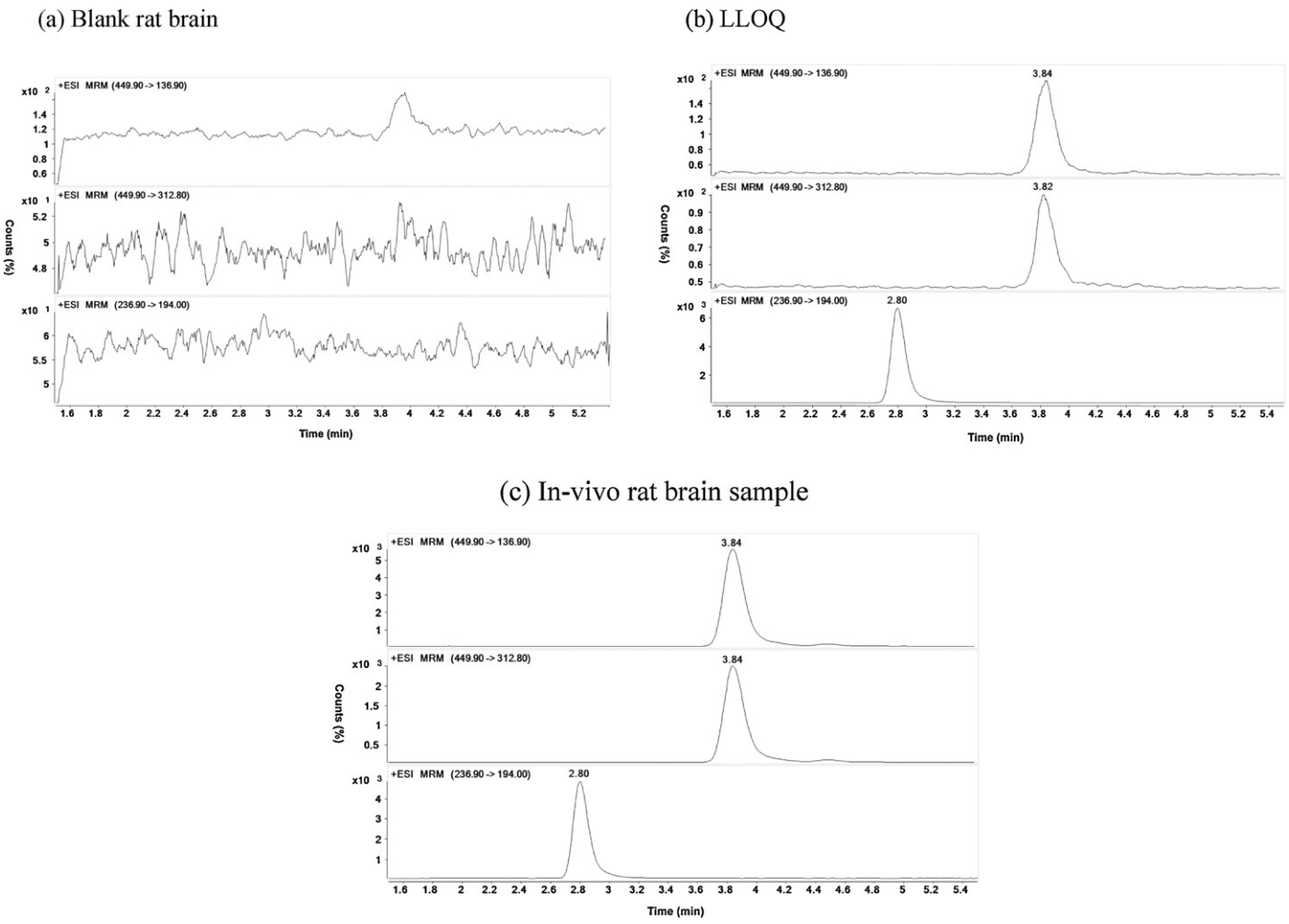

Fig. 2. Typical MRM chromatograms of FLZ in rat brain (a) a drug free brain, (b) a drug free brain spiked with FLZ at LLOQ (1.0 ng/g) and IS and (c) an in vivo rat brain sample showing FLZ (63.42 ng/g) obtained following intravenous administration of FLZ.

Table 2
Standard curve statistics of FLZ mean values of three batches.

	Nominal concentrations (ng/g)								Calculation curve parameters		
	1.0	2.0	3.0	10	30	100	300	400	Slope	Intercept	*r*
	Back-calculated concentrations (ng/g)										
Batch 1	1.02	1.89	3.02	11.2	29.5	95.9	302	397	0.044	0.021	0.9984
Batch 2	0.86	2.80	3.00	9.84	29.0	97.3	305	404	0.040	0.024	0.9933
Batch 3	0.95	2.52	2.85	9.01	29.6	107	313	411	0.042	0.029	0.9952
Mean	0.94	2.40	2.96	10.0	29.4	100	307	404	0.042	0.025	0.9956
RE (%)	−6.0	20	−1.3	0	−2.0	0	2.3	1.0			
RSD (%)	8.6	20	3.2	12	1.1	6.1	1.9	1.8	4.8	17	0.26

Table 3
Intra- and inter-day precision and accuracy of the HPLC–MS/MS method for the determination of FLZ in rat brain homogenate and plasma ($n = 5$ and 3 days, five replicates per day).

	Spiked	Intra-batch precision and accuracy ($n = 5$)			Inter-batch precision and accuracy ($n = 3$)		
		Measured (mean ± SD)	RSD (%)	Accuracy (%)	Measured (mean ± SD)	RSD (%)	Accuracy (%)
Brain (ng/g)	1.0	1.11 ± 0.13	12	111	1.07 ± 0.05	4.7	107
	3.0	2.99 ± 0.17	5.7	99.7	2.96 ± 0.02	0.68	98.7
	30	27.8 ± 0.8	2.9	92.7	28.8 ± 2.1	7.3	96.0
	300	298 ± 3	1.1	99.3	299 ± 2	0.67	99.7
Plasma (ng/ml)	1.0	1.05 ± 0.11	11	105	1.06 ± 0.11	11	106
	3.0	3.10 ± 0.04	1.3	103	2.93 ± 0.18	6.2	97.7
	30	31.3 ± 0.2	0.64	104	30.0 ± 1.1	3.7	100
	300	319 ± 7	2.2	106	304 ± 13	4.3	101

Table 4
Stability of FLZ in rat brain ($n = 3$).

Spiked (ng/g)	Short (12 h)		48 h (auto sampler)		3rd freeze–thaw		45 days at −80 °C	
	Mean ± SD (ng/g)	Accuracy (%)	Mean ± SD (ng/g)	Accuracy (%)	Mean ± SD (ng/g)	Accuracy (%)	Mean ± SD (ng/g)	Accuracy (%)
3.0	3.25 ± 0.09	108	2.92 ± 0.15	97.3	3.13 ± 0.30	104	2.92 ± 0.12	97.3
30	28.9 ± 1.5	96.3	28.8 ± 0.6	96.0	30.9 ± 2.0	103	29.3 ± 0.5	97.7
300	296 ± 7	98.7	298 ± 5	99.3	325 ± 24	108	317 ± 5	106

Table 5
Accuracy for determination of FLZ in rat brain homogenate after dilution for 100 times and in plasma after dilution for 100 and 500 times ($n = 5$).

	Spiked	Measured (mean ± SD)	RSD	Accuracy (%)
Brain (ng/g)	300	2.98 ± 0.16	5.4	99.3
	3000	32.2 ± 1.6	5.0	107
	30,000	309 ± 10	3.3	103
Plasma (100 times) (ng/ml)	300	3.21 ± 0.09	2.9	107
	3000	33.2 ± 0.9	2.8	111
	30,000	323 ± 10	3.1	108
Plasma (500 times)	1500	2.59 ± 0.19	7.4	86.3
	15,000	30.7 ± 2.6	8.5	102
	150,000	327 ± 8	2.5	109

97.7% to 106% for plasma. The results indicated that the precision and accuracy of this method were adequate for bio-analytical purposes.

3.3.5. Stability

The aim of the stability study was to obtain information on the stability of the analyte during the preparation, the multiple-freeze/thaw cycles, on the auto-sampler and after storing for a long time. The recovery of FLZ was between 96.0% and 108% in all tested samples (Table 4), suggesting that FLZ kept stable in above four conditions.

3.3.6. Dilution integrity

Dilution integrity experiments carried out at five replicates by 100 times dilution with methanol in brain, while 100 times and 500 times with saline in plasma. Assay precision and accuracy were determined in a similar manner as described in Section 2.5.4. The accuracy of diluted QCs was in the range of 86.3–111%; while precision values ranged from 2.5% to 8.5% for FLZ (Table 5). The results indicated that samples with concentration over the upper limit of calibration curve could be analyzed by appropriate dilution.

3.4. In vivo pharmacokinetic studies in brain

The described analytical method was successfully applied to the pharmacokinetic study of FLZ in rat brain after intravenous administration (35 mg/kg). Prior to the samples analysis, some of the plasma samples were diluted 500 times or 100 times with saline and some brain homogenate samples were diluted 100 times with methanol, because of that some of the plasma and brain FLZ concentrations exceeded the upper limit of standard curve. The presence of drug in brain vasculature also must be considered when brain concentrations were measured in whole brain homogenates. Correction for residual blood volume was necessary since the drug found in brain homogenates might come from the vascular contamination. It must be excluded in order to assess accurately the penetration of the drug into the brain. Therefore FLZ concentration in the brain after intravenous dosing was corrected using 15 μl/g of brain tissue as the vascular space to deduct the residual blood volume.

3.4.1. PK profile in blood, whole brain and different districts of brain

The mean concentration–time profiles of FLZ in plasma, the whole brain and different regions of brain were illustrated in Fig. 3. The profiles of the whole brain and various regions of brain had the similar shapes. Peak brain levels for FLZ were seen at the first sampling time after intravenous administration, demonstrating that FLZ could enter into the brain rapidly with no lag time. Then both of the plasma and brain concentration versus time profiles of FLZ declined rapidly within 2 min, then gradually eliminated. Through the statistic analysis using DAS 2.0 software, the pharmacokinetic parameters in rat plasma and brain were presented in Table 6. The area under the curve (AUC) were from 321 to 508 μg/l h for the brain tissues and 4891 μg/l h for plasma; the mean residence time (MRT) were from 0.17 h to 0.22 h for the brain tissues and 0.28 h for plasma and the elimination half-life ($t_{1/2}z$) were from 0.43 h to 0.64 h for the brain tissues and 0.57 h for plasma. The maximum concentration (C_{max}) was from 4553 to 7322 μg/l for the brain tissues. The penetration ratio of FLZ to brain was 0.073, which indicated that FLZ was obstructed by BBB.

Since FLZ has the protective effects for Parkinson's disease [2–4] and the nigrostriatal area in the midbrain was the onset of PD [22,23], we therefore investigate whether FLZ could be distributed to the onset of region and show a certain target. The results indicated that FLZ could across BBB to all the seven regions collected in this study, but FLZ did not show target effect on distribution in these regions after intravenous administration.

3.4.2. Effects of P-gp and BCRP inhibitors on FLZ penetration to rat brain

The above study demonstrated that it was not easy to cross the BBB for FLZ. In order to elucidate the mechanism of low penetration ratio of FLZ, the brain concentrations of FLZ were measured in rats that were pre-treated with the efflux inhibitors zosuquidar or ko143. The plasma concentration of dosed zosuquidar group, significantly decreased about 19% and 38% compared with the

Table 6
Pharmacokinetic parameters of FLZ in rat blood and different brain regions after intravenous administration of FLZ (35 mg/kg).

Parameters	Values								
	Plasma	Cerebral cortex	Cerebellum	Medulla oblongata	Mid-brain	Thalamus	Hippocampus	Striatum	Whole brain
$AUC_{(0-\infty)}$ (μg/l h)	4891	336	508	435	321	339	323	329	358
$MRT_{(0-\infty)}$ (h)	0.28	0.21	0.21	0.22	0.20	0.20	0.17	0.19	0.18
$t_{1/2}z$ (h)	0.57	0.43	0.55	0.64	0.45	0.47	0.49	0.47	0.78
T_{max} (h)	–	0.0042	0.0042	0.0042	0.0042	0.0042	0.0042	0.0042	0.0042
C_{max} (μg/l)	–	4882	7322	6285	4906	5039	5014	4553	6128

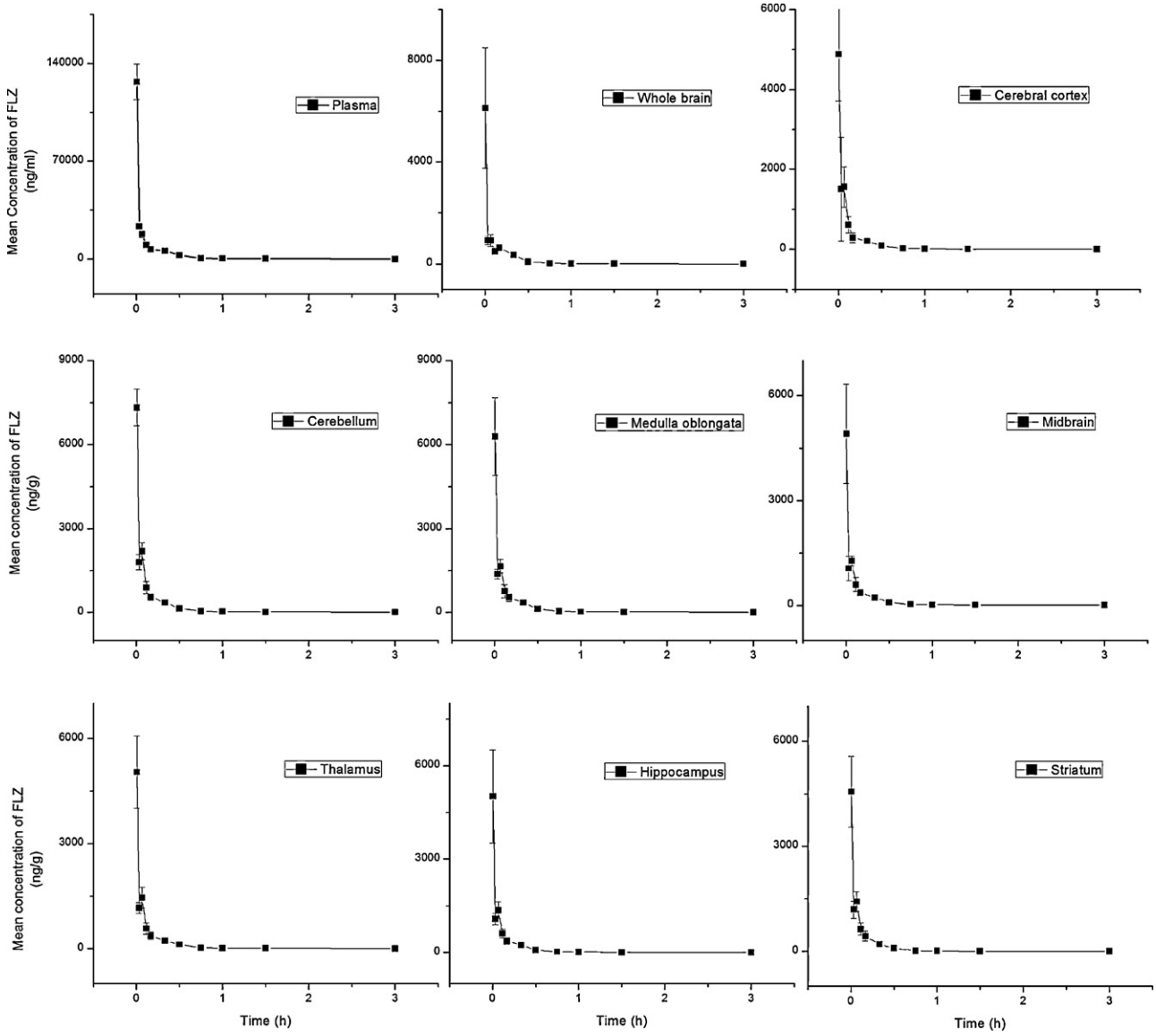

Fig. 3. Mean concentration-time profiles of FLZ after intravenous administration of FLZ (35 mg/kg) in plasma, whole brain and different brain regions (mean ± SD, $n = 5$).

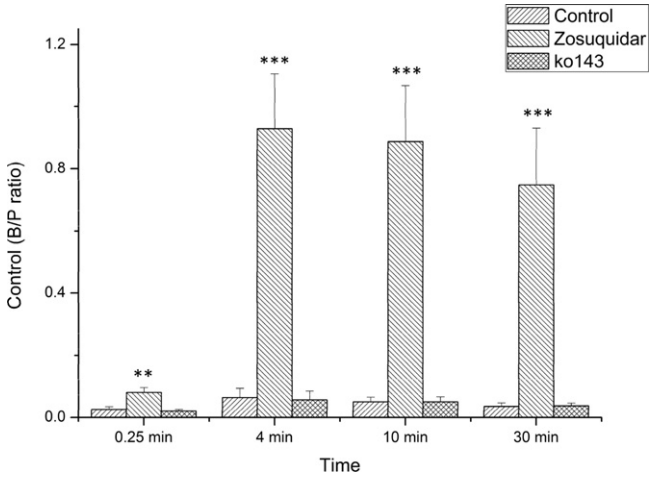

Fig. 4. Effect of pharmacological inhibition of drug efflux transporters on brain distribution of FLZ in rats. The rats received 35 mg/kg FLZ via tail vein injection 10 min after intravenous administration of 20 mg/kg zosuquidar or 7.5 mg/kg ko143. The values are presented as mean ± SD. $^{***}p < 0.001$, $^{**}p < 0.01$, compared with control group.

control group at 0.25 min and 4 min post-dose respectively, while FLZ levels at the other time points did not change significantly. And there is no significant change of FLZ plasma concentrations in pre-treated with ko143 group compared with the control group. The brain-to-plasma ratio of FLZ in the group treated with P-gp inhibitor zosuquidar increased about 3.1-fold at 0.25 min post-dose and about 14.5-fold to 20.8-fold at the other three time points compared with the control group ($p < 0.01$) (Fig. 4). While the brain-to-plasma ratio of FLZ in the groups treated with the BCRP inhibitor ko143 did not increase with any significant extent.

Drug penetration into the CNS is often limited by active efflux proteins in the BBB, such as P-gp and BCRP. Previous studies have shown that zosuquidar·3HCl is a potent and selective P-gp inhibitor because it appears to possess a very low affinity for enzymes of the cytochrome P-450 family and for the drug-transporting proteins MRP-1, MRP-2 or BCRP [24,25]. ko143, as the most potent analog of fumitremorgin (FTC), appears to be first highly potent and specific BCRP inhibitor applicable in vivo safely [26].

Our study indicated that the efflux protein of P-gp significantly limited the amount of FLZ penetrating into brain, while BCRP shows no effect. A study on dasatinib by Chen et al. [27] illustrated that

P-gp and BCRP efflux transporters may work in concert in limiting delivery of dasatinib across the BBB, although P-gp shows limit effect, while BCRP alone shows no effect. de Varies et al. [28] also reported such a synergistic effect of the two transporters for topotecan, another dual substrate of P-gp and BCRP. Therefore, further investigations are needed to study whether the "synergistic effect" of the two transporters exits on FLZ. The findings will highlight the need to better understand the role of P-gp and BCRP on FLZ brain penetration.

4. Conclusion

In this paper, a sensitive and reliable HPLC–MS/MS quantitative method was developed and validated to determine FLZ concentration in rat brain for the first time. The method showed excellent sensitivity, linearity, precision and accuracy. Based on this validated method, penetration ration of FLZ and its regional distribution in rat brain after intravenous administration were investigated successfully. In addition, the effects of P-gp and BCRP transporters on FLZ across BBB were also studied using this method for the first time.

Acknowledgment

This work was financially supported by the Natural Science Foundation of China (No. 81672697).

References

[1] P. Xie, X.Z. Jiao, X.T. Liang, W.H. Feng, H.L. Wei, G.T. Liu, Synthesis and antioxiactivity of squamosamide cycnc analogs, Acta Acad. Med. Sin. 26 (2004) 372–378.
[2] D. Zhang, J.J. Zhang, G.T. Liu, The novel squamosamide derivative (compound FLZ) attenuated 1-methyl, 4-phenyl-pyridinium ion (MPP+)-induced apoptosis and alternations of related signal transduction in SH-SY5Y cells, Neuropharmacology 52 (2007) 423–429.
[3] W. Feng, H. Wei, G.T. Liu, Pharmacological study of the novel compound FLZ against experimental Parkinson's models and its active mechanism, Mol. Neurobiol. 31 (2005) 295–300.
[4] D. Zhang, J.J. Zhang, G.T. Liu, The novel squamosamide derivative FLZ protects against 6-hydroxydopamine-induced apoptosis through inhibition of related signal transduction in SH-SY5Y cells, Eur. J. Pharmacol. 561 (2007) 1–6.
[5] X.C. Kong, D. Zhang, C. Qian, G.T. Liu, X.Q. Bao, FLZ, a novel HSP27 and HSP70 inducer, protects SH-SY5Y cells from apoptosis caused by MPP(+), Brain Res. 1383 (2011) 99–107.
[6] X.Q. Bao, X.C. Kong, C. Qian, D. Zhang, FLZ protects dopaminergic neuron through activating protein kinase B/mammalian target of rapamycin pathway and inhibiting RTP801 expression in Parkinson's disease models, Neuroscience 202 (2012) 396–404.
[7] D. Zhang, X. Hu, S.J. Wei, J. Liu, H. Gao, L. Qian, B. Wilson, G. Liu, J.S. Hong, Squamosamide derivative FLZ protects dopaminergic neurons against inflammation-mediated neurodegeneration through the inhibition of NADPH oxidase activity, J. Neuroinflamm. 5 (2008) 21.
[8] N. Li, G.T. Liu, The novel squamosamide derivative FLZ enhances BDNF/TrkB/CREB signaling and inhibits neuronal apoptosis in APP/PS1 mice, Acta Pharmacol. Sin. 31 (2010) 265–272.
[9] Y. Hou, Y.B. Yu, G. Liu, Y. Luo, A natural squamosamide derivative FLZ reduces amyloid-beta production by increasing non-amyloidogenic AbetaPP processing, J. Alzheimers Dis. 18 (2009) 153–165.
[10] C.L. Graff, G.M. Pollack, Drug transport at the blood–brain barrier and the choroid plexus, Curr. Drug Metab. 5 (2004) 95–108.
[11] M. Demeule, A. Regina, J. Jodoin, A. Laplante, C. Dagenais, F. Berthelet, A. Moghrabi, R. Beliveau, Drug transport to the brain: key roles for the efflux pump P-glycoprotein in the blood–brain barrier, Vascul. Pharmacol. 38 (2002) 339–348.
[12] J. Enokizono, H. Kusuhara, A. Ose, A.H. Schinkel, Y. Sugiyama, Quantitative investigation of the role of breast cancer resistance protein (Bcrp/Abcg2) in limiting brain and testis penetration of xenobiotic compounds, Drug Metab. Dispos. 36 (2008) 995–1002.
[13] J. Enokizono, H. Kusuhara, Y. Sugiyama, Effect of breast cancer resistance protein (Bcrp/Abcg2) on the disposition of phytoestrogens, Mol. Pharmacol. 72 (2007) 967–975.
[14] H. Potschka, M. Fedrowitz, W. Loscher, P-glycoprotein-mediated efflux of phenobarbital, lamotrigine, and felbamate at the blood–brain barrier: evidence from microdialysis experiments in rats, Neurosci. Lett. 327 (2002) 173–176.
[15] A.H. Schinkel, P-glycoprotein, a gatekeeper in the blood–brain barrier, Adv. Drug. Deliv. Rev. 36 (1999) 179–194.
[16] D.J. Begley, Delivery of therapeutic agents to the central nervous system: the problems and the possibilities, Pharmacol. Ther. 104 (2004) 29–45.
[17] W.M. Pardridge, The blood–brain barrier: bottleneck in brain drug development, NeuroRx 2 (2005) 3–14.
[18] L.B. Li, J.L. Zhang, Y.X. Wang, H.L. Wei, G.T. Liu, Establishment of a HPLC method for preclinical pharmacokinetic study of the novel anti-Parkinson's disease candidate drug FLZ in rats, Biomed. Chromatogr. 22 (2008) 867–872.
[19] G. Paxinos, C. Watson, The Mouse Brain in Stereotaxic Coordinates, third edition, People's Medical Publishing House, Beijing, 2005.
[20] E.A. Brown, R. Griffiths, C.A. Harvey, D.A. Owen, Pharmacological studies with SK&F 93944 (temelastine), a novel histamine H1-receptor antagonist with negligible ability to penetrate the central nervous system, Br. J. Pharmacol. 87 (1986) 569–578.
[21] S. Raje, J. Cao, A.H. Newman, H. Gao, N.D. Eddington, Evaluation of the blood–brain barrier transport, population pharmacokinetics, and brain distribution of benztropine analogs and cocaine using in vitro and in vivo techniques, J. Pharmacol. Exp. Ther. 307 (2003) 801–808.
[22] J.P. Covy, B.I. Giasson, Alpha-synuclein, leucine-rich repeat kinase-2, and manganese in the pathogenesis of parkinson disease, Neurotoxicology (2011).
[23] W.M. Panneton, V.B. Kumar, Q. Gan, W.J. Burke, J.E. Galvin, The neurotoxicity of DOPAL: behavioral and stereological evidence for its role in Parkinson disease pathogenesis, PLoS One 5 (2010) e15251.
[24] A.H. Dantzig, R.L. Shepard, K.L. Law, L. Tabas, S. Pratt, J.S. Gillespie, S.N. Binkley, M.T. Kuhfeld, J.J. Starling, S.A. Wrighton, Selectivity of the multidrug resistance modulator, LY335979, for P-glycoprotein and effect on cytochrome P-450 activities, J. Pharmacol. Exp. Ther. 290 (1999) 854–862.
[25] R.L. Shepard, J. Cao, J.J. Starling, A.H. Dantzig, Modulation of P-glycoprotein but not MRP1- or BCRP-mediated drug resistance by LY335979, Int. J. Cancer 103 (2003) 121–125.
[26] J.D. Allen, A. van Loevezijn, J.M. Lakhai, M. van der Valk, O. van Tellingen, G. Reid, J.H. Schellens, G.J. Koomen, A.H. Schinkel, Potent and specific inhibition of the breast cancer resistance protein multidrug transporter in vitro and in mouse intestine by a novel analogue of fumitremorgin C, Mol. Cancer. Ther. 1 (2002) 417–425.
[27] Y. Chen, S. Agarwal, N.M. Shaik, C. Chen, Z. Yang, W.F. Elmquist, P-glycoprotein and breast cancer resistance protein influence brain distribution of dasatinib, J. Pharmacol. Exp. Ther. 330 (2009) 956–963.
[28] N.A. de Vries, J. Zhao, E. Kroon, T. Buckle, J.H. Beijnen, O. van Tellingen, P-glycoprotein and breast cancer resistance protein: two dominant transporters working together in limiting the brain penetration of topotecan, Clin. Cancer Res. 13 (2007) 6440–6449.

Journal of Pharmaceutical and Biomedical Analysis 66 (2012) 240–251

Contents lists available at SciVerse ScienceDirect

Journal of Pharmaceutical and Biomedical Analysis

journal homepage: www.elsevier.com/locate/jpba

Comparative studies on the interactions of honokiol and magnolol with human serum albumin

Zhengjun Cheng

Chemical Synthesis and Pollution Control Key Laboratory of Sichuan Province, China West Normal University, Nanchong 637002, China

ARTICLE INFO

Article history:
Received 7 December 2011
Received in revised form 6 March 2012
Accepted 7 March 2012
Available online 15 March 2012

Keywords:
Human serum albumin
Honokiol
Magnolol
Fluorescence spectroscopy
Binding constants

ABSTRACT

In this study, the binding modes of honokiol (HK) and magnolol (MG) with human serum albumin (HSA) have been established under imitated physiological condition, which was very important to understand the pharmacokinetics and toxicity of HK or MG. The experimental results proved that the fluorescence of HSA was quenched by HK or MG through a static quenching procedure. The binding constants of HK–HSA and MG–HSA complexes were 5.304 and 263.755 $\times$ 10^4 L mol^{-1} at 298 K, respectively. The binding process was a spontaneous molecular interaction procedure, in which the hydrophobic interaction played a major role in the formation of the HK–HSA complex, whereas, the binding interaction between MG and HSA might involve the hydrophobic interaction strongly and electrostatic interaction. In addition, the effect of HK/MG on the secondary structure of HSA was analyzed using CD, UV–vis absorption, Fourier transform infrared (FT-IR), synchronous fluorescence and three-dimensional fluorescence spectra. According to Förster no-radiation energy transfer theory, the binding distance of HSA to HK or MG was calculated to be 1.842 or 1.238 nm. Besides, the effects of common ions on the binding constants of HSA–HK/MG systems were also discussed.

© 2012 Elsevier B.V. All rights reserved.

1. Introduction

Of all the proteins, human serum albumin (HSA) is the most abundant protein in plasma and constitutes approximately half of the proteins found in human blood [1], which is composed of a single polypeptide chain of 585 amino acid residues, with three α-helical domains (I, II and III), each containing two sub-domains (A and B) stabilized by seventeen disulfide bridges [2]. Specifically, aromatic and heterocyclic ligands were found to bind within two hydrophobic pockets in sub-domains IIA and IIIA, known as Sudlow's Site I and Site II, respectively [3]. The single tryptophan residue (Trp214) on HSA is located in Sudlow's Site I, which is a good binding site to drugs for measuring the drug-binding affinity [4]. The affinities of drugs to HSA would influence the concentrations of drugs at the binding sites and the duration of effectual drugs and consequently contribute to their magnitude of biological actions in vivo. In general, the weak binding between drug and HSA leads to a poor distribution, while the strong binding makes for a good distribution or decreasing the concentration of free drug in plasma. Therefore, pharmaceutical corporations need standardized screens for protein binding in a new drug design and for fixing dose limits. In recent years, some research groups [5–11] have reported the interactions of different drugs with HSA by different techniques, such as, spectroscopic (FTIR, CD, fluorescence, synchronous fluorescence, UV–vis absorption and 3D fluorescence), density functional theory (DFT) calculations, molecular docking and NMR spectroscopy.

Honokiol (HK) and magnolol (MG) (Scheme 1), the isomers of hydroxylated biphenolic compounds ($C_{18}H_{18}O_2$, MW = 266.33), are major bioactive components in *Magnolia officinalis reed* those have been used in traditional Chinese medicine for thousands of years [12]. They possess some special abilities to inhibit the glutamate-induced cell damage [13]; the formation of eicosanoids (PGD_2, PGE_2, LTC_4, LTB_4 and TXB_2), inflammatory pain [14]; endotoxin shock, protein kinase, NF-kB pathway, NADPH oxidase, bacteria in mouth, tumor promotion, activating retinoid receptor, detoxifying enzymes, glutathione-S-transferase, antioxidative enzymes [15]. HK and MG also regulate the release of neurotransmitters, such as acetylcholine and 5-hydroxytryptamine [16], and induce Ca^{2+} mobilization in rat cortical neurons and human neuroblastoma SH-SY5Y cells [16], and have neurotrophic properties, such as promotion of neurite outgrowth and neuronal survival under serum-deprived conditions in cultured rat cortical neurons [17], and stimulate glucose uptake in insulin-sensitive and insulin-resistant murine and human adipocytes using the insulin signaling pathway [18], and prevent age-related learning and memory impairment by preserving cholinergic neurons in the forebrain [19]. Besides, MG reduced fasting blood glucose and plasma insulin levels in Goto-Kakizaki diabetic rats and the glucose uptake in 3T3-L1 adipocytes [18], and inhibited cell growth and HER2-mediated tumor metastasis in human HER2-over-expressing

E-mail address: ncczj1112@126.com

0731-7085/$ – see front matter © 2012 Elsevier B.V. All rights reserved.
doi:10.1016/j.jpba.2012.03.010

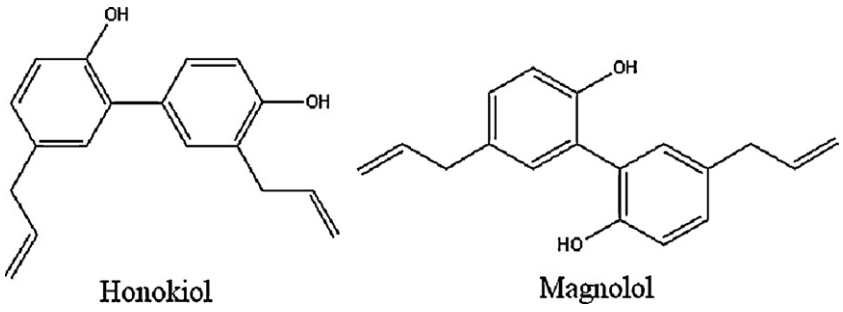

Scheme 1. Chemical structure of Honokiol and magnolol.

ovarian cancer cells [20]. HK have various biological effects [21] including the inhibition of estrogen receptor (ER)-negative MDA-MB-231 human breast cancer cells, alleviation of inflammatory arthritis, neuroprotection against oxidative stress, growth restraint of microbes, and suppression of metastasis, angiogenesis, invasion and proliferation in a wide range of cancer cell types. Lately, Wang et al. [22] reported that PEGylated liposomal HK improved the solubility, increased the drug concentration in plasma, and withstood the clearance. Besides, the ability to bind to human plasma protein of HK was studied, and the percent of protein bound of HK in human plasma was between 60% and 65%. However, in order to understand detailedly their pharmacological importance, the interactions of HSA with HK/MG have been investigated because the binding phenomena can provide the basic information of pharmacological actions, bio-information, bio-distribution, etc.

In this study, we have applied fluorescence, synchronous fluorescence, three dimensional fluorescence, UV–vis absorption, CD and FT-IR spectra techniques to explore the pharmacological effects of HK/MG on HSA under the simulative physiological conditions. The fluorescence quenching mechanisms, the number of the binding sites and the binding forces were investigated for the HK–HSA and MG–HSA systems. Besides, the binding sites on HSA by HK and MG were discussed using the site marker competitive experiments, and the effects of common ions on the binding constants of the HK–HSA and MG–HSA systems were also examined.

2. Materials and methods

2.1. Materials

Human Serum Albumin (HSA, 96% purity) purchased from Sigma (St. Louis, MO), was used without further purification and its molecular weight was assumed to be 66,000. All HSA solutions were prepared in the pH 7.4 buffer solution (0.10 mol L^{-1} Tris base, 0.10 mol L^{-1} HCl, and the pH was adjusted to 7.4 by adding 0.1 mol L^{-1} NaOH), and HSA stock solution was kept in the dark at 4 °C. The pH measurements were carried out on a PHS-3 C digital pH-meter (Jiangsu, Jiangfen Electroanalytical Instrument Co., Ltd, China) with a combined glass electrode. Honokiol (HK) and magnolol (MG) are of analytical grade and purchased from solid dose of traditional Chinese Medicine National Engineering Research and Manufacturing Center (Jiangxi, China). Other chemicals were of analytical reagent grade and used without further purification, and doubly distilled water was used throughout the experiment.

2.2. Fluorescence quenching measurements

All fluorescence spectra were performed on a Cary Eclipse fluorescence spectrofluorometer (Varian, USA) equipped with a xenon lamp source and 1.0 cm quartz cell and a thermostat bath.

Fluorometric titration experiments: 3.0 mL solution containing appropriate concentration of HSA was titrated by successive additions of 20% ethanol HK/MG solution with the concentration of 6.0×10^{-4} mol L^{-1} (to give a final concentration of $(1.0–8.0) \times 10^{-6}$ mol L^{-1} for HK, $(1.6–16.0) \times 10^{-6}$ mol L^{-1} for MG). The titrations were done manually using the microsyringe, and their fluorescence intensities are recorded, respectively. Since the stock solution of HK or MG was prepared in 20% ethanol, the quenching effect of 20% ethanol was also evaluated. The results showed that the effect of 20% ethanol on the interaction of HK/MG with HSA could be negligible for the amount used in our experiments. The excitation and emission slit widths were both set at 5 nm. An excitation wavelength of 280 nm was chosen and the temperature of samples was kept by recycle water during the experiment. All experiments were measured at four temperatures (293, 298, 304 and 310 K).

Three-dimensional fluorescence spectra were measured under the following conditions: the initial excitation wavelength was set at 200 nm with increment of 2 nm, and the emission wavelength was recorded from 200 to 500 nm at a scanning rate 24,000 nm/min.

2.3. Binding studies in the presence of site probes

The displacement experiments were performed in the presence of three site markers (ibuprofen, phenylbutazone and digitoxin) using the fluorescence titration methods. It is kept the concentration of HSA and the site probe (5.0 μM each) and varied the concentrations of the drug. An excitation wavelength of 280 nm was selected and the fluorescence spectra were recorded in the range of 250–500 nm. The binding constants of drug–protein–probe were evaluated by the Stern–Volmer equation.

2.4. UV–vis absorption studies

The UV–vis absorption spectra were collected at room temperature on a UV-3600 spectrophotometer (Shimadzu, Japan) in 1.0 cm quartz cells and an s-1700 thermoelectric single cell holder. And the UV–vis absorption spectra of HSA in the presence and absence of HK/MG were recorded in the range of 240–500 nm. The concentration of HSA was fixed at 5.0 μM while that of HK/MG was changed from 0 to 24.0 μM.

2.5. FT-IR measurements

FT-IR spectra were carried out on a Nicolet-6700 FT-IR spectrometer via the attenuated total reflection (ATR) at a resolution of 4 cm^{-1} and 64 scans at 298 K. The FT-IR spectra of HSA (0.10 mM) in the presence and absence of HK/MG were recorded in the range of 4000–400 cm^{-1}. The molar ratios of HSA to the drug (HK or MG) were maintained at 1:1 and 1:3, respectively. The corresponding absorbance contributions of the buffer and free HK/MG solutions were recorded and digitally subtracted with the same instrumental parameters.

2.6. CD measurements

Circular dichroism (CD) measurements were performed on a Jasco-810 automatic recording spectropolarimeter (Japan) using a 0.1 cm cell at room temperature. The CD spectra were recorded in the range of 190–260 nm and the scan rate were 100 nm/min with a response time of 4 s. CD determinations of pure HSA and HSA–HK/MG complexes were carried out using the same solutions of HK/MG at a corresponding concentration as the reference. The results were expressed as ellipticity (mdeg), which was obtained directly from the instrument. The α-helix contents of free and combined HSA were calculated from the following two equations [23]:

$$\mathrm{MRE} = \frac{\text{Observed CD } (\mathrm{m}deg)}{C_\mathrm{p} n l \times 10} \quad (1)$$

$$\alpha\text{-helix}\,(\%) = \frac{(-\mathrm{MRE}_{208} - 4000) \times 100}{33000 - 4000} \quad (2)$$

where C_p is the molar concentration of protein, n is the number of amino acid residues, l is the path length and MRE_{208} is the observed MRE value at 208 nm.

3. Results and discussion

3.1. Fluorescence quenching of HSA by HK or MG

The fluorescence spectra of HSA in the presence of different concentrations of HK/MG were shown in Fig. 1. With gradual increase in the MG concentration, the fluorescence intensity of HSA was found to be decreased accompanying the simultaneous enhancement in the fluorescence of MG (λ_{emi} = 402 nm). It could be seen from Fig. 1(A) and (B) that the intensity of the tryptophan fluorescence (λ_{emi} = 338 nm) was specifically quenched with a slight blue or red shift (from 338 to 332 nm for the HK–HSA complex, from 338 to 342 nm for the MG–HSA complex) in their maxima emission wavelength, implying that the microenvironment around HSA changed after the addition of HK or MG [24,25]. To make the trends more clear, the normalized fluorescence F/F_0 of the spectra was plotted in inset of Fig. 1, where F and F_0 were the fluorescence intensities of HSA before and after the addition of HK/MG. As shown in inset of Fig. 1, the extinction of HSA tryptophan by MG decreased more rapidly than that of HK. At the concentration of 7.0 μM, HK was found to cause 42.1% quenching of HSA, while MG quenched 46.2% for HSA. From the slopes of the curves, it could be concluded that the binding affinity of MG to HSA was much stronger than that of HK.

Fluorescence quenching can occur by different mechanisms, which are usually classified into dynamic and static quenching. In order to clarify the quenching mechanism of HK–HSA and MG–HSA complexes, their fluorescence spectra data were analyzed using the Stern–Volmer equation [26]:

$$\frac{F_0}{F} = 1 + K_{sv}[\mathrm{Q}] = 1 + K_q \tau_0 [\mathrm{Q}] \quad (3)$$

where F_0 and F denote the fluorescence intensities in the absence and presence of quencher, respectively; K_{sv} is Stern–Volmer quenching constant; K_q is the biomolecule quenching rate constant; [Q] is the concentration of quencher (HK or MG); τ_0 is the average lifetime of protein without the quencher, and the fluorescence lifetime of the biopolymer is 10^{-8} s [27]. In order to confirm the quenching mechanism, we assumed that the fluorescence quenching of HK–HSA and MG–HSA systems was a dynamic quenching process. Such, the fluorescence intensities of two systems analyzed by plotting F_0/F versus [Q] at four temperatures (293, 298, 304 and 310 K) were shown in Fig. 2, and the calculated K_{sv} and K_q values were listed in Table 1. For the dynamic quenching, the maximum

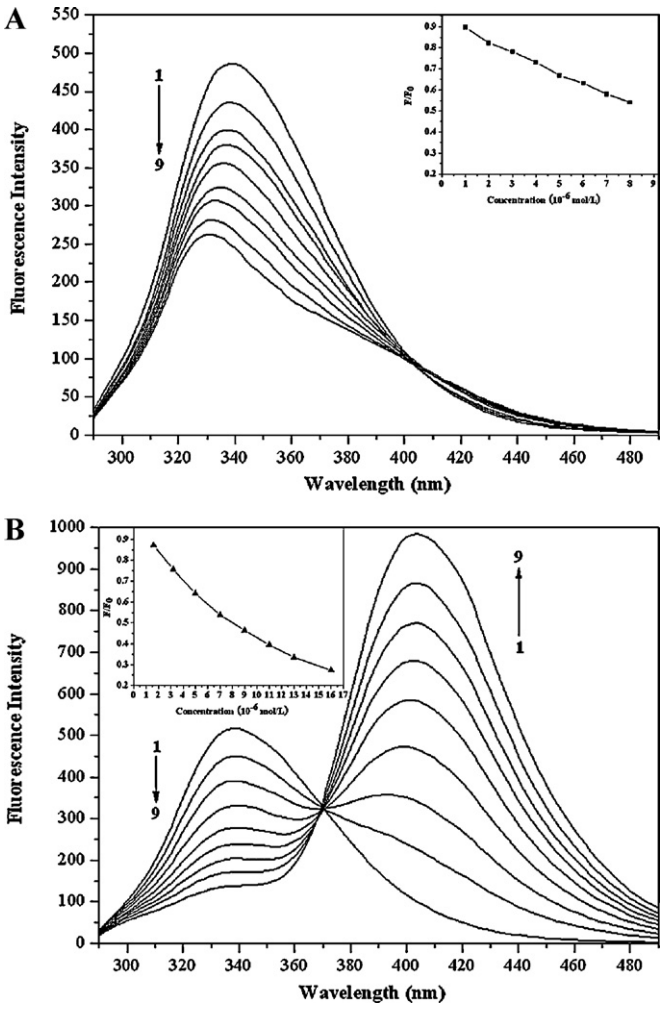

Fig. 1. Effect of (A) HK and (B) MG on the fluorescence intensity of HSA. Inset shows normalized fluorescence intensities of HK (■) and MG (▲) with different HSA concentrations. Conditions: T = 298 K, λ_{ex} = 280 nm; buffer, Tris–HCl; pH 7.4; c(HSA) = 5.0 μM; c(HK) 1–9: 0, 1.0, 2.0, 3.0, 4.0, 5.0, 6.0, 7.0 and 8.0 μM; c(MG) 1–9: 0, 1.6, 3.2, 5.0, 7.0, 9.0, 11.0, 13.0 and 16.0 μM, respectively.

scattering collision quenching constant of various quenchers with the biopolymers is 2×10^{10} L mol^{-1} s^{-1} [28]. Besides, the dynamic and static quenching also can be distinguished by the values of K_{sv}, that is to say, it is decreased with an increasing temperature for the static quenching and the reverse result will be observed for the dynamic quenching [24]. As shown in Table 1, the values of K_{sv} decreased with rising temperature, and the quenching rate constant K_q value was much greater than 2×10^{10} L mol^{-1} s^{-1}, indicating that the quenching mechanism of the HK–HSA and MG–HSA binding reactions was initiated by the complex formation rather than by the dynamic collision.

Besides, fluorescence quenching mechanisms can be also confirmed by the analysis of Stern–Volmer plots at different concentrations of HSA. The value of K_{sv} is expected to depend on the concentration of HSA in a static quenching process, whereas its value does not change at any concentration of HSA in only a dynamic process [29]. The plot of F_0/F versus [Q] yields K_{sv} as the slope (Fig. 3). The corresponding values of K_{sv}, R and SD for HSA–HK/MG systems were shown in Table 2. It could be seen that the values of K_{sv} decreased with increasing concentrations of HSA for two systems. The results reconfirmed that the quenching of HSA–HK and HSA–MG systems was initiated by the static quenching.

Table 1
The parameters of Stern–Volmer plots for the quenching of HSA by HK or MG at different temperatures.

$T(K)$	HSA–HK				HSA–MG			
	K_{sv} ($\times 10^{-5}$ M^{-1})	K_q ($\times 10^{-13}$ M^{-1} s^{-1})	R	SD	K_{sv} ($\times 10^{-5}$ M^{-1})	K_q ($\times 10^{-13}$ M^{-1} s^{-1})	R	SD
293	1.070	1.070	0.9921	0.0359	1.855	1.855	0.9935	0.1139
298	1.039	1.039	0.9948	0.0280	1.737	1.737	0.9920	0.1186
304	0.993	0.993	0.9921	0.0333	1.629	1.620	0.9911	0.1177
310	0.904	0.904	0.9940	0.0262	1.280	1.280	0.9955	0.0651

R is the correlation coefficient for the Stern–Volmer plots.

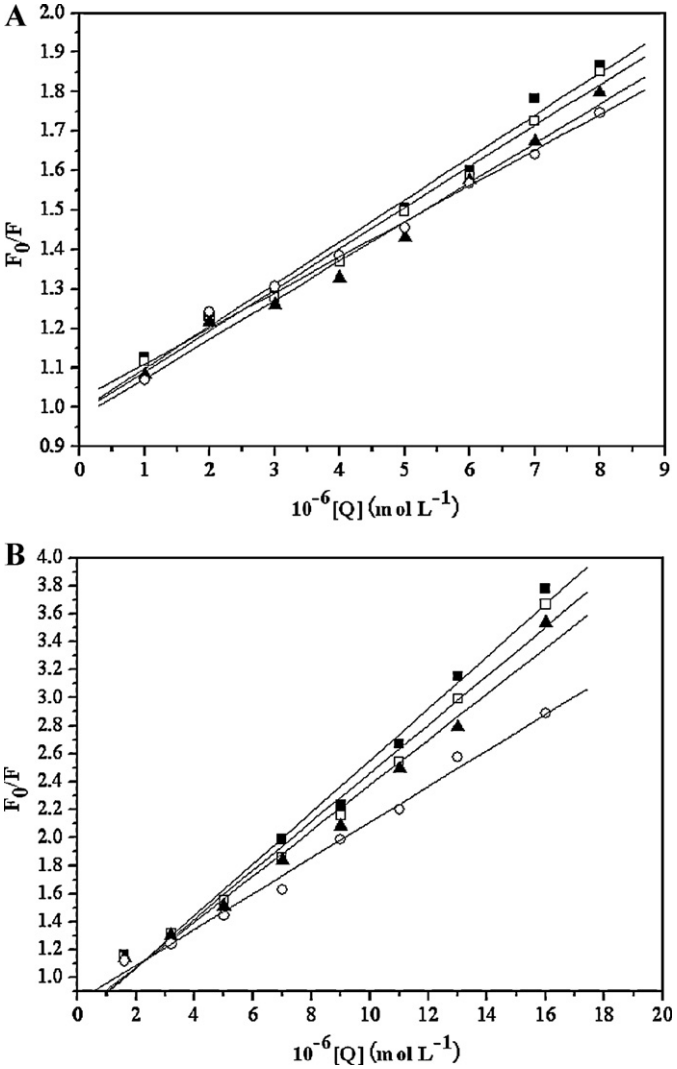

Fig. 2. Stern–Volmer plots for HSA with HK (A) and MG (B) at (■) 293 K, (□) 298 K, (▲) 304 K, and (O) 310 K.

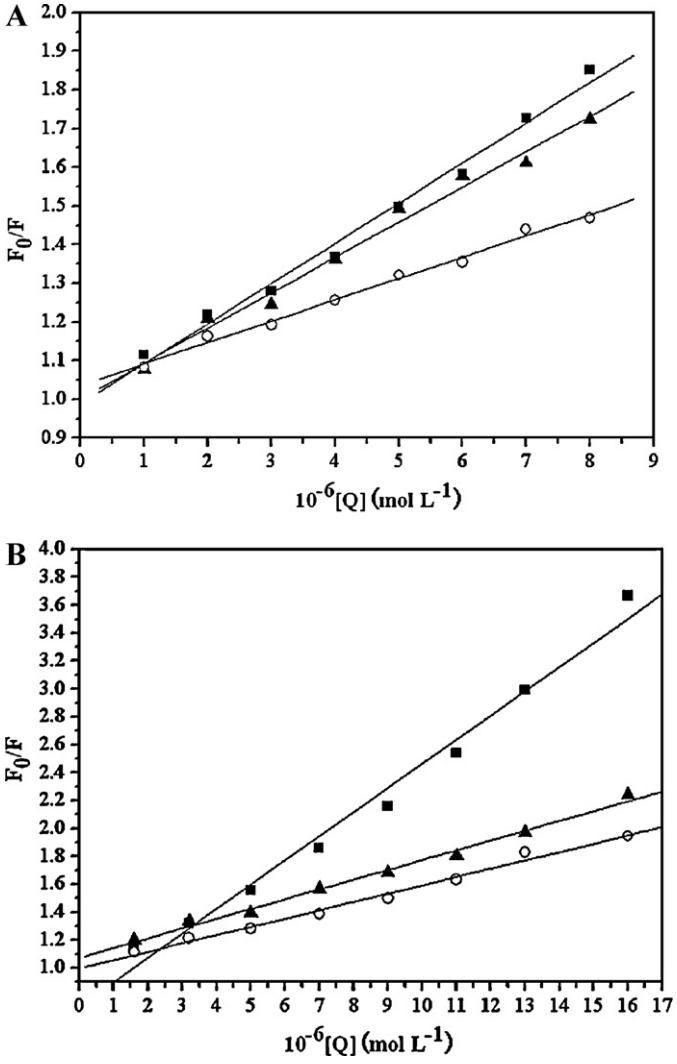

Fig. 3. Stern–Volmer plots for HK–HSA (A) and MG–HSA (B) systems at different concentrations of HSA at 298 K: (■) [HSA] = 5.0 μM, (▲) [HSA] = 6.0 μM, and (O) [HSA] = 7.0 μM.

Table 2
The parameters of Stern–Volmer plots for the HSA–HK/MG system at pH 7.40.

$T(K)$	HSA–HK				HSA–MG			
	[HSA] ($\times 10^6$ M)	K_{sv} ($\times 10^{-4}$ M^{-1})	R	SD	[HSA] ($\times 10^6$ M)	K_{sv} ($\times 10^{-4}$ M^{-1})	R	SD
298	5.0	1.039	0.9948	0.0280	5.0	1.737	0.9920	0.1186
	6.0	0.913	0.9937	0.0273	6.0	0.699	0.9962	0.0330
	7.0	0.552	0.9959	0.0132	7.0	0.595	0.9944	0.0340

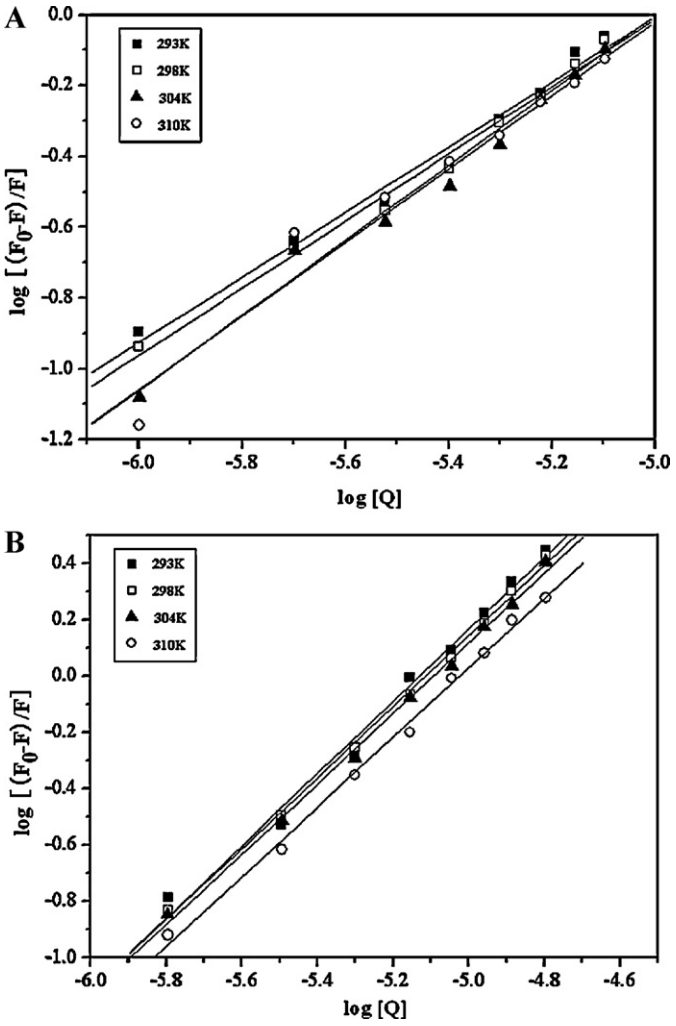

Fig. 4. Plots of $\log[(F_0 - F)/F]$ vs. log[Q] for the HSA–HK (A) and HSA–MG (B) systems at four different temperatures; c_{HSA} = 5.0 μM; pH = 7.4.

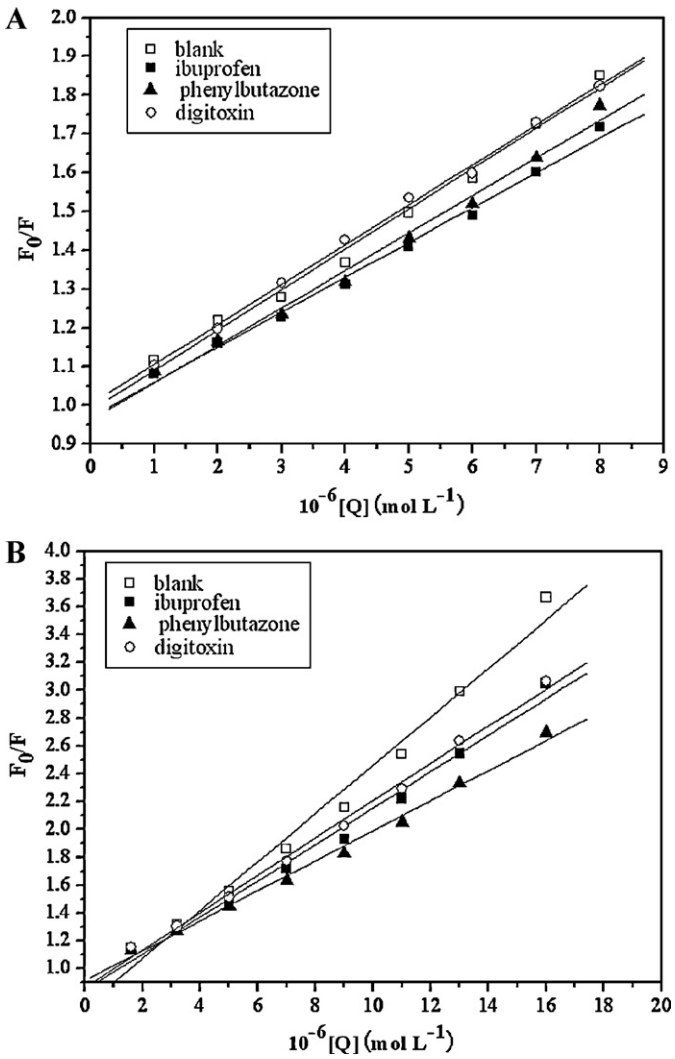

Fig. 5. Stern–Volmer plots for the HSA–HK (A) and HSA–MG (B) systems in the absence and presence of the site markers (T = 298 K, pH = 7.4).

3.2. Binding constant and binding sites of HSA with HK or MG

For the quenching process, under the assumption that HSA has the same independent binding sites, the following equation was employed for the determination of the binding constants (K) and the number of binding sites (n) [30]:

$$\log\left(\frac{F_0 - F}{F}\right) = \log\ K + n\ \log[\mathrm{Q}] \quad (4)$$

where F_0, F, and [Q] are the same as in Eq. (3), K is binding constant of HSA with HK/MG and n is the number of binding sites per albumin molecule. The binding constants and the number of binding sites could be calculated by plotting $\log[(F_0 - F)/F]$ versus log[Q] as shown in Fig. 4. From the slope of the linear fitting plots, the number of binding sites n, and the intercept ($\log K$), the binding constants K were calculated and listed in Table 3. It could be inferred from the values of n that there was about one independent class of the binding sites on HSA for HK/MG during their interaction. Hence, HK or MG most likely bound to the hydrophobic pocket located in subdomain IIA or IIIA [31]. The results also indicated that the binding force of MG to HSA was stronger than that of the HK–HSA complex.

3.3. Identification of binding sites on HSA

In order to further identify HK and MG binding sites on HSA, the site marker competitive experiments were conducted by using the drugs specifically bound to a know site or region on HSA. The first crystallographic analyzes of HSA [32] revealed that it comprised three structurally homologous domains (I, II, III): I (residues 1–195), II (196–383), III (384–585), each of which was composed of two subdomains (A and B) and was stabilized by 17 disulfide bonds and 1 free thiol at Cys34. The binding sites on HSA for endogenous and exogenous ligands may be in these domains, and the principal regions of the binding sites of serum albumins are located in the hydrophobic cavities in subdomains IIA and IIIA. Many ligands could bind specifically to serum albumins, such as, phenylbutazone and warfarin for site I, ibuprofen and flufenamic acid for site II, and digitoxin for site III [33]. In order to ascertain the binding sites on HSA for HK or MG, the displacement experiments have been performed using the site probes (for example, phenylbutazone, ibuprofen and digitoxin). The emission spectra of ternary mixtures of HK/MG, HSA and the site probe were recorded. That is to say, HK or MG was gradually added to the solution of HSA with the site marker held in equimolar concentrations (5.0×10^{-6} mol L^{-1}). Thus, the fluorescence quenching data were analyzed using the Stern–Volmer equation (Fig. 5), and their binding constants and corresponding R values were shown in Table 4. Obviously, the binding constant of MG–HSA with phenylbutazone (PB) was 62.06% of that without PB, while the binding constants of MG–HSA with and without ibuprofen (IB) or digitoxin (DIG) had only a

Table 3
The binding constants K, the number of binding sites n, and the thermodynamic parameters of HSA–HK and HSA–MG systems at different temperatures.

System	T (K)	K ($\times 10^{-4}$ L mol^{-1})	n	R^a	ΔG° (kJ mol^{-1})	ΔH° (kJ mol^{-1})	ΔS° (J mol^{-1} K^{-1})	R^b
	293	3.911	0.92	0.9916	−25.639			
	298	5.304	0.95	0.9946	−27.390			
HSA–HK						76.921	350.036	0.9750
	304	14.494	1.04	0.9915	−29.490			
	310	19.258	1.06	0.9808	−31.590			
	293	362.160	1.28	0.9946	−36.746			
	298	263.755	1.26	0.9988	−36.764			
HSA–MG						−35.688	3.612	0.9909
	304	221.462	1.25	0.9984	−36.786			
	310	156.027	1.23	0.9978	−36.807			

[a]The correlation coefficient for K values.
[b]The correlation coefficient for the van't Hoff plot.

Table 4
The effects of the site probe on the binding constants of HSA to HK/MG.

	Blank		With IB		With PB		With DIG	
	K_{sv} ($\times 10^{-5}$ M^{-1})	R	K_{sv} ($\times 10^{-5}$ M^{-1})	R	K_{sv} ($\times 10^{-5}$ M^{-1})	R	K_{sv} ($\times 10^{-5}$ M^{-1})	R
HSA–HK	1.039	0.9948	0.901	0.9965	0.967	0.9946	1.03	0.9988
HSA–MG	1.737	0.9920	1.309	0.9938	1.078	0.9969	1.338	0.9975

small difference. Besides, the binding constant of HK–HSA with IB was less than those of without IB or with PB or with DIG. These results revealed that PB displaced MG (or IB displaced HK) from the binding site while IB and DIG (or PB and DIG) had a little effect on the binding constant between MG and HSA (or between HK and HSA). Hence, the binding of MG to HSA mainly located within site I (subdomain IIA), and the binding between HK and HSA mainly located within site II (subdomain IIIA).

3.4. Thermodynamic parameters and binding forces

The active force between the drug and biological macromolecule may mainly include hydrogen bond, van der waals force, electrostatic force, and hydrophobic interaction force. The thermodynamic parameters, such as, enthalpy change (ΔH°), entropy changes (ΔS°), and free energy change (ΔG°) are important to propose the binding mode. For this reason, the binding studies were carried out at four temperatures (293, 298, 304 and 310 K) and evaluated by the van't Hoff equation [34]:

$$\ln K = -\frac{\Delta H^\circ}{RT} + \frac{\Delta S^\circ}{R} \quad (5)$$

where R is the gas constant, T is the experimental temperature, and K is the binding constant at the corresponding T. At these temperatures (293, 298, 304 and 310 K), HSA does not undergo any structural degradation. The $\ln K$ versus $1/T$ plot enabled the determination of the ΔH° and ΔS° values (Fig. 6). If the temperature changes little, the ΔH° value is regarded as a constant. Thus, the value of ΔG° can be calculated using the equation given below [34]:

$$\Delta G^\circ = \Delta H^\circ - T\,\Delta S^\circ = -RT\,\ln K \quad (6)$$

The values of ΔH°, ΔS° and ΔG° were summarized in Table 3. The negative values of ΔG° demonstrated the easy formation of the HK–HSA or MG–HSA complex and it was an exothermic reaction. The ΔH° and ΔS° values of the binding reaction between MG and HSA were found to be −35.688 kJ mol^{-1} and 3.612 J mol^{-1} K^{-1}, respectively. Thus, the formation of the MG–HSA complex was an exothermic reaction accompanied by a positive ΔS° value. From the point of view of water structure, a positive ΔS° value is frequently taken as a typical evidence for the hydrophobic interaction. Furthermore, specific electrostatic interaction between ionic species in aqueous solution are characterized by the negative ΔH° and positive ΔS° values, while the positive ΔH° and ΔS° values arise from typical hydrophobic interaction [35]. Obviously, it is not possible to account for the thermodynamic parameters of MG–HSA complex based on a single intermolecular force model. Therefore, the binding interaction of MG to HSA might involve the hydrophobic interaction strongly as evidenced by the positive ΔS° value and the electrostatic interaction could also not be excluded. Besides, the values of ΔH° and ΔS° for the binding reaction between HK and HSA were found to be 76.921 kJ mol^{-1} and 350.036 J mol^{-1} K^{-1}. The results indicated that the hydrophobic interaction played a major role in the formation of the HSA–HK complex. Obviously, the above results were in good agreement with the results coming from the identification of binding sites on HSA.

3.5. Energy transfer between HK/MG and HSA

The Förster resonance energy transfer in biochemistry is important because it can evaluate the distance between drugs and tryptophan residues responsible for the natural intrinsic fluorescence of protein. The binding distance (r) between a protein residue (donor) and a bound drug molecule (acceptor) can be calculated by Förster's non-radiative energy transfer theory [36]. The efficiency

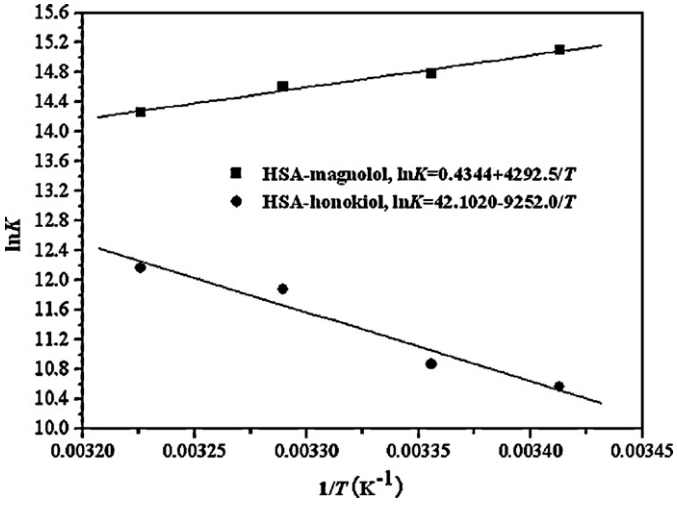

Fig. 6. van't Hoff plots for the HSA–HK and HSA–MG systems in Tris–HCl buffer, pH = 7.4.

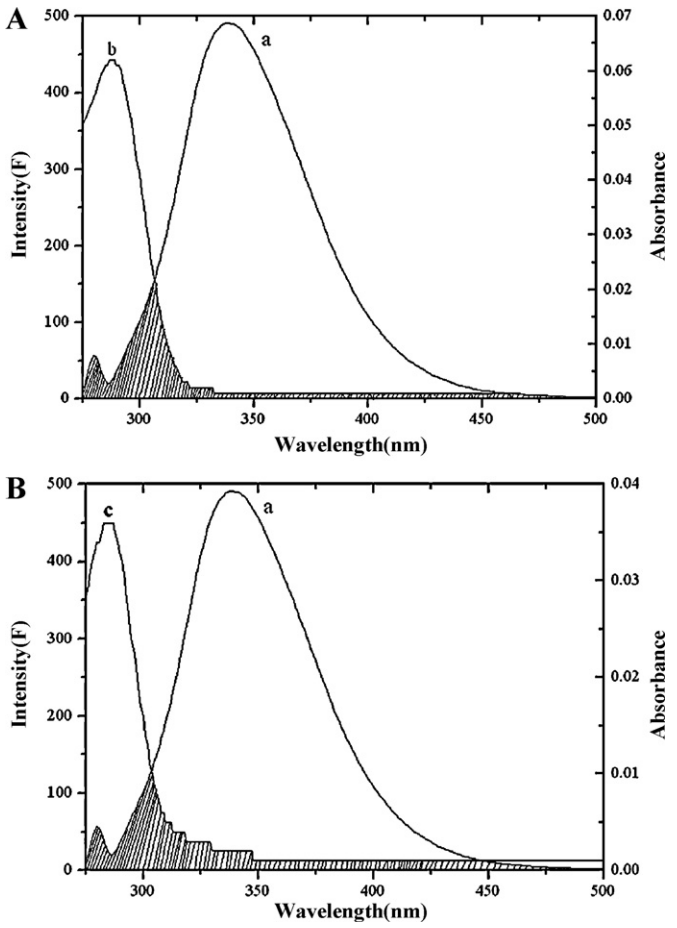

Fig. 7. The spectral overlaps of UV–vis absorption spectra of HK (A) and MG (B) with the fluorescence emission spectrum of HSA. (a) The fluorescence emission spectrum of HSA; (b) the UV–vis absorption spectrum of HK; (c) the UV–vis absorption spectrum of MG. c(HSA) = 5.0 μM, c(HK) = 6.0 μM, c(MG) = 13.0 μM, T = 298 K.

of energy transfer (E) is related to the distance (R_0) between donor and acceptor by:

$$E = 1 - \frac{F}{F_0} = \frac{R_0^6}{R_0^6 + r^6}. \quad (7)$$

In Eq. (7), r represents the distance between the donor and acceptor, and R_0 is the critical distance when the transfer efficiency equals to 50%. The value of R_0 is calculated using the equation [8]

$$R_0^6 = 8.8 \times 10^{-25} k^2 n^{-4} \Phi J \quad (8)$$

where k^2 is the orientation factor related to the geometry of the donor–acceptor dipole, n is the refractive index of medium, Φ is the fluorescence quantum yield in the absence of energy transfer, and J is the overlap between the fluorescence spectrum of the donor and the absorption spectrum of the acceptor, J is given by [9]

$$J = \frac{\int_0^\infty F(\lambda)\varepsilon(\lambda)\lambda^4 \, d\lambda}{\int_0^\infty F(\lambda)\, d\lambda} \quad (9)$$

where $F(\lambda)$ is the fluorescence intensity of the donor at wavelength λ, $\varepsilon(\lambda)$ is the molar absorption coefficient of the acceptor at wavelength λ. The value of J can be evaluated by integrating the overlap (Fig. 7) of the absorption spectrum of HK/MG with the fluorescence emission spectrum of HSA; R_0 can be evaluated from Eq. (8) using $k^2 = 2/3$, $n = 1.336$, $\Phi = 0.118$ for HSA [37]; r is evaluated by Eq. (7). All the results were shown in Table 5. The values of r indicated that the donor and acceptor were close to each other and hence had strong binding interactions between them [38]. Further, the observed donor–acceptor distance was less than 8 nm, indicating again that the static quenching interaction occurred between HSA and HK/MG.

Table 5
The calculated J, R_0, E and r values of HK–HSA and MG–HSA systems.

System	J (cm^3 L mol^{-1})	E (%)	R_0 (nm)	r (nm)
HK–HSA	8.342×10^{-16}	36.9	1.667	1.842
MG–HSA	2.790×10^{-16}	66.6	1.389	1.238

3.6. Conformational investigations

When drugs interacted with HSA, the intramolecular forces that responsible for maintaining the secondary or tertiary structures of protein can be affected, which may further result in a conformational change of protein. In order to investigate the structural change of HSA induced by HK or MG, UV–vis absorption, synchronous fluorescence, three-dimensional fluorescence, FTIR and CD spectra of free HSA and their complex were determined.

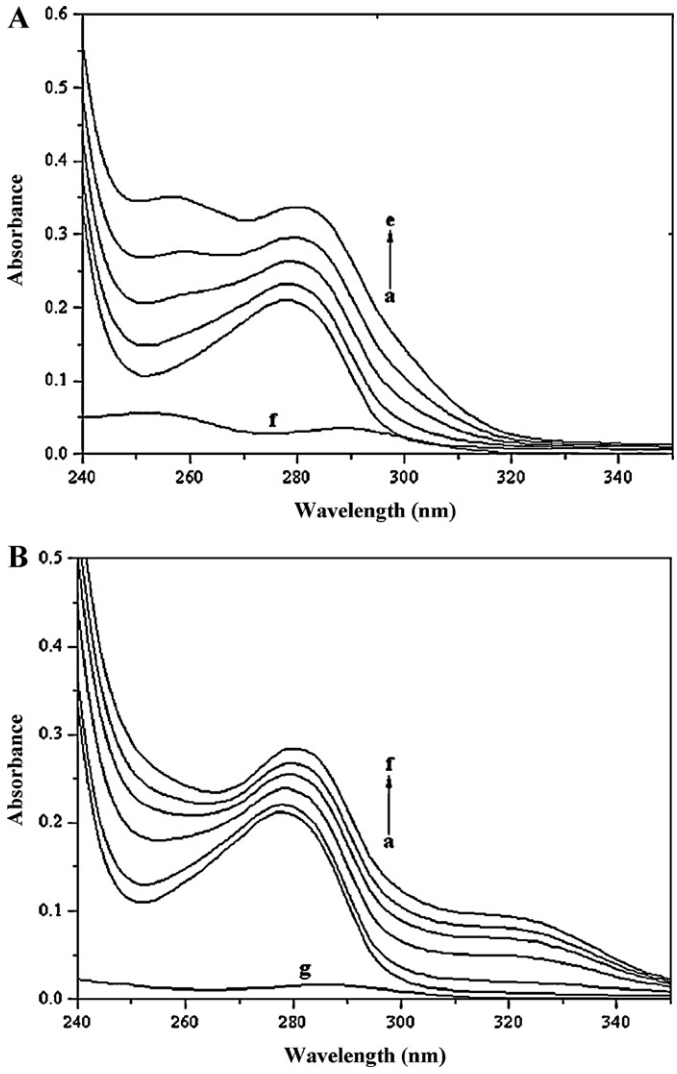

Fig. 8. The UV–vis spectra of HSA in the presence of different concentrations of HK (A) or MG (B); c(HSA) = 5.0×10^{-6} mol L^{-1}; HK/(10^{-6} mol L^{-1}) a–e: 0, 4.0, 10.0, 16.0, 24.0, and MG/(10^{-6} mol L^{-1}) a–f: 0, 4.0, 10.0, 16.0, 20.0, 24.0, respectively; the concentrations of 10.0 μM (f) and 10.0 μM (g) are used for HK and MG only; pH 7.4; T = 298 K.

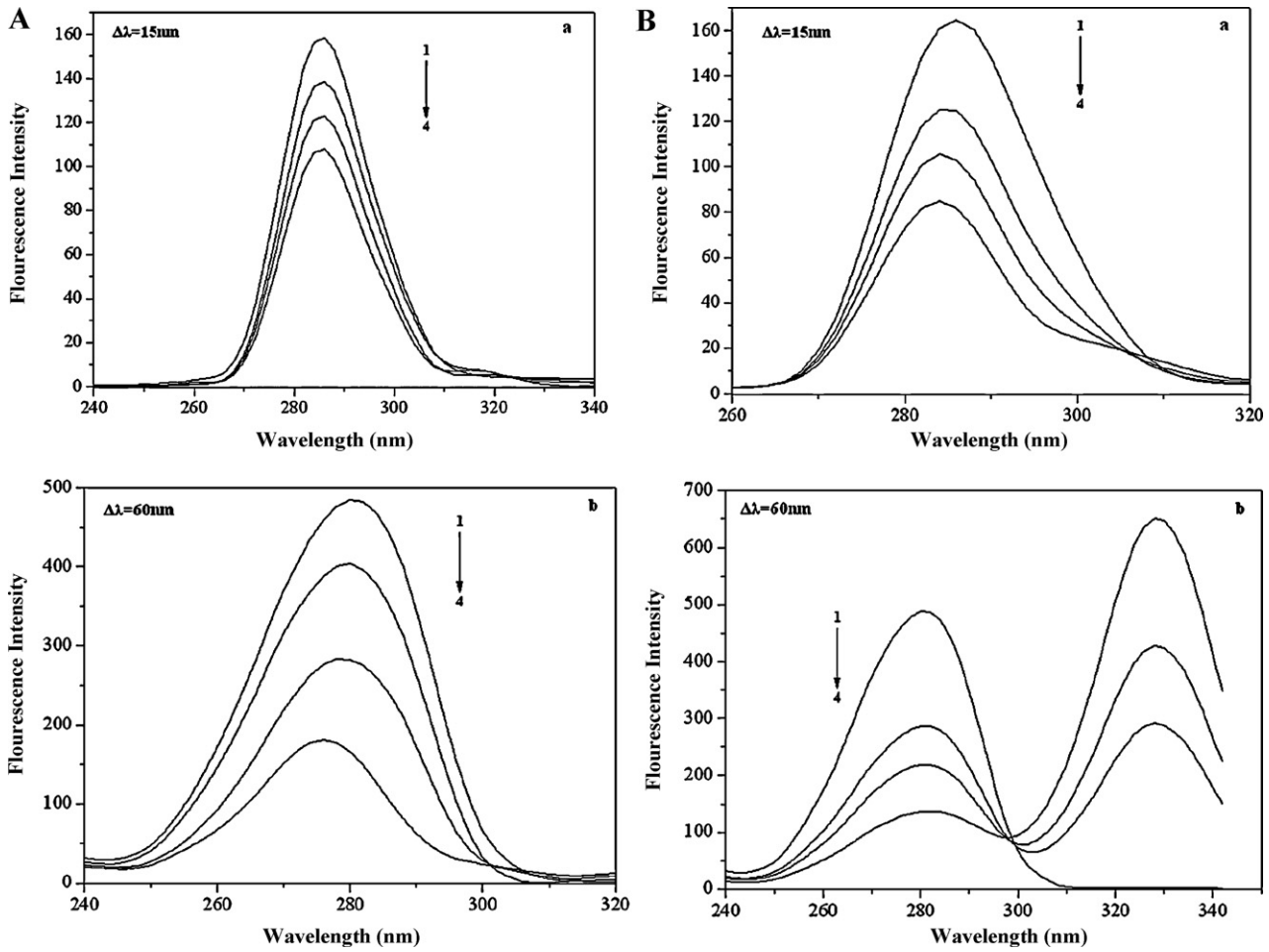

Fig. 9. Synchronous fluorescence spectra of (A) HK and (B) MG with HSA: (a) observing the tyrosine residues at $\Delta\lambda = 15$ nm and (b) observing the tryptophan residues at $\Delta\lambda = 60$ nm. (A) HK ($\times 10^6$ mol L^{-1}) 1–4: 0.0, 2.0, 6.0, and 10.0. (B) MG ($\times 10^6$ mol L^{-1}) 1–4: 0.0, 6.0, 10.0, and 18.0. The concentration of HSA is 5.0 μM. $T = 298$ K.

3.6.1. UV–vis absorption spectra

UV–vis absorption measurement is a very simple and effective method to explore the structural change of protein and detect the complex formation [39]. Fig. 8 was the UV–vis absorption spectra of HK, MG, HSA, HSA–HK and HSA–MG systems. As could be seen in Fig. 8, the absorption spectra intensities of HSA increased with the addition of HK or MG, moreover, the absorption spectra maxima shifts toward longer wavelength region, which suggested that it was due to the complex formation between HSA and HK/MG and the binding of HK/MG to HSA caused the conformational change of protein [40].

3.6.2. Synchronous fluorescence spectroscopy studies

Synchronous fluorescence spectroscopy introduced by Llody [41], which is a kind of simple and effective means to measure the fluorescence quenching and the possible shift of maximum emission wavelength and is related to the alteration of the polarity around the chromophore microenvironment. It can be obtained by simultaneously scanning excitation and emission monochromators. As the wavelength interval ($\Delta\lambda = \lambda_{em} - \lambda_{ex}$) is 15 nm, synchronous fluorescence offers characteristics of the tyrosine residues, while when $\Delta\lambda$ is 60 nm, it provides the characteristic information of tryptophan residues [42]. Such, when $\Delta\lambda$ was set at 15 and 60 nm, the shift of the maximum emission wavelength revealed the alteration of polarity microenvironment around tyrosine and tryptophan residues, respectively. By investigating the synchronous fluorescence spectra of tyrosine and tryptophan residues, we could explore the conformational change of HSA. The fluorescence spectra of tyrosine and tryptophan residues of HSA at various concentrations of HK/MG were shown in Fig. 9(A and B), respectively.

As shown in Fig. 9, the fluorescence intensity quenching of tryptophan residues was stronger than that of tyrosine residues, suggesting that tryptophan residues contribute greatly to the

Table 6
Three-dimensional fluorescence characteristic parameters of HSA, HK–HSA and MG–HSA systems, c(HSA) = 5.0 μM, c(HK) = 1.0 μM, c(MG) = 8.0 μM.

Peak	HSA		HSA–HK			HSA–MG		
	Peak position $\lambda_{ex}/\lambda_{em}$ (nm/nm)	Intensity F_0	Peak position $\lambda_{ex}/\lambda_{em}$ (nm/nm)	Intensity F	F_0/F	Peak position $\lambda_{ex}/\lambda_{em}$ (nm/nm)	Intensity F	F_0/F
A	302/305	113.8	302/305	175.1		302/305	134.1	
B	280/340	735.9	282/340	658.4	1.12	282/340	352.1	2.09
C	236/335	241.8	236/340	201.5	1.20	236/340	119.2	2.03

quenching of the intrinsic fluorescence. In the HK–HSA system, there was no significant shift of the maximum emission wavelength with $\Delta\lambda = 15$ nm (Fig. 9(A, a)) and a slightly blue shift (from 280 to 276 nm) of the maximum emission wavelength with $\Delta\lambda = 60$ nm (Fig. 9(A, b)), which implied that the interaction of HK with HSA did not affect the conformation of the region around tyrosine residues and affect the conformation of the region around tryptophan residues. However, in the MG–HSA system, a slightly blue shift (from 286 to 284 nm) of the maximum mission wavelength of tyrosine residues (Fig. 9(B, a)) and a slightly red shift (from 280 to 282 nm) of the maximum mission wavelength of tryptophan residues (Fig. 9 (B, b)), indicating that the conformation of HSA altered and the hydrophobicity around both the residues increased.

3.6.3. Three-dimensional fluorescence spectra analysis

The three-dimensional fluorescence spectra can provide total information regarding the fluorescence characteristics by changing excitation and emission wavelength simultaneously, so it is a powerful method to study the conformational change of protein.

The three-dimension fluorescence spectra of HSA, HK–HSA, and MG–HSA systems were shown in Fig. 10, and the corresponding characteristic parameters were summarized in Table 6. By comparing the spectral changes of HSA in the absence and presence of HK/MG, the microenvironment and conformation changes of HSA could be obtained. As shown in Fig. 10, peak A is the Rayleigh scattering peak ($\lambda_{ex} = \lambda_{em}$), whereas the strong peak B mainly reveals the spectral characteristic of tryptophan and tyrosine residues of HSA, and another strong fluorescence peak C shows the behavior of polypeptide backbone structures of HSA. It could be seen from Fig. 10 that the fluorescence intensity of peak A increased with the addition of HK/MG. It could be attributed to the HSA–HK or HSA–MG complex that made the volume of HSA increased, which in turn resulted in the enhancement of the scattering effect [43]. The fluorescence intensities of peaks B and C decreased and the maximum emission wavelength of peak C slightly red shifted (from 335 to 340 nm) with the addition of HK or MG for HSA (Table 6). This suggested that the interaction between HSA and HK/MG induced a slight unfolding of the polypeptide backbone of HSA, and HK/MG was located at the vicinity of tryptophan residues on HSA. The results were in accordance with the CD, synchronous and steady fluorescence spectral data.

3.6.4. FT-IR spectra analysis

The interactions of HSA with drugs were characterized by FTIR spectroscopy. Since there was no major spectral shifting for protein amide I band at 1655 cm^{-1} (mainly C = O stretch) and amide II band at 1548 cm^{-1} (C–N stretching coupled with N–H bending modes)

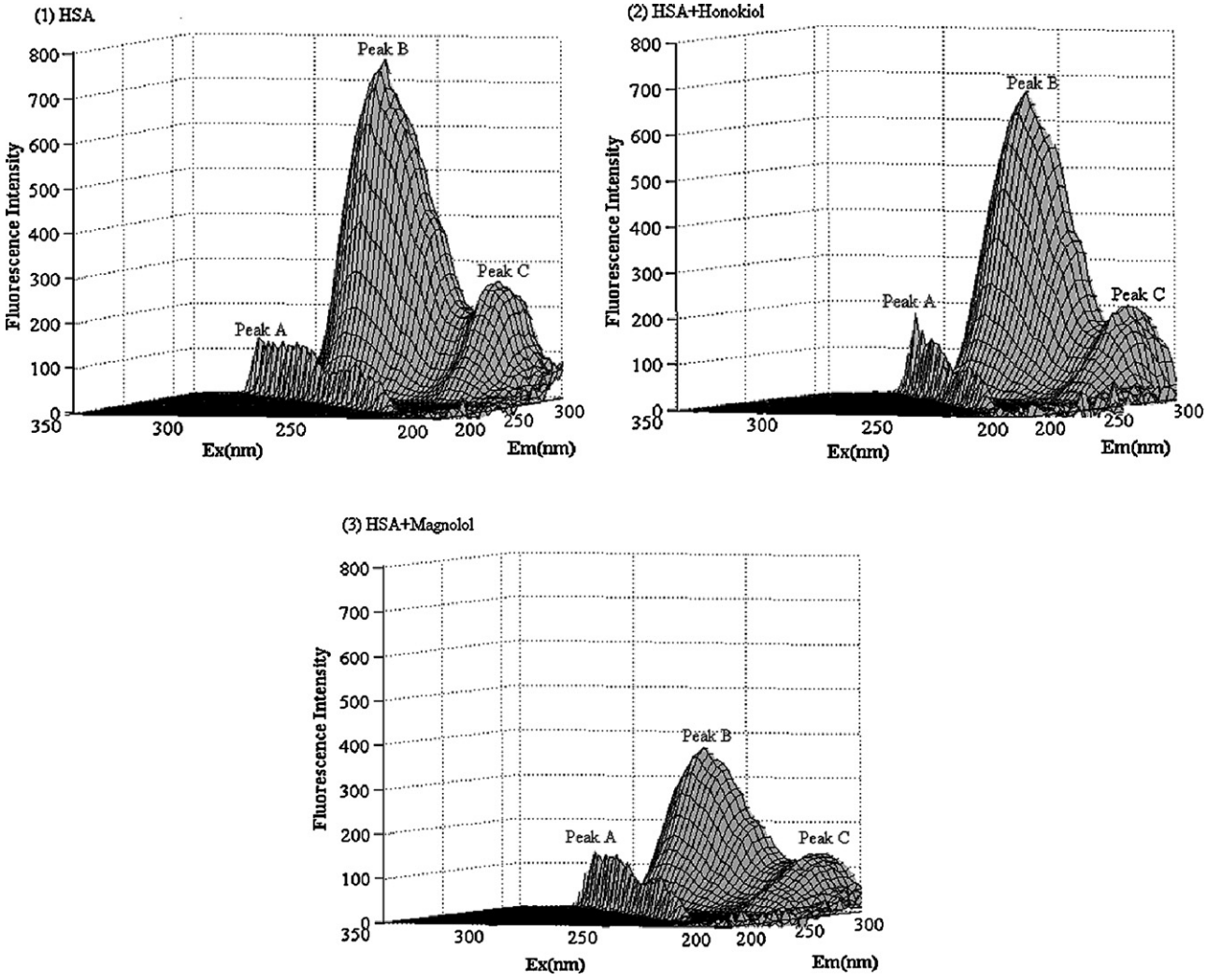

Fig. 10. The three-dimensional fluorescence spectra of HSA (1), HSA–HK system (2), HSA–MG system (3). Conditions: c(HSA) = 5.0 μM, c(HK) = 1.0 μM, c(MG) = 8.0 μM, pH = 7.4, T = 298 K.

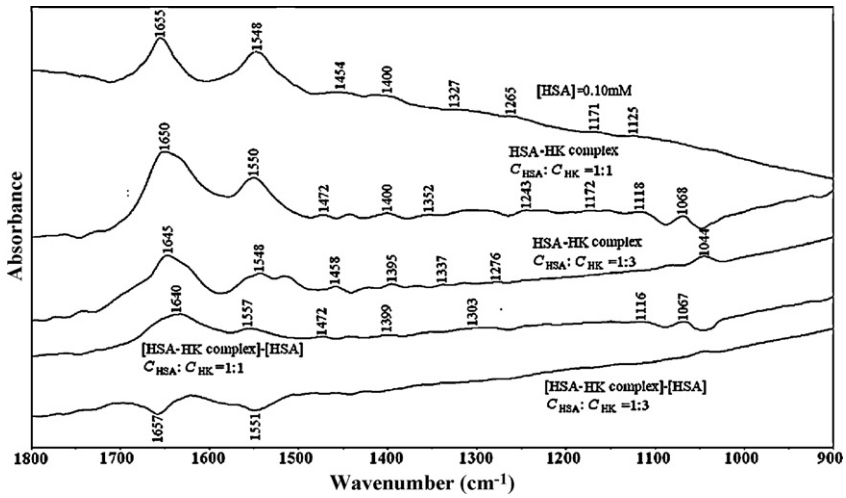

Fig. 11. FTIR spectra in the 1800–900 cm^{-1} for free HSA (0.10 mM), the HSA–HK complex (the molar ratio of HSA/HK was maintained at 1:1 and 1:3, respectively), and their corresponding difference spectra (indicated in the figure). The contribution of HK was subtracted from different spectra in this region.

in the presence of HK/MG, the difference spectra [(protein solution + drug solution) – (protein solution)] were obtained in order to monitor the intensity changes of these vibrations, and their results were shown in Figs. 11 and 12.

At low the molar ratio of HSA to HK or MG (1:1), the intensity changes were observed for HSA amide I band at 1650 or 1648 cm^{-1} and amide II band at 1550 or 1547 cm^{-1}, and positive features were observed for amide I and II bands at 1640 and 1557 cm^{-1} (HK), 1642 and 1546 cm^{-1} (MG) in the difference spectra of drugs–HSA complexes (Figs. 11–12). The results suggested that the increase in intensity of the amide I and II bands was due to HK or MG binding to the C = O, C—N, and N—H groups of protein [44]. However, when the molar ratio of HSA to drug (HK or MG) increased to 1:3, negative features were observed in the difference spectra for amide I and II bands at 1657 and 1551 cm^{-1} (HK), 1657 and 1551 cm^{-1} (MG) in the HSA–HK or HSA–MG system (Figs. 11 and 12). For the HK–HSA or MG–HSA complex, the intensity of the amide I band at 1655 cm^{-1} decreased, indicating that the percentage content of protein α-helical structure reduced at high HK or MG concentration [44]. For the amide I band of protein in other ligand-protein complexes, similar infrared spectral changes observed, where major conformational changes of protein occurred [44,45].

3.6.5. CD spectra analysis

To further investigate whether any conformational changes of HSA molecules occurred in the binding reaction, the measurement of CD spectra was performed. The CD spectra of HSA in the absence and presence of HK/MG were shown in Fig. 13. As Fig. 13 showed, HSA exhibited two negative ellipticities at 208 and 220 nm in the UV region, which were characteristic of the typical α-helix structure of protein. The addition of HK/MG caused a decrease in band intensity at all wavelengths of the far-UV CD, clearly indicating the decrease of the α-helix structure of protein. As could be seen from Fig. 13, when the molar ratio of drug/HSA was 12.5:1, the changes of the α-helix content of HSA induced by the compounds follow the order: MG > HK. The results explained possibly that the binding affinity of MG to HSA was higher than that of HK to HSA. The larger protein of unfolding of MG than HK was mostly derived from the increased hydrophobicity, because of the fact that hydrophobic interaction played an important role in the binding process, which was coincident with the results of thermodynamic parameters. The decreased contents of α-helix structure indicated that HK/MG bound to the amino acid residues of the main polypeptide chain of HSA and destroyed the hydrogen-networks [46]. However, the CD spectra of HSA in the absence and presence of HK/MG

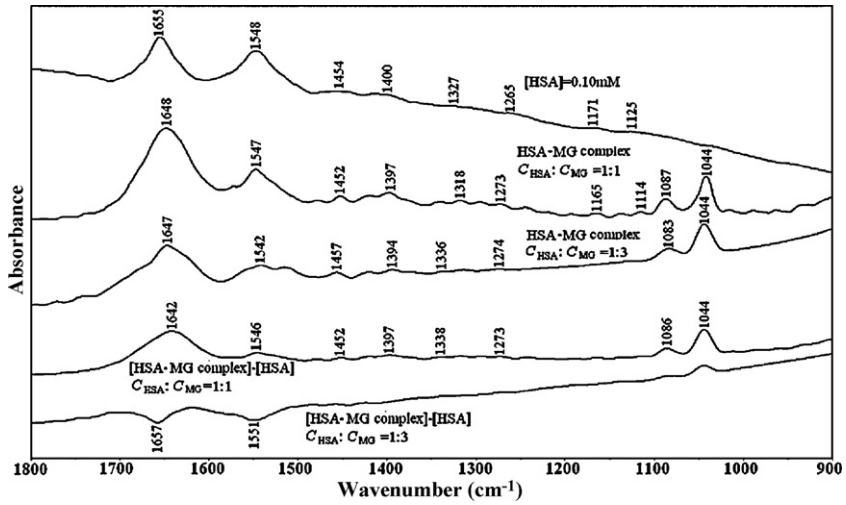

Fig. 12. FTIR spectra in the 1800–900 cm^{-1} for free HSA (0.10 mM), the HSA–MG complex (the molar ratio of HSA/MG was maintained at 1:1 and 1:3, respectively), and their corresponding difference spectra (indicated in the figure). The contribution of MG was subtracted from different spectra in this region.

Table 7
The effects of common ions on the binding constants of HK–HSA and MG–HSA systems. c(HSA) = 5.0 μM, and the concentrations of eight ions are 15.0 μM, T = 298 K.

Ions	HSA–HK			HSA–MG		
	K ($\times 10^{-4}$ L mol^{-1})	R	SD	K ($\times 10^{-6}$ L mol^{-1})	R	SD
–	5.304	0.9946	0.0327	2.638	0.9988	0.0220
Ca^{2+}	9.043	0.9964	0.0257	0.078	0.9992	0.0156
Zn^{2+}	15.104	0.9975	0.0220	0.050	0.9998	0.0085
Mn^{2+}	16.062	0.9992	0.0127	0.242	0.9993	0.0160
Fe^{3+}	4.944	0.9971	0.0219	0.098	0.9961	0.0353
Cu^{2+}	0.701	0.9971	0.0182	0.064	0.9994	0.0128
Cl^{-}	3.052	0.9981	0.0169	0.183	0.9951	0.0406
CH_3COO^{-}	12.260	0.9987	0.0159	0.331	0.9999	0.0019
CO_3^{2-}	5.284	0.9954	0.0278	0.284	0.9999	0.0071

were similar in shape, suggesting that the structure of BSA after the addition of HK/MG was also predominantly α-helix [37].

3.7. Influences of common ions on the interactions of HSA with HK/MG

Metal ions are vital to human body and play an essentially structural role in many proteins based coordinate bonds. In plasma, there are some metal ions, which can affect the interactions of drugs to serum albumins. Hence, in the text, the effect of common ions (such as, Ca^{2+}, Zn^{2+}, Mn^{2+}, Fe^{3+}, Cu^{2+}, Cl^{-}, CH_3COO^{-}, and CO_3^{2-}) on the binding constants of HSA with HK/MG were investigated at 298 K. The binding constants of HSA–HK/MG systems in the presence of above ions were evaluated and their values were listed in Table 7. As could be seen in Table 7, from the MG–HSA system, their binding constants decreased in the presence of anyone among above eight common ions, whereas, the binding constants of the MG–HSA system decreased in the presence of anyone among four common ions (Fe^{3+}, Cu^{2+}, Cl^{-} and CO_3^{2-}), suggesting that these common ions might compete for the same binding sites on HSA. This implied that there was the competition between the drug (HK or MG) and the corresponding common ion when both of them existed in the serum albumin solution at the same time. Moreover, the binding constants between HSA and HK markedly increased in the presence of anyone among Ca^{2+}, Zn^{2+}, Mn^{2+} and CH_3COO^{-} ions, which possibly resulted from two aspects as follows: the metal ion-HK complexes were formed via metal ion bridge, might enhance the binding capability of HK to HSA; or four ions (Ca^{2+}, Zn^{2+}, $Mn^{2+}$and CH_3COO^{-}) changed the conformation of HSA, which was more favorable for HK binding to HSA. Therefore, in the presence of above common ions, it may be prolonged or shortened to the storage time of the drug (HK or MG) in blood plasma. In such an event, it necessitated to readjust the dose limits of the drug in the presence of these common ions.

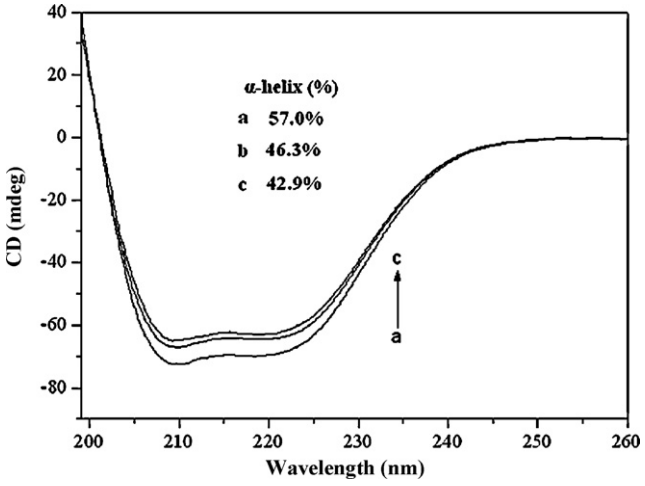

Fig. 13. CD spectra of HSA in the absence (a) and presence of HK (b) and MG (c). The concentration of HSA was 1.0 μM, and the concentrations of HK and MG were all 12.5 μM.

4. Conclusions

In the paper, the binding properties of HK/MG to HSA were characterized by measuring fluorescence and FT-IR. Structural analysis showed that HK bind HSA via the hydrophobic interaction with the number of bound HK per protein was 0.95, and MG bind HSA via the hydrophobic interaction strongly and electrostatic interaction with the number of bound MG per protein was 1.26. The distances between protein and drugs were calculated using Förster no-radiation energy transfer theory and were found to be 1.842 and 1.238 nm for the HSA–HK and HSA–MG complexes, respectively. The shorter distance in the latter complex indicated more efficient energy transfer than in the former. This was also confirmed by estimating the quenching rate constant (K_q) and binding constant (K) in each complex. The results of synchronous fluorescence spectra suggested that the conformation of HSA altered and the hydrophobicity around tryptophan residues increased, and CD spectra showed that the conformational change of HSA induced by MG was more remarkable than that of HK. In our experiment, the binding constants of the HK–HSA complex markedly increased in the presence of anyone among four common ions (Ca^{2+}, Zn^{2+}, Mn^{2+} and CH_3COO^{-}), however, for the MG–HSA complex, their binding constants decreased in the presence of anyone among above eight common ions. In addition, the site marker competitive experiments indicated that MG was located in site I (subdomain IIA) on HSA, and the binding of HK to HSA mainly located within site II (subdomain IIIA).

Acknowledgement

The author gratefully acknowledges financial support by the Education Department of Sichuan Province (12ZA171).

References

[1] C.B. Berde, B.S. Hudson, R.D. Simoni, L.A. Sklar, Human serum albumin: spectroscopic studies of binding and proximity relationships for fatty acids and bilirubin, J. Biol. Chem. 254 (1979) 391–400.
[2] X.M. He, D.C. Carter, Atomic structure and chemistry of human serum albumin, Nature 358 (1992) 209–215.
[3] (a) G. Sudlow, D.J. Birkett, D.N. Wade, The characterization of two specific drug binding sites on human serum albumin, Mol. Pharmacol. 11 (1975) 824–832; (b) G. Sudlow, D.J. Birkett, D.N. Wade, Further characterization of specific drug binding sites on human serum albumin, Mol. Pharmacol. 12 (1976) 1052–1061.
[4] H.N. Hou, Z.D. Qi, Y.W. OuYang, F.L. Liao, Y. Zhang, Y. Liu, Studies on interaction between Vitamin B12 and human serum albumin, J. Pharm. Biomed. Anal. 47 (2008) 134–139.
[5] Y.J. Hu, Y. Liu, X.H. Xiao, Investigation of the interaction between berberine and human serum albumin, Biomacromolecules 10 (2009) 517–521.

[6] S. Neelam, M. Gokara, B. Sudhamalla, D.G. Amooru, R. Subramanyam, Interaction studies of coumaroyltyramine with human serum albumin and its biological importance, J. Phys. Chem. B 114 (2010) 3005–3012.
[7] Y.Y. Yue, J.M. Liu, J. Fan, X.J. Yao, Binding studies of phloridzin with human serum albumin and its effect on the conformation of protein, J. Pharm. Biomed. Anal. 56 (2011) 336–342.
[8] I. Matei, S. Ionescu, M. Hillebrand, Interaction of fisetin with human serum albumin by fluorescence, circular dichroism spectroscopy and DFT calculations: binding parameters and conformational changes, J. Lumin. 131 (2011) 1629–1635.
[9] Y.L. Wang, T. Zhang, J. Xu, W.H. Du, Comparison of the binding affinity of chlorogenic acid with two serum albumins, Int. J. Biol. Macromol. 48 (2011) 81–86.
[10] P. Bourassa, I. Hasni, H.A. Tajmir-Riahi, Folic acid complexes with human and bovine serum albumins, Food Chem. 129 (2011) 1148–1155.
[11] X.M. Zhou, Q. Yang, X.Y. Xie, Q. Hu, F.M. Qi, Z.U. Rahman, X.G. Chen, NMR, multi-spectroscopic and molecular modeling approach to investigate the complexes between C.I. Acid Orange 7 and human serum albumin in vitro, Dyes and Pigments 92 (2012) 1100–1107.
[12] C.C. Shen, C.L. Ni, Y.C. Shen, Y.L. Huang, C.H. Kuo, T.S. Wu, C.C. Chen, Phenolic constituents from the stem bark of *Magnolia officinalis*, J. Nat. Prod. 72 (2009) 168–171.
[13] Y.R. Lin, H.H. Chen, C.H. Ko, M.H. Chan, Neuroprotective activity of honokiol and magnolol in cerebellar granule cell damage, Eur. J. Pharmacol. 537 (2006) 64–69.
[14] Y.R. Lin, H.H. Chen, C.H. Ko, M.H. Chan, Effects of honokiol and magnolol on acute and inflammatory pain models in mice, Life Sci. 81 (2007) 1071–1078.
[15] C. Zhao, Z.Q. Liu, Comparison of antioxidant abilities of honokiol and magnolol to scavenge radicals and to protect DNA, Biochimie 93 (2011) 1755–1760.
[16] H.F. Zhai, K. Nakade, Y. Mitsumoto, Y. Fukuyam, Honokiol and magnolol induce Ca^{2+} mobilization in rat cortical neurons and human neuroblastoma SH-SY5Y cells, Eur. J. Pharmacol. 474 (2003) 199–204.
[17] Y. Fukuyama, K. Nakade, Y. Minoshima, R. Yokoyama, H. Zhai, Y. Mitsumoto, Neurotrophic activity of honokiol on the cultures of fetal rat cortical neurons, Bioorg. Med. Chem. Lett. 12 (2002) 1163–1166.
[18] A.J. Alonso-Castro, R. Zapata-Bustos, F. Domínguez, A. García-Carrancá, L.A. Salazar-Olivo, Magnolia dealbata Zucc and its active principles honokiol and magnolol stimulate glucose uptake in murine and human adipocytes using the insulin-signaling pathway, Phytomedicine 18 (2011) 926–933.
[19] N. Matsui, K. Takahashi, M. Takeichi, T. Kuroshita, K. Noguchi, K. Yamazaki, H. Tagashira, K. Tsutsui, H. Okada, Y. Kido, Y. Yasui, N. Fukuishi, Y. Fukuyama, M. Akagi, Honokiol and magnolol prevent learning and memory impairment and cholinergic deficit in SAMP8 mice, Brain Res. 1305 (2009) 108–117.
[20] T.C. Chuang, S.C. Hsu, Y.T. Cheng, W.S. Shao, K.H. Wu, G.S. Fang, C.C. Ou, V.C. Wang, Magnolol down-regulates HER2 gene expression, leading to inhibition of HER2-mediated metastatic potential in ovarian cancer cells, Cancer Lett. 311 (2011) 11–19.
[21] E.J. Park, H.Y. Min, H.J. Chung, J.Y. Hong, Y.J. Kang, T.M. Hung, U.J. Youn, Y.S. Kim, K. Bae, S.S. Kang, S.K. Lee, Down-regulation of c-Src/EGFR-mediated signaling activation is involved in the honokiol-induced cell cycle arrest and apoptosis in MDA-MB-231 human breast cancer cells, Cancer Lett. 277 (2009) 133–140.
[22] X.H. Wang, L.L. Cai, X.Y. Zhang, L.Y. Deng, H. Zheng, C.Y. Deng, J.L. Wen, X. Zhao, Y.Q. Wei, L.J. Chen, Improved solubility and pharmacokinetics of PEGylated liposomal honokiol and human plasma protein binding ability of honokiol, Int. J. Pharm. 410 (2011) 169–174.
[23] D.J. Li, M. Zhu, C. Xu, B.M. Ji, Characterization of the baicaleinebovine serum albumin complex without or with Cu^{2+} or Fe^{3+} by spectroscopic approaches, Eur. J. Med. Chem. 46 (2011) 588–599.
[24] R.H. Liu, X.Y. Yu, W. Gao, D.H. Ji, F.X. Yang, X.F. Li, J. Chen, H.W. Tao, H.W. Huang, P.G. Yi, Study on the interaction between salvianic acid A sodium and bovine serum albumin by spectroscopic methods, Spectrochim. Acta A 78 (2011) 1535–1539.
[25] J. Zhang, X.J. Wang, Y.J. Yan, W.S. Xiang, Comparative studies on the interaction of genistein, 8-chlorogenistein, and 3′,8-dichlorogenistein with bovine serum albumin, J. Agric. Food Chem. 59 (2011) 7506–7513.
[26] Z.J. Cheng, Y.T. Zhang, Spectroscopic investigation on the interaction of salidroside with bovine serum albumin, J. Mol. Struct. 889 (2008) 20–27.
[27] J.R. Lakowicz, G. Weber, Quenching of fluorescence by oxygen: a probe for structural fluctuation in macromolecules, Biochemistry 12 (1973) 4161–4170.
[28] M.R. Eftink, C.A. Ghiron, Fluorescence quenching studies with proteins, Anal. Biochem. 114 (1981) 199–212.
[29] M.X. Xie, X.Y. Xu, Y.D. Wang, Interaction between hesperetin and human serum albumin revealed by spectroscopic methods, Biochim. Biophys. Acta 1724 (2005) 215–224.
[30] D.M. Chipman, V. Grisaro, N. Sharon, The binding of oligosaccharides containing N-acetylplucosamine and N-acetylmuramic acid to lysozyme, J. Biol. Chem. 242 (1967) 4388–4394.
[31] H. Gao, L.D. Lei, J.Q. Liu, Q. Kong, X.G. Chen, Z.D. Hu, The study on the interaction between human serum albumin and a new reagent with antitumor activity by spectrophotometric methods, J. Photochem. Photobiol. A 167 (2004) 213–221.
[32] D.C. Carter, J.X. Ho, Structure of serum albumin, Adv. Protein Chem. 45 (1994) 153–203.
[33] Z. Chi, R. Liu, Y. Teng, X. Fang, C. Gao, Binding of oxytetracycline to bovine serum albumin: Spectroscopic and molecular modeling investigations, J. Agric. Food Chem. 58 (2010) 10262–10269.
[34] R.S. Kumar, P. Paul, A. Riyasdeen, G. Wagniéres, H. van den Bergh, M.A. Akbarsha, S. Arunachalam, Human serum albumin binding and cytotoxicity studies of surfactant–cobalt(III) complex containing 1,10-phenanthroline ligand, Colloid Surface B 86 (2011) 35–44.
[35] D.P. Ross, S. Subramanian, Thermodynamics of protein association reactions: forces contributing to stability, Biochemistry 20 (1981) 3096–3102.
[36] T. Forster, O. Sinanoglu, Modern Quantum Chemistry, Academic Press, New York, 1965, pp. 93–137.
[37] B. Sandhya, A.H. Hegde, S.S. Kalanur, U. Katrahalli, J. Seetharamappa, Interaction of triprolidine hydrochloride with serum albumins: Thermodynamic and binding characteristics, and influence of site probes, J. Pharm. Biomed. Anal. 54 (2011) 1180–1186.
[38] C.Q. Jiang, M.X. Gao, X.Z. Meng, Study of the interaction between daunorubicin and human serum albumin, and the determination of daunorubicin in blood serum samples, Spectrochim. Acta A 59 (2003) 1605–1610.
[39] Z.J. Cheng, Y.T. Zhang, Fluorometric investigation on the interaction of oleanolic acid with bovine serum albumin, J. Mol. Struct. 879 (2008) 81–87.
[40] K.S. Witold, H.M. Henry, C. Dennis, De-termination of protein secondary structure by transform infrared spectroscopy: a critical assessment, Biochemistry 32 (1993) 389–394.
[41] J.B.F. Llody, Synchronized excitation of fluorescence emission spectra, Nat. Phys. Sci. 231 (1971) 64–65.
[42] Z.X. Chi, R.T. Liu, B.J. Yang, H. Zhang, Toxic interaction mechanism between oxytetracycline and bovine hemoglobin, J. Hazard. Mater. 180 (2010) 741–747.
[43] D.J. Li, Y. Wang, J.J. Chen, B.M. Ji, Characterization of the interaction between farrerol and bovine serum albumin by fluorescence and circular dichroism, Spectrochim. Acta A 79 (2011) 680–686.
[44] S. Dubeau, P. Bourassa, T.J. Thomas, H.A. Tajmir-Riahi, Biogenic and synthetic polyamines bind bovine serum albumin, Biomacromolecules 11 (2010) 1507–1515.
[45] P. Bourassa, C.D. Kanakis, P. Tarantilis, M.G. Pollissiou, H.A. Tajmir-Riahi, Resveratrol, Genistein, and curcumin bind bovine serum albumin, J. Phys. Chem. B 114 (2010) 3348–3354.
[46] F.L. Cui, J. Fan, J.P. Li, Z.D. Hu, Interactions between 1-benzoyl-4-p-chlorophenyl thiosemicarbazide and serum albumin: investigation by fluorescence spectroscopy, Bioorg. Med. Chem. 12 (2004) 151–157.

Journal of Pharmaceutical and Biomedical Analysis 66 (2012) 252–257

Contents lists available at SciVerse ScienceDirect

Journal of Pharmaceutical and Biomedical Analysis

journal homepage: www.elsevier.com/locate/jpba

Near infrared spectroscopy and multivariate calibration for simultaneous determination of glucose, triglycerides and high-density lipoprotein in animal plasma

Ana Carolina de Oliveira Neves[a], Aurigena Antunes de Araújo[b], Bruna Laís Silva[b], Patrícia Valderrama[c], Paulo Henrique Março[c], Kássio Michell Gomes de Lima[a,*]

[a] Universidade Federal do Rio Grande do Norte, Instituto de Química, Grupo de Pesquisa em Quimiometria Aplicada, CEP 59072-970 Natal, RN, Brazil
[b] Department of Biophysics and Pharmacology, UFRN, 59072-970 Natal, Brazil
[c] Universidade Tecnológica Federal do Paraná, Coordenação de Licenciatura em Química, BR 369, Km 0.5, CEP 87301-006 Campo Mourão, PR, Brazil

ARTICLE INFO

Article history:
Received 23 December 2011
Received in revised form 13 March 2012
Accepted 13 March 2012
Available online 23 March 2012

Keywords:
NIR
Glucose
Triglycerides
High-density lipoprotein
Multivariate calibration

ABSTRACT

The quantitative analysis of glucose, triglycerides and high-density lipoprotein (HDL) in rat plasma without sample pre-treatment using direct near-infrared spectroscopy was studied. Comparison was made of several multivariate calibration techniques and algorithms for data pre-processing and variable selection, including partial least squares (PLS), interval partial least squares (iPLS), genetic algorithm (GA) and successive projections algorithm (SPA). Variable selection yielded good results for the correlation coefficient and Root Mean Square Error of Prediction (RMSEP) values for the three parameters, especially triglycerides. The RMSEP values for glucose, triglycerides and HDL produced by the PLS model were 6.08, 16.07 and 2.03 mg dl^{-1}, respectively. *F* tests and *t*-tests were performed to compare the results of the models with each other and with a reference method. These results suggests that the PLS method can be used to simultaneously determine the concentrations of glucose, triglycerides and HDL in complicated biological fluids with NIR spectroscopy, offering an alternative analysis in animals.

© 2012 Elsevier B.V. All rights reserved.

1. Introduction

The values of hematological parameters in rats used in experiments are influenced by the housing and environment around the animal. Although each rat species has mechanisms to maintain proper values of these parameters, variations arise from sex, strain and genotype as well as age, diet, handling of the animals and the surrounding environment. Further, animals subjected to an experiment may respond differently depending on their environmental conditions and may be influenced by various ecological factors that vary by geographical region [1].

For biochemical laboratory measurements, quantitative methods must be suitably accurate and precise over the expected range of values required. In the literature, the vast majority of the biochemical analyses of rat hematological parameters, including glucose levels, triglycerides and cholesterol [2–5], are made by enzymatic methods. Plasma glucose levels are determined in animals that have fasted for 12 h using a colorimetric enzymatic assay with glucose oxidase. Triglycerides are determined using a colorimetric enzymatic assay with glycerol-3-phosphate oxidase, in which lipases act on triglycerides to generate glycerol, which is subsequently converted into glycerol phosphate and then oxidized to water and hydrogen peroxide by glycerol-3-phosphate oxidase. Hydrogen peroxide then reacts with 4-aminoantipyrine and 4-chlorophenol through an oxidative reaction catalyzed by peroxidase, producing a quinone imine (red) with a color intensity that is proportional to the original concentration of triglycerides in the sample. Cholesterol (HDL), in turn, is determined by a colorimetric enzymatic assay with cholesterol oxidase. In this method, cholesterol oxidase catalyzes the oxidation of cholesterol to produce hydrogen peroxide, which is then converted to red-colored (quinine imine) as described above where the color intensity is proportional to the original concentration of cholesterol in the sample. However, all of these methods for determining glucose, triglycerides and HDL in the plasma of animals suffer from inherent difficulties that affect the speed of analysis and the results. These problems include the need for specific reagents and temperature control, problems of chemical interference and the time required for analysis.

NIR spectroscopy has been applied successfully for the qualitative and quantitative analysis of several classes of compounds in areas such as the pharmaceutical industry [6], food safety [7], environmental studies [8], and clinical practice [9], among others. In the analysis of biochemical compounds, its advantages

* Corresponding author. Tel.: +55 84 3215 3828; fax: +55 83 3211 9224.
E-mail address: kassio@ufrnet.br (K.M.G. de Lima).

0731-7085/$ – see front matter © 2012 Elsevier B.V. All rights reserved.
doi:10.1016/j.jpba.2012.03.023

include an absence of specific reagents and non-destructive and non-invasive measurements. Various types of biomedical samples, including glucose [10,11], human serum albumin [12], cholesterol [13], urea [14] and hematocrit [15], have been investigated by NIR spectroscopy.

Hazen et al. [10] determined the total protein, albumin protein, globulin protein, triglycerides, cholesterol, urea, glucose and lactate plasma levels using NIR spectroscopy and multivariate calibration. PLS models gave RMSEP values of 3.23 mg dl^{-1} for glucose. Kang et al. [16] employed NIR spectroscopy and multivariate tools for the quantification of cholesterol, glucose and urea in bovine samples. The best predicted results for cholesterol, glucose and urea had a RMSEP of 6.68, 10:35 and 1.28 mg dl^{-1}, respectively. Kasemsumran et al. [17] developed a PLS models using NIR spectroscopy for the determination of glucose in cattle blood serum samples. The authors obtained models showing values of the RMSEP of 25.31 mg dl^{-1} and a correlation coefficient of 0.99 with eight latent variables. In another experiment, Petter et al. [18] proposed to determinate the LDL and high density lipoprotein (HDL) content in human serum by employing near-infrared (NIR) spectroscopy and multivariate calibration techniques (PCR and PLS). The authors used as an adsorbent (TiO(2) beads) for selectively immobilizing LDL and HDL-cholesterol and further analyzing the incubated and washed samples via NIR diffuse reflection spectroscopy. In this work, the pretreated serum samples were predicted by the PLSR model while the standard deviation (SD) from the reference to the NIR predicted values for six test samples in a concentration range from 500 to 2500 ppm were lower than 10%. Finally, Filho and Poppi [19] studied the use of NIR spectroscopy and multivariate calibration methods to measure triglyceride levels in human plasma. The authors compared the performance of techniques such as PLS, MLR and genetic algorithms as methods for variable selection. For the measurement of triglyceride levels, the methodology showed errors of approximately 9%, which is an acceptable relative error for this parameter.

However, several complicating factors remain. The major difficulties in the analysis of blood components by NIR are the weakness of the NIR signals from blood components compared to those from other components, especially water, and the complexity of overlapping bands. To overcome these difficulties, various chemometric algorithms have been applied to NIR data from serum, whole blood, and human tissues. The methods used for variable selection, such as iPLS (interval partial least squares) [20], GA (genetic algorithm) [21] and SPA (successive projections algorithm) [22], allow for improved multivariate models using a spectrum of variables with more relevant information. These algorithms eliminate variables that do not directly correlate with the property of interest, such as those that add only noise, nonlinearities, or irrelevant information. They also eliminate potential interferences and variables that generate a lower signal/noise ratio (which is indicative of low sensitivity).

Another tool used to improve NIR results is outlier detection, which selects samples that depart from the bulk of the data due to instrumental errors, the presence of another population, laboratory errors, and so on. The calibration and prediction sets in this work were optimized based on data with extreme leverage, unmodeled residuals in spectral data, and unmodeled residuals in the dependent variables [23].

In this work, a quantitative analysis of glucose, triglycerides and HDL in rat plasma was performed without sample pre-treatment, using direct NIR absorption measurements. A comparison of several multivariate calibration techniques, including PLS, iPLS, SPA, GA and outlier detection, was performed to determine the best models. Additionally, several data pre-processing methods were compared to determine which method was best to analyze this kind of data. These methods will be useful as an alternative to the existing methods for the simultaneous monitoring of glucose, triglycerides and HDL in plasma.Experimental

2.1. Animals

Twenty-three adult male Labina rats, weighing 300 g on average, were provided by the Animal Department of Biophysics and Pharmacology, Federal University of Rio Grande do Norte. All the animals were exposed to the same environmental conditions: light controlled in a 12/12 h light/dark cycle, temperature, and food and water ad libitum. The food of the animals was removed to induce fasting for 12 h before sacrifice. This study used two groups of rats, designated as control and experimental groups, with four subgroups in each group. The control group received saline injected intraperitoneally (ip), while the experimental group received a single dose of 4 mg kg^{-1} tobramycin ip. The data used in this study were obtained from a pre-clinical experimental study performed on rats which aimed the evaluation of the biochemical parameters (Glucose, HDL and triglycerides) during the use of tobramycin (antibiotic) over a period of 04 weeks. This study attempted to simulate the conditions of the dose quantity and duration of antibiotic therapy with tobramycin in humans, since it is used for the antibiotic treatment of serious infections potentially caused by *Pseudomonas aeruginosa* [24,25]. Each week, a subset of each group was euthanized with sodium thiopental at a dosage of 50 mg kg^{-1}, according to a protocol approved by the Ethics Committee on Animal Use, and blood was taken for the biochemical evaluation of glucose, triglyceride and HDL levels.

2.2. Reference method

Blood samples from sacrificed animals were collected in 15 ml conical Falcon tubes (16.5 mm × 120 mm) and left at room temperature (25 °C) to clot. Serum was obtained by centrifugation at 3000 rpm for 10 min. Blood glucose levels were measured using a previously described glucose oxidase method [1], using an analytical kit supplied by Bioclin, Brazil and following the instructions provided. The absorbance of the samples was determined using a BioPlus 2000. HDL cholesterol esters were measured using an analytical assay kit supplied by Bioclin, Brazil, following the instructions provided. Triglycerides were measured by the glycerol kinase method, using a kit supplied by Bioclin, Brazil and following the instructions provided. The concentration ranges of glucose, triglycerides and HDL were 73–130, 22–135 and 25.4–52.7 mg dl^{-1}, respectively. The estimated standard deviations for these measurements in rat plasma were 17.4, 24.7 and 11.4 mg dl^{-1}, respectively [1]. The study was approved by the Ethics and Research 36, UFRN.

2.3. Instrumentation

Spectral measurements were performed using a MB 160 Bomem FT-NIR spectrophotometer (ABB Bomem, Quebec, Canada). NIR spectra were obtained over a range of 1100–2500 nm with a resolution of 8 cm^{-1}. The time measurement was 41 s (50 scans) per spectrum. Absorbance spectra of rat plasma were obtained against an empty quartz cell (1 mm optical path, NSG precision cells, Inc., model 21UV1). The sample was introduced into a quartz cell using a disposable 1 ml syringe. After each measurement, the cell was cleaned using a sequence of 1 M acetic acid, ultra-pure water and finally acetone to dry the cell. Temperature was kept at 25 °C through the experiments.Data analysis

Data analysis was performed using MATLAB version 6.5 (The Math-Works, Natick, USA) using the PLS-toolbox (Eigenvector Research, Inc., Wenatchee, WA, USA, version 6.01). Different preprocessing methods were used, including the derivative and smoothing Savitzky–Golay methods, with varying the number of

window points (3, 5 and 7). The samples were divided into calibration (17 samples) and prediction (6 samples) sets by applying the classic Kennard-Stone (KS) selection algorithm [26] to the NIR spectra. The lowest root mean square error of prediction (RMSEP) is obtained when using the optimum number of PLS factors, which is found using the variance of the matrix of the instrumental responses. The prediction set was used to test the predictive ability of the PLS models. The predicted results for the calibration models developed by PLS using the spectral regions selected by iPLS, GA, and SPA were compared to those found by PLS using the whole region. Finally, the best models results for each parameter were compared before and after applying outlier detection.

3. Results and discussion

The organic matrix of this study, serum was obtained from animals receiving tobramycin in order to simulate the conditions of treatment period (04 weeks) held in humans. As this pharmacological, tobramycin, has the adverse effect is renal toxicity. The toxicity results from accumulation and retention of aminoglycoside (tobramycin) in the renal proximal tubular cells [27,28] and the levels of glucose, HDL and triglycerides were measured each week.

The absorbance spectra of 23 blood plasma samples of rats were directly measured with single-beam spectra. A representative spectrum is given in Fig. 1. The strong absorption band near to 1450 nm was assigned to the combination of OH symmetric and antisymmetric stretching modes, and a saturated feature of approximately 1940 nm was assigned to the combination of OH stretching and bending vibrations. For the clinical analyses, the presence of water is problematic because it shows a strong absorption in the same range as biological species such as glucose, triglycerides and cholesterol. Because of this, it is necessary to pre-process the data to decrease or remove water absorption effects. Here, to avoid the strong absorption of water, the region approximately at 1900–2000 nm was eliminated before the development of the calibration models for analytes (glucose, triglycerides and HDL). However there are informative NIR regions of glucose, triglycerides and cholesterol between 1100–1900 nm and 2000–2500 nm [13] for multivariate models. The bands arising from combinations of the stretching and deformation modes of CH and NH groups are found in this region, making it suitable for collecting useful information about the three analytes and for establishing PLS models.

3.1. Glucose

The results obtained for the calibration models in the NIR region for glucose in rat plasma are shown in Table 1. In addition to the PLS models, the results of the PLS–SPA, PLS-GA and iPLS models are shown. Only the best results from the tested pre-processing techniques are presented. *F* tests were performed for all the models using the prediction set. The results showed no significant difference (95% confidence level) between the best PLS model, the PLS (4)[1] and the other models, except for the PLS (4) first derivative (3 pts), the PLS (3) first derivative (7 pts), the PLS (3) second derivative (5 pts), the iPLS (3) using 400 spectral variables and the iPLS (4) using 600 spectral variables. Therefore, variable selection was important in this work because it enabled the use of models that require a small number of spectral variables. The RMSEP values of all the models were less than the reproducibility value of the BIOCLIN (Brazil) reference method, except for the PLS (4) first derivative (3 pts). The correlation coefficients for the prediction set ranged from 0.17 to 0.97 for all the models. It was observed that, in the NIR spectral region, models with derivative data showed higher RMSEP values than models with raw or smoothed data. Some important spectral information may have been lost when the derivative spectra were employed. The number of latent variables used for the PLS, iPLS, SPA and GA models using NIR spectra was 3 or 4. With the PLS models, a narrow spectral region (1105.05–1892.3 nm and 1997.27–2461.97 nm) was enough to predict the glucose parameter. The strategy of using GA models had the advantage of using few variables (321) to build the PLS models.

Two outliers were excluded from the calibration set, and the best PLS model for glucose was developed by applying a smoothing with 3 pts. For this model, the lowest Root Mean Square Error of Cross Validation (RMSECV) and RMSEP were 12.10 and 6.08, respectively. The correlation coefficient for the validation set was 0.98 and was obtained using four latent variables. This model was not significantly different when compared with the reference values according to a *t*-test (95% confidence level). Fig. 2 shows that the correlation between the measured and predicted values for glucose in rat plasma was predicted from NIR spectroscopy with error values similar to that of the reference method (17.4 mg dl^{-1}) [1].

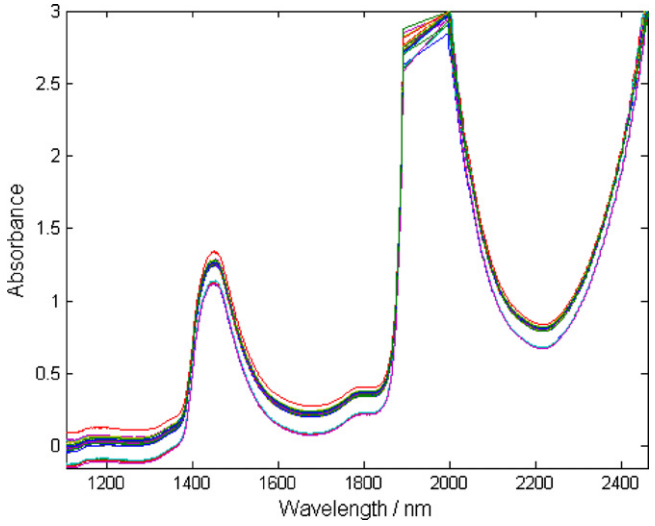

Fig. 1. NIR spectra of 23 samples of blood plasma of rats.

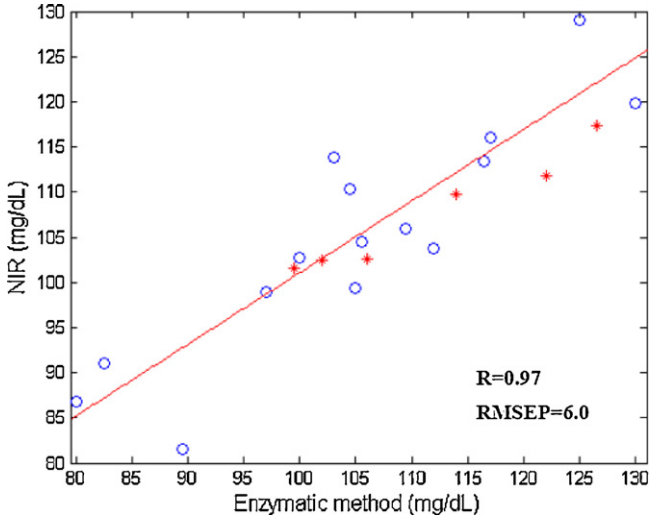

Fig. 2. Correlation among the measured and the predicted values for both calibration and prediction sets for glucose in rat blood plasma for the best model, PLS (4)[1], by NIR spectroscopy. (○) calibration set; (✱) validation set.

Table 1
Results for calibration and the external validation set for glucose: root mean square error of cross validation (RMSECV) and prediction (RMSEP), correlation coefficient (*R*) and the number of used spectral variables (Size). The number of PLS factors or in PLS, iPLS, PLS-SPA and PLS-GA models are represented in parentheses.

Models[a]	Calibration		Prediction		Size
	R	RMSECV (mg dl^{-1})	*R*	RMSEP (mg dl^{-1})	
PLS (4)	0.87	13.17	0.85	8.01	1223
PLS (4), smoothing 3 pts	0.84	13.46	0.93	6.32	1221
PLS (4), smoothing 5 pts	0.80	14.78	0.96	5.50	1219
PLS (4) First deriv. 3 pts	0.92	20.36	0.17	19.47	1221
PLS (4) First deriv. 5 pts	0.87	21.36	0.36	14.21	1219
PLS (3) First deriv. 7 pts	0.80	15.67	0.20	14.77	1217
PLS (3) Sec. deriv. 5 pts	0.88	26.00	0.83	12.14	1219
iPLS (3)	0.99	13.80	0.24	12.49	122
iPLS (3)	0.82	14.06	0.30	16.31	400
iPLS (4)	0.87	13.26	0.47	16.13	600
PLS-SPA (3)	0.80	13.46	0.11	12.02	17
PLS-GA (4)	0.90	9.63	0.84	10.80	321
PLS (4)[1]	0.90	12.11	0.97	6.08	1221

[a] Pts, points; deriv., derivative; sec., second.; [1] one application of outliers detection.

3.2. Triglycerides

Table 2 shows the results for the analysis of triglycerides in rat plasma. In general, better values were obtained for the RMSEP with smoothed data (3 pts), when compared with the models obtained with original raw or preprocessed data. For the suitable NIR spectral region (1105.05–1892.3 nm and 1997.27–2461.97 nm) the RMSEP values obtained for all of the models were similar, except for the PLS (3) first derivative (3 pts), PLS (1) first derivative (7 pts) and PLS (2) second derivative (5 pts) models. An *F*-test was performed for all of the PLS models using the prediction set, and the results showed no significant differences at the 95% confidence level among the best model, the PLS (3) smoothing (3 pts) model, and the other models, except for the three models already mentioned that presented the highest RMSEP values (30.80–37.30 mg dl^{-1}). For this parameter, variable selection using the iPLS, SPA and GA algorithms produced good results. For example, according to Table 2, for the PLS-SPA (3) model, a correlation coefficient of 0.91 was obtained for the prediction set using only seventeen spectral variables, and a RMSEP was obtained with a value under of the reproducibility value of the BIOCLIN (Brazil) reference method (24.7 mg dl^{-1}) [1]. The best variable selection algorithm for this parameter was found to be the iPLS algorithm. When 122 spectral variables were used to build the iPLS (3) model, a correlation coefficient for the prediction set of 0.96 was found; this value was close to that obtained for the best model (0.96). This model presented a higher RMSEP value, though it was still below that of the reference error.

Outlier detection was applied to the best model, but no improvement of the results was observed. To build the PLS (3)[1] model, three samples of the calibration set were excluded. After this selection, the same PLS (3)[1] was submitted to a second outlier detection, resulting in one outlier identified in the calibration set and another outlier in the prediction set. These two samples were excluded, and a new model PLS (3)[2] was built.

Fig. 3 shows the correlation between the measured values for triglycerides in rat plasma and those predicted by the best model, PLS (3) smoothing (3 pts), based on NIR spectroscopy. A *t*-test was performed and showed a significant difference (95% confidence level) between this model and the reference method. Because this result was not satisfactory, the *t*-test was applied at a 96% confidence level, resulting in no significant difference when compared to the reference method. The model provided a RMSEP value that was similar to the one observed by Filho et al. (20 mg dl^{-1}) [19].

3.3. Cholesterol

Table 3 shows the results for the cholesterol models. In general, the best values were obtained for the RMSEP with derivative data (3 pts), instead of original raw data or preprocessed data, in the spectral region from 1105.05 to 1892.3 nm and 1997.27 to 2461.97 nm. For all of the fourteen models presented in Table 3, the RMSEP values were below the reproducibility value of the BIOCLIN (Brazil) reference method (11.4 mg dl^{-1}). However, the correlation coefficients for the prediction set ranged from −0.62

Table 2
Results for calibration and the external validation set for triglycerides: root mean square error of cross validation (RMSECV) and prediction (RMSEP), correlation coefficient (*R*) and the number of used spectral variables (Size). The number of PLS factors or in PLS, iPLS, PLS-SPA and PLS-GA models are represented in parentheses.

Models[a]	Calibration		Prediction		Size
	R	RMSECV (mg dl^{-1})	*R*	RMSEP (mg dl^{-1})	
PLS (3)	0.77	26.16	0.94	21.58	1223
PLS (3), smoothing 3 pts	0.80	25.75	0.96	16.07	1221
PLS (3), smoothing 5 pts	0.78	24.54	0.94	16.75	1219
PLS (3) First deriv. 3 pts	0.89	34.25	0.40	35.75	1221
PLS (3) First deriv. 5 pts	0.78	38.84	0.80	21.34	1219
PLS (1) First deriv. 7 pts	0.56	28.41	0.75	30.79	1217
PLS (2) Sec. deriv. 5 pts	0.61	32.19	0.41	37.29	1219
iPLS (3)	0.75	27.03	0.96	21.19	122
iPLS (3)	0.76	25.90	0.93	26.00	400
iPLS (4)	0.74	25.74	0.94	24.83	600
PLS-SPA (3)	0.80	28.83	0.91	20.62	17
PLS-GA (3)	0.73	25.62	0.90	20.64	357
PLS (3)[1]	0.81	24.18	0.91	20.91	1221
PLS (3)[2]	0.83	23.06	0.93	15.76	1221

[a] Pts, points; deriv., derivative; sec., second.; [1] one application of outliers detection; [2] two applications of outliers detection.

Table 3
Results for calibration and the external validation set for HDL: root mean square error of cross validation (RMSECV) and prediction (RMSEP), correlation coefficient (R) and the number of used spectral variables (Size). The number of PLS factors or in PLS, iPLS, PLS-SPA and PLS-GA models are represented in parentheses.

Models[a]	Calibration		Prediction		Size
	R	RMSECV (mg dl^{-1})	R	RMSEP (mg dl^{-1})	
PLS (4)	0.88	6.22	0.05	8.24	1223
PLS (4), smoothing 3 pts	0.87	5.91	0.03	8.60	1221
PLS (4), smoothing 5 pts	0.87	5.76	0.02	8.77	1219
PLS (4) First deriv. 3 pts	0.87	10.51	0.65	4.56	1221
PLS (2) First deriv. 5 pts	0.76	8.04	-0.35	7.64	1219
PLS (3) First deriv. 7 pts	0.80	9.62	-0.01	7.39	1217
PLS (2) Sec. deriv. 5 pts	0.64	8.92	0.64	4.63	1219
iPLS (3)	0.87	5.75	-0.62	8.00	122
iPLS (3)	0.75	7.51	0.06	7.43	400
iPLS (4)	0.72	7.92	0.24	6.83	600
PLS-SPA (4)	0.77	13.80	0.51	6.30	17
PLS-GA (4)	0.98	3.49	0.81	3.31	334
PLS (4)[1]	0.98	3.75	0.95	1.66	334
PLS (4)[2]	0.99	4.60	0.98	2.03	334

[a] Pts, points; deriv., derivative; sec., second.; [1] one application of outliers detection; [2] two applications of outliers detection.

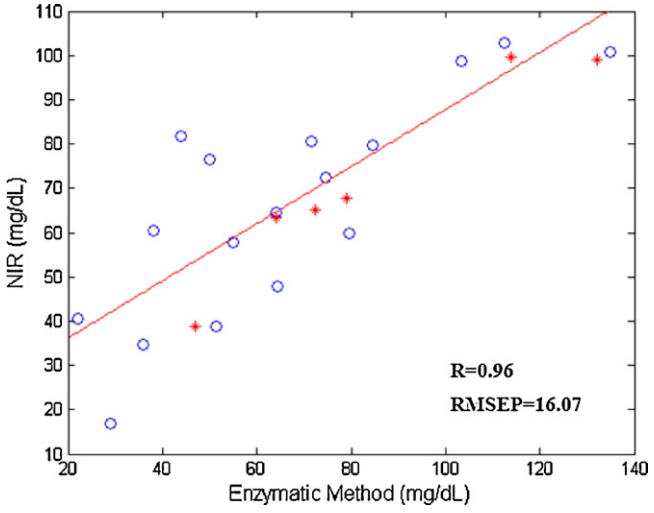

Fig. 3. Correlation among the measured and the predicted values for both calibration and prediction sets for triglycerides in rat blood plasma for the best model, PLS (3) smoothing 3 pts, by NIR spectroscopy. (○) calibration set; (✱) validation set.

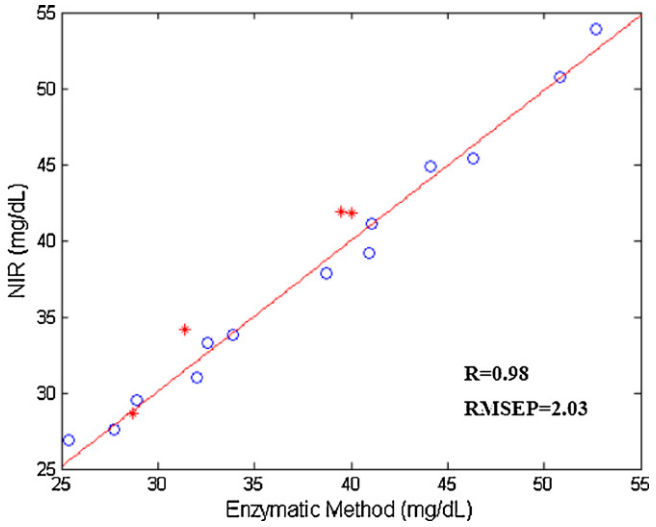

Fig. 4. Correlation among the measured and the predicted values for both calibration and prediction sets for HDL in rat blood plasma for the best model, PLS (4)^2, by NIR spectroscopy. (○) calibration set; (✱) validation set.

to 0.98, indicating that some models were unsatisfactory. For the specified NIR spectral region, the RMSEP values were similar for several models: the PLS (4) first derivative (3 pts), the PLS (2) second derivative (5 pts), the iPLS (4) using 600 spectral variables, the PLS-GA (4), the PLS (4)^1 after one application of outlier detection and the PLS (4)^2 after two applications of outlier detection. An F test was performed on these models using their prediction sets, and the results shows no significant differences (95% confidence level) among them. Another important issue for this parameter is variable selection. Using the GA method to choose the main spectral variables for use in the models, the correlation coefficient obtained for the prediction set was 0.81, and the RMSEP was 3.31 (334 spectral variables). This model was submitted to outlier detection, and two samples of the calibration set and one sample of the prediction set were excluded to give a new model, the PLS(4)^1. This latter model generated a correlation coefficient for the prediction set of 0.95 and a RMSEP of 1.66. Then, the PLS (4)^1 model was submitted to an additional round of outlier detection, and this excluded three more samples (two of the calibration set and one of the prediction set) in addition to the previous three. For the PLS (4)^2 model, (two more samples of the calibration set were excluded) the lowest RMSECV and RMSEP values were 4.60 and 2.03, respectively. The correlation coefficient for the validation set, obtained using 4 latent variables, was 0.98. Fig. 4 shows the correlation between the measured values of HDL in rat plasma and those predicted from NIR spectroscopy by the PLS (4)^2 model.

4. Conclusions

In this work, it was demonstrated that it is possible to obtain promising results considering the concentration range used in the calibration/validation sets (The RMSEP values for glucose, triglycerides and HDL found in this work were 6.08, 16.07 and 2.03 mg dl^{-1}, respectively) for the quantitative analyses of glucose, triglycerides and cholesterol in the blood plasma of rats with NIR spectroscopy and multivariate regression methods. The optimal combination of the informative regions from the iPLS, GA and SPA models directly improved the predicted values of triglycerides concentrations in blood plasma. For glucose and cholesterol, the models built using a GA method showed better results than those obtained using SPA or iPLS algorithms. For comparison, PLS models built by Petter el al. to HDL (in serum human samples by NIR) showed errors smaller than 10% [18]. In this work errors were found for HDL as being 4.9%. Furthermore, the relative errors found (PLS models) in this work for glucose and triglycerides were 4.1% and 13.4%, respectively. An important aspect of this approach is that

no reagents are necessary except for the aqueous solutions used to clean and rinse the optical cell. In addition to increasing the speed of the analysis, the proposed method may also provide a reduction in waste production compared to traditional methods.

Acknowledgements

The authors wish to thank the CAPES for a fellowship for A.C.O. Neves, the Programa de Pós-Graduação em Química (PPGQ) da UFRN and the Laboratório de Farmacologia da UFRN for providing the blood samples.

References

[1] J.A. Dantas, C.R. Ambiel, R.K.N. Cuman, S. Baroni, C.A.B. Amado, Valores de referência de alguns parâmetros fisiológicos de ratos do Biotério Central da Universidade Estadual de Maringá, Estado do Paraná, Acta Sci. Health Sci. 28 (2006) 165–170.
[2] M.R.V. Santos, V.H. Souza, I.A.C. Menezes, J.L. Bitencourt, J.M. Resende-Neto, A.S. Barreto, F.C. Andrade, R.M. Marçal, F. Teixeira-Silva, L.J. Quintans-Júnior, A.P.O. Barbosa, Parâmetros bioquímicos, fisiológicos e morfológicos de ratos (Rattus novergicus linhagem Wistar) produzidos pelo Biotério Central da Universidade Federal de Sergipe, Scientia Plena 6 (2010) 1–6.
[3] D.S.C.N. Pinheiro, C.B.F. Favali, A.A.S. Filho, P.V. Costa, Parâmetros Hematológicos de Camundongos e ratos do Biotério Central da Universidade Federal do Ceará, Bol. Inf. Cobea 3 (1997) 6–9.
[4] L.E. Lillie, N.J. Temple, L.Z. Florence, Reference values for young normal Sprague-Dawley rats: weight gain, hematology and clinical chemistry, Hum. Exp. Toxicol. 15 (1996) 612–616.
[5] S.T. Wolford, R.A. Schroer, F.X. Gohs, P.P. Gallo, M. Brodeck, H.B. Falk, R. Ruhren, Reference range database for serum chemistry and hematology values in laboratory animals, J. Toxicol. Environ. Health 18 (1986) 161–188.
[6] A.C.O. Neves, G.M. Soares, S.C. de Morais, F.S.L. da Costa, D.L. Porto, K.M.G. de Lima, Dissolution testing of isoniazid, rifampicin, pyrazinamide and ethambutol tablets using near-infrared spectroscopy (NIRS) and multivariate calibration, J. Pharm. Biomed. Anal. 57 (2012) 115–119.
[7] M.R.C. Inacio, M.F. Moura, K.M.G. de Lima, Classification and determination of total protein in milk powder using near infrared reflectance spectrometry and the successive projections algorithm for variable selection, Vib. Spectrosc. 57 (2011) 342–345.
[8] P. Geladi, H. Bärring, E. Dåbakk E, J. Trygg, H. Antti, S. Wold, B. Karlberg, Calibration transfers for predicting lake-water pH from near infrared spectra of lake sediments, J. Near Infrared Spectrosc. 7 (1999) 251–264.
[9] A. Sakudo, Y.H. Kato, H. Kuratsune, K. Ikuta, Non-invasive prediction of hematocrit levels by portable visible and near-infrared spectrophotometer, Clin. Chim. Acta 408 (2009) 123–127.
[10] K.H. Hazen, M.A. Arnold, G.W. Small, Measurement of glucose and other analytes in undiluted human serum with near-infrared transmission spectroscopy, Anal. Chim. Acta 371 (1998) 255–267.
[11] H.M. Heise, A. Bittner, Multivariate calibration for near-infrared spectroscopic assays of blood substrates in human plasma based on variable selection using PLS-regression vector choices, Fresenius J. Anal. Chem. 362 (1998) 141–147.
[12] S. Kasemsunram, Y.P. Du, K. Murayama, M. Huehne, Y. Ozaki, Near-infrared spectroscopic determination of human serum albumin, γ-glubulin, and glucose in a control serum solution with searching combination moving window partial least squares, Anal. Chim. Acta 512 (2004) 223–230.
[13] A. Bittner, R. Marbach, H.M. Heise, Multivariate calibration for protein, cholesterol and triglycerides in human plasma using short-wave near-infrared spectrometry, J. Mol. Struct. 349 (1995) 341–344.
[14] J.L. Pezzaniti, T. Jeng, L. McDowell, G.M. Oosta, Preliminary investigation of near-infrared spectroscopic measurements of urea, creatinine, glucose, protein, and ketone in urine, Clin. Biochem. 34 (2001) 239–246.
[15] S. Zhang, B.R. Soller, S. Kaur, K. Perras, T.J.V. Salm, Investigation of noninvasive in vivo blood hematocrit measurement using NIR reflectance spectroscopy and partial least-squares regression, Appl. Spectrosc. 54 (2000) 294–299.
[16] N. Kang, S. Kasemsumran, Y.W. Woo, H. Kim, Y. Ozaki, Optimization of informative spectral regions for the quantification of cholesterol, glucose and urea in control serum solutions using searching combination moving window partial least squares regression method with near infrared spectroscopy, Chemom. Intell. Lab. Syst. 82 (2006) 90–96.
[17] S. Kasemsumran, Y.P. Du, K. Maruo, Y. Ozaki, Improvement of partial least squares models for in vitro and in vivo glucose quantifications by using near-infrared spectroscopy and searching combination moving window partial least squares, Chemom. Intell. Lab. Syst. 82 (2006) 97–103.
[18] C.H. Petter, N. Heigl, R. Bakry, G.K. Bonn, A. Ritsch, C.W. Huck, Quantification of low-density and high-density lipoproteins in human serum by material enhanced infrared spectroscopy (MEIRS), Curr. Med. Chem. 16 (2009) 4601–4608.
[19] P.A.C. Filho, R.J. Poppi, Determination of triglycerides in human plasma using near-infrared spectroscopy and multivariate calibration methods, Anal. Chim. Acta 446 (2001) 39–47.
[20] L. Norgaard, A. Saudland, J. Wagner, J.P. Nielsen, L. Munck, S.B. Engelsen, Interval partial least-squares regression (iPLS): a comparative chemometric study with an example from near-infrared spectroscopy, Appl. Spectrosc. 54 (2000) 413–419.
[21] M. Ferrand, B. Huquet, S. Barbey, F. Barillet, F. Faucon, H. Larroque, O. Leray, J.M. Trommenschlager, Determination of fatty acid profile in cow's milk using mid-infrared spectrometry: Interest of applying a variable selection by genetic algorithms before a PLS regression, Chemom. Intell. Lab. Syst. 106 (2011) 183–189.
[22] M.C.U. Araujo, T.C.B. Saldanha, R.K.H. Galvao, T. Yoneyama, H.C. Chame, V. Visani, The successive projections algorithm for variable selection in spectroscopic multicomponent analysis, Chemom. Intell. Lab. Syst. 57 (2001) 65–73.
[23] P. Valderrama, J.W.B. Braga, R.J. Poppi, Variable selection, outlier detection, and figures of merit estimation in a partial least-squares regression multivariate calibration model. A case study for the determination of quality parameters in the alcohol industry by near-infrared spectroscopy, J. Agric. Food Chem. 55 (2007) 8331–8338.
[24] C. Arich, A. Gouby, C. Bengler, J.L. Ardilouze, A. Dubois, P. Joubert, S. Hansel, C. Janbon, S. Fabre, Comparison of the efficacy of cefotaxime alone and the combination cefazolin–tobramycin in the treatment of enterobacterial septicemia, Pathobiology 35 (1987) 613–615.
[25] M. Joshi, J. Bernstein, J. Solomkin, B.A. Wester, O. Kuye, Piperacillin/tazobactam plus tobramycin versus ceftazidime plus tobramycin for the treatment of patients with nosocomial lower respiratory tract infection. Piperacillin/tazobactam Nosocomial Pneumonia Study Group, J. Antimicrob. Chemother. 43 (1999) 389–397.
[26] R.W. Kennard, L.A. Stone, Computer aided design of experiments, Technometrics 111 (1969) 137–148.
[27] J.P. Fillastre, J. Hemet, P. Tulkens, J.P. Morin, G. Viotte, B. Olier, M. Godin, Comparative nephrotoxicity of four aminoglycosides: biochemical and ultrastructural modifications of lysosomes, Adv. Nephrol. Necker Hosp. 12 (1983) 253–275.
[28] A.M. Lerner, M.P. Reyes, L.A. Cone, D.C. Blair, W. Jansen, G.E. Wright, R. Lorber, Randomised, controlled trial of the comparative efficacy, auditory toxicity, and nephrotoxicity of tobramycin and netilmicin, Lancet 1 (1983) 1123–1126.

Journal of Pharmaceutical and Biomedical Analysis xxx (2012) xxx–xxx

Contents lists available at SciVerse ScienceDirect

Journal of Pharmaceutical and Biomedical Analysis

journal homepage: www.elsevier.com/locate/jpba

Short communication

Simultaneous determination of adenine nucleotides, creatine phosphate and creatine in rat liver by high performance liquid chromatography–electrospray ionization-tandem mass spectrometry

Yang Jiang[a], Chengjun Sun[a], Xueqin Ding[b], Ding Yuan[c], Kefei Chen[c], Bo Gao[b], Yi Chen[d], Aimin Sun[b,*]

[a] West China School of Public Health, Sichuan University, No. 17, Section 3, South Renmin Road, Chengdu, Sichuan 610041, People's Republic of China
[b] Analytical & Testing Center, Sichuan University, No. 29, Wangjiang Road, Chengdu, Sichuan 610064, People's Republic of China
[c] Regenerative Medicine Research Center, West China Hospital, Chengdu, Sichuan 610041, People's Republic of China
[d] Laboratory of Aging and Geriatrics Research, West China Hospital, Chengdu, Sichuan 610041, People's Republic of China

ARTICLE INFO

Article history:
Received 1 December 2011
Received in revised form 13 March 2012
Accepted 14 March 2012
Available online xxx

Keywords:
Adenine nucleotides
Creatine
Creatine phosphate
HPLC–ESI-MS/MS
Rat liver

ABSTRACT

A high performance liquid chromatography–electrospray ionization-tandem mass spectrometric method (HPLC–ESI-MS/MS) was developed for simultaneous determination of adenosine 5′-triphosphate (ATP), adenosine 5′-diphosphate (ADP), adenosine 5′-monophosphate (AMP), creatine phosphate (CP), and creatine in rat liver. After extraction with pre-cooled (4 °C) methanol/water (1:1, v/v), the analytes were separated on a porous graphitic carbon (Hypercarb) column (2.1 mm × 150 mm, 5 μm) using a programmed gradient elution with a mobile phase consisting of 2 mmol/L ammonium acetate in water and 2 mmol/L ammonium acetate in acetonitrile (pH = 10.0). The analytes were detected in a way of multiple reaction monitoring (MRM) under negative scan mode by a triple quadrupole mass spectrometer with electrospray ionization (ESI). An external calibration method with linear ranges from 10 to 5000 ng/mL for the five target compounds was used for quantification with a correlation coefficients ≥ 0.9973. The limits of detection and limits of quantification for all analytes were in ranges from 0.50 to 1.5 ng/mL and 1.6 to 0.5 ng/mL, respectively. The average recoveries spiked in three levels were from 77.2% to 102% and precisions expressed in RSDs were from 0.2% to 4.8%. The established method was successfully applied to determination of ATP, ADP, AMP, CP and creatine in liver tissue.

© 2012 Published by Elsevier B.V.

1. Introduction

Adenosine 5′-triphosphate (ATP), adenosine 5′-diphosphate (ADP) and creatine phosphate (CP) are important biomolecules for energy storage and conversion in tissues. Molecules of 5′-monophosphate (AMP) and creatine are involved in metabolism of these energy biomolecules. Liver is one of the most complex and metabolically active organs and performs many functions, such as biosyntheses and detoxification in which a large amount of energy molecules are needed. Concomitantly, liver cells are rich in active mitochondria that can provide abundant energy for cellular metabolism. In steatosis, energy metabolism of hepatocyte mitochondrial is impaired [1], implying alterations in energy biomolecules. Therefore, simultaneous quantification of adenine nucleotides, creatine phosphate and creatine in liver tissue is of great importance for understanding the energy state and evaluating the function of liver cells.

High-performance liquid chromatography (HPLC) has been widely used for determination of the aforementioned compounds in biological samples [2,3]. Considering high polarity and non-volatility of the analytes, as well as background interference of biological matrix, several HPLC–MS methods have been developed for analysis of the energy-related biomolecules [4–8]. However, these methods only focused on the determination of adenine nucleotides or creatine and in some cases [4,5] ion-pairing reagents were added to mobile phase, which could result in contamination of ion source and frequent cleaning was required. Besides, the sample matrixes of these methods were mainly kidney tissues [4], cells [5,6] urine [7]. Until now, there seems no LC–MS/MS method in multiple reaction monitoring (MRM) mode reported on simultaneous determination of adenine nucleotides, CP and creatine in liver tissue.

In this study, a simple and reliable HPLC–ESI-MS/MS method was developed for the first time for simultaneous determination of ATP, ADP, AMP, CP and creatine. Using porous graphitic carbon (PGC, Hypercarb) column, ion-pairing reagents were avoided and reasonable retention time for the analytes was achieved. To ensure high specificity, quantification was performed in MRM

* Corresponding author.
E-mail address: sunaiminsc@sina.com (A. Sun).

0731-7085/$ – see front matter © 2012 Published by Elsevier B.V.
doi:10.1016/j.jpba.2012.03.027

Please cite this article in press as: Y. Jiang, et al., Simultaneous determination of adenine nucleotides, creatine phosphate and creatine in rat liver by high performance liquid chromatography–electrospray ionization-tandem mass spectrometry, J. Pharm. Biomed. Anal. (2012), doi:10.1016/j.jpba.2012.03.027

mode. Moreover, methanol–water solution was used for sample extraction, and the procedure was rapid, simple as well as compatible with ESI-MS/MS analysis compared with the common perchloric acid-based extraction [4,6]. The method was successfully applied to analysis of ATP, ADP, AMP, CP and creatine in liver tissue of 8 normal rats. In addition, this assay is potentially useful in studying energy metabolism of fatty liver that is used as marginal donor liver, which is of great significance to further research on human liver transplantation.

2. Materials and methods

2.1. Chemicals and reagents

Standards of ATP, ADP, AMP, CP and creatine were purchased from Sigma (St. Louis, MO, USA). HPLC-grade acetonitrile (ACN) and methanol were purchased from Honeywell Burdick & Jackson (Muskegon, MI, USA). Other chemicals used were of analytical grade. Water used in the experiment was obtained from a Milli-Q system (18.2 MΩ cm, Millipore, Bedford, MA, USA).

2.2. Instrumentation

The HPLC–MS/MS system, Surveyor Plus HPLC System and TSQ Quantum Ultra Mass Spectrometer (Thermo Fisher Scientific, USA), is equipped with an autosampler, ESI electrospray ionization source, and TSQ mass analyzer. LCQUAN quantitative software was applied for data acquisition and processing. Other instruments used in sample preparation included a high speed refrigerated centrifuge (HC-2518 R, Zonkia, Hefei, China), a vacuum freeze dryer (Labconco, USA), a vortex shaker (QL-861, Kylin-Bell, Haimen, China), and a pH meter (PHS-3C, SPSIC, Shanghai, China).

2.3. Chromatographic conditions

The chromatographic separation was performed on a Hypercarb column (2.1 mm × 150 mm, 5 μm) from Thermo (Thermo Fisher Scientific, USA). The standards and samples were separated using a mobile phase consisting of 2 mmol/L ammonium acetate in water (solvent A) and 2 mmol/L ammonium acetate in acetonitrile (solvent B), which were both adjusted with ammonia to pH 10.0. The gradient elution program was: 0–2 min, 98% A; 2–4 min, 98–85% A; 4–10 min, 85% A; 10–13 min, 50% A; and then back to 98% A to reconditioning the column for 7 min. The flow rate of the mobile phase was 200 μL/min, and the column temperature was maintained at 35 °C.

2.4. Mass spectrometric parameters

ESI ionization was performed in the negative ion mode with a spray voltage of 3000 V. Sheath gas pressure and aux gas pressure were 40 arb and 10 arb, respectively. Capillary temperature was set at 350 °C. Quantification was performed in the multiple reaction monitoring (MRM) mode. The optimized parameters, such as quantification and confirmation ion transitions, collision energy (CE), tube lens for each compound, were summarized in Table 1.

2.5. Preparation of standard solutions

Proper amounts of ATP, ADP, AMP, CP and creatine were accurately weighed and dissolved in water to prepare stock standard solutions at 1.0 mg/mL. Mixed working standard solution was prepared by dilution of the stock standards solution in methanol–water (1:1, v/v). Then mixed working standard solution was serially diluted to prepare the concentration series of 10, 50, 250, 500, 2000 and 5000 ng/mL. Stock standard solutions were stable for one week stored at −20 °C, and mixed working standard solution was freshly prepared prior to use.

Table 1
Multiple reaction monitoring MRM transitions for quantification of the five target compounds.

Analyte	Precursor	Product	Collision energy (V)	Tube lens	Retention time (min)
ATP	506	159[a]	35	113	7.42
		177[b]	24		
		408[b]	22		
ADP	426	134[b]	24	97	7.33
		159[b]	24		
		328[a]	19		
AMP	346	79[a]	36	95	7.23
		134[b]	35		
		211[b]	15		
CP	210	79[a]	35	76	1.74
		97[b]	10		
		121[b]	15		
Creatine	130	59[b]	13	63	2.62
		88[a]	13		
		112[b]	14		

[a] Quantitation ion.
[b] Confirmation ion.

2.6. Sample preparation

The freeze-dried (−70 °C for 36 h) samples of rat liver were quickly ground and blended in a mortar. An aliquote of 10 mg of powdered liver tissue was placed into a 1.5 mL scaled Eppendorf tube containing 500 μL pre-cooled (4 °C) methanol to precipitate proteins by vortex shaking for 1 min. And then 500 μL pre-cooled (4 °C) water was immediately added to extract the analytes by vortex shaking for 3 min. After centrifugation of the extract at −10 °C for 20 min at 16,000 × *g*, the supernatant was stored at −20 °C prior to the LC–MS/MS analysis.

3. Results and discussion

3.1. Optimization of chromatographic conditions

3.1.1. Selection of column for separation

Several different chromatographic columns were tested, including Hypersil Gold C_{18} column (150 mm × 2.1 mm, 5 μm) from Thermo, Ultra C_8 column (15 mm × 2.1 mm, 5 μm) from Restek, Spursil C18-EP (150 mm × 2.1 mm, 3 μm) from Dikma, Hypercarb column (100 mm × 4.6 mm, 5 μm) and Hypercarb column (150 mm × 2.1 mm, 5 μm) from Thermo. Due to their high polarity, all the target compounds were weakly retained on these columns except Hypercarb column. Wang et al. also found that various reversed-phase columns could not provide reasonable retention time for adenine nucleotides [6]. The retention mechanism of porous graphitic carbon (PGC, Hypercarb) is different from conventional silica-bonded stationary phase, which can provide remarkable retention and selectivity for polar compounds. In addition, Hypercarb column is stable throughout the pH range of 0–14. Moreover, HPLC with PGC column would be more compatible for MS detection because the ion source contamination from buffer salts or ion-pairing agents could be avoided. Therefore, Hypercarb column was selected in this study. Fig. 1 shows the LC–MS/MS chromatogram of a standard mixture of the five target compounds in MRM mode.

Please cite this article in press as: Y. Jiang, et al., Simultaneous determination of adenine nucleotides, creatine phosphate and creatine in rat liver by high performance liquid chromatography–electrospray ionization-tandem mass spectrometry, J. Pharm. Biomed. Anal. (2012), doi:10.1016/j.jpba.2012.03.027

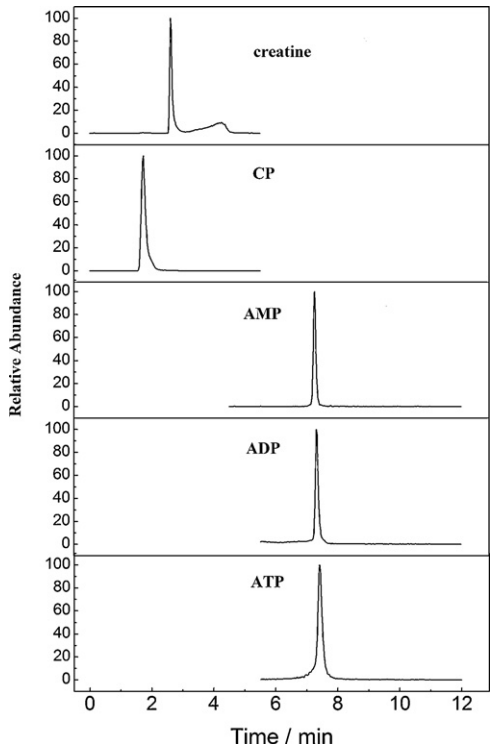

Fig. 1. The LC–MS/MS chromatograms of a standard mixture of the five target compounds (2000 ng/mL) in MRM mode.

3.1.2. Selection of mobile phase for separation

The composition of the mobile phase was optimized through several steps on the Hypercarb column. Firstly, the effect of methanol and acetonitrile as organic mobile phase using the same LC gradient and ammonium acetate concentration was investigated. There was no elution for the analytes in 30 min when substituting methanol for acetonitrile. Xing et al. also reported that acetonitrile was much more effective in displacing adenine nucleotides from the PGC column and exhibited a stronger elution capability than methanol [8]. Therefore, acetonitrile was selected for further experiments in this study. Secondly, based on the literatures [6,8], different concentrations of ammonium acetate (2, 5 and 10 mmol/L) were tested. It was found that the increase of salt concentration resulted in suppression of MS signal intensity, because of salt precipitation in ion source and ion transportation tube. Hence, 2 mmol/L ammonium acetate was added in the mobile phase, and reasonable retention and separation as well as good sensitivity and reproducibility were obtained. Thirdly, the pH of the mobile phase was also examined using acetic acid and ammonia for adjusting the pH of the mobile phase. In the preliminary experiments, it was found that the ESI-MS/MS intensity of adenine nucleotides considerably decreased when the pH was lower than 8. Hence, the influence of the mobile phase pH on the detection sensitivity of the analytes was investigated over the pH range of 8–11. With the increase of pH, the signal intensity of ESI-MS/MS for ATP and ADP was greatly enhanced, while the intensity of AMP and CP was not. However, there was significant decrease for creatine. By comprehensive consideration, the mobile phase's pH was adjusted to 10.0 for the analysis of the target compounds.

3.2. Optimization of mass spectrometric conditions

Due to high polarity of the analytes, the ESI ion source was selected. The mass spectrometric conditions were optimized for each compound by continuously infusing corresponding standard solutions at a flow rate of 10 μL/min using a syringe infusion pump. During the method development, MS parameters in both positive and negative ionization modes were tuned for ATP, ADP, AMP, CP and creatine. However, it was found that the response was much higher in the negative ionization mode for ATP, ADP, AMP and CP than that in the positive mode due to their acidic nature. Therefore, precursor ions and product ions were detected in ESI negative mode and quantification was performed in MRM mode. Fig. 2 shows chemical structures and full scan product ion of precursor ions of ATP, ADP, AMP, CP and creatine. Three product ions were monitored, one for quantification and the other two for confirmation. The optimized MS parameters are described in Section 2.4.

3.3. Sample extraction

In the previous literatures, perchloric acid [4,6], acetonitrile/water [9] and methanol [5] were used for extraction. Considering good water solubility of the analytes, we evaluated different solvents for the extraction, including 0.42 mol/L perchloric acid, acetonitrile:water (1:1), methanol:water (7:3) and methanol:water (1:1). For the perchloric acid extract, we found that the pH of the extract should be carefully monitored at 7 after KOH solution was used to neutralize perchloric acid, otherwise redundant acid or base would be not compatible with MS system and further interfere with the detection. Cordell et al. [5] reported that the perchloric acid extract was not compatible with LC–MS because of the presence of a precipitate when evaporating the neutralized samples. Hence, we tested several organic solvents that can precipitate proteins. The recoveries for the acetonitrile:water (1:1) extraction varied from 10% to 33%. Methanol:water (7:3) system demonstrated a lower than 20% recovery for ATP and a lower than 50% recovery for CP. With the proportion of water increase to 50%, the recoveries for the five target compounds varied from 68.7% to 87.0%. Therefore, methanol:water (1:1, v/v) was used for extraction, which was easy to prepare and more MS-compatible, compared with the perchloric acid-based extraction.

3.4. Method validation

3.4.1. Linearity, limit of detection and limit of quantification

Table 2 shows the equations of the external standard curves, correlation coefficients, linear range, limits of detection (LODs), and limits of quantification (LOQs) for the five target compounds. Good linearities ($r \geq 0.9973$) were obtained for all the five analytes. Here, the LODs and LOQs were defined as the concentration with a signal-to-noise ratio of 3 and 10, respectively.

3.4.2. Accuracy and precision

Accuracy of the method was evaluated by the recoveries of spiked liver tissue samples and precision was evaluated using relative standard deviations (RSDs). Three levels of mixture standard solutions were added to each sample and then analyzed using the established method. Each level was performed in six replicates. The results are shown in Table 3. In the three spiked levels, the averaged recoveries of this method were from 77.2% to 102%. The RSDs of method ranged from 0.2% to 4.8%.

3.5. Application of the method

This method has been successfully applied to determination of ATP, ADP, AMP, CP and creatine in liver tissue from eight normal rats. The collection of rat liver tissues was conducted in accordance with the experimental protocols approved by the Experimental Animal Center of Sichuan University. The results are summarized in Table 4 and a typical LC–MS/MS chromatogram from rat liver is displayed in Fig. 3. In the previous studies, HPLC method was

Please cite this article in press as: Y. Jiang, et al., Simultaneous determination of adenine nucleotides, creatine phosphate and creatine in rat liver by high performance liquid chromatography–electrospray ionization-tandem mass spectrometry, J. Pharm. Biomed. Anal. (2012), doi:10.1016/j.jpba.2012.03.027

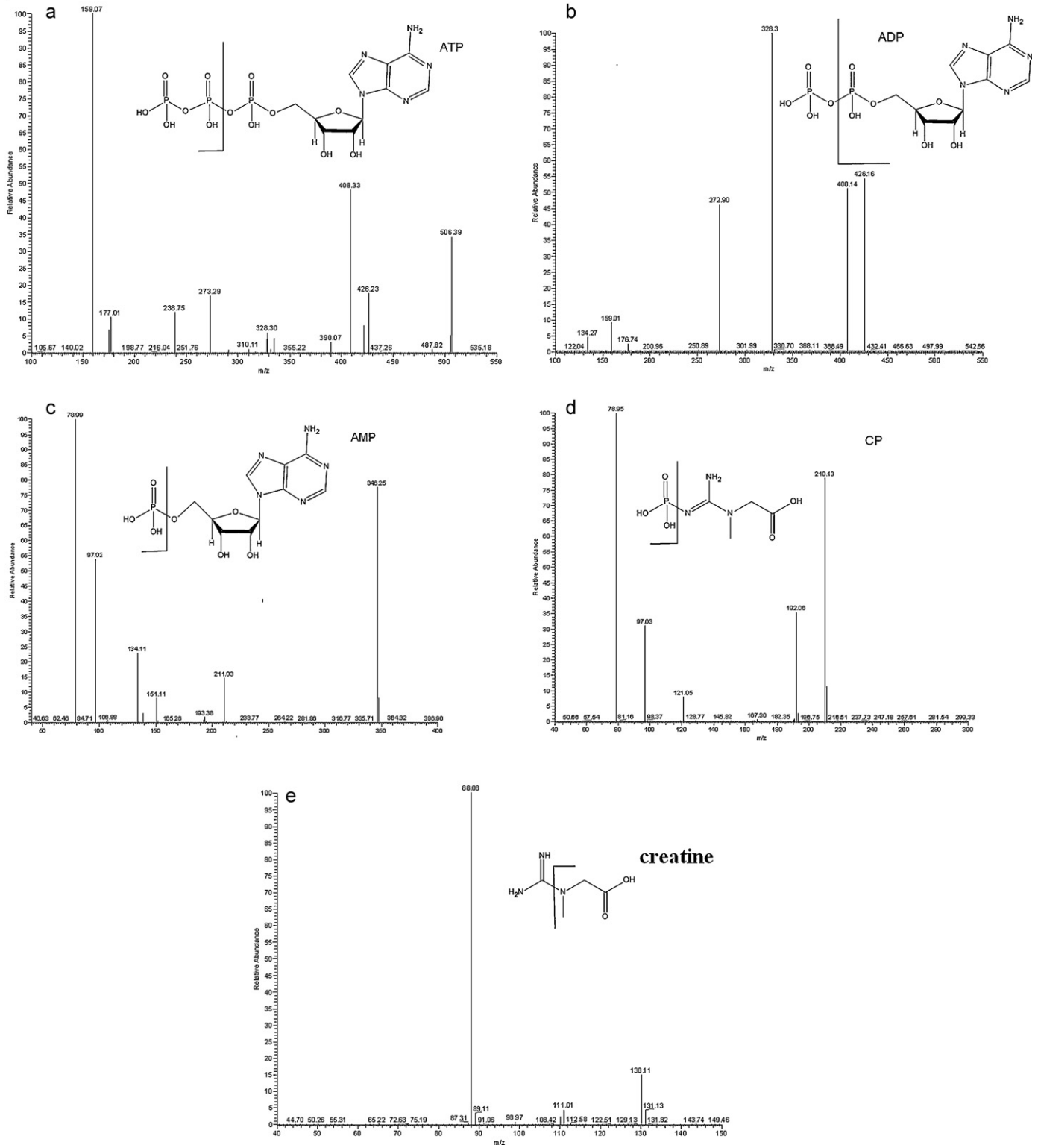

Fig. 2. Chemical structures and full scan product ion of precursor ions of ATP (a), ADP (b), AMP (c), CP (d) and creatine (e).

Table 2
Linear regression, LODs and LOQs for the five target compounds.

Analyte	Calibration curve	r	Linear range (ng/mL)	LOD (ng/mL)	LOQ (ng/mL)
ATP	$y = 259.4x - 2343$	0.9995	10–5000	0.5	1.6
ADP	$y = 338.5x - 1694$	0.9992	10–5000	0.5	1.6
AMP	$y = 369.0x - 516.9$	0.9999	10–5000	0.5	1.6
CP	$y = 214.9x - 2058$	0.9982	10–5000	1.0	3.3
Creatine	$y = 712.6x - 495.4$	0.9973	10–5000	1.5	5.0

Please cite this article in press as: Y. Jiang, et al., Simultaneous determination of adenine nucleotides, creatine phosphate and creatine in rat liver by high performance liquid chromatography–electrospray ionization-tandem mass spectrometry, J. Pharm. Biomed. Anal. (2012), doi:10.1016/j.jpba.2012.03.027

Table 3
Accuracy and precision of the method for the five target compounds ($n = 6$).

Analyte	Background (ng/mL)	Spiked (ng/mL)	Mean found (ng/mL)	Recovery (%)	RSD (%)
ATP	706.5	250	240.2	96.1	2.6
		500	488.3	97.7	2.2
		1000	1011	101	2.4
ADP	1132	250	242.9	97.1	4.8
		500	488.9	97.8	3.3
		1000	1006	101	2.4
AMP	445.8	250	244.1	97.6	3.9
		500	501.3	100	2.4
		1000	984.2	98.4	2.7
CP	69.3	200	156.2	78.1	1.4
		500	386.2	77.2	0.2
		1000	810.7	81.1	0.3
Creatine	188.5	250	255.5	102	2.1
		500	495.9	99.2	1.3
		1000	983.7	98.4	1.4

Table 4
The analytical results of the five target compounds in liver tissues by using the proposed method (mg/kg).

Sample no.	ATP	ADP	AMP	CP	Creatine
1	5606	2707	492.4	24.28	188.8
2	6470	2092	374.4	40.96	197.7
3	3026	1969	521.8	29.63	229.8
4	1414	1049	301.4	9.032	127.4
5	6105	2830	484.2	9.628	176.6
6	4305	2551	471.7	9.771	141.4
7	4548	3469	419.5	16.87	202.9
8	5172	4250	507.2	18.06	202.5
Mean ± SD	4581 ± 1683	2615 ± 971.3	446.6 ± 76.06	19.78 ± 11.31	183.4 ± 33.97

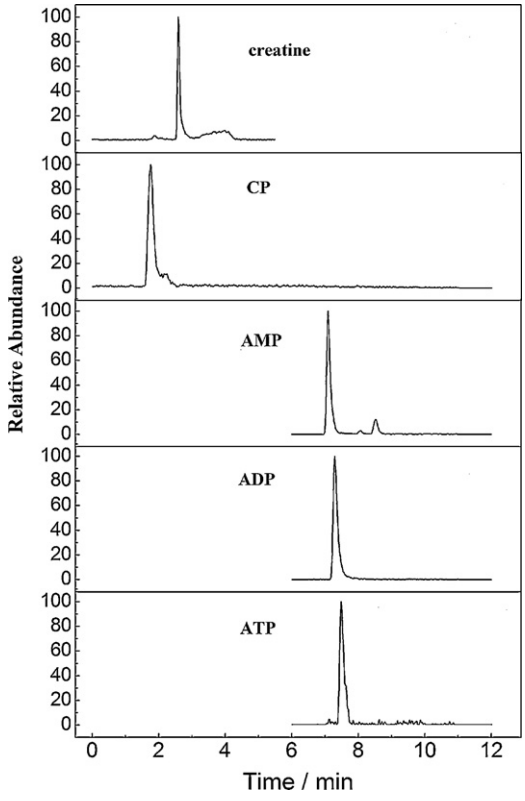

Fig. 3. Chromatograms of the five target compounds in rat liver.

widely used in determination of adenine nucleotides in liver tissue. Mikami et al. reported the change levels of ATP, ADP and AMP in rat liver induced by intense exercise [10]. And the contents of ATP, ADP and AMP in rat liver tissues during different day times were also reported by Abadi [11]. However, there is no report about simultaneous determination of ATP, ADP, AMP, CP and creatine in liver tissue by LC–MS/MS.

4. Conclusion

In this paper, a HPLC–ESI-MS/MS method was developed for simultaneous determination of ATP, ADP, AMP, CP and creatine in liver tissue. The use of porous graphitic carbon (PGC, Hypercarb) column enhanced retention of adenine nucleotides and meanwhile offered MS-compatible chromatographic conditions because no ion-pair agents were needed. In addition, the sample pre-treatment procedure was rapid, simple and well compatible with ESI-MS/MS analysis. This method has been successfully applied to simultaneous determination of ATP, ADP, AMP, CP and creatine in liver tissue from 8 normal rats. Moreover, the method can be expended for studying energy metabolism of fatty liver that is used as marginal donor liver, which is of great significance to further research on human liver transplantation.

Acknowledgement

The authors are grateful to the financial support from application infrastructure fund (2010JY0007) of Department of Science and Technology of Sichuan Province, China.

Please cite this article in press as: Y. Jiang, et al., Simultaneous determination of adenine nucleotides, creatine phosphate and creatine in rat liver by high performance liquid chromatography–electrospray ionization-tandem mass spectrometry, J. Pharm. Biomed. Anal. (2012), doi:10.1016/j.jpba.2012.03.027

References

[1] G. Vial, H. Dubouchaud, K. Couturier, C. Cottet-Rousselle, N. Taleux, A. Athias, A. Galinier, L. Casteilla, X.M. Leverve, Effects of a high-fat diet on energy metabolism and ROS production in rat liver, J. Hepatol. 54 (2011) 48–356.
[2] M.D. Scott, L.J. Baudendistel, T.E. Dahms, Rapid separation of creatine, phosphocreatine and adenosine metabolites by ion-pair reversed-phase high-performance liquid chromatography in plasma and cardiac tissue, J. Chromatogr. 576 (1992) 149–154.
[3] M.G. Volonté, G. Yuln, P. Quiroga, A.E. Consolini, Development of an HPLC method for determination of metabolic compounds in myocardial tissue, J. Pharm. Biomed. Anal. 35 (2004) 647–653.
[4] J. Klawitter, V. Schmitz, J. Miljus, D. Leibfritz, U. Christians, Development and validation of an assay for the quantification of 11 nucleotides using LC/LC–electrospray ionization-MS, Anal. Biochem. 365 (2007) 230–239.
[5] R.L. Cordell, S.J. Hill, C.A. Ortori, D.A. Barrett, Quantitative profiling of nucleotides and related phosphate-containing metabolites in cultured mammalian cells by liquid chromatography tandem electrospray mass spectrometry, J. Chromatogr. B 817 (2008) 115–124.
[6] J. Wang, T. Lin, J.P. Lai, Z.W. Cai, M.S. Yang, Analysis of adenosine phosphates in HepG-2 cell by a HPLC–ESI-MS system with porous graphitic carbon as stationary phase, J. Chromatogr. B 877 (2009) 2019–2024.
[7] S. Young, E. Struys, T. Wood, Quantification of creatine and guanidinoacetate using GC–MS and LC–MS/MS for the detection of cerebral creatine deficiency syndromes, Curr. Protoc. Hum. Genet. (2007) 17.3.1–17.3.18.
[8] J. Xing, A. Apedo, A. Tymiak, N. Zhao, Liquid chromatographic analysis of nucleosides and their mono-, di- and triphosphates using porous graphitic carbon stationary phase coupled with electrospray mass spectrometry, Rapid Commun. Mass Spectrom. 18 (2004) 1599–1606.
[9] J.L. Au, M.H. Su, M.G. Wientjes, Extraction of intracellular nucleosides and nucleotides with acetonitrile, Clin. Chem. 35 (1989) 48–51.
[10] T. Mikami, J. Kitagawa, Intense exercise induces the degradation of adenine nucleotide and purine nucleotide synthesis via de novo pathway in the rat liver, Appl. Physiol. 96 (2006) 543–550.
[11] R.H.H.B. Abadi, Analysis of free nucleotide pools of mouse liver tissue by high-pressure liquid chromatography (HPLC), Biochem. Biophys. 40 (2003) 209–212.

Please cite this article in press as: Y. Jiang, et al., Simultaneous determination of adenine nucleotides, creatine phosphate and creatine in rat liver by high performance liquid chromatography–electrospray ionization-tandem mass spectrometry, J. Pharm. Biomed. Anal. (2012), doi:10.1016/j.jpba.2012.03.027

Journal of Pharmaceutical and Biomedical Analysis 66 (2012) 264–270

Contents lists available at SciVerse ScienceDirect

Journal of Pharmaceutical and Biomedical Analysis

journal homepage: www.elsevier.com/locate/jpba

Application of ionic surfactant as a carrier and emulsifier agent for the microextraction of fluoroquinolones

Behnam Ebrahimpour, Yadollah Yamini*, Morteza Moradi

Department of Chemistry, Tarbiat Modares University, P.O. Box 14115-175, Tehran, Iran

ARTICLE INFO

Article history:
Received 8 December 2011
Received in revised form 13 March 2012
Accepted 14 March 2012
Available online 24 March 2012

Keywords:
Ion pair based surfactant assisted microextraction
Fluoroquinolones
Aliquat-336
High-performance liquid chromatography
Natural water
Urine sample

ABSTRACT

A simple microextraction method based on emulsification of organic extraction solvent in aqueous sample using an ionic surfactant was evaluated for extraction and preconcentration of trace amounts of ofloxacin and ciprofloxacin as polar model drugs. In this method, the surfactant was used as carrier and disperser agent simultaneously. The target analytes were converted into their ion-pair complexes with Aliquat-336 and then extracted into an organic solvent (1-octanol) dispersed in aqueous solution. After extraction and phase separation, the organic solvent on top of the solution was withdrawn into the syringe and 20 μL of it was injected into a HPLC instrument for analysis. The factors influential to extraction were investigated and optimized. Under optimum extraction conditions, the limits of detection (LODs) as small as 0.06 and 0.02 ng mL^{-1} and linear dynamic range of 0.1–100 and 0.06–100 ng mL^{-1} were obtained for ofloxacin and ciprofloxacin, respectively. For analysis of real samples such as waste water, river water and urine samples, solid-phase extraction (SPE) was applied prior to liquid phase microextraction in order to avoid/remove matrix effect. The obtained results indicate that the proposed method is efficient, fast and inexpensive for extraction and determination of fluoroquinolones in environmental aqueous and urine samples.

© 2012 Elsevier B.V. All rights reserved.

1. Introduction

Pharmaceuticals are an emerging environmental concern. Especially, the presence of endocrine disruptor chemicals in the aquatic environment has become a cause for increasing concern in recent years [1]. The fluoroquinolones (FQs) have emerged as one of the most important class of antibiotics and comprise a relatively large and constantly expanding group of substances. This group of synthetic drugs has shown excellent activity against both pathogenic Gram-negative and Gram-positive bacteria [2]. These compounds are widely used in human medicine for the treatment of pulmonary, urinary and digestive infections with good localized action on infected sites [3]. Low amounts of fluoroquinolones are found in plasma and their main excretion pathway is in urine. Due to the possible development of resistance of human pathogens to antibiotics, there is nowadays concern about the possibility of exposure to low levels of these compounds in the environment [4].

Environmental risk assessment studies combine the hazard with the likeliness of exposure, basing their evaluation on predicted environmental concentrations and laboratory data; however, measured environmental concentrations are indispensable for providing accurate data on the real concentrations, likewise details of the fate of pharmaceuticals in different environmental compartments. It is, therefore, necessary to develop precise, specific, and sensitive techniques for rapid detection and identification of FQs in the environmental and biological samples.

Several spectrophotometric and chromatographic methods [5–10] have been reported for detection of FQs in different matrixes. Among these methods, HPLC has been widely applied because of its high sensitivity and selectivity as well as its ability to minimize interferences. Although the development of modern analytical instruments allows enhancement in aspects of analysis, but the available analytical instrumentations have insufficient sensitivity for the analysis of natural samples in many cases. Liquid–liquid extraction (LLE) and solid-phase extraction (SPE) have been applied for clean-up and preconcentration of pharmaceutics [11,12]. These methods suffer from some drawbacks such as being time-consuming and requiring large volumes of organic solvents [13]. It is worthy to note that consuming a large amount of solvent would influence trace analysis. Modern trends in analytical chemistry are towards the simplification and miniaturization of sample preparation, as well as the minimization of the used organic solvent. In this sense, different liquid-phase and solid phase microextraction techniques have been explored as alternatives to conventional sample preparation procedures [14].

* Corresponding author. Tel.: +98 21 82883417; fax: +98 21 88006544.
E-mail address: yyamini@modares.ac.ir (Y. Yamini).

0731-7085/$ – see front matter © 2012 Elsevier B.V. All rights reserved.
doi:10.1016/j.jpba.2012.03.028

Dispersive liquid–liquid microextraction (DLLME) is a new microextraction technique which was reported in 2006 by Assadi et al. [15]. In this method, an appropriate mixture of extraction and dispersive solvents is injected rapidly into an aqueous sample with a syringe, resulting in the formation of a cloudy solution. Phase separation is performed by centrifugation and the enriched analyte in the sediment phase is determined. It is simple, rapid, and efficient, with suitable extraction recovery and preconcentration factors. One of the major disadvantages of DLLME is the small partition coefficients of analytes between organic/aqueous phases due to the presence of disperser solvent in the aqueous phase. A new version of DLLME namely surfactant-assisted dispersive liquid–liquid microextraction (SA-DLLME) based on surfactant, as disperser agent, was reported in 2010 [16]. In this method, a mixture of aqueous solution including surfactant and extraction solvent is quickly injected into the aqueous sample so as to form an emulsified solution. In comparison with the traditional DLLME, SA-DLLME uses small amounts of environmentally friendly emulsifier agents.

The main drawback of DLLME or SA-DLLME is their inability to extract hydrophilic compounds into the extraction solvent. To overcome this limitation, a new method for extraction of ionic and polar compounds to organic solvent has been reported, namely ion pair based surfactant assisted microextraction (IP-SAME) [17]. Two inherent specificities of ionic surfactants in extraction phenomena are: (1) the surfactants are capable of forming an emulsion between the organic and aqueous phases resulting in large surface area between analyte and extraction solvent; (2) surfactants are one of the most appropriate carriers for ionic compounds and make the ionic species extractable via ion pair formation phenomenon.

In the present work, an IP-SAME method prior to HPLC–UV was proposed for simultaneous extraction and determination of trace amounts of ofloxacin (OFL) and ciprofloxacin (CIP) antibiotics which have both acidic and basic functional groups (as studied polar models) from environmental water and human urine samples.

2. Experimental

2.1. Chemicals and supplies

Standards of the drugs (OFL, CIP) were purchased from Razi Drug Company (Tehran, Iran) and used without further purification. Analytical grade 1-octanol, 1-dodecanol, and toluene were supplied by Merck (Darmstadt, Germany). Tetradecyl trimethyl ammonium bromide, TTAB ($C_{17}H_{38}BrN$) and sodium dodecyl sulfate (SDS: $C_{12}H_{25}OSO_3Na$) were purchased from Sigma–Aldrich (St. Louis, MO, USA). Sodium hexadecyl sulfate (SHS: $C_{16}H_{33}OSO_3Na$) was purchased from Wako Pure Chemical Industries (Osaka, Japan). Three caprylil methyl ammonium chloride, Aliquat-336 ($C_{25}H_{54}ClN$) was obtained from Fluka (Buchs, Switzerland). Other reagents were of analytical grade and obtained from Merck. The water was purified on a Milli-Q ultra-pure water purification system from Millipore (Milford, MA, USA). Microliter syringes (25–500 μL) were purchased from Hamilton (Bonaduz, Switzerland). A centrifuge from Sepand Teb Azema (Tehran, Iran) was applied to phase separation.

2.2. Standards and real samples preparation

Stock standard solutions of each analyte were prepared separately by dissolving proper amounts of each drug in methanol at 1000 μg mL^{-1} level and stored at 4 °C. The stock solutions were diluted with methanol to reach secondary mix stock solutions with certain concentrations (1–200 μg mL^{-1}). Mixtures of standard working solutions for extraction at different concentrations were prepared by dilution with ultra-pure water for optimization of parameters. The working solutions were freshly prepared by diluting the mixed standard solutions in ultra-pure water for the required concentrations.

Tap water samples were collected from our lab (Tehran, Iran). River water sample as surface water was taken from Haraz River (Mazandaran, Iran). Also, waste water sample was collected from a pharmaceutical factory (Tehran, Iran).

Human urine samples for obtaining calibration curve and figures of merit were collected from healthy male volunteers. The samples were centrifuged for 5 min at 4000 rpm and filtered through a 0.45 μm pore size cellulose acetate filter from Millipore (Madrid, Spain). The filtrates were collected in glass containers, which had been carefully cleaned with hydrochloric acid. They were then washed with deionized water and stored at 4 °C to prevent bacterial growth and proteolysis. Five milliliters of this urine sample were spiked by mixed standard solution to obtain desired concentrations and diluted to 10 mL with deionized water. These samples were subsequently submitted to SPE prior to IP-SAME procedure. Urine samples were obtained from healthy volunteers: one of them consumed a single oral dose of 500 mg of ciprofloxacin while others consumed 300 mg of ofloxacin. These samples were collected 60 h after administration of tablets and the urinary volumes were recorded as well.

2.3. HPLC analysis

Chromatographic analysis was performed with a HPLC system including a Varian 9012 HPLC pump (Walnut Creek, CA, USA), a six-port Cheminert HPLC valve from Valco (Houston, USA) with a 20 μL sample loop and equipped with a Varian 9050 UV-vis detector. An ODS column (250 mm × 4.6 mm, with 5 μm particle size) from Technochroma (Barcelona, Spain) was applied to separate the FQs under gradient elution conditions. A mixture of 10 mmol L^{-1} sodium perchorate, 25 mmol L^{-1} citric acid buffer (pH 3.4) and acetonitrile (81:19) for 15 min and then 100% acetonitrile for 5 min at flow rate of 1.0 mL min^{-1} were used as the mobile phase and the analytes were detected at 280 nm.

2.4. Solid-phase extraction procedure

Extraction cartridges (C_{18}, 6 mL) were placed on a home-designed setup which could be connected to vacuum pump to adjust the flow rate. Based on preliminarily experiments, optimum conditions for solid-phase extraction steps were obtained as follows: the cartridges were rinsed with 2 mL of methanol followed by 2 mL of purified water at flow rate of 1 mL min^{-1} (conditioning step). Care was taken that the cartridge did not run dry. Then 10 mL of the spiked urine samples or 30 mL of water samples with adjusted pH at 6.0 were loaded onto the cartridge and drained at flow rate of 1 mL min^{-1} by applying vacuum (loading step). The cartridges were then washed with 2 mL of water followed by vacuum suction for 1 min and 1 mL of acetonitrile (washing) for 1 min, finally 1 mL of methanol containing 2% HCl were used to elute the adsorbed analytes (elution), which were transferred into a home-designed centrifuge vial, and were diluted to 10 mL before being submitted to IP-SAME procedure.

2.5. Extraction procedure

Aliquots of 10 mL sample solution containing analytes was adjusted to pH 10 and placed in a 12 mL home-made glass tube (especially used for low density organic solvent collection). 1.0 mL of pure water (pH = 10) containing 60 μL of extraction solvent (14% (w/v) of Aliquat-336 as emulsifier in 1-octanol) was injected rapidly into the sample solution by using 5.00 mL gas-tight syringe. As a result, a cloudy solution (water, Aliquat-336 and 1-octanol) was

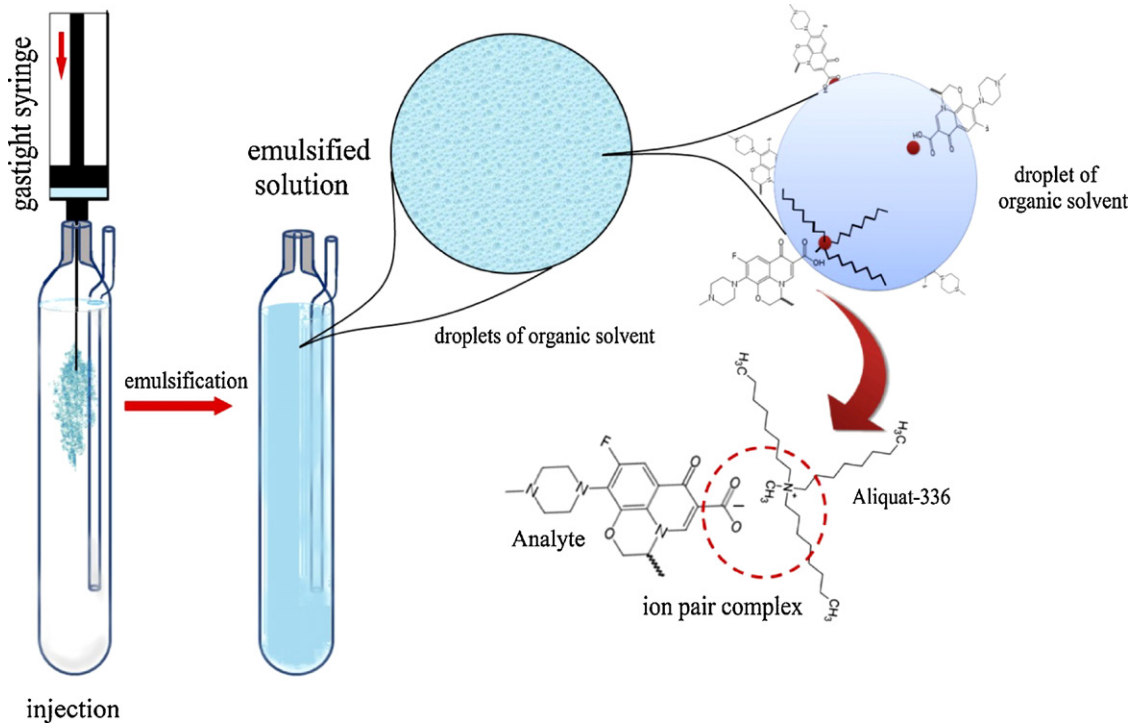

Fig. 1. Schematic design of the extraction procedure.

formed in the test tube. In this step, the extraction solvent was dispersed into the aqueous sample as very fine droplets. This process greatly enlarged the contact area between the extraction solvent and aqueous phase. Afterwards, the complex of FQs with Aliquat-336 was extracted into the fine droplets of extraction solvent. The formed emulsion was centrifuged at 4000 rpm for 5 min to separate the phases. The schematic design of procedure is shown in Fig. 1. Twenty microliters of the collected phase was taken using a 50 μL microsyringe and directly injected into the HPLC instrument.

3. Results and discussion

3.1. Optimization of IP-SAME

In order to optimize the IP-SAME of FQs from aqueous solutions, several parameters that control the optimum performance of extraction were studied. These parameters were separately evaluated to develop the optimized extraction conditions.

3.1.1. Effect of extraction solvent

Selecting a suitable extraction solvent is crucial in IP-SAME. It should have low solubility in water, high affinity for the analytes, good chromatographic behavior, and lower density than water. In this work, several organic solvents were studied as extraction solvent, including 1-dodecanol, 1-octanol and toluene, and their extraction efficiency was studied (Fig. 2).

In order to pick up a constant volume of the collected phase (30 μL), 1.0 mL of ultra-pure water containing 1 mmol L^{-1} TTAB as emulsifier agent and different volumes of the extraction solvents (45, 50, and 55 μL) of 1-dodecanol, 1-octanol and toluene, respectively, were injected into the sample solution (pH = 10). The average peak area (triplicates) and the standard deviation for the different extraction solvents are depicted in Fig. 2. As can be seen, the extraction efficiencies that were obtained for the analytes by using 1-octanol were the highest among other solvents. Polarity of 1-octanol is higher than two other examined solvents, so 1-octanol has better ability to stabilize and solve formed ion pair. Also, because of lower viscosity, dispersion of 1-octanol in aqueous medium was occurred with higher performance in comparison with 1-dodecane. Therefore, 1-octanol was selected as the extraction solvent for the rest of this study.

3.1.2. The pH and surfactant optimization

The pH value of solution determines the dominant form of the analytes. For analytes with both acidic and basic functional groups, cationic and anionic forms are dominant in acidic and basic ranges of pH, respectively.

The structure of FQs investigated in the present study and their physicochemical parameters (log *P*, pK_a) are provided in Table 1. These compounds are highly polar and may exist with different charges depending on pH of the sample. As shown in Table 1, their partition coefficients into organic solvents are low which are related to the existence of highly hydrophilic groups in their structure. FQs molecules have four relevant ionizable functional

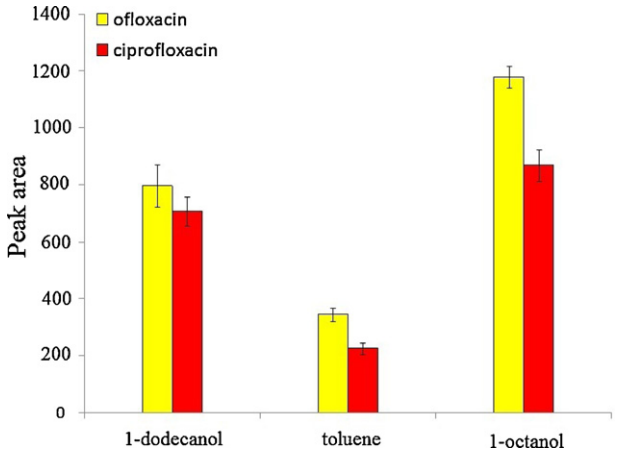

Fig. 2. Effect of extraction solvent on the peak area of the analytes. Analytes concentration, 100 ng mL^{-1}; sample volume, 10 mL; pH = 10; 1 mmol L^{-1} of TTAB.

Table 1
The chemical structure.

Analyte	Chemical structure	Log *P*	MW[a]	pK_a
Ofloxacin	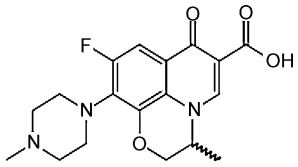	−0.48	361.37	6.05,8.22
Ciprofloxacin	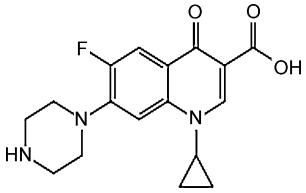	0.28	331.34	3.01,6.14,8.76,10,58

[a] Molecular weight.

groups, one carboxylic group and three basic nitrogen sites, which means that their acid–base chemistry possibly involves four protons [18]. The pK_a values of the studied fluoroquinolones are listed in Table 1, where p$K_{a,1}$ is assigned to the carboxylic group, whereas the remaining pK_a values (pK_{a2}, pK_{a3}, pK_{a4}, two reported for ofloxacin) are assigned to specific nitrogen sites [19]. This type of chemical structure of FQs causes that these compounds are presented in aqueous solution as permanently charged molecules in the whole pH range. Since FQs have both (acidic and basic) functional groups, they are ionizable and form ion pair complex with any of the surfactants. Therefore, the extraction efficiency will be affected by ion pair formation.

In the present study, the pH was better to be selected in a range that the surfactant formed ion pair complex, and an emulsified medium was formed as well. Therefore, to achieve the best conditions, the effect of pH and surfactant type was investigated synchronously. For this purpose, the extraction efficiency of two cationic surfactants (Aliquat-336 and TTAB) in the basic pH and two anionic surfactants (SDS and SHS) in the acidic pH was investigated.

Based on the obtained results illustrated in Fig. 3, Aliquat-336 gives the best extraction recoveries. Thus, Aliquat-336 at pH = 10.0, in addition to emulsifying the 1-octanol in sample solution, forms ion pair complexes with analyte ions and efficiently extracts them into the organic solvent. At pH > 10 the extraction was decreased, may be due to competition of OH^- with the analytes to form ion pair with Aliquat-336. Therefore, Aliquat-336 as an anionic carrier and pH = 10.0 were selected as the optimal options.

3.1.3. Surfactant concentration

The concentration of surfactant in IP-SAME is a critical factor. Variations in Aliquat-336 concentration (as the emulsifier) cause changes in the volume of the sedimented organic solvent. To avoid this and also to achieve a constant volume of the sedimented organic solvent, 1-octanol volumes containing various amounts of Aliquat-336 were utilized. Constant experimental conditions were used that included the use of different 1-octanol volumes containing 1.0%, 2.0%, 4.0%, 6.0%, 8.0%, 10.0%, 12.0% and 14.0% (w/v) Aliquat-336 in 1-octanol. In this step, the volume of the collected phase was kept constant (25 μL). As the Aliqut-336 concentration increased from 1.0 to 14.0 (w/v), the extraction efficiency was increased due to making finer droplets, causing an improved mass transfer into the organic phase and well ion pair formation. Further increase in concentration of surfactant made the organic solvent so viscose that solvent injection to the column would not be practical. Based on the obtained results, the best extraction recoveries were achieved by using 14% Aliquat-336 in 1-octanol.

3.1.4. Influence of ionic strength

By addition of NaCl to the aqueous solution, the influence of salt addition on the extraction efficiency of IP-SAME was investigated. The results indicate that the presence of salt significantly

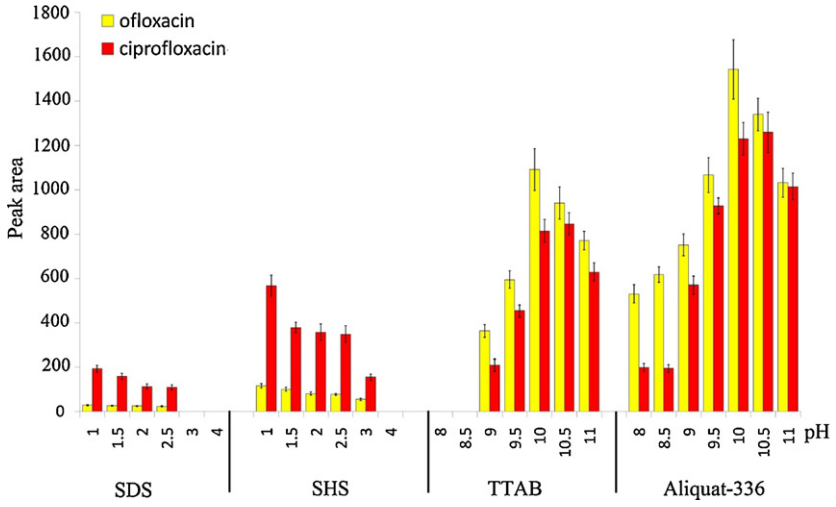

Fig. 3. Effect of sample pH and surfactant on peak area of the analytes. Analytes concentration, 100 ng mL^{-1}; sample volume, 10 mL; 60 μL of 1-octanol as extraction solvent.

Table 2
Calibration graph data, LODs, DLRs, RSD, PF and Ex for the analytes.

Sample	Analyte	R^2	LOD (ng mL^{-1})	DLR (ng mL^{-1})	RSD[a] (%)	PF	ER%
Water (distilled)	OFL	0.9949	0.06	0.1–100	4.6	324	81
	CIP	0.9993	0.02	0.06–100	4.9	368	92
Tap water	OFL	0.9928	0.2	0.5–200	5.5	204	51
	CIP	0.9978	0.1	0.3–200	5.6	228	57
Tap water (SPE)	OFL	0.9949	0.04	0.1–100	7.1	540	45
	CIP	0.9936	0.01	0.03–100	8.2	648	54
Urine (SPE)	OFL	0.9993	0.8	2.0–400	7.9	130	65
	CIP	0.9989	1.0	3.0–400	8.4	62	31

[a] RSD% were calculated at 10 ng mL^{-1} (n = 5).

reduces the extraction efficiency. Two main competitive effects occur in LPME when an increase in the ionic strength takes place, namely, salting-out effect and change of the physical properties of the Nernst diffusion film. In the case of the salting-out effect, salt addition has a favorable impact on the extraction, since it decreases water solubility of the analyte, thus improving mass transfer to the organic phase. On the contrary, it has been reported that the diffusion rate of the analyte into the extractant phase may decrease due to the change in the properties of the Nernst diffusion film. Furthermore, it should be taken into account that the addition of salt reduces the water solubility of the extractant phase, thereby involving the dilution of the enriched extract at increasing concentration of salt. Also, the presence of the salt decreases the efficiency of emulsification, so extraction efficiency decreases. In this work salt addition causes a negative effect on the extraction of the ion pair, which is more pronounced at large NaCl concentrations. Therefore, further experiments were performed without salt addition.

3.1.5. Influence of extraction solvent volume

The volume of extraction solvent is a crucial parameter that has an important effect on the extraction efficiency. The volume of collected extraction solvent was increased as the extraction solvent volume increased while the perconcentration factor of the analytes was decreased. The collected volume of the organic solvent on the top of the solution after phase separation should be more than 20 μL (volume of HPLC loop is 20 μL). It was observed that insufficient extraction solvent was collected when the volume less than 60 μL was used. To study the effect of extraction solvent volume, different volumes of organic solvent were subjected to IP-SAME while other parameters were kept constant. According to the obtained results, 60 μL was selected as the optimum volume of the organic solvent.

3.2. Method validation

3.2.1. Evaluation of method performance

In order to evaluate the practical applicability of the proposed extraction method, the figures of merit (i.e. limit of detection (LOD), linearity and *PF*) were investigated using spiked ultra-pure water under the optimum conditions (volume of 1-octanol, 60 μL; emulsifier and complexation agent, 14% (w/v) Aliquat-336 in 1-octanol; pH, 10.0; and without salt addition) whose results are provided in Table 2. Solutions containing the drugs in the range of 0.02–100 ng mL^{-1} were extracted at optimum conditions. The linear dynamic ranges from 0.06 to 100 ng mL^{-1} for OFL and from 0.1 to 100 ng mL^{-1} for CIP with the coefficients of determination (R^2) > 0.994 were obtained. The relative standard deviation (RSD%) for extraction and determination of the drugs was less than 4.9% based on three replicates. LODs of 0.02 and 0.06 ng mL^{-1} were acquired based upon signal-to-noise ratio of 3 (S/N = 3) for CIP and OFL, respectively. Also under the optimum conditions, preconcentration factors were 368 and 324 for CIP and OFL, respectively. These *PF*s correspond to extraction recoveries (*ER*s) of 92 and 81%, respectively. *ER*s were calculated based on the following equation:

$$ER\% = \left(PF \times \frac{V_{org}}{V_{aq}} \right) \times 100 \quad (1)$$

where V_{org} and V_{aq} are the volumes of extraction (organic solvent) and sample phases, respectively.

3.3. Application of the method

In order to assay the ability of the method to extract the drugs from complex matrices, the proposed procedure was applied to extract the drugs from the tap, waste and river waters and also from urine samples under optimal conditions.

3.3.1. Analysis of spiked samples

The results revealed that the analyzed water samples (tap, waste and river water) were free of OFL and CIP. Tap water samples were spiked with the standard solutions in the range of 0.1–200 ng mL^{-1} and the IP-SAME-HPLC method was applied to their analysis.

The extraction recoveries of fluoroquinolones from surface and waste water under optimal conditions were not remarkable and the obtained values of extraction recoveries were very low. However, it is known that significant increase in preconcentration of analytes could be obtained by dilution of the samples [20,21]. Unfortunately, the values of preconcentration factor (*PF*) were still low compared to distilled water after dilution. The improvement of the *PF* could be resulted from the reduction of the matrix effect which could in turn be achieved by solid-phase extraction (SPE). Therefore, due to high matrices effect, SPE was used to analyze the waste water, river water and urine samples. Due to its simple matrix, tap water sample can be analyzed directly with IP-SAME procedure or with SPE-IP-SAME. The results of analysis are shown in Table 2. Accuracy was calculated as the relative recoveries (recovery%) for the analysis of known amounts of target analytes added to actual water samples (tap water, river water and waste water) using the proposed method (Table 3). Based on the obtained results, by using SPE prior to IP-SAME the matrix of different samples has low effects on the recoveries.

3.3.2. Analysis of real urine samples

The proposed method was also applied to determination of the fluoroquinolones in human urine samples. Urine samples belonged to healthy volunteers: one of them consumed a single oral dose of 500 mg of ciprofloxacin and the others consumed 300 mg of ofloxacin. The samples taken from individuals were collected 60 h after administration of tablets and the urinary volumes were recorded as well (as mentioned in Section 2.2). Table 4 provides the results of three-replicate urine analyses from one healthy volunteer and two drug consumers. It was found that the concentration of CIP in urine 1 and concentration of OFL in the urine 2 samples were

Table 3
Determination of OFL and CIP in water samples.

Sample	Drug	$C_{initial}$	C_{added}	C_{found}	RSD (%)	Recovery (%)
Tap water	CIP	n.d.[a]	5	4.9	6.2	98.0
			30	29.6	6.8	98.7
	OFL	n.d.	5	4.8	6.7	96.0
			30	29.5	7.1	98.3
Waste water	CIP	n.d.	5	4.7	6.7	94.0
			30	28.1	7.3	93.7
	OFL	n.d.	5	4.6	6.8	92.0
			30	28.7	7.1	95.7
River water	CIP	n.d.	5	4.6	7.5	92.0
			30	28.1	7.8	93.7
	OFL	n.d.	5	4.8	8.6	96.0
			30	28.9	7.8	96.3

Table 4
Determination of OFL and CIP in urine samples.

Sample	Drug	$C_{initial}$	C_{added}	C_{found}	RSD (%)	Recovery (%)
Urine 1	CIP	63	30	86.3	7.3	92.7
	OFL	n.d.[a]	30	27.8	7.4	92.6
Urine 2	CIP	n.d.	30	29.5	6.8	98.3
	OFL	37	30	70.6	7.6	105.3
Urine[b] 3	CIP	n.d.	5	4.6	8.4	92.1
			30	28.1	8.1	93.6
	OFL	n.d.	5	4.5	8.0	90.0
			30	27.9	7.8	93.0

[a] Not detected.
[b] From a healthy volunteer.

63 and 37 ng mL^{-1}, respectively. Determining the accuracy of the method, these samples were spiked with 30.0 ng mL^{-1} of each analyte. The relative recoveries obtained by the method were in the range of 90.0–105.3%. The relative standard deviations for determination of FQs in the examined real urine samples were also in the range of 6.8–8.4%. Fig. 4 shows the chromatograms of the non-spiked and 30 ng mL^{-1} spiked urine sample taken from the healthy volunteer and Fig. 5 demonstrates the chromatograms yielded from analysis of the two urine samples from volunteers who used a tablet of mentioned drugs. Analyses were performed before and 60 h after oral administration.

Urine samples from one of the volunteers who received a 300 mg tablet of ofloxacin were collected before consuming the tablet as well as 4, 12, 20, 32 and 40 h after the drug consumption. The results of analysis indicate that ofloxacin in urine reaches its maximum amount 20 h after oral administration and

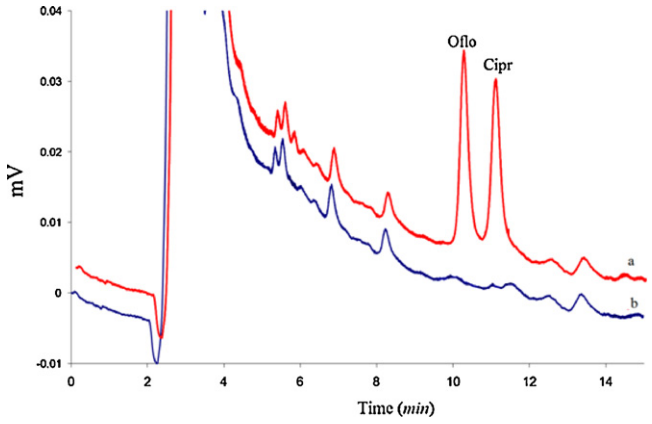

Fig. 4. The chromatograms of non-spiked (a) and 30 ng mL^{-1} spiked (b) urine sample.

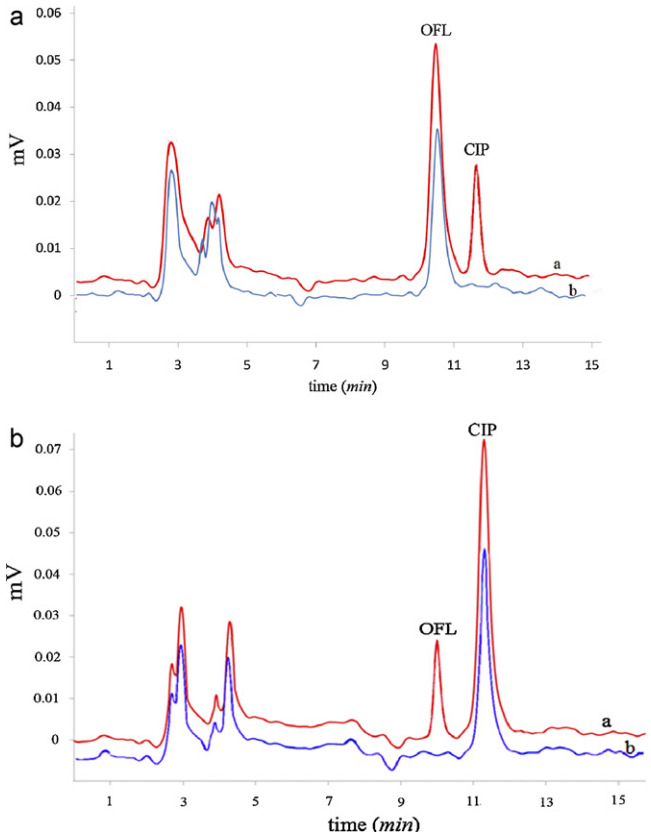

Fig. 5. The chromatograms of non-spiked (a) and 30 ng mL^{-1} spiked (b) urine samples from volunteers: (A) 60 h after administration of 300 mg tablet of ofloxacin; (B) 60 h after administration of 500 mg tablet of ciprofloxacin.

then decreases. Chromatograms obtained from analysis of these samples are shown in Fig. 6.

3.4. Comparison of the applied method with other reported methods

The results of a comparison made between the figures of merit of the proposed method and some of the published methods for extraction and determination of OFL and CIP in literature are provided in Table 5. Obviously, the proposed method has a good sensitivity and proper precision with a suitable dynamic linear range. Besides, the obtained LODs for the drugs by the present

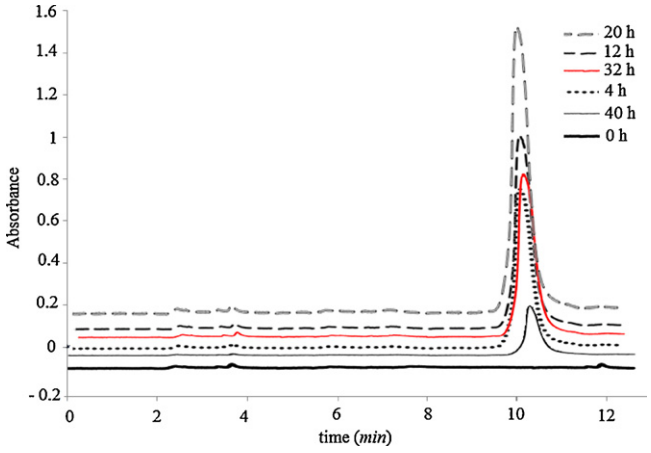

Fig. 6. The chromatograms of SPE-IP-SAME from real urine samples collected from a volunteer at different times who consumed a 300 mg tablet of ofloxacin.

Table 5
Comparison of proposed method with other methods for extraction and determination of the drugs.

Analysis method	Matrice	Coprofloxacin				Ofloxacin				Ref.
		LOD[a]	DLR	RSD%	PF	LOD	DLR	RSD%	PF	
HF-LPME-HPLC (DAD)	Water	0.01	0.03–1000	–	50	–	–	–	–	[22]
SD-LLLME-CE (UV)	Urine	10.78	40–1000	5.8	–	23.24	40–1000	4.8	–	[23]
HPLC (PIF)	Urine	4.5	40–120	4.6	–	10	40–120	5.5	–	[24]
HPLC–MS-SPF[b]	Urine	0.1	0.3–10	–	–	–	–	–	–	[25]
UA-DLLME–LC–UV	Water	–	–	–	–	0.36	10–2000	2.2	100	[26]
SPME-LC–MS–MS	Water	0.017	0.1–10	<8.6	–	0.007	0.1–10	8.6	–	[27]
SPE-LC-ESI-MS	Urine	17.0	58–1000	5.3	–	21.0	71–1000	5.3	–	[28]
IP-SAME-HPLC-UV	Water	0.02	0.06–100	4.9	368	0.06	0.1–100	4.6	324	This method
	Urine	1.0	3.0–400	8.4	62	0.6	2.0–400	7.9	130	

[a] Concentrations were reported as ng mL^{-1}.
[b] Solid-phase spectrofluorimetery.

method with sample volume of 10 mL are better than or comparable with those obtained by applying other methods. All of the results reveal that the optimized method is not only a good sample preconcentration technique but also an excellent sample clean-up procedure that can be used for the trace analysis of fluoroquinolone drugs in different and complicated matrices.

4. Conclusions

The aim of the present research was to develop an efficient method for extraction, clean-up and determination of trace amounts of polar compounds with both acidic and basic functional groups in natural waters and urine samples. IP-SAME was used for extraction and determination of ciprofloxacin and ofloxacin as model analytes. The proposed method is particularly environmentally friendly, precise, reproducible and linear over a broad concentration range and also provides high preconcentration factors.

The optimized method was applied to extraction of the drugs from water and urine samples. The obtained results indicated that the proposed method is a simple, inexpensive and relatively fast extraction technique with little consumption of organic solvent for extraction and determination of the FQ drugs in different matrices.

References

[1] S. Xie, B. Xiang, M. Zhang, H. Deng, Determination of medroxyprogesterone in water samples using dispersive liquid–liquid microextraction with low solvent consumption, Microchim. Acta 168 (2010) 248–253.
[2] A. Linder, E.S. Huang, M.A. Steinman, R. Gonzales, R.S. Stafford, Fluoroquinolone prescribing in the United States: 1995 to 2002, Am. J. Med. 118 (2005) 259–268.
[3] O. Ballesteros, I. Toro, V. Sanz-Nebot, A. Navalón, J.L. Vílchez, J. Barbosa, Determination of fluoroquinolones in human urine by liquid chromatography coupled to pneumatically assisted electrospray ionization mass spectrometry, J. Chromatogr. B 798 (2003) 137–144.
[4] A. Espinosa-Mansilla, A. Muñoz de la Peña, D. González Gómez, F. Salinas López, Determination of fluoroquinolones in urine and serum by using high performance liquid chromatography and multiemission scan fluorimetric detection, Talanta 68 (2006) 1215–1221.
[5] H. Nakata, K. Kannan, P.D. Jones, J.P. Giesy, Determination of fluoroquinolone antibiotics in wastewater effluents by liquid chromatography–mass spectrometry and fluorescence detection, Chemosphere 58 (2005) 759–766.
[6] K. Mitami, H. Kataoka, Determination of fluoroquinolones in environmental waters by in-tube solid-phase microextraction coupled with liquid chromatography–tandem mass spectrometry, Anal. Chim. Acta 562 (2006) 16–22.
[7] S. Jianzhong, G. Liming, X. Fei, R. Qinxiong, X. Xi, L. Xiaowei, D. Shuangyang, Adsorption strategy of plasmid DNA nanoparticulate: preparative purification by a simple custom expanded bed column, Chromatographia 71 (2010) 383–388.
[8] M. Ferdig, A. Kaleta, T.D. Vo, W. Buchberger, Improved capillary electrophoretic separation of nine (fluoro)quinolones with fluorescence detection for biological and environmental samples, J. Chromatogr. A 1047 (2004) 305–311.
[9] E. Turiel, G. Bordin, A.R. Rodriguez, Trace enrichment of (fluoro) quinolone antibiotics in surface waters by solid-phase extraction and their determination by liquid chromatography–ultraviolet detection, J. Chromatogr. A 1008 (2003) 145–155.
[10] H. Jing-Fang, L. Bo, Y. Qiong-Wei, F. Yu-Qi, Determination of fluoroquinolones in eggs using in-tube solid-phase microextraction coupled to high-performance liquid chromatography, Anal. Bioanal. Chem. 384 (2006) 1228–1235.
[11] A. Hernandez, C. Aguilar, F. Borrull, M. Calull, Determination of ciprofloxacin, enrofloxacin and flumequine in pig plasma samples by capillary isotachophoresis–capillary zone electrophoresis, J. Chromatogr. B 772 (2002) 163–172.
[12] Z.J. Yang, W.D. Qin, Separation of fluoroquinolones in acidic buffer by capillary electrophoresis with contactless conductivity detection, J. Chromatogr. A 1216 (2009) 5327–5332.
[13] A. Young, G. Lai, B. Hung, A. Yuen, Y. He, Determination of trace chloroanilines in environmental water samples using hollow fiber-based liquid phase microextraction, Chromatographia (2011), doi:10.1007/s10337-011-2022-6.
[14] F. Pena-Pereira, I. Lavilla, I. Bendicho, Miniaturized preconcentration methods based on liquid–liquid extraction and their application in inorganic ultratrace analysis and speciation: a review, Spectrochim. Acta 64B (2009) 1–15.
[15] M. Rezaee, Y. Assadi, M.R. Milani Hosseini, E. Aghaee, F. Ahmadi, S. Berijani, Determination of organic compounds in water using dispersive liquid–liquid microextraction, J. Chromatogr. A 1116 (2006) 1–9.
[16] M. Moradi, Y. Yamini, A. Esrafili, S. Seidi, Application of surfactant assisted dispersive liquid–liquid microextraction for sample preparation of chlorophenols in water samples, Talanta 82 (2010) 1864–1869.
[17] M. Moradi, Y. Yamini, J. Kakehmam, A. Esrafili, M. Ghambarian, A new strategy to simultaneous microextraction of acidic and basic compounds, J. Chromatogr. A 1218 (2011) 3945–3951.
[18] A. Saleh, Y. Yamini, M. Faraji, M. Rezaee, M. Ghambarian, Ultrasound-assisted emulsification microextraction method based on applying low density organic solvents followed by gas chromatography analysis for the determination of polycyclic aromatic hydrocarbons in water samples, J. Chromatogr. A 1216 (2009) 6673–6679.
[19] Z. Qiang, C. Adams, Potentiometric determination of acid dissociation constants (pK_a) for human and veterinary antibiotics, Water Res. 38 (2004) 2874–2890.
[20] A. Drapała, J.Å. Jönsson, P. Wieczorek, Peptides analysis in blood plasma using on-line system of supported liquid membrane and high-performance liquid chromatography, Anal. Chim. Acta 553 (2005) 9–14.
[21] M. Corbera, M. Hidalgo, V. Salvadó, P.P. Wieczorek, Determination of glyphosate and aminomethylphosphonic acid in natural water using the capillary electrophoresis combined with enrichment step, Anal. Chim. Acta 540 (2005) 3–7.
[22] M. Ramos, M. Bello, R. Fernandez-Torres, J.A. Ocaña, M.C. Mochon, Hollow fiber-based liquid phase microextraction (HF-LPME) as a new approach for the HPLC determination of fluoroquinolones in biological and environmental matrices, J. Pharm. Biomed. Anal. 55 (2011) 332–341.
[23] W. Gaoa, G. Chena, Y. Chenb, X. Zhangb, Y. Yina, Z. Huc, Application of single drop liquid–liquid–liquid microextraction for the determination of fluoroquinolones in human urine by capillary electrophoresis, J. Chromatogr. B 879 (2011) 291–295.
[24] A. Espinosa-Mansilla, A. Muñoz de la Peña, D. González Gómez, F. Salinas, HPLC determination of enoxacin, ciprofloxacin, norfloxacin and ofloxacin with photoinduced fluorimetric (PIF) detection and multiemission scanning. Application to urine and serum, J. Chromatogr. B 822 (2005) 185–193.
[25] A. Navalón, O. Ballesteros, R. Blanc, J. Vílchez, Determination of ciprofloxacin in human urine and serum samples by solid-phase spectrofluorimetry, Talanta 52 (2000) 845–852.
[26] H. Yan, H. Wang, X. Qin, B. Liu, J. Du, Ultrasound-assisted dispersive liquid–liquid microextraction for determination of fluoroquinolones in pharmaceutical wastewater, J. Pharm. Biomed. Anal. 54 (2011) 53–57.
[27] K. Mitani, H. Kataoka, Determination of fluoroquinolones in environmental waters by in-tube solid-phase microextraction coupled with liquid chromatography–tandem mass spectrometry, Anal. Chim. Acta 562 (2006) 16–22.
[28] S. Bailac, D. Barrón, V. Sanz-Nebot, J. Barbosa, Determination of fluoroquinolones in chicken tissues by LC-coupled electrospray ionisation and atmospheric pressure chemical ionization, J. Sep. Sci. 29 (2006) 131–137.

Journal of Pharmaceutical and Biomedical Analysis 66 (2012) 271–277

Contents lists available at SciVerse ScienceDirect

Journal of Pharmaceutical and Biomedical Analysis

journal homepage: www.elsevier.com/locate/jpba

UPLC–MS/MS determination of paeoniflorin, naringin, naringenin and glycyrrhetinic acid in rat plasma and its application to a pharmacokinetic study after oral administration of Si—Ni—San decoction

Jing Wen, Ying Qiao, Jie Yang, Xinyu Liu, Yang Song, Zhigang Liu, Famei Li*

Department of Analytical Chemistry, Shenyang Pharmaceutical University, 103 Wenhua Road, Shenyang 110016, PR China

ARTICLE INFO

Article history:
Received 27 October 2011
Received in revised form 17 March 2012
Accepted 19 March 2012
Available online 28 March 2012

Keywords:
Pharmacokinetics
Si—Ni—San decoction
UPLC–MS/MS

ABSTRACT

A UPLC–MS/MS method was developed for the simultaneous determination of paeoniflorin, naringin, naringenin and glycyrrhetinic acid in rat plasma. A Waters BEH C_{18} column was used with a gradient mobile phase system of methanol–water containing 2 mM ammonium acetate. The analysis was performed on a positive ionization electrospray mass spectrometer via multiple reaction monitoring (MRM). One-step protein precipitation with acetonitrile was used to extract the analytes from plasma. The limits of quantification were 9.800 ng/ml for paeoniflorin, 5.100 ng/ml for naringin, 5.200 ng/ml for naringenin and 10.60 ng/ml for glycyrrhetinic acid, respectively. The intra- and inter-day precision (relative standard deviation, RSD) ranged 4.9–12% and 2.8–13%, respectively. The accuracy (relative error, RE) was from −7.3% to 7.5% at all quality control (QC) levels. The validated method was applied to a pharmacokinetic study in rats after oral administration of Si—Ni—San decoction.

Crown Copyright © 2012 Published by Elsevier B.V. All rights reserved.

1. Introduction

Si—Ni—San is a traditional Chinese medicine composed of Radix Bupleuri, Radix Paeoniae Alba, Fructus Aurantii Immaturus and Radix Glycyrrhiza (1:1:1:1). The Chemical constituents of Si—Ni—San mainly include saponins (including saikoside and paeoniflorin, etc.), flavonoid glycosides (including naringin, hesperidin and liquiritin, etc.) and organic acids (including glycyrrhizic acid and benzoic acid, etc.), etc. Pharmacological studies have shown that Si—Ni—San had significant therapeutic effect on various experimental liver injury models [1]. It has been reported that the activities of Si—Ni—San were stronger than those of single drugs, which was the result of each constituent affecting the different target of liver injury [2]. Several reports [3–6] have indicated that saikosaponin, paeoniflorin, naringin and glycyrrhizin had played an important role in Si—Ni—San. Our previous work has shown that paeoniflorin, naringin, naringenin and glycyrrhetinic acid, active components of Si—Ni—San decoction were absorbed into the blood and could be detected after oral administration.Paeoniflorin is one of the main active ingredients in Radix Paeoniae which has been used as a phytochemical marker for the quality control of Radix Paeoniae in Chinese Pharmacopoeia [7]. Pharmacological studies have exhibited that paeoniflorin has liver protecting [8], anti-inflammatory [9], anti-coagulant [10], antioxidant [11] and neuronprotective [12] effects. Naringin is a flavonoid present in many Citrus fruits and traditional Chinese medicines. Like most flavonoids, naringin has anti-inflammatory [13], anti-ulcer [14] and antioxidant [15] activities. Early research has shown that orally administered naringin can be metabolized into naringenin and naringenin glucuronide [16–18]. Naringenin, the aglycone of naringin, has also been found to exhibit anti-ulcer [19,20], antioxidant [15] and anticancer [21] effects. Glycyrrhizic acid (GL) is one of the bioactive ingredients in Radix Glycyrrhiza. GL has been used in the treatment of hepatitis and chronic hepatitis [22–24]. GL also has anti-inflammatory, antiviral and antioxidant activities [25]. After orally administered, GL is converted to glycyrrhetinic acid (GA) by intestinal bacteria in rats [26,27]. It was found that GL was subjected to presystemic metabolism and enterohepatic circulation [28,29]. For the identification of metabolites of Si—Ni—San see [30]. Despite the number of pharmacological studies of the four components, there is no report on LC or LC–MS methods for the pharmacokinetic study of the four components.

In the present paper, we developed and validated a sensitive and selective UPLC–MS/MS method for the simultaneous determination of paeoniflorin, naringin, naringenin and glycyrrhetinic acid in rat plasma. The method was applied to a pharmacokinetic study in rats after oral administration of Si—Ni—San decoction.

* Corresponding author. Tel.: +86 24 2398 6289; fax: +86 24 2398 6289.
E-mail address: lifamei@syphu.edu.cn (F. Li).

0731-7085/$ – see front matter Crown Copyright © 2012 Published by Elsevier B.V. All rights reserved.
doi:10.1016/j.jpba.2012.03.040

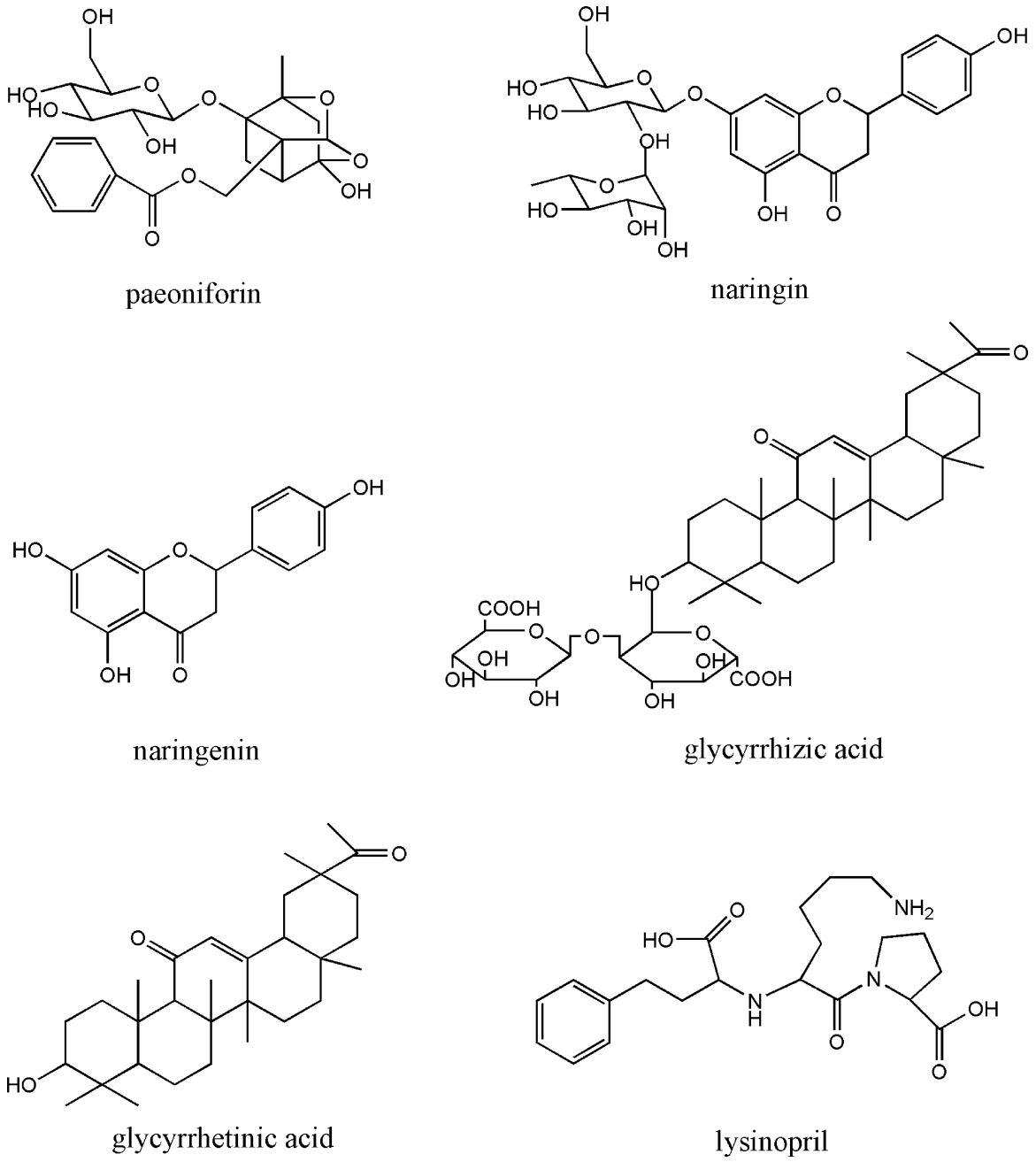

Fig. 1. Chemical structures of paeoniflorin, naringin, naringenin, glycyrrhizic acid, glycyrrhetinic acid and lysinopril. (I.S.)

2. Experimental

2.1. Chemicals and reagents

The reference standards of paeoniflorin, naringin, glycyrrhetinic acid and lysinopril (internal standard, I.S.) (purity >98%) were purchased from the National Institute for the Control of Pharmaceutical and Biological Products (Beijing, China). The reference standard of naringenin (purity >98%) was purchased from Baozetang Medical Technology Co. Ltd. (Jiangsu, China). The structures of these compounds are shown in Fig. 1. Radix Bupleuri was purchased from Northeast Big Pharmacy (Shenyang, China). Radix Paeoniae Alba and Fructus Aurantii Immaturus were purchased from Weikang Big Pharmacy (Shenyang, China). Radix Glycyrrhiza was purchased from Beijing Tongrentang Pharmacy (Shenyang, China). The above four medicinal materials were authenticated by Professor Jincai Lu (College of Traditional Chinese Materia Medica, Shenyang Pharmaceutical University). Methanol of HPLC grade was obtained from Tedia (Fairfield, OH, USA). Ammonium acetate of HPLC grade was obtained from Dikma (Richmond Hill, NY, USA). All other reagents were of analytical grade.

2.2. Instrumentation and analytical conditions

2.2.1. Liquid chromatography

Chromatography was performed on an ACQUITY UPLC™ system (Waters Corp., Milford, MA, USA) with cooling autosampler and column oven. An ACQUITY UPLC™ BEH C_{18} column (100 mm × 2.1 mm, 1.7 μm) was employed. The column temperature was maintained at 35 °C and a gradient elution with methanol

(A)–water (2 mM ammonium acetate) (B) was used. The gradient program was as follows: 0–2.5 min, 25–90% A, 2.5–4.5 min, 90% A. The flow rate was set at 0.25 ml/min. The autosampler was conditioned at 4 °C and the injection volume was 10 μl for analysis.

2.2.2. Mass spectrometry

Triple-quadrupole tandem mass spectrometric detection was carried out on a Micromass Quattro micro™ API mass spectrometer (Waters Corp, Milford, USA) with an electrospray ionization (ESI) interface. The ESI source was operated in positive ionization mode. Quantification was performed using MRM of the transitions of m/z 497.9 → 178.9 for paeoniflorin, m/z 581.2 → 273.0 for naringin, m/z 272.9 → 152.8 for naringenin, m/z 470.9 → 134.8 for glycyrrhetinic acid and m/z 406.2 → 246.1 for I.S., respectively.

The optimal MS parameters obtained were as follows: capillary voltage 3.0 kV; cone voltage for paeoniflorin, naringin, naringenin, glycyrrhetinic acid and I.S. was 13, 15, 30, 20 and 30 kV, respectively; source temperature 100 °C and desolvation temperature 450 °C. Nitrogen was used as desolvation and cone gas with a flow rate of 500 and 30 l/h. Argon was used as the collision gas at a pressure of approximately 2.8×10^{-3} mbar. The optimized collision energy for paeoniflorin, naringin, naringenin, glycyrrhetinic acid and I.S. was 20, 18, 25, 37 and 23 eV, respectively. All data collected in centroid mode were processed using MassLynx™ NT 4.1 software with a QuanLynx™ program (Waters Corp., Milford, MA, USA).

2.3. Preparation of standards and quality control (QC) samples

The standard stock solutions (196.0, 204.0, 208.0 and 212.0 μg/ml) of paeoniflorin, naringin, naringenin and glycyrrhetinic acid were prepared by dissolving required amount of the reference standards in methanol. The working solutions of calibration curve were prepared by mixing and diluting the stock solutions of each compound with methanol. Standard solution of I.S. was prepared by dissolving lysinopril in methanol at a final concentration of 11.30 μg/ml.

The standard plasma samples of calibration curve were prepared by spiking 20 μl of the above working solution into 100 μl of blank plasma to yield the concentration at 9.800, 19.60, 98.00, 490.0, 980.0, 1960, 3920 ng/ml for paeoniflorin, 5.100, 10.20, 51.00, 255.0, 510.0, 1020, 2040 ng/ml for naringin, 5.200, 10.40, 52.00, 260.0, 520.0, 1040, 2080 ng/ml for naringenin and 10.60, 21.20, 106.0, 530.0, 1060, 2120, 4240 ng/ml for glycyrrhetinic acid, respectively. Low, medium, and high concentrations of QC samples were chosen to be 19.60, 313.6, 3136 ng/ml for paeoniflorin, 10.20, 163.2, 1632 ng/ml for naringin, 10.40, 166.4, 1664 ng/ml for naringenin and 21.20, 339.2, 3392 ng/ml for glycyrrhetinic acid, respectively.

2.4. Plasma sample preparation

I.S. solution (20 μl) was pipetted into 1.5 ml EP tubes and evaporated to dryness under a gentle stream of nitrogen. The residue was vortex-mixed with 100 μl of plasma samples for 30 s and then 150 μl of acetonitrile was added. The mixture was vortex-mixed for 60 s and centrifuged at 13,000 rpm for 10 min to separate the precipitated protein, 10 μl of the supernatant were injected into the UPLC–MS/MS system for analysis.

2.5. Method validation

2.5.1. Selectivity

The selectivity was investigated by comparing the chromatograms of blank plasma obtained from six rats with those of corresponding standard plasma sample spiked with paeoniflorin, naringin, naringenin, glycyrrhetinic acid and I.S. and plasma sample after oral administration of Si—Ni—San decoction.

2.5.2. Linearity and lower limit of quantification (LLOQ)

Calibration curves were prepared using the standard plasma samples described in Section 2.3, and constructed from the peak-area ratios of each analyte to I.S. versus plasma concentrations using a $1/x^2$ weighted linear least-squares regression model. The LLOQ is defined as the lowest concentration on the calibration curve at which an acceptable accuracy (RE) within ±20% and a precision (RSD) below 20% can be obtained.

2.5.3. Precision and accuracy

Five replicates of QC samples of each analyte at three QC levels were included in each run to determine the intra- and inter-day (3 days) precision of the assay. Accuracy was determined as the percentage difference between the mean concentrations determined and the nominal concentrations. According to the guidance of FDA, the RSD determined at each concentration level is required not exceeding 15% and RE within ±15% of the actual value.

2.5.4. Extraction recovery and matrix effect

Extraction recovery of the four analytes was evaluated at three QC levels and for the I.S. at one concentration by comparing the peak areas obtained from plasma samples with the analytes spiked before and after extraction. Matrix effect was evaluated by comparing the peak areas of the analytes obtained from plasma samples with the analytes spiked after extraction to those from the neat standard solutions at the same concentration. An endogenous matrix effect was implied if the ratio is less than 85% or more than 115%.

2.5.5. Stability

Stability of the four analytes in plasma was assessed by analyzing QC samples of three levels during the sample storage and processing procedures. Short-term stability was assessed by analyzing QC samples kept at room temperature for 4 h, which exceeded the routine preparation time of samples. Long-term stability was evaluated by keeping QC samples at −20 °C for 15 days. Freeze–thaw stability was investigated after three freeze (−20 °C) and thaw (room temperature) cycles. Post-preparation stability was assessed by analyzing the extracted QC samples kept in the autosampler at 4 °C for 12 h. All stability testing QC samples were determined using calibration curve of freshly prepared.

2.6. Pharmacokinetic study

Healthy male SD rats, weighing 200–240 g, were obtained from the Animal Center of Shenyang Pharmaceutical University (Shenyang, China). All protocols of animal experiments were approved in accordance with the Regulations of Experimental Animal Administration issued by the State Commission of Science and Technology of the People's Republic of China. The rats were fasted for 12 h but with free access to water prior to the experiments.

Si—Ni—San extractum was dissolved with 0.5% CMC-Na yielding a concentration of 2.5 g/ml (expressed in grams of crude drugs per ml). The rats were given orally with 40 g/kg Si—Ni—San (equivalent to 2.2 mg/g for paeoniflorin, 21.5 mg/g for naringin and 5.8 mg/g for glycyrrhizic acid). Blood samples (0.3 ml) were collected in 1.5 ml heparinized polythene tubes before dosing and 0.17, 0.33, 0.50, 0.75, 1.0, 2.0, 4.0, 6.0, 8.0, 10, 12, 14, 24, 30, 48, 60 and 72 h after dosing. The blood samples were immediately centrifuged at 13,000 rpm for 10 min and the plasma was stored at −20 °C until analysis.

The maximum plasma concentrations (C_{max}) and the time to reach the maximum concentrations (T_{max}) were obtained directly

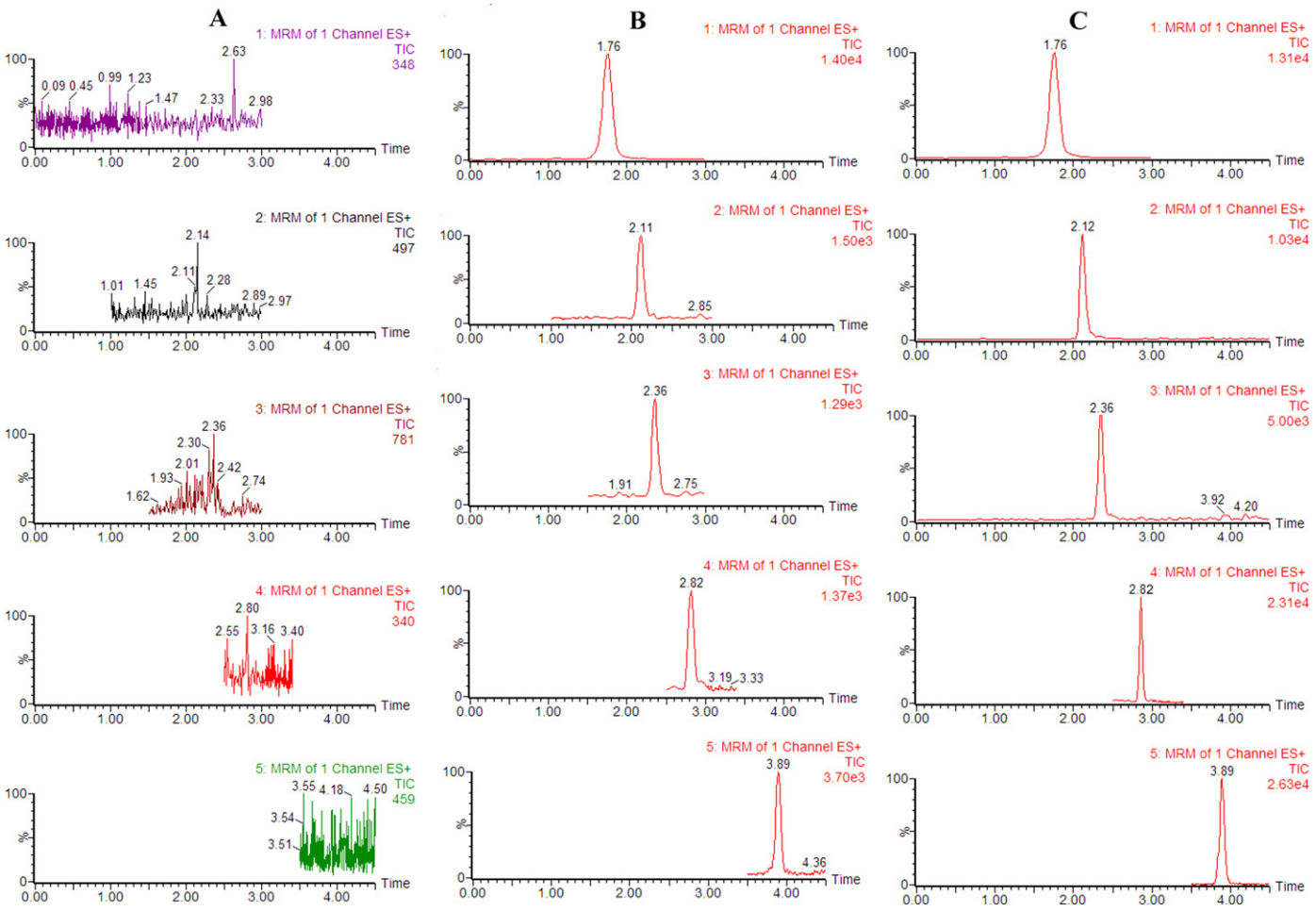

Fig. 2. Representative MRM chromatograms of paeoniflorin (channel 2), naringin (channel 3), naringenin (channel 4), glycyrrhetinic acid (channel 5) and I.S. (channel 1) in rat plasma: (A) blank plasma sample; (b) Blank plasma sample spiked with paeoniflorin, naringin, naringenin, glycyrrhetinic acid at the LLOQ and I.S.; (C) plasma sample from a rat 8.0 h after oral administration of Si—Ni—San decoction at a dose of 40 g/kg.

from the observed data. The elimination rate constant (k_e) was calculated on the slope of the linear regression of log-transformed concentration versus time using the last four measurable points. The elimination half-life ($t_{1/2}$) was calculated using $0.693/k_e$. The area under plasma concentration–time curve (AUC_{0-t}) to the last measurable plasma concentration (C_t) was estimated by using the linear trapezoidal rule. The area under the plasma concentration–time curve to time infinity ($AUC_{0-\infty}$) was calculated as $AUC_{0-\infty} = AUC_{0-t} + C_t/K_e$. The mean residence time (MRT) was calculated as $AUMC_{0-\infty}/AUC_{0-\infty}$. Data were expressed in mean and standard deviation (SD) for each group. The significance of difference was assessed by Student's t-test.

3. Results and discussion

3.1. Analysis method optimization

In our study, various mobile phase conditions were tried to obtain optimized responses, suitable retention times and good peak shapes for the analytes. Methanol, acetonitrile, 5 mM ammonium acetate, 0.1% formic acid and 100% water were tested as potential mobile phases. Finally a gradient elution with methanol and water containing 2 mM ammonium acetate was chosen to obtain satisfactory sensitivity and good peak shapes. The gradient program (Section 2.2.1) was used for short analytical time (4.5 min) and avoiding "cross-talk" peaks. Lysinopril was selected as the internal standard for its similarity in the retention and ESI ionization to those of analytes. For the MS condition, both positive and negative scan modes were tested and the positive mode was selected due to higher sensitivity. MRM mode was used to monitor both quasi-molecule and fragment ions, which made the method more specific. ESI source temperature, capillary and cone voltage, flow rate of desolvation gas and cone gas were optimized to obtain highest intensity of protonated molecules of the four analytes.

3.2. Sample extraction

Liquid–liquid extraction (LLE) was initially developed with different solvents, however, it could not eliminate the interferences from the sample matrix. Protein precipitation (PPT) was explored to extract the four analytes from plasma samples. The recovery of PPT with acetonitrile was higher than with methanol. Satisfactory recovery and higher responses were obtained with 150 μl acetonitrile.

3.3. Method validation

3.3.1. Selectivity

The selectivity was evaluated by extracting blank rat plasma from six different matrices and comparing the MS/MS responses

Table 1
Precision and accuracy data for the determination of paeoniflorin, naringin, naringenin and glycyrrhetinic acid in rat plasma ($n = 3$ days and five replicates per day).

Component	Added (ng/ml)	Found (ng/ml) (mean ± SD)	Intra-day RSD (%)	Inter-day RSD (%)	Relative error (%)
Paeoniflorin	9.800	9.437 ± 0.660	4.8	14	−3.7
	19.60	19.19 ± 1.57	6.9	13	−2.1
	313.6	315.8 ± 20.2	5.5	9.7	0.7
	3136	3371 ± 185	5.1	8.0	7.5
Naringin	5.100	5.125 ± 0.431	5.7	15	0.5
	10.20	10.68 ± 1.22	12	13	4.7
	163.2	167.6 ± 12.7	6.9	10	2.7
	1632	1647 ± 86.0	5.2	4.4	0.9
Naringenin	5.200	5.425 ± 0.522	8.9	13	4.1
	10.40	10.12 ± 0.67	5.1	12	−2.7
	166.4	177.1 ± 10.7	6.0	7.7	6.4
	1664	1753 ± 89	5.4	4.4	5.3
Glycyrrhetinic acid	10.60	10.21 ± 1.00	9.9	9.2	−3.7
	21.20	20.98 ± 1.29	4.9	11	−1.0
	339.2	332.0 ± 24.2	7.7	6.7	−2.1
	3392	3145 ± 217	7.4	2.8	−7.3

Table 2
Pharmacokinetic parameters of paeoniflorin, naringin, naringenin and glycyrrhetinic acid after oral administration of Si—Ni—San decoction at a dose of 40 g/kg ($n = 6$, mean ± SD).

Component	Paeoniflorin	Naringin	Naringenin	Glycyrrhetinic acid
C_{max} (ng/ml)	870.9 ± 238.3	368.9 ± 195.3	1034 ± 402.0	3972 ± 342.0
T_{max} (h)	0.70 ± 0.11	0.75 ± 0.17	13.6 ± 0.89	27.6 ± 3.28
K_e (h)	0.25 ± 0.11	0.13 ± 0.04	0.15 ± 0.04	0.07 ± 0.01
$t_{1/2}$ (h)	3.19 ± 1.54	5.76 ± 2.12	5.00 ± 1.46	9.40 ± 1.15
AUC_{0-t} (ng h/ml)	2282 ± 652.3	1436 ± 554.8	12,242 ± 6381	77,481 ± 16,674
$AUC_{0-\infty}$ (ng h/ml)	2489 ± 817.1	1492 ± 535.8	12,284 ± 6377	78,817 ± 16,707
$MRT_{0-\infty}$ (h)	4.11 ± 2.34	9.96 ± 1.64	16.25 ± 1.64	32.85 ± 4.07

at the retention times of the four analytes to the responses of the LLOQ. The representative chromatograms of blank plasma, blank plasma spiked with LLOQ and plasma sample obtained after oral administration of Si—Ni—San decoction are shown in Fig. 2. Under the established chromatographic condition, no endogenous interference from the plasma was observed and all the four analytes as well as I.S. were not interfered with each other.

3.3.2. Linearity and LLOQ

Typical equations for the calibration curves and correlation coefficients (r) were $y = 3.74 \times 10^{-3}x + 1.07 \times 10^{-2}$, $r = 0.9953$ for paeoniflorin, $y = 1.31 \times 10^{-3}x + 4.97 \times 10^{-3}$, $r = 0.9967$ for naringin, $y = 5.39 \times 10^{-3}x + 2.85 \times 10^{-3}$, $r = 0.9988$ for naringenin, and $y = 8.09 \times 10^{-4}x + 1.90 \times 10^{-3}$, $r = 0.9949$ for glycyrrhetinic acid. The calibration curves of the four analytes were linear in the ranges of 9.800–3920 ng/ml, 5.100–2040 ng/ml, 5.200–2080 ng/ml and 10.60–4240 ng/ml, respectively. The LLOQ of the four analytes were 9.800 ng/ml, 5.100 ng/ml, 5.200 ng/ml and 10.60 ng/ml, respectively, with precision (RSD) below 20% and accuracy (RE) within ±20% (Table 1).

3.3.3. Precision and accuracy

The intra- and inter-day precision and accuracy were determined by measuring five replicates of QC samples at three concentration levels. The precision and accuracy are shown in Table 1. The intra- and inter-day precision ranged 4.9–12% and 2.8–13%, respectively. The accuracy derived from QC samples was within −7.3 to 7.5% for three QC levels.

3.3.4. Extraction recovery and matrix effect

The extraction recoveries from QC samples at three concentrations levels were 87.50 ± 3.75%, 90.45 ± 6.98%, 84.94 ± 1.56% for paeoniflorin, 84.55 ± 8.32%, 87.83 ± 5.50%, 86.65 ± 1.34% for naringin, 95.62 ± 7.14%, 90.51 ± 8.75%, 90.90 ± 1.76% for naringenin and 89.98 ± 5.73%, 93.35 ± 1.61%, 91.76 ± 8.06% for glycyrrhetinic acid, respectively, whereas 83.11 ± 5.34% for I.S..

With regard to matrix effect, all the calculated values were between 90.93% and 109.8%. No significant matrix effect for paeoniflorin, naringin, naringenin, glycyrrhetinic acid and I.S. was observed, indicating that no co-eluting substance influenced the ionization of the analytes and I.S..

3.3.5. Stability

The concentrations of paeoniflorin, naringin, naringenin and glycyrrhetinic acid measured in the stability study were between 89.5% and 102.9% of the initial values, indicating that the analytes in rat plasma were stable for 4 h at room, 15 days at −20 °C, three freeze–thaw cycles and 12 h after pretreatment.

3.4. Pharmacokinetic application

The validated UPLC–MS/MS method was applied to a pharmacokinetic study of four major components in rats after oral administration of Si—Ni—San decoction. The mean plasma concentration–time curves of paeoniflorin, naringin, naringenin and glycyrrhetinic acid are presented in Fig. 3 and the pharmacokinetic parameters of the four components are shown in Table 2.

As seen from Table 2, the T_{max} are 0.70 h for paeoniflorin, 0.75 h for naringin, 13.6 h for naringenin and 27.6 h for glycyrrhetinic acid, respectively. Naringin is quickly absorbed into the body and also quickly eliminated after oral administration of Si—Ni—San decoction. Another small peak can be seen at 12 h (Fig. 3B), which may be due to the enterohepatic circulation of naringin in rats. Its metabolite, naringenin is produced slowly after oral administration of Si—Ni—San decoction. Glycyrrhetinic acid could not been detected in Si—Ni—San decoction in vitro. However, the C_{max} of glycyrrhetinic acid is 3972 ng/ml after oral administration of Si—Ni—San decoction. Therefore, the pharmacokinetic studies of the four analytes need to be further investigated.

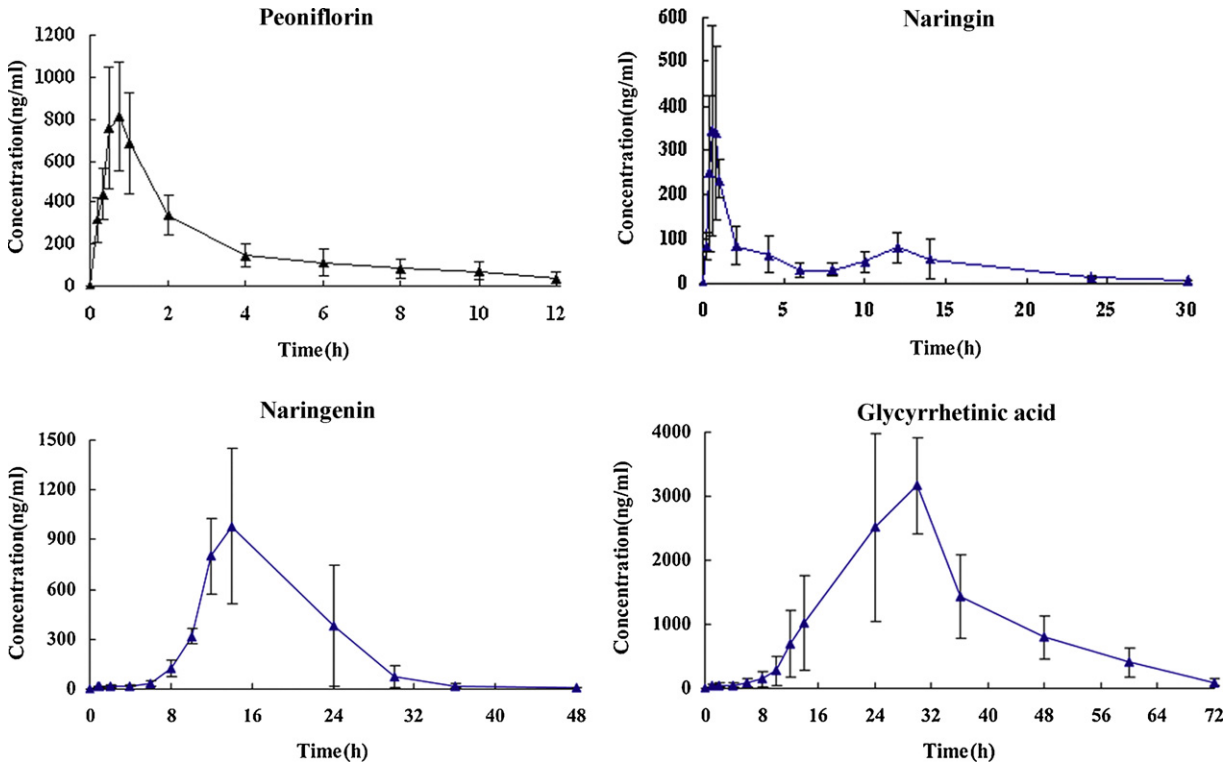

Fig. 3. The mean (±SD, $n = 6$) plasma concentration–time curves of paeoniflorin (A), naringin (B), naringenin (C) and glycyrrhetinic acid (D) following oral administration of Si—Ni—San decoction.

Acknowledgment

This work is supported by grant from the National Foundation of Natural Sciences of China (no. 81102786).

References

[1] J.Y. Jiang, C. Zhou, Q. Xu, Alleviating effects of Si—Ni—San, a traditional Chinese prescription, on experimental liver injury and its mechanisms, Biol. Pharm. Bull. 26 (2003) 1089–1094.
[2] J.Y. Jiang, Q. Xu, Effect of Si—Ni—San and its individual component drugs on experimental liver injury, Chin. J. Nat. Med. 2 (2004) 45–49.
[3] L. Zhang, Y. Dong, Y. Sun, T. Chen, Q. Xu, Role of four major components in the effect of Si—Ni—San, a traditional Chinese prescription, against contact sensitivity in mice, J. Pharm. Pharmacol. 58 (2006) 1257–1264.
[4] Y. Sun, T. Chen, Q. Xu, Si—Ni—San, a traditional Chinese prescription, and its drug-pairs suppress contact sensitivity in mice via inhibition of the activity of metalloproteinases and adhesion of T lymphocytes, J. Pharm. Pharmacol. 55 (2003) 839–846.
[5] Y. Sun, T.T. Cai, Y. Shen, X.B. Zhou, T. Chen, Q. Xu, Si—Ni—San, a traditional Chinese prescription, and its active ingredient glycyrrhizin ameliorate experimental colitis through regulating cytokine balance, Int. Immunopharmacol. 9 (2009) 1437–1443.
[6] Y. Sun, Y. Dong, H.J. Jiang, T.T. Cai, L. Chen, X. Zhou, T. Chen, Q. Xu, Dissection of the role of paeoniflorin in the traditional Chinese medicinal formula Si—Ni—San against contact dermatitis in mice, Life Sci. 84 (2009) 337–344.
[7] Pharmacopoeia Commission of PRC, Pharmacopoeia of the People's Republic of China, Chemical Industry Press, Beijing, 2010, pp. 96–97.
[8] J. Song, X.D. Wang, J.N. Zhao, Y. Dai, Z.W. Deng, Influence on experimental liver injury of extraction from Peony and Licorice decoction, Pharmacol. Clin. Chin. Mater. Med. 26 (2010) 40–42.
[9] J. Yamahara, T. Yamada, H. Kimura, T. Sawada, H. Fujimura, Biologically active principles of crude drugs. II. Anti-allergic principles in Shoseiryu-To anti-inflammatory properties of paeoniflorin and its derivatives, J. Ethnopharmacol. 5 (1982) 921–929.
[10] Y.K. Koo, J.M. Kim, J.Y. Koo, S.S. Kang, K. Bae, Y.S. Kim, J.H. Chung, H.S. Yun-Choi, Platelet anti-aggregatory and blood anti-coagulant effects of compounds isolated from *Paeonia lactiflora* and *Paeonia suffruticosa*, Pharmazie 65 (2010) 624–628.
[11] T. Chen, Z.P. Guo, X.Y. Jiao, Y.H. Zhang, J.Y. Li, H.J. Liu, Protective effects of paeoniflorin against hydrogen peroxide-induced oxidative stress in human umbilical vein endothelial cells, Can. J. Physiol. Pharmacol. 89 (2011) 445–453.
[12] L. Xiao, Y.Z. Wang, J. Liu, X.T. Luo, Y. Ye, X.Z. Zhu, Effects of paeoniflorin on the cerebral infarction, behavioral and cognitive impairments at the chronic stage of transient middle cerebral artery occlusion in rats, Life Sci. 78 (2005) 413–420.
[13] M. Jain, H.S. Parmar, Evaluation of antioxidative and anti-inflammatory potential of hesperidin and naringin on the rat air pouch model of inflammation, Inflamm. Res. 60 (2011) 483–891.
[14] M.J. Martin, E. Marhuenda, C. Perez-Guerrero, J.M. France, Antiulcer effect of naringin on gastric lesions induced by ethanol in rats, Pharmacology 49 (1994) 144–150.
[15] Y.T. Chen, R.T. Zheng, Z.J. Jia, Y. Ju, Flavonoids as superoxide scavengers and antioxidants, Free Radic. Biol. Med. 9 (1990) 19–21.
[16] K. Ishii, T. Furuta, Y. Kasuya, Determination of naringin and naringenin in human plasma by high-performance liquid chromatography, J. Chromatogr. B 683 (1996) 225–229.
[17] K. Ishii, T. Furuta, Y. Kasuya, Determination of naringin and naringenin in human urine by high-performance liquid chromatography utilizing solid-phase extraction, J. Chromatogr. B 704 (1997) 299–305.
[18] S.L. Hsiu, T.Y. Huang, Y.C. Hou, D.H. Chin, P.D. Chao, Comparison of metabolic pharmacokinetics of naringin and naringeninin rabbits, Life Sci. 70 (2002) 1481–1489.
[19] N.S. Parmar, The gastric anti-ulcer activity of naringenin, a specific histidine decarboxylase inhibitor, Int. J. Tissue React. 5 (1983) 415–420.
[20] V. Motilva, de la Lastra C. Alarcón, M.J. Martín, Ulcer-protecting effects of naringenin on gastric lesions induced by ethanol in rat: role of endogenous prostaglandins, J. Pharm. Pharmacol. 46 (1994) 91–94.
[21] G. Ekambaram, P. Rajendran, V. Magesh, D. Sakthisekaran, Naringenin reduces tumor size and weight lost in N-methyl-N′-nitro-Nnitrosoguanidine-induced gastric carcinogenesis in rats, Nutr. Res. 28 (2008) 106–112.
[22] J. Eisenburg, Treatment of chronic hepatitis B. Part 2. Effect of glycyrrhizic acid on the course of illness, Fortschr. Med. 110 (1992) 395–398.
[23] C. Feng, H. Wang, C. Yao, J. Zhang, Z. Tian, Diammonium glycyrrhizinate, a component of traditional Chinese medicine Gan-Cao, prevents murine T-cell-mediated fulminant hepatitis in IL-10- and IL-6-dependent manners, Int. Immunopharmacol. 7 (2007) 1292–1298.
[24] J. Yang, L. Zhou, J. Wang, G. Wang, A.K. Davey, The disposition of diammonium glycyrrhizinate and glycyrrhetinic acid in the isolated perfused rat intestine and liver, Planta Med. 74 (2008) 1351–1356.
[25] M.N. Asl, H. Hosseinzadeh, Review of pharmacological effects of *Glycyrrhiza* sp. and its bioactive compounds, Phytother. Res. 22 (2008) 709–724.
[26] S. Takeda, K. Ishihara, Y. Wakui, S. Amagaya, M. Maruno, T. Akao, K. Kobashi, Bioavailability study of glycyrrhetic acid after oral administration of glycyrrhizin in rats; relevance to the intestinal bacterial hydrolysis, J. Pharm. Pharmacol. 48 (1996) 902–905.

[27] Z. Wang, Y. Kurosaki, T. Nakayama, T. Kimura, Mechanism of gastrointestinal absorption of glycyrrhizin in rats, Biol. Pharm. Bull. 17 (1994) 1399–1403.
[28] B.A. Ploeger, J. Meulenbelt, J. DeJongh, Physiologically based pharmacokinetic modeling of glycyrrhizic acid, a compound subject to presystemic metabolism and enterohepatic cycling, Toxicol. Appl. Pharmacol. 162 (2000) 177–188.
[29] B. Ploeger, T. Mensinga, A. Sips, W. Seinen, J. Meulenbelt, J. DeJongh, The pharmacokinetics of glycyrrhizic acid evaluated by physiologically based pharmacokinetic modeling, Drug Metab. Rev. 33 (2001) 125–147.
[30] Z. Yan, Y. Chen, T. Li, J. Zhang, X. Yang, Identification of metabolites of Si—Ni—San, a traditional Chinese medicine formula, in rat plasma and urine using liquid chromatography/diode array detection/triple-quadrupole spectrometry, J. Chromatogr. B 885–886 (2012) 73–82.

Journal of Pharmaceutical and Biomedical Analysis 66 (2012) 278–281

Contents lists available at SciVerse ScienceDirect

Journal of Pharmaceutical and Biomedical Analysis

journal homepage: www.elsevier.com/locate/jpba

Everolimus quantification in peripheral blood mononuclear cells using ultra high performance liquid chromatography tandem mass spectrometry

Francois Roullet-Renoleau[a], Florian Lemaitre[a], Marie Antignac[b], Noel Zahr[c], Robert Farinotti[a], Christine Fernandez[a,b,*]

[a] Clinical Pharmacy Department – EA 4123, College of Pharmacy, Paris 11 University, 5 rue Jean Baptiste Clement, 92296 Chatenay Malabry, France
[b] Saint Antoine Hospital – AP-HP, Pharmacy Department – 184 rue du Fbg Saint Antoine, 75012 Paris, France
[c] Pitie Salpetriere Hospital – AP-HP, Pharmacology Department – 47 boulevard de l'hopital, 75013 Paris, France

ARTICLE INFO

Article history:
Received 5 November 2011
Received in revised form 22 February 2012
Accepted 20 March 2012
Available online 29 March 2012

Keywords:
Everolimus
Liquid chromatography tandem mass spectrometry
Peripheral blood mononuclear cells
Therapeutic drug monitoring

ABSTRACT

A reliable ultra high performance liquid chromatography tandem mass spectrometry method has been developed for the determination of everolimus in human peripheral blood mononuclear cells (PBMCs). Protein precipitation was used for sample preparation. Analysis was performed on an UPLC Waters Acquity system. Chromatography was carried out using a cartridge column MassTrak TDM C18 (2.1 × 10 mm) with 0.1% formic acid and 2 mM of ammonium acetate in water and 0.1% formic acid and 2 mM of ammonium acetate in methanol mixture as a mobile phase delivered at a flow rate of 0.4 mL/min in gradient mode. The assay was linear over a range of 0–12.5 ng/mL. The analysis of quality control samples at 2.5, 5.0 and 10.0 ng/mL demonstrated good precision with relative standard deviation of less than 15%. Recoveries at concentrations of 2.5, 5.0 and 10.0 ng/mL were all greater than 83%. The method was successfully applied to the analysis of everolimus in PBMCs from blood samples of transplant recipients.
© 2012 Elsevier B.V. All rights reserved.

1. Introduction

Everolimus (EVE) is a macrolide lactone with potent immunosuppressive properties, used in combination with cyclosporine, tacrolimus or mycophenolate mofetil to prevent organ rejection after solid organ transplantation [1]. Similar to sirolimus, EVE is a proliferation signal inhibitor. It prevents cellular rejection through a combination with the immunophilin FK506-binding protein 12 (FKBP-12) which inhibits selectively the Mamalian Target of Rapamycin (m-TOR) activity. The clinical use of EVE is complicated by a narrow therapeutic index, the potential for drug interactions and a significant interpatient and intrapatient variability, in part due to (1) its metabolism by cytochrome P450 3A4, 3A5 and 2C8 enzymes and (2) its transport by P-glycoprotein (P-gp, ABCB1), encoded by the human *ABCB1* gene [1].

Therapeutic drug monitoring (TDM) and dosage individualization are necessary due to the unpredicted concentrations levels found in patients, together with their narrow therapeutic window. Elevated blood concentrations can cause significant toxicity or under dosing can lead to transplant rejection.

As EVE is highly bound to red blood cells, lymphocytes and granulocytes, TDM is undertaken in whole blood.

P-glycoprotein plays an important role in excluding substrate drugs from lymphocytes [2]. The expression and activity of this protein are variable between individuals due to genetic (*ABCB1* gene polymorphisms) and environmental (xenobiotics) factors [3]. The P-glycoprotein level of expression can influence intracellular drug concentrations and, therefore, drug efficacy. Hence, lymphocytes are expected to be a more specific biological matrix than whole blood to reflect EVE efficacy. Quantification in human peripheral blood mononuclear cells was already described for other immunosuppressive agents such as cyclosporine A, tacrolimus or mycophenolate mofetil [4,5]. The authors of these works found, interestingly, that PBMC and whole blood concentrations were not correlated. To date, no method has been developed for évérolimus quantification in PBMC.

The aim of this study was to develop and validate a selective and sensitive analytical procedure for the measurement of EVE in peripheral blood mononuclear cells (PBMCs) by liquid chromatography tandem mass spectrometry (LC–MS/MS). This method was applied to the analysis of patient samples in order to study the correlation between EVE concentrations in blood and PBMC.

* Corresponding author at: Saint Antoine Hospital – AP-HP, Pharmacy Department – 184 rue du Fbg Saint Antoine, 75012 Paris, France. Tel.: +33 1 48 29 21 64; fax: +33 1 48 29 21 42.
E-mail address: christine.fernandez@sat.aphp.fr (C. Fernandez).

0731-7085/$ – see front matter © 2012 Elsevier B.V. All rights reserved.
http://dx.doi.org/10.1016/j.jpba.2012.03.042

2. Materials and methods

2.1. Chemicals, biologicals and material

EVE was supplied by Novartis (Huningue, France). Ascomycin was chosen as internal standard (IS) because no isotopically labelled internal standard was available. Ascomycin was purchased from Sigma–Aldrich (Saint Quentin Fallavier, France). Acetonitrile, water and methanol were of mass spectrometry grade and purchased from local suppliers.

Orthophosphoric acid was from Merck (Darmstadt, Germany), Ammonium Acetate from Prolabo (Fontenay sous Bois, France), Argon from Messer (Puteaux, France).

For PBMC isolation from whole blood, RPMI 1640 + L-glutamine medium was purchased from Gibco (Cergy-Pontoise, France). BD Vacutainer CPT and Falcon tubes were from Becton Dickinson (Franklin Lakes, USA).

2.2. Sample preparation

2.2.1. Isolation and purification of PBMCs

PBMCs were isolated from whole blood (treated patients or blank blood for calibration points and quality controls) by density gradient centrifugation. Peripheral venous blood (approximately 8 mL) was collected into a BD Vacutainer CPT tube and centrifuged at 1800 × *g* for 25 min. The PBMC layer was collected and washed twice with 10 mL of RPMI + L-glutamine at 4 °C. PBMCs counting was performed on two aliquots of 250 μL (Sysmex cell counter – Sysmex Corporation, Kobe, Japan). After centrifugation at 3000 × *g* for 10 min, the supernatant was discarded. The cell pellet was resuspended in 1.5 mL of methanol for cell lysis and EVE extraction (see below). The whole procedure was performed at 4 °C to block EVE efflux from cells.

2.2.2. Preparation of standard and quality control (QC) samples

Stock solutions of EVE (1 mg/mL) were prepared in methanol at a concentration of. Working solutions (10 μg/mL) were also prepared in methanol. The stock solution of IS (1 mg/mL) was prepared in DMSO. This solution was diluted extemporaneously in water to obtain the 2 ng/mL working solution. Stock solutions were stable for at least 3 months at −30 °C.

Aliquots of blank PBMC (1 million PBMCs per sample) were spiked with the 10 μg/mL EVE solution in order to prepare calibration points at concentrations ranging from 0 to 12.5 ng/mL and 3 QC samples at 2.5, 5 and 10 ng/mL.

2.2.3. Cells lysis and EVE extraction

Clinical samples, calibration points and QC samples were processed in the same way.

PBMCs resuspended in methanol, as previously described in Section 2.2.1, were mixed for 2 h using a Vortex Shaker Vibrax VX2 (IKA Werke, Staufen, Germany) at room temperature. After centrifugation at 2300 × *g* for 5 min, the whole volume of supernatant was collected and evaporated to dryness, at room temperature, under a nitrogen flow. The residue was reconstituted with methanol and 50 μL were transferred into conical test tubes for EVE extraction: 200 μL of zinc sulfate 0.1 M, 250 μL of water containing the IS and 150 μL of acetonitrile were added to each sample. After vortex mixing and centrifugation (15,000 × *g* for 4 min), the supernatants was transferred into vials for LC–MS/MS analysis and 20 μL were injected.

Blood samples from transplant recipients were treated following the same method: to 50 μL of blood, 200 μL of zinc sulfate 0.1 M, 250 μL of water containing 20 μg/mL IS and 150 μL of acetonitrile were added to each sample and vortexed. After centrifugation (15,000 × *g* for 4 min), 20 μL of each supernatant were injected in the LC–MS/MS system. This method was previously validated in our lab and is currently used for routine monitoring.

2.3. LC–MS/MS apparatus and conditions

Chromatography was performed on a Waters® Acquity™ UPLC system. Instrument control and data acquisition were processed by Masslynx v4.1 (Waters, Saint Quentin en Yvelines, France). Rapid separation was obtained using a cartridge column MassTrak TDM C18 (2.1 × 10 mm) (Waters, Saint Quentin en Yvelines). Samples were injected into the cartridge maintained at 55 °C. EVE and IS were eluted under gradient conditions, at a flow rate of 0.4 mL/min. The mobile phase was made by mixing solvent A (2 mmol/L ammonium acetate and 0.1% (v/v) formic acid in water) and solvent B (2 mmol/L ammonium acetate and 0.1% (v/v) formic acid in methanol) following a linear gradient (50%A – 50%B from 0 to 0.6 min, 100%B from 0.6 to 1.2 min and 50%A – 50% B from 1.2 min to the end of run). High purity argon was used as collision gas. Ionization was achieved in the positive ion mode using the following settings: capillary voltage 1.0 kV, collision energy 20 eV and 15 eV for IS and EVE, respectively. Sample cone voltage was 30 V and 25 V for IS and EVE, respectively. Source block temperature was set at 120 °C, desolvation gas flow and temperature were maintained at 900 L/h and 350° collision gas pressure 3.6 mbar.

EVE and IS were detected in multiple reaction monitoring (MRM) mode with a dwell time of 0.1 s per channel. MRM transitions were m/z 975.5 → 908.5 for EVE and m/z 809.5 → 756.5 for IS, these transitions have been reported by others for whole blood LC–MS/MS methods (Moes et al.). The extractor voltage was 2 V and RF lens voltage 0.3 V.

Peak area ratios of EVE and IS (m/z 809.5 → 756.5) were used for quantification. The retention times for EVE and IS were approximately 0.99 and 1.1 min, respectively.

2.4. Method validation

The validation of the method was based on the recommendations published by the ICH (International Conference on Harmonization) [6,7].

2.4.1. Selectivity

The assay selectivity was assessed by analysing extracts from PBMCs extracts from different cardiac transplant recipients.

2.4.2. Limit of quantitation and calibration curves

The lowest limit of quantification (LLOQ) for EVE was experimentally chosen as the minimal concentration in PBMCs samples which could be confidently determined: the deviation between measured and nominal concentration should not deviate more than ±15%. Calibration curves were established with standard solutions at a concentration of 0–1.25–2.5–3.75–5–7.5–10–12.5 ng/mL, all analyzed in triplicates. Back-calculated values of the lowest calibration samples with a bias and CV% below ±15%, enabled to determine the LLOQ values.

2.4.3. Accuracy and precision

Replicate analysis ($n = 6$) of QC samples at the three concentrations (2.5, 5.0 and 10.0 ng/mL) were used for the intra-assay precision and accuracy determination. Inter-assay accuracy and precision were determined by repeated analysis performed on 3 different days. The concentration in each sample was determined using calibration standards prepared on the same day. The precision being calculated as the coefficient of variation (CV%) within a single run (intra-assay) and between different assays (inter-assays), and the accuracy as the percentage of deviation between nominal and measured concentration.

During the analysis of patient samples, QC samples (2.5, 5.0 and 10.0 ng/mL) were assayed. The analytical series were accepted only if the percentage of deviation (bias) between theoretical and back-calculated (experimental) concentrations for each calibration level and quality control samples were less than ±15%.

2.4.4. Matrix effect and recovery

The quantitative determination of the matrix effect was assessed. Five QC samples at 5 ng/mL (EVE) and 2 ng/mL (IS) were prepared as follows:

- pure standard solutions samples (in methanol) directly injected onto column;
- PBMCs extract samples from five different sources, spiked whith EVE and IS *after* extraction;
- PBMCs samples from five different sources (same as previously) spiked with EVE and IS *before* extraction.

The recovery and of EVE in the presence of PBMCs matrix was assessed by comparing the peak areas of EVE either in methanol, or added before and after extraction of five different batches of PBMCs, as well as the corresponding peak areas ratios of EVE to IS.

The extraction recoveries of EVE and IS were calculated as the absolute peak-area response in PBMCs samples spiked with drugs *before* extraction, expressed as the percentage of the response of the same amount of drugs (prepared in methanol) added into blank PBMCs extracts *after* the extraction procedure. Recovery studies were done in triplicate QC samples.

2.5. Application to clinical sample analysis

Trough steady-state EVE concentrations were determined in blood samples from 36 cardiac maintenance transplant recipients who received a graft at least 6 months before the beginning of the study. Patients were treated with EVE (0.5–5 mg/day; mean dose = 1.339 mg/day; sd = 0.785) and were at steady-state conditions (at least 5 days after the last dose modification). Patients were also treated with cyclosporine A or tacrolimus. 7 mL of blood were collected in order to measure EVE in whole blood as a routine drug monitoring procedure with a validated method adapted from Sallustio et al. [8]. The same sample was used for the separation and analysis of PBMC. Hence, this study did not require additional blood samples than the ones collected for routine follow up. Patients were informed and gave their consent to enter the study.

2.6. Statistics

The correlation between whole blood and PBMC concentrations was performed using a Pearson test, considering the 0.05 value as significant.

3. Results and discussion

The proposed method enables the quantification of EVE in PBMCs extracts by liquid chromatography coupled with tandem MS/MS. A typical chromatographic profile of a blank PBMC sample and a PBMC extract from an heart transplant recipient before oral administration of 1.5 mg of EVE is shown in Fig. 1.

3.1. Method validation

The validation of the method has been performed in accordance with ICH requirements which include selectivity, limit of quantitation, range, accuracy and precision. None of the PBMC extracts from cardiac transplant recipients had any interference at the retention

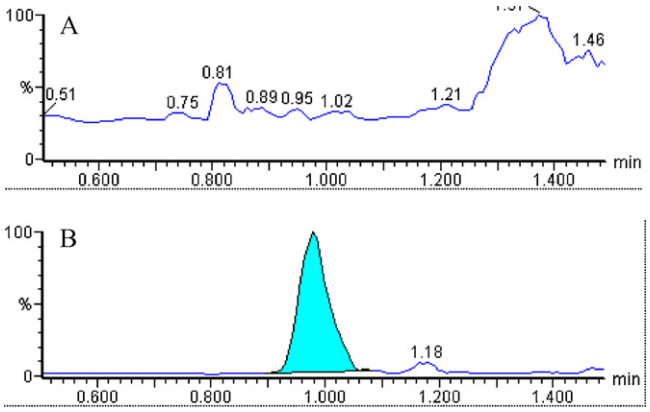

Fig. 1. Typical chromatograms for EVE. (A) Chromatogram of a blank PBMC sample and (B) chromatogram of a PBMC extract from an heart transplant recipient before oral administration of 1.5 mg of EVE (0.08 ng/10^6 PBMCs).

times of EVE and IS. The lowest achievable limit of quantification obtained for EVE was 1.25 ng/mL.

Calibration curves for EVE were linear over a range of 0–12.5 ng/mL on all three days with correlation coefficient values ranging from 0.984 to 0.997.

The mean intra-assay precision was similar over the entire concentration range and always less than 12.5%. Overall, the mean inter-day precision was good, with average CVs within 6.4–12.0%. The intra-assay deviation (bias) from the nominal concentrations of EVE was between −0.2 and −3.4% (Table 1).

Matrix effect obtained for EVE at a concentration of 5 ng/mL and IS at a concentration of 2 ng/mL were respectively 91.7% and 91.6%. The mean recoveries ($n = 3$) for EVE (2.5, 5.0 and 10.0 ng/ml) were 87.1, 83.4 and 79.4% respectively. Mean recovery ($n = 3$) for internal standard was 82.1%.

3.2. Application to clinical sample analysis

The method was applied to blood trough (C0) samples from 36 patients who underwent heart transplant under EVE therapy. Blood sampling was performed at T0, before drug administration. PBMC density ranged from 0.5 to 12.5 millions cells per millilitre. EVE PBMC concentrations ranged from 0.04 to 0.47 fg/cell. These data suggest a weak correlation ($r^2 = 0.558$, $p = 0.0002$) between PBMC concentration and blood concentration reported to dosage (Fig. 2).

4. Discussion

A sensitive and selective analytical method was developed for the quantification of EVE in human PBMCs. To our knowledge, it is the first method described for the intracellular quantification of EVE. As EVE acts on the m-TOR kinase located in T-lymphocyte, lymphocyte concentrations of should reflect drug efficacy, better than whole drug concentrations do. In previous papers, calcineurin inhibition has also been correlated with cyclosporine concentration in human PBMCs [9]. Furthermore, Falck et al. put forth the

Table 1
Recovery, accuracy, intra-day and inter-day precision for EVE in PBMCs.

Theoretical EVE concentration (ng/mL)	Extraction recovery ($n = 6$)	Accuracy % ($n = 18$)	CV%	
			Intraday (n=)	Interday (n=)
2.5	87.1	99.5	12.1	12.0
5.0	83.4	96.6	6.4	6.4
10.0	79.4	99.8	8.5	11.0

CV, coefficient of variation.

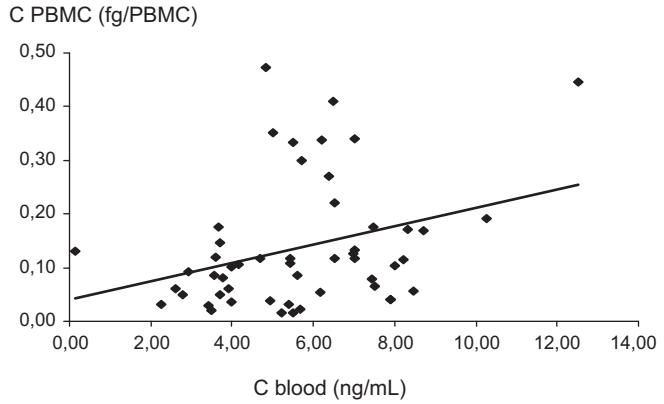

Fig. 2. Relation between EVE whole blood concentrations and PBMC concentrations reported to daily dose in patients treated with EVE ($n = 36$, C PBMC: intracellular concentration of EVE in fg/PBMC and C blood: whole blood concentrations of EVE in ng/mL) ($y = 0.0171x + 0.0413$, $r = 0.32$).

hypothesis that T-lymphocyte concentrations of cyclosporine A could be an earlier marker of renal graft rejection [10]. They reported that T-lymphocyte concentrations of cyclosporine A decreased in rejector patients few days before an event of graft rejection whereas blood concentrations (C_0 as well as C_2 or AUC_{0-12}) where not different between rejector patients and non-rejector patients.

Crettol et al. have shown that intracellular cyclosporine concentrations correlated ($r = 0.30$) [11] significantly with cyclosporine whole blood concentrations. On the opposite, Ansermot et al. have shown a large interindividual variability in PBMC cyclosporine A concentrations and the lack of correlation between PBMC and whole blood levels [12]. The authors point out that whole blood concentrations may not predict PBMC drug levels. This hypothesis is confirmed by Barbari et al. who have reported that renal transplant patients with acute rejection have lower cyclosporine PBMC levels but similar blood trough levels than patients with no signs of organ rejection [13].

Our work is the first step towards this kind of study for EVE. We have shown a weak correlation between EVE whole blood and PBMC concentrations ($r^2 = 0.558$). This result suggests that EVE concentrations in PBMC do not reflect EVE whole blood concentrations. It could be explained by the transport of EVE by P-gp, an efflux pump protein located in lymphocyte cell membrane which excludes the drug towards the plasma compartment. P-gp functionality is modified by genetic disposition (polymorphism) and environmental parameters (xenobiotics). This variability could explain some discrepancies between PBMC and whole blood concentrations.

5. Conclusion

We have developed a sensitive method for EVE quantification in PBMC using LC–MS/MS. For cyclosporine A, lower intracellular drug amounts were measured in patients with acute rejection, despite lack of differences in whole blood concentrations between patients with or without rejection. Hence, intracellular concentration measurements could correlate better with clinical events than whole blood concentrations do.

Despite the time needed for PBMC isolation and EVE extraction, this method is a new potential tool to monitor heart transplant recipients and elucidate the mechanism behind the lack of immunosuppressive effect during acute rejection episodes.

Next step will be the clinical evaluation of the influence of EVE PBMC concentrations on the risk of graft rejection. The influence of genetic covariates (P-glycoprotein polymorphism) and co-medications (cyclosporine A) on EVE PBMC concentrations will be further explored as they could modulate the immunosuppressive effect of the drug.

References

[1] G.I. Kirchner, I. Meier-Wiedenbach, M.P. Manns, Clinical pharmacokinetics of everolimus, Clin. Pharmacokinet. 43 (2004) 83–95.
[2] A. Capron, M. Mourad, M. De Meyer, L. De Pauw, D.C. Eddour, D. Latinne, L. Elens, V. Haufroid, P. Wallemacq, CYP3A5 and ABCB1 polymorphisms influence tacrolimus concentrations in peripheral blood mononuclear cells after renal transplantation, Pharmacogenomics 11 (2010) 703–714.
[3] M. Eichelbaum, M.F. Fromm, M. Schwab, Clinical aspects of the MDR1 (ABCB1) gene polymorphism, Ther. Drug Monit. 26 (2004) 180–185.
[4] N. Ansermot, M. Fathi, J.L. Veuthey, J. Desmeules, D. Hochstrasser, S. Rudaz, Quantification of cyclosporine A in peripheral blood mononuclear cells by liquid chromatography–electrospray mass spectrometry using a column-switching approach, J. Chromatogr. B: Analyt. Technol. Biomed. Life Sci. 857 (2007) 92–99.
[5] A. Capron, F. Musuamba, D. Latinne, M. Mourad, J. Lerut, V. Haufroid, P.E. Wallemacq, Validation of a liquid chromatography–mass spectrometric assay for tacrolimus in peripheral blood mononuclear cells, Ther. Drug Monit. 31 (2009) 178–186.
[6] International Conference of Harmonization, Q2A Text on Validation of Analytical Procedures, March 1995.
[7] International Conference of Harmonization, Q2B Validation of Analytical Procedures: Methodology, May 1997, vol. 4, 2010, pp. 413–419.
[8] B.C. Sallustio, B.D. Noll, R.G. Morris, Comparison of blood sirolimus, tacrolimus and everolimus concentrations measured by LC–MS/MS, HPLC-UV and immunoassay methods, Clin. Biochem. 44 (2011) 231–236.
[9] T.D. Batiuk, F. Pazderka, J. Enns, L. DeCastro, P.F. Halloran, Cyclosporine inhibition of calcineurin activity in human leukocytes in vivo is rapidly reversible, J. Clin. Invest. 96 (1995) 1254–1260.
[10] P. Falck, A. Asberg, H. Guldseth, S. Bremer, F. Akhlaghi, J.L. Reubsaet, P. Pfeffer, A. Hartmann, K. Midtvedt, Declining intracellular T-lymphocyte concentration of cyclosporine a precedes acute rejection in kidney transplant recipients, Transplantation 85 (2008) 179–184.
[11] S. Crettol, J.P. Venetz, M. Fontana, J.D. Aubert, N. Ansermot, M. Fathi, M. Pascual, C.B. Eap, Influence of ABCB1 genetic polymorphisms on cyclosporine intracellular concentration in transplant recipients, Pharmacogen. Genomics 18 (2008) 307–315.
[12] N. Ansermot, M. Rebsamen, J. Chabert, M. Fathi, M. Gex-Fabry, Y. Daali, M. Besson, M. Rossier, S. Rudaz, D. Hochstrasser, P. Dayer, J. Desmeules, Influence of ABCB1 gene polymorphisms and P-glycoprotein activity on cyclosporine pharmacokinetics in peripheral blood mononuclear cells in healthy volunteers, Drug Metab. Lett. 2 (2008) 76–82.
[13] A.G. Barbari, M.A. Masri, A.G. Stephan, N. Mourad, B. El-Ghoul B, G.S. Kamel, H.E. Kilani, A.S. Karam, Cyclosporine lymphocyte maximum level: a new alternative for cyclosporine monitoring in kidney transplantation, Exp. Clin. Transplant. 1 (2005) 293–300.

Journal of Pharmaceutical and Biomedical Analysis 66 (2012) 282–286

Contents lists available at SciVerse ScienceDirect

Journal of Pharmaceutical and Biomedical Analysis

journal homepage: www.elsevier.com/locate/jpba

Development of a monoclonal antibody-based ELISA for the hedgehog inhibitors cyclopamine and KAAD-cyclopamine

Stephen T. Lee[a,*], Kip E. Panter[a], Dale R. Gardner[a], Benedict T. Green[a], Kevin D. Welch[a], Jianjun Zhang[b], Cheng-Wei Tom Chang[b]

[a] Poisonous Plant Research Laboratory, Agricultural Research Service, United States Department of Agriculture, 1150 E. 1400 N., Logan, UT 84341, USA
[b] Department of Chemistry and Biochemistry, Utah State University, 0300 Old Main Hill, Logan, UT 84322, USA

ARTICLE INFO

Article history:
Received 14 February 2012
Received in revised form 19 March 2012
Accepted 20 March 2012
Available online 29 March 2012

Keywords:
Cyclopamine
Cancer
Enzyme-linked immunoassay
Hedgehog pathway

ABSTRACT

Cyclopamine (**1**) was isolated from the plant *Veratrum californicum* Durand (Liliacea) and identified as the teratogen responsible for severe craniofacial birth defects including cyclops in the offspring of sheep grazing on mountain ranges in central Idaho. More recently, cyclopamine (**1**) was found to inhibit the hedgehog (Hh) signaling pathway which plays a critical role in embryonic development and is implicated in several types of cancer. Thus, cyclopamine (**1**) and cyclopamine derivatives have been targeted as potential pharmaceutical treatments for certain cancers and other diseases associated with the Hh signaling pathway. A monoclonal antibody-based competitive inhibition enzyme-linked immunosorbent assay was developed to detect and measure cyclopamine (**1**) and cyclopamine derivatives in biological samples. The limits of detection of the assay for cyclopamine (**1**), 3-keto-*N*-aminoethyl aminocaproyl digyrocinnamoyl-cyclopamine (**8**), and *N*-(4-L-rhamnopyranosyl-1H-1,2,3-triazol-1-yl)-methylcyclopamine (**11**) were 2.9 pg, 0.41 pg and 2.6 pg, respectively. This assay was also found to be useful for the detection and measurement of cyclopamine (**1**) in sera from mice that had been dosed with cyclopamine (**1**). The simple ELISA method described herein demonstrates the potential of using these techniques for the rapid screening of biological samples for the presence and levels of cyclopamine (**1**) and other cyclopamine derivatives that are Hh inhibitors with anticancer potential.

Published by Elsevier B.V.

1. Introduction

Cyclopamine (**1**) (11-deoxojervine) a steroidal alkaloid, was isolated from the plants *Veratrum grandifloru* (Maxim. ex Baker) Loes. In 1965 and *Veratrum californicum* Durand (Liliacea) in 1968–1969 [1–3]. Cyclopamine (**1**) was identified as the primary teratogen of *Veratrum californicum* that was responsible for numerous cyclopic and other craniofacial malformations in the offspring of in sheep grazing on mountain ranges in central Idaho during the first half of the 20th century [2,3].

More recently, molecular biologists reported that the mechanism of cyclopamine (**1**) action is the inhibition of the hedgehog (Hh) signal transduction pathway [4,5]. The Hh signaling pathway plays an integral role in cell growth and differentiation in embryonic development, but is much less active in adults. Several reports have implicated abnormally elevated Hh signaling in cancers [6–8]. Thus cyclopamine (**1**) [9] and cyclopamine derivatives such as 3-Keto-*N*-aminoethyl aminocaproyl digyrocinnamoyl-cyclopamine (KAAD-cyclopamine) (**8**) [10] and *N*-(4-L-rhamnopyranosyl-1H-1,2,3-triazol-1-yl)-methylcyclopamine (*N*-RPT-methylcyclopamine) (**11**) [11] have been targeted as potential cancer treatment drugs. KAAD-cyclopamine (**8**) was 10–20 times more potent in the inhibition of the Hh pathway in stem cells compared to cyclopamine (**1**) and *N*-RPT-methylcyclopamine (**11**) had higher activity against a lung cancer cell line than cyclopamine (**1**) [10,11].

We previously developed a competitive inhibition enzyme-linked immunosorbent assay (ELISA) for cyclopamine (**1**), and other structurally related compounds using polyclonal antibodies [12]. The limit of detection for cyclopamine (**1**) using the polyclonal antibody based ELISA was 90.0 pg. While the production of polyclonal antibodies was relatively fast and inexpensive, interest in this assay by researchers using cyclopamine (**1**) and related compounds to study the Hh pathway and potential anticancer agents led us to consider developing an ELISA using a monoclonal antibody. We hypothesized that using a monoclonal antibody specific to cyclopamine (**1**) we may be able to achieve lower limits of detection by the reduction of non-specific antibodies inherent in polyclonal antibody production that often lead to higher background signal in ELISA assays. Also the ability to produce unlimited quantities of

* Corresponding author. Tel.: +1 435 752 2941; fax: +1 435 753 5681.
E-mail address: stephen.lee@ars.usda.gov (S.T. Lee).

0731-7085/$ – see front matter. Published by Elsevier B.V.
http://dx.doi.org/10.1016/j.jpba.2012.03.043

identical and specific antibody using an immortal cell line was critical due to the interest of others in transferring this assay to their own laboratories.

This report describes the development of a monoclonal antibody-based competitive inhibition enzyme-linked immunosorbent assay to detect and measure cyclopamine (**1**) and cyclopamine derivatives in biological samples. This monoclonal ELISA has significantly lower limits of detection for cyclopamine (**1**) and related compounds and different selectivity than the previously reported polyclonal based ELISA. ELISAs offer advantages over classical instrumental techniques such as minimal sample preparation, the ability to run many samples simultaneously, and in many cases lower limits of detection (LOD). Immunoassays are performed in aqueous media and are uniquely suited for the analysis of pharmaceuticals in biological samples. We demonstrate the applicability of this assay for the detection and measurement of cyclopamine (**1**) spiked into sheep sera and in a mouse model.

2. Materials and methods

2.1. Chemicals and materials

Polyoxyethylene sorbitan monolaurate (Tween 20), bovine albumin (BSA) fraction V, and phosphate buffered saline tablets were obtained from Sigma Chemical Co. (St. Louis, MO, USA).

Cyclopamine (**1**), jervine (**2**), *N*-methylcyclopamine (**3**), dihydrojervine (**4**), tetrahydrojervine (**5**), cyclopamine-3-one-4-ene (**6**), veratramine (**7**), rubijervine (**9**), isorubijervine (**10**) were from a collection at the Poisonous Plant Research Laboratory, Logan, UT, USA. KAAD-cyclopamine was purchased from EMD Biosciences, Inc (La Jolla, CA, USA). *N*-RPT-Methylcyclopamine (**11**) was obtained from Dr. Cheng-Wei Tom Chang at Utah State University (Logan, UT, USA) and cycloposine (**12**) was a gift from and Infinity Pharmaceuticals (Cambridge, MA, USA).

Enzyme-linked immunosorbent assays (ELISAs) were performed on 96-well NUNC F96 Maxisorp polystyrene microtiter plates purchased from VWR Scientific Products (Denver, CO, USA). Microtiter plates were read with a Spectra Max microplate reader from Molecular Devices Corporation (Sunnyvale, CA, USA) at 450 nm. Nonlinear curve fitting of the data was performed using Prism version 4.04 (GraphPad Software, San Diego, CA, USA).

2.2. HPLC–ESI/MS/MS method

High performance liquid chromatography–electrospray ionization/tandem mass spectrometry (HPLC–ESI/MS/MS) analysis of cyclopamine (**1**) containing samples were performed using a Surveyor HPLC and autosampler system coupled to a ThermoFinnigan LCQ Advantage Max mass spectrometer (ThermoFinnigan, San Jose, CA, USA). Samples (dissolved in 50/50 0.1% formic acid/acetonitrile) (20 μL) were injected onto a Betasil C-18 reversed phase column (100 × 2.1 mm i.d.) (Thermo Electron Corporation, Waltham, MA, USA) protected by a guard column of the same adsorbent. The column was eluted with a gradient flow (0.300 mL/min) of 0.1% formic acid in water (solvent A) and acetonitrile (solvent B). The mobile phase program was started at a composition of 80:20 (A:B) for 2 min, changed by linear gradient to 40:60 over 1 min, and held at 40:60 for 7 min for a total run time of 10 min. Flow from the HPLC column was connected directly to the electrospray source (ESI) of the mass spectrometer (MS). The mass spectrometer was run in MS^2 mode, scanning product ions over a mass range of 110–500 Da after fragmentation of the protonated cyclopamine (**1**) molecular ion MH^+ (*m*/*z* 412.3) using a relative collision energy setting of 37%. Cyclopamine (**1**) eluted from the column at a retention time of 4.5 min. The cyclopamine (**1**) peak areas were measured from reconstructed ion chromatograms generated from the combined ion count from selected MS/MS fragment ions (*m*/*z* 321, 377, 394).

Calibration standards were prepared as follows: a stock solution of cyclopamine (**1**) (1 mg/mL) was prepared in chloroform. A 20 μL aliquot was diluted in 0.98 mL of acetonitrile, followed by 100 μL dilution in 1.9 mL and 200 μL in 1.8 mL followed by serial dilutions to give 100, 50, 25, 12, 6.25, and 3.1 ng/mL standards in acetonitrile. A 75 μL aliquot of each standard was then added to 75 μL of blank mouse sera and the samples. For treated mouse sera, the frozen samples were thawed, centrifuged and then a 0.075 mL aliquot was placed into a 1.5 mL conical vial and 0.075 mL of acetonitrile was added. The samples were vortexed and then centrifuged for 10 min. The clear liquid was removed and placed into a micro autosample vial and analyzed for cyclopamine (**1**) by HPLC-ESI/MS/MS LC–MS//MS.

2.3. Cyclopamine 3-succinate protein conjugates

Cyclopamine (**1**) was conjugated to fetuin and BSA proteins as described previously [12]. The fetuin and BSA protein conjugates are designated as CYCLO-SA-FET and CYCLO-SA-BSA, respectively, throughout this report.

2.4. Monoclonal antibody

CYCLO-SA-FET and CYCLO-SA-BSA were sent to ProMab Biotechnologies, Inc. (Richmond, CA, USA). CYCLO-SA-FET was used as the antigen in generating the monoclonal antibodies and CYCLO-SA-BSA was used as the coating conjugate. All immunizations and subsequent steps in production of Hybridoma cells/purified antibodies were completed by ProMab Biotechnologies, Inc.

2.5. ELISA procedure

Cyclopamine-protein coating conjugates were dissolved in carbonate buffer (0.05 M, pH 9.6) and 100 μL added to each well of the microtiter plate. The microtiter plates were incubated (2 h, RT and then 16 h, 4 °C). The plates were then inverted to remove excess coating solution and covered with an adhesive plate sealer and stored in a plastic bag (−20 °C) for up to 6 months. Before use, the plates were washed (3×) with saline-Tween buffer (0.15 M NaCl, 0.5% Tween 20) and blotted dry. A 50 μL aliquot of samples or standards diluted in the assay buffer (1% BSA, PBS) were added to the wells followed by 50 μL of antiserum diluted in the assay buffer. The plates were then incubated (1 h, 37 °C). After the 1 h incubation, the plates were washed with saline-Tween buffer (3×) and then Anti-Mouse IgG (Fc Specific)-peroxidase, antibody produced in goat (Sigma–Aldrich, Inc., Saint Louis, MO, USA) (50 μL), diluted 1/9000 in assay buffer, was added to all wells and the plates incubated (1 h, 37 °C). The plates were then washed with saline-Tween buffer (3×) and 100 μL of 3,3′,5,5′-Tetramethylbenzidine (TMB) Liquid Substrate System for ELISA (Sigma–Aldrich, Inc., Saint Louis, MO, USA) was added to each well. After 15 min (37 °C) the reaction was stopped by the addition of 50 μL of 0.5 M H_2SO_4 to each well. The absorbances were measured at 450 nm (OD_{450}).

The optimum dilutions for both the coating conjugate and antiserum were determined by checkerboard assays. The concentration of the coating conjugate and antibody were selected based on the combination at which the greatest difference in optical density was observed at 450 nm (OD_{450}s) between the wells of no free cyclopamine (**1**) and the presence of cyclopamine (**1**) at 156 pg/well.

Eleven steroidal alkaloids (Fig. 1) were selected for cross-reactivity studies: jervine (**2**), *N*-methylcyclopamine (**3**),

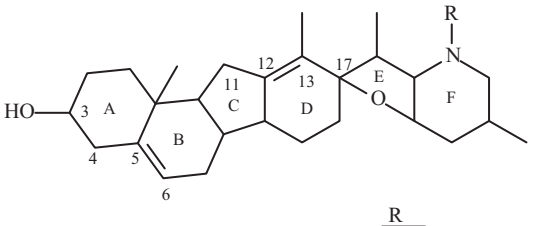

	R
Cyclopamine (**1**)	H
N-Methylcyclopamine (**3**)	CH_3

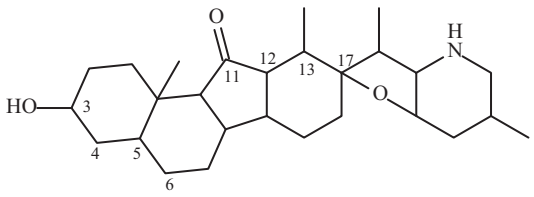

	C-4, C-5	C-5, C-6	C-12, C-13
Jervine (**2**)	—	=	=
Dihydrojervine (**4**)	—	=	—
Tetrahydrojervine (**5**)	—	—	—

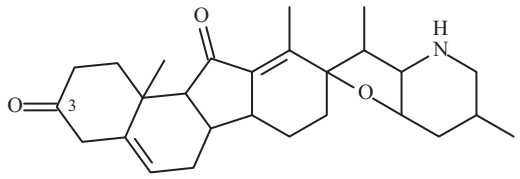

Cyclopamine-3-one-4-ene (**6**)

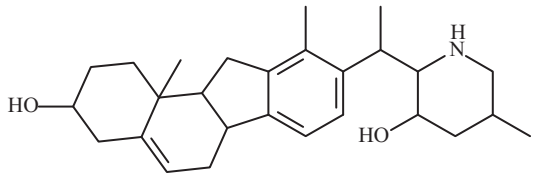

Veratramine (**7**)

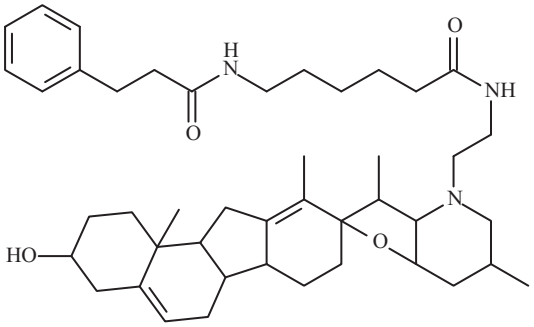

KAAD-Cyclopamine (**8**)

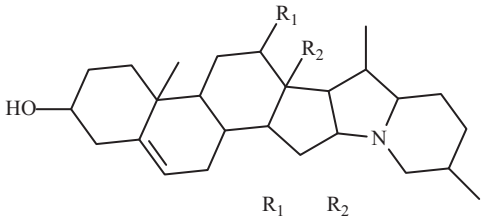

	R_1	R_2
Rubijervine (**9**)	OH	CH_3
Isorubijervine (**10**)	H_2	CH_2OH

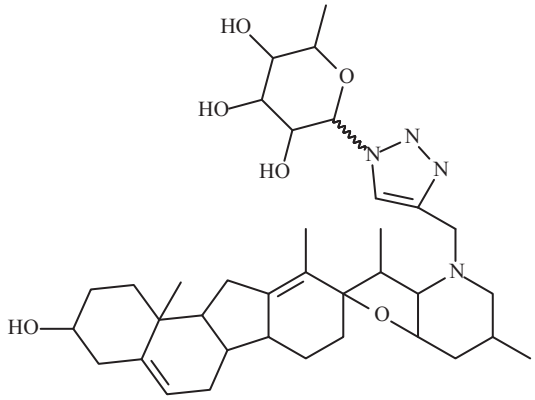

N-(4-L-rhamnopyranosyl-1H-1,2,3-triazol-1-yl)-Methylcyclopamine (**11**)

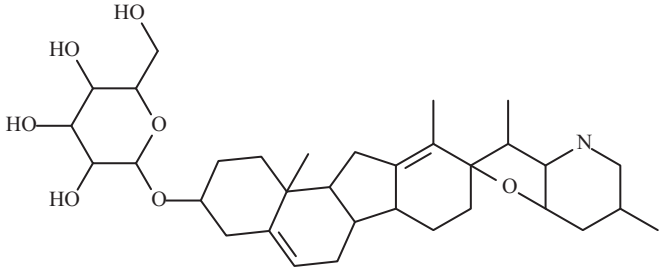

Cycloposine (**12**)

Fig. 1. Chemical structures of cyclopamine (**1**) and other steroidal alkaloids tested for cross-reactivity.

dihydrojervine (**4**), tetrahydrojervine (**5**), cyclopamine-3-one-4-ene (**6**), veratramine (**7**), KAAD-cyclopamine (**8**), rubijervine (**9**), isorubijervine (**10**), *N*-RPT-methylcyclopamine (**11**), and cycloposine (**12**). All steroidal compounds were tested for cross-reactivity over the range of $0.015–4.0 \times 10^4$ pg/well. The data for each compound were fit to a four parameter equation:

$$y = \frac{(a-d)}{[1+(x/c)^b]} + d \quad (1)$$

to yield inhibition and/or calibration curves. In this equation a and d are the upper and lower asymptotes, b is the slope of the linear portion of the curve, and c is the midpoint of the linear portion of the curve. The constant c in Eq. (1) has been reported as I_{50} values for ELISA assays [13]. We also report the absolute I_{50} values as calculated from the equation of the curve. The limit of detection (LOD) was conservatively defined in this study as the I_{80} values, as calculated from the equation of the curve. Table 1 reports the constant c, the 95% confidence intervals for c, the calculated I_{50} values, and the limit of detection (LOD) (I_{80}) for each compound.

Table 1
ELISA assay and inhibition data for steroidal alkaloids.

Steroidal alkaloids[a]	c[b] (pg)	(95% CI[c]) (pg)	I_{50} (pg)	LOD (I_{80}) (pg)
Cyclopamine (**1**)	13	13–14	14	2.9
Jervine (**2**)	98	89–108	98	19
N-Methylcyclopamine (**3**)	15	13–17	15	2.4
Dihydrojervine (**4**)	9.3×10^2	$(6.9–13) \times 10^2$	8.8×10^2	18×10^2
Tetrahydrojervine (**5**)	1.5×10^3	$(0.86–2.7) \times 10^3$	1.2×10^3	1.5×10^2
Cyclopamine-3-one-4-ene (**6**)	6.2×10^2	$(4.7–8.2) \times 10^2$	4.7×10^2	64
Veratramine (**7**)	4.6×10^5	[d]	4.3×10^2	27
KAAD-Cyclopamine (**8**)	31	26–36	16	0.41
Isorubijervine (**10**)	4.7×10^2	$(3.6–6.2) \times 10^2$	6.4×10^2	1.1×10^2
N-RPT-Methylcyclopamine (**11**)	10	9.6–11	9.7	2.6

[a] $n = 42$ for cyclopamine, $n = 6$ for veratramine, $n = 9$ for all other steroidal alkaloids.
[b] c is the concentration of the midpoint of the linear portion of the curve.
[c] Confidence intervals.
[d] Confidence intervals not calculated due to poor fit of Eq. (1) to the data.

2.6. Spiked sera preparation

Blood was drawn from a sheep into serum blood collection vacutainers (Becton, Dickinson and Co. Franklin Lakes, NJ, USA) and incubated (20 min, RT), centrifuged (2100 rpm, 30 min, RT), and the sera removed with a pipette. The sera was spiked with cyclopamine (**1**) to produce concentrations of 10.0 and 100 ppb (pg/μL), vortexed and refrigerated for a minimum of 16 h. The spiked serum was allowed come to room temperature and 20 μL of the spiked sera was diluted with 980 μL of assay buffer and 50 μL of the diluted sera was applied to the microtiter plates.

2.7. Dosing mice with cyclopamine (*1*) and sera preparation

Cyclopamine (**1**) was prepared for intravenous (IV) injection into mice by first dissolving 1 mg of cyclopamine (**1**) in 1 mL of 100% ethanol. A 10 μg/mL (10,000 ppb) cyclopamine (**1**) solution in PBS was prepared by addition of 100 μL of the 1 mg/ml cyclopamine (**1**) in ethanol to 4900 μL PBS buffer (pH 7.4). A 1 μg/mL (1000 ppb) cyclopamine (**1**) solution was prepared by a 1:10 dilution of the 10 μg/μL with PBS buffer. Three mice (C57B/6 mice, Jackson Laboratories, Bar Harbor, ME, USA) for each dilution were in injected via the tail vein with 250 μL aliquots of the 10 μg/μL and 1 μg/μL cyclopamine (**1**) solutions in PBS. Blood was collected 10 min after injection via retro-orbital puncture. The blood was incubated (20 min, RT) and serum was obtained after centrifugation (2100 rpm, 20 min, RT). Mouse sera (20 μL) was diluted with 980 μL of assay buffer and 50 μL of the diluted sera was applied to the microtiter plates.

All animal procedures were conducted under veterinary supervision and were approved by the Utah State University Animal Care and Use Committee.

3. Results and discussion

3.1. ELISA development

Cyclopamine (**1**) was conjugated to a high molecular weight protein to elicit an immune response. The conjugation procedure included the reaction of the C-3 hydroxyl group of the alkaloid with succinic anhydride to form a hemisuccinate, followed by activation of the carboxylic acid moiety with *N*-hydroxysuccinimide and reaction with the protein to form a 5 atom length succinate linker [12].

A competitive inhibition ELISA assay was developed with the monoclonal antibody provided by ProMab Biotechnologies Inc. using the CYCLO-SA-FET immuno-conjugate, and using the CYCLO-SA-BSA conjugate as a coating conjugate.

Checkerboard assays using the monoclonal antibody raised against the CYCLO-SA-FET immunogen with CYCLO-SA-BSA coating conjugate resulted in an optimum dilution of monoclonal antibody of 1/240,000 with the coating conjugate at 50 pg/well for a competitive inhibition ELISA assay.

3.2. Cyclopamine (*1*) ELISA and cross-reactivity

Inhibition curves for rubijervine (**9**) and cycloposine (**12**) showed no cross-reactivity with the antibodies over the concentration range studied in this assay. The inhibition curves in Fig. 2 and the I_{50} values reported in Table 1 show cyclopamine (**1**), *N*-methylcyclopamine (**3**), KAAD-cyclopamine (**8**), and *N*-RPT-methylcyclopamine (**11**) equally cross-react and are recognized by the antibody. Fig. 2 and Table 1 also show that the antibody has some affinity to jervine (**2**), while dihydrojervine (**4**), tetrahydrojervine (**5**), veratramine (**7**), and cyclopamine-3-one-4-ene (**6**) are recognized to an even lesser degree. The presence of a ketone at the C-11 position imparts enough structural dissimilarity to markedly reduce antibody recognition of jervine (**2**). Saturation of jervine (**2**) at the C-5, C-6 and C-12, C-13 positions such as in dihydrojervine (**4**) and tetrahydrojervine (**5**) further reduces antibody recognition of these compounds. These compounds are all C-nor-D-homo steroids with a fused furanopiperidine functional group attached spiro at the C-17 of the steroid. Compounds lacking this backbone structure such as rubijervine (**9**) and isorubijervine (**10**) are not well recognized by the antibody. In addition, veratramine (**7**) which does not possess an ether bridged furan ring is not well recognized by the

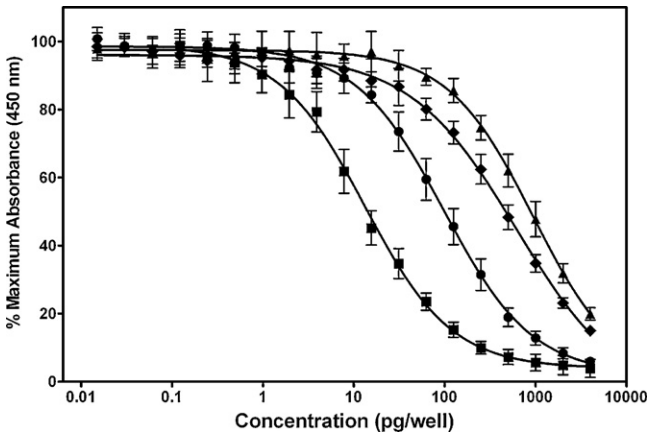

Fig. 2. Representative inhibition curves for selected steroidal alkaloids including cyclopamine (**1**) (■), jervine (**2**) (●), cyclopamine-3-one-4-ene (**6**) (♦), and dihydrojervine (**4**) (▲). $n = 42$ for cyclopamine (**1**), $n = 9$ for other steroidal alkaloids. The error bars represent the standard deviation of points.

antibody. The addition of a ketone at the C-3 and double bond at C-4, C-5 reduces antibody recognition of cyclopamine-3-one-4-ene (**6**) compared to cyclopamine (**1**) while attachment of a glucosyl residue at the C-3 hydroxyl results in no recognition of the antibody to cycloposine (**12**). From these data, we conclude that the assay is specific for steroidal alkaloids possessing the structural features of cyclopamine (**1**) and can be alkylated with functional groups at the nitrogen of cyclopamine (**1**) such as of *N*-methylcyclopamine (**3**), KAAD-cyclopamine (**8**) and *N*-RPT-methylcyclopamine (**11**). The LOD (I_{80}) for cyclopamine (**1**), *N*-methylcyclopamine (**3**), KAAD-cyclopamine (**8**), and *N*-RPT-methylcyclopamine (**11**) were 2.9 pg, 2.4 pg, 0.41 pg, and 2.6 pg, respectively. This LOD for cyclopamine (**1**), 2.9 pg, is over an order of magnitude lower than the LOD of 90 pg for the previously reported polyclonal antibody-based ELISA [12].

3.3. ELISA LOD comparison with HPLC-ESI/MS/MS

The LOD, defined as three times the signal to noise, for cyclopamine (**1**) using the HPLC-ESI/MS/MS method described herein was 7.0 pg. If the same definition is used for the ELISA assay with the LOD defined as the lowest concentration of free cyclopamine with an absorbance reading less than the blank by three times the standard deviation the of the blank as calculated from the cyclopamine (**1**) standard curve, the LOD for cyclopamine (**1**) is 0.91 pg. Whether a conservative estimate of the LOD using the I_{80} value of cyclopamine (**1**) of 2.9 pg or the latter value based on signal to noise of 0.91 pg, these values compare favorably to HPLC-ESI/MS/MS LOD of 7.0 pg.

3.4. Determination of cyclopamine (*1*) in sera

We evaluated the applicability of this assay for the detection and measurement of cyclopamine (**1**) in sera. Samples were quantified against a 16-point cyclopamine (**1**) standard curve over the range of 0.122–4000 pg. The standard curve was determined by fitting the standards to Eq. (1). The r^2 for the standard curve was 0.9886. Average recoveries for 9 replicates at concentrations of 10.0 and 100 ppb cyclopamine (**1**) in sheep sera were 77 and 98%, respectively, with relative standard deviations of 8.3 and 10%.

Sera from mice dosed IV with cyclopamine (**1**) was quantitated using the ELISA method against a 15 point cyclopamine (**1**) standard curve over the range of 0.122–2000 pg. The standard curve was determined by fitting the standards to Eq. (1). The r^2 for the standard curve was 0.9886. The concentrations of cyclopamine (**1**) in sera from the 3 mice injected with the 10,000 ppb were all 21 ppb while the concentrations of cyclopamine (**1**) in sera from the 3 mice injected with the 1000 ppb ranged from 1.5 to 3.0 ppb.

The concentration of cyclopamine (**1**) in mice serum was also determined using HPLC-ESI/MS/MS. A five point standard curve ranging from 3.1 to 50.0 ng/mL (ppb) in mouse sera was prepared by serial dilution. The r^2 for the standard curve was 0.9973. Using the HPLC-ESI/MS/MS method the concentrations of cyclopamine (**1**) in sera from the 3 mice injected with the 10,000 ppb ranged from 15 to 16 ppb while the 3 mice injected with the 1000 ppb ranged from 1.6 to 2.4 ppb. It should be noted that the levels of cyclopamine (**1**) in sera from the mice injected with 1000 ppb cyclopamine ($\leq$3.0 ppb) were near the LOD for both the ELISA and HPLC-ESI/MS/MS methods and are therefore estimates.

4. Conclusions

An ELISA for cyclopamine (**1**) was developed. The limits of detection of the assay for cyclopamine (**1**), *N*-methylcyclopamine (**3**), KAAD-cyclopamine, and *N*-RPT-methylcyclopamine (**11**) were 2.9 pg, 2.4 pg, 0.41 pg and 2.6 pg, respectively. This assay was also used for the detection and measurement of cyclopamine (**1**) in sera from mice injected with cyclopamine (**1**). The simple ELISA method described demonstrates the potential of using these techniques for the rapid screening of biological samples for the presence and levels of cyclopamine (**1**) and other cyclopamine derivatives that are potential Hh inhibitors and anticancer drugs.

Acknowledgements

We thank Isabelle McCollum and J. Charles Hailes for technical assistance.

References

[1] T. Masamune, Y. Mori, M. Takasugi, A. Murai, S. Ohuchi, N. Sato, N. Katsui, C-N or-D-homosteroids and related alkaloids. IV. 11-Deoxojervine, a new alkaloid from *Veratrum* species, Bull. Chem. Soc. Jpn. 38 (1965) 1374–1378.
[2] R.F. Keeler, Teratogenic compounds of *Veratrum californicum* (Durand)-IV. First isolation of veratramine and alkaloid Q and a reliable method for isolation of cyclopamine, Phytochemistry 7 (1968) 303–306.
[3] R.F. Keeler, Teratogenic compounds of *Veratrum californicum* (Durand)-VI. The structure of cyclopamine, Phytochemistry 8 (1969) 223–225.
[4] M.K. Cooper, J.A. Porter, K.E. Young, P.A. Beachy, Teratogen-mediated inhibition of target tissue response to Shh signaling, Science 280 (1998) 1603–1607.
[5] J.P. Incardona, W. Gaffield, R.K. Kapur, H. Roelink, The teratogenic alkaloid cyclopamine inhibits Sonic hedgehog signal transduction, Development 125 (1998) 3553–3562.
[6] N. Dahmane, J. Lee, P. Robins, P. Heller, A. Ruiz i Altaba, Activation of the transcription factor Gli1 and the Sonic hedgehog signaling pathway in skin tumours, Nature 389 (1997) 876–881.
[7] D.M. Berman, S.S. Karhadkar, A. Maitra, R. Montes de Oca, M.R. Gerstenblith, K. Briggs, A.R. Parker, Y. Shimada, J.R. Eshleman, D.N. Watkins, P.A. Beachy, Widespread requirement for Hedgehog ligand stimulation in growth of digestive tract tumors, Nature 425 (2003) 846–851.
[8] S.S. Karhadkar, G.S. Bova, N. Abdallah, S. Dhara, D. Gardner, A. Maitra, J.T. Isaacs, D.M. Berman, P.A. Beachy, Hedgehog signalling in prostate regeneration, neoplasia and metastasis, Nature 431 (2004) 707–712.
[9] G. Feldmann, S. Dhara, V. Fendrich, D. Bedja, R. Beaty, M. Mullendore, C. Karikari, H. Alvarez, C. Iacobuzio-Donahue, A. Jimeno, K.L. Gabrielson, W. Matsui, A. Maitra, Blockade of Hedgehog signaling inhibits pancreatic cancer invasions and metastases: a new paradigm for combination therapy in solid cancers, Cancer Res. 67 (2007) 2187–2196.
[10] J. Taipale, J.K. Chen, M.K. Cooper, B. Wang, R.K. Mann, L. Milenkovic, M.P. Scott, P.A. Beachy, Effects of oncogenic mutations in smoothend and patched can be reversed by cyclopamine, Nature 406 (2000) 1005–1009.
[11] J. Zhang, M. Garrossian, D.R. Gardner, A. Garrossian, Y.T. Chang, Y.K. Kim, C.W.T. Chang, Synthesis and anticancer activity studies of cyclopamine derivatives, Bioorg. Med. Chem. Lett. 18 (2008) 1359–1363.
[12] S.T. Lee, K.E. Panter, W. Gaffield, B.L. Stegelmeier, Development of enzyme-linked immunosorbent assay for the *Veratrum* plant teratogens: cyclopamine and jervine, J. Agric. Food Chem. 51 (2003) 582–586.
[13] D.M. Roseman, X. Wu, M.J. Kurth, Enzyme-linked immunosorbent assay detection of pyrrolizidine alkaloids: immunogens based on quaternary pyrrolizidinium salts, Bioconjug. Chem. 7 (1996) 187–195.

Journal of Pharmaceutical and Biomedical Analysis 66 (2012) 287–297

Contents lists available at SciVerse ScienceDirect

Journal of Pharmaceutical and Biomedical Analysis

journal homepage: www.elsevier.com/locate/jpba

The metabonomics of combined dietary exposure to phthalates and polychlorinated biphenyls in mice

Jie Zhang[a,1], Lijuan Yan[b,1], Meiping Tian[a], Qiansheng Huang[a], Siyuan Peng[a], Sijun Dong[a,**], Heqing Shen[a,*]

[a] Key Lab of Urban Environment and Health, Institute of Urban Environment, Chinese Academy of Sciences, Xiamen 361021, PR China
[b] Xiamen Entry–Exit Inspection and Quarantine Bureau, Xiamen 361012, PR China

ARTICLE INFO

Article history:
Received 31 December 2011
Received in revised form 22 March 2012
Accepted 23 March 2012
Available online 3 April 2012

Keywords:
Metabonomics
Exposure
Phthalate
Polychlorinated biphenyl

ABSTRACT

Humans undergo simultaneous daily exposure to a multitude of endocrine-disrupting compounds (EDCs). In present study, after combined exposure to endocrine disruptors DEHP and Aroclor 1254 for 12 days, a liquid chromatography/time-of-flight mass spectrometer method combining both reversed-phase (RP) and hydrophilic interaction chromatography (HILIC) separations was carried out to investigate the metabolic responses in mice. The metabolic profiles of endogenous metabolites could differentiate the dose and control groups in both RPLC and HILIC modes. Moreover, the male mice and female mice in different groups could be obviously clustered in their own regions with combined model. Fourteen lysoPCs, PC(18:4/18:1), lysoPE(18:2/0:0), phenylalanine and tryptophan were identified as potential biomarkers for the combined toxicity of DEHP and Aroclor 1254. Different change trends could be observed for the identified lysoPCs, due to their different levels of uptake and metabolism in mice. Moreover, gender-specific differences in several lysoPCs (e.g. lysoPC(18:0), lysoPC(22:6), lysoPC(20:3), and PC(18:4/18:1)) were observed for treated mice. The metabonomic results indicated the combined exposure led to a disturbance of lipid metabolism. The mRNA expressions of PLA2, ACOX1, CPT1, FAS and SCD1 involved in lipid metabolism were investigated. Among them, significant increases of FAS and SCD1 expressions in the liver induced by the exposure could be observed for both male and female mice, contributing to the hepatic lipid accumulation in mice. Besides lipid metabolism, tryptophan metabolism and phenylalanine metabolism may also be involved with the toxic responses to these EDCs. The present study not only improves the understanding of the combined toxicity of phthalates and PCBs but also shows that the metabonomic approach may prove to be a promising technique for the toxicity research of EDCs.

© 2012 Elsevier B.V. All rights reserved.

1. Introduction

Recently, the environmental endocrine-disrupting compounds (EDCs) have drawn increasing amounts of attention because of their potential health impacts on animals and humans. Phthalates and polychlorinated biphenyls (PCBs) are two typical classes of EDCs. Phthalates are used as plasticizers in a large variety of consumer products to impart flexibility and resilience to plastic products. Because phthalates are not covalently bound with the plastics in which they are mixed, they can easily migrate into the environment. PCBs are a family of chlorine-containing compounds that are used as lubricants, heat-transfer fluid and plasticizers. Although the production of PCBs was banned ten years ago, they are still ubiquitous pollutants frequently found in various environmental samples due to their extensive use and chemical stability. Therefore, humans are unavoidably exposed to these chemicals through ingestion, inhalation, transcutaneous absorption and medical transfusions. The potential public health risks associated with phthalate and PCB exposure include not only metabolic and endocrine disruption but also carcinogenesis [1,2].

Many studies deal with exposure to single compounds to assess their toxicity, which is important for obtaining basic toxicological information. However, humans are usually simultaneously exposed to a large number of chemicals [3]. How to evaluate the combined toxicity of these chemicals remains a big challenge. Given the constant exposure to the ubiquitous phthalates and PCBs, the evaluation of their combined effects is of great theoretical and practical significance. To date, very few toxicological studies concerning systemic metabolic response to phthalates and PCBs have been reported.

* Corresponding author. Tel.: +86 592 6190771; fax: +86 592 6190771.
** Corresponding author. Tel.: +86 592 6190779; fax: +86 592 6190779.
E-mail addresses: sjdong@iue.ac.cn (S. Dong), hqshen@iue.ac.cn (H. Shen).
[1] These authors contributed equally to the present article.

0731-7085/$ – see front matter © 2012 Elsevier B.V. All rights reserved.
http://dx.doi.org/10.1016/j.jpba.2012.03.045

Traditional toxicological methods are ideal if the component to be measured in response to an alteration in the experimental conditions has been previously identified. However, these methods have obvious limitations for components without any previous knowledge when we deal with novel environment chemicals. Metabonomics represents a potentially powerful method that offers enormous advantages over traditional methods, especially for EDC research [4]. Metabonomics has been defined as "quantitative measurement of the dynamic multiparametric metabolic response of living systems to pathophysiological stimuli or genetic modification" [5]. Over the past 10 years, increasing numbers of studies have demonstrated that metabonomic data are useful for assessment of toxic mechanisms, prediction of toxicity and identification of clinical biomarkers [6]. In our recent studies, a metabonomic approach was successfully used for the investigation of diabetes mellitus [7]. Metabolite profiles based on nuclear magnetic resonance (NMR) spectroscopy measurements of blood and urine in animal models exposed to individual or combined chemicals in a single class of phthalates or PCBs have been recently reported, and many pathways were found to contribute to metabolic and endocrine disruption associated with PCB exposure [8–11]. Liquid chromatography (LC) coupled to mass spectrometry (MS) is believed to have the potential to become the workhorse of metabonomic analysis. An approach using LC–MS and GC–MS was adopted by Ravenzwaay et al. [12] to investigate the metabolic profiling of rat blood after oral administration of DEHP and DBP. High doses of DEHP and DBP mixture induced a significantly different metabolite profile from those induced by the individuals. However, the combined metabonomic toxicities of phthalates and PCBs are not addressed.

For this purpose, we designed a study to investigate the effect of two representative phthalate and PCBs, specifically, di(2-ethylhexyl)phthalate (DEHP) and Aroclor 1254. DEHP is the most frequently used congener among phthalates and is believed to have great relevance to many metabolic pathways. Aroclor 1254 is a commercial PCB mixture containing 54% chlorine by weight and has been widely used in toxicity research. In the present study, Kunming mice were administered oral DEHP and Aroclor 1254 for 12 days. The reversed-phase liquid chromatography (RPLC) and hydrophilic interaction chromatography (HILIC) coupled to mass spectrometry (MS) were used to acquire the metabonomic datasets from mice serum samples, and the principal component analysis (PCA) was applied to discriminate the global serum metabolite profiles. The metabonomic approach was used to investigate the potential mechanisms and the candidate biomarkers underlying the combined exposure to phthalates and PCBs in mice.

2. Experimental

2.1. Chemicals and solvents

DEHP (purity > 98.5%), and formic acid (HPLC grade) were purchase from Acros (Morris Plains, NJ, USA). Arcolor 1254 (analytical grade), leucine–enkephalin (purity > 95%) and all standards (purity > 95%) were purchased from Sigma–Aldrich (St. Louis, MO, USA). Both methanol and acetonitrile (HPLC grade) were obtained from Fisher Scientific (Fair Lawn, NJ, USA). Distilled water (18.2 MΩ) was obtained from a Milli-Q system (Bedford, MA, USA).

2.2. Animals and dosing

A total of 24 Kunming mice were obtained from the Shanghai Laboratory Animal Center, China. All animal studies were conducted according to the China Animal Welfare legislation. After acclimating for 1 week, the animals were housed in stainless-steel cages in an air-conditioned room at the temperature of 26 ± 2 °C, a relative humidity of 50 ± 5%, and a 12 h light/12 h dark cycle. All of the mice were randomized according to body weight and were assigned to two groups: a control group (4 male mice, 4 female mice) and a dose group (8 male mice, 8 female mice). The dose group was administered oral DEHP (15 mg/kg bw/day) and Aroclor 1254 (7.5 mg/kg bw/day) which were dissolved in corn oil, while the control group was fed with pure corn oil. The doses in the present study were chosen based on previous reports about toxicological research of individual DEHP and Aroclor 1254 treatment (for DEHP, Refs. [9,13,14]; for Aroclor 1254, Refs. [15–17]). Although the doses used were higher than environmental exposure level, they were similar to (even much lower than) the doses used in above peer-reviewed reports. In fact, dosing animals at higher levels than probable human exposures (especially for POPs) is the default approach to investigate the toxic response to the chemicals when human model is unavailable.

2.3. Sample collection

After 12 days of dosing, the mice were euthanized after the final dose. Blood was withdrawn by eyeball removal immediately after euthanasia and placed into ice-cold tubes. Sera were isolated by centrifugation (3500 × *g*, 10 min at 4 °C) and frozen at −80 °C prior to metabonomic analysis. A quality control (QC) was prepared by pooling and mixing the same volume of each sample. The livers were removed immediately after sacrifice, weighed, and then stored at −80 °C until required for quantitative real-time PCR analysis.

2.4. Metabolite profiling

The sera were thawed at room temperature before analysis. A volume of 600 μL cold methanol was added to 200 μL serum and was shaken vigorously, and the mixture was stored for 10 min and subsequently centrifuged at 12,000 × *g* for 10 min at 4 °C. The supernatant was filtered through a syringe filter (0.2 μm) prior to UPLC–MS analysis.

All of the chromatographic separations were performed on an ACQUITY ultra performance liquid chromatography system (Waters Corp, Milford, USA). A 100 cm × 2.1 mm ACQUITY 1.7 μm C18 column and a 100 cm × 2.1 mm ACQUITY 1.7 μm HILIC column were used for reversed-phase and HILIC separations, respectively. For reversed-phase separation, mobile phase A was 0.1% formic acid, while mobile phase B was ACN modified by the addition of 0.1% formic acid. The linear gradient increased from 5% to 95% B in 16 min at a flow rate of 0.3 mL/min. For HILIC separation, mobile phase A was 95% ACN in water (0.1% formic acid), while mobile phase B was 50% ACN in water (0.1% formic acid). The linear gradient increased from 5% to 45% B in 15 min at a flow rate of 0.3 mL/min. In both separation modes, the column was maintained at a temperature of 35 °C, and the sample injection volume was 5 μL. The QC sample was injected every 10 samples during the whole sequence to evaluate the stability of the analysis. Blank (methanol) runs were carried out randomly between samples to examine chromatographic carryover.

A LCT Premier XE time-of-flight mass spectrometer (Waters Corp, Manchester, UK) was used to acquire the metabolic profiling. The mass spectrometer was used in full-scan positive-ion mode in the range of *m*/*z* 100–1000 with capillary voltage of 2.4 kV, cone voltage 35 V, desolvation gas 750 L/h at 300 °C, cone gas 50 L/h, and source temperature 110 °C. The mass spectrometer was operated in W optics mode with 14,000× resolution using dynamic range extension. The data acquisition rate was 0.2 s with a 0.1 s interscan delay. All analyses were acquired using lock spray to ensure accuracy and reproducibility. Leucine enkephalin was used as the lock

mass at a concentration of 2 μg/mL and flow rate of 20 μL/min. Data were collected in centroid mode, the lockspray frequency was 10 s, and acquired data were averaged over 10 scans.

For the further identification of potential biomarkers, a micrOTOF-Q tandem mass spectrometer (Bruker Daltonics, Billerica, USA) was used. The capillary and cone voltage were set at 3 kV and 35 V, respectively. The desolvation gas was set to 750 L/h at a temperature of 350 °C, the cone gas was set to 30 L/h, and the source temperature was set to 110 °C.

2.5. Data analysis

UPLC–MS data were analyzed with MarkerLynx v4.1, which converts three-dimensional LC–MS data (m/z, retention time and ion intensity) to a two-dimensional data table as of ion peaks (m/z and retention time pairs) and their respective intensities (peak areas). Peak detection, retention time correction, and alignment were performed using the following parameters: mass range 100–1000, mass tolerance 0.01, masses per retention time 50, minimum intensity 1%, mass window 0.05, retention time window 0.10, and noise elimination level 6. The data table of each sample was normalized to total intensity to correct for the different enrichment factors of serum among individuals. The missing peak intensities were assumed to be due to low abundance of those metabolite ions below the limit of detection. The peaks with missing values in more than 80% of the samples were excluded. The processed data table was imported to SIMCA-P+ software (Umetrics, Uppsala, Sweden) for principal component analysis (PCA). Non-linear iterative partial least squares (NIPALS) algorithm was implemented in this software to compute the first few principal components even when missing values exist. For the identification of potential biomarkers, the following databases were used: HMDB (http://www.hmdb.ca), Massbank (http://www.massbank.jp), and KEGG (http://www.kegg.com).

Data were presented as mean ± SD. Comparisons between individual group means were made using t test. p values below 0.05 were considered to be statistically significant. The statistical analysis was performed by SPSS software package (SPSS Inc., Chicago, USA).

2.6. Quantitative real-time PCR (qRT-PCR)

Quantitative PCR was applied to assess the expression of selected genes involved in important metabolic pathways. Total RNA was extracted from liver samples with trizol reagent. Reverse-transcription of cDNA synthesis was performed with 1 μg total RNA using PrimeScript® RT reagent Kit (TaKaRa Bio, Otsu, Japan). The qRT-PCR was carried out in a 25 μL final volume and performed in triplicate using SYBR Green Master Mix reagents in a Light cycler 480 detection system (Roche Applied Science, Indianapolis, USA) according to the manufacturer's protocol. PCR primers were listed in Table 1. The conditions for quantitative PCR were as follows: 95 °C for 10 min followed by 40 cycles at 95 °C for 15 s, and 60 °C for 30 s. Gene expression levels were normalized to β-actin expression levels. Three replicates of quantitative PCR were performed for each sample. The fold changes of the tested genes were analyzed by the $2^{-\Delta\Delta Ct}$ method. Values were reported as mean ± SD. Comparisons between individual group means were made using t test. p values below 0.05 were considered to be statistically significant.

Table 1
Primer sequences used for qRT-PCR analysis.

Gene	Forward primer (5′–3′)	Reverse primer (5′–3′)	Product size (bp)
Acox	cccaagacccaagagttcatt	tcacggatagggacaacaaag	161
Scd1	gtgaggcgagcaactgactat	gacggatgtcttcttccaggt	155
Fasn	gcagtttcttgatgtggaacac	aggctgtggtgactcttagtga	114
Cpt1	ccactgatgaaggagggagac	tatgggttggggtgatgtaga	226
Pla1	cagtgccagataaaccaagtga	tacagaaagtcccaacaacagg	91
Pla2	agcagagaacaaatgccaaga	aaatggaggggaagaagaggta	107
β-Actin	catccgtaaagacctctatgccaac	atggagccaccgatccaca	171

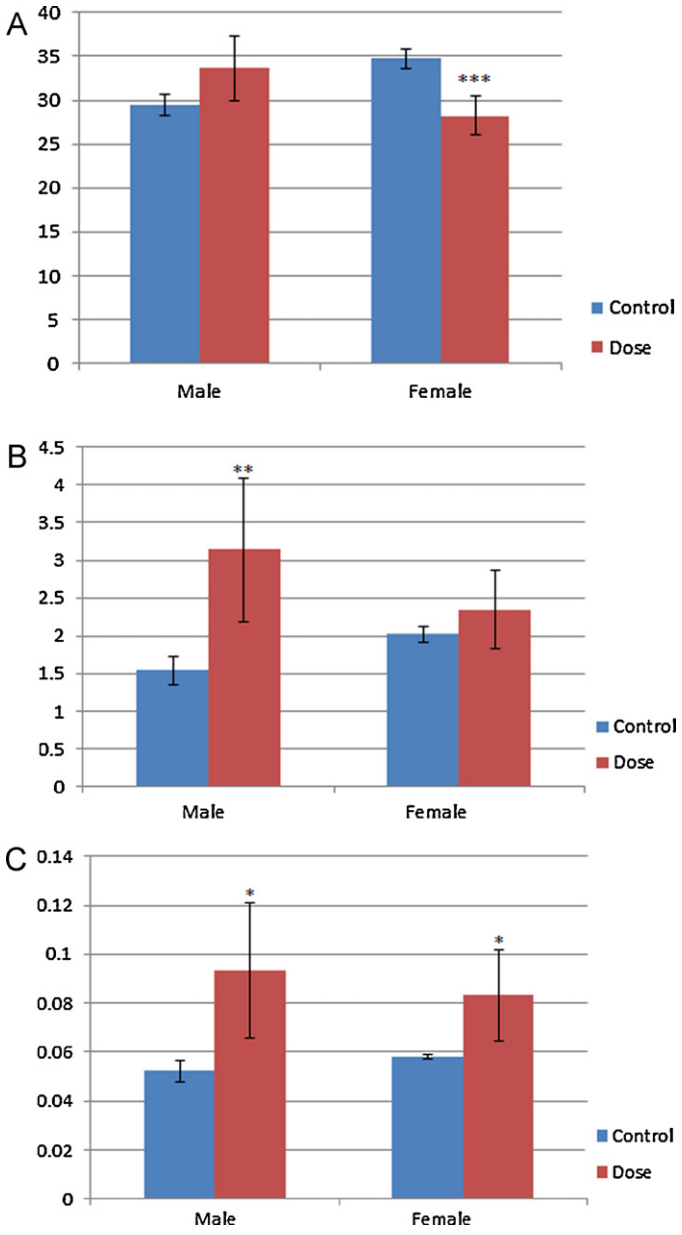

Fig. 1. Comparison of final body weights, liver weights and ratios of liver to body weight of mice after combined dietary exposure to DEHP and Aroclor 1254. *$p < 0.05$, **$p < 0.01$ and ***$p < 0.001$ compared to the control value.

3. Results and discussion

3.1. Effects of combined dietary exposure to DEHP and Aroclor 1254 on body weights and liver weights of mice

There was no significant difference in the body weights of male mice after treatment with DEHP and Aroclor 1254 for 12 days, whereas a significant body weight reduction of about 16% ($p < 0.001$) was observed for female mice (Fig. 1A). The combined exposure for male mice significantly enhanced their liver weights

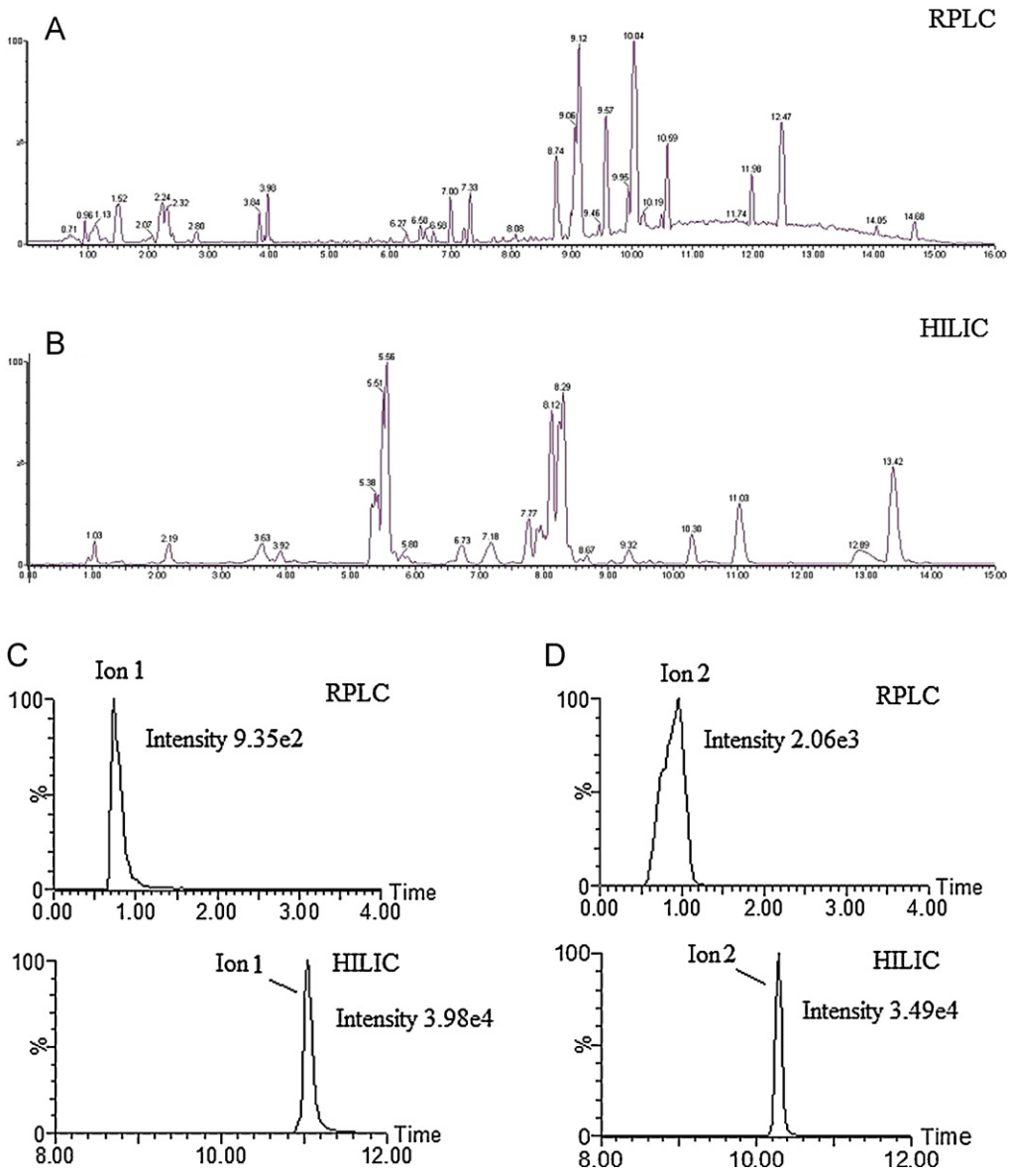

Fig. 2. Typical serum base peak chromatograms of treated mouse in RPLC (A) and HILIC (B) modes.

($p = 0.0099$), while no significant difference of liver weight could be observed for female mice ($p = 0.26$) (Fig. 1B). However, the ratios of liver to body weight show marked increases by 79% ($p = 0.017$) and 43% ($p = 0.025$) for male and female mice compared to the controls (Fig. 1C), respectively.

3.2. Metabonomic profiling

The sera from control group and dose group were subjected to metabonomic analysis. The goal of metabonomics is to acquire information on all detectable metabolites in a biological system. Liquid chromatography (LC) coupled to mass spectrometry (MS) provides a useful approach to metabolic profiling. Reversed phase (RP) is the most widely used chromatographic mode, primarily due to its versatility and feasibility for separating a large variety of metabolites. Recently, a novel separation mode, hydrophilic interaction chromatography (HILIC), has gained popularity. HILIC can separate polar metabolites that have limited retention on traditional reversed-phase packings, and it provides completely different selectivity. HILIC has been used as a complementary or alternative technique to reversed-phase packings in many metabonomic studies [18]. In this study, the separation parameters of serum on RPLC and HILIC were individually optimized, and the typical base peak chromatograms are shown in Fig. 2A and B. Different metabolite profiling could be obviously observed in the two chromatographic modes, suggesting that HILIC acted as a suitable complementary mode for separating serum metabolites, especially for highly polar metabolites. For example, as shown in Fig. 2C and D, two metabolite ions (m/z 162.112 and m/z 204.123) were not be retained on reversed-phase column and coeluted together at 0.8 min (dead time). The polar metabolite ions presented low MS responses in RPLC separation due to their suffering to serious ion suppression, and consequently their MS responses could not reflect accurate concentration differences. However, these metabolite ions were well separated on HILIC column with retention time of 10.2 and 11.1 min, respectively. The relatively high proportion of organic solvent used in HILIC separation could also significantly improved their MS responses. The intensity of the metabolite ion at m/z 162.112 and 204.123 in HILIC separation were improved by 41 and 16 folds respectively compared to those in RPLC separation. The combination of RPLC and HILIC coupled to MS increased metabonome coverage and provided a more exact

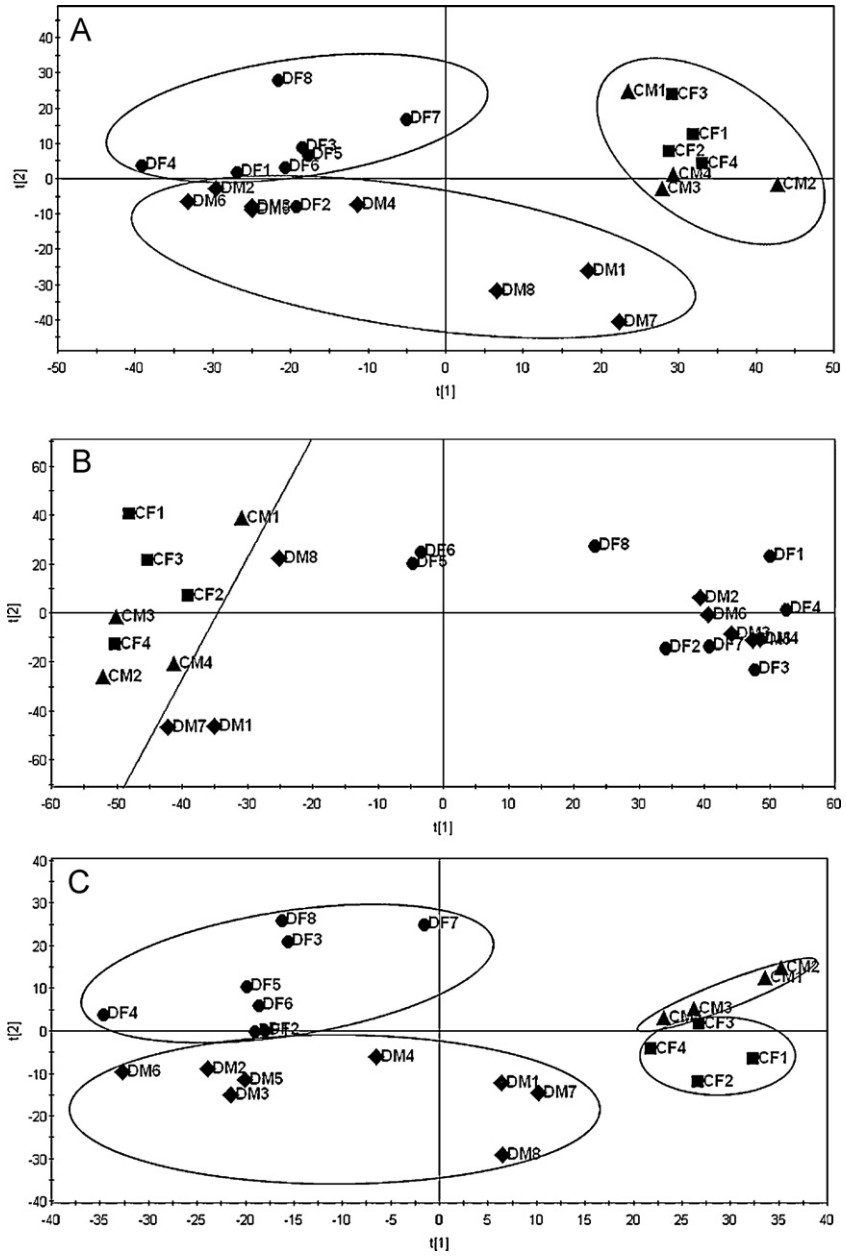

Fig. 3. PCA score plots generated from RPLC datasets (A), HILIC datasets (B) and combined datasets (C). ▲CM: male mice in control group; ■CF: female mice in control group; ♦DM: male mice in dose group; ●DF: female mice in dose group.

quantitative analysis for most metabolites. The stability and reproducibility of chromatographic separation and mass measurement during the entire sequence were assessed with our previously described method [7]. Briefly, a QC sample was injected every 10 samples to monitor the stability of the analysis. The variations in retention time and *m*/*z* values of randomly selected peaks (e.g. *m*/*z* 213.9855 at 0.56 min, *m*/*z* 160.0757 at 1.29 min, *m*/*z* 246.1701 at 3.00 min, *m*/*z* 310.2013 at 5.16 min, *m*/*z* 550.3866 at 12.82 min and *m*/*z* 282.2792 at 14.28 min) which covered the whole separation were below 0.1 min and 10 mDa, respectively. These parameters were applied in further data analysis and biomarker identification.

3.3. Multivariate statistical analysis

Many aligned individual peaks were detected and extracted from metabolic profiling by MarkerLynx. Any peaks with missing values in more than 80% of the samples were excluded using home-made software. Finally, the processed peak tables were fed to SIMCA-P+ for principal components analysis (PCA). PCA is a multivariate analysis tool that requires no prior knowledge of class membership and was used in this study to detect inherent trends within the datasets and to screen potential biomarkers. In a PCA model, $R2X_{(cum)}$ is the cumulative SS (sum of squares) for the variation of all data explained by the extracted components, and $Q2_{(cum)}$ is the total variation of the data that can be predicted by the same components, as estimated from cross-validation. The PCA score plot shows distinct clusters if the metabolic states are different between the selected groups. Each point in the PC plot represents one sample. As shown in Fig. 3A, the dose group and control group were obviously separated, and the samples of treated male mice and female mice could also been clustered in their own regions. The dose group appears to form a sparser cluster than was observed for the control group, perhaps due to the severe metabolic disorder induced by liver damage. For HILIC dataset, the dose group

Table 2
Identified metabolites in mouse serum and their associated metabolic pathways.

No.	Metabolite	Chemical formula	Adduct	Measured mass (Da)	Adduct MW (Da)	MW Difference (Da)	Trend	*p* value[a]	Pathway
1	PC(18:4/18:1)	$C_{44}H_{78}NO_8P$	$[M+H]^+$	780.5541	780.553772	0.000305	↑	0.00005	Phospholipid metabolism
2	LysoPE(18:2/0:0)	$C_{23}H_{44}NO_7P$	$[M+H]^+$	478.2928	478.292816	0.000031	↑	0.00023	Phospholipid metabolism
3	LysoPC(16:1)	$C_{24}H_{48}NO_7P$	$[M+H]^+$	494.3244	494.324097	0.000305	↑	0.0004	Phospholipid metabolism
4	sn1-LysoPC(16:0)	$C_{24}H_{50}NO_7P$	$[M+H]+$	496.3393	496.339752	0.000458	↑	0.00009	Phospholipid metabolism
			$[2M+H]^+$	991.6755	991.672241	0.003235	↑	0.00032	
5	sn2-LysoPC(16:0)	$C_{24}H_{50}NO_7P$	$[M+H]^+$	496.3390	496.339752	0.000763	↑	0.00001	Phospholipid metabolism
			$[2M+H]^+$	991.6736	991.672241	0.001343	↑	0.00002	
6	sn1-LysoPC(18:2)	$C_{26}H_{50}NO_7P$	$[M+H]^+$	520.3393	520.339783	0.000488	↑	0.00386	Phospholipid metabolism
7	sn2-LysoPC(18:2)	$C_{26}H_{50}NO_7P$	$[M+H]^+$	520.3396	520.339783	0.000183	↑	0.00248	Phospholipid metabolism
8	sn1-LysoPC(18:1)	$C_{26}H_{52}NO_7P$	$[M+H]^+$	522.3554	522.355408	0.000008	↑	0.00001	Phospholipid metabolism
9	sn2-LysoPC(18:1)	$C_{26}H_{52}NO_7P$	$[M+H]^+$	522.3546	522.355408	0.000793	↑	0.00020	Phospholipid metabolism
10	sn1-LysoPC(18:0)	$C_{26}H_{54}NO_7P$	$[M+H]^+$	524.3713	524.371033	0.000244	↑	0.00221	Phospholipid metabolism
11	sn2-LysoPC(18:0)	$C_{26}H_{54}NO_7P$	$[M+H]^+$	524.3714	524.371033	0.000366	↑	0.00648	Phospholipid metabolism
12	LysoPC(20:3)	$C_{28}H_{52}NO_7P$	$[M+H]^+$	546.3547	546.355408	0.000732	↑	0.00275	Phospholipid metabolism
13	sn1-LysoPC(20:4)	$C_{28}H_{50}NO_7P$	$[M+H]^+$	544.3399	544.339783	0.000122	↓	0.00012	Phospholipid metabolism
14	sn2-LysoPC(20:4)	$C_{28}H_{50}NO_7P$	$[M+H]^+$	544.3397	544.339783	0.000061	↓	0.00016	Phospholipid metabolism
15	sn1-LysoPC(22:6)	$C_{30}H_{50}NO_7P$	$[M+H]^+$	568.3394	568.339783	0.000366	↓	0.00013	Phospholipid metabolism
16	sn2-LysoPC(22:6)	$C_{30}H_{50}NO_7P$	$[M+H]^+$	568.3402	568.339783	0.000427	↓	0.00048	Phospholipid metabolism
17	Tryptophan	$C_{11}H_{12}N_2O_2$	$[M+H]^+$	205.0966	205.097153	0.000549	↓	0.00002	Tryptophan metabolism
18	Phenylalanine	$C_9H_{11}NO_2$	$[M+H]^+$	166.0854	166.086258	0.000854	↓	0.00003	Phenylalanine metabolism

[a] Control group versus dose group.

and control group were separated, whereas the gender clustering could not be observed in the score plot (Fig. 3B). The larger values of $R2X_{(cum)}$ (0.72) and $Q2_{(cum)}$ (0.54) (first two components) of RPLC also confirm that RPLC could provide better differentiation over HILIC (first three components, $R2X_{(cum)} = 0.54$, $Q2_{(cum)} = 0.44$).

To evaluate the performance of the combination of RPLC and HILIC, the data tables derived from individual RPLC and HILIC models were combined into a single spreadsheet. The combined spreadsheet was directly fed to SIMCA-P+ analysis without any normalization. The $R2X_{(cum)}$ and $Q2_{(cum)}$ values of the combined datasets were 0.75 and 0.55 (calculated from first two components) respectively, which were slightly higher than those built on the RPLC datasets, indicating the combined model may be of stronger ability to differentiate metabolic changes than single model. As shown in Fig. 3C, the control group forms a tight cluster, while the dose group clusters more loosely and apart from the control group. Furthermore, it should be noted that the clustering of gender could be observed within the individual groups, thereby suggesting that male and female mice demonstrated different metabolic profiles to the same treatment.

3.4. Biomarker identification

A number of ions were found predominantly in the loading plot, whose long distances from the origin represent their significant contribution to PCA differentiation. These metabolites may be candidate biomarkers to reflect metabolic changes induced by dietary exposure to DEHP and Aroclor 1254, and the significance of differences of these metabolites between control and dose groups were presented in Table 3. The method of biomarker identification has been described in our previous report [7]. Briefly, a pooled serum sample was prepared by mixing all samples in equal proportion, and it was subsequently analyzed to acquire the retention time, accurate molecular weight, isotopic pattern and MS/MS spectra for targeted metabolites using the combination of high resolution time-of-flight mass spectrometer (HRTOF-MS) and quadrupole time-of-flight hybrid tandem mass spectrometer (QTOF-MS).

As an illustrative example, Fig. 4A shows the MS and MS/MS spectra of one selected metabolite with a retention time of 10.02 min. The accurate mass of the ion was found to be 496.3393. The assistant software in MassLynx was used to determine the elemental composition for the peak at m/z 496.3393. The accurate mass cutoffs and i-FIT value were strictly restricted to 10 mDa and 10, respectively. The top five candidates in the calculated list could be potential biomarker. The molecular formula of the candidates and MS/MS spectrum were searched using Human Metabolome Database (HMDB) and Massbank, and lysoPC(16:0) was found to be the most likely metabolite. Next, the retention time and MS/MS spectrum of the commercial standard were matched with the targeted metabolite, leading us to identify the metabolite as lysoPC(16:0). The same method was used for the identification of other selected metabolites. When commercial standards were not available, the metabolites were putatively identified by comparing the acquired structure information with metabolite databases and previous literature.

Many biomarkers were classified as lysophospholipids (lysoPCs) that could be used as clinical diagnostic indicators to reveal pathophysiological changes. LysoPCs have two forms with the fatty acyl groups at positions 1 (sn1) or 2 (sn2) on glycerol backbone. As regioisomers, the two forms have identical molecular weights, meaning that discrimination is relatively difficult. Two metabolites at m/z 496.339 could be observed in the MS spectra with retention times of 9.56 and 10.02 min. With the method mentioned above, they were putatively identified as lysoPC(16:0). Sn1-lysoPC was usually eluted later than corresponding sn2-lysoPC on a reversed-phase column due to its higher hydrophobicity. Therefore, the metabolites (m/z 496.339), which eluted at 10.02 and 9.56 min, were identified as sn1-lysoPC(16:0) and sn2-lysoPC(16:0), respectively (Fig. 4A and B). The specific forms of lysoPC(16:0) were further confirmed based on their own MS/MS spectra. Sn1-lysoPC(16:0) generated prominent phosphocholine cations at m/z 184, while sn2-lysoPC(16:0) yielded more fragment ions at m/z 104. The major fragmentation pathways of lysoPC isomers were shown in Fig. 4C. The ratio of these two characteristic fragment ions could be an effective parameter to discriminate sn1- and sn2-lysoPC.

3.5. Biological significance of biomarkers

Among the identified biomarkers in Table 2, most of them are closely involved with phospholipid metabolism, including PC(18:4/18:1), lysoPE(18:2/0:0) and fourteen lysoPCs. The other biomarkers are tryptophan and phenylalanine.

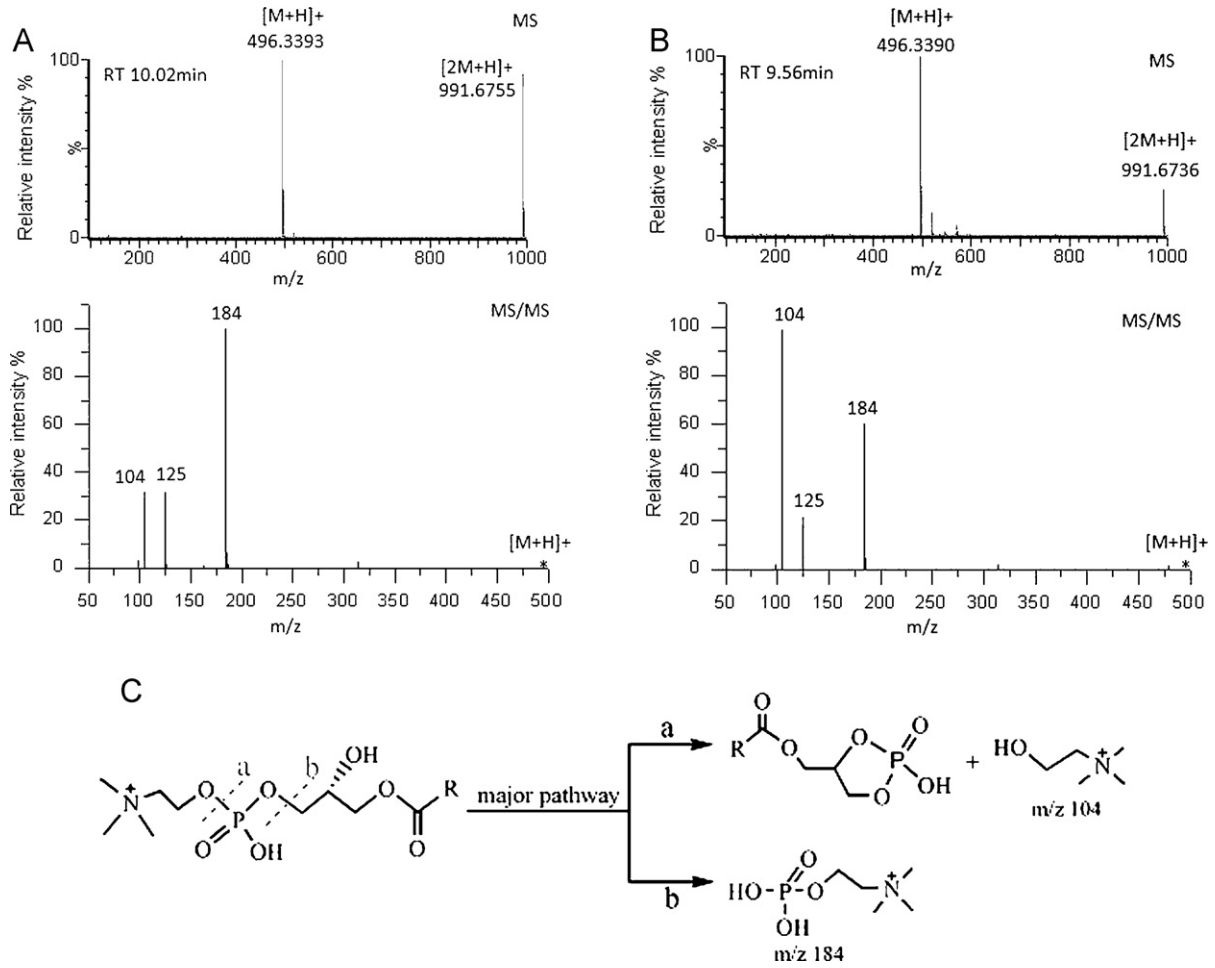

Fig. 4. MS and MS2 spectra of sn1-lysoPC(16:0) (A) and sn2-lysoPC(16:0) (B) and their major fragmentation pathway (C) in positive ion mode. R is a fatty acid chain.

Table 3
Relative abundance of identified markers in mouse serum. CM: male mice in control group; CF: female mice in control group; DM: male mice in dose group; DF: female mice in dose group.

No.	Metabolite	Relative abundance (mean ± SD)		p^a	Relative abundance (mean ± SD)		p^b
		CM	DM		CF	DF	
1	PC(18:4/18:1)	19.05 ± 3.07	42.42 ± 2.28	<0.001	35.43 ± 2.36	40.15 ± 6.21	0.181
2	LysoPE(18:2/0:0)	34.79 ± 3.80	51.41 ± 9.51	0.008	36.46 ± 6.94	47.55 ± 6.37	0.020
3	LysoPC(16:1)	23.98 ± 8.68	55.47 ± 21.64	0.021	18.89 ± 3.52	41.52 ± 9.12	<0.001
4	sn1-LysoPC(16:0)	677.22 ± 43.60	779.22 ± 38.32	0.002	664.20 ± 25.24	721.33 ± 12.50	<0.001
5	sn2-LysoPC(16:0)	263.88 ± 24.90	343.53 ± 19.68	<0.001	276.41 ± 21.68	321.49 ± 11.43	<0.001
6	sn1-LysoPC(18:2)	536.68 ± 12.86	585.52 ± 51.08	0.095	521.89 ± 29.56	596.68 ± 54.36	0.030
7	sn2-LysoPC(18:2)	207.38 ± 21.37	236.28 ± 20.10	0.044	203.42 ± 27.28	247.98 ± 30.62	0.034
8	sn1-LysoPC(18:1)	265.00 ± 22.37	357.37 ± 38.78	0.001	229.12 ± 58.86	348.96 ± 41.37	0.002
9	sn2-LysoPC(18:1)	61.45 ± 3.61	83.16 ± 16.76	0.031	52.77 ± 9.67	78.51 ± 10.81	0.002
10	sn1-LysoPC(18:0)	397.62 ± 24.18	470.36 ± 36.81	0.005	414.12 ± 19.04	434.01 ± 20.12	0.132
11	sn2-LysoPC(18:0)	178.39 ± 17.93	215.49 ± 19.84	0.010	176.36 ± 22.76	192.69 ± 16.47	0.182
12	LysoPC(20:3)	118.66 ± 11.88	150.47 ± 31.53	0.085	97.22 ± 18.80	167.87 ± 48.57	0.020
13	sn1-LysoPC(20:4)	105.95 ± 17.56	53.09 ± 25.82	0.004	105.52 ± 5.48	68.05 ± 25.34	0.017
14	sn2-LysoPC(20:4)	58.37 ± 14.71	27.96 ± 11.29	0.003	55.86 ± 4.89	39.04 ± 12.22	0.027
15	sn1-LysoPC(22:6)	251.00 ± 15.43	156.96 ± 26.04	<0.001	213.34 ± 29.82	168.96 ± 45.56	0.111
16	sn2-LysoPC(22:6)	43.63 ± 3.51	23.77 ± 3.61	<0.001	34.21 ± 7.40	27.86 ± 9.76	0.282
17	Tryptophan	213.86 ± 8.62	168.29 ± 24.60	0.005	240.38 ± 33.20	181.22 ± 14.22	0.001
18	Phenylalanine	196.65 ± 5.35	179.26 ± 8.51	0.004	205.97 ± 13.37	163.59 ± 14.62	<0.001

[a] CM group versus DM group.
[b] CF group versus DF group.

LysoPC is a class of compounds that have a constant polar head and fatty acyls of different chain lengths, position, double bond and saturation degree. LysoPC is present as a minor phospholipid in the cell membrane (≤3%) and in the blood plasma (8–12%). The composition of phospholipid is highly sensitive to industrial, radioactive, and chemical pollution of the environment. As shown in Fig. 5, phosphatidylcholine (PC) is hydrolyzed by phospholipase A (PLA) to generate free fatty acid (arachidonic acid,

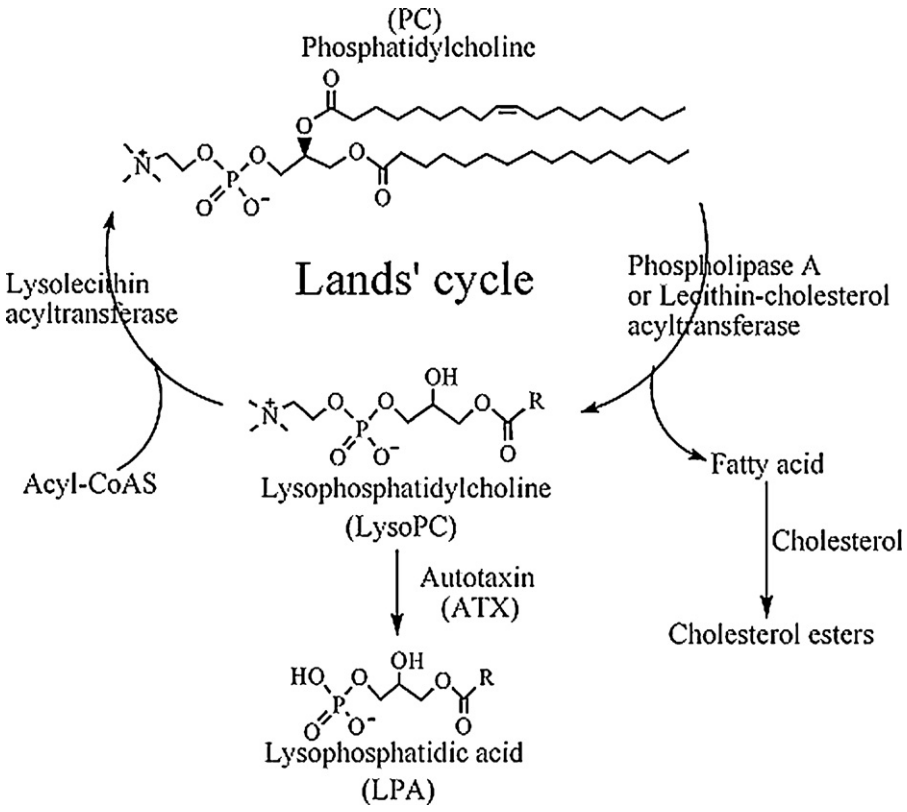

Fig. 5. Scheme of lysoPC metabolism in Lands' cycle. PC is hydrolyzed by PLA to generate free fatty acid and lysoPC. The fatty acid liberated from PC is converted to cholesterol esters, and lysoPC is changed to LPA by ATX. LysoPC is also converted to PC in the presence of acyl-CoA by LPLATs.

AA) and lysoPC, both of which have important functions in the Lands' cycle. Fatty acid released from PC is converted to cholesterol esters. LysoPC is converted to PC in the presence of acyl-CoA by LPLATs, or it is changed to lysophosphatidic acid (LPA) by autotaxin (ATX). Interestingly, we observed a significant increase of several lysoPC levels in the dose group compared to the control group, such as lysoPC(16:0), lysoPC(16:1), lysoPC(18:2), lysoPC(18:1), lysoPC(18:0) and lysoPC(20:3) (Table 2). Moreover, we observed a decrease in other identified lysoPCs, such as lysoPC(20:4) and lysoPC(22:6) (Table 2). The phenomena could be explained by different uptake and metabolism of lysoPCs in mice after the treatment of DEHP and Aroclor 1254. A recent paper [12] has reported the increase of lysoPC(16:0) concentration in rat blood after the exposure to 3000 ppm DEHP for 28 days, which was in agreement with our data. The specific lysoPC forms have different abundances in serum due to their different biological and biophysical properties, but they were observed to have similar change trends. For example, the combined exposure resulted in a significant increase for both sn1-lysoPC(16:0) and sn2-lysoPC(16:0). LysoPC augments inflammation through effects on adhesion molecules and growth factors, monocytes, and macrophages. The exposure to DEHP in rats was reported to increase the hepatic contents of PC by inducing alterations in the activities of several enzymes that participate in the biosynthesis of PC [19]. In a more recent report, the composition of phospholipids in the liver was also reported to show a great change after single oral administration of oil solutions of hexane–ether extracts from potable water sources with different contents of benzopyrene and PCBs [20]. In this study, PC(18:4/18:1) and lysoPE(18:2/0:0) were elevated in dose group after combined exposure, which could be explained by the disturbance of PLA or ATX activities and the abnormal lysoPC consumption in inflammatory response.

Phthalates and PCBs have been approved to be endocrine disrupting chemicals. Therefore, they maybe result in gender specific changes of metabolic pathways. With further inspection of these data, we found the combined dietary exposure to DEHP and Arocolor 1254 had different influence on the concentrations of some lysoPCs in dosed male mice and female mice. As shown in Table 3, there was no significant difference in sn1-lysoPC(18:2) and lysoPC(20:3) levels of dosed male mice compared to the controls, whereas significant increases of these two lysoPCs were observed for dosed female mice. After the exposure, lysoPC(18:0), lysoPC(22:6) and PC(18:4/18:1) showed significant changes for dosed male mice, while no difference was observed for dosed female mice. The different change of lysoPCs in male and female mice exposed to DBP and DEHP were also observed in previous report using NMR-based metabonomic strategy [12]. In DEHP-treated mice some gender specific genes could disturbs the growth hormone signaling in the liver and contributes to endocrine disruption [9]. Our data support gender specific endocrine disruption associated with the combined exposure. However, the exact mechanism of endocrine disruption induced by DEHP and Aroclor 1254 remains unknown.

LysoPC is generated following PLA2 hydrolysis of PC, which is the initiating event in many eicosanoid-based signal transduction pathways. PLA2 is secreted by cells in response to inflammatory stimuli, and is proven to regulate the inflammatory process by catalyzing the production of lipid mediators. Several studies suggest that the exposure of different cell types to PCBs stimulated the release of arachidonic acid (a polyunsaturated fatty acid presented in phospholipids) from the intracellular phospholipids via a mechanism that involves PLA2 [21,22]. However, the inhibition of PLA2 was observed in platelet exposed to mono(2-ethylhexyl)phthalate (MEHP), major metabolite of DEHP in blood [23]. In this study, the

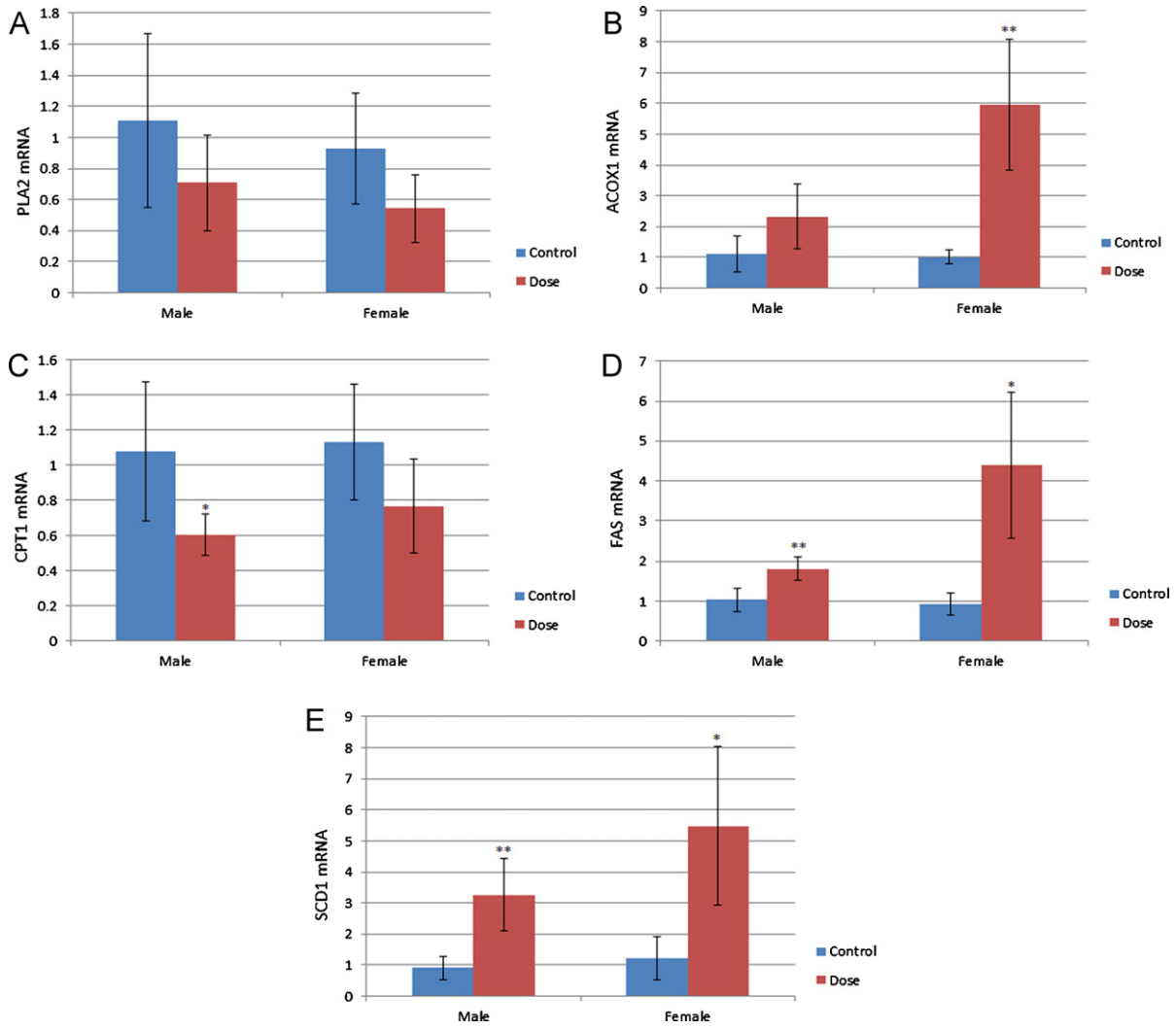

Fig. 6. Effects of DEHP and Aroclor 1254 on mRNA expressions of PLA2 (A), ACOX1 (B), CPT1 (C), FAS (D) and SCD1 (E) genes. Relative expressions of these genes were determined using qRT-PCR normalized to the expression in untreated male mice. Values shown are the mean ± SD. $^{*}p < 0.05$, and $^{**}p < 0.01$ compared to the control value.

mRNA express of PLA2 showed no significant difference for dosed male mice, whereas a slight decrease ($p = 0.053$) was observed for dosed female mice (Fig. 6A) after the combined exposure. Considering the complexity of phospholipid metabolism, the change of lysoPCs in dosed mice may be induced by the abnormal expression of other enzymes (e.g. ATX). Furthermore, the metabolites are downstream of both transcription and translation, so metabonomics could provide a more direct and sensitive measurement of the response to chemical exposure.

LysoPCs are a class of phospholipids that are intermediates in the metabolism of lipids. The disturbance of lysoPC metabolism observed in this study indicted the adverse effect of DEHP and Aroclor 1254 on lipid metabolism. Many other studies also suggest mitochondrial dysfunction and abnormality of fatty acid metabolism probably may be the most important mechanisms for the hepatotoxicity of PCBs and phthalates [11,13]. Here, the mRNA expression of several hepatic genes (such as acyl-coenzyme A oxidase 1(ACOX1), carnitine palmitoyl transferase 1 (CPT1), fatty acid synthetase (FAS), and stearoyl-CoA desaturase-1(SCD1)) was measured in the different groups of mice. ACOX1 and CPT1 are key enzymes of fatty acid oxidation and regarded as peroxisome proliferator-activated receptor (PPAR) responsive genes. PPAR has a central role in energy balance, lipid metabolism, and inflammatory responses. DEHP and its active metabolite MEHP could interfere with PPAR nuclear receptors and may thereby affect metabolic homeostasis [24]. In present study, the hepatic mRNA expression of ACOX1 was not changed ($p = 0.10$) in dosed male mice, whereas a significant increase ($p = 0.008$) was observed for dosed female mice (Fig. 6B). However, the expression of CPT1 showed a marked decrease ($p = 0.014$) for male mice and a slight but not significant decrease ($p = 0.088$) for female mice after combined exposure (Fig. 6C). These data suggested that the exposure to DEHP and Aroclor 1254 had different influence for male and female mice on the mRNA expression of ACOX1 and CPT1. The mRNA expressions of FAS and SCD1 which play a very important role in fatty acid synthesis, showed a significant increase in the liver for both male and female mice exposed to DEHP and Aroclor 1254 (Fig. 6D and E). Furthermore, the changes of FAS and SCD1 expression were found to be more pronounced in female mice than in male mice. For example, the mean FAS expression level in dosed male mice was increased by 1.6-fold ($p = 0.0099$), while the counterpart in female mice increased by 4.8-fold ($p = 0.024$). Meanwhile, the more significant elevation of SCD1 expression was observed in female mice (4.5-fold, $p = 0.041$) than male mice (3.6-fold, $p = 0.0049$) compared to the controls. The elevated expression of FAS and SCD1 increased hepatic lipid accumulation in mice after combined exposure. The high level of SCD1 has been reported to be critically linked to the metabolic perturbations found in metabolic diseases [25]. Overall,

combined abnormal mRNA expressions of ACOX1, CPT1, FAS and SCD1 would thus contribute to the increased ratio of liver to body weight in mice exposed to DEHP and Aroclor 1254.

Tryptophan is one of the 10 essential amino acids, and it plays an important role in the production of the nervous system. There is a significant decrease in the tryptophan concentration for both male and female mice exposed to DEHP and Aroclor 1254 (Table 3). DEHP treatment increased liver weights, peroxisomal proliferation and NAD+ synthesis from tryptophan in Sprague-Dawley rats [26]. Moreover, DEHP was reported to reduce mRNA expression of aminocarboxymuconate-semialdehyde decarboxylase (ACMSDase) involved in modulating the flux of tryptophan [27]. However, Aroclor 1254 tended to cause an increase of tryptophan, due to its significant inhibition of tryptophan hydroxylase (TPH) in the brains of both fish and mammals [28]. Therefore, the combined exposure definitely has different effects on tryptophan metabolism from those of individual exposure. Whether the tryptophan level is increased or decreased perhaps depends on the exact dose and dose composition of DEHP and Aroclor 1254. Phenylalanine is another essential amino acid that cannot be synthesized by humans. Toxicogenomic data has shown that an early gene-expression change concerning phenylalanine catabolism was associated with DEHP treatment [29]. A recent study has reported a decrease in phenylalanine concentration in aqueous liver extract of mice that were administered high doses of DEHP [12]. In the present study, phenylalanine concentration in serum was found to significant decrease in the dose group (Table 3), which was in agreement with previous report [12].

4. Conclusion

A LC–MS-based metabonomic method combining with PCA was used for the investigation of metabolic changes in mice serum after oral administration of endocrine disruptors DEHP and Aroclor 1254 for 21 days. Clear differentiation between the dose and control groups was observed for either RPLC or HILIC modes. Moreover, the male mice and female mice in different groups could be obviously clustered in their own regions with combined datasets of RPLC and HILIC modes, thereby indicating that the combined model could provide better classification than either single mode. Eighteen metabolites were identified and considered as potential biomarkers, including phenylalanine, tryptophan, PC(18:4/18:1), lysoPE(18:2/0:0) and fourteen lysoPCs. The metabonomic results indicated the combined exposure led to a disturbance of lipid metabolism, tryptophan metabolism and phenylalanine metabolism. Significant increases of FAS and SCD1 expressions in the liver induced by the exposure could be observed for both male and female mice, contributing to the hepatic lipid accumulation in mice. The present study improves the understanding of the combined toxicity of phthalates and PCBs, and it provides insight regarding the application of metabonomic approach in toxicity research of EDCs.

Acknowledgments

This work is financially supported by the Chinese Academy of Sciences (CAS) Knowledge Innovation Programs (KZCX2-EW-QN408), the CAS 100 Talents Program (09i4061a70), and the Xiamen Science and Technology Fund (3502Z20112017).

References

[1] K. Srogi, Levels and congener distributions of PCDDs, PCDFs and dioxin-like PCBs in environmental and human samples: a review, Environ. Chem. Lett. 6 (2008) 1–28.
[2] U. Heudorf, V. Mersch-Sundermann, J. Angerer, Phthalates: toxicology and exposure, J. Hyg. Environ. Health 210 (2007) 623–634.
[3] A. Kortenkamp, Ten years of mixing cocktails: a review of combination effects of endocrine-disrupting chemicals, Environ. Health Perspect. 115 (2007) 98–105.
[4] D.G. Robertson, P.B. Watkins, M.D. Reily, Metabolomics in toxicology: preclinical and clinical applications, Toxicol. Sci. 120 (2011) S146–S170.
[5] J.K. Nicholson, J.C. Lindon, E. Holmes, 'Metabonomics': understanding the metabolic responses of living systems to pathophysiological stimuli via multivariate statistical analysis of biological NMR spectroscopic data, Xenobiotica 29 (1999) 1181–1189.
[6] J.G. Bundy, M.P. Davey, M.R. Viant, Recent developments in environmental metabolomics, Metabolomics 5 (2008) 3–21.
[7] J. Zhang, L.J. Yan, L. Lin, W.G. Chen, X.Y. Song, X.M. Yan, W. Hang, B.L. Huang, Metabonomics research of diabetic nephropathy and type 2 diabetes mellitus based on UPLC-oaTOF-MS system, Anal. Chim. Acta 650 (2009) 16–22.
[8] S. Sumner, R. Snyder, J. Burgess, C. Myers, R. Tyl, C. Sloan, T. Fennell, Metabolomics in the assessment of chemical-induced reproductive and developmental outcomes using non-invasive biological fluids: application to the study of butylbenzyl phthalate, J. Appl. Toxicol. 29 (2009) 703–714.
[9] A. Eveillard, F. Lasserre, M. de Tayrac, A. Polizzi, S. Claus, C. Canlet, L. Mselli-Lakhal, G. Gotardi, A. Parisd, H. Guillou, P.G. Martin, T. Pineau, Identification of potential mechanisms of toxicity after di-(2-ethylhexyl)-phthalate (DEHP) adult exposure in the liver using a systems biology approach, Toxicol. Appl. Pharmacol. 236 (2009) 282–292.
[10] M.L. Whitfield Åslund, A.J. Simpson, M.J. Simpson, 1H NMR metabolomics of earthworm responses to polychlorinated biphenyl (PCB) exposure in soil, Ecotoxicology 20 (2011) 836–846.
[11] C.F. Lu, Y.M. Wang, Z.G. Sheng, G. Liu, Z. Fu, J. Zhao, J. Zhao, X.Z. Yan, B.Z. Zhu, S.Q. Peng, NMR-based metabonomic analysis of the hepatotoxicity induced by combined exposure to PCBs and TCDD in rats, Toxicol. Appl. Pharmacol. 248 (2010) 178–184.
[12] B. Ravenzwaay, G.C. Cunha, V. Strauss, J. Wiemer, E. Leibold, H. Kamp, T. Walk, W. Mellert, R. Looser, A. Prokoudine, E. Fabian, G. Krennrich, M. Herold, The individual and combined metabolite profiles (metabolomics) of dibutylphthalate and di(2-ethylhexyl)phthalate following a 28-day dietary exposure in rats, Toxicol. Lett. 198 (2010) 159–170.
[13] J.N. Feige, A. Gerber, C. Casals-Casas, Q. Yang, C. Winkler, E. Bedu, M. Bueno, L. Gelman, J. Auwerx, F.J. Gonzalez, B. Desvergne, The pollutant diethylhexyl phthalate regulates hepatic energy metabolism via species-specific PPARα-dependent mechanisms, Environ. Health Perspect. 118 (2010) 234–241.
[14] N.C. Noriega, K.L. Howdeshell, J. Furr, C.R. Lambright, V.S. Wilson, L.E. Gray, Pubertal administration of DEHP delays puberty, suppresses testosterone production, and inhibits reproductive tract development in male Sprague-Dawley and Long-Evans rats, Toxicol. Sci. 111 (2009) 163–178.
[15] L.E. Elabbas, M. Herlin, M.A. Finnilä, F. Rendel, N. Stern, C. Trossvik, W.J. Bowers, J. Nakai, J. Tuukkanen, M. Viluksela, R.A. Heimeier, A. Akesson, H. Håkansson, In utero and lactational exposure to Aroclor 1254 affects bone geometry, mineral density and biomechanical properties of rat offspring, Toxicol. Lett. 207 (2011) 82–88.
[16] J.B. Silkworth, E.A. Carlson, C. McCulloch, K. Illouz, S. Goodwin, T.R. Sutter, Toxicogenomic analysis of gender, chemical, and dose effects in livers of TCDD- or aroclor 1254-exposed rats using a multifactor linear model, Toxicol. Sci. 102 (2008) 291–309.
[17] P.R. Kodavanti, C. Osorio, J.E. Royland, R. Ramabhadran, O. Alzate, Aroclor 1254, a developmental neurotoxicant, alters energy metabolism- and intracellular signaling-associated protein networks in rat cerebellum and hippocampus, Toxicol. Appl. Pharmacol. 256 (2011) 290–299.
[18] S. Cubbon, C. Antonio, J. Wilson, J. Thomas-Oates, Metabolomic applications of HILIC–LC–MS, Mass Spectrom. Rev. 29 (2010) 671–684.
[19] H. Mizuguchi, N. Kudo, T. Ohya, Y. Kawashima, Effects of tiadenol and di-(2-ethylhexyl)phthalate on the metabolism of phosphatidylcholine and phosphatidylethanolamine in the liver of rats: comparison with clofibric acid, Biochem. Pharmacol. 57 (1999) 869–876.
[20] V.V. Urnysheva, L.N. Shishkina, Effect of the toxic chemicals in low doses on phospholipid composition of the animal liver, Biol. Bull. 31 (2004) 163–168.
[21] P.K. Tithof, E. Schiamberg, M. Peters-Golden, P.E. Ganey, Phospholipase A2 is involved in the mechanism of activation of neutrophils by polychlorinated biphenyls, Environ. Health Perspect. 104 (1996) 52–58.
[22] K. Matsusue, Y. Ishii, N. Ariyoshi, K. Oguri, A highly toxic PCB produces unusual changes in the fatty acid composition of rat liver, Toxicol. Lett. 91 (1997) 99–104.
[23] R.S. Labow, E. Meek, G.A. Adams, G. Rock, Inhibition of human platelet phospholipase A2 by mono(2-ethylhexyl)phthalate, Environ. Health Perspect. 78 (1988) 179–183.
[24] P.J. Lapinskas, S. Brown, L.M. Leesnitzer, S. Blanchard, C. Swanson, R.C. Cattley, J.C. Corton, Role of PPAR-alpha in mediating the effects of phthalates and metabolites in the liver, Toxicology 207 (2005) 149–163.
[25] S. García-Serrano, I. Moreno-Santos, L. Garrido-Sánchez, C. Gutierrez-Repiso, J.M. García-Almeida, J. García-Arnés, J. Rivas-Marín, J.L. Gallego-Perales, E. García-Escobar, G. Rojo-Martinez, F. Tinahones, F. Soriguer, M. Macias-Gonzalez, E. García-Fuentes, Stearoyl-CoA desaturase-1 is associated with insulin resistance in morbidly obese subjects, Mol. Med. 17 (2011) 273–280.
[26] M. Shin, M. Ohnishi, S. Iguchi, Peroxisome-proliferator regulates key enzymes of the tryptophan-NAD+ pathway, Toxicol. Appl. Pharmacol. 158 (1999) 71–80.

[27] T. Fukuwatari, S. Ohsaki, S. Fukuoka, R. Sasaki, K. Shibata, Phthalate esters enhance quinolinate production by inhibiting alpha-amino-beta-carboxymuconate-epsilon-semialdehyde decarboxylase (ACMSD), a key enzyme of the tryptophan pathway, Toxicol. Sci. 81 (2004) 302–308.
[28] I.A. Khan, P. Thomas, Disruption of neuroendocrine control of luteinizing hormone secretion by Aroclor 1254 involves inhibition of hypothalamic tryptophan hydroxylase activity, Biol. Reprod. 64 (2001) 955–964.
[29] R.A. Currie, V. Bombail, J.D. Oliver, D.J. Moore, F.L. Lim, V. Gwilliam, I. Kimber, K. Chipman, J.G. Moggs, G. Orphanides, Gene ontology mapping as an unbiased method for identifying molecular pathways and processes affected by toxicant exposure: application to acute effects caused by the rodent non-genotoxic carcinogen diethylhexylphthalate, Toxicol. Sci. 86 (2005) 453–469.

Journal of Pharmaceutical and Biomedical Analysis 66 (2012) 298–305

Contents lists available at SciVerse ScienceDirect

Journal of Pharmaceutical and Biomedical Analysis

journal homepage: www.elsevier.com/locate/jpba

Validation of a dried blood spot LC–MS/MS approach for cyclosporin A in cat blood: Comparison with a classical sample preparation

Rayane Mohamed[a,*], Laura Mercolini[b], Suzanne Cuennet-Cosandey[a], Jacques Chavent[a], Maria Augusta Raggi[b], Mathieu Peyrou[a]

[a] Novartis Animal Health, Novartis centre de Recherche Santé Animale SA, CH-1566 Saint Aubin, Switzerland
[b] University of Bologna, Faculty of Pharmacy, I-40126 Bologna, Italy

ARTICLE INFO

Article history:
Received 11 November 2011
Received in revised form 22 March 2012
Accepted 23 March 2012
Available online 2 April 2012

Keywords:
Cyclosporin A
Dried blood spot
LC–MS/MS
Pharmacokinetics

ABSTRACT

A rapid, selective and sensitive bioanalytical method was developed and validated for cyclosporin A (CsA) in cat blood samples using dried blood spot (DBS) coupled with high pressure liquid chromatography hyphenated to positive electrospray tandem mass spectrometry (HPLC–ESI-MS/MS). CsA was quantified using a structural analog cyclosporin D (CsD) as internal standard in multiple reaction monitoring mode (MRM) using the transitions 1220 → 1203 for CsA and 1234 → 1217 for CsD. A 5-μL blood aliquot was spotted onto a DBS card, then after a drying step, blood spots were punched out from the cards and extracted with MeOH before injection into a LC–MS/MS system. The linear range of the method was 5–2000 ng/mL, with accuracy and precision within the FDA acceptance criteria (i.e., ±15% and ±20% for the lowest level). In the study presented herein a comparison was made between this new methodology, based on the use of DBS, and a previously developed solid phase extraction (SPE) procedure, applied to blood samples from a cat pharmacokinetic study. Good correlation (r^2 = 0.97) was demonstrated between the data obtained with the two methods. The DBS methodology revealed to be cheaper, faster, less solvent-consuming and requiring less blood volume from animals than the previous SPE method. Thus, the proposed HPLC–ESI-MS/MS method, based on DBS, has demonstrated to be a suitable and advantageous approach for the analysis of CsA in cat blood.

© 2012 Elsevier B.V. All rights reserved.

1. Introduction

In human medicine cyclosporin A (CsA) (Fig. 1a) is used since decades as an immunosuppressant drug for solid organs transplant recipient. In addition, the drug has been also used for the treatment of immune-mediated diseases such as rheumatoid arthritis, psoriasis and atopic dermatitis. In veterinary medicine, CsA has been found to be highly valuable in dogs and cats for the control of immune-mediated diseases and allergic disorders, such as perianal fistulas [1,2], atopic dermatitis [3–5] and other immune-mediated skin diseases [6]. CsA has also been used for renal transplantation in cats with end-stage renal disease. The success of transplantation is highly dependent on effective and safe immunosuppressive therapy. Pharmaceuticals concentration measurement in whole blood is acknowledged to be an acceptable alternative to classical plasma concentrations measurements by the regulatory authorities [7–9]. Nowadays, the use of dried blood spot (DBS) for sample collection and analysis in pharmacokinetics and toxicokinetic studies is largely reported in the literature [10–12]. The main advantages of DBS are the low blood volume required (5–25 μL) which is compliant with the overall objectives of the 3Rs (reduce, refine and replace), simplification of sample collection, storage and reduction of transportation costs. However there are still some improvements to bring to the use of DBS for bioanalytical purposes, as the procedure can be tedious and time-consuming. Indeed, blood has to be spotted on an absorbent storage card; then spots are allowed to dry and then punched out from the card for extraction with a suitable solvent [13]. One alternative to overcome these issues is the DBS automation; some attempts were reported in the literature but still with some limitations, such as manual pre-punching or manual autosampler feeding before analysis [14,15].

As shown in Fig. 1a, CsA is a lipophilic cyclic polypeptide. Over the years immunoassays have been largely used for its measurements, however this technique suffers from a lack of specificity and the cross reactivity of immunoassay antibodies can lead to false estimation of CsA concentrations [16,17]. Liquid chromatography hyphenated to tandem mass spectrometry (LC–MS/MS) is considered as the method of choice for measuring CsA concentrations in different biological matrices such as blood [18,19], plasma [20,21] or urine [22]. This technique provides a high level of specificity and sensitivity which are required in complex biofluid matrice analysis.

* Corresponding author at: Novartis Animal Health Research Center, CH-1566 Saint Aubin, Switzerland. Tel.: +41 26 679 1604; fax: +41 26 679 1228.
E-mail address: rayane.mohamed@novartis.com (R. Mohamed).

0731-7085/$ – see front matter © 2012 Elsevier B.V. All rights reserved.
http://dx.doi.org/10.1016/j.jpba.2012.03.049

To the best of our knowledge, this paper is the first article about dried blood spots for cat blood samples. As cat is specie used in pre-clinical studies and is major specie for veterinary R&D, it is important to assess such technology in the light of potential interspecies differences. The main advantage of developing such approach for cats is related to the withdrawal of lower blood volumes, in order to overcome the restriction linked to the relatively small total blood volume in cats compared to other species, such as dogs or monkeys. Up to day, only two reports in the scientific literature describe the use of DBS for CsA measurements in human matrices [23,24]. Here we described a rapid, sensitive and accurate method for the measurements of CsA in DBS obtained from cat blood samples. Data generated during a previous pharmacokinetic (PK) study using a SPE procedure were compared to this innovative DBS–LC–MS/MS methodology. Method validation was performed according to international bioanalytical guidelines [25].

2. Experimental

2.1. Chemical and reagents

Cyclosporin A (CsA) and cyclosporin D (CsD) – used as internal standard – (Fig. 1b) were obtained through Novartis Pharma Reference Standards Units (Ringaskiddy, Ireland). Acetonitrile (ACN), methanol (MeOH), water (H_2O) all LC–MS graded and formic acid (HCOOH) were provided by Sigma Aldrich (Buchs, Switerland). Ammonium acetate was from Fluka (Buchs, Switzerland).

2.2. Standards solutions

Stock solution (0.1 mg/mL) of CsA and CsD were prepared by dissolving the standard reference in a mixture acetonitrile/water (6/4, v/v). Further dilutions were prepared in the same mixture solvents. Stock solutions and dilutions were stored at +4 °C until use.

2.3. Cat blood samples

Cat blood samples were provided by Novartis Animal Health Research Center. K+, EDTA was added as anticoagulant. Neutral blood was taken from healthy cat not exposed to cyclosporin A. Incurred samples are from a previous internal PK study.

2.4. Sample preparation

2.4.1. Manual DBS procedure

Frozen cat blood samples were allowed to thaw at room temperature. An aliquot of 5 μL of blood spiked with cyclosporin D (CsD) used as the internal standard at 400 ng/mL was carefully transferred onto a 903 Protein Saver card (Whatman, Bottmingen, China). The internal standard was added directly into the matrix by prior spiking 4 μL of CsD at 2000 ng/mL into 20 μL of cat blood samples. The blood was left to dry for 2 h at room temperature in a dark and dry place. A 6 mm diameter circle was punched out from the card using a Harris Uni-Core Punch, 6 mm, 4/pk with two 2.5 in. × 3 in. cutting mats (Whatman, Bottmingen, China) and placed into a NuncU96 well Plate 128 × 86 mm (VWR International, Dietikon, CH) with 100 μL of methanol. The plate was then shaken for 15 min and centrifuged at 1000 × *g* (ThermoScientific Multifuge X3R, Waltham, USA) for 1 min. The supernatant (10 μL) was injected into a Symbiosis (Spark Holland, Emmen, The Netherlands) pumps systems coupled to a 4000QTRAP mass spectrometer (AB Sciex, Concord, Canada).

2.4.2. Solid phase extraction procedure

Frozen cat blood samples were allowed to thaw at room temperature and each 0.5 mL aliquot was poured into a 4.5 mL polypropylene test tube. CsD (50 μL at 500 ng/mL) was added, followed by 0.5 mL water containing 0.1% phosphoric acid and 1.0 mL acetonitrile. The extracts were submitted to vortex and centrifuged at 3500 × *g* for 15 min at 20 °C. The supernatant was transferred into a new tube and 1 mL water was added. The extracts were loaded onto a Varian Versaplate 100 mg C8 solid phase extraction cartridges, previously conditioned with 1 mL ACN and 1 mL H_2O. After loading, the extracts were washed with 1.5 mL acetonitrile/water 30:70 (v/v) and cartridges were allowed drying before elution with 1.5 mL acetonitrile. The extracts were evaporated under a gentle nitrogen stream at 40 °C and the dry residue was resuspended with 125 μL acetonitrile/water 60:40 (v/v) before injection (10 μL).

2.5. LC–ESI-MS/MS

Analyses were performed on a 4000 QTRAP mass spectrometer, equipped with a TurboIonspray ionization source (AB Sciex, Concord, Canada) and coupled to Symbiosis pumps systems (Spark

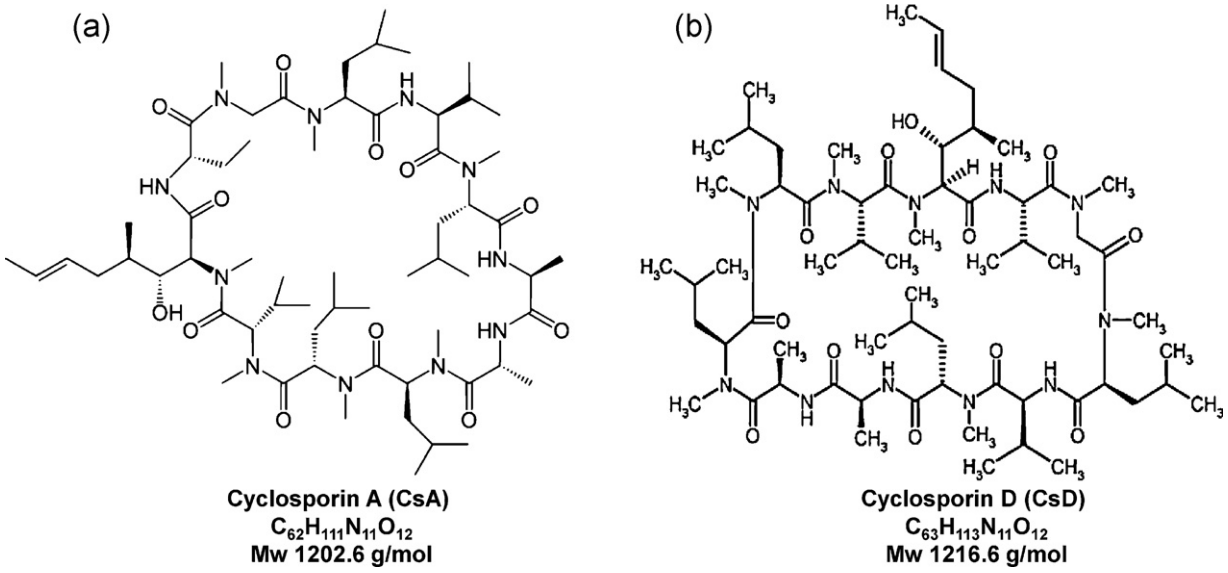

Fig. 1. Chemical structures of (a) cyclosporin A (CsA) and (b) cyclosporin D (CsD).

Holland, Emmen, NL). HPLC analyses were run on a Macherey-Nagel Nucleodur 100-3C18ec (C18 modified, particle size 3 μm), CC 125/2, 125 × 2 mm HPLC column equipped with a precolumn cartridge, 8 × 3 mm, with the same packing material as the main column (Macherey Nagel, Oesingen, CH). Mobile phases were constituted with solvent A: water containing 2 mM ammonium acetate/MeOH/formic acid (95:5:0.1, v/v/v) and solvent B: water containing 2 mM ammonium acetate/MeOH/formic acid (5:95:0.1, v/v/v). The total flow rate was 0.6 mL/min and the gradient program was: 0 min 80%B; 0–0.5 min 95%B, 0.5–1.5 min 95%B; 1.5–1.6 min 80%B; 1.6–5 min 80%B. Injection was performed with a Symbiosis Reliance autosampler module (Spark Holland, Emmen, NL) and 10 μL volume was injected onto the column. The column was heated at 80 °C with a-1100 Series G1316A Agilent column oven (Agilent Technologies, Santa Clara, USA). MS tuning was performed in positive electrospray ionization (ESI) by infusing (Pump-11, Havard Apparatus, Holliston, MA, USA) individual solution of CsA and CsD (1 μg/mL in acetonitrile/water; 60/40; v:v) mixed with a HPLC flow made of solvents A and B (50/50, v/v; 0.1 mL/min) using a T-connector. Nitrogen was used for the nebulizer (GS1 and GS2) and curtain (CUR) gases at pressures of respectively 40, 50 and 20 psi. The block source temperature was maintained at 450 °C with a capillary voltage set at 5.5 kV. Nitrogen was also used as collision gas at a medium pressure selection. MS/MS detection was realized using the selected reaction monitoring (SRM) acquisition mode. The most intense fragment ion of each compound was selected using a dwell time of 100 ms. Quantitative analysis was performed using the respective SRM signal. Data processing was performed using Analyst 1.5.1 software (AB Sciex).

2.6. Linearity and accuracy

Quantification was performed using neutral cat blood samples (K+, EDTA as anticoagulant) collected at Novartis Animal Health Research Center (St. Aubin, CH). CsD was used as internal standard. Calibration curves were prepared on the analysis day by spiking frozen cat blood sample at 5, 10, 20, 40, 100, 200, 400, 1000 and 2000 ng/mL. A quadratic regression using a $1/x$ weighing type was used. Considering the blood spot volume (i.e., 5 μL) and the solvent dilution factor (i.e., 20 times), those levels correspond to 2.5, 5, 10, 20, 50, 100, 200, 500 and 1000 pg injected on column. Acceptance criteria for accuracy was ±15% (except at the LLOQ ±20%).

2.7. Quality control samples

Quality control samples (QC) were prepared in the same way as the calibration samples, except that a distinct set of stock solution and further dilutions was used. Four concentrations levels were evaluated i.e., 10, 40, 400 and 2000 ng/mL. Acceptance criteria for QC accuracy was ±15% (except for the LLOQ ±20%).

2.8. Method validation

A partial validation was performed by injecting on three different days a 9-point calibration curve ranged from 5 to 2000 ng/mL corresponding to 2.5–1000 pg injected on column. Along with the calibration curve, quality control samples were measured on each day at four different concentration levels ($n = 4$ at each level). The carry-over was assessed by measuring the peak area obtained at the expected retention time of CsA (i.e., 2.9 min) of respectively a solvent sample placed directly after the ULOQ (i.e., 2000 ng/mL) and at the LLOQ (i.e., 5 ng/mL). The area obtained in the blank solvent should not exceed more than 20% of the LLOQ area value. The overall recovery (including extraction recovery and matrix effect) was measured by plotting the area response obtained for a blood sample spiked at a specific concentration versus a neat standard solution corresponding to the same amount injected on column. The lower limit of quantification (LLOQ) was considered as the lowest standard on the calibration curve with a response of at least 5 times higher than the averaged blank noise, identifiable and reproducible with a precision of 20% and accuracy between 80 and 120%. The limit of detection (LOD) was determined as the smallest detectable peak above at least 3 times the baseline noise.

Table 1
MRMs followed for CsA and CsD along with their chromatographic retention times.

Analyte	MRM	Collision energy (eV)	Retention time (min)
CsA	1220 → 1203	25	2.9
CsD	1234 → 1217	25	3.1

2.9. Stability study

A stability study was performed by preparing quality control samples at three different concentration levels ($n = 2$ at each concentration). These samples were spotted on the cards according to the procedure described earlier and let dry for 2 h at room temperature. Reference time referred as t_0 corresponds to the samples processed right after the drying step. The others samples were kept in Ziploc bags containing desiccant in the dark at room temperature. They were processed at time $t + 3$ h, $t + 24$ h, $t + 48$ h, $t + 6$ days and $t + 9$ days. According to our internal procedure, the bias between the mean measured value after stability testing and the mean measured value at t_0 (i.e., % difference stored versus fresh) should be in the range of ±15% for every level.

2.10. Influence of fresh blood versus frozen blood

A 8-points calibration curve was prepared in fresh blood collected on healthy animals the morning of the DBS preparation. Data obtained were compared to those generated by building a calibration curve with frozen neutral cat blood samples. To assess the differences between the two conditions, a Deming regression is used. Confidence intervals are constructed by the jackknife method [26]. The data are also submitted to a Bland–Altman plot.

2.11. Comparison with a classical SPE–LC–MS method

Data generated in a previous pharmacokinetic study using a SPE procedure, were compared to those obtained with an advanced DBS–LC–MS/MS methodology. To assess the differences between the two conditions, a Deming regression is used. Confidence intervals are constructed by the jackknife method [26]. The data are also submitted to a Bland–Altman plot.

3. Results and discussion

3.1. LC–ESI-MS/MS

Full mass spectra and the respective fragment ions patterns obtained under collision induced dissociation (CID) were acquired for CsA and CsD to determine their respective multiple reaction monitoring (MRM) parameters (Table 1). Only ammonium adducts $(M+NH_4)^+$ species were observed for both species at $m/z = 1220$ and $m/z = 1234$, respectively for CsA and CsD, due certainly to steric hindrance caused by the cyclic structure of both CsA and CsD (Fig. 1a and b). Several HPLC columns and chromatographic conditions were tested. The lipophilic properties of CsA lead us to use a gradient starting with a high percentage of organic solvent (i.e., 80%) and a column oven temperature set at 80 °C. Lower temperatures were tested for the column oven resulting all with poor peak shapes especially for CsD (data not shown). The retention time for CsA was

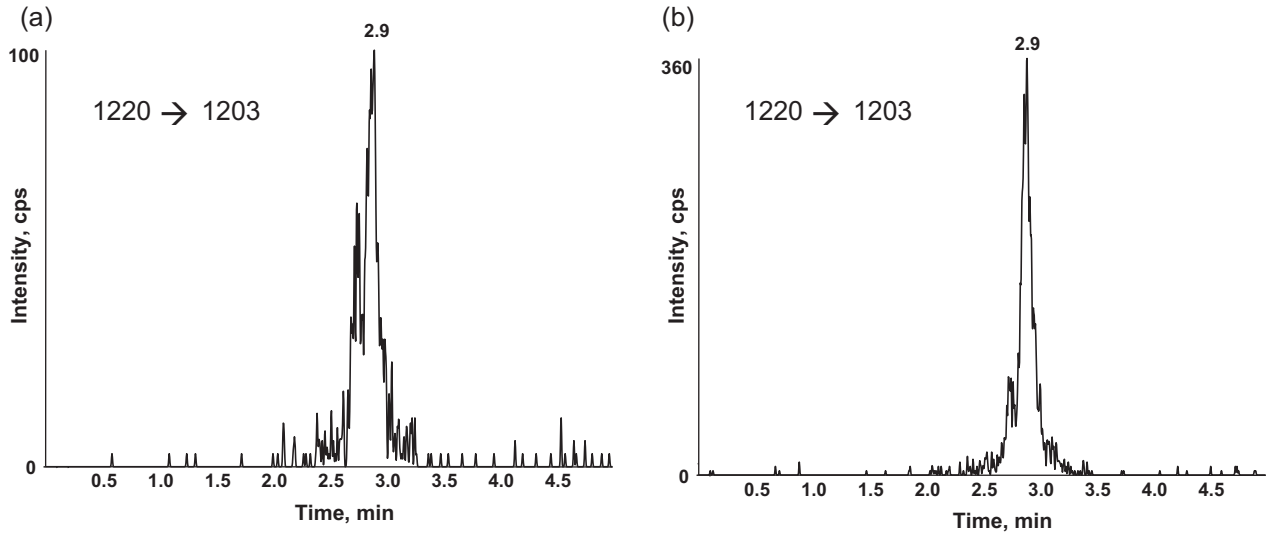

Fig. 2. Extracted ion chromatograms for CsA for (a) blank cat blood sample containing neither CsA nor CsD and (b) the same blank cat blood sample spiked with CsA at 5 ng/mL (i.e., LLOQ).

2.9 min and the total analysis time of 5.0 min. A co-eluting interference was observed in the CsA retention window preventing the decrease the limit of quantification below 5 ng/mL (Fig. 2). This interference might be the result from a slight memory effect, as CsA is very hydrophobic and might bind onto the HPLC column. Overall this effect was below 20% of the averaged response obtained at the LLOQ and therefore had a minor impact on the data quality.

3.2. DBS optimization

Multiple factors were evaluated to assess the DBS extraction efficiency. The nature and volume of the extraction solvent, the spot size and the spot drying conditions were assessed. The different trials showed that a 5 μL blood spot extracted with MeOH provided the best results not only in terms of signal intensity but also in terms of sample cleanliness. An extraction volume of 100 μL was optimal to obtain a good MS/MS intensity without being affected significantly by the dilution phenomenon. It is noteworthy to say that higher extraction volumes (i.e., 250 μL and 500 μL) were tested and the resulting intensity signals were respectively 6.5 and 55 times lower than for 100 μL. These intensity factors did not match with the expected dilution factors i.e., 2.5 and 5 times. One hypothesis could be a lower efficiency of the extraction using larger volumes. Indeed after being punched, the spot was placed into a well of 8 mm diameter and 120 mm height, the extraction solvent was added and vortex horizontally. Considering the dimensions of the well using a 250 and 500 μL extraction volume can decrease the yield efficiency, as the vortexing step may not be optimal for such volumes. Different drying conditions, such as microwave heating were evaluated, but the results showed higher variability than by drying at room temperature in the dark (data not shown).

A medium concentration (100 ng/mL) extracted ion chromatogram for a DBS obtained from a cat blood spiked with CsA and CsD (400 ng/mL) is shown in Fig. 3.

3.3. Influence of using fresh blood versus frozen blood

The use of frozen blood is convenient in bioanalysis studies as it allows performing the analysis later on after blood collection without spoiling the quality of the results which represents a big advantage especially for multi-sites studies. The effect of hematocrit (HT) is well described when using DBS techniques [13]. Since blood viscosity is related to the HT, it can have an impact on the flow and diffusion properties over the card. In our case the fresh cat blood samples have a HT values ranging between 0.33 and 0.49 L/L while frozen blood represents the worst case scenario in terms of viscosity properties. In this study we evaluated the potential accuracy deviation between frozen and fresh blood samples by preparing 2 series of calibration curves with both blood types. For the fresh blood, collection was performed in the early morning prior submission to DBS procedure. The results demonstrated excellent correlation between fresh and frozen blood, with coefficient correlation $r^2 = 0.9976$ (Fig. 4). Because typical linear regression assumes that only one variable can be affected by error, the data were also processed in SAS 9.2.2, using the Deming regression model in order to validate the results [26]. The Deming regression is a two-dimensional model accounting for measurement error in observations from both datasets, and so it is best suited for method comparison; a correlation of 1.001 was obtained. Therefore, the use of frozen matrix is suitable for the DBS extraction of cyclosporin A in cat blood allowing more flexibility during sample collection. This

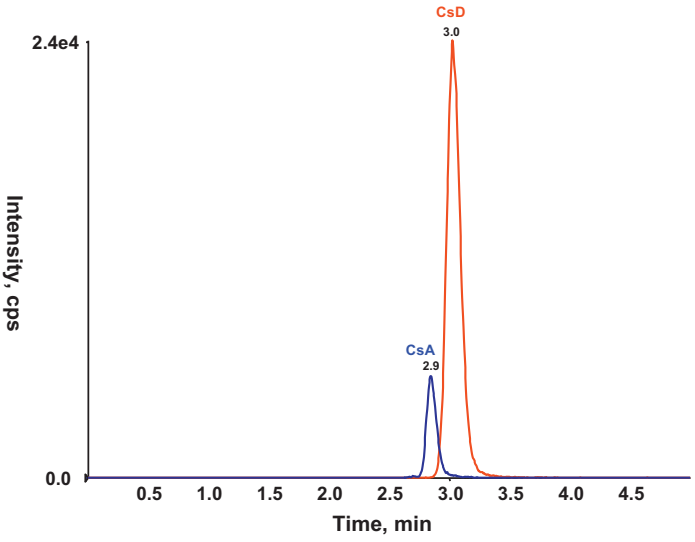

Fig. 3. Medium concentration (100 ng/mL) extracted ion chromatogram for a DBS obtained from a cat blood spiked with CsA and CsD (400 ng/mL).

Table 2
Method validation data.

	Coefficient of correlation, *r*	Slope, *b*	Intercept, *c*	*a*
Linearity 5-2000 ng/mL				
Day 1	0.9998	0.00142	0.00763	9.39E−09
Day 2	0.9994	0.00138	0.00685	2.86E−08
Day 3	0.9994	0.00137	0.00404	1.29E−07
Mean	0.9995	0.0014	0.00617	5.57E−08
S.D.	0.0002	0.0000	0.00189	6.42E−08

	Theoretical conc. (ng/mL)			
	9.94	39.75	397.52	1987.60
	Calculated concentrations (ng/mL)			
Inter- and intra-day precision				
Day 1	9.47	60.88	373.10	2004.61
	9.30	39.97	398.61	2089.83
	10.47	41.78	399.72	2194.20
	9.63	41.35	386.99	2030.09
Mean	9.72	45.99	389.61	2079.68
Accuracy (%)	97.8	115.7	98.0	104.6
Precision as CV%	5.4	21.6	3.2	4.1
N	4	4	4	4
Day 2	10.06	36.01	382.39	1935.27
	10.44	40.16	399.50	1866.03
	9.40	37.13	416.72	2115.86
	10.30	43.36	427.12	2181.42
Mean	10.05	39.16	406.435	2024.65
Accuracy (%)	101.1	98.5	102.2	101.9
Precision as CV%	4.6	8.4	4.8	7.3
N	4	4	4	4
Day 3	10.17	42.49	393.39	1918.66
	9.81	41.66	394.97	1909.42
	10.39	40.89	394.84	1830.85
	10.13	39.08	404.38	1883.13
Mean	10.13	41.03	396.89	1885.52
Accuracy (%)	101.9	103.2	99.8	94.9
Precision as CV%	2.3	3.6	1.3	2.1
N	4	4	4	4
Grand mean	9.97	42.06	397.64	1996.61
Overall accuracy (%)	100.3	105.8	100.0	100.5
Precision as CV (%)	4.27	14.53	3.46	5.06
N	12	12	12	12

	5 ng/mL – 2.5 pg injected on column	100 ng/mL – 50 pg injected on column	2000 ng/mL – 1000 pg injected on column
Overall recovery			
n_1	77	67	74
n_2	51	74	66
n_3	77	77	71
Mean	68	73	70
S.D.	15.01	5.13	4.04
RSD	22%	7%	6%

	Sample ID	Peak area Cyclosporin A	Carry-over (% of LLOQ response) Cyclosporin A
Carry over			
Day 1	C at LLOQ	2101	
	C at ULOQ	581008	
	Solvent	497	23.6
Day 2	C at LLOQ	2295	
	C at ULOQ	492005	
	Solvent	189	8.2
Day 3	C at LLOQ	2058	
	C at ULOQ	670018	
	Solvent	317	15.4
		Mean (%)	15.8

LOD = 3.5 ng/mL; LLOQ = 5 ng/mL.

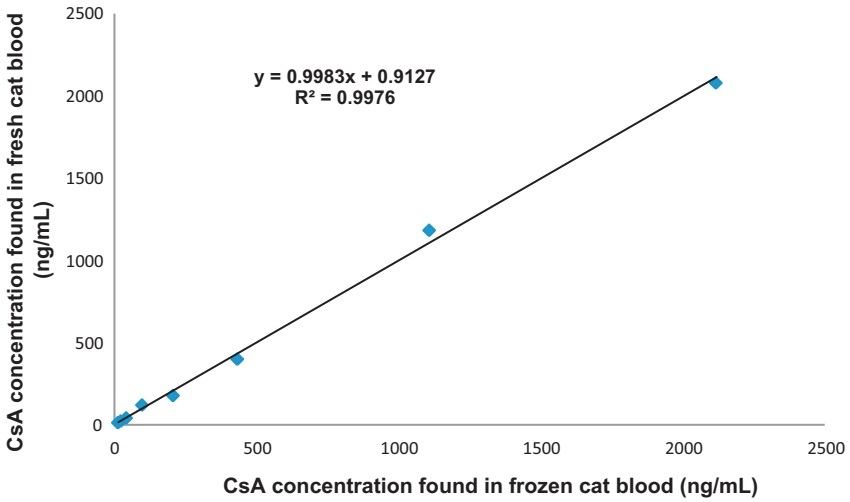

Fig. 4. Comparison between frozen blood samples and fresh blood samples for DBS sampling.

is compliant with a former test conducted by Wilhelm et al. [23] to assess HT impact on CsA concentration obtained by DBS for human blood samples.

3.4. Method validation

Validation of the method was performed according to the US FDA guidelines for industry [25], the data are summarized in Table 2. One calibration curve along with quality control samples ($n = 4$) were analyzed on three separate days. Data obtained from the 3 individual calibration curves demonstrate that the method was linear for CsA from 5 to 2000 ng/mL with an averaged correlation coefficient r^2 of 0.9995. This method covers a larger range than the one obtained with the classical SPE method (i.e., 3–125 ng/mL) and is more sensitive than the previous published ones with DBS [23,24]. The mean accuracy obtained during these three days was

Table 3
Stability data.

Timepoints	Sample ID	Theoretical conc. (ng/mL)	Observed conc. (ng/mL)	Accuracy (%)	% Difference (stored versus fresh)
t_0	QC10	9.94	9.47	−3.9	N/A
	QC10		9.63		
	QC400	397.50	373.10	−4.4	N/A
	QC400		386.99		
	QC2000	1987.60	2004.61	1.5	N/A
	QC2000		2030.09		
t + 3 h	QC10	9.94	9.30	−0.5	3.5
	QC10		10.47		
	QC400	397.50	398.61	0.4	5.0
	QC400		399.72		
	QC2000	1987.60	2089.83	7.8	6.2
	QC2000		2194.20		
t + 24 h	QC10	9.94	9.40	−0.9	3.1
	QC10		10.30		
	QC400	397.50	416.72	6.1	11.0
	QC400		427.12		
	QC2000	1987.60	2115.86	8.1	6.5
	QC2000		2181.42		
t + 48 h	QC10	9.94	10.39	3.2	7.4
	QC10		10.13		
	QC400	397.50	394.84	0.5	5.1
	QC400		404.38		
	QC2000	1987.60	1830.85	−6.6	−7.9
	QC2000		1883.13		
t + 6 days	QC10	9.94	8.47	−2.5	1.4
	QC10		10.91		
	QC400	397.50	391.50	−2.0	2.5
	QC400		387.51		
	QC2000	1987.60	1925.85	−2.9	−4.3
	QC2000		1934.51		
t + 9 days	QC10	9.94	7.33	−22.1	−18.9
	QC10		8.16		
	QC400	397.50	388.71	−1.5	3.0
	QC400		394.16		
	QC2000	1987.60	1957.25	−0.6	−2.1
	QC2000		1993.97		

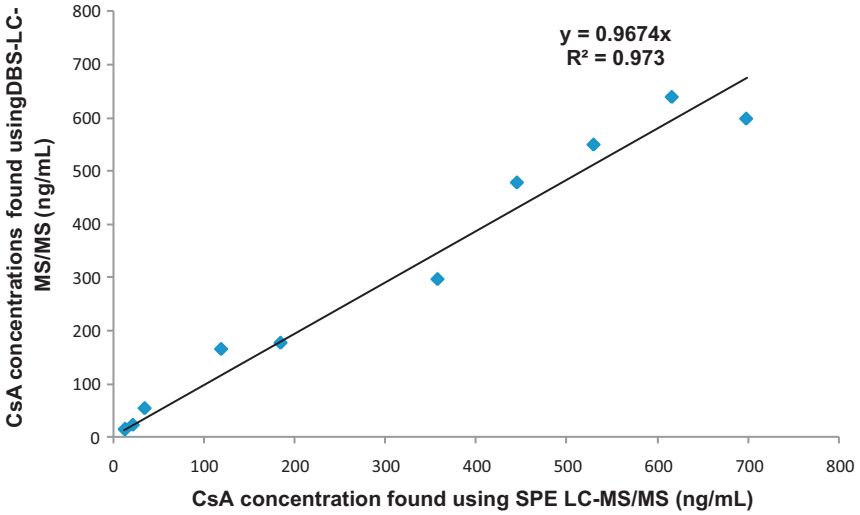

Fig. 5. CsA concentration correlation obtained with DBS and SPE extraction.

ranged between 100.3 and 105.8% while the mean precision (%CV) was ranged between 3.46 and 14.56%. It is noteworthy to say that this relatively high CV value was mainly due to one outlier during the 1st validation day. Carry-over was assessed and a light effect fluctuating from 8.2% to 23.6% was observed over the three days. Overall the mean carry over did not exceed 20% which is compliant guidelines acceptance criteria. The mean overall recoveries ($n = 3$) measured showed consistency ($6 < CV < 22\%$) and were between 68 and 73%. A way to improve the recovery sample would be to pull the extraction liquid more vigorous through the spot, our method entails a 15-min shaking step and this was enough to correctly quantify high and low concentration samples (Fig. 5). The LOD and LLOQ were respectively of 3.5 ng/mL and 5 ng/mL.

3.5. Stability study

A stability study was performed to ensure that DBS processing does not affect the quality results over the time. Indeed, during pharmacokinetics studies there is usually a delay of time between the blood collection and analysis. If the samples are to be shipped within the same continent up to 2 working days can be counted and even more for transcontinental shipment. The stability study demonstrated that CsA was stable for 9 days in dried blood spot placed at room temperature in the dark under a dry atmosphere (Table 3) with bias variations less than 15.0%. However a slight degradation seemed to occur on day 9 for the lowest concentration tested (i.e., 10 ng/mL), as a bias variation was observed at 18.9%.

3.6. Comparison of the DBS versus a classical SPE extraction

The described DBS procedure was applied during a pharmacokinetic study where CsA was orally administered to cats at 7 mg/kg dose. The results obtained for one PK profile was then compared to the one obtained with the classical SPE extraction procedure, developed during the previous study. A good correlation was demonstrated between the 2 methodologies yielding the equation $y = 0.9674x$ with a correlation coefficient of $r^2 = 0.973$ ($n = 11$) (Fig. 5) and where x represents the concentrations found using SPE extraction and y is the concentrations found using DBS extraction. The comparison using the Deming regression generated a correlation of 1.052, therefore no significant difference is observed between the two methods. In addition, the total amount of solvent used for the SPE extraction was around 125 mL for 20 samples while for the same amount of sample the DBS procedure used only 2 mL of solvent. The volume of blood sample has also drastically decreased as for 20 samples 10 mL of blood were required for the SPE and whereas DBS procedure required only 100 μL. Those data are compliant with all the ethical and animal welfare initiatives to reduce the impact of blood sampling on animals.

4. Conclusion

A rapid, sensitive and selective DBS extraction for the measurement of CsA in cat blood samples by means of an original HPLC–ESI-MS/MS was developed. This methodology was compared to an existing one based on SPE extraction and proved to be cheaper, faster, less solvent-consuming and required less blood volume from animals. Moreover, a suitable stability has been demonstrated for CsA in DBS placed at room temperature in the dark and under a dry atmosphere for 9 days.

The method was validated according to FDA guidelines for bioanalytical method and demonstrated to be precise and accurate. This methodology could also be extended to others animal species or even in human as CsA in used in both areas.

Blood samples can be stored frozen before applying DBS, which is very useful for their routine use for pharmacokinetics studies (provided that appropriate training is giving to the personnel). It is noteworthy to mention that the hematocrit effect is analyte-dependent and should be assessed case by case.

Even if the method developed in this study represents an advance in the analytical field, there is still some improvement to be made to fully implement such methodology in bioanalytical laboratories for high throughput analysis as the manual punching step can be tedious and time-consuming. Fully automated system should overcome this issue in the next future.

References

[1] K.A. Mathews, S.A. Ayres, C.A. Tano, S.M. Riley, H.R. Sukhiani, C. Adams, Cyclosporin treatment of perianal fistulas in dogs, Can. Vet. J. 38 (1997) 39–41.
[2] K.A. Mathews, H.R. Sukhiani, Randomized controlled trial of cyclosporine for treatment of perianal fistulas in dogs, J. Am. Vet. Med. Assoc. 211 (1997) 1249–1253.
[3] J. Fontaine, T. Olivry, Treatment of canine atopic dermatitis with cyclosporine: a pilot clinical study, Vet. Rec. 148 (2001) 662–663.
[4] T. Olivry, J. Steffan, R.D. Fisch, P. Prelaud, E. Guaguere, J. Fontaine, D.N. Carlotti, Randomized controlled trial of the efficacy of cyclosporine in the treatment of atopic dermatitis in dogs, J. Am. Vet. Med. Assoc. 221 (2002) 370–377.
[5] J. Steffan, D. Alexander, F. Brovedani, R.D. Fisch, Comparison of cyclosporine A with methylprednisolone for treatment of canine atopic dermatitis: a parallel, blinded, randomized controlled trial, Vet. Dermatol. 14 (2003) 11–22.

[6] D.C. Robson, G.G. Burton, Cyclosporin: applications in small animal dermatology, Vet. Dermatol. 14 (2003) 1–9.
[7] ICH. Harmonised Tripartate Guideline, Code S3A Toxicokinetics: the Assessment of Systemic Exposure in Toxicity Studies, 1-1-1995.
[8] FDA, Fed. Regist. 60 (1995) 11264–11268.
[9] ICH. Common Technical Document Code M4. The Common Technical Document for the Registration of Pharmaceutical for Human Use, 1999.
[10] T. Koal, H. Burhenne, R. Romling, M. Svoboda, K. Resch, V. Kaever, Quantification of antiretroviral drugs in dried blood spot samples by means of liquid chromatography/tandem mass spectrometry, Rapid Commun. Mass Spectrom. 19 (2005) 2995–3001.
[11] M. Barfield, N. Spooner, R. Lad, S. Parry, S. Fowles, Application of dried blood spots combined with HPLC–MS/MS for the quantification of acetaminophen in toxicokinetic studies, J. Chromatogr. B: Analyt. Technol. Biomed. Life Sci. 870 (2008) 32–37.
[12] P. Abu-Rabie, N. Spooner, Direct quantitative bioanalysis of drugs in dried blood spot samples using a thin-layer chromatography mass spectrometer interface, Anal. Chem. 81 (2009) 10275–10284.
[13] W. Li, F.L. Tse, Dried blood spot sampling in combination with LC–MS/MS for quantitative analysis of small molecules, Biomed. Chromatogr. 24 (2009) 49–65.
[14] J. Deglon, A. Thomas, A. Cataldo, P. Mangin, C. Staub, On-line desorption of dried blood spot: a novel approach for the direct LC/MS analysis of micro-whole blood samples, J. Pharm. Biomed. Anal. 49 (2009) 1034–1039.
[15] A. Thomas, J. Deglon, S. Lenglet, F. Mach, P. Mangin, J.L. Wolfender, S. Steffens, C. Staub, High-throughput phospholipidic fingerprinting by online desorption of dried spots and quadrupole-linear ion trap mass spectrometry: evaluation of atherosclerosis biomarkers in mouse plasma, Anal. Chem. 82 (2010) 6687–6694.
[16] L.J. Dusci, L.P. Hackett, G.M. Chiswell, K.F. Ilett, Comparison of cyclosporine measurement in whole blood by high-performance liquid chromatography, monoclonal fluorescence polarization immunoassay, and monoclonal enzyme-multiplied immunoassay, Ther. Drug Monit. 14 (1992) 327–332.
[17] N. Ansermot, M. Fathi, J.L. Veuthey, J. Desmeules, S. Rudaz, D. Hochstrasser, Quantification of cyclosporine and tacrolimus in whole blood. Comparison of liquid chromatography–electrospray mass spectrometry with the enzyme multiplied immunoassay technique, Clin. Biochem. 41 (2008) 910–913.
[18] C. Seger, K. Tentschert, W. Stoggl, A. Griesmacher, S.L. Ramsay, A rapid HPLC–MS/MS method for the simultaneous quantification of cyclosporine A, tacrolimus, sirolimus and everolimus in human blood samples, Nat. Protoc. 4 (2009) 526–534.
[19] A. Meinitzer, G. Gartner, S. Pilz, M. Stettin, Ultra fast liquid chromatography–tandem mass spectrometry routine method for simultaneous determination of cyclosporin A, tacrolimus, sirolimus, and everolimus in whole blood using deuterated internal standards for cyclosporin A and everolimus, Ther. Drug Monit. 32 (2010) 61–66.
[20] C. Alvarez, I.W. Wainer, Development of an automatic solid phase extraction and liquid chromatography mass spectrometry method by using a monolithic column for the analysis of cyclosporin A in human plasma, Talanta 79 (2009) 280–283.
[21] J. Denes, M. Katona, A. Hosszu, N. Czuczy, Z. Takats, Analysis of biological fluids by direct combination of solid phase extraction and desorption electrospray ionization mass spectrometry, Anal. Chem. 81 (2009) 1669–1675.
[22] Z.G. Fang, B.G. You, Y.G. Chen, J.K. Zhang, Y.Q. Liu, X.N. Zhang, Q. Zhang, Analysis of cyclosporine A and its metabolites in rat urine and feces by liquid chromatography–tandem mass spectrometry, J. Chromatogr. B: Analyt. Technol. Biomed. Life Sci. 878 (2010) 1153–1162.
[23] A.J. Wilhelm, J.C. den Burger, R.M. Vos, A. Chahbouni, A. Sinjewel, Analysis of cyclosporin A in dried blood spots using liquid chromatography tandem mass spectrometry, J. Chromatogr. B Analyt. Technol. Biomed. Life Sci. 877 (2009) 1595–1598.
[24] E. Hinchliffe, J.E. Adaway, B.G. Keevil, Simultaneous measurement of cyclosporin A and tacrolimus from dried blood spots by ultra high performance liquid chromatography tandem mass spectrometry, J. Chromatogr. B Analyt. Technol. Biomed. Life Sci. (2011).
[25] FDA, Guidance for Industry. Bioanalytical Method Validation, 1-5-2001.
[26] A.M. Deal, V.W. Pate, S. El Rouby. SAS® Macro for Deming Regression, Paper CC-014 Presented at SESUG 2009, 2009. Available from: http://analytics.ncsu.edu/sesug/2009/CC014.Deal.pdf.

Journal of Pharmaceutical and Biomedical Analysis 66 (2012) 306–313

Contents lists available at SciVerse ScienceDirect

Journal of Pharmaceutical and Biomedical Analysis

journal homepage: www.elsevier.com/locate/jpba

Determination of total and unbound sufentanil in human plasma by ultrafiltration and LC–MS/MS: Application to clinical pharmacokinetic study

Teijo I. Saari*[,1], Jörg Fechner[1], Harald Ihmsen, Jürgen Schüttler, Christian Jeleazcov

Department of Anesthesiology, University of Erlangen-Nürnberg, Krankenhausstraße 12, 91054 Erlangen, Germany

ARTICLE INFO

Article history:
Received 15 March 2012
Accepted 23 March 2012
Available online 3 April 2012

Keywords:
Sufentanil
Unbound
Liquid chromatography
Mass spectrometry
Pharmacokinetic
Target-controlled infusion (TCI)

ABSTRACT

A sensitive and specific liquid chromatography–tandem mass spectrometry (LC–MS/MS) method was developed and validated for the quantification of sufentanil total and unbound drug concentrations. Unbound drug was separated by an ultrafiltration step before sample preparation. Both the ultrafiltrate and plasma samples were extracted with solid-phase extraction and substituted with deuterated sufentanil used as an internal standard. Separation was performed by gradient elution using UPLC-like system and analysed by MS/MS consisting of an electrospray ionization source. Calibration curves showed linearity in the concentration range of 5–2500 pg/ml for analysis of both total and unbound concentrations of sufentanil. The lower limit of quantification was 5 pg/ml for both total and unbound sufentanil plasma drug concentrations. Intra- and interassay precision and accuracy did not exceed 15%. Method was applied to pharmacokinetic study in patients undergoing coronary artery bypass grafting.

© 2012 Elsevier B.V. All rights reserved.

1. Introduction

Sufentanil (N-{4-(methoxymethyl)-1-[2-(2-thienyl)ethyl]-4-piperidyl}-propionanilide) is a synthetic opioid analgesic widely used in clinical anesthesia and analgesia. Sufentanil is the most potent of the synthetic opioids and it is about five to ten times stronger than fentanyl [1]. The determination of sufentanil in biological fluids is associated with numerous analytical difficulties. Due to its efficacy at low dosages, the therapeutic plasma concentrations used for analgesia are in the range of 0.4–1 ng/ml [2,3] and until recent years the plasma concentrations of this compound were well below the limit of detection of most analytical instruments. Most of the previous pharmacokinetic studies involving sufentanil have been conducted using novel radioimmunoassay [4,5] that has many limitations [5]. Recently, more sensitive methods based on liquid chromatography separation with tandem mass spectrometry detection have been published [6–8].

Target controlled infusion (TCI)-systems have been introduced for instantaneous calculation of the infusion rate necessary to achieve and maintain a given therapeutic drug plasma concentration based on population pharmacokinetic parameters [9,10]. Compared to bolus dosing, TCI systems provide more stable analgesia and better hemodynamic control [11,12]. Also, smaller amounts of opioid are administered with TCI [13]. Recently, we have been studying low and high intraoperative dosing of sufentanil with respect to postoperative opioid consumption, pain and hyperalgesia in patients undergoing cardiac surgery. These phenomena are dependent on the unbound plasma drug concentrations and an alteration in a protein binding may result in clinically significant changes in the sufentanil pharmacokinetics [14]. Sufentanil is highly bound to plasma proteins [15,16], thus the effects of protein binding on the concentration–time course and the pharmacokinetics of sufentanil are of importance. However, data regarding the influence of drug binding to plasma proteins on pharmacodynamic parameters are scarce, and the unbound instead of the total concentration is recommended to be used whenever possible in pharmacokinetic–pharmacodynamic (PK–PD) models for drugs that are highly or weakly bound to plasma proteins [14,17]. Therefore, a method for determining the unbound drug concentrations had to be established, since we are not aware of any published reports describing the analysis of both total and unbound sufentanil concentrations in human plasma. For analysis of unbound drug concentrations, the plasma samples should be treated by equilibrium dialysis, ultracentrifugation or ultrafiltration techniques before extraction and analysis [17–19].

A method to determine the plasma levels of total and unbound sufentanil in patients undergoing cardiac surgery with cardiopulmonary bypass was developed. Although the method described here is derived from a previous study [7], it has been considerably modified. The preparation of human plasma samples is

* Corresponding author at: Anästhesiologische Klinik, Universitätsklinikum Erlangen, Krankenhausstraße 12, 91054 Erlangen, Germany.
Tel.: +49 9131 8533680; fax: +49 9131 8536147.
E-mail addresses: teijo.saari@gmail.com, teijo.saari@kfa.imed.uni-erlangen.de (T.I. Saari).
[1] These authors contributed equally to this work.

0731-7085/$ – see front matter © 2012 Elsevier B.V. All rights reserved.
http://dx.doi.org/10.1016/j.jpba.2012.03.050

preceded by ultrafiltration to facilitate the analysis of unbound sufentanil. Furthermore, an UPLC-like system is utilised for more efficient separation and sensitive analysis [20]. Finally, we used deuterated sufentanil as an internal standard to improve the precision and accuracy of the method as well as the robustness of the quantification against matrix effect. Tandem mass spectrometry is used for specific and reliable detection and quantification of the analytes.

2. Materials and methods

2.1. Drugs and chemicals

Sufentanil and the internal standard Sufentanil-D5 (Fig. 1) was purchased from LGC-Standards (Wesel, Germany), trifluoroacetic acid (TFA) was from Sigma–Aldrich (Steinheim, Germany). Methanol (HPLC-grade), acetonitrile, ethanol (99.95% LC–MS Grade), acetic acid, ammonia (30%) and perchloric acid were purchased from Roth (Karlsruhe, Germany). Deionised water was prepared with a Simplicity system from Millipore (Schwalbach, Germany). All eluents were degased in an ultrasonic bath and perfused with helium gas. Drug free human plasma was obtained from Recipe Chemicals (München, Germany).

2.2. Standard solution and calibration standards

Stock solutions of sufentanil and Sufentanil-D5 were 100 μg/ml, and sufentanil calibration standards were prepared with methanol and stored at −20 °C. Quality control (QC) samples were prepared to drug free plasma and blank study plasma samples (zero samples) by adding 50 μl sufentanil standards to 450 μl drug free plasma. The calibration samples for the determination of total and unbound sufentanil (2500, 500, 250, 50, 25, 5 pg/ml) were prepared in the same way using drug free plasma.

2.3. Extraction procedure

2.3.1. Unbound sufentanil

For the estimation of the unbound concentrations of sufentanil, plasma proteins with protein bound sufentanil had to be separated. An aliquot (500 μl) of plasma was filled in the Centrifree filter unit (Millipore) and centrifuged at 5000 × *g* at 20 °C for 20 min. The volume of the ultrafiltrate was estimated. For the assay ultrafiltrated samples were supplied together with IS (50 μl of 5000 pg/ml Sufentanil-D5) and 500 μl of perchloric acid (100 mM) to ISOLUTE solid phase extraction cartridges (Biotage, Uppsala, Sweden), which had been conditioned with 2 ml of methanol followed by 2 ml water. The cartridges were rinsed twice with 1 ml water/methanol (50:50, v/v), containing 5% ammonia under a slight vacuum. For descaling the residual water, the cartridges were centrifuged for 5 min at 3000 × *g*. The analytes were then eluted with 100 μl ethanol containing 5% acetic acid.

2.3.2. Total sufentanil

Total sufentanil was estimated out of an aliquot of 500 μl plasma without ultrafiltration. The extraction procedure was the same as described above except that after the supplementation of IS and perchloric acid the samples were centrifuged for 3 min at 3000 × *g* before extraction.

2.4. Equipment

The extracted samples were analysed with HPLC and tandem mass spectrometry. Chromatographic separation was carried out with the Waters Alliance HPLC system (Waters, Eschborn, Germany). The system was upgraded and modified by Fischer Analytics (Bingen, Germany) to allow UPLC-like pressures of more than 400 bar. For chromatographic separation, a Kinetex (C18, 50 mm × 2.1 mm, 1.7 μm, 100 Å) analytical column (Phenomenex, Aschaffenburg, Germany) protected by a HPLC Guard Cartridge system (C18 Security Guard, Phenomenex) was used. The analytes were detected with a Waters Quattro Micro tandem mass spectrometer equipped with an electrospray ionization interface (ESI). Data were collected and analysed with MassLynx™ V4.0 software.

2.5. HPLC conditions

The chromatographic separation of the analytes was accomplished by gradient elution. The separation was started with mobile phase consisting of 0.02% trifluoroacetic acid in water–acetonitrile (70:30, v/v). The percentage of acetonitrile was raised to 80% after 0.2 min and held constant for 3 min after which column was reequilibrated with starting conditions (70:30, v/v) for the next 4 min. Total chromatographic time was 7 min. Changes in mobile phase composition were achieved using step gradient. The mobile phase flow was kept at 500 μl/min and 25 μl of the extracted sample were injected. With a column temperature of +20 °C, the retention times for sufentanil and sufentanil-D5 were 1.5 min.

2.6. Mass spectrometry conditions

Ionization and analysis were accomplished in positive electrospray mode with multiple-reactions monitoring (MRM). The optimal settings for mass spectrometry were as follows: ion source temperature was set at 120 °C, the capillary and cone voltages were set to 5 kV and 30 V, respectively and the cone gas flow was 50 l/min. Desolvation gas temperature was 350 °C and the flow was

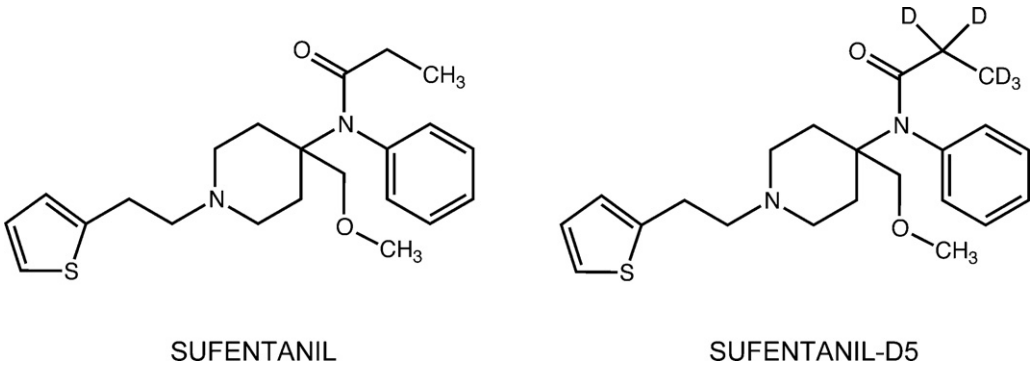

Fig. 1. Chemical structures of sufentanil and sufentanil-D5 (internal standard).

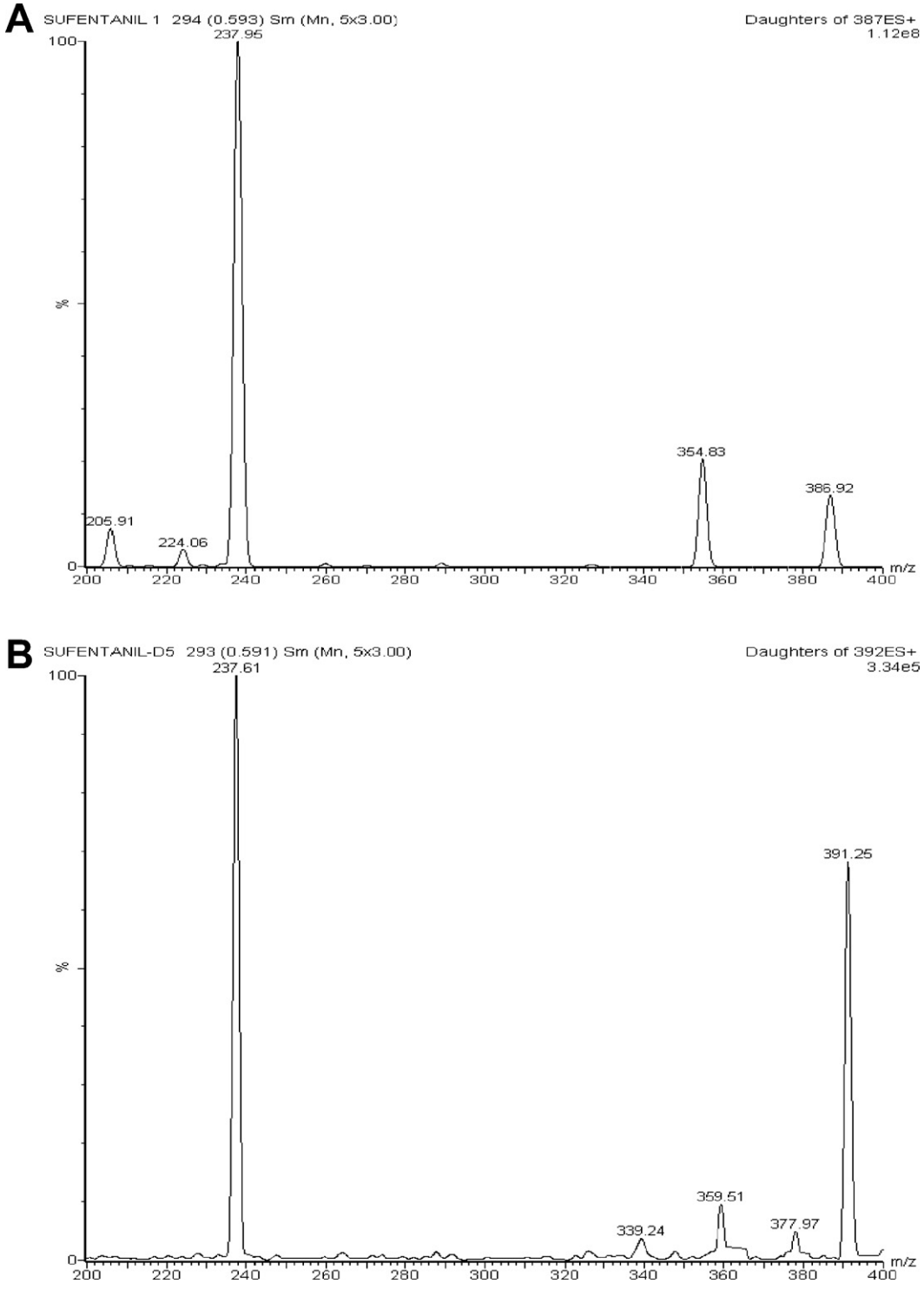

Fig. 2. (A) Positive product ion mass spectra of sufentanil and internal standard with precursors at *m*/*z* 386.92 and 391.25, respectively.

set 650 l/min. Nitrogen was used as the desolvation and cone gas and argon was used as the collision gas. To avoid soiling the mass spectrometer with the matrix, the effluent was directed with an automatic divert valve to a waste container for the first 0.5 min. The valve was then switched to the mass spectrometer ion source and after 3 min again to the waste container. The product ions were 238.27 *m*/*z* for sufentanil (387.14 → 238.27 *m*/*z*) and 238 for the IS (392 → 238). Dwell time was 400 ms for all ion transitions monitored.

2.7. Method validation

The method was validated according to the Food and Drug Administration (FDA) guidelines on recovery, linearity, precision, accuracy, selectivity, and specificity [21].

2.7.1. Loss of sufentanil during filtration and extraction recovery

The filtration procedure was examined for a loss of sufentanil because of unspecific binding to filter materials. Unspecific

binding was evaluated by determining the sufentanil levels before and after passage of the filter units, using standard sufentanil samples (50 pg/ml sufentanil in water). The concentrations were estimated before and after the passage of the filter units. The efficiency of the extraction procedure of the sufentanil and internal standard from human plasma was analysed in triplicate at concentrations of 5, 250 and 2500 pg/ml in human plasma. Recovery was calculated by comparison of the results obtained for samples extracted according to the analytical procedure of total plasma concentration with those obtained for the standard solutions added to the blank plasma extracts, corresponding to 100% recovery.

2.7.2. Linearity

Assay linearity was evaluated on 3 consecutive days by constructing freshly prepared plasma calibration samples over the concentration range of 5–2500 pg/ml for total and unbound sufentanil. Calibration curves were generated with QuanLynx software (v. 4.0; Waters) using linear regression.

2.7.3. Precision and accuracy

The lower limit of quantification (LLOQ) for sufentanil was defined as the lowest standard on the calibration curve with a peak response at least five times that of the blank response (S/N ratio) and with precision of 20% and accuracy of 80–120%. For the assessment of the interday accuracy and precision of the method at least five replicates of low-, mid and high concentration QC samples were run on 3 consecutive days. Intraday accuracy and precision were evaluated by analysis of three calibration standards and five replicates of each QC sample concentration in 1 day. The precision was determined as the intra-assay and inter-assay relative standard deviations (%RSD) of the determined concentrations in percentages [%RSD = 100(SD/*M*)], where M is the mean and SD is the standard deviation of *M*. Accuracy was expressed as the relative error from nominal concentration [%RE = (experimentally obtained concentration − nominal concentration) (100/nominal concentration)]. The acceptance criteria for accuracy were ±15% deviation from nominal values and for precision % RSD less than 15%.

2.7.4. Selectivity and specificity

Test for selectivity was carried out in six lots of blank patient plasma. In the first set, the blank human plasma was directly injected after extraction (without analyte and IS), while the other set was spiked with IS and LLOQ concentration of sufentanil. The acceptance criterion requires that at least 90% of selectivity samples should be free from any interference at the retention time of analyte and IS. The specificity of the assay was evaluated by comparing chromatograms of a blank plasma sample, a blank plasma sample spiked with sufentanil (5 pg) and IS; and a patient's plasma sample containing sufentanil.

2.8. Stability

Short-term stability, post-processing stability, stability after three freeze–thaw cycles and stock solution stability were evaluated according to the analytical procedure of total plasma concentration. For this purpose, QC samples were prepared at three concentrations: 5, 250 and 2500 pg/ml. For the analysis of short-term stability the samples were maintained at room temperature (+24 °C) for 9 h after which they were stored overnight at 10 °C before analysis. Post-processing stability was evaluated by maintaining the samples in the autoinjector at room temperature (+24 °C) for six days, followed by injection into the chromatographic system. For the evaluation of stability after three freeze–thaw cycles, the QC samples were frozen at −75 °C for 24 h. After this period, the samples were again thawed and frozen for 24 h and this process was repeated until the third thawing cycle when the samples were extracted and analysed. The stability of stock solutions was evaluated after maintaining them at room temperature (+24 °C) for 9 h after which they were stored overnight at +10 °C before analysis. The results were compared to those obtained for freshly prepared samples and are expressed as relative error (%RE). The solutions were considered stable if the deviation from nominal value was within ±15.0%.

2.9. Application to clinical pharmacokinetic study

We used this method to study the pharmacokinetics of unbound and total sufentanil during coronary artery bypass surgery with cardio-pulmonary bypass (CPB), with special regard to protein binding. This study was performed in accordance with the guidelines for Good Clinical Practice and the Declaration of Helsinki. Written informed consent was obtained from 42 patients, and we report here the data for a population of the first 13 patients. The study was approved by the Institutional Review Board (Ethikkommission der Medizinischen Fakultät der Friedrich-Alexander-Universität Erlangen-Nürnberg, Erlangen, Germany). Anesthesia was induced and maintained with continuous infusions of propofol (Disoprivan® 2%, AstraZeneca, Wedel, Germany) as anesthetic and sufentanil (Sufenta®, Janssen-Cilag, Neuss, Germany) as analgesic drug given by TCI. The target concentrations ranging from 0.4 to 1.5 ng/ml were used and sufentanil administration was stopped at last skin suture. Higher target concentrations were used at the induction of anesthesia after which the target was set to 0.8 ng/ml. Timed blood samples for the pharmacokinetic measurements were drawn from an artery line into ethylenediaminetetraacetic acid-containing tubes (S-Monovette® Kalium EDTA, Sarstedt, Nürnbrecht, Germany) immediately before the induction of anesthesia and five more samples were drawn during the operation (before skin incision, 5 min before CPB, 15 and 45 min after the beginning of CPB, 15 min after the end of CPB). The last blood sample was drawn at the skin closure. To determine the arterial sufentanil concentrations, 8 ml blood were drawn per sample, after 1 ml blood had been drawn and discarded. After each sample collection, the intra-arterial catheter was flushed with 2 ml of heparinised NaCl-solution. Plasma was separated immediately and stored at 5 °C on ice until extraction and assay which was accomplished within 12 h after blood sampling.

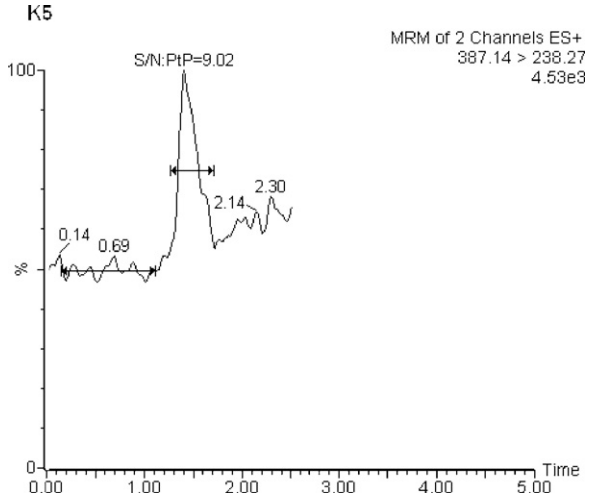

Fig. 3. A representative chromatogram of plasma sample spiked with the LOD concentration of sufentanil. Limit of detection was found to be 0.375 pg with a signal to noise ratio (S/N) of 9.02.

Table 1
Accuracy and precision data of the analytical method for the measurement of total and unbound plasma concentrations of sufentanil in human plasma.

Sufentanil									
Intraday					Interday				
Nominal concentration (pg/ml)	Mean ± SD	%RSD	%RE	*n*	Nominal concentration (pg/ml)	Mean ± SD	%RSD	%RE	*n*
5	4.7 ± 0.19	4.1	−5.6	6	5	4.9 ± 0.50	10.12	−2.0	20
50	51.6 ± 2.1	4.0	3.2	5					
250	247 ± 8.3	3.4	−1.3	6	250	242 ± 9.8	4.0	−3.3	16
500	506 ± 10	2.0	1.1	6					
2500	2441 ± 29	1.2	−2.3	5	2500	2529 ± 161	6.3	1.2	17

%RSD, relative standard error; %RE, relative error.

3. Results and discussion

We describe an analytical method to measure unbound and total concentrations of sufentanil from human plasma samples, and application of this method to the pharmacokinetic study determining the concentration–time course of sufentanil during coronary artery bypass surgery with CPB. To our knowledge there are no previous studies in the literature to describe the analysis of unbound plasma concentrations of sufentanil. The method was validated according to the Food and Drug Administration (FDA) guidelines [21].

The unbound sufentanil concentrations were analysed with similar method to that used for total sufentanil concentration, except for a procedure prior to the analysis to separate the free drug from the drug bound to plasma proteins. In the present study the Centrifree® filter units were used to get ultrafiltrate in which the amount of unbound drug corresponds to that in original plasma sample. Protein bound fraction of the drug does not cross the filter membrane in the filter unit and consecutively does not reach the ultrafiltrate [22]. The ultrafiltration procedure has been recently used successfully to determine unbound plasma concentrations of various drugs [23–26]

We modified the previously published methods also by using HPLC-system upgraded to be used in UPLC-like pressures to further improve the analytical performance of the system. Furthermore deuterated sufentanil was utilised as an internal standard to increase the robustness against possible matrix effects and to increase the accuracy and precision of the method.

3.1. Recovery of sufentanil

Plasma ultrafiltration caused a 17.5% unspecific loss of sufentanil after the passage of the filter (±SD 5.4; %CV = 6.5; $n = 9$). No inconsistency was observed in the recovery of sufentanil. The extraction recoveries of sufentanil determined at three QC concentration levels of 5, 250 and 2500 pg/ml were 87 ± 10%, 77 ± 12% and 81 ± 4% ($n = 3$), respectively.

3.2. Chromatography and mass spectrometry

To obtain good chromatographic separation, a mobile phase containing a low acid concentration and low percentage of organic modifier has been suggested previously [7]. Contrary to the results of Martens-Lobenhoffer [7], a gradient elution with increased amount of acetonitrile (up to 80%) was successfully utilised. We also employed a flow-rate of 0.5 ml/min during the whole run without any loss in quality of chromatographic separation.

A positive ionization mode with ESI was used, since previous reports have shown it superior compared to other modes [6]. Analytical conditions for mass spectrometry were tested to obtain a high intensity of $[M+H]^+$ ions of the analytes. The positive product ion mass spectra of sufentanil and IS show high abundances of fragment ions (Fig. 2). The product ion for sufentanil was 238 as reported previously [7]. The precursor → product ion transformations of m/z 387 → 238 and m/z 392 → 238 were used for MRMs for sufentanil and IS, respectively. No interference from endogenous substances in the blank plasma lots or from other metabolites was observed in the retention time of sufentanil.

3.3. Linearity and limits of detection and quantification

We found a linear calibration curve for total and unbound sufentanil concentration range from 5 to 2500 pg/ml. A typical equation for the calibration function is $y = 1.11158x$ ($r^2 = 0.99987$). The limit of detection (LOD) was 0.375 pg with a S/N ratio of 9.02. The lower limit of quantitation was set at 5 pg/ml. A representative chromatogram of plasma spiked with the LOD concentration of sufentanil and IS is presented in Fig. 3.

3.4. Precision and accuracy

The validation data regarding intraday and interday precision and accuracy are summarised in Table 1. The measurement of total and unbound sufentanil by our method showed good intraday and interday precision and accuracy. Compared to previous studies, utilization of deuterated sufentanil as IS resulted in notable

Table 2
Stability analysis of the analytical method for the measurement of total and unbound plasma concentrations of sufentanil in human plasma.

	Accuracy, mean ± SD (%RE)		
	5 pg/ml ($n = 3$)	250 pg/ml ($n = 3$)	2500 pg/ml ($n = 3$)
Short-term stability[a]	4.9 ± 0.6 (−1.33)	246 ± 5.5 (−1.73)	2530 ± 36 (1.19)
Freeze and thaw stability	5.0 ± 0.6 (−0.67)	248 ± 6.6 (−0.80)	2661 ± 118 (6.43)
Stock solution stability	5.4 ± 0.38 (7.33)	239 ± 9.5 (−4.13)	2475 ± 149 (−1.00)
Post-preparative stability[b]	4.5 ± 0.34 (−10.4)	233 ± 6.6 (−6.93)	2337 ± 32 (−6.51)

[a] Short-term stability, 9 h in room temperature (24 °C).
[b] Post-preparative stability, 6 days in autosampler (24 °C).

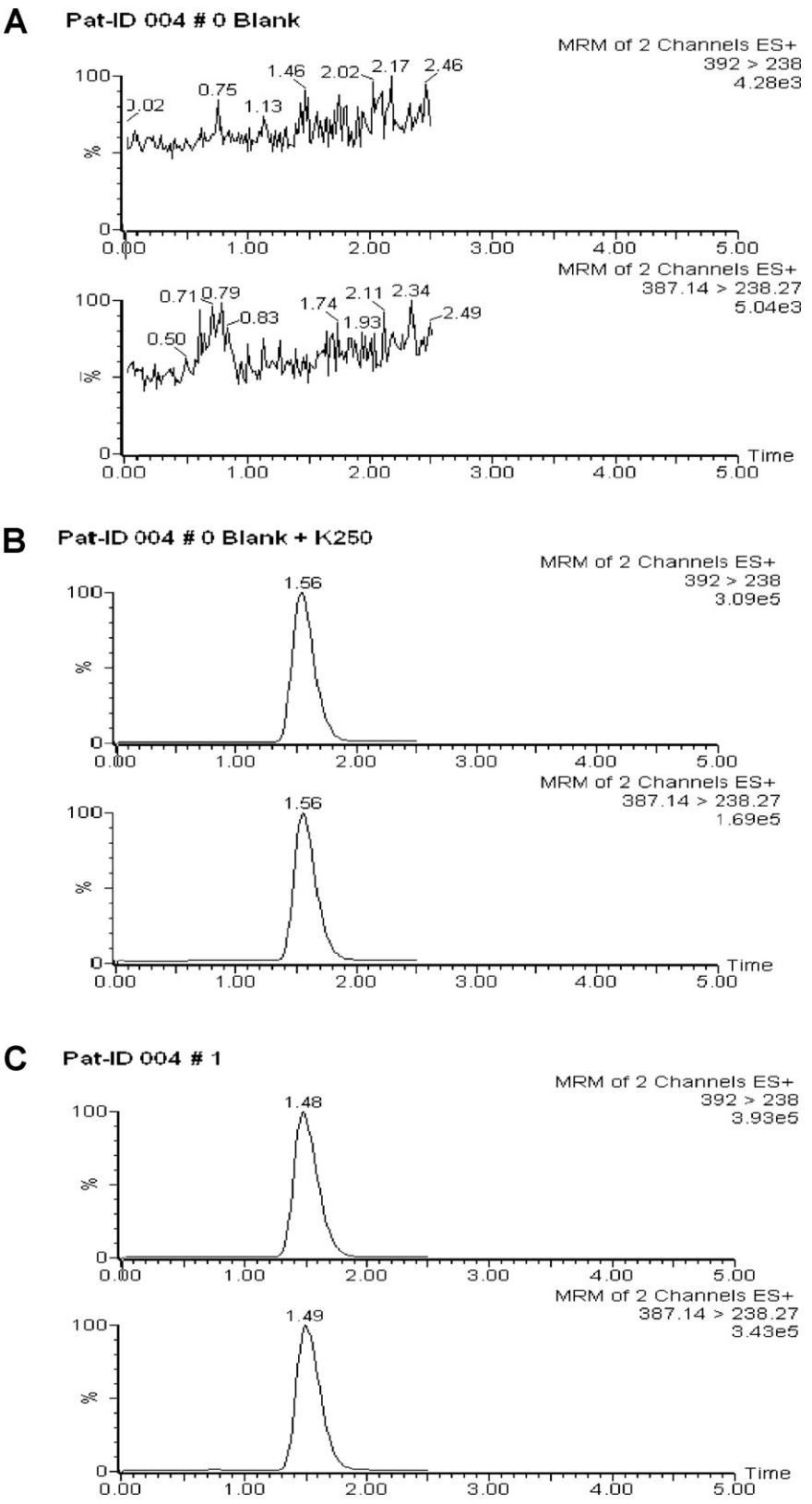

Fig. 4. Multiple reactions monitoring MS/MS chromatograms of (A) a blank plasma sample; (B) a blank plasma sample spiked with sufentanil (250 pg) and internal standard; and (C) a patient's plasma sample from the pharmacokinetic study spiked with internal standard with a measured sufentanil concentration of 401 pg/ml. The retention times for sufentanil and internal standard were 1.48 and 1.49 min, respectively.

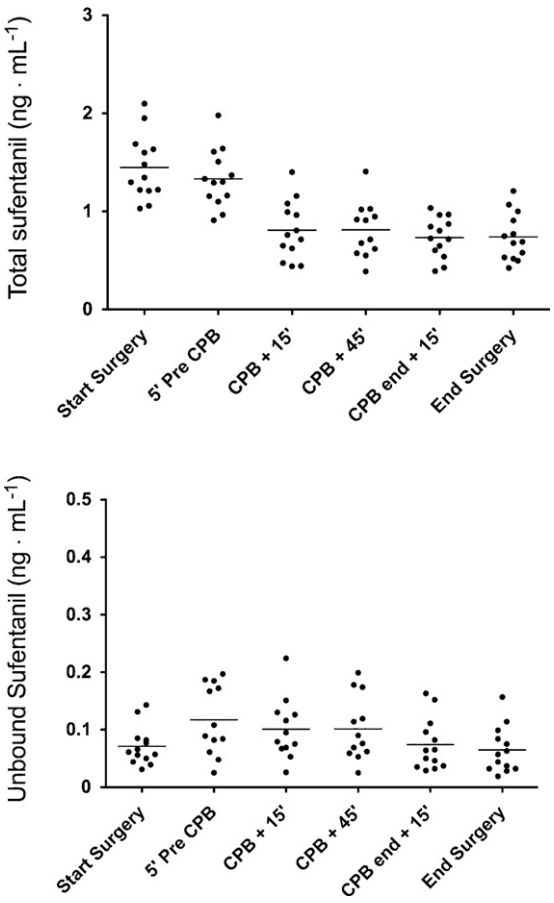

Fig. 5. Plasma concentrations of total and unbound sufentanil in 13 patients undergoing coronary artery bypass grafting with cardiopulmonary bypass. CPB, cardiopulmonary bypass.

improvement in intra- and interday accuracy and accuracy and prediction.

3.5. Selectivity and specificity

Specificity was evaluated by comparing chromatograms of blank patient plasma with corresponding drug-free plasma sample spiked with sufentanil and IS and with a blank patient samples from the pharmacokinetic study. None of the six blank plasma lots caused a significant interference at the retention times of the analytes or internal standards. The signal response ratios (blank interference/LLOQ standard) were within the acceptable criteria for all studied compounds (Fig. 4). The matrix effect at QC concentration level of 5 pg/ml was $100 \pm 9\%$ ($n = 6$) indicating that no co-eluting substance influenced the ionization of the analytes.

3.6. Stability

No significant degradation of sufentanil was observed during the short-term (9-h) storage at room temperature, or after three freeze–thaw cycles storage at $-75\,^{\circ}C$, suggesting that no stability related problems are to be expected during routine analysis (Table 2). The degradation was less than 15% for all compounds. Also the stock solutions showed no significant degradation after short term storage at room temperature.

3.7. Pharmacokinetic application

This method was applied to a pharmacokinetic study to determine both total and unbound concentrations of sufentanil from plasma samples drawn from patients undergoing coronary artery bypass grafting. These patients had received several other drugs to treat their acute and chronic diseases, but none of these drugs or their metabolites were found to interfere with the present assay. Plasma concentrations of total and unbound sufentanil receiving sufentanil are presented in Fig. 5. Although individual sufentanil plasma concentrations show quite a large interindividual variability, the plasma concentrations of both total and unbound sufentanil were more than 10-fold higher than LLOQ of the method.

4. Conclusion

We describe a sensitive and specific analytical method for determining both total and unbound plasma concentrations of sufentanil. Compared to previously published analytical methods for sufentanil drug concentration measurement, this method shows improved accuracy and precision due to the utilization of deuterated sufentanil as internal standard. The method could monitor plasma concentrations as low as 5 pg/ml, which is enough to detect sufentanil plasma drug concentrations during the whole concentration–time course after intraoperative administration of sufentanil when the drug is used as an analgesic. The method was used successfully to determine both total and unbound sufentanil plasma concentration from patients undergoing coronary artery bypass grafting and receiving several other drugs concomitantly.

Funding

This work was funded by a grant of the German Federal Ministry of Education and Research (BMBF, FKZ 01EX1015B). The sponsor had no involvement in study design; in the collection, analysis, and interpretation of data; in the writing of the report; and in the decision to submit the paper for publication.

Acknowledgements

The authors thank Rainer Knoll, Dipl. Bioingenieur (Department of Anesthesiology, University of Erlangen-Nürnberg, Erlangen, Germany) for his kind help in conducting the drug analysis.

References

[1] L.E. Mather, Clinical pharmacokinetics of fentanyl and its newer derivatives, Clin. Pharmacokinet. 8 (1983) 422–446.
[2] E. Iannuzzi, M. Iannuzzi, V. Cirillo, G. Viola, R. Parisi, A. Cerulli, M. Chiefari, Peri-intubation cardiovascular response during low dose remifentanil or sufentanil administration in association with propofol TCI. A double blind comparison, Minerva Anestesiol. 70 (2004) 109–115.
[3] J. Vuyk, Pharmacokinetic and pharmacodynamic interactions between opioids and propofol, J. Clin. Anesth. 9 (1997) 23S–26S.
[4] M. Michiels, R. Hendriks, J. Heykants, Radioimmunoassay of the new opiate analgesics alfentanil and sufentanil. Preliminary pharmacokinetic profile in man, J. Pharm. Pharmacol. 35 (1983) 86–93.
[5] R.J.H. Woestenborghs, P.M. Timmerman, M.L.J.E. Cornelissen, F.A. Van Rompaey, E. Gepts, F. Camu, J.J.P. Heykants, D.R. Stanski, Assay methods for sufentanil in plasma. Radioimmunoassay versus gas chromatography–mass spectrometry, Anesthesiology 80 (1994) 666–670.
[6] L. Liang, S. Wan, J. Xiao, J. Zhang, M. Gu, Rapid UPLC–MS/MS method for the determination of sufentanil in human plasma and its application in target-controlled infusion system, J. Pharm. Biomed. Anal. 54 (2011) 838–844.
[7] J. Martens-Lobenhoffer, Very sensitive and specific determination of sufentanil in human serum applying liquid chromatography–two stage mass spectrometry, J. Chromatogr. B: Anal. Technol. Biomed. Life Sci. 769 (2002) 227–233.
[8] L. Palleschi, L. Lucentini, E. Ferretti, F. Anastasi, M. Amoroso, G. Draisci, Quantitative determination of sufentanil in human plasma by liquid chromatography–tandem mass spectrometry, J. Pharm. Biomed. Anal. 32 (2003) 329–336.

[9] E. Gepts, Pharmacokinetic concepts for TCI anaesthesia, Anaesthesia 53 (1998) 4–12.
[10] S.E. Kern, D.R. Stanski, Pharmacokinetics and pharmacodynamics of intravenously administered anesthetic drugs: concepts and lessons for drug development, Clin. Pharmacol. Ther. 84 (2008) 153–157.
[11] N. Derrode, F. Lebrun, J.-C. Levron, M. Chauvin, B. Debaene, Influence of peroperative opioid on postoperative pain after major abdominal surgery: sufentanil TCI versus remifentanil TCI. A randomized, controlled study, Br. J. Anaesth. 91 (2003) 842–849.
[12] M.M.R.F. Struys, M. Sahinovic, B.J. Lichtenbelt, H.E.M. Vereecke, A.R. Absalom, Optimizing intravenous drug administration by applying pharmacokinetic/pharmacodynamic concepts, Br. J. Anaesth. 107 (2011) 38–47.
[13] P. Richebé, O. Pouquet, S. Jelacic, S. Mehta, J. Calderon, W. Picard, C. Rivat, A. Cahana, G. Janvier, Target-controlled dosing of remifentanil during cardiac surgery reduces postoperative hyperalgesia, J. Cardiothorac. Vasc. Anesth. 25 (2011) 917–925.
[14] S. Schmidt, D. Gonzalez, H. Derendorf, Significance of protein binding in pharmacokinetics and pharmacodynamics, J. Pharm. Sci. 99 (2009) 1107–1122.
[15] C. Meistelman, D. Benhamou, J. Barre, J.-C. Levron, V. Mahe, X. Mazoit, C. Ecoffey, Effects of age on plasma protein binding of sufentanil, Anesthesiology 72 (1990) 470–473.
[16] W.E. Meuldermans, R.M. Hurkmans, J.J. Heykants, Plasma protein binding and distribution of fentanyl, sufentanil, alfentanil and lofentanil in blood, Arch. Int. Pharmacodyn. Ther. 257 (1982) 4–19.
[17] J.D. Wright, F.D. Boudinot, M.R. Ujhelyi, Measurement and analysis of unbound drug concentrations, Clin. Pharmacokinet. 30 (1996) 445–462.
[18] D. Jung, M. Mayersohn, D. Perrier, The "ultra-free" ultrafiltration technique compared with equilibrium dialysis for determination of unbound thiopental concentrations in serum, Clin. Chem. 27 (1981) 166–168.
[19] M.L. Howard, J.J. Hill, G.R. Galluppi, M.A. McLean, Plasma protein binding in drug discovery and development, Comb. Chem. High Throughput Screen. 13 (2010) 170–187.
[20] M.I. Churchwell, N.C. Twaddle, L.R. Meeker, D.R. Doerge, Improving LC–MS sensitivity through increases in chromatographic performance: comparisons of UPLC–ES/MS/MS to HPLC–ES/MS/MS, J. Chromatogr. B: Anal. Technol. Biomed. Life Sci. 825 (2005) 134–143.
[21] Guidance for Industry, Bioanalytical Method Validation, U.S. Department of Health and Human Services, Food and Drug Administration, Center for Drug Evaluation and Research (CDER), Center for Veterinary Medicine (CVM), 2001.
[22] Millipore Corporation, Centrifree Ultrafiltration Devices, Package Insert. www.millipore.com (accessed 12.03.12).
[23] E.R. Gardner, W. Dahut, W.D. Figg, Quantitative determination of total and unbound paclitaxel in human plasma following abraxane treatment, J. Chromatogr. B: Anal. Technol. Biomed. Life Sci. 862 (2008) 213–218.
[24] L. Zeng, C.E. Nath, P.J. Shaw, J.W. Earl, A.J. McLachlan, HPLC-UV assay for monitoring total and unbound mycophenolic acid concentrations in children, Biomed. Chromatogr. 23 (2009) 92–100.
[25] A.D. Pranger, J.-W.C. Alffenaar, A.M.A. Wessels, B. Greijdanus, D.R.A. Uges, Determination of moxifloxacin in human plasma, plasma ultrafiltrate, and cerebrospinal fluid by a rapid and simple liquid chromatography–tandem mass spectrometry method, J. Anal. Toxicol. 34 (2010) 135–141.
[26] N. Moraes, G. Lauretti, M. Napolitano, Enantioselective analysis of unbound tramadol, O-desmethyltramadol and N-desmethyltramadol in plasma by ultrafiltration and LC–MS/MS: application to clinical pharmacokinetics, J. Chromatogr. B 880 (2012) 140–147.

Journal of Pharmaceutical and Biomedical Analysis 66 (2012) 314–324

Contents lists available at SciVerse ScienceDirect

Journal of Pharmaceutical and Biomedical Analysis

journal homepage: www.elsevier.com/locate/jpba

Determination of dalcetrapib by liquid chromatography–tandem mass spectrometry

Katja Heinig[a], Franz Bucheli[a], Olaf Kuhlmann[a,*], Manfred Zell[a], Axel Pähler[a], Elke Zwanziger[a], Günter Gross[b], Joseph Tardio[b], Tomohiro Ishikawa[c], Tomoko Yamashita[d]

[a] Non-Clinical Drug Safety, Pharma Research and Early Development, F. Hoffmann-La Roche Ltd., Basel, Switzerland
[b] Formulation Research, Pharma Research and Early Development, F. Hoffmann-La Roche Ltd., Basel, Switzerland
[c] Clinical Research Planning Department, Pharmaceutical Division, Japan Tobacco Inc., Tokyo, Japan
[d] Drug Metabolism and Pharmacokinetics Research Laboratories, Central Pharmaceutical Research Institute, Japan Tobacco Inc., Osaka, Japan

ARTICLE INFO

Article history:
Received 23 January 2012
Received in revised form 28 March 2012
Accepted 30 March 2012
Available online 6 April 2012

Keywords:
Dalcetrapib
Thioester
Liquid-chromatography–tandem mass spectrometry
Column switching
Dithiothreitol
N-ethylmaleimide

ABSTRACT

The cholesteryl ester transfer protein modulator dalcetrapib is currently under development for the prevention of dyslipidemia and cardiovascular disease. Dalcetrapib, a thioester, is rapidly hydrolyzed *in vivo* to the corresponding thiophenol which in turn is further oxidized to the dimer and mixed disulfides (where the thiophenol binds to peptides, proteins and other endogenous thiols). These forms co-exist in an oxidation–reduction equilibrium *via* the thiol and cannot be stabilized without influencing the equilibrium, hence specific determination of individual components, *i.e.*, in order to distinguish between the free thiol, the disulfide dimer and mixed disulfide adducts, was not pursued for routine analysis. The individual forms were quantified collectively as dalcetrapib-thiol (dal-thiol) after reduction under basic conditions with dithiothreitol to break disulfide bonds and derivatization with N-ethylmaleimide to stabilize the free thiol. The S-methyl and S-glucuronide metabolites were determined simultaneously with dal-thiol with no effect from the derivatization procedure. Column-switching liquid chromatography–tandem mass spectrometry provided a simple, fast and robust method for analysis of human and animal plasma and human urine samples. Addition of the surfactant Tween 80 to urine prevented adsorptive compound loss. The lower limits of quantitation (LLOQ) were 5 ng/mL for dal-thiol, and 5 ng/mL for the S-methyl and 50 ng/mL for the S-glucuronide metabolites. Using stable isotope-labeled internal standards, inter- and intra-assay precisions were each <15% (<20% at LLOQ) and accuracy was between 85 and 115%. Recovery was close to 100%, and no significant matrix effect was observed.

© 2012 Published by Elsevier B.V.

1. Introduction

Dalcetrapib (RO4607381; JTT-705), which targets cholesteryl ester transfer protein (CETP) activity and increases high-density lipoprotein cholesterol, is in Phase III clinical development to assess its impact on atherosclerosis and cardiovascular outcomes [1]. Dalcetrapib (dal-ester), a thioester, undergoes rapid hydrolysis by nonspecific esterases in biological fluids and in the intestine to generate the pharmacologically active free thiol which binds to CETP (data on file). It is well known that sulfhydryl-containing peptides, proteins and low molecular weight compounds (such as glutathione or cysteine) exist in the body as mixed disulfides [2]. Oxidation of thiol drugs to form disulphide bonds either with itself or endogenous thiols has been reported for tiopronin [3], clopidogrel [4] or captopril [5]. Similarly, dalcetrapib free thiol is expected to form dimers and mixed disulfides with endogenous thiols, and binds to plasma proteins ('active form' dalcetrapib-thiol [dal-thiol]) (Fig. 1). Disulfide dimer and endogenously bound thiol are considered to co-exist in body fluids in oxidation–reduction equilibrium *via* the free thiol. In animals, dal-thiol undergoes extensive metabolism *via* glucuronic acid conjugation, methylation and hydroxylation (but not sulfation) to form pharmacologically inactive S-methyl (dal-S-Me) [6] and S-glucuronide (dal-S-Glu) metabolites [7], which are further metabolized to a variety of secondary oxidation products. In a mass balance study of orally administered dalcetrapib in healthy male volunteers [8], dal-thiol was the principal component in human plasma, while pharmacologically inactive dal-S-Me and dal-S-Glu were the most abundant metabolites.

An analytical method was needed to allow determination of drug exposure in non-clinical pharmacokinetic and toxicokinetic studies as well as in clinical studies. Specifically, a reliable measurement of free, bound, or the sum of all forms and metabolites had to be established. Liquid chromatography–tandem mass

* Corresponding author. Tel.: +41 61 6882532; fax: +41 61 6882908.
E-mail address: olaf.kuhlmann@roche.com (O. Kuhlmann).

0731-7085/$ – see front matter © 2012 Published by Elsevier B.V.
http://dx.doi.org/10.1016/j.jpba.2012.03.056

spectrometry (LC–MS/MS) was selected as the available method of choice to provide selective and sensitive bioanalysis. Thiol compounds typically present challenges for bioanalysis due to their high reactivity and need to be stabilized before measurement, for example, by pH adjustment or derivatization with alkylating agents such as maleimides or methylacrylate. Disulfides are usually converted to thiols by treatment with reducing agents (*e.g.*, dithiothreitol (DTT) or tributylphosphine) and derivatized for analysis. Comprehensive summaries of analytical procedures for thiols and disulfide can be found in previous literature reviews [9–11]. Simultaneous analysis of thiols and disulfides using differential labeling has been described [11,12], but these laborious multi-step procedures present practical difficulties for the routine analysis of large numbers of samples during drug development. This manuscript describes the development and validation of a column-switching method using LC–MS/MS to determine thioester, free thiol, disulfide dimer, and mixed disulfides as combined 'active form' (dal-thiol, as N-ethylmaleimide [NEM] derivative), and principal metabolites. The method was further refined to facilitate routine handling of large sample batches from clinical and preclinical studies during drug development, and to permit simultaneous analysis of total 'active form' (dal-thiol) and dal-S-Me and dal-S-Glu metabolites. Stability of dalcetrapib thioester in biological media was investigated and the equilibrium status of various components of dalcetrapib 'active form' and the potential for their quantitation are discussed; in this regard, the sum of 'active form' (dal-thiol) following thiolysis with DTT and alkylation with NEM was selected for routine quantification, with simultaneous measurement of the dal-S-Me and dal-S-Glu metabolites. Findings are presented following method validation based on internationally accepted guidelines and application of the method to animal and human study samples.

2. Experimental

2.1. Chemicals, solutions and standards

Ethanol (Lichrosolv for HPLC) was obtained from Merck (Darmstadt, Germany), and acetonitrile (HPLC grade S) from Rathburn (Walkerburn, U.K.). Ammonium formate (p.a.), formic acid 98–100% (Suprapur grade) and Tween 80 were purchased from Fluka (Buchs, Switzerland). DTT was purchased from AppliChem (Darmstadt, Germany) and NEM from Acros Organics (Geel, Belgium). Solutions of 0.1N NaOH and HCl were prepared from Merck Titrisol ampoules. Water used for preparation of all solutions was from a Milli-Q apparatus (Millipore, Billerica, MA, USA).

Dalcetrapib (dal, MW 389.6) and isotopically (D_{10} at cyclohexane ring) labeled dalcetrapib used as internal standard (dal-IS, MW 399.66) and the NEM derivative reference dal-NEM (MW 444.64) were provided by F. Hoffmann-La Roche Ltd. (Basel, Switzerland). The free thiophenol of dalcetrapib (thiol, MW 319.51), thiophenol dimer (dimer, MW 637.01), dal-S-Me (MW 333.54) and dal-S-Glu (MW 496.24) were obtained from Japan Tobacco Inc. (Osaka, Japan). Stable isotope labeled dal-S-Me ($^{13}CD_3$ at methyl group, MW 337.55) and dal-S-Glu (D_{10} at cyclohexane ring, MW 505.70) used as internal standards were synthesized at F. Hoffmann-La Roche. Stock solutions of analytes (1 mg/mL) were prepared in ethanol and further diluted with ethanol to give spiking solutions. Small aliquots of spiking solutions were added to blank plasma or to blank urine containing 0.2% Tween 80 for the preparation of calibration standards and quality control (QC) samples: Method 1, 5–4000 ng/mL dal-thiol; 5–4000 ng/mL (5–2000 ng/mL, Method 2) dal-S-Me; 50–10,000 ng/mL (50–4000 ng/mL, Method 2) dal-S-Glu. Calibration standards and QC materials were prepared freshly before use. Internal standard stock solution (1 mg/mL dal-IS) was prepared in ethanol and further diluted to a 200 ng/mL working solution.

A stock solution of DTT in water was prepared at 23.14 mg/mL (150 mM). DTT working solution was obtained by mixing 5 mL DTT stock solution, 20 mL 0.1 N NaOH and 75 mL ethanol/water 70:30 (v/v). A NEM stock solution of 125 mg/mL (1 M) was prepared in acetonitrile; the NEM working solution comprised 5 mL NEM stock solution, 20 mL 0.1 N HCL and 75 mL ethanol. Reagent stock solutions were stable for at least 1 month and working solutions for up to 1 week if stored chilled.

Blank animal plasma was prepared either from EDTA or heparin blood (rat, mouse, hamster, cynomolgus monkey and rabbit) in laboratories at F. Hoffmann-La Roche. Human heparin plasma was purchased from TRINA Bioreactives (Greifensee, Switzerland). Urine was supplied by donors from our own laboratories. Human gastrointestinal fluids were collected in the Roche Clinical Pharmacology Unit (Strasbourg) under fasted or stimulated conditions.

2.2. Sample preparation

2.2.1. Derivatization procedure with DTT/NEM for dal-thiol

To 50 μL plasma or urine, 300 μL ethanol (double blank only) or internal standard solution was added for protein precipitation, followed by 100 μL of DTT working solution. After vortex-mixing (Heidolph model Reax 2000; Heidolph Instruments, Schwabach, Germany), the sample solution was left to react for approximately 30 min at room temperature. For derivatization, 100 μL of NEM working solution was added. After vortex-mixing and centrifugation (6 min at 15,000 rpm; 10 °C, Heraeus Multifuge 3 S-R, Thermo Electron LED, Zürich, Switzerland), supernatant was transferred to the injection vial.

2.2.2. Protein precipitation (without derivatization)

To investigate the stability of dalcetrapib thioester, 10 volumes ethanol was added to plasma after the desired storage time, mixed, centrifuged (6 min at 15,000 rpm) and supernatant was transferred into a new vial. For free thiol or dimer analysis, ethanol or acetonitrile was used for protein precipitation; the ratio of plasma to solvent ranged from 1:2 to 1:10 (v/v).

2.2.3. Derivatization with NEM before protein precipitation

5 μL aliquots of 1 M NEM stock solution were added to 50 μL plasma, followed by protein precipitation (*i.e.* with 500 μL of ethanol).

2.2.4. Derivatization with NEM after protein precipitation

Organic solvent (*i.e.* 500 μL of ethanol) was added to 50 μL plasma, followed by addition of 5 μL of 1 M NEM stock solution.

2.2.5. Pretreatment with DTT (without NEM derivatization)

Procedures as described in Section 2.2.1 but with addition of 100 μL of ethanol instead of NEM solution.

2.3. Liquid chromatography–mass spectrometry

2.3.1. Method 1

A schematic of the column-switching LC–MS/MS system is shown in Fig. 2 and details of the LC program are provided in Table 1.

The following conditions were used to optimize sample preparation, to investigate the feasibility of determining thioester and entities of the 'active form' (free thiol, dimer, adducts) separately and to perform initial stability tests. Furthermore, the method served for quantitation of dal-thiol in plasma from clinical and preclinical studies and for exploratory determination of metabolites dal-S-Me and dal-S-Glu. Sample solution (5–50 μL)

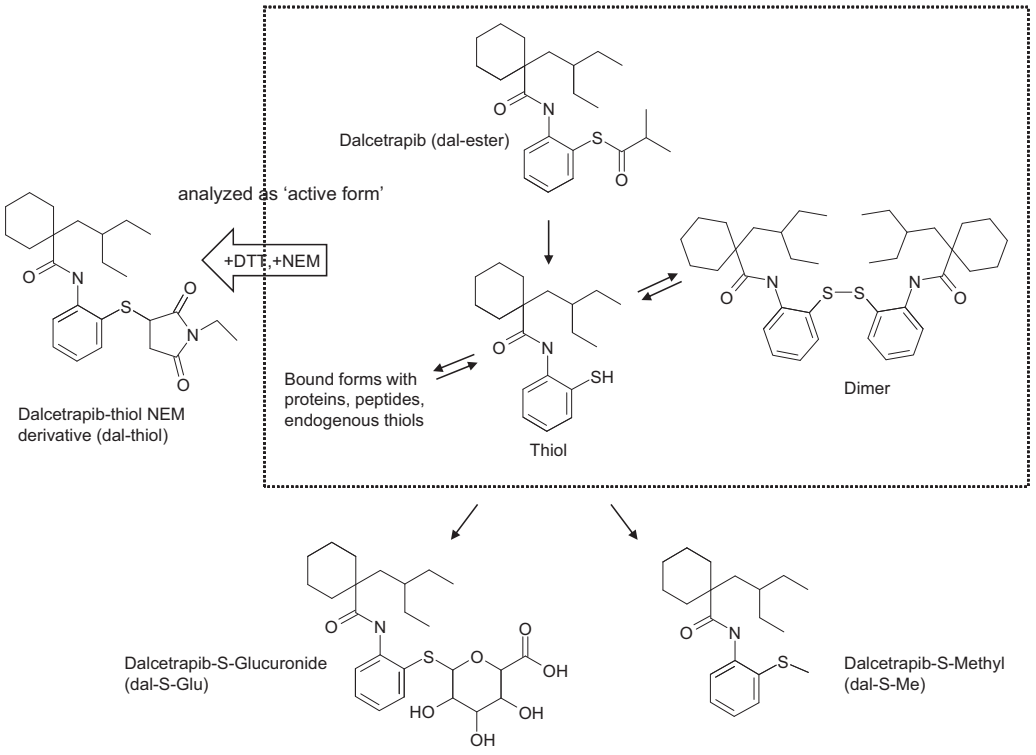

Fig. 1. Structures of dalcetrapib, 'active form' components, N-ethylmaleimide (NEM) derivative and measured metabolites. DTT, dithiothreitol.

Table 1
HPLC program for Method 1. Initial conditions: binary gradient pumping mode, total flow (pumps A and B, analytical column [AC]) 0.3 mL/min, pump B% 0, pump C flow (on trapping column [TC]) 0.5 mL/min, dilution flow (DIL) 2 mL/min. *Changed settings for analysis of dimer.

Time (min)	Module	Events	Parameter	Comment
0.39	System controller	Event	3	Stop DIL pump
0.40	Pumps	C Flow	0.5	Increase flow on TC
0.41	Pumps	C Flow	2	
0.60	System controller	Event	24	Switch valve – connect TC and AC
0.61	System controller	Solenoid valve	B	Organic rinse of TC
1.00	Pumps	%B	0	Start gradient on AC
1.20 (*2.7)	System controller	Event	4	Switch valve to separate TC and AC
1.60 (*3.2)	System controller	Solenoid valve	A	Re-equilibrate TC
2.50	Pumps	%B	100	Gradient finished, rinse AC
3.90	Pumps	%B	100	With 100% solvent B
3.91	Pumps	%B	0	Re-equilibrate AC
4.40	System controller	Stop		

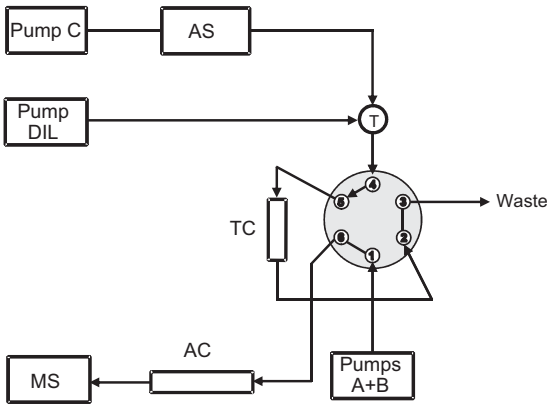

Fig. 2. Column-switching HPLC system (trapping process shown). AS: autosampler; TC: trapping column; AC: analytical column; pump C: trapping pump; pump DIL: dilution pump (only used in Method 1); T: T junction; pumps A and B: analytical pumps; MS: mass spectrometer.

was injected by a SIL-HTc autosampler with integrated system controller SCL-10AD (Shimadzu, Kyoto, Japan). An XTerra RP_{18}, 5 μm, 10 mm × 2.1 mm (Waters, Milford, MA, USA) was used as trapping column (TC). Pump C (LC-10ATvp, Shimadzu) delivered mobile phase C_a for trapping (5 mM ammonium formate and 0.2% formic acid in water–acetonitrile 80:20 v/v) or alternatively C_b for rinsing after the trapping process (5 mM ammonium formate and 0.2% formic acid in water–acetonitrile 10:90 v/v). The dilution pump (L-6000A, Merck-Hitachi, Tokyo, Japan) was connected *via* a T-junction with the trapping pump and delivered 5 mM ammonium formate, 0.2% formic acid in water to provide aqueous dilution of injection solution before entering the TC. The electrically driven switching valve 7000E (Labsource, Reinach, Switzerland) directed effluent from the TC either to waste or onto the analytical column (AC, XTerra MS C18 3.5 μm, 2.1 mm × 50 mm, Waters) or, for analysis of the thiophenol dimer only, a Luna phenyl–hexyl column, 3 μm, 2 mm × 10 mm (Phenomenex, Torrance, US). A high-pressure gradient HPLC system comprising two LC-10ADvp pumps (A and B, Shimadzu) delivered the mobile phases A (5 mM ammonium formate, 0.2% formic acid in water–acetonitrile 50:50, v/v) and B

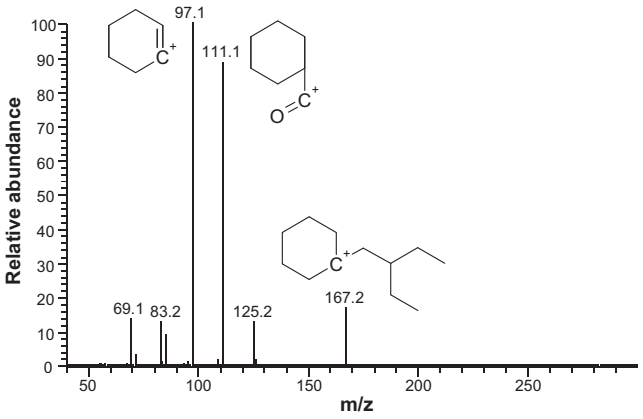

Fig. 3. Product ion spectrum of dal-ester and proposed structure of fragments; the same fragment ions were observed for free thiol, dimer, dal-S-Me, dal-S-Glu and NEM derivative of thiol.

(5 mM ammonium formate, 0.2% formic acid in water–acetonitrile 10:90, v/v).

A TSQ Quantum Ultra triple-quadrupole mass spectrometer (Thermo Fisher Scientific, SanJose, CA, USA) equipped with an electro-spray ionization source was used in the positive selected reaction ion monitoring (SRM) mode. Sheath, auxiliary and sweep gases were nitrogen set at 60, 10 and 5 instrument units, respectively. Argon was used as collision gas at 1.0 mTorr. Spray voltage was set at 4500 V and the capillary temperature at 300 °C. SRM was used for analyte detection. The selected transitions (m/z) were 445 → 97 for dal-thiol (dalcetrapib 'active form'), 496 → 97 for dal-S-Glu, 334 → 97 for dal-S-Me, 455 → 107 for dal-IS, 390 → 97 for dalcetrapib thioester (dal-ester), 320 → 97 for free thiol and 637 → 97 for the dimer. Fig. 3 shows the product ion spectra. Collision energies were optimized between 20 and 30 eV and the tube lens voltage between 60 and 110 V, depending on the compound. Data acquisition was performed in centroid mode at unit mass resolution (setting 0.7 Da). The scan time was 80 ms and the scan width 0.2 amu. Data acquisition was performed with software Xcalibur 1.3 distributed by Thermo Fisher Scientific.

2.3.2. Method 2

Modified LC–MS/MS conditions were used for routine analysis of large sample batches from clinical and preclinical studies for dal-thiol, dal-S-Me and dal-S-Glu during the major part of Phase III drug development and for the performance of (long-term) stability investigations. Column-switching LC was employed as described for Method 1 with the following modifications: Rheos 2000 and 2200 pumps (Flux Instruments, Buchs, Switzerland) were used for trapping/rinsing and analytical separation, respectively. Solvent C_a was water/methanol (95:5 v/v) and C_b acetonitrile/water (90:10 v/v). TC was a Gemini C18 Mercury 2 mm × 10 mm (Phenomenex). A Capcell PAK, C18 MG, 2.0 mm × 35 mm, 5 μm column (Shiseido) was used as AC and 2 μL-aliquots of sample solution were injected by a PAL autosampler (CTC Analytics, Zwingen, Switzerland), removing the requirement for online dilution. At 0.5–3.0 min after injection, analytes and IS were transferred to the AC. The TC was rinsed with C_b for 3.0–4.0 min then re-conditioned with C_a at 2 mL/min. A gradient on the AC was run from mobile phase A (70%, 0.0025% ammonium hydroxide in water) and B (30%, 0.0025% ammonium hydroxide in methanol) to 100% B at 0.3 mL/min between 0.2 and 1.5 min. After 4 min the AC was reconditioned with 30% B. Total run time was 5 min.

Mass spectrometric detection was performed on a TSQ Quantum instrument using +4 kV ESI voltage, 350 °C capillary temperature, sheath and auxiliary gases of 60 and 5 units, respectively. Collision gas pressure was 1.5 mTorr and collision energy 15 eV. Compounds were monitored at m/z 445 → 167 for dal-thiol → 167 for dal-S-Me, 496 → 167 for dal-S-Glu, 455 → 177 for dal-IS, 338 → 167 for dal-S-Me-IS, and 506 → 330 for dal-S-Glu-IS at 0.1 amu scan width and 50 ms scan time. Xcalibur 2.0 and LCQuan 2.5 software were used for data acquisition and peak integration.

2.4. Data handling and method validation

Calibration curves ($y = a + bx$) were obtained by weighted linear least-squares regression (weighting factor $1/x^2$) of measured peak-area ratios analyte/internal standard (y) *versus* analyte concentration (x). Method validation was performed according to current FDA and EMA guidelines [13,14].

2.4.1. Selectivity, precision and accuracy

Selectivity was evaluated by analyzing blank samples (including pre-dose, control and placebo samples) from all species for interference from endogenous compounds. Intra-assay precision and accuracy were evaluated in human and animal plasma and in human urine by analyzing spiked samples at five concentrations (including the lower limit of quantification [LLOQ] and upper limit of quantitation [ULOQ]) against one calibration set ($n = 5$ for Method 1, $n = 6$ for Method 2). Inter-assay precision and accuracy were evaluated for Method 1 by analyzing spiked samples at five concentrations including the LLOQ and ULOQ, on five occasions, using a separate calibration set each time. Inter-assay data for Method 2 were calculated from three intra-assay batches ($n = 18$). Acceptance criteria for the intra- and the inter-assay precision studies included a CV ≤ 15% except for LLOQ (≤20%). Mean values for each concentration level were required to be within 85% and 115% of nominal except at LLOQ (80% and 120%). Where no co-eluting internal standard was available (for metabolites in Method 1), the required CV and deviation from accuracy each had to be <20% (25% at LLOQ).

2.4.2. Recovery and matrix effect

Three sets of spiked samples were compared for determination of recovery and matrix effect for dal-thiol, (a) standard QC materials: dal-ester was spiked to blank matrix prior to the extraction/work-up procedure, and samples were handled as described for the methods, (b) recovery reference: NEM reference was spiked to blank matrix, (c) 100% reference: NEM reference was added to matrix-free solution. Comparing the analyte response of (a) with (b) provided the method recovery (derivatization efficiency) while comparing (b) with (c) revealed the matrix effect. Three QC levels were analyzed at least in triplicate. Similar procedures were performed for dal-S-Me and dal-S-Glu, spiking analytes to matrix (a), to extract (b) and to matrix-free solution (c).

2.4.3. Stability

Stability of the stock solutions was investigated by comparing analyte responses in stock *versus* freshly prepared solutions. Matrix stability was determined by spiking with low and high QC concentrations of dal-ester and metabolites, and analyzing (at least in triplicate) after the storage period. Analytes were considered stable under the chosen conditions if the difference between the measured concentration and the nominal QC concentration was lower than ±15%. Short term (room temperature), long-term (frozen), freeze-thaw, and extract stability were investigated, as well as the influence of light, different plasma batches and anticoagulants. Stability was also examined in pooled mouse, rat and cynomolgus monkey plasma. For this purpose, samples were measured against a calibration curve in human plasma immediately (100% reference) and again after storage (in triplicate), with stability calculated as deviation post-storage from 100% reference value.

2.4.4. Reproducibility

Reproducibility of sample re-analysis (ISR) was examined for 5–10% of samples from various animal and human studies and was successful if at least two thirds of repeat results deviated by <20% from original data. Cross-validation of LC–MS/MS Methods 1 and 2 and of a previously used LC–UV method was performed for human plasma (using spiked QCs and pooled study samples) employing the following criteria: at least 75% of results for QC samples should be within ±15% of nominal values and within ±15% at the lowest concentration level. At least 75% of results for *ex vivo* samples should be within ±15% of their originally determined value.

2.4.5. Application to study samples

The method described was successfully applied to the analysis of more than 2500 samples from pharmacokinetic and toxicokinetic studies in rats, mice, hamsters, rabbits, and cynomolgus monkeys [7]. Moreover, approximately 200 urine and 8500 plasma samples from clinical studies were analyzed at the laboratory of F. Hoffmann-La Roche Ltd., Basel, before the method was transferred to a bioanalytical CRO. Repeated analysis of study samples on different occasions was performed to further evaluate assay quality and robustness. For all studies, repeated analyses fulfilled the acceptance criteria for cross-validation of bioanalytical methods, *i.e.*, ≥75% of samples had to be within ±15% of the original value.

3. Results and discussion

3.1. LC–MS/MS method development

3.1.1. Method 1

A column-switching system was used for on-line solid-phase extraction of the deproteinized plasma samples. The method was considered suitable for determination of dal-ester, free thiol, dimer, dal-thiol (NEM derivative), dal-S-Me and dal-S-Glu. The XTerra RP_{18} TC proved to be robust for at least 800 injections, and provided sufficient retention of analytes. Other columns, such as Atlantis dC18 (2.1 mm × 10 mm, 5 μm) were also suitable for trapping, but tolerated fewer injections. Online aqueous dilution of the injection solution containing a high content of organic solvent was performed to reduce elution strength and allow trapping of larger sample volumes, if needed. Mobile phase C_a was used for trapping of compounds and rinsing of the TC; 20% acetonitrile proved to be optimal to facilitate washing out of polar and less polar matrix components without loss of analytes. Although dal-thiol and dal-S-Me metabolite are relatively non-polar, a higher content of organic solvent was unsuitable since this reduced retention of dal-S-Glu that was required for simultaneous analysis. Mobile phase C_b, containing 90% acetonitrile, was used to purge the TC and the capillaries between the autosampler and TC, to remove lipophilic sample constituents from the TC and minimize carry-over. The same solution was used to efficiently rinse the autosampler injection port between injections. The organic solvent content of mobile phase A was adjusted to elute compounds of interest in a narrow band from the TC. Solvent content had to be sufficiently low to permit good gradient formation; 50% acetonitrile was sufficient for compound elution from the TC, and a gradient to 90% acetonitrile was used on the AC. The XTerra MS C18 (3.5 μm) column showed sufficient selectivity to separate interfering peaks, and addition of formic acid to the mobile phases provided good peak shapes for the analytes dal-ester, free thiol, metabolites and dal-thiol (NEM derivative) (Fig. 4A and B). Compounds showed good separation both from each other and from endogenous interference. The dimer, however, showed a long retention time, large peak width and insufficient response, which was resolved by replacing the 50 mm C18 AC by a short 10 mm phenyl–hexyl column and prolonging elution time from the TC (Fig. 4C).

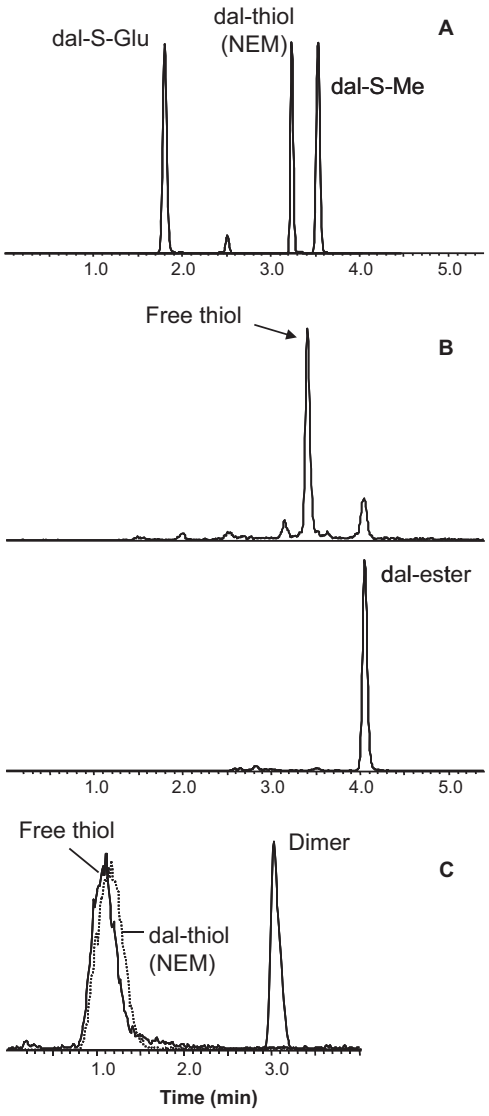

Fig. 4. Chromatograms (overlaid from separate injections) of (A) dal-S-Me, dal-S-Glu and dal-thiol (NEM derivative), (B) free thiol and dal-ester without derivatization and (C) dimer, free thiol and dal-thiol (NEM derivative): 10 mm column, Method 1.

Method 1 was used in human and animal study samples for stability tests of dal-ester, investigations on determination of free thiol and dimer, and for quantification of dalcetrapib 'active form' dal-thiol, dal-S-Me and dal-S-Glu (Fig. 5).

3.1.2. Method 2

The requirement for routine analysis of the dal-S-Me and dal-S-Glu metabolites together with dal-thiol prompted the synthesis of stable isotope-labeled internal standards and re-development of the LC–MS/MS method. The Gemini column, being relatively low cost and highly robust, was employed as TC. Use of a basic analytical mobile phase provided high signal-to-noise, particularly for dal-S-Glu, and fewer endogenous compound peaks in the analysis of dal-S-Me compared with Method 1 (Figs. 5 and 6); thus providing improved precision during routine analysis. A Capcell PAK column, stable at higher pH, was employed as the AC. Ionization still occurred in positive electrospray mode despite the basic eluent. This approach termed "wrong-way-round" ionization

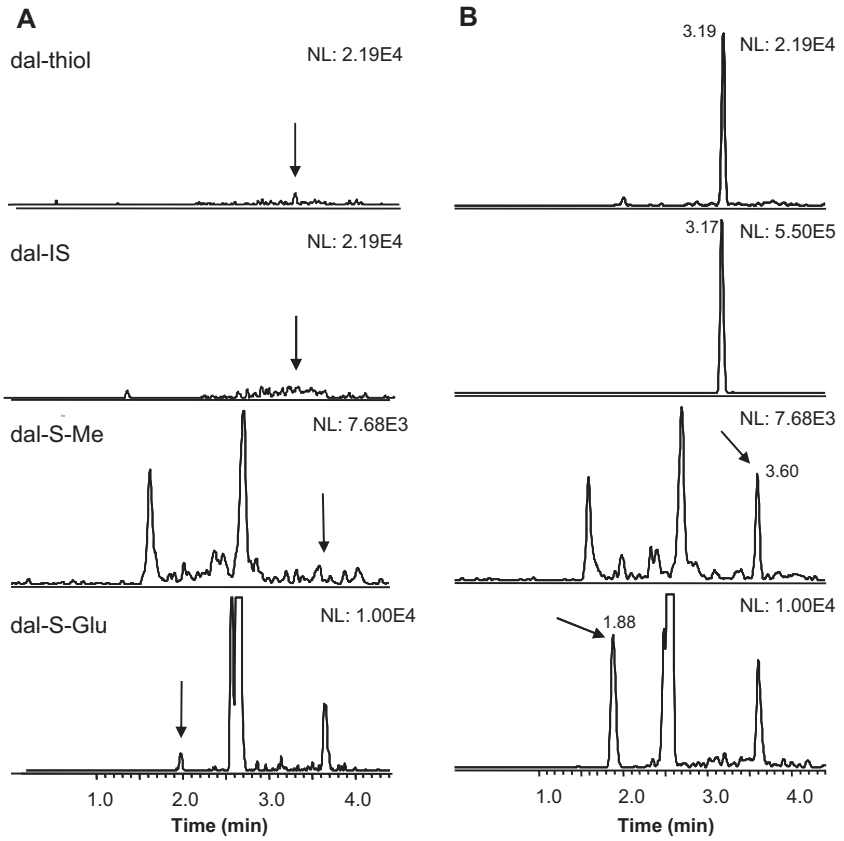

Fig. 5. Extracted ion chromatograms of dal-thiol (NEM derivative), dal-S-Me and dal-S-Glu and of internal standard dal-IS in (A) human double blank plasma and (B) human plasma spiked at lower limit of quantification (B), Method 1.

[15] has previously been used successfully to improve sensitivity of LC–MS/MS analyses [16–18].

3.2. Sample preparation procedures

3.2.1. Derivatization procedure to determine total 'active form' of dalcetrapib (dal-thiol)

The derivatization agent NEM has proved to be reliable with no concerns regarding diastereomer formation with dalcetrapib [19,20]. Investigations were performed to optimize and simplify the procedure, to more rapidly provide a sample extract suitable for direct injection into the column-switching LC–MS/MS system. Reactions could be performed at room temperature and immediately; it was not necessary to wait for 10 min after NaOH addition. The reaction time with DTT was investigated (1–60 min); no dal-ester remained after 20 min so reaction time was set to 30 min. Protein precipitation before derivatization resulted in improved recovery of dal-thiol from plasma compared to matrix-free solution. Greater recovery from plasma was obtained when protein precipitation was undertaken using ethanol, compared to acetonitrile. Maintaining the derivatization step with NEM was preferred to measuring the free SH after DTT treatment alone, to prevent potential reactions of the free SH in the injection solution and to obtain better sensitivity as the MS response for SH (at m/z 320) was significantly lower than for the derivative (at m/z 445). HCl was added to neutralize the final sample solution to prevent hydrolysis of dal-thiol (NEM derivative) to the free thiol.

Thus, the entire derivatization procedure was performed in only three steps; protein precipitation with pure ethanol containing dal-IS, DTT reaction with NaOH in ethanol/water, and derivatization for 30 min with NEM and HCl in ethanol, and was easily automated for turnaround of large sample numbers from clinical trials. After centrifugation, the sample extract could be injected without further work-up. The metabolites dal-S-Me and dal-S-Glu were determined simultaneously with dal-thiol without being affected by the derivatization procedure.

Spiking the same concentration of thioester, thiol or dimer to plasma and performing the treatment with DTT and NEM resulted in the same signal intensity for the NEM derivate peaks, not only for freshly spiked but also for samples stored at room temperature or frozen. This confirms that this derivatization method is independent of whether the drug is present in the biological matrix as free form, dimerized or bound, *i.e.* to plasma proteins.

The above described sample preparation method was varied as appropriate to investigate derivatization with NEM before or after protein precipitation without cleavage of disulfide bonds by DTT (Section 3.4).

3.2.2. Urine analysis

In human urine, a significant decrease in measured analyte concentration immediately after spiking was associated with non-specific compound loss due to adsorption on container walls. To prevent this, it was necessary to add a solubilizing agent or surfactant [21,22] to improve drug solubility and compete for binding sites on the solid surface. Previous experiences with the surfactant Tween 80 for small molecule drugs [22] and a peptide (taspoglutide) [23] revealed it was able to stabilize drugs and also to re-dissolve already adsorbed analytes in urine. In the final procedure, preparation of calibration and quality control samples, collection and storage of study samples and all sample workup steps were carried out in glass containers, and 0.2% Tween 80 was added to calibration, QC and study samples.

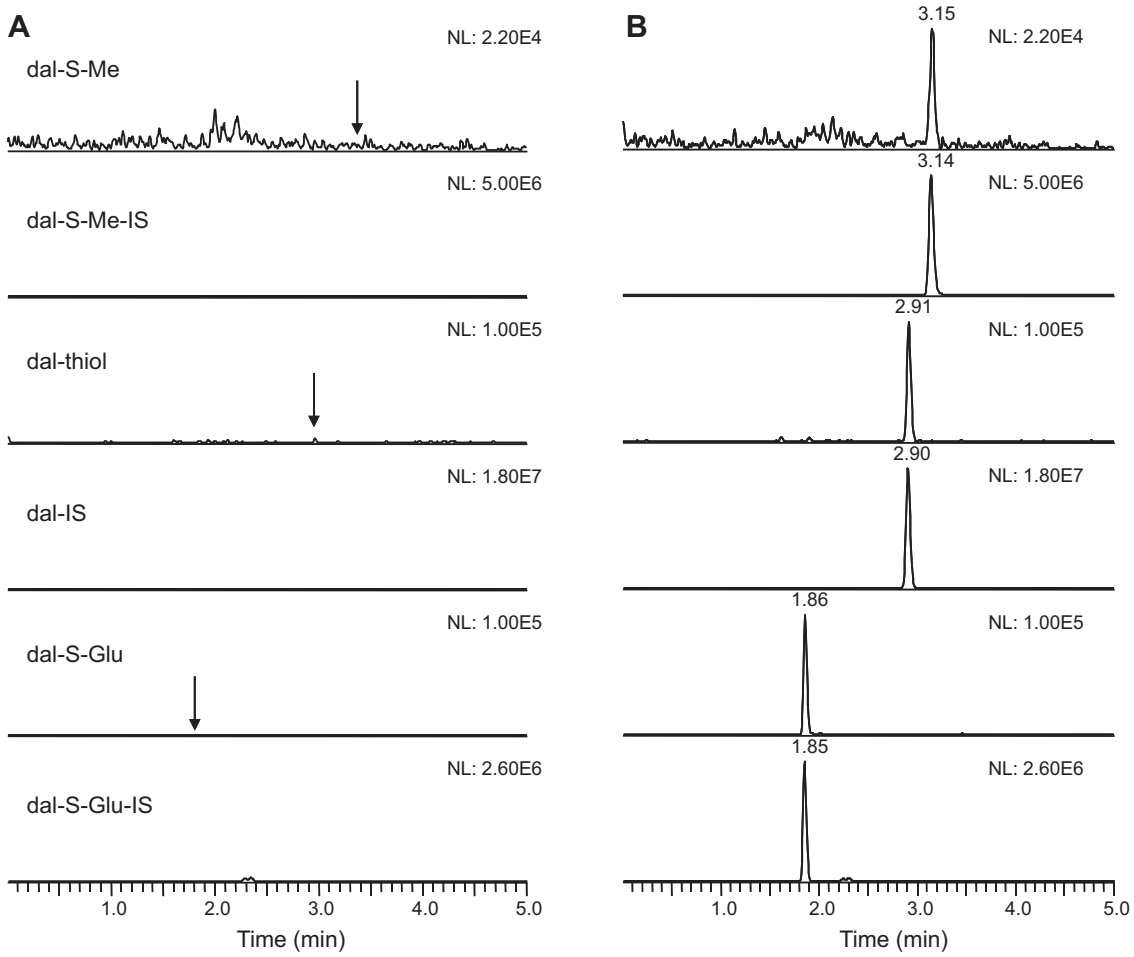

Fig. 6. Extracted ion chromatograms of dal-thiol (NEM derivative), dal-S-Me and dal-S-Glu and of internal standard dal-IS in (A) human double blank plasma and (B) human plasma spiked at lower limit of quantification (B), Method 2.

3.3. Stability of dalcetrapib thioester

3.3.1. Gastrointestinal tract

In vivo, rapid hydrolysis of dal-ester occurs in the human gastrointestinal tract with a half-life of approximately 15 min. *In vitro* studies showed dal-thioester in gastric fluid of four fasted subjects to be stable with ~99% remaining by 26.5 h. However, coincident with the higher pH of stimulated gastric fluid, variable degrees of hydrolysis were observed; in separate samples, 1.5, 2.7, 58.4, and 86.5% remained after 120 min. In human intestinal fluid, hydrolysis to the free thiol was almost instantaneous with a half-life of ~4 s (Fig. 7). These findings suggest that while speed of hydrolysis appears to be independent of stimulation, hydrolysis *per se* may be associated both with increased pH and pancreatin level. The principal component in human gastric and intestinal fluid after hydrolysis of dal-thioester was the dimer. Moreover, recently published observations in dual portal and peripheral vein cannulated cynomolgus monkeys that the metabolism of dalcetrapib-thiol to dalcetrapib-S-Glu (glucuronidation) appears to occur almost instantly, whereas methylation to dalcetrapib-S-Me occurs much more slowly, confirm a high influence of glucuronidation of the free thiol on first-pass effect [7].

3.3.2. Solutions and plasma

Previous work has shown that dal-ester is also hydrolyzed in plasma and liver (unpublished data, Japan Tobacco), thus, no attempt was made to detect dal-ester *ex vivo*, *i.e.*, following the addition of esterase inhibitor. Stability tests were conducted primarily to characterize dal-ester conversion in spiked standards for determination of 'active form' dal-thiol (see Section 2.2.2). We confirmed that hydrolysis was rapid in animal plasma *ex vivo*: only about 2% of dal-ester was detected 15 min after spiking in cynomolgus monkey and dog plasma, and ester bond cleavage was immediate in rat plasma due to high esterase levels. Stability was enhanced in acidified conditions, while under basic conditions conversion occurred rapidly. As a result, NaOH was added to thioester-spiked calibration and QC samples before derivatization with DTT and NEM to ensure complete ester cleavage.

3.4. Free thiol, bound thiol or total 'active form'?

3.4.1. Determination of unchanged free thiol

As predicted, free thiol was unstable in solution; dimer was detected immediately after dissolution and thiol concentration decreased with storage. The process was accelerated by addition of acid but could not be prevented under basic conditions. Stability was only slightly improved in acetonitrile compared with ethanol.

Free thiol was unstable at room temperature both in plasma and in plasma supernatant after protein precipitation using either ethanol or acetonitrile. Improved stability was observed when the spiked plasma or the supernatant post-precipitation was immediately stored at −20 °C: no relevant decrease of thiol was obtained overnight. A higher thiol peak was obtained when protein precipitation was carried out with ethanol compared with acetonitrile,

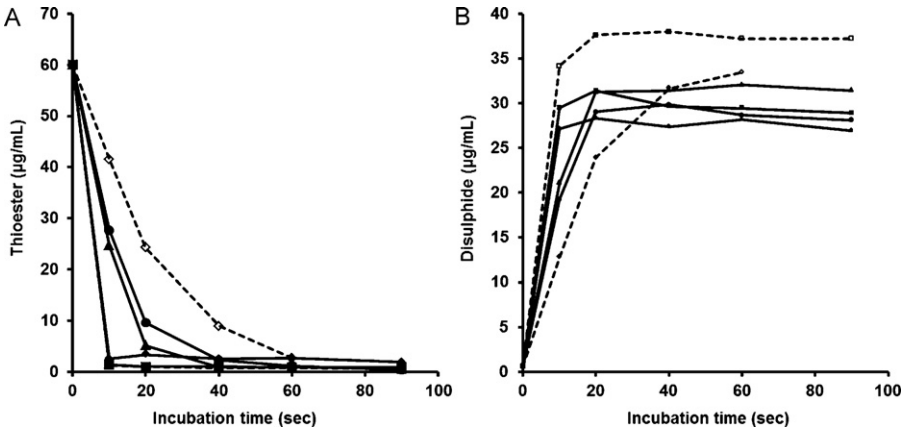

Fig. 7. Stability of dalcetrapib in human intestinal fluid. Concentration of (A) thioester and (B) disulfide after incubation (60 µg/mL) in intestinal fluid from fasted ($n = 4$, solid lines) or stimulated ($n = 2$, dashed lines) subjects. Fasted subjects: 1001, 1002, 1005, 1006. Stimulated subjects: 2005, 2006.

very likely due in part to higher recovery and/or a shift of equilibrium from bound to free thiol with ethanol.

3.4.2. Determination of stabilized free thiol

After addition of NEM to plasma to stabilize the sulfhydryl group, the resulting thiol derivative was stable both in plasma and in supernatant after protein precipitation. The derivative peak was increased when protein precipitation was performed before NEM addition.

Although NEM can be added immediately after sampling, the equilibrium could be changed by thiol capture with possible re-dissociation of disulfide bonds and, even if the sample is frozen immediately, further sample preparation may change the equilibrium. This was confirmed in a hamster study where samples prepared by derivatization with NEM alone prior to protein precipitation were compared to samples prepared by the 'active form' method (protein precipitation, DTT treatment, NEM derivatization). Concentrations attained after NEM derivatization were 100- to 1000-fold lower than with 'active form' method, and a meaningful correlation between data sets could not be obtained. In spiked samples containing both thiol and dimer and subjected to derivatization with NEM, the NEM derivative peak increased with time suggesting that re-dissociation of dimer to thiol occurs.

3.4.3. Determination of dimer

A dimer peak was detected when disulfide dimer was dissolved in organic solvent. This disappeared completely after addition of base because of lower solubility, whereas addition of acid increased the dimer peak. Formation of thiol was not detected in matrix-free dimer solutions. Dal-dimer spiked to plasma could not be recovered by protein precipitation with ethanol; a thiol peak detected in the supernatant led to the conclusion that ethanol favors dissociation of dimer to free thiol. Protein precipitation using acetonitrile (two- or three-fold plasma volume) resulted in the detection of dimer due to better recovery and solubility in acetonitrile compared with ethanol and only very small amounts of thiol. The dimer was found to be very unstable in plasma during storage at room temperature; detection was only possible when precipitation was performed with acetonitrile immediately after spiking, but stability could be improved by acidifying the plasma. However, under acidic conditions any thiol present was converted to dimer, leading to overestimation of dimer level.

3.4.4. Discussion

Experiments performed *in vitro* may not be equivalent to processes in living organisms (intake of thioester and conversion to free thiol, dimer and endogenously bound forms). Nevertheless, based on the *in vitro* data presented above we conclude that specific determination of these individual components is technically difficult and of limited relevance. Any sample preparation step changed the equilibrium between free and bound thiol in the sample, and instability and lack of reproducibility prevented the generation of reliable data. As a consequence, for routine analysis, free thiol, disulfide dimer and mixed disulfide adducts were determined collectively as dal-thiol ('active form') after reduction under basic conditions with DTT to break disulfide bonds and stabilize the free thiol by derivatization with NEM. This sum parameter is considered to be an appropriate surrogate for drug exposure, since bound thiol may act as a 'drug reserve' to provide the desired pharmacological effect after re-dissociation. This mechanism and the concept of total drug measurement were reported for other thiol drugs before, *e.g.* [24,25]. Dal-thiol 'active form' quantitation allows for inter-individual and inter-species comparison regardless of shifts in the oxidation–reduction equilibrium and independent of the formulation used. Consequently determination of 'active form' is used in the analysis of all animal and human samples generated during drug development.

3.5. Validation results for dal-thiol, dal-S-Me and dal-S-Glu

3.5.1. Selectivity and specificity

No significant interferences (from endogenous compounds, dal-ester or other metabolites) co-eluting with dal-thiol, dal-S-Me and dal-S-Glu were observed in blank plasma from different species, or in blank urine. Any interfering peak was always <20% of the response at LLOQ. Typical chromatograms obtained with Methods 1 and 2 are shown in Figs. 5A and 6A, respectively. No influence from co-administered drugs (atorvastatin, simvastatin, ketoconazole or rosiglitazone) was observed.

3.5.2. Linearity and limit of quantitation

The lower limits of quantitation (LLOQ), defined here as the minimum concentration that could be measured routinely with an inaccuracy of <20% CV (*i.e.*, an accuracy between 80 and 120%) were 5 ng/mL for dal-thiol, 5 ng/mL for dal-S-Me and 50 ng/mL for dal-S-Glu. This sensitivity was sufficient to support pharmacokinetic, toxicokinetic and clinical studies. Typical chromatograms for the lowest calibration standard obtained with Methods 1 and 2 are shown in Figs. 5B and 6B, respectively. Using Method 1, the calibration curves were linear up to 4000 ng/mL for dal-thiol and dal-S-Me and up to 10,000 ng/mL for dal-S-Glu. Linear ranges for

Table 2
Assay quality parameters in human heparin plasma (Method 1).

Inter-assay		Intra-assay			
Added concentration (ng/mL)	Precision/accuracy (%)	Added concentration (ng/mL)	Precision/accuracy (%)	Matrix effect (%)	Percent recovery
Dal-thiol					
5	4.19/99.8	5	6.1/96.8		
10	5.26/97.8	15	5.1/101.8	99.8 (5.5)	106.7 (9.1)
200	1.95/98.5	300	4.3/105.4	95.9 (7.2)	106.4 (2.0)
2000	3.13/99.7	3000	1.2/97.1	110.4 (2.4)	95.2 (3.2)
4000	2.19/108.7	4000	1.9/95.2		
Dal-S-Me					
5	5.8/98.0	5	3.1/95.7		
10	2.8/96.8	15	2.8/101.3		113.7 (3.9)[a]
200	0.7/98.2	300	3.5/108.6		n.d.
2000	3.2/101.7	3000	0.8/106.2		110.5 (1.3)[a]
4000	4.7/107.8	4000	2.7/100.0		
Dal-S-Glu					
50	10.6/107.9	50	5.1/94.5		
100	4.8/102.8	150	4.0/94.6		112.3 (2.7)[a]
500	2.7/89.5	3000	5.0/99.9		n.d.
5000	4.4/109.0	8000	2.1/100.1		113.5 (3.0)[a]
10,000	3.5/110.5	10,000	0.8/112.7		

$n = 5$.
n.d., not determined.
Numbers in brackets: CV%.
[a] Determined as overall recovery (combined matrix effect and extraction recovery).

the metabolites for Method 2 were 5–2000 ng/mL for dal-S-Me and 50–4000 ng/mL for dal-S-Glu.

3.5.3. Precision and accuracy

Inter- and intra-assay precision and accuracy for dal-thiol, dal-S-Me and dal-S-Glu in human plasma for Methods 1 and 2 are shown in Tables 2 and 3, respectively. Using Method 1, intra-assay precision and accuracy for dal-thiol in hamster, cynomolgus monkey, rabbit, rat and mouse plasma and human urine, intra-assay precision and accuracy for dal-thiol using Method 1 were <15% CV and 85–115%, respectively. Due to lack of co-eluting analog or stable labeled internal standards for dal-S-Me and dal-S-Glu in Method 1, acceptance criteria for precision and accuracy were set to <20% CV and 80–120%, respectively, which were attained for plasma from all analyzed animal species and for human urine. For Method 2, stable isotope-labeled internal standards were available for all analytes, and inter- and intra-assay precision was <15% (<20% at LLOQ), accuracy 85–115%, for all matrices (rat, cynomolgus monkey, dog and mouse plasma and human urine).

3.5.4. Matrix effect and recovery

No significant matrix effect was observed for dal-thiol, dal-S-Me and dal-S-Glu in human plasma (Tables 2 and 3). Furthermore, no matrix effect was detected for any measured analyte in animal plasma (98–102%, 91–101% and 94–107% in rat, cynomolgus monkey and mouse, respectively). The matrix effect in human urine for dal-thiol was insignificant (98–103%) whereas slight signal suppression was observed for dal-S-Me (83–87%) and dal-S-Glu (82–86%); this was however compensated by the IS (data on file).

Recovery for dal-thiol in terms of derivatization and extraction in human plasma was close to 100% (Tables 2 and 3 for Methods 1 and 2, respectively). Recovery of dal-S-Me and dal-S-Glu (Method 2 only) was >85% for animal and human plasma, and human urine (see Table 3 for human data, animal data on file).

Table 3
Assay quality parameters in human heparin plasma (Method 2).

Added concentration (ng/mL)	Inter-assay precision/accuracy (%)	Intra-assay precision/accuracy (%)	Matrix effect (%)	Recovery (%)
Dal-thiol				
5	6.4/104.3	3.6/110.2		
15	4.1/107.0	1.6/111.3	100.4 (3.3)	100.5 (2.5)
300	2.6/103.7	1.8/102.6	98.9 (2.6)	100.4 (1.6)
3000	3.0/102.9	2.4/105.3	100.5 (1.0)	99.3 (0.7)
4000	2.6/102.8	2.0/104.8		
Dal-S-Me				
5	7.1/113.4	2.0/119.1		
15	5.5/97.5	4.9/97.3	103.1 (1.6)	97.6 (3.1)
300	3.5/99.5	3.6/100.7	98.0 (3.3)	100.2 (1.6)
1500	3.1/98.1	3.5/98.7	100.1 (1.4)	100.7 (0.4)
2000	3.6/98.6	3.1/98.5		
Dal-S-Glu				
50	9.6/99.9	8.3/94.4		
150	7.5/100.0	4.8/98.7	101.3 (13.2)	108.0 (13.7)
600	5.6/100.9	4.4/96.2	103.6 (2.4)	102.0 (2.6)
3000	3.4/100.6	2.5/98.3	105.8 (2.9)	103.2 (2.4)
4000	6.3/104.8	4.3/103.3		

$n = 6$ (inter-assay $n = 18$).
Numbers in brackets: CV%.

Table 4
Stability–concentration loss % of stored *versus* freshly prepared quality control (QC) samples, Method 2.

Matrix	Condition	QC level	dal-thiol	dal-S-Me	dal-S-Glu
Human plasma	Freeze-thaw (4 cycles)	Low	−0.6	−0.6	+6.1
		High	−9.3	−5.1	−2.9
	20 h room temp.	Low	+2.3	−2.4	+1.4
		High	+0.9	+1.3	+1.6
	12 months −25 (±5) °C	Low	−2.5	+4.0	+4.5
		High	−4.3	+3.9	+2.0
Extract (plasma)	54 h 8 °C	Low	−4.7	−2.0	−2.6
		High	+0.3	−1.2	+2.2
Human urine	Freeze-thaw (4 cycles)	Low	−4.7	−4.7	−7.3
		High	−6.7	−6.0	−7.0
	27 h room temp.	Low	+3.3	−4.7	0.0
		High	−6.7	+9.3	+5.3
	6 months −25 (±5) °C	Low	−2.0	−7.3	−6.7
		High	−3.3	−4.7	−0.3
Extract (urine)	187 h 8 °C	Low	−7.3	−5.3	−8.7
		High	−5.3	0.0	−4.3

$n = 3$.

3.5.5. Cross-validation results

Measurement of dal-thiol by LC–MS/MS using Method 1 provided results comparable to the previously used LC–UV method (data on file): measured concentrations for 70% of pooled ($n = 30$) study samples and for 90% of QC samples ($n = 30$) deviated by <20%: a deviation >30% was observed for one sample only. Dal-thiol concentrations determined by LC–MS/MS Method 2 deviated by <20% from those obtained with Method 1 for all pooled study samples ($n = 18$) and QC materials ($n = 15$). For dal-S-Me and dal-S-Glu, the deviation between Methods 1 and 2 were <20% for 93% and 87%, respectively. In conclusion, no significant difference was seen between the LC–MS/MS and LC–UV methods in determining dal-thiol and its metabolites.

3.5.6. Reproducibility

For Method 1, 5–9% of samples from five clinical studies were re-analyzed to determine reproducibility. Deviations of repeats from original values were <20% for 78–95% of study samples. For Method 2, at least 5% of samples were re-analyzed: repeat values deviated by <20% for at least two thirds of samples. Thus, the acceptance criteria were fulfilled for both methods.

3.5.7. Stability of dal-thiol and metabolites in spiked samples

As described earlier, dal-ester is degraded rapidly in the gastrointestinal tract following oral administration to the free thiol, which immediately forms the dimer and other sulfide bonds. Hence, stability of dal-thiol (dalcetrapib 'active form') in study samples may not be correctly mirrored in dal-thiol measurement after *ex vivo* spiking of dal-ester. Nevertheless, such stability investigations are valuable to determine appropriate storage and handling conditions for solutions, spiked calibration standards and QC samples. For the metabolites it can be assumed that spiked samples appropriately model their stability in study samples. Stock solutions of dal-ester, dal-S-Me and dal-S-Glu were stable for at least 3 months in the refrigerator and 6 months at −25 °C (Table 4). Loss of dal-thiol occurred after storage of dal-ester solutions or matrix spikes in direct sunlight (≥50% after 1 h), all solutions, standards and samples were therefore protected from light. Furthermore, depending on the time interval between matrix spiking and sample preparation, irretrievable degradation of dal-ester occurred in EDTA and heparin plasma older than 2 months. However, when sample preparation was performed at room temperature within 1 h of spiking, recovery of dal-thiol was complete without significant difference between EDTA and heparin, and independent of blank plasma storage time before spiking. Nevertheless, standards and QCs were prepared in heparin plasma less than 1 month old, and study samples were collected using heparin as anticoagulant. For some animal screening studies EDTA was used, and sample workup was performed within 30 min.

Dal-thiol, dal-S-Me and dal-S-Glu proved stable in human heparin plasma and in human urine (containing Tween 80) for at least three freeze-thaw cycles, 20 h at room temperature and 6 months at −25 °C. Substances were stable in injection solutions in the autosampler for at least 54 h (Table 4). Dal-thiol was stable in EDTA hamster and cynomolgus monkey plasma for 3 months at −20 °C while dal-S-Me and dal-S-Glu were stable in rat, cynomolgus monkey, mouse and dog heparin plasma for ≥3 freeze-thaw cycles, 20 h at room temperature and 6 months at −25 °C (data on file).

Table 5
Stability of dal-thiol in (A) pooled incurred EDTA plasma samples using Method 1 and in (B) pooled incurred heparin plasma samples; each expressed as mean concentration loss % for repeat *versus* original determination A.

A

	Mouse	Rat	Cynomolgus monkey
18 h at room temperature	−9.3	−7.2	−13.5
6 weeks at −20 °C	−12.9	−6.3	+0.2

B

Concentration pool	Dog Low/high	Rat Low/high	Cynomolgus monkey Low/high	Mouse Low/high	Human
Room temperature	10.7/−4.0 (24 h)	−12.7/−11.5 (24 h)	−0.3/−7.2 (25.5 h)	−8.5/2.7 (24 h)	−3.6 (18 h)
−25 °C	1.9/−7.2 (3 months)	−9.9/−12.1 (7 months)	−10.4/−4.8 (12 months)	3.4/−13.3 (7 months)	−6.2 (3 months)

3.5.8. Incurred sample stability

To reliably determine appropriate storage conditions and time frames for test samples, the stability of dal-thiol was assessed in study samples by comparing repeat values after various storage periods with original data from fresh samples. No significant decrease of dal-thiol was apparent in pooled plasma samples containing either EDTA (Table 5A) or heparin (Table 5B) from different species.

4. Conclusion

The hydrolysis of dalcetrapib-thioester to the thiol and formation of a disulfide is rapid under physiological conditions. *In vitro* data indicated that the individual forms are in redox equilibrium with each other *via* the thiol and could not be stabilized without influencing the equilibrium. Reliable quantitation could only be achieved by reducing all forms (thiol, disulfides, dal-ester) under basic conditions and analyzing total 'active form' (dal-thiol) after total cleavage of disulfide bonds with DTT and derivatization. Derivatization with NEM provided stability and sufficient response in mass spectrometric detection. The derivatization procedures had no impact on the dal-S-Me and dal-S-Glu metabolites which could be determined together with dal-thiol.

Online solid-phase extraction *via* column-switching and LC–MS/MS provided a robust, simple, selective and rapid method to determine dal-thiol and its dal-S-Me and dal-S-Glu metabolites. Sufficient sensitivity, minimal matrix effects and excellent recoveries were obtained without elaborate off-line sample preparation. Good reproducibility of repeated analyses and incurred samples stability strengthened the reliability of the method. This method is in use for all preclinical and clinical studies of dalcetrapib.

Acknowledgments

The authors thank Dr. Berthold Lausecker for support and discussions, and Swiss BioAnalytics (Birsfelden, Switzerland) for contributions to method development and validation. Medical writing support was provided by Prime Healthcare Ltd. with support from F. Hoffmann-La Roche Ltd.

References

[1] G.G. Schwartz, A.G. Olsson, C. Ballantyne, P.J. Barter, I.M. Holme, D. Kallend, L.A. Leiter, E. Leitersdorf, J.J. McMurray, P.K. Shah, J-C. Tardif, B.R. Chaitman, R. Duttlinger-Maddux, J. Mathieson, dal-OUTCOMES Committees and Investigators, rationale and design of the dal-OUTCOMES trial: efficacy and safety of dalcetrapib in patients with recent acute coronary syndrome, Am. Heart J. 158 (2009) 896–901.

[2] K. Shimada, K. Mitamura, Derivatization of thiol-containing compounds, J. Chromatogr. B 659 (1994) 227–241.

[3] K. Matsuura, K. Murai, Y. Fukano, H. Takashina, Simultaneous determination of tiopronin and its metabolites in rat blood by LC–ESI–MS–MS using methyl acrylate for stabilization of thiol group, J. Pharm. Biomed. Anal. 22 (2000) 101–109.

[4] M. Takahashi, H. Pang, K. Kawabata, N.A. Farid, A. Kurihara, Quantitative determination of clopidogrel active metabolite in human plasma by LC–MS/MS, J. Pharm. Biomed. Anal. 48 (2008) 1219–1224.

[5] K. Hayashi, M. Miyamoto, Y. Sekine, Determination of captopril and its mixed disulphides in plasma and urine by high-performance liquid chromatography, J. Chromatogr. 338 (1985) 161–169.

[6] H. Okamoto, F. Yonemori, K. Wakitani, T. Minowa, K. Maeda, H. Shinkai, A cholesterol ester transfer protein inhibitor attenuates atherosclerosis in rabbits, Nature 406 (2000) 203–207.

[7] O. Kuhlmann, K. Heinig, Dalcetrapib pharmacokinetics and metabolism in the Cynomolgus monkey, Xenobiotica 41 (2011) 430–436.

[8] M. Derks, R. Busse-Reid, O. Kuhlmann, A. Paehler, [^{14}C]-dalcetrapib ADME following a single oral dose in healthy male subjects, Clin. Pharmacol. Ther. 87 (2010) S24.

[9] N.R. Srinivas, R.N.V.S. Mamidi, Bioanalytical considerations for drugs containing free sulfhydryl groups, Biomed. Chromatogr. 17 (2003) 285–291.

[10] R.E. Hansen, J.R. Winther, An introduction to methods for analyzing thiols and disulfides: reactions, reagents, and practical considerations, Anal. Biochem. 394 (2009) 147–158.

[11] T. Toyo'oka, Recent advances in separation and detection methods for thiol compounds in biological samples, J. Chromatogr. B 877 (2009) 3318–3330.

[12] B. Seiwert, U. Karst, Simultaneous LC/MS/MS determination of thiols and disulfides in urine samples based on differential labeling with ferrocene-based maleimides, Anal. Chem. 79 (2007) 7131–7138.

[13] US FDA. Guidance for Industry: Bioanalytical Method Validation. Rockville, MD, USA: US Department of Health and Human Services, FDA, Center for Drug Evaluation and Research, 2001. www.fda.gov/downloads/Drugs/GuidanceComplianceRegulatoryInformation/Guidances/UCM070107.pdf.

[14] European Medicines Agency. Draft Guideline on Validation of Bioanalytical Methods. EMEA/CHMP/EWP/192217/2009 (2009) www.ema.europa.eu/pdfs/human/ewp/19221709en.pdf.

[15] B.A. Mansoori, D.A. Volmer, R.K. Boyd, Wrong-way-round electrospray ionization of amino acids, Rapid Commun. Mass Spectrom. 11 (1997) 1120–1130.

[16] L. Peng, T. Farkas, Analysis of basic compounds by reversed-phase liquid chromatography–electrospray mass spectrometry in high-pH mobile phases, J. Chromatogr. A 1179 (2008) 131–144.

[17] E. Stokvis, H. Rosing, L. López-Lázaro, I. Rodriguez, J.M. Jimeno, J.G. Supko, J.H. Schellens, J.H. Beijnen, Quantitative analysis of the novel depsipeptide anticancer drug Kahalalide F in human plasma by high-performance liquid chromatography under basic conditions coupled to electrospray tandem mass spectrometry, J. Mass Spectrom. 37 (2002) 992–1000.

[18] K. Heinig, T. Wirz, M. Yuan, M. Tingler, W. Mylott, Determination of taspoglutide in plasma and urine using ultra-performance liquid chromatography and tandem mass spectrometry with wrong-way-round electrospray ionization, J. Biomed. Chromatogr. 25 (2011) 1215–1221.

[19] M. Jemal, D.J. Hawthorne, High performance liquid chromatography/ionspray mass spectrometry of N-ethylmaleimide and acrylic acid ester derivatives for bioanalysis of thiol compounds, Rapid Commun. Mass Spectrom. 8 (1994) 854–857.

[20] M. Jemal, S. Khan, D.S. Teitz, J.A. McCafferty, D.J. Hawthorne, LC/MS/MS determination of omapatrilat, a sulfhydryl-containing vasopeptidase inhibitor, and its sulfhydryl- and thioether-containing metabolites in human plasma, Anal. Chem. 73 (2001) 5450–5456.

[21] C. Chen, L. Bajpai, N. Mollova, K. Leung, Sensitive and cost-effective LC–MS/MS method for quantitation of CVT-6883 in human urine using sodium dodecylbenzenesulfonate additive to eliminate adsorptive losses, J. Chromatogr. B 877 (2009) 943–947.

[22] W. Li, S. Luo, H.T. Smith, F.L.S. Tse, Quantitative determination of BAF312, a S1P-R modulator, in human urine by LC–MS/MS: prevention and recovery of lost analyte due to container surface adsorption, J. Chromatogr. B 878 (2010) 583–589.

[23] K. Heinig, T. Wirz, Determination of taspoglutide in human and animal plasma using liquid chromatography–tandem mass spectrometry with orthogonal column-switching, Anal. Chem. 81 (2009) 3705–3713.

[24] R. Głowacki, D. Gryglik, K. Kuśmierek, E. Bald, Urinary mesna and total mesna measurement by high performance liquid chromatography with ultraviolet detection, Talanta 66 (2005) 534–539.

[25] K. Kuśmierek, G. Chwatko, R. Głowacki, E. Bald, Determination of endogenous thiols and thiol drugs in urine by HPLC with ultraviolet detection, J. Chromatogr. B 877 (2009) 3300–3308.

Journal of Pharmaceutical and Biomedical Analysis 66 (2012) 325–333

Contents lists available at SciVerse ScienceDirect

Journal of Pharmaceutical and Biomedical Analysis

journal homepage: www.elsevier.com/locate/jpba

A new UPLC-MS/MS method for the determination of irinotecan and 7-ethyl-10-hydroxycamptothecin (SN-38) in mice: Application to plasma and brain pharmacokinetics

Lauriane Goldwirt[a,b,*], Florian Lemaitre[a,b], Noel Zahr[a], Robert Farinotti[a,b], Christine Fernandez[a,b]

[a] Pitié Salpetrière Hospital – AP-HP, Pharmacy Department, 47, Boulevard de l'hôpital, 75013 Paris, France
[b] Clinical Pharmacy Department – EA 4123, College of Pharmacy, Paris 11 University, 5, rue Jean Baptiste Clement, 92296 Chatenay Malabry, France

ARTICLE INFO

Article history:
Received 31 December 2011
Received in revised form 2 April 2012
Accepted 4 April 2012
Available online 11 April 2012

Keywords:
Irinotecan
SN-38
LC–MS/MS
Pharmacokinetics
Brain distribution
Carboxylesterase

ABSTRACT

A sensitive and accurate liquid chromatography method with mass spectrometry detection using MRM in positive ion mode was developed and validated for the simultaneous quantification of irinotecan (CPT-11) and 7-ethyl-10-hydroxycamptothecin (SN-38) in mouse plasma and brain. Camptothecin (CPT) was used as internal standard. A single step protein precipitation was used for plasma sample preparation, and a liquid–liquid extraction was needed for brain sample preparation. The method was validated with respect to selectivity, extraction recovery, linearity, intra- and inter-day precision and accuracy, limit of quantification and stability.

Limits of quantification were 5 ng/mL for CPT-11 and SN-38 in plasma samples and 1.25 ng/g in brain. Linear calibration curves were obtained over concentration ranges of 5–5000 ng/mL in plasma and 1.25–1250 ng/g in brain for CPT-11 and SN-38. The intra-day and inter-day variation (relative standard deviation, R.S.D.) found to be less than 15% for both substances in both media. Stability studies showed that plasma carboxylesterase had to be inactivated in order to prevent in vitro conversion of CPT-11 into SN-38. Zinc sulfate (1 M) was used to inactivate the enzyme before sample storage. Brain samples did not require enzyme inactivation. This method was successfully applied to perform brain and plasma pharmacokinetic studies of CPT-11 and SN-38 in mice after intraperitoneal administration.

© 2012 Elsevier B.V. All rights reserved.

1. Introduction

Irinotecan (CPT-11), 7-ethyl-10-[4-(1-piperidino)-1-piperidino]carbonyloxycamptothecin, is a semisynthetic analog of a naturally occurring alkaloid, camptothecin (CPT) (Fig. 1). It acts by inhibiting DNA topoisomerase I [1]. In humans, CPT-11 is metabolized by an endogenous carboxylesterase-mediated hydrolyzation into a highly active metabolite, 7-ethyl-10-hydroxycamptothecin (SN-38). SN-38 is further converted to inactive glucuronide by UGT1A (uridine diphosphate glucuronosyltransferase) [2]. Chemical structures of CPT-11 and SN-38 are displayed in Fig. 1. SN-38 is a few log orders more cytotoxic than the parent molecule [3].

In humans, carboxylesterases (CEs) are present in intestinal mucosa, plasma, liver and also in brain [4]. They catalyze the hydrolysis of esters, amides and thioesters and play an important role in endobiotic and xenobiotic metabolism. Previous studies showed that CPT-11 would rapidly converted to SN-38 after in vitro incubation in mouse or rat serum, plasma or tissue homogenate, since rats and mice, the two most widely used animal models in pharmacokinetic studies, express high levels of CEs in their plasma which differs markedly between humans and rodents [5–7].

CPT-11 has been marketed for the treatment of colorectal cancer for both first- and second line-therapy and for other solid tumours [8]. CPT-11 has also shown activity against brain tumour (glioblastoma, neuroblastoma) [9,10].

The lactone form of CPT-11 and SN-38 has a closed α-hydroxy-δ-lactone ring, which can be hydrolyzed to form the open-ring hydroxyl acid (carboxylate form). As the rate of hydrolysis of lactone to carboxylate is dependent on pH, ionic strength) and protein concentration [11,12], we chose to convert and quantify CPT-11 and SN-38 as total lactone forms. Various methods have been developed for the analysis of CPT-11 in several types of biological samples plasma, whole blood, and tissues (kidney, liver, spleen, lung, heart, intestine and tumour, but none of them was applied to CPT-11 and SN-38 analysis in brain pharmacokinetics, furthermore, there was no description of CPT-11 stability in brain tissue [13,14]. However, as CPT-11 is used in brain tumour treatment, its quantification in brain during animal experiments is of major interest in order

* Corresponding author at: Clinical Pharmacy Department – EA 4123, College of Pharmacy, Paris 11 University, 5 rue Jean Baptiste Clement, 92296 Chatenay Malabry, France.
E-mail address: lauriane.goldwirt@u-psud.fr (L. Goldwirt).

0731-7085/$ – see front matter © 2012 Elsevier B.V. All rights reserved.
http://dx.doi.org/10.1016/j.jpba.2012.04.003

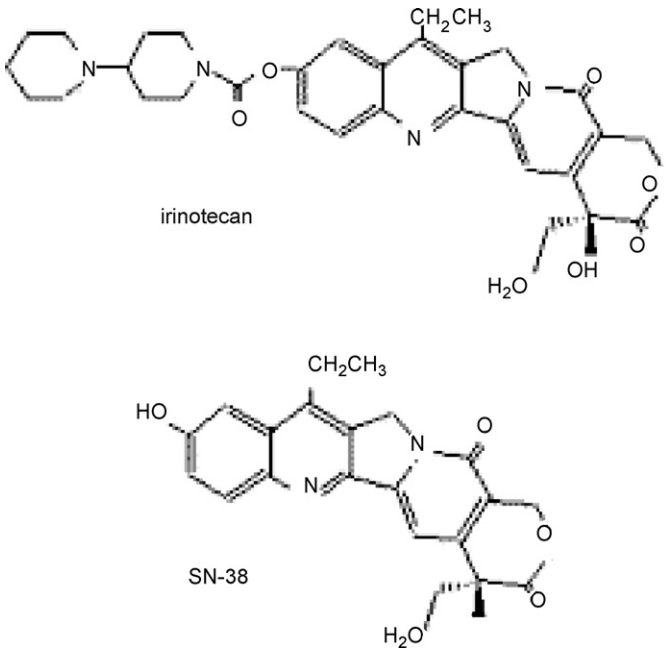

Fig. 1. Chemical structure of CPT-11 and SN-38.

to assess how the drug is distributed in the central nervous system. The understanding of the whole brain distribution can lead to solutions to overcome drug resistance.

Many quantification methods were developed using high-performance liquid chromatography (HPLC) with fluorimetric detection, or liquid chromatography tandem mass spectrometry (LC–MS/MS) [13,15–17] after solid-phase extraction or multi-step liquid–liquid extraction [18,19]. In order to reach an optimized lower limit of quantification for CPT11 and SN-38, liquid chromatography with tandem mass spectrometry was chosen to set this new quantification method in mice plasma and brain. This method was applied to the pharmacokinetic study of CPT-11 and SN-38 after intraperitoneal administration of CPT-11.

2. Materials and methods

2.1. Chemical reagents and animals

CPT-11 ((*S*)-4,11-diethyl-3,4,12,14-tetrahydro-4-hydroxy-3,14-dioxo-1H-pyrano[3′,4′:6,7]indolizino[1,2-b]quinolin-9-ylester), (purity ≥99%), SN-38 (7-ethyl-10-hydroxycamptothecin) (purity ≥98%) and (S) (+) camptothecin (internal standard, IS) (95% purity) were purchased from Sigma–Aldrich Corporation (St. Louis, MO). LC grade acetonitrile (>99.8%), LCMSMS grade water, and zinc sulfate ($ZnSO_4{\cdot}7H_2O$) for analysis were purchased from Merck (Darmstadt, Germany). Formic acid (The Second Reagent Factory, Shanghai, China) was of analytical grade. Ammonium acetate AnalaR Normapur Reagent was purchased from VWR BDH Prolabo (Haasrode, Belgium).

Female Swiss mice of 20–30 g were purchased from Janvier Laboratories (France). Studies involving animals and their care were performed according to the guidelines issued by the European Economic Community for the care and use of laboratory animals (Official Journal of the European Community, 18/2/86-authorization L3600) and according to our animal facility recommendations. Water and food were freely available throughout the studies. At the end of the experiments, animals were anesthetized using isoflurane, their blood was collected by cardiac puncture, they were sacrificed by cervical dislocation and brain was removed. Brain was washed using a 0.9% sodium chloride solution and immediately stored at −20 °C.

2.2. Instrument and analytical conditions

Chromatography was performed on an Acquity UPLC system (Waters Corp., Milford, MA, USA) with an autosampler temperature of 6 °C. Separation was performed at 25 °C on a Waters Acquity UPLC BEH C18 column (2.1 mm × 50 mm, 1.7 μm particle size) with a linear gradient elution using ammonium acetate buffer (10 mM; pH 3.5) with 0.1% formic acid (A) and acetonitrile (B) as the mobile phase. The elution program was as follows: 20% B (initial), 20–70% B (3 min), 70–98% B (0.2 min), 98% B (0.7 min), and 98–20% B (0.2 min). The flow rate was 0.4 mL/min and the injection volume was 20 μL. Solid–liquid extraction of plasma samples was performed with Isolute C18 500 mg/10 mL H (XL) cartridge (Biotage, Sweden).

Mass spectrometric detection was performed on an Acquity Tandem Quadripole Detector (Waters Corp., Milford, MA, USA) in positive ESI mode. Nitrogen was used as the desolvation gas (900 L/h) and cone gas (30 L/h). For collision-induced dissociation, argon was used as the collision gas at a flow rate of 0.22 mL/min. The cone voltage and collision energy were set at 30 V and 60 eV for CPT-11, 30 V and 40 eV for SN-38, and 30 V and 30 eV for camptothecin used as internal standard (IS). The other parameters were as follows: capillary voltage, 3.0 kV; source temperature, 120 °C; desolvation temperature, 350 °C. Quantitation was performed using multiple reaction monitoring (MRM) of the transitions of m/z 587.49 → 167.11 for CPT-11 lactone, m/z 393.37 → 249.23 for SN-38 lactone and m/z 349.28 → 305.30 for IS.

2.3. Calibration standards and quality control sample preparation

Individual stock solutions of CPT-11 (1 mg/mL), SN-38 (1 mg/mL) and IS (1 mg/mL) were prepared by accurately weighing the required amounts into separate volumetric flasks and dissolving in methanol for CPT-11 and dimethylsulfoxide for SN-38 and IS. CPT-11, SN-38 and IS stock solutions were stored at −20 °C and were stable at least 3 months.

Intermediate working and final working solutions containing CPT-11 and SN-38 were extemporaneously prepared in an ammonium acetate buffer (10 mM; pH 3.5)/acetonitrile mixture (80/20).

Plasma calibration standards and quality controls (CQ) were prepared by spiking blank plasma with the appropriate amount of working solutions. Plasma CQ samples were prepared at four concentrations of 5, 50, 500 and 5000 ng/mL, and calibration standards were prepared at 7 concentrations ranging from 5 ng/mL to 10,000 ng/mL.

Brain calibration standards and quality controls were prepared by spiking 400 mg blank brain aliquots with 100 μL of appropriate working solutions before tissue homogenization. Brain CQ samples were prepared at four concentrations of 1.25; 12.5; 125 and 1250 ng/g, and calibration standards were prepared at 7 concentrations ranging from 1.25 to 1250 ng/g.

2.4. Sample preparation

2.4.1. Plasma sample preparation

The IS solution (200 μL, 500 ng/mL in acetonitrile) was added to 100 μL of plasma, 50 μL of ammonium acetate buffer (10 mM; pH 3.5). Twenty microL of zinc sulfate (1 M) was added in stabilized plasma samples. The mixture was then precipitated with 200 μL of methanol and 200 μL of zinc sulfate (100 mM). After vortex mixing for 1 min, the samples were centrifuged at 15,000 rpm

for 15 min. Twenty microL of the supernatant were injected into the chromatographic system.

2.4.2. Brain sample preparation

The IS solution (200 μL, 500 ng/mL in acetonitrile) was added to small slices of brain (400 mg) (calibration and CQ samples were previously spiked with CPT-11 and SN-38 working solutions), which were individually homogenized using an Ultraturax® with 2.5 mL of ammonium acetate buffer (10 mM; pH 3.5) and 2.5 mL of zinc sulfate (100 mM), and then centrifuged at 4000 rpm for 10 min at 25 °C. The supernatant was transferred into an Isolute solid–liquid extraction column, previously conditioned by acetonitrile and ammonium acetate buffer (10 mM; pH 3.5). After rinsing the column with 2 mL of ammonium acetate buffer (10 mM; pH 3.5), elution was performed with 4 mL of acetonitrile. Samples were evaporated to dryness under a nitrogen stream at ambient temperature. The dry residue was reconstituted with 250 μL of 80/20 ammonium acetate buffer/acetonitrile mixture and 20 μL were injected in the chromatographic system.

2.5. Method validation

The analytical methodology was validated according to the guidelines outlined in the US Food and Administration guidance for industry on bioanalytical method validation [20,21]. As part of the validation, assay precision, accuracy, recovery, linearity, specificity and stability were assessed.

2.5.1. Specificity

Specificity was assessed by analyzing blank plasma and brain homogenates ($n = 6$), blank plasma and brain homogenates spiked with CPT-11 and SN-38 ($n = 6$).

2.5.2. Linearity of calibration curves and lower limits of quantification

Calibration curves were generated by plotting the peak area ratios (analyte/internal standard) versus the theoretical concentration. Linearity of the calibration curve was evaluated by a linear regression analysis using a $1/(\text{concentration})^2$ weighting.

The lower limit of detection (LLOD) was defined as the amount of CPT-11 and SN-38 that could be detected with a signal-to-noise ratio of 3. The lower limit of quantification (LLOQ) was defined as the lowest drug concentration that could be determined with a relative error and precision (relative standard deviation, R.S.D.) of less than 20%.

2.5.3. Precision and accuracy

Intra-day assay accuracy and precision were established through the performance of five replicates of the QC samples at the four concentrations described. Inter-day assay accuracy and precision were established through the performance of five consecutive intra-day runs. Assay accuracies were evaluated by the deviation of the mean concentration measurement of the replicates versus the theoretical concentration value expressed as a percentage (%Bias). Assay precisions were evaluated from the relative standard deviation (RSD) of the concentration measurements and expressed as the percent coefficient of variation (% CV) from the mean concentration of the replicates. Intra- and inter-run accuracies and precisions for QC concentrations of less than or equal to ±15% were deemed to be acceptable.

2.5.4. Recovery and matrix effect

Extraction recoveries in mice plasma for the two analytes (CPT-11 and SN-38) were determined at the four levels of QC. They were calculated as the ratio of analyte peak area from extracted QC plasma to mean peak area from extracted blank plasma spiked with the neat solutions.

The matrix effect variation (plasma and brain) was evaluated using extracted blank samples prepared from different mice plasma and brain spiked with the analytes at four QCs concentrations. Matrix effects for the compounds (CPT-11 and SN-38) were determined as the ratio of analyte peak area from extracted blank plasma and brain spiked with the neat solutions to the mean peak area of the neat solutions at the same concentration prepared in solvent ammonium acetate (10 mM; pH 3.5)–acetonitrile (80:20, v/v).

2.6. Carboxylesterase inhibition

2.6.1. Plasma carboxylesterase inhibition for stability experiments

Several conditions for carboxylesterase inhibition were assessed to prevent the post sample-collection transformation of CPT-11 into its active metabolite SN-38 in plasma. Five hundred microL fresh mouse plasma samples were spiked with 100 μL of CPT-11 (50 μg/mL). Twenty microL of zinc sulfate (1 M) were added to 100 μL plasma for enzyme inactivation.

The conditions tested without inactivation were immediate analysis, immediate freezing and analysis after a freeze-thaw cycle, analysis after 24 h of storage at room temperature, and analysis after 1 h of storage at 4 °C.

To assess carboxylase inactivation zinc sulfate (1 M) was added at $t = 0$ min after spiking fresh mice plasma with CPT-11. Analysis was performed on stabilized plasma samples kept 1 h at 4 °C and on stabilized plasma samples after a freeze-thaw cycle.

Results are expressed as molar ratios of SN-38/(CPT-11 + SN-38).

2.6.2. Brain carboxylesterase inhibition

In order to expose CPT-11 to brain carboxylesterase, mice brains were homogenized left 1 h at ambient temperature before extraction and analysis: NaCl (0.9%) to preserve physiological conditions, and zinc sulfate (100 mM)–ammonium acetate buffer (10 mM; pH 3.5) (50:50, v/v) to assess the technique condition. Samples were analyzed in five replicates and results were expressed as molar ratios of SN-38/(CPT-11 + SN-38).

2.7. Pharmacokinetic analysis and brain distribution study

Swiss mice were treated by intraperitoneal route with a single dose of irinocan (40 mg/kg), and sacrificed at 0.5, 0.75, 1, 1.5, 2, 4, 6 and 8 h post-injection (3 mice per time point). Blood was collected via cardiac puncture with a heparinized syringe and drawn in polyethylene tubes. Samples were immediately centrifuged at 5000 rpm for 15 min and plasma removed, stabilized with zinc sulfate (1 M) and stored at −20 °C until analysis. Brains were collected and directly frozen at −20 °C in polyethylene tubes. CPT-11 levels in mice plasma and brains were measured using their respective assay procedures as described above. The pharmacokinetic parameters $t_{1/2}$ (biological half-life), and AUC_{0-t} (area under curve from time 0 to the last measured concentration calculated using the trapezoidal rule) (WinNonlin; Pharsight Corporation, Mountain View, Calif). T_{max} (the time to reach peak concentration) was obtained from the time point corresponding to peak concentration of CPT-11 and SN-38 in mice plasma. C_{max} (the peak concentration) was determined directly from concentration versus time plot.

3. Results and discussion

3.1. Optimization of MS conditions

CPT-11, SN-38 and camptothecin were scanned with ESI positive ion mode following analysis of standard lactone solutions. CPT-11 yielded a quasi-molecular ion with an m/z 587.49 $[M+H]^+$,

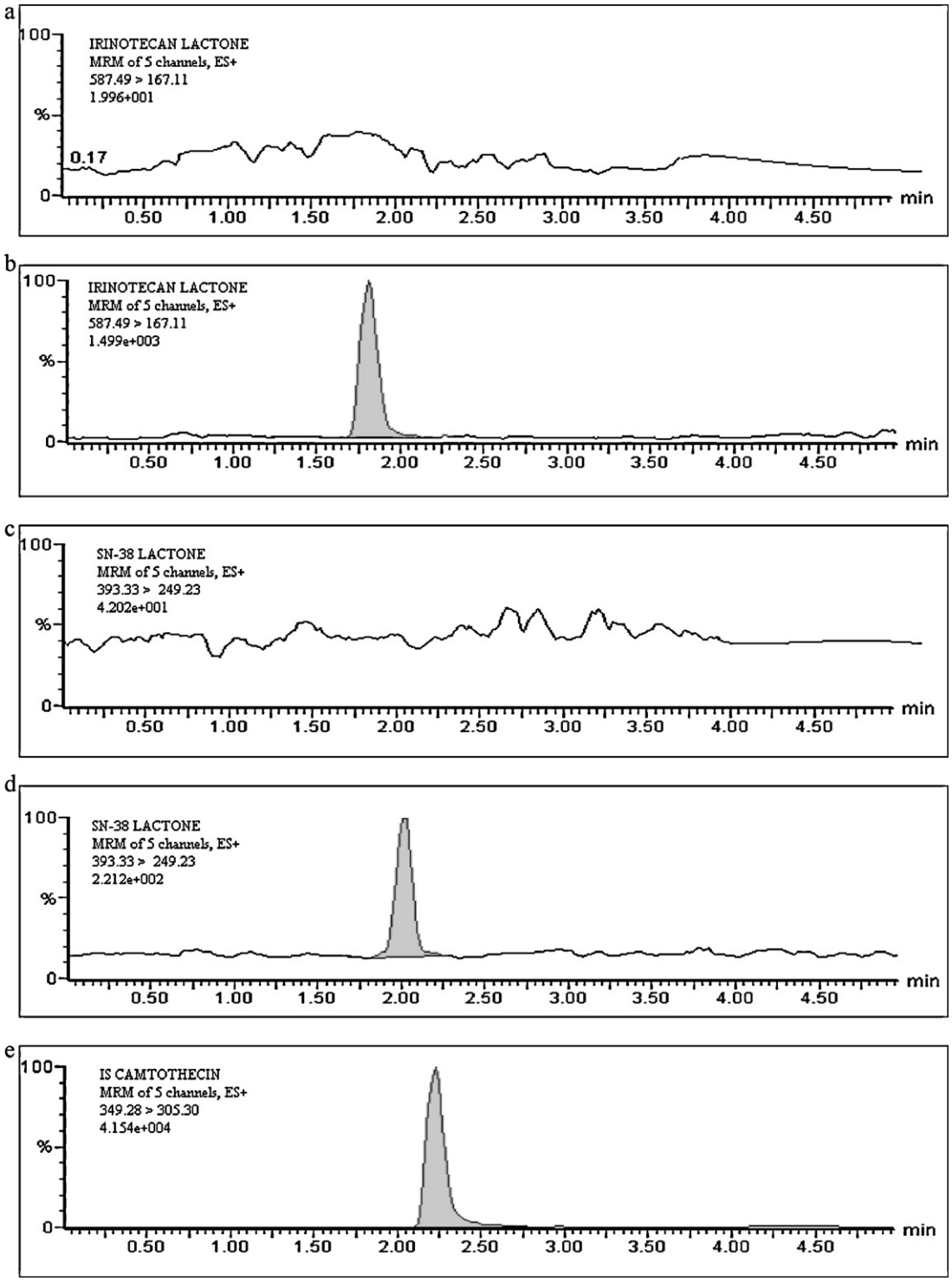

Fig. 2. Chromatograms of CPT-11 and SN-38 in plasma. (a and c) Blank plasma samples corresponding to CPT-11 and SN-38 analysis, respectively. (b and d) Plasma samples spiked with 5 ng/mL of CPT-11 and SN-38 (LLOQ). (e) Internal standard (for chromatographic conditions, see text).

SN-38 an m/z 393.37 $[M+H]^+$, while the IS molecule showed a quasi-molecular ion with m/z 349.28 $[M+H]^+$. These ions were chosen as parent ions for fragmentation in the MRM mode. The product ions m/z 167.11, m/z 249.23 and m/z 305.30 were selected as the target ions of CPT-11, SN-38 and IS, respectively. The collision energy in the LC–MS/MS mode was modulated to optimize the sensitivity, and the optimal values were found to be 60, 40 and 30 eV for CPT-11, SN-38 and IS, respectively. Source temperature and desolvation temperature were set at 120 °C and 350 °C, respectively.

3.2. Chromatographic conditions

The LC mobile phase was optimized by testing various percentages of organic solvent and different modifiers in water. The addition of acid base modifiers – ammonium acetate buffer (10 mM; pH 3.5) with 0.1% formic acid – to the mobile phase improved the sensitivity by promoting the ionization of CPT-11, SN-38 and IS. To achieve symmetrical peak shapes, good resolution and a short chromatographic run time, a mobile phase consisting

Table 1
Standard curves, correlation coefficients and linear ranges of CPT-11 and SN-38 in different samples (for chromatographic conditions, see text).

Biosample	Molecule	Standard curve ($n = 6$)	Correlation coefficient (r^2)	Linear range
Plasma	CPT-11	$0.0103x + 0.00694$	0.999805	5–5000 (ng/mL)
	SN-38	$0.0011x + 0.00265$	0.998024	5–5000 (ng/mL)
Brain	CPT-11	$0.000423x + 0.001068$	0.995389	1.25–1250 (ng/g)
	SN-38	$0.000591x + 0.001147$	0.992794	1.25–1250 (ng/g)

Table 2a
Precision, accuracy, extraction recovery and matrix effect for irinotecan and SN-38 in plasma samples and brain tissue of mice (for chromatographic conditions, see text).

Biosamples	QC concentration (ng/mL)	Intra-day ($n = 5$)		Inter-day ($n = 5$)		Mean extraction recovery (%)	Matrix effect (%)
Plasma		Precision (R.S.D. %)	Accuracy (mean %)	Precision (R.S.D. %)	Accuracy (mean %)		
CPT-11	5	7.3	90.9	11.9	93.0	107.9	65.4
	50	12.7	96.2	14.8	97.7	91.2	132.9
	500	11.6	102.2	9.7	98.2	104.3	114.9
	5000	1.2	101.3	12.2	109.7	85.8	128.5
SN-38	5	5.7	101.6	8.8	101.0	97.5	120.0
	50	9.5	87.8	9.6	86.1	89.0	137.6
	500	6.1	98.6	14.4	96.2	93.0	127.8
	5000	5.4	100.8	6.7	97.3	101.4	117.0
Biosamples	QC concentration (ng/g)	Intra-day ($n = 5$)		Inter-day ($n = 5$)		Mean extraction recovery (%)	Matrix effect (%)
Brain		Precision (R.S.D. %)	Accuracy (mean %)	Precision (R.S.D. %)	Accuracy (mean %)		
CPT-11	1.25	3.9	98.0	5.1	102.3	4.2	93.8
	12.5	6.4	96.2	8.4	98.2	5.5	106.1
	125	3.7	115.8	7.7	111.2	5.3	101.1
	1250	6.6	94.4	9.3	93.4	6.1	114.4
SN-38	1.25	5.3	96.7	5.8	100.7	19.8	340.8
	12.5	5.8	91.6	9.1	93.9	36.4	304.9
	125	2.4	87.9	3.5	87.8	33.7	313.5
	1250	4.8	92.9	4.3	88.6	38.5	286.7

R.S.D.: relative standard deviation.
CPT11: irinotecan.
SN-38: 7-ethyl-10-hydroxycamptothecin.

Table 2b
Precision, accuracy for irinotecan and SN-38 in plasma samples stabilized with zinc sulfate.

Biosamples	QC concentration (ng/mL)	Intra-day ($n = 5$)		Inter-day ($n = 5$)	
Plasma		Precision (R.S.D. %)	Accuracy (mean %)	Precision (R.S.D. %)	Accuracy (mean %)
CPT-11	5	10.1	101.6	12.9	98.4
	50	6.2	108.3	6.5	91.7
	500	2.4	109.8	4.1	90.2
	5000	4.7	98.9	7.1	101.1
SN-38	5	10.8	88.7	15.1	111.3
	50	7.1	110.9	7.9	89.1
	500	4.4	105.8	5.3	94.2
	5000	6.4	89.1	10.1	110.9

R.S.D.: relative standard deviation.
CPT11: irinotecan.
SN-38: 7-ethyl-10-hydroxycamptothecin.

Table 3
Carboxylesterase inhibition assays in mouse plasma.

Time of inactivation with $ZnSO_4$ (1 M)	Sample storage conditions before analysis	Molar ratio: SN-38/(CPT-11 + SN-38) (%) ($n = 3$)		
		Mean		Sd
No inactivation	No storage, immediate analysis	0.519	±	0.001
	One freeze thaw cycle	12.27	±	0.001
	24 h at room temperature	99.89	±	0.001
	1 h at +4 °C	13.03	±	0.005
With inactivation occurring at $t = 0$ min	Analysis after 1 h at +4 °C following inactivation	1.155	±	0.001
	One freeze thaw cycle	1.627	±	0.003

CPT11: irinotecan.
SN-38: 7-ethyl-10-hydroxycamptothecin.

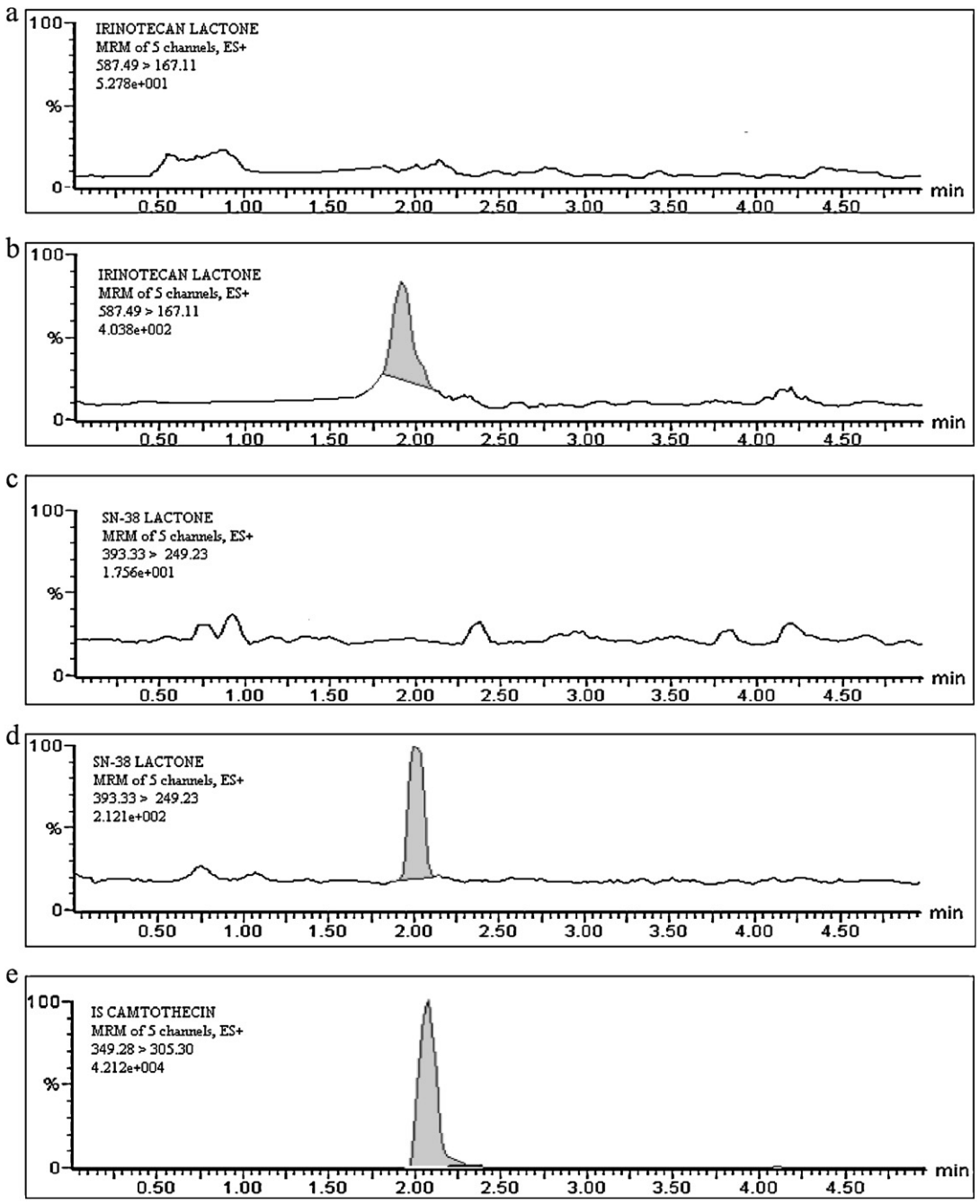

Fig. 3. Chromatograms of CPT-11 and SN-38 in brain. (a and c) Blank brain samples corresponding to CPT-11 and SN-38 analysis, respectively. (b and d) Brain samples spiked with 1.25 ng/g of CPT-11 and SN-38 (LLOQ). (e) Internal standard (for chromatographic conditions, see text).

of acetonitrile and ammonium acetate buffer (10 mM; pH 3.5) with 0.1% formic acid was used in the experiments. With a mobile phase gradient, retention times were 1.8, 2.1 and 2.3 min for lactone forms of CPT-11, SN-38 and IS respectively, which were short and suitable for high throughput sample determination in pharmacokinetic studies.

In order to insure total lactonization of all components, it was necessary to be able to detect carboxylate forms. An infusion of CPT-11 and SN-38 carboxylate solutions in methanol was used to determine their transitions: m/z 605.39 → 303.46 for CPT-11 carboxylate, m/z 411.30 → 347.35 for SN-38 carboxylate. Carboxylate forms of CPT-11 were chromatographically separated from lactone form but identified as lactone forms in the detection system, due to the high source temperature involving a loss of H_2O. This was not observed for SN-38 carboxylate forms. Retention times of CPT-11 and SN-38 carboxylate in the chromatographic system were 0.9 and 1.2 min respectively (Figs. 2 and 3). Throughout the development and validation of the assay, it was possible to ensure that the lactonization of the samples was complete and stable during pre-treatment, chromatographic separation and MRM detection, because no carboxylate (neither CPT-11 nor SN-38) was detected.

3.3. Method validation

The selectivity assays ($n = 6$ for brain and plasma) showed that there was no endogenous interference at the retention times of CPT-11, SN-38, and IS. The calibration curves of the peak area (Y) to the concentration (C) were constructed using $1/x^2$ weighted

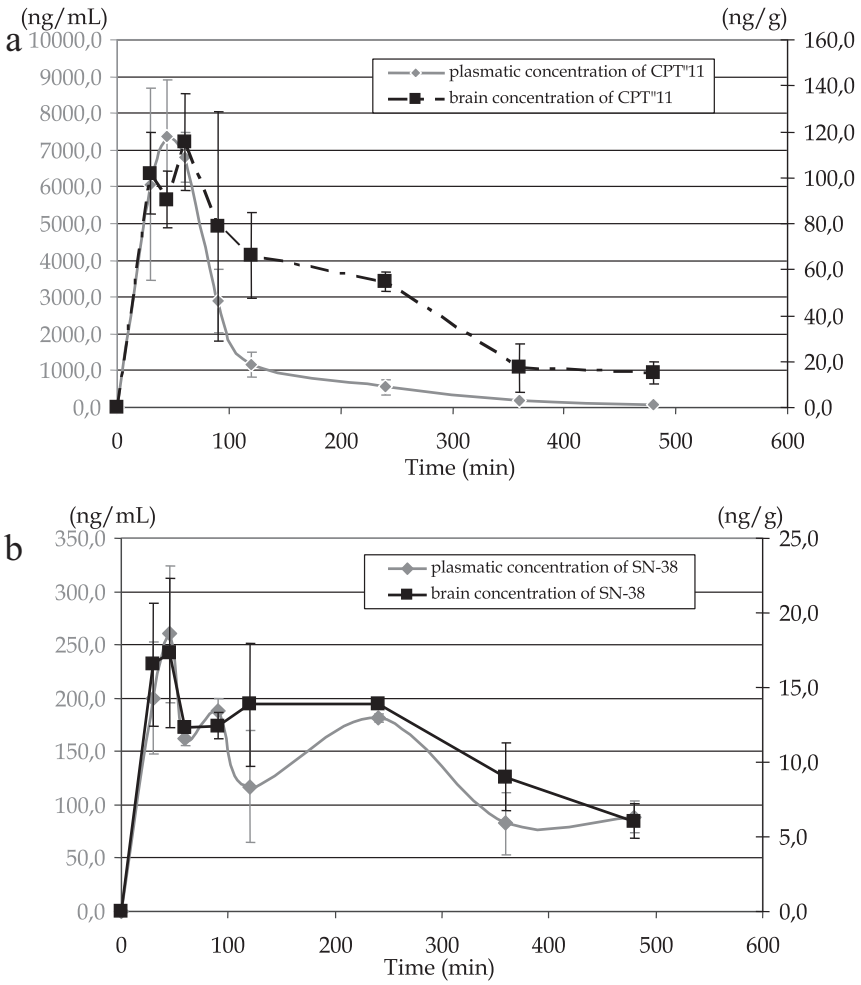

Fig. 4. Concentration–time profiles of CPT-11 (CPT-11) (a) and SN-38 (b) in plasma and brain tissue following intraperitoneal administration of CPT-11 (40 mg/kg) in mice (mean ± s.e.m.; $n = 3$).

linear least-square regression models. The calibration curves ($n = 6$), correlation coefficients and linear ranges of CPT-11 and SN-38 in plasma and brain tissue are listed in Table 1. The calibration curves were prepared daily and showed good linearity in the corresponding range for CPT-11 and SN-38 ($r^2 > 0.99$).

The current assay offered an LLOQ of 5 ng/mL in plasma and 1.25 ng/g in brain tissue. The limits were sufficient for pharmacokinetics and tissue distribution studies following a single intraperitoneal administration (40 mg/kg) of CPT-11.

Accuracy and precision assessed by analyzing QC samples at different concentrations ($n = 5$) are presented in Table 2a (plasma without inactivation and brain samples). Accuracy and precision were also assessed in plasma stabilized with zinc sulfate (1 M), as presented in Table 2b. The results suggested that this method was accurate and reproducible for the quantification of CPT-11 and SN-38 in mice plasma and brain tissue.

Extraction recoveries and matrix effect are shown in Table 2a. Extraction recoveries for CPT-11 and SN-38 in brain were low but reproducible and compatible with in vivo analysis. The extraction procedure of CPT-11 and SN-38 in brain samples was developed taking into account the imperatives to ensure an extraction yield adequate for a sufficient detection and the lack of brain matrix traces (lipids, proteins). Solid–liquid extraction responded to these imperatives, and although the extraction yield of irinotecan and SN-38 is small, it remains compatible with the limit of detection.

The low recovery of SN-38 brain extraction procedure contributes to the high matrix effect reported. Overlap between the matrix and SN-38 is responsible for this huge matrix effect. However, this matrix effect was reproducible and did not alter accuracy or precision. With this method, the recovery was quite low for SN-38 in brain, despite several attempts, improving this extraction recovery was not possible. Other techniques (liquid–liquid extraction single-step protein precipitation) were tested but unsuccessfully as they exhibit higher extraction recoveries but much lower specificity, incompatible with LC-MS/MS analysis.

3.4. Carboxylesterase inhibition

Considering the high activity of carboxylesterase in mice plasma, inactivating this enzyme rapidly after collection was a major concern. Several conditions to inhibit carboxylesterases were assessed to prevent the post sample-collection transformation of CPT-11 into its active metabolite SN-38 in mouse plasma and brain tissue.

3.4.1. Carboxylesterase inhibition in mouse plasma

The main purpose was to find a reagent able to inactivate the enzyme and compatible with MS/MS practice. Results are presented in Table 3 and are expressed as the ratio between the number of moles of SN-38 newly formed and the number of moles of CPT-11 initially present, which is the number of moles of CPT-11 dosed into the sample added to the quantity of newly formed SN-38.

Table 4
Pharmacokinetic parameters of CPT-11 and SN-38 following peritoneal administration of 40 mg/kg of CPT-11 to mice ($n = 27$).

		$t_{1/2}$ (min)	T_{max} (min)	C_{max} (ng/mL or ng/g)	AUC (min ng/mL) or (min ng/g)
CPT-11	Plasma	80	45	7363	646,086
	Brain	130	90	245	42,345
SN-38	Plasma	346	45	260	63,465
	Brain	272	45	41	10,370

CPT11: irinotecan.
SN-38: 7-ethyl-10-hydroxycamptothecin.

With a 99.89% conversion of CPT-11 into SN-38 in samples stored during 24 h at room temperature, the post-collection inactivation of mouse plasma carboxylesterase appeared to be essential. Freezing samples is not effective enough to inactivate the enzyme (12.27% transformation). In fact, thawing reactivates the enzyme which is not denatured at low temperature (−20 °C). These results show that 13.03% of CPT-11 is converted into SN-38 within 1 h versus 1.155% when zinc sulfate (1 M) is added. Hence, adding zinc sulfate (1 M) inactivates carboxylesterase (the only enzyme responsible for hydrolysis of irinotecan into SN-38) and stops SN-38 production.

To date, only two methods for the quantification of CPT-11 and SN-38 in rat or mouse plasma with enzyme inactivation have been described [15,22]. Nevertheless, it was not possible for us to use sodium dodecyl sulfate, or phosphate buffer as described in these studies, because of the concentration at which they had to be used was incompatible with MSMS detection. Conversely, zinc sulfate exhibits a strong capacity of protein denaturation, and it is compatible with mass spectrometry analyses. As no reactivation occurs in plasma samples stabilized with zinc sulfate (1 M) after thawing. Zinc sulfate (1 M) can be considered as an efficient mice plasma carboxylesterase denaturant.

3.4.2. Carboxylesterase inhibition in mouse brain tissue

As no transformation of CPT-11 into SN-38 occurred in brain samples homogenized in NaCl (0.9%) left 1 h at ambient temperature, nor in zinc sulfate, it has been concluded that no carboxylesterase activity occurred in brain homogenates. Although enzymatic activity of murine cerebral carboxylesterase has been described in literature [23], these results show that CPT-11 was stable under our sample storage conditions but do not mean that CPT-11 could not be metabolized in vivo into SN-38 in mouse brain.

3.5. Pharmacokinetics and tissue distribution study

The validated analytical method was successfully applied to a pharmacokinetic study after intraperitoneal administration of CPT-11 to mice (40 mg/kg by intraperitoneal route). CPT-11 and SN-38 were detected throughout the pharmacokinetic study. Plots of CPT-11 and SN-38 plasma and brain concentrations versus time are displayed in Fig. 4a and b respectively. After intraperitoneal injection of CPT-11, plasma and brain C_{max} were observed. CPT-11 and SN-38 pharmacokinetics profiles show an enterohepatic circulation previously reported in the literature (Fig. 4) [24]. T_{max} in plasma and brain are close showing that CPT-11 rapidly crosses the blood brain barrier. The main pharmacokinetic parameters were calculated (Table 4). AUC brain to AUC plasma ratios for CPT-11 and SN-38 are found to be 6.55% and 16.3% respectively. High AUC brain/AUC plasma of SN-38 could be explained by (1) in situ metabolism of CPT-11 or (2) by an efflux transport from brain back to plasma lower for SN-38 than for CPT-11, as these drugs are both substrates of many efflux transporters (i.e. P-glycoprotein, BCRP) [25]. Up to date, comparison of CPT-11 and SN-38 affinity with efflux transporters has never been described.

4. Conclusion

The UPLC–MS/MS method described in this paper is a simple, rapid and reliable method for the determination of CPT-11 and SN-38 in mouse plasma and brain tissue. Storage and extraction procedures were optimized in order to limit in vitro conversion of CPT-11 into SN-38. This method was successfully applied to pharmacokinetics and tissue distribution studies after CPT-11 intraperitoneal administration. This method is currently being applied to study the influence of drug combination on CPT-11 brain distribution.

References

[1] S. Basili, S. Moro, Novel camptothecin derivatives as topoisomerase I inhibitors, Expert Opin. Ther. Pat. 19 (2009) 555–574.
[2] A. Sparreboom, M.J. de Jonge, P. de Bruijn, E. Brouwer, K. Nooter, W.J. Loos, R.J. van Alphen, R.H. Mathijssen, G. Stoter, J. Verweij, Irinotecan (CPT-11) metabolism and disposition in cancer patients, Clin. Cancer Res. 4 (1998) 2747–2754.
[3] R.H.J. Mathijssen, R.J. van Alphen, J. Verweij, W.J. Loos, K. Nooter, G. Stoter, A. Sparreboom, Clinical pharmacokinetics and metabolism of irinotecan (CPT-11), Clin. Cancer Res. 7 (2001) 2182–2194.
[4] M. Hosokawa, Structure and catalytic properties of carboxylesterase isozymes involved in metabolic activation of prodrugs, Molecules 13 (2008) 412–431.
[5] T. Tsuji, N. Kaneda, K. Kado, T. Yokokura, T. Yoshimoto, D. Tsuru, CPT-11 converting enzyme from rat serum: purification and some properties, J. Pharmacobiodyn. 14 (1991) 341–349.
[6] J.A. Crow, A. Borazjani, P.M. Potter, M.K. Ross, Hydrolysis of pyrethroids by human and rat tissues: examination of intestinal, liver and serum carboxylesterases, Toxicol. Appl. Pharmacol. 221 (2007) 1–12.
[7] N. Kaneda, H. Nagata, T. Furuta, T. Yokokura, Metabolism and pharmacokinetics of the camptothecin analogue CPT-11 in the mouse, Cancer Res. 50 (1990) 1715–1720.
[8] M. Potmesil, Camptothecins: from bench research to hospital wards, Cancer Res. 54 (1994) 1431–1439.
[9] H.S. Friedman, W.P. Petros, A.H. Friedman, L.J. Schaaf, T. Kerby, J. Lawyer, M. Parry, P.J. Houghton, S. Lovell, K. Rasheed, T. Cloughsey, E.S. Stewart, O.M. Colvin, J.M. Provenzale, R.E. McLendon, D.D. Bigner, I. Cokgor, M. Haglund, J. Rich, D. Ashley, J. Malczyn, G.L. Elfring, L.L. Miller, Irinotecan therapy in adults with recurrent or progressive malignant glioma, J. Clin. Oncol. 17 (1999) 1516–1525.
[10] M.D. Prados, K. Lamborn, W.K.A. Yung, K. Jaeckle, H.I. Robins, M. Mehta, H.A. Fine, P.Y. Wen, T. Cloughesy, S. Chang, M.K. Nicholas, D. Schiff, H. Greenberg, L. Junck, K. Fink, K. Hess, J. Kuhn, A phase 2 trial of irinotecan (CPT-11) in patients with recurrent malignant glioma: a North American Brain Tumor Consortium study, Neuro Oncol. 8 (2006) 189–193.
[11] J. Fassberg, V.J. Stella, A kinetic and mechanistic study of the hydrolysis of camptothecin and some analogues, J. Pharm. Sci. 81 (1992) 676–684.
[12] T.G. Burke, Z.H. Mi, Preferential binding of the carboxylate form of camptothecin by human serum albumin, Anal. Biochem. 212 (1993) 285–287.
[13] S. Bardin, W. Guo, J.L. Johnson, S. Khan, A. Ahmad, J.X. Duggan, J. Ayoub, I. Ahmad, Liquid chromatographic-tandem mass spectrometric assay for the simultaneous quantification of Camptosar and its metabolite SN-38 in mouse plasma and tissues, J. Chromatogr. A 1073 (2005) 249–255.
[14] F.A. de Jong, R.H.J. Mathijssen, P. de Bruijn, W.J. Loos, J. Verweij, A. Sparreboom, Determination of irinotecan (CPT-11) and SN-38 in human whole blood and red blood cells by liquid chromatography with fluorescence detection, J. Chromatogr. B: Analyt. Technol. Biomed. Life Sci. 795 (2003) 383–388.
[15] Z. Zhang, J. Yao, X. Wu, J. Zou, J. Zhu, An accurate assay for simultaneous determination of irinotecan and its active metabolite SN-38 in rat plasma by LC with fluorescence detection, Chromatographia 70 (2009) 399–405.
[16] M. Ramesh, P. Ahlawat, N.R. Srinivas, Irinotecan and its active metabolite, SN-38: review of bioanalytical methods and recent update from clinical pharmacology perspectives, Biomed. Chromatogr. 24 (2010) 104–123.
[17] H. Sumiyoshi, Y. Fujiwara, T. Ohune, N. Yamaoka, K. Tamura, M. Yamakido, High-performance liquid chromatographic determination of irinotecan (CPT-11) and its active metabolite (SN-38) in human plasma, J. Chromatogr. B: Biomed. Sci. Appl. 670 (1995) 309–316.
[18] I. Barilero, D. Gandia, J.-P. Armand, A. Mathieu-Boué, M. Ré, A. Gouyette, G.G. Chabot, Simultaneous determination of the camptothecin analogue CPT-11 and its active metabolite SN-38 by high-performance liquid chromatography: application to plasma pharmacokinetic studies in cancer patients, J. Chromatogr. B: Analyt. Technol. Biomed. Life Sci. 575 (1992) 275–280.
[19] L.P. Rivory, M. Findlay, S. Clarke, J. Bishop, Trace analysis of SN-38 in human plasma by high-performance liquid chromatography, J. Chromatogr. B: Biomed. Sci. Appl. 714 (1998) 355–359.
[20] Guidance for Industry: Bioanalytical Method Validation, 2001, http://fda.gov/cder/guidance/index.htm.

[21] V.P. Shah, K.K. Midha, J.W.A. Findlay, H.M. Hill, J.D. Hulse, I.J. McGilveray, G. McKay, K.J. Miller, R.N. Patnaik, M.L. Powell, A. Tonelli, C.T. Viswanathan, A. Yacobi, Bioanalytical method validation—a revisit with a decade of progress, Pharm. Res. 17 (2000) 1551–1557.
[22] A. Kurita, N. Kaneda, High-performance liquid chromatographic method for the simultaneous determination of the camptothecin derivative irinotecan hydrochloride, CPT-11, and its metabolites SN-38 and SN-38 glucuronide in rat plasma with a fully automated on-line solid-phase extraction system, PROSPEKT, J. Chromatogr. B: Analyt. Technol. Biomed. Life Sci. 724 (1999) 335–344.
[23] S.M. Ghiasuddin, D.M. Soderlund, Hydrolysis of pyrethroid insecticides by soluble mouse brain esterases, Toxicol. Appl. Pharmacol. 74 (1984) 390–396.
[24] I. Younis, S. Malone, H. Friedman, L. Schaaf, W. Petros, Enterohepatic recirculation model of irinotecan (CPT-11) and metabolite pharmacokinetics in patients with glioma, Cancer Chemother. Pharmacol. 63 (2009) 517–524.
[25] N.F. Smith, W.D. Figg, A. Sparreboom, Pharmacogenetics of irinotecan metabolism and transport: an update, Toxicol. In Vitro 20 (2006) 163–175.

Journal of Pharmaceutical and Biomedical Analysis 66 (2012) 334–338

Contents lists available at SciVerse ScienceDirect

Journal of Pharmaceutical and Biomedical Analysis

journal homepage: www.elsevier.com/locate/jpba

Short communication

Quantitation of slow release triptorelin in beagle dog plasma by liquid chromatography–tandem mass spectrometry

Jiangbin Han[a], Jiye Sun[a], Chunjie Sha[a], Jinfeng Zhang[b], Yunyun Gai[a], Youxin Li[a], Wanhui Liu[a,b,*]

[a] State Key Laboratory of Long-acting and Targeting Drug Delivery System, Shandong Luye Pharmaceutical Co. Ltd, Yantai 264003, PR China
[b] School of Pharmacy, Yantai University, Yantai 264003, PR China

ARTICLE INFO

Article history:
Received 27 December 2011
Received in revised form 18 February 2012
Accepted 23 February 2012
Available online 3 March 2012

Keywords:
Triptorelin
LC–MS/MS
Quantitation
Pharmacokinetics
Plasma

ABSTRACT

A sensitive method based on liquid chromatography–tandem mass spectrometry has been developed for the determination of triptorelin levels in beagle dog plasma. Plasma samples were applied to Oasis® HLB solid-phase extraction (SPE) cartridges. Extracted samples were evaporated under a stream of nitrogen and then reconstituted with 100 μl methanol:water:formic acid (60:40:0.08, v/v/v). The separation was achieved on a Venusil MP-C18 column (2.1 mm × 50 mm, 3 μm, Agela) with a gradient elution. Detection utilized a Qtrap5500 system operated in the positive ion mode with multiple reaction monitoring of the analyte at m/z 656.5 → 249.1 and of the I.S. at m/z 510.8 → 120.1. The proposed method was validated by assessing the specificity, linearity, precision and accuracy, recovery, matrix effects, and stability. Linear calibration curves were obtained in the concentration range of 0.01–10 ng/ml (the correlation coefficients were above 0.995). The lower limit of quantification (LLOQ) of the method was 0.01 ng/ml. The method was successfully applied to a pharmacokinetic study of a slow release triptorelin formulation in beagle dogs following a single intramuscular injection.

Crown Copyright © 2012 Published by Elsevier B.V. All rights reserved.

1. Introduction

Peptides and proteins are becoming increasingly common pharmacotherapies for the treatment of many human diseases. For example, peptides are emerging as a novel class of therapeutic agents in the pharmaceutical industry, especially in cancer chemotherapy. Peptide therapeutic agents are often synthetic analogs of endogenous peptides, such as hormones or neurotransmitter peptides.

Recent findings have suggested that the regression of various hormone-dependent disorders and of prostate tumors can be achieved after the administration of luteinizing hormone–releasing hormone (LHRH) agonists [1–4]. Natural LHRH is rapidly degraded in the blood (elimination $t_{1/2}$, 3–4 min) by enzymatic cleavage at position 6, position 10, or both; however, the replacement of the amino acids at these positions allowed the synthesis of analogs with enhanced resistance to enzymatic degradation, resulting in a 10–200-fold increased potency compared with natural LHRH [5,6]. Among these analogs, triptorelin ([D-Trp6]-LHRH) has been widely used, and its biological and clinical effects are well documented [7].

Triptorelin, 5-oxoPro-His-Trp-Ser-Tyr-D-Trp-Leu-Arg-Pro-Gly-NH_2, is a synthetic peptide used in hormonal therapy for the treatment of prostate cancer. This peptide inhibits the production of hormones by the pituitary gland, leading to a reduction in the level of the male hormone testosterone. Prostate cancer is often sensitive to the levels of these hormones in the body, and reducing the levels of these hormones may result in slowing of the growth of the cancer [8].

Although expected effects are obtained with daily injections of triptorelin, depot formulations are needed to increase the flexibility of administration; this increased flexibility will increase the convenience for patients and possibly improve patient compliance. A microsphere-based, slow release formulation of triptorelin acetate 3.75 mg has been developed. This formulation is injected intramuscularly, and the drug is released over 1 month.

With this type of formulation, the assessment of the release of and the plasma concentration of triptorelin is of particular importance to assure the desired biological effects.

Pharmacokinetic studies of triptorelin have been performed using a radioimmunoassay (RIA) [9], which was shown to be sensitive. The limit of detection (LOD) of this method was approximately 0.01 ng/ml using 500 μl of plasma. Nevertheless, this method has limitations due to the high cost and the cross-reactivity with structurally similar peptides, which interfere with the precise quantitation of the triptorelin level in plasma.

In the present study, we developed a highly specific and sensitive liquid chromatography–electrospray ionization tandem mass

* Corresponding author at: State Key Laboratory of Long-acting and Targeting Drug Delivery System, Shandong Luye Pharmaceutical Co. Ltd, Yantai 264003, PR China. Tel.: +86 535 3808288.
E-mail address: wanhui@luye.cn (W. Liu).

0731-7085/$ – see front matter Crown Copyright © 2012 Published by Elsevier B.V. All rights reserved.
doi:10.1016/j.jpba.2012.02.021

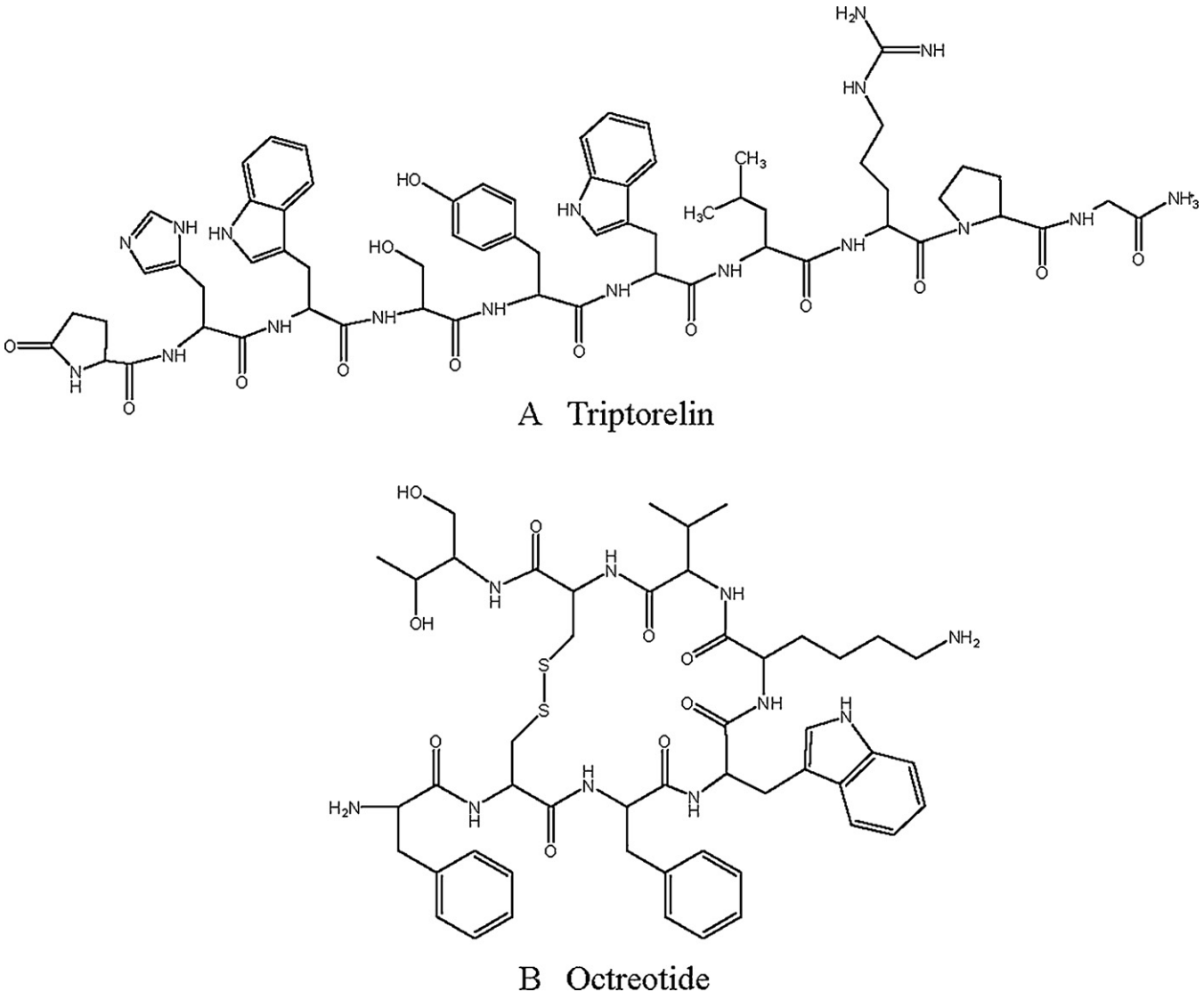

Fig. 1. Structures of (A) triptorelin and (B) octreotide (internal standard).

spectrometry (LC–ESI-MS/MS) method for the determination of triptorelin levels in beagle dog plasma, and we applied this method to the evaluation of the slow release profile of triptorelin acetate biodegradable microspheres after the intramuscular injection of 0.3 mg/kg per month (peptide base). To the best of our knowledge, this is the first report of the use of the LC–MS/MS method for the determination of the plasma concentration of triptorelin.

2. Experimental

2.1. Reagents and chemicals

Triptorelin acetate (peptide base content 86%,) was supplied by the National Institute for the Control of pharmaceutical and biological products (Beijing, PR China). Octreotide acetate (purity > 99%) (Fig. 1) for use as internal standard (I.S.) was purchased from Shanghai TASH Biotechnology (Shanghai, PR China). HPLC grade methanol was purchased from Merck Scientific (New Jersey, USA). HPLC grade formic acid and acetic acid were supplied by Fluka (St. Louis, MO, USA). Millipore Milli-Q gradient purified water (Molsheim, France) was used throughout the study. Oasis® HLB cartridges (30 mg, 1 cm^3) was purchased from Waters (Milford, MA, USA). Centrifuge tubes were supplied by Eppendorf (Hamburg, Germany).

2.2. Preparation of calibration standards and quality control (QC) samples

A stock solution of triptorelin acetate (containing triptorelin 1 mg/ml) in methanol–water–formic acid (80:20:0.04, v/v/v) was diluted with methanol–water–formic acid (60:40:0.08, v/v/v) to give a series of standard solutions with triptorelin concentrations in the range 0.01–10 ng/ml. A series of calibration standards was then prepared by spiking blank plasma samples (100 μl) with 100 μl of aliquots of standard solutions to give triptorelin concentrations in plasma of 0.01, 0.03, 0.1, 0.3, 1, 3 and 10 ng/ml. Low, medium and high QC samples were prepared by spiking blank plasma samples with QC solutions (0.03, 0.3 and 8 ng/ml) prepared independently in the same way.

2.3. Sample preparation

All frozen dog plasma samples were thawed at room temperature prior to preparation. After vortexing, 100 μl of IS solution (Octreotide, 5 ng/ml), 100 μl of methanol–water–formic acid (60:40:0.08, v/v/v), and 500 μl of methanol were added to 100 μl of plasma. The mixture was vigorously vortexed for 1 min and centrifuged at 15,000 × *g* for 10 min. The supernatant was

mixed with 600 μl of water and then transferred to an Oasis HLB SPE column, which had been previously activated by successive applications of 1 ml of methanol and 1 ml of Milli-Q water. The column was then washed with 1 ml of methanol–water (60:40, v/v). The peptide adsorbed on the two monomers (hydrophilic N-vinylpyrrolidone and lipophilic divinylbenzene) surface was eluted with 1 ml of methanol (containing 1% formic acid). The eluate was placed in the glass tubes and evaporated under a gentle stream of nitrogen at 40 °C. The residue was reconstituted in 100 μl of methanol–water–formic acid (60:40:0.08, v/v/v) solution. A 10 μl aliquot was transferred into the LC–MS/MS system.

2.4. LC–MS/MS

The HPLC system (Agilent 1290 series) consisted of a binary pump, an autosampler, a column oven maintained at 40 °C and a Venusil MP-C18 (2.1 mm × 50 mm, 3 μm, Ageale, TianJin, PR China). The mobile phase consisted of solvent A (0.02% acetic acid in MilliQ water) and solvent B (methanol) at a flow rate of 0.6 ml/min. The gradient involved: 10% B for 1.2 min; a linear increase to 60% B over 1.1 min; 60% B for 0.4 min, an increase to 98% B in 0.01 min; 98% B for 1.3 min (to wash the column); a decrease to 10% B in 0.01 min; and 10% B for 1.5 min (to equilibrate the column).

Detection was performed on a Qtrap 5500 mass spectrometer (Applied Biosystems Sciex, Ontario, Canada) with an ESI source operated in the positive ion mode. Multiple reaction monitoring (MRM) involved triptorelin at m/z 656.5 → 249.1 transition and octreotide at m/z 510.8 → 120.1 transition. Optimized MS conditions were as follows: curtain gas, gas 1 and gas 2 (all nitrogen) 35, 55 and 55 units respectively; ion spray voltage 5500 V; source temperature 575 °C; declustering potentials 50 V for triptorelin and 55 V for octreotide; collision energies 42 eV (m/z 656.5 → 249.1) and 90 eV (m/z 656.5 → 110.1) for triptorelin and 60 eV for octreotide.

2.5. Assay validation

Assay validation was performed according to FDA guidelines [10]. The specificity was determined by analyzing blank plasma samples from six different subjects. The linearity was assessed by weighted ($1/x^2$) least-squares linear regression of the analyte:I.S. peak area ratios for the calibration curves. The precision (represented by the relative standard deviation, RSD) and the accuracy (represented by the relative error, RE) were evaluated based on assay of the LLOQ, QC samples in three consecutive days, six replicates for each day. The matrix effects were evaluated by comparing the peak areas of the analyte in post-extraction spiked blank plasma samples with the peak areas of the standard solutions [11]. To evaluate the precision and accuracy of the method with respect to the sample dilution process, QC samples of 40 ng/ml were diluted five-fold before being analyzed in six replicates on the day of method validation. The recovery was determined by comparing the peak areas of the QC samples with the peak areas of the post-extraction spiked blank plasma. The stability of the stock solution at 4 °C for two months was evaluated. The long-term and short-term stability were studied by assaying samples after storage for one month at −35 °C and after storage at room temperature for 2 h, respectively. The stability during three successive freeze–thaw cycles and in processed samples stored at room temperature (25 °C) for 6 h was also evaluated.

2.6. Application of the method to a pharmacokinetic study in beagle dog

The method was applied to determine the plasma concentrations of triptorelin in healthy beagle dogs (males, $N = 5$) after the intramuscular injection of triptorelin acetate biodegradable microspheres (0.3 mg/kg peptide base). Blood samples (0.5 ml at each time point) were collected from the antebrachium vein prior to dosing and at 0.25, 1, 6, and 24 h, and 2, 3, 4, 6, 9, 11, 14, 16, 19, 23, 26, and 30 d after dosing. The plasma concentration–time profiles for triptorelin in each subject were analyzed by noncompartmental analysis using DAS 2.1.

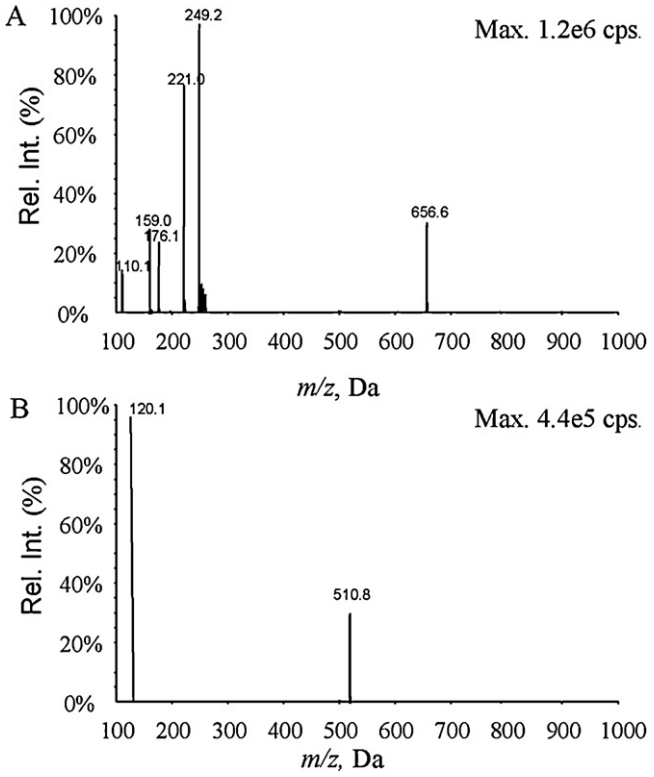

Fig. 2. Full-scan product ion scans of $[M+H]^{2+}$ for (A) triptorelin and (B) octreotide.

3. Results and discussion

3.1. Method development

The full-scan product ion spectra of the $[M+H]^{2+}$ ions of triptorelin and octreotide are shown in Fig. 2. Even though both the m/z 656.5 → 249.1 and m/z 656.5 → 110.1 transitions had the same signal in the extracted ion chromatogram when the collision gas (CAD) was set to 9 units, a better peak shape and a better signal-to-noise ratio were obtained for the m/z 656.5 → 249.1 transition than the m/z 656.5 → 110.1 transition due to the former having a higher selectivity. Thus, the m/z 656.5 → 249.1 transition was selected as the basis for quantification. The m/z 510.8 → 120.1 transition was used to monitor octreotide.

The chromatographic conditions were optimized based on the signal-to-noise and the peak shapes of the analyte and I.S. The Venusil MP-C18 column was chosen because it gave the best resolution and peak shapes. Mobile phase A solutions containing 0.02%, 0.05%, or 1.0% formic acid; 0.02%, 0.05%, or 1.0% acetic acid; or 0.01% or, 0.02% trifluoroacetic acid were evaluated. Either methanol or acetonitrile was used as mobile phase B and 0.02% acetic acid aqueous solution–methanol was selected because it provided the highest sensitivity. Using a flow rate of 0.6 ml/min, the retention times for the analyte and I.S. were 2.33 and 2.26 min, respectively.

Solid-phase extraction (SPE) was chosen as the sample preparation method. During the development of our method, we

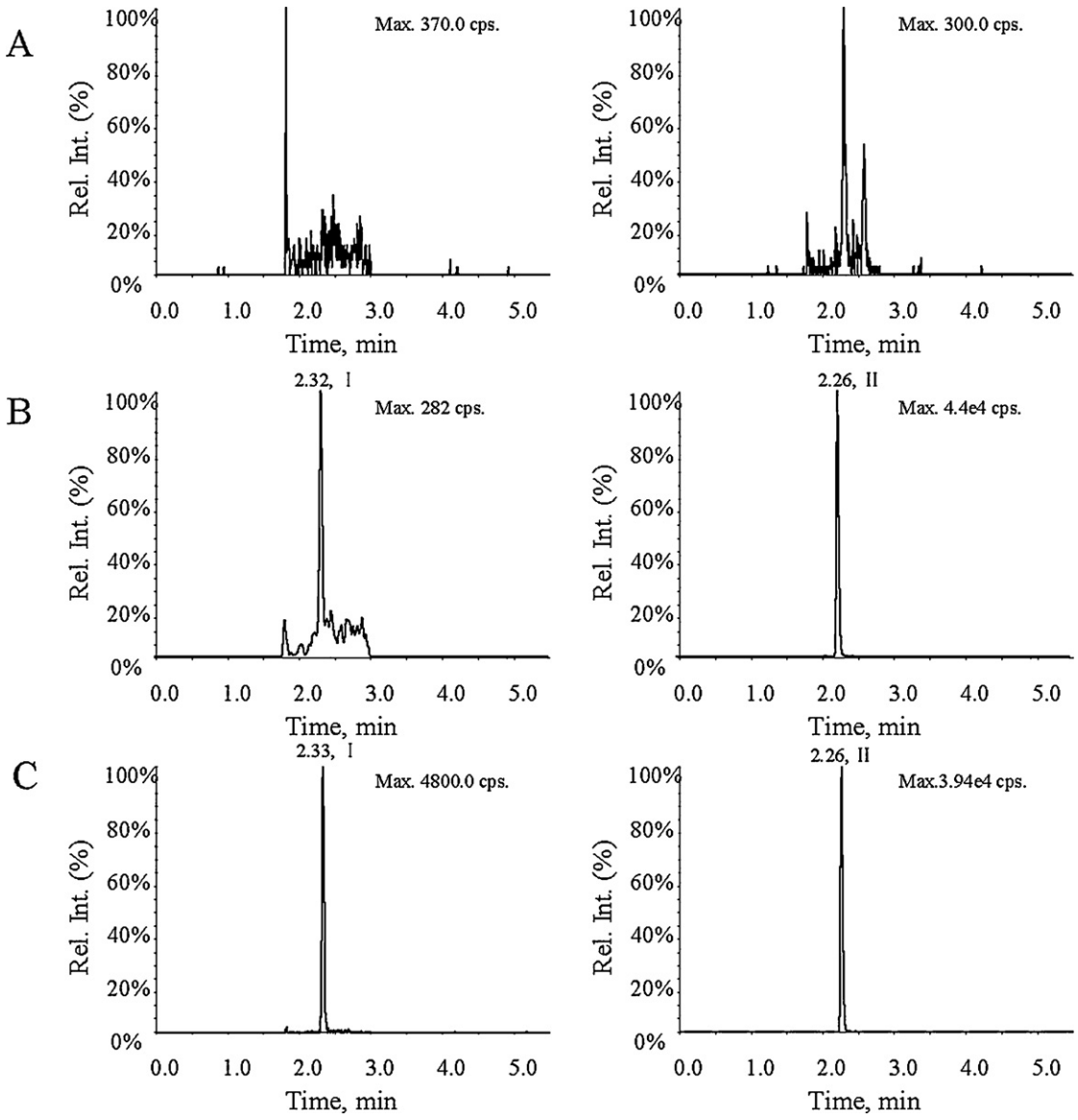

Fig. 3. Representative MRM chromatograms of triptorelin and octreotide in beagle dog plasma. (A) Blank plasma; (B) blank plasma spiked with 0.01 ng/ml triptorelin (I) and 5 ng/ml octreotide (II); (C) plasma sample from a beagle dog volunteer 6 d of triptorelin after intramuscular injection triptorelin acetate biodegradable microspheres 0.3 mg/kg (as peptide base).

investigated a variety of SPE cartridges (Oasis MAX cartridge, Oasis MCX cartridge, Oasis HLB cartridge) for plasma pre-treatment, and we optimized the different loading, washing and elution steps. The Oasis HLB cartridge provided a higher and more stable recovery than other SPE cartridges that we used. Compared with methanol, 1% formic acid in methanol could improve the recovery of triptorelin from the 40% to approximately 70% and was therefore was used as the elution solvent.

3.2. Method validation

The assay was found to be free from interference because there were no endogenous peaks in the plasma at the retention times of triptorelin and octreotide. Representative chromatograms of blank plasma, plasma spiked with triptorelin at the LLOQ (0.01 ng/ml) and a study sample taken 6 d after intramuscular injection of triptorelin acetate biodegradable microspheres are shown in Fig. 3. The assay was linear in the range of 0.01–10 ng/ml ($y = 0.561x + 0.000899$, $r = 0.9978$), with intra- and inter-day precisions of <13.8% and <14.8%, respectively, and an accuracy in the range of −1.05 to 1.52% (Table 1). The matrix effects were shown to be minimal based on the ratios of peak areas for triptorelin in the low, medium and high post-extraction spiked blank plasma samples to the peak areas in the corresponding standard solutions; these ratios were 104.7 ± 9.3%, 97.0 ± 2.8% and 104.9 ± 4.5%, respectively. The precision and accuracy of the dilution process were found to be acceptable, with an RSD < 3.96, an RE < −1.5%. The recoveries of triptorelin from the low, medium and high QC samples were also satisfactory, with concentrations of 70.6 ± 5.2%, 72.4 ± 1.2% and 64.0 ± 2.0% of the nominal values, respectively. In terms of stability (Table 2), triptorelin was shown to be stable under all of the conditions examined.

3.3. Pharmacokinetic study

The mean concentration–time profile of triptorelin after the intramuscular injection of triptorelin acetate biodegradable microspheres is shown in Fig. 4. The mean peak in the plasma

Table 1
Precision and accuracy for the determination of triptorelin in beagle dog plasma (in three consecutive days, six replicates for each day).

Spiked conc. (ng/ml)	Calculated conc. (mean ± SD, ng/ml)	Intra-day RSD (%)	Inter-day RSD (%)	Accuracy RE (%)
0.0100	0.0101 ± 0.0014	13.8	14.8	1.2
0.030	0.0301 ± 0.0023	7.09	10.03	0.39
0.300	0.305 ± 0.019	6.5	1.01	1.52
8.00	7.92 ± 0.44	3.64	2.98	−1.05

Table 2
Stability of triptorelin under various conditions (data are means ± SD of 3 replicates).

Storage conditions	Initial conc. (ng/ml)	Final conc. (ng/ml)	RE (%)
Beagle dog plasma at room temperature for 2 h	0.03	0.032 ± 0.001	5.6
	0.30	0.29 ± 0.02	−3.3
	8.00	8.01 ± 0.27	0.1
Processed samples at room temperature for 6 h	0.03	0.032 ± 0.001	7.9
	0.30	0.29 ± 0.01	−2.6
	8.00	7.80 ± 0.42	−2.5
Beagle dog plasma after three freeze/thaw cycles	0.03	0.031 ± 0.001	4.2
	0.30	0.30 ± 0.01	−0.9
	8.00	8.04 ± 0.25	0.5
Beagle dog plasma for 1 month at −35 °C	0.03	0.028 ± 0.001	−6.8
	0.30	0.29 ± 0.02	−4.1
	8.00	7.81 ± 0.36	−2.4
The stability of the stock solution for 2 months at 4 °C	0.03	0.032 ± 0.002	6.7
	0.30	0.31 ± 0.02	3.7
	8.00	8.47 ± 0.35	5.9

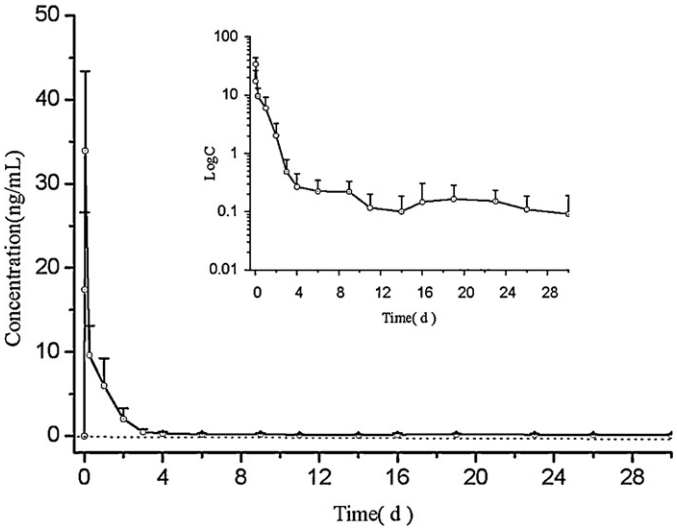

Fig. 4. Plasma concentration–time profile of intramuscular injection triptorelin acetate biodegradable microspheres 0.3 mg/kg (as peptide base) to healthy beagle dog. Data are mean + SD for 5 dogs (5 males).

concentration (C_{max}) was 33.9 ± 9.5 ng/ml at a time (T_{max}) of 1 h after the injection was given. The mean area under the plasma concentration–time curve (AUC_{0-t}) was 20.89 ± 7.44 ng d/ml and the mean elimination half-life ($t_{1/2}$) was 4.34 ± 1.47 d. From the first day to the third day following administration, the triptorelin plasma concentration continuously decreased from 33.9 ng/ml to 0.487 ng/ml, and then reached a plateau at concentrations of 0.091–0.268 ng/ml.

Acknowledgements

This work was supported by the National Basic Research Program of China (973 Program) (No. 2010CB735602 and No. 2012CB724003). We also would like to thank Taishan Scholar Projects for their kind support in the method development.

References

[1] T.W. Redding, G. Schally, Inhibition of prostate tumor growth in two rats models by chronic administration of D-Trp-6 analogue of luteinizing hormone–releasing hormone, Proc. Natl. Acad. Sci. U.S.A. 78 (1981) 6509–6512.
[2] W.R. Miller, W.N. Scott, R. Morris, M.M. Fraser, R.M. Sharpe, Growth of human breast cancer cells inhibited by a luteinizing hormone–releasing hormone agonist, Nature 313 (1985) 231–233.
[3] F. Labile, A. Belanger, A. Dupont, K. Edmond, Y. Lacoursiere, G. Monfette, Combined treatment with LHRH agonist and pure antiandrogen in advanced carcinoma of prostate, Lancet 84 (1984) 1090.
[4] A. Corbin, From contraception to cancer: a review of the therapeutic applications of LHRH analogues as antitumor agents, Yale J. Biol. Med. 55 (1982) 27–47.
[5] T.W. Redding, A.J. Kastin, D. Gonzales-Barcena, The half-life, metabolismand excretion of titrated luteinizing hormone–releasing hormone (LH–RH) in man, J Clin. Endocrinol. Metab. 37 (1973) 626–631.
[6] A.V. Schally, D.H. Coy, A. Arimura, LHRH agonists and antagonists, Int. Gynaecol. Obstet. 18 (1980) 318–324.
[7] A.V. Schally, A.M. Comaru-SchaUy, T.W. Redding, Antitumor effects of analogs of hypothalamic hormones in endocilne-dependent cancers, Proc. Soc. Exp. Biol. Med. 175 (1984) 259–281.
[8] H. Villavicencio, B.J. Rubio, R. Regalado, G. Chéchile, J. Palou, F. Algaba, Grade, local stage and growth pattern as prognostic factors in carcinoma of the penis, Eur. Urol. 32 (1997) 442–447.
[9] E. Eric, D. Katy, C. Maryvonne, R. Catherine, D. Fernand, Radioimmunoassay of [D-Trp6]-luteinizing hormone–releasing hormone: its application to animal pharmacokinetic studies after single injection and long-acting formulation administration, Regul. Pept. 14 (1986) 155–167.
[10] Guidance for Industry Bioanalytical Method Validation, U.S. Department of Health and Human Services, Food and Drug Administration, Center for Drug Evaluation and Research (CEDR), Center for Veterinary Medicine (CVM), BP, May 2001. http://www.fda.gov/cder/guidance/4252fnl.htm.
[11] W.M.A. Niessen, P. Manini, R. Andreoli, Matrix effects in quantitative pesticide analysis using liquid chromatography–mass spectrometry, Mass Spectrom. Rev. 25 (2006) 881–899.

Journal of Pharmaceutical and Biomedical Analysis 66 (2012) 339–344

Contents lists available at SciVerse ScienceDirect

Journal of Pharmaceutical and Biomedical Analysis

journal homepage: www.elsevier.com/locate/jpba

Short communication

Sample preparation method to minimize chemical shift variability for NMR-based urinary metabonomics of genetically hypertensive rats

Kazuki Akira*, Hiroyuki Hichiya, Maki Shuden, Mayu Morita, Hidemichi Mitome

College of Pharmaceutical Sciences, Matsuyama University, 4-2 Bunkyo-cho, Matsuyama, Ehime 790-8578, Japan

ARTICLE INFO

Article history:
Received 20 January 2012
Received in revised form 21 February 2012
Accepted 24 February 2012
Available online 3 March 2012

Keywords:
Metabonomics
Urine
pH
Chemical shift
NMR

ABSTRACT

Urinary metabonomics based on proton nuclear magnetic resonance (^{1}H NMR) has been widely employed to study metabolic differences associated with gene function and pathophysiological and toxicological stimuli. However, the chemical shift variability of ^{1}H NMR signals, which is due to differences in pH and ionic strength among urine samples, remains an outstanding problem for efficient data mining. Thus, we have proposed an improved sample preparation method where urine samples are lyophilized and reconstituted in a buffer solution (pH 7.40) so that the extent of urine concentration becomes constant based on creatinine concentration. In order to examine the usefulness of the proposed method, urine samples taken from spontaneously hypertensive rats (SHR) and stroke-prone SHR (SHRSP) were treated not only by the proposed method but also by the usual method where urine with various concentrations is mixed with an equivalent volume of buffer solution (pH 7.40). Consequently, the pH of the urine samples prepared by the proposed method was precisely controlled to 6.89–7.01, whereas the pH of samples by the usual method was in the range of 6.81–7.18. The chemical shift variations of various metabolites having ionizable groups such as succinate, α-ketoglutarate, *cis*-aconitate, taurine, and glycine were significantly reduced with decreases in pH variability. A preliminary multivariate statistical analysis was carried out for the ^{1}H NMR spectral data obtained by the proposed method, where the metabolic profiles were distinguished between the SHR and SHRSP. The proposed sample preparation method will be particularly useful to closely inspect NMR-based urinary metabonomic data for the exploration of metabolic changes.

© 2012 Elsevier B.V. All rights reserved.

1. Introduction

Metabonomics based on proton nuclear magnetic resonance (^{1}H NMR) and multivariate statistical analysis is an important approach for measuring metabolic responses for genetic and environmental factors [1–3]. This approach has been successfully applied to disease diagnosis and for the evaluation of drug toxicity [4].

In ^{1}H NMR-based metabonomic studies, urine is often analyzed because of the non-invasive nature and relatively high concentrations of metabolites. Although urine is a complex mixture of a wide range of organic compounds, it provides highly resolved ^{1}H NMR spectra and more ^{1}H resonances compared with plasma or serum [2]. However, chemical shift variability is well-known for various metabolites in urine samples because of the physiological variations of pH and ionic strength, which can lead to false interpretations of the metabonomic data [5–10]. Thus, in the standard procedures, the pH consistency is controlled by mixing urine with a buffer, and the ^{1}H NMR spectra are segmented into small buckets (<0.04 ppm) that are larger than the anticipated chemical shift variations and integrated to provide variables for the subsequent multivariate statistical analysis [10–12]. The optimal buffer concentrations [5,6] and sophisticated bucketing [10,13] have been investigated in a few research groups. Although these procedures are effective, the chemical shift variations across bucket borders due to the insufficient pH control and variable ionic strength are a significant problem for the multivariate analysis. This problem is more significant when smaller buckets or full resolution NMR data are used to enhance information output [9,14–16]. More sophisticated techniques such as peak alignment have been proposed to solve the problem of chemical shift variability [10,17]. However, these techniques are not always effective, especially for unknown signals and severely overlapping signals [6]. Thus, improved sample preparation is still required to reduce chemical shift variability.

In our laboratory, ^{1}H NMR-based urinary metabonomics has been applied to explore the metabolic changes characteristic of spontaneously hypertensive rats (SHR) and stroke-prone SHR (SHRSP), which are widely used as animal models for essential hypertension [18–20]. In the course of our studies, we have also noted the problem of chemical shift variability in urine samples, in spite of the combined use of a buffer solution and bucketing. Thus, it

* Corresponding author. Tel.: +81 89 926 7097; fax: +81 89 926 7162.
E-mail address: akira@cc.matsuyama-u.ac.jp (K. Akira).

0731-7085/$ – see front matter © 2012 Elsevier B.V. All rights reserved.
doi:10.1016/j.jpba.2012.02.020

was considered that one of the simplest approaches to solving this problem was to make urine concentration constant in a series of NMR measurements. In this paper, a sample preparation method has been proposed, where urine is lyophilized and reconstituted in a buffer so that the extent of the urine concentration becomes constant based on the urinary creatinine concentration, and the usefulness of the method has been investigated using urine from the SHR and SHRSP with regard to the chemical shift variability. In addition, the samples prepared by the proposed method were preliminarily subjected to ^{1}H NMR-based metabonomics of the two substrains.

2. Experimental

2.1. Animal experiments

Six male SHR/Izm and six male SHRSP/Izm aged seven weeks were purchased from Disease Model Cooperative Research Association (Kyoto, Japan). Animal studies were conducted under approved guidelines (Guidelines for Proper Conduct of Animal Experiments, Science Council of Japan, 2006) and were reviewed by an institutional animal use committee. Collection of 24 h urine and measurements of blood pressures were performed according to the method described previously [19], with the only exception that urine was collected from about 12 a.m. at 10 weeks of age. The volume of intact urine, including a small amount of washing water (1–2 ml) for the metabolism cages, was 8–13 ml and 13–22 ml for the SHR and the SHRSP, respectively. All urine samples were filtered through DISMIC-25CS filters (hydrophilic, pore size 0.20 μm; Advantec Toyo, Tokyo, Japan), and stored frozen at −80 °C until required for NMR spectroscopy and other analyses.

2.2. Sample preparation

In the usual sample preparation method [18–20], 350 μl of urine was mixed with 350 μl of a 0.2 M sodium phosphate buffer (pH 7.40) and 100 μl of D_2O containing sodium 3-trimethylsilyl[2,2,3,3-D_4]propionate (TSP, 424 μg/ml), and the supernatant (650 μl) after centrifugation (2400 × *g*, 15 min) was obtained for NMR measurements. The method proposed in this study was as follows. Seven-hundred microliters of urine were freeze-dried and the residue was reconstituted in a buffered solution, which was made by mixing a 0.1 M sodium phosphate buffer (pH 7.40) with D_2O in a ratio of 7:1 (v/v). Also, the buffered solution contained TSP as the chemical shift reference in a concentration of 49.6 μg/ml. The volume of buffered solution used for the reconstitution was adjusted to 0.8–2.0 ml so that the resulting creatinine concentration was 286 μg/ml, which was the creatinine concentration of a reconstituted sample from the SHRSP. This concentration corresponded to the higher level of the creatinine concentrations of the samples prepared by the usual method. The concentration of the phosphate buffer in the reconstituted samples was the same as in the samples prepared by the usual method. The reconstituted samples were centrifuged at 2400 × *g* for 15 min at 25 °C, and the supernatant (650 μl) placed in a 5-mm o.d. NMR tube was used for the NMR measurements.

2.3. ^{1}H NMR spectroscopy

^{1}H NMR was measured on a Bruker Avance 500 spectrometer (11.75 T) at a probe temperature of 300 K with the water resonance suppressed using a NOESYPRESAT pulse sequence [21]. Sixty-four free-induction decays were collected into 65,536 data points with a spectral width of 10,331 Hz, a 14.5 μs pulse width (90° pulse angle), an acquisition time of 3.172 s, and a relaxation delay of 3 s to ensure full T_1 relaxation. The spectra were Fourier transformed after application of a line-broadening function of 0.3 Hz and referenced to a chemical shift of TSP at δ 0.0. The assignments of the resonances were made on the basis of literature assignments [22,23] and standard additions.

2.4. Multivariate statistical analysis

All NMR spectra were phased, baseline corrected, and treated using AMIX software (version 3.9.7; Bruker BioSpin, Yokohama, Japan) as described previously [18–20]. The NMR spectra (δ 0.50–9.50) were automatically reduced to 225 integrated segments of equal width (0.04 ppm). The region between δ 4.20 and 6.52 was removed, and then each integral value of a spectrum was divided by the integral intensity of creatinine signal (CH_3, 3.042–3.055 ppm) in order to normalize each spectral data set and compensate for variations in urine volumes. The normalized data sets were then subjected to principal components analysis, one of multivariate statistical analysis, after mean-centering and Pareto scaling. Scores plots of the principal components (PCs) were constructed to visualize the separation of the urine samples between the SHR and SHRSP. Loadings plots were constructed to show the importance of each variable (bucket) and metabolite to the separation.

3. Results and discussion

3.1. Sample preparation method

In the usual sample preparation method, all the urine samples were almost doubly diluted resulting in various urine concentrations. On the other hand, in the proposed sample preparation method (see Section 2.2), the urine concentrations can be freely adjusted to a certain level, and, if necessary, be increased to improve signal-to-noise ratios in NMR spectra when urine is freeze-dried and reconstituted in a buffered solution. The improved signal-to-noise ratios result in the detection of more minor metabolites, leading to the increased metabolic information. In addition, if a deuterated buffer is used, NMR spectra can be obtained without water suppression, which is sometimes troublesome due to difficulties with phase adjustment and baseline correction. Another simple approach to control urinary pH and reduce chemical shift variations may be to dilute urine with a buffer to a certain constant level less than that of the most diluted urine in a series of samples. However, such a solution is not recommended due to problems associated with water suppression as well as lowering in signal-to-noise ratios.

Some indication to reflect urine concentration is necessary for the proposed sample preparation. A variety of indices have been reported for the correction of urinary concentrations of components, including specific gravity, osmolality, and creatinine concentration in urine [24–26]. These are also possible markers for the extent of urine concentration. Specific gravity and osmolality are considered to be unsuitable for such markers because they change due to precipitation of salts when urine samples that have been kept in a freezer are thawed. Although urine volume is also an index for urine concentration when urine is collected in a specified time, for example 24 h, it cannot be used for spot urine. On the other hand, creatinine is often used in clinical settings [27]. Creatinine is also used for the normalization of ^{1}H NMR spectral data in urinary metabonomic studies [19,28]. Thus, in the proposed sample preparation method, urinary creatinine concentration was used as the reference to make urine concentrations constant.

Urine was obtained from the SHR and SHRSP as described above (Section 2.1). As shown in Table 1, the body weight of the SHRSP was smaller than that of the SHR, and the blood pressure

Table 1
Characteristics of the 10-week-old SHR and SHRSP.

Strain	Body weight (g)	Blood pressure (mmHg)		Concentration of creatinine (mg/dl)	Amount of creatinine excreted in 24 h (mg/kg body weight/day)
		Systolic	Diastolic		
SHR ($n=6$)	246.8 ± 6.9	188.2 ± 11.9	145.7 ± 17.7	64.9 ± 12.5	27.1 ± 1.9
SHRSP ($n=6$)	224.9 ± 4.2*	230.1 ± 18.6*	186.2 ± 32.5*	40.9 ± 6.7*	29.9 ± 2.0*

Data expressed as mean ± standard deviation. Statistical analysis was done using an unpaired *t*-test.
Creatinine concentrations in urine were measured by a kit (Cre-EN Kainos, KAINOS, Tokyo, Japan) based on an enzymatic method.
* $P<0.05$ *vs.* SHR.

of the former was higher than that of the latter. The average 24-h urine volume of the SHRSP was 1.6 times more than that of the SHR, whereas the average creatinine concentration in urine of the latter (64.9 ± 12.5 mg/dl) was 1.6 times higher than that of the former (40.9 ± 6.7 mg/dl). The correlation coefficient between the urine volume and creatinine concentration from the 12 rats was −0.931. These results support the validity of using urinary creatinine concentration as an index of urine concentration. Any creatinine concentrations of the intact urine from the SHR were higher than those from the SHRSP. The highest creatinine concentration in the intact urine of the SHR was 2.5 times higher than the lowest one of the SHRSP. Urine from the SHR and the SHRSP was considered to be suitable for the present study because of the large difference in urine concentration. Thus, the usefulness of the proposed method was investigated using these urine samples in terms of the variations of pH and chemical shifts.

3.2. pH variations

The deviations in pH values of the intact urine and the urine samples prepared in both the usual and proposed methods are shown in Fig. 1. The urine samples from the SHRSP showed higher pH values on average compared with those from the SHR in both the intact urine and the urine samples prepared by the usual method, which was thought to be due to the lower urine concentration in the SHRSP. In fact, in the intact urine and the urine samples prepared by the usual method, strong inverse correlations with correlation coefficients of −0.881 and −0.960 were found between the pH values and the urine concentration represented by creatinine concentrations, respectively. These results indicate that creatinine concentration is a good marker of urine concentration for the adjustment of urinary pH. The range of hydrogen ion concentrations in the intact urine became narrower owing to the buffer capacity after treatment by the usual method, although the pH deviation of the usual method (pH 6.81–7.18) was similar to that of the intact urine (pH 5.97–6.34). On the contrary, in the proposed method, there was no appreciable difference in the pH values between the two substrains, and the pH values were more closely controlled to 6.89–7.01. Therefore, the proposed method was expected to be effective for the reduction of chemical shift variability.

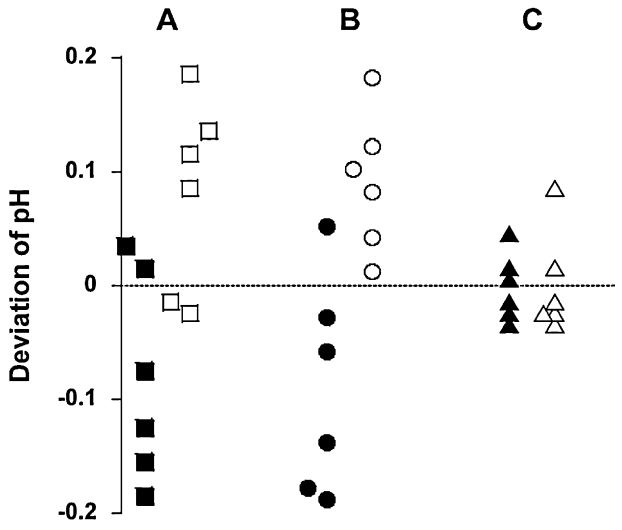

Fig. 1. pH variations of the intact urine (A) and the NMR samples prepared by the usual (B) and proposed methods (C). The pH was measured using a Seven Easy pH meter (METTLER TOLEDO, Tokyo, Japan) equipped with a glass electrode (U402-M3-S7/200) and a NTC 30 kΩ temperature probe at room temperature (24–26 °C). The pH meter readings of the NMR samples were regarded as the pH because the volume of D_2O contained in the samples was small. The mean ± standard deviation (relative standard deviation, %) of pH of the intact urine and the NMR samples prepared by the usual and the proposed methods were 6.15 ± 0.12 (1.93), 7.00 ± 0.12 (1.72), and 6.92 ± 0.04 (0.52), respectively. Key: filled squares, circles, and triangles, SHR; open squares, circles, and triangles, SHRSP.

3.3. Chemical shift variations

A typical ^{1}H NMR spectrum of rat urine is shown in Fig. 2. There was no appreciable difference in the spectra between the two sample preparation methods, except the signal due to acetate (δ 1.92) was obviously less intense in the proposed method because of the high volatility. Six metabolites such as succinate, α-ketoglutarate, citrate, *cis*-aconitate, taurine, and glycine were selected to examine the chemical shift variations because the chemical shifts of such metabolites having ionizable groups are generally sensitive to pH and ionic strength [6].

As shown in Fig. 3, in the usual method, the peak positions of the six metabolites varied over a range of 0.005 ppm (2.5 Hz). The largest variation was observed for *cis*-aconitate (methylene proton). The peak positions in the SHR showed a trend to shift to a lower magnetic field compared with those in the SHRSP in the usual method, which indicated insufficient pH control by the buffer. These shifts of peak positions cause erroneous bucket integrals if the bucket border lies around the average peak position (2.411 ppm), which disturbs the exact search of metabolic changes. The major reason for this difference in chemical shifts between the two substrains was considered to be the enhanced acidity of the SHR urine due to the higher urine concentration.

The peak positions were highly correlated with the pH in the NMR samples prepared by the usual method. The correlation coefficients between the peak positions and the pH were −0.808 for citrate, −0.974 for succinate, −0.871 for α-ketoglutarate, −0.993 for *cis*-aconitate, −0.979 for taurine and −0.948 for glycine. In addition, the correlation coefficients between the peak positions and the creatinine concentrations were 0.653 for citrate, 0.969 for succinate, 0.851 for α-ketoglutarate, 0.963 for *cis*-aconitate, 0.959 for taurine and 0.939 for glycine. These results indicate that creatinine concentration is a superior index of urine concentration when attention is paid to the chemical shift variability.

On the other hand, in the proposed method, the deviations and standard deviations of the peak positions were significantly reduced, and there was no appreciable difference in peak positions between the two substrains except for citrate. The citrate peak in the samples from the SHR still showed a trend to shift to a lower

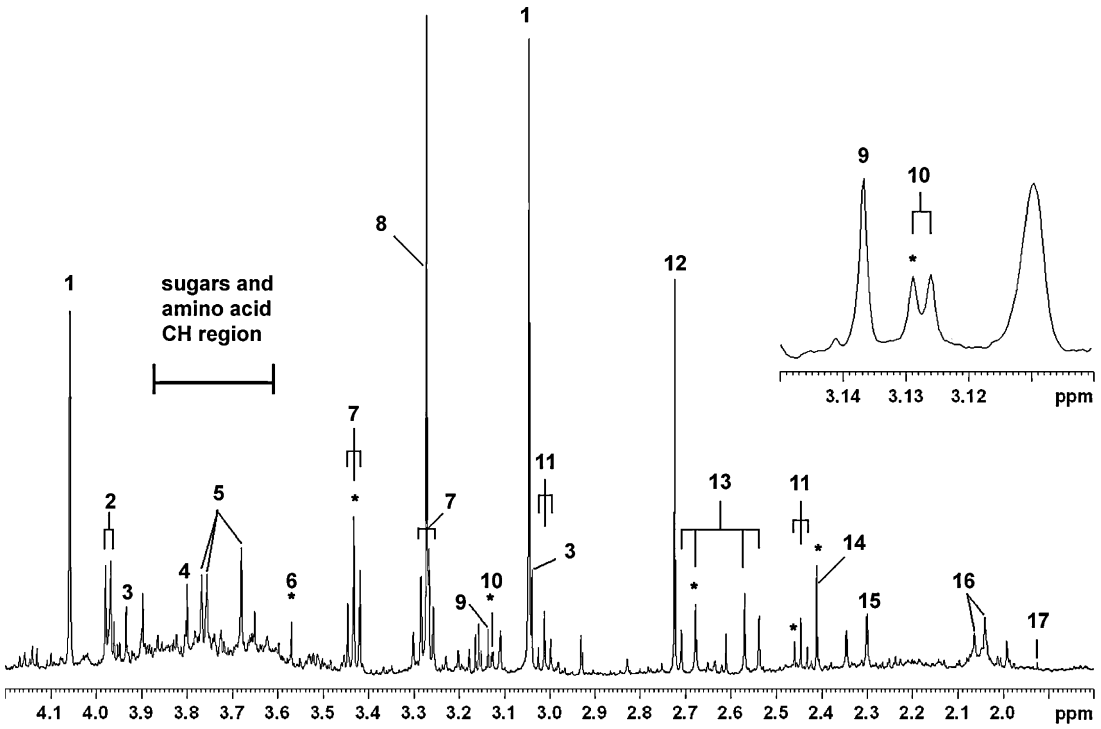

Fig. 2. A typical ^{1}H NMR spectrum of rat urine. A spectrum of an SHRSP urine sample prepared by the proposed method is illustrated. Key: 1, creatinine; 2, hippurate; 3, creatine; 4, guanidinoacetate; 5, phenylacetylglycine; 6, glycine; 7, taurine; 8, trimethylamine *N*-oxide; 9, malonate; 10, *cis*-aconitate; 11, α-ketoglutarate; 12, dimethylamine; 13, citrate; 14, succinate; 15, *p*-cresol glucuronide; 16, *N*-acetyls of glycoproteins; 17, acetate. The asterisks indicate the peaks used for the examination of chemical shift variations.

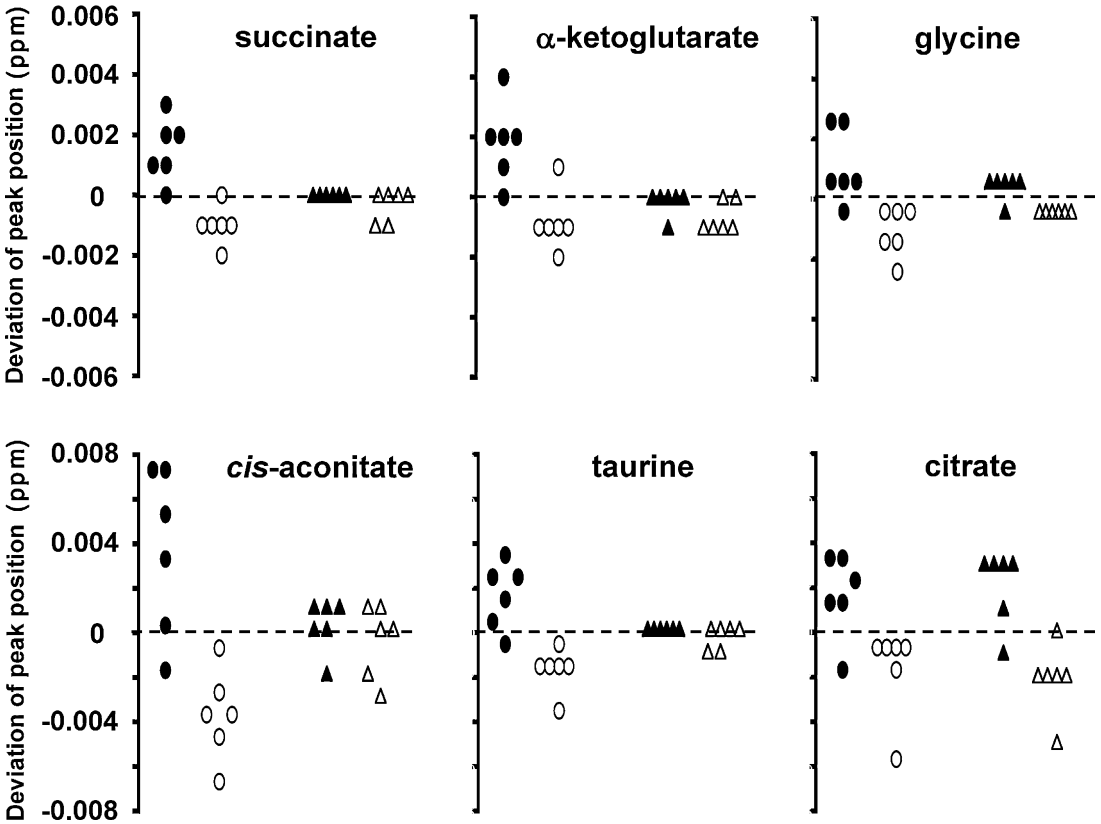

Fig. 3. Chemical shift variations of the six metabolites in the urine samples prepared by the usual and proposed methods. Filled and open ellipses indicate the samples from the SHR and SHRSP, respectively, in the usual method. Filled and open triangles indicate the samples from the SHR and SHRSP, respectively, in the proposed method. The peaks with asterisks in Fig. 2 were used for the evaluation of chemical shift variations. The mean ± standard deviation of peak positions (ppm) in the usual and proposed methods was 2.411 ± 0.0015 and 2.412 ± 0.0004 for succinate, 2.461 ± 0.0018 and 2.461 ± 0.0005 for α-ketoglutarate, 3.569 ± 0.0015 and 3.570 ± 0.0005 for glycine, 3.124 ± 0.0048 and 3.126 ± 0.0014 for *cis*-aconitate, 3.432 ± 0.0021 and 3.433 ± 0.0004 for taurine, and 2.682 ± 0.0025 and 2.680 ± 0.0027 for citrate, respectively.

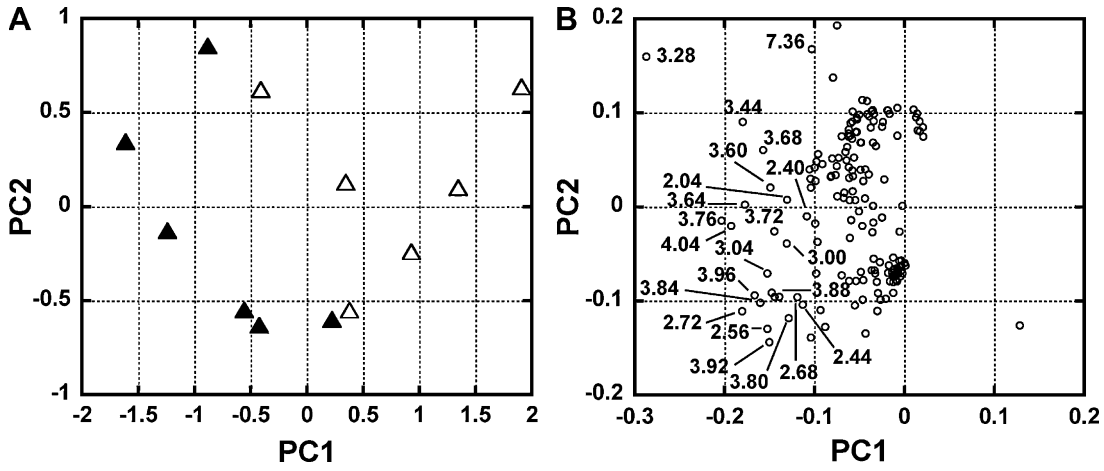

Fig. 4. PC1–PC2 scores (A) and loadings plots (B) of the ^{1}H NMR spectral data obtained by the proposed method. Filled and open triangles in panel A indicate the SHR and SHRSP, respectively. The loadings of 168 variables (buckets) are plotted in panel B with the middle δ values of 0.04 ppm regions. The metabolites included in each bucket were as follows: citrate in 2.56, 2.68, and 2.72; α-ketoglutarate in 2.44, 3.00, and 3.04; succinate in 2.40; hippurate in 3.96, phenylacetylglycine in 3.68, 3.76, and 7.36; trimethylamine *N*-oxide in 3.28; creatine in 3.04 and 3.92; taurine in 3.44.

magnetic field. The above smaller correlation of citrate peak positions with pH in the usual method and the poor control of citrate chemical shifts in the proposed method indicate that the chemical shift variation of this metabolite is largely due to some factors other than pH. The nature of citrate to form complexes with some urinary metals seems to be the major factor [7]. From these experimental results, the proposed method was demonstrated to minimize the chemical shift variations of the representative metabolites besides exceptional citrate. The proposed method is expected to be effective for most chemical shift variations encountered in the NMR spectroscopic analysis of urine from various species. It seems that there are many ^{1}H signals sensitive to pH and ion strength and their chemical shift variations are not easily recognized, particularly in the crowded regions. Such variations can be also reduced by the proposed method.

3.4. Multivariate statistical analysis

The SHRSP, which are well-known as the only animal model for stroke [29], are a substrain derived from the SHR [30], and both strains cause hypertension without exception. Thus, the metabolic differences between the two hypertensive substrains are of great interest because they are expected to provide insights into stroke which is one of the major causes of death. However, such differences have not been clarified so far. Thus, the NMR spectral data from the samples prepared by the improved method were preliminarily analyzed by principal components analysis. Consequently, the two strains were separated on the PC maps almost along the PC1 axis, as shown in Fig. 4. The results indicate that there were metabolic changes between the two substrains. The PC1 loadings in Fig. 4 suggest a decreased excretion of most urinary metabolites in the SHRSP based on creatinine output; particularly citrate, α-ketoglutarate, succinate, hippurate, phenylacetylglycine, trimethylamine *N*-oxide, creatine, and taurine. Details of the metabolic changes are works in progress.

4. Conclusions

In summary, the proposed sample preparation method is one of the best ones to eliminate chemical shift variability in ^{1}H NMR-based urinary metabonomics. The reduction of chemical shift variations enables not only more accurate multivariate analysis but also high resolution data analysis by bucketing into smaller bins. The proposed sample preparation is recommendable especially for the NMR-based metabonomic identification of urinary metabolites and biomarkers related to disease and drug toxicity.

References

[1] J.C. Lindon, J.K. Nicholson, Spectroscopic and statistical techniques for information recovery in metabonomics and metabolomics, Annu. Rev. Anal. Chem. 1 (2008) 45–69.
[2] J.C. Lindon, J.K. Nicholson, E. Holmes, J.R. Everett, Metabonomics: metabolic processes studied by NMR spectroscopy of biofluids, Concepts Magn. Reson. 12 (2000) 289–320.
[3] J.C. Lindon, E. Holmes, M.E. Bollard, E.G. Stanley, J.K. Nicholson, Metabonomics technologies and their applications in physiological monitoring, drug safety assessment and disease diagnosis, Biomarkers 9 (2004) 1–31.
[4] J.P. Shockcor, E. Holmes, Metabonomic applications in toxicity screening and disease diagnosis, Curr. Top. Med. Chem. 2 (2002) 35–51.
[5] M. Lauridsen, S.H. Hansen, J.W. Jaroszewski, C. Cornett, Human urine as test material in ^{1}H NMR-based metabonomics: recommendations for sample preparation and storage, Anal. Chem. 79 (2007) 1181–1186.
[6] C. Xiao, F. Hao, X. Qin, Y. Wang, H. Tang, An optimized buffer system for NMR-based urinary metabonomics with effective pH control, chemical shift consistency and dilution minimization, Analyst 134 (2009) 916–925.
[7] V.M. Asiago, G.A.N. Gowda, S. Zhang, N. Shanaiah, J. Clark, D. Raftery, Use of EDTA to minimize ionic strength dependent frequency shifts in the ^{1}H NMR spectra of urine, Metabolomics 4 (2008) 328–336.
[8] A.M. Weljie, J. Newton, P. Mercier, E. Carlson, C.M. Slupsky, Targeted profiling: quantitative analysis of ^{1}H NMR metabolomics data, Anal. Chem. 78 (2006) 4430–4442.
[9] O. Cloarec, M.E. Dumas, J. Trygg, A. Craig, R.H. Barton, J.C. Lindon, J.K. Nicholson, E. Holmes, Evaluation of the orthogonal projection on latent structure model limitations caused by chemical shift variability and improved visualization of biomarker changes in ^{1}H NMR spectroscopic metabonomic studies, Anal. Chem. 77 (2005) 517–526.
[10] T. De Meyer, D. Sinnaeve, B. Van Gasse, E. Tsiporkova, E.R. Rietzschel, M.L. De Buyzere, T.C. Gillebert, S. Bekaert, J.C. Martins, W. Van Criekinge, NMR-based characterization of metabolic alterations in hypertension using an adaptive, intelligent binning algorithm, Anal. Chem. 80 (2008) 3783–3790.
[11] E. Holmes, P.J.D. Foxall, J.K. Nicholson, G.H. Neild, S.M. Brown, C.R. Beddell, B.C. Sweatman, E. Rahr, J.C. Lindon, M. Spraul, P. Neidig, Automatic data reduction and pattern recognition methods for analysis of ^{1}H nuclear magnetic resonance spectra of human urine from normal and pathological states, Anal. Biochem. 220 (1994) 284–296.
[12] E. Holmes, J.K. Nicholson, A.W. Nicholls, J.C. Lindon, S.C. Connor, S. Polley, J. Connelly, The identification of novel biomarkers of renal toxicity using automatic data reduction techniques and PCA of proton NMR spectra of urine, Chemom. Intell. Lab. Syst. 44 (1998) 245–255.
[13] F. Dieterle, A. Ross, G. Schlotterbeck, H. Senn, Metabolite prejection analysis for fast identification of metabolites in metabonomics. Application in an amiodarone study, Anal. Chem. 78 (2006) 3551–3561.
[14] Y. Yang, C. Li, X. Nie, X. Feng, W. Chen, Y. Yue, H. Tang, F. Deng, Metabonomic studies of human hepatocellular carcinoma using high-resolution magic-angle spinning ^{1}H NMR spectroscopy in conjunction with multivariate data analysis, J. Proteome Res. 6 (2007) 2605–2614.
[15] C. Xiao, H. Dai, H. Liu, Y. Wang, H. Tang, Revealing the metabonomic variation of rosemary extracts using ^{1}H NMR spectroscopy and multivariate data analysis, J. Agric. Food Chem. 56 (2008) 10142–10153.

[16] M. Li, B. Wang, M. Zhang, M. Rantalainen, S. Wang, H. Zhou, Y. Zhang, J. Shen, X. Pang, M. Zhang, H. Wei, Y. Chen, H. Lu, J. Zuo, M. Su, Y. Qiu, W. Jia, C. Xiao, L.M. Smith, S. Yang, E. Holmes, H. Tang, G. Zhao, J.K. Nicholson, L. Li, L. Zhao, Symbiotic gut microbes modulate human metabolic phenotypes, Proc. Natl. Acad. Sci. U. S. A. 105 (2008) 2117–2122.
[17] J. Forshed, R.J.O. Torgrip, K.M. Aberg, B. Karlberg, J. Lindberg, S.P. Jacobsson, A comparison of methods for alignment of NMR peaks in the context of cluster analysis, J. Pharm. Biomed. Anal. 38 (2005) 824–832.
[18] K. Akira, M. Imachi, T. Hashimoto, Investigations into biochemical changes of genetic hypertensive rats using ^{1}H nuclear magnetic resonance-based metabonomics, Hypertens. Res. 28 (2005) 425–430.
[19] K. Akira, S. Masu, M. Imachi, H. Mitome, M. Hashimoto, T. Hashimoto, ^{1}H NMR-based metabonomic analysis of urine from young spontaneously hypertensive rats, J. Pharm. Biomed. Anal. 46 (2008) 550–556.
[20] K. Akira, S. Masu, M. Imachi, H. Mitome, T. Hashimoto, A metabonomic study of biochemical changes characteristic of genetically hypertensive rats based on ^{1}H NMR spectroscopic urinalysis, Hypertens. Res. (2012), doi:10.1038/hr.2011.182.
[21] J.K. Nicholson, P.J.D. Foxall, M. Spraul, R.D. Farrant, J.C. Lindon, 750 MHz ^{1}H and ^{1}H–^{13}C NMR spectroscopy of human blood plasma, Anal. Chem. 67 (1995) 793–811.
[22] M.E. Bollard, E. Holmes, J.C. Lindon, S.C. Mitchell, D. Branstetter, W. Zhang, J.K. Nicholson, Investigations into biochemical changes due to diurnal variation and estrus cycle in female rats using high-resolution ^{1}H NMR spectroscopy of urine and pattern recognition, Anal. Biochem. 295 (2001) 194–202.
[23] J.C. Lindon, J.K. Nicholson, in: J.C. Lindon, G.E. Tranter, J.L. Holmes (Eds.), Biofluids studied by NMR, Encyclopedia of Spectroscopy and Spectrometry, vol. 1, Academic Press, London, 2000, pp. 98–116.
[24] B.C. White, K.M. Jamison, C. Grieb, D. Lally, C. Luckett, K.S. Kramer, J. Phillips, Specific gravity and creatinine as corrections for variation in urine concentration in humans, gorillas, and woolly monkeys, Am. J. Primatol. 72 (2010) 1082–1091.
[25] A.H. Garde, A.M. Hansen, J. Kristiansen, L.E. Knudsen, Comparison of uncertainties related to standardization of urine samples with volume and creatinine concentration, Ann. Occup. Hyg. 48 (2004) 171–179.
[26] B.M. Warrack, S. Hnatyshyn, K.H. Ott, M.D. Reily, M. Sanders, H. Zhang, D.M. Drexler, Normalization strategies for metabonomic analysis of urine samples, J. Chromatogr. B 877 (2009) 547–552.
[27] A.M. Cote, M.A. Brown, E. Lam, P. Von Dadelszen, T. Firoz, R.M. Liston, L.A. Magee, Diagnostic accuracy of urinary spot protein: creatinine ratio for proteinuria in hypertensive pregnant women: systematic review, Br. Med. J. 336 (2008) 1003–1006.
[28] Y. Wang, D. Lawler, B. Larson, Z. Ramadan, S. Kochhar, E. Holmes, J.K. Nicholson, Metabonomic investigations of aging and caloric restriction in a life-long dog study, J. Proteome Res. 6 (2007) 1846–1854.
[29] K. Okamoto, Y. Yamori, A. Nagaoka, Establishment of the stroke-prone spontaneously hypertensive rat (SHR), Circ. Res. 34/35 (1974) I143–I153 (Suppl.).
[30] K. Okamoto, K. Aoki, Development of a strain of spontaneously hypertensive rats, Jpn. Circ. J. 27 (1963) 282–293.

Journal of Pharmaceutical and Biomedical Analysis 66 (2012) 345–348

Contents lists available at SciVerse ScienceDirect

Journal of Pharmaceutical and Biomedical Analysis

journal homepage: www.elsevier.com/locate/jpba

Short communication

Isolation and structural elucidation of abietic acid as the main adulterant in an herbal drug for the treatment of psoriasis

Yi He, Yumei Zhang, Jing Lu*, Ruichao Lin

National Institutes for Food and Drug Control, Tiantan Xili 2, Beijing 100050, China

ARTICLE INFO

Article history:
Received 16 December 2011
Received in revised form 1 March 2012
Accepted 2 March 2012
Available online 23 March 2012

Keywords:
Abietic acid
NMR
HPLC–DAD–MS
Herbal drug
Psoriasis

ABSTRACT

An herbal drug for the treatment of psoriasis showed severe clinical adverse reactions. The main component of adulterant was isolated from the drug and its chemical structure was elucidated as abietic acid using NMR, HR–MS, and HPLC–DAD–MS. Although abietic acid had ever been used in clinical study for the treatment of psoriasis, it is not an approved drug. Its adulteration is very dangerous for the patients.

© 2012 Elsevier B.V. All rights reserved.

1. Introduction

Psoriasis is a common, chronic, immune-mediated disease that affects approximately 2% of the world population. Although this disease is rarely fatal, psoriasis has a significant adverse effect on the quality of life by its complications such as inflammatory arthropathy, disability, and myocardial infarction [1–4]. It is believed that psoriasis results from interplay between multiple genetic and environmental factors, but its pathogenesis is still incompletely understood [4,5]. Current therapies for psoriasis are far from satisfactory. Many therapies are associated with significant side effects including renal injury, liver abnormalities, vasculitis, and even cancer [4,6]. Therefore, some patients turn to herbal medicine for the treatment of psoriasis.

An example of such an herbal drug, YXD capsule was composed of *Scutellariae Radix*, *Moutan Cortex*, *Coptidis Rhizoma*, *Lonicerae japonicae Flos*, *Rehmanniae Radix*, *Zaocys*, *Schizonepetae Herba*, *Notopterygii Rhizoma et Radix*, *Angelicae dahuricae Radix*, *Saposhnikoviae Radix*, *Forsythiae Fructus*, *Cicadae Periostracum*, *Haematitum*, *Olibanum*, and *Glycyrrhizae Radix et Rhizoma*. It was sent to our institute because several batches of the product caused severe adverse reactions including one case of death and one case of deafness.

Abietic acid is an abietane diterpenoid and one of the major components of rosin (colophony), in which its concentration could reach 54% [7,8]. In vivo and in vitro studies showed that abietic acid had anti-obesity, lipoxygenase inhibition, testosterone 5α-reductase inhibition, and anti-inflammation effect [9–12]. Oral preparations of abietic acid had been used in clinical study for the treatment of psoriasis in China [13–15], but it has not been approved as drug so far.

In this paper, we describe the isolation and structure elucidation of abietic acid from YXD capsules using NMR, HR–MS, and HPLC–DAD–MS.

2. Materials and methods

2.1. Sample and chemicals

YXD capsules were commercial products obtained from Ningxia Hui Autonomous Region, China. Abietic acid (purity: about 75%, GC) was purchased from Sigma–Aldrich (St. Louis, MO, USA). Silica gel was obtained from Qingdao Haiyang Chemical Co., Ltd. (Qingdao, Shandong, China). Deuterated chloroform used for NMR analysis was purchased from Cambridge Isotope Laboratories (Andover, MA, USA). All chemical reagents were either high-performance liquid chromatography (HPLC) or analytical grade obtained from Mallinckrodt Baker Inc. (Phillipsburg, NJ, USA), Fisher Scientific (Pittsburgh, PA, USA), and Beijing Chemical Works (Beijing, China). Water was purified with MilliQ system (Millipore, Billerica, MA, USA).

* Corresponding author.
E-mail address: lujing@nicpbp.org.cn (J. Lu).

0731-7085/$ – see front matter © 2012 Elsevier B.V. All rights reserved.
doi:10.1016/j.jpba.2012.03.007

2.2. Extraction and isolation

The contents of two capsules (0.8 g, pale-brown powder) were suspended in water, followed by partition with chloroform. The chloroform extract was applied to flash column chromatography (silica gel) and eluted with the mixture of petroleum ether (b.p. 60–90 °C) – ethyl acetate (98:2). Further purification was performed on a Delta Prep 4000 preparative chromatography system (Waters Corporation, Milford, MA, USA) using Prep Nova-Pak HR C18 (Waters Corporation, 6 μm, 40 mm × 100 mm) as stationary phase and 70% methanol (5 mL/min) as mobile phase to afford compound **1** (100 mg).

2.3. NMR and MS analysis

^{1}H-, ^{13}C- and 2D NMR spectra were measured on a Bruker DRX-500 spectrometer (Bruker BioSpin, Rheinstetten, Germany). Chemical shifts were reported in ppm using the solvent peak as an internal standard. MS spectra were determined on Autospec-Ultima ETOF MS spectrometer (EI-MS, Micromass Ltd., Wythenshawe, Manchester, UK) and ZAB-HS MS spectrometer (HR–EI-MS, VG Analytical, Wythenshawe, Manchester, UK).

2.4. HPLC–DAD–MS analysis

The sample solution was prepared by shaking 0.1 g of the capsule's contents with 20 mL methanol, and the reference solution was prepared by dissolving 5 mg of abietic acid in 10 mL of methanol.

HPLC–DAD–MS analysis was performed using the Agilent 1200 Series HPLC system and 6410B Triple Quadrupole LC/MS system (Agilent Technologies, Palo Alto, CA, USA). The sample solution was separated by using a Phenomenex Kinetex C18 column (2.6 μm, 2.10 mm × 100 mm, Phenomenex Inc., Torrance, CA, USA) with injection volume of 2 μL. The mobile phase was the mixture of acetonitrile and 0.1% formic acid with a flow rate of 0.2 mL/min, and the detection wavelength was set at 241 nm.

MS detection was performed in positive electrospray ionization (ESI+) mode. The LC effluent was directly introduced into the ESI source without split. Nitrogen was used as desolvation gas. The optimized interface and MS conditions were as follows: gas temperature 300 °C, gas flow 10 L/min, nebulizer pressure 35 psi, source voltage 4 kV, fragmentor voltage 100 V, and collision energy 10 eV (for MS/MS).

3. Results and discussion

Compound **1** was obtained as a colourless amorphous powder. The molecular formula was determined to be $C_{20}H_{30}O_2$ by HR–EI-MS (*m/z* 302.2246 $[M]^+$; calculated for $C_{20}H_{30}O_2$, 302.2249). Its degree of unsaturation can thus be calculated as 6. Furthermore, the characteristic fragment ion peaks at *m/z* 287 $[M-CH_3]^+$, 259 $[M-C_3H_7]^+$, and 257 $[M-COOH]^+$ of EI-MS suggested the existence of a methyl group, a propyl group, and a carboxyl group, which were also supported by the HR–EI-MS (*m/z* 287.2014 $[M-CH_3]^+$, calculated for $C_{19}H_{27}O_2$, 287.2011; *m/z* 259.1685 $[M-C_3H_7]^+$, calculated for $C_{17}H_{23}O_2$, 259.1698; *m/z* 257.2254 $[M-COOH]^+$, calculated for $C_{19}H_{29}$, 257.2269).

The ^{1}H NMR signals (Table 1) at δ 5.38 (1H, m, H-7) and 5.77 (1H, m, H-14) suggested the presence of ethylenic bond; whereas the ^{13}C NMR spectrum of **1** (Table 1) showed a carboxylic carbon signal at δ 183.7 (C-8) and four olefinic carbon signals at δ 145.2, 135.6, 122.3 and 120.4. Based on the calculation of unsaturation degree, **1** could be estimated as a tricyclic compound. The heteronuclear multiple quantum coherence (HMQC) spectrum showed that the protons at δ_H 5.38 (H-7) and 5.77 (H-14) were connected to the carbons at δ_C 120.5 (C-7) and 122.3 (C-14), respectively. In the heteronuclear multiple bond correlations (HMBC, Table 1) spectrum, the long range correlations between H-7 and C-14, and between H-14 and C-7 suggested that those ethylenic carbons were adjacent to each other.

Table 1
NMR spectral data of compounds **1** (δ in ppm, *J* in Hz)[a].

Position	δ_H	δ_C	HMBC[b]
1	1.14 (m)	38.3	
2	1.59 (m)	18.0	
3	1.79 (m)	37.2	
4	–	46.3	
5	2.07 (m)	44.9	
6	1.87 (m)	25.6	
7	5.38 (m)	120.4	C-5, C-6, C-9, C-14
8	–	135.6	
9	1.94 (m)	50.9	
10	–	34.5	
11	1.79 (m)	22.5	
12	2.07 (m)	27.4	
13	–	145.2	
14	5.77 (s)	122.3	C-7, C-8, C-9, C-12, C-15
15	2.21 (m)	34.9	
16	1.01 (d, *J* = 4.5)	20.9	C-13, C-17
17	1.00 (d, *J* = 4.5)	21.4	C-13, C-16
18	–	183.7	
19	1.26 (s)	16.8	C-3, C-5, C-18
20	0.83 (s)	14.0	C-1, C-5, C-9

[a] Data were recorded in $CDCl_3$ at 500 MHz (^{1}H) and 125 MHz (^{13}C).
[b] HMBC correlations are from proton(s) stated to the indicated carbon.

By comparison of UV and NMR data with those reported in the literature [9,16], compound **1** was identified to be abietic acid (Fig. 1).

As shown in Fig. 2, the HPLC–DAD chromatography, UV spectrum, and MS spectrum obtained from HPLC–DAD–MS confirmed the presence of abietic acid in the capsules.

The presence of abietic acid could not be explained by the literature search on the chemical composition of labeled ingredients. Therefore, it is adulterated. The range of the concentration of abietic acids in rosin is very large (varying from 20 to 54%) [7,8]. Little literature reported about the chemical difference among crude abietic acid, processed (purified) rosin, and natural rosin. So it is also very hard to determine which adulterant was actually added in this herbal drug.

Oral preparations of abietic acid had side-effects including nausea, discomfort in the stomach, loss of appetite, loose or solid stool, dizziness and fatigue, drug eruptions, and sleepiness [13–15]. Rosin has been regarded as a common allergen [7,17]. In an ancient book

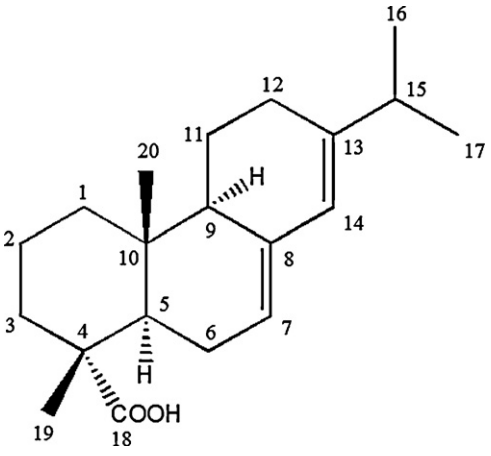

Fig. 1. Structure of abietic acid.

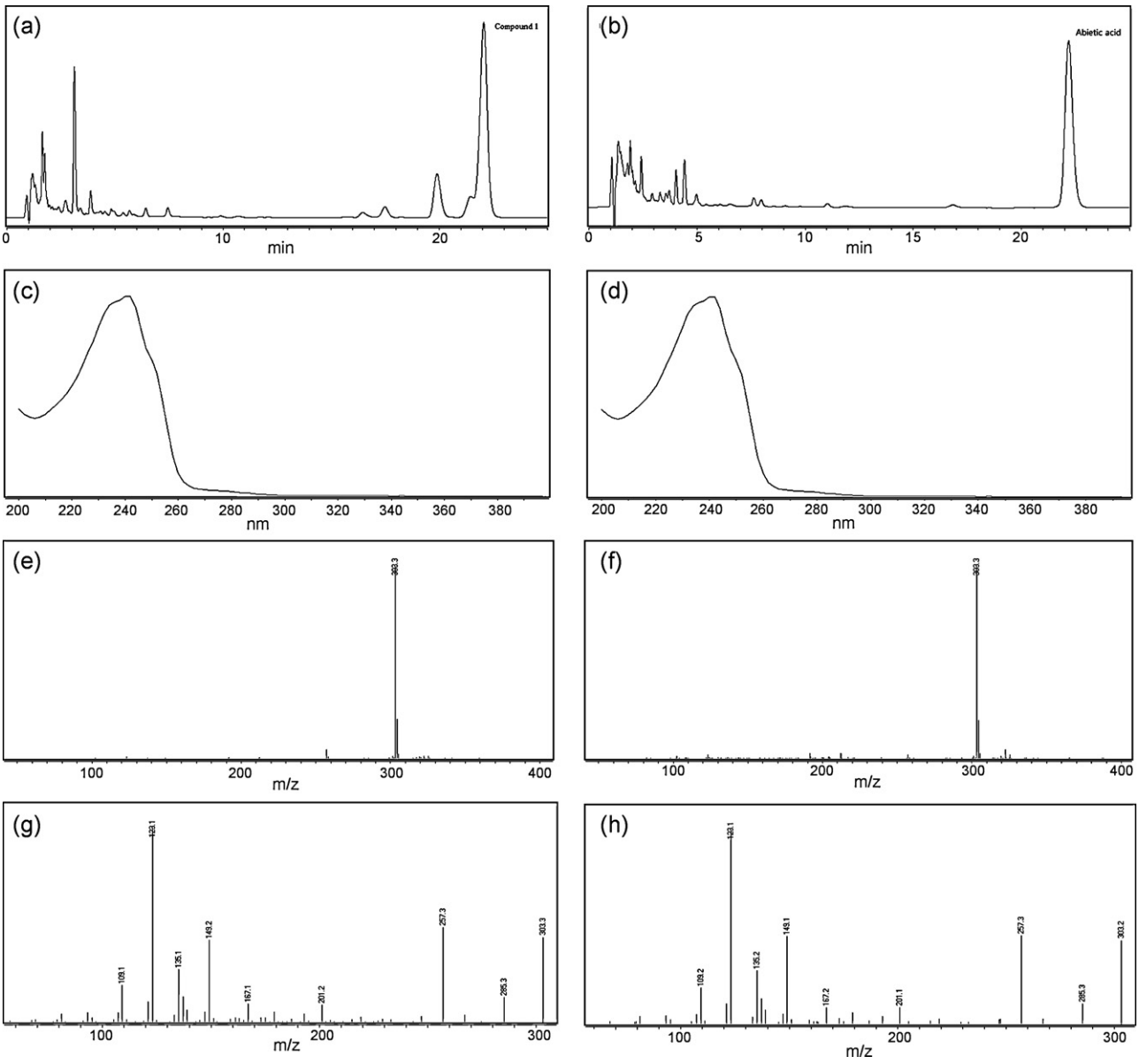

Fig. 2. HPLC–DAD chromatograms of the YXD capsule sample (a) and abietic acid reference (b); the UV spectra of compound **1** (c) and abietic acid reference (d); mass spectra of compound **1** (e) and abietic acid reference (f); MS/MS spectra of the *m/z* 303 ion of compound **1** (g) and abietic acid reference (h).

of traditional Chinese medicine "Xu Yi Shuo" (AD 1522), it was recorded that someone died after ingesting rosin without careful purification [15]. The severe adverse reactions of YXD capsule may be caused by the adulterant.

4. Conclusion

In this study, the main component of adulterant, abietic acid, was isolated from an herbal drug by flash column chromatography and preparative HPLC, and its chemical structure was elucidated using NMR, HR–MS, HPLC–DAD–MS. In view of the fact that abietic acid is not an approved drug till present, its adulteration is very dangerous for the patients, and the severe adverse reactions of YXD capsule may be caused by the adulterant.

References

[1] J.M. Gelfand, A.L. Neimann, D.B. Shin, X. Wang, D.J. Margolis, A.B. Troxel, Risk of myocardial infarction in patients with psoriasis, JAMA 296 (2006) 1735–1741.
[2] S.R. Rapp, S.R. Feldman, M.L. Exum, A.B. Fleischer, D.M. Reboussin, Psoriasis causes as much disability as other major medical diseases, J. Am. Acad. Dermatol. 41 (1999) 401–407.
[3] C.L. Leonardi, J.L. Powers, R.T. Matheson, B.S. Goffe, R. Zitnik, A. Wang, A.B. Gottlieb, Etanercept as monotherapy in patients with psoriasis, N. Engl. J. Med. 349 (2003) 2014–2022.
[4] B.J. Nickoloff, F.O. Nestle, Recent insights into the immunopathogenesis of psoriasis provide new therapeutic opportunities, J. Clin. Invest. 113 (2004) 1664–1675.
[5] P. Rahman, J.T. Elder, Genetic epidemiology of psoriasis and psoriatic arthritis, Ann. Rheum. Dis. 64 (2005) ii37–ii39.
[6] W. Weger, Current status and new developments in the treatment of psoriasis and psoriatic arthritis with biological agents, BJP 160 (2010) 810–820.
[7] S. Sadhra, I.S. Foulds, C.N. Gray, Oxidation of resin acids in colophony (rosin) and its implications for patch testing, Contact Dermatitis 39 (1998) 58–63.
[8] J. Zhang, X. Bi, X. An, C. Wu, Study on rosin decarboxylation under microwave irradiation, J. Southwest Forestry Coll. 24 (2004) 55–57.
[9] S. Roh, M. Park, Y. Kim, Abietic acid from resina pini of *Pinus* species as a testosterone 5α-reductase inhibitor, J. Health Sci. 56 (2010) 451–455.
[10] K. Hwang, J. Ahn, S. Kim, J. Park, T. Ha, Abietic acid has an anti-obesity effect in mice fed a high-fat diet, J. Med. Food 14 (2011) 1052–1056.
[11] N.N. Ulusu, D. Ercil, M.K. Sakar, E.F. Tezcan, Abietic acid inhibits lipoxygenase activity, Phytother. Res. 16 (2002) 88–90.

[12] M.A. Fernández, M.P. Tornos, M.D. García, B. De las Heras, A.M. Villar, M.T. Sáenz1, Anti-inflammatory activity of abietic acid, a diterpene isolated from *Pimenta racemosa* var. grissea, J. Pharm. Pharmacol. 53 (2001) 867–872.
[13] C. Mi, H., Shi, F. Li, A botanical drug for treating psoriasis and preparation process of its crude drug abietic acid, Chinese patent CN 1883519A (27 December 2006).
[14] Y. Dong, C., Wang, Q., Xu, C., Tang, X., Xia, S. Han, Medicine for treating psoriasis, Chinese patent CN 1397341A (19 February 2003).
[15] Editorial board of China herbal, State administration of traditional Chinese medicine, China Herbal, book two, Shanghai Science and Technology Publishers, Shanghai, 1999, pp. 303–305.
[16] S. Budavari, M.J. O'Neil, A. Smith, P.E. Heckelman, J.F. Kinneary, The Merck Index, 12th ed., Merck Research Laboratories, Division of Merck & Co., Inc., New Jersey, 1996, pp. 1–2.
[17] A.M.R. Downs, J.E. Sansom, Colophony allergy: a review, Contact Dermatitis 41 (1999) 305–310.

Journal of Pharmaceutical and Biomedical Analysis 66 (2012) 349–351

Contents lists available at SciVerse ScienceDirect

Journal of Pharmaceutical and Biomedical Analysis

journal homepage: www.elsevier.com/locate/jpba

Short communication

Development of a p38δ mitogen activated protein kinase ELISA assay for the quantitative determination of inhibitor activity

Márcia Goettert[a], Nouran Shaalan[b], Ralph Graeser[c], Stefan A. Laufer[a,*]

[a] Department of Pharmaceutical and Medicinal Chemistry, Institute of Pharmacy, Eberhard Karls University of Tübingen, Auf der Morgenstelle 8, 72076 Tübingen, Germany
[b] Department of Pharmaceutical Biology, Faculty of Pharmacy & Biotechnology, German University of Cairo, Egypt
[c] ProQinase GmbH, Breisacher Str. 117, D-79106 Freiburg, Germany

ARTICLE INFO

Article history:
Received 26 February 2012
Accepted 6 March 2012
Available online 15 March 2012

Keywords:
p38δ
ELISA
MAPK
Small-molecule inhibitors
RA

ABSTRACT

The p38 mitogen activated protein kinase (MAPK) has emerged as a target for treating inflammatory diseases, like rheumatoid arthritis (RA). Expression of p38δ is induced in rheumatoid arthritis synovial fibroblasts (RASFs) by a cytokine-independent pathway substantially different from other MAPK pathways. To identify inhibitors of p38δ MAPK, we developed a direct ELISA assay based on a previously described p38α assay for monitoring the phosphorylation of ATF-2. This work presents a straightforward assay for evaluating the potency of small-molecule inhibitors. To validate the assay under optimized conditions, we used reference compounds and achieved results comparable to published data.

© 2012 Elsevier B.V. All rights reserved.

1. Introduction

Mitogen activated protein kinase (MAPK) p38 isoforms play an important role in the regulation of a variety of cellular processes, including pro-inflammatory cytokine activity [1]. To date, little is known about the distinct p38 isoforms. However, some specific physiological functions are suggested by the distinct expression patterns of the different p38 isoforms. The p38 MAPK pathway is activated by proinflammatory cytokines and by cellular stress, including mechanical stress, osmotic shock, and UV light. Cytokines, like TNF-α, IL-1, and IL-6, engage specific cell receptors to activate p38 MAPKs. In turn, p38α induces pro-inflammatory cytokine production, which then leads to a vicious circle [2,3]. The balance of pro- and anti-inflammatory factors plays an important role in self-limited physiological inflammatory responses; loss of this balance can contribute to chronic inflammatory diseases, like Rheumatoid Arthritis (RA). Pro-inflammatory cytokines play an important role in the continuous stimulation of rheumatoid arthritis synovial fibroblasts (RASFs) and other inflammatory cells in the joints [3,4].

The MAPK pathway also regulates the expression of matrix metalloproteases (MMPs). MMP overexpression can cause degradation of components of the extracellular matrix. This is important in regulating cytokines and adhesion molecules, and it is associated with cancer cell invasion and metastasis [4–6].

Typically, the levels of pro-inflammatory cytokines and MMPs are chronically increased in RA. The activation of p38 MAPK appears to be critically involved in their regulation. Interestingly, RASFs characterization has shown that cellular activation can be driven and maintained by both cytokine-dependent and cytokine-independent pathways. All p38 MAPK isoforms have been reported to be activated in RA synovial tissue, but the α and γ isoforms are the most abundantly expressed [3]. Ospelt et al. showed that a specific isoform, p38δ, could be induced in RASFs by a cytokine-independent pathway [5]. Other studies showed that p38δ was predominantly expressed in RA synovial tissue at the site of invasion and bone destruction; the other three p38 isoforms were found in the non-attached lining and sublining of the synovium [3]. Additionally, p38δ induces the production of MMP-1, MMP-3, IL-6, and IL-8. Other works have also described fibroblast-mediated joint destruction through a cytokine-independent pathway. Moreover, a substantial number of patients with RA that received selective cytokine-blockers (biologicals) did not show delays in disease progression. This implied that other, cytokine-independent pathways of inflammation and joint destruction might be involved in RA [2,4].This interesting

Abbreviations: MAPK, mitogen-activated protein kinase; RASFs, rheumatoid arthritis synovial fibroblast; ATF-2, activating transcription factor 2; ELISA, enzyme-linked immunosorbent assay; MMPs, matrix metalloproteases; RA, rheumatoid arthritis; TBS, tris-buffered saline; BB, blocking buffer; KB, kinase buffer; NSB, non-specific binding; BSA, bovine serum albumin; DTT, dithiothreitol; β-Gly, β-glycerolphosphate; TMB, Substrate A (solution containing hydrogen peroxide) and Substrate B (solution containing 3,3′,5,5′ tetramethylbenzidine).

* Corresponding author. Tel.: +49 7071 2972459; fax: +49 7071 295037.
E-mail address: stefan.laufer@uni-tuebingen.de (S.A. Laufer).

0731-7085/$ – see front matter © 2012 Elsevier B.V. All rights reserved.
doi:10.1016/j.jpba.2012.03.008

insight into the differential expression and activation of p38 isoforms has promoted p38δ as an attractive target for treating chronic inflammatory diseases, like RA. In addition, this approach could lead to potential RA-targeting drugs that lack immunosuppressive activity.

2. Experimental

2.1. Materials

Activated p38δ MAP kinase and ATF-2 were purchased from ProQinase Tools & Tests GmbH (Freiburg, Germany). The monoclonal anti-phospho-ATF-2 ($Thr^{69/71}$) peroxidase linked antibody, bovine serum albumin (BSA), dithiothreitol (DTT), and Tween-20 were purchased from Sigma-Aldrich GmbH (Kappelweg, Germany). The TMB Substrate Reagent Set was purchased from BD Biosciences (Erembodegem, Belgium). Reference Standard AS601245, Titrisol® 2 N sulfuric acid (H_2SO_4), and $MgCl_2 \cdot 6H_2O$ pure were purchased from Merck KGA (Darmstadt, Germany). Reference Standard SP600125 and BIRB796 were synthesized in our laboratory (University of Tuebingen). β-Glycerolphosphate (β-Gly), ATP disodium salt hydrate, Tris–HCl, NaCl, and Tris–base were purchased from Fluka (Buchs, Switzerland).

2.2. Assay development and validation

In the present work, we describe the development of a direct enzyme-linked immunosorbent assay (ELISA) for quantifying p38δ MAPK activity after inhibitor treatment. This assay is applicable to routine inhibitor screening. Although similar to existing methods, this assay has the advantages of being easy to perform, accurate, fast, and it does not require radioisotopes.

Because activating transcription factor 2 (ATF-2) can be phosphorylated by MAPKs, we used ATF-2 to measure p38δ kinase activity [7–9]. Thus, in the presence of a candidate p38δ inhibitor, the degree of ATF-2 phosphorylation is inversely correlated with the inhibitor potency. The assay was designed to directly detect ATF-2 phosphorylation with a monoclonal peroxidase-labeled antibody, which was successfully established in a previously described p38α MAPK and JNK3 assay [10,11]. The use of a monoclonal antibody contributes to assay stability and specificity, because it precludes the risk of secondary antibody cross reactivity [11]. However, assays that include bisubstrate enzyme reactions can result in inconstant K_m values for each substrate. Therefore, crucial parameters (concentrations of ATP, ATF-2 substrate, enzyme, antibody, and incubation time) had to be adjusted to optimize the assay.

The inhibitory potency of some potential inhibitors was compared with those reported in the literature by analyzing 3 replicates of each sample. The percent of inhibition is calculated with the following equation:$\text{Inhibition}\,(\%) = 100 - \left(OD_{SAMPLE} - OD_{NSB} / OD_{STIM} - OD_{NSB}\right) \times 100$

2.3. p38δ assay protocol

A Nunc Maxisorp flat-bottomed plate (96 wells; VWR-International GmbH; Bruchsal, Germany) was coated with 0.5 μg ATF-2/50 μl (1:192 in TBS buffer pH 7.8) and incubated overnight at 4 °C. Next, the plate was blocked with blocking buffer (BB – TBS buffer, pH 7.8, 0.025% BSA, and 0.05% Tween-20) for 30 min at room temperature. We prepared a kinase reaction buffer (KB; 500 μl 1 M Tris, pH 7.5; 100 μl 1 M $MgCl_2$, 100 μl 1 M β-Gly, 100 μl 10 mg/ml BSA solution, 10 μl 1 M DTT, 5 μl 10 mM ATP, 10 μl 100 mM Na_3VO_4 and 9175 ml bidistilled water). The KB was used to dilute the kinase at 1:1560 to generate a final concentration of 300 pg/μl. This was used for the inhibitor dilution and transferred to the plate with ATF-2. The reaction was incubated for 50 min at 37 °C. Then, the plate was blocked with BB for 15 min. The antibody was diluted 1:5000 in BB adjusted to pH 6.5. Then, 50 μl of antibody solution was added to each well and incubated for 1 h at 37 °C. After each incubation step, the wells were washed three times with double-distilled water and dried for 5 min at 37 °C. To detect the anti-phospho-ATF-2 complex, the TMB substrate (50 μl/well) was added, and after incubating for 5–10 min at room temperature, a dark blue color developed. The reaction was stopped with 25 μl of 2 N H_2SO_4 per well. The absorbance was measured at 450 nm with an ELISA reader equipped with SOFTmax PRO software.

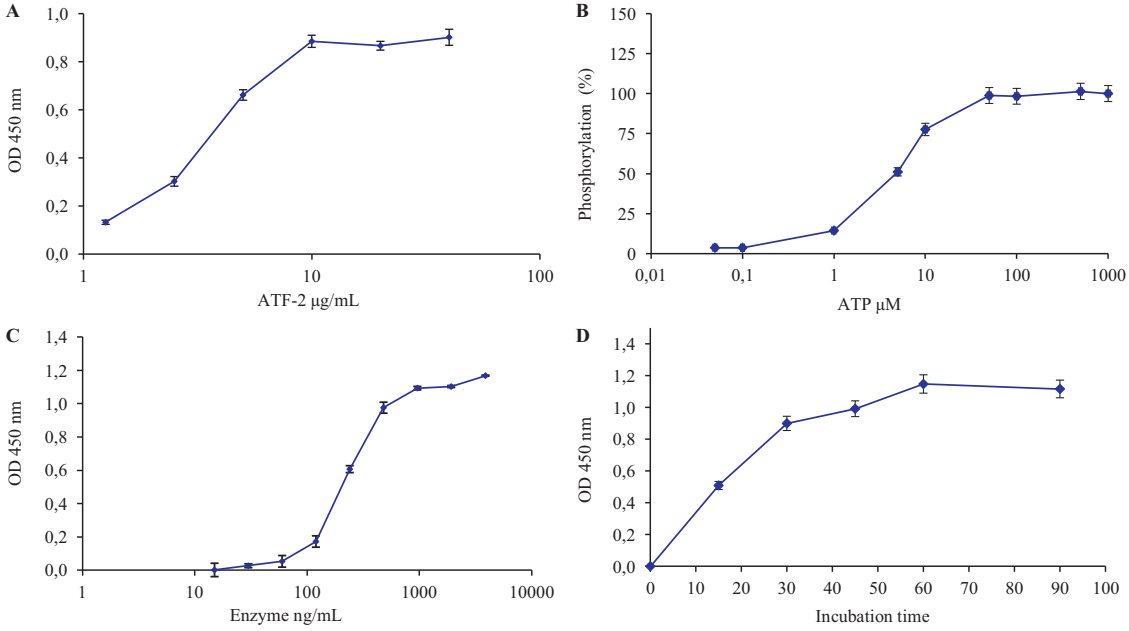

Fig. 1. Determination of the assay conditions. (A) ATF-2 titration, 10 μg/ml; (B) K_m value for ATP, 5 μM; (C) titration of the protein kinase p38δ, 300 pg/ml; (D) determination of the incubation time for the p38δ assay, 50 min.

Table 1
Inhibition of p38δ MAPK by different inhibitors.

Compound	% inhibition 10 μM	% inhibition 1 μM
BIRB796	89.59 ± 1.6*	45.04 ± 5.0*
Literature data	89.0 ± 0.0 [14]	53.0 ± 8.0 [14]; 60.0 ± 5.0 [15]
SP600125	ND	19.55 ± 4.5*
Literature data		18.0 ± 2.0 [15]
AS601245	50.49 ± 5.3*	24.16 ± 8.2*
Literature data	72.0 ± 2.0 [15]	32.0 ± 10.0 [15]

Note: Comparison of published percentage of inhibition (μM) and the results of this study (with asterisks) ± SEM; ND, not determined.

* Mean of three repeats in triplicate determination.

3. Results and discussion

3.1. Assay optimization and validation

First, the concentration of ATF-2 had to be sufficiently high to serve as phosphate acceptor for the kinase reaction. Also, excess of ATF-2 should be present to avoid limiting the reaction. We selected a 10 μg/ml concentration. Next, the monoclonal anti-phospho-ATF-2 ($Thr^{69/71}$) peroxidase antibody concentration was determined by titration. We found that the signal increased linearly over the dilution range tested, and that a dilution of 1:5000 yielded a good signal–noise ratio.

The ATP concentration is crucial for assaying inhibitors that compete with ATP for the binding pocket of the kinase. All four p38 MAPKs can phosphorylate ATF-2, but with different affinities; thus, the particular concentration had to be optimized. In contrast to classic radioactive assays, the ATP concentration in an ELISA is no limited. Thus, the optimal ATP concentration used in an assay should be close to the K_m value to avoid false positive or false negative results with a given test compound [12]. For the final test, we chose the half saturation (50%) concentration of 5 μM (Fig. 1).

With the optimized ATF-2, ATP, and antibody concentrations, we next determined the optimum p38δ concentration within a linear range of activity to achieve maximum assay sensitivity. We found that an enzyme concentration of 300 pg/μl was within the linear range of activity. For screening purposes, the incubation time should also produce a signal within the linear range of detection, where measurements are most sensitive to the activity of competitive inhibitors [12,13]. We found that saturation was achieved after 60 min of incubation. We determined that 50 min of incubation provided a good tradeoff between linearity and signal strength for our assay. After optimizing the assay parameters (10 μg/ml ATF-2, 300 pg/μl p38δ, 5 μM ATP, 1:5000 antibody dilution, and 50 min incubation), we determined the inhibitory potency of some potential inhibitors and compared the results with those reported in the literature (Table 1).

Because p38δ is a novel target, no specific inhibitors are currently identified. However, p38δ inhibition was reported as a "side effect" in testing some known inhibitors of other MAPKs (BIRB796 p38α; SP600125 JNK3 and AS601245 panJNK).

4. Conclusions

This novel in vitro-screening assay is applicable for the detection of small molecule inhibitors of p38δ MAPK. The assay showed good precision and accuracy, and it was simple and rapid to perform (3 h total assay time). Furthermore, for maximum assay sensitivity, we used an ATP concentration in the recommended range (K_m value) and achieved results well comparable to literature data. This assay will facilitate investigations of p38δ as a therapeutic target for RA. It will enable the identification of potent inhibitors and may be instrumental in exploring the mechanisms underlying p38δ activity.

References

[1] T. Efimova, A. Broome, R.L. Eckert, A regulatory role for p38δ MAPK in keratinocyte differentiation, J. Biol. Chem. 278 (2003) 34277–34285.
[2] A. Korb, M. Tohidast-Akrad, E. Cetin, R. Axmann, J. Smolen, G. Schett, Differential tissue expression and activation of p38 MAPK α, β, γ, and δ isoforms in rheumatoid arthritis, Arthr. Rheum. 54 (2006) 2745–2756.
[3] G. Schett, J. Zwerina, G. Firestein, The p38 mitogen-activated protein kinase (MAPK) pathway in rheumatoid arthritis, Ann. Rheum. Dis. 67 (2008) 909–916.
[4] L.C. Hubner, O. Distler, I. Tarner, R.E. Gay, T. Pap, Synovial fibroblast: key players in rheumatoid arthritis, Rheumatology 45 (2006) 669–675.
[5] C. Ospelet, D. Kyburz, M. Pierer, R. Seibl, M. Kurowska, O. Distler, M. Neidhart, U. Muller-Ladner, T. Pap, R.E. Gay, S. Gay, Toll-like receptors in rheumatoid arthritis joint destruction mediated by two distinct pathways, Ann. Reum. Dis. 63 (Suppl. II) (2004) 90–92.
[6] M.R. Junttila, R. Ala-aho, T. Jokilehto, J. Peltonen, M. Kallajoki, R. Grenman, P. Jaakkola, J. Westermarck, V.-M. Kähari, p38α and p38α mitogen-activated protein kinase isoform regulates invasion and growth of head and neck squamous carcinoma cells, Oncogene 26 (2007) 5267–5279.
[7] H. van Dam, D. Wilhelm, I. Herr, A. Steffen, P. Herrlich, P. Angel, ATF-2 is preferentially activated by stress-activated protein kinases to mediate c-Jun induction in response to genotoxic agents, EMBO J. 14 (1995) 1798–1811.
[8] T. Yamasaki, A. Takahashi, J. Pan, N. Yamaguchi, K.K. Yokoyama, Phosphorylation of activation transcription factor-2 at serine 121 by protein kinase C controls c-Jun-mediated activation of transcription, J. Biol. Chem. 284 (2009) 8567–8581.
[9] W.F. Waas, H.H. Lo, K.N. Dalby, The kinetic mechanism of the dual phosphorylation of the ATF-2 transcription factor by p38 mitogen-activated protein (MAP) kinase alpha: implications for signal/response profiles of MAP kinase pathways, J. Biol. Chem. 276 (2001) 5676–5684.
[10] M. Goettert, R. Graeser, S.A. Laufer, Optimization of a nonradioactive immunosorbent assay for p38α mitogen-activated protein kinase activity, Anal. Biochem. 406 (2010) 233–234.
[11] M. Goettert, S. Luik, R. Graeser, S.A. Laufer, A direct ELISA assay for quantitative determination of the inhibitory potency of small molecules inhibitors for JNK3, J. Pharm. Biomed. Anal. 55 (2011) 236–240.
[12] R.A. Copeland, Mechanistic consideration in high-throughput screening, Anal. Biochem. 320 (2003) 1–12.
[13] R. Copeland, Enzymes: A Practical Introduction to Structure, Mechanism and Data Analysis, John Wiley & Sons, New York, 2000, pp. 188–263.
[14] Y. Kuma, G. Sabio, J. Bains, N. Shpiro, R. Márquez, A. Cuenda, BIRB796 inhibits all p38 MAPK isoforms in vitro and in vivo, J. Biol. Chem. 280 (2005) 19472–19479.
[15] J. Bain, L. Plater, M. Elliott, N. Shpiro, C.J. Hastie, H. MacLauchlan, I. Klevernic, J.S.C. Arthur, D.R. Alessi, P. Cohen, The selectivity of protein kinase inhibitors: a further update, Biochem. J. 408 (2000) 297–315.

Journal of Pharmaceutical and Biomedical Analysis 66 (2012) 352–355

Contents lists available at SciVerse ScienceDirect

Journal of Pharmaceutical and Biomedical Analysis

journal homepage: www.elsevier.com/locate/jpba

Short communication

A single serum dilution enzyme-linked immunosorbent assay for determining anti-human papillomavirus (HPV) antibody titres in humans immunised with prophylactic HPV vaccines

Yingji Jin [a], Hyoung Jin Kim [a], Ga Won Yim [b], Young Tae Kim [b], Don Yong Chang [a], Hong-Jin Kim [a,*]

[a] College of Pharmacy, Chung-Ang University, 221 Huksuk-Dong, Dongjak-Gu, Seoul 156-756, Republic of Korea
[b] Division of Gynecologic Oncology, Department of Obstetrics and Gynecology, Yonsei University College of Medicine, Seoul, Republic of Korea

ARTICLE INFO

Article history:
Received 5 December 2011
Received in revised form 6 March 2012
Accepted 8 March 2012
Available online 15 March 2012

Keywords:
Enzyme-linked immunosorbent assay
Human papillomavirus
Serology
Virus-like particle

ABSTRACT

Two types of prophylactic human papillomavirus (HPV) vaccines are currently available. However, there is no simple monitoring system for assessing acquired immunity that can cope simultaneously with large numbers of serum samples. Approximately 30% of women with normal cytology are known to be seropositive for HPV types 16 and 18 because of the high prevalence of these HPV types. Therefore, to be useful the monitoring system has to discriminate clearly between vaccine recipients and other serology groups. However, there has never been any focus on developing a method to satisfy this condition. In this study, we developed a high-throughput single-serum-dilution enzyme-linked immunoassay (ELISA) system for determining anti-HPV antibody titres following vaccination. We optimised the conditions for each ELISA step to increase its accuracy and precision and to avoid the high background of non-specific reactions that is a major problem for serology assays. The new ELISA system has superior linearity, accuracy and reproducibility. Moreover, it clearly discriminated between antibody levels in vaccine recipients and those in other serology groups such as individuals with normal cervical cytology and those with cervical cancer. Therefore, this single-serum-dilution ELISA should be very useful for assessing the acquired immunity of HPV vaccine recipients.

© 2012 Elsevier B.V. All rights reserved.

1. Introduction

Two prophylactic vaccines for preventing genital human papillomavirus (HPV) infection are currently available: one is quadrivalent (Gardasil®, Merck) and the other bivalent (Cervarix™, GlaxoSmithKline) [1]. The antibody levels elicited by the two prophylactic HPV vaccines are significantly higher than those elicited by natural HPV infection and highly efficacious for protecting against HPV infection [2]. A current study has revealed that serum antibody levels induced by natural HPV infection do not protect against reinfection with HPV [3]. Therefore, antibody levels in excess of those elicited by natural HPV infection have been regarded as the best guide to estimate the potential for protecting against HPV infection [4]. The difference between serum antibody levels in natural HPV infection and vaccination is known to exceed 100-fold [5]. Therefore, precise analysis of serum antibody levels following vaccination is theoretically impossible if the ELISA system is set to measure antibody levels caused by natural HPV infection. Indeed, the serum dilution range for measuring antibody levels by natural HPV infection was not suitable for discriminating between vaccine recipients and other serology groups (Supplementary material-I). For an accurate analysis, the antibody levels in sera have to be determined by the traditional method of end-point titration [6]. However, the end-point method cannot cope with large numbers of sera and is not suitable for evaluating vaccine efficacy over long periods of time. Therefore, the development of a high throughput assay system for measuring antibody levels of vaccine recipients is a high priority.

In this study, we have developed such a method. In the assay we use HPV16 and 18 L1 VLPs as coating antigens and detect type-specific human serum IgG bound to the VLPs using HRP-conjugated anti-human IgG antibody. We have optimised the system so that for the first time there is no interference from antibody levels due to natural HPV infection.

2. Materials and methods

2.1. Preparation of HPV16 and 18 L1 VLPs

HPV16 and 18 L1 VLPs were prepared as described previously [7]. The purity of the VLPs was confirmed to be more than 95%.

* Corresponding author. Tel.: +82 2 820 5613; fax: +82 2 816 7338.
E-mail address: hongjink@cau.ac.kr (H.-J. Kim).

0731-7085/$ – see front matter © 2012 Elsevier B.V. All rights reserved.
doi:10.1016/j.jpba.2012.03.011

2.2. Serum samples

We obtained serum samples from Korean women who participated in previous studies [8,9]. The samples were from children (age 1–10 years), women with normal cervical cytology (age 24–69 years), women with high-grade cervical intraepithelial neoplasia (CIN, age 22–74 years) and women with cervical cancer (age 26–74 years). The four women in the vaccination group received three doses of Cervarix™, and blood samples were also obtained from them. The procedures for vaccination and collection of blood were approved by the institutional review board of the College of Medicine, Yonsei University.

2.3. Titration of anti-HPV16 and 18 L1 IgGs by the single serum dilution ELISA method

The volumes of solution used for ELISA were as follows: coating, 100 μl; blocking, 300 μl; serum and secondary antibody reaction, 100 μl; wash, 250 μl; substrate reaction 100 μl. ELISA plates with 96 wells (Cat. No. 655061, Greiner bio one, Germany) were coated overnight with 100 ng of purified HPV16 or 18 L1 VLP prepared in PBS containing 1 M NaCl. The 1 M NaCl in the coating buffer significantly increased the sensitivities (data not shown). The ELISA sensitivity as a function of the coating amounts were described in Supplementary material-II. To prepare the references we used sample no. 1 from the vaccination group (Supplementary material-III and IV). The anti-HPV16 and 18 L1 IgG titres of the reference serum were determined by the end-point serial dilution ELISA method as described in Supplementary material-III and IV, yielding titres for HPV16 and 18 of 204,800 each. The reference sera were prepared by two-fold serial dilution in commercial human male serum (Sigma, USA). The references and serum samples were diluted 1:400 with 1% skim milk (Cat. No. 30620074-1, Bioworld, USA) in PBS containing 0.05% Tween 20 (PBS-T) and incubated in 96-well plates at 37 °C for 2 h. The sensitivities according to the serum dilution were presented in Supplementary material-V. After three washes with PBST, each plate was incubated with HRP-conjugated goat anti-human IgG antibody (diluted 1:5000 with 1% skim milk in PBST, Cat. No. A8667, Sigma, USA) at 37 °C for 1 h. The anti-human IgG antibody is specifically reacted with the whole molecule of human IgG. The plates were developed with *o*-phenylenediamine (Sigma, USA) and measured absorbance at 492 nm. The IgG levels for HPV16 and 18 were determined from the reference curves. The limits of detection (LoD) and of quantification (LoQ) were determined as described previously [10]. LOD and LOQ were estimated by a signal-to-noise ratio of 3:1 and 10:1, respectively. The equations for LOD and LOQ are as follows: LOD = 3.3 × standard deviation (SD)/slope of the calibration curve (S), LOQ = 10 × SD/S. Coefficient variation (CV) was determined by the equation as follows: SD/observed mean titre × 100 [11].

2.4. Statistical analysis

The statistical significance of differences between groups was determined using two-tailed Student's *t*-tests. $P < 0.01$ was considered significant.

3. Results and discussion

3.1. Sensitivities of ELISAs as a function of blocking agent

As shown in Fig. 1, 5% skim milk effectively blocked non-specific binding in sera of women with normal cytology. However, bovine serum albumin (BSA, Bioworld, USA), fetal bovine serum (FBS, Sigma, USA) and Tween 20 (Sigma, USA) did not prevent non-specific binding and actually reduced the sensitivity of detection in the vaccination group. Interestingly, the lowest background and highest sensitivity was obtained in the absence of any blocking agent. Therefore, we omitted any blocking step, which had the additional advantage of reducing the time for the ELISA. The ELISA plates are manufactured from polystyrene which strongly bound to proteins. However, the components contained in the sera of children and normal cytology groups rarely caused non-specific reactions in the non-blocking condition, while non-specific reactions occurred in the conditions blocked with BSA, FBS and Tween 20 (Supplementary material-VI). Therefore, the components of human sera are thought to preferentially bind with BSA, FBS and Tween 20 rather than the non-blocked polystyrene. In addition, we assume that the decreases of sensitivities when using a blocking agent occurred because the components contained in the blocking agents interfered with the specific binding between anti-HPV antibodies and coated VLPs. These results suggest that the non-blocking condition can be considered to increase the sensitivity and reduce the background OD in the other ELISA system aimed at measuring antibody levels contained in human sera.

3.2. Evaluation of the single serum dilution ELISA

To confirm whether the reactions of the ELISA were specific for HPV 16 and 18, the anti-HPV16 or 18 antibodies contained in the sera of vaccine recipients were pre-incubated with the corresponding purified VLPs to block the reaction between type-specific serum antibodies and VLPs on the plate. In the ELISA measuring anti-HPV16 L1 IgG, pre-incubation with HPV16 L1 VLP blocked the reaction between anti-HPV16 L1 IgG and coated HPV16 L1 VLP, while pre-incubation with HPV18 L1 VLP did not (Fig. 2A), and the equivalent result was obtained in the reciprocal experiment (Fig. 2B). These results indicate that our ELISA system is highly type-specific. The references for both HPV16 and 18 showed excellent linearity ($R^2 = 0.99$, data not shown). LoD and LoQ for HPV16 were 355 and 1076, respectively, and for HPV18 they were 389 and 1180. The LoD and LoQ values refer to antibody titres presented as natural numbers. The inter-assay coefficient of variation (CV) and recovery (%) for HPV16 and HPV18 were confirmed to be superior (Table 1).

3.3. Titration of the anti-HPV16 and 18 L1 IgGs of the normal cytology, high grade CIN, cervical cancer and vaccination groups using the single serum dilution ELISA

To evaluate the applicability of the single-serum dilution ELISA, we measured the antibody titres of the normal cytology, high grade CIN, cervical cancer and vaccination groups. There was no overlap in antibody titre between the vaccination group and other tested groups, and both the anti-HPV16 and 18 L1 IgG titres of the vaccination group were significantly higher than other groups (Fig. 3). These results indicate that our single-serum dilution ELISA method is highly suitable for assessing antibody titres induced by prophylactic HPV vaccines and for comparing antibody levels between vaccine recipients and other serology groups such as individuals with normal cervical cytology and those with cervical cancer.

To assess the anti-HPV IgG levels of non-vaccinated groups, sera should be diluted 1:100 or 1:200 because their antibody levels cannot be effectively detected in high-serum dilution ratios [8]. However, the antibody levels of vaccine recipients were detectable despite the fact that the sera were diluted 1:3200, indicating that the antibody titrations for vaccine recipients cannot be compatible with those for non-vaccinated recipients in a type of ELISA system (Supplementary material-V). For this reason, the original antibody levels of the vaccine recipients were not comparably presented in the previous ELISA system for non-vaccine recipients (Supplementary material-I). Our results suggest that a suitable serum dilution range for vaccine recipients is 1:400 to 1:3200, and

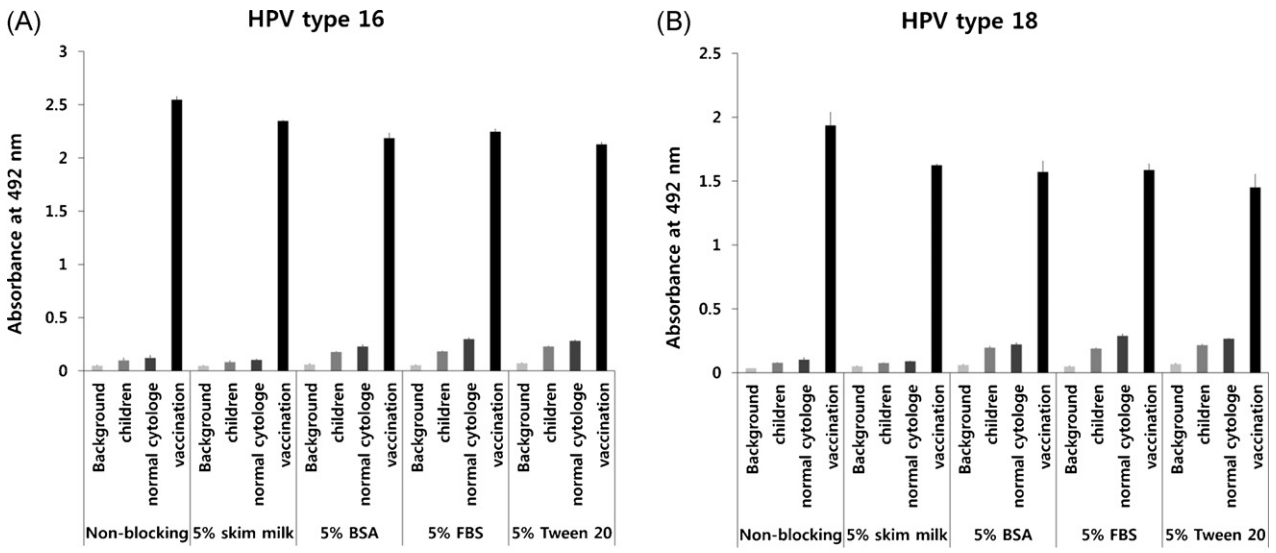

Fig. 1. The sensitivity of the ELISA as a function of blocking agent. To investigate the blocking conditions with the highest sensitivity and lowest non-specific reactions, the OD values of the background, children, normal cytology and vaccination group were compared. The ELISA plates were coated with purified HPV16 (A) or 18 VLP (B) and blocked for 2 h with each blocking agent prepared in PBST. Thereafter, each serum was diluted to 1:400 and incubated at 37 °C for 2 h. Other reactions were performed as described in Materials and Methods (Section 2.3). Data are the means ± SD of duplicate assays.

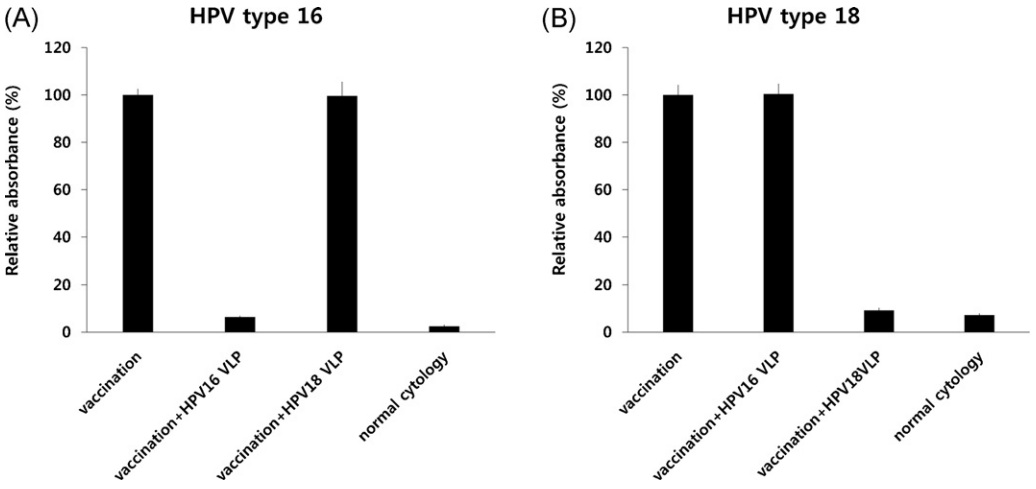

Fig. 2. Evaluation of the type specificity of the single-serum dilution ELISA. The ELISA plates were coated with HPV16 or 18 L1 VLP (100 ng per well). Sera of the vaccination group were reacted with the purified HPV16 or 18 L1 VLP prior to the reaction with the VLP coated on the plates. Fifty microliters of the serum, which was diluted 1:200, mixed with 50 μl of purified HPV16 or 18 L1 VLP (20 μg/ml) and incubated at RT for 10 min in a test tube. The incubated mixtures were added to the plate and further incubated at 37 °C for 2 h. Subsequent reactions were performed as described in Materials and Methods. Panels A and B are the results of the type specificity tests for HPV16 and 18, respectively. The OD value of vaccination group in each assay was set at 100%. Data are the means ± SD of triplicate.

the antibody levels of vaccine recipients can be determined without interference of those by natural HPV infection in the suggested serum dilution range.

Although there was a report using reference sera to calibrate the anti-HPV antibody levels, the serially diluted sera had to be applied for the titrations [12]. Therefore, there has not been an ELISA system that uses the single-serum dilution. In addition, previous methods have some defects such as requiring a blocking step that exceeds 2 h and specialised techniques or equipment [8,13]. A routinely applicable monitoring system for evaluating vaccine efficacy is expected to be continuously required to standardise antibody levels for boosting immunisation. In addition,

Table 1
Inter-assay precision and accuracy of single-serum dilution ELISA for HPV type 16 and 18. Serum antibody levels were presented on a natural and logarithmic number scale (natural number/$\log_{10}$ scale number).

HPV type	Expected (titer/$\log_{10}$ titer)	*N*	Observed (titer/$\log_{10}$ titer)	SD	CV (%)	Recovery (%)
16	High (25600/4.4)	5	25555/4.4	1566/0.02	6.1/0.5	99.8/99.9
	Medium (3200/3.5)	5	3627/3.6	286/0.03	7.8/0.8	113.4/101.7
	Low (400/2.6)	5	428/2.6	70/0.07	16.4/2.6	107.1/101.0
18	High (25600/4.4)	5	24698/4.4	595/0.01	2.4/0.2	96.5/99.8
	Medium (3200/3.5)	5	3452/3.5	404/0.05	11.7/1.4	107.9/101.0
	Low (400/2.6)	5	430/2.6	50/0.05	11.6/1.9	107.5/101.2

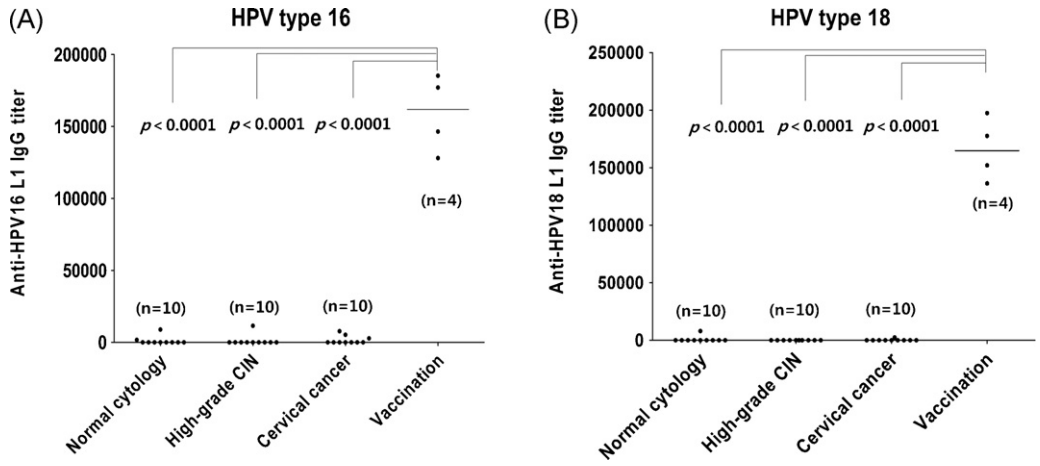

Fig. 3. Anti-HPV16 and 18 L1 IgG titres of the groups with normal cytology, high-grade CIN, and cervical cancer, and of the vaccination group, determined by single serum dilution ELISA. To measure the anti-HPV16 L1 IgG (A) and anti-HPV18 L1 IgG (B) titres, ten sera from the normal cytology, high-grade CIN and cervical cancer groups and four from the vaccination group were used. Antibody titres were deduced from the reference curves for HPV16 VLP and 18 VLP and are presented as dot plots. The horizontal bars indicate median IgG titres.

such a system is essential for investigating effective dosing schedules. Therefore, an ELISA has to be not only convenient but also effective in order to be widely applicable. Our system can cope with approximately 40 serum samples per plate at the same time, does not require specialised techniques or a blocking step and is compatible with these demands for routine and convenient application of the ELISA system. We anticipate that our ELISA system will provide an opportunity to increase the effectiveness of HPV vaccines.

4. Conclusion

The optimised single-serum dilution ELISA showed superior specificity, linearity, accuracy and reproducibility. Our ELISA system can clearly discriminate the anti-HPV antibody levels between vaccinated and non-vaccinated recipients, suggesting that the system is useful to assess acquired immunity from the vaccination.

Acknowledgements

This research was supported by a Grant (PA100009) from the 2010 Seoul R&BD Program for the commercialisation of a patent of the Republic of Korea.

Appendix A. Supplementary data

Supplementary data associated with this article can be found, in the online version, at doi:10.1016/j.jpba.2012.03.011.

References

[1] I.H. Frazer, Measuring serum antibody to human papillomavirus following infection or vaccination, Gynecol. Oncol. 118 (2010) S8–S11.
[2] M. Ferguson, D.E. Wilkinson, T. Zhou, in: WHO meeting on the Standardization of HPV Assays and the role of the WHO HPV Laboratory Network in Supporting Vaccine Introduction, held on 24–25 January 2008 Geneva, Switzerland, Vaccine 27 (2009) 337–347.
[3] R.P. Viscidi, M. Schiffman, A. Hildesheim, R. Herrero, P.E. Castle, M.C. Bratti, A.C. Rodriguez, M.E. Sherman, S. Wang, B. Clayman, R.D. Burk, Seroreactivity to human papillomavirus (HPV) types 16, 18, or 31 and risk of subsequent HPV infection: results from a population-based study in Costa Rica, Cancer Epidemiol. Biomarkers Prev. 13 (2004) 324–327.
[4] T.F. Schwarz, Clinical update of the AS04-adjuvanted human papillomavirus-16/18 cervical cancer vaccine, Cervarix Adv. Ther. 26 (2009) 983–998.
[5] M. Stanley, D.R. Lowy, I. Frazer, Chapter 12: prophylactic HPV vaccines: underlying mechanisms, Vaccine 24 (Suppl. 3) (2006), S3/106–S3/113.
[6] K. Miura, A.C. Orcutt, O.V. Muratova, L.H. Miller, A. Saul, C.A. Long, Development and characterization of a standardized ELISA including a reference serum on each plate to detect antibodies induced by experimental malaria vaccines, Vaccine 26 (2008) 193–200.
[7] H.J. Kim, S.Y. Kim, S.J. Lim, J.Y. Kim, S.J. Lee, H.-J. Kim, One-step chromatographic purification of human papillomavirus type 16 L1 protein from *Saccharomyces cerevisiae*, Protein Exp. Purif. 70 (2010) 68–70.
[8] N.H. Jeong, M.K. Woo, N.W. Lee, S.J. Hur, K.S. Choi, H.J. Kim, Human papillomavirus 16 and 18 L1 serology in Korean women with high-grade cervical intraepithelial neoplasia and cervical cancer, Arch. Pharm. Res. 32 (2009) 1013–1020.
[9] N.H. Jeong, N.W. Lee, M.K. Woo, H.J. Kim, Serologic response to human papillomavirus type 16 virus-like particles in Korean women with cervical precancerous and cancerous lesions, Arch. Pharm. Res. 32 (2009) 383–389.
[10] G. Murtaza, M. Ahmad, M.A. Madni, M.W. Asghar, A new reverse phase HPLC method with fluorescent detection for the determination of salbutamol sulfate in human plasma, B. Chem. Soc. Ethiopia 23 (2009) 1–8.
[11] M.P. Molloy, E.E. Brzezinski, J. Hang, M.T. McDowell, R.A. VanBogelen, Overcoming technical variation and biological variation in quantitative proteomics, Proteomics 3 (2003) 1912–1919.
[12] D.M. Harper, E.L. Franco, C. Wheeler, D.G. Ferris, D. Jenkins, A. Schuind, T. Zahaf, B. Innis, P. Naud, N.S. De Carvalho, C.M. Roteli-Martins, J. Teixeira, M.M. Blatter, A.P. Korn, W. Quint, G. Dubin, Efficacy of a bivalent L1 virus-like particle vaccine in prevention of infection with human papillomavirus types 16 and 18 in young women: a randomised controlled trial, Lancet 364 (2004) 1757–1765.
[13] A.V. Ramanakumar, P. Thomann, J.M. Candeias, S. Ferreira, L.L. Villa, E.L. Franco, Use of the normalized absorbance ratio as an internal standardization approach to minimize measurement error in enzyme-linked immunosorbent assays for diagnosis of human papillomavirus infection, J. Clin. Microbiol. 48 (2010) 791–796.

Journal of Pharmaceutical and Biomedical Analysis 66 (2012) 356–358

Contents lists available at SciVerse ScienceDirect

Journal of Pharmaceutical and Biomedical Analysis

journal homepage: www.elsevier.com/locate/jpba

Short communication

Determination of eight amino acids in mice embryonic stem cells by pre-column derivatization HPLC with fluorescence detection

Liyuan Zhang[1], Yubo Li[1], Huifang Zhou, Lixin Li, Yuming Wang, Yanjun Zhang*

Tianjin Key laboratory of TCM Chemistry and Analysis, School of Traditional Chinese Materia Medica, Tianjin University of TCM, Tianjin 300193, China

ARTICLE INFO

Article history:
Received 13 October 2011
Accepted 8 March 2012
Available online 17 March 2012

Keywords:
Pre-column derivatization
HPLC
Mice embryonic stem cells
Dansyl chloride
Amino acid

ABSTRACT

A precise, accurate, and selective pre-column derivatization HPLC method with fluorescence detection was validated and used for the determination of amino acids (proline, valine, methionine, isoleucine, leucine, tryptophan, phenylalanine, and lysine) in mice embryonic stem (ES) cells. The cell sample was derivatized by dansyl chloride, and the analytes were separated on a C_{18} column. The method provided good reproducibility and sensitivity for the quantification of the eight analytes with average recovery factors of less than 107.43% and higher than 91.25%, respectively. Intra-day precision was between 2.0% and 4.9%, and inter-day precision was between 2.9% and 6.0%. The %RSD values for repeatability were below 8.8. This assay can be readily utilized as a precise, sensitive, and highly accurate quality-control method for amino acids in mice ES cells.

Crown Copyright © 2012 Published by Elsevier B.V. All rights reserved.

1. Introduction

Embryonic stem (ES) cells are derived from the inner cell mass of early embryos [1,2]. They are characterized by their capacity for self-renewal and potential for differentiation into the cells of all three germ layers [3–7]. The recent studies not only provide a valuable model for the investigation of developmental biology, but also offer a potential in vitro system on which to test the toxic effects of some drugs [8–11]. Thus, the use of ES cells in vitro culture methods is of wide interest.

The quantitative determination of amino acids in biological samples has a certain significance in the understanding of the changes in amino acids and the pathology of some diseases [12]. Most groups of amino acids have weak luminescence, due to the high sensitivity, an HPLC method with fluorescence detection would have higher selectivity and sensitivity, allowing researchers to focus on the characteristics of the samples [13].

An understanding of intracellular amino acid concentrations can provide important information on cell growth and metabolism. Changes of endogenous amino acid concentrations in ES cells can cause embryo toxicity and teratogenicity. However, because intracellular amino acid concentrations are usually low, the method must be sensitive enough. A study was thus undertaken to assess the applicability of the proposed pre-column derivatization HPLC method with fluorescence detection for the determination of amino acids in mice ES cells and adapt it to our requirements.

2. Experimental

2.1. Chemicals

Reference standards of the eight amino acids (purity 98%) were purchased from the National Institute for the Control of Pharmaceutical and Biological Products (Beijing, China), HPLC-grade acetonitrile and methanol were obtained from Fisher Co. Ltd. (USA). Dansyl chloride and other reagents were of analytical grade.

2.2. Preparation of Li_2CO_3 buffer, standard solutions, and derivatization reagent

Li_2CO_3 powder (0.2960 g) was dissolved in water (100 mL) at a concentration of 40 mmol/L, pH was adjusted to 9.5 with acetic acid. Stock solutions of the eight amino acids in Li_2CO_3 buffer solution were prepared, respectively. Standard solutions were prepared by diluting the stock solutions with Li_2CO_3 buffer solution to obtain series concentrations. Dansyl chloride (0.0270 g) was dissolved in acetonitrile (100 mL) to a concentration of 1 mmol/L.

2.3. Cell sample preparation and pretreatment

The following describes the preparation and pretreatment of cell samples [14]. R1 mES cells (Institute of Biochemistry and Cell Biology, Shanghai Institutes for Biological Sciences, Chinese Academy of Sciences) were cultured in a T25 flask containing MEF feeder cells.

* Corresponding author. Tel.: +86 022 59596223.
E-mail address: tianjin_tcm001@sina.com (Y. Zhang).
[1] Liyuan Zhang and Yubo Li contributed equally to this work as co-first authors.

0731-7085/$ – see front matter Crown Copyright © 2012 Published by Elsevier B.V. All rights reserved.
doi:10.1016/j.jpba.2012.03.014

mES cells were routinely grown as a monolayer in the presence of a leukemia inhibitory factor (1000 U/mL, Gibco) to maintain their undifferentiated status and then passaged every second day. The ES cell medium consisted of high-glucose DMEM (4.5 g glucose/L, Gibco) supplemented with 15% FBS (Biochrom s0615), 50 U/mL penicillin, 50 mg/mL streptomycin, 1% nonessential amino acids (Gibco), and 0.1 mM β-mercaptoethanol (Sigma). Cells were incubated in a 37 °C incubator supplied with 5% CO_2.

2.4. Preparation of sample solutions

The preparation of sample solutions was performed as in Refs. [15,16]. In brief, the cell sample was removed from the −80 °C refrigerator, vortexed, and then centrifuged (10,000 r/min, 15 min). 100 μL of the supernatant was transferred and evaporated under a stream of nitrogen gas to dryness (60 °C). Then, 100 μL Li_2CO_3 buffer solution was added to the residue, followed by 100 μL derivatization solution. The sample solution was vortexed for 30 s and then sealed, and derivatization was carried out at 60 °C for 30 min in water. After the addition of 10 μL methylamine hydrochloride and vortex mixing, the derivatized sample was transferred to a vial after filtration.

2.5. HPLC conditions

Analysis was carried out on a Shimadzu HPLC system (LC-20A, Japan) equipped with an RF-10AXL fluorescence detector. The analyte was separated on an analytical column Diamonsil C_{18} (5 μm, 150 mm × 4.6 mm). The mobile phase consisted of sodium acetate buffer containing 0.02% trithylamine (pH 7.2; 0.02 M) (A) and sodium acetate buffer (pH 7.2; 0.1 M)–acetonitrile–methanol (20:40:40, v/v/v) (B). Using a gradient program of 45–50% (v/v) B in 0–5 min, 50–54% B in 5–25 min, 54–85% B in 25–40 min, 85% B in 40–45 min, and 85–45% B in 45–60 min. The mobile phase was filtered under a vacuum through a 0.45 μm membrane filter and degassed before use. Analysis was carried out at a flow rate of 0.9 mL/min, and the column temperature was set to 30 °C. The fluorescence excitation and emission wavelengths were 330 and 508 nm, respectively, and the injection volume was 10 μL.

3. Results and discussion

3.1. Method validation

3.1.1. Specificity and linearity

As shown in Fig. 1,the selectivity of the analysis is shown by a symmetrical resolution of the peaks with no interference around the retention time of the analyte. Good linear regression equations (correlation coefficients >0.99) were obtained within the tested ranges.

3.1.2. LOD and LOQ

The LODs were 0.17, 0.16, 0.11, 0.26, 0.27, 0.35, 0.11, and 0.060 μmol/L of the eight amino acids, respectively. Their corresponding LOQs were 0.50, 0.48, 0.33, 0.77, 0.81, 1.0, 0.34, and 0.18 μmol/L, respectively, indicating the high sensitivity of the HPLC method used in this study.

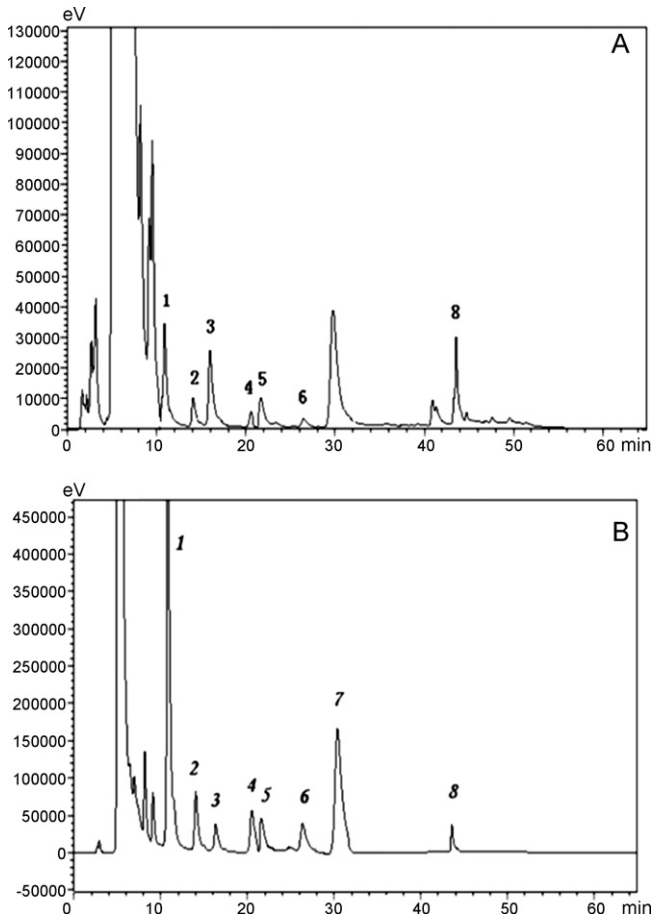

Fig. 1. HPLC chromatograms of cell sample (A) and amino acid standard (B): 1, proline; 2, valine; 3, methionine; 4, isoleucine; 5, leucine; 6, tryptophan; 7, phenylalanine; 8, lysine.

3.1.3. Precision, repeatability, stability and recovery

The intra-day precision was between 2.0% and 4.9%, and inter-day precision was between 2.9% and 6.0%. The %RSD values for repeatability were 7.6, 7.0, 4.7, 7.5, 7.6, 7.8, 8.8, and 7.5 for the eight analytes, respectively, and the sample solution was found to be stable for 12 h at room temperature (RSD < 7.3%). The results demonstrate that the method is precise, sensitive, and highly accurate in simultaneously determining eight amino acids. The recoveries of eight analytes were between 91.25% and 107.43%, and their RSDs were between 0.4% and 2.5%.

3.2. Contents of eight analytes

The method developed as described above was tested by its application in the analysis of the contents of eight amino acids in mice ES cells. Three batches of cell samples were tested, all of which showed good reproducibility. The mean contents of the eight amino acids in mice ES cells are summarized in Table 1. As shown in Table 1, a high degree of variability in the content of the eight amino acids was observed; this could be due to the different actions

Table 1
The results (μmol/L) of determination of eight amino acids in mice embryonic stem cells.

Batch	Proline	Valine	Methionine	Isoleucine	Leucine	Tryptophan	Phenylalanine	Lysine
1	10.88	16.66	45.00	5.49	10.19	4.85	19.61	5.78
2	11.21	17.00	45.70	6.39	9.89	5.11	19.53	5.99
3	11.52	17.90	47.73	6.34	10.10	5.62	20.69	6.28

the eight amino acids played in the cell or the different biochemical pathways in which the eight amino acids participated.

4. Conclusion

In this work, a specific, sensitive, and confirmatory HPLC-fluorescence detection method for the simultaneous determination of eight amino acids in mice ES cells was developed. The proposed method was found to be accurate and precise, and was fully validated, and applied to the preparation of the samples.

Acknowledgments

This study was supported by China Postdoctoral Science Foundation (200902281), National Basic Research Program of China (973 Program) (2011CB505300, 2011CB505302) and Program for Changjiang Scholars and Innovative Research Team in University (IRT0973).

References

[1] M.J. Evans, M.H. Kaufman, Establishment in culture of pluripotential cells from mouse embryos, Nature 292 (1981) 154–156.
[2] J.A. Thomson, J. Itskovitz-Eldor, S.S. Shapiro, M.A. Waknitz, J.J. Swierqiel, V.S. Marshall, J.M. Jones, Embryonic stem cell lines derived from human blastocysts, Science 282 (1998) 1145–1147.
[3] M.K. Carpenter, M.S. Inokuma, J. Denham, T. Mujtaba, C.P. Chiu, M.S. Rao, Enrichment of neurons and neural precursors from human embryonic stem cells, Exp. Neurol. 172 (2001) 383–397.
[4] B.E. Reubinoff, P. Itsykson, T. Turetsky, Neural progenitors from human embryonic stem cells, Nat. Biotech. 19 (2001) 1134–1140.
[5] J.M. Zhou, J.X. Chu, X.J. Chen, An improved protocol that induces human embryonic stem cells to differentiate into neural cells in vitro, Cell Biol. Int. 32 (2008) 80–85.
[6] X.J. Li, Z.W. Du, E.D. Zarnowska, M. Pankratz, L.O. Hansen, R.A. Pearce, S.C. Zhang, Specification of motoneurons from human embryonic stem cells, Nat. Biotech. 23 (2005) 215–221.
[7] J.M. Zhou, F.Y. Xing, J.J. Shi, Z.F. Fang, X.J. Chen, F. Chen, Quality of embryonic bodies and seeding density effects on neural differentiation of mouse embryonic stem cells, Cell Biol. Int. 32 (2008) 1169–1175.
[8] M. Festag, C. Sehner, P. Steinberg, An in vitro embryotoxicity assay based on the disturbance of the differentiation of murine embryonic stem cells into endothelial cells. I: Establishment of the differentiation protocol, Toxicol. In vitro 21 (2007) 1619–1630.
[9] T.C. Stummann, L. Hareng, S. Bremer, Embryotoxicity hazard assessment of cadmium and arsenic compounds using embryonic stem cells, Toxicology 252 (2008) 118–122.
[10] M. Murabe, J. Yamauchi, Y. Fujiwara, Y. Miyamoto, M. Hiroyama, A. Sanbe, A. Tanoue, Estimation of the embryotoxic effect of CBZ using an ES cell differentiation system, Biochem. Biophys. Res. Commun. 356 (2007) 739–744.
[11] M. Murabe, J. Yamauchi, Y. Fujiwara, M. Hiroyama, A. Sanbe, A. Tanoue, A novel embryotoxic estimation method of VPA using ES cells differentiation system, Biochem. Biophys. Res. Commun. 352 (2007) 164–169.
[12] M. Kang, D.Z. Wang, L.R. Zhang, Quantitative analysis of free amino acids by reversed-phase high performance liquid chromatography with DABS-CI pre-column derivatization technique, Anti-infect. Pharm. 1 (2004) 117–122.
[13] Y.H. Ping, X.H. Yang, H.H. Liu, The application of HPLC-fluorescence derivatization in biopharmaceutical analysis, Jiangxi Med. Lab. Sci. 24 (2006) 61–64.
[14] L. Zhao, X.L. Du, J.M. Wang, L. Chen, Culture of mouse embryonic stem cells, Prog. Modern Biomed. 7 (2007) 916–918.
[15] Y.Y. Ding, M.X. Xie, Z.W. Deng, The study of the conditions of dansyl chloride as pre-column derivatization of amino acid, J. Beijing Normal University (Nat. Sci.) 37 (2001) 526–529.
[16] X.W. Zhu, X.X. Gao, F. An, X.J. Guo, Determination of 22 kinds of free amino acid in urine of hypertensive patient by pre-column derivatization HPLC with fluorescence detection, China Pharm. 21 (2010) 2823–2825.

Journal of Pharmaceutical and Biomedical Analysis 66 (2012) 359–364

Contents lists available at SciVerse ScienceDirect

Journal of Pharmaceutical and Biomedical Analysis

journal homepage: www.elsevier.com/locate/jpba

Short communication

Rapid HILIC method with fluorescence detection using derivatization reaction utilizing *o*-phthaldialdehyde for determination of degradation product of aliskiren

Michal Douša*, Jiří Břicháč, Jiří Svoboda, Robert Klvaňa

Zentiva, a.s. Praha, U Kabelovny 130, 102 37 Praha 10, Czech Republic

ARTICLE INFO

Article history:
Received 30 September 2011
Accepted 8 March 2012
Available online 17 March 2012

Keywords:
Aliskiren
HILIC
3-Amino-2,2-dimethylpropanamide (ADPA)
Degradation product
Related substances

ABSTRACT

A rapid procedure based on direct extraction and HILIC separation of aliskiren (ALI) degradation product – 3-amino-2,2-dimethylpropanamide (ADPA) with fluorescence detection has been developed. The formation of ADPA from ALI under different conditions was studied. The evaluation of HILIC method robustness was performed using multifactorial experiments with fixed factors (one-level Plackett–Burman design). XBridge HILIC column with isocratic elution using mobile phase 10 mM K_2HPO_4 pH 7.2–acetonitrile (26:74; v/v) was employed. Fluorescence detection after post column derivatization using *o*-phthaldialdehyde (OPA) reagent was performed at excitation and emission wavelength of 345 nm and 450 nm, respectively. The reported method has an advantage of a simple sample pre-treatment and quick and very sensitive measurement. The method was successfully applied for the analysis of commercially available ALI samples.

© 2012 Elsevier B.V. All rights reserved.

1. Introduction

Essential hypertension affects approximately one billion individuals worldwide. It has been identified as a major risk factor for cardiovascular diseases such as stroke, myocardial infarction, and congestive heart failure [1,2]. ALI (Fig. 1) belongs to the pharmacotherapeutic group of renin inhibitor and issued for the treatment of hypertension. ALI blocks the renin system at its rate-limiting step by directly inhibiting the catalytic activity of renin [3,4]. It is manufactured as film-coated tablets in strengths of 150 and 300 mg and the recommended dose is 150 mg once daily.

Validated analytical methods for the determination of ALI in pharmaceutical formulations were reported using spectrophotometric [5] and stability-indicating LC methods [6]. Micellar electrokinetic chromatography method for simultaneous determination of ALI and hydrochlorothiazide in pharmaceutical preparations was reported as well [7]. The validated HPLC method with fluorescence detection was used for the determination of ALI in animal and human plasma and urine [8].

3-Amino-2,2-dimethylpropanamide (ADPA) is an important analyte whose amount has to be tightly controlled in the final active pharmaceutical ingredient (API). Not only does it enter the synthetic sequence in the final stage in excess amounts (up to 3 equiv.) [9,10], but it is also formed by the decomposition of ALI at elevated temperatures and during prolonged storage. The amide functional group in position 1 is exposed to an intramolecular attack of the amino group in position 5 (Fig. 2), which leads to the formation of the corresponding ALI-lactam. Similarly, an intramolecular attack of the hydroxy group in position 4 leads to the formation of corresponding ALI-lactone, which represents the major decomposition pathway in neutral environment. Both attacks are accompanied by the release of a molecule of the ADPA. As the final crystallizations are typically carried out at elevated temperatures to ensure slower crystal formation and higher purity of the API, some level of the ADPA has always been observed. ADPA with the corresponding degradation products have been detected both in in-house batches and in commercial samples. Presence of the ADPA in the final product also significantly biases other analytical methods such as an assay by titration. Hence, finding a suitable method to reliably verify the ADPA content is a key task in ALI analytical chemistry.

ADPA has only a weak UV absorbance in the low wavelength range (<205 nm) and HPLC with photometric detection does not allow sensitive determination of ADPA. On other hand, successful approach to analysis of amino compounds by HPLC is to employ pre-column derivatization leading to hydrophobic and highly absorbing UV or fluorescence derivates which can be effectively separated and sensitively quantified. The reaction of *o*-phthaldialdehyde (OPA) in presence of thiols (such as 2-mercaptoethanol) with primary amino group leads to highly fluorescent 1-alkyl-2-thioindoles derivate [11,12]. The reaction is relatively rapid, it proceeds at laboratory temperature. However, the stability of 1-alkyl-2-thioindoles products is not sufficient due to the spontaneous rearrangements [13].

* Corresponding author. Fax: +420 272701331.
E-mail addresses: hplc@hplc.cz, michal.dousa@seznam.cz (M. Douša).

0731-7085/$ – see front matter © 2012 Elsevier B.V. All rights reserved.
doi:10.1016/j.jpba.2012.03.015

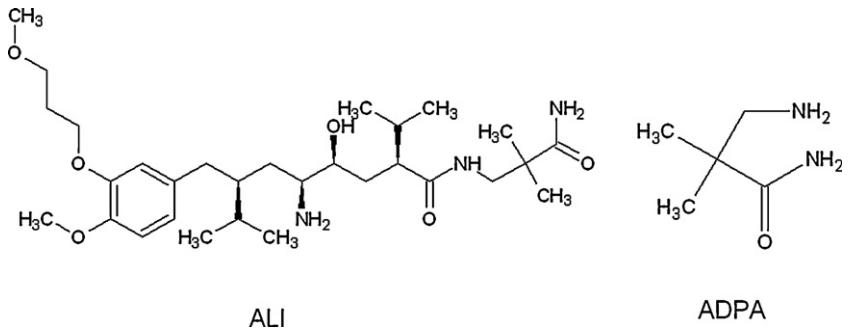

Fig. 1. The structure of ALI and ADPA.

For that reason, the reaction is often applied as a post-column derivatization [14].

The objective of the presented work is to develop a rapid and sensitive quantitative HILIC method for the determination of ADPA in API and in dosage forms of ALI. The developed method was successfully applied for the determination of ADPA content in commercially available ALI samples (both API and dosage forms).

2. Experimental

2.1. Reagents and chemicals

Acetonitrile (ACN) of HPLC gradient grade (J.T. Baker, USA) and water purified on Milli-Q system (Millipore, USA) were used for preparation of solutions and mobile phases. All other chemicals were of analytical grade or pure grade quality (Sigma–Aldrich, Czech Republic). The different batches of ALI were obtained from Dr. Reddy's (India), Changzhou Pharmaceutical Factory (China) and Zentiva (Czech Republic). The samples of dosage forms were purchased at a local pharmacy (Novartis, Switzerland) and obtained from Zentiva (Czech Republic). The standards of ADPA, ALI and ALI-lactone were prepared in-house (Zentiva, Czech Republic; purity >99.6%).

2.2. Sample and standard preparation

The standards of ADPA, ALI and ALI-lactone were dissolved in sample solvent consisting of a mixture of ACN and water in ratio 75:25 (v/v) to obtain the standard stock solution (concentration of 1.0 mg/ml). The system suitability test solution was prepared by spiking of ALI standard stock solution by ADPA to obtain concentration of 0.15% with respect to ALI. The reference solution was prepared by diluting of ADPA standard stock solution to obtain concentration of 1.5 μg/ml (concentration of 0.15% with respect to ALI sample solution).

API sample solution was prepared by weighing 10 mg of ALI sample into a 10 ml volumetric flask. Sample solvent (about 8 ml) was added and sample was dissolved by sonication for 2 min in an ultrasonic bath UCC4 (TESON, Slovakia) to obtain ALI preparation solution. After cooling to the laboratory temperature, the flask was made up to the mark by sample solvent.

To prepare the dosage form sample solution, twenty tablets containing 150 or 300 mg of ALI were accurately weighed and crushed to a fine powder. Amounts of powdered tablets equivalent to 250 mg of ALI was transferred to a 250 ml volumetric flask. After addition of 150 ml sample solvent, the flasks were shaken and sonicated for 5 min. The samples were made up to volume with sample solvent and centrifuged for 5 min.

2.3. Chromatographic apparatus and conditions

All chromatographic experiments were carried out on an Acquity UPLC system with a fluorescence detector W2475 (all Waters, USA). The system was controlled and acquired data processed by the Empower software (Waters, USA).

Chromatographic separations were performed on an XBridge HILIC column (150 mm × 4.6 mm, 3.5 μm; Waters, USA). The mobile phase consisted of aqueous solutions of 10 mM K_2HPO_4 adjusted with phosphoric acid to pH 7.2 and ACN in ratio of 26:74 (v/v). The mobile phase flow rate was 0.8 ml/min and column temperature was maintained at 35 °C. The injection volume was 10 μl and analytes were monitored after postcolumn derivatization using the fluorescence detection at excitation wavelength of 345 nm and emission wavelength of 450 nm. Postcolumn addition of a derivatization mixture was performed using postcolumn reaction system PCRS-1000 (reactor volume 250 μl; 0.42 mm I.D.) (Science Instruments and Software, Czech Republic). The reaction system was

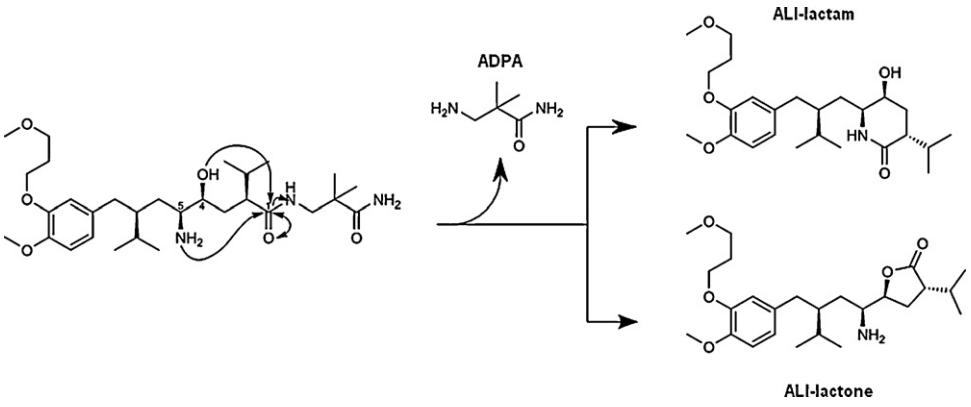

Fig. 2. Degradation of ALI by intramolecular attack of the amino or the hydroxy group, accompanied by the release of an ADPA and formation of ALI-lactam or ALI-lactone.

placed between a chromatographic column and the detector and connected to the column with a low-dead-volume PEEK mixing tee (Valco Instruments Company, USA). The reaction temperature was 25 °C. As the postcolumn derivatization reagent, mixture of 6 mmol/l OPA and 28 mmol/l 2-mercaptoethanol in 0.05 mol/l sodium tetraborate (pH 10.5) was used and delivered at a flow rate 0.3 ml/min.

2.4. LC–MS apparatus and conditions

The LC–high resolution MS analysis was performed using HTC Pal autosampler (CTC analytics, Switzerland) connected to Rheos allegro UHPLC pump (Flux systems, Switzerland) in combination with an LTQ XL Orbitap mass spectrometer (Thermo Scientific, USA). 10 μl of the sample was injected onto a XBridge HILIC 150 mm × 4.6 mm, 3.5 μm column (Waters, USA). A mobile phase consisted of 10 mM ammonium formate–ACN, pH 7.2 (26:74, v/v) and flow rate was 800 μl/min. Mass detection was carried out after electrospray ionization (ESI) in positive-ion full scan mode. The settings of the mass spectrometer were as follows: source voltage, 4.0 kV; capillary temperature, 300 °C and scan rage from m/z 50 to m/z 650. Nitrogen was used as sheath gas (pressure 45 arbitrary units) and auxiliary gas (pressure 10 arbitrary units). Data acquisition was performed using Xcalibur software (Thermo Scientific, USA).

3. Results and discussion

3.1. Degradation studies

The formation of ADPA and ALI-lactone from ALI was evaluated using forced degradation studies of the ALI [15]. The samples were subjected to acid hydrolysis (0.1 M HCl at 90 °C for 30 min), alkaline hydrolysis (0.1 M NaOH at 90 °C for 30 min), oxidative hydrolysis (3% hydrogen peroxide at 90 °C for 30 min), dry heated degradation (90 °C for 30 min) and UV light degradation (254 nm for 24 h). The results of degradation studies are shown in Fig. 3. The significant formation of ADPA and ALI-lactone was observed during acid and alkaline hydrolysis. The peaks with relative retention time (RRT) related to ALI – RRT 0.80, RRT 0.83 and RRT 1.33 are unknown primary amino positive related substances of ALI originating in acid and alkaline hydrolysis.

3.2. Optimization of HILIC method

The composition of the mobile phase was optimized to achieve the retention factor of ADPA $k \geq 1.0$, symmetry factor $A_S \leq 1.5$, plate number $N > 5000$ and resolution between ALI and ADPA $R_S \geq 2.0$. The hold-up volume of the column was determined using injection of toluene. Chromatographic data were calculated in agreement with European Pharmacopoeia (*Ph.Eur.*) [16]. Various proportions of CAN an phosphate buffer in the mobile phase were tested to achieve optimal separation. All the experiments were performed with 10 mM phosphate buffer pH 7.2. Acceptable resolution was achieved with isocratic elution and acetonitrile using flow rate 0.8 ml/min at temperature of 35 °C in ratio 26:74.

3.3. Validation parameters of HILIC method

The method was fully validated according to ICH Q2(R1) guideline [17].

3.3.1. System suitability

The system suitability test was performed before each run to assure that the analytical method can be used within the employed HPLC system with a satisfactory performance. Repeatability of injections expressed as relative standard deviation (RSD, %) of peak area of ADPA and resolution between ALI and ADPA for the five consecutive injections of a system suitability test solution were limited to ≤1.5% and $R_S \geq 3.0$, respectively. For all measurements performed during the validation, the resolution more than 9.0 and RSD of peak areas ≤1.0% was achieved.

Table 1
The calculated coefficients of regression equation of accuracy for API and dosage forms.

	API	Dosage forms
a	(-0.003 ± 0.022)	(-0.02 ± 0.035)
b	(1.014 ± 0.101)	(0.998 ± 0.112)
r	0.9998	0.9992

3.3.2. Limit of detection (LOD), limit of quantification (LOQ) and linearity

LOD and LOQ were calculated for ADPA based on a detector signal-to-noise ratio (S/N). The baseline noise was measured in a blank experiment in the region of retention time of ADPA using chromatographic software. The LOD ($S/N = 3$) and LOQ ($S/N = 10$) were found to be 0.006 μg/ml (0.0006% with regard to the concentration of ALI) and 0.020 μg/ml (0.002% with regard to the concentration of ALI), respectively.

The calibration curve was constructed ranging from LOQ to 120% of the general specification limit (from LOQ to 0.18% with regard to the concentration of ALI) by plotting the peak area against the concentration (five concentrations points). Calibration equation was calculated using linear regression analysis showing slope 426 404 010 and y-intercept −53 794. Excellent linearity was achieved exhibiting correlation coefficient of 0.9999. The linearity of calibration curve was investigated using other statistical test including quality coefficient QC [18]. The linearity of calibration model is considered valid if the quality coefficient QC fulfills the criterion QC < 5%. The calculated QC was 0.69%.

3.3.3. Precision, accuracy and determination of ADPA in commercially available samples

The accuracy of the ADPA was evaluated in triplicate at three concentration levels (0.05, 0.15 and 0.18% regarding to the concentration of the ALI). The determined content (c_d) was compared with the expected one (c_e) using linear regression. The coefficients of regression equations (significance level $P = 0.95$) for API and dosage forms are shown in Table 1. The first and second constants were not statistically different from zero and one, respectively. It can be concluded that analytical method gives accurate results for determination of ADPA.

The precision of ADPA was evaluated by determining real samples of API and dosage forms in five consecutive injections. Table 2

Table 2
The content of ADPA determined in different APIs and dosage forms batches.

Samples (producer)	Content (%)	RSD (%)
API ALI (Changzhou Pharmaceutical Factory, China)	0.12	1.1
API Aliskiren (Dr. Reddy's, India)	0.19	0.9
API ALI (Changzhou Pharmaceutical Factory, China)	0.34	1.8
API ALI (Zentiva, Czech Republic)	0.01	0.8
Rasilez 150 mg (Novartis, Switzerland)	0.03	2.1
Rasilez 300 mg (Novartis, Switzerland)	0.03	2.6
Dosage form 300 mg, batch 01 (Zentiva, Czech Republic)	0.18	1.2
Dosage form 300 mg, batch 02 (Zentiva, Czech Republic)	0.17	1.9

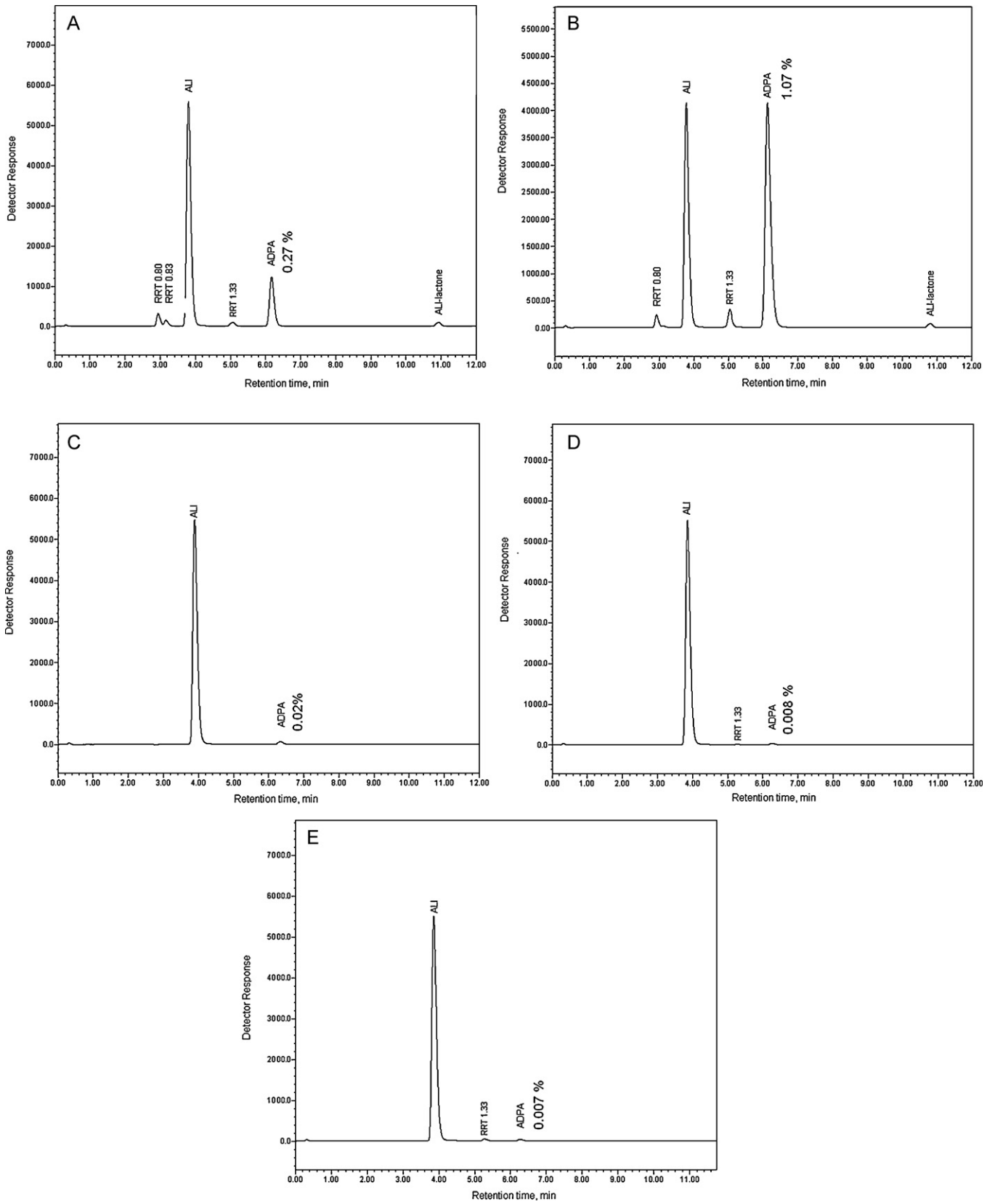

Fig. 3. Degradation studies. Typical chromatograms obtained after API degradation under various stress conditions (ADPA contents depicted). (A) Acid degradation, (B) alkaline degradation, (C) peroxide degradation, (D) dry heated degradation, and (E) UV degradation.

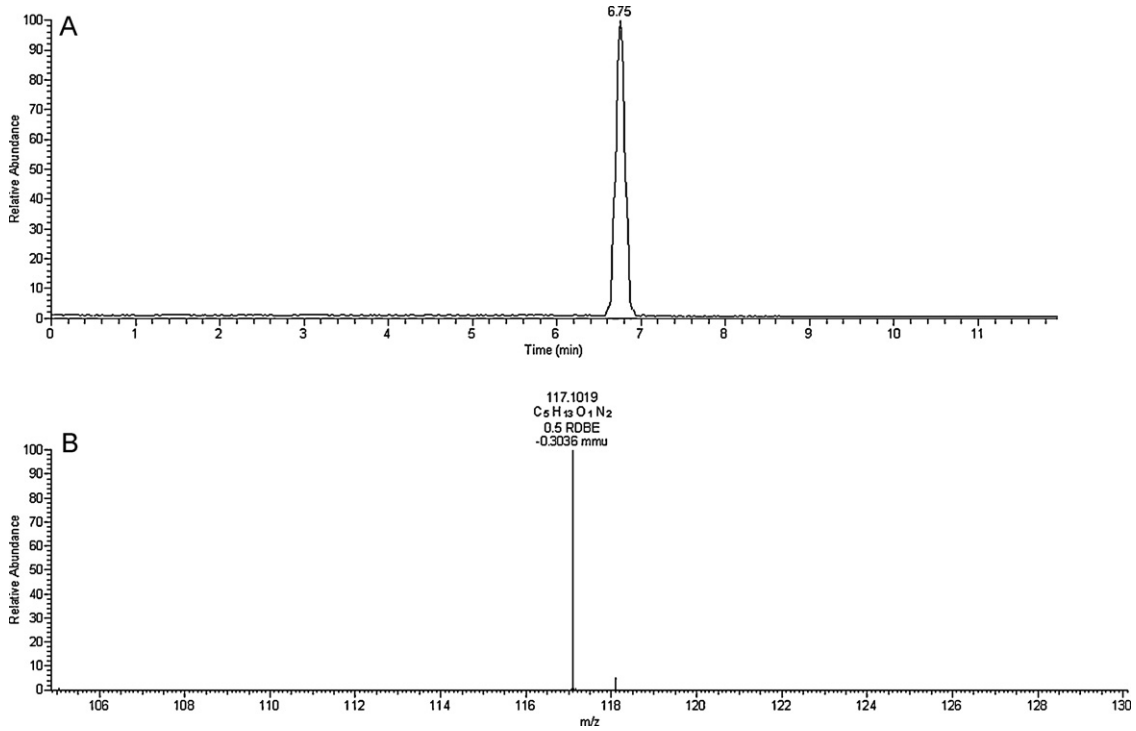

Fig. 4. LC–high resolution MS analysis of aliskiren spiked with ADPA. (A) Extracted ion chromatogram of *m*/*z* 117. (B) Mass spectrum of ADPA obtained at RT 6.8 min. Difference between theoretical and measured molecular weight is depicted (for conditions see Section 2).

summarizes the results of ADPA content in four API batches and in dosage forms.

3.3.4. Robustness

The robustness of method was examined by Placket–Burman partial factorial design [19,20] and the algorithm of Vander Heyden for the evaluation was used. Twelve experiments ($N = 12$) Plackett–Burman design for 11 factors were performed. Seven factors investigated in the robustness evaluation are summarized in Table 3 and results of studied responses (resolution, *N* and content of ADPA) are given in Table 4. There are 4 dummy (D) effects available to estimate the critical effect (E_{critical}). Effects are statistically significant if the *t*-value calculated for an effect is larger than a critical *t*-value or if the $|E_X|$ value is larger than a critical effect value E_{critical}:

$$|E_X| \geq E_{\text{critical}} = t_{(\text{critical})}(\text{SE})_e$$

where $(\text{SE})_e$ is the standard error on $|E_X|$, $t_{(\alpha/2,nDi)}$ is a tabulated *t*-value for $\alpha = 0.05$, $(1 - \alpha/2) = 0.975$. $(\text{SE})_e$ is estimated from the dummy factor effects and represents the experimental error in the design. The robustness is to be studied for system suitability test solution and sample solution of API. The interpretation of studied responses of robustness test is described in Table 5.

Table 3
The factors examined in the robustness tests and their levels.

	Factors	Level (−)	Nominal level	Level (+)
F1	Column temperature (°C)	30	35	40
F2	Volume fraction of ACN	0.70	0.74	0.80
F3	Mobile phase flow (ml/min)	0.70	0.80	0.90
F4	pH mobile phase	6.8	7.2	7.6
F5	Derivatization reagent flow (ml/min)	0.20	0.30	0.40
F6	Volume injection (μl)	9	10	11
F7	Mobile phase buffer concentration (mM)	5	10	15

The significant effect of volume fraction of ACN on resolution (R_S) should be expected. However, the plate count was not significantly affected by small variation of volume fraction of ACN. The

Table 4
The Plackett–Burman design (−) low factor level, (+) high factor level and results of the experiments.

Experiment No.	F1	F2	(D1)	F3	(D2)	F4	(D3)	F5	F6	F7	(D4)	Responses		
												R_S	*N*	ADPA (%)
1	(+)	(+)	(−)	(+)	(+)	(+)	(−)	(−)	(−)	(+)	(−)	9.94	11 731	0.103
2	(−)	(+)	(+)	(−)	(+)	(+)	(+)	(−)	(−)	(−)	(+)	9.51	9 282	0.103
3	(+)	(−)	(+)	(+)	(−)	(+)	(+)	(+)	(−)	(−)	(−)	25.40	7 274	0.101
4	(−)	(+)	(−)	(+)	(+)	(−)	(+)	(+)	(+)	(−)	(−)	8.75	7 010	0.103
5	(−)	(−)	(+)	(−)	(+)	(+)	(−)	(+)	(+)	(+)	(−)	10.46	7 162	0.097
6	(−)	(−)	(−)	(+)	(−)	(+)	(+)	(−)	(+)	(+)	(+)	13.84	11 620	0.103
7	(+)	(−)	(−)	(−)	(+)	(−)	(+)	(+)	(−)	(+)	(+)	9.72	6 222	0.099
8	(+)	(+)	(−)	(−)	(−)	(+)	(−)	(+)	(+)	(−)	(+)	6.57	8 800	0.104
9	(+)	(+)	(+)	(−)	(−)	(−)	(+)	(−)	(+)	(+)	(−)	13.22	7 278	0.103
10	(−)	(+)	(+)	(+)	(−)	(−)	(−)	(+)	(−)	(+)	(+)	7.92	6 991	0.102
11	(+)	(−)	(+)	(+)	(+)	(−)	(−)	(−)	(+)	(−)	(+)	20.15	11 241	0.103
12	(−)	(−)	(−)	(−)	(−)	(−)	(−)	(−)	(−)	(+)	(−)	14.06	8 912	0.106

Table 5
The interpretation of the significance of effects on the response.

Factors		R_S	N	ADPA (%)
F1	E(F1)	3.41	262	−0.0002
F2	E(F2)	−6.29*	−223	0.0014
F3	E(F3)	3.74	1 369	0.0006
F4	E(F5)	0.32	1 369	−0.0008
F5	E(F6)	−1.98	−2 768*	−0.0026*
F6	E(F7)	−0.59	450	−0.0001
F7	E(F8)	−3.22	−253	−0.0021
Dummy 1	E(D1)	3.96	−845	−0.0016
Dummy 2	E(D2)	−2.08	296	−0.0019
Dummy 3	E(D3)	1.89	−1 025	−0.0004
Dummy 4	E(D4)	−2.35	798	0.0002
Critical effect $E_{critical}$ (α = 0.05%)		4.72	1 359	0.0022

* Statistically significant effect.

change of derivatization reagent flow rate showed a high significant effect on the N and content of ADPA. This is in agreement with the theory describing the contribution of the coil volume to the extracolumn peak broadening which results in a decrease of separation efficiency [21,22]. In summary, the reported method is robust under described conditions. The flow rate of derivatization reagent is crucial parameter of the method and this parameter has to be under control.

3.3.5. Selectivity

Due to the results of degradation studies it can be concluded that proposed HILIC method is selective for the determination of ADPA in API and dosage form.

3.4. LC/MS confirmation

The HILIC results were further verified using LC–high resolution MS. Confirmation of the elemental composition of ADPA was based on the precise measurement of the molecular weight. ADPA eluted at 6.8 min and molecular ion $[M+H]^+$ of m/z 117.1019 with the elemental composition $C_5H_{13}ON_2$ was detected (see Fig. 4). ALI-lactone ($[M+H]^+$ of m/z 436) and an unknown impurity with retention time 1.33 min ($[M+H]^+$ of m/z 288) was also detected by LC–MS (data not shown).

4. Conclusion

ADPA forming by the decomposition of ALI at elevated temperatures and during prolonged storage was detected using highly selective HILIC method and confirmed by means of LC–MS. The rapid and efficient HILIC method for the measurement of ADPA in commercially available ALI samples has been described and validated. Preparation of samples in series and short chromatographic run also offer to adopt developed method in routine laboratory assays.

References

[1] A.V. Chobanian, G.L. Bakris, H.R. Black, W.C. Cushman, L.A. Green, J.L. Izzo Jr., D.W. Jones, B.J. Materson, S. Oparil, J.T. Wright Jr., E.J. Roccella, The Seventh Report of the Joint National Committee on Prevention, Detection, Evaluation, and Treatment of High Blood Pressure: The JNC 7 Report, JAMA 289 (2003) 2560–2572.
[2] R.L. Antikainen, V.A. Moltanochov, C. Chukwuma, K.A. Kuulasmaa, P.M. Marques-Vidal, S. Sans, L. Wilhelmsen, J.A. Tuomilehto, Trends in the prevalence, awareness, treatment and control of hypertension: the WHO MONICA Project, Eur. J. Cardiovasc. Prev. Rehabil. 13 (2006) 13–21.
[3] K.K. Daugherty, Aliskiren, Am. J. Health Syst. Pharm. 65 (2008) 1323–1332.
[4] S. Vaidyanathan, V. Jarugula, H.A. Dieterich, D. Howard, W.P. Dole, Clinical pharmacokinetics and pharmacodynamics of aliskiren, Clin. Pharmacokinet. 47 (2008) 515–531.
[5] M. Wrasse-Sangoi, L.T. Secretti, I.F. Diefenbach, C.M.B. Rolim, M.S. Sangoi, Development and validation of an UV spectrophotometric method for the determination of aliskiren in tablets, Quim. Nova 33 (2010) 1330–1334.
[6] M. Wrasse-Sangoi, M.S. Sangoi, P.R. Oliveira, L.T. Secretti, C.M.B. Rolim, Determination of aliskiren in tablet dosage forms by a validated stability-indicating RP-LC method, J. Chromatogr. Sci. 49 (2011) 170–175.
[7] M.S. Sangoi, M. Wrasse-Sangoi, P.R. Oliveira, C.M.B. Rolim, M. Steppe, Simultaneous determination of aliskiren and hydrochlorothiazide from their in pharmaceutical preparations using validated stability-indicating MEKC method, J. Chromatogr. Sci. 34 (2011) 1859–1866.
[8] G. Lefevre, S. Gauromb, Automated quantitative determination of the new rennin inhibitor CGP60536 by high-performance liquid chromatography, J. Chromatogr. B 738 (2000) 129–136.
[9] R. Goeschke, J.K. Maibaum, W. Schiling, S. Stutz, P. Rigollier, Y. Yamaguchi, N.C. Cohen, P. Herold, Delta-amino-gamma-hydroxy-omega-aryl alkanoic acid amides with enzyme especially renin inhibiting activities, EP 0678503 (B1) (1999).
[10] P. Herold, S. Stutz, F. Spindler, Process for the preparation of substituted octanoyl amides, EP 1296935 (B1) (2009).
[11] M. Roth, Fluorescence reaction for amino acids, Anal. Chem. 43 (1971) 880–882.
[12] R.F. Chen, C. Scott, E. Trepman, Flourescence properties of o-phthaldialdehyde derivates of amino acids, Biochim. Biophys. Acta 576 (1979) 440–455.
[13] S.S. Simons, D.F. Johnson, The structure of the fluorescent adduct formed in the reaction of o-phthalaldehyde and thiols with amines, J. Am. Chem. Soc. 98 (1976) 7098–7099.
[14] M. Roth, A. Hampai, Column chromatography of amino acids with fluorescence detection, J. Chromatogr. 83 (1973) 353–356.
[15] ICH Q1A(R2), Stability Testing of New Drug Substances and Products; Step 4 Version, 2003.
[16] European Pharmacopoeia, 6th ed., Council of Europe, Strasbourg, 2009, pp 4407–4413.
[17] ICH Q2(R1), Validation of Analytical Procedures; Step 4 Version, 2005.
[18] J. Van Loco, M. Elskens, Ch Croux, H. Beernaert, Linearity of calibration curves: use and misuse of the correlation coefficient, Accredit. Qual. Assur. 7 (2002) 281–285.
[19] B. Dejaegher, M. Dumarey, X. Capron, M.S. Bloomfield, Y. Vander Heyden, Comparison of Plackett–Burman and supersaturated designs in robustness testing, Anal. Chim. Acta 595 (2007) 59–71.
[20] Y. Vander Heyden, F. Questier, D.L. Massart, A ruggedness test strategy for procedure related factors: experimental set-up and interpretation, J. Pharm. Biomed. Anal. 17 (1998) 153–168.
[21] R. Aris, On the dispersion of a solute in a fluid flowing through a tube, Proc. R. Soc. A 35 (1965) 67–77.
[22] M. Martin, C. Eon, G. Guiochon, Study of the pertinency of pressure in liquid chromatography. II. Problems in equipment design, J. Chromatogr. A 108 (1975) 229–241.

Journal of Pharmaceutical and Biomedical Analysis 66 (2012) 365–370

Contents lists available at SciVerse ScienceDirect

Journal of Pharmaceutical and Biomedical Analysis

journal homepage: www.elsevier.com/locate/jpba

Short communication

Application of a rapid and sensitive liquid chromatography–tandem mass spectrometry method for determination of bumetanide in human plasma for a bioequivalence study

Dinesh S. Patel[a,b], Naveen Sharma[b], Mukesh C. Patel[a], Bhavin N. Patel[b,c,**], Pranav S. Shrivastav[c,*], Mallika Sanyal[d]

[a] Chemistry Department, Pramukh Swami Science and H.D. Patel Arts College, Sarva Vidyalaya Campus, Kadi 382 715, Gujarat, India
[b] Bio-Analytical Laboratory, Cliantha Research Limited, Bodakdev, Ahmedabad 380054, Gujarat, India
[c] Department of Chemistry, School of Sciences, Gujarat University, Navrangpura, Ahmedabad 380009, Gujarat, India
[d] Department of Chemistry, St. Xavier's College, Navrangpura, Ahmedabad 380009, Gujarat, India

ARTICLE INFO

Article history:
Received 29 December 2011
Received in revised form 20 February 2012
Accepted 12 March 2012
Available online 21 March 2012

Keywords:
Bumetanide
LC–MS/MS
Solid phase extraction
Bioequivalence study
Incurred sample reanalysis

ABSTRACT

A rapid, selective and sensitive liquid chromatography–tandem mass spectrometry (LC–MS/MS) assay has been proposed for the determination of bumetanide in human plasma using tamsulosin as internal standard (IS). The analyte and IS were extracted from 200 μL of human plasma via solid phase extraction and the chromatographic separation was achieved on Peerless Basic C18 (100 mm × 4.6 mm, 3 μm) column under isocratic conditions. Detection of bumetanide and IS was done by tandem mass spectrometry, operating in positive ionization and multiple reaction monitoring (MRM) acquisition mode. The protonated precursor to product ion transitions monitored for bumetanide and IS were m/z 365.2 → 240.2 and 409.2 → 228.2 respectively. The method was fully validated as per the US FDA guidelines. The limit of detection and lower limit of quantitation of the method were 0.03 and 0.30 ng/mL respectively with a linear dynamic range of 0.30–200.0 ng/mL for bumetanide. The intra-batch and inter-batch precision (% CV) was ≤6.9% while the mean extraction recovery was >90% across quality control levels. The method is selective in presence of four diuretic drugs and some commonly used medications by healthy volunteers. It was successfully applied to a bioequivalence study of 2 mg bumetanide tablet formulation in 10 healthy Indian male subjects under fasting condition. The reproducibility in the measurement of study data was demonstrated by reanalysis of 42 incurred samples.

© 2012 Elsevier B.V. All rights reserved.

1. Introduction

Bumetanide [BUM, 3-butylamino-4-phenoxy-5-sulfamoylbenzoic acid] is one of the most potent loop diuretics of the sulfamyl category which produces rapid onset and short duration of action [1,2]. It is used in the treatment of edema associated with congestive heart failure, hepatic and renal diseases, including the nephritic syndrome [3,4]. BUM is also a potent inhibitor of Na^+–K^+–$2Cl^-$ co-transport in the thick ascending limb of the loop of Henle [5]. It is frequently used in patients in whom high doses of furosemide (a loop diuretic) are ineffective. BUM is about 40–60 times more potent as a diuretic than furosemide on a weight basis and it has greater oral bioavailability (80%) [6]. Following oral administration of 1 mg or 2 mg dose, diuresis occurs in 30–60 min. Peak activity is reached between 1 and 2 h. BUM is eliminated rapidly in humans, with a half-life of between 1 and 1.5 h. The plasma protein-binding is in the range of 94–96% [7].

Several methods are reported for the analysis of BUM in different biological matrices, either alone [8–12], or in combination with other diuretic drugs for antidoping studies [13–16]. As a single analyte, BUM has been determined in plasma of non-human primates [8], urine [10,11], human serum [12], brain tissue [12], and human plasma [9,10]. An HPLC-fluorescence method has been developed by Bokens et al. [9] in human plasma. The calibration curves were linear in the concentration range of 0.5–25 ng/mL employing 1.0 mL plasma for processing by LLE. Wells et al. [10] have determined BUM in plasma and urine by HPLC and discussed the application of the method to BUM disposition studies in neonates treated with extracorporeal membrane oxygenation. Recently, Li et al. [12] have developed a sensitive (1 ng/mL) and rapid (5 min) isotope dilution LC–MS/MS method for quantitative analysis of BUM in human

* Corresponding author. Tel.: +91 079 26300969; fax: +91 079 26308545.
** Corresponding author at: Department of Chemistry, School of Sciences, Gujarat University, Navrangpura, Ahmedabad 380009, Gujarat, India. Tel.: +91 79 26853088; fax: +91 79 26853093.
E-mail addresses: bhavinpatel27@rediffmail.com (B.N. Patel), pranav_shrivastav@yahoo.com, pranav_shrivastav@rediffmail.com (P.S. Shrivastav).

0731-7085/$ – see front matter © 2012 Elsevier B.V. All rights reserved.
doi:10.1016/j.jpba.2012.03.018

Table 1
Summary of chromatographic methods developed for analysis of bumetanide in biological matrices.

Sr. no.	Extraction procedure (sample volume); internal standard; mean recovery	Column; elution process; mobile phase; flow rate; injection volume	Detection technique; analytical run time; retention time; linear dynamic range; application	Ref.
1[a]	LLE with 5.0 mL DEE in presence of H_2SO_4 (1000 μL plasma); 4-benzyl-3-*n*-butylamino-5-sulfamoyl benzoic acid; 71.0%	Waters μBondapak C18 (300 mm × 4.0 mm, 10 μm); isocratic; methanol–0.1% KH_2PO_4 in distilled water, pH 4.0 (60:40, v/v); 2.0 mL/min; 30 μL	HPLC-fluorescence (excitation: 338 nm, emission: 440 nm); 10 min; 5.7 min; 1.0–100 ng/mL; measurement of bumetanide (0.03 mg/kg) concentration in five cynomolgus monkeys	[8]
2	LLE with 6.0 mL DEE in presence of H_2SO_4 (1000 μL plasma); 3-*n*-butylamino-4-phenoxy-5-methyl sulfamoyl benzoic acid; 90.0%	Waters Corasil C18 (220 mm × 3.9 mm, 37–50 μm); isocratic; acetonitrile-0.03 M sodium phosphate buffer, pH 3.0 (125:200, v/v); 1.0 mL/min; 100 μL	HPLC-fluorescence (excitation: 340 nm, emission: 440 nm); 12 min; 4.48 min; 0.5–25 ng/mL; pharmacokinetic study with 0.5 mg bumetanide in a healthy volunteer	[9]
3	PP with acetonitrile followed by SPE on C18 Bond Elut cartridge (200 μL plasma); piretanide; 95.0%	Radial Pak C18 (100 mm × 8.0 mm, 5 μm); isocratic; methanol–water–glacial acetic acid (66:34:1, v/v/v); 1.2 mL/min; 100 μL	HPLC-fluorescence (excitation: 228 nm, emission: 418 nm); 8.0 min; 6.5 min; 5.0–500 ng/mL; bumetanide disposition studies in neonates treated with extracorporeal membrane oxygenation	[10]
4	PP with acetonitrile (15 μL serum, 0.5 g rat brain); d_5-bumetanide; >97.0%	Waters Atlantis T3 (100 mm × 2.1 mm, 3 μm); gradient; formic acid in water and methanol; 0.25–0.40 mL/min; 10 μL	LC–ESI-MS/MS; 5.0 min; 4.15 min; 1.0–1250 ng/mL; pharmacokinetic study with 0.30 mg/kg bumetanide in P70 long Evans rat serum and brain	[12]
5	SPE on Bond Elut Plexa extraction cartridges in presence of H_3PO_4 (200 μL plasma); tamsulosin hydrochloride; 90.5%	Peerless Basic C18 (100 mm × 4.6 mm, 3 μm); isocratic; methanol: 5 mM ammonium trifluoroacetate in deionized water (80:20, v/v); 0.6 mL/min; 15 μL	LC–ESI-MS/MS; 3.5 min; 1.52 min; 0.3–200 ng/mL; bioequivalence study with 2 mg bumetanide in 10 healthy Indian male volunteers	PM

LLE: liquid–liquid extraction; DEE: diethylether; PP: protein precipitation; SPE: solid phase extraction; PM: present method.

serum and brain tissue. The salient features of chromatographic methods developed for BUM in biological matrices are summarized in Table 1.

In the present study a sensitive, selective, rugged and rapid LC–MS/MS method has been proposed for the determination of BUM in human plasma. The method is extensively validated as per the United States Food and Drug Administration (USFDA) guidelines and is adequately sensitive for routine subject sample analysis. The method requires only 200 μL human plasma for SPE, minimum usage of organic solvents and demonstrates excellent performance in terms of ruggedness and efficiency (3.5 min per sample). The dynamic linear range was validated from 0.30 to 200 ng/mL. The method is selective in presence of four diuretic drugs namely acetazolamide, indapamide, clopamide and spironolactone. Ion suppression/enhancement was studied by post column infusion of analyte and post extraction spiking technique. The proposed method has been successfully applied to a bioequivalence study of 2 mg bumetanide tablet formulation in 10 healthy Indian males under fasting condition. The authenticity in the measurement of study data is demonstrated through reanalysis of incurred samples.

2. Experimental

2.1. Chemicals and materials

Reference standard material of bumetanide (98.9%) was procured from Industriale Chimica (Saronno, VA, Italy), while tamsulosin hydrochloride (IS, 99.5%) was from Zydus Cadila (Ahmedabad, India). HPLC grade methanol and analytical grade *ortho*-phosphoric acid (88.0%) were obtained from S.D. Fine Chemicals Ltd. (Mumbai, India). Ammonium trifluoroacetate (ATFA, 98%) was procured from Acros Organics (NJ, USA). Varian Bond Elut Plexa (1 cc, 30 mg) extraction cartridges were procured from Varian Inc. (Palo Alto, CA, USA).

Water used for LC–MS/MS was prepared using Milli Q water purification system from Millipore (Bangalore, India). Control buffered (K_2EDTA) human plasma was procured from Clinical Department, BA Research India Limited (Ahmedabad, India) and was stored at −20 °C.

2.2. LC–MS/MS instrumentation and settings

A Shimadzu liquid chromatography system (Kyoto, Japan) with Peerless Basic C18 (100 mm length × 4.6 mm inner diameter, with 3.0 μm particle size) column from Chromatopak Analytical Instrumentation India Pvt. Ltd. (Mumbai, India) was used in this study. The mobile phase consisted of methanol: 5 mM ammonium trifluoroacetate in deionized water, pH 6.0 (80:20, v/v). The autosampler temperature was maintained at 4 °C and the flow rate was set at 0.60 mL/min for isocratic conditions. Ionization and detection of analyte and IS was performed on a triple quadrupole mass spectrometer, API-3000 equipped with Turbo Ion spray®, from MDS SCIEX (Toronto, Canada) operating in the positive ion mode. Quantitation was done using MRM mode to monitor protonated precursor → product ion transition of m/z 365.2 → 240.2 for BUM and 409.2 → 228.2 for IS. All the parameters of LC and MS were controlled by Analyst software version 1.4.2. The source dependant parameters maintained for BUM and IS were Gas 1 (Nebulizer gas): 10 psi, ion spray voltage (ISV): 4500 V, turbo heater temperature (TEM): 500 °C, entrance potential (EP): 10 V, collision activation dissociation (CAD): 5 psi, curtain gas (CUR): 10 psi. The compound dependent parameters like declustering potential (DP), focusing potential (FP) collision energy (CE) and cell exit potential (CXP) were optimized at 30, 180, 25 and 15 V for BUM and 45, 285, 34 and 15 V for IS respectively. Quadrupole 1 and quadrupole 3 were maintained at unit resolution. A dwell time of 300 ms was set for both BUM and IS.

2.3. Preparation of standard stock and plasma samples

The standard stock solution of BUM (100.0 μg/mL) and working solution of IS (100.0 μg/mL) were prepared by dissolving requisite amount in methanol. The calibration standards (CSs) and quality control (QC) samples [LLOQ QC (0.30 ng/mL), lower limit of quantitation quality control; LQC (0.90 ng/mL), low quality control;

MQC-2/MQC-1 (12.00/80.00 ng/mL), medium quality control; HQC (150.0 ng/mL), high quality control; ULOQ QC (200.0 ng/mL), upper limit of quantitation quality control] were prepared by spiking blank plasma with respective working solutions (5% of total volume of plasma). CSs were made at 0.30, 0.60, 2.00, 4.00, 10.00, 25.00, 50.00, 100.0, 160.0 and 200.0 ng/mL for BUM. The spiked plasma samples at all the levels were stored at −20 °C for validation and subject sample analysis.

2.4. Protocol for sample preparation

Aliquots of 200 μL plasma solution containing 10 μL of working solution of BUM and 190 μL blank plasma were transferred into riavials, 25 μL of deionized water (for CS and QC samples)/25 μL of 80% methanol–water solution (for study samples) was added and vortexed to mix. Further, 100 μL working solution of IS (100.0 ng/mL) and 100 μL of 15% (v/v) *ortho*-phosphoric acid solution was added and vortexed again. Prior to loading plasma samples, Varian Bond Elut Plexa extraction cartridges were prewashed with 1.0 mL of methanol, followed by 1.0 mL of deionized water and centrifuged for 1 min at 1811 × *g* after each step. Plasma samples were then applied to these conditioned cartridges and after centrifugation for 2 min at 1811 × *g*, washing was done with 1.0 mL of deionized water, followed by centrifugation for 1 min at 1811 × *g*. Elution was carried out with 1.0 mL of methanol followed by centrifugation for 1 min at 1811 × *g*. The eluent was evaporated to dryness under gentle stream of nitrogen (15 psi) at 40 °C. The residue was taken up in 300 μL of mobile phase solution and 15.0 μL was used for injection in the chromatographic system.

2.5. Method validation

The method was validated for selectivity, sensitivity, interference check, carryover check, linearity, precision and accuracy, reinjection reproducibility, limit of detection (LOD), recovery, ion suppression/enhancement, matrix effect, stability and dilution reliability following the USFDA guidelines [17].

Test for selectivity was carried out in 12 different lots of blank human plasma including hemolyzed and lipemic plasma collected with K_2EDTA as an anticoagulant. They were processed with and without the analyte and IS to check for any interference peaks. The potential interferences from the common drugs were determined. These included acetaminophen, aspirin, caffeine, cetrizine, chlorpheniramine maleate, ibuprofen and pseudoephedrine. Additionally, the interference of four diuretic drugs (acetazolamide, indapamide, clopamide and spironolactone) was studied which are used in doping analysis along with BUM for ionization (ion suppression/enhancement), analytical recovery (precision and accuracy) and chromatographic interference (interference with MRM of analyte and IS). The MRM transitions in the positive ionization mode for acetazolamide (223/181), indapamide (366/132), clopamide (346/250) and spironolactone (405/339) were studied.

Carry over experiment was performed to verify any carryover of analyte, which may reflect in subsequent runs. The design of the study comprised of the following sequence of injections i.e. double blank plasma sample → two samples of LLOQ → double blank plasma → ULOQ sample → double blank plasma to check for any interference due to carry over.

The linearity of the method was determined by analysis of eight calibration curves containing ten non-zero concentrations. The area ratio response for BUM/IS obtained from multiple reaction monitoring was used for regression analysis. Each calibration curve was analyzed individually by using least square weighted ($1/x^2$) linear regression.

Intra-batch and inter-batch (on three consecutive validation days) accuracy and precision were evaluated at six QC levels (LLOQ QC, LQC, MQC-2, MQC-1, HQC and ULOQ QC) in six replicates for BUM. The deviation (% CV) at each concentration level from the nominal concentration was expected to be within ±15%. Reinjection reproducibility was performed by re-injecting one validation batch.

The relative recovery, matrix effect and process efficiency were evaluated as reported previously [18] at HQC, MQC-1, MQC-2 and LQC levels in six replicates. Relative recovery (RE) was calculated by comparing the mean area response of samples spiked before extraction to that of samples spiked after extraction at each QC level. The recovery of IS was similarly estimated. Absolute matrix effect (ME) was assessed by comparing the mean area response of samples spiked after extraction with the mean area response of neat standard solutions prepared in mobile phase. The overall 'process efficiency' (% PE) was calculated as (ME × RE)/100. The relative matrix effect on analyte quantification was also checked in eight different batches/lots of K_2EDTA plasma including hemolyzed and lipemic plasma. From each batch, four samples at LQC and HQC levels was prepared (spiked after extraction) and checked for the % accuracy and precision (% CV). The deviation of the standards and QCs should not be more than ±15%. Matrix ion suppression effects on the MRM LC–MS/MS sensitivity were evaluated by the post column analyte infusion experiment [19]. Any dip in the baseline upon injection of double blank plasma would indicate ion suppression, while a peak at the retention time of BUM and IS indicates ion enhancement.

All stability results were evaluated by measuring the area ratio response (BUM/IS) of stability samples against freshly prepared comparison standards at LQC and HQC levels. Stock solutions of BUM and IS were checked for short term stability at room temperature and long term stability at 4 °C. Bench top stability, processed sample stability at room temperature and at refrigerated temperature (4 °C), freeze–thaw stability at −20 °C and long term stability at −20 °C and −70 °C were performed at LQC and HQC levels using six replicates at each level.

Dilution integrity experiment was carried out at 5 times the ULOQ concentration i.e. 1000 ng/mL and at HQC level for BUM. Six replicate samples each of 1/10 of 5× ULOQ (100.0 ng/mL) and 1/10 of HQC (15.00 ng/mL) concentration were prepared and their concentrations were calculated, by applying the dilution factor of 10 against the freshly prepared calibration curve for BUM.

2.6. Bioequivalence study and incurred sample reanalysis

The study plan was defined as "An open label, randomized, two period, two treatment, two sequence, balanced, crossover, single dose oral bioequivalence study of test (2 mg bumetanide tablets of a generic company) and a reference (BUMEX®, 2 mg bumetanide tablets from Sandoz Inc., Princeton, NJ 08540, USA) formulation in 10 healthy Indian subjects under fasting conditions". All the subjects were informed of the aim and risk involved in the study and written consent were obtained. The procedures followed while dealing with human subjects were based on International Conference on Harmonization, E6 Good Clinical Practice guidelines [20]. The subjects for study were fasted 10 h before administration of the drug formulation. Blood samples were collected in vacutainers containing K_2EDTA anticoagulant before (0.0) and at 0.25, 0.5, 0.75, 1.0, 1.25, 1.5, 1.75, 2.0, 2.25, 2.5, 2.75, 3.0, 3.5, 4.0, 4.5, 5.0, 6.0, 8.0, 10.0 and 12.0 h of administration of drug. Blood samples were centrifuged at 2415 × *g* at 4 °C for 10 min and plasma was separated, stored at −20 °C until use. An incurred sample re-analysis (ISR) was also conducted by computerized random selection of 42 subject samples (10% of total study samples analyzed) near C_{max} and the elimination phase. The percent change in the value should not be more than ±20% [21].

3. Results and discussion

3.1. Method development

Mass spectrometry: The tuning of MS parameters was carried out in positive as well as negative ionization modes for BUM and IS using 500.0 ng/mL tuning solution. The response observed was much higher in positive ionization mode for analyte and IS compared to the negative mode due to their basic nature with low background noise, resulting in higher sensitivity. The analyte and IS gave predominant singly charged protonated precursor $[M+H]^+$ ions at *m*/*z* of 365.2 and 409.2 for BUM and IS respectively in Q1 full scan spectra. Fragmentation was initiated using sufficient nitrogen for CAD and by applying 25.0 V collision energy to break the precursor ion for BUM. In the product ion mass spectrum of BUM, the most abundant ion was observed at *m*/*z* 240.2, which was produced by elimination of sulfamoyl and carboxylic acid groups from the precursor ion. The major product ion of IS in Q3 mass spectra was observed at *m*/*z* 228.2 by applying 34.0 V collision energy. This fragment can be ascribed to methoxybenzene-1-sulfonamide containing substructure formed due to C—N bond cleavage of the parent molecule. To attain an ideal Taylor cone and a better impact on spectral response, an optimum potential of 4500 V was kept which gave consistent and stable signal. Fine tuning of nebulizer gas and CAD gas was done to get a consistent and stable response.

Chromatography: The chromatographic conditions were suitably optimized to achieve a short run time, symmetric peak shapes, minimum matrix interference and solvent consumption. The separation and ionization of BUM and IS were affected by the composition of mobile phase. Methanol–water and acetonitrile–water in various proportions (60:40, 70:30, 80:20 and 90:10, v/v) were tested as the mobile phase on four different columns namely, Hypurity C8 (100 mm × 4.6 mm, 5 μm), Hypurity C18 (50/100 mm × 4.6 mm, 5 μm), BDS Hypersil C18 (100 mm × 4.6 mm, 5 μm) and Peerless Basic C18 (100 mm × 4.6 mm, 3 μm). The ionization of BUM and IS was augmented by addition of an acidic additive in the mobile phase. Thus, formic acid (0.01–0.005%) and ATFA (2–10 mM) were attempted to improve the response. When formic acid was added in the mobile phase, the peak shape of BUM was unacceptable at lower concentration levels. The response of analyte and IS was distinctly increased by addition of ATFA. Both BUM and IS were found to have higher response and better peak shapes in the mobile phase containing 5 mM ATFA. In addition, the effect of flow rate was also studied from 0.3 to 0.9 mL/min, which was also responsible for acceptable chromatographic peak shapes. Though desired separation and adequate response was observed on Hypurity C8 and C18 columns, the run time was too long (≥6.0 min). This limitation was overcome by use of BDS Hypersil C18 column, however, the peak shape with little tailing prevented its further use. Peerless Basic C18 (100 mm × 4.6 mm, 3 μm) column helped in the separation and elution of BUM and IS in a short time with desired sensitivity and negligible matrix interference.

Plasma extraction: Due to high drug protein binding, protein precipitation (PP) was tried initially using methanol and acetonitrile as precipitating agents but the response was insufficient with some ion suppression. Thus, LLE was carried out in different solvent systems like dichloromethane, diethyl ether, heptane and methyl *tert*-butyl ether (MTBE), alone and in combination under acidic conditions as reported previously [8,9]. However, the response was inconsistent especially at the LLOQ level in majority of all these solvent systems, except MTBE which gave an average recovery in the range of 60–65% at different QC levels. Finally, SPE with Bond Elut Plexa extraction cartridges was tested in presence of H_3PO_4 to break drug–protein binding. Consistent and quantitative recovery (~90%) was obtained at all QC levels.

3.2. System suitability, selectivity, interference and carryover check

During method validation, the precision (% CV) of system suitability test was observed in the range of 0.12–0.37% for the retention time and 1.12–2.36% for the area response of BUM and IS. All plasma samples studied were found free from any endogenous interference. Fig. 1(a)–(c) demonstrates the selectivity results with the chromatograms of double blank plasma (without IS), blank plasma (with IS), peak response of BUM at LLOQ concentration. No interference was observed for commonly used medications, which is evident from the real subject sample chromatograms of BUM at 0.50 h after oral administration of 2 mg tablet formulation (Fig. 1(d)). Under the optimized experimental conditions, the retention time for acetazolamide, indapamide, clopamide and spironolactone was observed at 1.12, 1.85, 1.63 and 2.21 min respectively. However, due to their different MRM transitions there was no interference in the quantification of BUM. The % accuracy results for BUM at both the QC levels was within 97.3–103.4%. Almost negligible area (less than 0.5% of LLOQ area) was observed in double blank plasma run after ULOQ, which suggests no carry-over of the analyte in subsequent runs.

3.3. Linearity, sensitivity, accuracy and precision

All eight calibration curves were linear over the concentration range of 0.30–200.0 ng/mL with correlation coefficient $r \geq 0.999$. A straight-line fit was made through the data points by least square regression analysis to give the mean linear equation $y = (0.0093 \pm 0.0017)x + (0.0003 \pm 0.0002)$ where y is the peak area ratio of the analyte/IS and x the concentration of the analyte. The LLOQ of the method was 0.30 ng/mL at a signal-to-noise ratio (S/N) ≥ 32 and an LOD of 0.03 ng/mL. The intra-batch precision (% CV) ranged from 0.9 to 3.4 and the accuracy was within 96.7 to 106.7%. For the inter-batch experiments, the precision varied from 3.3 to 6.9 and the accuracy was within 96.7 to 103.8%.

3.4. Recovery, matrix effect, matrix factor, ion suppression

The RE, ME and PE data at different QC levels are presented in Table 2. The relative recovery of the analyte is the 'true recovery', which is unaffected by the matrix as it is calculated by comparing the area ratio response (analyte/IS) of extracted (spiked before extraction) and unextracted (spiked after extraction) samples. Further, the relative matrix effect which compares the precision (% CV) values between different lots (sources) of plasma (spiked after extraction) samples varied from 0.1 to 3.7 for BUM at the LQC and HQC levels. Results of post-column analyte infusion experiment should no ion suppression or enhancement at the retention time of BUM and IS. The average matrix factor value calculated as the response of post spiked sample/response of neat solution (in mobile phase) at the LLOQ level was 0.97, which indicates a minor suppression of about 3%.

3.5. Stability and dilution reliability

The stock solution of BUM was stable at room temperature for 6 h and at 4 °C for 81 days. The intermediate stock solution of BUM in methanol-deionized water (80:20, v/v) was stable at room temperature for 27 h and at 4 °C for 15 days with % change of 0.6 and 1.4 respectively. The values for the percent change for all the stability experiments of BUM are compiled in Table 3.

The precision values for dilution integrity of 1/10 of 5× ULOQ (100.0 ng/mL) and 1/10 of HQC (15.00 ng/mL) concentration were 1.4 and 0.5% respectively, while the accuracy results were within 100.6 and 102.5.

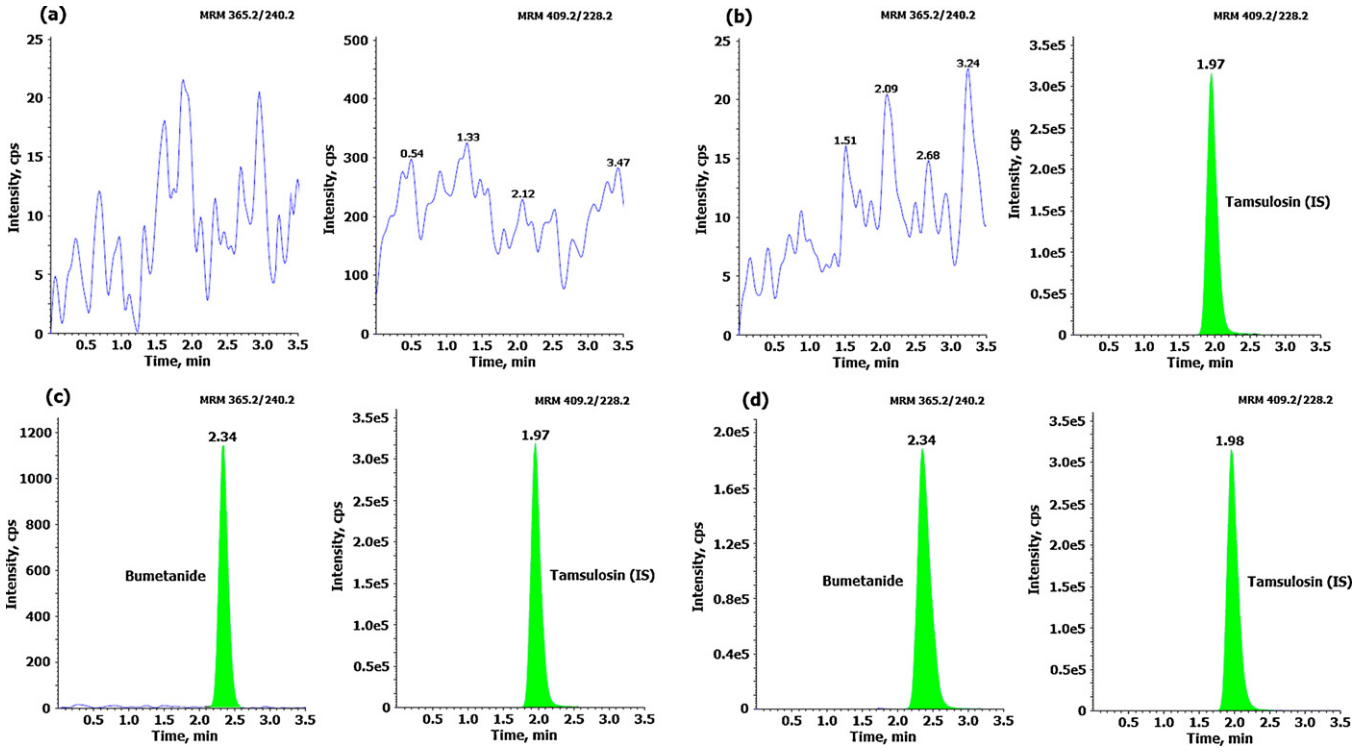

Fig. 1. MRM ion-chromatograms of bumetanide (m/z 365.2 → 240.2) and tamsulosin (IS, m/z 409.2 → 228.2) in (a) double blank plasma (without analyte and IS), (b) blank plasma with IS, (c) bumetanide at LLOQ and IS (d) real subject sample at 0.5 h after administration of 2 mg dose of bumetanide tablet.

Table 2
Absolute matrix effect, relative recovery and process efficiency for bumetanide.

A (% CV)	B (% CV)	C (% CV)	Absolute matrix effect [B/A × 100]	Relative recovery [C/B × 100]	Process efficiency [C/A × 100]
LQC					
11,791 (3.03)	11,425(3.63)	10,304 (2.96)	96.9 (93.1)[a]	90.9 (87.2)[a]	88.1 (81.2)[a]
MQC-2					
158,712 (4.62)	154,745 (4.41)	137,973 (3.13)	97.5 (93.8)[a]	89.2 (89.5)[a]	86.9 (83.9)[a]
MQC-1					
1,040,811 (3.96)	1,022,076 (4.11)	952,006 (2.38)	98.2 (94.7)[a]	93.1 (91.7)[a]	91.4 (86.8)[a]
HQC					
1,922,539 (4.35)	1,901,391 (4.33)	1,689,667 (2.54)	98.9 (95.3)[a]	88.8 (92.7)[a]	87.8 (88.3)[a]

A: mean area response of six replicate samples prepared in mobile phase (neat samples).
B: mean area response of six replicate samples prepared by spiking in extracted blank plasma.
C: mean area response of six replicate samples prepared by spiking before extraction.
CV: coefficient of variation.
[a] Values for internal standard, tamsulosin.

Table 3
Stability results for bumetanide under different conditions.

Stability	Storage condition	Level	Mean stability sample[a] (μg/mL)	% CV	% change
Bench top stability	Room temperature (25 h)	LQC	0.89	2.2	−1.1
		HQC	145.5	1.0	−3.0
Processed sample stability (extracted samples)	Auto sampler (4 °C, 97 h)	LQC	0.94	4.3	4.4
		HQC	158.2	2.4	5.5
Processed sample stability (extracted samples)	Room temperature (69 h)	LQC	0.89	2.2	−1.1
		HQC	144.3	3.0	−3.8
Freeze and thaw stability	After 6th cycle at −20 °C	LQC	0.87	4.6	−3.3
		HQC	164.7	3.9	9.8
Long term stability	91 days at −20 °C	LQC	0.90	4.1	0.0
		HQC	142.9	1.4	−4.7
Long term stability	91 days at −70 °C	LQC	0.84	3.1	−6.7
		HQC	145.8	7.5	−2.8

$\%\ \text{change} = \frac{\text{mean stability samples} - \text{mean comparison samples}}{\text{mean comparison samples}} \times 100.$
LQC: low quality control; HQC: high quality control; CV: coefficient of variation.
[a] Mean of six replicates at each level.

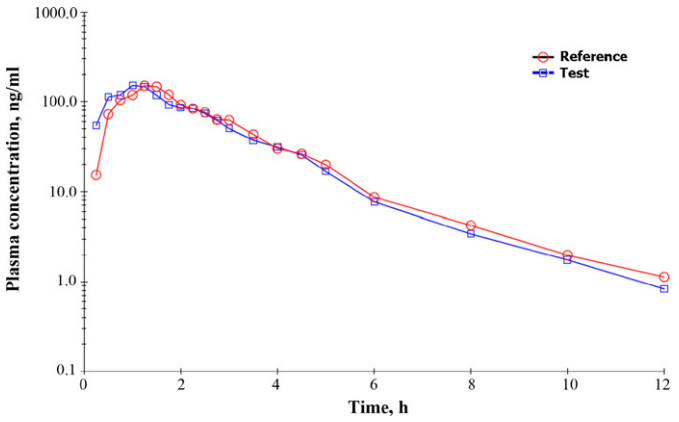

Fig. 2. Mean plasma concentration-time profile of bumetanide after oral administration of test (2 mg bumetanide tablets of a generic company) and a reference (BUMEX®, 2 mg bumetanide tablets from Sandoz Inc., Princeton, NJ 08540, USA) formulation to 10 healthy subjects under fasting condition.

3.6. Application of the method on human subjects

The mean pharmacokinetic profile for the treatment, under fasting condition is presented in Fig. 2. The mean pharmacokinetic parameters viz. C_{max}, $AUC_{0-12\,h}$, AUC_{0-inf}, T_{max} and $t_{1/2}$, calculated for test/reference formulation were $112.77 \pm 30.52/111.38 \pm 30.50$, $268.03 \pm 51.78/255.60 \pm 70.33$, $270.13 \pm 52.15/258.00 \pm 71.34$, $1.06 \pm 0.37/1.19 \pm 0.61$and $1.76 \pm 0.31/1.88 \pm 0.33$ respectively. The C_{max}, T_{max} and AUC_{0-t} values obtained under fasting conditions were higher compared to reported work with Japanese volunteers using 2 mg bumetanide tablet formulation [4,22]. This may be due genetic difference, race, age, gender (body size and muscle mass), type of food, etc. which may result in pharmacokinetic differences. The mean log-transformed ratios of the parameters and their 90% CIs were all within the defined bioequivalence range. The % change in the randomly selected subject samples for incurred sample reanalysis was within 10 to −11.5%.

4. Conclusion

The method presented has the highest sensitivity and employs minimum plasma volume (200 μL) for processing compared to other procedures [8–11]. Moreover, the total analysis time (extraction and chromatography) is the shortest compared to all these methods. The run time per sample analysis of 3.5 min suggests high throughput of the proposed method. The method is selective in presence of four diuretic drugs. Also, the on-column loading of BUM at ULOQ was 2 ng per sample injection volume. This is considerably less compared to other reported procedures, which helps in maintaining the efficiency and the lifetime of the column. Incurred sample reanalysis results demonstrated reproducibility of the proposed method in healthy subject samples.

Acknowledgments

The authors are indebted to Mr. Vijay Patel, Executive Director, Mr. Anshul Dogra, Study Director and Mrs. Arpana Prasad, R & D Supervisor, Cliantha Research Limited for their continuous support, motivation and assistance during the course of this project.

Appendix A. Supplementary data

Supplementary data associated with this article can be found, in the online version, at doi:10.1016/j.jpba.2012.03.018.

References

[1] M.J. Asbury, P.B.B. Gatenby, S. O'Sullivan, E. Bourke, Bumetanide: potent new loop diuretic, Br. Med. J. 1 (1972) 211–213.
[2] A. Ward, R.C. Heel, Bumetanide: a review of its pharmacodynamic and pharmacokinetic properties and therapeutic use, Drugs 28 (1984) 426–464.
[3] S.G. Karlander, R. Henning, O. Lundvall, Renal effects of bumetanide, a new saluretic agent, Eur. J. Clin. Pharmacol. 6 (1973) 220–223.
[4] N. Yagi, H. Kenmotsu, Y. Shimode, K. Oda, H. Sekikawa, M. Takada, Bioavailability and diuretic effect of bumetanide following rectal administration of suppositories containing weak acids in human subjects, Biol. Pharm. Bull. 16 (1993) 1124–1129.
[5] R. Greger, P. Wangemann, Loop diuretics, Ren. Physiol. 10 (1987) 174–183.
[6] J.L. McCrindle, T.C. Li Kam Wa, W. Barron, L.F. Prescott, Effect of food on the absorption of frusemide and bumetanide in man, Br. J. Clin. Pharmacol. 42 (1996) 743–746.
[7] P.N.V. Tata, R. Venkataramanan, K. Swroop, S.K. Sahota, Bumetanide, Anal. Profiles Drug Subs. Excipients 22 (1993) 107–144.
[8] L.M. Walmsley, L.F. Chasseaud, J.N. Miller, Determination of bumetanide in the plasma of non-human primates by high-performance liquid chromatography, J. Chromatogr. 226 (1981) 441–449.
[9] H. Bokens, C. Bourscheidt, R.F. Muller, Determination of bumetanide in plasma by high-performance liquid chromatography, J. Chromatogr. 434 (1988) 327–329.
[10] T.G. Wells, I.R. Hendry, G.L. Kearns, Measurement of bumetanide in plasma and urine by high-performance liquid chromatography and application to bumetanide disposition, J. Chromatogr. 570 (1991) 235–242.
[11] M.J. Legorburu, R.M. Alonso, R.M. Jiménez, E. Ortiz, Quantitative determination of the loop diuretic bumetanide in urine and pharmaceuticals by high-performance liquid chromatography with amperometric detection, J. Chromatogr. Sci. 39 (2001) 425–430.
[12] Y. Li, R. Cleary, M. Kellog, J.S. Soul, G.T. Berry, E.E. Jensen, Sensitive isotope dilution liquid chromatography/tandem mass spectrometry method for quantitative analysis of bumetanide in serum and brain tissue, J. Chromatogr. B 879 (2011) 998–1002.
[13] X. Zheng, M. Lu, L. Zhang, Y. Chi, L. Zheng, G. Chen, An online field-amplification sample stacking method for the determination of diuretics in urine by capillary electrophoresis-amperometric detection, Talanta 76 (2008) 15–20.
[14] V. Morra, P. Davit, P. Capra, M. Vincenti, A.D. Stilo, F. Botre, Fast gas chromatographic/mass spectrometric determination of diuretics and masking agents in human urine. Development and validation of a productive screening protocol for antidoping analysis, J. Chromatogr. A 1135 (2006) 219–229.
[15] T.F. Tsai, M.R. Lee, Liquid-phase microextraction combined with liquid chromatography–electrospray tandem mass spectrometry for detecting diuretics in urine, Talanta 75 (2008) 658–665.
[16] G.J. Murray, J.P. Danaceau, Simultaneous extraction and screening of diuretics beta-blockers, selected stimulants and steroids in human urine by HPLC–MS/MS and UPLC–MS/MS, J. Chromatogr. B 877 (2009) 3857–3864.
[17] Guidance for Industry, Bionanalytical Method Validation, US Department of Health and Human Services, Food and Drug Administration Centre for Drug Evaluation and Research (CDER), Centre for Veterinary Medicine (CVM), May 2001.
[18] B.K. Matuszewski, M.L. Constanzer, C.M. Chavez-Eng, Strategies for the assessment of matrix effect in quantitative bioanalytical methods based on HPLC–MS/MS, Anal. Chem. 75 (2003) 3019–3030.
[19] R. King, R. Bonfiglio, C. Fernandez-Metzler, C. Miller-Stein, T. Olah, Mechanistic investigation of ionization suppression in electrospray ionization, J. Am. Soc. Mass Spectrom. 11 (2000) 942–950.
[20] Guidance for Industry: ICH E6 Good Clinical Practice, U.S. Department of Health and Human Services, Food and Drug Administration, Centre for Drug Evaluation and Research (CDER), Centre for Biologics Evaluation and Research (CBER), 1996.
[21] M. Yadav, P.S. Shrivastav, Incurred sample reanalysis: a decisive tool in bioanalytical research, Bioanalysis 3 (2011) 1007–1024.
[22] N. Yagi, T. Kjuchi, H. Satoh, Y. Ishikawa, M. Takada, H. Sekikawa, Bioavailability and diuretic effect after administration of retarded capsules of bumetanide in human subjects, Biol. Pharm. Bull. 22 (1999) 275–280.

Journal of Pharmaceutical and Biomedical Analysis 66 (2012) 371–375

Contents lists available at SciVerse ScienceDirect

Journal of Pharmaceutical and Biomedical Analysis

journal homepage: www.elsevier.com/locate/jpba

Short communication

A validated HPLC assay for the determination of R-(−)-gossypol in human plasma and its application in clinical pharmacokinetic studies

Hongxia Lin[a], Murugesan K. Gounder[a,*], Joseph R. Bertino[a], Ah-Ng Tony Kong[a,b], Robert S. DiPaola[a], Mark N. Stein[a]

[a] The Cancer Institute of New Jersey, Robert Wood Johnson Medical School, University of Medicine and Dentistry of New Jersey, 195 Little Albany Street, New Brunswick, NJ 08901, United States
[b] Department of Pharmaceutics, Ernest-Mario School of Pharmacy, Rutgers, The State University of New Jersey, 160 Frelinghuysen Road, Piscataway, NJ 08854, United States

ARTICLE INFO

Article history:
Received 31 January 2012
Received in revised form 13 March 2012
Accepted 14 March 2012
Available online 24 March 2012

Keywords:
R-(−)-gossypol
HPLC–UV
Pharmacokinetics

ABSTRACT

R-(−)-gossypol acetic acid (AT-101), a natural BH3 mimetic, is investigated in a Phase I/II clinical trial for the treatment of advanced solid tumor malignancies. Gossypol undergoes rapid degradation in solution phase, which causes major technical difficulty for its quantitation in plasma. We developed and validated a sensitive HPLC assay for pharmacokinetic evaluation of gossypol. Acetonitrile deproteinization method was chosen for sample preparation and Schiff's base derivative, R-(−)-gossypol-diamino-propanol (GDP), was used as internal standard. Chromatographic separation of gossypol in plasma was performed using a Zorbax Eclipse XDB column C_{18} at 30 °C. The mobile phase consists of 10 mmol/L KH_2PO_4 (pH 3.0) and acetonitrile (20:80) at 1.0 mL/min flow rate. Linearity ranged over 56–3585 ng/mL ($R^2 = 0.9997 \pm 0.0003$, $n = 4$), and the limit of detection was 28 ng/mL. The intra- and inter-assay precision was less than 13.7% and the bias ranged from −7.4 to 7.0%. The method was successfully applied to characterize the pharmacokinetics of AT-101 in a Phase I clinical trial. The validated assay is accurate, and sensitive with minimum loss and rapid analysis time and suitable for quantification of gossypol for pharmacokinetics evaluation.
Published by Elsevier B.V.

1. Introduction

Gossypol [1,1′,6,6′,7,7′-hexahydroxy-5,5′-diisopropyl-3,3′-dimethyl-(2,2′-binaphthelene)8,8′-dicarboxaldehyde], a natural compound isolated from cottonseed and roots, has been investigated extensively as a male contraceptive agent [1,2]. Recently gossypol and its analogs apogossypolone and apogossypol are shown to have anti-proliferative and cytotoxic effects on a variety of human cancer cell lines, e.g. prostate: VCap, PC-3, and DU145 [3,4], breast: MCF-7 [5], colon: HT-29 [6], leukemia: HL-60 [7], and diffuse large cell lymphoma WSU-DLCL2 [8], and tumor growth inhibition in preclinical xenograft models [9,10]. R-(−)-gossypol, the biologically more potent gossypol enantiomer (AT-101, Ascenta Pharmaceuticals Inc.) has received development support from National Cancer Institute (USA), and a phase I/II clinical trial was initiated for determining the safety and the maximum tolerated dose of AT-101 in combination with paclitaxel and carboplatin in patients with advanced solid tumor malignancies. Previous phase I and II studies on safety evaluation of AT-101 as a single agent, and in combination with docetaxel or topotecan [11–15] showed some possible survival benefit. As a promising anti-tumor agent, a better understanding of the pharmacokinetics is necessary for the correlation of its therapeutic effect. Previously high performance liquid chromatography (HPLC) methods were reported for the quantitative analyses of gossypol in human, and dog plasma using electrochemical (EC) [16,17] or ultraviolet (UV) detector [18], and its analog apogossypol in mouse plasma by liquid chromatography-mass spectrometry (LC/MS–MS) [19]. However, HPLC–UV method was not fully validated for the quantitative analysis of gossypol in human plasma. In this present study, we report a fully validated HPLC–UV method for quantitative analysis of gossypol in human plasma using R-(−)-gossypol-diamino-propanol (GDP), as internal standard (a stable Schiff's base gossypol derivative), for the evaluation of clinical pharmacokinetics of AT-101 in patients with advanced solid tumor malignancies.

2. Experimental

2.1. Chemicals and reagents

R-(−)-gossypol was a gift from Ascenta Therapeutics Inc (Malern, PA). (R)-(−)-1-amino-2-propanol (D-alaninol), and dimethylformamide, glutathione (reduced) were purchased from Sigma–Aldrich Co. (St. Louis, MO). HPLC grade solvents

* Corresponding author. Tel.: +1 732 2357211; fax: +1 732 2357493.
E-mail address: goundemk@umdnj.edu (M.K. Gounder).

0731-7085/$ – see front matter. Published by Elsevier B.V.
doi:10.1016/j.jpba.2012.03.029

methanol and acetonitrile were purchased from Fisher Scientific Inc. (Pittsburg, PA). The control plasma used for the preparation of calibration standards was obtained from the New Brunswick affiliated hospital blood bank (New Brunswick, NJ).

2.2. Instrument and chromatographic conditions

A Finnigan Surveyor LC system equipped with Surveyor quaternary pump, Surveyor auto-sampler and Surveyor PDA and Xcaliber software (Thermo Electron Inc, CA) was used for the analysis and data acquisition. Chromatographic separation of R-(−)-gossypol in plasma was performed using a Zorbax Eclipse XDB C_{18} column (4.6 mm × 150 mm, Agilent, Santa Clara, CA) at 30 °C. The auto-sampler was maintained at 4 °C. The UV detector was set at 254 nm and the mobile phase consisted of 10 mM KH_2PO_4 (pH 3.0) and acetonitrile (20:80) at the flow rate of 1.0 mL/min. The retention times of R-(−)-gossypol and the internal standard (IS) were 9.7 min and 6.1 min.

2.3. Preparation of stock and working solutions

The stock solution of R-(−)-gossypol acetic acid (1 mg/mL) was prepared in acetonitrile and was stable for 3 months at −70 °C. Since gossypol is unstable in water, methanol, ethanol and alcoholic solvents [20], antioxidant glutathione-reduced (20 mM) was added to control blank plasma and patient blood samples to stabilize the drug. The working calibration standards were prepared in plasma by serial dilution of stock standard solution at the concentrations ranging from 0.028 to 3.58 μg/mL.

2.4. Preparation of internal standard solution

The internal standard GDP was synthesized as described by Dowd and Pelitire's method [21]. Briefly, 5 mg R-(−)-gossypol was added to the complexing reagent consisting of 0.2 mL (R)-(−)-1-amino-2-propanol, 1.0 mL glacial acetic acid and 8.8 mL dimethylformamide and was heated at 95 °C for 30 min. After cooling down, the mixture was diluted to 100 times with acetonitrile and used as IS. Under the chromatographic conditions GDP gave a single peak with a retention time ~6 min. The identity of Schiff's base R-(−)-gossypol-diamino-propanol was further confirmed by mass spectrometry *m/z* 633.1 (Thermo-Finnigan triple Quad TSQ quantum). The plasma standards and the IS solutions were stored in polypropylene tubes at −70 °C and thawed on the day of analysis.

2.5. Sample preparation

The calibration standards and patient samples were thawed on ice, and aliquots of 300 μL samples were pipetted into 1.5 mL polypropylene microfuge tubes and spiked with 10 μL (8.6 nM) of IS. The samples were deproteinized with 600 μL acetonitrile and vortex mixed for 30 s. After centrifuged at 13,000 rpm (17,900 × *g*) for 10 min at 4 °C, an aliquot of 100 μL supernatant was injected into the HPLC system for analysis. Extraction of gossypol from plasma in different solvents such as chloroform, dichloromethane, and acetone was attempted; however, on drying even under nitrogen atmosphere, we found gossypol degraded and ended up with poor recovery. Therefore, we choose to deproteinize standards and samples with acetonitrile and direct inject the acetonitrile extracts without further reduction in sample volume.

2.6. Method validation

The selectivity of the method was tested by comparing the chromatograms from four different batches of blank human plasma with the corresponding gossypol spiked plasma. Peak areas of endogenous compounds co-eluting with the analyte were less than 20% of the peak area of the LLOQ standard (lower limit of quantitation). The calibration standards were prepared and assayed on three different days to demonstrate the linearity of this method. Linearity was assessed by the least square linear regression. The lower limit of detection (LOD) was defined as signal/noise ratio of 3. The LLOQ was defined as the lowest analyte concentration that can be determined with precision less than 20% relative standard deviation (RSD). The precision and accuracy of the assay were evaluated at three concentrations (quality control 0.112, 0.896 and 3.58 μg/mL). Three replicate samples were prepared and analyzed on the same day for intraday and continuous days ($n = 4$) for inter-day accuracy and precision following FDA guide lines [22]. The assay precision was expressed as relative standard deviation and accuracy was calculated as bias. The intra- and inter-day precision was required to be below 15%, and the accuracy to be within ±15%. The extraction recovery of R-(−)-gossypol and IS in plasma was measured at three QC concentrations and expressed as the ratio of the peak responses.

The stability of gossypol in plasma was performed under the different storage conditions. The stability test conditions included analysis of QC samples after three cycles of freeze and thaw, storage at room temperature for 4 h and at −70 °C for 1 month. Post preparation stability was accessed by re-analyzing the samples after 24 h in auto-sampler at 4 °C. All the stability test samples were analyzed in triplicate and determined with freshly prepared calibration standard. The analyte was considered to be stable in plasma when 85–115% of the initial concentration was found.

2.7. Pharmacokinetics application in patients

The method was applied to evaluate the pharmacokinetics of gossypol in an Institutional Review Board approved phase I clinical trial in patients with advanced solid tumors. AT-101 was administered orally at 40 mg b.i.d. on Days 1, 2 and 3 of a 21 days cycle. On day 1 of each cycle 1 h after AT-101 treatment, patients were treated with i.v. infusion of paclitaxel at 150 mg/m^2 (3 h) followed by i.v. infusion of carboplatin (0.5 h, AUC 5). Following gossypol administration, blood samples (4 mL) were collected in EDTA tubes at predose and at 1, 2, 3, 4, 4.5, 5, 6, 8, 10, and 24 h post administration. Blood samples were placed on ice and transported immediately to the laboratory, and 3 mL whole blood decanted into appropriately labeled polypropylene tubes containing 300 μL of 200 mM of freshly prepared reduced glutathione in PBS. The contents were mixed and centrifuged at 2300 rpm for 5 min at 4 °C and the plasma was transferred to vials and stored at −70 °C for future analysis. The pharmacokinetic parameters C_{max}, half-life ($t_{½}$), area under concentration–time curve (AUC), apparent clearance (CL) were estimated using WinNonlin 2.1 software (Pharsight Corp., Palo Alto, CA). The data was analyzed using non-compartmental model for PK modeling.

3. Results and discussion

3.1. Method development

Chromatographic conditions, especially the composition of mobile phase was optimized to achieve resolution of gossypol, IS and other components in plasma. Since gossypol is reported to decompose in methanol even at 5 °C, and is stable in acetonitrile [20], we tested mobile phase with different ratios of acetonitrile and water, and acetonitile:water (80:20) was selected for mobile phase. For the selection of IS, we evaluated two of the previously reported compounds gossypol dimethyl ether [17], and apogenein [19]. Gossypol dimethyl ether is not commercially available and has to

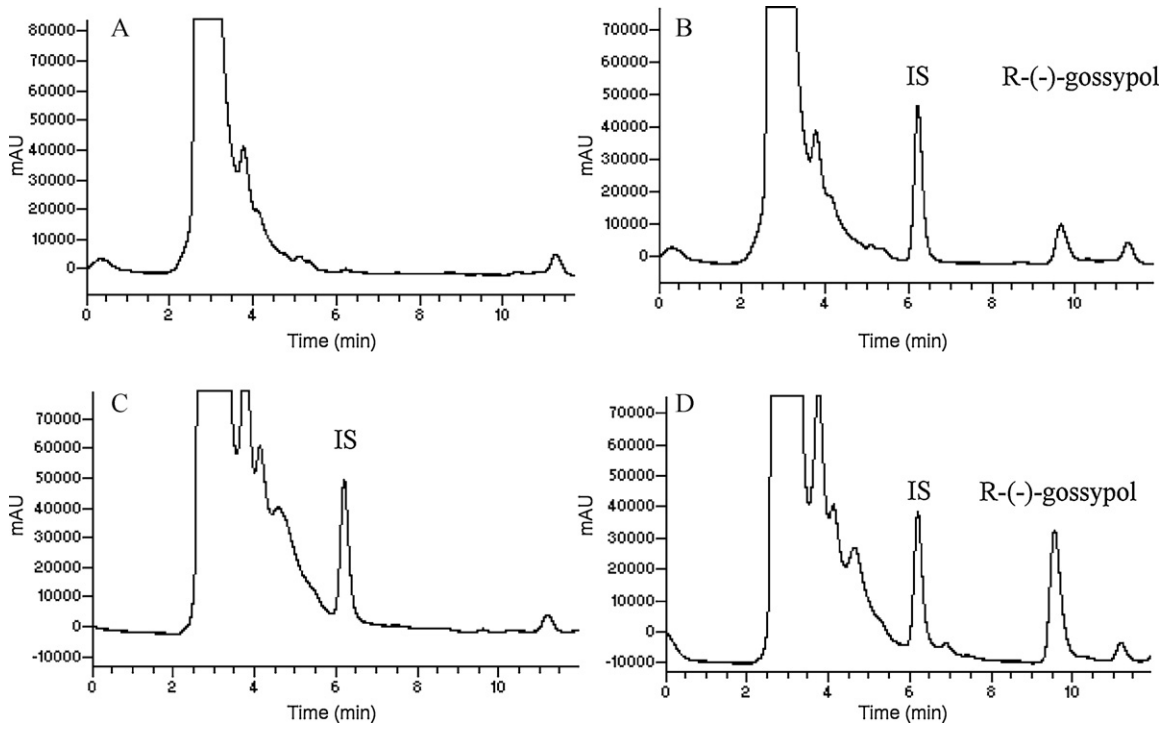

Fig. 1. Representative HPLC chromatogram from extractions of a blank plasma (A); 224.0 ng/mL gossypol with IS (B); and a patient plasma sample at predose (C) and 4.5 h (D).

be synthesized in multiple steps from gossypol to gossypol hexamethyl ether, which is then demethylated to yield gossypol dimethyl ether, a cumbersome and time consuming procedure [23]. In addition the purity and yield have to be determined. When we used apigenein as an IS, the retention time was close to the void volume and found not suitable for HPLC–UV analysis. Since gossypol and Schiff's base derivative of gossypol have different chromatographic retention times, but have similar UV absorption characteristics, we derivatized R-(−)-gossypol to Schiff's base R-(−)-gosspol-diaminopropanol by following the simple one step procedure and used as IS. Under the chromatographic conditions, GDP separated as a single chromatographic peak with no interference from gossypol at 254 nm. Fig. 1 shows the typical chromatograms of blank plasma (A), blank plasma spiked with gossypol and IS (B), a patient plasma sample at predose (C) and 4.5 h after oral treatment of AT-101 (D).

3.2. Sample preparation method

Sample preparation is important for the acceptable recovery and reproducible results. Since gossypol is unstable in aqueous and alcoholic solutions at room temperature, the stability of gossypol in plasma with different antioxidants was investigated in detail. The percentage of gossypol remaining in plasma as a function of storage time was plotted at 4 °C and room temperature (not shown). R-(−)-gossypol showed good stability in mobile phase acetonitrile/water (80:20), which was retained without oxidation after 24 h at 4 °C. At room temperature in plasma more than 60% of R-(−)-gossypol was degraded over 24 h, when compared to freshly prepared samples, whereas, similarly prepared samples stored at 4 °C retained about 74.5% in plasma over 24 h. The stability of R-(−)-gossypol (5 μg/mL) in plasma with 20 mM reduced glutathione and 1% ascorbic acid at 4 °C can improve the stability of R-(−)-gossypol. However, at room temperature, none of these antioxidants increased the stability of gossypol in plasma. Based on instability of gossypol in water phase, we choose the single step ice cold acetonitirle plasma-deproteinization extraction procedure and performed all operations on ice. It is necessary to add 20 mM glutathione for preparing patient plasma samples during storage. As shown in Table 1, the stability of quality control samples with 20 mM glutathione was investigated under the various conditions throughout the validation process. The results show quality control plasma samples with 20 mM glutathione can keep gossypol stable at −70 °C for 1 month or on ice for 4 h. The acetonitrile extracts of samples were stable at 4 °C autosampler in 24 h. However, the freeze-thaw stability after 3 cycles showed significant degradation of gossypol at the lower concentration, therefore the patient samples should not be thawed repeatedly.

3.3. Method validation

The HPLC assay showed acceptable linearity over the range of 0.056–3.585 μg/mL (R^2 = 0.9997 0.0003, n = 4) with the LOD of

Table 1
Stability of R-(−)-gossypol in human plasma by HPLC assay (n = 3, Mean ± S.D.).

Added concentration (μg/mL)	Remained concentration (%)			
	On ice, 4 h	Three freeze-thaw cycles	−80 °C, 1 month	Autosampler, 4 °C, 24 h[a]
0.112	100.1 ± 2.4	71.9 ± 4.5	99.3 ± 4.0	95.6
0.896	101.5 ± 2.0	81.6 ± 1.7	109.3 ± 5.3	97.3
3.585	103.8 ± 6.1	86.9 ± 1.1	111.8 ± 5.6	100.6

[a] n = 2.

Table 2
Precision and accuracy of R-(−)-gossypol.

	Intraday ($n = 3$)			Interday (n = 4)		
Conc. norminal (μg/mL)	Measured (μg/mL) Mean ± S.D.	Precision (%)	Accuracy (Bias%)	Measured (μg/mL) Mean ± S.D.	Precision (%)	Accuracy (Bias%)
0.056(LLOQ)	0.058 ± 0.002	2.9	−7.3	0.060 ± 0.005	13.2	7.0
0.112	0.105 ± 0.002	1.6	−6.4	0.114 ± 0.008	7.4	1.7
0.896	0.892 ± 0.014	1.5	0.2	0.869 ± 0.021	2.4	−3.1
3.585	3.575 ± 0.120	3.5	0.3	3.584 ± 0.018	0.5	0.02

Table 3
Plasma pharmacokinetic parameters of R-(−)-gossypol (Cycle 1 Day 1).

Patients[a]	$AUC_{(0-10\,h)}$ (μg/mL × h)	Clearance (L/h)	$t_{1/2}$ (h)	C_{max} (μg/mL)
#1	1.74	17.86	3.19	0.32
#2	5.12	6.35	3.14	0.92
#3	3.69	8.64	3.11	0.68
#4	4.34	7.90	2.91	0.87
#5	2.74	9.21	4.30	0.49
Average	3.53	9.99	3.33	0.66
SD	1.33	4.53	0.55	0.25

[a] Treated with combination of AT-101 40 mg bid,(p.o.), paclitaxel (150 mg/m^2, i.v. 3 h), followed by carboplatin (AUC 5, i.v. 30 min).

28 ng/mL and LLOQ of 56 ng/mL. Table 2 summarizes the intra and inter-day precision and accuracy. Intra-day and inter-day precisions were less than 13.2%. Accuracy (bias) ranged from −7.4 to 7.0%. The direct deproteinization method showed satisfactory intra and inter-assay precision and accuracy for quantitation of gossypol in plasma. In the PK studies, the measured concentrations of R-(−)-gossypol at 12 h post dose were within calibration range and the limits of detection.

The recovery of R-(−)-gossypol and IS in control plasma at the different concentrations was compared to the same concentration in acetonitrile:water (80:20). The recovery of R-(−)-gossypol and IS in plasma standards was consistent. The extraction recoveries of gossypol and IS in plasma were in the range of 87.8–101.1%.

3.4. Application in pharmacokinetic studies

This HPLC assay was applied to determine the concentration of R-(−)-gossypol in plasma of solid tumor patients treated with AT-101, paclitaxel and carboplatin. The large inter-individual variation following oral administration could be due to food and other factors (transporters) in the gastrointestinal tract which might affect the absorption of gossypol. The calculated pharmacokinetic parameters are listed in Table 3. Average of R-(−)-gossypol $AUC_{0-10\,h}$ was 3.53 ± 1.33 μg/mL × h. The pharmacokinetic parameters of gossypol ($t_{1/2}$, C_{max}) were comparable with a previous study using HPLC coupled with electrochemical detector [16].

4. Conclusions

A simple and sensitive HPLC assay was developed and fully validated for quantitation of R-(−)-gossypol in plasma. The method was developed using 300 μL of human plasma for determination of gossypol with a lower limit of quantitation (56 ng/mL) using GDP as the internal standard. The HPLC assay is applicable for R-(−)-gossypol quantitation in clinical pharmacokinetics studies.

Acknowledgments

The authors gratefully acknowledge NCI and the Cancer Institute of New Jersey for support. The authors acknowledge the assistance of the Tissue Analytic Service of CINJ for patient sample collection.

References

[1] G.Z. Liu, K.C. Lyle, J. Cao, Clinical trial of gossypol as a male contraceptive drug. Part I. Efficacy study, Fertil. Steril. 48 (1987) 459–461.
[2] E.M. Coutinho, C. Athayde, G. Atta, Z.P. Gu, Z.W. Chen, G.W. Sang, E. Emuveyan, A.O. Adekunle, J. Mati, J. Otubu, M.M. Reidenberg, S.J. Segal, Gossypol blood levels and inhibition of spermatogenesis in men taking gossypol as a contraceptive. A multicenter, international, dose-finding study, Contraception 61 (2000) 61–67.
[3] N. McGregor, L. Patel, M. Craig, S. Weidner, S. Wang, K.J. Pienta, AT-101 (R-(−)-gossypol acetic acid) enhances the effectiveness of androgen deprivation therapy in the VCaP prostate cancer model, J. Cell. Biochem. 110 (2010) 1187–1194.
[4] S.R. Volate, B.T. Kawasaki, E.M. Hurt, J.A. Milner, Y.S. Kim, J. White, W.L. Farrar, Gossypol induces apoptosis by activating p53 in prostate cancer cells and prostate tumor-initiating cells, Mol. Cancer Ther. 9 (2010) 461–470.
[5] W. Ye, H.L. Chang, L.S. Wang, Y.W. Huang, S. Shu, Y. Sugimoto, M.K. Dowd, P.J. Wan, Y.C. Lin, Induction of apoptosis by (−)-gossypol-enriched cottonseed oil in human breast cancer cells, Int. J. Mol. Med. 26 (2010) 113–119.
[6] M. Zhang, H. Liu, R. Guo, Y. Ling, X. Wu, B. Li, P.P. Roller, S. Wang, D. Yang, Molecular mechanism of gossypol-induced cell growth inhibition and cell death of HT-29 human colon carcinoma cells, Biochem. Pharmacol. 66 (2003) 93–103.
[7] L.H. Huang, J.Q. Hu, W.Q. Tao, Y.H. Li, G.M. Li, P.Y. Xie, X.S. Liu, J. Jiang, Gossypol inhibits phosphorylation of Bcl-2 in human leukemia HL-60 cells, Eur. J. Pharmacol. 645 (2010) 9–13.
[8] Y. Sun, J. Wu, A. Aboukameel, S. Banerjee, A.A. Arnold, J. Chen, Z. Nikolovska-Coleska, Y. Lin, X. Ling, D. Yang, S. Wang, A. Al-Katib, R.M. Mohammad, Apogossyplone, a nonpeptidic small molecule inhibitor targeting Bcl-2 family proteins, effectively inhibits growth of diffuse large cell lymphoma cells in virtro and in vito, Cancer Biol. Ther. 7 (2008) 1418–1426.
[9] L. Xu, D. Yang, S. Wang, W. Tang, M. Liu, M. Davis, J. Chen, J.M. Rae, T. Lawrence, M.E. Lippman, (−)-Gossypol enhances response to radiation therapy and results in tumor regression of human prostate cancer, Mol. Cancer Ther. 4 (2005) 197–205.
[10] Y. Meng, W. Tang, Y. Dai, X. Wu, M. Liu, Q. Ji, M. Ji, K. Pienta, T. Lawrence, L. Xu, Natural BH3 mimetic (−)-gossypol chemosensitizes human prostate cancer via Bcl-xL inhibition accompanied by increase of Puma and Noxa, Mol. Cancer Ther. 7 (2008) 2192–2202.
[11] G. Sonpavde, V. Matveev, J.M. Burke, J.R. Caton, M.T. Fleming, T.E. Hutson, M.D. Galsky, W.R. Berry, P. Karlov, J.T. Holmlund, B.A. Wood, M. Brookes, L. Leopold, Randomized phase II trial of docetaxel plus prednisone in combination with placebo or AT-101, an oral small molecule Bcl-2 family antagonist, as first-line therapy for metastatic castration-resistant prostate cancer, Ann. Oncol. (November) (2011), doi:10.1093/annonc/mdr555.
[12] R.S. Heist, J. Fain, B. Chinnasami, W. Khan, J.R. Molina, L.V. Sequist, J.S. Temel, P. Fidias, V. Brainerd, L. Leopold, T.J. Lynch, Phase I/II study of AT-101 with topotecan in relapsed and refractory small cell lung cancer, J. Thorac. Oncol. 5 (2011) 1637–1643.
[13] G. Liu, W.K. Kelly, G. Wilding, L. Leopold, K. Brill, B. Somer, An open-label, multicenter, phase I/II study of single-agent AT-101 in men with castrate-resistant prostate cancer, Clin. Cancer Res. 15 (2009) 3172–3176.
[14] N. Ready, N.A. Karaseva, S.V. Orlov, A.V. Luft, O. Popovych, J.T. Holmlund, B.A. Wood, L. Leopold, Double-blind, placebo-controlled, randomized phase 2 study of the proapoptotic agent AT-101 plus docetaxel, in second-line non-small cell lung cancer, J. Thorac. Oncol. 6 (2011) 781–785.
[15] M.Q. Baggstrom, Y. Qi, M. Koczywas, A. Argiris, E.A. Johnson, M.J. Millward, S.C. Murphy, C. Erlichman, C.M. Rudin, R. Govindan, A phase II study of AT-101 (Gossypol) in chemotherapy-sensitive recurrent extensive-stage small cell lung cancer, J. Thorac. Oncol. 6 (2011) 1757–1760.
[16] D.F. Wu, Y.W. Yu, Z.M. Tang, M.Z. Wang, Pharmacokinetics of (+/−)-, (+)-, and (−)-gossypol in humans and dogs, Clin. Pharmacol. Ther. 39 (1986) 613–618.
[17] P. Bushunow, M.M. Reidenberg, J. Wasenko, J. Winfield, B. Lorenzo, S. Lemke, B. Himpler, R. Corona, T. Coyle, Gossypol treatment of recurrent adult malignant gliomas, J. Neurooncol. 43 (1999) 79–86.
[18] N. Sattayasai, J. Sattayasai, V. Hahnvajanawong, High-performance liquid chromatographic determination of gossypol in plasma, J. Chromatogr. 307 (1984) 235–239.
[19] L. Coward, G. Gorman, P. Noker, C. Kerstner-Wood, M. Pellecchia, J.C. Reed, L. Jia, Quantitative determination of apogossypol, a pro-apoptotic analog of gossypol, in mouse plasma using LC/MS/MS, J. Pharm. Biomed. Anal. 42 (2006) 581–586.
[20] A.A. Nomeir, M.B. Abou-Donia, Gossypol: high-performance liquid chromatographic analysis and stability in various solvents, J. Am. Chem. Soc. 59 (1982) 546–549.

[21] M.K. Dowd, S.M. Pelitire, HPLC preparation of the chiral forms of 6-methoxy-gossypol and 6,6′-dimethoxy-gossypol, J. Chromatogr. B: Analyt. Technol. Biomed. Life Sci. 867 (2008) 69–77.
[22] V.P. Shah, K.K. Midha, S. Dighe, I.J. McGilveray, J.P. Skelly, A. Yacobi, T. Layloff, C.T. Viswanathan, C.E. Cook, R.D. McDowall, et al., Analytical methods validation: bioavailability, bioequivalence and pharmacokinetic studies, Conference report, J. Pharm. Res. 9 (1992) 588–592.
[23] R. Adams, T.A. Geissman, Structure of gossypol VII. Gossypol dimethyl ether, J. Am. Chem. Soc. 60 (1938) 2163–2166.

Journal of Pharmaceutical and Biomedical Analysis 66 (2012) 376–380

Contents lists available at SciVerse ScienceDirect

Journal of Pharmaceutical and Biomedical Analysis

journal homepage: www.elsevier.com/locate/jpba

Short communication

Development and validation of a useful HPLC–UV method for quantification of total and phosphorylated-ribavirin in blood and erythrocytes of HCV+ patients

Antonio D'Avolio*, Amedeo De Nicolò, Marco Simiele, Stefano Turini, Danilo Agnesod, Lucio Boglione, Jessica Cusato, Lorena Baietto, Giuseppe Cariti, Andrea Calcagno, Mauro Sciandra, Giovanni Di Perri, Stefano Bonora

Laboratory of Clinical Pharmacology and Pharmacogenetic, Department of Infectious Diseases, University of Turin, Amedeo di Savoia Hospital, Turin, Italy[1]

ARTICLE INFO

Article history:
Received 15 February 2012
Accepted 14 March 2012
Available online 28 March 2012

Keywords:
HPLC–UV
Anemia
HCV
Intracellular
Ribavirin

ABSTRACT

Ribavirin-induced hemolytic anemia is the main cause of discontinuation of the combination therapy with alpha-interferon-2b and ribavirin for the treatment of hepatitis C virus (HCV) infection. The determination of intracellular ribavirin levels in blood, including the levels of its phosphorylated metabolites, might be useful for predicting ribavirin-induced anemia, which could be caused by the accumulation of these molecules within the erythrocytes. In this work, we simplified and validated a previously developed assay method, to make it suitable for routine monitoring of cellular ribavirin. Whole blood diluted with a five-fold volume of ice-cold distilled underwent a process of acid phosphatase digestion to convert phosphorylated ribavirin metabolites to free ribavirin. The resulting mixture, spiked with an internal standard, was treated with a protein precipitation protocol in acetonitrile, followed by reverse-phase high-performance liquid chromatography analysis. The calibration curve for ribavirin levels in whole blood was linear at concentrations from 625 to 320,000 ng/mL (r^2 = 0.998). Accuracy, intra-day and inter-day precision for ribavirin and phosphorylated-ribavirin quality controls were all below 9.0%. We tested this method by monitoring blood ribavirin concentrations in 13 HCV+ patients, receiving alpha interferon-plus ribavirin combination therapy.

© 2012 Elsevier B.V. All rights reserved.

1. Introduction

Ribavirin (RBV), a guanosine analogue broad-spectrum antiviral agent, is used for the treatment of hepatitis C virus (HCV) in combination with pegylated alpha-interferon (2a and 2b). Despite the strong beneficial effects of RBV, and its relative plasma concentrations in this therapy on HCV infection [1,2], a loss of hemoglobin occurs in a substantial population of HCV patients [3]. Progressive loss of hemoglobin can lead to anemia; this effect can be counteracted by reducing the ribavirin dose, possibly compromising the therapeutic efficacy of the regimen or using erythropoietin as an adjunctive treatment. Current studies suggest that an excessive RBV accumulation in erythrocytes is responsible for anemia [4–6]. Once incorporated within erythrocytes, RBV is converted into phosphorylated (RBV-P) metabolites by intracellular phosphorylation. These metabolites would decrease intracellular ATP levels, resulting in a reduction of erythrocyte integrity, which could be followed by hemolysis [7,8]. It should therefore be possible to predict the occurrence of ribavirin-induced anemia by determining ribavirin concentrations both in red blood cells and plasma [1–5]. A high-performance liquid chromatography (HPLC) method was previously developed to quantify ribavirin levels in erythrocytes [9]. Since phosphorylated metabolites are the main form of intracellular ribavirin, whole-blood samples were treated with acid phosphatase to convert phosphorylated forms of RBV in non-phosphorylated forms; then they were extracted via solid phase extraction (SPE) and finally analyzed. However, the analytical procedures used in previous studies were too laborious to be used for routine monitoring of intracellular ribavirin. In this study, we modified the analytical procedure in order to validate a new HPLC method and in order to evaluate its feasibility for the routinely determination of intraerythrocytic RBV and RBV-P levels in patient samples.

2. Materials and methods

2.1. Chemicals

Acetonitrile HPLC grade and methanol HPLC grade were purchased from J.T. Baker (Deventer, Holland). HPLC grade water

* Corresponding author. Tel.: +39 011 4393979; fax: +39 011 4393882.
E-mail address: antonio.davolio@unito.it (A. D'Avolio).

[1] UNI EN ISO 9001:2008 Certificate Laboratory; Certificate No. IT-64386; Certification for: "Design, development and application of determination methods for anti-infective drugs. pharmacogenetic analyses." www.tdm-torino.org..

0731-7085/$ – see front matter © 2012 Elsevier B.V. All rights reserved.
doi:10.1016/j.jpba.2012.03.030

Table 1
Chromatographic condition (gradient). Mobile phase A (KH_2PO_4 50 mM with *ortho*-phosphoric acid, final pH 3.23) and mobile phase B (acetonitrile).

Time (min)	% Mobile phase A	% Mobile phase B	Flow (mL/min)
0.0	100	0	1.0
2.0	100	0	1.0
4.0	92	8	1.0
7.0	92	8	1.0
7.1	70	30	1.0
8.1	70	30	1.0
8.2	100	0	1.0
14.0	100	0	1.0

was produced with Milli-DI system coupled with a Synergy 185 system by Millipore (Milan, Italy). Blank blood were taken from healthy donors, kindly supplied by the Blood Bank of the Maria Vittoria Hospital (Turin, Italy). Ribavirin monophosphate (RMP) was purchased from Toronto Research Chemicals Inc. (North York, Canada). Ribavirin (1-β-D-ribofuranosyl-1,2,4-triazole-3-carboxamide), thymidine (internal standard), acid phosphatase type 4 prepared from sweet potato, *ortho*-phosphoric acid KH_2PO_4, Tris–HCl buffer, acetate buffer, KOH powder and all other chemicals were purchased from Sigma–Aldrich Corp. (Milan, Italy). The enzyme was stored in a refrigerator at 4 °C to prevent degradation.

2.2. HPLC instruments and chromatographic conditions

The HPLC system consisted in a binary pump model 515, a 717 autosampler and a 2487 UV detector (Waters, Milan, Italy). Chromatographic separation was performed by an Atlantis 3 μ dC18 column (150 mm × 4.6 mm I.D., Waters, Milan, Italy), protected by a Security-Guard with C18 (4.0 mm × 3.0 mm I.D., Phenomenex, CA, USA), at 35 °C using a column thermostat.

UV absorbance was monitored at 235 nm. The chromatographic conditions used in this method were very similar to those used in our previous method developed for plasma samples [10]. The run was performed with a gradient (Table 1) of two different phases: mobile phase A (KH_2PO_4 50 mM with *ortho*-phosphoric acid, final pH 3.23) and mobile phase B (acetonitrile).

2.3. Stock solutions, standards and quality controls

A stock solution of RBV, RMP and thymidine were made in pure water at final concentration of 1 mg/mL. RBV and RMP were stored at −20 °C until use (less than 1 month). Stock solution of thymidine was stored at 4 °C (less than 6 months).

Standard solutions and quality controls were prepared from aliquots of whole blood from healthy donors, spiked with scalar concentrations of ribavirin, in order to create 10 standard points (STDs) of the calibration curve, plus zero point (ribavirin-free blood). The concentrations of the standard points of the calibration curve were: 625 ng/mL, 1250 ng/mL, 2500 ng/mL, 5000 ng/mL, 10,000 ng/mL, 20,000 ng/mL, 40,000 ng/mL, 80,000 ng/mL, 160,000 ng/mL, 320,000 ng/mL.

Similarly, four quality controls (QCs), high (H), medium (M), low (L) and very-low (VL) were prepared starting from the same whole blood aliquots spiked with RBV. While, another stock of QCs with the same concentrations was prepared with RMP (subtracting the weight of the phosphate group to achieve the same final free-RBV concentrations). RBV and RMP concentration in QC-H, QC-M, QC-L and QC-VL were 200,000 ng/mL, 100,000 ng/mL, 50,000 ng/mL and 7500 ng/mL, respectively.

Internal standard (IS) was prepared by diluting 200 μL of a stock solution of thymidine (1 mg/mL) in 4 mL of a solution of water–methanol 50:50, with a final concentration of 50 μg/mL.

STDs, QCs and patient samples were stored at −80 °C until analysis.

2.4. Specificity and selectivity

Interference from endogenous compounds was investigated by the analysis of six different blank blood samples. No potential concomitant drugs were investigated.

2.5. Enzyme digestion and extraction procedure

20 μL of blood sample (four aliquots for each patient sample), STDs and QCs were treated with a lysis solution, made up 300 μL of a Tris–HCl buffer 30 mM (pH 8.0) and 100 μL of pure water. Then, 25 μL of acetate buffer 1 M (pH 4) and 40 μL of IS solution were added to all samples. Two of the four aliquots from each patient were treated with 0.5 units of acid phosphatase, in order to evaluate the amount of total RBV (RBV + RBV-P); the other two aliquots, not-treated, were used to quantify the amount of not-phosphorylated-RBV (RBV). All samples were then incubated in a water bath at 37 °C for 1 h.After incubation, all samples were treated with 2.5 μL of KOH 10 N to alkalize the solution, ensuring the rapid deactivation of acid phosphatase. At this point, 1500 μL of acetonitrile was added to all samples in order to achieve protein precipitation. Afterwards the samples, after being placed on Vortex for 10″, were centrifuged (Jouan BR4i) at 9600 × *g* for 10 min at 4 °C. After centrifugation, the supernatant was transferred to glass shots and it was dried in a vacuum-centrifuge at 50 °C. Dry pellets were reconstituted with 125 μL of mobile phase A, transferred in total recovery vials and loaded in the autosampler. 30 μL was injected in the HPLC system.

Plasma samples of the same patients were analyzed according to our previous published paper [10].

2.6. Accuracy, precision, and limit of quantification

Intra-day, inter-day accuracy and precision of the method were determined by performing 10 validation sessions. RBV and RBV-P QCs were analyzed in duplicate. Accuracy was calculated as the mean percent deviation from the nominal concentrations.

Inter-day and intra-day precisions were expressed as the relative standard deviation at each QC concentration. The calibration curve was obtained using the standard points described above.

Limit of detection (LOD) in blood was defined as the concentration that yields a signal-to-noise ratio of 3. Percentage of deviation from the nominal concentration (measure of accuracy) and relative standard deviation (measure of precision) at the concentration considered as the limit of quantification (LOQ) was <20%, as requested by FDA guidelines [11].

2.7. Recovery

Average recovery of RBV and RBV-P was determined by comparing the peak area of the extracts obtained from QC samples (200,000 ng/mL, 100,000 ng/mL, 50,000 ng/mL and 7500 ng/mL) with those obtained by direct injection of the same amount of drug.

2.8. Patients recruiting and calculation of intraerythrocyte RBV concentrations

The method was tested on 13 patients in therapy with RBV and peg-INFα 2a or 2b. Samples were collected after 2 weeks of treatment. Blood sampling at the end of the dosing interval (Ctrough), was performed after written informed consent has been given. All patients were HCV+-positive mono-infected without history of previous infection or treatment. The concentrations

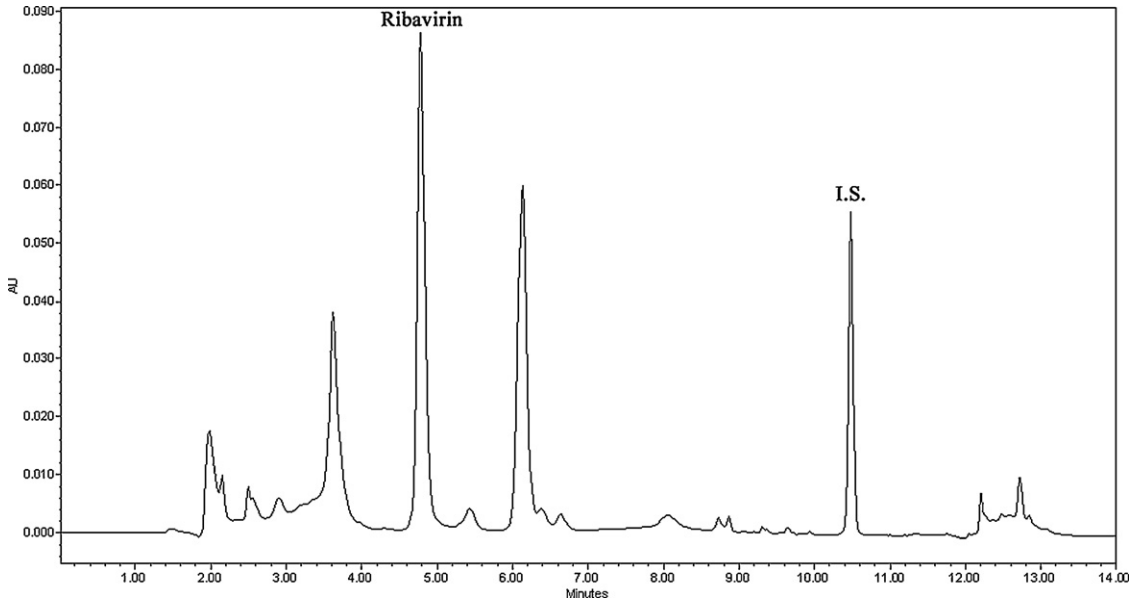

Fig. 1. STD 10 chromatogram with Ribavirin and internal standard (IS).

of phosphorylated-RBV were obtained by subtracting the non-phosphorylated fraction (determined on the aliquots untreated with acid phosphatase) to the total blood RBV (determined on the aliquots treated with the enzyme). Erythrocyte concentrations of total and phosphorylated RBV were calculated by normalizing blood concentrations on the basis of corresponding hematocrit and by the subtraction of the plasmatic fraction of RBV. The following formula was used: $C_{rbc} = \{(C_w 100) - [C_p(100 - HCT)]\}/HCT$, where HCT is the hematocrit, C_{rbc} is RBV concentration in the red blood cells and C_w and C_p are the whole blood and plasma RBV concentrations, respectively [9].

3. Results

3.1. Sensibility and specificity

A typical HPLC chromatogram of RBV and IS in whole blood samples is shown in Fig. 1. Peaks representing RBV and IS were observed at retention times of 4.8 ± 0.15 and 10.5 ± 0.15 min, respectively. We did not observe any difference in retention times for RBV and IS between treated and untreated samples. No interfering peaks generated from endogenous substances were observed in the chromatogram for "blank" whole blood (Fig. 2).

3.2. Accuracy, precision, and limit of quantification

Relative standard errors for intra- and inter-day assay precision were determined by 10 different validation sessions. Results of the validation of the method are shown in Table 2. LOD and LOQ were 312 and 625 ng/mL, respectively. Calibration curves were linear in our concentrations range (625–320,000 ng/mL), with a mean regression linear coefficient (r^2) of 0.998.

3.3. Recovery

Multiple aliquots ($n = 8$) at each different concentration were tested. Mean recovery of RBV and RBV-P were 80.1% (R.S.D. = 5.3%).

3.4. Analysis of samples from patients

Blood samples were obtained at a median of 12.15 h (IQR 11.75–12.9) after last drug intake. Average of total RBV and

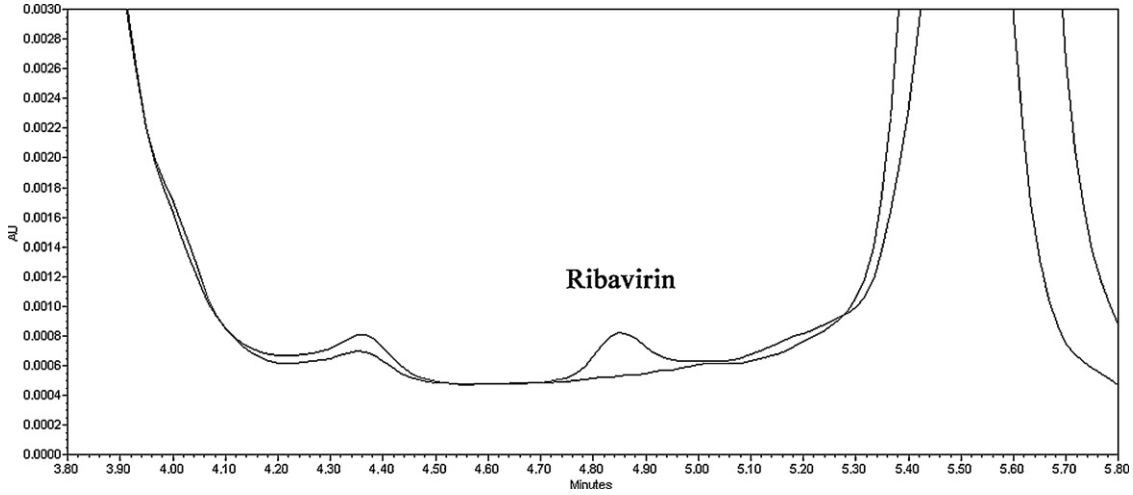

Fig. 2. Overlapping of STD 1 (LOQ) with ribavirin and blank plasma chromatograms.

Table 2
Intra-day and inter-day precision for the analysis of ribavirin (A) and phosphorylated-ribavirin (B) in blood QCs ($n = 10$) [mean R.S.D.%].

(A)

QC, spiked RBV concentration (ng/mL)	Accuracy %	Intra-day R.S.D.%	Inter-day R.S.D.%
QC-H (200,000)	1.48	3.00	3.89
QC-M (100,000)	1.80	2.87	4.63
QC-L (50,000)	0.02	2.93	3.91
QC-VL (7500)	−6.65	3.97	8.07

(B)

QC, spiked RBV-P concentration (ng/mL)	Accuracy %	Intra-day R.S.D.%	Inter-day R.S.D.%
QC-H (200,000)	7.50	3.47	8.21
QC-M (100,000)	0.78	4.53	5.99
QC-L (50,000)	7.80	2.79	7.09
QC-VL (7500)	3.46	4.86	6.05

Table 3
Mean concentrations of RBV forms determined in samples from patients (minimum and maximum value concentrations range reported in brackets) after 2 and 4 weeks of standard therapy.

RBV-forms	2 weeks (ng/mL)	4 weeks (ng/mL)
Not-phosphorylated (RBV) blood	6497 (1719–15,466)	8287 (3070–18,990)
Phosphorylated (RBV) blood	118,556 (85,783–189,396)	121,340 (70,693–188,506)
Total (RBV) blood	125,053 (90,226–193,306)	129,627 (75,694–196,686)
Phosphorylated (RBV) intra-RBC	298,792 (198,571–503,713)	330,540 (187,515–512,473)
Total (RBV) intra-RBC	313,244 (217,674–542,506)	349,737 (198,554–557,149)

RBV-P blood concentrations was 129,627 ng/mL and 121,340 ng/mL, respectively. Maximum and minimum values observed were 196,686 and 75,694 ng/mL for total RBV and 188,506 and 70,693 ng/mL for RBV-P, respectively (summarized in Table 3).

The method here reported was used to calculate the intraerythrocytic levels of RBV in the first month of treatment in 13 HCV-positive patients according to the aforementioned formula. The mean RBV intra-RBC concentration was of 349,737 ng/mL, ranging from 198,554 to 557,149 ng/mL (data reported in Table 3). The mean plasma concentration in the same patients was 2007 ng/mL, with an intra-RBC/plasma ratio of 183.

4. Discussion and conclusion

In this work we further simplified the quantification assay of ribavirin in whole-blood samples. The advantage of this method is the elimination of the SPE step required by previously published papers, making our method faster and cheaper. Precisely, our extraction differs from previously methods [4–9] in the use of the protein precipitation instead of PBA columns extraction and in the use of UV detector instead of mass spectrometry detector [12,13].

Moreover, we have introduced for the first time the quality controls for RBV-P, which allowed us to evaluate the goodness of the enzymatic digestion. We have chosen an incubation time of 1 h as earlier experiments have shown that it was enough to achieve the complete dephosphorylation of phosphorylated RBV (data not shown).

As a whole, the validation procedure reported good precision and accuracy <15%, as requested by the FDA guidelines. The LOQ value allows an accurate quantification for all real-life specimens.

As already extensively described in previous papers [4,5] we observed RBV intra-erythrocyte accumulation in patients treated with pegylated interpheron and ribavirin.

The feasibility of our new procedure was tested in measuring concentrations in routine samples withdrawn from patients. Using our method on blood samples from 13 HCV-positive naïve patients we confirmed the data obtained from previous studies. Moreover, we underlined a strong accumulation in RBCs and obtained, at the same time, a cross-confirmation of the usefulness of our method.

In conclusion, we can confirm the eligibility of this HPLC–UV method for the simple, accurate and precise routinely dosage of blood and intra-erythrocytes RBV concentrations, and that this assay is feasible in laboratories without mass spectrometer instrumentations. Moreover, it is also possible to indirectly determine the concentrations of phosphorylated RBV within the erythrocytes. In literature the correlation between these concentrations and hemoglobin reduction during treatment has already underlined [4–6]. However, a cut-off value for red blood cells toxicity has not yet been identified. In addition, it is not still clear if there is a correlation between erythrocyte RBV concentrations and the reaching of sustained virological response (SVR) [5].

The use of a simple assay method, like that described in this paper, could be an important tool to answer these questions and it could, at the same time, allow the investigation of the hypothesis that erythrocyte concentrations could be a new parameter for the early routine evaluation of toxicity in patients treated with ribavirin-containing anti-HCV therapy.

Conflicts of interest

The authors disclose no conflicts.

References

[1] D. Aguilar Marucco, D. Gonzalez de Requena, S. Bonora, C. Tettoni, M. Bonasso, T. De Blasi, A. D'Avolio, M. Sciandra, M. Siccardi, L. Baietto, L. Trentini, A. Sinicco, G. Cariti, G. Di Perri, The use of trough ribavirin concentration to predict sustained virological response and haematological toxicity in HIV/HCV-co-infected patients treated with ribavirin and pegylated interferon, J. Antimicrob. Chemother. 61 (2008) 919–924.
[2] A. D'Avolio, A. Ciancio, M. Siccardi, L. Baietto, M. Simiele, G. Cariti, A. Calcagno, A. Smedile, J. Cusato, S. Bonora, M. Rizzetto, G. Di Perri, Ribavirin pharmacokinetics and IL28B plus CYP27B1 SNPs as predictors of response to Peg-IFN/RBV treatment in HCV 1/4 infected patients, Hepatology 54 (2011) 2278–2279.
[3] M.W. Fried, Side effects of therapy of hepatitis C and their management, Hepatology 36 (2002) S237–S244.
[4] Y. Inoue, M. Homma, Y. Matsuzaki, M. Shibata, T. Matsumura, T. Ito, K. Mitamura, N. Tanaka, Y. Kohda, Liquid chromatography assay for routine monitoring of cellular ribavirin levels in blood, Antimicrob. Agents Chemother. 48 (2004) 3813–3816.
[5] R. Kubota, T. Komiyama, N. Kumagai, M. Kimijima, K. Mitsuki, J. Uetake, F. Kaneko, S. Tsunematsu, K. Tsuchimoto, Optimal erythrocyte ribavirin level to reduce the risk of anemia and obtain an early virological response in patients with chronic hepatitis C caused by genotype 1b infection, Hepat. Res. Treat. 2010 (2010), doi:10.1155/2010/495928, Article ID 495928.
[6] M. Homma, Y. Matsuzaki, Y. Inoue, M. Shibata, K. Mitamura, N. Tanaka, Y. Kohda, Marked elevation of erythrocyte ribavirin levels in interferon and ribavirin-induced anemia, Clin. Gastroenterol. Hepatol. 2 (2004) 337–339.
[7] Y. Hitomi, E.T. Cirulli, J. Fellay, J.G. McHutchison, A.J. Thompson, C.E. Gumbs, K.V. Shianna, T.J. Urban, D.B. Goldstein, Inosine triphosphate protects against ribavirin-induced adenosine triphosphate loss by adenylosuccinate synthase function, Gastroenterology 140 (2011) 1314–1321.
[8] L. De Franceschi, G. Fattovich, F. Turrini, K. Ayi, C. Brugnara, F. Manzato, F. Noventa, A.M. Stanzial, P. Solero, R. Corrocher, Hemolytic anemia induced by ribavirin therapy in patients with chronic hepatitis C virus infection: role of membrane oxidative damage, Hepatology 31 (2000) 997–1004.
[9] M. Homma, A.L. Jayewardene, J. Gambertoglio, F. Aweeka, High-performance liquid chromatographic determination of ribavirin in whole blood to assess disposition in erythrocytes, Antimicrob. Agents Chemother. 43 (1999) 2716–2719.
[10] A. D'Avolio, A. Ibanez, M. Sciandra, M. Siccardi, D.G. de Requena, S. Bonora, G. Di Perri, Validation of liquid/liquid extraction method coupled with HPLC–UV

for measurement of ribavirin plasma levels in HCV-positive patients, J. Chromatogr. B: Analyt. Technol. Biomed. Life Sci. 835 (2006) 127–130.
[11] FDA, Guidance for industry: Bioanalytical method validation, http://fda.gov/cder/guidance/4252fnl.pdf, 2001.
[12] L.T. Yeh, M. Nguyen, C.C. Lin, A sensitive and specific method for the determination of total ribavirin in human red blood cells by liquid chromatography-tandem mass spectrometry, J. Chromatogr. Sci. 41 (2003) 255–260.
[13] L.T. Yeh, M. Nguyen, S. Dadgostari, W. Bu, C.C. Lin, LC–MS/MS method for simultaneous determination of viramidine and ribavirin levels in monkey red blood cells, J. Pharm. Biomed. Anal. 43 (2007) 1057–1064.

Journal of Pharmaceutical and Biomedical Analysis 66 (2012) 381–386

Contents lists available at SciVerse ScienceDirect

Journal of Pharmaceutical and Biomedical Analysis

journal homepage: www.elsevier.com/locate/jpba

Short communication

Structural elucidation of impurities in 5-n-butyl-4-{4-[2-(1H-tetrazole-5-yl)-1H-pyrrol-1-yl]phenylmethyl}-2,4-dihydro-2-(2,6-dichlorophenyl)-3H-1,2,4-triazol-3-one (Ib), a novel nonpeptide angiotensin AT1 receptor antagonist

Ting Gao[a,b], Yaxuan Liu[a,b], Yibing Ji[a,b,*], Xiaoming Wu[c], Jinyi Xu[c]

[a] Key Laboratory of Drug Quality Control and Pharmacovigilance, Ministry of Education, Nanjing 210009, China
[b] Department of Analytical Chemistry, China Pharmaceutical University, Nanjing 210009, China
[c] College of Pharmacy, China Pharmaceutical University, Nanjing 210009, China

ARTICLE INFO

Article history:
Received 2 February 2012
Received in revised form 10 March 2012
Accepted 16 March 2012
Available online 31 March 2012

Keywords:
Ib
Impurity
Mass spectrometry
NMR
Structural elucidation

ABSTRACT

5-n-butyl-4-{4-[2-(1H-tetrazole-5-yl)-1H-pyrrol-1-yl]phenylmethyl}-2,4-dihydro-2-(2,6-dichlorophenyl)-3H-1,2,4-triazol-3-one (Ib), a new nonpeptide angiotensin AT1-receptor antagonist, has been observed to play a positive role in the treatment of hypertension in preclinical tests. Four process impurities of Ib were detected by LC–UV and LC/ESI-MS, and the impurities isolated by preparative HPLC chromatography were characterized by LC–MS/MS, high resolution MS (HRMS), NMR and IR analyses. The structures of impurities were confirmed as 5-n-butyl-4-{4-[2-chloro-5-(1H-tetrazole-5-yl)-1H-pyrrol-1-yl]phenylmethyl}-2,4-dihydro-2-(2,6-dichlorophenyl)-3H-1,2,4-triazol-3-one (I), 5-n-butyl-4-{4-[2-bromo-5-(1H-tetrazole-5-yl)-1H-pyrrol-1-yl]phenylmethyl}-2,4-dihydro-2-(2,6-dichlorophenyl)-3H-1,2,4-triazol-3-one (II), 5-n-butyl-4-{4-[4-chloro-2-(1H-tetrazole-5-yl)-1H-pyrrol-1-yl]phenylmethyl}-2,4-dihydro-2-(2,6-dichlorophenyl)-3H-1,2,4-triazol-3-one (III) and 5-n-butyl-4-{4-[4-bromo-2-(1H-tetrazole-5-yl)-1H-pyrrol-1-yl]phenylmethyl}-2,4-dihydro-2-(2,6-dichlorophenyl)-3H-1,2,4-triazol-3-one (IV), respectively. All of the four impurities were produced as the by-products of the bromination reaction by NBS (N-bromosuccinimide) in the synthesis of Ib.

© 2012 Elsevier B.V. All rights reserved.

1. Introduction

Compound Ib, designated as 5-n-butyl-4-{4-[2-(1H-tetrazole-5-yl)-1H-pyrrol-1-yl]phenylmethyl}-2,4-dihydro-2-(2,6-dichlorophenyl)-3H-1,2,4-triazol-3-one, is a new nonpeptide angiotensin II AT1-receptor antagonist with high potency and low side effects, designed and synthesized in the department of Medicinal Chemistry of China Pharmaceutical University [1]. Several pharmacological studies have shown that Ib was potentially efficient in the treatment of hypertension [2–4], and it also showed a good effect of inhibiting cardiac hypertrophy induced by L-thyroxin in rat [5].

During process development studies of Ib, four impurities were detected by HPLC with the level approaching or exceeding the 0.10% identification threshold [6]. Hence, a comprehensive study was carried out using suitable chromatographic and spectrometric techniques.

2. Experimental

2.1. Materials and reagents

Ib was supplied by the Department of Medicinal Chemistry of China pharmaceutical University. HPLC grade acetonitrile and methanol were purchased from Tedia Company, Inc. (USA) and Jiangsu Hanbang Chemical Co. (Nanjing, China), respectively. Purified water (Robust, Guangdong, China) was used in the preparation of solutions. Other chemicals were of analytical grade.

2.2. HPLC–UV

Chromatographic studies were performed on Agilent 1200 series HPLC instrument (Agilent Technologies, USA) with a UV detector and Shimadzu HPLC system equipped with SPD-M20A diode-array UV detector (Shimadzu Corporation, Kyoto, Japan). Sample solutions were injected onto a Diamonsil C18 column

* Corresponding author at: Department of Analytical Chemistry, China Pharmaceutical University, 24 Tongjia Xiang, Nanjing 210009, China. Tel.: +86 25 83271310; fax: +86 25 83271310.
E-mail addresses: gaoting1736@126.com (T. Gao), jiyibing@jlonline.com, jiyibing1970@163.com (Y. Ji).

0731-7085/$ – see front matter © 2012 Elsevier B.V. All rights reserved.
doi:10.1016/j.jpba.2012.03.031

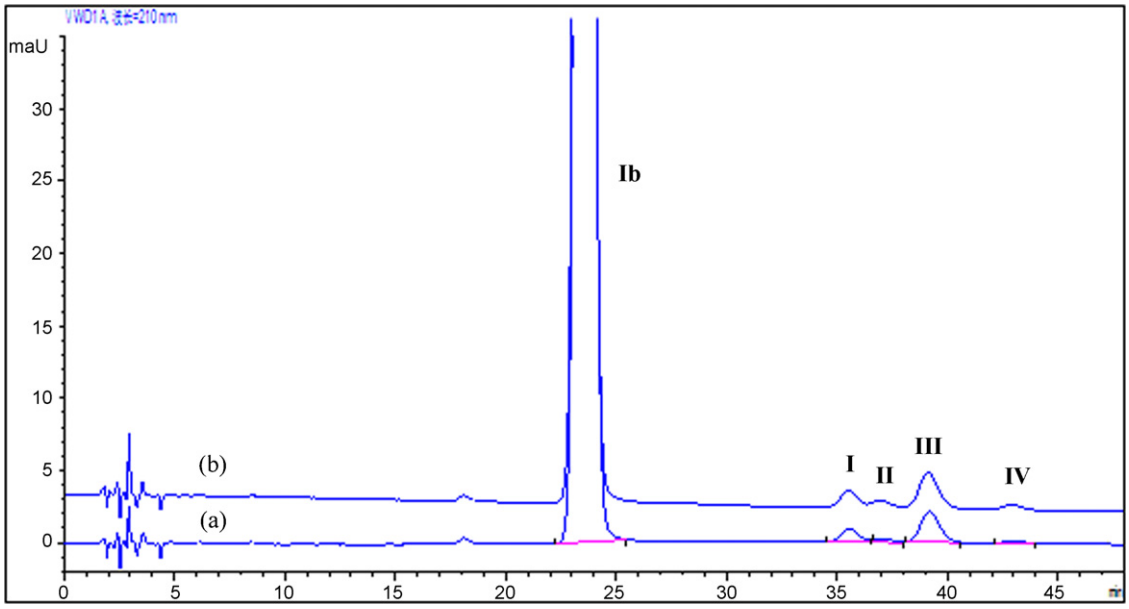

Fig. 1. Typical HPLC chromatogram of Ib (RT 23.5) with four impurities. (a) HPLC chromatogram of samples of Ib API and (b) HPLC chromatogram of Ib spiked at 0.1% (w/w) with the four isolated impurities.

(Dikma) with 25 cm × 4.6 mm i.d. dimension and 5 μm particle size, maintained at 30 °C. The mobile phase consisting of A: 0.1% (v/v) phosphoric acid in water (pH adjusted to 3.5 with triethylamine), and B:acetonitrile in the ratio of 51:49 (v/v) with flow rate of 1 ml/min was used, and UV detector wavelength was fixed at 210 nm. The sample solution (200 μg/ml) was prepared in mobile phase and 20 μl was injected.

2.3. Mass spectrometry

Samples were analyzed by a Thermo Scientific TSQ Quantum MS/MS system equipped with electro-spray ionization interface (Thermo Scientific, San Jose, CA, USA). The HPLC conditions for LC/MS and MS/MS analyses matched those described above except that the mobile phase A was ammonium acetate (5 mM). The spray voltage was set at 4000 V and the temperature of capillary was maintained at 350 °C. The fluid was nebulized by high-purity nitrogen. The sheath gas and auxiliary gas were set at 30 and 10 arbitrary units, respectively. The product ions were generated by collision-induced dissociation of the selected precursor ions using ultra purity argon (Ar) as collision gas (pressure set at 1.5 mTorr).

Q-TOF Micro™ mass spectrometer (Waters, Manchester, UK) was used for accurate mass determination. Leucine enkephalin ($C_{28}H_{37}N_5O_7$) was used as an external lock mass (556.2771 Da).

2.4. Preparative HPLC

The impurities were isolated using Shimadzu preparative HPLC system (Shimadzu Corporation, Kyoto, Japan). Ib was dissolved to 45 mg/ml, and 2 ml injections were made on a 2 cm ID × 25 cm L column. A mixture of 0.05% (v/v) trifluoroacetic acid (TFA) aqueous solution and methanol in the ratio of (34/66, v/v) was used as mobile phase at a flow rate of 20 ml/min and the detector wavelength was set at 210 nm. The collected fractions concentrated by evaporation under high vacuum were freeze dried and the HPLC purity of impurities was above 97.0%.

2.5. NMR

The ^1H, ^{13}C and DEPT measurements were recorded on a Bruker AVANCE 500 NMR spectrometer (Fallanden, Switzerland) instrument at 303K. The ^1H–^1H-COSY, HSQC and HMBC were also performed using the same instrument. The samples were dissolved in $CDCl_3$ and tetramethylsilane (TMS) as internal standard.

2.6. IR spectroscopy

The IR spectra of isolated impurities were recorded in the solid state KBr powder dispersion using a FT-IR spectrometer (FT-IR 8400, Shimadzu, Japan).

3. Results and discussion

3.1. Detection of impurities by HPLC

The HPLC analysis of Ib samples using in-house validated method, revealed the presence of four impurities ranging from 0.05% to 0.90% (by area normalization). The impurities were marked

Table 1
Summary of analytical results of the impurities in Ib.

	RRT	λ_{max} (nm)	Proposed formula $[M+Na]^+$	Measured masses (Da)	Calculated masses (Da)	Error (ppm)	$[M+H]^+$ (m/z)	MS/MS fragment ions (m/z)
Ib	1.00	248	$C_{24}H_{22}N_8OCl_2Na$	531.1197	531.1191	1.1	509	224, 196, 168, 167
Impurity-I	1.51	271	$C_{24}H_{21}N_8OCl_3Na$	565.0808	565.0802	1.1	543	258, 230, 195, 167
Impurity-II	1.58	271	$C_{24}H_{21}N_8OCl_2BrNa$	609.0301	609.0296	0.8	587	286, 274, 195, 167
Impurity-III	1.67	270	$C_{24}H_{21}N_8OCl_3Na$	565.0809	565.0802	1.2	543	286, 258, 230, 195, 167
Impurity-IV	1.83	270	$C_{24}H_{21}N_8OCl_2BrNa$	609.0302	609.0296	1.0	587	302, 274, 195, 167

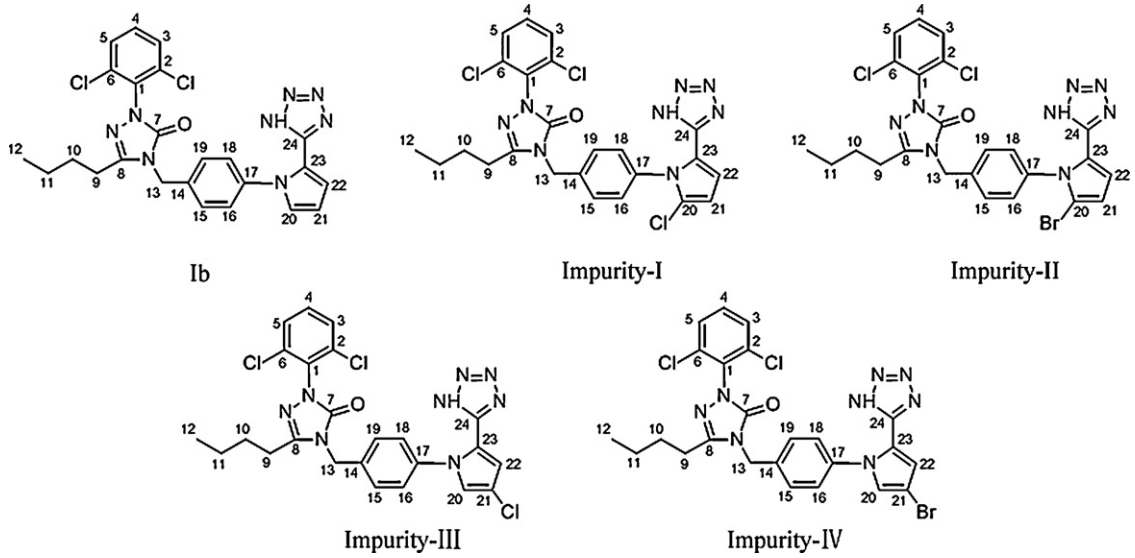

Fig. 2. Chemical structures of Ib and impurities.

as impurity-I (RT 35.6 min), impurity-II (RT 37.1 min), impurity-III (RT 39.2 min) and impurity-IV (RT 43.0 min), respectively. The isolated impurity standards were spiked in Ib sample and to confirm the identity of their retention times (Fig. 1). The chemical structures of Ib and the impurities are shown in Fig. 2.

3.2. Structural elucidation of related impurities by mass spectrometry

Structural elucidation of the impurities was carried out employing LC–UV/PDA, LC/MS, MS/MS and HRMS analyses. The HPLC RRT, UV λ_{max} values, calculated and measured exact masses and MS/MS fragment ions are summarized in Table 1.

The ESI mass spectrum of Ib displayed a molecular ion peak $[M+H]^+$ at *m/z* 509, and the characteristic ^{37}Cl isotopic peak (i.e. ~65% relative abundance) shows the presence of two chlorine atoms in the structure. The MS^2 spectrum of Ib showed four prominent peaks at *m/z* 224, 196, 168 and 167. The formation of these product ions can be rationalized by considering the fragmentation pattern as depicted in Fig. 3a.

Impurity-I and impurity-III both yielded a pseudomolecular ion peak $[M+H]^+$ at *m/z* 543, with a mass difference of 34 Da in comparison to Ib. The even molecular mass (542 Da) implies the existence of even number of nitrogen atoms. The $[M+Na]^+$ accurate masses of impurity-I and impurity-III were 565.0808 Da and 565.0809 Da, respectively, the closest possible molecular formula being $C_{24}H_{21}N_8ONaCl_3^+$ for $[M+Na]^+$. The isotopic patterns of impurity-I at *m/z* 565.0808, 567.0805, 569.0737 and 571.0502 consistent with the Cl_3 isotope distribution clearly indicated the presence of three chlorine atoms in the structure. Also, the impurity-III had the similar isotopic patterns consistent with the Cl_3 isotope ratios.

MS^2 spectra of impurity-I and impurity-III showed the same four product ion peaks at *m/z* 258, 230, 195 and 167. The peak at *m/z* 258 was produced from the loss of the 5-n-butyl-2-(2,6-dichlorophenyl)-3H-1,2,4-triazol-3-one (part A). The most abundant ion at *m/z* 230 can be produced by elimination of a N_2 unit from *m/z* 258. The ion at *m/z* 195 can be due to the loss of chlorine (−35 Da) from *m/z* 230, but the ion at *m/z* 195 of impurity-I was much stronger than in impurity-III indicating that the chlorine atom of impurity-I is more labile than in impurity-III. The fragment ion at *m/z* 195 generated *m/z* 167 by the neutral loss of a N_2 molecule (−28 Da). The probable fragmentation pathway is shown in Fig. 3b. Based on mass spectrometric analysis, impurity-I and impurity-III were suspected to be the chlorinated impurities of Ib, but the location of the chlorine could not be deduced from the MS/MS data. Hence, further analysis by NMR was necessary.

Impurity-II and impurity-IV both yielded a molecular ion peak $[M+H]^+$ at *m/z* 587, 78 Da higher than Ib. The even molecular mass (586 Da) indicates that the compound contains an even number of nitrogen atoms. The $[M+Na]^+$ accurate masses of impurity-II and impurity-IV, measured by HRMS were 609.0301 Da and 609.0302 Da, respectively, and these measured values gave the same best possible elemental composition of $C_{24}H_{21}N_8ONaCl_2Br^+$. The isotopic patterns of impurity-II at *m/z* 609.0301, 611.0254, 613.0447 and 615.0272 with isotope ratios of approximately 62:100:45:6 clearly indicated the presence of one bromine and two chlorine atoms in the structure. Impurity-IV also had the similar isotopic patterns.

MS^2 spectra of impurity-II and impurity-IV showed the same product ion peaks at *m/z* 274, 195 and 167. The peak at *m/z* 274 can be produced by elimination of the part A along with a N_2 group. The ion at *m/z* 195 corresponded to the loss of bromine (−79 Da) from *m/z* 274, but the ion at *m/z* 195 of impurity-II had a higher relative abundance than in impurity-IV indicating that the bromine atom of impurity-II is more labile. The fragment ion at *m/z* 167 can be due to the neutral loss of a N_2 molecule (−28 Da) from *m/z* 195. The proposed fragmentation mechanism is given in Fig. 3b. This indicated that the impurity-II and impurity-IV were the brominated impurities of Ib with no information on the position of the substitution. So, NMR analysis was necessary.

3.3. Structural elucidation of related impurities by NMR

The isolated impurity samples were used for NMR analysis. ^1H, ^{13}C, DEPT, ^1H–^1H-COSY, HSQC and HMBC experiments were employed. The carbon atoms are numbered as in Fig. 2. ^1H NMR spectra of Ib has ten resonances in the aromatic region, consistent with ten aromatic protons on one pyrrole ring and two benzene rings. The characteristic n-butyl and benzyl protons were also observed in the ^1H NMR spectra of Ib. ^{13}C and DEPT NMR data showed signals of one methyl, four methylene, ten methine and eight quaternary carbon atoms. The ^1H and ^{13}C NMR spectral assignments for Ib are presented in Table 2.

Table 2
NMR assignment for Ib and impurities.

Position	Ib			Impurity-I			Impurity-II			Impurity-III			Impurity-IV		
	δ_H (J/Hz)[a]	δ_C	DEPT[b]	δ_H (J/Hz)[a]	δ_C	DEPT[b]	δ_H (J/Hz)[a]	δ_C	DEPT[b]	δ_H (J/Hz)[a]	δ_C	DEPT[b]	δ_H (J/Hz)[a]	δ_C	DEPT[b]
1	–	135.7	Q	–	135.7	Q	–	135.7	Q	–	135.6	Q	–	135.6	Q
2	–	131.8	Q	–	131.8	Q	–	131.8	Q	–	131.6	Q	–	131.6	Q
3	7.43 (1H, d, J = 8)	128.8	CH	7.44 (1H, d, J = 8.5)	128.8	CH	7.43 (1H, d, J = 8)	128.8	CH	7.44 (1H, d, J = 8)	128.8	CH	7.45 (1H, d, J = 8)	128.8	CH
4	7.34 (1H, m)	131.4	CH	7.35 (1H, m)	131.4	CH	7.34 (1H, m)	131.4	CH	7.36 (1H, m)	131.5	CH	7.36 (1H, m)	131.6	CH
5	7.43 (1H, d, J = 8)	128.8	CH	7.44 (1H, d, J = 8.5)	128.8	CH	7.43 (1H, d, J = 8)	128.8	CH	7.44 (1H, d, J = 8)	128.8	CH	7.45 (1H, d, J = 8)	128.8	CH
6	–	131.8	Q	–	131.8	Q	–	131.8	Q	–	131.6	Q	–	131.6	Q
7	–	153.5	Q	–	153.4	Q	–	153.5	Q	–	153.5	Q	–	153.6	Q
8	–	148.9	Q	–	148.9	Q	–	149.0	Q	–	149.0	Q	–	149.0	Q
9	2.53 (2H, t, J = 7.5)	25.7	CH_2	2.55 (2H, t, J = 7.5)	25.7	CH_2	2.54 (2H, t, J = 7.5)	25.8	CH_2	2.54 (2H, t, J = 7.5)	25.7	CH_2	2.54 (2H, t, J = 7.5)	25.7	CH_2
10	1.68 (2H, m)	27.4	CH_2	1.66 (2H, m)	27.5	CH_2	1.65 (2H, m)	27.5	CH_2	1.67 (2H, m)	27.4	CH_2	1.67 (2H, m)	27.5	CH_2
11	1.40 (2H, m)	22.0	CH_2	1.38 (2H, m)	22.0	CH_2	1.37 (2H, m)	21.9	CH_2	1.39 (2H, m)	22.0	CH_2	1.40 (2H, m)	22.0	CH_2
12	0.89 (3H, t, J = 7.2)	13.6	CH_3	0.88 (3H, t, J = 7.5)	13.6	CH_3	0.88 (3H, t, J = 7.5)	13.6	CH_3	0.89 (3H, t, J = 7.5)	13.6	CH_3	0.90 (3H, t, J = 7.5)	13.6	CH_3
13	4.89 (2H, s)	44.3	CH_2	5.01 (1H, s)	44.5	CH_2	5.02 (1H, s)	44.6	CH_2	4.95 (1H, s)	44.4	CH_2	4.95 (2H, s)	44.5	CH_2
14	–	134.9	Q	–	136.0	Q	–	136.6	Q	–	135.5	Q	–	135.6	Q
15	7.13 (1H, d, J = 8)	127.4	CH	7.31 (1H, d, J = 8.5)	127.4	CH	7.31 (1H, d, J = 8)	127.4	CH	7.19 (1H, d, J = 8.5)	127.4	CH	7.19 (1H, d, J = 8)	127.4	CH
16	7.07 (1H, d, J = 7.5)	126.0	CH	7.23 (1H, d, J = 8.5)	129.2	CH	7.20 (1H, d, J = 8.5)	129.4	CH	7.11 (1H, d, J = 8)	126.3	CH	7.11 (1H, d, J = 8)	126.3	CH
17	–	138.8	Q	–	136.7	Q	–	137.3	Q	–	138.3	Q	–	138.2	Q
18	7.07 (1H, d, J = 7.5)	126.0	CH	7.23 (1H, d, J = 8.5)	129.2	CH	7.20 (1H, d, J = 8.5)	129.4	CH	7.11 (1H, d, J = 8)	126.3	CH	7.11 (1H, d, J = 8)	126.3	CH
19	7.13 (1H, d, J = 8)	127.4	CH	7.31 (1H, d, J = 8.5)	127.4	CH	7.31 (1H, d, J = 8)	127.4	CH	7.19 (1H, d, J = 8.5)	127.4	CH	7.19 (1H, d, J = 8)	127.4	CH
20	6.97 (1H, d, J = 3.5)	127.7	CH	–	122.8	Q	–	109.5	Q	6.92 (1H, s)	124.2	CH	6.97 (1H, s)	126.6	CH
21	6.96 (1H, m)	116.3	CH	6.98 (1H, d, J = 4)	114.3	CH	6.97 (1H, d, J = 4)	115.1	CH	–	117.3	Q	–	98.4	Q
22	6.38 (1H, d, J = 3.5)	110.8	CH	6.33 (1H, d, J = 4)	109.0	CH	6.43 (1H, d, J = 4)	113.1	CH	6.85 (1H, s)	115.0	CH	6.92 (1H, s)	117.4	CH
23	–	117.1	Q	–	118.5	Q	–	120.5	Q	–	114.6	Q	–	118.2	Q
24	–	–	–	–	–	–	–	–	–	–	–	–	–	–	–
NH	–	–	–	–	–	–	–	–	–	–	–	–	–	–	–

Refer the structural formula for numbering (Fig. 2). s: singlet; d: doublet; t: triplet; m: multiplet; Q: quaternary atom.

[a] ^1H–^1H coupling constants.

[b] Hybridization (degree of bonding) of carbon atoms.

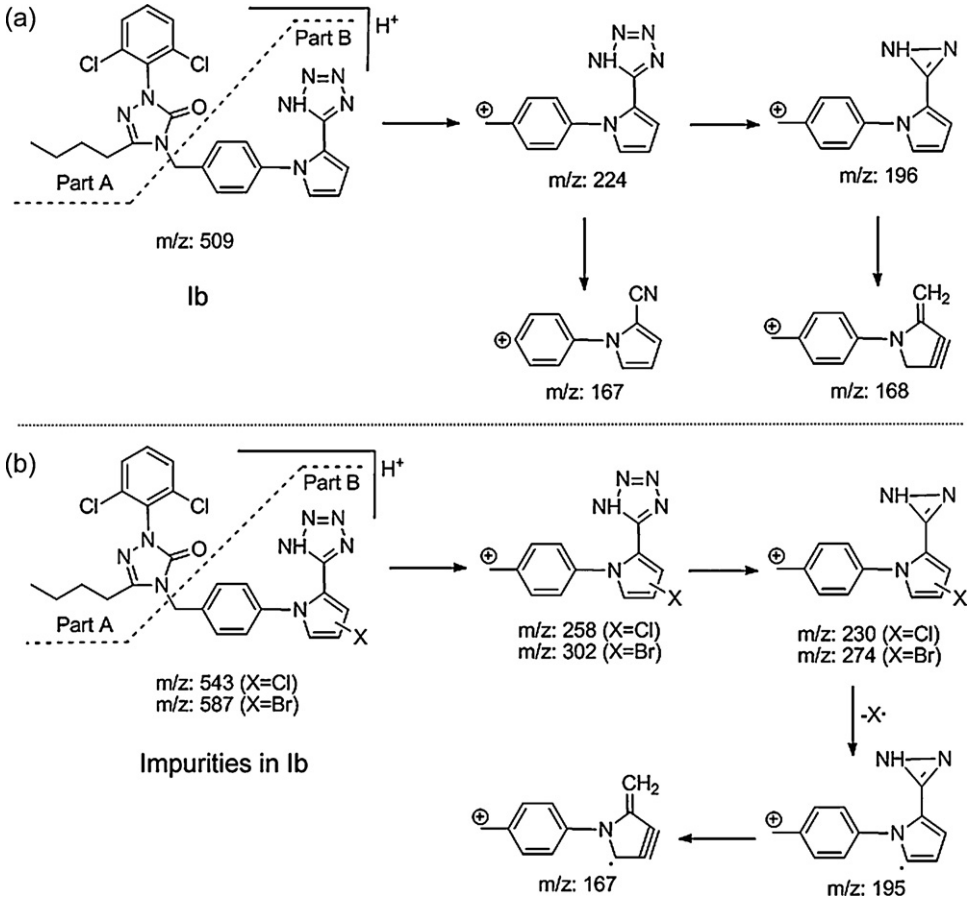

Fig. 3. Fragmentation pattern of (a) Ib and (b) impurities in Ib.

In comparison with Ib, the ^{1}H NMR spectrum of impurity-I showed the same number of aliphatic and benzene protons with similar splitting patterns. However, the number of protons and the splitting patterns were found to be different on the pyrrole ring. Two doublets at δ 6.98 ppm (J = 4) and δ 6.33 ppm (J = 4), both integrating for 1H were observed in the spectrum of impurity-I, and the DEPT spectra displayed positive signals for nine methine groups (Table 2). Furthermore, the two doublets both had the obvious correlations with C-20 and C-23 in the HMBC spectra of impurity-I, and a cross peak between H-20 and C-17 exhibited in HMBC experiment of Ib was absent in the impurity-I. Therefore, the substitution of chlorine atom was on the C-20 of the pyrrole ring, and the structure of impurity-I was confirmed as 5-n-butyl-4-{4-[2-chloro-5-(1H-tetrazole-5-yl)-1H-pyrrol-1-yl]phenylmethyl}-2,4-dihydro-2-(2,6-dichlorophenyl)-3H-1,2,4-triazol-3-one (Fig. 2).

The NMR spectra of impurity-II were similar with those of impurity-I, except that the signal at 109.5 ppm for impurity-II observed in ^{13}C corresponding to C-20 can be attributed to the effect of the attached heavy atom (Br) on the nuclear shielding constant. So, the location of the bromine atom in impurity-II was also on the C-20 of the pyrrole ring, and the structure of impurity-II was confirmed as 5-n-butyl-4-{4-[2-bromo-5-(1H-tetrazole-5-yl)-1H-pyrrol-1-yl]phenylmethyl}-2,4-dihydro-2-(2,6-dichlorophenyl)-3H-1,2,4-triazol-3-one (Fig. 2).

It was found that the signals of aliphatic protons and benzene protons in ^{1}H NMR spectra were identical with those in impurity-III and Ib. However, significant differences in their ^{1}H NMR spectra were found in the pyrrole moiety. Two singlets at δ 6.92 ppm and δ 6.85 ppm, both integrating for 1H were observed in the ^{1}H NMR spectra of impurity-III. Moreover, the signal at 117.3 ppm for impurity-III observed in ^{13}C corresponding to carbon number C-21 and its absence in DEPT confirmed the substitution of chlorine atom at position C-21 of the pyrrole ring (Table 2). The assignment was further proved by HSQC and HMBC spectra. From these spectral information, the structure of impurity-III was confirmed as 5-n-butyl-4-{4-[4-chloro-2-(1H-tetrazole-5-yl)-1H-pyrrol-1-yl]phenylmethyl}-2,4-dihydro-2-(2,6-dichlorophenyl)-3H-1,2,4-triazol-3-one (Fig. 2).

^{1}H NMR and ^{13}C NMR spectral data of impurity-IV showed chemical shift similarity with impurity-III except of the upfield shift of C-21 (98.4 ppm) observed in ^{13}C due to the heavy atom effect of bromine. Besides, the signal at 98.4 ppm was absent in DEPT, confirming the bromine atom located on the C-21 of the pyrrole ring. The HSQC and HMBC spectra further supported the assignment. The ^{1}H and ^{13}C NMR spectral assignments for impurity-IV are shown in Table 2. Thus, the structure of impurity-IV was confirmed as 5-n-butyl-4-{4-[4-bromo-2-(1H-tetrazole-5-yl)-1H-pyrrol-1-yl]phenylmethyl}-2,4-dihydro-2-(2,6-dichlorophenyl)-3H-1,2,4-triazol-3-one (Fig. 2).

In the IR spectra, Ib and four impurities showed similar absorption bands of $\nu_{C=O}$ 1695 cm^{-1}, $\nu_{N-H\ (stretch)}$ 3140 cm^{-1}, $\nu_{N-H\ (bending)}$ 1610 cm^{-1}, $\nu_{C-N\ (stretch)}$ 1201 cm^{-1}, aromatic ring (ν_{Ar-H} 3023 cm^{-1}, 3063 cm^{-1} and $\nu_{C=C}$ 1400 cm^{-1}, 1450 cm^{-1}, 1458 cm^{-1}, 1487 cm^{-1}) and alkane (ν_{C-H} 2862 cm^{-1}, 2928 cm^{-1}, 2961 cm^{-1}). The IR spectra further supported the structure of impurities.

3.4. Formation of the impurities

According to the structures of impurities and the synthetic procedure of Ib, the four impurities were all produced as by-products in the NBS bromination reaction. The bromination step of the intermediate 1-(4-methyl)phenyl-1H-pyrrole-2-carbonitrile with N-bromosuccinimide (NBS) in CCl_4 using azobisisobutyronitrile (AIBN) as initiator to form an α-bromo derivative was employed in the synthesis of Ib, accompanied by the formation of chlorinated and dibrominated by-products. Hence, the quality of the intermediates and the conditions of NBS bromination reaction must be strictly controlled in the synthesis of Ib.

Acknowledgements

The financial supports of the Program for New Century Excellent Talents in University (No. NCET-08-0847) and the technological specialized project for "significant new formulation of new drugs" of China (Grant No. 2009ZX09102) are gratefully acknowledged.

References

[1] J.Y. Xu, Y.X. Zhou, X.M. Wu, K. Tang, Q.J. Wang, Synthesis and bioactivity of 1-aryl-3-alkyl-1,4-dihydro-4-substitued-5H-1,2,4,-triazolinones-5, J. China Pharm. Univ. 30 (1999) 323–327.
[2] Y. Wang, W. Wang, Q.J. Wang, J.H. Wu, J.Y. Xu, X.M. Wu, [Ca2+]i and PKC-α are involved in the inhibitory effects of Ib, a novel nonpeptide angiotensin II subtype AT1 receptor antagonist, on angiotensin II-induced vascular contraction in vitro, Biochem. Biophys. Res. Commun. 364 (2007) 118–123.
[3] J.H. Wu, Q.J. Wang, J.Y. Guo, Z.Y. Hu, Z.Y. Yin, J.Y. Xu, X.M. Wu, Characterization of angiotensin II antagonism displayed by Ib, a novel nonpeptide angiotensin AT1 receptor antagonist, Eur. J. Pharmacol. 589 (2008) 220–224.
[4] J.H. Wu, Q.J. Wang, S. Hu, J.Y. Xu, X.M. Wu, Antihypertensive effects of a new angiotensin type 1 receptor antagonist 1b on rats, J. China Pharm. Univ. 36 (2005) 563–566.
[5] J. Zhang, Q.J. Wang, J.Y. Xu, X.M. Wu, Effects of a new angiotensin type 1 receptor antagonist 1b on the cardiac hypertrophy induced by L-thyroxin in rat, J. China Pharm. Univ. 37 (2006) 157–160.
[6] International Conference on Harmonisation of technical requirements for registration of pharmaceuticals for human use, ICH Q3A(R), in: Impurities in New Drug Substances, 2003, pp. 1–13.

Journal of Pharmaceutical and Biomedical Analysis 66 (2012) 387–391

Contents lists available at SciVerse ScienceDirect

Journal of Pharmaceutical and Biomedical Analysis

journal homepage: www.elsevier.com/locate/jpba

Short communication

A novel ion-pair RP-HPLC method for determination of five components in compound α-ketoacid tablets

Di Zhang, Peng Zhang, Qikun Jiang, Ying Kong, Meng Zhu, Tianhong Zhang*

School of Pharmacy, Shenyang Pharmaceutical University, 103 Wenhua Road, Shenyang 110016, China

ARTICLE INFO

Article history:
Received 3 January 2012
Received in revised form 18 March 2012
Accepted 19 March 2012
Available online 28 March 2012

Keywords:
Compound α-ketoacid tablets
Simultaneous determination
Ion-pair
RP-HPLC

ABSTRACT

A sensitive and reliable ion-pair reversed-phase high-performance liquid chromatographic (RP-HPLC) method has been developed and validated for the simultaneous determination of D,L-α-hydroxymethionine calcium (HMACa), D,L-α-ketoisoleucine calcium (KILCa), α-ketovaline calcium (KVCa), α-ketoleucine calcium (KLCa) and α-ketophenylalanine calcium (KPACa) in the compound α-ketoacid tablets using tetrabutylammonium hydroxide as an ion-pair reagent. The analytes were separated on a C_{18} column (250 mm × 4.6 mm, 5 μm) with the mobile phase of methanol–potassium dihydrogen phosphate buffer (pH 3.0; 50 mM) (37:63, v/v) at a flow rate of 0.6 mL min^{-1}. The UV detection wavelength was set at 210 nm. Good linearity with correlation coefficients larger than 0.9990 (n = 6) for all analytes were achieved. The average recoveries were within the range of 99.6–100.9%, and the RSDs of the results were within the acceptable limit of 2.0%, which showed that this method was accurate and precise. The limits of detection were 10.44, 5.94, 3.44, 3.60 and 1.63 ng mL^{-1}, and the limits of quantification were 34.80, 19.80, 10.32, 12.00 and 5.44 ng mL^{-1} for HMACa, KILCa, KVCa, KLCa and KPACa, respectively. The method is simple and accurate for quality control of the compound α-ketoacid tablets.
© 2012 Elsevier B.V. All rights reserved.

1. Introduction

Compound α-ketoacid tablets are enteral medicinal products which can not only improve the nutritional status but also prevent and treat chronic renal insufficiency when used in connection with a low protein diet [1–3]. Compound α-ketoacid tablets have shown positive influences on the progression of uraemic symptoms, which were reported to prevent degradation of the body's own protein and reduce proteinuria [4]. Besides, it could significantly modify immune functions in patients with chronic renal failure [5]. Apart from the fact that calcium supplementation can improve renal osteodystrophy, it also has a positive clinical effect on secondary hyperthyroidism [6,7].

Compound α-ketoacid tablets (Fresenius, Germany) contain five keto- or hydroxy-amino acids in the form of calcium salts, including D,L-α-hydroxymethionine calcium (HMACa), D,L-α-ketoisoleucine calcium (KILCa), α-ketovaline calcium (KVCa), α-ketoleucine calcium (KLCa) and α-ketophenylalanine calcium (KPACa). It is challengeable to carry out the quality control analysis of compound α-ketoacid tablets due to its complicated compositions. To date, only one method was reported for the simultaneous determination of HMACa, KILCa, KVCa, KLCa and KPACa using ion exclusion chromatography (IEC) [8], IEC has been one convenient way to determine weakly acidic or basic compounds based on a Donnan exclusion mechanism [9–11], in this mode of chromatography, negatively charged ions were separated on cation-exchange columns, positively charged ions were separated on anion-exchange columns containing cationic quaternary ammonium functional groups [12], however, its sensitivity and repeatability were shown to be comparatively poor. The chromatographic system was equipped with a hydrogenous cation exchange column which was difficult to preserve, and the run time of the method was relatively long.

The aim of the present study was to develop and validate a simple, rapid, sensitive and reliable ion-pair RP-HPLC method for the simultaneous determination of five calcium salts in the compound α-ketoacid tablets, which has been successfully applied to the determination of all analytes in commercial brands of their combined tablet formulation.

2. Experimental

2.1. Chemicals and reagents

D,L-α-Hydroxymethionine calcium (HMACa), D,L-α-ketoisoleucine calcium (KILCa), α-ketovaline calcium (KVCa), α-ketoleucine calcium (KLCa) and α-ketophenylalanine calcium (KPACa) were provided by laboratory of Shenyang Pharmaceutical

* Corresponding author. Tel.: +86 24 23984159; fax: +86 24 23986320.
E-mail address: zhangdi048349@126.com (T. Zhang).

0731-7085/$ – see front matter © 2012 Elsevier B.V. All rights reserved.
doi:10.1016/j.jpba.2012.03.038

Table 1
The quantitative composition of the tablets.

Compound			
Keto and hydroxy analogues		*Amino acids*	
D,L-α-Hydroxymethionine calcium	59 mg	L-Lysine monoatsetat	105 mg
D,L-α-Ketoisoleucine calcium	67 mg	L-Threonine	53 mg
α-Ketovaline calcium	86 mg	L-Triptaphan	23 mg
α-Ketoleucine calcium	101 mg	L-Histidine	38 mg
α-Ketophenylalanine calcium	68 mg	L-Tyrosine	30 mg
Excipients		*Skin pill*	
Corn starch	44 mg	Talc	9.1 mg
Polivinilpirrolidon	6 mg	Polyethylene 6000	1.48 mg
Magnesium stearate	15 mg	Hinolinovy yellow E104	0.72 mg
Talc	19.57 mg	Eudragit E12.5	5.9 mg
Colloidal silicon dioxide	4.4 mg	Triatsetin	0.43 mg
Polyethylene 6000	12.8 mg	Titanium dioxide	7.4 mg
Polivinilpirrolidon soluble	43.2 mg		

University with their corresponding purities of 99.96%, 99.94%, 99.91%, 99.94%, and 99.76% determined by area normalization method, respectively, and the structures were validated by comparing the chemical and spectroscopic (UV, NMR and MS) data. Compound α-ketoacid tablets were purchased from Beijing Fresenius KaBi Medicine Co., Ltd (Beijing, China). Analytical reagent grade of hydrochloric acid, potassium dihydrogen phosphate, triethylamine (TEA), and tetrabutylammonium hydroxide were purchased from Shenyang Economic and Technological Development Zone reagent factory (Shenyang, China), Xilong Huagong Co., Ltd (Guangdong, China), Bodi Huagong Co., Ltd (Tianjin, China) and Yongda chemical reagent Co., Ltd (Tianjin, China), respectively. Purified water was purchased from Wahaha Group Co., Ltd (Hangzhou, China). HPLC grade of methanol was obtained from Concord Technology Co., Ltd (Tianjin, China).

2.2. Instrumentation and chromatographic conditions

The separations were performed with a HPLC system consisting of L-2130 binary pump, L-2400 UV detector set at 210 nm, L-2300 column oven maintained at 30 °C and L-2200 autosampler (Hitachi, Japan). The data acquisition was achieved with L-2000 Elite workstation software. Compounds were separated on a C_{18} column (250 mm × 4.6 mm, particle size 5 μm, Beijing Tai-Ke-mei Scientific Co., Ltd., Beijing, China). The mobile phase was methanol-potassium dihydrogen phosphate buffer (50 mM, containing 0.3% TEA, containing 0.16% tetrabutylammonium hydroxide, pH 3.0 adjusted with hydrochloric acid) (37:63, v/v), pumped at a flow rate of 0.6 mL min^{-1}.

2.3. Preparation of standard solutions

Stock solutions of HMACa, KILCa, KVCa, KLCa and KPACa were prepared by dissolving accurately weighed reference substances in water to get final concentrations of 0.58, 0.66, 0.86, 1.00 and 0.68 mg mL^{-1}, respectively.

Working solutions were prepared by diluting 0.6 mL of each stock solution in a 5 mL volumetric flask with water to get final concentrations of 69.6 mg L^{-1} HMACa, 79.2 mg L^{-1} KILCa, 103.2 mg L^{-1} KVCa, 120.0 mg L^{-1} KLCa and 81.6 mg L^{-1} KPACa.

2.4. Sample preparation

Ten tablets were accurately weighed and their average weight was calculated. The quantitative compositions of the tablets are listed in Table 1. The tablets were finely powdered, and the powder consisted of 18.0 mg HMACa, 20.0 mg KILCa, 26.0 mg KVCa, 30.0 mg KLCa and 20.0 mg KPACa was weighed into a 25 mL volumetric flask and 18.0 mL water was added, the volumetric flask was sonicated for 20 min to dissolve and then made up to volume with water, the solution was filtered through a 0.45 μm millipore filter. The filtrate was further diluted by diluting 1.0–10.0 mL with water.

3. Results and discussions

3.1. Optimization of chromatographic conditions

The structures of HMACa, KILCa, KVCa, KLCa and KPACa are illustrated in Fig. 1.

In order to achieve simultaneous determination of the five components with perfect separation and short analysis time, different chromatographic conditions were attempted. The high polarity of all analytes suggested that they could be separated on C_{18} column with high ratio of aqueous phase. Methanol and acetonitrile were attempted as organic phase, but the peak shape of KVCa and KPACa were wide, unsymmetrical and tailed after addition of acetonitrile, hence methanol was selected as organic phase. In order to achieve better peak shape, detection sensitivity and higher response, specified amount of potassium dihydrogen phosphate was added and tetrabutylammonium hydroxide was selected as ion-pair reagent. To minimize the peak tailing, TEA (0.3%) was added as an organic modifier. Aqueous phase of different pH values were attempted, and finally pH 3.0 was chosen with the best separation condition. Therefore, the mobile phase composition was selected as methanol–potassium dihydrogen phosphate buffer (50 mM, containing 0.3% TEA, containing 0.16% tetrabutylammonium hydroxide, pH 3.0 adjusted with hydrochloric acid) (37:63, v/v). Under these optimized conditions, the analyte peaks were well resolved and free from tailing. The resolution were >2 for all the peaks. The elution order was KVCa (t_R = 6.8 min), HMACa (t_R = 8.6 min), KILCa (t_R = 9.9 min), KLCa (t_R = 10.7 min) and KPACa (t_R = 12.5 min), at flow rate of 0.6 mL min^{-1}. The equilibration times were about 30 min.

The five components showed maximum response at 205 nm. In order to avoid interference of methanol, the chromatogram was recorded at 210 nm, the analytes also respond well at the selected wavelength.

3.2. Method validation

The analytical method was validated with respect to parameters such as specificity, linearity, limit of detection (LOD), limit of quantification (LOQ), precision, accuracy, stability and robustness.

3.2.1. Specificity

Chromatograms representing sample solution, working solution and negative control solution are presented in Fig. 2. Fig. 2(a) shows a sample chromatogram without any interference peaks

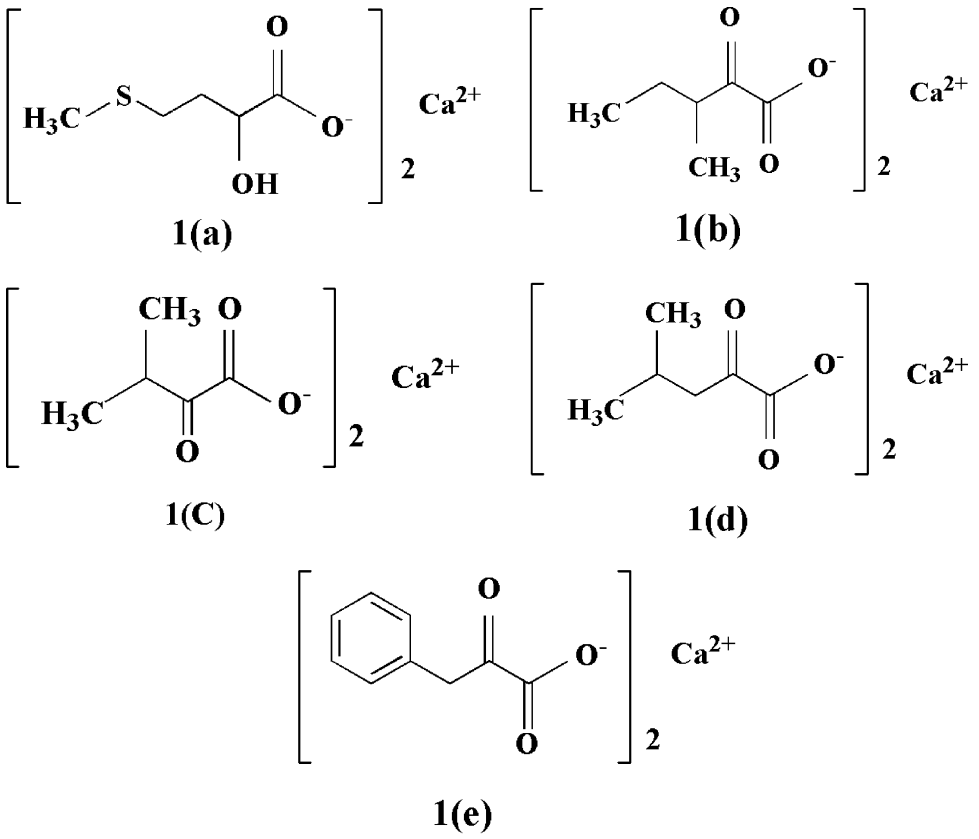

Fig. 1. Structures of HMACa: 1(a); KILCa: 1(b); KVCa: 1(c); KLCa: 1(d); KPACa: 1(e).

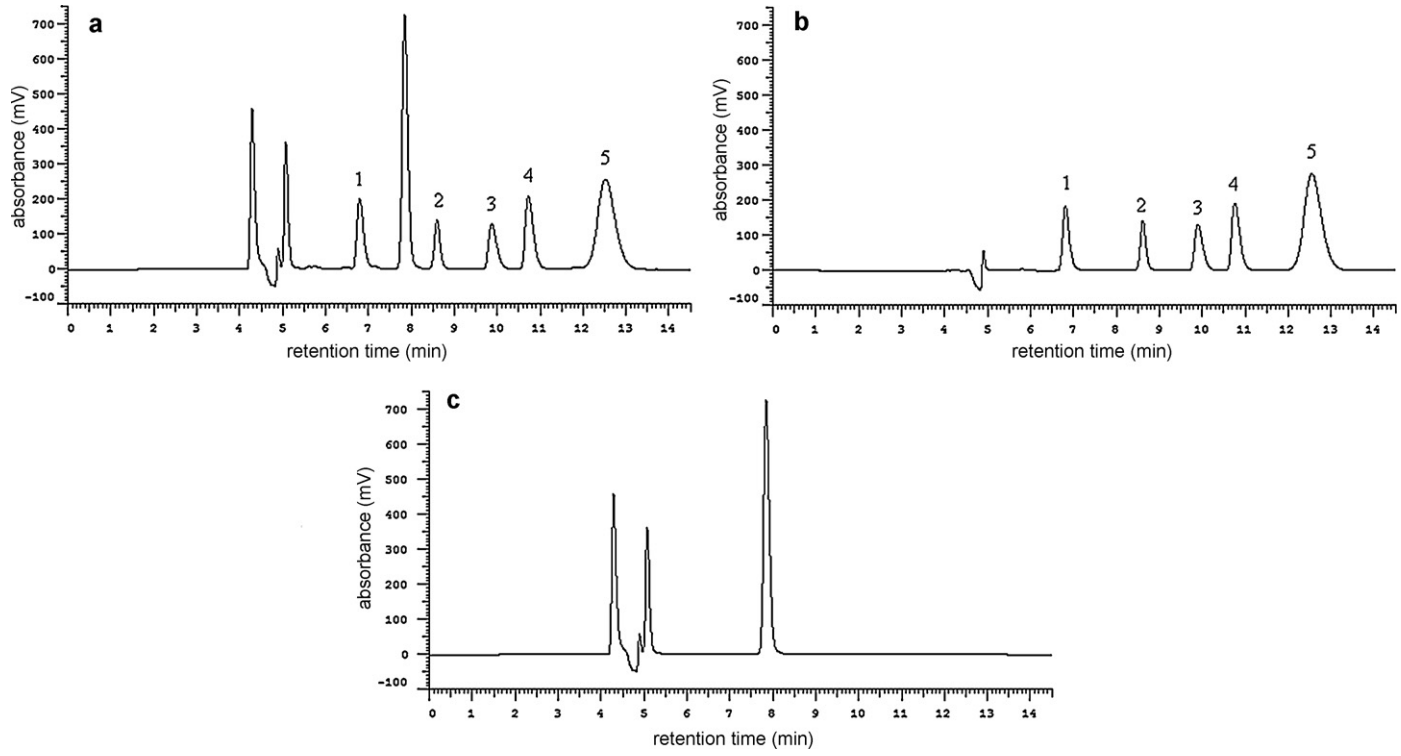

Fig. 2. Representative chromatograms: (a) sample solution; (b) working solution; (c) negative control solution. Peaks: 1, KVCa; 2, HMACa; 3, KILCa; 4, KLCa; 5, KPACa.

Table 2
Regression equation, SD, r, linear range, S_{yx}, LOD and LOQ of the method.

Compound	Regression equation	SD (intercept)	r	Range ($\mu g\,mL^{-1}$)	S_{yx}	LOD ($ng\,mL^{-1}$)	LOQ ($ng\,mL^{-1}$)
HMACa	$y = 2 \times 10^7 x + 1.7 \times 10^4$	11,203	0.9993	11.6–116	32,705	10.44	34.80
KILCa	$y = 2 \times 10^7 x + 7.0 \times 10^3$	5618	0.9998	13.2–132	20,480	5.94	19.80
KVCa	$y = 2 \times 10^7 x + 4.8 \times 10^4$	4889	0.9998	17.2–172	27,041	3.44	10.32
KLCa	$y = 2 \times 10^7 x - 1.4 \times 10^4$	5988	0.9999	20.0–200	24,329	3.60	12.00
KPACa	$y = 1 \times 10^8 x + 6.8 \times 10^4$	47,284	0.9999	13.6–136	70,373	1.63	5.44

Table 3
Results of the intermediate precision study.

	Compound									
	HMACa		KILCa		KVCa		KLCa		KPACa	
	Content[a] (%)	RSD (%) $n = 6$	Content[a] (%)	RSD (%) $n = 6$	Conten[a] (%)	RSD (%) $n = 6$	Content[a] (%)	RSD (%) $n = 6$	Content[a] (%)	RSD (%) $n = 6$
Day 1	99.2	1.06	100.6	1.25	101.3	0.69	101.9	1.19	100.9	1.15
Day 2	99.7	0.59	100.6	1.04	101.2	0.50	102.4	0.46	101.0	0.96
Day 3	99.1	0.44	100.2	1.39	101.5	0.31	102.0	1.33	100.6	0.59
Mean	99.3		100.5		101.3		102.1		100.8	
RSD (%) $n = 18$	0.76		1.17		0.53		1.03		0.89	
Day 4	99.1	0.83	100.4	0.98	100.9	0.38	102.3	0.50	100.9	0.15
Day (3–4)	99.1		100.3		101.2		102.2		100.8	
RSD (%) $n = 12$	0.63		1.15		0.45		0.97		0.44	

[a] Each content is the average of six measurements.

at 210 nm. Chromatogram of the standards is shown in Fig. 2(b). The negative control solution was injected, the separation was not interfered by the peaks found as could be seen in Fig. 2(c). The chromatographic run time of 13.5 min was sufficient for sample analysis that allows analyzing large number of samples in a short period of time.

3.2.2. Linearity

Linearity of the proposed method was evaluated, by the analysis of working solutions of HMACa, KILCa, KVCa, KLCa and KPACa at six different concentrations which were injected in triplicate. The linear ranges were 11.6–116 $\mu g\,mL^{-1}$ for HMACa, 13.2–132 $\mu g\,mL^{-1}$ for KILCa, 17.2–172 $\mu g\,mL^{-1}$ for KVCa, 20.0–200 $\mu g\,mL^{-1}$ for KLCa and 13.6–136 $\mu g\,mL^{-1}$ for KPACa. The linearity results are listed in Table 2. The results showed excellent correlations within the tested concentrations ranges.

3.2.3. Limit of detection (LOD) and limit of quantification (LOQ)

The lowest concentration of working solution was diluted with water to a series of appropriate concentrations, and aliquots of diluted solutions were injected into HPLC for analysis. The LOD and LOQ for each analyte under the chromatographic conditions were determined at the signal to noise ratio (S/N) of 3 and 10, respectively. The results of LOD and LOQ are listed in Table 2.

3.2.4. Precision

Repeatability was studied by the determination of six sample solutions. The samples were given the same treatment as described in Section 2.4. The RSDs of the results were 0.99% (HMACa), 0.72% (KILCa), 0.51% (KVCa), 0.54% (KLCa) and 0.75% (KPACa), respectively.

The precision was examined on the mixed standards for six times within 1 day. The relative standard deviations (RSDs) were 1.04%, 0.37%, 1.15%, 1.11% and 0.89% for HMACa, KILCa, KVCa, KLCa and KPACa, which were well within the acceptable limit of 2.0%.

Intermediate precision of the method was evaluated by assaying the sample solutions on four consecutive days by five analysts using the same experimental conditions. On the fourth day, analysis was made on a different instrument and those results were compared with day 3. On each day, two freshly prepared sample solutions were injected in triplicate. The results are shown in Table 3. The RSDs were less than 2.0% suggesting that the results were precise for the study.

3.2.5. Accuracy

A recovery test was used to evaluate the accuracy of the developed method. The amount equal to half of the quantity described in Section 2.4 was weighed; recovery test was carried out by adding known amount of each standard corresponding to three concentration levels 80%, 100% and 120% of the drugs in the sample described above in triplicate. The samples were given the same treatment as described in Section 2.4. The recoveries were calculated as follow formula: Recovery (%) = $100 \times (amount\ found - original\ amount)/amount\ added$. The results indicated that the method is highly accurate (Table 4).

3.2.6. Stability studies

The stability was evaluated using a freshly prepared sample solution. The five components did not show evidence of significant degradation for at least 10 h when kept at room temperature. The relative error (RE) was taken as a measure of stability, which are well within the acceptable limit of 2.0%. The stability allowed a large batch of samples to be processed in one assay run.

3.2.7. Robustness

Robustness of the method was determined by analyzing the same sample under various conditions of pH, flow rate, percentage of methanol in the mobile phase and column oven temperature. The reproducibility of the results and the resolutions has proven that the method is robust.

3.3. Pharmaceutical formulation analysis

Three batches of compound α-ketoacid tablets were analyzed using the described method. Quantification was carried out in triplicates, and the obtained results are listed in Table 5, which indicated that the amounts of each component in the tablets of all brands were within the requirements of 90.0–110.0% of the corresponding label claims.

Table 4
Accuracy of the method.

Theoretical (% of target level)	Original amount[a] (mg)	Amount added[a] (mg)	Amount found[a] (mg)	Recovery[a] (%)	Mean recovery[b] (%)	RSD (%) $n = 9$
HMACa					100.5	0.88
80	8.75	7.21	16.05	101.2		
100	8.75	9.01	17.82	100.7		
120	8.75	10.81	19.53	99.7		
KILCa					100.9	0.59
80	9.94	8.08	18.14	101.5		
100	9.94	10.27	20.23	100.2		
120	9.94	12.04	22.10	101.0		
KVCa					100.1	1.15
80	12.75	10.43	23.07	98.9		
100	12.75	13.01	25.79	100.2		
120	12.75	15.62	28.58	101.3		
KLCa					100.5	0.89
80	14.98	12.03	26.98	99.8		
100	14.98	15.03	30.10	100.6		
120	14.98	18.05	33.21	101.0		
KPACa					99.5	0.79
80	10.09	8.06	18.05	98.8		
100	10.09	10.03	20.17	100.5		
120	10.08	12.00	22.00	99.3		

[a] Mean value of three determinations.
[b] Mean value of nine determinations.

Table 5
Sample quantification results.

Batch	81DL454	81DK402	81DB047
Compound			
HMACa			
Labeled values[a]	17.50	17.51	17.51
Found values[a]	18.01	17.05	17.59
Content[a] (%)	102.9	97.4	100.5
RSD(%) $n = 3$	1.27	1.37	0.60
KILCa			
Labeled values[a]	19.88	19.88	19.88
Found values[a]	20.11	19.13	19.88
Content[a] (%)	101.2	96.2	100.0
RSD(%) $n = 3$	0.35	0.43	1.64
KVCa			
Labeled values[a]	25.51	25.52	25.52
Found values[a]	26.55	24.81	25.87
Content[a] (%)	104.1	97.2	101.4
RSD(%) $n = 3$	0.82	0.24	0.79
KLCa			
Labeled values[a]	29.96	29.97	29.97
Found values[a]	31.78	29.53	31.05
Content[a] (%)	106.1	98.5	103.6
RSD(%) $n = 3$	0.73	0.71	1.17
KPACa			
Labeled values[a]	20.17	20.18	20.18
Found values[a]	20.53	19.76	20.14
Content[a] (%)	101.8	97.9	99.8
RSD(%) $n = 3$	0.54	1.09	0.58

[a] Each content is the average of three measurements.

4. Conclusion

An ion-pair RP-HPLC method for simultaneous determination of HMACa, KILCa, KVCa, KLCa and KPACa were developed and validated in this study. The method has the advantage of simplicity, convenience, accuracy and precision compared to the previous report. The specificity, linearity, precision, accuracy, sample stability and robustness were all well within the acceptable limits. In conclusion, the developed method could be used for the assay of the five components in the compound α-ketoacid tablets.

Acknowledgements

The authors express sincere thanks to Prof. Youjun Xu (Shenyang Pharmaceutical University) and his students for their cooperation and assistance.

References

[1] J.H. Chang, D.K. Kim, J.T. Park, E.W. Kang, T.H. Yoo, B.S. Kim, K.H. Choi, H.Y. Lee, D. Han, S.K. Shin, Influence of ketoanalogs supplementation on the progression in chronic kidney disease patients who had training on low-protein diet, Nephrology 14 (2009) 750–757.
[2] Q.H. Jin, Effect of ketosteril and low protein diet on nutritional status and renal function in patients with chronic kidney disease, Chin. J. Prev. Contr. Chron. Non-commun. Dis. 1 (2008) 47–48.
[3] N.L. Lifshin, A. Nikolaev, V.M. Ermolenko, A trial of the long-term use of a low-protein diet and ketosteril in chronic kidney failure, Ter. Arkh. 66 (1994) 51–55.
[4] M. Jaworska, Z. Szulinska, M. Wilk, Development of a capillary electrophoretic method for the analysis of amino acids containing tablets, J. Chromatogr. A 993 (2003) 165–172.
[5] Y.X. Gao, L. Cui, Y. Xu, L.Q. Liu, H. Dong, L.M. Zhou, The effects of ketosteril on immune functions in patients with chronic renal failure, Inner Mongolia Med. J. 10 (2006) 890–892.
[6] M. Sun, W.J. Lu, W.W. Sheng, Y.M. Wu, Z.W. Yan, Effect of low-protein diet plus α-ketonic acid on parathyroid hormone in chronic renal failure, J. Chin. Mod. Med. 6 (2005) 527–528.
[7] F.L. Zheng, Z.Q. Bi, X.W. Li, Effects of alpha-ketoacids therapy on protein metabolism and secondary hyperparathyroidism in predialysis patients, Chin. J. Internal Med. 32 (1993) 396–399.
[8] J. Chen, Determination of compound α-keto acid tablets by ion exclusion chromatography, Chin. Pharm. 10 (2010) 1481–1483.
[9] M. Mori, H. Itabashi, M. Ikedo, K. Tanaka, Ion-exclusion chromatography with the direct UV detection of non-absorbing inorganic cations using an anion-exchange conversion column in the iodide-form, Talanta 70 (2006) 174–177.
[10] L. Yang, L. Liu, B.A. Olsen, M.A. Nussbaum, The determination of oxalic acid, oxamic acid, and oxamide in a drug substance by ion-exclusion chromatography, J. Pharm. Biomed. Anal. 22 (2000) 487–493.
[11] J.C. Dias, E. Suzuki, C.L. Albuquerque, A.L. Ferreira, A.R.M.S. Brito, L.T. Kubota, Determination of short-chain fatty acids in dietary fiber extracts using ion-exclusion chromatography with suppressed conductivity detection, J. Pharm. Biomed. Anal. 49 (2009) 1128–1132.
[12] K.L. Ng, B. Paull, P.R. Haddad, K. Tanaka, Retention modeling of electrostatic and adsorption effects of aliphatic and aromatic carboxylic acids in ion-exclusion chromatography, J. Chromatogr. A 850 (1999) 17–27.

Journal of Pharmaceutical and Biomedical Analysis 66 (2012) 392–398

Contents lists available at SciVerse ScienceDirect

Journal of Pharmaceutical and Biomedical Analysis

journal homepage: www.elsevier.com/locate/jpba

Short communication

Metabolite profiles of icariin in rat plasma by ultra-fast liquid chromatography coupled to triple-quadrupole/time-of-flight mass spectrometry

Qian Qian[a,b], Song-Lin Li[a], E. Sun[a], Ke-Rong Zhang[c], Xiao-Bin Tan[a], Ying-Jie Wei[a], Hong-Wei Fan[d], Li Cui[a], Xiao-Bin Jia[a,b,*]

[a] Key Laboratory of New Drug Delivery System of Chinese Meteria Medica, Jiangsu Provincial Academy of Chinese Medicine, 100 Shizi Road, Nanjing 210028, Jiangsu Province, China
[b] Department of Pharmaceutics, Jiangsu University, Zhenjiang 212013, China
[c] ChinaAsia Pacific Application Support Center, AB Sciex, Shanghai 200233, China
[d] Clinical Pharmacology Laboratory, Nanjing First Hospital to Nanjing Medical University, 68 Changle Road, Nanjing 210006, China

ARTICLE INFO

Article history:
Received 4 January 2012
Received in revised form 26 March 2012
Accepted 29 March 2012
Available online 5 April 2012

Keywords:
Icariin
UFLC–TOF/MS
Metabolites

ABSTRACT

In this work, the metabolite profiles of icariin in rat plasma were qualitatively investigated, and the possible metabolic pathways of icariin were subsequently proposed. After oral administration of icariin, rat plasma samples were collected and pretreated by protein precipitation. Then these pretreated samples were injected into a Venusil ASB-C18 column with mobile phase consisted of 0.1% formic acid water and 0.1% formic acid acetonitrile and detected by Ultra fast liquid chromatography coupled to time-of-flight mass spectrometry (UFLC–TOF/MS). A total of 19 metabolites, namely, icariside I (M1), icaritin (M2), desmethylicaritin and its isomer (M3–M6), icaritin-3-O-gluA (M7), icaritin-7-O-gluA (M8), icariside II and its isomer (M9 and M10), icaritin-3,7-di-O-gluA (M11), 1,3-isoprene alcohol icaritin and its isomer (M12, M13 and M18), 1,3-isoprene alcohol icariside II (M14), allylic alcohol icaritin and its isomer (M15 and M16), 1,3-isoprene icariside II (M17) and icaritin-3-O-rha-7-O-gluA (M19) were detected and tentatively identified, and 9 of them, including M7 and M8 and M12–M18 were reported for the first time. The metabolites profiles in plasma revealed that glucuronide conjugates of isoflavonoids and flavonoid aglycones were the major circulating forms of icariin.

© 2012 Elsevier B.V. All rights reserved.

1. Introduction

Herba Epimedii, the dried aerial parts of *Epimedium brevicornu* Maxim, *Epimedium sagittatum* Maxim, *Epimedium pubescens* Maxim and *Epimedium koreanum* Nakai, are traditionally used as tonic, aphrodisiac and antirheumatic medical herbs for cardiovascular, bone loss and impotence diseases in East Asian countries [1]. Flavonoids are reported to be the bioactive components of Herba Epimedii, and most of the flavonoids belong to the 8-prenylflavonoids [2]. Icariin (Fig. 1), one of the most abundant flavonoids of Herba Epimedii, has lots of pharmacological and biological activities, including prevent osteoporosis, pencil erection, anti-cancer and anti-depression [3–5]. Hence, icariin is considered to be a key active ingredient of Herba Epimedii. Our previous work used caco-2 model and the rat intestinal perfusion model to study the absorption and metabolism of icariin in rat intestine. Also the metabolites of icariin were identified as icariside II (one of two) [6,7].

Like many medicinal herbs, Herba Epimedii-containg products are commonly taken p.o. In the past decades, the metabolism of icariin has been studied extensively by NMR [8], CE [9], HPLC/MS/MS [10], etc. However, because of the limitations of the instrument, it was difficult to detect many trace metabolites under certain conditions, which consequently restrict the bioavailability studies on this herb in animals. To the best of our knowledge, only six metabolites of icariin, including icariside I, icaritin, desmethylicaritin, icariside II, icaritin-3,7-di-O-gluA and icaritin-3-O-rha-7-O-gluA have been reported in rat plasma following administration of icariin [8–11].

Due to their excellent sensitivity and high throughput, triple quadrupole instruments have been the workhorse instrument for the quantitative portion of this application. Accurate mass instruments such as time of flight (TOF) and orbital trapping analyzers have been used for metabolite identification due to their high mass accuracy and resolution [12,13]. Unfortunately, orbital trapping involves a compromise between resolution and speed. Traditional TOF technology has shown limitations in linearity and requires internal calibration to maintain mass accuracy. Modifying study designs, sample preparation procedures, or chromatography in order to accommodate instrument limitations is not acceptable.

In present paper, the apparatus and techniques used in study of metabolic products for the further realization of in vivo course of rats have higher sensitivity. On the one hand, the highly innovative design of the system we used combines a proven high performance triple quadrupole front end with the accelerator TOF Analyzer, a

* Corresponding author.
E-mail address: xiaobinjia_nj@126.com (X.-B. Jia).

0731-7085/$ – see front matter © 2012 Elsevier B.V. All rights reserved.
http://dx.doi.org/10.1016/j.jpba.2012.03.053

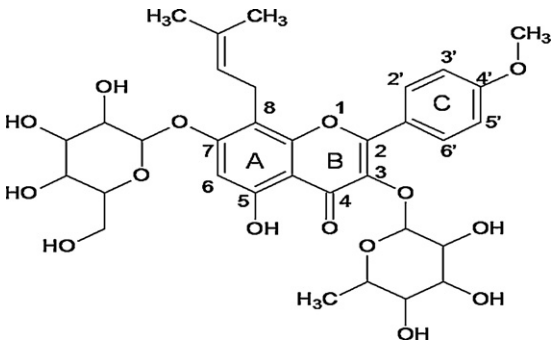

Fig. 1. The structure of icariin.

state of the art accurate mass analyzer with unprecedented performance and stability. This results in the linearity and sensitivity of a high performance triple quadrupole, combined with seed, high mass accuracy (2 ppm or less) and high resolution (30,000) of an accurate mass instrument, even at low mass for small molecules.

On the other hand, five key features of the metabolite pilot software were used for rapid metabolite identification of icariin, namely: (i) Intuitively supports the high resolution accurate mass metabolite identification workflows of the triple TOF LC/MS/MS system; (ii) Metabolites are detected through a combination of powerful peak finding algorithms; (iii) Automatic structure driven processing parameters; (iv) Integrated MS/MS fragment interpretation and structure editor; (v) Multiple sample correlation function for time course studies and inter-species comparison of metabolites.

In this study, an UFLC–TOF/MS method was developed for the analyses of metabolites in rat plasma after oral administration of pure icariin. A total of 19 metabolites (Table 1) were detected and tentatively identified, and 9 of them were reported for the first time.

2. Experimental

2.1. Materials

Icariin (purity >98%) was purchased from National Institute for the Control of Pharmaceutical and Biological Products (Beijing, China). HPLC grade acetonitrile (ACN) and methanol were purchased from Merck (Darmstadt, Germany). MS grade formic acid was purchased from Nanjing Chemical Reagent Co., Ltd. The ultrapure water was purified by the Milli-Q water purification system (Millipore, Bedford, MA, USA). All the other reagents and chemicals were of analytical grade.

2.2. Animal protocol

Male Sprague-Dawley rats weighing between 200 and 250 g were obtained from SLEK Lab Animal Center of Shanghai (Shanghai, China). Animals were housed under standard conditions of temperature, humidity, and light. Food and water were provided ad libitum. The rats were fasted overnight before the day of the experiment. The studies were approved by the Animal Ethics Committee of Jiangsu Provincial Academy of Chinese Medicine.

Sample collection: Icariin preparation containing 20% polyethylene glycol (PEG) 400 was orally administered to six male rats at a single dose of approximate 120 mg/kg body weight. Before administration, a jugular vein cannula was implanted for blood sampling, and blank blood samples were collected. The peak time of icariin was about 30 min [10], therefore, 15, 30 and 60 min was taken as the sampling point. A volume of 0.8 mL plasma sample was collected from jugular vein at 15, 30 and 60 min and hepatic portal at 70 min, respectively, into heparinized tubes after dosing. All blood samples were then centrifuged for 10 min at 3000 rpm, 4 °C, and the supernatants (i.e., the plasma) were stored at −70 °C until additional extraction and analysis.

2.3. Sample preparation

The samples were prepared as follows: briefly, 800 μL of methanol was added to 200 μL of plasma sample to precipitate the protein. After vortex-mixing for 3 min, samples were separated by centrifugation at 14,000 rpm for 10 min, and then the supernatant was transferred to another tube and evaporated to dryness at 40 °C under a gentle stream of nitrogen. The residue was reconstituted in 200 μL initial mobile phase ACN-water (95:5) followed by vortex-mixing and centrifugation at 14,000 rpm for 15 min. Then, 40 μL of an aliquot of the supernatant was injected into the UFLC system.

2.4. Instrumentation and conditions

The controls and samples were analyzed on a triple TOF™ 5600 MS/MS system (AB SCIEX, Canada) coupled to a Prominence™ UFLC system (Shimadzu, Japan). Separations were accomplished on a Venusil ASB-C18 column (2.1 mm × 100 mm, 3 μm) (Agela, USA). The mobile phase consisted of 0.1% formic acid water (solvent A) and 0.1% formic acid ACN (solvent B).

The linear gradient elution program was as follows: 0–1 min, 5% B; 1–5 min, 5–21% B; 5–10 min, 25–60% B; 10–14 min, 60–90% B; 14–19 min, 90% B, 19–19.1 min, 90–5% B; 19–25 min, 5% B; The flow rate was kept at 0.3 mL/min, and the injecting volume was set at 10 μL.

The mass spectrometer was operated in the positive ESI mode with a Duo Spray TM source (AB SCIEX, Canada), and mass range was set at *m/z* 100–1000. The following parameter settings were used: ion spray voltage: 5500 V; ion source heater: 550 °C; curtain gas: 30 psi; ion source gas 1, 60 psi; For the TOFMS-IDA-4 MS/MS analysis, TOFMS, the survey scan, and MS/MS experiments were run with 250 ms accumulation time for TOFMS and 100 ms accumulation time in MS/MS experiments. Collision energy (CE) is 35; collision energy spread (CES) is 15 in MS/MS experiment. In addition, information-dependent acquisition (IDA) was used to trigger acquisition of MS/MS spectra for ions matching the IDA criteria. Real time Multiple Mass Defect Filter (MMDF) was used in IDA criteria. Gives IDA priority to ions was matching the mass defect window to acquire MS/MS spectra.

3. Results and discussion

Studies on liquid chromatography coupled with mass spectrometry (LC–MS) for metabolite identification of natural products and herbs have been increased greatly over these years. Though the coupling of LC and MS has provided an alternative tool for online structural characterization and rapid identification of compounds in complex biological samples, the output signals still contain a great deal of noise embedding the useful information together with false peaks and spikes. A formidable challenge in LC–MS method development and analysis is actually the data interpretation. The two most used visualization techniques are the summation of all mass channels to total ion chromatograms (TICs) and to show only the most abundant signal at each scan in a base peak chromatogram (BPC). However, it is impossible to detect peak of trace levels from TIC or BPC. The only alternative is a manual review of each extracted ion chromatograms (XICs) [14,15].

Fig. 2 shows the TICs and the XICs of plasma samples in the positive ion mode respectively. By comparing with the blank and biological fluids, lots of endogenous interferences were observed in TICs, but no endogenous interferences were observed in XICs.

Table 1
Accurate mass measurement for the protonated molecules of metabolites in rat plasma.

No.	Formula	t_R (min)	Calculated m/z	Experimental m/z	ppm error
P	$C_{33}H_{40}O_{15}$	8.23	677.2440	677.2442	0.30
M1	$C_{27}H_{30}O_{11}$	8.22	531.1861	531.1862	0.21
M2	$C_{21}H_{20}O_6$	13.32	369.1333	369.1332	−0.19
M3	$C_{20}H_{18}O_6$	8.9	355.1176	355.1173	−0.90
M4	$C_{20}H_{18}O_6$	9.24	355.1176	355.1174	−0.62
M5	$C_{20}H_{18}O_6$	9.32	355.1176	355.1173	−0.90
M6	$C_{20}H_{18}O_6$	9.09	355.1176	355.1176	−0.06
M7	$C_{27}H_{28}O_{12}$	8.43	545.1654	545.1649	−0.83
M8	$C_{27}H_{28}O_{12}$	8.11	545.1654	545.1645	−1.56
M9	$C_{27}H_{30}O_{10}$	10.16	515.1912	515.1905	−1.30
M10	$C_{27}H_{30}O_{10}$	10.75	515.1912	515.1908	−0.72
M11	$C_{33}H_{36}O_{18}$	8.13	721.1974	721.197	−0.61
M12	$C_{21}H_{18}O_7$	9.55	383.1125	383.113	1.23
M13	$C_{21}H_{18}O_7$	12.25	383.1125	383.1123	−0.60
M14	$C_{27}H_{28}O_{11}$	9.55	529.1704	529.1702	−0.45
M15	$C_{21}H_{20}O_7$	8.87	385.1282	385.1284	0.57
M16	$C_{21}H_{20}O_7$	9.21	385.1282	385.1281	−0.21
M17	$C_{27}H_{28}O_{10}$	11.87	513.1755	513.1752	−0.62
M18	$C_{21}H_{18}O_7$	9.06	383.1125	383.1122	−0.86
M19	$C_{33}H_{38}O_{16}$	8.43	691.2233	691.2228	−0.67

3.1. Identification of icariin

Both negative and positive modes of ESI mass spectra were examined in this study. Generally in the negative mode, fewer product ions were observed in tandem mass experiments, while in positive ion mode, $[M+H]^+$ ions of sufficient abundance could be subjected to MS^n analysis and provided more structural information.

LC–MS/MS spectra of the metabolites of icariin were obtained via fragmentation of molecular ions that used for more precise structural identification of metabolites. The chromatographic and mass spectrometry conditions were optimized with icariin. Full scan mass spectrum analysis of icariin showed the presence of $[M+H]^+$ (m/z 677.2442) (Fig. 3A) and two isotope peaks (m/z 678.2470, 679.2499). The MS–MS product ion spectrum of icariin was shown in Fig. 3B. Icariin was eluted at 8.23 min (Fig. 3C). Fragmentation of icariin in the ion trap lead to three product ions at m/z: 531.1871, 369.1340 and 313.0711. The most abundant product ion at m/z 369.1340 was produced by the loss of rhamnose and glucose (308 Da). The product ions at m/z 531.1871 were formed by the loss of rhamnose (146 Da). The product ion at m/z 313.0711 was 56 Da less than m/z 369 by the loss of C_4H_7 (56 Da), which is produced

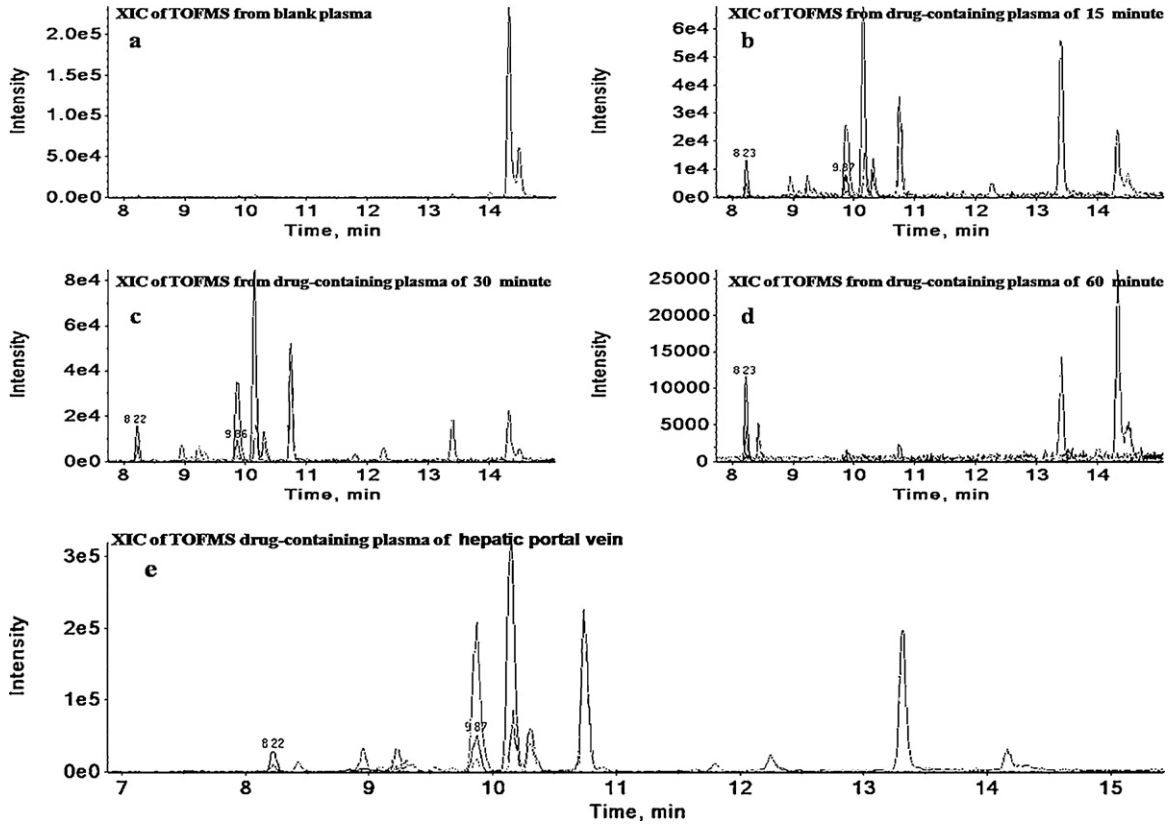

Fig. 2. The representative XICs of plasma. (a) The blank plasma; (b) the plasma of 15 min; (c) the plasma of 30 min; (d) the plasma of 60 min and (e) the plasma of hepatic portal.

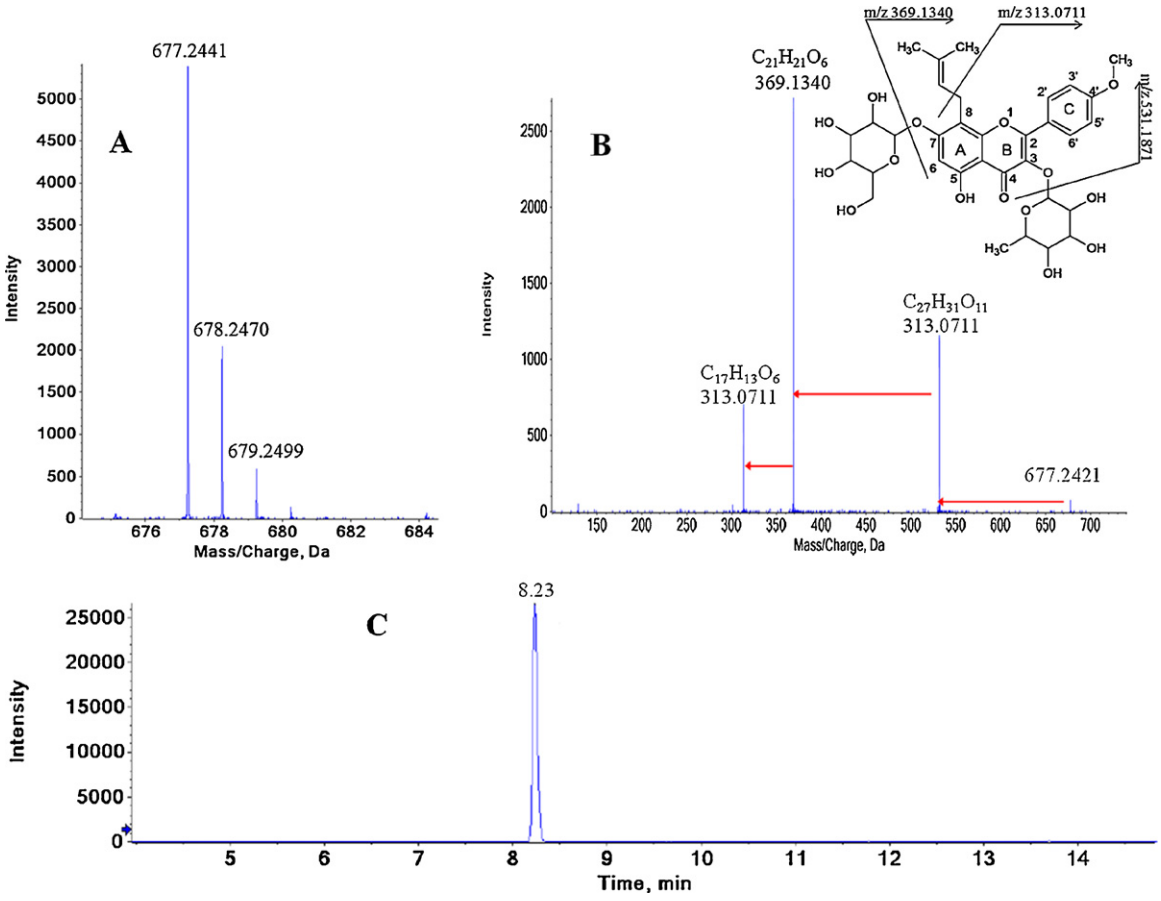

Fig. 3. Low collision energy mass spectrum (A), high collision energy spectrum (B) and XICs (C) of icariin.

by the rearrangement at isopentene group at the position 8 of the A-ring. It could be concluded that the ions at *m*/*z* 531, 369 and 313 were the characteristic product ions of icariin. 308, 146, and 56 Da were the characteristic neutral losses of icariin. These characteristic product ions and neutral losses were the sound bases to identify metabolites of icariin.

3.2. Identification of metabolites

The full scan mass spectrum of fragment ions of rat plasma after administration of icariin was compared with blank plasma samples to find out the possible metabolites in rat plasma. Based on the method mentioned above, the parent medicine and its main nineteen metabolites (M1–M19) were found as potential metabolites in hepatic portal vein. Among them, eighteen peaks (M1–M18) were also found in the plasma of 15 min. All peaks can be found in the plasma of 30 min, and ten peaks (M1–M3, M7 and M8, M10–13 and M19) were also found in the plasma of 60 min (Table 2).

As can be seen from Table 2, the targets were present in higher concentration in plasma of hepatic portal vein than in plasma of jugular vein. All metabolites were tentatively identified. The retention times of M7, M8, M11 and M19 were longer than that of icariin, which indicate that the phase II metabolites were produced.

TOF/MS spectra of these metabolites were shown in Fig. 4. Among them, the MS and MS/MS spectra and the retention time of the molecular ion at *m*/*z* 677 (P) were the same as those of icariin, the retention time of which was 8.23 min. The MS^2 spectra of M1 (*m*/*z* 531.1862), M2 (*m*/*z* 369.1332), M7 and M8 (*m*/*z* 545.1649), M9 and M10 (*m*/*z* 515.1905), M11 (*m*/*z* 721.197) and M19 (*m*/*z* 691.2228), along with the corresponding main fragment ions at *m*/*z* 369, 313, were the same as the parent icariin and *m*/*z* 677.2442 and its product ions at *m*/*z* 531, 369, 313 basically.

Among them, the molecular ion of M1 (*m*/*z* 531), M9 and M10 (*m*/*z* 515), M2 (*m*/*z* 369) were produced by neutral loss of 146, 162 and 308 Da diagnostic of rhamnose and glucose from the parent compound respectively. The results indicated they all should be the desugarization product of icariin. Therefore, M1 (Fig. 4A) should be

Table 2
The relative peak area of metabolites in plasma of different collection times.

	15 min ($\times 10^4$)	30 min ($\times 10^4$)	60 min ($\times 10^4$)	Hepatic portal vein ($\times 10^4$)
P	4.51	5.78	4.02	13.3
M1	1.50	1.71	1.25	4.94
M2	0.267	8.11	6.99	120
M3	2.66	2.82	0.339	16.0
M4	2.86	3.06	N/A	16.4
M5	1.61	2.60	N/A	12.6
M6	94.7	0.892	N/A	3.86
M7	10.4	0.175	2.42	7.54
M8	24.2	0.193	0.133	1.46
M9	3.24	3.79	N/A	17.0
M10	9.69	16.4	0.633	78.2
M11	0.492	0.588	0.552	2.55
M12	2.28	2.27	0.141	13.0
M13	1.59	1.50	0.204	6.47
M14	1.45	1.85	N/A	10.3
M15	3.18	2.30	N/A	12.5
M16	1.47	1.73	N/A	16.0
M17	0.617	0.712	N/A	2.82
M18	2.09	1.75	N/A	11.9
M19	N/A	0.227	2.04	5.31

N/A, not available.

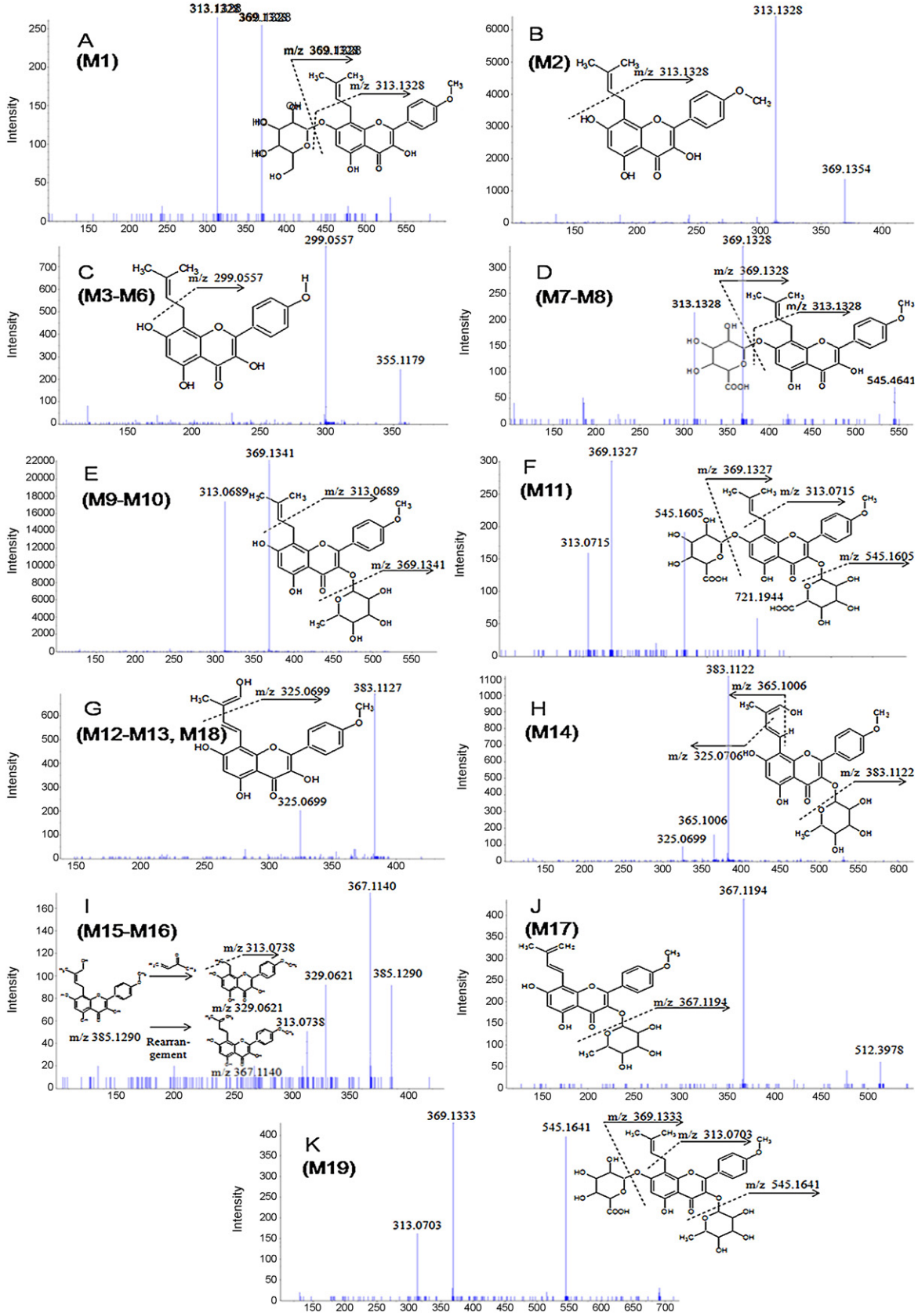

Fig. 4. Mass spectra of metabolites of icariin. (A) Icariside I, M1; (B) icaritin, M2; (C) desmethylicaritin, M3–M6; (D) icaritin-3-O-gluA or icaritin-7-O-gluA, M7 and M8; (E) icariside II, M9 and M10; (F) icaritin-3,7-di-O-gluA (M11); (G) 1,3-isoprene alcohol icaritin, M12, M13 and M18; (H) 1,3-isoprene alcohol icariside II, M14; (I) allylic alcohol icaritin, M15 and M16; (J) 1,3-isoprene icariside II, M17 and (K) icaritin-3-O-rha-7-O-gluA, M19.

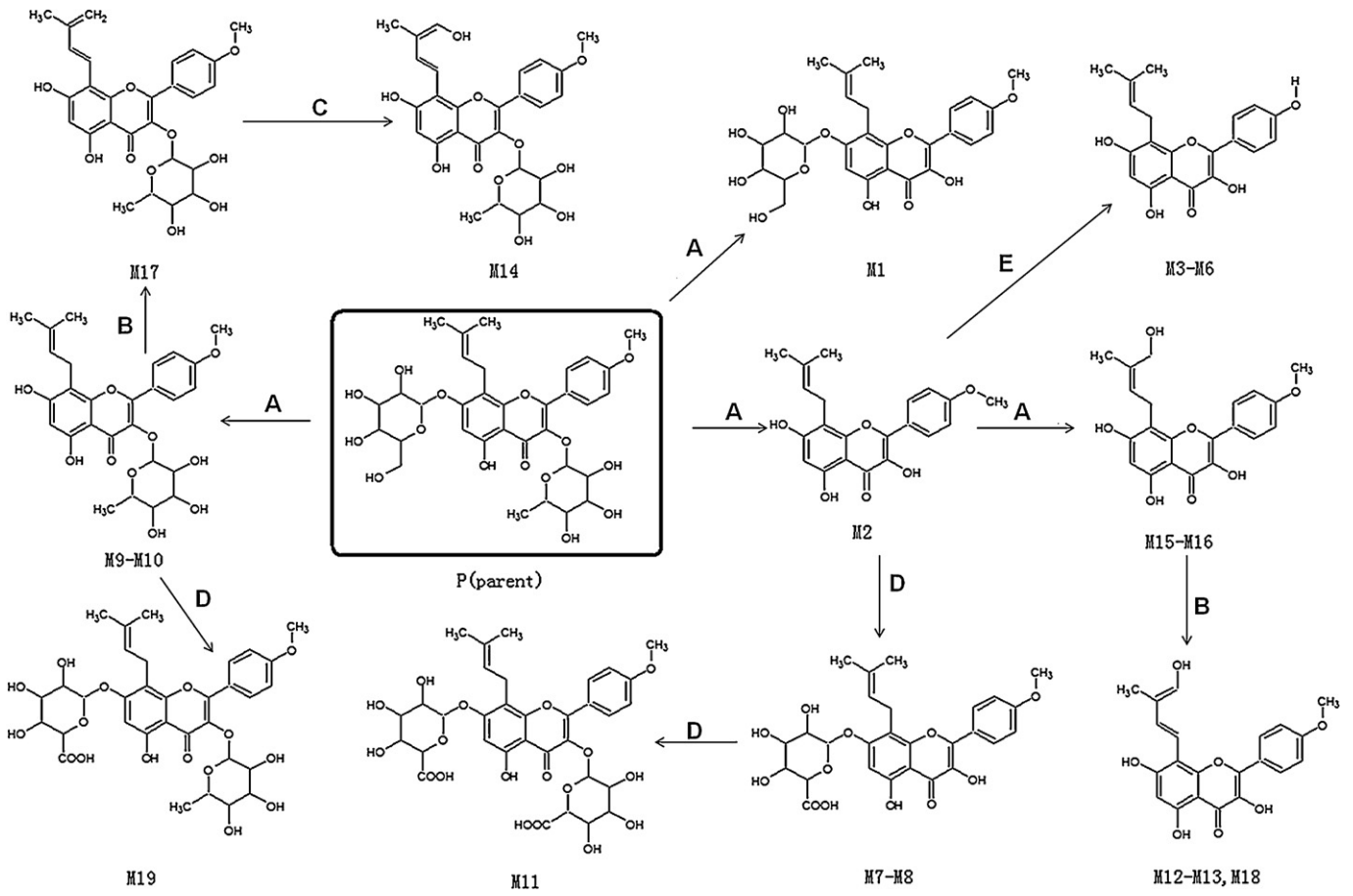

Fig. 5. Proposed major metabolic pathway of icariin in rat. (A) Desugarization; (B) dehydrogenation; (C) hydroxylation; (D) glucuronidation and (E) demethylation.

icariside I along with the loss of rhamnose at the position 3 of the B-ring of icariin. Simultaneously, M9 and M10 (Fig. 4E) should be icariside II along with the loss of glucose at the position 7 of the A-ring of icariin. And M2 (Fig. 4B) should be icaritin along with the loss of glucose and rhamnose at the position 7 of the A-ring and the position 3 of the B-ring of icariin.

Furthermore, the molecular ion at *m*/*z* 545 (M7 and M8) and *m*/*z* 721 (M11), were 176 and 352 Da more than M2, respectively, which were the mono-glucuronide and di-glucuronide of icaritin. Simultaneously, the molecular ion at *m*/*z* 691 (M19) was 176 Da more than M9 and M10. Therefore, M19 (Fig. 4K) should be the mono-glucuronide of icariside II. According to the structure of the icaritin and icariside II, M7 and M8 (Fig. 4D) is called icaritin-3-O-gluA or icaritin-7-O-gluA, M11 (Fig. 4F) is called icaritin-3-O-gluA-7-O-gluA and M19 is called icaritin-3-O-rha-7-O-gluA.

The molecular ion at *m*/*z* 355.1179 (M3–M6) and its product ions at *m*/*z* 299.0557 (Fig. 4C) were all 14 Da less than *m*/*z* 369 (M2) and its product ions at *m*/*z* 313, respectively. Therefore, M3–M6 was identified as the desmethylicaritin, and the demethylation position was at the unique saturated C—O bond at the position 4′ of the C-ring. However, mechanism formation of isomeric was not clear.

The molecular ion at *m*/*z* 383.1127 (M12, M13 and M18) and its product ions at *m*/*z* 325.0699 (Fig. 4G) were all 14 Da more than *m*/*z* 369 (M2) and its product ions at *m*/*z* 313, respectively. So, M12, M13 and M18 could be characterized as oxidation products of M2, and the oxidation position was at terminal methyl of isopentene group at the position 8 of the A-ring, coupled with migration of the double-bond of the isopentene group.

The MS^2 spectra of the molecular ion at *m*/*z* 529.1704 (M14) showed the abundant second order fragment ions at *m*/*z* 383.1122, 365.1036, and 325.0706 (Fig. 4H), which at *m*/*z* 383.1122 and *m*/*z* 325.0706 were the same as the M12, M13 and M18. It has been shown that ion *m*/*z* 365.103 is produced by the McLafferty rearrangement at isopentene group at the position 8 of the A-ring. Hence M14 is called 1,3-isoprene alcohol icariside II.

The molecular ion at *m*/*z* 513.1755 (M17) and its product ions at *m*/*z* 367.1194 (Fig. 4J) were all 2 Da less than *m*/*z* 515 (M9 and 10) and its product ions at *m*/*z* 369, respectively. Therefore, M17 was identified as the dehydrogenation product of icariside II, and the dehydrogenated position was at isopentene group at position 8 of the A-ring.

The molecular ion at *m*/*z* 385.1290 (M15 and M16) were all 16 Da more than *m*/*z* 369 (M2). So, M15 and M16 could be characterized as oxidation products of M2, and the oxidation position was at terminal methyl of isopentene group at the position 8 of the A-ring. Furthermore, the mass spectral fragmentation pattern of the molecular ion at *m*/*z* 367.1140, *m*/*z* 329.0621 and *m*/*z* 313.0738 was showed at Fig. 3I.

In conclusion, there are four phase II metabolites of icariin: M7, M8, M11 and M19. And only M11 was the di-glucuronide of icaritin. The relative quantity of all metabolites was analyzed based on MultiQuant software (Table 2). It was found from Table 2 that the majority of the metabolites had excellent response in plasma of 15 and 30 min, but decreased significantly in plasma of 60 min. Only M7, M8 and M19 also had excellent response in plasma of 60 min. The results suggested that icaritin was quickly metabolized and degraded.

Double peaks appeared in the plasma concentration–time curves in rates orally administrated of icariin was reported in literature [16,17]. There might be hepato-enteral circulation in excretion

of icariin. Analyzing the common points between M7, M8 and M19, we found that the mono-glucuronide react with the effects of enterohepatic circulation of icariin.

4. Conclusions

In conclusion, an UFLC–TOF/MS was applied to the complex metabolites of icariin in rat plasma. A total of 19 metabolites were detected and tentatively identified from the plasma samples, and 9 of them were reported for the first time. M1–M6, M9 and M10 and M12–M18 were the phase I metabolites of icariin in rat, such as demethylation, dehydrogenation and desugarization. The phase II metabolites of icariin in rat included one di-glucuronides (M11) and three mono-glucuronides (M7, M8 and M19) which had excellent response in plasma of 60 min. The metabolite profile in plasma revealed that glucuronide conjugates of isoflavonoids, as well as aglycones and sub-aglycones were the major circulating forms of icariin in Fig. 5. The possible metabolic pathways of icariin were subsequently proposed. The experimental results showed that the main phase I metabolism of icariin in rat was desugarization and oxidative dehydrogenation reactions. We speculated from the plasma concentration that icaritin was the main metabolite of icariin. Though the structures of metabolites cannot be determined conclusively by LC–MS/MS alone, the present method is still very valuable and dependable for the further study of the metabolism of icariin.

Acknowledgments

This work was supported by the Natural Science Foundation of China (Nos. 30572372, 30973944, and 30973978), the science and technology projects fund of Jiangsu Province (No. LZ09067).

References

[1] Editorial Committee of Pharmacopoeia of Ministry of Health PR China, The Pharmacopeoia of People's Republic of China (Part 1), China, Chemical Industry Press, Beijing, 2010, pp. 306–308.
[2] H.P. Ma, X.R. He, Y. Yang, M.X. Li, D.J. Hao, The genus Epimedium: an ethnopharmacological and phytochemical review, J. Ethnopharmacol. 134 (2011) 519–541.
[3] D.W. Zhang, Y. Cheng, N.L. Wang, J.C. Zhang, M.S. Yang, X.S. Yao, Effects of total flavonoids and flavonol glycosides from Epimedium koreanum Nakai on the proliferation and differentiation of primary osteoblasts, Phytomedicine 15 (2008) 55–61.
[4] X. Huang, D.Y. Zhu, Y.J. Lou, A novel anticancer agent, icaritin, induced cell growth inhibition, G1 arrest and mitochondrial transmembrane potential drop in human prostate carcinoma PC-3 cells, Eur. J. Pharmacol. 564 (2007) 26–36.
[5] H. Ning, Z.C. Xin, G.T. Lin, L. Banie, T.F. Lue, C.S. Lin, Effect s of icariin on phosphodiesterase-5 activity in vitro and cyclic guanosine monophosphate level in cavernous smooth muscle cells, Urology 68 (2006) 1350–1354.
[6] Y. Chen, J.Y. Wang, X.B. Jia, X.B. Tan, M. Hu, Role of intestinal hydrolase in the absorption of prenylated flavonoids present in Yin Yanghuo, Molecules 16 (2011) 1336–1348.
[7] Y. Chen, Y.H. Zhao, X.B. Jia, M. Hu, Absorption mechanisms of prenylated flavonoids present in the heat-processed Epimedium koreanum Nakai (Yin Yanghuo), Pharm. Res. 25 (2008) 2190–2199.
[8] M. Liu, H.P. Liu, X.M. Lu, C. Li, Z. Xiong, F. Li, Simultaneous determination of icariin, icariside II and osthole in rat plasma after oral administration of the extract of Gushudan(a Chinese compound formulation) by LC–MS/MS, J. Chromatogr. B 860 (2007) 113–120.
[9] F. Qiu, Y.J. Chen, Y.H. Kano, X.S. Yao, Metabolism of orally administered icariin in rats, Acta Pharmaceutica Sinica 34 (1999) 222–226.
[10] J. Liu, Y.J. Lou, Determination of icariin and metabolites in rat serum by capillary zone electrophoresis: rat pharmacokinetic studies after administration of icariin, J. Pharm. Biomed. Anal. 36 (2004) 365–370.
[11] H.Y. Zhao, M.X. Fan, L. Fan, J.H. Sun, D. Guo, Liquid chromatography–tandem mass spectrometry analysis of metabolites in rats after administration of prenylflavonoids from Epimediums, J. Chromatogr. B 878 (2010) 113–1124.
[12] D.F. Toh, L.S. New, H.L. Koh, E.C. Chan, Ultra-high performance liquid chromatography/time-of-flight mass spectrometry (UHPLC/TOFMS) for timedependent profiling of raw and steamed panax notoginseng, J. Pharm. Biomed. Anal. 52 (2010) 43–50.
[13] C.Y. Li, L.W. Qi, P. Li, Correlative analysis of metabolite profiling of Danggui Buxue Tang in rat biological fluids by rapid resolution LC–TOF/MS, J. Pharm. Biomed. Anal. 54 (2011) 186–191.
[14] M. Fredriksson, P. Petersson, M. Jörntïen-Karlsson, B.O. Axelsson, D. Bylund, An objective comparison of pre-processing methods for enhancement of liquid chromatography–mass spectrometry data, J. Chromatogr. A 1172 (2007) 35–150.
[15] H.Y. Zhao, J.H. Sun, M.X. Fan, L. Fan, L. Zhou, Z. Li, J. Han, B.R. Wang, D.A. Guo, Analysis of phenolic compounds in Epimedium plants using liquid chromatography coupled with electrospray ionization mass spectrometry, J. Chromatogr. A 1190 (2008) 57–181.
[16] C.S. Wu, J.L. Zhang, T.H. Zhou, B.L. Guo, Y.L. Wang, J.F. Hou, Simultaneous determination of seven flavonoids in dog plasma by ultra-performance liquid chromatography–tandem mass spectrometry and its application to a bioequivalence study of bioactive components in Herba Epimedii and Er-Xian Decoction, J. Pharm. Biomed. Anal. 54 (2011) 186–191.
[17] S.P. Wong, P. Shen, L. Lee, J. Li, E.L. Yong, Pharmacokinetics of prenylflavonoids and correlations with the dynamics of estrogen action in sera following ingestion of a standardized Epimedium extract, J. Pharm. Biomed. Anal. 50 (2009) 216–223.

Journal of Pharmaceutical and Biomedical Analysis 66 (2012) 399–401

Contents lists available at SciVerse ScienceDirect

Journal of Pharmaceutical and Biomedical Analysis

journal homepage: www.elsevier.com/locate/jpba

Short communication

A novel approach to signal normalisation in atmospheric pressure ionisation mass spectrometry

Michael Vogeser[a,*], Fabian Kirchhoff[a], Roland Geyer[b]

[a] Institute of Clinical Chemistry, University of Munich, Munich, Germany
[b] Tecan Trading AG, Männedorf, Switzerland

ARTICLE INFO

Article history:
Received 27 January 2012
Received in revised form 28 March 2012
Accepted 30 March 2012
Available online 5 April 2012

Keywords:
Internal standardisation
Post column infusion
Ion suppression, atmospheric pressure ionisation (API)
Liquid chromatography–tandem mass spectrometry (LC–MS/MS)

ABSTRACT

The aim of our study was to test an alternative principle of signal normalisation in LC–MS/MS. During analyses, post column infusion of the target analyte is done via a T-piece, generating an "area under the analyte peak" (AUP). The ratio of peak area to AUP is assessed as assay response. Acceptable analytical performance of this principle was found for an exemplary analyte. Post-column infusion may allow normalisation of ion suppression not requiring any additional standard compound. This approach can be useful in situations where no appropriate compound is available for classical internal standardisation.

© 2012 Elsevier B.V. All rights reserved.

1. Introduction

Liquid chromatography tandem–mass spectrometry has found an important role in clinical chemistry. In contrast to ligand-binding based assays, method development is typically straightforward with LC–MS/MS. The principle of internal standardisation–ideally involving stable isotope-labelled compounds – enables highest analytical reliability. By this approach, matrix effects which may be relevant in the entire process of extraction, chromatography and mass spectrometric detection can be compensated. For many of the clinically relevant endogenously occurring small molecule analytes (such as steroid hormones), stable isotope labelled compounds are available. This is in contrast to most analytes in therapeutic drug monitoring (TDM) where only few stable isotope labelled compounds are available. Consequently, in most TDM methods "homologues" are used as IS, representing compounds of *similar* molecular structure with respect to the target analyte. However, already minor differences (as functional groups) in the molecular structure between target analyte and IS can result in substantial differences in a compound's ionisation and fragmentation behaviour. Whenever the ionisation efficacy of a target analyte and such a related internal standard compound, respectively, is modulated in an non-equal manner by matrix constituents, inaccuracy arises in LC–MS/MS methods [1]. Thus, the reliability of LC–MS/MS applications, in particular in the field of TDM, is critically determined by the appropriateness of available candidate IS substances. Therefore, the search for suitable compounds is typically a major challenge in the development of LC–MS/MS methods in TDM today. Unsuited IS compounds (differing "too much" from the target analyte), typically lead to non-linearity of response and/or unacceptable reproducibility.

We here describe a novel principle for monitoring and normalisation of signal generation in LC–MS/MS, not requiring any compound in addition to the target analyte.

2. Materials and methods

2.1. Instrumental set-up

The analytical principle described herein is based on the continuous post-column infusion of a pure solution of the target analyte *throughout* an analytical series. This instrument configuration generates a background signal in the signal-trace of the target analyte; the actual peak of the chromatographic separation is superimposed to this background-signal [2]. Despite introducing the reference solution of the target analyte at a *continuous* rate, the intensity of the background signal is highly *variable* in LC–MS/MS, displaying the actual modulation of target analyte ionisation by

* Corresponding author at: Institute of Clinical Chemistry, University of Munich, Marchioninistr. 15, 81375 Munich, München, Germany. Tel.: +49 89 7095 3221; fax: +49 89 7095 8888.
E-mail address: michael.vogeser@med.uni-muenchen.de (M. Vogeser).

0731-7085/$ – see front matter © 2012 Elsevier B.V. All rights reserved.
http://dx.doi.org/10.1016/j.jpba.2012.03.055

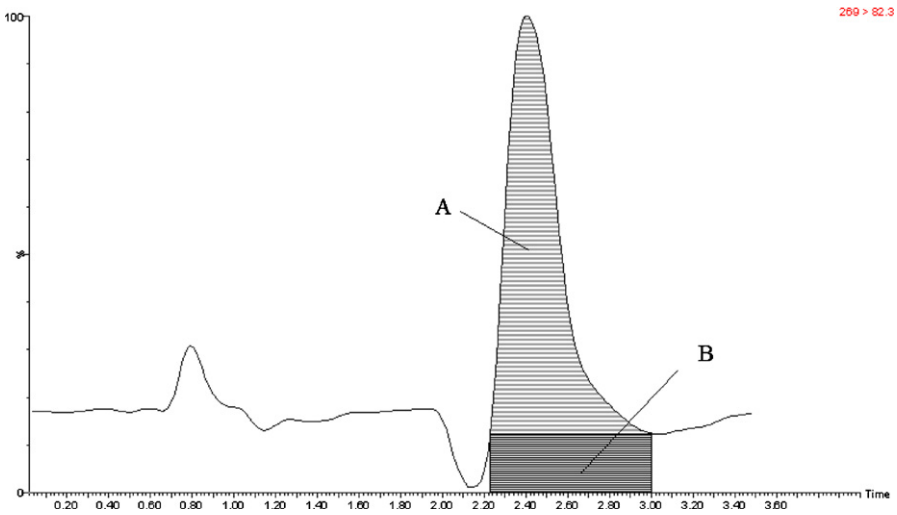

Fig. 1. Principle of internal standardisation by continuous post-column infusion of the target analyte and representative chromatogram of HMR 1726 quantification with LC–MS/MS; (A) peak area; (B) area-under-the-peak (AUP).

matrix compounds eluting from the chromatographic system. This post-column infusion set-up is widely used to investigate the ion-suppression characteristics of LC–MS/MS methods. Upon injection of a biological, matrix-based sample, ionisation yield typically decreases drastically for a time period of seconds to minutes due to matrix constituents. During method development, it is tried to minimise the extent of this ion-suppression range (in particular by efficient sample preparation) and to obtain elution of the target analyte outside this range by appropriate chromatographic retention of the analyte. Notably, the extent of the ion-suppression range can be variable from sample to sample.

The key feature of the analytical principle described here is that a peak integration line is drawn and that in – a second step – the area of the quadrangle *below* this integration line (characterizing the background signal) is recorded. A representative chromatogram applying post-column infusion is shown in Fig. 1. The "area above the peak integration line" is denoted with A, the "area under the peak" (AUP) with B. (A time interval of ion suppression resulting from residual sample matrix components and preceding the analyte peak can be observed in a typical pattern.) The ratio of the analyte peak area to the AUP can be calculated as the *response* of the analysis (A/B; Fig. 1). In case of ion-suppression occurring during the target analyte peak elution, the area of both, the peak above the integration line and the AUP will be diminished alike, resulting in an unaffected ratio of the two areas (i.e. response). Thus, any sample-individual ion suppression (or enhancement) effect should be compensated by this instrumental configuration and mode of data analysis.

2.2. Evaluation

In order to test this latter principle of quantification involving continuous post-column infusion without use of a separate IS substance, we performed experiments on an exemplary analyte, the drug metabolite HMR1726 (also referred to as A//1726 or teriflunomide). This compound is the active metabolite of leflunomide, an immunosuppressant drug used for the treatment of autoimmune disorders [3,4].

The detailed mass spectrometric and chromatographic conditions are given as Supplemental file.

We performed a validation protocol including four independent series in order to investigate the performance of this quantification method. Calibrator samples and quality control samples were prepared by spiking drug free serum. Furthermore, to study the precision of the method, aliquots of pooled leftover serum from patients treated with leflunomide were analysed in fourfold determination in each series.

3. Results and discussion

Applying normalisation by post-column infusion, linear calibration functions were observed in all series ($r > 0.99$). Accuracy and imprecision was below 15% for the QC samples and the serum pool (Table 1).

In most cases, LC–MS/MS methods applying classical internal standardisation realise a clearly higher degree of accuracy and precision, however, the validation results were in accordance with the FDA guidelines for bioanalytical method validation [5]. Indeed, for a LC–MS/MS method employing isotope dilution internal standardisation for the quantification of HMR 1726 CVs $\leq$ 7.1% have been observed [4].

In five analyses among the total of 64 performed during our method validation, atypical ion suppression patterns – displayed by a low AUP – were observed in a sporadic manner. In these cases, both, the peak area and the AUP of the affected QC samples were substantially smaller compared to all other analyses of the same sample. This may be explained by concomitant elution of substances interfering with the processes of ionisation which have cumulated within the chromatographic system. Using the quantitative post-column infusion principle of normalisation we obtained results in accordance with the expected concentrations in all these five cases.

While post-column infusion of a solution of a target analyte is widely used in the context of the validation of LC–MS/MS methods with respect to ionisation modulation characteristics, the approach to use this set-up for normalisation of API signal generation *within*

Table 1
Results of the method validation study for the quantification of HMR 1726 in serum by LC–MS/MS applying the principle of continuous post-column infusion for normalisation of the efficacy of atmospheric pressure ionisation (fourfold determination in four series).

	Accuracy (%; mean)	Inter-assay imprecision (CV %)
15.8 μg/l (QCL)	112.7	14.9%
88.2 μg/l (QCM)	110.4	14.0%
180 μg/l (QCH)	102.3	7.2%
Pool (mean 33.5 μg/l)	–	10.5%

analytical is novel. Two previous articles report methods also aiming to realise real-time signal normalisation in LC–MS/MS: Stahnke et al. [6] have reported a similar instrument configuration; in this method, however, not a solution of the target analyte itself but instead one single solution of an unrelated compound was infused for the generation of a reference signal in the analysis of more than 100 different pesticides. Since the modulation of ion generation by matrix compounds or ion source related factors can be highly analyte-specific, we assume that our approach – based on continuous infusion of a solution of the *actual* target analyte – might be more reliable. Kaufmann and Butcher [7] describe superimposition of analyte spikes during chromatography which is technically far more demanding compared to the technology described here.

In the test reported here we used a syringe pump and a T-piece tube connection set-up in order to obtain a continuous introduction of the analyte to the ion source. This is also applicable in gradient methods; in the case of isocratic chromatographic systems, alternatively, the target analyte can as well simply be added to the mobile phase allowing a very simple configuration.

At present, an evident shortcoming of our normalisation approach is the fact that positioning of the integration lines and construction of integration areas has to be performed "manually" in the software system. Inclusion of this post-column-infusion monitoring/normalisation principle into MS/MS-quantification software solutions with calculation of the AUP seems desirable. In order to obtain good reproducibility of the AUP it is essential that the chromatographic performance is stable and in particular that any peak tailing is constant.

It must be noted that the principle described in this article cannot equalise between-sample variation of autosampler injection volume or of pre-ionisation analyte extraction procedures like solid phase extraction; only the ionisation process of a LC–MS/MS method can be monitored and normalised by this principle. Thus the availability of a related compound to be used as a "classical" internal standard which undergoes the entire analytical process including chromatographic separation certainly remains desirable for any analyte. However, autosampler precision is very high in many systems, so that the application of our principle also seems potentially applicable for clinical and biomedical research analyses in cases where all available candidate internal standard compounds are actually found to be inappropriate.

We have described in this article the *proof-of-concept* for a novel approach which can be useful for the monitoring and normalisation of between sample variations in the ionisation efficacy of LC-API–MS. Our evaluation results and experiences justify further validation of this approach for different analytes and the development of appropriate software solutions for application of this principle also in a routine setting. Further work will have to address the suitability of the approach described herein also in multi-analyte methods and over extended calibration concentration ranges. Furthermore a potential impact of this technology on the analytical sensitivity in trace concentration ranges has to be assessed. However, the principle may probably help to increase the reliability of LC–MS/MS analyses of "orphan" analytes for which appropriate IS compounds are not available. This may include entirely new compounds in the context of drug development, new illicit drugs in clinical toxicology but also endogenous compounds addressed in the development of innovative "metabolomic" multimethods.

Appendix A. Supplementary data

Supplementary data associated with this article can be found, in the online version, at http://dx.doi.org/10.1016/j.jpba.2012.03.055.

References

[1] M. Vogeser, C. Seger, Pitfalls associated with the use of liquid chromatography–tandem mass spectrometry in the clinical laboratory, Clin. Chem. 56 (2010) 1234–1244.
[2] T.M. Annesley, Ion suppression in mass spectrometry, Clin. Chem. 49 (2003) 1041–1044.
[3] F. Behrens, M. Koehm, H. Burkhardt, Update 2011: leflunomide in rheumatoid arthritis – strengths and weaknesses, Curr. Opin. Rheumatol. 23 (2011) 282–287.
[4] H. Rakhila, T. Rozek, A. Hopkins, S. Proudman, L. Cleland, M. James, M. Wiese, Quantitation of total and free teriflunomide (A77 1726) in human plasma by LC–MS/MS, J. Pharmaceut. Biomed. Anal. 55 (2011) 325–331.
[5] US Department of Health and Human Services. Guidance for industry – bioanalytical method validation. Food and Drug Administration, Center for Drug Evaluation and Research, 2001.
[6] H. Stahnke, T. Reemtsma, L. Alder, Compensation of matrix effects by postcolumn infusion of a monitor substance in multiresidue analysis with LC–MS/MS, Anal. Chem. 81 (2009) 2185–2192.
[7] A. Kaufmann, P. Butcher, Segmented post-column addition; a concept for continuous response control of liquid chromatography/mass spectrometry peaks affected by signal suppression/enhancement, Rapid. Commun. Mass. Spectrom. 19 (2005) 611–617.

Journal of Pharmaceutical and Biomedical Analysis 66 (2012) 402–410

Contents lists available at SciVerse ScienceDirect

Journal of Pharmaceutical and Biomedical Analysis

journal homepage: www.elsevier.com/locate/jpba

Identification of the components of bitespiramycin by liquid chromatography–mass spectrometry

Ming-juan Wang[a,b], Jing Xue[a], Wen-bo Zou[a], Yan Wang[a], Chang-qin Hu[a,*], Jos Hoogmartens[b], Erwin Adams[b]

[a] Department of Antibiotics, National Institutes for Food and Drug control, Beijing 100050, PR China
[b] Katholieke Universiteit Leuven, Faculteit Farmaceutische Wetenschappen, Laboratorium voor Farmaceutische Analyse, O&N2, PB 923, Herestraat 49, B-3000 Leuven, Belgium

ARTICLE INFO

Article history:
Received 21 December 2011
Received in revised form 7 March 2012
Accepted 8 March 2012
Available online 15 March 2012

Keywords:
Liquid chromatography–mass spectrometry
Bitespiramycin
Component identification
Macrolide antibiotics

ABSTRACT

Reversed-phase liquid chromatography coupled with electrospray ionization tandem mass spectrometry (LC/ESI-MS/MS) was used to characterize the components of bitespiramycin, a group of 4″-acylated spiramycins produced by bioengineered strains. In total 38 components were characterized in commercial samples, including 12 impurities that had never been reported before and 12 other that were partially characterized. The structures of these unknown compounds were deduced by comparison of their fragmentation patterns with those of known major components. Their ultraviolet spectra were used to confirm the presence of an α-, β-, γ-, δ-unsaturated butadiene in the macrocyclic lactone. Compared with the classical method, LC/ESI-MS/MS is particularly advantageous in terms of sensitivity and efficiency to characterize minor components at trace levels in multi-component antibiotics.

© 2012 Elsevier B.V. All rights reserved.

1. Introduction

Bitespiramycin (former name: shengjimycin complex) is produced by the bioengineered strain WSJ-1 (Institute of Medicinal Biotechnology, Chinese Academy of Medical Sciences & Peking Union Medical College, Beijing), which was obtained by integrating the 4″-*O*-acyltransferase gene to a spiramycin (SPM)-producing strain. Since the 4″-*O*-acyltransferase lacks specificity to substrates, the products formed are a group of 4″-acylated SPMs. Besides the major components (4″-isovaleryl SPM III/II/I, 4″-butyryl/isobutyryl SPM II/III, 4″-propionyl SPM II/III, 4″-acetyl SPM II/III), several minor components (including SPM III, II, neo-SPM III, 4″-(3-methyl-2-butenoyl) SPM III, deforosaminyl 4″-isovaleryl SPM III) were also isolated and structurally identified [1–7]. Their structures are shown in Fig. 1.

Some scientific literature exists on the separation and identification of active components of this kind of macrolide antibiotics [1–9,11–18]. The mass spectra of these macrolides revealed that the fragile positions were the hydroxyls linked to the glycosides at positions 5 and 9, forming aglycone (AG) moieties at *m/z* 349 (SPM I and its derivatives), 391 (SPM II and its derivatives), or 405 (SPM III and its derivatives). Neutral losses of mycarose (−144 u) or acylated mycarose (−186/200/214/228 u, corresponding to 4″-acetyl/propionyl/(iso)butyryl/isovaleryl, respectively) and forosamine (−159 u) yielded AG-mycaminose moieties. The presence of the characteristic disaccharide ion with *m/z* 360, 374, 388 or 402 would further reveal that the 4″-*O*-substituent was acetyl, propionyl, butyryl/isobutyryl or isovaleryl, respectively. In some cases, doubly protonated ions of SPMs derivatives were also observed [8,11,12,15].

Though main components in bitespiramycin have been identified [1–7,15], most of its minor components are still unknown. To ensure the safety of commercial bitespiramycin, it is necessary to characterize as much as possible impurities. The aim of this work is to identify the unknown compounds in commercial bitespiramycin samples by liquid chromatography coupled with ion trap mass spectrometry, using the spectra of the major components as templates. The chromatographic properties of known components in bitespiramycin are also reported to illustrate the retention behavior of macrolide antibiotics in reversed-phase high-performance liquid chromatography (RP-HPLC), which will be helpful in identifying the structures of unknown impurities and confirming the proposed structures.

2. Experimental

2.1. Reagent and samples

HPLC-grade acetonitrile was obtained from Fisher Scientific (Fairlawn, NJ, USA). Analytical grade ammonium acetate was

* Corresponding author. Tel.: +86 10 67095308; fax: +86 10 65115148.
E-mail address: hucq@nicpbp.org.cn (C.-q. Hu).

0731-7085/$ – see front matter © 2012 Elsevier B.V. All rights reserved.
doi:10.1016/j.jpba.2012.03.013

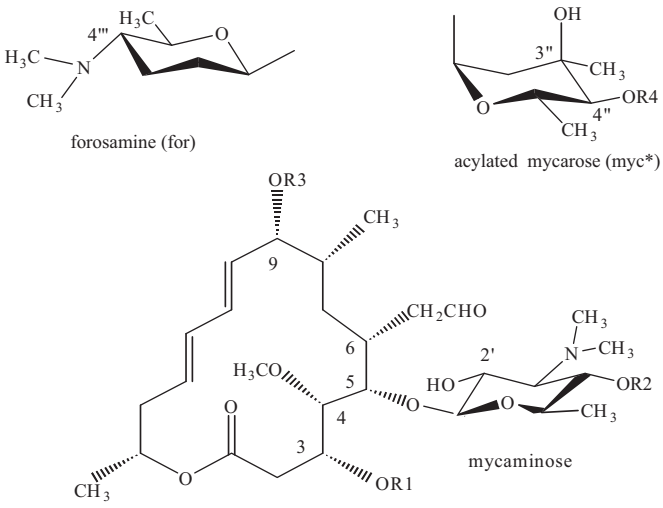

Components	R1	R2	R3	R4	$[M+H]^+$	Peak No.
4″-isovaleryl SPM III	$COCH_2CH_3$	myc[a]	for	$COCH_2CH(CH_3)_2$	983.7	20
4″-isovaleryl SPM II	$COCH_3$	myc[a]	for	$COCH_2CH(CH_3)_2$	969.7	17
4″-isovaleryl SPM I	H	myc[a]	for	$COCH_2CH(CH_3)_2$	927.6	14
4″- (iso)butyryl SPM III	$COCH_2CH_3$	myc[a]	for	COC_3H_7[b]	969.7	16
4″- (iso)butyryl SPM II	$COCH_3$	myc[a]	for	COC_3H_7[b]	955.6	13
4″-propionyl SPM III	$COCH_2CH_3$	myc[a]	for	$COCH_2CH_3$	955.6	12
4″-propionyl SPM II	$COCH_3$	myc[a]	for	$COCH_2CH_3$	941.7	9
4″-acetyl SPM III	$COCH_2CH_3$	myc[a]	for	$COCH_3$	941.7	8
4″-acetyl SPM II	$COCH_3$	myc[a]	for	$COCH_3$	927.5	6
SPM III	***$COCH_2CH_3$***	***myc***	***for***	***H***	***899.7***	***4***
SPM II	***$COCH_3$***	***myc***	***for***	***H***	***885.5***	***3***
SPM I	***H***	***myc***	***for***	***H***	***843.5***	***ND***
4″-(3-methyl-2-butenoyl) SPM II	***$COCH_3$***	***Myc[a]***	***for***	***$COCH=C(CH_3)_2$***	***967.5***	***15***
neo-SPM III	***$COCH_2CH_3$***	***H***	***for***	***/***	***755.8***	***1***
deforosaminyl 4″-isovaleryl SPM III	***$COCH_2CH_3$***	***myc[a]***	***H***	**$COCH_2CH(CH_3)_2$**	***842.5***	***13***

([a] Refers to acylated mycarose;

[b] R4 may have two possible forms: 4″-butyryl ($COCH_2CH_2CH_3$) or isobutyryl ($COCH(CH_3)_2$), both of which are reported in literature;

ND = Not detected

Known minor components in bitespiramycin are reported in boldface, italic form;

Fig. 1. Chemical structures of bitespiramycin major components and some known minor components.

supplied by Merck (Darmstadt, Germany). A milli-Q water purification system (Millipore, USA) was used to further purify glass-distilled water. Bitespiramycin samples examined (batch no: 200906001, 200906002, 200906003) were obtained from Shenyang Antibiotic Factory (Liaoning, China).

2.2. Instrumentation

The liquid chromatography–mass spectrometry (LC–MS) system consisted of a 3201 S1-2 binary pump, a 3202 S1-2 vacuum degasser, a 3014 S1-2 column heater, a 3012 S1-2 column switch system, a 3133 S1-2 sampler from SHISEIDO (Tokyo, Japan), an Accela PDA detector (Thermo Fisher Scientific Inc., Massachusetts, USA) and a 3200Q TRAP mass detector (Applied Biosystem Inc., California, USA), controlled by Analyst® software (version 1.4.2).

2.3. Chromatographic conditions

A mobile phase containing acetonitrile 10 mmol L^{-1} ammonium acetate (50:50, v/v) was used at a flow rate of 0.5 mL min^{-1}. The CAPCELL PAK C_{18} column (type: MG III, size: 150 mm × 2.0 mm i.d., 5 μm) (Shiseido, Japan) was maintained at 35 °C. Samples were prepared in a mixture of acetonitrile and water (50:50, v/v) at a concentration of about 1.0 mg mL^{-1}. The injection volume was 20 μL. Ultraviolet detection was performed from 200 to 400 nm (extraction: 232 nm).

2.4. Mass spectrometry

Tuning and MS/MS investigation of bitespiramycin major components (4″-isovaleryl SPM II/III) were carried out according to the manufacturer's instruction. The optimized mass spectrometric conditions were as follows: electrospray ionization (EPI) positive ionization mode, declustering potential (DP) 50, entrance potential (EP) 10, collision energy (CE) 40, curtain gas: 20.0, ion source gas 1: 65.0, ion source gas 2: 60.0, ion spray voltage (IS): 5500.0, temperature (TEM): 500.0, interface heater: on. The acquisition of the first-order mass spectra (Q1 scan) was from 500 to 1100 u. The ions of interest were isolated in the ion trap and activated at CE of 40 to get enhanced product ion (EPI) spectra in the range of 200–1000 u. Each protonated molecule $[M+H]^+$ was confirmed based on our previous studies [11] and literature data [15,18]. The presence of minor adduct ions of $[M+Na]^+$and $[M+K]^+$ will further confirm each $[M+H]^+$. In the case of peaks containing multiple components, the "precursor Ion (Prec)" method of Analyst® software was used to confirm the individual protonated molecule.

3. Results and discussion

3.1. Development of the LC/MS method

Based on Ref. [11], the system using 10 mmol L^{-1} ammonium acetate–acetonitrile was selected for separation of the bitespiramycin complex. Two brands of C_{18} columns (Extend C_{18} column (150 mm × 4.6 mm i.d., 5 μm) [11] and CAPCELL PAK C_{18} column (type: MG III, size: 150 mm × 2.0 mm i.d., 5 μm) [13]) were evaluated. The CAPCELL PAK C_{18} column gave better results in terms of peak shape and separation.

To improve the separation, the parameters, such as pH value, concentration of buffer solution and type and percentage of organic modifier, were investigated. Separation improved at basic pH, but this increased the retention time (more than 120 min for 4″-isovaleryl spiramycin III) and reduced the sensitivity of the MS detector. Using an acidic mobile phase, the separation was poorer. Therefore, the pH of the ammonium acetate solution was not adjusted. Higher concentrations of ammonium acetate gave a somewhat better separation, but to ensure complete volatility of the mobile phase, its final concentration was kept at 10 mmol L^{-1}. Methanol was also evaluated as organic modifier, but due to the presence of the $[M+CH_3OH+H]^+$ adduct, which reduces the abundance of the ions of interest, acetonitrile was finally selected. Though some peaks in the total ion chromatogram (TIC) consisted of more than two components (see Section 3.3), the final LC–MS method is acceptable since MS has additional separation capability. At least 27 peaks were detected by both the diode array detector (DAD) and MS detector, including impurities at the 0.1% level. Typical LC–UV–TIC chromatograms of a commercial sample are shown in Fig. 2.

3.2. Fragmentation pathway and chromatographic behavior of known components

3.2.1. Fragmentation pathway of known components

In accordance with other macrolide antibiotics [8,11–14], most product ions of major components in bitespiramycin were formed by cleavage of glycosidic bonds, as shown in Fig. 3. The neutral losses of 159 u, 186/200/214/228 u and 191 u correspond to the cleavage of forosamine at C-9 (product ion: F1), 4″-acetyl/propionyl/(iso)butyryl/isovaleryl mycarose (product ion: F2) and mycaminose (product ion: F5) at C-5, respectively. Product ion F3 originates by the loss of both forosamine and acylated mycarose. Further fragmentation of the aglycone ion (F5) with *m*/*z* 349 (SPM I and its derivatives), 391 (SPM II and its derivatives) or 405 (SPM III and its derivatives) was the same as described by Pendela et al. for SPM I, II or III [12]. The presence of the characteristic disaccharide ion (F4) with *m*/*z* 360, 374, 388 or 402 further confirmed that the 4″-acylated substituent group was acetyl, propionyl, butyryl/isobutyryl or isovaleryl, respectively [11–13]. No obvious doubly protonated molecules of SPMs derivatives were observed under the experimental conditions used.

The MS/MS spectra of known minor components, i.e. 4″-(3-methyl-2-butenoyl) SPM II, deforosaminyl 4″-isovaleryl SPM III (platenomycin), neo-SPM III and SPM III/II (see Fig. 1 for their structures) show similar fragmentation pathways, as demonstrated in Fig. 3. For example, in case of 4″-(3-methyl-2-butenoyl) SPM II, since its 4″-substituent is —COCH=C$(CH_3)_2$ (2 u less than 4″-isovaleryl (—$COCH_2CH(CH_3)_2$), the neutral loss of its acylated mycarose is 226 u instead of 228 u and the corresponding disaccharide ion is at *m*/*z* 400 instead of 402. For deforosaminyl 4″-isovaleryl SPM III, due to lack of forosamine, the MS/MS spectrum has no apparent F1 product ion and its consecutive neutral losses correspond to 4″-isovaleryl mycarose (−228 u), the hydroxyl group at C-9 (−18 u) and mycaminose (−191 u). The presence of the disaccharide ion at *m*/*z* 402 further confirms that its 4″-substituent is isovaleryl. The MS/MS spectra of neo-SPM III and SPM III/II were the same as in literature [8,11–14].

3.2.2. Chromatographic behavior of known components

The retention behavior of the components of the bitespiramycin complex can be linked to their hydrophobic properties (Figs. 1 and 2): the more hydrophobic the R1 or R2 substituent, the longer the retention time (RT). For example, $RT_{(4''\text{-isovaleryl SPM III})} > RT_{(4''\text{-isovaleryl SPM II})} > RT_{(4''\text{-isovaleryl SPM I})}$, and $RT_{(4''\text{-isovaleryl SPM III})} > RT_{(4''\text{-(iso) butyryl SPM III})} > RT_{(4''\text{-propionyl SPM III})} > RT_{(4''\text{-acetyl SPM III})} > RT_{(\text{SPM III})}$. It was also found that the influence of 4″-acylated mycarose on the chromatographic behavior of the bitespiramycin components was larger than that of R1 of the macrocyclic lactone or forosamine. For example, $RT_{(4''\text{-isovaleryl SPM II})} > RT_{(4''\text{-(iso) butyryl SPM III})}$, $RT_{(4''\text{-(iso) butyryl SPM II})} > RT_{(4''\text{-propionyl SPM III})}$, $RT_{(4''\text{-propionyl SPM II})} > RT_{(4''\text{-acetyl SPM III})}$, indicated that the RTs of bitespiramycin components were more influenced by the R2

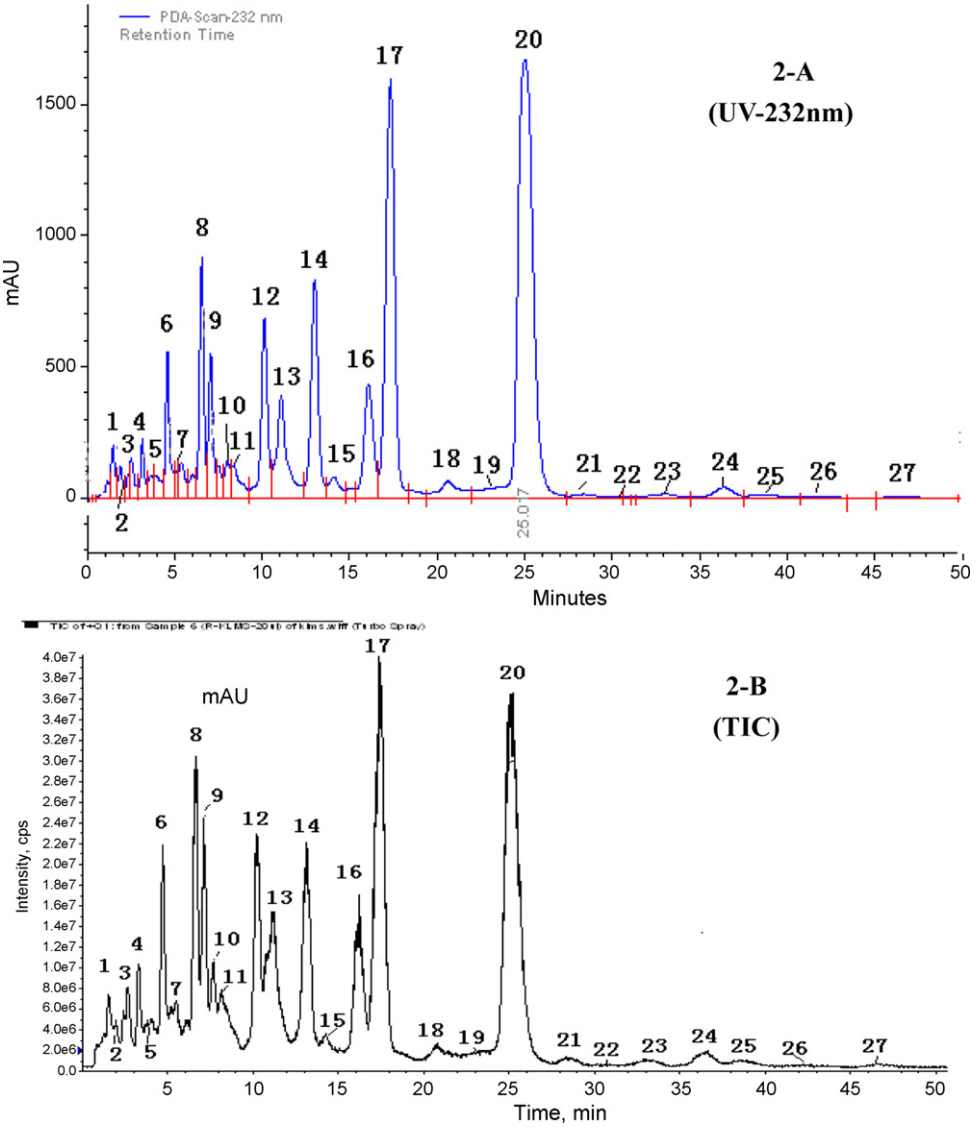

Fig. 2. Typical LC-UV and TIC-chromatograms of a commercial bitespiramycin sample. Column: CAPCELL PAK C_{18} column (type: MG III, size: 150 mm × 2.0 mm i.d., 5 μm), maintained at 35 °C. Mobile phase: acetonitrile 10 mM ammonium acetate solution (50:50, v/v). Flow rate: 0.5 mL min^{-1}. Sample concentration: ~1.0 mg mL^{-1}. Injection volume: 20 μL. For peak identification of known peaks, see Fig. 1.

group of the acylated mycarose than by the R1 substituent of the macrocyclic lactone. By comparison of the retention behavior of deforosaminyl 4″-isovaleryl SPM III (peak 13) and neo-SPM III (lack of acylated mycarose, peak 1), it could be found that the effect of acylated mycarose on the RTs was much greater than that of forosamine. Similar retention behavior was also observed in acetylspiramycin components: the RTs of leucomycin A8 (8.1 min) and meleumycin B2 (10.8 min) (lack of forosamine) were much longer than those of neo-SPM II (2.8 min) and III (3.5 min) [13].

The chromatographic behavior of known components can be very helpful to confirm the proposed structures of unknown related substances. For example, 3-*O*-butanoyl 4″-isovaleryl SPM ($[M+H]^+$ *m*/*z* 997.8) in peak 24 and 4″-(iso)hexanoyl SPM III ($[M+H]^+$ *m*/*z* 997.8) in peak 25 have a longer carbon chain substituent either at the 3-position of the macrocyclic lactone (3-*O*-butanoyl 4″-isovaleryl SPM) or at the 4″-position of the acylated mycarose (4″-(iso) hexanoyl SPM III) than 4″-isovaleryl SPM III ($[M+H]^+$ *m*/*z* 983.7) in peak 20 and both the former have longer RTs. Meanwhile, $RT_{(4''\text{-(iso)hexanoyl SPM III})} > RT_{(3\text{-}O\text{-butanoyl 4''-isovaleryl SPM})}$ confirms that the R2 group of the acylated mycarose has more influence on the RTs of bitespiramycin components than the R1 substituent of the macrocyclic lactone. All the above results are well consistent with their proposed structures elucidated by LC/ESI-MS/MS (see Sections 3.3.2 and 3.3.4, respectively).

3.3. Investigation of unknown components in commercial bitespiramycin samples

Three commercial samples from the same origin were screened for unknown components. The similarity of the different batches indicated that the production process was repeatable. Based on the fragmentation behavior of known bitespiramycin components (Fig. 3), the unknown components were further investigated by LC–MS.

As bitespiramycin is a group of hybrid antibiotics produced by a bioengineered strain, its related substances may arise from the fermentation process. Identification of unknown components in commercial samples was discussed based on their structural differences compared to the major components. The characterization results are summarized in Table 1. The proposed structures of 12 new related substances that had never been reported before are

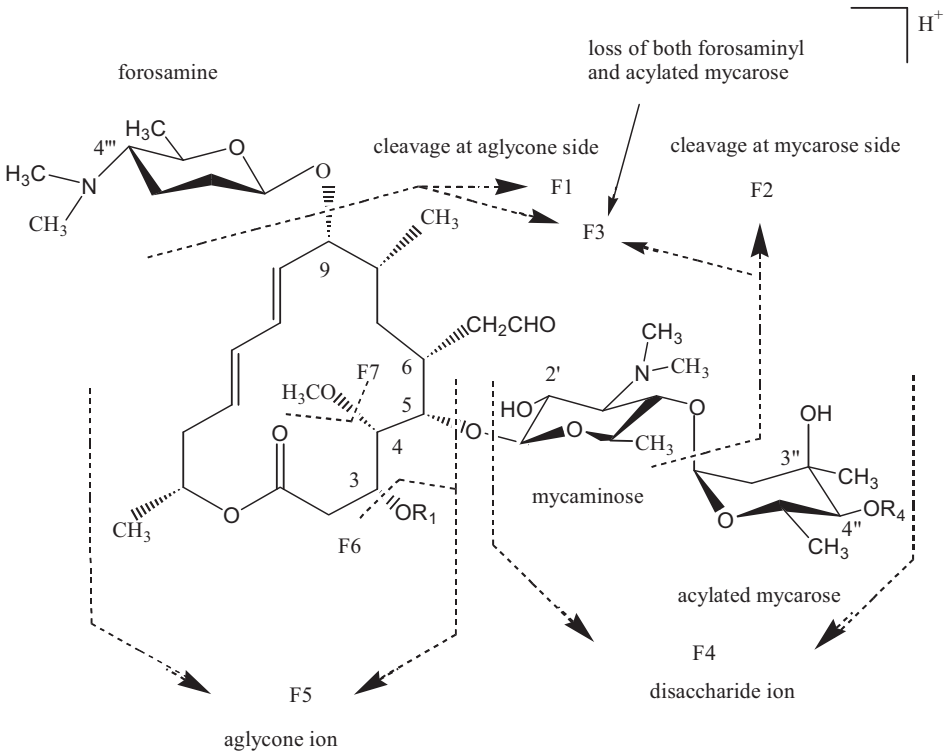

Components	$[M+H]^+$	F1	F2	F3	F4	F5	F6	F7
4″-isovaleryl SPM III	983.7	824.5	755.6	596.5	402.7	405.4	331.3	299.3
4″-isovaleryl SPM II	969.7	810.5	741.4	582.4	402.7	391.4	331.3	299.3
4″-isovaleryl SPM I	927.6	768.8	699.6	540.6	402.7	349.5	331.3	299.3
4″- (iso)butyryl SPM III	969.7	810.5	755.5	596.4	388.3	405.3	331.3	299.3
4″- (iso)butyryl SPM II	955.6	796.7	741.7	582.6	388.3	391.4	331.3	299.3
4″-propionyl SPM III	955.6	796.6	755.7	596.6	374.5	405.5	331.3	299.3
4″-propionyl SPM II	941.7	782.7	741.7	582.6	374.6	391.5	331.3	299.3
4″-acetyl SPM III	941.5	782.7	755.8	596.6	360.5	405.4	331.3	299.3
4″-acetyl SPM II	927.5	768.6	741.7	582.6	360.4	391.5	331.3	299.3
4″-(3-methyl-2-butenoyl) SPM II	*967.5*	*808.4*	*741.5*	*582.4*	*400.3*	*391.3*	*331.3*	*299.3*
neo-SPM III	*755.8*	*596.5*	*/*	*596.5*	*/*	*405.4*	*331.3*	*299.3*
deforosaminyl 4″-isovaleryl SPM III	*842.5*	*/*	*614.5*	*596.4*	*402.4*	*405.4*	*331.4*	*299.3*
SPM III	*899.6*	*740.6*	*755.6*	*596.5*	*318.4*	*405.5*	*331.4*	*299.3*
SPM II	*885.5*	*726.4*	*741.6*	*582.4*	*318.3*	*391.4*	*331.4*	*299.3*

Fig. 3. Fragmentation pathway of known bitespiramycin components. (Known minor components in bitespiramycin are written in italic.)

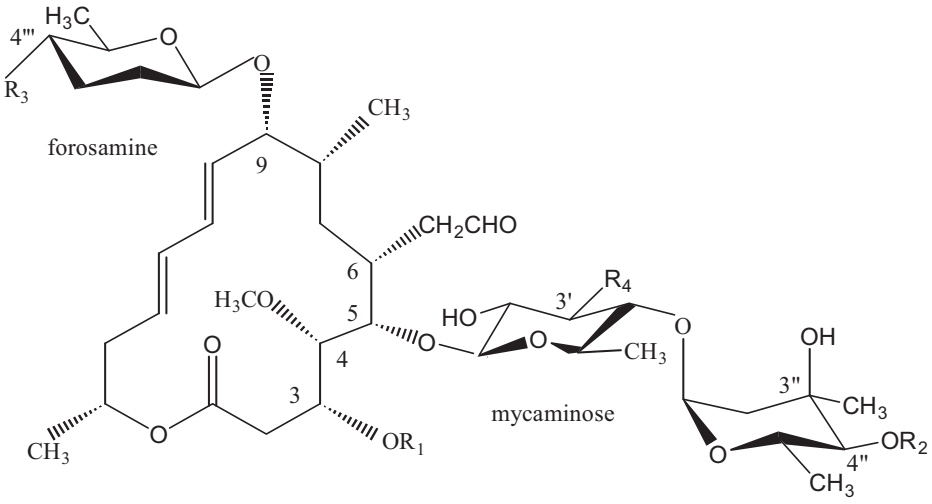

Identication (Peak No[a])	R1	R2	R3	R4
4″-propionyl SPM I (peak 7)	H	$COCH_2CH_3$	$-N(CH_3)_2$	$-N(CH_3)_2$
4″- (iso)butyryl SPM I (peak 10)	H	$COCH_2CH_2CH_3$	$-N(CH_3)_2$	$-N(CH_3)_2$
	H	$COCH(CH_3)_2$	$-N(CH_3)_2$	$-N(CH_3)_2$
4"-(iso)hexanoyl SPM II (peak 21)	$COCH_3$	COC_5H_{11} [b]	$-N(CH_3)_2$	$-N(CH_3)_2$
4"-(iso)hexanoyl SPM III (peak 25)	$COCH_2CH_3$	COC_5H_{11} [b]	$-N(CH_3)_2$	$-N(CH_3)_2$
4"- acryl SPM III (peak 22)	$COCH_2CH_3$	$COCH=CH_2$	$-N(CH_3)_2$	$-N(CH_3)_2$
4″-(3-methyl-2-butenoyl) SPM III (peak 18)	$COCH_2CH_3$	$COCH=C(CH_3)_2$	$-N(CH_3)_2$	$-N(CH_3)_2$
3-*O*-butanoyl-4″-isovaleryl SPM (peak 24)	$COCH_2CH_2CH_3$	$COCH_2CH(CH_3)_2$	$-N(CH_3)_2$	$-N(CH_3)_2$
3,4-anhydro-4″-isovaleryl SPM I (peak 23)	– [c]	$COCH_2CH(CH_3)_2$	$-N(CH_3)_2$	$-N(CH_3)_2$
4‴-*N*-demethyl-4″-acetyl SPM III (peak 3)	$COCH_2CH_3$	$COCH_3$	$-NHCH_3$	$-N(CH_3)_2$
4‴-*N*-demethyl-4″-propionyl SPM III (peak 5)	$COCH_2CH_3$	$COCH_2CH_3$	$-NHCH_3$	$-N(CH_3)_2$
4‴-*N*,*N*-didemethyl-4″-isovaleryl SPM II (peak 7)	$COCH_3$	$COCH_2CH(CH_3)_2$	$-NH_2$	$-N(CH_3)_2$
4‴-*N*-demethyl-4″-isovaleryl SPM II (peak 8)	$COCH_3$	$COCH_2CH(CH_3)_2$	$-NHCH_3$	$-N(CH_3)_2$

[a] Refer to Fig. 2 for the peak numbers.

[b] R2 substituent has seven possible forms: $-CO(CH_2)_4CH_3$, $-COC(CH_3)_2CH_2CH_3$, $-COCH_2C(CH_3)_3$, $-COCH(CH_3)CH(CH_3)_2$, $-COCH_2CH(CH_3)CH_2CH_3$, $-COCH_2CH_2CH(CH_3)_2$, $-COCH(CH_3)CH_2CH_2CH_3$.

[c] Lacks the R1 substituent and has a double bond between C-3 and C-4. The stereochemistry will change correspondingly.

Fig. 4. Proposed structures for the related substances characterized in this work.

Table 1
List of bitespiramycin major components and its related substances in commercial samples.

Peak no.[a]	$[M+H]^+$	Identification	Structure	Comment
1	755.8	Neo-SPM III	Fig. 1	Known minor component
2		Unknown		
3	885.5	SPM II	Fig. 1	Known minor component
	927.5	Isomer 1 of 4″-acetyl SPM II		
	927.5	4‴-*N*-demethyl-4″-acetyl SPM III	Fig. 4	
4	899.6	SPM III	Fig. 1	Known minor component
5	941.5	Isomer 1 of 4″-acetyl SPM III		
	941.5	4‴-*N*-demethyl-4″-propionyl SPM III	Fig. 4	
6	**927.5**	**4″-Acetyl SPM II**	Fig. 1	**Major component**
7	955.5	Isomer 1 of 4″-propionyl SPM III		
	955.5	Isomer 1 of 4″-(iso)butyryl SPM II	Fig. 4	
	941.5	4‴-*N*, *N*-didemethyl-4″-isovaleryl SPM II	Fig. 4	
	941.5	Isomer 2 of 4″-acetyl SPM III		
	899.6	4″-Propionyl SPM I	Fig. 4	
8	**941.5**	**4″-Acetyl SPM III**	Fig. 1	**Major component**
	955.6	4‴-*N*-demethyl-4″-isovaleryl SPM II	Fig. 4	
9	**941.5**	**4″-Propionyl SPM II**	Fig. 1	**Major component**
10	913.6	4″-(Iso)butyryl SPM I	Fig. 4	
11	955.5	Isomer 2 of 4″-(iso)butyryl SPM II		
	955.5	Isomer 2 of 4″-propionyl SPM III		
12	**955.6**	**4″-Propionyl SPM III**	Fig. 1	**Major component**
13	**955.6**	**4″-(Iso)butyryl SPM II**	Fig. 1	**Major component**
	842.5	Deforosaminyl 4″-isovaleryl SPM III	Fig. 1	Known minor component
14	**927.6**	**4″-Isovaleryl SPM I**	Fig. 1	**Major component**
15	967.5	4″-(3-Methyl-2-butenoyl) SPM II	Fig. 1	Known minor component
16	**969.7**	**4″-(Iso)butyryl SPM III**	Fig. 1	**Major component**
17	**969.7**	**4″-Isovaleryl SPM II**	Fig. 1	**Major component**
18	981.6	4″-(3-Methyl-2-butenoyl) SPM III	Fig. 1	
19	984.1	Isomer 1 of 4″-isovaleryl SPM III		
20	**983.7**	**4″-Isovaleryl SPM III**	Fig. 1	**Major component**
21	909.6	4″-Isovaleryl SPM I with an aberrant mycaminose (173 u)		
	983.7	4″-(Iso)hexanoyl SPM II	Fig. 4	
	983.7	Isomer 2 of 4″-isovaleryl SPM III		
22	953.7	4″-Acryl SPM III	Fig. 4	
23	909.6	3,4-Anhydro-4″-isovaleryl SPM I	Fig. 4	
24	913.6	4″-Isovaleryl SPM4 with an aberrant macrocylic lactone (*m*/*z* 335)[b]		
	997.8	3-*O*-butanoyl 4″-isovaleryl SPM	Fig. 4	
25	997.8	4″-(Iso)hexanoyl SPM III	Fig. 4	
26		Unknown		
27	955.8	4″-Isovaleryl SPM with an aberrant macrocylic lactone (*m*/*z* 395) and an aberrant mycaminose (173 u)[c]		

Bold indicates major components.
[a] Refer to Fig. 2 for the peak numbers.
[b] The *m*/*z* value of the aberrant macrocyclic lactone is 4 u higher than 3, 4-anhydro macrocylic lactone.
[c] The molecular weight of the aberrant macrocylic lactone is 4 u higher than SPM II and its neutral loss of the aberrant mycaminose corresponds to 173 u.

shown in Fig. 4. Twelve other components (most are isomers) were partially characterized.

3.3.1. *Isomers of major components and derivatives of SPM I*

As observed in other macrolide antibiotics [10–13], isomers of the major components with same *m*/*z* values and similar product ions were also found in bitespiramycin, e.g. isomer of 4″-acetyl SPM II in peak 3, isomers of 4″-acetyl SPM III in peaks 5 and 7, isomers of 4″-propionyl SPM III in peaks 7 and 11, isomers of 4″-(iso)butyryl SPM II in peaks 7 and 11 and isomers of 4″-isovaleryl SPM III in peaks 19 and 21, respectively. Most of them co-eluted with other components. However, positional isomers and even spatial isomers cannot be distinguished by LC/MS only. Further nuclear magnetic resonance (NMR) experiments are necessary to confirm their exact structures.

Besides 4″-isovaleryl SPM I, other SPM I derivatives were also observed, including 4″-propionyl SPM I in peak 7 and 4″-(iso)butyryl SPM I in peak 10, which formed by fragmentation the aglycone ion F5 (see Fig. 3) at *m*/z 349 and had characteristic ions at *m*/*z* 331 (F6), 299 (F7) and 281, indicating that they were derivatives of SPM I. The neutral losses of 4″-propionyl SPM I and 4″-(iso)butyryl SPM I were 159 u, 200/214 u and 191 u, demonstrating the presence of forosamine, 4″-propionyl/(iso)butyryl mycarose and mycaminose, respectively.

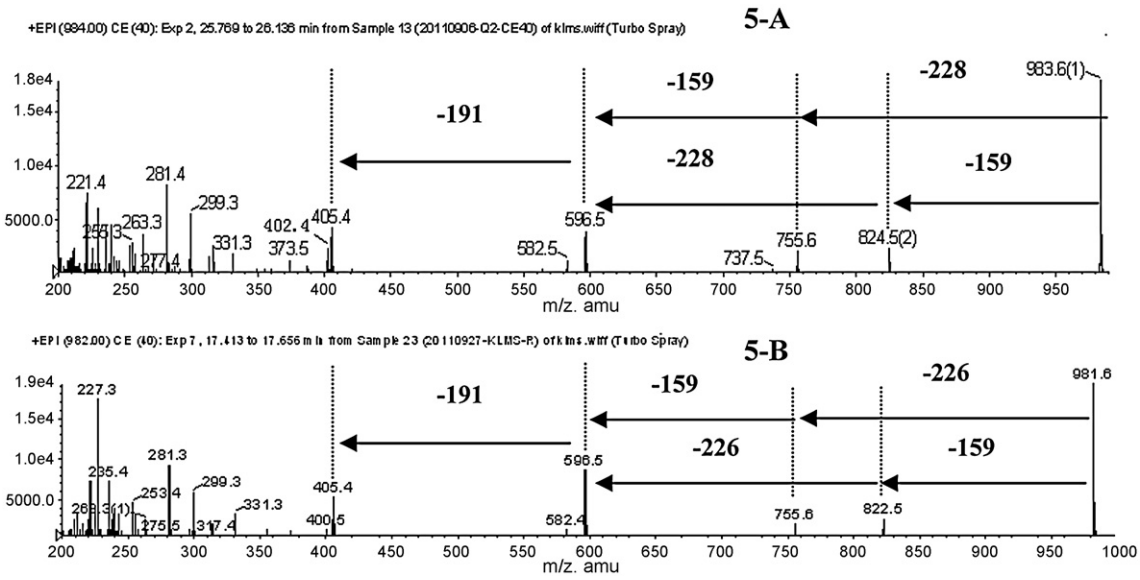

Fig. 5. Comparison of MS/MS spectra of 4″-isovaleryl SPM III (5-A, *m*/*z* 983.6) and 4″-(3-methyl-2-butenoyl) SPM III (5-B, *m*/*z* 981.6).

3.3.2. Unknown compounds with different 4″-substituent

Since the 4″-*O*-acyltransferase lacks specificity to substrates, the products formed are a group of hybrid antibiotics. Besides 4″-isovaleryl, 4″-(iso)butyryl, 4″-propionyl, 4″-acetyl SPM II/III, other 4″-substituent derivatives were also observed: (I) 4″-(iso)hexanoyl SPM II and III in peaks 21 and 25, respectively, whose neutral losses of acylated mycarose were both 242 u, 14 u higher than those of 4″-isovaleryl SPM II/III, while the presence of the disaccharide ion at *m*/*z* 416 further confirmed the proposed structure. (II) Similar to the known minor component 4″-(3-methyl-2-butenoyl) SPM II (Fig. 1), the protonated molecule of the compound in peak 18 ($[M+H]^+$ *m*/*z* 981.6), its neutral loss of acylated mycarose (226 u) and characteristic disaccharide ion at *m*/*z* 400.3 were all 2 u less than those of 4″-isovaleryl SPM III (their MS/MS spectra are shown in Fig. 5). This indicated that the 4″-substituent was also 3-methyl-2-butenoyl ($-COCH{=}C(CH_3)_2$). (III) Similarly, the MS/MS spectrum of the compound in peak 22 ($[M+H]^+$ *m*/*z* 953.7) revealed the presence of 4″-acryl ($-COCH{=}CH_2$), which was confirmed by the neutral loss of acylated mycarose (198 u) and its corresponding disaccharide ion at *m*/*z* 372.4, which were both 2 u less than those of 4″-propionyl SPM III.

Other neutral losses of the above compounds (see (I)–(III)) were all 159 u and 191 u, which revealed that the forosamine and mycaminose sugars were normal. The aglycone ions at *m*/*z* 405 or 391 and corresponding characteristic ions at *m*/*z* 331 and 299 indicated that they were derivatives of SPM III or II.

3.3.3. Unknown components with aberrant forosamine sugar

Several impurities were observed with an aberrant forosamine sugar in the samples. For example, the MS/MS spectrum of a compound in peak 3 ($[M+H]^+$ *m*/*z* 927.5) was similar to that of 4″-acetyl SPM III, except for the initial loss corresponding to forosamine. Instead of 159 u, a loss of 145 u was observed, which indicated that the impurity had an aberrant forosamine sugar. For SPM, the difference of 14 u was attributed to a difference in the degree of methylation of the amino group [12]. Such impurities were also observed in acetylspiramycin [13]. So, the compound above was identified as 4‴-*N*-demethyl-4″-acetyl SPM III. Similarly, the impurities in peaks 5 ($[M+H]^+$ *m*/*z* 941.5) and 8 ($[M+H]^+$ *m*/*z* 955.6) were identified as 4‴-*N*-demethyl-4″-propionyl SPM III and 4‴-*N*-demethyl-4″-isovaleryl SPM II, which have aberrant forosamine sugars 14 u less than those of 4″-propionyl SPM III and 4″-isovaleryl SPM II, respectively. The compound in peak 7 ($[M+H]^+$ *m*/*z* 941.5) was identified as 4‴-*N*,*N*-didemethyl-4″-isovaleryl SPM II, whose fragmentation behavior was similar to that of 4″-isovaleryl SPM II, but its aberrant forosamine sugar was 28 u less.

3.3.4. Unknown components with aberrant macrocyclic lactone

One compound in peak 24 ($[M+H]^+$ *m*/*z* 997.8) was characterized as 3-*O*-butanoyl 4″-isovaleryl SPM. The loss of 88 u (corresponding to butanoic acid), 14 u higher than derivatives of SPM III, was observed at position C-3. Its protonated molecule and product ions F1, F2, F3 and F5 (Fig. 3) were all 14 u higher than those of 4″-isovaleryl SPM III, while F4 (disaccharide ion), F6 and F7 were the same, indicating the structural difference was located at C-3.

The protonated molecule of the compound in peak 23 ($[M+H]^+$ *m*/*z* 909.6) and its product ions F1, F2, F3 and F5 were all 18 u less than those of 4″-isovaleryl SPM I and further loss of water at C-3 was not observed. Based on the above observation and the literature [11–13], the compound was proposed to be 3,4-anhydro-4″-isovaleryl SPM I, which lacks the R1 substituent and has a double bond between C-3 and C-4 (3,4-anhydro). The stereochemistry will change accordingly.

The compound in peak 24 ($[M+H]^+$ *m*/*z* 913.6) was identified as 4″-isovaleryl SPM with an aberrant macrocyclic lactone (*m*/*z* 335): Its neutral losses were 159 u, 228 u and 191 u, which revealed the presence of forosamine, 4″-isovaleryl mycarose and mycaminose, respectively. The latter two sugars were confirmed by the *m*/*z* of the disaccharide ion at 402. However, its aglycone ion (F5) at *m*/*z* 335 and corresponding ions at *m*/*z* 303 and 285 were all 4 u more than those of the 3,4-anhydro macrocyclic lactone. Its UV spectrum showing maximum absorbance at 230 nm indicated the presence of an α-, β-, γ-, δ-unsaturated butadiene structure in the macrocyclic lactone. Further investigation will be needed to confirm the exact structure of the aberrant macrocyclic lactone (*m*/*z* 335).

The compound in peak 27 ($[M+H]^+$ *m*/*z* 955.8) was identified as 4″-isovaleryl SPM with an aberrant macrocyclic lactone (*m*/*z* 395) and an aberrant mycaminose (173 u): its neutral losses were 159 u, 228 u and 173 u, which revealed the presence of forosamine, 4″-isovaleryl mycarose and an aberrant mycaminose (173 u), respectively. And its aglycone ion (F5) at *m*/*z* 395 and corresponding ions at *m*/*z* 335 (F6), 303 (F7) and 285 were all 4 u more

than those of 4″-isovaleryl SPM II. The presence of an α-, β-, γ-, δ-unsaturated butadiene structure in the macrocyclic lactone was revealed by its UV maximum absorbance at 230 nm. To find out the details of aberration, other techniques will be needed. The proposed structure of the aberrant mycaminose (173 u) is discussed in Section 3.3.5.

3.3.5. Unknown components with aberrant mycaminose

One compound in peak 21 ($[M+H]^+$ m/z 913.6) was characterized as 4″-isovaleryl SPM I with an aberrant mycaminose (173 u). The latter might be the dehydrated form of mycaminose (191 u) or a modified form of forosamine (159 u) where one of the N-methyls was replaced by N-ethyl. To confirm the exact structure of the aberrant mycaminose (173 u) in peaks 21 and 27, other techniques, such as NMR, will be needed.

4. Conclusion

A powerful LC/MS method has been developed to characterize the minor components in bitespiramycin. Due to the high sensitivity of mass spectrometry, this method was particularly advantageous to detect impurities at trace levels in commercial bulk samples. In this work, besides 9 major components and 5 known minor components, 24 other minor components were found in commercial samples, including 12 new related substances that had never been reported before. It should be noted that because isomer structures could not be distinguished by LC/MS, the other 12 were only partially characterized and need further investigation by other techniques, such as NMR. However, due to their low amount and the fact that the impurities cannot be easily purified, NMR experiments are not considered straightforward at the moment.

The retention times of both the known major components and newly identified minor components on the reversed phase column are related to their structures: their retention behavior can be linked to their hydrophobic properties and the influence of 4″-acylated mycarose on the chromatographic behavior of the bitespiramycin components was larger than that of R1 of the macrocyclic lactone or forosamine (see Fig. 1). The information was very helpful to confirm the proposed structures of unknown related substances. Similar results were also observed by Hu et al. [11].

References

[1] Y.F. Liu, C.H. Sun, W.Z. Jin, Isolation and structural identification of shengjimycin A and B, the major components of shengjimycin, Chin. J. Antibiot. 22 (1997) 328–333.
[2] C.H. Sun, W.Z. Jin, 4-Isobutyrylspiramycin, a novel naturally occurring compound, Chin. J. Antibiot. 23 (1998) 253–258.
[3] C.H. Sun, W. Jiang, Y.G. Jin, W.Z. Wang, Isolation and structural identification of 4″-isovaleryl spiramycin I (shengjimycin E), Chin. J. Antibiot. 25 (2000) 1–4.
[4] W. Jiang, C.H. Sun, W.Z. Jin, Chemical studies on minor components of shengjimycins I. Isolation and structure identification of 4″-isobutyryl-spiramycin II (shengjimycin $B_{2\beta}$), Chin. J. Antibiot. 27 (2002) 209–212.
[5] W. Jiang, C.H. Sun, W.Z. Jin, Chemical studies on minor components of shengjimycins. II Structure identification of shengjimycin A_0, B_3 and C_2, Chin. J. Antibiot. 27 (2002) 387–391.
[6] W.Z. Jin, C.H. Sun, W. Jiang, J. Huang, Chemical studies of shengjimycin components, Chin. J. Antibiot. 27 (2002) 705–708.
[7] W. Jiang, C.H. Sun, W.Z. Jin, Chemical studies on minor components of shengjimycins II. Structure identification of shengjimycin B_0, Chin. J. Antibiot. 28 (2003) 385–387.
[8] X.G. Shi, S.Q. Zhang, J.P. Fawcett, D.F. Zhong, Acid catalysed degradation of some spiramycin derivatives found in the antibiotic bitespiramycin, J. Pharm. Biomed. Anal. 36 (2004) 593–600.
[9] A. Kondo, T. Nakatani, Y. Kuzuya, H. Suzuki, H. Sano, K. Yamaguchi, K. Shirahata, K. Takahashi, K. Kita, Y. Nishiie, Studies on acetylspiramycin. 1. Separation and chemical structures of acetylspiramycin components, Jpn. J. Antibiot. 43 (1990) 1152–1163.
[10] A. Kondo, K. Sato, K. Shuto, K. Yamashita, S. Ichikawa, K. Takahashi, K. Kita, Y. Nishiie, H. Sano, K. Yamaguchi, Studies on acetylspiramycin. II. Biological activities of spiramycin components, Jpn. J. Antibiot. 43 (1990) 1521–1529.
[11] M. Hu, C.Q. Hu, Identification of the components of 16-membered macrolide antibiotics by LC/MS, Anal. Chim. Acta 535 (2005) 89–99.
[12] M. Pendela, C. Govaerts, J. Diana, J. Hoogmartens, A. Van Schepdael, E. Adams, Characterization of impurities in spiramycin by liquid chromatography/ion trap mass spectrometry, Rapid Commun. Mass Spectrom. 21 (2007) 599–613.
[13] M.J. Wang, M. Pendela, C.Q. Hu, S.H. Jin, J. Hoogmartens, A. Van Schepdael, E. Adams, Impurity profiling of acetylspiramycin by liquid chromatography–ion trap mass spectrometry, J. Chromatogr. A 1217 (2010) 6531–6544.
[14] M.J. Gonzàlez de la Huebra, V. Ursula, B. Guy, R.R. Adela, Characterisation of dirithromycin and spiramycin using high performance chromatography and direct infusion mass spectrometry, Anal. Chim. Acta 503 (2004) 247–256.
[15] X.G. Shi, D.F. Zhong, Analysis of multicomponent in bitespiramycin by high-performance liquid chromatography–mass spectrometry, J. Chin. Mass Spectrom. 24 (2003) 460–463.
[16] J.Y. Li, C.Y. Ma, H.Y. Wang, Y.H. Wang, L.Z. Wu, Y.G. Wang, On-line identification of 4″-isovalerylspiramycin I in the genetic engineered strain of *S. spiramyceticus* F21 by liquid chromatography with electrospray ionization tandem mass spectrometry, ultraviolet absorbance detection and nuclear resonance spectrometry, J. Chromatogr. A 1217 (2010) 1419–1424.
[17] D.F. Zhong, X.G. Shi, L. Sun, X.Y. Chen, Determination of three major components of bitespiramycin and their major active metabolites in rat plasma by liquid chromatography–ion trap mass spectrometry, J. Chromatogr. B 791 (2003) 45–53.
[18] Y.L. Yang, J.N. Yang, M. Hu, C.Q. Hu, Determination of the components of bitespiramycins by HPLC, Acta Pharm. Sin. 44 (2009) 1183–1186.

Journal of Pharmaceutical and Biomedical Analysis

Editors

B. Chankvetadze, Department of Chemistry, School of Exact and Natural Sciences, Tbilisi State University, 0179 Tbilisi, Georgia. E-mail: jpba_bezhan@yahoo.com

S. Görög, Chemical Works of Gedeon Richter Ltd., P.O. Box 27, H-1475 Budapest 10, Hungary. E-mail: s.gorog@richter.hu

J. Haginaka, Faculty of Pharmaceutical Sciences, Mukogawa Women's University, 11-68 Koshien Kyuban-cho, Nishinomiya 663-8179, Japan. E-mail: jpba@mukogawa-u.ac.jp

R. Moaddel, Baltimore, MD. 21224. USA. Tel: - +1-301-792-6579.

S. Pinzauti, Department of Pharmaceutical Sciences, University of Florence, Polo Scientifico, Via U. Schiff 6, 50019 Sesto Fiorentino, Italy. E-mail: pinz@unifi.it

Editorial Advisory Board

S.W. Baertschi (Indianapolis, IN, USA)
C. Barbas (Madrid, Spain)
C. Bertucci (Bologna, Italy)
F. Bressolle (Montpellier, France)
P.S. Callery (Morgantown, WV, USA)
A. Cifuentes (Madrid, Spain)
S. Fanali (Monterotondo Scalo, Italy)
S. Furlanetto (Florence, Italy)
M. Ganzera (Innsbruck, Austria)
R. Gotti (Bologna, Italy)
P. Hubert (Sart-Tilman Liège, Belgium)
U. Holzgrabe (Würzburg, Germany)
K. Jozwiak (Lublin, Poland)
K. Kakehi (Higashi-Osaka, Japan)
R. Kaliszan (Gdansk, Poland)
S.P. Li (Macau, China)
B.K. Matuszewski (West Point, PA, USA)
N. Medlicott (Dunedin, New Zealand)
R.H.H Neubert (Halle/Saale, Germany)
B.A. Olsen (Indianapolis, IN, USA)
K.W. Phinney (Gaithersburg, MD, USA)
S. Pichini (Rome, Italy)
M.A. Raggi (Bologna, Italy)
K.E. Scriba (Jena, Germany)
K. Shimada (Sendai, Japan)
S. Singh (S.A.S. Nagar, India)
E. Szökö (Budapest, Hungary)
T-H. Tsai (Taipei, Taiwan)
Y. Vander Heyden (Brussels, Belgium)
J.-L. Veuthey (Geneva, Switzerland)
I.D. Wilson (Macclesfield, UK)
G. Xu (Dalian, China)

Author enquiries
For enquiries relating to the submission of articles (including electronic submission) please visit this journals homepage at http://www.elsevier.com/locate/jpba. Contact details for questions arising after acceptance of an article, especially those relating to proofs, will be provided by the publisher. You can track accepted articles at http://www.elsevier.com/trackarticle. You can also check our Author FAQs at http://www.elsevier.com/authorFAQ and/or contact Customer Support via http://support.elsevier.com.

Funding body agreements and policies
Elsevier has established agreements and developed policies to allow authors whose articles appear in journals published by Elsevier, to comply with potential manuscript archiving requirements as specified as conditions of their grant awards. To learn more about existing agreements and policies please visit http://www.elsevier.com/fundingbodies

Orders, claims, and journal enquiries: please contact the Elsevier Customer Service Department nearest you:
St. Louis: Elsevier Customer Service Department, 3251 Riverport Lane, Maryland Heights, MO 63043, USA; phone: (877) 8397126 [toll free within the USA]; (+1) (314) 4478878 [outside the USA]; fax: (+1) (314) 4478077; e-mail: JournalCustomerService-usa@elsevier.com
Oxford: Elsevier Customer Service Department, The Boulevard, Langford Lane, Kidlington, Oxford OX5 1GB, UK; phone: (+44) (1865) 843434; fax: (+44) (1865) 843970; e-mail: JournalsCustomerServiceEMEA@elsevier.com
Tokyo: Elsevier Customer Service Department, 4F Higashi-Azabu, 1-Chome Bldg, 1-9-15 Higashi-Azabu, Minato-ku, Tokyo 106-0044, Japan; phone: (+81) (3) 5561 5037; fax: (+81) (3) 5561 5047; e-mail: JournalsCustomerServiceJapan@elsevier.com
Singapore: Elsevier Customer Service Department, 3 Killiney Road, #08-01 Winsland House I, Singapore 239519; phone: (+65) 63490222; fax: (+65) 67331510; e-mail: JournalsCustomerServiceAPAC@elsevier.com